Tokyo Medical and Dental University
Global Center of Excellence (GCOE) Program
International Research Center for Molecular Science in Tooth and Bone Diseases

東京医科歯科大学　グローバルCOEプログラム

歯と骨の分子疾患科学 国際教育研究拠点

平成24年度 実績報告書

東京医科歯科大学

Tokyo Medical and Dental University
Global Center of Excellence (GCOE) Program
International Research Center for Molecular Science in Tooth and Bone Diseases

東京医科歯科大学　グローバルCOEプログラム

歯と骨の分子疾患科学
国際教育研究拠点

～デント・メドミクスのインテリジェンスハブ～

平成20年～平成24年

平成24年度 実績報告書

ご 挨 拶

東京医科歯科大学においては、大山喬史学長のリーダーシップのもと、5年間にわたり、文部科学省による大学院教育の高度化事業としてグローバルCOEプログラムを推進しております。世界的な研究のトップ拠点としての本プログラムは、我が国の大学院の教育研究機能を一層充実・強化し、国際的に卓越した研究基盤の上で、世界をリードする創造的な人材養成を図ることを目的としております。東京医科歯科大学においては、歯と骨に関わる臨床及び基礎の疾患科学の国際的に卓越した教育研究拠点の形成をこの5年間推進し、国際的な競争力のある大学創りを展開して参りました。『歯と骨の分子疾患科学の国際教育研究拠点-デント・メドミクスのインテリジェンスハブ』を表題として掲げる、本拠点は平成20年度の医学の領域において高い評価のもとに採択されると共に、平成22年度の中間評価においても医学領域の14件のグローバルCOEプログラムの中で、トップランクの2つの拠点に与えられる最高位の評価を受け、平成23年度及び平成24年度においてもこれを反映する支援を文部科学省より受けてグローバルCOEの活動が展開されてきております。

『歯と骨の分子疾患科学の国際教育研究拠点』を推進するにあたり、全ての事業推進担当者がそれぞれの最先端の研究領域に関わる大学院教育を毎週の総合プレゼンテーションにおいて英語による発表と討論を主体として展開し、これにより、学部や研究所を超えた組織の融合的な研究教育の場として異なる専門の3名以上の事業推進担当者が毎週出席して教育にあたり、また、各回の総合プレゼンテーションに対する学生からの評価を毎週フィードバックし、現在も高いレベルの双方向の評価に基づく大学院教育の場として根付いております。歯と骨の国際教育研究拠点としてこれまでの大学院においてはなかった英語面接により競争的に選抜された“特別選抜学生”である“Advanced International Super Student”（AI・スーパースチューデント）に対する重点的な教育と経済的な支援、さらには、年に2回の学生のプログレスを含めた複数の教員によるアドバイスと評価を英語の面談にて実施し、これにより密度の高い教育を推進しております。これと共に、国際的に活躍する大学院生の養成を目指し、海外の主要な歯と骨の研究拠点であるハーバード大学、トロント大学、カルフォルニア大学サンフランシス校と提携し、毎年の学生の派遣と当該大学における海外のトップ研究者をチューターとする教育を展開し、また、高学年の学生は、海外の拠点におけるレクチャーを行う事により、積極的な指導者としての経験を積みつつあります。東京医科歯科大学の拠点においては、“国際PIシャペロン”として優れた若手の研究者を、既にポスドクを終了し、更なる発展を目指す若手研究者として養成し、国際的なトップレベルの研究のみならず、「さきがけ」をはじめとする科学研究費を自ら獲得し、更には選抜した学生の教育に直接関わるなど、近い将来の歯と骨の領域の研究教育を担う人材として養成し国立大学の教員を輩出しております。また、本プログラムの特徴として、毎年の国際外部評価委員による審査とその評価を行うことにより、ハーバード大学を初めとする国際的なトップの大学の教員の立場からのアドバイスと優れたフィードバックを得ると共に、本拠点の存在と意義を世界的にも発信しております。その成果の一つとして、ハーバード大学においては、東京医科歯科大学との連携を出発点にヨーロッパの大学との提携が開始されるなどの発展がなされています。

また、国内的にも、東京医科歯科大学の大学院生の海外派遣プログラムを本学のみならず、国内の優れた本領域の他大学の大学院生を選抜し、本学の海外チューター拠点とする大学に本学のスーパースチューデントと共に派遣するなど、国際的な波及効果を年々高めつつあります。

本教育研究拠点はこれまで、歯と骨の領域の疾患科学である歯学・医学において学術の急速な発展に伴う専門家や再分化に対応する深い専門性を持つと共に、イノベーションに対応する学術領域の垣根を越えた研究の推進を実現しており、本拠点なくしては、得られなかった新領域の創生が図られ、またこれに伴い、新しい領域における若手の教育研究が推進されています。国際的にも、欧米の世界的な研究教育拠点との交流の強化と発展のみならず、アジアにおける本学のリーダーシップを推進し、各国における指導的な人材を本学のGCOE拠点より継続的に且つ発展しつつ供給しております。実際に、これまでスーパースチューデントとして育成された大学院生が米国でのNIHの米国人若手研究者でも取得の困難なK awardを獲得する例をはじめ、トップレベル大学の研究者として活躍していると共に、アジアの優れた研究拠点の大学の若手の指導者として教育研究の中心として活躍する成果が挙げられております。東京医科歯科大学では、これらの若手の世界的なネットワークをさらに発展させる為、本学での教育研究を受けて世界各地で活躍するこれらの本拠点で育成された若手研究者と現在大学院においてスーパースチューデントとして教育されている学生及び国際PIシャペロンとして本拠点において活動する若手との交流を『学生主体のシンポジウム』等の開催により深め本学の大学院学生に対する世界的なネットワーキングとロールモデルを見つつ、発展する為の仕組みを形成しつつあります。また、海外のチューターと海外のトップ研究拠点のリーダーとの連携は、本学学生のこれらの大学への派遣のみならず、海外からの研究者、教育者の招聘をこの5年間に50回以上行いつつ、小グループでこれらの世界的研究者と学生との綿密なディスカションを主体とするMeet-the-Professorシステムを機能させ、本学からの発信及び、本学学生の世界的なエキスパートとのネットワーキングも進展させつつあります。これらの教育研究は、大山学長の御指導のもと、全ての事業推進担当者の先生方がそれぞれ新しい領域を開拓しつつ、未来の国際的指導者を育成する活動を展開している努力の賜物ですし、歯と骨の伝統ある本学の多くの先輩方の業績に基づくものです。

大山学長をはじめ、理事の先生方のリーダーシップのもとに、全事業推進担当者の先生方の不断のご努力によってなされた教育研究の成果が本報告書に集約されており、拠点としての活動が達成されております。今後とも皆様の益々のご支援を賜りますようお願い申し上げます。

野田　政樹
Masaki Noda

東京医科歯科大学

平成24年度

グローバルCOEプログラム実績報告書

歯と骨の分子疾患科学の国際教育研究拠点

専攻等名

医歯学総合研究科器官システム制御学系専攻・口腔機能再構築学系専攻・生体支持組織学系専攻
顎顔面頸部機能再建学系専攻・先端医療開発学系専攻・生体環境応答学系専攻・疾病生命科学研究部
生体材料工学研究所・難治疾患研究所

野田　政樹 Masaki Noda
拠点リーダー／医歯学総合研究科・器官システム制御学系専攻・教授
分子薬理学／医学博士・歯学博士

拠点形成統括および先端硬組織分子再建科学の研究

田上　順次 Junji Tagami
医歯学総合研究科・口腔機能再構築学系専攻・教授
齲蝕制御学／歯学博士

先端硬組織分子再建科学

高柳　広 Hiroshi Takayanagi
医歯学総合研究科・生体支持組織学系専攻・教授
分子情報伝達学／医学博士

硬組織分子喪失病態学

森田　育男 Ikuo Morita
医歯学総合研究科・顎顔面頸部機能再建学系専攻・教授
分子細胞機能学／薬学博士

先端硬組織分子再建科学

小村　健 Ken Omura
医歯学総合研究科・口腔機能再構築学系専攻・教授
顎口腔外科学／医学博士

硬組織疾患ゲノム科学

春 日 井　昇 平 Shohei Kasugai
医歯学総合研究科・口腔機能再構築学系専攻・教授
インプラント・口腔再生医学／歯学博士

先端硬組織分子再建科学

須 田　英 明 Hideaki Suda
医歯学総合研究科・口腔機能再構築学系専攻・教授
歯髄生物学／歯学博士

先端硬組織分子再建科学

和泉　雄一 Yuichi　Izumi
医歯学総合研究科・生体支持組織学系専攻・教授
歯周病学／歯学博士

硬組織分子喪失病態学

柳 下　正 樹 Masaki Yanagisita
医歯学総合研究科・生体支持組織学系専攻・教授
硬組織病態生化学／医学士

先端硬組織分子再建科学

山 口　朗 Akira Yamaguchi
医歯学総合研究科・口腔機能再構築学系専攻・教授
口腔病理学／医学博士

先端硬組織分子再建科学

森 山　啓 司 Keiji Moriyama
医歯学総合研究科・顎顔面頚部機能再構築学系専攻・教授
顎顔面矯正学／医学博士

硬組織分子喪失病態学

大 川　淳 Atsushi Okawa
医歯学総合研究科　先端医療開発学系専攻・教授
整形外科学／医学博士

先端硬組織分子再建科学

宮坂　信之 Nobuyuki Miyasaka
医歯学総合研究科・生体環境応答学系専攻・教授
膠原病・リウマチ内科学／医学博士

硬組織分子喪失病態学

宗田　大 Takeshi Muneta
医歯学総合研究科・生体支持組織学系専攻・教授
運動器外科学／医学博士

先端硬組織分子再建科学

稲澤　譲治 Johji Inazawa
難治疾患研究所・教授
分子細胞遺伝学／医学博士

硬組織疾患ゲノム科学

三木　義男 Yoshio Miki
難治疾患研究所・教授
分子遺伝／医学博士

硬組織疾患ゲノム科学

石野　史敏 Fumitoshi Ishino
難治疾患研究所・教授
エピジェネティクス／理学博士

硬組織疾患ゲノム科学

澁谷　浩司 Hiroshi Shibuya
医歯学総合研究科・器官システム制御学系専攻・教授
分子細胞生物学／理学博士

硬組織基礎生命科学

小川　佳宏 Yoshihiro Ogawa
医歯学総合研究科・器官システム制御学系専攻・教授
分子代謝医学／医学博士

硬組織基礎生命科学

水島　昇 Noboru　Mizushima
医歯学総合研究科・器官システム制御学系専攻・教授
細胞生理学／医学博士

硬組織分子喪失病態学

中川 一路 Ichiro　Nakagawa
医歯学総合研究科・口腔機能再構築学系専攻・教授
細菌感染制御学／歯学博士

硬組織分子喪失病態学

四 宮　謙 一 Kenichi Shinomiya
医歯学総合研究科・先端医療開発学系専攻・非常勤講師
脊椎・脊髄神経外科学／医学博士、横浜市立みなと赤十字病院・院長

先端硬組織分子再建科学

秋 吉　一 成 Kazunari Akiyoshi
生体材料工学研究所・素材研究部門・非常勤講師
有機材料学／工学博士、京都大学 大学院工学研究科高分子化学・教授

先端硬組織分子再建科学

萩 原　正 敏 Masatoshi Hagiwara
疾患生命科学研究部・高次生命制御研究部門・非常勤講師
形質発現制御学／医学博士、京都大学 大学院医学研究科形態形成機構学・教授

硬組織基礎生命科学

国際PIシャペロン、AISS・QAISS

Takuya Notomi, Ph.D.
（納富拓也）
Research Assistant Professor
Department of Molecular Pharmacology

Alireza Sadr, D.D.S., Ph.D.
Research Assistant Professor
Department of Cariology and Operative Dentistry

Masatsugu Oh-hora, M.D., Ph.D.
（大洞将嗣）
Research Associate Professor
Department ofCell Signaling

Iimura Tadahiro, D.D.S., Ph.D.
（飯村忠浩）
Research Associate Professor
Department of Oral Pathology

Naoto Haruyama, D.D.S., Ph.D.
（春山　直人）
Research Associate Professor
Department of Maxillofacial Orthognathics

Hideyuki Iwai, M.D., Ph.D.
（岩井秀之）
Research Assistant Professor
Department of Medicine & Rheumatology

Kunikazu Tsuji, M.D., Ph.D.
（辻邦和）
Research Assistant Professor
Department of Orthopedic Surgery

Lee Jiyoung, Ph.D.
（李知英）
Research Assistant Professor
Department of Epigenetics

Naoki Sawada, M.D., Ph.D.
（澤田直樹）
Research Assistant Professor
Department of Molecular Medicine and Metabolism

Patricia Makishi
Dept. of Cariology and Operative Dentistry
「レジンセメントと象牙質界面における
ナノリーケージについて」

許　ジン
（Xu Jing）
歯髄生物学
視床下部性神経ペプチドによる
中枢性骨代謝制御機構の解明
Uncovering the molecular mechanism of central control of bone remodeling by hypothalamic neuropeptides

Reena Rodriguez
Dept. of Oral Impltantology & Regenerative Dental Medicine
「Epigallocatechin-3-gallate 含有Gelatin Hydrogelを
用いた骨再生に関する研究」

則武　加奈子
Kanako Noritake
Dept. of Oral Impltantology & Regenerative Dental Medicine
「スーパーGBR膜「ハイドロゲルシート」の開発」

郝　佳
（Hao Jia）
インプラント・口腔再生医学　hydeoxyapatiteコーティングインプラント埋入時にZoledronic Acidを局所投与した際の骨形成に与える影響と細菌接着について
Bacterial adhesion and bone formation effect of Zoledronic Acid immobilized hydroxyaptite implants

Paksinee Kamolratanakul
Dept. of Molecular Pharmacology
「ナノゲルscaffoldを用いたEP4アゴニストとBMPの
骨再生能に関する研究」

中川　朋美
Tomomi Nakagawa
Dept. of Molecular Pharmacology
「悪性黒色腫の骨の転移における転写因子Cizの
役割の解明」

鈴木　尋之
Hiroyuki suzuki
Dept. of Maxillofacial Orthognathics
「可溶型fibroblast growth factor receptor2（FGFR2）の
頭蓋冠縫合部早期癒合症に対する治療効果」

Erik Idrus
Dept. of Cell Signaling
「RANKL刺激によるNFATc1制御遺伝子と
microRNAの同定」

Gamaralalage Amodini Rajakaruna
Dept. of Periodontology
「歯周病とバージャー病の関連の解明」

藤田　浩二
Koji Fujita
Dept. of Orthopaedic and Spinal Surgery
「Vitamin Eの骨代謝に対する影響について」

木原　翼
Tasuku Kihara
Oral pathology
骨芽細胞分化と骨再生におけるCCN3の役割
The role of CCN3 in osteoblast differentiation and bone regeneration

古田　繭子
Mayuko Furuta
分子細胞遺伝学（Molecular Cytogenetics）
新たなRNA創薬に寄与する癌制御性microRNAの機能的スクリーニング
Exploration of novel tumor-suppresive microRNAs using functional genomics-assisted approach

安藤　彰子
Akiko Ando
バイオイメージングを用いた歯周組織幹細胞の同定
Identification of periodontal stem cells by bio-imaging approaches

Bharti Pariksha
歯周病学
歯周治療が全身の炎症に与える影響
Effect of Periodontal Treatment on systemic inflammation.

辻　香織

Kaori Tsuji
顎顔面矯正学
Zinc finger 型転写因子POKEMONの破骨細胞における役割の解明
Investigation of the role of zinc finger transcription factor, POKEMON in osteoclasts

許　レン
XU Ren
整形外科（Orthopaedic and Spinal Surgery）
視床下部性神経ペプチドによる中枢性骨代謝制御機構の解明
Uncovering the molecular mechanism of central control of bone remodeling by hypothalamic neuropeptides

周　夢宇

Zhou Mengyu
歯髄生物学（Pulp Biology and Endodontics）
歯根形成のメカニズム-SCAP（根尖部幹細胞）からの象牙芽細胞およびセメント芽細胞分化に関与する因子の解明
The mechanisms of root formation- Elucidation of the signaling molecules on odontoblast and cementoblast differentiation from SCAP

Smriti Aryal A. C

分子薬理学（Molecular Pharmacology）
細胞骨格による骨代謝制御の分子機構 -Nckの骨の細胞機能調節に於ける役割の解明-
Molecular Mechanisms Underlying Cytoskeletal Regulation of Bone Metabolim-Role of Nck Proteins in Bone Cell Function-

Chokechanachaisakul Uraiwan

歯髄生物学（Pulp Biology and Endodontics）
ラットを用いた歯髄生物学
Rat's pulp biology

Kunawarote Sitthikorn

う蝕制御学
う蝕象牙質に対する接着性能の改良
Improve Bond strength to Caries-affected dentin

Ilnaz Hariri

う蝕制御学
高度に石灰化した接着界面構造の作成と機械的性質の評価
Generation of hyper mineralized adhesive Interface and study on its mechanical properties

AL-BARI MD. ABDUL ALIM

分子情報伝達学（Cell Signaling）
破骨細胞分化を制御するphosphatidylinositol-3,4,5-trisphosphate結合タンパク質の同定と機能解析
Identification and analysis of phosphatidylinositol-3,4,5-trisphosphatebinding proteins（PIP_3BPs）that regulate osteoclast differentiation

古市　祥子

Akiko Furuichi
インプラント・口腔再生医学
酸素ナノバブル水の骨組織における生体活性評価
Evaluation for the biologically activity of oxygen nano bubbles solution（OXNB）

Hamid Nurrohman

う蝕制御学（Cariology and Operative Dentistry）
人口口腔装置を用いたバイオフィルムによるう蝕形成後の”Super Dentin”のナノ構造解析
The effect of collagenolytic inhibitors on the quality of acid-base resistant zone in dentin

Chui Chanthoeun

歯周病学（Periodontology）
歯周組織の除菌のための新しい治療様式の開発:LEDと光感受性色素を用いた抗菌的光線力学療法の効果に関する基礎的研究
Development of a New Treatment Modality for Periodontal Disinfection: Basic Study on the Effect of Antimicrobial Photodynamic Therapy using the Combination of an LED
light Source and a Photosensitizing Dye

Samir Kumar Pal

口腔病理学（Oral Pathology）
口腔扁平上皮癌による骨破壊におけるThrombospondin-1の役割
The Role of Thrombospondin-1（TSP-1）in Bone Destruction by Oral Squamous Cell Carcinoma

Hoi　Chin　Hew

遺伝子応用医学
新規プロラインキナーゼC（PKC）アポトーシス標的分子Evi-1の同定
Identification of Evi − 1 as a novel PKC Apoptosis Regulatory Target

村松　智輝

Tomoki Muramatsu
分子細胞遺伝学（Molecular Cytogenetics）
食道扁平上皮癌の発生・進展におけるYAP増幅・発現亢進の分子病理学的意義
Significance of YAP amplification/overexpression in the pathogenesis of esophageal squamous cell carcinoma

鈴木　允文

Suzuki Takafumi
歯周病学
骨吸収を引き起こす咬合性外傷の分子機構について解析する-TRPV4の役割-
Molecular mechanism underlying occlusal trauma, induced-bone loss Role of TRPV4

宮嶋　大輔

Daisuke Miyajima
顎顔面外科（分子薬理）
骨代謝における負のMCSFシグナルによる新制御機構の解析 -Dok　アダプター分子による破骨細胞制御と骨粗鬆症-
Novel Insights into Negative Molecular Regulation of MCSF Signaling in Bone Metabolism -Function of Dok Adaptor Molecules in Osteoclasts and Osteoporois -

Atukorallaya Devi Sewvandini Atukorala

硬組織構造生物学
咽頭鰓弓および咽頭鰓発生への外胚葉上皮の関わり
Tracing the fate of ectoderm during the pharyngeal arch development

Kandakar Abu Shameem Md. Saadat

分子発生学

RB/E2F経路の制御と骨肉腫形成過程におけるDRIL1の役割

The Role of DRIL1in the Regulation of RB/E2F Pathway and Tumorigesis of Osteosarcoma

関根　由莉奈

高次生命科学

ナノゲル　リポソーム複合体ハイブリッドゲルの設計と医療応用

Design and Application of Hydrid Hydrogels with Nanogel-coated Liposomes complex

馬　成山

（Ma Chengshan）

整形外科学

骨リモデリングにおける中枢神経制御の経路

A Novel Central-Control Pathway of Bone Remodeling

妻沼　有香

歯周病学

歯根膜細胞シートのインプラント両方への応用

Application of periodontal ligament cell sheet for implant therapy.

Bhargava Suhas Srilatha

インプラント・口腔再生医学

Y-TZPジルコニアの表面処理が骨芽細胞と線維芽細胞に及ぼす影響

Surface modified Y-TZP Zirconia: its effect on osteoblasts and fibroblasts in vitro

MD ABDULLA AL MASUD KHAN

硬組織薬理学

TNFαとRANKLアンタゴニストであるW9ペプチドの骨形成における役割

A Role of TNF- α and RANKL antagonist peptide W9 on osteogenesis

滝沢　文彦

発生発達病態学

マクロファージToll-like receptor 4 シグナルにおける細胞内カルシウムおよびTransient Receptor potential Vanilloid 2の役割の解析

Role of intracellular calcium and Transient Receptor potential Vanilloid 2 in macrophage Toll-like receptor 4 signaling

白　樺

Bai Hua

Dept. of Moleclurar Cytogenetics

「ヒト癌におけるオートファジー関連遺伝子LC3Av1遺伝子の機能解析」

Bakhsh, Turki Abdulsalam A.

う蝕制御学

コンポジットレジン接着界面の長期的な挙動について、SS-OCTを用いた定量的評価

SS-OCT as a new tool for long term quantitative evaluation on the resin-dentin interface in a bonded restoration

Warunee Pluemsakunthai

インプラント・口腔再生医学

ウサギ頭蓋骨欠損モデルにおける改良PRF含有αTCPの骨再生における有用性の検討

The effect of platelet rich fibrin（PRF）preparation with Alpha-tricalcium phosphate（α -TCP）enhance bone regeneration in rabbit calvarium

森田　淳平

顎顔面矯正学

可溶型線維芽細胞成長因子受容体2を用いたアペール症候群の新規治療方法の開発 - アペール症候群表現型の救済 -

The development of novel treatment for Apert syndrome by a soluble form of FGFR2-Rescue of Apert phenotypes

Bijaya Baobam

細菌感染制御学

オートファジーおよび免疫応答におけるA群レンサ球菌認識機構の解析

Molecular analysis of recognition mechanisms of Group A Streptococcus in autophagic degradation system and immune responses

山田　梓

歯周病学

ヒト歯根膜幹細胞の骨芽細胞/セメント芽細胞分化を誘導する因子の探索

The search of factoers inducing osteoblastic/cementoblastic differentiation in human Periodontal Ligament Stem Cells

南原　弘美

歯周病学

歯周病原細菌によるWnt5a遺伝子発現機構の解析

The modulation of Wnt5a expression by periodontopathic bacteria

中根　綾子

小児歯科学

慨定量的in situ　蛍光イメージングによる骨細胞の慨日リズムの可視化と、成長発達過程におけるその機能解析

Quantitative in situ fluorescent imaging approach for functional dynamics of osteocytes through circadian oscillation during growth and development

Nurmaa Dashzeveg

バイオ情報学

骨肉腫におけるP53によって誘導されるアポトーシス関連遺伝子の解析

Discovery of pro-apoptotic genes induced by p5 3 in osteosarcoma

荻田　真弓

歯周病学

ヒト歯根膜細胞におけるレーザー照射およびサイトカイン刺激によるhuman-beta-defensin（HBDs）発現の探査

The expression of HBDs by laser irradiation, various cytokines and bacterial components in human PDL cells

山口　佑季

バイオ情報学

哺乳類の特徴的形質における哺乳類特異的遺伝子群の役割

The role of mammalian specific genes in mammalian characteristics

大上　えりか

顎顔面外科学
口腔扁平上皮癌が生産する破骨細胞性骨吸収制御因子の同定
Identification of osteoclastic bone resorption regulatory factors produced by oral squamous cell carcinoma

湯浅　将人
整形外科学
デキサメタゾン併用によるBone morphogenetic proteinによる骨形成に対する有効性の検討
The efficiency of bone formation by BMP with dexamethasone

宮部　斉重
膠原病・リウマチ内科学
関節リウマチ病態形成におけるLPA/LPA受容体、ATXの関与
Pathogenic roles of LPA/LPA receptors and ATX on the rheumatoid arthritis

山田　剛史
整形外科学
骨髄由来間葉系細胞（MSC）の質 - 骨形成抑制因子の同定 -
The significance of the quality of the human bone marrow mesenchymal cells（hBMMCs）in the bone formation

Rojbani Hisham Khalifa

インプラント・口腔再生医学
ブラッククミン（Nigella　Sativa）の骨再生における効果の検討
Effect of Nigella Sativa on Bone Formation

チェン康

（Chang Kang）
インプラント・口腔再生医学　歯科用インプラント周囲骨における直流電流装置を用いた骨形成促進作用に関する研究
A direct current device for accelerating bone formation in tissues surrounding a dental implant.

Osama Zakaria

インプラント・口腔再生医学
異なる表面性状を有する歯科用インプラント周囲骨における電気的刺激を用いた骨形成促進作用に関する研究
Electrical stimulation for acceleratioing Peri-implant bone formation of different implant surfaces

岩崎　陽平
分子薬理学
骨に対するPTH作用におけるCB2の調節作用の解析 -
骨細胞集団および中枢神経系の骨量調節における連関の解明 -
Analysis of regulatory effect of CB2 to thePTH effect to Bone.-Relevance of Bone Cell Assembly（BCA）and Central Nervous System（CNS）in the maintenance of bone-

長谷川　久紀

膠原病・リウマチ内科学
関節リウマチ（RA）の新規治療標的となるmicroRNAの探究
Identification of microRNA as a new therapeutic target for rheumatoid arthritis.

福田　真

膠原病・リウマチ内科学
関節リウマチ病態形成におけるFROUNTの関与
Pathogenic roles of FROUNT on Rheumatoid Arthritis

佐藤　潔
顎口腔外科学
口腔扁平上皮癌の顎骨浸潤における癌関連線維芽細胞の役割
Roles of carcinoma-associated fibroblasts in bone invasion by oral squamous cell carcinoma

Marwa Madi
インプラント・口腔再生医学
インプラント周囲炎を誘発させた状態における、HA薄膜スパッタリングインプラントと、他の表面性状インプラントの比較
Experimental periimplantitis at HA sputtered coated implants in comparison to other surface treatments

渡辺　千穂
顎顔面矯正学
骨代謝におけるRNA stabitlityの機能解析
Functional analysis of RNA stability in bone metabolism

細矢　匡

膠原病・リウマチ内科学
TEAM1-TREM1-Ligand 相互作用修飾による自己免疫疾患の新規治療法の開発
Development of new treatment of autoimmune diseases by modifying interaction between TREM1 and TREM-Logand

徐　成
（Cheng Xu）
整形外科学
骨形成におけるmicroRNAの役割
Role of microRNA in bone formation

木村　直樹

膠原病・リウマチ内科学
腫瘍による筋炎発症のメカニズムの解析
Analysis of cancer-associated autoimmune myosis

Prasansuttiporn Taweesak

う蝕制御学
次亜塩素酸ナトリウム処置後象牙質に対するrosmarinic acidの接着強さ及び耐久性への影響
Effect of rosmarinic acid on bond strength and bond longevity to NaOCL-treated dentin.

Adorno Quevedo Carlos Gabriel
歯髄生物学
ラット歯髄の慢性炎症後にみられるリンパ管新生
Lymphangiogenesis in the rat dental pulp following induced chronic inflammation

安岡　潤一
高次生命科学
カチオン性ナノゲルによる新規核酸デリバリーシステム
Novel nucleic acid Delivery Systems by Cationic Nanogel

鈴木　晶子

膠原病・リウマチ内科学
マウス膠原病モデルの病態における体液調整因子の働きを明らかにする。
The role of circulating plasma volume regulation factors in murine arthritis and myositis model

土戸　優志

高次生命科学
新規ナノゲルによるタンパク質デリバリー
Protein Delivery by Novel Nanogel

宮原　宇将

インプラント・口腔再生医学
ナノゲルを用いた骨再生に関する研究
A research on bone regeneration by using Nanogel

Thitthaweerat Suppason
う蝕制御学
次亜塩素酸ナトリウムとロスマリン酸の失活歯への接着強さと長期接着耐久性に及ぼす影響
Influence of NaOCIand rosmarinic acid on bond strength and long-term bond durability in endodontically treated tooth

Md.Sofiqul Islam

う蝕制御学
フラボノイドによる、象牙質コラーゲン保護と脱灰象牙質の再石灰効果 - 新しい根面蝕歯 - 治療アプローチ
Flavonoid Reserves Dentin Collagen and Promotes human Root Dentin Lesion Re-mineralization in vitro

Gerardo Jose Joves Mendez

う蝕制御学
塩化カルシウム・フッ素含有ボンディングシステムを用いた歯質接着界面の強化
Reinforcement of adhesive interface using a CaCl2/ fluoride-incorporated bonding system

芦垣　紀彦

歯周病学
歯周病原細菌が慢性腎不全を悪化させる病因の解析
Periodontal bacteria aggravate chronic renal failure by subtotal nephrectomy in mice

Paveenarat Aukkarasongsup
顎顔面矯正学
低酸素状態下のマウス歯根幕細胞におけるペリオスチン遺伝子発現制御メカニズムの解析：低酸素応答領域の同定とHIF－1経路関わり
Analysis of periostion gene expression in mouse periodontal ligament cells under hypoxia: identification of HRE and HIF-1 pathway

渡辺　高

顎顔面外科学
in situ蛍光イメージング解析による、骨の分化・再生におけるRunk2タンパク細胞内動態の新規調節機構の解析
Investigation of novel subcelular bynamics of Runx2 during bone differentiation and regeneration by in situ fluorescent imaging analysis

坂野　若詠
う蝕制御学
新規象牙質接着システムの開発及び評価について
Developing resin composite restoration with adhesive system

Rumana Khanom
口腔病理学
シグナル分子としてのケラチン17が癌の骨浸潤に果たす役割の解析
The functional role of leratin 1 7 as a signaling molecule in bone invasion of oral cancer

Duarte Puerto Carolina Lizeth
顎顔面矯正学
磁気制御されたRelaxin と　BMP-2ナノ粒子を用いた骨縫合の拡大
Sutural Expansion Assisted With Magnetically Controlled Site Specific Relaxin and BMP-2 Nanoparticles

于　淼
（Yu Miao）
インプラント・口腔再生医学
尾部懸垂マウスを用いた、骨再生におけるメカニカルストレスの関与に関する研究
The role of mechanical stress in bone regeneration using tail suspension mice

上園　将慶
顎顔面矯正学 低浸襲かつ早期に骨接合する新規矯正用デバイスの開発
Development of minimally invasive and rapidly osseointegratable orthodontic devices

Amir Nazari

う蝕制御学
う蝕脱灰象牙質を高度石灰化組織へと変化させるための再石灰化技術の創造
Developing a Dentin Remineralising Method（DRM）to Transform Carious Demineralised Dentin into Hypermineralised Substrate

Gombo Bolortuya

Dept. of Pulp Biology and Endodontics
「インテグリン発現を評価することによる象牙芽細胞の成熟とシグナル伝達に対する低出力レーザー療法の効果」

伊達　佑生

Yuki Date
Dept. of Oral Impltantology & Regenerative Dental Medicine
「歯根発生に関する因子の同定」

大城　暁子
健康推進歯学
FDC-SPの口腔内組織での機能
The roles of FDC-SP in oral tissues

Aslam Al Mehdi

Dept. of Periodontology
「歯周疾患は動脈疾患の進行に重要なリスクファクターとなる」

松本　力

Tsutomu Matsumoto
口腔病理学
矯正的歯の移動における骨細胞の役割
The role of osteocyte in orthodontic tooth movement

Wayakanon Praween

分子細胞機能学（Cellular Physiological Chemistry）
アニュラーギャップジャンクションの形成機構
The Mechanisms of Annular Gap Junction Formation

青井　陽子
Yoko Aoi
Dept. of Cellular Physiological Chemistry
「低酸素下におけるサイトカイン産生変動機序～
メチル化の関与」

下田　麻子
Asako Shimoda
有機材料（Organic materials）
ナノゲル架橋ハイドロゲルによるタンパク質デリバリー
Design of Nanogel-assembled hydrogel for protein delivery

高橋　治子
Haruko Takahashi
有機材料（Organic materials）
Polysaccharide nano-ball を用いた新規ナノキャリアの開発
Design of Funtional Polysaccharide nano-ball as new nanocarrier

半場　秀典
う蝕制御学
Creating “acid resistant enamel” : de- /re-mineralization methods

馬　騰
分子発生学
Effect of p53 activating chemical compounds on p53 phosphorylation and p53-mediated apoptosis in osteosarcoma and oral squamous cell carcinoma

島田　泰如
顎口腔外科学
Molecular pathogenesis of Keratocystic Odontogenic Tumors

Zayar Lin
インプラント・口腔再生医学
Application of oral mucosal fibroblasts as a source of cell-mediated bone regeneration therapy

葉　暢暢
歯周病学
Periodontal disease and preterm low birth weight The cross reaction between antibodies of periodontal pathogens and β2GPI

Dawud Abduweli
硬組織構造生物学
Pharyngeal Dentition of Medaka: Tooth Replacement and Stem Cell Niche

白川　純平
顎口腔外科学
Stem Cell G0/G1 Control for Bone Formation by Molecular Link between Mechanical Stimulation and PTHR Signaling

Suphanantachat Supreda
歯周病学
Determination of gene expression profile during cementogenesis using next generation sequencing system

カハル　アブラ
運動器外科学
Roles of BMP-7 in joint homeostasis

小野　岳人
分子情報伝達学
Elucidating effects of inflammatory responses on bone system

顧　潔
歯髄生物学
Analysis of receptive mechanism and recognition in the CNS of pulpal sensation

瀧本　昇陽
歯髄生物学
Regulation of inflammation and induction of regeneration in the dental pulp by MMP-3

吉崎　正子
顎顔面矯正学
Investigation on inhibitory effects of soluble Apert FGFR2-nanogel complex on premature fusion of cranial sutures

Mandurah, Mona Mohammad M.
う蝕制御学
Study on evaluation of sclerotic dentin–resin interface using SS-OCT and nanoindentation

山下　優
インプラント・口腔再生医学
In Vivo Study in a Rat Calvarial Defect Model on the application of combined PRF Membrane with Novel GBR of Cholesterol-bearing Pullulan Nanogel Scaffold for increased bone regeneration

Lodha Ena
う蝕制御学
Enhancement of bleaching action and reminerralization using iontophoresis

Rajapakshe Mudiyanselage Anupama Rasadari Rajapakshe
硬組織病態生化学
Histological observation of the inflamed gingival tissue at the site of periodontitis.

Mohd Haidil Akmal Bin Mahdan
う蝕制御学
Effect of long term water strage and thermal cycling on bonding durability in crown and root canal dentin in vitro

Thanatvarakorn Ornnicha
う蝕制御学
Comparative Study on Effect of Long-term Artificial Saliva Immersion and Acid Challenge on the Dentin Permeability Reduction by Two Desensitizers

横山　和佳
膠原病・リウマチ内科学
Pathogenic Roles of CCL25/CCR9 on Rheumatoid Arthritis

松尾　祐介
膠原病・リウマチ内科学
Identification of the origin of pathogenic fibroblast-like synoviocytes in murine arthritis

中里　洋子
膠原病・リウマチ内科学
Analysis of cancer-associated autoimmune myositis

Maheswari Kuppusamy
インプラント・口腔再生医学
Periosteal elevation in rat calvarium using different Titanium mesh

Alaa Abdulahad Turkistani

う蝕制御学
In Vitro Evaluation of Demineralization Around Indirect Composite Restorations
Using SS-OCT

Uehara Daniela Tiaki

分子細胞遺伝学
Investigation of Causative Genomic Aberrations in Subjects with Congenital Diseases of Unknown Etiology

Mohannad Issa Michael Nassar

う蝕制御学
Glutathione Effect on Dentinal Matrix Metalloproteinase

竹中　健智
膠原病・リウマチ内科学
Analysis of the functions of HUMAN TREM-1-ligand in rheumatoid arthritis for the development of new safer anti-rheumatic drugs

Khunkar, Sahar Jameel M

う蝕制御学
In vitro study on potential effect of a natural plant extract, Miswak, on inhibition of enzymatic collagen degradation and on lesion development in bovine root dentin

Thanit Prasitsak
分子発生学
The Role of Foxc1 in Brain Vascular Development

Surapornsawasd Thunyaporn
顎顔面矯正学
Molecular Characterization of Human BCOR Mutations in root formation of OFCD syndrome

喬　華
う蝕制御学
The relationship between dentin permeability and adhesives for the resin coating technique

橋田　之彦

顎顔面外科学（分子細胞機能学）
Effect of intercellular cAMP level on two different phenotypes (osteogenic and osteoclastogenic) in osteoblast

小倉　健司

顎顔面矯正学
Roles of RANKL produced by periodontal tissues in orthodontic tooth movement

齋藤　鉄也
膠原病・リウマチ内科学
Identification of the Origin of Pathogenic Fibroblast-like Synoviocytes in Murine Models of Arthritis

梅澤　夏佳

膠原病・リウマチ内科学
The role of CRTAM（Class I-restricted T cell associated molecule）in C-protein induced myositis

川崎　真希理

分子薬理学
Functional analysis of ciliary protein Bbs3 in bone metabolism.

李　慧

顎顔面外科学（分子細胞遺伝学）
Oncogenic / tumor-suppressive microRNA (miRNA)

Nuylan, Michelle Loyola
分子細胞遺伝学
Exploration of therapeutic approach based on the inactivated-type NOTCH1 mutation in esophageal and oral squamous cell carcinoma

ALSAYED, EHAB ZAKI E

う蝕制御学
Long-term Evaluation of Enamel Coated by Resin Thin Film using SS-OCT

Baba Bista

う蝕制御学
Effect of Elasticity of Current One-step Self-etch Adhesives on Marginal Adaptation of the Restorations

Kong Kalyan

う蝕制御学
The Effect of Lasers on Bleaching Bovine teeth with low concentration Hydrogen Peroxide and Titanium Dioxide Photocatalyst

Nadila Wali

分子遺伝学
ヒト乳癌骨転移における 切断型BRCA2タンパク質機能の解明

Sahani Mayurbhai Himatbhai

細胞生理学
Molecular dissection of non-canonical Atg12_Atg5 conjugation system in Plasmodium falciparum.

山田　峻之

顎顔面外科学（分子薬理）
Discovery of new molecular targets for β_Adrenergic Receptor(AR) that exceeds PTH anabolic action

東京医科歯科大学
歯と骨の分子疾患科学の国際教育研究拠点

グローバルCOEプログラム活動概要

平成20年度から24年度に至るまでの5年間で10回の国際シンポジウムを開催すると共に、毎週の先進的な歯及び骨に関わる骨と生命科学に関わる総合プレゼンテーションを毎週3名以上の推進担当者の教授の参加のもとに行い、その数は117回を数え参加者総数7,000名に上っております。また、世界的な研究者の招聘講演は歯科学、医科学及び生命科学の領域から61回を数え、学生並びに若手研究者に対する個別のディスカッションと教育の場として機能しております。さらに東京医科歯科大学を拠点とする国際教育に加え選抜した大学院生に対し積極的に世界のトップ拠点の大学院教育を受けさせるためにすでに毎年ハーバード大学に大学院生を派遣し、カナダのトロント大学における大学院活動並びにカリフォルニア大学サンフランシスコ校の医学系の学生教育に対しても本学の大学院生が派遣され、これらの大学における教員のもとで自らの研究発表をし、また教育を受ける機会を設定しております。これに加え、平成21年度には海外のトップクラスの歯と骨の領域の企業研究所への派遣を行い、メルク等の会社組織の中での研究の実地の場における教育が行われております。特別選抜大学生の選抜試験は年2回行われ英語による選抜のもと選ばれた大学院生に対する教育及び経済的な支援が行われると共に若手の優秀な研究者対する拠点内での競争的な研究費の申請による訓練、さらには事業推進担当者の教授が新たな分野を開拓するイノベーション研究プログラムを開始し、拠点内部の教授によるピアレビュー並びに若手研究者や大学院生による教授のプレゼンテーションへの評価などの透明性の高い評価システムのもとにこのプログラムの推進を行っております。さらに国際的な外部評価はこれまでに10回を数え、より高度な国際的拠点としての進展を目指していると共に社会への公開の為、ホームページを充実しこれまで7万件を超えるアクセスを頂いております。

1. 目的・必要性 (Objectives)

東京医科歯科大学は“歯”と“骨”の疾患科学において世界的な拠点であること特徴とする。本拠点形成の目的は、世界で最も高年齢化の進行する我国にあって、人々が生きるために必須の“歯”と“骨”の分子疾患科学について、21世紀COEの成果を発展的に継承し、世界最先端の研究を展開して、合わせて次世代を担う国際的に活躍する若手研究者を養成する世界でも類のない国際教育研究拠点を形成することである。

2. 人材育成計画 (Education Plan)

(1) 国際PIシャペロン（PI-Chaperon（PIC））制度

国際PIシャペロン（PIC）制度とは、国際公募により選抜され、国際的に活躍する自立した研究者を目指す(Principal Investigator)、シャペロン型（大学院生を指導し共に研究する）のPostDoc終了後の（PDは採用しない）若手研究者育成制度である。さらに挑戦的な学際領域を開拓して（Prime Innovation）未来の領域を作り上げ、国際的に競争力のある創造性豊かなプロジェクトを遂行する（Project with Imagination）ことの3つのPIをキーワードとする若手研究者を育成するシステムである。英語のインタビューにより、全て外部より採用する。またGrant Writing等の指導ではGrant査読者やStudy Section担当者による教育を含め国際的視点でのトレーニングを行う。

(2) アドバンスト・I・スーパースチューデント（AI-SS）制度

アドバンスト・I・スーパースチューデントとは選抜され重点的な大学院教育と経済支援を受け、国際的に発展する力をつけるスーパースチューデント（SS）である。21世紀COEにおいては、本拠点は重点教育・経済支援の対象となるSS制度を創出し、優れた大学院生の教育、育成を達成した。本拠点においては、これを発展させ，(i) 国際的に活躍する（International），(ii) 国際的に大学院生同士で相互に切磋琢磨する（Interactive），(iii) 個性の輝く（Individual Identity）の“3つのI”をキーワードとする指導的人材の育成を目指す新制度を創設する。新たに、(1) 国際教育としての国際メンター制度、(2) 国際“Interactive”プログラムによる、一流の大学院であるUCSF、ハーバード大（米国）トロント大（カナダ）における大学院の教育（学生発表会）に参加し、海外拠点の大学院生との交流ならびに現地海外教員による教育

を受け、(3) 個を伸ばす国際教育プログラムとして国際コンティニュエータープログラム（AISS-ICP）などを自ら選択しつつ教育を創造する。医歯学系大学院留学生数は全国一位だが更に海外の若手のリクルート、キャリアパスの担当部を其々設置して強化する。

3. 研究活動計画 (Research Plan)

拠点の研究においては、歯と骨の疾患領域における世界最高レベルの研究として硬組織の喪失と形成に関わる疾患のメカニズムならびにその診断・治療基盤研究を推進する。具体的研究目的は以下の3点である。即ち、【研究目的1】歯と骨の喪失に至る疾患の分子病態成立のメカニズムの解明、【研究目的2】歯と骨の先進的再建の為の治療法の基盤研究の推進、【研究目的3】歯と骨の疾患の統合的機能情報研究の推進である。これらの有機的融合により新たな歯と骨の疾患分子の統合研究（デントメドミクス）を創成する。この目的のために、歯学部、医学部、難治疾患研究所、生体材料工学研究所、研究部の五つの部局が横断的体制をとり、個々の先進研究をさらに発展させるとともにこれらを合わせた新領域のイノベーションを推進する。

4. 組織構成 (Administration)

学部・研究所を越えた横断的体制をとり、先進研究をさらに発展させる。

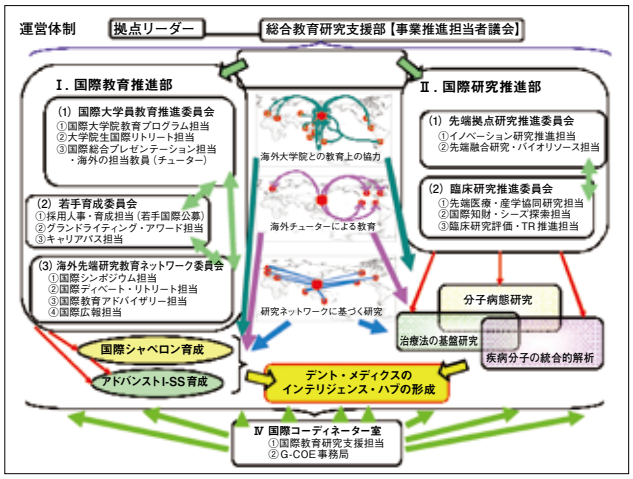

5. 中間評価結果 (Middle Evaluation Result)

（文部科学省発表2011年1月7日）

「グローバルCOEプログラム」（平成20年度採択拠点）中間評価について

http://www.mext.go.jp/a_menu/koutou/globalcoe/1301052.htm

グローバルCOEプログラム　平成20年度採択拠点中間評価結果一覧（総括評価内訳）

【医学系】

現行の努力を継続することによって、当初目的を達成することが可能と判断されるとされた12件に選ばれ、更にこの中で特に秀れた2件として評価された。

拠点番号	拠点プログラム名	機関名
F07	歯と骨の分子疾患科学の国際教育研究拠点	東京医科歯科大学

専攻等名	拠点リーダー名	連携先機関名（※）	特に優れている拠点 12件中2件
医歯学総合研究科器官システム制御学系専攻	野田政樹		◎

グローバルCOE プログラム 平成20年度採択拠点中間評価【特に優れている拠点】概要

【医学系】

F07「歯と骨の分子疾患科学の国際教育研究拠点」
東京医科歯科大学医歯学総合研究科器官システム制御学系専攻

特に人材育成面において、国際PI シャペロン教員やアドバンスト・I・スーパースチューデントなどユニークなシステムが立ち上がり、世界の著名大学の教員をメンターに採用するなどメンター制度も効率的に活用され、若手研究者育成に大変優れた成果があがっている。

また、毎週1 回の国際総合プレゼンテーション、海外のトップ研究者を招く海外研究者講演会、国際シンポジウムの開催などが積極的、生産的になされるとともに、海外の先端的研究者による国際外部評価会など、拠点の活動に対する評価システムをうまく構築しており、教育にかなりの努力が払われている。

研究活動においても、世界トップレベルの業績が得られ、基礎的研究の実績のみならず、臨床研究活動も進展している。

運営面では、大学及び拠点リーダーの強いリーダーシップの下で精力的に拠点が運営され、国際化に向けた取組みも盛んで、歯科と医科の融合もうまくなされている。

6. 国際外部評価会
(International Advisory Review)

実施日

2012.11.14

歯と骨のGCOE国際外部評価会
International Advisory Review

EVALUATION FORM（7名回答）

【評価者】

Lynda F. Bonewald
Professor, Department of Oral Biology Faculty, University of Missouri Kansas City

Irma Thesleff
Professor, Institute of Biotechnology, University of Helsinki

Gregory J. Seymour
Professor, Dean, Faculty of Dentistry, University of Otago

Nawarat Wara-aswapati Charoen
Associate Professor, Dean, Faculty of Dentistry, Department of Periodontology, Khon Kaen University

Young Ku
Professor, School of Dentistry, Department of Periodontology, Seoul National University

Seung-Hak Baek
Professor, School of Dentistry, Department of Orthodontics, Seoul National University

Young-Chel Park
President, World Implant Orthodontic Association Professor, Department of Orthodontics, College of Dentistry, Yonsei University

【評価】

A. Overall Evaluation on the Global COE Program

1. Overall evaluation on the Global COE program activities

Excellent	Good	Fair	Poor	N/A
7				

2. Research

2-1. Evaluation on the researches in the Global COE program

Excellent	Good	Fair	Poor	N/A
7				

2-2. Collaboration within the Global COE program

Excellent	Good	Fair	Poor	N/A
7				

2-3. Clinical aspects of the Global COE program

Excellent	Good	Fair	Poor	N/A
4	2			1

3. Education

3-1. Efforts to promote young scientists in the Global COE program

Excellent	Good	Fair	Poor	N/A
7				

3-2. International collaborative efforts

Excellent	Good	Fair	Poor	N/A
6				1

4. Management

4-1. Administrative structure of the Global COE program

Excellent	Good	Fair	Poor	N/A
6				1

4-2. Is the budget of the Global COE program spent efficiently?

Excellent	Good	Fair	Poor	N/A
5				2

5. Perspective

Will the GCOE program contribute to the future development of the bone and tooth field?

Excellent	Good	Fair	Poor	N/A
6				1




7. 国際教育活動 (International Education)

歯と骨のGCOEの大学院生（AISS/QAISS）による海外活動リスト

2012年4月10日Harvard School of Dental Medicine Research Day
参加者：Chiho Watanabe, Makiri Kawasaki, Nurmaa Dashzeveg



2012年4月11日 Harvardでの本学の大学院生（AISS）・Chiho Watanabe, Makiri Kawasaki, Nurmaa Dashzeveg によるレクチャー

2012年6月13日 Dr. Yu Suk Choi（UCSD）とのディスカッション

2012年9月25日 Dr. Le Duong（MSD） とのディスカッション

2012年10月11日UCSF Research Day
参加者：Masayoshi Uezono, Ye ChangChang


2012年10月12日UCSFでの大学院生（QAISS, AISS）・Masayoshi Uezono, Ye ChangChangによるレクチャー

8. Meet the Professor

2012年10月29日
Dr. Bjorn Olsenと学生のディスカッション

9：50 -10：50 Students Discussion1
（司会：納富拓也、春山直人、学生14名）
11：30-12：30 Students Discussion2
（司会：飯村忠浩、岩井秀之、学生15名）
13：30-14：30 Students Discussion3
（司会：辻　邦和、李　知英、学生14名）
14：30-15：30 Students Discussion4
（司会：澤田直樹、大洞将嗣、学生14名）
15：30-16：30 Students Discussion5
（司会：Sadr Alireza、学生15名）

Dr. Bjorn Olsenと国際PIシャペロンのディスカッション
13：30-13：50　納富拓也
13：50-14：10　春山直人
14：10-14：30　飯村忠浩
14：30-14：50　岩井秀之
15：10-15：30　辻　邦和
15：30-15：50　李　知英
15：50-16：10　澤田直樹
16：10-16：30　Sadr Alirezar

2012年10月31日 プログラム卒業生・Dr. Mikihito Hayashi, Dr. Paksinee Kamolratanakul, Dr. Koji Fujita, Dr. Noriaki Ono, Dr. Shingo Sato, Dr. Hiroyuki Inose, Dr. Ganburged Ganjargal, Dr. Yoshio Ohyama, Dr. Yukiko Maeda, Dr. Verica Pavlic, Dr. Ayako Kimura, Dr. Mara Gomez Floresとのディスカッション

2012年11月12日　9：30〜11：30
Dr. Martha J. Somermanとのディスカッション
（司会：森山啓司教授、Sadr Alireza　学生16名）

Dr. Irma Thesleff
（司会：春山直人、辻邦和、李知英　学生14名）

Dr. Lynda F. Bonewald
（司会：飯村忠浩、納富拓也　学生18名）

Dr. Nawarat Wara-aswapati Charoen
（司会：渡辺久、南原弘美　学生10名）

Dr. Gregory J. Seymour
（司会：大洞将嗣、岩井秀之、学生12名）

2013年1月22日　16：30〜17：30
Dr. Michael Rosenblattとのディスカッション

2013年2月4日　9：00〜9：50
Dr. Mark Bartoldとのディスカッション
（司会：澤田直樹、岩井秀之、学生18名）

Dr. Steven Offenbacher
（司会：辻邦和、納富拓也、学生17名）

Dr. Panos N. Papapanou
（司会：飯村忠浩、春山直人、学生18名）

Dr. Denis F. Kinane
（司会：大洞将嗣、李知英、学生18名）

9. 総合プレゼンテーション (Presentation)

ポスター	プレゼンテーションタイトル	日　付
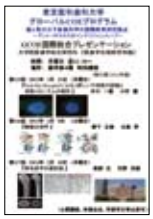	第117回『骨免疫学の最前線』	2013年3月4日
	第116回『糖鎖生物学』	2013年2月18日
	第115回『Nod-like ReceptorによるA群レンサ球菌の認識と排除メカニズムの解析』	2013年1月21日
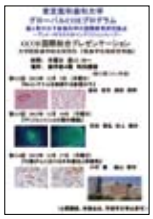	第114回　小村　健　『口腔がんにおける外科療法と再建術』	2012年12月17日
	第113回　花田　信弘『ディフェンシンと口腔の健康』	2012年12月10日
	第112回　澁谷　浩司『Wntシグナルを制御する新規分子』	2012年12月3日
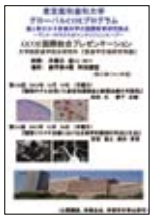	第111回『関節リウマチ治療における生物学的製剤の利点と欠点』	2012年11月26日
	第110回『動物モデルを用いた変形性関節症と新規治療の可能性』	2012年11月19日
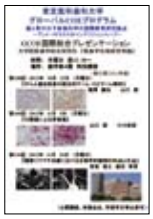	第109回『口腔癌による骨破壊』	2012年11月5日
	第108回『がんと遺伝疾患の統合的ゲノム・エピゲノム解析』	2012年10月22日
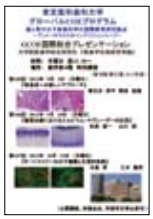	第107回『オートファジーの分子機構と生理的役割』	2012年10月15日
	第106回『歯周治療におけるエルビウム・ヤグレーザーの応用』	2012年9月10日
	第105回『骨造成への新しいアプローチ』	2012年9月3日
	第104回『哺乳類の進化に関わるジェネティクスとエピジェネティクス』	2012年6月18日
	第103回『下顎前突症患者に対する歯科矯正・顎矯正治療』	2012年6月11日
	第102回『新型ワンステップ接着材の性能』	2012年6月4日
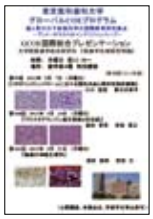	第101回『歯痛の神経生理学』	2012年5月21日
	第100回『プロスタグランジン産生制御と抗炎症』	2012年5月14日
	第99回『メタボリックシンドロームにおける慢性炎症と異所性脂肪蓄積』	2012年5月7日
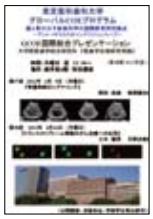	第98回「トランスクリプトーム情報のがん治療への応用」	2012年4月16日
	第97回「骨量制御のシグナリング」	2012年4月9日

平成24年度　総合プレゼンテーション　AISS大学院学生による教員への評価・アンケート集計

平成24年度	H24/4/11 ～ H24/12/17	参加者						The quality of content						The method of the presentations was						Overall evaluation of your attitude (effort,motivation and commitment)					
		教授	シャペロン・コーディネーター	学生日本人	学生外国人	一般	合計	Excellent (%)	Good (%)	Excellent & Good (%)	回収枚数	Excellent	Good	Excellent (%)	Good (%)	Excellent & Good (%)	回収枚数	Excellent	Good	Excellent (%)	Good (%)	Excellent & Good (%)	回収枚数	Excellent	Good
1	第97回	3	8	15	31	10	67	95%	5%	100%	44	42	2	86%	14%	100%	44	38	6	82%	14%	95%	44	36	6
2	第98回	3	3	13	32	2	53	76%	24%	100%	38	29	9	63%	24%	87%	38	24	9	58%	34%	92%	38	22	13
3	第99回	4	7	15	31	17	74	73%	25%	98%	40	29	10	75%	20%	95%	40	30	8	63%	30%	93%	40	25	12
4	第100回	4	6	18	32	17	77	76%	18%	93%	45	34	8	71%	22%	93%	45	32	10	69%	22%	91%	45	31	10
5	第101回	5	5	20	26	3	59	84%	13%	97%	38	32	5	84%	13%	97%	38	32	5	82%	16%	97%	38	31	6
6	第102回	3	3	9	29	16	60	95%	5%	100%	40	38	2	95%	5%	100%	40	38	2	88%	13%	100%	40	35	5
7	第103回	4	6	11	28	5	54	92%	3%	94%	36	33	1	94%	0%	94%	36	34	0	94%	0%	94%	36	34	0
8	第104回	3	3	9	23	11	49	75%	21%	96%	28	21	6	71%	25%	96%	28	20	7	71%	21%	93%	28	20	6
9	第105回	2	3	9	29	14	57	85%	15%	100%	33	28	5	91%	6%	97%	33	30	2	79%	21%	100%	33	26	7
10	第106回	3	5	14	30	12	64	74%	18%	92%	39	29	7	72%	21%	92%	39	28	8	67%	23%	90%	39	26	9
11	第107回	3	2	7	31	16	59	66%	31%	97%	32	21	10	66%	31%	97%	32	21	10	59%	31%	91%	32	19	10
12	第108回	3	4	10	27	11	55	76%	21%	97%	34	26	7	76%	21%	97%	34	26	7	68%	18%	85%	34	23	6
13	第109回	4	4	10	31	4	53	74%	23%	97%	39	29	9	79%	18%	97%	39	31	7	67%	26%	92%	39	26	10
14	第110回	3	6	5	25	1	40	62%	35%	96%	26	16	9	54%	38%	92%	26	14	10	58%	27%	85%	26	15	7
15	第111回	3	4	8	19	5	39	81%	5%	86%	21	17	1	90%	5%	95%	21	19	1	76%	14%	90%	21	16	3
16	第112回	4	3	7	26	2	42	55%	31%	86%	29	16	9	55%	28%	83%	29	16	8	52%	28%	79%	29	15	8
17	第113回	2	3	2	33	6	46	69%	29%	97%	35	24	10	60%	31%	91%	35	21	11	60%	34%	94%	35	21	12
18	第114回	2	4	9	27	4	46	45%	45%	91%	33	15	15	48%	39%	88%	33	16	13	45%	33%	79%	33	15	11
	合計	58	79	191	510	156	994				630														

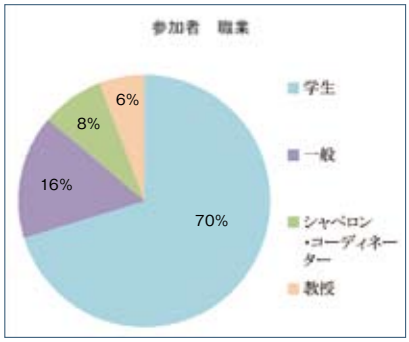

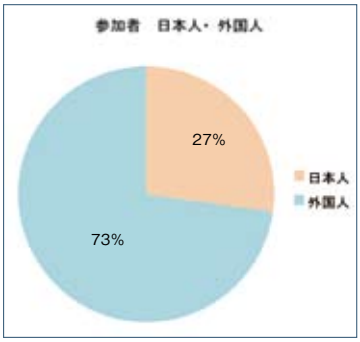

平均 (Overall evaluation)

Excellent (%)	Good (%)	その他
69%	23%	8%

開催回数　18回
アンケート回収枚数　630枚
出席者数　教授58名を含む994名
学生評価　Excellent ＆ Good率　平均　91%

学生	701名
一般	156名
シャペロン・コーディネーター	79名
教授	58名

日本人	191名
外国人	510名

10. 国際シンポジウム (International Symposium)

ポスター	タイトル	講演者	日　付
	第8回グローバルCOE国際シンポジウム Molecular Science in Oral-Systemic Medicine ～Winter Seminar～	Panos N. Papapanou, Steven Offenbacher, Denis Kinane, Fusanori Nishimura, Shogo Takashiba, Yasushi Furuichi, Koji Inagaki, Mark Bartold, Shinya Murakami, Yuichi Izumi,	2013年 2月3日～4日
	第7回グローバルCOE国際シンポジウム Molecular Science in Oral-Systemic Medicine ～Autumn Seminar～	Martha J. Somerman, Peter A. Mossey, Lynda F. Bonewald, Irma Thesleff, Gregory J. Seymour, Nawarat Wara-aswapati Charoen, Young Ku, Seung-Hak Baek, Young -Chel Park, Kenjiro Kosaki, Satoshi Fukumoto, Takashi Tsuji, Kazuhisa Yamazaki, Tetsu Takahashi, Kiyoshi Harada, Naoto Haruyama, Keiji Moriyama	2012年 11月12日～14日
	International Research Day	Bjorn Olsen, Mikihito Hayashi, Koji Fujita, Hiroyuki Inose, Noriaki Ono, Yoshio Ohyama, Yukiko Maeda, Ayako Kimura, Paksinee Kamolratanakul, Shingo Sato, Tingjiao LiuMara Gomez Flores, Ganburged Ganjargal, Verica Pavlic	2012年 10月30日～31日

Autumn Seminar

大山学長とAutumn Seminar講演者（2012年11月12日）

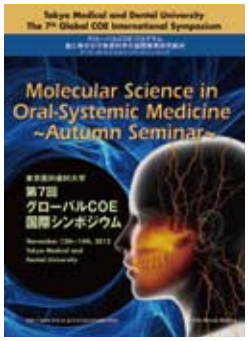


Dr. Somerman


Dr. Bonewald


Dr. Kosaki


Dr. Moriyama


Dr. Mossey


Dr. Thesleff


Dr. Fukumoto


Dr. Tsuji


Dr. Haruyama


Dr. Seymour


Dr. Nawarat


Dr. Ku


Dr. Yamazaki


Dr. Takahashi


Dr. Baek


Dr. Park


Dr. Harada


Dr. Izumi

Dr. Somerman

NIDCR/NIH: Today's Discovery, Tomorrow's Cure

Martha J. Somerman D.D.S., Ph.D.
Director NIDCR,
NIH and Chief Laboratory for Oral Connective Tissue Biology,
NIAMS, NIH. Bethesda, Maryland

This presentation will focus on research supported by National Institute of Dental and Craniofacial Research/ National Institutes of Health, with an emphasis on advances made toward improvements in treatment of dental-oral-craniofacial pathologies/conditions. Research topics, from basic to translational to clinical, will include: a) current and planned genomic analysis/genomic wide association studies applied to analysis of dental-oral-craniofacial pathologies/anomalies/disorders and will include cleft lip/palate, caries and periodontal diseases and Sjogren's Syndrome; b) salivary diagnostics for oral-systemic diseases; c) oral cancer from the oral cancer genome project to assays for diagnosis and early detection of head and neck cancer; d) public health challenges, e.g., acute/chronic pain linked to temporomandibular joint disorders and associated co- morbidities and human papilloma virus-related oral cancers; e) The microbiome project, where data have been obtained by sampling 6 sites (nasal passages, gastrointestinal tract, urogenital tract, skin and oral cavity (9 sites)) and are being analyzed for the role of these microbes in human health and disease; and f) clinical research within the clinical research center at NIH and also nationally/internationally. The emphasis will be on advances in research supported by NIDCR /NIH that have and will continue to improve the quality of health for all communities.

Dr. Bonewald

The Osteocyte as a Regulator of Bone Remodeling

Lynda F. Bonewald, Ph.D.
University of Missouri-Kansas City

As the skeleton matures, the ratio of osteocytes to other bone cells such as osteoblasts and osteoclasts increases to approximately 90-95% osteocytes in the adult skeleton. The osteocyte is a terminally differentiated cell localized within mineralized matrix thereby unable to divide while within this environment. Osteocytes can remain viable for decades in the bone matrix. To remain viable, these cells are exposed to bone fluid which provides nutrients but also allows the osteocyte to send molecular messages to other cells. Osteocytes are connected to each other and cells on the bone surface and the marrow space via their dendritic processes representing another mode of osteocyte communication. The morphology and other properties allow this cell to be exquisitely sensitive to mechanical loading and unloading which is translated into signals such as sclerostin or RANKL to regulate osteoblastic bone formation and osteoclastic bone resorption. Many of the effects of osteotropic factors such as parathyroid hormone are mediated through osteocytes. Therefore, the osteocyte is a major regulator of bone modeling and remodeling. Effects of aging on the skeleton may be through changes in the osteocyte. Maintaining or optimizing osteocyte function may abrogate bone loss and maintain bone mass.

Dr. Kosaki

Clinical molecular diagnostics of congenital malformation syndrome using in-solution hybridization-based enrichment and massively parallel sequencing

Kenjiro Kosaki, M.D., Ph.D., F.A.C.M.G.
Center for Medical Genetics,
Keio University School of Medicine

As catalogued in genetic textbooks like "Smith's Recognizable Patterns of Human Malformation" and "Inborn Errors of Development" several hundreds of genes have been shown to cause human congenital disorders. The identification of these causative genes has offered us a wonderful opportunity to delineate the molecular basis of these disorders. Molecular diagnosis offers valuable information to the patients and their families in terms of prognosis, preventing complications, and providing accurate genetic counseling. Theoretically, any gene can be tested by the direct sequencing of PCR products amplified from the patient's genomic DNA. However, identifying pathogenic mutations has been difficult when the causative gene has a large number of exons. In such cases, direct sequencing is expensive, technically demanding, and time consuming. Recently, next generation sequencing [NGS] has been introduced. We are currently developing a sensitive and specific mutation analysis system covering most of the genes enlisted in the Smith's textbook with targeted enrichment and massively parallel sequencing. In this symposium, we would like to share our strategies with the audience.

Generally speaking, there are two NGS approaches for diagnostic sequencing in genetic disorders: PCR-based targeted enrichment followed by long-read sequencing and in-solution hybridization-based enrichment followed by short-read sequencing. In-solution hybridization-based enrichment was adopted because PCR method does not allow multiplex enrichment of thousands of sequences. A proof-of-principle experiment was performed on thirty patients with neurofibromatosis type was performed and the ability of NGS protocol to identify likely disease-causing mutations was demonstrated in comparison with the current methodology, Sanger sequencing. Our diagnostic protocol illustrates a drastic change in the clinical molecular diagnostics of congenital malformation syndromes and provides a paradigm for other genetic conditions.

Dr. Moriyama

New biological insights of tooth movement in response to mechanical stress

Keiji Moriyama, D.D.S., Ph.D.
Section of Maxillofacial Orthognathics,
Tokyo Medical and Dental University Graduate School
Tokyo, Japan

Orthodontic tooth movement is a dynamic biological phenomenon, which is triggered by the loss of equilibrium in the mechanical environment surrounding the tooth upon orthodontic force application. To date, it is widely accepted that periodontal tissue, including cementum, periodontal ligament (PDL) and alveolar bone, play indispensable roles in tooth movement due to its unique biomechanical, cellular, and molecular natures, although the precise underlying mechanisms are yet to be fully elucidated.

To investigate the involvement of periodontal tissue in mechanical stress, we prepared an experimental tooth movement model in vivo and demonstrated that the forced mechanical stress stimulated the transcription of periostin, which is a 90 kDa secreted extracellular matrix (ECM) implicated in cellular adhesion and migration. In contrast, occlusal hypofunction decreases the expression of both periostin and twist, a basic helix-loop-helix transcription factor, which binds to periostin promoter to stimulate its transcription.

On the other hand, osteocytes are thought to be the major bone cell type responsible for sensing mechanical strain and coordinating signals of bone resorption and formation. Recently it has been reported that targeted deletion of osteocytes by diphtheria-toxin (DT) injection into the mice expressing DT receptor specifically in osteocytes results in bone loss, whereas the bone mass does not decrease in response to unloading experiment by tail suspension of these mice. To further elucidate the roles of osteocytes in bone remodeling triggered by mechanical loading/unloading, we conducted tooth movement in the osteocyte-ablated mice and compared the distance of tooth movement as well as the histological changes between the groups with or without intraperitoneal DT injection. The distance of tooth movement in DT-injected mice was significantly smaller than that in DT-uninjected mice on day 12. Interestingly, the number of TRAP-positive osteoclasts decreased in DT-injected mice after day 8, compared with that in DT-uninjected mice. These results suggest that osteocytes are involved in osteoclast formation in response to the change of mechanical environment, and that osteocytes play a crucial role in mechanical stress-induced bone remodeling during tooth movement.

Dr. Mossey

A global approach to the challenge of orofacial clefting

Peter A. Mossey, B.D.S., Ph.D.

Professor of Craniofacial Development and Dentofacial Orthopaedics,
University of Dundee

Background : Birth defects in general and craniofacial anomalies, the most common of which is non syndromic cleft lip and /or palate CL/P, have emerged as a component part of the World Health Organisation's Non Communicable Diseases (NCD) agenda; and it was agreed at the 63rd World Health Assembly in May 2010 that due to the rising tide of birth defects, these should be prioritised in health policy by member states around the world. This has led to the inclusion of CL/P in the subsequent Global Burden of Disease (GBD) agenda and it has become apparent that in the absence of intervention there is a very high neo-natal mortality associated with cleft lip and palate in the developing world. There is also convincing evidence that death and disability due to congenital malformations has been grossly under represented in the GBD hitherto and this issue requires concerted global attention.

Global epidemiology : in consensus meetings co-ordinated by the WHO between 2000 and 2004, efforts to co-ordinate the descriptive epidemiology of CL/P around the world has resulted in a meta analytic approach co-ordinated by the International Clearing House for birth defects (ICBD) based in Rome, Italy. This has collected information from registries around the world in a format that allows data comparison and an estimate of global birth prevalence of CL/P; and also establishes an infrastructure that facilitates the planning of health services to meet the burden imposed by orofacial cleft care.

Global oral health inequalities research network (GOHIRN) : The IADR have established a new overarching network that identifies the importance of oral diseases as a major public health issue and that major inequalities in oral health exist both within and between countries. This group will work with major international stakeholders to address issues such as the Millennium Development Goals and work to address oral health inequalities using a "common risk factor" approach alongside other major non-communicable diseases such as cardiovascular disease, cancers, diabetes, obesity and respiratory disorders. The objectives will be to influence clinicians, educators, policy makers, researchers and research funders around the world.

European cleft research : for the last decade significant advances have been made around the world in (a) improving the evidence base for best treatment protocols in the management of infants born with CL/P and (b) significant advances in knowledge of genetic and environmental aetiology. A series of European initiatives from SCANDCleft, EUROCleft, the European Science Foundation (ESF), EUROCRAN and now EUROCleftNet have made a significant contribution and present future opportunities in the co-ordination of global research efforts and aim towards establishing standardised research protocols which will ultimately allow inter-centre comparisons.

Genomics approach : This presentation will provide the compelling evidence for a strong genetic component in non-syndromic CL/P and will describe the genetic approaches for the identification of causative genes. This will include selected candidate gene association studies, linkage studies, genome wide association studies (GWAS), array comparative genomic hybridisation (CGH) and informative animal models. Unique insights into the molecular pathogenesis of CL/P through candidate gene pathways will include interferon regulatory factor 6 (IRF6), ventral anterior homeobox 1 (VAX 1) and the MSX1 and BMP signalling pathways.

In the context of determining the genetic aetiology of clefts, it is also important to consider the implications of heterogeneity, cleft sub-phenotypes, inter-population differences and gene / environment interaction and strategies for future studies to enhance understanding of the molecular pathogenesis of CL/P through functional genomics, epigenetics, gene expression and considering an array of approaches to identify rarer missense mutations in the pathogenesis of common, complex diseases.

The clinical implications of an improved characterisation of genetic aetiology in terms of prevention will be discussed.

Dr. Thesleff

Mechanisms of tooth renewal

Irma Thesleff, D.D.S., Ph.D.

Institute of Biotechnology, University of Helsinki, Finland

The capacity for tooth renewal is quite limited in mammals. The major mechanism of tooth renewal in vertebrates is tooth replacement and in fish and reptiles teeth can be replaced continuously. However, in mammals the deciduous dentition, or part of it, can be replaced by a second set of functional teeth, and there is maximally one round of tooth replacement. The mechanisms of tooth replacement have remained largely unknown mainly because mice do not replace their teeth. We have used the ferret as a model animal and performed morphological and molecular analyses of tooth replacement. The replacement teeth are formed successionally from their deciduous predecessors. They develop from the so called dental lamina associated with the outer enamel epithelium of the preceding tooth. We have recently localized putative stem/progenitor cells in the dental lamina epithelium during tooth replacement. These observations have also indicated that there may be a capacity for continued tooth replacement in mammals.

In addition to replacement, some mammalian teeth can be renewed by continuous growth which compensates for tooth wear. We have examined the mechanisms of the continuous growth of the mouse incisor. Our results together with work from other laboratories have indicated that there is a stem cell niche in the proximal end of the incisor in the so called labial cervical loop. The maintenance and differentiation of the epithelial stem and progenitor cells is regulated by a complex network of stimulatory and inhibitory molecules affecting Fgf, Tgfbeta, Bmp, Wnt and Hh signal pathways. The stem cells responsible for tooth renewal have been identified in the cervical loop. We have recently demonstrated that these cells express the stem cell marker Sox2 and that the Sox2 positive cells contribute to all epithelial cell lineages of the incisor. Taken together, the current data indicate that tooth renewal is based on epithelial stem and progenitor cells which seem to have a conserved common genetic signature in different types of tooth renewal, and that their maintenance and differentiation is regulated by a network of same conserved signal pathways that regulates tooth morphogenesis.

Dr. Fukumoto

Role of dental epithelium- stem cell interactions during dental cell differentiation

Satoshi Fukumoto, D.D.S., Ph.D.

Division of Pediatric Dentistry,
Tohoku University Graduate School of Dentistry

Tooth morphogenesis is characterized by reciprocal interactions between the dental epithelium and mesenchymal cells derived from the cranial neural crest, which result in the formation of the proper number and shapes of teeth. Multiple extracellular signaling molecules, including BMPs, FGFs, WNTs, and Shh, have been implicated in these interactions for tooth development. The epithelial cells then subsequently give rise to enamel-forming ameloblasts, while the dental pulp stem cells (DPSCs) form dentin-forming odontoblasts and dental pulp cells. Epithelial-mesenchymal interactions regulate the growth and morphogenesis of ectodermal organs such as teeth. The interactions between DPSCs and the epithelium have not yet been clearly elucidated. Dental pulp stem cell line (SP) that was comprised of enriched side population cells and that displayed a multipotent capacity to differentiate into odontogenic, osteogenic, adipogenic, and neurogenic cells. We then analyzed interactions between SP cells and cells from the rat dental epithelial cell line (SF2). SP cells differentiated into odontoblasts that expressed dentin sialophosphoprotein when cultured with SF2 cells. This differentiation was regulated by BMP-2 and -4 and was inhibited by the BMP antagonist Noggin.

Stem cell research has identified and established several types of stem cells, including induced pluripotent stem (iPS) cells, which are generated from a variety of somatic cell types via introduction of transcription factors that mediate pluripotency and has great potential for tissue-specific regenerative therapies. Further, ameloblasts secrete enamel-specific extracellular matrices, including ameloblastin (AMBN), and these are lost upon tooth eruption following transformation and apoptosis. This makes it impossible to repair or replace damaged enamel in an erupted tooth. Since ameloblasts are lost upon tooth eruption, identifying alternative sources of these cells becomes important. Since dental epithelial cells, which differentiate into enamel secreting ameloblasts, disappear in adults after tooth development, our strategy to create ameloblasts from mouse iPS cells may have direct application in regenerative tooth medicine. We found that mouse iPS cells cultured with mitomycin-C treated SF2 cells displayed an epithelial cell-like morphology. These cells expressed the epithelial cell markers p63 and cytokeratin-14, and the ameloblast markers AMBN, but did not express the endodermal cell marker Gata6 or the mesodermal cell marker brachyury. This is the first demonstration of differentiation of iPS cells into ameloblasts through interactions with the dental epithelium.

A number of factors are thought to give iPS cells the capacity for direct or indirect differentiation into ameloblasts. Possible direct effectors include gap junctions, intercellular binding molecules, adhesion factors and extracellular matrices secreted by dental epithelium. Growth factors might also be involved, because conditioned medium from SF2 cells induced AMBN expression in iPS cells. AMBN is also a candidate factor for dental cell differentiation of iPS cells, as SF2 cells expressing low levels of AMBN did not induce the differentiation of iPS cells. AMBN has diverse functions in various cellular physiologies, such as cell growth, differentiation, cell polarization and attachment, although the detailed mechanisms of AMBN signaling require additional investigation. AMBN-null mice display severe enamel hypoplasia due to impaired dental epithelial cell proliferation, polarization and differentiation into ameloblasts, as well as loss of cell attachment activity with immature enamel matrix. These results suggest that AMBN is necessary for both in vivo and in vitro ameloblast differentiation.

Co-culturing with dental epithelial cells appears to induce stem cell differentiation that favors an odontogenic cell fate and this might be a useful approach in tooth bioengineering.

Dr. Tsuji

Tooth Regenerative Therapy as a Future Dental Treatment

Takashi Tsuji, Ph.D.

Graduate School of Innovation Studies (Intellectual Property Management),
Tokyo University of Science

Oral functions such as enunciation, mastication and occlusion, are an important aspect of good health and quality of life. These oral functions are achieved in harmony with the teeth, masticatory muscles and the temporomandibular joint under the control of the central nervous system. Damage, loss and the onset of disease in teeth, including dental caries and periodontal disease, thus cause fundamental problems for oral functions and associate health issues. Various therapies for these dental disorders have been established using artificial materials such as root canal treatments and prosthesis procedures. Furthermore, after the loss of a tooth, the tooth functions are traditionally restored by replacement with an artificial tooth, the use of a bridge, and also osseo-integrated dental implants.

To restore the partial loss of organ functions and to repair damaged tissues, an attractive concept in regenerative therapy is stem cell transplantation into various tissues and organs. Dental tissue-stem cells have been identified and will have utility for the development of stem cell transplantation therapy to restore the partial loss of organ function and thereby achieve dental tissue repair such as caries and periodontal diseases. The ultimate goal of regenerative therapy is to develop fully functioning bioengineered organs that can replace lost or damaged organs following disease, injury or aging. For the success of tooth replacement regenerative therapy, a bioengineered tooth must be capable of erupting in the lost tooth region in an adult oral environment and achieve full functionality, including sufficient masticatory performance, biochemical cooperation with the periodontal tissues and proper responsiveness to noxious stimulations via neurons in the maxillofacial region.

To generate whole tooth, the approach is to recreate organogenesis through the epithelial-mesenchymal interactions that occur in the developing embryo and thereby develop fully functioning bioengineered organs from the resulting bioengineered organ germ generated via three-dimensional cell manipulation using immature stem cells in vitro. We previously developed a bioengineering method for forming a three-dimensional organ germ in the early developmental stages, termed the "bioengineered organ germ method" (Nature Methods 4, 227-230, 2007). This method was adoptable to generate various organ germs such as tooth, hair follicles (Nature Commun. 3, 784, 2012, Sci. Rep. 2, 424, 2012), salivary gland and lacrimal gland. Recently, we reported fully functioning bioengineered tooth replacements after the transplantations of a bioengineered tooth germ (PNAS 106, 13475-13480, 2009) or mature tooth unit comprising the bioengineered tooth and periodontal tissues such as periodontal ligament and alveolar bone (PLoS ONE, 6, e21531, 2011) into a lost tooth region. The bioengineered molar tooth germ could erupt and reach occlusion with an opposing tooth after transplantation in the mouse adult oral environment. The bioengineered tooth unit, which was controlled for length and shape, was successfully transplanted into a properly-sized bony hole in the alveolar bone through bone integration by recipient bone remodeling. These bioengineered teeth displayed physiological tooth functions such as mastication, periodontal ligament function for bone remodeling and responsiveness to noxious stimulations. Tooth regenerative therapy has the potential to provide essential functional recovery and ultimately replace the current artificial materials used in dental treatments.

In this presentation, I would like to talk and discuss about the strategies and recent progress of the research and development for the establishment of tooth regenerative therapies.

Dr. Haruyama

Amelogenins: Multifaceted enamel matrix proteins in hard tissue biology

Naoto Haruyama, D.D.S., Ph.D.

GCOE Program, International Research Center for Molecular Science in Tooth and Bone Diseases, Tokyo Medical and Dental University

Amelogenins are the most abundant extracellular matrix proteins secreted by ameloblasts during tooth development and are important for enamel formation. Recently, amelogenins have been detected not only in ameloblasts, which are differentiated from the epithelial cell lineage, but also in other tissues, including mesenchymal tissues at low levels, suggesting that amelogenins possess other functions in these tissues.

In the first part of this presentation, the emerging evidences for the additional roles of full-length amelogenin (M180) and leucine-rich amelogenin peptide (LRAP) in mesenchymal cells, such as chondrocytes and osteoblasts, will be introduced.

Experiments utilizing a chondrogenic cell line, ATDC5, revealed that the supplement of recombinant mouse M180- or LRAP-protein into chondrogenesis-stimulating medium increased alkaline phosphatase (ALP) activity and glycosaminoglycan secretion at 14 and 21 days of culture, respectively, as compared with the control. Quantitative PCR (Q-PCR) analysis indicated that LRAP increased the gene expression levels of Runx2, Col2a1, and Aggrecan at 7 days of differentiation. Moreover, both M180 and LRAP significantly increased the gene expression levels of ALP, Aggrecan, Col10a1, and Osteopontin at 28 days of culture. BrdU assay and Q-PCR analysis for Wnt signalling indicated that both M180 and LRAP reduced the cell proliferation, but induced the cell differentiation possibly through altered non-canonical Wnt signalling.

Interestingly, amelogenin null mice showed increased osteoclastogenesis and root resorption in periodontal tissues. Recombinant amelogenin proteins suppress osteoclastogenesis in vivo and in vitro, suggesting that amelogenin, especially LRAP, was involved in preventing idiopathic root resorption by regulating osteoclastogenesis (odontoclastogenesis). To identify extended functions of LRAP in bone formation and resorption, we then engineered transgenic (TgLRAP) mice using a murine 2.3kb α 1(I)-collagen promoter to drive expression of LRAP. Although LRAP expression did not affect bone structure in these mice, the ovariectomized (OVX) TgLRAP mice resisted bone loss induced by ovariectomy resulting in higher bone mineral density compared to OVX wild type (WT) mice. The quantitative analysis of calcein intakes indicated that the OVX TgLRAP mice had increased bone formation compared to sham operated WT mice. The parameters for bone resorption in tissue sections showed increased number of osteoclasts in OVX WT, but not in OVX TgLRAP compared to sham operated WT or TgLRAP mice. in vitro calvarial cell cultures isolated from the TgLRAP mice showed increased ALP activity and increased formation of mineralization nodules. The TgLRAP calvarial cells also showed inhibitory effects on osteoclastogenesis in vitro. Gene expression comparison by Q-PCR in calvarial cells indicated that bone formation makers such as Runx2, ALP and Osteocalcin were increased in TgLRAP, compared to WT cells. Meanwhile, Rankl expression was decreased in TgLRAP cells in vitro, supporting the bone phenotypes in OVX mice. These results suggest that the LRAP have distinct roles to maintain the bone metabolism.

Although amelogenins are implicated in tissue-specific epithelial-mesenchymal or mesenchymal-mesenchymal signaling, the precise molecular mechanism has not been characterized. To obtain a clue for the mechanism, the results of a yeast two-hybrid assay aimed at identifying protein-binding partners for LRAP will be introduced in the last part of this presentation.

The therapeutic application of an enamel matrix derivative (EMDOGAIN®) rich in amelogenins resulted in the regeneration of cementum, alveolar bone, and periodontal ligament in the treatment of experimental or human periodontitis, indicating the attractive potential of amelogenin in hard tissue formation. Gaining further insights into the cell functions modulated by the multifunctional amelogenin proteins will lead to the development of new therapeutic approaches for treating dental diseases and disorders.

Dr. Seymour

The periodontal - systemic connection: Molecular mechanisms and their significance in overall health care

Gregory J. Seymour, BDS, MDSc, Ph.D.

Sir John Walsh Research Institute, Faculty of Dentistry, University of Otago, New Zealand

The relationship between poor oral health and systemic diseases has, over the last two decades, been increasingly recognized. A large number of epidemiological studies have now clearly established the link between poor oral health and cardiovascular diseases, poor glycaemic control in diabetics, as well as a number of other diseases. The vast majority of studies investigating the relationship between periodontal disease and cardiovascular disease show a significant positive association even after adjusting for confounders, such that the focus is now on the biological mechanisms which under pin this relationship as well as on the role of periodontal treatment in reducing the risk of further cardiovascular events. A number of hypotheses have been postulated to explain the association between periodontal disease and atherosclerosis. These include (i) common susceptibility which may involve a common susceptibility gene(s) but where there is no direct link between the two diseases, (ii) direct infection of the arterial wall by oral organisms, including the recognised periodontal pathogens, following bacteraemia, (iii) systemic inflammation and increased levels of circulating cytokines with atherogenic potential and finally (iv) molecular mimicry between stress proteins expressed on the periodontal bacteria and heat shock protein 60 (HSP60) expressed on stressed endothelial cells. With respect to this final mechanism, antibodies to both Porphyromonas gingivalis GroEL antigen and human HSP60, which cross-react with one another, have been identified in the serum of patients with cardiovascular disease, the levels of which are significantly correlated with the extent of periodontal disease and with the numbers of periodontal pathogens. In addition, cross-reactive P. gingivalis GroEL and HSP60 specific T cell have been identified in the peripheral blood, as well as in the atherosclerotic plaques of patients with atherosclerosis. These data, together with the observation that enhanced atherosclerosis in P. gingivalis infected Apo-E deficient mice is associated with increased levels of anti- P. gingivalis GroEL antibodies, provide strong support for the role of molecular mimicry contributing to the association between periodontal disease and cardiovascular disease.

Although a number of studies have shown an improvement in endothelial function following periodontal therapy, there is a distinct lack of evidence showing that the treatment of periodontal disease impacts on clinical cardiovascular outcomes. Such studies, by necessity, need to involve several thousand subjects followed over a long period of time – up to ten years and are probably too expensive and too difficult to undertake.

Overall however, the relationship between poor oral health and systemic diseases has become a significant issue, and despite the lack of direct clinical evidence, there is sufficient strong basic biological evidence to explain the underlying mechanism, such that these associations can no longer be ignored in overall health strategies.

Dr. Nawarat

Oral - Systemic Connection: Roles of the Host Factors

Nawarat Wara-aswapati, D.D.S., DMSc.

Department of Periodontology, Faculty of Dentistry, Khon Kaen University, Khon Kaen, Thailand

Periodontitis is an inflammatory disease caused by gram-negative periodontopathic bacteria which can induce the production of host inflammatory mediators, eventually leading to the breakdown of tooth-supporting tissues. Emerging evidence has suggested the association of periodontal diseases with several systemic diseases such as diabetes mellitus (DM), cardiovascular diseases (CVDs), adverse pregnancy outcomes, respiratory diseases, Alzheimer's disease and cancer. Host immune responses play a vital role in the periodontal-systemic connection.

In this lecture, we will discuss the association of host factors, Wnt5a and trefoil factors (TFFs), with periodontitis. Wnt5a is secreted by activated antigen-presenting cells and Wnt5a signaling is essential for the general inflammatory response of human macrophages during sepsis. TFFs are secreted molecules involved in cytoprotection against tissue damage and immune response. Recently, we have investigated the mechanisms by which P. gingivalis modulates Wnt5a expression. In addition, we determined if TFF expression in saliva and gingival tissues was associated with periodontal pathology. Our results suggested that Wnt5a and TFF3 may be involved in the pathogenesis of periodontal disease and play a role in the periodontal-systemic connection.

Dr. Ku

The biologic effect of oligopeptides derived from fibronectin and its application to biomimetics

Young Ku, D.D.S., Ph.D.

Department of Periodontology, School of Dentistry, Seoul National University, Seoul, Korea

Fibronectin(FN) is a major glycoprotein in the extracellular matrix (ECM) and regulates various cellular events. It is consisted of disulfide-linked 235 kDa monomers, which are composed of three domains; types I, II and III. The Arg-Gly-Asp (RGD) and Pro-His-Ser-Arg-Asn (PHSRN) in 10^{th} and 9^{th} type III domain, respectively, are important cell adhesion. Oligopeptides based on FN are regarded as attractive biomolecules for biomaterials. We synthesized FN type III 7-10, 8-10 and 9-10 fragments and analyzed their biologic activities. We also synthesized PHSRN and RGD containing short oligopeptides with linkers and also via recombinant DNA technology and investigated their biological effects. Recently we evaluated the oligopeptides from fibrin binding domain based on FN and found that these peptides have enhancing biologic activities in some cell lines. We hypothesized that these peptides can be used as biomaterial surface modifiers which could enhance biocompatibility and wound healing.

Dr. Yamazaki

Periodontal disease and atherothrombotic diseases: Lessons from clinical and basic studies

Kazuhisa Yamazaki, D.D.S., Ph.D.
Laboratory of Periodontology and Immunology,
Division of Oral Science for Health Promotion,
Niigata University Graduate School of Medical and Dental Sciences

Over the past two decades, the relationship between poor oral health and systemic diseases has been increasingly recognized. There is considerable epidemiological evidence to support the concept that poor oral health may put patients at a significant risk for a variety of systemic conditions such as coronary heart disease (CHD). CHD is the leading cause of death in Japan and other developed countries. The major pathway underlying CHD pathology is atherosclerosis. Several risk factors for atherosclerosis have been identified, including smoking, hypertension, hyperglycemia, hypercholesterolemia and genetic factors. However, atherosclerosis can develop in the absence of these classic risk factors. Recent epidemiological studies have suggested a link between atherosclerosis and infection/inflammation. Associations have been reported with Chlamydia pneumoniae, Helicobacter pylori, and cytomegalovirus, as well as with dental infections, particularly those associated with periodontitis. Several biologically plausible mechanisms have been presented to explain the association, such as bacteremia, elevated levels of inflammatory markers, generation of cross-reactive immune responses by chronic infections, and induction of imbalanced cholesterol metabolism. There is evidence demonstrating the direct effect of periodontopathic bacteria on host cells, increased levels of high-sensitivity C-reactive protein and elevated levels of cross-reactive antibody between human heat-shock protein 60 and its orthologue, GroEL of Porphyromonas gingivalis. We have demonstrated that P. gingivalis induces several atherosclerosis-related molecules in human coronary arterial endothelial cells, and that high-sensitivity C-reactive protein (hs-CRP) and interleukin (IL)-6 protein levels are higher in cases of periodontitis and that successful treatment of periodontitis decreases the levels of both mediators. In addition, periodontitis patients have lower anti-atherogenic HDL cholesterols than periodontally healthy subjects. However, since the two disorders share several common risk factors, including cigarette smoking, age, and diabetes mellitus, and moreover, current research does not yet provide evidence of a causal relationship between the two diseases, media claim about an association between periodontitis and heart disease. Nevertheless, several animal studies aimed at clarifying the effect of periodontopathic bacterial infection on atherogenesis have successfully shown the formation of atheromatous plaque and the elevation of systemic inflammatory markers. Recently, we have shown by using mouse model that periodontal infection itself does not cause atherosclerosis, but it accelerates it by inducing systemic inflammation and deteriorating lipid metabolism, particularly when underlying hyperlidemia or susceptibility to hyperlipidemia exists. In this presentation, an update on the current understanding of the contribution of poor oral health to atherosclerosis and the possible mechanisms involved will be presented and discussed based mainly on our studies.

Dr. Takahashi

Paradigm shift of orhthognathic surgery in diagnosis, simulation, and guided surgery

Tetsu Takahashi, D.D.S., Ph.D.
Division of Oral and Maxillofacial Surgery,
Department of Oral Medicine and Surgery,
Tohoku University Graduate School of Dentistry

The traditional planning for orthognathic surgery using tracing and dental plaster models has remained mostly unchanged over the past 50 years. They present significant limitations and are often inadequate for the treatment of patients with complex CMF deformities. My topic is 3D surgical simulation for orthognathic surgery based on the occlusal relationship to predict surgical outcomes.

Before taking CT scanning, impression of the bite and upper and lower dental arches was taken using special impression tray and silicon impression material. 3-D virtual skull model with detailed dental occlusal and intercuspidation date was created by triple CT scan procedure. First the patient was vertically scanned with wax bite wafer in place in a natural seated position using standardized CT scanning protocol. Second, the tray and impression material was placed in the patient's mouth in the correct position, and the patient was scanned with a smaller field of view centered on the occlusal plane. Finally, the special tray and impression material was scanned more precisely using high-resolution standardized CT scanning protocol. These three scanning dates were installed to Maxilim software (Ver. 2.2.2, Medicim NV, Mechelen, Belgium). Acquiring the 3D integrated augmented skull model with dentition, 3D cephalometric analysis, virtual osteotomy and segmentation of each bony segment were undergone. The surgical simulation was then performed at the position of final occlusion by use of virtual elastics between upper and lower teeth.

Next step from the simulation, we need some intraoperative guides to acquire the actual results same as simulated results. There are two possibilities to make such guide, one is template to set on the osteotomy gap to indicate the amount of movement and another is surgical splint that made as an intermediate splint same as conventional model surgery. We have used 3D virtual surgical splints made from a transparent polycarbonate material (Tecanat Polycarbonate, Eisigner Industries, US) processed using computeter-aided design and computer-aided manufacturing techniques during the actual surgery.

3D virtual orthognathic surgery planning has powerful potential as a communication tool because it offers the possibility to visualize an integrated treatment plan of the patient as a single virtual anatomic model including the hard and soft tissue and teeth. Furthermore, the surgical guides help surgeons to indicate appropriate 3D location of maxillary segment during bimaxillary surgery. However, to make the paradigm shift from conventional planning to 3D virtual planning, some problems such as time consuming, costs, irradiation and quality of care have to be overcome near future.

Dr. Baek

Recent Paradigm Change in Three-Dimensional Imaging and CAD-CAM Technology for Virtual Orthodontic Treatment and Orthognathic Surgery

Seung-Hak Baek, D.D.S., M.S.D., Ph.D.
Dept. of Orthodontics, School of Dentistry, Seoul National University

Current rapid change of paradigm in the diagnosis and treatment for patients with malocclusion and facial deformity give a new horizon to the orthodontic treatment and orthognathic surgery in terms of efficiency and effectiveness.

This presentation will give you the up-to-date information of 3D-Digital processes which are currently being used in the diagnosis and treatment planning, and real treatment in the orthodontic treatment and orthognathic surgery for both clinical practice and research.

The purposes of this presentation are to discuss about the data acquisition from CT, intra-oral scanning, and surface scanning, the data manipulation including virtual segmentation of teeth, virtual diagnostic and final set-up of the models, virtual bracket positioning and jig fabrication, virtual orthognathic surgery, and virtual fabrication of surgical wafers, and the appliance fabrication and delivery for indirect bonding jig with customized base, and surgical wafers using CAD-CAM and SLA technology.

Dr. Park

Clinical and biomechanical considerations for correction of the dento-facial deformities

Young-Chel Park, D.D.S., Ph.D.
Dept. of Orthodontics Yonsei University Seoul, Korea

So far, the conventional orthognathic surgery has been widely used to treat the dentofacial deformity patient. However, some problems were found such as limited amount of movement in the skeletal tissue, high recurrence rate and difficulty to achieve the functional and esthetic balance. To minimize the limitation and side effects of the orthognathic surgery, orthopedic intervention has been widely used for the treatment of dento-facial deformities. As a result, orthopedic intervention such as distraction osteogenesis and rapid maxillary expansion has became an alternative option for treatment of hypoplasia in the patients with dento-facial deformity.

Biologic and biomechanical background of distraction osteogenesis for the treatment of maxillary hypoplasia in cleft lip and palate patient and in the hemi facial microsomia patient will be discussed with the clinical cases. Rapid maxillary expansion(RME) has been widely used to correct the vertical and transverse deficiency of the maxilla in the growing patients. It is possible to extend the indication of age and the range of maxillary expansion by using the surgically assisted RME and the mini screw assisted RME. The characteristics of surgically assisted RME and the mini screw assisted RME will also be discussed with the treated cases and related researches.

If the patient with dento-facial deformity was treated under accurate diagnosis and treatment planning with a proper biologic and biomechanical principles, accompanied with overcorrection and long term retention, it would be possible to improve the functional and esthetic balance

Dr. Harada

Orthognathic Surgery : The Considerations for its Accuracy and Safety

Kiyoshi Harada, D.D.S., Ph.D.
Maxillofacial Surgery Section,
Graduate School of Medical and Dental Sciences

Now orthognathic surgery is one of the most common surgical methods for the treatment of dento-facial deformity patients. Though there are many technique for orthognathic surgery, sagittal splitting of the mandibular ramus and Le Fort Ⅰ osteotomy of the maxilla are the most popular. Since these popular orthognathic surgeries have been well trained by oral surgeons, few major troubles have been reported during surgery recently. However, results of the orthognathic surgery should be based on the improvement of occlusal disharmony. The postoperative occlusal condition depends on accuracy of the surgical movement on the jaw bones. In addition, as a surgical basis, the techniques for accurate bone movement should be free from unexpected bleeding or jaw bone fracture. Since orthognathic surgery is becoming a common treatment method in the field of oral and maxillofacial surgery, safety must be guaranteed during surgery. In this lecture, several original techniques are introduced for accurate and safe movement of jaw bone during orthognathic surgery.

In the sagittal splitting of the mandibular ramus, the bilateral mandibular rami are split into the proximal and distal segments. The distal segment is moved posterior or anterior to improve the occlusal disharmony. However, the proximal segment must be maintained in its original position due to the presence of condyle. Improper positioning of the proximal segment, namely, condyle can cause various problems of temporomandibular joint and instability of the postoperative occlusion. Therefore, it is considered to be better that the pre-splitting position of the proximal segment should be recorded using a device. Even though beginners of the orthognathic surgery perform the sagittal splitting of the mandibular ramus, luxation of the temporomandibular joint can be prevented using this device during surgery.

In the maxillary osteotomy, accurate upward impaction is difficult because there are important blood vessels nourishing the maxilla in its posterior portion. Though some oral surgeons perform upward hammering of the maxilla for its upward movement, it's very danger. The presence of inferior concha and, in the similar situation, nasal-intubated endotracheal tube also interferes during upward movement of the maxillary segment. To solve these problems of upward movement of the maxilla, additional osteotomy to Le Fort Ⅰ or application of resin replica is performed during surgery.

These techniques have not only advantages, but also some disadvantages. I hope the accuracy and safety of orthognathic surgery will be discussed through this lecture to increase the quality of lives of the patients undergoing orthognathic surgery.

Winter Seminar

大山学長と Winter Seminar講演者（2013年2月3日）

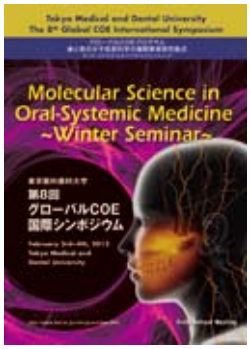

Dr. Offenbacher

Dr. Papapanou

Dr. Kinane

Dr. Nishimura

Dr. Takashiba

Dr. Furuichi

Dr. Inagaki

Dr. Bartold

Dr. Murakami

Dr. Izumi

Dr. Offenbacher

An Update in Periodontal Medicine: Managing Oral Infections to Improve Overall Health

Steven Offenbacher D.D.S., Ph.D., M. MSc.
Professor and Chair,
Department of Periodontology,
University of North Carolina at Chapel Hill

Periodontal Medicine was defined in 1996 as the effect of periodontal infections on systemic health. This discipline was initially established to study the observations that linked periodontal disease with an increased risk for heart attack, stroke and preterm delivery among pregnant women. Although this is an emerging field, current findings suggest that periodontitis is associated with mores severe and prevalent cardiovascular disease, kidney disease, chronic obstructive airway disease, diabetes and pregnancy complications. These associations appear to confer additional risk even after adjustments for relevant confounders like smoking, obesity, and other traditional risk factors. Current evidence suggest that the periodontal organisms gain access to the systemic circulation and that periodontal infections create an oral wound that serves as a portal for the systemic dissemination of oral pathogens. Once into the bloodstream these organisms elicit hepatic inflammation, vascular damage, and many appear capable of crossing the placental barrier in pregnant women. Thus, clinical periodontal disease represents an infected wound that can serve as a chronic portal for the systemic dissemination of oral pathogens that has the potential to mediate inflammatory damage to multiple organs systems. The evidence from humans and animal studies would suggest that once periodontal organisms enter into the circulatory system, they induce upstream and downstream mediators of the hepatic acute phase response resulting in increases in serum biomarkers such as sICAM (soluble intracellular adhesion molecule-1), IL-6 (interleukin 6), fibrinogen and CRP (C-Reactive Protein). Many of these inflammatory markers are predictive of cardiovascular, pregnancy and diabetes risk. It appears that, periodontal disease may, in part, explain the association between the observed increases in inflammatory biomarkers of the acute phase response, coagulation and vascular stress as associated with increased risk for certain systemic conditions.

During pregnancy, periodontal infection also appears to be a special threat to the placenta and fetus. Case-control and prospective cohort studies have suggested that there is a significant association between maternal periodontal disease and pregnancy complications that result in preterm delivery [gestational age (GA) <37 weeks] and low birth weight [LBW, birth weight <2500g]. Several studies suggest that periodontal disease independently enhances the risk of obstetric complications including preterm birth, growth restriction [birth weight less than 10th percentile of weight for gestational age, adjusting for baby gender and race], preeclampsia and very preterm birth [delivery less than 32 weeks gestation]. Periodontal disease represents a risk for these adverse pregnancy outcomes even after adjusting for a range of potential confounders including previous history of preterm birth, parity, maternal weight gain, smoking, and other infections. Data suggest that maternal periodontal infections may potentially represent a bona fide risk factor for preterm birth and growth restriction by serving as an infectious and inflammatory exposure to the placenta and fetus during pregnancy. This infectious and inflammatory stress which represents the toxicity of the oral biofilm appears to increase neonatal morbidity and may have life-long effects on the health of the offspring.

Estimates of the potential magnitude of the effect of periodontal disease on these conditions are significant, increasing the risk as much as traditional risk factors such as smoking. Furthermore, data from animal models of disease provide a compelling demonstration of biological feasibility. However, data supporting the reversibility of this association in humans is equivocal. Although some early treatment studies show promise, other studies do not show any systemic benefits from treatment. Clearly additional studies exploring the potential benefits of treating periodontal disease to reducing the risk for these systemic conditions are needed. However, since periodontal disease is both a preventable and treatable condition, it represents a potentially modifiable risk factor. Thus, if periodontal disease is proven to be causally related to these conditions, the findings could have a tremendous health care impact.

Dr. Papapanou

Periodontal Infections and Cardiovascular Disease : Biological Plausibility and Epidemiologic Evidence

Panos N. Papapanou, D.D.S., Ph.D.
Professer and Chair,
Section of Oral and Diagnostic Sciences,
Columbia University College of Dental Medicine

One of the key features of periodontal diseases is the intimate contact between the biofilm of the microbial plaque and the ulcerated epithelium of the periodontal pocket. This allows the subgingival bacteria, some of which have tissue-invading properties, to gain direct access to the underlying connective tissue and gingival microvasculature through the disrupted epithelial barrier. As a result, bacteremias are fairly common in patients with periodontitis and are triggered by mechanical stimulation of the gingival tissues. In addition, inflammatory mediators that are abundantly produced locally in the inflamed gingiva through cellular innate and adaptive immunity pathways can enter the blood stream, reach distant organs and also 'excite' the vascular endothelium. These phenomena have been shown to be important in the context of atherogenesis. The presentation will give an overview of the potential biologically plausible mechanisms through which periodontal infection/inflammation may lead to extra-oral pathology, and summarize the available epidemiologic evidence from cross-sectional, cohort and intervention studies that have investigated the association of periodontitis and cardiovascular/cerebrovascular disease. The public health implications of these findings will be discussed.

Dr. Kinane

The Role of Host Response Variations in Oral and Systemic Disease Interactions

Denis F. Kinane, B.D.S., Ph.D.
Morton Amsterdam Dean
Professor of Pathology and Periodontology
University of Pennsylvania, School of Dental Medicine

Variations in host response amongst humans are critical in determining who gets disease and who remains healthy given the same environmental challenges. Clearly initiating and environmental challenges are necessary in any disease, and in periodontal disease the subgingival biofilm and challenges such as smoking can fulfill these roles. This lecture will explore the relationship between oral disease, specifically periodontal disease, and other chronic inflammatory diseases such as diabetes, heart disease and pre-term pregnancies. The central role of the chronic inflammatory burden as a linking feature between these diseases and the specific potential effect of the periodontal biofilm as the major etiological agent will be addressed. Mechanistic links, particularly for cardiovascular disease, and the concept of shared risk factors will be covered also. The gatekeeper role of our surface epithelial layer and its variations will be explored in both its molecular variations and functions. Stimulation of TLRs by periodontal bacteria typically produces either a hyper-inflammatory response or an anti-microbial peptide response. These responses are understood to be regulated by epigenetic modifications. Likewise the changes in cellular receptor expression are mediated by micro RNAs which may also have a role in apoptotic responses. Features such as the lipid raft cellular receptors, in particular the TLR family as well as GPCRs will be reviewed as will the potential for signaling through these receptors in producing cytokine, and other cellular inflammatory and anti-inflammatory responses. The importance of genetics, specifically by SNP carriage, and the regulation of inflammation by both micro RNA affects and by chromatin remodeling and other epigenetic changes will be mentioned. The central role of chronic inflammation and how it contributes and is worsened in a variety of states will be considered. The audience should achieve an understanding and a realistic perspective of the interactions of these chronic diseases and knowledge on their prevention.

Dr. Nishimura

The Periodontal Host Response with Type 2 Diabetes

Fusanori Nishimura, D.D.S., Ph.D.
Professer and Chair,
Department of Dental Science for Health Promotion,
Hiroshima University Institute of Biomedical and Health Sciences

In the past decade, periodontal disease has been recognized as not merely a local infectious disease, but as chronic, subclinical, inflammatory disease for the host. The subjects with type 2 diabetes appear to respond to bacterial challenge in an exaggerated manner as compared with the subjects without diabetes through several possible mechanisms, and develop severer forms of inflammatory periodontal disease. Severe periodontal disease in such subjects, in turn, acts to reduce insulin sensitivity known as insulin resistance, thereby contributing to the induction of hyperglycemia as well as hyperinsulinemia, important risk factors for vascular complications. Additionally, recent studies suggested that such subclinical inflammatory state also promotes renal dysfunction, all of which are important risk factors for atherosclerosis. Finally, all such conditions act to increase the risk for coronary heart diseases, one of the leading causes of mortality and morbidity in subjects with diabetes. Thus, it is very important to elucidate molecular mechanisms as to why local periodontal inflammation is amplified to the level of influencing our overall systemic health.

Recently, macrophages have been suggested to infiltrate into adipose tissues, and to interact with adipocytes, thereby exacerbating adipose tissue inflammation. Furthermore, both cell types appear to express toll-like receptor-4 (TLR4), and free fatty acids have been found to act as endogenous ligand for TLR4. Based on these findings, we hypothesized that, in cases of infectious diseases such as severe periodontal disease and gut infection, classical exogenous ligand for TLR4 may further exacerbate inflammatory responses in adipose tissue, thereby contributing to the induction of many unwanted side effects such as insulin resistance. To prove this, we established co-culture system between adipocytes and macrophages and stimulated these cells with bacterial lipopolysaccharide (LPS). We found that stimulation of the cells with LPS markedly up-regulated inflammatory gene expression in adipocytes as well as protein productions from co-cultures. Some of these effects were confirmed in vivo model by using both genetically induced and environmentally induced obese model mice as well. Hence, our results suggest that, although the prevalence of extremely obese subjects as seen in western societies is very low in eastern Asia including Japan, once they develop severe periodontal diseases, the disease may up-regulate adipose tissue inflammation, especially in subjects with newly diagnosed type 2 diabetes who are slightly more obese than the subjects without diabetes. Current understanding on these mechanisms will be discussed in the context of developing new "order-made" diagnostic strategies to avoid such unwanted side effects.

Dr. Takashiba

Periodontal Medicine
– Prediction of Systemic Diseases on Periodontal Infection –

Shogo Takashiba, D.D.S., Ph.D.
Professer and Chair,
Department of Pathophysiology - Periodontal Medicine,
Okayama University Graduate School of Medicine,
Dentistry and Pharmaceutical Sciences

Epidemiological studies have suggested the relations among many systemic diseases and periodontitis. In those studies, clinical indices have been used as parameter to show severity of periodontitis. What is really involved in the pathogenicity of the systemic diseases that periodontitis relates? Direct pathogenicity of periodontal bacteria seems to be a small portion of the pathogenicity between these diseases. Host responses to the bacteria or denatured host proteins must be a large portion of pathogenicity such as immune responses to molecules mimicked to the bacterial antigens or involved in inflammation.

For further understanding the severity of periodontitis, we have been used both bacterial DNA to identify specific periodontal bacteria and immunoglobulin G (IgG) to determine the degree of sensitization by bacterial antigens. Increased IgG antibody level means activated acquired immune response and further host response that may cause failure of homeostasis, resulting tissue or organ damages. Real pathogenicity has not been well documented.

However, using these two parameters, we can understand the host responses of periodontitis patients. There are three groups; 1) major group with regular IgG response reflecting the severity of periodontal infection, 2) minor group with hypo-response (low IgG level) to severe periodontal infection, 3) minor group with hyper-response (high IgG level) to less periodontal infection.

In the first group, IgG antibody level changes according to the amount of bacterial DNA detected from periodontal lesion. Thus, it is easy to infer about the sensitization of host from these laboratory examinations. Furthermore, this group may be close to those whose periodontal conditions related to the some systemic diseases. Studies using this assumption have been conducted, suggesting relations between periodontitis and systemic disease somehow. In the second group, IgG antibody level stays lower level even though a lot of amount of bacterial DNA detected from periodontal lesion. The host may be in immuno-compromised condition. Bacteremia or aspiration pneumonia must be considered. In the third group, IgG v\level stays higher level even though very low amount of bacterial DNA detected from periodontal lesion. Hyper-immunoglobulinemia that may relate to injury of glomerulus must be considered. In addition, excessive immunoreaction may exist and injure tissues or organs. Because few studies using this assumption have been conducted, further studies must be performed for these systemic diseases.

In this lecture, I will show our recent studies as examples for the idea mentioned above. The definition of threshold of IgG titer against *Porphyromonas gingivalis*, utilization of the IgG titer test to explain chronic obstructive pulmonary disease, preliminary study to reveal the relation of the IgG titer and atherosclerosis related to diabetes.

Dr. Furuichi

Association between Periodontal Disease and Adverse Pregnancy Outcome

Yasushi Furuichi, D.D.S., Odont.Dr.
Professer and Chair,
Division of Periodentology & Endodontology,
Department of Oral Rehabilitation,
School of Dentistry, Health Sciences University of Hokkaido

Periodontal disease is an infectious disease with a certain extent of inflammatory lesion in the periodontium where numbers of microorganisms and inflammatory cells are in contact and varieties of inflammatory mediators are produced and/or infiltrated in. Chronic periodontitis becomes prominent at later ages of adulthood, but gingivitis proceeds at their younger ages. Adverse pregnancy outcome includes pre-term birth (PB: delivery earlier than 37 weeks of gestation) and low birth-weight (LBW: delivery weight less than 2,500 g). Incidence rate of PLBW (PB and /or LBW) are reported to be 4~15 % and varies among different countries and districts. PLBW is the main cause of mortality and morbidity of the new-born and be an ineligible burden not only from familial but also from socioeconomic aspects.

Both periodontal disease and adverse pregnancy outcome are multi-factorial in its pathogenesis and possess common risk factors such as smoking. Since the middle of 1990's, a number of epidemiological and experimental studies have been performed on the topic of the association between periodontal disease and PLBW and the results were reported in the literature. Such studies can be categorized into three groups according to the aims of the studies, i.e. analyzing the association between the both events, analyzing the mechanisms behind the association, and evaluating the effects of periodontal intervention on the association. Although there have been somewhat large discrepancies in the results of the association studies, significant positive associations have been reported in more than half of the large scaled epidemiological studies. Mechanisms of the association have been analyzed with employing microbiological, immune-pathological, and genomic methods. So far, there have been several studies showing interesting findings which may in part explain the mechanisms of the association. It could be concluded that the biggest controversies were found in the periodontal intervention studies and that periodontal treatments would not be recommended during the pregnancy in order to reduce the incidences of PLBW according to the results of the large scaled RCTs. However, it has also been claimed that periodontal treatment during the pregnancy in itself is beneficial in order to treat periodontal disease and maintain healthier periodontium of the pregnant women. It was also demonstrated that unsuccessful periodontal treatments resulted in higher risks of PLBW than successful periodontal treatments in a study. In this presentation, association between periodontal disease and adverse pregnancy outcome will be discussed from the three aspects mentioned above.

Dr. Inagaki

Interrelationships between Systemic Osteoporosis and Periodontal Disease : Association and Mechanisms

Koji Inagaki, D.D.S., Ph.D.
Professor,
Department of Dental Hygiene,
Aichi Gakuin University Junior College

Many studies have attempted to define the relationship between postmenopausal osteoporosis and periodontal disease. Most studies support a positive association between these common diseases; however, many are cross-sectional in nature, include relatively small sample sizes, and have inadequate control of potential confounding factors, such as age, gender, hormone intake, race, and smoking, limiting our understanding of the nature of the relationship between these diseases. Clinical conditions causing low estrogen environments in postmenopausal women allow T- and B-cell abnormalities, increased local production of the bone-active cytokines (i.e., Interleukin-1, -6 and -8, tumor necrosis factor- (TNF-) and a rise in prostaglandin E_2, resulting in the progression of periodontitis. In post-menopausal osteoporosis, lack of estrogen will affect the remodeling of the bone tissue in such a way that, in most patients with periodontitis, the amount of bone resorbed exceeds that being formed, resulting in net bone loss. Osteoporosis can be treated by a variety of methods, the hormone replacement therapy (HRT), the selective estrogen receptor modulators (SERM) and the bisphosphonates. The HRT or bisphosphonates treatments improve the clinical outcome of periodontal disease and may be an adjunctive treatment to preserve periodontal bone mass. This presentation reviews the current evidence on the mechanism of periodontal breakdown after menopause with long-term follow-up cases and the benefit to oral health by treatments for osteoporosis.

Dr. Bartold

Is There a Role for Stem Cells in Periodontal Regeneration?

Mark Bartold, D.D.S., Ph.D.
Professor of Periodontics & Director Colgate Australian
Clinical Dental Research Center
University of Adelaide

Although stem cells have received considerable attention in recent years, clonogenic bone marrow stromal stem cells (also know as mesenchymal stem cells) were first isolated and characterized almost 40 years ago. Since then considerable effort has been made in determining the therapeutic applications of mesenchymal stem cells. Mesenchymal stem cell properties such as multipotency and immunomodulation make these cells ideal candidates for tissue regeneration and tissue engineering. Most of us are familiar with the concept of embryonic stem cells and their potential use in tissue regeneration. Over the past 10 years, reports have appeared characterizing mesenchymal stem cells isolated from the periodontal tissues (periodontal ligament and gingiva) and their potential use in periodontal regeneration. More recently reports of isolation of induced pluripotent stem (iPS) cells from gingiva and periodontal ligament have appeared. Both mesenchymal stem cells and iPS cells from periodontal tissues provide an attractive source of cells for periodontal tissue engineering. It is now clear that in order for tissue engineering to reach its full regenerative potential an appropriate scaffold for cell delivery together with the incorporation of supplemental cytokines and growth factors will be necessary for the regenerative process to proceed both spatially and temporally. The precise roles of mesenchymal stem cells in tissue regeneration still need to be elucidated. For example, it is still unclear whether these cells act via direct differentiation in situ or through paracrine mediated processes leading to recruitment of local progenitor cells to enable tissue regeneration. In this presentation the biology and potential for clinical use of periodontal stem cells for periodontal regeneration will be explored.

Dr. Murakami

Periodontal Tissue Engineering
– The Future Perspective of Cytokine Therapy and Cell Therapy –

Shinya Murakami, D.D.S., Ph.D.
Professor and Chairman,
Department of Periodontology,
Osaka University Graduate School of Dentistry

It has been demonstrated that mesenchymal stem cells and progenitor cells of osteoblasts or cementoblasts can be identified within periodontal ligament (PDL). Thus, improving the biological potential of these cells and stimulating the periodontal regeneration are recognized as being clinically possible. One of the most physiologically efficient methods to stimulate these cells is the use of cytokines.

Basis Fibroblast Growth Factor (FGF-2) is known to be deeply involved in the proliferation, migration and differentiation of a variety of cells and to strongly induce angiogenesis. Utilizing beagle dogs and non-human primates, we revealed that topical application of recombinant FGF-2 induced statistically significant periodontal tissue regeneration in the experimentally-prepared intraosseous bone defects. Recently, a human clinical trial was conducted using FGF-2 in Japan. This was a randomized controlled double-blinded clinical trial of dose responses including placebo comparison. As a result, a significant difference in % increase in alveolar bone height at 2- or 3-walled intrabony defects of the patients was demonstrated by standardised radiographs between Placebo Group and 0.3% -FGF-2 Group at 9 months after the treatment. This suggests that topical application of FGF-2 can be efficacious in regeneration of periodontal tissue of periodontitis patients.

Based on the results of a series of *in vitro* analyses, we have suggested the following mode of action of FGF-2 to induce periodontal regeneration. During the early stages of periodontal tissue regeneration, FGF-2 stimulates the proliferation and migration of PDL cells while maintaining their multipotent nature, inducing differentiation into hard tissue-forming cells such as osteoblasts and cementoblasts. Furthermore, FGF-2 induces angiogenesis and increases extracellular-matrix production such as osteopontin, hyaluronan from PDL cells, thus leading to a local environment suitable for the periodontal regeneration. These results in the enhanced periodontal tissue regeneration are shown at the FGF-2-applied sites.

For ideal periodontal regeneration, it is crucial to fully introduce the concept of "tissue engineering". If we need to treat severe bony defects or horizontal bone destruction with FGF-2, it is essential to introduce the concept of a "scaffold" into the carrier of FGF-2 drug. An FGF-2 carrier that could provide a formable and osteoconductive scaffold for undifferentiated progenitor cells within PDL would dramatically increase both the dental and craniofacial applications of FGF-2 drug.

Furthermore, researchers, including our group, have found that mesenchymal stem cells can be obtained from various tissues such as bone marrow and adipose tissues. By using beagle dog models, we recently revealed that transplantation of adipose-tissue derived stem cells enhances periodontal regeneration at applied sites. The combined effects of 'cell therapy' and 'cytokine therapy' need to be assessed in the future, to allow the establishment of 'periodontal tissue engineering'.

Dr. Izumi

Clinical Application of Er:YAG Laser in Periodontal and Peri-implant Therapy

Yuichi Izumi D.D.S., Ph.D.
Professor and Chair,
Department of Periodontology,
Graduate School of Medical and Dental Sciences,
Tokyo Medical and Dental University

Recently, various lasers have been used for a wide range of oral conditions. Lasers have numerous advantageous physical properties such as ablation, hemostasis, bactericidal effect as well as photo-bio-modulation, making it suitable for treating inflammatory and infectious conditions. Thus, the use of lasers is considered safe and effective for treating oral diseases such as periodontitis and peri-implantitis.

Among various laser systems, in particular, the recent development of the Er:YAG laser has expanded the application of lasers to hard tissue treatment in periodontics since the 2.94 μm wavelength can be applied on both dental soft and hard tissues. The Er:YAG laser has various characteristics advantageous for soft and hard tissue management, such as easy and precise ablation, cutting, debridement and recontouring with minimal thermal damage to the surrounding tissues under water irrigation. Nowadays, the Er:YAG laser is effectively being used for various tissue managements such as gingival tissue ablation, dental root and implant fixture surface debridement, and osseous surgery.

In periodontal and peri-implant applications, the Er:YAG laser is capable of treating alveolar bone tissue either directly or indirectly during osseous management. Animal studies reported faster wound healing in bone tissue following Er:YAG laser ablation compared to bur cutting, as well as significantly enhanced and favorable new bone formation following surgical treatment of periodontitis or peri-implantitis using an Er:YAG laser compared to mechanical instrumentation. These positive results are considered to be due to the high decontamination and detoxification effects of the Er:YAG laser on the diseased site, the pronounced bleeding from the laser-treated bone surface, as well as the production of characteristic microstructures on the ablated bone and root surfaces, which possibly enhances fibrin and blood clot retention. In addition, potential photo-bio-modulation effects of low-level laser effect which induces a variety of biological responses may be partly involved in the increased bone formation. Given these observations and evidences, the Er:YAG laser has been recently established as one of the most promising laser systems for periodontal and peri-implant therapy.

In this presentation, the current clinical applications of Er:YAG laser for various treatments such as soft tissue management, non-surgical and surgical periodontal treatment, osseous surgery and peri-implant therapy will be discussed, based on scientific evidence from currently available basic and clinical studies as well as clinical cases.

International Research Day

Dr. Olsen

Dr. Hayashi

Dr. Kamolratanakul

Dr. Fujita

Dr. Ono

Dr. Sato

Dr. Inose

Dr. Ganjargal

Dr. Ohyama

Dr. Maeda

Dr. Pavlic

Dr. Kimura

Dr. Flores

Dr. Olsen

Vascular endothelial growth factor (VEGF) is a regulator of bone formation and osteoblastic differentiation

Bjorn Reino Olsen, M.D., Ph.D.
Dean for Research, Harvard School of Dental Medicine, Boston, MA

Vascular endothelial growth factor-A (VEGF) and its cell surface tyrosine kinase receptors (VEGFR1 and VEGFR2) are critical for cardiovascular development and postnatal homeostasis, but they also have important non-vascular functions. During cartilage development, VEGF serves as a survival factor for chondrocytes, and secretion of VEGF by hypertrophic chondrocytes during endochondral bone formation is essential for the invasion of mesenchymal stem cells, osteoclasts, sprouting endothelial cells and hematopoietic precursor cells into the hypertrophic cartilage and, thus, for establishment of primary ossification centers.

The mesenchymal stem cells, located in the perichondrium of cartilage templates of endochondral bones, respond to VEGF produced by hypertrophic chondrocytes, migrate into the cartilage via tunnels produced by osteoclasts and differentiate into the osteoblasts, osteocytes and stromal cells that form the primary spongiosa of endochondral bones. Paradoxically, not only do these stem cells respond to VEGF produced by hypertrophic chondrocytes, but they also express high levels of VEGF. This raises the question of how VEGF produced by hypertrophic chondrocytes can have a chemotactic effect on the stem cells when the VEGF receptors on their surface may be occupied by their own VEGF. To address this question as well as the broader question of what the function of VEGF, produced by mesenchymal stem cells, may be we generated mice in which expression of VEGF was knocked down in the stem cells. We took advantage of the fact that the transcription factor Osterix is expressed by mesenchymal stem cells before they differentiate into osteoblasts and used an Osterix-Cre based strategy to conditionally knock down VEGF expression in the cells.

These mice exhibited no major defects in their development but showed postnatal progressive osteoporosis with reduced bone density and increased bone marrow fat. In cultures of bone marrow-derived mesenchymal stem cells from the conditional mutant mice osteoblast differentiation was reduced while adipocyte differentiation was increased. In a series of in vitro experiments we found that VEGF stimulates expression and activity of Runx2, critical for osteoblast differentiation, while it represses the levels of PPAR γ 2, essential for adipocyte differentiation, in mesenchymal stem cells. VEGF was also found to interact with the nuclear envelope protein lamin A/C in that lamin A protein levels increased in the stem cells when levels of VEGF were reduced and levels of VEGF were reduced when levels of lamin A/C were reduced. Finally, we found that the effects of VEGF on osteoblast and adipocyte differentiation could not be explained by the canonical pathway for VEGF action, namely, secretion of VEGF and binding of VEGF to the cell surface receptors VEGFR1 and VEGFR2. Instead, the data support the conclusion that these effects of VEGF are due to a novel intracellular activity.

Previous studies of lamin A/C in mesenchymal stem cells have shown that decreased levels of this nuclear envelope protein results in reduced osteoblast and increased adipocyte differentiation. Our data suggest that VEGF mediates these effects of lamin A/C. Interestingly, mutations in lamin A/C are associated with premature aging and levels of VEGF expression are notably reduced in multiple cells types, including mesenchymal stem cells, with age. Coupled with the finding that bone marrow mesenchymal stem cells from patients with osteoporosis are more likely to differentiate into adipocytes than osteoblasts compared with cells from patients with normal bone mass, our data support the speculation that strategies aimed at preventing a reduction of intracellular VEGF levels in mesenchymal stem cells will be useful in preventing age-dependent osteoporosis.

For details and references, see Liu X, Hemmelhut AD, Jia S, Leimeon S, Burne E, Ferrara N, and Olsen BR. (2012) Intracrine VEGF regulates the balance between osteoblast and adipocyte differentiation. J. Clin. Invest. doi:10.1172/JCI63189
(The paper was published online August 13, 2012 and will be published in print in the September 1, 2012 issue of the journal)

1

Dr. Hayashi

Semaphorin 3A regulates bone homeostasis by inhibiting osteoclast and promoting osteoblast synchronously

Mikihito Hayashi, Ph.D.
Japan Science and Technology Agency, ERATO,
Takayanagi Osteonetwork project

Bone homeostasis is maintained by the crosstalk between bone-forming osteoblasts and bone-resorbing osteoclasts. Osteoclast differentiation is strictly controlled by osteoblast lineage cells to maintain adequate bone volume since excessive osteoclastic bone resorption has been implicated in the pathogenesis of various osteopenic conditions. However, an inhibitory factor of osteoclast differentiation derived from osteoblasts was not identified except for osteoprotegerin (Opg), a decoy receptor for RANKL. Here we show that a conditioned medium of Opg-deficient calvarial cells contains factors that inhibit osteoclast formation. By means of functional screening and mass spectrometric analysis, we identified that one of these factors is the axon guidance molecule Semaphorin 3A (Sema3A).

Sema3a$^{-/-}$ mice exhibited a severe low bone mass phenotype accompanied by enhanced osteoclast differentiation. Sema3A-induced inhibition was mediated by the modulation of DAP12-induced ITAM signaling. Neuropilin-1 (Nrp1), a receptor for Sema3A, competed with TREM2 for Plexin-A1, thereby functioning as a suppressor of the Plexin-A1-TREM2-DAP12-induced costimulatory signal. The inhibition of RhoA activation is also involved in the inhibitory effect of Sema3A on the migration of osteoclast precursor cells.

In addition to an osteoclastic phenotype, Sema3a$^{-/-}$ mice also showed a severe defect in osteoblast differentiation and an increase in adipocyte differentiation in bone marrow. These findings suggest that Sema3A promotes mesenchymal cell differentiation toward osteoblasts, but not adipocytes. Sema3A stimulated the canonical Wnt/ β -catenin signaling pathway, at least in part, through FARP2-mediated activation of Rac1 during osteoblast differentiation. The osteopenic phenotype in Sema3a$^{-/-}$ mice was recapitulated by mice in which the Sema3A-binding site of Nrp1 had been genetically disrupted.

We further investigated the therapeutic potential of Sema3A in a bone regeneration model of cortical bone defects induced by drill hole injury. The local administration of Sema3A into the injured site accelerated bone regeneration. Sema3A treatment reduced bone loss after ovariectomy by both inhibiting osteoclastic bone resorption and promoting osteoblastic bone formation synchronously. Thus, Sema3A is a promising new therapeutic target in bone and joint diseases. This study demonstrates that Sema3A expressed by osteoblast lineage cells functions as an osteoprotective factor with the capacity to bring both osteoblasts and osteoclasts into a condition which favors bone mineral increase.

5

Dr. Kamolratanakul

Achievement of bone regeneration and bone remodeling, the animal experimental studies to clinical trial in bone tissue engineering paradigms.

Paksinee Kamolratanakul, D.D.S., Ph.D.
Department of oral and maxillofacial surgery,
Chulalongkorn University, Bangkok, Thailand

In many cases of patients who suffer from bone disease or bone defect after surgical resection or trauma, bone reconstruction and bone repair are required.Various of the experimental researches are developed in order to achieve bone regeneration aspect. The appropriate animal models are selected to test the hypothesis based on concept of bone regeneration by tissue engineering. According to biological components involved in tissue engineering of bone; cells, scaffolds and signaling molecules are considered and utilized to create bone regeneration and balance of bone remodeling. Here, we emphasized on signaling molecules; PGE2 specific receptor agonist (EP4), PTH and TRPV4 which regulate bone repair and remodeling in different bone tissue engineering paradigms.

Owing to a role of EP4 on bone formation, critical-sized defect model demonstrated the combination of EP4 and low-dose BMP-2 in nanogel scaffold heals bone defect and regenerate proper newly-formed bone.

Consistently, PTH promotes bone formation when apply intermittently in normal condition but not in TRPV4 deficiency mice. Deletion of TRPV4 results in imbalance of bone remodeling, possibly via impairment of osteoclastogenesis. Consequently, PPRT g-induced bone formation is enhanced by TRPV4 deficiency, at least in TRPV4 heterozygous mice

Signaling molecules in various experimental conditions those mimics to clinical conditions may be the keys to achieve bone repair and regeneration, leading to development of clinical treatment in patient hereafter.

9

Dr. Fujita

Vitamin E decreases bone mass by stimulating osteoclast fusion.

Koji Fujita M.D., Ph.D.
Mayo clinic, Division of Endocrinology, Diabetes, Metabolism, & Nutrition

Bone homeostasis is maintained by the balance between osteoblastic bone formation and osteoclastic bone resorption. Osteoclasts are multinucleated cells that are formed by mononuclear preosteoclast fusion. Fat-soluble vitamins such as vitamin D are pivotal in maintaining skeletal integrity. However, the role of vitamin E in bone remodeling is unknown. We show that mice deficient in α -tocopherol transfer protein (Ttpa-/- mice), a mouse model of genetic vitamin E deficiency, have high bone mass as a result of a decrease in bone resorption. Cell-based assays indicated that α -tocopherol stimulated osteoclast fusion, independent of its antioxidant capacity, by inducing the expression of dendritic-cell-specific transmembrane protein, an essential molecule for osteoclast fusion, through activation of mitogen-activated protein kinase 14 (p38) and microphthalmia-associated transcription factor, as well as its direct recruitment to the Tm7sf4 (a gene encoding DC-STAMP) promoter. Indeed, the bone abnormality seen in Ttpa-/- mice was rescued by a Tm7sf4 transgene. Moreover, wild-type mice or rats fed an α -tocopherol-supplemented diet, which contains a comparable amount of α -tocopherol to supplements consumed by many people, lost bone mass. These results show that serum vitamin E is a determinant of bone mass through its regulation of osteoclast fusion.

13

Dr. Ono

Nestin-positive cells in endochondral bone development

Noriaki Ono, D.D.S., Ph.D.
Endocrine Unit, Massachusetts General Hospital and
Harvard Medical School, Boston, MA

Nestin-positive cells that support hematopoietic stem cells are putative mesenchymal stem cells in adult bone marrow. The relationship of these cells to osteoblast precursors is poorly understood. Previous studies have shown that, during early endochondral bone development, osterix-expressing osteoblast precursors in the perichondrium translocate to the marrow space, many of them in a pericyte-like manner. To determine the possible involvement of nestin-positive cells in this process, we studied triple-mutant mice carrying a green fluorescent protein under the nestin promoter (Nes+ or Nes-GFP) and a constitutive or an inducible cre recombinase under various promoters (Prx1-Cre, and Col2a1-CreER, Osx-CreER that activate a Rosa26 tomato reporter upon tamoxifen injection). At embryonic day 10.5 (E10.5), Nes+ cells were distributed throughout the limb bud, largely in a reticular pattern. All of these cells were in the Prx1-lineage, with some of them co-expressing the endothelial marker, CD31. When the distinct growth cartilage started to elongate at E12.5, Nes+ cells were found in the innermost portions of the perichondrium (PC), but not within the cartilage itself. At E13.5, Osx-lineage cells began to appear in the PC adjacent to the incipient hypertrophic cartilage. In this part of the PC, most of the Nes+ cells were either in the Osx lineage or positive for CD31 immunoreactivity, but not in the Col2 lineage. We thereafter chased the descendents of these Osx lineage cells (Osx-E13.5 cells) and Col2 lineage cells (Col2-E13.5 cells) using a pulse-chase protocol in which tamoxifen was given at E13.5 and mice were harvested at subsequent times. Both Osx-E13.5 cells and Col2-E13.5 cells translocated into the future marrow space, proliferated and differentiated into osteoblasts of the spongiosa. After 3 days of chase at E16.5, many of Osx-E13.5 cells, but none of Col2-E13.5 cells in the spongiosa expressed Nes-GFP. When chased further for 7 days until the time of birth (P0), Osx-E13.5 cells rarely expressed Nes-GFP in the spongiosa, while many Col2-E13.5 cells expressed Nes-GFP both in the perichondrium and spongiosa. Upon further chase by postnatal day 21, Osx-E13.5 cells disappeared almost completely with only a few cells remaining in the diaphysis, whereas Col2-E13.5 cells extensively contributed to chondrocyte, osteoblast/cyte and bone lining cell populations, with many co-expressing Nes-GFP. These findings indicate that Nes+ cells are heterogeneous in the embryonic perichondrium, and that a subset of Nes+ cells becomes Osx+ cells and a subset of Col2+ cells becomes Nes+ cells during endochondral bone development. In addition, while Osx-E13.5 cells do not indefinitely renew themselves, Col2-E13.5 cells contribute to multiple bone cell lineages at least until postnatal day 21

Dr. Sato

The pericyte as a cell of origin for sarcomas

Shingo Sato, M.D., Ph.D.
Developmental and Stem Cell Biology, the Hospital for Sick Children

Sarcomas are malignancies derived from mesenchymal tissues such as bone, muscle, fat, and cartilage. With modern surgical techniques, chemotherapy, and radiation therapy, the survival rate of sarcomas has much improved over the past three decades. However, the molecular mechanisms in the occurrence and growth of sarcomas have yet to be elucidated. Even the cell of origin for most sarcomas still remains unclear. Although there are several cases of in vitro evidence that sarcomas are derived from mesenchymal progenitor or stem cells, this hypothesis has not been proven in vivo.

We previously performed a high-throughput screening to identify cell surface makers in the tumor initiating cell population in sarcomas. This screen found that the expression of NG2 and CD146, both markers of pericytes, were enriched in the sarcoma initiating subpopulation. Pericytes are mesenchymal cells surrounding endothelial cells in capillaries, venules, and small arterioles, and cells have mesenchymal progenitor properties. These findings raise the possibility that sarcomas are derived from pericytes in which an oncogenic mutation occurs.

To test this hypothesis, we first generated Ng2-Cre; Rosa26R-LacZ mice to label NG2-expressing cells and their progenies, and confirmed by beta-galactosidase staining that LacZ was expressed in the expected cells, such as pericytes, in normal murine tissues.

We then crossed Ng2-Cre; Rosa26R-LacZ mice with p53+/- mice, which are known to develop several types of sarcomas, and used beta-galactosidase staining to investigate the expression of LacZ in murine sarcomas. We found that murine sarcomas expressed LacZ, showing that the sarcomas are derived from NG2- expressing cells, most likely from pericytes.

Furthermore, we generated Ng2-Cre mediated p53 conditional knockout mice (Ng2-Cre; $p53^{lox/lox}$ mice) to determine whether p53 inactivation in pericytes could induce sarcoma formation. Interestingly, almost all of Ng2-Cre; $p53^{lox/lox}$ mice developed some types of sarcomas, especially osteosarcoma, after 7 months of age. These findings show that sarcomas can arise from oncogenic mutations in pericytes. To determine important neoplastic changes in pericytes, we are currently comparing the gene expression profile, the genomic DNA sequence, or the copy number variation between sarcoma cells and pericytes harvested from the same Ng2-Cre; $p53^{lox/lox}$ mouse.

Identifying the cell of origin for sarcomas is important not only in understanding their underlying etiology, but also in developing novel therapeutic approaches to sarcomas based on suppressing the changes causing the cell of origin to undergo malignant change.

Dr. Inose

A microRNA regulatory mechanism of osteoblast differentiation

Hiroyuki Inose, M.D., Ph.D.
Department of Orthopedics, Tokyo Medical and Dental University

Growing evidence shows that microRNAs (miRNAs) regulate various developmental and homeostatic events in vertebrates and invertebrates. Osteoblast differentiation is a key step in proper skeletal development and acquisition of bone mass; however, the physiological role of non-coding small RNAs, especially miRNAs, in osteoblast differentiation remains elusive. Here, through comprehensive analysis of miRNAs expression during osteoblast differentiation, we show that miR-206, previously viewed as a muscle-specific miRNA, is a key regulator of this process. miR-206 was expressed in osteoblasts, and its expression decreased over the course of osteoblast differentiation. Overexpression of miR-206 in osteoblasts inhibited their differentiation, and conversely, knockdown of miR-206 expression promoted osteoblast differentiation. In silico analysis and molecular experiments revealed Connexin 43 (Cx43), a major gap junction protein in osteoblasts, as a target of miR-206, and restoration of Cx43 expression in miR-206-expressing osteoblasts rescued them from the inhibitory effect of miR-206 on osteoblast differentiation. Finally, transgenic mice expressing miR-206 in osteoblasts developed a low bone mass phenotype due to impaired osteoblast differentiation. Our data show that miRNA is a novel regulator of osteoblast differentiation.

Dr. Ganjargal

The role of fibrillin-1 in periodontal ligaments

Ganburged Ganjargal, D.D.S., Ph.D.
Prosthodontics and Orthodontics dept
Dental School Health Science University of Mongolia

Marfan syndrome is an autosomal dominant disease characterized by aneurysm and dilatation of the aortic root, tall stature, and ectopia lentis. These manifestations reflect excessive signaling of transforming growth factor (TGF)- β . Moreover, patients are frequently associated with severe periodontitis which is a chronic inflammation of the gingiva, periodontal ligament and alveolar bone. Elastic system fibers are generally formed by elastin and microfibrils, but PDLs are mainly composed of the latter. Compared with the wellknown function of collagen fibers to support teeth, little is known about the role of elastic system fibers in PDLs.

To clarify their role, we examined PDLs of mice underexpressing fibrillin-1 (mgR mice), which is one of the major microfibrillar proteins. The PDLs of homozygous mgR mice showed one-quarter of the elastic system fibers of wild-type (WT) mice. A close association between the elastic system fibers and the capillaries was noted in WT, homozygous and heterozygous mgR mice. Interestingly, capillaries in PDLs of homozygous mice were dilated or enlarged compared with those of WT mice. A comparable level of type I collagen, which is the major collagen in PDLs, was expressed in PDL-cells of mice with three genotypes. However, multi-oriented collagen fiber bundles with a thinner appearance were noted in homozygous mice, whereas well-organized collagen fiber bundles were seen in WT mice. There was a marked decrease in periostin expression, which is known to regulate the fibrillogenesis and crosslinking of collagen.

Recently, angiotensin II receptor blockers (ARBs) were discovered as an effective drug that can prevent aortic aneurysm and dilation in Marfan syndrome by inhibiting TGF- β signaling. To investigate the effect of ARB on the progression of periodontitis, the application of a potent ARB, telmisartan, was examined in a mouse model of Marfan syndrome (Mg Δ 1, Mg Δ and wild-type mice were challenged with Porphyromonas gingivalis that causes chronic periodontitis, with and without telmisartan application. The amount of resorption was significantly larger in the former than the latter. Immunoarray and ELISA demonstrated that interleukin (IL)-17 and tumor necrosis factor (TNF)- α levels were significantly higher in infected Mg Δ mice than infected wild-type mice. Telmisartan treatment significantly suppressed the alveolar bone resorption of infected Mg Δ mice and levels of TGF- β , IL-17, TNF- α in infected Mg Δ mice to levels seen in infected wild-type mice. This study suggests that ARB can prevent the severe periodontitis frequently seen in Marfan syndrome.

These observations suggest that the microfibrillar protein, fibrillin-1, is indispensable for normal tissue architecture and gene expression of PDLs.

Dr. Ohyama

Modulation of matrix mineralization by Vwc2-like proteins

Yoshio Ohyama, D.D.S., Ph.D.
Periodontology and Oral Biology, Boston University,
Boston, MA,

Objectives: Bone morphogenetic proteins (BMPs) have been applied to various clinical settings including craniofacial reconstruction, and bone/cartilage repair and regeneration for bone bioengineering. However, there are still several problems for the clinical use of BMPs; poor expression control of BMP genes, poor control of retention and release of BMPs, etc. There are a number of extracellular modulators identified as BMP antagonists, such as chordin and noggin, which exert inhibitory effects on BMP functions. However, at present, little is known about the extracellular modulators that promote BMP functions. We identified Willebrand factor C domain-containing protein 2-like (Vwc2l, also known as Brorin-like) as a new cysteine knot protein (CKP) family member. The objectives of this present study are to analyze the effect of Vwc2l on osteoblast mineralization and to investigate its molecular mechanism.

Methods: The expression of novel Vwc2l transcript variants was examined by PCR. The effect of Vwc2l protein on osteoblast mineralization in vitro was analyzed by mineralized nodule formation assay and the expression of Osterix, one of the key osteogenic markers, induced by these isoform proteins was demonstrated by real time PCR.

Results: Vwc2l transcript variants were detected in more ubiquitous tissues by RT-PCR. In osteoblasts, the induction of Vwc2l expression was observed at matrix mineralization stage. When Vwc2l was stably transfected into osteoblasts, the matrix mineralization was markedly accelerated in Vwc2l-expressing clones compared to that in the control. The expression of Osterix was significantly increased by addition of all Vwc2l isoform proteins.

Conclusion: Vwc2l is a novel secreted protein that promotes matrix mineralization by modulating Osterix expression.

Dr. Maeda

Global Small RNA Profiling During Osteoblast Differentiation

Yukiko Maeda, Ph.D.
Department of Medicine
University of Massachusetts Medical School

MicroRNAs (miRNAs) negatively and post-transcriptionally regulate expression of multiple target genes to support anabolic pathways for bone formation. By global miRNA array analysis, we found miR-218 was induced during osteoblast differentiation. Furthermore, we demonstrated miR-218 promoted commitment and differentiation of bone marrow stromal cells by activating a positive Wnt signaling loop. In a feed forward mechanism, miR-218 stimulates the Wnt pathway by down regulating three Wnt signaling inhibitors: Sclerostin (SOST), Dickkopf2 (DKK2) and secreted frizzled-related protein2 (SFRP2). In turn, miR-218 expression is up regulated in response to stimulated Wnt signaling and functionally drives Wnt related transcription and osteoblast differentiation, thereby creating a positive feedback loop.

To further explore undiscovered miRNAs which take potential role during osteoblasts differentiation, we performed a systemic profiling of small RNAs in skeletal tissue. Deep sequencing technology has the ability to identify all known and unknown small RNAs including novel miRNA and other non-coding RNAs. Therefore we used a Deep sequencing approach to analyze expression of small RNAs during osteoblast differentiation. Primary calvarial osteoblasts were collected from neonatal mice and small RNA libraries were generated at three differentiation points of osteoblasts (i.preosteoblast, ii. osteoblast, iii. mature osteoblast). Deep sequence data of these libraries consisted of 64.9~65.2% of miRNA, 32.3~33% of other ncRNAs such as piwi RNA and 1.3~1.8% of unknown and previously unidentified small RNAs. Of the 1112 known miRNAs, 42 miRNAs were up regulated and 45 miRNAs were down regulated more than two fold during differentiation. To understand the function of miRNA expression dynamics in osteoblast differentiation, the top 100 Target genes of the 18 significantly up regulated miRNAs and 24 significantly down regulated miRNAs were identified. Gene ontology analysis revealed that these targeted genes were enriched in Bone development and Wnt signaling category. To find miRNAs which regulate osteoblast differentiation, we transfected some of most up regulated miRNAs and most down regulated miRNA, miR-1983 into MC3T3E1 osteoblasts. We found miR-142 up regulated and miR-1983 down regulated the expression of osteoblast marker genes. In addition, miR-142 down regulated the target gene, TGF β receptor 1 . miR-1983 down regulated Wnt signaling targets, Tcf-1and Lef-1 mRNA level.

In summary, we performed global miRNA studies during osteoblast differentiation and revealed miRNAs that regulate osteoblast differentiation through modulation of Wnt and TGF β signaling.

Dr. Pavlic

Laser dentistry challenges in Bosnia and Herzegovina

Verica Pavlic, D.D.S., Ph.D.
Institute of Dentistry (Zavodzastomatologiju) , Banja Luka,
Bosnia and Herzegovina

During my PhD studies in Tokyo Medical and Dental University (TMDU) , I successfully completed research related to the effects of low-level Er:YAG laser irradiation on bone regeneration. Study showed promising results in enhanced MC3T3-E1 osteoblast proliferation following low-level Er:YAG laser irradiation with various combinations of laser settings (fluence 0.7~ 17.2 J/cm^2) , mainly by activation of MAPK/ERK. Results suggested use of low-level Er:YAG laser as a successful treatment modality for enhancing bone regeneration in various fields of medicine and dentistry.

After completing PhD project, for which I was multiply awarded, I returned back to my home country-Bosnia and Herzegovina (B&H) , where I started to work at University of Banja Luka, as an assistant professor in the Department of Dentistry, Section of Periodontology and Oral Medicine.

The current situation in B&H, regarding the use of lasers in dentistry, is typical for a low-income country, where lasers are still not fully incorporated in everyday dentistry, mainly due to the high costs of laser devices. Therefore, legal requirements on safe use of lasers are nonexistent or insufficient. In B&H a single law is regulating all non-ionic radiation, including lasers, but without any attention given to the distinct characteristics of lasers. Further, neither national standards nor internationally available standards on safe use of lasers are in use. Ministry of Health and Social Welfare recognized a need to address the issue of current or future laser usage in B&H, prescribing standards on potential laser hazards, laser safety measures and ways to ensure and improve patient safety in laser dentistry. As an expert on laser dentistry in B&H, I was privileged to be invited by B&H certification and accreditation body to develop and adapt national standards on safe use of lasers in B&H, based on internationally accepted standards and containing requirements related to use of dental lasers and laser safety. It is expected that future to these standards will provide a basic of safety practices in laser dentistry, and consequently, improve patient safety in laser dentistry in B&H and contribute in improving dental health care quality.

Apart from participating in creating a legal base for safe use of lasers in B&H dentistry, I am working on several projects, mainly related to the effects of low-level laser therapy on mouth diseases and conditions, such as recurrent aphthous stomatitis (RAS) , Herpes simplex infections, xerostomia···

Dr. Kimura

Molecular elucidation of pathophysiology of bone and cartilage disorders

Ayako Kimura, Ph.D.
Department of Molecular Bone and Cartilage Pathology,
Hard Tissue Genome Research Center,
Tokyo Medical and Dental University

Chondrocyte differentiation is strictly regulated by various transcription factors including Runx2 and Runx3. However, the physiological role of Runx1 in chondrocyte differentiation remains to be elucidated. To address that, we generated chondrocyte-specific Runx1-deficient mice (α 1 (II) Cre/Runx1flox mice) and mesenchymal cell-specific Runx1-deficient mice (Prx1Cre/Runx1flox mice) , because Runx1-/- mice die early in utero. Furthermore, we crossed them with Runx2 mutant mice to obtain chondrocyte-specific or mesenchymal cell-specific Runx1/Runx2 double mutant mice (α 1 (II) Cre/DKO mice and Prx1Cre/DKO mice, respectively) . α 1 (II) Cre/Runx1flox and α 1 (II) Cre/DKO mice were grossly normal. In contrast, Prx1Cre/Runx1flox mice displayed a delay in the calcification of the sternum, and Prx1Cre/DKO mice completely lacked the sternum. Histologically, in the prospective sternum of Prx1Cre/DKO mice, mesenchymal cell condensation developed normally; however, commitment to the chondrocytic lineage was seriously impaired. In line with that observation the expression of α 1 (II) collagen, Sox5 and Sox6 in the prospective sternum of Prx1Cre/DKO mice was severely attenuated by in situ hybridization, while Sox9 expression was unchanged. Molecularly, transient transfection of Runx1 or Runx2 in mesenchymal cell increased endogenous Sox6 and Sox5 expression, which led to α 1 (II) collagen induction. Thus, we demonstrated that Runx1 and Runx2 cooperatively regulate chondrocyte lineage commitment through the induction of Sox5 and Sox6.

Malignant fibrous histiocytoma (MFH) , which has an aggressive biological behavior and a poor prognosis, is the most common type of soft tissue sarcoma in older adults. However, the molecular pathogenesis of MFH is largely unknown. It has been suggested that genetic abnormalities are implicated in the cause of MFH, namely, genetic alterations, including aberration of DNA copy number such as gene amplifications and deletions, may lead to activation of oncogenes and inactivation of tumor suppressor genes. To identify genomic alterations involved in MFH oncogenesis, we performed DNA copy number analysis of MFH cases by using CGH array. We observed high-level amplification at chromosome region 2q11, 2q24, 2q31, 2q36, 4q16, 8p11, 16q22, 17p13, 22q11, Xq25 (ratio > 2) . In addition, we found homozygous deletion at chromosome 10q23, 13q13, 13q14, 17q13, which spanned known tumor suppressor genes including p53. These chromosome regions may harbor genes important for MFH oncogenesis and progression, and may be potentially useful for diagnostic purposes.

Dr. Flores

Proteomics for Alzheimer Disease for Biomarkers Discovery

Mara Gómez Flores, D.D.S., Ph.D.
Department of Cellular Biology, Center for Research and
Advanced Studies of the National Polytechnic Institute (CINVESTAV) ,
Mexico city, Mexico.

Alzheimer's disease (AD) is the most common type of dementia that affects around 24.3 million people worldwide, with rapid demographic growth in elderly population an is expected to increase in developing countries. AD has become one of the most severe progressive social, economical and medical burden in many countries all over the world. AD brains are characterized by the presence of extracellular deposits of amyloid- β (A β) containing plaques and intracellular neurofibrillary tangles (NFTs) composed by paired helical filaments of hyperphosphorylated Tau protein. AD, seems to be the result of a series of complex events involving both genetic and environmental factors; among the main factors are, the oxidative stress and the mitochondrial damage. Initial changes in brain might occur decades prior to the onset of clinical symptoms. One approach for early diagnosis might be the discovery of biomarkers present in initial stages of the disease and follow up by the disorder's progression as well as the identification of targets for developing new drugs. The main goal is, to identify related proteins in the evolution of AD, using target proteins with iTRAQ and analyze them through mass spectrometry. Our results showed the identification of over 604 proteins and we have found that some protein expression were up-regulated and down-regulated, compared to those found in normal brain. Previous reports have shown the participation of that GAPDH protein could be used as a biomarker for early diagnose, and is specific for AD. Moreover, we have identified other proteins related in mitochondrial damage and stress, proteins like transferring and Heat Shock Proteins. In conclusion, we intent to offer a broad approach about the expression of many different proteins in AD's brains and in normal (brain) ones, this would allow to have some specific biomarkers for early diagnose of AD.

11. 新聞記事 (Newspaper Reports)


Japan Medicine MONTHLY
CLINICAL & MEDICAL NEWS

関節リウマチ（RA）の治療薬として国内の臨床現場に生物学的製剤（Bio）が登場し、今年で10年目を迎える。その後も相次いで発売され、現在は6製剤。この間に国内のエビデンスと臨床実績を積み重ね、日本に見合った薬物療法の実践を目指してきた。国内でもデータや経験を基にBioを使いこなし、RA診療に臨む時代になったといえる。欧米では近年、診断、治療、寛解に関する基準や手法が新たに提唱され、国内でもそれらを積極的に臨床へ導入する動きがある。ここでも海外の仕組みを丸飲みするのではなく、国内エビデンスによる検証や、日常診療での有効活用の模索が行われている。特集では、Bioを中心に、国内で進展するRAの薬物療法などをリポートする。

宮坂信之　2012年6月25日


骨の減少抑える
たんぱく質発見
骨粗鬆症治療に期待
東京医科歯科大

骨の中が空洞化する「骨粗鬆症」など骨量が減る病気について、その減少をくい止めるたんぱく質を、東京医科歯科大の高柳広教授（骨免疫学）らが見つけた。国内に患者が1300万人いるとされる骨粗鬆症や関節リウマチなど骨の病気への治療の応用が期待される。

骨は、破壊（吸収）と新たな形成のバランスが保たれることで、健康な状態を保っている。このバランスが崩れ、吸収が多くなると骨が空洞化して骨粗鬆症になったり、逆の場合は骨が硬くなる「大理石骨病」などを引き起こす。現在の骨粗鬆症の治療は、吸収を抑えることが中心で、形成を保つ薬はほとんどないという。

高柳教授らは、もともと神経や免疫をコントロールする作用があることが知られていた「セマフォリン3A」（セマ3A）というたんぱく質に、骨の破壊を抑える効果があることを確認した。このたんぱく質を、マウスに静脈注射したところ、吸収の細胞を抑え、形成の細胞が促進され、骨量が通常に増えた。

また、老化するにつれて、骨量が減っているマウスの血中を調べたところ、セマ3Aの濃度が比例して減っていた。今後、臨床診断の指標になる可能性もある。

18日付の英科学誌ネイチャー（電子版）に掲載される。（石塚広志）

高柳 広　2012年4月19日　朝日新聞

12. HP (Home Page)

平成24年度　アクセス数　4,462

13. 海外研究者等招聘講演会 (Overseas Researcher Seminar)

ポスター	タイトル	講演者	日　付
	第60回グローバルCOE海外研究者講演会 「Fibrinolysis-The Fountain of Youth of Bone?」	Dr. Jonathan SchoeneckerM.D.	2013年3月11日
	第230回 Bone Biology Seminar 「Bone marrow endothelium: A hierarchically organised system with transplantable hemogenic stem cells giving rise to functional blood vessels as well as HSC.」	Dr. Susan Kaye NILSSON B.Sc. (Honours), Ph.D.	2013年3月5日

ポスター	タイトル	講演者	日　付
	第229回 Bone Biology Seminar 「The ERK MAPK pathway in skeletal development.」	Shunichi Murakami, M.D., Ph.D.	2013年1月31日
	第228回 Bone Biology Seminar 「Mechanisms of metastasis to bone : homing of breast cancer to bone」	Dr. Michael Rosenblatt, M.D.	2013年1月22日
	第56回グローバルCOE海外研究者講演会「Considerations for accurate and predictable surgical correction of facial asymmetry」	Prof Tae-Geon KWON	2012年10月18日
	第227回 Bone Biology Seminar「The Cathepsin K Inhibitor Reduces Bone Resorption While Maintaining Bone Formation.」	Dr. Le Duong, Ph.D.	2012年9月25日
	第53回グローバルCOE海外研究者講演会共催「Novel Skeletal Roles of Neural Molecules」「Role of CXCL10 in Osteolytic Bone Metastasis」「ARD1 controls osteoblast differentiation by acetylating Runx2」「Molecular genetic characterization of hereditary enamel and dentin defects」	Dr. Hong-Hee Kim, Ph.D. Dr. Zang Hee Lee, D.D.S., Ph.D. Dr. Jongwan Park, M.D., Ph.D. Dr. Jeong Wook Kim, D.D.S., Ph.D.	2012年8月27日
	第226回 Bone Biology Seminar「Mechanical derivation of multi-nucleated myotubes from human adipose-derived stem cells.」	Dr. Yu Suk Choi, Ph.D.	2012年6月13日

14. イノベーション研究活動推進 (Innovation)

【2012年度】

実施日：2012年7月9日　書類審査、7月30日ヒアリング

研究課題名：難治性硬組織疾患の病態オミックス先端拠点研究
研　究　者：分子細胞遺伝学　稲澤　譲治
分子薬理学　野田　政樹
顎口腔外科学　小村　健
顎顔面矯正学　森山　啓司
膠原病・リウマチ内科学　宮坂　信之
分子遺伝学　三木　義男
整形外科学　大川　淳

研究課題名：歯髄・歯肉の幹細胞の特性解析と再生医療への応用
研　究　者：歯髄生物学　須田　英明
運動器外科学　宗田　大

研究課題名：口腔癌顎骨浸潤の分子メカニズムの解明を目指したフロンティア研究拠点
研　究　者：口腔病理学　山口　朗
顎口腔外科学　小村　健

研究課題名：侵襲性歯周炎のエクソーム解析
研　究　者：歯周病学　和泉　雄一
分子細胞遺伝学　稲澤　譲治

研究課題名：幹細胞エクソソームを用いた新規組織再生法の開発
研　究　者：分子細胞機能学　森田　育男
京都大学大学院工学研究科　秋吉　一成

15. 国際PIシャペロンの活動 (International PI Chaperon Activity)

●2012年4月23日

国際PIシャペロンフォーラム

●6月28日、7月2日

国際PIシャペロン競争的研究費審査

16. 大学院生採用面接評価 (SS Interview and Evaluation for Selection)

複数教員による英語（年次）面接と評価　優秀賞受賞者

●第Ⅷ（2012年4月～）Award Winner

1位　Most Excellent Award 川崎真希理
2位　Excellent Award　中里洋子
3位　Excellent Award　葉暢暢

第Ⅷ期　AISS採用面接　点数分布

評価点数	全体平均　73.07点	該当者数
81－85	○○○○○○○○	8
76－80	○○○○○○○○○○	10
71－75	○○○○○○○○○○○○○○○	15
66－70	○○○○○○○○○	9
61－65	○○○	3
56－60	○○○○	4
51－55	○	1
合　計		50

●第Ⅸ（2012年10月～）Award Winner

1位　Most Excellent Award　小野岳人
2位　Excellent Award　Smriti Aryal A. C
3位　Excellent Award　Nurmaa Dashzeveg

第Ⅸ期　AISS採用面接点数分布

評価点数	全体平均　76.89点	該当者数
91－100	○○	2
86－90	○○○	3
81－85	○○○	3
76－80	○○○○○○	6
71－75	○○○○○○○○	8
66－70	○○○○○	5
61－65	○○○	3
合　計		30

17. プレゼンテーション型英語クラス (English Class)

開催日

Student Instruction：
2012年4月23日、5月21日、6月25日、7月23日、9月24日、11月6日、12月17日、2013年1月28日
Instructor：Mr. Kevin Cleary（本学准教授）
参加者　15名（2013年1月28日現在）

18. 歯と骨のGCOE　受賞リスト (Award List)

田上　順次

1. 日本歯科審美学会優秀発表賞　大槻　昌幸
2. 第５回日本歯科理工学会IADR-DMGC-J記念賞
   高垣　智博

高柳　広

1. 中島　友紀
   第30回日本骨代謝学会学会奨励賞
   平成24年7月
2. 岡本　一男
   平成23年度三浦記念リウマチ学術研究賞 (公益財団法人　日本リウマチ財団)
   平成23年7月29日
3. 林　幹人
   4th International Conference on Osteoimmunology Travel Award
   平成24年6月
   第30回日本骨代謝学会優秀演題賞
   平成24年7月
   第33 回日本炎症・再生医学会優秀演題賞
   平成24年7月

小村　健

1. 佐藤　潔, 坂本　啓, 栢森　高, 小村　健, 山口　朗: 口腔扁平上皮癌による骨破壊には腫瘍細胞と間質細胞が産生するRANKLが関与する．第30回日本口腔腫瘍学会総会優秀ポスター賞　2012年1月26-27日　埼玉
2. 上杉　篤史: The tumor suppressive microRNA miR-218 targets the mTOR component Rictor and ihibits AKT phosphorylation in oral cancer. 平成23年度難治疾患研究所発表会優秀論文賞　2012年3月8日　東京
3. 山本　信祐 : Identification of microRNAs negatively regulating NRF2 pathway. 平成23年度難治疾患研究所発表会ベストディスカッション賞　2012年3月8日　東京
4. 宮崎　英隆, 金　舞, 中島　雄介, 牧口　貴哉, 早田　隆司, 宇田川　雅敏, 樺沢　勇司, 小村　健, 横尾　聡 : 組織内レーザー照射法による血管病変の治療. 第57回日本口腔外科学会総会 優秀口演発表賞 2012年10月19-21日　横浜市

春日井　昇平

1. 宗像　源博　クインテッセンス出版株式会社　最優秀論文賞　2012年12月
2. 藤井　政樹　第42回日本口腔インプラント学会学術大会　最優秀発表賞　2012年9月23日
3. 鶴見　和久　第42回日本口腔インプラント学会学術大会　最優秀ポスター発表賞　2012年9月23日
4. 渕上　慧　第42回日本口腔インプラント学会学術大会　最優秀講演賞　2012年9月23日
5. Marwa Madi　FDI Poster Presentation　Award 8月29日

須田　英明

1. 西原　良治（指導　鈴木規元、石村瞳）．スーパーエンドα、βを用いた根管充填の速度および充填率に関する研究．D4研究体験実習学生発表会　歯学科長賞，2010年9月25日．

森山　啓司

1. 伊藤　洋介、川元　龍夫、森山　啓司．ビーグル犬におけるミニプレート顎間牽引の顎整形効果に関する検討．第71回日本矯正歯科学会大会・優秀発表賞、盛岡、平成24年9月26-28日．
2. 渡辺　千穂、江面　陽一、中元　哲也、早田　匡芳、納富　拓也、森山　啓司、野田　政樹．骨量制御の新転写後性分子機構：mRNA deadenylaseである Ccr4-not complex構成因子Cnot3の欠失による高回転型の骨量減少の解析．第30回日本骨代謝学会・ANZBMS travel award、東京、平成24年7月19－21日
3. 鎌田　秀樹、福岡　裕樹、山田　大輔、志賀　百年、川元　龍夫、森山　啓司．顔面非対称を伴う骨格性下顎前突症例における下顎骨形態の三次元的解析．第22回日本顎変形症学会総会・優秀ポスター賞、福岡、平成24年6月18-19日．
4. 片岡　恵一、小川　卓也、春山　直人、小林　起穂、阿彦　希、大宅　彩、東堀　紀尚、森山　啓司．創内型装置を用いて上顎骨延長法を行った口唇裂・口蓋裂症例における術後変化．第36回日本口蓋裂学会総会・学術集会・優秀ポスター賞、京都、平成24年5月24-25日

宗田　大

1. 2012年度お茶の水会医科同窓会研究奨励賞
   Arthritis Res Ther. 2010;12(6):R206. Epub 2010 Nov 5. “Intradiscal transplantation of synovial mesenchymal stem cells prevents intervertebral disc degeneration through suppression of matrix metalloproteinase-related genes in nucleus pulposus cells in rabbits.” Miyamoto T, Muneta T, Tabuchi T, Matsumoto K,

Saito H, Tsuji K, Sekiya I.

稲澤　譲治

1. 春木　茂男が「Frequent silencing of protocadherin 17, a candidate tumour suppressor for esophageal squamous-cell carcinoma.(Carcinogenesis. 31:1027-36. 2010発表)」の研究成果で平成22年度東京医科歯科大学　田中道子賞を受賞した。
2. 古田　繭子が東京医科歯科大学グローバルCOE（GCOE）プログラム研究発表で「Excellent Presentation-Special Award-」を受賞した。
3. 鶴田　智彦（現・永寿総合病院産婦人科勤務）が平成23年度日本産科婦人科学会「優秀論文賞婦人科腫瘍学部門」を受賞した。

小川　佳宏

1. 亀井　康富　日本肥満学会学術奨励賞
「肥満・生活習慣病における核内受容体・転写共役因子の病態生理的意義の解明」
2. 江原　達弥　日本肥満学会若手研究奨励賞
「マウス新生仔の肝臓における脂肪合成酵素GPAT1のDNAメチル化による遺伝子発現制御」

19. Research Day

●国際的トップ大学Research Dayへ派遣

Harvard University

Poster	Student	Degree/Program	Evaluator
8	Makiri Kawasaki	Visiting Scholar, Tokyo	Shigemi Nagai
9	Chiho Watanabe	Visiting Scholar, Tokyo	Shigami Nagai
11	Nurmaa Dashzeveg	Visiting Scholar, Tokyo	Nina Anderson

University of California San Francisco

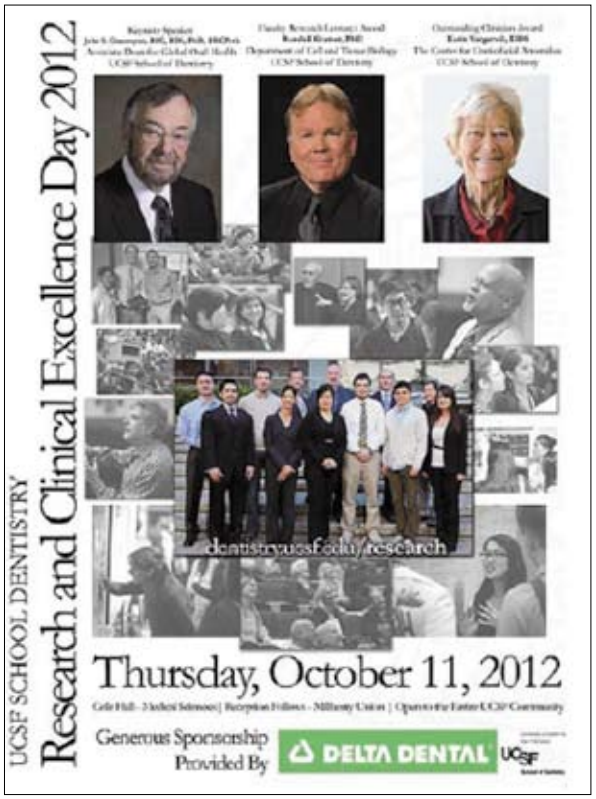

University of Toronto

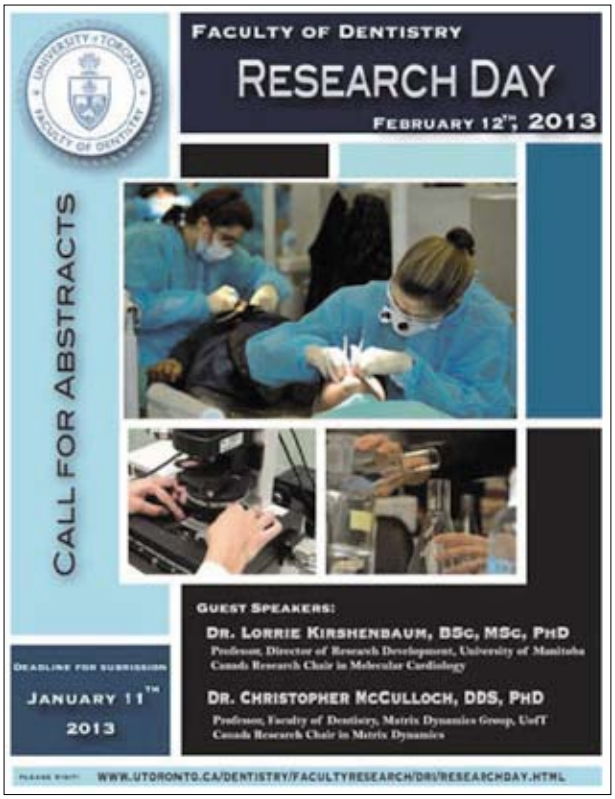

HARVARD
School of Dental Medicine

2012 STUDENT RESEARCH DAY
APRIL 10, 2012 ■ 8:30 AM-3:30 PM ■ REB LOBBY

8:30AM - 9:00AM BREAKFAST (REB LOBBY)

9:00 - 9:30AM WELCOME & PRESENTATION OF AWARDS (REB AUDITORIUM)

9:30AM - 11:30AM SESSION I: POSTER PRESENTATIONS (REB LOBBY)

Poster	Student	Degree/Program	Evaluator
1	Judy Rosenbloom	General Practice Resident	Stephanos Kyrkanindes
2	Danielle Herschler	General Practice Resident	Stephanos Kyrkanindes
3	Laila Dantas	General Practice Resident	Elsbeth Kalenderian
4	Karine Calixte	General Practice Resident	Elsbeth Kalenderian
5	Kyosuke Suwabe	Visiting Scholar, Iwate	Bjorn R. Olsen
6	Yasushi Tamada	Visiting Scholar, Iwate	Bjorn R. Olsen
7	Mikako Takahashi	Visiting Scholar, Iwate	Bjorn R. Olsen
8	Makiri Kawasaki	Visiting Scholar, Tokyo	Shigemi Nagai
9	Chiho Watanabe	Visiting Scholar, Tokyo	Shigemi Nagai
10	Ye Chang Chang	Visiting Scholar, Tokyo	Nina Anderson
11	Nurmaa Dashzeveg	Visiting Scholar, Tokyo	Nina Anderson
12	Arwa Farag	DMSc 2012 Oral Medicine	Shoichiro Kokabu
13	Martin Fu	DMSc 2012 Periodontology	Shoichiro Kokabu
14	Soo-Woo Kim	DMSc 2012 Periodontology	Xiu-Ping Wang
15	Tan Nguyen	DMSc 2012 Orthodontics	Xiu-Ping Wang
16	Daniel Ho	DMSc 2012 Periodontology	Xiu-Ping Wang
17	Mahshid Bahaderan	DMSc 2015 Orthodontics	Robert Wright
18	Brian Asbury	MMSc 2012 Orthodontics	Robert Wright
19	Imanoel Golshirazian	MMSc 2012 Orthodontics	Robert Wright
20	Yinayra Victoria	MMSc 2012 Orthodontics	Claudia Nicolae
21	Anisha Thondukolam	MMSc 2012 Periodontology	Claudia Nicolae
22	Hung-Hsiang Tso	MMSc 2012 Prosthodontics	Bruce Donoff
23	Ahmad Alnatour	MMSc 2012 Endodontics	Bruce Donoff
24	Thao Le	MMSc 2012 Endodontics	Bruce Donoff
25	Jeong Lee	MMSc 2012 Prosthodontics	Dorothy Pazin
26	Esther Hyun Kim	MMSc 2012 Endodontics	Dorothy Pazin
27	Muirzaddin Mokti	MMSc 2012 Implantology	Dorothy Pazin

20. リトリート (Retreat)

Fifth Retreat Meeting

【日程】

2012年11月12日（月）

9：30～11：30　海外研究者とのディスカッション

15：10～15：40　Poster Session 1（25演題）

2012年11月13日（火）

15：40～16：10　Poster Session 2（23演題）

【場所】

東京医科歯科大学　M&Dタワー2階ホワイエ

Sixth Retreat Meeting

【日程】

2013年2月4日（月）

9：00～9：45　海外研究者とのディスカッション

15：50～16：20　Poster Session 3（25演題）

【場所】

東京医科歯科大学　M&Dタワー2階ホワイエ

Important information.

From the next lecture series we would like to evaluate your understanding of the lectures every week as this course would be certified as one of formal lectures of the university. Please express your opinion and submit both the following questionnaire including your short comments on the contents of lecture at the end of each lecture:

Questionnaire

1. The name of the lecturer.
2. Your name and department.
3. Evaluation of the lecture

   The quality of the content of the lecture was

   (excellent, good, average, relatively poor, poor)

   The method of the presentations was

   (excellent, good, average, relatively poor, poor)

   Overall evaluation of your attitude (effort, motivation and commitment).

   (excellent, good, average, relatively poor, poor)

4. Your comments or questions to the lecturer.

臨床のお話でとても興味深く、より身近な課題として
とても勉強になりました。
正級の子供に対し、治療に入るのか（工期）、経過観察にするのか、今後明確な線引きのできる方法が知りたいと思いました。

Prof. F. Ishino, the GCOE Committee on International Education Programs

Prof. I. Morita, the GCOE Committee on Development of Young Scientists

Important information.

From the next lecture series we would like to evaluate your understanding of the lectures every week as this course would be certified as one of formal lectures of the university. Please express your opinion and submit both the following questionnaire including your short comments on the contents of lecture at the end of each lecture:

Questionnaire

1. The name of the lecturer.
2. Your name and department.
3. Evaluation of the lecture

   The quality of the content of the lecture was

   (excellent, good, average, relatively poor, poor)

   The method of the presentations was

   (excellent, good, average, relatively poor, poor)

   Overall evaluation of your attitude (effort, motivation and commitment).

   (excellent, good, average, relatively poor, poor)

4. Your comments or questions to the lecturer.

Thank you for your presentation.

As you mentioned about the effect of cancer chemotherapy using Paclitaxel in pathological & clinical eff, I would like to ask you about the criterias.

- what is the difference in each criteria, esp. grade 3 = complete response ?.
- Does it correlate between pathological and clinical effect of this cancer ?.

Prof. F. Ishino, the GCOE Committee on International Education Programs

Prof. I. Morita, the GCOE Committee on Development of Young Scientists

21. Illustrations of Achievement

Weekly Presentations

114 presentations GCOE
7,160 participants

Weekly Presentations Evaluation by Super Students (Excellent & Good)

Weekly Presentations Evaluation Questionnaire

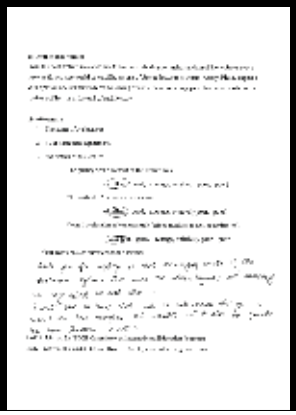

GCOE Seminars

Total 61 Sessions

1,191 participants

2012.4-2013.3 Total 9 Sessions (Dr. Donald B. Kimmel, Dr. Le Duong etc)
2011.4-2012.3 Total 10 Sessions (Dr. Mark I. Ryder, Dr. David E. Birk etc)
2010.4-2011.3 Total 17 Sessions (Dr. Irma Thesleff, Dr. Vicki Rosen etc)
2009.4-2010.3 Total 12 Sessions (Dr. Henry Kronenberg, Dr. Jack Martin etc)
2008.4-2009.3 Total 13 Sessions (Dr. Theresa A. Guise, Dr. Gerard Karsenty etc)

PhD Student Advisory Session

Total 4 Sessions

<2011>
4, 2012.1.26
Dr. Thomas John Martin
Dr. Henry Kronenberg
Dr. Erwin F. Wagner
Dr. Gerard Karsenty
Dr. Benjamin Alman
Dr. Naoyuki Takahashi
Dr. Shigeaki Kato

<2010>
3, 2011.2.4
Dr. Dennis Crawford
Dr. Alberto Gobbi
Dr. James Hui

<2009>
2, 2010.2.12
Dr. Peter Thomsen
Dr. Peter Schupbach

1, 2009.6.11
Dr. Roland Baron
Dr. Stephan E.
Dr. Harris Jerry
Dr. Feng Roberta Faccio

Annual Chaperone Competition and Grant Writing Tutorials

2009-2012
Evaluates for Competition

<Total 5 Competitions>
1, 2009.1.19
2, 2009.6.29
3, 2010.7
4, 2 011.7.5
5, 2012.6.28, 2012 7.2

Collaborative Research and Innovation

Johji Inazawa

2012.8.10
2011.9.5
2010.11.30
2009.6.29
2008.12

1, Yuichi Izumi, Masaki Noda (D, R)
2, Johji Inazawa, Masaki Noda, Ken Omura, Keiji Moriyama, Nobuyuki Miyasaka, Yoshio Miki, Atsushi Okawa, (M, D, R, B)
3, Hideaki Suda, Takeshi Muneta (D,M)
4, Ikuo Morita, Yuichi Izumi (Dc, Db)
5, Akira Yamaguchi, Ken Omura (Db, Dc)
6, Yuichi Izumi, Johji Inazawa (D, R)
7, Ikuo Morita, Kazunari Akiyoshi (D, B)
8, Masaki Yanagishita, Yuichi Izumi Db,Dc)

International Tutorials Meet-the-International Experts

International Advisory Review

Hideaki Suda

2009.1.23 Reynolds, Kubo, Yoshida
2009.6.11 Roland Baron, Stephan E. Harris, Roberta Faccio
2010.10.29 Derrik Rancourt
2011.1.31 Adam Engler
2011.2.4 Dennis C. Crawford, James Hui Hoi Po, Alberto Gobbi
2012.1.26 Thomas John Martin, Henry Kronenberg, Erwin F. Wagner, Gerard Karsenty, Benjamin Alman, Naoyuki Takahashi, Shigeaki Kato
2012.11.14 Lynda F. Bonewald, Irma Theslef, Gregory J. Seymour, Nawarat Wara-aswapati, Young Ku, Seung-Hak Baek, Young-Chel Park
2013.2.4 Steven Offenbacher, Panos Papapanou, Denis Kinane, Mark Bartold

2012 Annual International Advisory Review

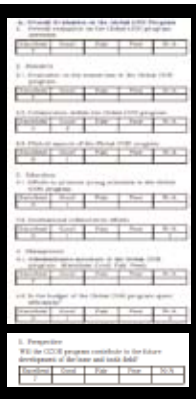

2011 Annual International Advisory Review

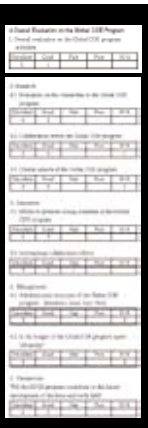

2010 Annual International Advisory Review

2009 Annual International Advisory Review

Grant Writing Workshop

日程：2009.7.30
2010.9.14

Participants：
Keiji Moriyama, Masaki Noda, Takuya Notomi, Masatsugu Ohora, Tadahiro Iimura, Hideki Iwai, Kunikazu Tsuji, Lee Jiyoung, Naoki Sawada, Sadr Alireza, Naoto Haruyama, Hiroyuki Nakamura

Total 2 Sessions

Annual Student Review and Competition（Total 9 Competitions）

Period	Number of Applicants	Number of Acceptances
Period Ⅰ(2008.10)	49	43
Period Ⅱ (2009.4)	28	10
Period Ⅲ (2009.10)	62	43
Period Ⅳ (2010.4.)	27	20
Period Ⅲ (2010.10)	67	31
Period Ⅵ (2011.4)	60	28
Period Ⅶ (2011.10)	39	23
Period Ⅷ(2012.4)	50	31
Period Ⅸ (2012.10)	30	20

Press Releases

Number of Press Releases	
2008	25
2009	42
2010	52
2011	54
2012	54

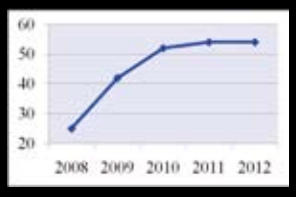

Home Page and Annual Reports

HP: Number of Visitors：71,485

373 page　477 page　469 page　438 page

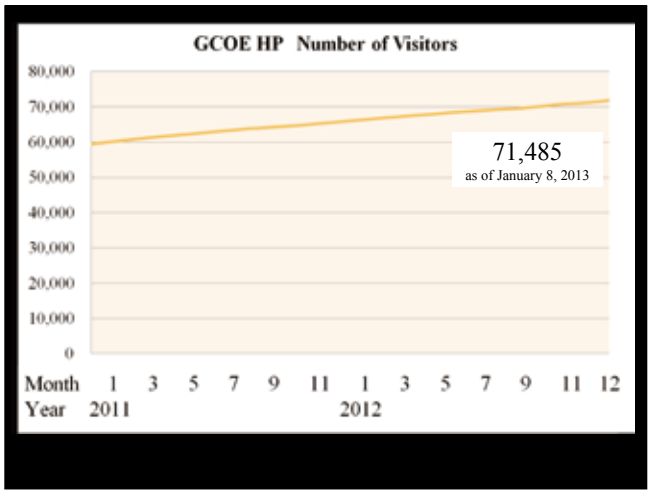
GCOE HP Number of Visitors
80,000
70,000
60,000
50,000
40,000
30,000
20,000
10,000
0
71,485
as of January 8, 2013
Month 1 3 5 7 9 11 1 3 5 7 9 11 12
Year 2011 2012


International Education at Affiliated Universities
Harvard U, UCSF, U. Toronto
29 Students
Harvard 12
UCSF 6
Toronto 11
2008 4人
2009 6人
2010 6人
2011 7人
2012 6人
Harvard 2009.4.14
Rajib Bhattacharjee
Ganburged Ganjargal
Yoko Aoi
Harvard 2010.4.13
Kanako Noritake
Bai Hua
Tomomi Sakuma
Harvard 2011.4.12
MD Abdulla Al Masud Khan
Daisuke Miyajima
Smriti Aryal A C
Harvard 2012.4.10
Chiho Watanabe
Makiri Kawasaki
Nurmaa Dashzeveg
UCSF 2010.10.6
Daisuke Miyajima
Paksinee Kamolratanakul
UCSF 2011.10.13
Azusa Yamada
Khandakar Abu Shameem
Md.Saadat
UCSF 2012.10. 11
Masayoshi Uezono
Ye Chang Chang
Toronto 2008.10.16
Begum Asma
Kanako Noritake
Chalida Nakalekha
Toronto 2009.2.10
Neil Alles
Toronto 2010.2.23
Noriko Ebe
Hao Jia
Xu Jing
Toronto 2011.2.15
Kaori Tsuji
Toronto 2012.2.15
Takehito Ono
Gamaralalage Amodini Rajakaruna
Toronto 2013.2.12
Norihiko Ashigaki

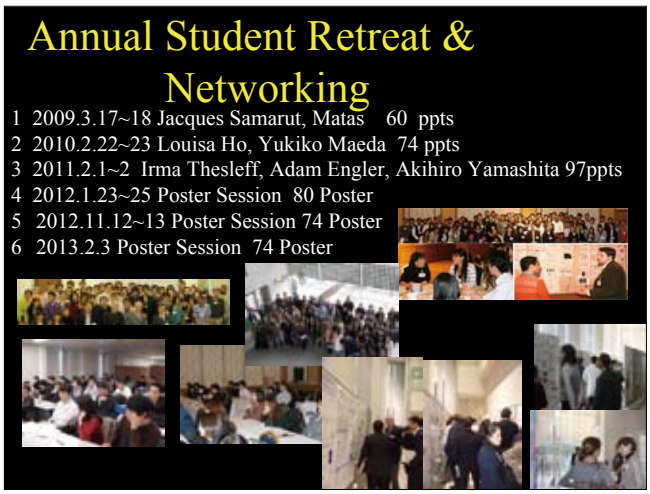
Annual Student Retreat & Networking
1 2009.3.17~18 Jacques Samarut, Matas 60 ppts
2 2010.2.22~23 Louisa Ho, Yukiko Maeda 74 ppts
3 2011.2.1~2 Irma Thesleff, Adam Engler, Akihiro Yamashita 97ppts
4 2012.1.23~25 Poster Session 80 Poster
5 2012.11.12~13 Poster Session 74 Poster
6 2013.2.3 Poster Session 74 Poster

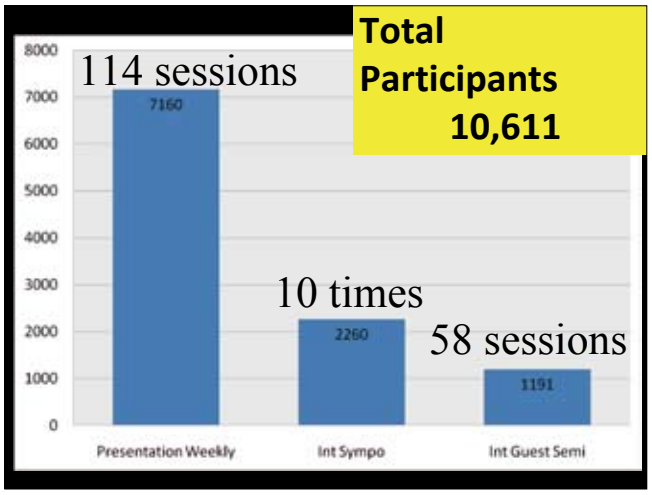
Total Participants 10,611
8000
7000
6000
5000
4000
3000
2000
1000
0
114 sessions
7160
10 times
2260
58 sessions
1191
Presentation Weekly
Int Sympo
Int Guest Semi

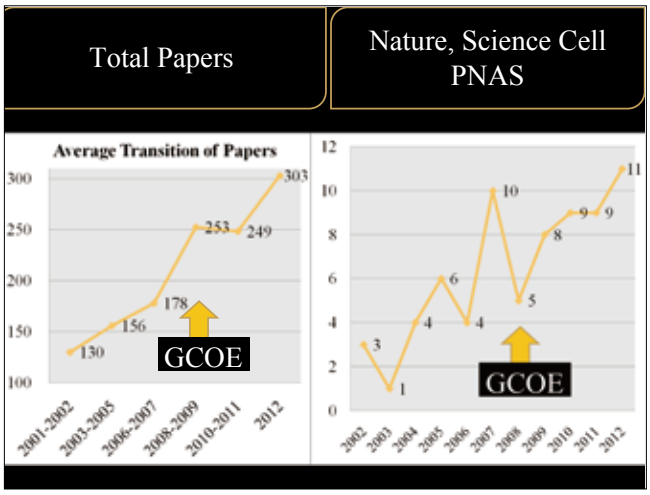
Total Papers
Nature, Science Cell PNAS
Average Transition of Papers
300
250
200
150
100
130
156
178
253
249
303
GCOE
2001-2002
2003-2005
2006-2007
2008-2009
2010-2011
2012
12
10
8
6
4
2
0
3
1
4
6
4
10
5
8
9
9
11
GCOE
2002
2003
2004
2005
2006
2007
2008
2009
2010
2011
2012

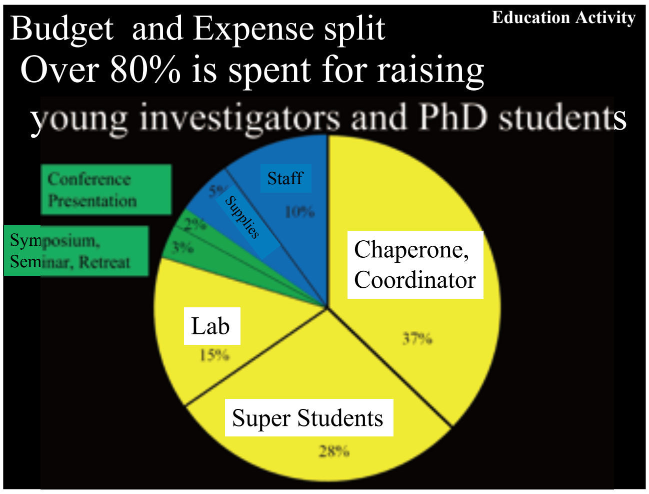
Education Activity
Budget and Expense split
Over 80% is spent for raising
young investigators and PhD students
Conference
Presentation
Symposium,
Seminar, Retreat
Staff
10%
5%
Supplies
2%
3%
Chaperone,
Coordinator
37%
Lab
15%
Super Students
28%

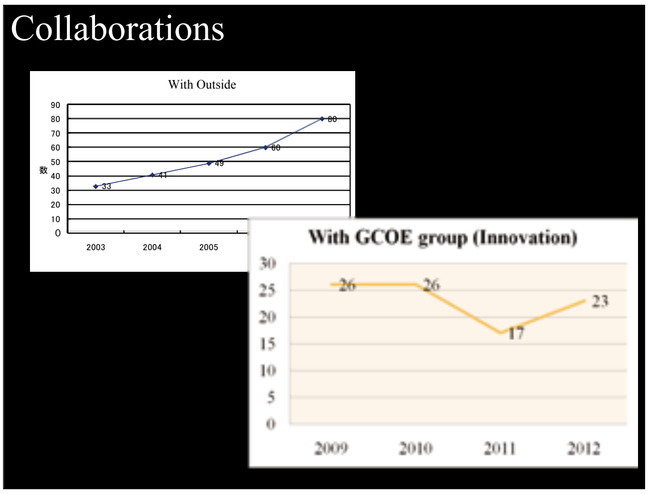
Collaborations
With Outside
90
80
70
60
50
40
30
20
10
0
数
33
41
49
60
80
2003
2004
2005
With GCOE group (Innovation)
30
25
20
15
10
5
0
26
26
17
23
2009
2010
2011
2012

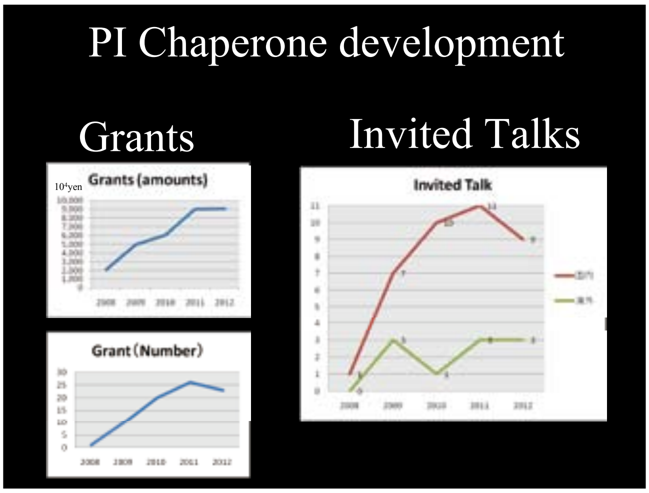
PI Chaperone development
Grants
Invited Talks
Grants (amounts)
10⁴yen
Grant (Number)
Invited Talk

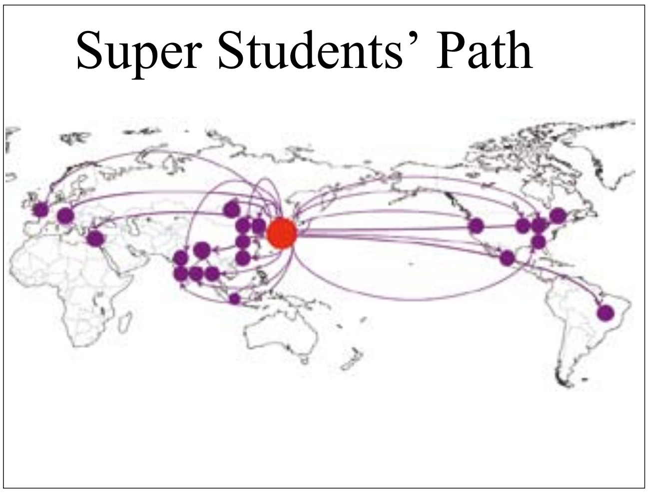
Super Students' Path

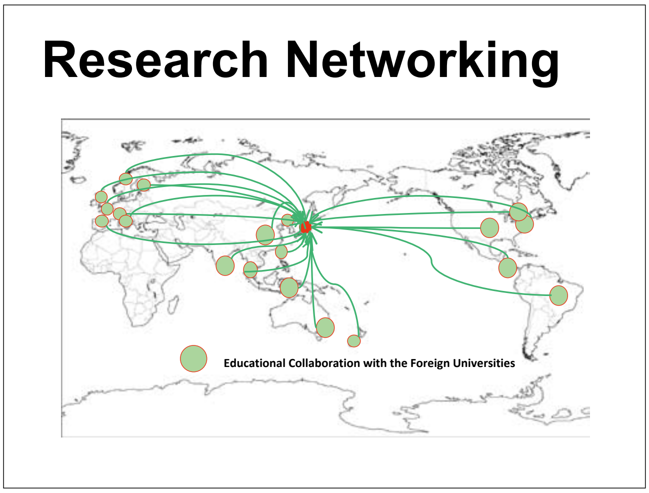
Research Networking
Educational Collaboration with the Foreign Universities

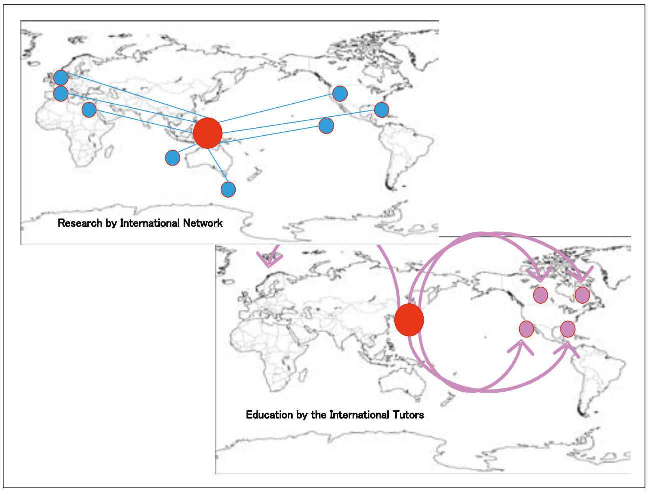
Research by International Network
Education by the International Tutors

International Tutors

We send our PhD students to participate in their graduate school programs or leaning techniques

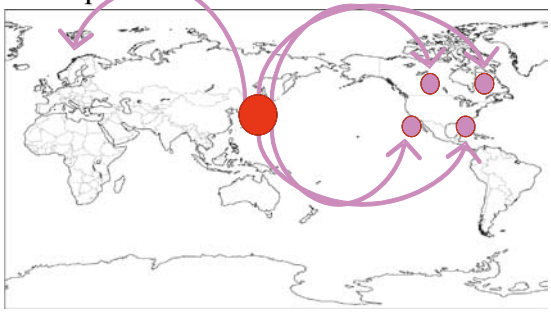

Collaboration with the Foreign Universities

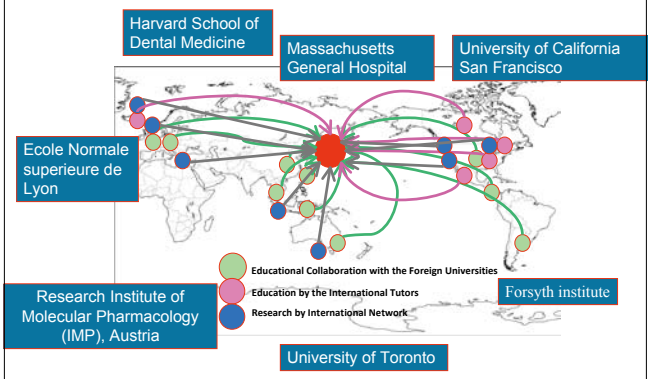

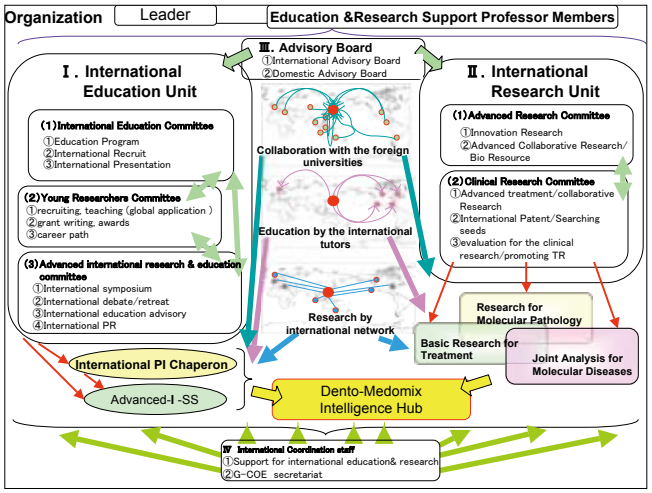

Support for Participation in Academic Societies

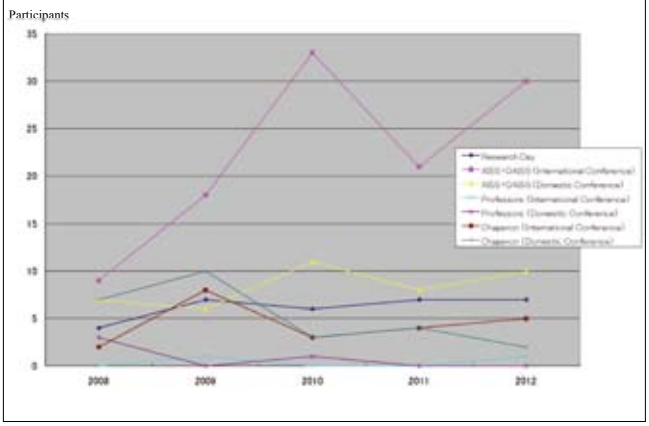

平成24年度

GCOEプログラム 実績報告書

CONTENTS

野田　政樹（分子薬理学分野）…… 50
田上　順次（う蝕制御学分野）…… 62
高柳　広（分子情報伝達学分野）…… 92
森田　育男（分子細胞機能学分野）…… 114
小村　健（顎口腔外科学分野）…… 126
春日井 昇平（インプラント・口腔再生医学分野）…… 144
須田　英明（歯髄生物学分野）…… 158
和泉　雄一（歯周病学分野）…… 182
柳下　正樹（硬組織病態生化学分野）…… 206
山口　朗（口腔病理学分野）…… 220
森山　啓司（顎顔面矯正学分野）…… 240
大 川　淳（整形外科学分野）…… 280
宮坂　信之（膠原病・リウマチ内科学分野）…… 296
宗田　大（運動器外科学分野）…… 320
稲澤　譲治（分子細胞遺伝学分野）…… 356
三木　義男（分子遺伝分野）…… 374
石野　史敏（エピジェネティクス分野）…… 394
澁谷　浩司（分子細胞生物学分野）…… 412
小川　佳宏（分子代謝医学分野）…… 414
水島　昇（細胞生理学分野）…… 430
中川　一路（細菌感染制御学分野）…… 454
秋吉　一成（有機材料学分野）…… 476
萩原　正敏（形質発現制御学分野）…… 484

分子薬理学分野

野田 政樹

医歯学総合研究科・器官システム制御学系専攻
分子薬理学・教授

1）研究の課題名

骨の形成を促進することは高齢化に伴う骨量減少に対する治療の上で重要な課題となっている。しかしながら現在において骨量を増加させる為の骨形成促進薬が限られており、また唯一の薬剤である副甲状腺ホルモン（PTH）についてもそのメカニズムはなお十分には明らかでない。そこで骨芽細胞における骨形成促進に関わる甲状腺ホルモンの機能解析を目的として、同様なGタンパク共益型受容体であるベータアドレナリン受容体のシグナルとの相互作用について相互作用の存在することを明らかにした（Proceedings of the National Academy of Sciences of the United States of America 2012）。さらに細胞骨格の制御因子であるプロフィリンに基づく細胞の制御機構を解明した（Journal of Biological Chemistry 2012）。

破骨細胞のチャンネル機能に関わる研究

骨量の急速な低下は破骨細胞による吸収の亢進に基づくがその破骨細胞の機能制御に関わる分子についての検索を行った。これまでに破骨細胞にはTPCが発現することまたそのTPCの機能についての解析を行い破骨細胞の分化レベルに対するTPC2の機能とその役割を明らかにした（Journal of Biological Chemistry 2012）。

骨に対するがん転移のメカニズム

骨は様々ながん細胞の転移の好発する臓器でそのメカニズムについてはなお十分には明らかでない。そこでメラノーマ細胞を用いてがん細胞のメカニズムの検討を行った。その結果、CIZ分子が転移を好発するがん細胞で高いレベルで発現していること、またCIZを強制発現することによりメラノーマ細胞の遊歩機能を亢進することを含めがん細胞の転移にこの分子が関わることを明らかにした（Journal of Cellar Physiology 2012）。

2）研究のイラストレーション

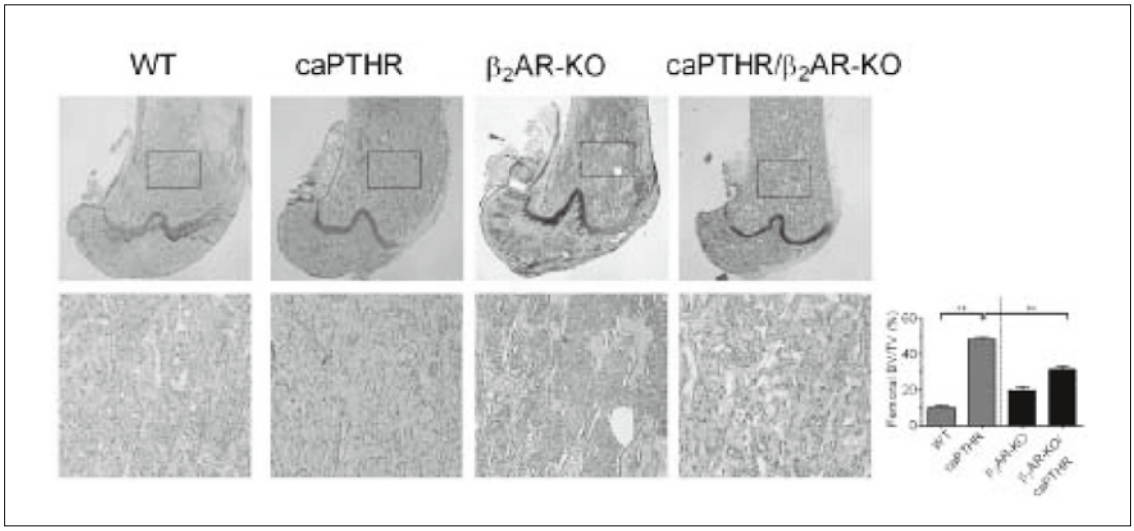

PNAS 2012

3）発表の研究内容についての英文要約

Osteoporosis treatment requires reagents to increase bone mass through distimiration of bone formation. Very few anabolic drags available currently. Parathyroid Hormone is the only available drug treat osteoporosis patients to prevent difuctures in hip as well as spine. However, the mechanisms in bold in patterned hormone action are not still understood. We have addressed the mechanisms underlying the functions of parathyroid hormone receptor and found that this receptor function requires the presence of the other G protein coupled receptor（β 2 adrenergic receptor）. We have further examined the role of the cytoskeleton as well as new channels in the regulation of a bone cell function.

4）本事業に関連して世界的な研究拠点形成に向けて、以下の点で改善・整備等されたこと

A（研究拠点体制）

若手教員ならびに これまでに選抜されたAISS 大学院生による研究体制が整えられた。

B（研究教育環境）

事業推進担当者ならびにシャペロンによる総合プレゼンテーションによる教育研究環境が整えられた。

C（人材確保）

国際公募による若手研究者が選抜された大学院生を教育するなど、優秀な人材が確保された。

D（人材育成）

若手研究者ならびに大学院生の中で英語による選抜で優れた者を選抜し、教育する体制が整えられた。

E（国際化）

大学院生が国際的に成果を発信しGCOE の中で国際的な研究者との交流に基づく活動が行われた。

5）GCOE事業を推進するに当たって力を入れた点

歯と骨の領域の研究を推進し世界最高水準の研究を行うとともに若手教育に重点を置き、また事業推進担当者間における研究交流を行うとともに海外の優れた研究者による若手教育とシニア研究者間のネットワーキングを推進する体制を整えた。

6）英文原著論文

1. Hanyu R, Wehbi V, Hayata T, Moriya S, Feinstein T, Ezura Y, Nagao M, Saita Y, Hemmi H, Notomi T, Nakamoto T, Schipani E, Takeda S, Kaneko K, Kurosawa H, Karsenty G, Kronenberg H, Vilardaga JP, Noda M. Anabolic action of parathyroid hormone regulated by the β 2-adrenergic receptor. Proceedings of the National Academy of Sciences of the United States of America;109（19）：7433-8, 2012
2. Miyajima D, Hayata T, Suzuki T, Hemmi H, Ezura Y, Nakamoto T, Notomi T, Amagasa T, Böttcher RT, Costell M, Fässler R, Noda M. Profilin1 regulates sternum development and endochondral bone formation. Journal of Biological Chemistry; 28;287（40）：33545-53, 2012
3. Notomi T, Ezura Y, Noda M. Identification of two pore channel 2 as a novel regulator of osteoclastogenesis. Journal of Biological Chemistry; 287（42）：35057-64, 2012
4. Sakuma T, Nakamoto T, Hemmi H, Kitazawa S, Kitazawa R, Notomi T, Hayata T, Ezura Y, Amagasa T, Noda M. CIZ/NMP4 is expressed in B16 melanoma and forms a positive feedback loop with RANKL to promote migration of the melanoma cells. Journal of Cellular Physiology; 227（7）：2807-12, 2012

7）平成24年度までの自己評価

これまでの研究成果として副甲状腺ホルモンの機能にアドレナリン受容体が関わる新たな複合GPCRのメカニズムを解明するとともに細胞骨格の骨の骨形成における働き、また新しいチャンネルに基づく破骨細胞の制御を明らかにした。さらに教育体制、研究体制がグローバルCOEの拠点として機能したものと評価できる。

8）学会発表（英文）

1. Watanabe C, Morita M, Ezura Y, Nakamoto T, Hayata T, Notomi T, Yamamoto T, Moriyama K, Noda M, Cnot3（Ccr4-not complex subunit 3）controls bone mass via regulating expression of genes including those related to osteoclastic activity. The 2nd Tri-University Consortium on Oral Science and Education, Beijing, China, July 27-28, 2012
2. Hayata T, Ezura Y, Noda M, Limb- and sternum-specific inactivation of Dullard gene causes severe defects in skeletal development via alteration of TGF-β signaling, 1st Asia-Pacific Bone and Mineral Research Meeting with the ANZBMS 22nd Annual Scientific Meeting, Perth, Australia, September 2-5, 2012
3. Watanabe C, Ezura Y, Nakamoto T, Hayata T, Notomi T, Moriyama K, Noda M, Analysis of high turnover type bone loss due to haploinsufficiency of Cnot3, a subunit of Ccr4-not complex（mRNA seadenylase）, 1st Asia-Pacific Bone and Mineral Research Meeting with the ANZBMS 22nd Annual Scientific Meeting, Perth, Australia, September 2-5, 2012
4. Ezura Y, Hayata T, Nakamoto T, Notomi T, Sekiya I,

Muneta T, Noda M, Identification of Signature Genes Selectively Expressed in Mesenchymal Stem Cells Derived from Synovial Joint Tissues, The 34th Annual Meeting of American Society for Bone and Mineral Research, Minneapolis, MN, USA, October 12 - 15, 2012

5. Nakamoto T,Motoyoshi T, Hada T, Kawasaki M, Sakuma T, Hayata T, Ezura Y, Noda M, Chondrocyte Metabolism in Inflammatory Arthritis is regulated by CIZ, The 34th Annual Meeting of American Society for Bone and Mineral Research, Minneapolis, MN, USA, October 12 - 15, 2012
6. Hayata T, Ezura Y, Asashima M, Nishinakamura R, Noda M, Limb- and Sternum-Specific Inactivation of Dullard Gene Causes Severe Defects in Skeletal Development via Alteration of TGF-β Signaling, The 34th Annual Meeting of American Society for Bone and Mineral Research, Minneapolis, MN, USA, October 12 - 15, 2012
7. Notomi T, Ezura Y, Noda M, Lysosomal calcium channel, TPC2, regulates osteoclastogenesis via generation of intracellular Ca^{2+} response and subsequent NFATc1 localization：a novel mechanism of osteoclastic Ca^{2+} signaling, The 34th Annual Meeting of American Society for Bone and Mineral Research, Minneapolis, MN, USA, October 12 - 15, 2012
8. Aryal S, Miyai K, Hayata T, Ezura Y, Notomi T, Nakamoto T, Pawson T, Noda M, Nck, an actin cytoskeleton modulator, controls expression of osteocytic genes, phosphate homeostasis by regulating FGF 23 expression in bone and maintains bone mass, The 34th Annual Meeting of American Society for Bone and Mineral Research, Minneapolis, MN, USA, October 12 - 15, 2012
9. Kawasaki M, Nakamoto T, Notomi T, Hayata T, Ezura Y, Noda M, The expression of Ift88 is dose-dependently decreased in cultured chondrocytes ATDC5 when treated with TGF-β 1, The 34th Annual Meeting of American Society for Bone and Mineral Research, Minneapolis, MN, USA, October 12 - 15, 2012
10. Shirakawa J, Nakamoto T, Notomi T, Hayata T, Ezura Y, Omura K, Noda M, PTH Enhances Mechanical Stress-iduced Osteoblast Proliferation in Calvarial Derived Osteoblasts via Up-regulation of CyclinD1 Expression, The 34th Annual Meeting of American Society for Bone and Mineral Research, Minneapolis, MN, USA, October 12 - 15, 2012
11. Moriya S, Nakamoto T, Notomi T, Hayata T, Ezura Y, Kaneko K, Noda M, Parathyroid hormone stimulates Tob1 expression in osteoblastic cells in vitro and in vivo, The 34th Annual Meeting of American Society for Bone and Mineral Research, Minneapolis, MN, USA, October 12 - 15, 2012

9）学会発表（和文）

1 江面陽一、早田匡芳、中元哲也、納富拓也、関矢一郎、宗田大、野田政樹
ヒト骨髄および滑膜由来間葉系細胞において異なるCpGメチル化を示す遺伝子群の探索と骨軟骨細胞分化の制御に関わる転写因子群の抽出：RUNX2 およびRUNX3, DLX5, ALX4遺伝子
Identification of Differentially Methylated Transcription Factor Genes in theHuman Synovium and Bone Marrow Derived Mesenchymal Cells：RUNX2, RUNX3, DLX5, and ALX4 Genes　第30回日本骨代謝学会　7月19日-21日, 2012年

2 早田匡芳、江面陽一、野田政樹
四肢及び胸骨特異的Dullard遺伝子欠損マウスは骨化遅延を示す
Limb- and Sternum-Specific Inactivation of Dullard Gene Causes Retardation of Ossification　第30回日本骨代謝学会　7月19日-21日, 2012年

3 中元哲也、平林恭子、Alexander Valentinitsch、川崎真希理、佐久間朋美、早田匡芳、江面陽一、Ernestina Schipani、Henry M. Kronenberg、野田政樹
PTHの骨形成促進作用はシャトリングタンパク質CIZによって抑制される
Anabolic Action of PTH/PTHrP Receptor Signaling in Bone is Suppressed by a Nucleocytoplasmic Shuttling Protein CIZ　第30回日本骨代謝学会　7月19日-21日, 2012年

4 納富拓也、江面陽一、野田政樹
Two Pore Channel 2を介したリソソーム由来Ca2+による新たな破骨細胞分化制御機構
Lysosomal calcium channel, TPC2, regulates osteoclastogenesis via regulation of intracellular calcium response　第30回日本骨代謝学会　7月19日-21日, 2012年

5 渡辺千穂、江面陽一、中元哲也、早田匡芳、納富拓也、森山啓司、野田政樹
骨量制御の新転写後性分子機構：mRNA deadenylaseであるCcr4-not complex構成因子Cnot3の欠失による高回転型の骨量減少の解析
Molecular mechanisms underlying mRNA stability in bone metabolism：Role of Ccr4-not complex subnuit3（Cnot3）　第30回日本骨代謝学会　7月19日-21日, 2012年

6 Smriti Aryal A.C、Kentaro Miyai、Yoichi Ezura、

Tadayoshi Hayata、Takuya Notomi、Tetsuya Nakamoto、Tony Pawson、Masaki Noda
骨芽細胞におけるアクチン細胞骨格調整因子、Nckの欠損は骨芽細胞の遊走と骨形成を阻害す
Deficiency of Nck, an Actin Cytoskeleton Modulator in the Osteoblast Inhibits Osteoblast Migration and Suppresses Bone Formation　第30回日本骨代謝学会　7月19日-21日, 2012年

7　川崎真希理、中元哲也、納富拓也、早田匡芳、江面陽一、野田政樹
一次繊毛タンパクBbs3は骨代謝に関与する
Ciliary protein Bbs3 is involved in bone metabolism
第30回日本骨代謝学会　7月19日-21日, 2012年

8　白川純平、江面陽一、中元哲也、早田匡芳、納富　拓也、小村健、野田政樹
PTH及びメカニカルストレスによる骨芽細胞におけるサイクリンD1発現の検討
Expression of cyclin D1 in osteoblasts by PTH and mechanical stress　第30回日本骨代謝学会　7月19日-21日, 2012年

9　守屋秀一、早田匡芳、中元哲也、納富拓也、江面陽一、金子和夫、野田政樹
骨芽細胞におけるGタンパク質共役型受容体（GPCR）によるRANKL制御の検討
GPCR control of RANKL expression in osteoblasts
第30回日本骨代謝学会　7月19日-21日, 2012年

10　平林恭子、中元哲也、野田政樹
β2アドレナリン受容体によるPTH受容体シグナル制御の解析
第22回日本歯科医学会総会　11月9日-11日, 2012年
大阪　日本

10）外部資金の獲得状況

グローバルCOE プログラム
研究題目：歯と骨の分子疾患科学の国際教育研究拠点ーデント・メドミクスのインテリジェンスハブー
代表：野田政樹
2008年－2012年
研究費　281,811 千円（2011年度）

日本学術振興会研究費補助金（萌芽）
研究題目：顎骨形成促進への新戦略の分子機構研究
代　　表：野田政樹
期　　間：2011-2012年
研究費：280万円

基盤研究（C）
研究題目：変形性関節症の治療を目指す間葉系幹細胞エピジェネティクスに関する分子生物学的解明
代表：江面陽一
2010年-2012年
研究費：100万円

若手研究（B）
研究題目：Dullardによる新規BMP/TGF-βシグナル抑制　機構の発見と軟骨代謝制御
代表：早田匡芳
2011年-2012年
研究費：112万円

基盤研究（C）
研究題目：転写因子CIZによる副甲状腺ホルモンの骨への作用の制御
代表：中元哲也
2010年-2012年
研究費：98万円

若手研究（B）
研究題目：神経伝達物質受容体・イオンチャネルによる電位変化を伴う力学的負荷感知機構の解明
代表：納富拓也
H23年-H24年
研究費：120万円

新学術領域研究
研究題目：膜電位操作回路による生体骨構築のための基盤研究-光照射による骨リモデリング制御―
代表：納富拓也
2012年-2013年
研究費：540万円

11）特別講演、招待講演、シンポジウム

・野田政樹：FASEB Summer Research Conferences?
2012年8月5日　Saxtons River, VT, USA
演題：Osteopontin Biology in Bone

・野田政樹：第14回日本骨粗鬆症学会
骨ドック・健診分科会
特別講演　2012年9月27日
演題：不動性骨粗鬆症のメカニズム
Osteopontin Biology

・野田政樹：第18回埼玉県骨粗鬆症研究会
特別講演　2012年11月10日
演題：廃用性骨委縮のメカニズム

12）主催学会

・第226回 Bone Biology Seminar
「Mechanical derivation of multi-nucleated myotubes from human adipose-derived stem cells.」
Dr. Yu Suk Choi, Ph.D. 2012年6月13日

・第227回 Bone Biology Seminar
「The Cathepsin K Inhibitor Reduces Bone Resorption While Maintaining Bone Formation.」
Dr. Le Duong, Ph.D. 2012年9月25日

・第228回 Bone Biology Seminar
「Mechanisms of metastasis to bone：homing of breast cancer to bone」
Dr. Michael Rosenblatt, M.D.　2013年1月22日

・第229回 Bone Biology Seminar
「The ERK MAPK pathway in skeletal development.」
Dr. Shunichi Murakami, M.D., Ph.D. 2013年1月31日

・第230回 Bone Biology Seminar
「Bone marrow endothelium：A hierarchically organised system with transplantable hemogenic stem cells giving rise to functional blood vessels as well as HSC.」
Dr. Susan Kaye NILSSON B.Sc.（Honours）, Ph.D.
2013年3月5日

・第231回 Bone Biology Seminar
「 Cancer-associated muscle dysfunction：role of ryanodine receptor remodeling and the bone microenvironment」
Dr. Theresa A. Guise, M.D.　2013年3月28日

13）新聞、雑誌、TV報道

1. 2012年4月25日
骨粗しょう症　骨形成治療に2受容体必須　化学工業日報
2. 2012年5月11日
骨粗鬆症における骨形成促進薬のメカニズム解明
科学新聞

14）GCOE総合講義

アナボリックな作用を持つ副甲状腺ホルモンの受容体が作用するメカニズムはこれまで十分に明らかではなかった。そこでこの分子とGPCRのベータアドレナリン受容体との相互作用の検討を行った結果、アナボリックな作用にはベータ2アドレナリン受容体の存在が必要であることが明らかとなった。この様な事は新たな複合体としての骨の形成作用を示すものである。

15）教室、分野や講座の准教授、講師、助教、特別研究員、ポスドク、指導を受けた大学院生の名前

准教授　　江面　陽一
助　教　　早田　匡芳
特任講師　中元　哲也（国際コーディネーター）
特任講師　納富　拓也（国際PI シャペロン）
大学院生
○ 渡辺　千穂
○ Smriti Aryal A. C.
○ 白川　純平
守屋　秀一
○ 川崎　真希理（学術振興会DC）
山田　峻之

○はAISS

化学工業日報 The Chemical Daily

2012年(平成24年) 4月25日(水曜日)

骨粗しょう症

骨形成治療に2受容体必須

PTHとアドレナリン

創薬に新たな可能性

東京医科歯科大

The Science News 科学新聞

2012年(平成24年) 5月11日(金曜日)

骨粗鬆症における骨形成促進薬のメカニズム解明

—東京医歯大の研究グループ成功—

Anabolic action of parathyroid hormone regulated by the β_2-adrenergic receptor

Ryo Hanyu[a,b,c,1], Vanessa L. Wehbi[d,1], Tadayoshi Hayata[a,c,1], Shuichi Moriya[a,b,1], Timothy N. Feinstein[d], Yoichi Ezura[a,c], Masashi Nagao[a,b], Yoshitomo Saita[a,b], Hiroaki Hemmi[a,c,e], Takuya Notomi[a,c], Tetsuya Nakamoto[a,c], Ernestina Schipani[f], Shu Takeda[c], Kazuo Kaneko[b], Hisashi Kurosawa[b], Gerard Karsenty[g], Henry M. Kronenberg[f], Jean-Pierre Vilardaga[d,2], and Masaki Noda[a,c,e,h,i,2]

[a]Department of Molecular Pharmacology, Medical Research Institute, [c]Global Center of Excellence Program for the International Research Center for Molecular Science in Tooth and Bone Disease, [h]Hard Tissue Genome Research Center; and [i]Advanced Bone Joint Science Center, Tokyo Medical and Dental University, 113-8510 Tokyo, Japan; [b]Department of Orthopedics, School of Medicine, Juntendo University, 113-8421 Tokyo, Japan; [d]Laboratory for G Protein-Coupled Receptor Biology, Department of Pharmacology and Chemical Biology, School of Medicine, University of Pittsburgh, Pittsburgh, PA 15261; [e]Medical Top Track Program, Medical Research Institute, Tokyo Medical and Dental University, 101-0062 Tokyo, Japan; [f]Endocrine Unit, Massachusetts General Hospital and Harvard Medical School, Boston, MA 02114; and [g]Department of Genetics and Development, College of Physicians and Surgeons, Columbia University, NY 10027

Edited by John T. Potts, Massachusetts General Hospital, Charlestown, MA, and approved March 26, 2012 (received for review June 6, 2011)

Parathyroid hormone (PTH), the major calcium-regulating hormone, and norepinephrine (NE), the principal neurotransmitter of sympathetic nerves, regulate bone remodeling by activating distinct cell-surface G protein-coupled receptors in osteoblasts: the parathyroid hormone type 1 receptor (PTHR) and the β_2-adrenergic receptor (β_2AR), respectively. These receptors activate a common cAMP/PKA signal transduction pathway mediated through the stimulatory heterotrimeric G protein. Activation of β_2AR via the sympathetic nervous system decreases bone formation and increases bone resorption. Conversely, daily injection of PTH (1–34), a regimen known as intermittent (i)PTH treatment, increases bone mass through the stimulation of trabecular and cortical bone formation and decreases fracture incidences in severe cases of osteoporosis. Here, we show that iPTH has no osteoanabolic activity in mice lacking the β_2AR. β_2AR deficiency suppressed both iPTH-induced increase in bone formation and resorption. We showed that the lack of β_2AR blocks expression of iPTH-target genes involved in bone formation and resorption that are regulated by the cAMP/PKA pathway. These data implicate an unexpected functional interaction between PTHR and β_2AR, two G protein-coupled receptors from distinct families, which control bone formation and PTH anabolism.

bone anabolism | bone cells

Osteoporosis, a severe bone disorder and one of the most representative age-related diseases in the modern world, reduces bone strength and increases fracture risks associated with morbidity. The N-terminal fragment of the parathyroid hormone [PTH(1–34)], sold under the name Forteo (Lilly), is the only anabolic drug to date that can increase bone mass in humans and animals (1–4). Previous studies showed that PTH(1–34) treatment reduces the risk of fracture by ~65% in osteoporotic patients (5–7). So far, the use of PTH(1–34) has been limited to severe cases of osteoporosis and for a period of only 18 or 24 mo because of the potential risks of osteosarcoma and hypercalcemia, as observed in rat studies (8). To further overcome these limitations, a precise understanding of the physiological, cellular, and molecular bases of the anabolic action of PTH on bone is necessary.

PTH directly acts on bone and kidney, and indirectly on intestine, to regulate calcium ion (Ca^{2+}) levels in the blood and extracellular fluids. In the kidney, PTH induces expression of the 1-α-hydroxylase by acting on proximal tubules, which, in turn, increases the active form of vitamin D (1-α-25 dihydroxy vitamin D_3) involved in calcium reabsorption from the intestine. In bone, PTH acts on osteoblasts (bone-forming cells) to increase bone formation and induces expression of receptor activator of nuclear factor-κB ligand (RANKL), a cytokine that stimulates development and activation of osteoclasts (bone-resorbing cells), which, in turn, enhances calcium release from bone. PTH binds to the PTH receptor type 1 (PTHR), a G protein-coupled receptor (GPCR) predominantly expressed in osteoblasts and in distal and proximal renal tubules among other tissues (e.g., vascular smooth muscles, T lymphocytes). Previous genetic studies showed that the sympathetic tone reduces bone mass by suppressing bone formation and by enhancing bone resorption via activation of the β_2AR expressed in osteoblasts (9, 10). Given that β_2AR and PTHR are both coexpressed in osteoblastic cells (11), we hypothesize that PTH actions on bone might be modulated by the presence of the sympathetic system. Here, we examined this hypothesis by comparing the effects of intermittent injection of PTH (1–34) on bone metabolism in wild-type (WT) mice and in β_2AR-deficient mice (β_2AR-KO). We found that β_2AR deficiency suppressed the osteoanabolic action of PTH by blocking expression of intermittent (i)PTH-target genes involved in osteoblast activity and bone formation. We further found that iPTH treatment-induced increase in bone mass in aged osteoporotic mice is blunted by β_2AR deficiency.

Results

β_2AR Is Necessary for the Osteoanabolic Action of PTH. WT mice subjected to intermittent PTH(1–34) treatment (noted thereafter iPTH) showed an increase in the trabecular content compared with the control (untreated) group (WT) (Fig. 1*A*). In contrast, the trabecular content remained unchanged in mice lacking the β_2AR (β_2AR-KO) after iPTH treatment (β_2AR-KO) (Fig. 1*A*), which expressed the same level of PTHR as WT mice (Fig. S1). Quantification of cancellous bone volume over tissue volume (BV/TV) in long bone showed that iPTH treatment increased bone volume in WT mice but not in β_2AR-KO mice (Fig. 1*B*). We also observed that the capacity of iPTH treatment to increase the thickness of trabecular bone (Tb.Th) was lost in β_2AR-KO mice (Fig. 1*C*). Such an observation was not limited to long bone because we observed that the lack of β_2AR also suppressed iPTH treatment-induced increase in the BV/TV parameter of cancellous bone in vertebral bone (Fig. 1 *D* and *E*).

Author contributions: J.-P.V. and M. Noda designed research; R.H., V.L.W., T.H., S.M., Y.E., M. Nagao, T. Notomi, T. Nakamoto, and M. Noda performed research; T.N.F., Y.E., Y.S., H.H., E.S., S.T., K.K., H.K., G.K., and H.M.K. contributed new reagents/analytic tools; Y.E., H.M.K., J.-P.V., and M. Noda analyzed data; and J.-P.V. and M. Noda wrote the paper.

The authors declare no conflict of interest.

This article is a PNAS Direct Submission.

[1]R.H., V.L.W., T.H., and S.M. contributed equally to this work.

[2]To whom correspondence may be addressed. E-mail: jpv@pitt.edu or noda.mph@tmd.ac.jp.

This article contains supporting information online at www.pnas.org/lookup/suppl/doi:10.1073/pnas.1109036109/-/DCSupplemental.

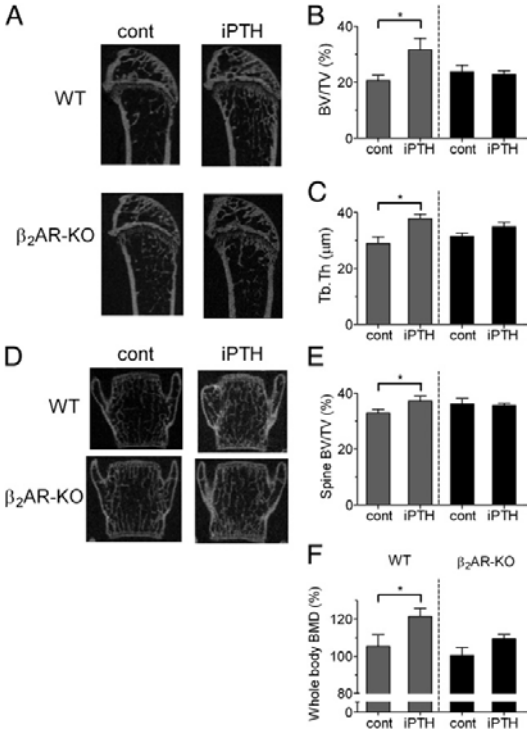

Fig. 1. β_2AR control of PTH-induced bone formation. (*A–C*) 2D micro-CT (μ-CT) images of the distal metaphyses of the femur in WT mice and β_2AR-KO mice treated either with vehicle (cont) or iPTH (*A*) and corresponding values for BV/TV (*B*) and trabecular thickness (*C*). (*D* and *E*) 2D μ-CT images of spine in WT mice and β_2AR-KO mice (*D*) and associated BV/TV parameter obtained from the secondary trabeculae of the fourth lumbar vertebrae (*E*). (*F*) Whole-body BMD was measured before and after iPTH treatment or vehicle (cont), and the ratio of posttreatment per pretreatment values are expressed as percentages. Data are expressed as means ± SD for $n = 4–5$ (*$P < 0.05$).

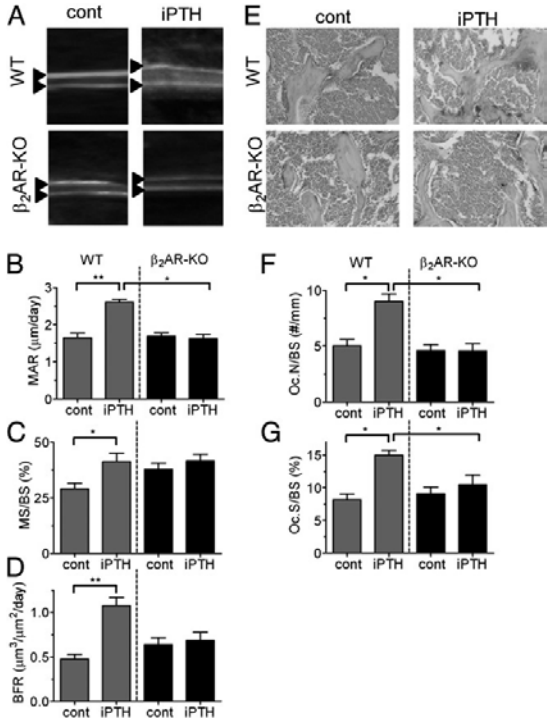

Fig. 2. β_2AR control of PTH-induced increase in the levels of dynamic bone formation and bone resorption parameters. (*A*) Calcein band in the distal metaphyses of the femur were visualized to obtain dynamic histomorphometry parameters in WT mice and β_2AR-KO mice treated either with vehicle or iPTH. (*B–D*) Parameters of osteoblast activity. (*B*) Levels of MAR. (*C*) Lineralizing surface per bone surface (MS/BS). (*D*) Bone formation rate (BFR). (*E*) Secondary trabecular regions of the epiphyses of tibiae were examined for osteoclasts based on TRAP staining in vehicle-treated (cont) and iPTH-treated (iPTH) WT mice and β_2AR-KO mice. (*F* and *G*) Parameters of osteoclast activity. (*F*) Osteoclast number per bone surface (Oc.N/BS). (*G*) Osteoclast surface over bone surface area (Oc.S/BS). Data are expressed as means ± SD of $n = 4–5$) (*$P < 0.05$; **$P < 0.01$).

Intermittent PTH treatment increased not only the level of morphological parameters but also the level of mineral content in bone measured by dual energy X-ray absorptiometry (DEXA) (Fig. 1*F*). This increase was suppressed in mice lacking the β_2AR (β_2AR-KO) (Fig. 1*F*). These data indicate that the absence of β_2AR suppresses the capacity of intermittent injection of PTH(1–34) to induce structural changes in both long bone and spine associated with an increase in bone mass.

Given that the anabolic effect of iPTH results from a tight balance between bone formation and bone resorption (12), we next examined whether the absence of β_2AR affects the action of iPTH on bone formation. The capacity of iPTH treatment to increase the amount of bone deposited between two timed administrations of calcein labeling, an indicator of bone mineralization in WT mice, was lost in β_2AR-KO (Fig. 2*A*). Quantification of these calcein intervals revealed that the absence of β_2AR suppressed the increase in mineral apposition rate (MAR) by iPTH (Fig. 2*B*), which is an indicator of the activity of individual osteoblasts. Analyses of dynamic parameters of bone formation further indicated that iPTH increased the mineralizing surface over the bone surface (MS/BS), which reflects the quantity of osteoblasts forming the bone matrix in WT mice but not in β_2AR-KO mice. There was a slight elevation in the baseline level in β_2AR-KO in MS/BS. However, iPTH did not increase MS/BS in β_2AR-KO mice (Fig. 2*C*). iPTH treatment increased bone formation rate (BFR), an indicator of the amount of bone formation within a unit time period, in WT mice but not in β_2AR mice (Fig. 2*D*).Therefore, the absence of β_2AR suppressed the increase of bone formation parameters triggered by iPTH treatment.

With respect to bone resorption, iPTH treatment enhanced the number of osteoclasts, which are shown as tartrate-resistant acid phosphatase (TRAP)-positive cells over the bone surface (Oc.N/BS), in WT mice, but not in β_2AR-KO mice (Fig. 2 *E* and *F*). iPTH treatment also increased osteoclast surface over bone surface (Oc.S/BS) in WT mice, which is a rough indicator of osteoclastic activity (Fig. 2 *E* and *G*). In contrast, β_2AR deficiency suppressed this increase (Fig. 2*G*). Thus, these histomorphometry analyses indicated that the lack of β_2AR suppressed the capacity of iPTH treatment to promote osteoclastic number and activity. Taken together, these data indicate that the presence of β_2AR is necessary for the actions of iPTH on both bone formation and bone resorption.

Given that PTHR is expressed in several extraskeletal cell types (proximal and distal tubule cells in kidneys, smooth muscle cells, T lymphocytes), it was unclear whether the suppression of PTH(1–34) osteoanabolism, which was caused by the absence of β_2AR, originated directly from osteoblasts or was a secondary

consequence of a systemic PTH(1–34) action or β_2AR action on extraskeletal tissues. We ruled out this latter possibility by using mice genetically engineered to have increased PTHR signaling activity in osteoblasts only. These mice express a constitutively active PTHR variant (hereafter noted caPTHR) that carries a His/Arg substitution at amino acid 223, which constitutively activates the G_S/cAMP/PKA signaling pathway, and which has been associated with Jansen-type metaphyseal dysplasia (11, 13). Previous studies showed that the osteoblastic expression of caPTHR stimulates an anabolic response in trabecular bone, which is in contrast to the decrease of net bone mass observed after continuous perfusion of PTH (13).We now observed that mice with osteoblast-specific expression of caPTHR increased the levels of trabecular bone content in the presence but not in the absence of β_2AR (caPTHR/β_2AR-KO) (Fig. 3*A*). Quantification of BV/TV indicated that β_2AR deficiency mostly suppressed the capacity of caPTHR to increase bone mass (Fig. 3*B*). As was the case in β_2AR-deficient mice (β_2AR-KO), deletion of β_2AR in caPTHR transgenic mice (caPTHR/β_2AR-KO) blocked increases in mineral apposition rate and BFR triggered by constitutive signaling of caPTHR (Fig. 3*D*). These data, thus, indicate that the absence of β_2AR interferes with PTHR signaling in osteoblasts associated with bone formation.

We next observed that the constitutive activation of PTHR in osteoblasts increased the appearance of osteoclasts (Fig. 3*E*). Quantification of osteoclasts indicated that β_2AR deficiency suppressed the capacity of caPTHR to increase levels of osteoclast number, as well as osteoclast surface (Fig. 3*F*). Thus, the deletion of β_2AR in caPTHR mice recapitulated the loss of the osteoanabolic action of PTH observed in β_2AR-KO mice after iPTH treatment. These data indicate that the β_2AR control of the anabolic action of PTH is likely mediated by a mechanism operating in osteoblasts.

β_2AR Control of PTH-Target Gene Expression. We next determined whether β_2AR deficiency modulated the expression of PTH-target genes involved in bone formation/resorption. To this end, we measured mRNA levels of a series of regulatory proteins in the bone of caPTHR mice and caPTHR/β_2AR-KO mice. Expression levels of alkaline phosphatase (ALP) (a marker of early to late stage osteoblast differentiation), type I collagen α1 (Col1α1) (the most abundant structural protein for bone and connective tissues), bone sialoprotein (BSP) (a specific marker of osteoblasts), RANKL (a critical regulatory factor for osteoclastogenesis), and osteoprotegerin (OPG) (the soluble decoy receptor for RANKL) were increased in caPTHR mice compared with WT mice (Fig. 4*A*). These increases were largely suppressed in caPTHR/β_2AR-

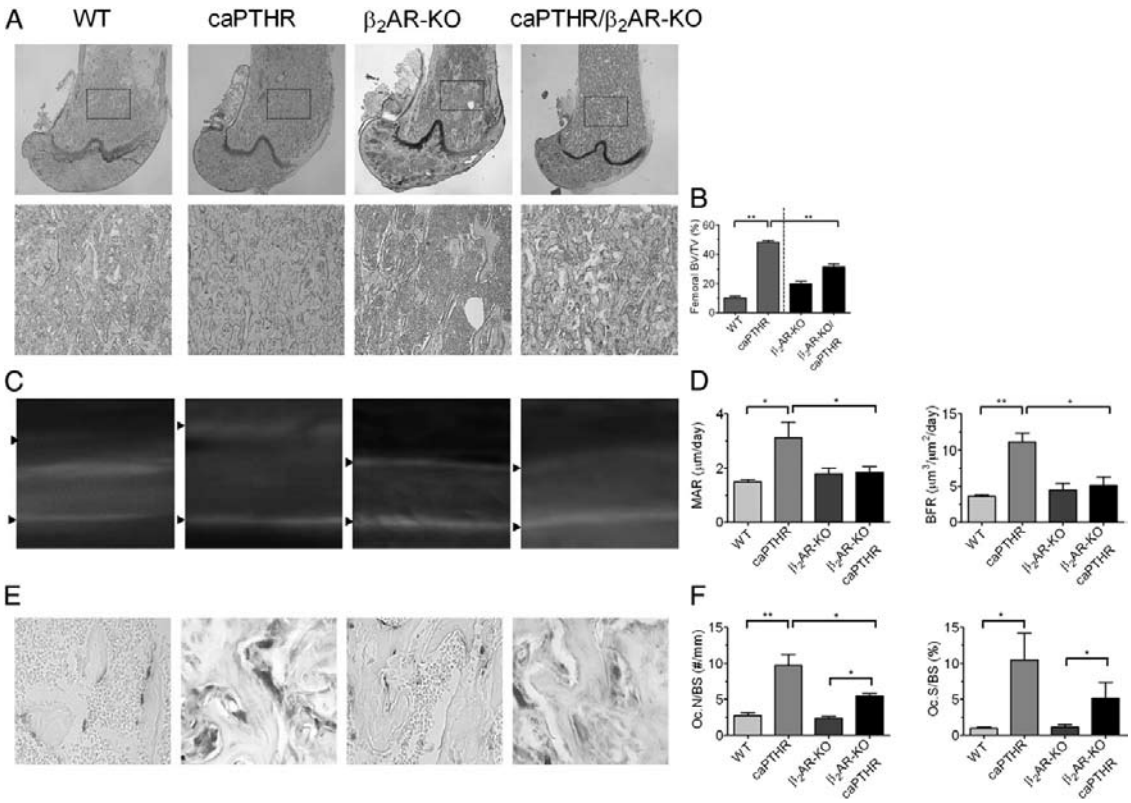

Fig. 3. β_2AR is required for anabolic action of constitutively active PTHR specifically expressed in osteoblasts. (*A*) Upper images represent Masson–Goldner staining in histological sections of WT, caPTHR, β_2AR-KO, and caPTHR/β_2AR-KO mice. Lower images represent enlargement corresponding to sections shown in the upper images. (*B*) BV/TV measured from the secondary trabeculae of the distal metaphyses of the femora. (*C*) Calcein band in the distal metaphyses of the femur were visualized to obtain dynamic histomorphometry parameters in WT, caPTHR, β_2AR-KO, and caPTHR/β_2AR-KO mice. (*D*) MAR and BFR. (*E*) TRAP staining of decalcified sections of the distal metaphyses of the femora. (*F*) Osteoclast number per bone surface (Oc.N/BS) and osteoclast surface per bone surface (Oc.S/BS). Data are expressed as means ± SD (n = 5–6; $^*P < 0.05$; $^{**}P < 0.01$).

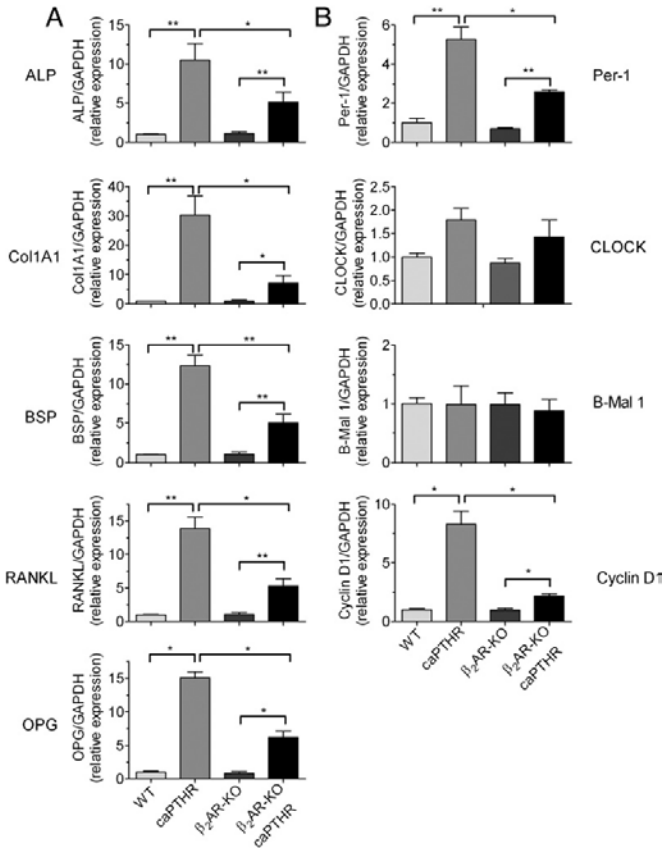

Fig. 4. Expression of PTH target genes regulated by β_2AR. (*A* and *B*) Expression of ALP, Col 1α, BSP, RANKL, OPG (*A*) and Per-1, B-MAL, CLOCK, and cyclin D1 (*B*), all normalized to GAPDH mRNA expression, in bone samples from WT and β_2AR-KO mice. Results are expressed in arbitrary units as means ± SD (n = 5–6/group; $*P < 0.05$; $**P < 0.01$).

KO mice (Fig. 4*A*). We also found that β_2AR deficiency reduced the capacity of intermittent injection of PTH to increase the gene expression of ALP, Col1α1, and Runt-related transcription factor (Runx)2 (Fig. S2). The negative effect of β_2AR deficiency can also take place just 1 h after a single PTH injection, as observed for gene expression of c-fos and RANKL (14–17) (Fig. S3). These increases were reduced in β_2AR-KO mice. These observations indicated that the inhibitory effect of β_2AR deficiency on PTH anabolism depends on the regulation of the expression of genes related to osteoblast activity and bone metabolism.

Because the action of the sympathetic tone in bone is associated with genes involved in the circadian rhythm, we next compared the expression levels of clock genes in WT, β_2AR-KO, caPTHR, and caPTHR/β_2AR-KO mice. We previously observed that caPTHR increases the steady-state levels of Period-1 (Per-1) mRNA expression in vivo (18). We now found that the increase in Per-1 mRNA expression triggered by constitutively active PTHR signaling was reduced in caPTHR/β_2AR-KO mice (Fig. 4*B*). The expression level of B-Mal, another clock gene, was not affected regardless of the presence or absence of either caPTHR or β_2AR, and CLOCK gene expression was not significantly modulated by β_2AR deficiency (Fig. 4*B*). We conclude that the central clock gene transcription system remains intact in β_2AR and caPTHR-β_2AR transgenic mice and that Per-1 is a specific target of PTH signaling in osteoblasts that is modulated by β_2AR in vivo.

PTH activates bone formation, in part, by stimulating osteoblast proliferation. Expression of caPTHR in osteoblasts enhanced the expression level of cyclin D1, a regulatory protein involved in the cell cycle of early osteoclasts (Fig. 4*B*). In contrast, β_2AR deficiency suppressed this enhancement. Overall, these data indicate the existence of a functional interaction between PTHR and β_2AR signaling in osteoblasts that allows the anabolic action of PTH via up-regulation of genes involved in cell proliferation and that is also necessary for bone formation.

β_2AR Control of iPTH-Induced Bone Formation in an Osteoporosis Model. Next, we tested the anabolic action of iPTH in a mouse model for osteoporosis. To this end, we used >50-wk old mice that showed a significant reduction in bone mass compared with younger 10 wk-old mice. Trabecular patterns of these aged mice were sparse (Fig. 5*A* vs. Fig. 1*A*: WT, control), and iPTH treatment produced additional trabecular bone (Fig. 5*A*, WT, iPTH). Aged mice that lack β_2AR showed more trabecular bone in the distal femur but did not show an increase in bone after iPTH treatment (Fig. 5*A*). Quantification of trabecular BV/TV indicated that baseline levels were lower in aged mice (~5%) than in younger adult mice (~20%) (Fig. 5*B* vs. Fig. 1*B*: WT, control). iPTH treatment was effective and significantly increased BV/TV levels in aged WT mice under condition of low bone mass (Fig. 5*B*, WT). The absence of β_2AR increased bone volume levels by

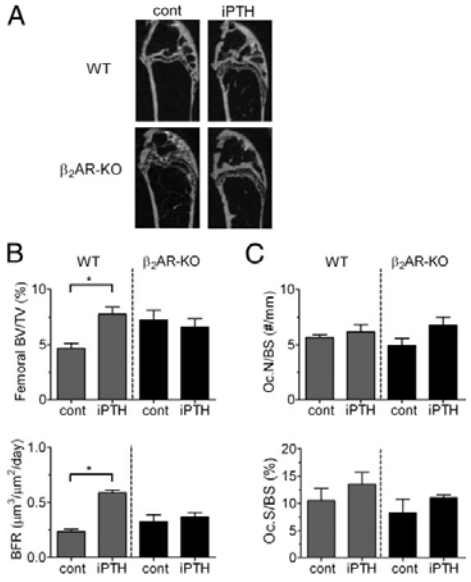

Fig. 5. Effect of β_2AR deficiency in aged mice. Aged mice of >50 wk were subjected to iPTH or vehicle (cont) injection for 4 wk. (*A*) 2D μ-CT images of the distal end of femur in WT mice and β_2AR-KO mice treated either with vehicle (cont) or iPTH . (*B*) BV/TV and BFR. (*C*) Osteoclast number per bone surface (Oc.N/BS) and osteoclast surface per bone surface (Oc.S/BS). Data are expressed as means ± SD of $n = 4–5$ (*$P < 0.05$).

2–3%. In contrast to WT, iPTH-induced increase in bone volume (BV/TV) was not observed in β_2AR-KOmice (Fig. 5 *A* and *B)*. The higher BV/TV level in β_2AR-KO compared with WT aged mice at baseline, presumably resulting from reduced age-related bone resorption, might hide some of the changes that could be caused by iPTH treatment. Despite the uncertainty in differentiating the effect of iPTH and β_2AR deficiency in aged mice, the data indicate, without ambiguity, that the absence of β_2AR blocks PTH-induced increases in BFR (Fig. 5*B*).

Further analysis of dynamic parameters of bone metabolism indicated that the BFR was reduced by ∼50% in old WT mice compared with young WT (10-wk-old) mice (0.2 vs. 0.4 $\mu m^3/\mu m^2$ per d; Fig. 5*B* vs. Fig. 2*D*). iPTH injection enhanced BFR levels approximately twofold in WT (Fig. 5*B*). β_2AR deficiency in these aged mice slightly elevated the baseline levels of BFR. In contrast to WT, β_2AR deficiency failed to respond to iPTH treatment with regard to BFR (Fig. 5*B*). Bone resorption parameters showed that the osteoclast number and the osteoclast surface were similar in old and young mice (Fig. 5*C*). In contrast to bone formation parameters, osteoclastic parameters in aged mice were not significantly altered by iPTH injection regardless of the presence or absence of β_2AR (Fig. 5*C*). These data indicated that in a mouse model for osteoporosis, β_2AR is required for iPTH-induced increase in bone mass, and this is mainly based on β_2AR requirement for iPTH activation of bone formation.

Discussion

Given that the sympathetic tone via the β_2AR has been reported to exert negative effects on bone mass by activating bone resorption and suppressing bone formation (10, 19), we initially predicted that mice lacking the β_2AR would improve the anabolic effect of iPTH treatment. Surprisingly, our results indicate the opposite. They support the unexpected feature that β_2AR deficiency suppresses the bone-anabolic effect mediated by iPTH (Figs. 1 and 2). Our in vivo studies further show that β_2AR deficiency in mice expressing a constitutively active PTHR selectively in osteoblasts suppresses bone formation. This impaired capacity to promote bone formation is accompanied by a reduced expression of several PTH-target genes encoding proteins involved in bone matrix formation (ALP, Col1α1, and BSP), in osteoblast proliferation (cyclin D1), and in the regulation of circadian protein expression (Per-1) in β_2AR-deficient caPTHR transgenic mice. The reduction in iPTH-induced increases of gene expression in β_2AR-KO mice compared with WT mice further supports the conclusion that PTHR signaling in osteoblasts requires the presence of β_2AR for its anabolic action in bone, at least in part, through the regulation of genes encoding proteins necessary for the osteoblastic function. However, additional factors may also be involved in the lack of PTH anabolism seen in β_2AR-KO mice. Among them are the levels of CART (cocaine amphetamine regulated transcript), a neuropeptide in the brain and in the circulation that is a major inhibitor of osteoclastogenesis by suppressing RANKL expression, which could be different in WT and β_2AR-KO and, thus, be one of the possible mechanisms whereby bone resorption is blunted in the β_2AR-KO mice, as we observed in our experiments. Other factors might also originate from osteoclasts, given that the BFR in caPTHR/β_2AR-KO mice remains unchanged compared with β_2AR-KO mice.

In summary, our studies demonstrate that the β_2AR plays a critical role in the osteoanabolic action of PTH by controlling expression of PTH-target genes involved in osteoblast activation and bone formation.

Materials and Methods

Adrb2-*deficient mice.* Breeding pairs of *Adrb2* heterozygous (*Adrb2*$^{+/-}$) with a genetic background of C57/BL6 were used to generate *Adrb2* WT and homozygous mutant (*Adrb2*$^{-/-}$) mice for this study (21).

Adrb2-*deficient Col1α1-caPTHR transgenic mice.* *Adrb2*$^{-/-}$ mice (noted as β_2AR-KO mice) with a genetic background of C57/BL6 and α1(I) collagen-caPTHR transgenic mice with a genetic background of FVB/N were used (11).

In vivo PTH administration. Ten-week-old (young adult mouse model) or 54-wk-old (aging mouse model) female mice were given s.c. injections of vehicle (saline) or hPTH (1–34) (Bachem) at a concentration of 80 μg/kg body weight for 5 d/wk over 4 wk. For some experiments, 4-wk-old mice were used.

Other methods are described in *SI Materials and Methods*.

ACKNOWLEDGMENTS. This work was supported by the Japanese Ministry of Education [Global Center of Excellence (COE) Program, International Research Center for Molecular Science in Tooth and Bone Diseases Grants-in-Aid 18109011, 18659438, 18123456, 20013014, and 23659868), grants from the Japan Space Forum (to M. Noda), and National Institutes of Health Grant R01DK087688 (to J.-P.V).

1. Delmas PD (2002) Different effects of antiresorptive therapies on vertebral and nonvertebral fractures in postmenopausal osteoporosis. *Bone* 30:14–17.
2. Kurland ES, et al. (2000) Parathyroid hormone as a therapy for idiopathic osteoporosis in men: Effects on bone mineral density and bone markers. *J Clin Endocrinol Metab* 85:3069–3076.
3. Orwoll ES, et al. (2003) The effect of teriparatide [human parathyroid hormone (1-34)] therapy on bone density in men with osteoporosis. *J Bone Miner Res* 18:9–17.
4. Sosa Henríquez M, Díez Pérez A (2007) [Parathyroid hormone in the treatment of osteoporosis]. *Med Interna* 24:87–97.
5. Lindsay R, et al. (1997) Randomised controlled study of effect of parathyroid hormone on vertebral-bone mass and fracture incidence among postmenopausal women on oestrogen with osteoporosis. *Lancet* 350:550–555.
6. Cosman F, et al. (2001) Parathyroid hormone added to established hormone therapy: Effects on vertebral fracture and maintenance of bone mass after parathyroid hormone withdrawal. *J Bone Miner Res* 16:925–931.
7. Keaveny TM, et al. (2008) Femoral bone strength and its relation to cortical and trabecular changes after treatment with PTH, alendronate, and their combination as assessed by finite element analysis of quantitative CT scans. *J Bone Miner Res* 23:1974–1982.
8. Saag KG, et al. (2007) Teriparatide or alendronate in glucocorticoid-induced osteoporosis. *N Engl J Med* 357:2028–2039.
9. Takeda S, et al. (2002) Leptin regulates bone formation via the sympathetic nervous system. *Cell* 111:305–317.
10. Elefteriou F, et al. (2005) Leptin regulation of bone resorption by the sympathetic nervous system and CART. *Nature* 434:514–520.

11. Calvi LM, et al. (2001) Activated parathyroid hormone/parathyroid hormone-related protein receptor in osteoblastic cells differentially affects cortical and trabecular bone. *J Clin Invest* 107:277–286.
12. Neer RM, et al. (2001) Effect of parathyroid hormone (1-34) on fractures and bone mineral density in postmenopausal women with osteoporosis. *N Engl J Med* 344: 1434–1441.
13. Calvi LM, Schipani E (2000) The PTH/PTHrP receptor in Jansen's metaphyseal chondrodysplasia. *J Endocrinol Invest* 23:545–554.
14. McCauley LK, et al. (2001) Parathyroid hormone stimulates fra-2 expression in osteoblastic cells in vitro and in vivo. *Endocrinology* 142:1975–1981.
15. Ma YL, et al. (2001) Catabolic effects of continuous human PTH (1–38) in vivo is associated with sustained stimulation of RANKL and inhibition of osteoprotegerin and gene-associated bone formation. *Endocrinology* 142:4047–4054.
16. Fu Q, Jilka RL, Manolagas SC, O'Brien CA (2002) Parathyroid hormone stimulates receptor activator of NFkappa B ligand and inhibits osteoprotegerin expression via protein kinase A activation of cAMP-response element-binding protein. *J Biol Chem* 277:48868–48875.
17. Tyson DR, Swarthout JT, Partridge NC (1999) Increased osteoblastic c-fos expression by parathyroid hormone requires protein kinase A phosphorylation of the cyclic adenosine 3′,5′-monophosphate response element-binding protein at serine 133. *Endocrinology* 140:1255–1261.
18. Hanyu R, et al. (2011) Per-1 is a specific clock gene regulated by parathyroid hormone (PTH) signaling in osteoblasts and is functional for the transcriptional events induced by PTH. *J Cell Biochem* 112:433–438.
19. Kondo H, et al. (2005) Unloading induces osteoblastic cell suppression and osteoclastic cell activation to lead to bone loss via sympathetic nervous system. *J Biol Chem* 280: 30192–30200.
20. Kitahara K, et al. (2003) Osteopontin deficiency induces parathyroid hormone enhancement of cortical bone formation. *Endocrinology* 144:2132–2140.
21. Chruscinski AJ, et al. (1999) Targeted disruption of the beta2 adrenergic receptor gene. *J Biol Chem* 274:16694–16700.

う蝕制御学分野

田上 順次

医歯学総合研究科・口腔機能再構築学系専攻
齲蝕制御学・教授

1）研究課題名

波長405nm半導体レーザーが可視光応答型酸化チタン光触媒を用いた歯の漂白材の効果に及ぼす影響

Effect of 405nm diode laser on tooth bleaching with visible-light activating titanium dioxide photocatalyst

波長405nm青紫半導体レーザーが、過酸化水素と可視光応答型酸化チタン光触媒（VL-TiO2）を含有する歯の漂白材の効果に及ぼす影響についてin vitroで検討した。過酸化水素、VL-TiO2、メチレンブルー（MB）および純水から成る試験液を調製し、試作波長405nm青紫半導体レーザーを各種照射条件で7分間照射し、30秒ごとにMB濃度を測定し、漂白効果を評価した。その結果、405nm半導体レーザー光は、漂白に有効であり、連続波では出力が高いほど、高い漂白効果を示した。また、パルス波では、平均出力が同じであれば、Duty比、パルス幅は漂白効果に影響を及ぼさないことが明らかになった。また、405nm青紫色半導体レーザーと波長470nmのアルゴンレーザーについて、同様の方法で比較したところ、同じ出力で、405nm半導体レーザーは高い漂白効果を示した。

Super Toothに関する研究

Study on Super Tooth

接着材料と歯質との界面の詳細なる観察から、セルフエッチングシステムを用いた場合に接着界面にはう蝕抵抗性を示す層が確認され、これは接着材料によってエナメル質や象牙質が修飾されて強化された層であることから、Super toothと称している。このSuper toothを確実に形成することができれば、一生涯に渡り歯を長持ちさせることが可能となり、QOLの向上に貢献できる。Super toothの形成メカニズムについては未だ不明な点が多いが、ボンディング材に含まれる機能性モノマーの種類によってその形成が全く異なり、リン酸エステル系モノマーであるMDPを含む接着システムにおいてはエナメル質においてもSuper enamelの形成が確認されるものの、同様にリン酸エステル系モノマーであるPhenyl-Pを用いた場合、接着界面にABRZの形成は認められず、さらに接着界面の酸に対する脆弱性を示すことがわかった。したがって、Super toothの形成には機能性モノマーとHAPとの化学的結合能の強さが重要な要因であり、さらにこの層は、樹脂含浸層とは異なる層である可能性が高いこともわかってきた。

レジンコーティングの応用に関する研究

Study on dental coating materials

間接修復法において、露出した象牙質を保護するために、接着材で象牙質表面をコーティングするレジンコーティング法の研究を中心に行っている。レジンコーティング法の応用によって、レジンセメントの歯質接着性の向上や、窩壁適合性の向上、さらに象牙質、歯髄の保護などの効果を有する。最近では、薄膜コーティング材料も開発、市販され、これを使用することによってクラウンの支台歯への応用も可能となった。さらに薄膜コーティング法は、健全歯質への応用による歯の強化などについても検討しており、薄膜コーティング材料は10μm前後のコーティング膜を形成するが、歯ブラシ摩耗w10000回行っても消失せず、臨床的にも十分な耐摩耗性が認められた。将来的にはこのような材料を健全歯質に塗布することによって、Super Toothを形成し、歯の摩耗やバイオフィルムの付着を抑制することが期待される。

マイクロCTを用いた歯の脱灰・再石灰化の評価

Micro CT measurement of de/re-mineralization to tooth structures

初期う蝕に関する治療方法については未だ確立されておらず、さらに高齢者の根面う蝕についての研究も十分とはいえない。従来、歯の脱灰、再石灰化の評価にはマイクロラジオグラフィー（TMR）が利用されていたが、

試料の非破壊での観察は不可能であった。申請者らは、高性能で非破壊的に歯の脱灰、再石灰化を観察可能な装置であるマイクロCTを利用して歯の脱灰・再石灰化の評価を行っている。マイクロCTは、解析ソフトとフィルターとの工夫によって、エナメル質初期う蝕に対してTMRと遜色のない画像解析が可能であることを報告した。さらにCPP-ACP ペーストのエナメル質塗布による脱灰抑制効果やフッ化物配合象牙質知覚過敏抑制コート材の象牙質脱灰抑制効果などについて評価している。将来的にはマイクロCTが硬組織の脱灰、再石灰化の研究の中心的な役割を果たす計測機器となる可能性は高い。

コンポジットレジン修復物の色調適合性に関する研究

Color matching of resin composite restoration

コンポジットレジンの透過光特性の違いは、コンポジットレジン修復物の色調に固有の特徴を与えていると思われる。しかしながら、コンポジットレジンの透過光特性、特に拡散透過性に着目した研究は少ない。自動変角光度計を用いてコンポジットレジンの透過光特性（正透過性、拡散透過性）について評価を行った結果、特に拡散透過性の増加は、コンポジットレジンの背景色遮蔽性の向上と関連があり、また積層充填により形成されるcomposite-composite接合部は、拡散透過性を上げ、背景色遮蔽性を上げることができることが判明した。コンポジットレジン修復物の拡散透過性を上げることにより、窩洞が浅い場合でも、透明感を失わずに背景色の遮蔽を行うことができ、コンポジットレジン修復物の色調適合性を向上させる可能性があることが示唆された。

一方、コンポジットレジンなどの半透明性材料は周囲媒体との境界部において、周囲色調を反映することにより、色調変位を起こし、これにより境界部の色差が不明瞭となり、色調が適合しているかのように見える。これをカメレオン効果と呼ぶ。カメレオン効果は、周囲媒体と半透明材料との相互協調関係により発現すると考えられる。コンポジットレジン修復物のカメレオン効果を適切に評価するために、ヒト歯牙を用いてカメレオン効果の研究を行った結果、コンポジットレジン修復物境界部のカメレオン効果は、コンポジットレジン側のみならず歯牙側の色調変化により引き起こされ、その変化は歯牙側の方が大きいことが判明した。さらにその色調変化は、拡散透過性の高いコンポジットレジンの方が大きくなる可能性が示唆された。

各種接着システムの象牙質接着強さに及ぼす残存象牙質厚さの影響について

Effect of remaining dentin thickness on bond strength of various adhesive systems to dentin

レジンの接着強さは、平坦面の象牙質被着体に対して評価されることが多いが,残存象牙質厚さが少ないとレジンの象牙質への接着強さが低下することが報告されている。そこで本研究では、各種ボンディングシステムを使用したレジンの接着強さに及ぼす残存象牙質厚さの影響について検討した。ヒト抜去大臼歯の咬合面エナメル質を削除し,スチールバーで仕上げした象牙質平坦面を作製し、3種の接着システム;Clearfil SE Bond, Single Bond or Clearfil Tri-S Bondを用い製造者指示に従い処理した後、Z100のレジンを3×5×2mmに築盛し、実験:用ハロゲンランプ電圧可変光照射器を用い,出力600 mW/cm2で40秒間光照射を行い重合硬化させた。37℃暗所水中に24時間保管後、試料中央部から長軸方向に、レジンー象牙質界面の接着面積が約1mm^{2}の試片を切り出した。これら試片の残存象牙質厚さ（RDT）を測定した後,試片の両端を試験装置にシアノアクリレートで接着し、これをEZ　testに装着して,クロスヘッドスピード1mm/minで微小引張接着強さを測定した。微小引張接着強さは、RDTにより RDT<2 mm; 2≤RDT<3 mm; 3≤RDT<4 mm; RDT≥ 4 mmの4群に分けた。Clearfil SE Bondの接着強さは、RDTと相関があったが、Single Bondの接着強さはRDTの影響を受けないことが明らかとなった。レジンの象牙質接着強さへ及ぼすRDTの影響は、ボンディングシステムにより異なる傾向を示すことが判明した。

学生模型実習における修復物適合性のSS-OCTによる3D評価

3D evaluation of composite resin restoration at practical training using swept-source optical coherence tomography (SS-OCT)

東京医科歯科大学4学年の学生67名を対象とした模型実習において、顎模型に装着した右上6番のメラミン歯に齲蝕を想定し、コンポジットレジン修復を行わせた。終了後、修復を行ったメラミン歯を回収し、コンポジットレジンの形態と適合性を評価した。評価項目として、窩洞外形、修復物の適合状態、表面の仕上げ研磨状態の3項目とし、それぞれの完成度に応じて採点した。修復物内面の適合状態は、SS-OCTを用いて非破壊で行い、3D立体画像構築を取り入れて総合的な判定を試みた。また、SS-OCTによる断層画像を学生に公開し

た。SS-OCTを用いることにより、メラミン歯に修復したコンポジットレジンの内部の状態を観察することができた。窩洞外形では、分離型の2窩洞の修復が39、連結した1窩洞の修復が28であり、修復物の適合状態は、内面に大きなギャップや空隙のみられるものが23であった。仕上げ研磨の状態は概ね良好であり、不良なものは6のみであった。また、3項目すべてが不良であったものは2、2項目が不良であったものは12であった。学生が行ったコンポジットレジン修復を、SS-OCTの3D画像を用いて評価し、内部の適合状態を学生に還元することによって、コンポジットレジン修復における充填操作の重要性を指摘することができた。窩洞外形や仕上げ研磨が良好であっても、コンポジットレジンの内面にギャップや空隙のみられる修復がみられ、SS-OCTの非破壊断層画像を用いた教育は有用性が高いと考えられた。

SS-OCTによる隣接面う蝕の臨床診断

Diagnosis of proximal caries using swept-source optical coherence tomography（SS-OCT）in vivo

直視による診断の困難な臼歯部隣接面う蝕は、X線写真による診断が一般に行われている。しかしながら隣接面う蝕に対するX線写真の感度は低く、中等度以上の深さに進行してからフイルム上の変化として捉えられることが多い。隣接面う蝕の診断を目的とし、口腔内用プローブを装着した試作歯科用OCTを用いて実際の臨床患者における臼歯隣接面の観察を行い、X線画像による画像と比較した。隣接面う蝕が疑われる53人の患者を対象とし、健全部を含めた75の隣接歯面を抽出し、デンタルX線写真ならびにSS-OCT画像を撮影した。X線写真とSS-OCT画像、ならびに視診を組み合わせた総合的な診断から、隣接面う蝕の明らかな症例に対しては切削介入によるう蝕治療を行い、コンポジットレジン修復を行った。う蝕の除去は、う蝕検知液をガイドとして行い、う蝕除去後の窩洞の深さを臨床的なう蝕の進行度として記録した。健全または早期エナメル質脱灰と思われる歯面に対しては、歯面清掃とフッ素塗布を行い、視診による診断が明らかな症例のみを実験の対象とした。臨床での診断ならびにう蝕治療に関与していない歯科医師6名を選出し、先に得られたX線写真とSS-OCT画像から、隣接面う蝕の進行度を、0:健全部、1:エナメル質脱灰、2:エナメル質う蝕、3:象牙質初期う蝕、4:象牙質進行う蝕　の5段階で判定した。臨床的なう蝕の進行度を評価基準として、X線写真とSS-OCT画像の感度、特異度、ROC曲線のAz値を算出し、比較した。

隣接面う蝕に対するSS-OCTの感度、特異度、Az値は、それぞれ0.93, 0.64、0.78であり、X線写真から得られた結果よりも有意に高かった。SS-OCTを用いると、識別困難な隣接面う蝕を、他のin vitroの実験結果と同様、輝度の上昇として画像表示することができ、有用性の高いことが示唆された。

リン酸化オリゴ糖カルシウムおよびフッ素配合ガム咀嚼後エナメル質初期う蝕の再石灰化効果

Effects of a chewing gum containing phosphoryl oligosaccharides of calcium（POs-Ca）and fluoride on remineralization

人工初期エナメル質う蝕サンプルを口腔内装置に装着した状態で、Placeboガム、POs-CaガムおよびPOs-Ca+Fガムを1日3回14日間摂取させ、①TMR、②広角X線回折、③微小硬さ試験および④TOF-SIMS（飛行時間型イオン分析）を用いて、ヒト口腔内環境下における各種ガムの再石灰化効果について比較検討した。その結果、ミネラル回復率は、POs-Caは21.9 ± 10.6 %、POs-Ca Fでは26.3 ± 9.4%と、いずれもControl群の15.0 ± 11.4%よりも有意に高いミネラル密度の回復が認められた（$p<0.05$）。微小硬さ変化では、POs-CaならびにPOs-Ca Fにおいて脱灰部よりも再石灰化部において硬さの回復を認めた。また、表層18 μmまでの1 μm深さごとの硬さ値について追加測定したところ、表層から2 μm付近において、POs-Ca FがPOs-Caより有意に高い硬さ値を示した。一方、再石灰化部のハイドロキシアパタイトの結晶量および結晶配向性を評価した結果、POs-Ca Fでは24.9 ± 5.4%と、POs-Caの16.4 ± 4.1 %およびControl群の11.1 ± 4.8%よりもハイドロキシアパタイトの結晶回復率が有意に高いことが判明した。またこれらのアパタイト結晶は、同一の方向性をもって配列していることも確認された。さらに、初期エナメルう蝕最表層部におけるフッ素分布について二次イオン質量分析を行った結果、POs-Ca F咀嚼後の再石灰化部において、その脱灰部では認められないフッ素分布が確認された。以上より、口腔内環境におけるPOs-Caおよびフッ化物配合ガムのエナメル質初期の再石灰化効果が認められた。

人工う蝕罹患象牙質に対する塩化カルシウム・フッ素含有ボンディングシステムを用いた歯質接着界面の強化

Reinforcement of adhesive interface using a CaCl2/fluoride-incorporated bonding system on artificial caries affected dentin model

本研究では、2ステップフッ素徐放性接着システムに

塩化カルシウムを添加し、う蝕罹患象牙質に対する接着強さへの効果、及びう蝕象牙質の再石灰化への効果について検討する。本研究には、プライマーに異なる濃度の塩化カルシウム（0, 10, 20%）を添加した試作2ステップ接着システムを使用する。まず、健全ヒト小臼歯の歯冠部より象牙質を切り出し、#600耐水研磨紙で検索した後、中央にテープを貼り、その周囲をネイルバーニッシュする。テープを除去したのち、pH4.5に調整した人工脱灰液7日間浸漬し人工う蝕を作成する。その後、表面を600番の耐水研磨紙にて1.6kg重の荷重で研削する。OCT（光干渉断層計）にて脱灰深さ（400-500 μm）と確認する。試料を2群（24時間後と8週間後）に分け、再石灰化溶液に浸漬する。試料にボンディング及びコンポジットレジン築盛をした後、スティック状に切り出し微小引張り試験を行う。微小引張り試験後の試料は、破壊形態を観察する。また、微小硬さ試験によって試作ボンディングシステムの接着界面における再石灰化効果を検討する。さらにAcid-base resistant zone（酸-塩基抵抗層、ABRZ）の観察にはTEM観察方法を用いる。ABRZ内に存在するミネラルをSAEDによって解析することによって、試作プライマーのレジンーう蝕罹患象牙質接着界面における再石灰化に及ぼす効果について詳細に検討する。本実験から期待される成果は、象牙質接着耐久性の向上に貢献するだけではなく、コンポジットレジン修復の長期耐久性にも大いに役立つと考えられる。

マイクロCTによる光重合型コンポジットレジンの重合収縮挙動の評価

Evaluation of resin composite polymerization by three dimensional micro-CT imaging

コンポジットレジンの重合時に発生する重合収縮は避けられない事象である。歯質と修復物との間の接着界面にギャップやマイクロリーケージクを引き起こし、術後疼痛、細菌侵入による二次う蝕や歯髄炎の原因となることが考えられる。従来から化学重合型レジンは重合時、窩洞の中心方向に向かって収縮し、光重合型コンポジットレジンは光の照射方向に収縮すると考えられてきた。これらの重合収縮時における挙動は有限要素法やレーザースペクトル法により研究、解析されているが、重合に伴う収縮の挙動を直接観察できる手法は少ない。本実験ではコンポジットレジンで作られた疑似一級窩洞に、実験用に試作したコンポジットレジンを充填し、光照射前と光照射後の試作コンポジットレジンをマイクロCTにより撮影し収縮挙動の解析を行った。

X線造影性のないコンポジットレジン、SOLARE（A3、GC）に疑似一級窩洞を作成し、実験用試作コンポジットレジンをセラミックプライマー（クラレメディカル）とメガボンド（クラレメディカル）を塗布した窩洞に充填した。続いて光照射（D-LUX2000、DENTRADE）前、光照射後それぞれに、試料の3D画像をマイクロCT（SMX100CT、島津製作所）にて撮影した。得られた3D画像よりマーカーとなるフィラーを専用ソフト（ラトックシステムエンジニアリング）を使って抽出し、窩洞内の全てのマーカーフィラーの重合前、重合後の座標を測定する。

接着破壊メカニズムの解明

The analysis of failure mechanics of adhesive interface

近年の目覚ましい接着歯学の発展に伴い、“Minimal Intervention”コンセプトに基づく接着レジンを用いた保存修復治療は、臨床的有効性と経済的効率の観点から患者に大きな利益をもたらすものであると期待されている。十分な耐久性を兼ね備え、歯とより強固に接着するボンディングシステムを構築するためには、「歯とレジンとの接着機構がどのように破壊されるか」という接着破壊のメカニズムを解明することが重要である。しかし接着界面の破壊は極めて短時間に起こるため、肉眼はおろか、通常のビデオカメラ撮影（毎秒40フレーム程度）を行ってスロー再生をしても破壊様相を観察することはできない。したがってこれまで特殊な撮影方法を用いて使用して接着界面のリアルタイム動的観察を試みてきた。そして2012年微小引張り接着試験におけるレジン-象牙質接着界面の亀裂発生および亀裂進展の観察に成功した。しかしなお、理論上起こると考えられる接着界面内部の変形や3次元的な亀裂の進展を解析するには至っていない。本研究ではさらに破壊メカニズムの解明を進展させるためリアルタイム波動解析的手法を用いて歯とレジンとの接着界面の破壊メカニズムを解明する予定である。

コンポジットレジンの吸水量が色調変化に与える影響について

The Effect of water sorption of composite resins on color changes

近年、コンポジットレジンは機械的性能ならびに審美性が向上し、臨床的に満足できる結果を得られるようになってきている。しかし、継時的な色調の変化はまだ依然として問題となっている。その原因としては、重合開始材、重合率、食物由来の色素、紫外線、温度変化、吸

水など様々なものが報告されている。このなかでも今回は吸水に着目して研究を行った。吸水率に影響を与える因子としてはレジンモノマーの種類、フィラー含有量、フィラーの種類、重合率などが報告されているが、表面粗さと吸水に関する報告はない。そこで本研究では、異なる粘度のコンポジットレジンを用い、その研削条件を3種類設けて、色調変化と吸水の関係に関する検討を行った。粘度が高いほど色調変化を表す⊿E*の値は小さくなる一方、研削条件は⊿E*の値に影響を与えなかった。また、吸水率に関しても粘度が高くなるほど吸水率が低くなった。また⊿E*と吸水率の間には有意な相関が確認できた。結論として、すべてのコンポジットレジンにおいて肉眼で明らかに認識できる色調変化が見られ、コンポジットレジンの色調の安定にはさらなる研究が必要であることがわかった。

2級コンポジットレジン修復におけるエナメル質と象牙質に対する窩洞適合性と微小引張り強さ

Contemporary adhesives: marginal adaptation and microtensile bond strength of class II composite restorations

本研究では、4種類の接着システムを用いて2級コンポジットレジン修復を行い、隣接面エナメル質と象牙質への窩洞適合性と接着強さに及ぼす影響について検討した。窩洞適合性において、エナメル質では、すべての材料において95.4%以上の連続マージンが観察された。一方、象牙質では60.2%から84.8%の連続マージンが認められ、Clearfil SE Bond と Clearfil Tri-S Bond は、Adper Scotchbond Multi Purpose と Adper Scotchbond 1 XT より有意に多い連続マージンが認められた（$p<0.05$）。微小引張り接着強さにおいて、Adper Scotchbond Multi Purpose、Adper Scotchbond 1 XT、Clearfil SE Bond、Clearfil Tri-S Bondはそれぞれエナメル質に対して、40.5、37.3、30.8、23.2 MPa、象牙質に対して37.7、33.0、37.3、29.0 MPaの接着強さを示した。接着システムの違いはエナメル質に対する窩洞適合性に影響を及ぼさないが、象牙質に対してはエッチ＆リンスシステムと比較してセルフエッチシステムの優れた窩洞適合性が得られた。Adper Scotchbond Multi Purposeは、エナメル質と象牙質に対して最も高い接着強さが得られた。Clearfil SE Bondは、象牙質に対して最も安定した接着強さが得られ、エナメル質に対しても良好な接着強さが得られた。

レジンコーティング後の象牙質透過性の経時的変化

Change of dentin permeability in different storage media after resin coating

本研究では、レジンコーティングと保管液が象牙質透過性に及ぼす経時的変化について検討した。

直径7mmの牛歯象牙質ディスクを36個作製し、象牙質透過性を測定した。その後、試料を3グループに分け、無処理（コントロール）、メガボンド、メガボンド+プロテクトライナーFでコーティングを行った。さらに、それぞれのグループを2つに分け、脱イオン水もしくは人工唾液にて1日、1ヶ月、3ヶ月保管を行った後、再び象牙質透過性を測定し、象牙質透過性の減少率を測定した。コントロール群において、脱イオン水に保管すると象牙質透過性は一定ではなかった一方で、人工唾液に保管すると象牙質透過性が経時的に減少した。レジンコーティングを施すと象牙質透過性が有意に低下し、特に、メガボンドのみよりも、メガボンド+プロテクトライナーFでコーティングを施すと象牙質透過性が有意に低下することがわかった。また、保管液は象牙質透過性に影響を及ぼすことがわかった。

マイクロCT法を用いたミネラル脱灰・再石灰化の非破壊定量解析

Non-destructive quantitative analyses of de/remineralization using micro-computed tomography（μCT）

マイクロCT法は微小焦点X線をサンプルに照射,回転することで3D画像を構築する方法である.従来,歯質の脱灰・再石灰化評価には,包埋・切断を必要とするマイクロラジオグラフィー（TMR）法が用いられているが,マイクロCT法に定量的な手法を応用することで経時的なミネラル変化を測定することができる.本研究は,エナメル質表層下脱灰病変を持つヒト抜去歯牙を用い,最適な条件を検証するために,ソフトウェア補正と各種条件に分けて,0.5 mmAlのみ、0.5 mmAlと0.3 mmCuもしくは 0.5 mmAlと0.4 mmCuのフィルターを設定した.観察部位を切り出し,TMR法を用いて,同部位のミネラル密度プロファイルを算出し,マイクロCT法と比較を行った.結果,AlとCuをフィルターとした条件において,ミネラル関連の値において高い相関性が得られた.

齧歯動物歯髄における樹状細胞サブセットの解析

Identification of several subpopulations ofDCs in rodent dental pulp

樹状細胞（DC）の共刺激分子発現やサイトカイン産生は、所属リンパ節（RLN）に遊走するDC の抗原提示能に多

大な影響を与える。歯髄は、粘膜や皮膚と同様に最前線に位置し生体防御機能を発揮している。本研究では、抗原を捕捉後RLNに遊走するDCを4つのサブセットに分類し、その経時的遊走能の変化と共刺激分子発現を検討した。RLNに遊走する歯髄DCは、CD11C. CD207, CD103, CD326, CD11b の表現型から、F1（$CD11c^{hi}$CD207-粘膜下樹状細胞（SMDC））, F2（$CD11c^{int/lo}$CD207-新規リクルートSMDC）, CD103+ F3（$CD11c^{int/lo}CD207^{+}$レジデントSMDC）, CD103- F3（ランゲルハンス細胞、LC）の4サブセットに分類できた。CD207+ SMDCは、CD103の発現によりLCと区別することができた。F1 DCは最も早く遊走し、CD86, CD273, CD274を高く発現していた。これに対して、$CD103^{-}$および$CD103^{+}$ F3 DC共に、遅れての遊走が認められ、$CD103^{-}$ LCでは、共刺激分子発現誘導は制限されていた。F1 SMDCとF3 LCでは、遊走時期と共刺激分子発現の違いから、異なる役割を担っていることが示唆された。

ヒト唾液タンパク質のモデルとしてのカゼインが歯質の脱灰/再石灰化、エナメル質酸蝕およびアパタイト成長（歯石形成）現象に及ぼす影響

Influence of casein as a model of salivary proteins on tooth de-/remineralization, acid enamel erosion and apatite growth（calculus formation）

唾液タンパク質が歯質の脱灰や再石灰化に強い影響を及ぼすことは既に知られていが、これに関連したインビトロモデル研究においては、これまでほとんどその影響は考慮されていない。その理由として、新鮮唾液の確保が容易でないこと、あるいは確保しても実験中にも変質（タンパク分解）しやすいために実験結果の再現性に疑念が残る、などが指摘できる。そのため、インビトロの結果と実際の口腔での現象とのあいだに、深刻な食い違いが見られる場合がある。そこで本研究では、脱灰/再石灰化現象やペリクル膜成分に関係する唾液タンパク質の一つであるPRP（Proline-Rich Protein）の分子構造に類似し、かつ市販品として容易に入手できるタンパク質としてミルクカゼインに注目した（一種のリンタンパク質）。種々の濃度のカゼインを含む人工唾液（カルシウムやリン酸も含有）を作製して、①エナメル質/象牙質の脱灰/再石灰化（う蝕の進行）②アパタイトの成長・沈着（歯石形成）③エナメル質の酸蝕（歯質の損失）に与える影響を研究課題として取り組んでいる。この研究を通して、実際の口腔で起こっているこれらの現象の真実（メカニズム）に迫るとともに、これらの研究課題をインビトロで研究する場合の標準試験法として確立し、それぞれの課題研究の中で臨床的に有用な技術開発（①う蝕予防/再石灰化促進 ②歯石予防　③酸蝕予防/修復）にも繋げたいと考えている。現在、①と②についてインビトロ実験を進めている。例えば、種々の濃度のカゼインあるいはフッ化物イオン（F-）を含む人工唾液にアパタイト粉末（結晶）を浸漬すると、カゼインの濃度に応じて顕著な結晶成長の抑制および歯面への石灰化沈着の抑制を確認した（電顕観察）。

根面う蝕に関与する唾液中のバイオマーカーの加齢による変化

Age related changes in saliva and their effect on root caries

根面う蝕の発生要因として、唾液中のコラゲナーゼ活性や、唾液の緩衝能も重要な因子であることから、若年者と高齢者の唾液の性状を比較し、高齢者の根面う蝕の発症状態について、唾液中のバイオマーカーの違いの分析を試みた。来院患者　若年者、高齢者20名を対象にインフォームドコンセントの取得後、口腔内検査を行い、DMFT、根面う蝕、口腔清掃状態等を記録した。根面う蝕指数（Root Caries Index）は、根面露出面総数における、（齲蝕根面数＋処置済根面数）の割合で算出した。その後、無刺激唾液を5分間採取し、唾液容量、初期pH、酸緩衝能、さらに各種バイオマーカーの分析を行った。唾液バイオマーカーは、唾液中カルシウム濃度、酵素活性（コラゲナーゼ、アミラーゼ）、Glutathione酸化的ストレスマーカー、マトリックスメタロプロテアーゼ（MMP8）、マトリックスメタロプロテアーゼ阻害因子（TIMP-1）の測定分析を行った。若年者、高齢者2群間で統計的有意差があったものはDMFT、根面う蝕指数, 唾液容量, カルシウム、コラゲナーゼ酵素活性、マトリックスメタロプロテアーゼであった。ピアソンの相関関係による統計処理で、有意な相関関係（$p < 0.05$）が見られたのは、DMFTとコラゲナーゼ酵素活性、DMFTとマトリックスメタロプロテアーゼ、唾液容量とコラゲナーゼ酵素活性、アミラーゼ酵素活性とカルシウム量、アミラーゼ酵素活性とマトリックスメタロプロテアーゼ阻害因子、コラゲナーゼ酵素活性とマトリックスメタロプロテアーゼであった。高齢者の根面う蝕指数（Root Caries Index）と酸化的ストレスマーカー間では有意な相関関係は見られなかった（$P = 0.543$）。これは酸化的ストレスマーカーが、一般には年齢とともに低い値は示すが、個人の身体的状態に大きく作用され、また実際に根面う蝕の発生は複雑な要素が関与しているので、今回は明瞭な相関は得られなかったと思われる。

還元型グルタチオンの、接着歯学への応用（解毒剤、コラーゲン分解酵素活性阻害剤としての利用）

Reduced glutathione detoxification of 2-hydroxyethylmethacrylate and its effect on resin-dentin bond strength

グルタチオンは、体内、細胞内で最高の解毒剤であり抗酸化物質である。グルタチオンは細胞中に還元型（GSH）と酸化型（GSSG）が存在する。還元型では、システイン中のチオール基がフリーラジカルを抑制する能力を持ち、フリーラジカルと同等量のチオール基が還元する（H++ e-）。グルタチオン抱合による解毒は、システイン残基のチオール基に様々な物質を結合することによる。グルタチオン-S-トランスフェラーゼによってこれらの結合反応が触媒されが、また、ある種の金属イオンは非酵素的にグルタチオンと結合する。HEMAは接着性レジン剤に含まれ、その低い分子量、また親水性から歯質への浸透がよく、歯髄に近い深い窩洞ではその使用により、歯髄細胞への影響が危惧され、臨床予後を悪化させる要因と考えられる。本研究ではグルタチオンの、HEMAの解毒作用をラット由来の歯髄細胞を用いて、細胞毒性試験を行った。またリン酸処理後の歯面に塗布し、接着試験を行い、グルタチオンの象牙質接着性へ影響を調べた。この結果、グルタチオンの、HEMAの解毒作用がみられ、さらにグルタチオンの使用で、接着強さが向上したことが分かった。

ヘスペリジンによるヒト歯根面象牙質脱灰後のコラーゲンの保護と、再石灰化への影響

In Vitro Evaluation of Hesperidin to Preserve Dentin Collagen

歯質象牙質は70%が無機質（ヒドロキシアパタイト）、20%が有機物（膠原繊維（コラーゲン繊維）と非膠原性タンパク質）からなり、う蝕のメカニズムを考える上で、酸による無機質の脱灰抑制とあわせて、有機質の保護を考慮しなければならない。近年、有機質の保護が確立できれば、これを足場にしてう蝕脱灰部の再石灰化が有意に起こると考えられている。フラボノイド（flavonoid）は天然に存在する安全性の高い有機化合物群で，少量でも抗酸化作用を有し、天然の架橋剤としてコラーゲンを保護すると報告されている。本研究では天然フラボノイドのヘスペリジンを歯質象牙質に作用させ、う蝕の進行への影響を評価した。方法:象牙質う蝕モデルとしてpHを調整した脱灰、再石灰溶液にて8日間保存した。この間、象牙質にヘスペリジンン溶液にて一日2時間作用させた。最終脱灰量、コラーゲン崩壊度を定量分析し、x線を用いたミネラルプロファイル測定による脱灰部の分析を行った。また同じフラボノイドのグレープシード抽出物と、う蝕予防に使用されるクロロヘキシジンとの効果を比較検討した。結果考察:ヘスペリジン群は有意に脱灰量、コラーゲン崩壊度を抑制していた。脱灰部の分析を行った結果、表層のみならず、やや深部まで再石灰化が見られた。これらの結果より、ヘスペリジンは、う蝕の脱灰抑制、再石灰化促成に何らかの効果があることが分かった。作用メカニズムは、今後さらなる研究が必要だが、う蝕の発生また進行をコントロールするうえで、生体に安全なフラボノイドは有効な薬理作用を持つと予測され、将来の治療薬と期待される。

ヘスペリジン配合セルフエッチングプライマーの象牙質接着性への影響

Effect of hesperidin incorporation in a self-etching primer on dentin adhesive

歯科接着修復学は、健全な歯質を保存しつつ接着歯学の技術で審美的機能的に修復を目指すものである。象牙質は有機質を含むため、有機質の経時的劣化が接着力の低下に影響を及ぼしている。よって、有機質の保護強化が現在の課題で、様々な実験が行われている。我々はヘスペリジンの抗酸化作用、天然の架橋剤として作用を利用し、歯科修復材の前処理剤として応用させる試みを行った。市販の歯科接着材のプライマー（前処理剤）にヘスペリジン0～10%を配合させた。牛、ヒト歯質象牙質を使い、歯科接着剤で接着後、0.9X0.9㎜の接着断面ので、引っ張り接着試験を行い、グレープシード抽出物と、クロロヘキシジン群と比較した。また、電子顕微鏡レベルで破断面の観測を行った。結果考察:ヘスペリジン配合群は接着強さが上がり、1%で最も有意な差が出た。これらはグレープシード抽出物と、クロロヘキシジン群に比べても、有意に高い値であった。これらの結果より、ヘスペリジンはプライマー（前処理剤）に配合した場合、その架橋作用により有機物コラーゲンを保護すると考えられ、高いに接着力につながったと思われる。今期は1年水中保管したサンプルの接着試験、界面のTEM観察により、コラーゲン保護材としての効果を臨床応用を検討する予定である。

天然由来接着性ポリフェノール重合体の接着歯学への応用～革新的ナノ接合能の確立へ～

Mussel-mimetic bio-adhesive polymers: the alternative to petroleum adhesives

岩盤上のムール貝などが水中で行う接着と、古来より接着剤や塗布剤として使用される漆の接着の歯科材料へ応

用を目指すものである。ムール貝の接着は、水中でも材質を問わず動的で且つリバーシブルなものであり、また漆は木質に塗布されると、強固な薄膜を形成し、高い接着能や耐水性能を持つことは知られている。これらの接着には、ドーパと呼ばれる水酸基を2個持つカテコール性アミノ酸分子が関わり、水中でも安定的に共有結合並みの接着力を発現するためだと考えられている。この度、天然ポリフェノール由来のカテコール性重合体の創製に成功した、北陸先端科学技術大学院大学マテリアルサイエンス研究科との共同研究が発足し、このプロジェクトに携わる予定である。このカテコール性接着剤は、既存の接着剤の接着機構であるアンカー効果とは違った全く別の機構、つまりナノレベルで化学結合性の接着機能を持つ。ベンゼン環同士のスタッキングが水中で強く働き、多数のフェノール性水酸基が、被着材の酸化部位やOH基と強結合型の水素結合を形成するといわれている。更に疎水性である長鎖アルキル基の存在により、水中でも抜群の安定接着を発現出来きる、画期的な素材である。この革新的天然由来接ポリフェノール接着素材を使ううえで、接着性の向上、さらに、操作性、生体適合性、そして審美性など課題要素は多々あり、それぞれ評価していく予定である。

ナノインデンテーションによる新しいコンポジットレジン修復システム象牙質界面層の硬さ

Nanoindentation hardness of resin-dentin interface of a new composite system

本研究の目的は、ナノインデンテーション法を用いて、新規接着修復システムであるプライムフィルの接着界面の硬さを、従来のオールインワン接着システムと比較することである。プライムフィルは、従来システムと異なり、接着界面（プライマー層）への光照射が不要であり、専用の低粘度レジンに含まれる重合開始剤との接触により重合が開始される。ヒト抜去歯を研磨し象牙質平面を出し、その後、プライムフィル（PF）プライマー（トクヤマデンタル）、ボンドフォース（BF;トクヤマデンタル）、またはGボンドプラス（GB;ジーシー）で処理した。BF、GBはメーカー指示に従い乾燥後、450mW/cm^{2}のハロゲン照射器を用いて10秒間光照射した。一方、PFは乾燥のみとした。次に、低粘度レジン（PF:PFフロー;トクヤマデンタル、BF:エステライトフロークイック;トクヤマデンタル、GB:MIフロー;ジーシー）を2mmの厚さで充填し、メーカー指示に従い光照射した。37℃水中に24時間保管後、ダイヤモンドカッターを用いて試料を接着界面に垂直に切断し、ダイヤモンドスラリー（～0.1μm）を用いて鏡面研磨した。硬さは、ナノインデンテーション試験機を用い、Berkovich tipにより、最大荷重2mN、0.2 mN/s rateの条件にて、接着層の中心付近15点を測定した。接着界面の硬さは、PF: 508（138）、BF:432（107）、GB: 288（67）であった。新規に開発された、プライマーと低粘度レジンの組み合わせからなるシステムは、接着界面において従来のオールインワン接着システムと同等以上のレジンの重合性および硬さが得られた。

レジン性薄膜で被覆されたエナメル質について、SS-OCTを用いた長期評価

Protection of Enamel against Demineralization by Resin Coating Evaluated under OCT

これまで咬合面をシーラントで被覆してう蝕を予防する技術は知られていた。最近、歯全体を薄膜で被覆できるポリマーが開発された。本研究では、その長期耐久性や脱灰に対する抵抗性を、SS-OCT（非破壊で断層画像が得られる装置）を用いて検討した。牛歯からエナメル質試料を作製し、4種類の薄膜材料でエナメル質全表面を被覆した。これらの試料に5000回の熱的およびブラッシング負荷を与えた。その後、同試料を一定期間脱灰した（1～14日間）。これら一連の操作毎に、SS-OCTにて同試料の断層画像を取得した。脱灰完了後、微小エックス線法にて脱灰抵抗性を評価し、SS-OCT画像との関連性を検討した。 本研究の成果は、フッ化物などを含む機能性薄膜技術を使用することで、いわゆる”Super tooth”の実現に貢献できた。またSS-OCTがその臨床診断装置としても期待できた。

OCTを用いたレジンインレーの適合性とレジンコーティングの有効性の評価

Effect of resin coating on sealing of indirect composite inlays using SS-OCT

SS-OCTは非破壊で組織や修復物の断層画像を得ることができる。さらに間接修復で露出した象牙質を保護するために、接着材で象牙質表面をコーティング方法がある。本研究では、間接法による接着修復物の窩洞の適合性を、SS-OCTを用いて調査した。ヒト抜去歯に直径4mm、深さ1.8mmの1級窩洞を形成し、レジンインレーを接着させ、レジンコーティングの有無が適合性に及ぼす影響を比較した。レジンコーティングの場合に2ステップ接着剤を用いて窩洞を処理し、充填にはフローアブルコンポジットレジンによるライナーを行った。全群で充填操作24時間および5000回の熱サイクル後、OCT画像にお

けるコンポジットレジン辺縁の輝度変換部分をギャップとして判定した。結果、レジンコーティングを窩洞に施すことにより、修復物の適合性が向上することが判明した。特に熱応力試験においてはレジンコーティングの長所が明らかになった。

エナメル質表層部のPOs-CaならびにPOs-Ca+Fによる再石灰化:SS-OCTによる評価

Remineralization of Enamel subsurface lesion by POs-Ca and POs-Ca+F in vitro: evaluation by SS-OCT

波長走査型光干渉断層計（SS-OCT）は、組織の断層画像を非破壊で観察することができる。エナメル質の再石灰化に、POs-Caが有効であることが報告されており、フッ化物との併用により、さらに高い効果が期待される。本研究では、POs-CaならびにPOs-Ca+Fのエナメル質表層部再石灰化に及ぼす影響につき、SS-OCTを用いて評価した。牛歯エナメル質を所定の期間人工脱灰液に浸漬し、POs-CaならびにPOs-Ca+F液で4〜14日間再石灰化を行った。これら一連の操作毎に、SS-OCTにて同試料の断層画像を取得した。その後、試片を薄切研磨し、ナノインデンテーション法より脱灰深さとナノ硬さにつき評価した。人工脱灰エナメル質のSS-OCT画像では、脱灰層を輝度の上昇として識別することができ、その深さは再石灰化期間が長くなると浅く変化していた。OCT減衰係数変化から得られたパラメーターとエナメル質の硬さとの強い相関関係が明らかになった。そのOCT画像処理方法は臨床的にエナメル質脱灰および再石灰の定量的評価に用いることが可能と考えられた。

2）研究のイラストレーション

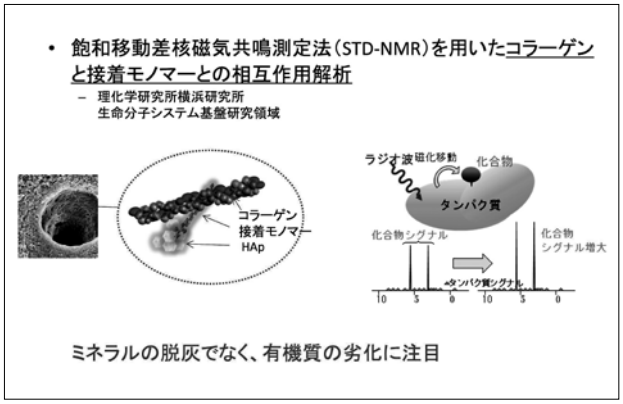

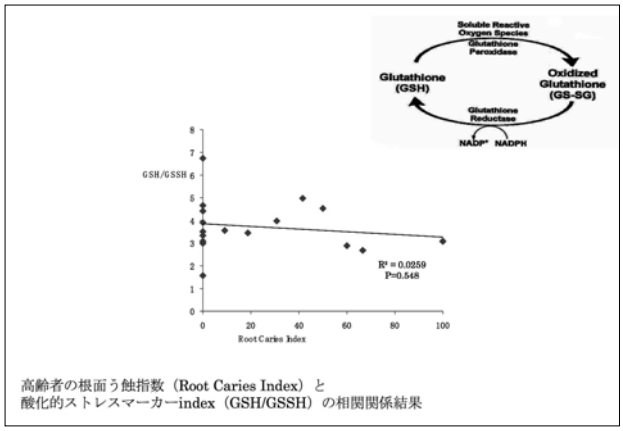

高齢者の根面う蝕指数（Root Caries Index）と
酸化的ストレスマーカーindex（GSH/GSSH）の相関関係結果

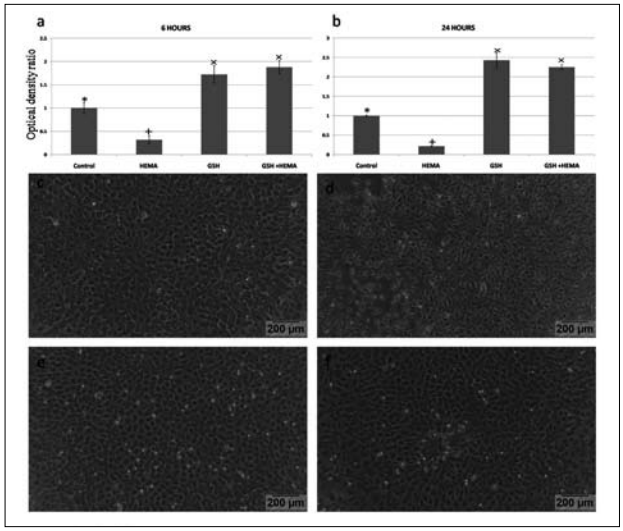

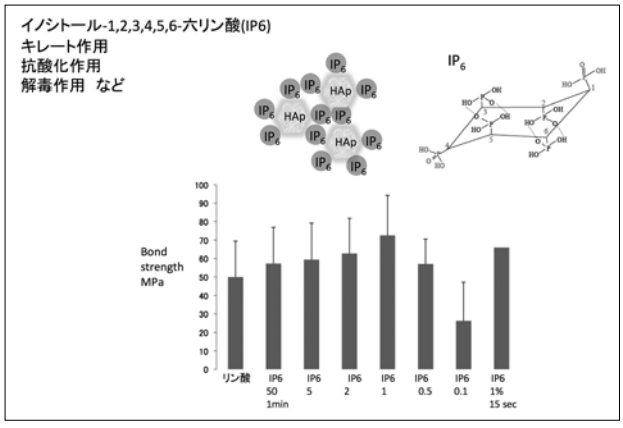

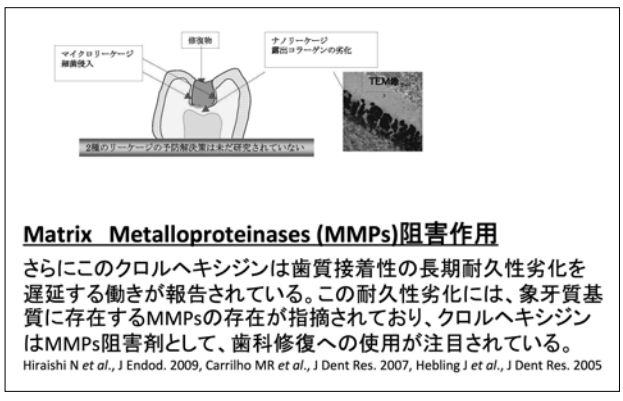

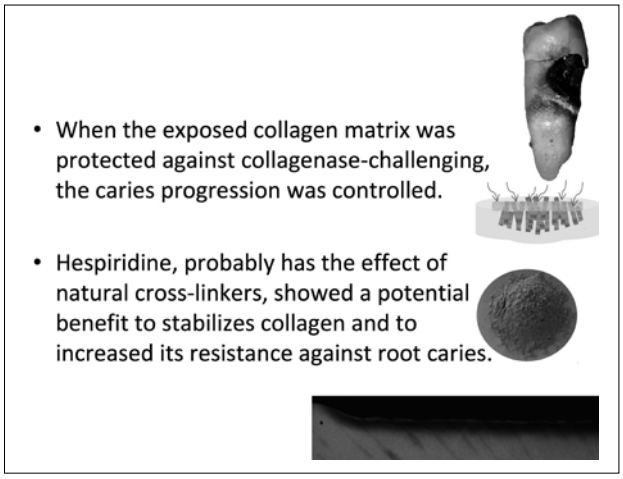

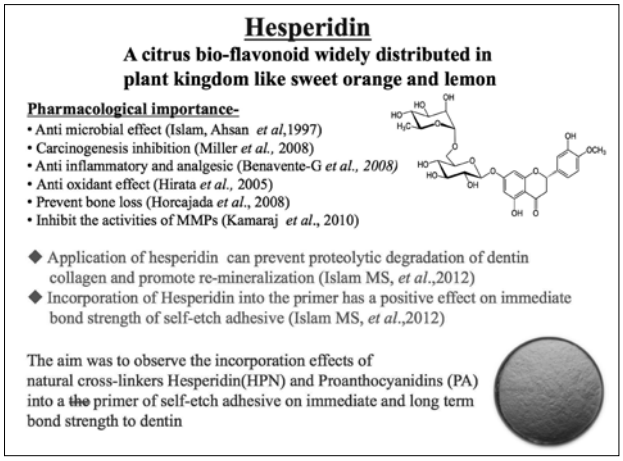

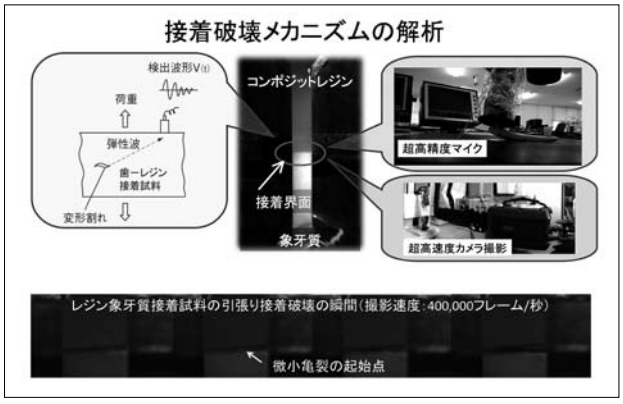

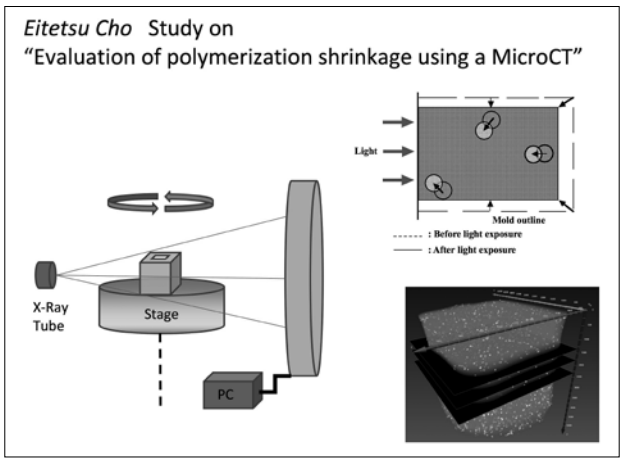

3）発表の研究内容についての英文要約

Effect of 405nm diode laser on tooth bleaching with visible-light activating titanium dioxide photocatalyst

Visible light activating titanium dioxide photocatalyst (VL-TiO2) may improve efficacy of hydrogen peroxide (H2O2) bleaching agents used in dentistry while contributing to their safety by lowering the required concentration of peroxide. The objective of this study was to evaluate the effects of a 405 nm diode laser on bleaching reaction of H2O2 and VL-TiO2 on methylene blue (MB) dye. The experimental solution was prepared with H2O2, VL-TiO2, MB and pure water. The final concentration of H2O2 was 3.5% and that of MB was 10 ppm. The experimental solution of 3 ml in a quartz cell was irradiated by a 405 nm diode laser with various powers, duty cycles and pulse durations for 7 min. In all irradiation conditions, the increase in laser irradiation time gradually decreased the MB concentration. Irradiation by higher output power showed more reduction of MB concentration. Pulse durations as short as 5 ms with duty cycle reduced to 25% did not affect the degree of the reduction in MB concentration compared to continuous wave irradiation at the same average output power. It was concluded that using 405 nm diode laser, the bleaching effects of VL-TiO2

depended on the irradiation time and the average output power, regardless of pulse duration or duty cycle.

Study on Super tooth

Dentin bonding systems have been dramatically simplified and improved during therecent decades. Monomer penetration into dentin and its polymerization in situ creates a hybridlayer, which is essential to obtain good bonding to dentin. Moreover, the presence of an acid—baseresistant zone below the hybrid layer has been documented with self-etching adhesive systems inan artificial secondary caries attack. When ultrastructure of the acid—base resistant zone isassessed by SEM and TEM observations, formation of the acid—base resistant zone is considered tobe due to the monomer penetration potential and fluoride release in the adhesive systems.Natural dentin has a limited potential to resist an acid attack of secondary caries; however, theacid—base resistant zone does not purely consist of dentin in morphology, it is rather acombination of dentin and the adjacent hybrid layer. Therefore, the reinforced dentin has beencalled ‘‘Super Dentin’’ bearing the ability to prevent primary and secondary caries. Prospectively,the great potential of adhesive technology in creation of the ‘‘Super Dentin’’ would lead to thedevelopment of new materials for mechanical, chemical and biological protection of the dentalstructures.

Study on dental coating materials

It has been proposed that a resin coating can serve as a means to protect dentalstructure after preparation of the tooth for indirect restorations, sealing the exposed dentin.The resin coating is applied on the cut surfaces immediately after tooth preparation andbefore making an impression by assembling a dentin bonding system and a flowablecomposite. Resin coatings minimize pulp irritation and improve the bond strength betweena resin cement and tooth when bonding the restoration to tooth. Recently, thin-film coatingdental materials based on all-in-one adhesive technology were introduced for resin coatingof indirect restorations. The thin coating materials are applied in a single clinical step andcreate a barrier-like film layer on the prepared dentin. The thin coatings play an importantrole in protecting the dentin from physical, chemical, and biological irritation. In addition,these thin-film coating materials reportedly prevent marginal leakage beneath inlays orcrown restorations. In light of the many benefits provided by such a protective layer, theseall-in-one adhesive materials may therefore also have the potential to cover exposed rootdentin surfaces and prevent caries formation.

Micro CT measurement of de/re-mineralization to tooth structures

Transverse microradiography（TMR）is consideredas the gold standard technique for the evaluation ofenamel lesions. Micro-computed tomography（μCT）has the advantage of non-destructive measurements,but the beam-hardening effect withpolychromatic x-rays is a major drawback. To date,no study has validated μCT against TMR. Theobjective of this study was to validate μCT measurementsof enamel lesions under various x-rayconditions and software beam-hardening correction（BHC）against TMR. Human molars with naturalwhite-spot lesions were scanned for 5 min by μCTat 100 kV in different conditions: 50 μA（0.5-mm Alfilter）, 165 μA（0.5-mm Al/0.3-mm Cu）, and 200 μA（0.5-mm Al/0.4-mm Cu）, with or without BHC.Grayscale values were converted into mineral densityvalues using phantoms. Thin sections at thesame positions were then prepared for TMR. Lesiondepth（LD; μm）and mineral loss（ΔZ; vol%μm）were compared between μCT and TMR by Pearson' scorrelations. μCT measurements correlated wellwith TMR under all conditions（$p < 0.001$, $r > 0.86$for LD and ΔZ）, except for 0.5-mm Al without BHC（$p > 0.05$）. Even without BHC, combined Al/Cufilters successfully reduced the beam-hardeningeffect. μCT can be used as a non-destructive alternativeto TMR with comparable parameters for thestudy of enamel lesions.

Color matching of resin composite restoration

This study is focused on light transmission properties of resin composite for improvement of color matching of resin composite restoration. Resin composite showed that there was significant correlation between the diffused light transmission property and translucency. Additionally, resin composite placed in layers exhibited reduced straight-line lighttransmission and increased diffusion transmission compared with bulk-filled resin composite. The layering technique and/or higher light diffusion property of resin composite would producesuperiorcolor rendition in resincompositerestoration with shallow cavity. Resin composite restored in the human tooth cavities produced the color shiftingof resin composite and tooth at the border. For deep cavity, resin composites with higherdiffused light transmission property showed higher color shifting at the border, while forshallow cavity, the straight-line as well as diffused light transmission of resin compositeaffected the color shifting at the border. Clinically, diffused light transmission propertyof resin composites may contribute to the color shifting at the border of resin compositerestoration regardless of cavity depth, resulting in better color matching.

Effect of remaining dentin thickness on bond strength of various adhesive systems to dentin

The aim of this study was to evaluate the effect of remaining dentin thickness（RDT）on resin composite

bond strength to dentin surfaces when using various adhesive systems. One of three adhesives, Clearfil SE Bond, Single Bond or Clearfil Tri-S Bond, followed by Z100 resin composite were built up on flat dentin surfaces of human molars. The teeth were sectioned obtaining beams with cross-sectional areas of approximately 1 mm2. RDT was measured and microtensile bond strength was determined. Resulting data were categorized into four groups: RDT<2 mm; 2≤RDT<3 mm; 3≤RDT<4 mm; RDT≥ 4 mm. Clearfil SE Bond showed a correlation between μTBS and RDT. Single Bond showed no significant difference in μTBS for any RDT. The bond strength of resin composite to the different RDT flat dentin surfaces was affected by the adhesive system used.

3D evaluation of composite resin restoration at practical training using swept-source optical coherence tomography (SS-OCT)

Internal adaptation of restorations to the cavity wall is one of the important topics in clinical dentistry, and necessary to be stressed at dental education. In this study, swept-source optical coherence tomography (SS-OCT) was used for detection of marginal and internal defects in the composite resin restorations as an educational device for undergraduate dental students. Class 1 and Class 2 composite restorations to melamine resin molar tooth were assigned to the students and prepared by the students during the skill test, and SS-OCT imaging was performed to evaluate students' works. SS-OCT could detect the internal gaps and voids within the restorations in tomography images synthesized based on the backscatter signal from within the restoration. It is suggested that the SS-OCT is a promising diagnostic modality, as well as an educational tool for the detection of internal gaps in adhesive restorations. The internal adaptation of composite resin restorations of melamine resin teeth performed by undergraduate students could be evaluated on tomograms using SS-OCT. The imaging modality enabling quick and non-invasive observation and evaluation of restorations is beneficial in educational settings, since importance of filling manipulations in composite resin restoration can be indicated at the practical training.

Diagnosis of proximal caries using swept-source optical coherence tomography (SS-OCT) in vivo

The aim of this study was to determine the diagnostic accuracy of swept-source optical coherent tomography (SS-OCT) in detecting and estimating the depth of proximal caries in posterior teeth in vivo. SS-OCT images and bitewing radiographs were obtained form 70 proximal surfaces of 53 patients. Six examiners scored the locations according to a caries lesion depth scale (0-4) using SS-OCT and the radiographs. The results were compared with clinical observations obtained after the treatment. SS-OCT could detect the presence of proximal caries in tomograms that were synthesizedbased on the backscattered signal. SS-OCT showed significantly higher sensitivity and Az values of ROC analysis than radiographs for the detection of cavitated enamel lesions and dentin caries (Student's t-test, $p < 0.05$). SS-OCT appears to be a more reliable and accurate method than bitewing radiographs for the detection and estimation of the depth of proximal lesions in the clinical environment.

Effects of a chewing gum containing phosphoryl oligosaccharides of calcium (POs-Ca) and fluoride on remineralization

The aim of thisstudy was to assess the effect of a chewing gum containing phosphoryl oligosaccharides of calcium (POs-Ca) and fluoride on remineralization of enamel subsurface lesions, in a double-blind, randomized controlled in situ trial. 36 volunteer subjects wore removable buccal appliances with three different insets of bovine enamel with subsurface demineralized lesions. For 14 days, the subjects chewed one of the three chewing gums (placebo, POs-Ca, POs-Ca+F), three times a day. After each treatment period, the insets were subjected to laboratory tests; mineral level determined by transverse microradiography (TMR), hydroxyapatite (HAp) crystallites assessed by synchrotron radiation wide-angle X-ray diffraction, nanoindentation hardness and fluoride ion mapping by time-of-flight secondary ion mass spectrometry. Addition of POs-Ca to the chewing gum resulted in significant remineralization of enamel subsurface lesions. Although POs-Ca+F gum was not superior in TMR recovery rate when compared with POs-Ca gum, other results highlighted the importance of fluoride ion bioavailability in formation of HAp crystallites and reinforcement of enamel subsurface lesions in situ.

Reinforcement of adhesive interface using a CaCl2/ fluoride-incorporated bonding system on artificial caries affected dentin model

Intrafibrillar and interfibrillar remineralization starting from the base of the demineralized dentin can be achieved via the slow release of calcium ions from set Portland cement. Also, adding calcium chloride to this cement significantly improved sealing ability and marginal adaptation. In addition, μTBS using 2-step adhesive systems has revealed relatively reduction when applied to caries affected dentin compared to etch-and-rinse, but the etch dentin surface is over-dried or over-wet, the collagen matrix collapses and prevents effective infiltration of the primer, thereby resulting in low bond strengths and excessive microleakage though. Fluoride adhesive systems have also improved bond strength because of fluoride ions released and penetration

into dentin and creation of good chemical union and apatite crystals formation. To evaluate the effect of calcium chloride added to a primer in a 2-step fluoride releasing bonding system on the bond strength to caries affected dentin and to determine remineralization of demineralized dentin using SEM/TEM observation. It is expected to be found an improvement on bond strength using this primer with calcium and fluoride bonding, and future observation of remineralization formation in caries affected dentin, which will have an important significance in durability and success of the restorations.

Evaluation of resin composite polymerization by three dimensional micro-CT imaging

Light-cured composites undergo shrinkage during polymerization. The aim of this study was to evaluate regional shrinkage within a light-cured composite during polymerization by microcomputed tomography and mechanical properties by nanoindentation in bonded or non-bonded class-I cavity.The magnitude and direction of regional polymerization shrinkage depends on boundary conditions, depth and conversion degree. Polymerization shrinkage effect is most significant at the deepest part of the cavity. The application of micro-CT combined with sophisticated image analysis is a novel approach to investigate shrinkage mechanisms of dental composites.

The analysis of failure mechanics of adhesive interface

The purpose of this study is to analyze the failure mechanics of adhesive interface using visual methods and gain further information about the response of dentin adhesive interfaces to load. The microscopic video rate recording produced a wealth of additional information regarding the nature and complexity of interfacial failures. In the results, the propagation of the crack along the interface in real time was observed. The dynamic pattern and the site of failure were found to be dependent on variations such as bonding systems. The valuable information may aid the selection of adhesive for a given clinical situation and the development of new adhesives.

The Effect of water sorption of composite resins on color changes

The purpose of our study was to evaluate the shade changes of resin composites after immersion in staining solutions. Methods: Disks of three resin composites made by same brands (Estelite Sigma Quick (SQ), Estelite Flow Quick (FQ), Estelite Flow Quick - High Flow (HF); Tokuyama) of A2 shade were prepared with 2.0 mm thicknesses and were final polished with 280-, 600-, 2000-grit SiC paper. Their color was measured after specimen preparation and after 1-day immersion in staining solutions on black and white backings according to the CIELAB color scale on a spectrophotometer, and color difference (ΔE^*) between bulk-filled and layered specimens were calculated. The data were statistically analyzed using two-way ANOVA and t-test with Bonferroni test for multiple comparisons. The ΔE^* value of HF was statistically lower than that of SQ in all polishing groups.On the other hand, the polishing method did not statistically affect ΔE^* valuesin each materials. ΔE^* values of resin composite. The water sorption value of HF was significant lower than SQ and FQ after 24 hrs water-strorage. There were visible shade changes ($\Delta E^* > 2.5$) in all resin composite after 1-day immersion in staining solution. The condition of final polish did not affect ΔE^* values and there were significant difference betweem SQ and HF.

Contemporary adhesives: marginal adaptation and microtensile bond strength of class II composite

The marginal adaptation (in terms of % continuous margin) and microtensile bond strength (μTBS) of the enamel and dentin of direct class II composite restorations were evaluated. 32 class II cavities were prepared with one proximal box limited within the enamel and one proximal box extending into the dentin. The teeth (n=8/group) were restored with: Adper Scotchbond Multi Purpose (SMPP), Adper Scotchbond 1 XT (S1XT), Clearfil SE Bond (CSEB), or Clearfil Tri-S Bond (CTSB) and incrementally placed composite restorations. Marginal adaptation was evaluated by SEM. The teeth were sectioned and trimmed to obtain specimens for μTBS testing.All adhesive systems exhibited continuous margins with enamel of over 95.4%, whereas continuous margins with dentin ranged from 60.2 to 84.8%. The mean μ TBSs [MPa] for enamel were 40.5 (SMPP), 37.3 (S1XT), 30.8 (CSEB) and 23.2 (CTSB), and for dentin, they were 37.7 (SMPP), 33.0 (S1XT), 37.3 (CSEB) and 29.0 (CTSB).The self-etch adhesive systems showed excellent marginal adaptation to dentin. SMPP provided the highest bond strength to both enamel and dentin, whereas CSEB was the most predictable adhesive for dentin and an acceptable adhesive for enamel.

Title: Change of dentin permeability in different storage media after resin coating

To evaluate the effects of the resin coating strategy and the storage media on change of dentin permeability. Thirty-six dentin disks were prepared from bovine incisors. They were divided into the following three groups: dentin surface was left uncoated (control), coated with an adhesive (Clearfil SE Bond; SE), and coated with a combination of an adhesive (SE) and a flowable composite (Clearfil Protect Liner F; PLF) (SE+PLF). Furthermore, the specimens were divided into two sub-groups according to the storage media: deionized water and artificial saliva.

The reduction rates of dentin permeability were measured using a fluid filtration system working under liquid pressure of 6.9 KPa after the immersion periods of 1 day, 1 month and 3 months.In the control groups, the dentin permeability of the specimens stored in artificial saliva was significantly reduced after 1 month ($p<0.05$), while the dentin permeability of the specimens stored in deionized water was unstable. The resin coating groups of SE and SE+PLF had a significant effect on the reduction of dentin permeability in both deionized water and artificial saliva for each storage period ($p<0.05$). However, the reduction rates of dentin permeability tended to decrease over storage time.

Non-destructive quantitative analyses of de/remineralization using micro-computed tomography (μCT)

Micro-computed tomography (μCT) has the advantage of non-destructive measurements, but beam-hardening effect with polychromatic X-rays is a major drawback. No study to date has validated μCT against TMR; the objective was to validate μCT measurements of enamel lesions under various X-ray conditions and software beam-hardening correction (BHC) against TMR. Human molars with natural white-spot lesions were scanned for 5 min by μCT at 100 kV with different conditions; 50 μA (0.5-mm Al filter), 165 μA (0.5-mm Al/0.3-mm Cu) and 200 μA (0.5-mm Al/0.4-mm Cu) with or without BHC. Grayscale values were converted into Mineral density values using phantoms. Thin sections at the same positions were then prepared for TMR. Lesion depth (LD; μm) and mineral loss (ΔZ; vol%μm) were compared between μCT and TMR by Pearson's correlations. μCT measurements correlated well with TMR under all conditions ($p < 0.001$, $r > 0.86$ for LD and ΔZ), except for 0.5-mm Al without BHC ($p > 0.05$). Even without BHC, combined Al/Cu filters successfully reduced beam-hardening effect; μCT can be used as a non-destructive alternative of TMR with comparable parameters for study on enamel lesions.

Identification of several subpopulations ofDCs in rodent dental pulp

Dendritic cells (DCs) are abundantly found in the tissues of the front line of defense, such as skin and mucosa, and are essential immunocompetent cells in innate and adaptive immunity. DCs are separated into several subpopulations depending on their surface markers, and each subpopulation is believed to have distinct functions. In the dental pulp, presence of DCs was reported, but their functional evaluation has not been performed. Here, we report the localization of several populations of DCs in rodent dental pulp with slight inflammation. $CD11c^+$DCs/macrophages were localized in the pulp-dentin border of the central pulp beneath the dental fissure and the pulp horn of treated cusp. $CD103^+$ cells were detected in the perivascular region of the inner pulp. $CD207^+$ cells were not observed in the dental pulp, however they were present in the oral mucosa (data not shown). $F4/80^+$ cells with dendritic morphology were distributed in the perivascular region of the inner pulp, the subodontoblastic layer and the pulp-dentin border of the pulp horn of treated cusp. Several subpopulations of DCs exist in the rodent dental pulp, and progress of pulplal inflammation may be regulated by these DCs.

Influence of casein as a model of salivary proteins on tooth de-/remineralization, acid enamel erosion and apatite growth (calculus formation)

It is known that salivary proteins have significant influence on tooth de-/remineralization. However, little attention has been paid to the influence in in vitro study. The main reasons are as follows: difficulties to collect fresh saliva and less repeatability of experimental data due to denaturationduring the experiment, leading to serious differences in in vitro (without saliva) and in vivo experiments.

In such backgrounds, we had interest in milk casein as a model salivary protein of Proline-Rich Protein that has been demonstrated to have significant influence on tooth de-/remineralization, and to be regarded as the main constituent of pellicle. We prepared artificial saliva solutions which contained calcium and phosphate with different concentrations of casein, then examined the influence of casein on ①enamel/dentin de-/remineralization (caries progress) ②apatite growth and its deposition on tooth surface (calculus formation) ③acid erosion. Through thesestudies, we intend to approach the real mechanisms occurring in oral cavity, and establish a standard experimental protocol for these study topics above. Moreover we wish to develop more effective and clinically applicable technologies for the prevention.

Age related changes in saliva and their effect on root caries

The objectives were as follows: To compare salivary factors: (saliva flow rate [SFR], pH, buffering capacity, collagenase type-1, Calcium [Ca], matrix metalloproteinase-8 [MMP-8], α´-amylase, tissue inhibitor of metalloproteinase-1 [TIMP-1], reduced-glutathione/oxidized-glutathione [GSH:GSSG]) and oral-hygiene factors (oral-hygiene index [OHI-S], calculus index [CI-S], debris index [DI-S]) between elderly and young adults and to detect any correlation between salivary factors, root caries index (RCI) and DMFT index. Elderly patients showed statistically significant higher DMFT, collagenase and MMP-8 values when compared to young adults ($p<0.05$). Younger patients showed statistically significant higher SFR and Ca values when compared to elderly ($p<0.05$). There was no statistical difference

between the two age groups regarding pH, buffering capacity, ά-amylase, TIMP-1 and GSH:GSSG ($p>0.05$). A significant positive correlation was found between DMFT and collagenase ($p<0.05$, $R^2=0.469$), DMFT and MMP-8 ($p<0.05$, $R^2=0.162$), ά-amylase and Ca ($p<0.05$, $R^2=0.313$), collagenase and MMP-8 ($p<0.05$, $R^2=0.174$), ά-amylase and TIMP-1 ($p<0.05$, $R^2=0.369$) while a significant negative correlation between SFR and collagenase was detected ($p<0.05$, $R^2=0.239$). The positive correlation between ά-amylase and Ca can be explained by Ca stabilization effect on amylase. A positive correlation was found between DMFT, collagenase and MMP-8; however this correlation was not observed with RCI which reflects the multifactorial etiology of root caries.

Reduced glutathione detoxification of 2-hydroxyethylmethacrylate and its effect on resin-dentin bond strength

This study evaluated the influence of reduced glutathione (GSH) application on HEMA cytotoxicity on rat pulpal cells, and evaluated the effect of etched-dentin treatment with GSH on the immediate microtensile bond strength (μTBS) of etch-and-rinse adhesive. The cytotoxicity of HEMA (10 mM), GSH (10 mM) or GSH with HEMA (10 mM each) was compared (6 hours and 24 hours) using a transwell insert model, followed by morphological observation of cells. Etched dentin surfaces were rinsed and treated with one of the following solutions: 2% GSH, 5% GSH or 10% GSH, bonded with Adper Single Bond Plus (3M, ESPE) and restored with resin composite. After 1 day of water-storage at 37 °C, the specimens were subjected to μTBS testing. There were statistically significant differences among the groups. HEMA elicited remarkable toxic effect, while GSH protected the cells from HEMA-induced damage. Pretreatment with 5% GSH significantly increased the immediate μTBS, while 10% GSH had a negative effect, and 2% had no significant difference from the control group. Conclusions: GSH had a protective effect against HEMA cytotoxicity and had a positive influence on μTBS at controlled concentrations.

In Vitro Evaluation of Hesperidin to Preserve Dentin Collagen

This study was aimed to investigated the effect of various plant-derived agents (hesperidin, proanthocyanidin, epigallocatechin gallate and genipin) on the stability of dentin collagen matrix to resist collagenase degradation. The dentin specimens were treated with 0.5 % test solution and subjected to ultimate tensile strength (UTS) and swelling ratio measurements. Demineralized human dentin powder was incubated with 0.02 %, 0.1 % and 0.5 % of each test agent and followed by bacterial collagenase digestion. The extent of collagen degradation was investigated using hydroxyproline assay. The UTS and swelling ratio measurements revealed that the mechanical property of dentin was improved by the use of these natural agents (Figure 1). The greatest reduction in collagen degradation was shown following the use of hesperidin, proanthocyanidin, and epigallocatechin gallate at 0.5% (Figure 2). The use of hesperidin, proanthocyanidin, and epigallocatechin gallate could improve the mechanical properties of collagen and resist enzymatic degradation, leading to functional repair of pathological dentin lesion.

Effect of hesperidin incorporation in a self-etching primer on dentin adhesive

Degradation of collagen at resin-dentin interface deteriorates durable composite restorations. This study was attempted to evaluate the immediate and long term effect of natural cross-likers incorporation into a primer of a self-etch adhesive on the micro tensile bond strength (μTBS) to dentin. Citrus fruits derived hesperidin (HPN) 0.5 to 5 wt% or grape seed derived proanthocyanidin (PA) 0.5wt% was incorporated into the Clearfil SE primer (Kuraray Noritake Dental Inc.. I beam restored specimens were further sub-divided for immediate (one day) and long term (one year storage in artificial saliva) tensile bond strength test and nano-indentation measurement of resin-dentin interface. The immediate μTBS significantly increased with HPN 0.5% (87.6 ± 8.9 MPa), HPN 1.0% (88.1 ± 10.1 MPa) and HPN 2.0% (89.7 ± 9.9 MPa) when compared with the control (77.4 ± 8.8 MPa). The long term μTBS was significantly higher with 1%HPN (70.3 ± 10.8 MPa) and 2%HPN (76.8 ± 10.2 MPa), when compared with the control (63.9 ± 10.1 MPa). The mechanical properties of bonded interface were improved with the use of HPN-in primers. The PA group failed to improve the μTBS and the mechanical properties. Incorporation of HPN into the self-etching primer had the positive effect on μTBS and mechanical properties of resin-dentin interface, which improved the long term bond durability.

Mussel-mimetic bio-adhesive polymers: the alternative to petroleum adhesives

The glue secreted by marine mussels bind strongly to virtually all inorganic and organic surfaces in aqueous environments, where conventional adhesives perform poorly. Kakeno et al. has applied the properties of mussel adhesive in synthetic mimics from plant-derived sources as 3,4-dihydroxycinnamic acid (caffeic acid; DHCA) and 4-hydroxycinnamic acid (p-coumaric acid; 4HCA) to synthesize poly- (DHCA-co-4HCA) by transesterification technique (Polymer Journal, 2011). This novel copolymer was found to show strong adhesive characteristics, which were equivalent to conventional superglues from petroleum resources. This strong adhesive action was due

to interactions between catechol groups present at the end of the polymer terminal chains and the substrate-surfaces. Further development has been made to produce another synthesis from 3,4-Dihydroxyhydrocinnamic acid (DHHCA) and 3- (3-Hydroxyphenyl) propionic acid (3HPPA), poly-(DHHCA-co-3HPPA) (Figure 1). In this preliminary study, we report the adhesion principle of novel plant-derived adhesives and their adhesive characteristics.

Nanoindentation hardness of resin-dentin interface of a new composite system

The study aimed to investigate the nanoindentation hardness of the interfacial resin layer using a new composite system in comparison to conventional light-cured all-in-one adhesive systems. The system is different from other composite systems in that the interfacial layer (primer) is not light cured upon application, but is activated in contact with the initiator- containing flowable composite.
Dentin surface of disks cut from human teeth were polished and treated by one of the materials in the study. After 24 hours of storage in water at 37° C the specimens were sectioned through the interface by a low speed diamond saw. The resin-dentin interface was fine-polished by diamond slurry and the hardness of interfacial resin layer was measured at 15 points in the middle of adhesive layer under a maximum force of 2 mN in a nanoindentation device (ENT-1100a, Elionix). The use of the newly developed dentin primer in combination with low-viscosity resin resulted in effective polymerization and hardness of the resin at the interfacial area, which was comparable or superior to conventional all-in-one adhesives, while saving clinical time. A better copolymerization between composite and the interfacial resin is achieved with no need for an oxygen inhibition-mediated reaction.

Protection of Enamel against Demineralization by Resin Coating Evaluated under OCT

New resin materials have been developed using advanced organic-inorganic biomaterial technology that have the potential to protect enamel as a thin coat. The aim of this work is to investigate the durability of enamel coating materials and their protective effects against subsurface demineralization using Optical Coherence Tomography (OCT). Resin-embedded tooth blocks are assigned to four different groups, in which enamel surface was partly covered by each of the four resin-based coating materials. Swept Source OCT at 1319 nm-wavelength was used to obtain cross-sectional images of the coated enamel before and after thermal aging. Then the specimens were subjected to OCT imaging after acid challenge for up to two weeks in a demineralization solution with the uncoated enamel surface serving as control. Coating layer film thickness differed among materials. All coats remained on the enamel surface after the thermal-cycling challenge. Nevertheless, their interfacial integrity was affected occasionally microgaps appeared as shown by OCT images. All coatings effectively prevented demineralization of the enamel, with no underneath lesion being detected by OCT. A sealed enamel surface by thin resin coatings containing active ingredients such as fluoride will remarkably contribute to the protection of smooth enamel surface from erosive acid challenge.

Effect of resin coating on sealing of indirect composite inlays using SS-OCT

The aim of this study is to use swept-source optical coherence tomography (SS-OCT) to investigate the effect of resin coating technique on the adaptation of indirect composite inlays luted with resin cements and to confirm the results with conventional microscopy. Round class-I cavities were prepared on flat occlusal surfaces of human third molars divided into three groups according to the resin cement used. Each group was divided into two subgroups, an experimental group that received resin coating and a control group without the resin coating. In the resin coated group, the cavity surface was prepared using a two-step self-etching system and low viscosity microfilled resin. Indirect composite inlays were cemented to the cavities using one of the resin cements. 3D optical evaluation of the restoration interface was conducted using SS-OCT on all groups. The optical sealing was affected by both the material and resin coating, and the interaction was also significant ($p<0.05$). Resin coating using a bonding agent and flowable composite benefits the adaptation of indirect restorations to dentin surface which is a key interface within a restoration. SS-OCT is a quick 3D imaging technique to study the interface without the difficulties of common leakage tests.

Remineralization of Enamel subsurface lesion by POs-Ca and POs-Ca+F in vitro: evaluation by SS-OCT

Early enamel lesions can be reverted if there are sufficient bioavailable calcium and phosphate in a buffered oral environment. The aim of this study was to characterize the changes of subsurface demineralized enamel lesions subjected to POs-Ca and POs-Ca+F solutions in vitro by SS-OCT. Blocks of bovine anterior teeth imbedded in resin cube were demineralized, and then subjected to POs-Ca and POs-Ca+F solution for up to 14 days. OCT images were recorded using SS-OCT in all groups. Then, the specimens were cross-sectioned, fine polished and subjected to nanoindentation. On SS-OCT images in demineralized area, reflectivity from superficial enamel increased and lesions appeared to be brighter than sound enamel. A boundary was observed suggesting the lesion front; which corresponded to the lesion depth. Both POs-Ca and POs-

Ca+F resulted in decreased reflectivity, suggesting mineral deposition and recovery through the lesion. There was a strong correlation between the OCT signal attenuation parameter and enamel lesion hardness for all groups. SS-OCT images demonstrated a potential for monitoring demineralization and remineralization and lesion depth measurements of early enamel lesions, paving the way for clinical use of this modality for monitoring of enamel white spots.

4）本事業に関連して世界的な研究拠点形成に向けて、以下の点で改善・整備等されたこと

A（研究拠点体制）

ペンシルバニア大学歯学部（米国）、ジョージア医科大学歯学部（米国）、UCSF（米国）、大学カンピナス大学歯学部（ブラジル）、アレキサンドリア大学歯学部（エジプト）、テヘラン大学歯学部（イラン）、King's College of London 歯学部（英国）、ミュンヘン大学歯学部（ドイツ）、モンペリエ大学歯学部（フランス）、ゲント大学歯学部（ベルギー）、ブルノ大学歯学部（チェコ共和国）、国際カトリック大学（スペイン）、グラナダ大学歯学部（スペイン）、マヒドン大学歯学部（タイ）、チュラロンコン大学歯学部（タイ）、チェンマイ大学歯学部（タイ）、シドニー大学歯学部（オーストラリア）、メルボルン大学歯学部（オーストラリア）、香港大学歯学部（中国）、北京大学歯学部（中国）、首都医科大学歯学部（中国）、延世大学歯学部（韓国）、鶴見大学歯学部（日本）、岡山大学歯学部（日本）、東北大学工学部（日本）との間で外国人研究者の受入れ、共同研究の継続および新たな立ち上げを行った。

内外の歯科器材メーカー12社（クラレ・ノリタケデンタル、GC、トクヤマデンタル、パナソニック電工、松風、サンメディカル、ニシカ、パナソニックヘルスケア、東洋水産、3M、デンツプライ、GSK）と、共同研究、器材の共同開発のための企画の立ち上げ、情報交換のための会議を行った。

B（研究教育環境）

各種研究設備の整備のため、獲得した外部資金や企業との委託研究による資金を充てた。分野内で調達できないものについては学外の施設の利用を推進した。特にOCTの実用化に向けて、試作機を導入して臨床評価を行った。また新技術を導入したOCT試作機の改良型を導入した。

各研究プロジェクトごとに、それぞれ年4-6回程度の成果報告会を行い、情報の共有、学生の教育を推進した。

C（人材確保）

外部資金により複数の特任教員を雇用し、特に歯の脱灰と再石灰化に関する研究と、抗MMP物質の根面う蝕の抑制効果に関する研究に取り組む学生の指導の強化および研究の推進を図った。さらに外国人研究者も多く受け入れて、大学院生や若手教員と共同で研究をおこなわせることで、相互の能力開発を図った。

D（人材育成）

多くの学生を国際学会に派遣して研究発表させて、諸外国の研究者と討論させる機会を提供した。各研究グループと定期的なミーティングを行い、研究内容に関する議論の場を多く持つよう心掛けた。学会発表に際しては、すべての演者にリハーサルを義務付けて、分野の教員、学生全員により、プレゼンテーションの内容、形式についての改善を行った。学生及び若手教員が内外の学会で学術賞を受賞した。

E（国際化）

国際学会だけでなく、海外での臨床家向けのプログラムにおいても講演を積極的に行い、現在臨床に携わる歯科医師にも当教室の研究成果を普及し、新たな留学生確保のための情報提供も行った。大学院生の約40%が留学生という状況を最近5年間維持している。東アジア、東南アジアだけでなく、中東からの学生も増加し、新たな国際ネットワーク形成が確立しつつある。特に母国政府の奨学金を受給する学生の受け入れが進んでいる。大学院向けの講義は長年英語で行ってきており、外国人留学生、研究者が活動しやすい環境を整備している。米国の臨床家向けのUSCの卒後研修プログラムで、分野の若手教員が講演の機会を得て、本プログラムの成果を普及することができた。

教室のホームページによる情報発信に際し、英語のページも充実させるとともに、最新情報を提供するように心がけた結果、国内外から多くのアクセスを得た。

5）GCOE事業を推進するに当たって力を入れた点

- 外部資金は決して十分とはいえないが、複数の特任教員を雇用して、これまでに十分な研究指導、推進ができなかった領域をカバーした。
- 分野内の打ち合わせは日本語と英語の併用、研究打ち合わせは英語を主体におこない、留学生や外国人研究者が積極的に参加できるようにした。
- 国際学会での研究発表の機会を多く提供できるよう、外部資金の獲得に努めている。

・研究拠点としてのアピールのため、臨床的なテーマのプログラムにおいても多くの講演、研究発表を行い、研究成果の臨床への貢献をアピールするよう心掛けた。

6）英文原著論文

1. ◎Bakhsh TA, Sadr A, Shimada Y, Mandurah M, Hariri I, AlsayedEZ, Tagami J, Sumi Y. Concurrent evaluation of composite internal adaptation and bond strength in a class-I cavity. J Dent（in press）.
2. Carvalho AO, Oliveira MT, Nikaido T, Tagami J, Giannini M.　Effect of adhesive system and application strategy on reduction of dentin permeability.Braz Oral Res 26（5）: 397-403, 2012
3. ◎Gando I, Ariyoshi M, Ikeda M, Sadr A, Nikaido T, Tagami J. Resistance of dentin coating materials against abrasion by toothbrush. Dent Mater J（in press）.
4. ◎Hamba H, Nikaido T, Sadr A, Nakashima S, Tagami J. Enamel Lesion Parameter Correlations between Polychromatic Micro-CT and TMR. J Dent Res 91（6）: 586-591, 2012.
5. ◎Hariri I, Sadr A, Nakashima S, Shimada Y, Tagami J, Sumi Y. Estimation of enamel and dentin mineral content from refractive index. Caries Res（in press）.
6. ◎Hariri I, Sadr A, Shimada Y, Tagami J, Sumi Y. Effects of structural orientation of enamel and dentin on light attenuation and local refractive index: an optical coherence tomography study. J Dent 40（5）: 387-96, 2012.
7. ◎Horie K,Nakajima M,Hosaka K, Kainose K, Tanaka A, Foxton RM, Tagami J. Influence of composite-composite join on light transmission characteristics of layered resin composite. Dent Mater 28（2）: 204-211, 2012.
8. ◎Ichikawa C, Nikaido T, Inoue G, Sadr A, Tagami J. Ultra-morphologies of the dentin acid-base resistant zone of two-step self-etching systems after long-term storage in water. J Adhes Dent 14（3）: 207-213, 2012.
9. ◎Imai K, Shimada Y, Sadr A, Tagami J, Sumi Y. Noninvasive cross-sectional visualization of enamel cracks by optical coherence tomography. J Endod 38（9）: 1269-1274, 2012.
10. ◎Islam S, Hiraishi N, Nassar M, Yiu C, Otsuki M, Tagami J.Effect of natural cross-linkers incorporation in a self-etching primer on dentine bond strength. J Dent 40（12）: 1052-1059,2012.
11. ◎Islam SM, Hiraishi N, Nassar M, Sono R, Otsuki M, Takatsura T, Yiu C, Tagami J. In vitro effect of hesperidin on root dentin collagen and de/re-mineralization.
    Dent Mater J 31（3）: 362-367, 2012.
12. ◎Jamleh A, Sadr A, Nomura N, Yahata Y, Ebihara A, Hanawa T, Tagami J, Suda H. Nano-indentationtesting of new and fractured nickel-titanium endodontic instruments. Int Endod J 45（5）: 462-468, 2012.
13. ◎Kitasako Y, Sadr A, Hamba H, Ikeda M, Tagami J. Gum containing calcium-fluoride reinforces enamel subsurface lesion in situ. J Dent Res 91（4）: 370-375, 2012.
14. ◎Kuribayashi M, Kitasako Y, Matin K, Sadr A, Shida K, Tagami J. Intraoral pH measurement of carious lesions with qPCR of cariogenic bacteria to differentiate caries activity. J Dent 40（3）: 222-228, 2012.
15. Li N, Nikaido T, Sadr A, Takagaki T, Chen JH, Tagami J. PhosphoricAcid-Etching Promotes BondStrength and Formation of Acid-Base Resistant Zone on Enamel. Oper Dent（in press）.
16. ◎Moosavi H, Hariri I, Sadr A, Thitthaweerat S, Tagami J. Effects of curing mode and moisture on nanoindentation mechanical properties and bonding of a self-adhesive resin cement to pulp chamber floor. Dent Mater（in press）.
17. ◎Mori F, Hiraishi N, Otsuki M, Tagami J.　Effect of mastication on flow and properties of saliva. Asian Pac J Dent 12（1）: 1-5, 2012.
18. ◎Nakagawa H, Sadr A, Shimada Y, Tagami J, Sumi Y. Validation of swept source optical coherent tomography（SS-OCT）for the diagnosis of smooth surface caries in vitro. J Dent（in press）.
19. Nakajima Y, Shimada Y, Miyashin M, Takagi Y, Tagami J, Sumi Y. Noninvasive cross-sectional imaging of incomplete crown fractures（cracks）using swept-source optical coherence tomography. Int Endod J 45（10）: 933-941, 2012.
20. ◎Nakata K, Nikaido T, Nakashima S, Nango N, Tagami J. An approach to normalizing micro-CT depth profiles of mineral density for monitoring enamel remineralization progress. Dent Mater J 31（4）: 533–540, 2012.
21. ◎Nazari A, Sadr A, Saghiri MA, Campillo-Funollet M, Hamba H, Shimada Y, Tagami J, Sumi Y. Non-destructive characterization of voids in six flowable composites using swept-source optical coherence tomography. Dent Mater（in press）.
22. ◎Nazari A, Shimada Y, Sadr A, Tagami J.Pre-etching vs. grinding in promotion of adhesion to intact enamel using self-etch adhesives. Dent Mater J 31（3）: 394-400 2012.
23. ◎Nazari A, Sadr A, Campillo-Funoller M, Nakashima S, Shimada Y, Tagami J, Sumi Y.Effect of hydration on assessment of early enamel lesion using swept-source optical coherence tomography. J Biophotonics（in press）.
24. ◎Nazari A, Sadr A, Shimada Y, Tagami J, Sumi Y. 3D assessment of void and gap formation in flowable resin composites using optical coherence tomography. J Adhes Dent（in press）.

25. ◎Nurrohman H, Nikaido T, Takagaki T, Sadr A, Ichinose S, Tagami J. Apatitecrystal protection against acid-attack beneath resin-dentin interface with fouradhesives: TEM and crystallography evidence. Dent Mater 28（7）: e89-98, 2012.
26. ◎Nurrohman H, Nikaido T, Takagaki T, Sadr A, Waidyasekera K, Kitayama S, Ikeda M, Tagami J.Dentin bonding performance and ability of four MMA-based adhesiveresins to prevent demineralization along the hybrid layer. J Adhes Dent. 14（4）: 339-348, 2012.
27. Oyanagi T, Tagami J, Matin K. Potentials of mouthwashes in disinfecting cariogenic bacteria and biofilms leading to inhibition of caries. Open Dent J 6: 23-30, 2012
28. ◎Prasansuttiporn T,Nakajima M, Foxton RM, Tagami J. Scrubbing effect of self-etching adhesives on bond strength to NaOCl-treated dentin. J Adhes Dent 14（2）: 121-127, 2012
29. ◎Shimada Y, Sadr A, Nazari A, Nakagawa H, Otsuki M, Tagami J, Sumi Y. 3D evaluation of composite resin restoration at practical training using swept-source optical coherence tomography（SS-OCT）. Dent Mater J 31（3）: 409-417, 2012.
30. ◎Takahashi R, Nikaido T, Tagami J, Hickel R, Kunzelmann KH. Contemporary adhesives: marginal adaptation and microtensile bond strength of class II composite restorations. Am J Dent 25（3）:181-188, 2012.
31. ◎Tano E, Otsuki M, Kato J, Sadr A, Ikeda M, Tagami J.　Effects of 405nm Diode Laser on Titanium Oxide Bleaching Activation. Photomed Laser Surg 30（11）: 648-54, 2012.
32. ◎Thanatvarakorn O, Nakashima S, Sadr A, Prasansuttiporn T, Ikeda M, Tagami J. In vitro evaluation of dentinal hydroraulic conductance and tubule sealing by a novel calcium-phosphate desensitizer. J Biomed Mater Res Part B（in press）.
33. ◎Thitthaweerat S, Nakajima M, Foxton RM, Tagami J. Effect of waiting interval in chemical activation mode of one-step dual-cure adhesives on bonding to root canal dentine. J Dent 40（12）: 1109-1118, 2012
34. ◎Tsubone M, Nakajima M,Hosaka K, Foxton RM, Tagami J. Color shifting effect at the border of resin composite restorations in human teeth. Dent Mater 28（8）: 811-817, 2012.
35. ◎Yahagi C, Takagaki T, Sadr A, Ikeda M, Nikaido T, Tagami J. Effect of liningwith a flowablecomposite on internal adaptation of direct composite restorationsusing all-in-one adhesive systems. Dent Mater J. 31（3）: 481-488, 2012.
36. Yiu CK, Hiraishi N, Tay FR, King NM. Effect of chlorhexidine incorporation into dental adhesive resin on durability of resin-dentin bond. J Adhes Dent 14（4）: 355-362, 2012.
37. ◎Yoshikawa T, Wattanawongpitak N, Cho E, Tagami J.Effect of remaining dentin thickness on bond strength of various adhesive systems to dentin. Dental Mater J 31（6）: 1-6, 2012.

7）総説ならびに著書

[総説]

（英文）

Nikaido T, Takahashi R, Ariyoshi M, Sadr A, Tagami J. Protection and reinforcement of tooth structures by dental coating materials. Coatings 2: 210-220, 2012

[著書]

（英文）

Bakhsh TA, Sadr A, Shimada Y, Khunkar S, Tagami J, Sumi Y. Relationship between non-destructive OCT evaluation of resins composites and bond strength in a cavity. Proceedings of SPIE 8208: 91（8）, 2012.

Sadr A, Mandurah M, Nakashima S, Shimada Y, Kitasako Y, Tagami J, Sumi Y. Monitoring of enamel lesion remineralization by optical coherence tomography: An alternative approach towards signal analysis. Proceedings of SPIE（in press）.

（和文）

田上順次、宮崎真至、松本勝利.コンポジットレジン修復の Art & Imagination 臨床に必須の知識と技術. 日本歯科評論 別冊. p 216. 2012年

加藤純二、金子潤、大槻昌幸、守矢佳世子. これで納得! デンタルホワイトニング. p 145、2012年

8）学会発表（英文）

1. ◎Baksh TA, Sadr A, Shimada Y, Mandurah M, Takagaki T, Tagami J. Ultrastructural assessment of tooth-resin interface using FIB-TEM technique. 90th IADR, Oral, Iguaçu Falls, Brazil, June 20-23, 2012.
2. ◎Gando I, Ariyoshi M, Nikaido T, Ikeda M, Sadr A, Tagami J. Wear resistance of surface coating materials by toothbrushing abrasion. 90th IADR, Oral, Iguaçu falls, Brazil, June 20-23, 2012.
3. ◎Hosaka K, Nakajima M, Takahashi M, Thitthaweerat S, Otsuki M, Tagami J. Effect of Dentin Surface Moisture on mTBS of Solvent-free 1-SEA. 90th IADR, Oral, Iguaçu Falls, Brazil, June 20-23, 2012.
4. ◎Inoue G, Kirihara M, Tagami J. Long-term effects of F-Ca-P containing solution on morphology and μTBS.

90th IADR, Poster, Iguaçu Falls, Brazil, June 20-23, 2012.

5. ◎Kirihara M, Inoue G, Nikaido T, Ikeda M, Alireza Sadr, Tagami J. Relationship between F-release and morphology of acid-base resistant zones. 90th IADR, Iguaçu Falls, Brazil, June 20-23, 2012.
6. ◎Takahashi M, Wiboonpin T, Hosaka K, Nakajima M, Tagami J. Color Changes of Resin Composite after Immersion in Staining Solutions. 90th IADR, Oral, Iguaçu Falls, Brazil, June 20-23, 2012.
7. Mayoral JR, Flores H, Sadr A, Shimada Y, Sumi Y, Roig M, Krejci I, Giner L, Tagami J. SS-OCT Real-time monitoring of resin composite placement by layering technique. 90th IADR, Poster, Iguaçu Falls, Brazil, June 20-23, 2012.
8. ◎Makishi P,Shimada Y, Sadr A, Bakhsh Ta, Hariri I, Tagami J, Sumi Y. Evaluation of Resin-Cements Marginal Adaptation to Class-V Cavity Using SS-OCT. 90th IADR, Oral, Iguaçu Falls, Brazil, June 20-23, 2012.
9. Nikaido T, Nurrohman H, Waidyasekera K, Takagaki T, Sadr A, Tagami J. Nanoleakage expression in hybrid layer and acid-base resistant zone. 90th IADR, Oral, Iguaçu Falls, Brazil, June 20-23, 2012.
10. ◎Takagaki T, Nikaido T, Sadr A, Tagami J　Raman Microscopic Analysis of ABRZ Using Different Functional Monomers. 90th IADR, Oral, Iguaçu Falls, Brazil, June 20-23, 2012.
11. ◎Mandurah M, Sadr A, Kitasako Y, Nakashima S, Shimada Y, Tagami J, Sumi Y, Tanaka T: Remineralization of enamel subsurface lesion by POs-Ca and POs-Ca+F: Evaluation by Nanoindentation and SS-OCT. 136th Japanese Society of Conservative Dentistry, Oral, Ginowan City, Okinawa, June 28-29, 2012.
12. ◎Baksh TA, Sadr A, Shimada Turkistani A, Tagami J, Sumi Y. Optical evaluation of composite adaptation in Class-II cavity　restoration using SS-OCT. 136th The Japanese Society of Conservative Dentistry, Oral, Ginowan City, Okinawa, June 28-29, 2012.
13. ◎Turkistani A, Sadr A, Shimada, Mandurah M, Tagami J, Sumi Y. Effact of Resin Coating on Sealing of Indirect Composite Inlays Using SS-OCT. Oral, 136th Japanese Society of Conservative Dentistry, Oral, Ginowan City, Okinawa, June 28-29, 2012.
14. Bista B, Nazari A, Shimada Y, Sadr A, Tagami J, Sumi Y. Evaluation of Current One-step Self-etch Adhesives using Optical Coherence Tomography. 12th Biennial Meeting of Asian Academy of Aesthetic Dentistry and 23rd congress of Japan Academy of Aesthetic Dentistry, Oral, Sapporo, July 20 -22, 2012.
15. ◎Kalyan K, Otsuki M, Tano E, Kato J, Shinoki T, Tagami J. Effect of Wavelength and Output Power of Lasers on Bleaching with Hydrogen Peroxide and Titanium Dioxide Photocatalyst. 12th Biennial Meeting of Asian Academy of Aesthetic Dentistry and 23rd congress of Japan Academy of Aesthetic Dentistry, Poster, Sapporo, July 20 -22, 2012.
16. Otsuki M, Tagami J. Comparison of various fluorescence-detecting oral cameras. 1st International Conference on Fluorescence based diagnostic of Oral Diseases, Oral, Montpellier, September 20-21, 2012.
17. ◎Islam MD, Hiraishi N, Nassar, Otsuki M, Tagami J. Effect of Cross-linker on resin-dentin Bond Strength of Self-etching Adhesive. SEA ADE 23rd Annual Scientific Meeting, Oral, Honk kong, November 2-4, 2012.
18. ◎Hiraishi N, Kaneko D, Taira S, Islam MS,Otsuki M,Tagami J. Mussel-mimetic bio-adhesive polymers: the alternative to petroleum adhesives. 137th The Japanese Society of Conservative Dentistry, Oral, Hiroshima, November 22-23, 2012.
19. ◎Islam MS,Hiraishi N, Otsuki M, Tagami J. In Vitro Evaluation of Plant-derived Agents to Preserve Dentin Collagen. 137th The Japanese Society of Conservative Dentistry, Poster, Hiroshima, November 22-23, 2012.
20. ◎Kalyan K, Kusanagai A, Otsuki M, Tagami J. Effect of different LED lights on bleaching with hydrogen peroxide and titanium dioxide photocatalyst. 137th The Japanese Society of Conservative Dentistry, Poster, Hiroshima, November 22-23, 2012.
21. ◎Nassar M, Hiraishi N, Islam MS, Otsuki M,Tagami J. Age-related Changes in Saliva and their Effect on Root Caries. 137th The Japanese Society of Conservative Dentistry, Poster, Hiroshima, November 22-23, 2012.
22. ◎Qiao H, Takahashi R, Nakashima S, Nikaido T, Tagami J. Change of dentin permeability in different storage media after resin coating. 137th The Japanese Society of Conservative Dentistry, Oral, Hiroshima, November 22-23, 2012.
23. ◎Romero Maria Jacinta R.H, Nakashima S, NIkaido T, Sadr A, Tagami J. Effect of casein as a model of salivary protein on hydroxyapatite growth in vitro. 137th The Japanese Society of Conservative Dentistry, Oral, Hiroshima, November 22-23, 2012.
24. ◎Shimada Y, Nakagawa H, Sadr A, Wada I, Nakajima M, Nikaido T, Otsuki M, Tagami J, Sumi Y. Non-invasive cross-sectional imaging of proximal caries using swept-source optical coherence tomography (SS-OCT) in vivo. 137th The Japanese Society of Conservative Dentistry, Oral, Hiroshima, November 22-23, 2012.
25. ◎Nassar M, Hiraishi N, Otsuki M,Tagami J, Aizawa M. The influence of Inositol Phosphate (IP6) Used as Etchant on Resin-Dentin Bond Strength. 31st The Japan Society of Adhesive Dentistry, Oral, Tokyo, December 8-9, 2012.
26. ◎Sadr A, Mandurah M, Shimada Y, Tagami J, Sumi Y. Monitoring of Enamel Lesion Remineralization by Optical Coherence Tomography: An Alternative Approach towards Signal Analysis. Lasers in

DentistryXIX, SPIE Photonics West, Oral, San Francisco, USA, February 2-7, 2013.

9）学会発表（和文）

1. 太嶋恵美,半場秀典,矢作智花,二階堂徹,田上順次. フッ化物含有コート材の象牙質における根面う蝕の抑制効果について. 第136回日本歯科保存学会春季学術大会、宜野湾市、沖縄、2012年6月28、29日
2. 田中　梓、中島正俊、田上順次.コンポジットレジン修復物のカメレオン効果に及ぼす歯牙の加齢変化による影響について.第136日本歯科保存学会春季学術大会、宜野湾市、沖縄、2012年6月28、29日
3. 中嶋省志, 二階堂徹, 清水明彦, 田上順次. カリオテスター^{TM}を用いた根面う蝕の脱灰程度の評価についてのインビトロ研究-TMR法による評価との比較. 第136回日本歯科保存学会春季学術大会、宜野湾市、沖縄、2012年6月28、29日
4. 松井七生子、髙垣智博、二階堂徹、池田正臣、田上順次. 2ステップセルフエッチングシステムにおけるボンド中の機能性モノマーの役割　第136回日本歯科保存学会春季学術大会、宜野湾市、沖縄、2012年6月28、29日
5. 和田郁美、島田康史、中嶋省志、サダルアリレザ、田上順次.非う蝕性歯頸部欠損のSS-OCTによる断層画像観察.第136回日本歯科保存学会春季学術大会、口頭、宜野湾市、沖縄、2012年6月28、29日
6. 關奈央子、二階堂徹、森尾郁子、田上順次. 歯学科四年次保存修復学基礎実習における留学生サブインストラクターの評価と意義. 第31回日本歯科医学教育学会、岡山、2012年7月21日
7. 荒牧音、ビンガレアル、大野建州、張晨陽、田上順次、東みゆき.咬頭切削後の所属リンパ節における歯髄から遊走する樹状細胞の解析.第54回歯科基礎医学会学術大会、郡山、2012年9月14～16日
8. 吉川孝子、趙永哲、田上順次. コンポジットレジンの窩底部重合促進効果について. 第60回日本歯科理工学会学術講演会、福岡、2012年10月13、14日
9. 鵜鷹佐知子、中嶋省志、二階堂徹、池田正臣、清水明彦、田上順次. 各種フッ化物塗布による脱灰象牙質の再石灰化促進効果 –TMRとカリオテスターTMによるインビトロ評価–　第137回日本歯科保存学会秋季学術大会、広島、2012年11月22、23日
10. 菅原豊太郎、中嶋省志、清水明彦、田上順次、桃井保子. フッ化物塗布はウシ歯根象牙質の脱灰を抑制した. 第137回日本歯科保存学会秋季学術大会、広島、2012年11月22、23日
11. 關奈央子、森尾郁子、山口陽子、田上順次. 歯学部における英語教育の必要性について. 第77回、口腔病学会学術大会、東京、2012年11月30日、12月1日
12. サダルアリレザ、アルセイイハブザキ、田上順次. ナノインデンテーションによる新しいコンポジットレジン修復システム象牙質界面層の硬さ. 第31回日本接着歯学会学術大会、東京、2012年12月8、9日
13. 平石典子、金子大作、平　修、大槻昌幸、田上順次. ポリフェノール類由来カテコール性接着剤樹脂の接着歯学への実用化. 第31回日本接着歯学会学術大会、東京、2012年12月8、9日

10）受賞

1. 日本歯科審美学会優秀発表賞　大槻昌幸
2. 第5回日本歯科理工学会IADR-DMGC-J記念賞　高垣智博

11）外部資金の獲得状況

受託研究

研究題目：口腔内エナメル質初期う蝕に対するフッ化物配合ガムの再石灰化効果
代表：田上順次
期間：平成24年～平成27年
研究費総額：150万円（間接経費を含む）

受託研究

研究題目：機能水による口腔洗浄技術に関する研究（機能水による口腔洗浄効果の検証）
代表：田上順次
期間：平成24年11月～平成25年3月
研究費総額：100万円

委託研究

研究題目：口腔内プローブを用いた光干渉断層計（OCT）の臨床応用
代表：田上順次
期間：平成22年～平成25年
研究費総額：150万円

委託研究

研究題目：近赤外光・レーザーを用いた新たな歯科疾患診断・治療用機器の開発に関する研究
代表：田上順次
期間：平成22年～平成24年
研究費総額：500万円

科学研究費補助金、基盤B
研究題目：光干渉断層計の歯冠修復領域への応用
代表：田上順次
期間：平成23年～25年
研究費総額：832万円

受託研究
研究題目：リン酸化オリゴ糖カルシウムの歯の再石灰化効果に関する研究
代表：田上順次
期間：平成20年～平成24年
研究費総額：1454万円

科学研究費補助金、挑戦的萌芽
研究題目：コラーゲンの高分子修飾と高密度石灰化ハイブリッドSuper Dentinの誘導形成
代表：田上順次
期間：平成23年～平成24年
研究費総額：106万円

科学研究費補助金、基盤C
研究題目：歯の漂白の評価のための変色歯モデルと評価システムの開発
代表：大槻昌幸
期間：平成21～平成24年
研究費総額：405万円

科学研究費補助金、基盤C
研究題目：象牙質接着界面に生成したう蝕抵抗層（ABRZA）とナノリーケージとの関係
代表：二階堂徹
期間：平成21年～平成24年
研究費総額：455万円

科学研究費補助金、基盤C
研究題目：レジン修復物の重合収縮応力緩和と接着性能同時向上効果を有する臨床技法の開発
代表：吉川孝子
期間：平成22年～平成24年
研究費総額：325万円

科学研究費補助金、基盤C
研究題目：Hidden cariesの非侵襲トモグラフィーを用いた3D評価
代表：島田康史
期間：平成24年～平成26年
研究費総額：546万円

科学研究費補助金、若手研究B
研究題目：アシッドベースレジスタントゾーンの精査と改質・スーパートゥースの構築
代表：井上剛
期間：平成22年～25年
研究費総額：300万円

科学研究費補助金、若手研究B
研究題目：マイクロCTによる光重合型コンポジットレジンの重合収縮挙動の観察の研究
代表：趙永哲
期間：平成23年～平成25年
研究費総額：182万円

科学研究費補助金、若手研究B
研究題目：接着破壊メカニズムの3次元動的解析-疎水性接着システム開発への応用-
代表：保坂啓一
期間：平成23年～平成25年
研究費総額：382万円

科学研究費補助金、若手研究B
研究題目：FIB-TEMを用いたエナメル質接着界面のナノレベル解析
代表：高垣智博
期間：平成24年～平成26年
研究費総額：429万

科学研究費補助金、若手研究B
研究題目：OCTを用いたコンポジットレジンの3次元及びリアルタイムの評価
代表：サダル　アリレザ
期間：平成24年～平成26年
研究費総額：377万

科学研究費補助金、基盤C
代表：平石典子
期間：平成22年～平成25年
研究費総額：380万円

12）特別講演、招待講演、シンポジウム

1. 田上順次.The 34th Annual Scientific Conference on Dental Research and Continuing Education「New era of adhesive dentistry: Self etching creates the super dentin基調講演. ホーチミン医科薬科大学歯学部、2012年4月7日
2. 田上順次.「New concept of dentin bonding and application OCT to operative dentistry」講演. 北京医学大学口腔学院、2012年4月14日
3. 田上順次.「Application of Swept Optical Coherent Tomography to dental clinic and research」講演.日中歯科医学大会、四川大学華西口腔医学院、2012年

4月27日
4. 田上順次.東京医科歯科大学歯科同窓会主催実習コース、「セラミックを超えたコンポジットレジンテクニック」講演、東京医科歯科大学、平成24年5月20日
5. Sadr A, Optical Coherence Tomography for Diagnosisand Monitoring of Caries Lesions, Faculty Development Program Invited Speaker, The University of British Columbia, May 23, 2012, Vancouver, Canada.
6. 田上順次.～これからの超高齢社会に向けて～「従来型修復治療から、新たな予防的修復治療への転換」(生涯歯を守り、長持ちさせるための提言).第30回日本顎咬合学会学術大会・総会のシンポジウムにて講演、東京国際フォーラム、平成24年6月10日
7. 田上順次.歯科用OCT装置の技術・研究打ち合わせ、「歯科医療、歯科産業の将来展望」講演、パナソニックヘルスケア株式会社、平成24年7月8 - 10日
8. 田上順次.機能性充填修復材料に関する製品評価会議、「GIOMER/MiCDミーティング」講演、株式会社松風研修センター4F、平成24年7月14日
9. 田上順次.「松風歯科クラブ臨床講座」講演、THE GRAND HALL、平成24年7月15日
10. 田上順次. Tri-University Consortium, Session 1, Current research status of the three universities「Promotion interdisciplinary international projects and educating research-oriented health care professionals」講演、Beijing Friendship Hotel、平成24年7月26 - 29日
11. Sadr A, Optical Coherence Tomography from Basic Research to Clinical Applications, Continuing Education Invited Speaker, University of Southern California, September 19, 2012, Los Angeles, USA.
12. 田上順次.「超高齢社会における歯の治療・管理と新しい修復治療」平塚市歯科医師会主催学術講演会、平塚市保健センター2階健康増進室、平成10月3日
13. 田上順次.「現代の虫歯事情とこれから注目されるであろう再石灰化ケアについて」講演、丸ビルホール&コンファレンススクエア、平成24年10月11日
14. 田上順次. 2012 International Quintessence Symposium (Sydney & Exhibition Centre)「Creating the "Super Tooth": New Concept of Bonding to Enamel & Dentin」講演. 平成24年10月18 - 22日
15. 田上順次. The new international course new materials and technologies in dental medicine「Scientific background of minimally invasive caries treatment」特別講義、マサリク大学医学部口腔科学科、平成24年10月29日 - 11月2日
16. Junji Tagami. New Era of Adhesive: Self Etching Technology Creates the "Super Dentin". Special lecture, Gent University, Gent, Belgium, Nov.15, 2012.
17. Junji Tagami. New Era of Adhesive: Self Etching Technology Creates the "Super Dentin". Special lecture, ACTA, Amsterdam, Netherland, Nov.16, 2012.
18. 田上順次　日本歯科保存学会秋季学術講演会　シンポジウムでの講演　「歯科用OCT画像診断」 広島国際会議場、広島市、2012年11月22日

13）主催学会

日本接着歯学会シンポジウム、2012年9月9日、東京医科歯科大学

14）教室、分野や講座の准教授、講師、助教、特別研究員、ポスドク、指導を受けた大学院生の名前

准教授	大槻　昌幸
准教授	佐々木　好幸
講師	二階堂　徹
	中島　正俊
助教	吉川　孝子
	島田　康史
	北迫　勇一
	岸川　隆蔵
	井上　剛
	趙　永哲
	保坂　啓一
	高垣　智博
	原田　直子

GCOE特任講師：Alireza SADR

特任講師	中嶋　省志
特任助教	平石　典子
大学院4年	今井　加奈子
	今村　友美
	鵜鷹　佐知子
	丸藤　伊織
	桐原　大
	栗林　恵美

坂野　若詠
美田　　瞳
Hamid NURROHMAN
Amir NAZARI
Taweesak PRASANSUTTIPORN
○Ilnaz HARIRI

大学院3年　Gerardo Jose Joves Mendez
田中　　梓
貝ノ瀬　公典
Mona Mohammad MANDURA
○Md. Sofiqul ISLAM
中川　寿一
Suppason THITTHAWEERAT
○Turki A BAKHSH

大学院2年　松井　七生子
和田　郁美
上杉　有美子
吉峰　斉昭
太嶋　恵美
永井　茂之
Mohannad NASSAR
Ornnicha　THANATVARAKORN
Haidil Akmal MAHDAN
○Ena LODHA
喬　　華

大学院1年　品川　淳一
小黒　玲奈
指宿　隆秀
会田　麻美
千葉　彩香
堀江　　圭
上野　智香
手塚　弘樹
佐藤　健人
佐藤　隆明
荒井　昌海
中村　真理愛
増子　律子
○Alaa TURKISTANI
Teerapong MAMANEE
Sahar Jameel KHUNKAR
○Ehab ALSAYAD
KONG Kalyan
Baba BISTA
Maria Jacinta Rosario Hernandez ROMERO
Zaher Bukhari
Patrycja Zakilina MAJKUT

RESEARCH REPORTS
Biomaterials & Bioengineering

Y. Kitasako[1,4], A. Sadr[2,4], H. Hamba[1,2], M. Ikeda[3], and J. Tagami[1,2]

[1]Cariology and Operative Dentistry, Department of Restorative Sciences, Graduate School of Medical and Dental Sciences, Tokyo Medical and Dental University, 5-45 Yushima 1-chome, Bunkyo-ku, Tokyo, Japan 113-8549; [2]Global Center of Excellence Program, International Research Center for Molecular Science in Tooth and Bone Diseases at Tokyo Medical and Dental University, Tokyo, Japan; [3]Clinical Oral Science, Department of Oral Health Care Sciences, Faculty of Dentistry, Tokyo Medical and Dental University, Bunkyo-ku, Tokyo, Japan; and [4]authors contributing equally to this work; *corresponding author, kitasako.ope@tmd.ac.jp

J Dent Res 91(4):370-375, 2012

Gum Containing Calcium Fluoride Reinforces Enamel Subsurface Lesions *in situ*

ABSTRACT

The aim of this study was to assess the effect of chewing gum containing phosphoryl oligosaccharides of calcium (POs-Ca) and a low concentration of fluoride (F) on the hardness of enamel subsurface lesions, utilizing a double-blind, randomized, and controlled *in situ* model. Fifteen individuals wore removable lingual appliances with 3 bovine-enamel insets containing subsurface demineralized lesions. Three times a day for 14 days, they chewed one of the 3 chewing gums (placebo, POs-Ca, POs-Ca+F). After the treatment period, cross-sectional mineral content, nanoindentation hardness, and fluoride ion mapping by time-of-flight secondary ion mass spectrometry (TOF-SIMS) were evaluated. Although there were no statistical differences in overall mineral content and hardness recovery rates between POs-Ca and POs-Ca+F subsurface lesions ($p > 0.05$), nanoindentation at 1-μm distance increments from the surface showed statistical differences in hardness recovery rate between POs-Ca and POs-Ca+F in the superficial 20-μm region ($p < 0.05$). Fluoride mapping revealed distribution of the ion up to 20 μm from the surface in the POs-Ca+F group. Nanoindentation and TOF-SIMS results highlighted the benefits of bioavailability of fluoride ion on reinforcement of the superficial zone of subsurface lesions *in situ* (NCT01377493).

KEY WORDS: chewing gum, enamel, remineralization, calcium, fluoride, hardness.

DOI: 10.1177/0022034512439716

Received November 5, 2011; Last revision January 26, 2012; Accepted January 28, 2012

INTRODUCTION

Sugar-free chewing gums may have an anticariogenic effect through the stimulation of saliva (Kandelman and Gagnon, 1990) and be an effective vehicle for bioavailable compounds such as calcium promoting enamel remineralization (Morgan *et al*., 2008). It has been suggested that low but slightly elevated levels of fluoride in saliva and plaque provided from drinking water and fluoride-containing products helped to prevent and reverse caries (Featherstone, 1999). Recently, manufacturers have been adding bioavailable calcium and fluoride in various forms to enhance the potential anticariogenic and remineralization potential of gums (Reynolds *et al*., 2003; Cai *et al.,* 2009; Cochrane *et al*., 2010; Kitasako *et al*., 2011; Shen *et al*., 2011).

In the studies focused on the beneficial effects of remineralizing agents, transverse microradiography (TMR) has been commonly performed to evaluate enamel mineral loss/gain through whole lesions (Featherstone and Zero, 1992; ten Cate *et al*., 1996). While useful for overall assessments, the x-ray-based technique may not provide information on any possible interactions between active ingredients and enamel structure. In contrast, depth-related properties of enamel subsurface lesions have also been described by microhardness (Featherstone *et al*., 1983; Kielbassa *et al*., 1999; Delbem *et al*., 2009). Some correlations have been described between microhardness and mineral content in demineralized lesions (Featherstone *et al*., 1983; Kielbassa *et al*., 1999); meanwhile, the trends may not be exactly the same in remineralization, depending on the composition of the minerals deposited and their crystalline structure (Kitasako *et al*., 2011).

Nanoindentation techniques have shown great utility for high-resolution profiling of local mechanical properties of biological samples such as enamel. Moreover, elemental analysis of the composition and/or the type of mineral at each lesion depth might be helpful to fully understand the remineralization process (Magalhães *et al*., 2009). Time-of-flight secondary ion mass spectrometery (TOF-SIMS) can measure tiny amounts of elements with small atomic sizes such as fluoride and has been recently used to investigate enamel caries lesions *in vitro* (Dickinson *et al*., 2007).

To date, no study has reported on the effect of chewing gum containing both calcium and fluoride on the hardness and fluoride distribution in enamel subsurface lesions *in situ*. The aim of this study was to examine cross-sectional nanoindentation hardness profiles at different structural levels of enamel subsurface lesions after chewing sugar-free gum containing bioavailable calcium and fluoride utilizing an *in situ* model. Fluoride ion mapping

was also performed at the superficial regions to aid our understanding of the role of fluoride added to the calcium-containing chewing gum. The null hypothesis tested was that there were no differences in the hardness of remineralized subsurface lesions with or without the addition of calcium and fluoride to the chewing gum.

MATERIALS & METHODS

Study Design and Protocol

This study was based on a double-blind, randomized, controlled *in situ* design with 3 sugar-free gums as described previously (Kitasako *et al.,* 2011). In brief, phosphoryl oligosaccharides of calcium (POs-Ca®; Ezaki Glico Co. Ltd., Osaka, Japan) is a form of soluble, bioavailable calcium produced by enzymatic hydrolyzation of potato starch (To-o *et al*., 2003), and added to a commercially available sugar-free gum. One of the gums was a sugar-free chewing gum without POs-Ca (placebo), and the other 2 contained 2.5 wt% POs-Ca or 2.5 wt% POs-Ca and 1.2% green tea extract containing 0.02 mg fluoride, namely, POs-Ca and POs-Ca+F.

Approval for this study was obtained from the Ethics Committee for Human Research at Tokyo Medical and Dental University. Fifteen healthy adults (eight males and seven females) were recruited (age 20-31 yrs) after informed consent was obtained. The volunteers were all residents of metropolitan Tokyo, where the tap water is not fluoridated (mean fluoride level: 0.07 ppm). The volunteers were examined to confirm that there was no current caries activity, periodontal condition, or any other oral disease, and that each individual had 22 or more permanent teeth. The volunteers were not taking any medication which could potentially influence their oral conditions. Health history questionnaires at baseline and health update questionnaires during the treatment periods were used to monitor the participants. They were randomly divided into three groups according to the crossover design.

Preparation of Enamel Subsurface Lesions

Enamel blocks (7 mm × 10 mm × 2 mm, width × length × depth) cut from the central part of bovine incisors were embedded in acrylic resin (Unifast Trad; GC, Tokyo, Japan). The outer enamel surface was polished, and one-third of the surface was covered with a nail varnish, to serve as the sound portion. Subsurface lesions were then formed on the remaining surface by the two-layer demineralization method, with 8% methylcellulose gel (Methocel MC; Fluka, Milwaukee, WI, USA) and 0.1 M lactate buffer (pH 4.6) at 37°C for 14 days (ten Cate *et al*., 1996). After demineralization, the blocks were sterilized by ethylene oxide gas sterilizer (Steri-Gas; 3M, Minneapolis, MN, USA). Another one-third of the surface was then covered by the nail varnish (demineralized; DEM), and the remaining exposed one-third of enamel surface served as the remineralization area (REM).

Intra-oral Appliances

Removable lower-buccal acrylic appliances housing the enamel blocks and covering premolars to molars were fabricated for each participant. Those wearing the appliances chewed 2 slabs of gum 3 times every day (at 8:00, 12:00, and 17:00) for 20 min each time. After chewing and before removing the intra-oral appliance, participants continued wearing the appliances for 20 additional min. They were asked to avoid eating, drinking, or brushing with the appliance inserted and to brush their teeth as usual 3 times a day with a non-fluoridated toothpaste. They were instructed to rinse the appliances briefly after removal with tap water and store them at 37°C in sealed and humidified containers until the next insertion. The treatment was performed in 3 periods of 2 wks each, during which the participants in each group received one of the gums randomly.

TMR (microradiography and microdensitometry)

Approximately 150-μm-thick sections were obtained from each block, and were microradiographed together with high-purity aluminum step wedges (12.5 μm × 21 steps) onto high-resolution plates (Konica Minolta Opto, Tokyo, Japan) by a Cu Kα x-ray generated at 20 kV and 20 mA for 13 min (PW-3830; Philips, Eindhoven, The Netherlands). The mineral profiles of DEM and REM areas were obtained from the digital images of the microradiographs, assuming 87 vol% as the maximum mineral content of enamel. Average mineral recovery rate was calculated from the ML (mineral loss or ΔZ) of DEM (ML_{DEM}) and REM (ML_{REM}) as follows: recovery rate (%R) = (ML_{DEM}–ML_{REM})/ML_{DEM} × 100.

Hardness Test

Sections from the same samples used for microradiography were embedded in epoxy resin (EpoxiCure; BUEHLER, Lake Bluff, IL, USA). To produce smooth cross-sectional surfaces suitable for nanoindentation, the surface on each sample was sequentially polished by silicon-carbide papers #600, #800, #1000, #1200, #1500, and #2000, followed by diamond slurries with particle sizes of 6 μm, 3 μm, 1 μm, 0.5 μm, and 0.25 μm, with a lapping machine (Maruto, Tokyo, Japan). Hardness profiles of the DEM and REM areas were measured with a nanoindentation device (ENT-1100a; Elionix, Tokyo, Japan) in two phases, namely, the whole lesion and the superficial zone. In the first phase, the hardness profile down to 150 μm below the enamel surface was assessed on all samples. A minimum of 160 indentations was performed along 16 lines, each with 10 points, across the polished cross-section, with a spacing of 10 μm between each 2 neighboring points. The first line of indentations was set within 10 μm from the enamel surface. In the second phase, the hardness profile of the superficial 20 μm was plotted for 5 samples in each group. For this purpose, 200 indentation points were programmed on 20 lines with 1 μm distance between each 2 adjacent lines in the axial direction and a lateral spacing of 10 μm between points. The first point was within resin approximately 2 μm above the visible enamel border. For all indentations, the maximum load was 2 mN at a loading rate of 0.2 mN/sec, with a Berkovich diamond tip. In total, over 20,000 indentations were performed. To calculate hardness (H) at each point, we divided the maximum load over the area projected under the load. In addition to the averaged hardness plot, mean hardness recovery rate (%) in each phase was also calculated as follows: recovery rate (%) = (H_{REM}–H_{DEM})/H_{DEM} × 100.

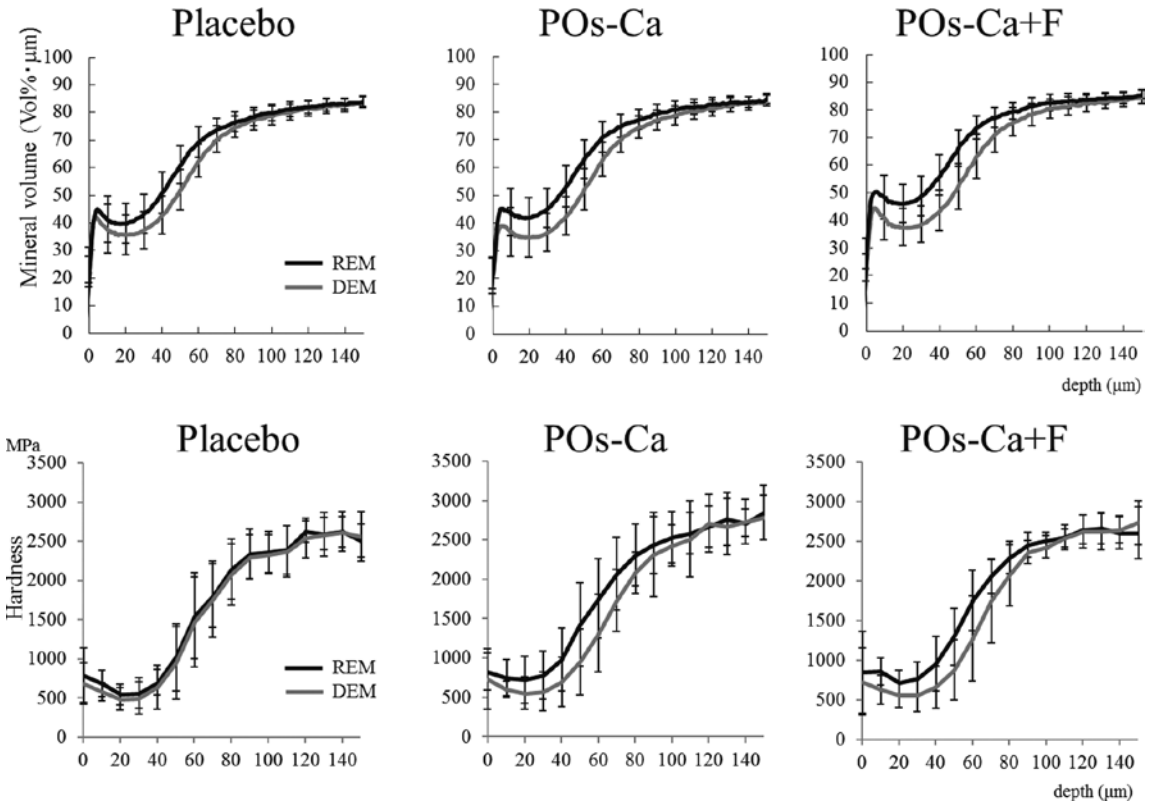

Figure 1. Mean TMR mineral content profiles (top) and hardness profiles (bottom) for 3 chewing gums. All gums resulted in some mineral gain. The hardness change for the placebo was not remarkable. DEM, demineralized area; REM, remineralized area.

TOF-SIMS

Analysis was performed with TOF-SIMS300 (ION-TOF, Münster, Germany) equipped with a pulsed Bi_3^{++} liquid ion gun operated at 25 kV. The system vacuum was held below 10^{-6} Pa throughout the measurements. The average primary ion current was 0.04 pA, and beam diameter was 0.2 to 0.3 μm in the burst alignment mode. Images were acquired in an area 100 μm × 100 μm with 256 × 256 pixel resolution. Fluoride mapping and profile were obtained from the top surface to 80 μm below the surface.

Statistical Analysis

Data were analyzed to determine normality. Mineral recovery rate and superficial hardness recovery were examined by *t* test with Bonferroni corrections. Overall hardness recovery rates were analyzed by Kruskal-Wallis test with Mann-Whitney U comparisons between each two groups. All statistical analyses were performed with SPSS software ($\alpha = 0.05$).

RESULTS

All participants completed the program without significant protocol violations or adverse events.

Mineral Content

Mean mineral density profiles of the DEM and REM areas in each gum are shown in Fig. 1, and recovery rates are presented in Fig. 2. POs-Ca and POs-Ca+F gums resulted in significantly greater mineral recovery rate than the placebo gum ($p < 0.05$), while there was no statistical difference between POs-Ca and POs-Ca+F ($p > 0.05$).

Nanoindentation Hardness

The mean hardness profiles of the DEM and REM in whole lesions are shown in Fig. 1, and those of the superficial zone are given in Fig. 3. REM showed remarkably improved hardness profiles compared with the corresponding DEM areas except for the placebo gum. Mean nanoindentation hardness recovery rates of the DEM and REM areas in each gum are shown in Fig. 2. The mean hardness recovery rates of both POs-Ca and POs-Ca+F gums in the whole lesions were significantly higher than that of the placebo ($p < 0.05$), while there were no significant differences between POs-Ca and POs-Ca+F gums ($p > 0.05$). However, in the superficial zone, there was a statistical difference in recovery rate among all 3 groups ($p < 0.05$).

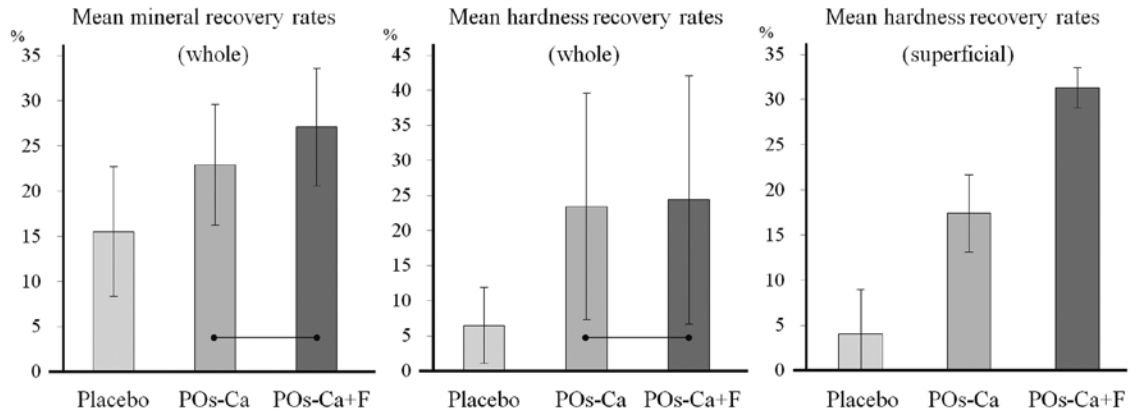

Figure 2. Mean mineral content recovery (%), hardness recovery (%) in whole lesions, and hardness recovery (%) in the superficial zone of 3 gums. In each graph, groups connected with a horizontal bar are not statistically significantly different ($p > 0.05$).

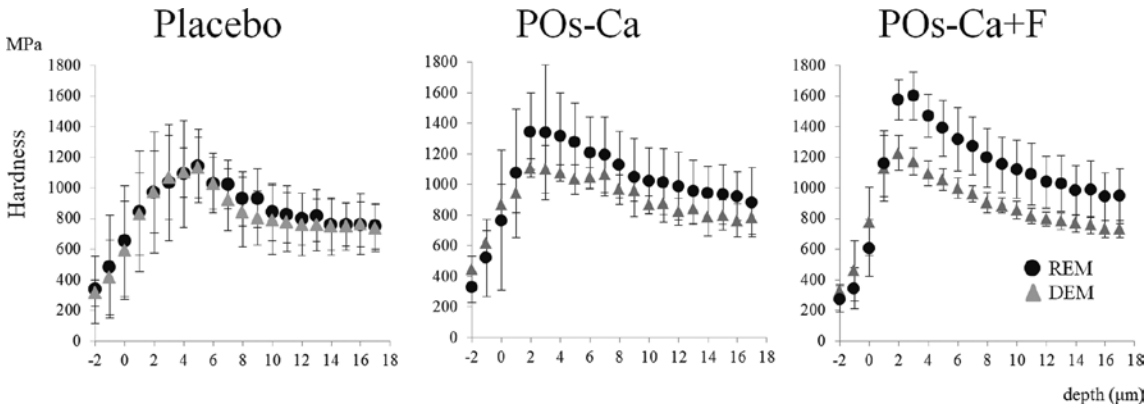

Figure 3. Mean hardness profiles of the 3 gums in the superficial zone of the lesion, starting from epoxy resin adjacent to the enamel surface. The placebo gum shows little improvement in hardness. DEM, demineralized area; REM, remineralized area.

TOF-SIMS Findings

Although fluoride was sparsely detected within the superficial lesion at the REM area of POs-Ca and the DEM area of POs-Ca+F, a high density of fluoride was detectable only within the REM area of POs-Ca+F (Fig. 4). Fluoride was detected up to approximately 20 μm from the surface at the REM area in POs-Ca+F.

DISCUSSION

The main finding in this study was that the bioavailable calcium (POs-Ca) effectively enhanced the hardness of demineralized enamel in the lesion body. Addition of a low level of fluoride to POs-Ca seemed to exert a synergistic effect through enhanced mineralization and hardness of the superficial zones.

The present report may be the first on the direct detection of cross-sectional changes in nanoindentation hardness and structural integrity at 1-μm-depth increments, and on fluoride distribution in the superficial zone of enamel remineralized by chewing gum containing calcium and fluoride in an *in situ* model. Nanoindentation hardness mapping with micrometer spacing between adjacent points increases data resolution; however, given the time required to perform each indentation, sensitivity of the test at a small load (2 mN), and the large amount of data produced, such a strategy is technically difficult for a large number of specimens. Considering these limitations, and taking into account the reproducibility of TMR and whole-lesion hardness data of the *in situ* cross-over design, 5 samples were subjected to the test for superficial hardness.

The testing of nanohardness at 1-μm-depth increments suggested that an enhanced reinforcement at the remineralized superficial lesions was induced by the chewing gum containing a low fluoride concentration. Moreover, the TOF-SIMS fluoride mapping and profile revealed that fluoride ion was detected up to 20 μm. It is noteworthy that the maximum levels of both superficial hardness and fluoride distribution were near the surface at approximately 2 μm depth. In line with this finding,

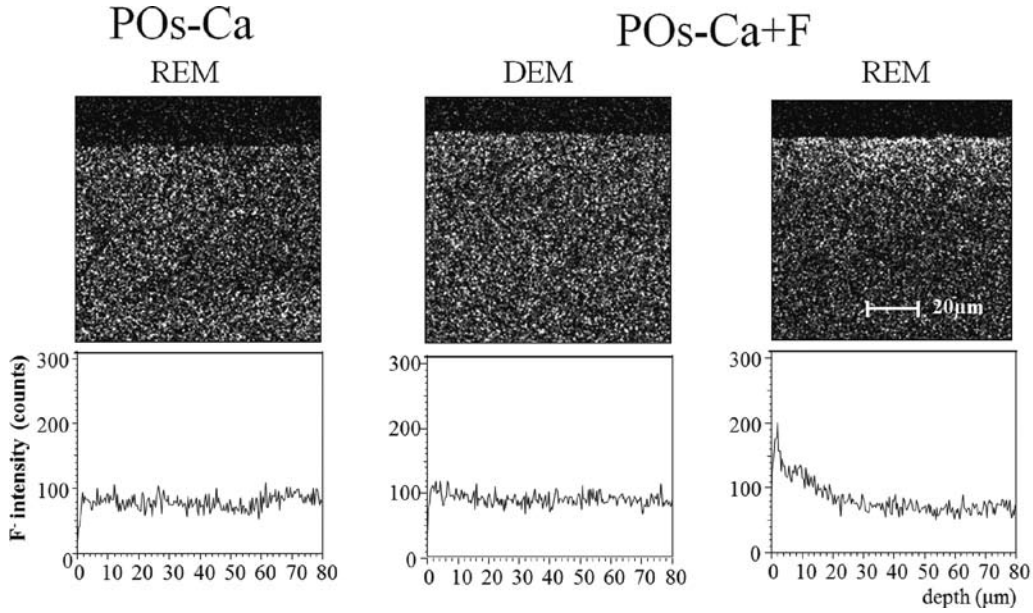

Figure 4. Representative TOF-SIMS image and profile of fluoride mapping at the superficial lesion after remineralization for POs-Ca and POs-Ca+F gums. DEM, demineralized area; REM, remineralized area. High density of fluoride was detectable within the superficial lesion at REM of POs-Ca+F up to 20 μm from the top surface of the subsurface lesion.

it was previously suggested that long-term exposure to low concentrations of fluoride (around 1 ppm) resulted in repair of the outer portion of enamel lesions, but did not significantly affect precipitation of mineral in the inner enamel (ten Cate, 2008). According to the results of the TMR and overall hardness profiles in this study, remineralization took place throughout the depth of the subsurface lesion in both POs-Ca gums. Our previous study showed high solubility of the POs-Ca: The chewing gum was shown to release 7.1 mM calcium ion, similar to the POs-Ca+F (7.3 mM), whereas a low level of fluoride ion concentration (up to 1.25 ppm) was extracted from POs-Ca+F (Kitasako *et al*., 2011). That finding, accompanied by TMR profiles, indicated that both calcium and fluoride ions were released from the POs-Ca+F gum in a bioavailable form without impairing their mutual effects. Even in the presence of low-level fluoride, POs-Ca could penetrate the lesion deeply, perhaps owing to its small size (average molecular mass, about 800; maximum chain length, about 4 nm) (Kamasaka *et al*., 1997; Tschoppe *et al*., 2011). These results are also in correspondence with those of wide-angle x-ray diffraction (WAXRD) in the previous report, which indicated additional benefits of a low fluoride concentration of the crystalline structure of remineralized enamel (Kitasako *et al*., 2011). It is therefore suggested that the increased hardness in the superficial area was a result of better crystalline structure, and formation of more acid-resistant and denser fluoridated apatite crystal, despite the fact that TMR did not show any differences between the two groups.

Both POs-Ca and POs-Ca+F showed remarkable similarities in mineral profiles around the lesion body which were in accordance with nanoindentation hardness profiles. However, mineral density changes in the placebo gum were not reflected in hardness profiles and hardness recovery, suggesting that the mineral deposition did not result in mechanical reinforcement of enamel in this gum, perhaps due to the lack of proper crystallization, as previously confirmed by the WAXRD for the placebo gum (Kitasako *et al*., 2011). Previously, mathematical relationships were assumed between hardness and mineral content; however, it was recently suggested that the hardness and the mineral content might describe two different properties of enamel (Buchalla *et al*., 2008). It appears that meaningful hardness differences obtained by submicrometer-depth increment measurements could not be derived from TMR mineral density profiles. Further cross-sectional nanoindentation studies might be useful for understanding the relationships between the parameters and remineralization mechanisms.

In conclusion, this *in situ* study demonstrated that fluoride containing POs-Ca gum was superior in hardness recovery of enamel subsurface lesions especially at the superficial layers when compared with POs-Ca and Placebo gums. The study highlights the importance of calcium and fluoride ion bioavailability in the reinforcement of demineralized enamel. Nanoindentation hardness measurement with small forces and submicron distance increments is a unique approach for local assessment of enamel changes after remineralization.

ACKNOWLEDGMENTS

This study was supported by Global COE, International Research Center for Molecular Science in Tooth and Bone Diseases at Tokyo Medical and Dental University. The author(s) declare no potential conflicts of interest with respect to the authorship and/or publication of this article.

REFERENCES

Buchalla W, Imfeld T, Attin T, Swanin MV Schmidlin PR (2008). Relationship between nanaohardness and mineral content of artificial carious enamel lesion. *Caries Res* 42:157-163.

Cai F, Shen P, Walker GD, Reynolds C, Yuan Y, Reynolds EC (2009). Remineralization of enamel subsurface lesions by chewing gum with added calcium. *J Dent* 37:763-768.

Cochrane NJ, Cai F, Huq NL, Burrow MF, Reynolds EC (2010). New approaches to enhanced remineralization of tooth enamel. *J Dent Res* 89:1187-1197.

Delbem AC, Sassaki KT, Vieira AE, Rodrigues E, Bergamaschi M, Stock SR, *et al.* (2009). Comparison of methods for evaluating mineral loss: hardness versus synchrotron microcomputed tomography. *Caries Res* 43:359-365.

Dickinson ME, Wolf KV, Mann AB (2007). Nanomechanical and chemical characterization of incipient in vitro carious lesions in human dental enamel. *Arch Oral Biol* 52:753-760.

Featherstone JD (1999). Prevention and reversal of dental caries: role of low level fluoride. *Community Dent Oral Epidemiol* 27:31-40.

Featherstone JD, Zero DT (1992). An *in situ* model for simultaneous assessment of inhibition of demineralization and enhancement of remineralization. *J Dent Res* 71(Spec Iss):804-810.

Featherstone JD, ten Cate JM, Shariati M, Arends J (1983). Comparison of artificial caries-like lesions by quantitative microradiography and microhardness profiles. *Caries Res* 17:385-391.

Kamasaka H, To-o K, Kusaka K, Kuriki T, Kometani K, Okuda S (1997). Effect of phosphoryl oligosaccharides on iron solubility under neutral conditions. *Biosci Biotechnol Biochem* 61:1209-1210.

Kandelman D, Gagnon G (1990). A 24-month clinical study of the incidence and progression of dental caries in relation to consumption of chewing gum containing xylitol in school preventive programs. *J Dent Res* 69:1771-1775.

Kielbassa AM, Wrbas KT, Schulte-Mönting J, Hellwig E (1999). Correlation of transversal microradiography and microhardness on in situ-induced demineralization in irradiated and nonirradiated human dental enamel. *Arch Oral Biol* 44:243-251.

Kitasako Y, Tanaka M, Sadr A, Hamba H, Ikeda M, Tagami J (2011). Effects of chewing gum containing phosphoryl oligosaccharides of calcium (POs-Ca) and fluoride on remineralization and crystallization of enamel subsurface lesions *in situ*. *J Dent* 39:771-779.

Magalhães AC, Moron BM, Comer LP, Wiegand A, Buchalla W, Buzalaf MA (2009). Comparison of cross-sectional hardness and transverse microradiography of artificial carious enamel lesions induced by different demineralising solutions and gels. *Caries Res* 43:474-483.

Morgan MV, Adams GG, Bailey DL, Tsao CE, Fischman SL, Reynolds EC (2008). The anticariogenic effect of sugar-free gum containing CPP-ACP nanocomplexes on approximal caries determined using digital bitewing radiography. *Caries Res* 42:171-184.

Reynolds EC, Cai F, Shen P, Walker GD (2003). Retention in plaque and remineralization of enamel lesions by various forms of calcium in a mouthrinse or sugar-free chewing gum. *J Dent Res* 82:206-211.

Shen P, Manton DJ, Cochrane NJ, Walker GD, Yuan Y, Reynolds C, *et al.* (2011). Effect of added calcium phosphate on enamel remineralization by fluoride in a randomized controlled in situ trial. *J Dent* 39:518-525.

ten Cate JM (2008). Remineralization of deep enamel dentine caries lesions. *Aust Dent J* 53:281-285.

ten Cate JM, Dundon KA, Vernon PG, Damato FA, Huntington E, Exterkate RA, *et al.* (1996). Preparation and measurement of artificial enamel lesions, a four-laboratory ring test. *Caries Res* 30:400-407.

To-o K, Kamasaka H, Nishimura T, Kuriki T, Saeki S, Nakabou Y (2003). Absorbability of calcium from calcium-bound phosphoryl oligosaccharides in comparison with that from various calcium compounds in the rat ligated jejunum loop. *Biosci Biotechnol Biochem* 67:1713-1718.

Tschoppe P, Zandim DL, Martus P, Kielbassa AM (2011). Enamel and dentine remineralization by nano-hydroxyapatite toothpastes. *J Dent* 39:430-437.

分子情報伝達学分野

高柳　広

医歯学総合研究科・生体支持組織学系専攻
分子情報伝達学・教授

1）研究の課題名

研究の題目

骨代謝制御ネットワークの解明：Elucidation of novel regulatory mechanisms in bone metabolism

研究内容

骨代謝は、骨自身だけではなく他臓器や組織の恒常性維持にも重要である事が明らかにされている。本研究は骨代謝制御ネットワークを、骨を構成する個々の細胞間から最終的に全身の組織、臓器レベルで解明する。この実現の為に、研究内容は3つの項目から構成されている。A）骨構成細胞に発現する遺伝子・タンパク質の網羅解析;B）コンディショナル遺伝子改変マウスを用いた骨代謝制御遺伝子の機能解析; C）骨による全身性制御機構の解明である。本年度はこれらの成果を4本の論文としてまとめ、そのうちNature誌に1本発表することができた。1）Semaphorin 3A（Sema3A）が破骨細胞の分化抑制と骨芽細胞の分化促進とを同時に行うことで骨保護作用を示すことを明らかにした。Sema3Aはその受容体であるneuropilin-1（Nrp1）と結合し、ITAMシグナルおよびRhoAの活性化を抑制することでRANKLにより誘導される破骨細胞の分化を抑制した。また、Sema3Aは古典的Wnt経路をつうじ骨芽細胞の分化を促進し脂肪細胞の分化を抑制することも明らかになった。Sema3Aノックアウトマウスおよび変異Nrp1ノックインマウスのどちらも著明な骨量の低下を示した。Sema3Aの投与の効果を検討したところ、破骨細胞の分化抑制および骨芽細胞の分化促進をともなう顕著な骨量の増加作用をもつことが明らかになった。以上から、Sema3Aは骨関連疾患の新規の治療薬となることが期待される。2）抑制性転写因子Leukemia/lymphoma-related factor（LRF）が、破骨細胞の分化を分化段階特異的な二層性に制御することを明らかにした。LRFは破骨細胞上に発現がするが、骨代謝における役割はほとんど解明されていなかった。破骨細胞分化段階特異的なLER欠損マウスを用いてLRFの生理的機能を解析した結果、LRFは破骨細胞分化初期では分化を抑制し、分化後期においては促進するという分化段階に応じて異なる役割を果たすことを明らかにした。3）クラスIA型PI3KがAKT経路を介して、破骨細胞の機能を制御することを明らかにした。破骨細胞特異的IA型PI3Kノックアウトマウスは破骨細胞の骨吸収不全による大理石骨病を発症した。分子メカニズムの解析により、IA型PI3Kは破骨細胞においてAktを活性化することにより、酸やプロテアーゼを含むリソソーム小胞の吸収窩側への分泌に必須な役割を果たしていることを解明した。

拠点内イノベーション研究

研究の題目

光メージングと分子生物学の融合によるオステオネットワークの解明を目指したフロンティア研究拠点

New frontier of osteonetwork research by combinational approaches of optical imaging and molecular biology

研究内容

骨のホメオスタシスは骨芽細胞による骨形成と破骨細胞による骨吸収のバランスで維持されており、これらの細胞系の分化・機能の制御機構を明らかにすることは骨生物学の大きな目標の一つである。近年では、骨組織に埋もれている骨細胞の機能が注目され、骨リモデリングにおける骨細胞、骨芽細胞、破骨細胞間の相互作用の解明も重要な研究課題となっている。また、骨組織の内部には、骨芽細胞、骨細胞、破骨細胞以外に間葉系幹細胞、造血・免疫系細胞、血管系細胞、脂肪細胞などの多くの細胞系が混在しているため、骨髄環境に存在する多くの細胞系の相互作用を明らかにすることも重要課題となっている。さらに、骨組織のホメオスタシスは、ホルモン、メカニカルストレスなどのバイオモデュレーターにより骨の外部から入力された刺激で制御されているので、骨組織と骨外の臓器・組織との相互作用を解析することも

重要となる。

このように臓器としての骨組織の重要性は広がりつつあり、骨組織のホメオスタシスを生物学的に理解するには、これら多くの細胞系の動的な相互作用を明らかにすることが極めて重要である。本研究グループでは、骨内外の細胞間の緊密なコミュニケーションをオステネットワークという新たな骨生物学のパラダイムとして捉え、ネットワークを構成する分子・細胞群を統合的かつ動的に解析することにより、骨をさらに深く理解することを目標とする。具体的には、骨組織に対する光イメージングの応用と遺伝子改変マウス作製を含めた網羅的分子生物学のテクニックを有機的に結合させ、研究を推進する。これら異分野として発展しつつある2つの先端科学的なアプローチを統合し、オステオネットワーク構成分子群の同定とその機能解明にチャレンジする。

2）研究のイラストレーション

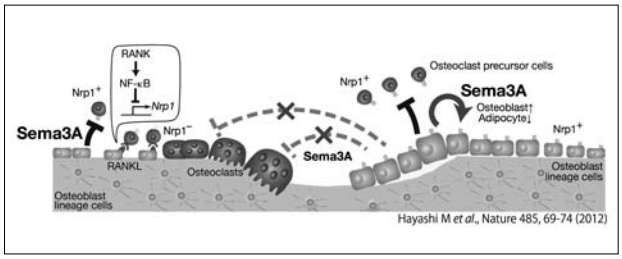

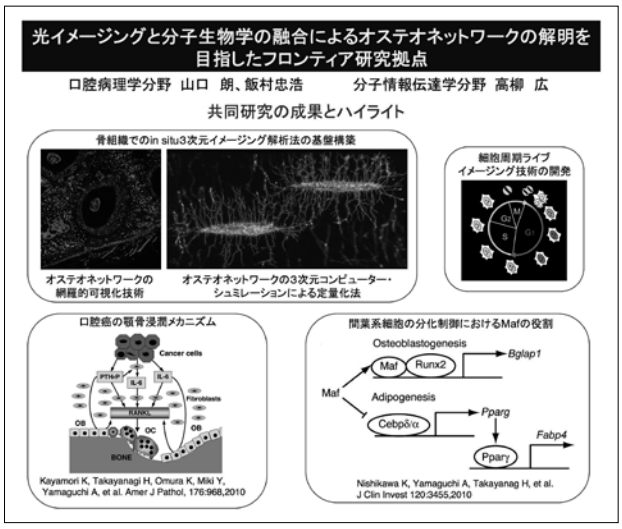

3）発表の研究内容についての英文要約

1）The bony skeleton is maintained by local factors that regulate bone-forming osteoblasts and bone-resorbing osteoclasts, in addition to hormonal activity. Osteoprotegerin protects bone by inhibiting osteoclastic bone resorption, but no factor has yet been identified as a local determinant of bone mass that regulates both osteoclasts and osteoblasts. Here we show that semaphorin 3A（Sema3A）exerts an osteoprotective effect by both suppressing osteoclastic bone resorption and increasing osteoblastic bone formation. The binding of Sema3A to neuropilin-1（Nrp1）inhibited receptor activator of nuclear factor-κB ligand（RANKL）-induced osteoclast differentiation by inhibiting the immunoreceptor tyrosine-based activation motif（ITAM）and RhoA signalling pathways. In addition, Sema3A and Nrp1 binding stimulated osteoblast and inhibited adipocyte differentiation through the canonical Wnt/β-catenin signalling pathway. The osteopenic phenotype in Sema3a −/− mice was recapitulated by mice in which the Sema3A-binding site of Nrp1 had been genetically disrupted. Intravenous Sema3A administration in mice increased bone volume and expedited bone regeneration. Thus, Sema3A is a promising new therapeutic agent in bone and joint diseases. 2）Cell fate determination is tightly regulated by transcriptional activators and repressors. Leukemia/lymphoma-related factor（LRF; encoded by Zbtb7a）, known as a POK family transcriptional repressor, is induced during the development of bone-resorbing osteoclasts, but the physiological significance of LRF in bone metabolism and the molecular mechanisms underlying the transcriptional regulation of osteoclastogenesis by LRF have not been elucidated. Here we show that LRF negatively regulates osteoclast differentiation by repressing nuclear factor of activated T cells c1（NFATc1）induction in the early phase of osteoclast development, while positively regulating osteoclast-specific genes by functioning as a coactivator of NFATc1 in the bone resorption phase. The stage-specific distinct functions of LRF were demonstrated in two lines of conditional knockout mice in which LRF was deleted in the early or late phase of osteoclast development. Thus, this study shows that LRF plays stage-specific distinct roles in osteoclast differentiation, exemplifying the delicate transcriptional regulation at work in lineage commitment. 3）Class IA phosphatidylinositol 3-kinases（PI3Ks）are activated by growth factor receptors and regulate a wide range of cellular processes. In osteoclasts, they are activated downstream of α（v）β（3）integrin and c-Fms, which are involved in the regulation of bone-resorbing activity. The physiological relevance of the in vitro studies using PI3K inhibitors has been of limited value, because they inhibit all classes of PI3K. Here, we show that the osteoclast-specific deletion of the p85 genes encoding the regulatory subunit of the class IA PI3K results in an osteopetrotic phenotype caused by a defect in the bone-resorbing activity of osteoclasts. Class IA PI3K is required for the ruffled border formation and vesicular transport, but not for the formation of the sealing zone. p85 α/β doubly deficient osteoclasts had a defect in M-CSF-induced Akt activation and the introduction of constitutively active Akt recovered the bone-resorbing activity. Thus, the class

IA PI3K-Akt pathway regulates the cellular machinery crucial for osteoclastic bone resorption, and may provide a molecular basis for therapeutic strategies against bone diseases.

4）本事業に関連して世界的な研究拠点形成に向けて、以下の点で改善・整備等されたこと

A（研究拠点体制）

他分野（特に免疫学）の学外研究者との協力し、世界的な成果を責任著者として3本の論文を発表できた。さらに学内共同研究の成果を論文として発表した。

B（研究教育環境）

GCOE AISS学生の博士号取得に向けた確実な研究指導を行った結果、GCOE AISS学生1名が博士号を取得し、残る3名のうち1名は論文revision中であり、2名は論文投稿に向け順調に研究を進めている。

C（人材確保）、D（人材育成）

昨年度に比べ、国内外から他分野に精通したポスドク、大学院生、技術補佐員をさらに増員し、学際的環境下で骨代謝研究を推進できる環境を整備した。

E（国際化）

海外において多数の講演を行った。さらに当研究室では、海外からのポスドクが常時研究に参画しており、ラボ内セミナーでの公用語は英語としている。

5）GCOE事業を推進するに当たって力を入れた点

GCOEシンポジウムや国際学会を積極的に活用して、世界の一線級の研究者と意見交換を行い、世界トップレベルの研究を意識した研究推進を行った。本年度も引き続き、GCOE拠点内にとどまらず東京医科歯科大学や他大学の研究者と広く密接な連携を行うことで、各分野の先端的な発想を自分の研究領域と融合させ、研究成果として結実させることを心がけた。

6）英文原著論文。

1. ◎Tsuji K, Negishi-Koga T, Sumiya E, Kukita A, Kato S, Maeda T, Pandolfi PP, Moriyama K, Takayanagi H. Stage-specific functions of LRF in the transcriptional control of osteoclast development.
   Proc Natl Acad Sci USA., 109（7）：2561, 2012
2. Otero K, Shinohara M, Zhao H, Cella M, Gilfillan S, Colucci A, Faccio R, Ross FP, Teitelbaum SL, Takayanagi H, Colonna M. TREM2 and β-catenin regulate bone homeostasis by controlling the rate of osteoclastogenesis.
   J Immunol., 188（6）：2612, 2012
3. Fujita K, Iwasaki M, Ochi H, Fukuda T, Ma C, Miyamoto T, Takitani K, Negishi-Koga T, Sunamura S, Kodama T, Takayanagi H, Tamai H, Kato S, Arai H, Shinohara K, Itoh H, Okawa A, Takeda S. Vitamin E decreases bone mass by stimulating osteoclast fusion
   Nat Med., 18（4）：589, 2012
4. ◎Hayashi M, Nakashima T, Taniguchi M, Kodama T, Kumanogoh A, Takayanagi H. Osteoprotection by Semaphorin 3A.
   Nature, 485（7396）：69, 2012
5. ◎Shinohara M, Nakamura M, Masuda H, Hirose J, Kadono Y, Iwasawa M, Nagase Y, Ueki K, Kadowaki T, Sasaki T, Kato S, Nakamura H, Tanaka S, Takayanagi H. Class IA phosphatidylinositol 3-kinase regulates osteoclastic bone resorption through Akt-mediated vesicle transport.
   J Bone Miner Res., doi：10.1002/jbmr.1703. [Epub ahead of print]
6. ◎Hara-Yokoyama M, Kukimoto-Niino M, Terasawa K, Harumiya S, Podyma-Inoue KA, Hino N, Sakamoto K, Itoh S, Hashii N, Hiruta Y, Kawasaki N, Mishima-Tsumagari C, Kaitsu Y, Matsumoto T, Wakiyama M, Shirouzu M, Kasama T, Takayanagi H, Utsunomiya-Tate N, Takatsu K, Katada T, Hirabayashi Y, Yokoyama S, Yanagishita M. Tetrameric Interaction of the Ectoenzyme CD38 on the Cell Surface Enables Its Catalytic and Raft-Association Activities.
   Structure, 20（9）：1585, 2012
7. ◎Al-Bari A, Shinohara M, Nagai Y, Takayanagi H. Inhibitory effect of chloroquine on bone resorption reveals the essential role of lysosomes in osteoclast differentiation and function.
   Inflamma Regener.,（in press）

7）総説ならびに著書

（英文）

1. O'Brien CA, Nakashima T, Takayanagi H. Osteocyte control of osteoclastogenesis..
   Bone, in press
2. Nakashima T, Mikihito Hayashi, Takayanagi H. New insights into osteoclastogenic signaling mechanisms.
   Trends Endocrinol Metabo, 582-590（9ページ）, 2012
3. Nakashima T, Takayanagi H. RANK and RANKL. Encyclopedia of Signaling Molecules
   Springer New York, Editor Sangdum Choi, 1581-1589（9ページ）, 2012
4. Negishi-Koga T and Takayanagi H Bone cell communication factors and Semaphorins BoneKEy Reports, 2012

5. Komatsu N and Takayanagi H
Autoimmune arthritis：the interface between the immune system and joints.
Adv Immunol, 45-71（26ページ）, 2012
6. Komatsu N and Takayanagi H
Inflammation and bone destruction in arthritis：synergistic activity of immune and mesenchymal cells in joints.
Front Immunol, 1-11（11ページ）, 2012

（和文）

1. 高柳広：骨免疫学の歴史と展望
医学のあゆみ、639-645（7ページ）、2012
2. 高柳広：骨代謝研究の進歩
細胞、2-3（2ページ）、2012
3. 林幹人、中島友紀、高柳広：骨リモデリングの制御機構
細胞、8-11（4ページ）、2012
4. 中島友紀、高柳広：新着論文要約と解説：RANKLはプロゲスチンによる乳癌の発生を制御している
O.li.v.e.、28-32（5ページ）、2012
5. 中島友紀、林幹人、高柳広：骨細胞による破骨細胞形成の制御機構
内分泌・糖尿病・代謝内科、457-464（8ページ）、2012
6. 中島友紀、林幹人、高柳広：骨細胞とリモデリング
リウマチ科、530-537（8ページ）、2012
7. 中島友紀、林幹人、高柳広：新 注目の海外文献（1）・授乳期マウスにおける骨細胞による骨小腔と骨細管の再構築の実証--ほか
CLINICAL CALCIUM、145-147（3ページ）、2012
8. 中島友紀、林幹人、高柳広：骨細胞による骨吸収制御
CLINICAL CALCIUM、85-96（12ページ）、2012
9. 中島友紀、高柳広：破骨細胞分化における正と負の転写制御
炎症と免疫、227-233（7ページ）、2012
10. 中島友紀、高柳広：骨代謝における骨細胞の新たな役割
Medical Practice、1925-1928（4ページ）、2012
11. 林幹人、中島友紀、高柳広：セマフォリンによる骨代謝
CLINICAL CALCIUM、1693-1699（7ページ）、2012
12. 林幹人、中島友紀、高柳広：Semaphorinシグナルによる骨代謝
アンチ・エイジング医学、704-709（6ページ）、2012
13. 中島友紀：骨細胞による骨恒常性の制御
リウマチ科、352-361（10ページ）、2012
14. 中島友紀、高柳広：関節リウマチ骨破壊のメカニズム
Jpn J Rehabil Med、683-689（7ページ）、2012
15. 中島友紀：骨細胞による骨リモデリング制御
The BONE、5-10（6ページ）、2012
16. 中島友紀、高柳広：骨免疫学からみたRA治療の新展開
最新医学、203-211（9ページ）、2012
17. 中島友紀、高柳広：骨を作りか変える指令細胞の発見
整形外科、50（1ページ）、2012
18. 林幹人、中島友紀、高柳広：セマフォリンによる骨代謝制御
CLINICAL CALCIUM、63-69（7ページ）、2012
19. 岡本一男、高柳広：骨免疫学 － オーバービュー
CLINICAL CALCIUM、11-19（9ページ）、2012
20. 岡本一男：骨免疫学-研究最前線　骨と免疫系のクロストーク　3.転写因子NFATc1と破骨細胞
医学のあゆみ、655-659（5ページ）、2012
21. 岡本一男：骨免疫学の歴史と新たな展開, 領域融合レビュー
オンラインジャーナル、2012
22. 岡本一男、高柳広：第IV部　学術的免疫研究の展開 26. 骨免疫学の新展開
免疫学update　－分子病態の解明と治療への展開－、2012予定
23. 篠原正浩、高柳広：炎症性関節炎における破骨細胞の制御」
臨床リウマチ、in press
24. 篠原正浩、高柳広：骨免疫学の最前線
腎と骨代謝、99-106（8ページ）、2012
25. 篠原正浩、高柳広：骨免疫学
炎症と免疫、105-108（9ページ）、2012

8）特許取得、特許申請

1. 発明の名称：骨形成促進剤（PCT/JP2012/003113）
発明者：高柳広、古賀貴子
出願日：2012年5月11日
出願人：国立大学法人　東京医科歯科大学
2. 発明の名称：骨形成促進剤
（特許出願番号：2011-108642）
発明者：高柳広、古賀貴子
出願日：2011年5月13日

出願人：国立大学法人　東京医科歯科大学

3. 発明の名称：骨量を増加させるための組成物
（特許出願番号：2012-42160）
発明者：林幹人、中島友紀、高柳広
出願日：2012年2月28日
出願人：国立大学法人　東京医科歯科大学

9）平成24年度までの自己評価

本年度は、Semaphorin 3Aが破骨細胞の分化抑制と骨芽細胞の分化促進とを同時に行うことで骨保護作用を示すことを明らかにし、Semaphorin 3Aが骨関連疾患の有望な新規治療薬となる可能性を示すことができた。この成果をもとに特許を出願した。また、破骨細胞分化段階特異的な抑制性転写因子Leukemia/lymphoma-related factor（LRF）欠損マウスを用いてLRFの生理的機能を解析した結果、LRFは破骨細胞分化初期では分化を抑制し、分化後期においては促進するという分化段階特異的な二層性に制御することを明らかにした。これらに加えて、クラスIA型PI3KがAKT経路を介して破骨細胞の機能を制御すること、リソソーム内のプロトンを中和するクロロキンが破骨細胞の分化も抑制することを明らかにした。以上、本年度は骨と免疫系が密接に関与している事を多数発見でき、主著論文4本（うち1本はNature誌）と共著論文3本、計7本の論文として発表した。本年度はGCOEプログラムの最終年度であるため、これまでの研究成果を精力的にまとめており、現在さらに2本の論文が投稿中である。

10）学会発表（英文）

1. ◎Authors：Masatsugu Oh-hora, Noriko Komatsu, Anjana Rao, Hiroshi Takayanagi.
Title：Physiological functions of store-operated calcium entry in immune system.
The 6th Global COE International Symposium
Poster Presentation
Tokyo, 2012 January 23-25
2. ◎Authors：Takehito Ono, Kazuo Okamoto, Hiroshi Takayanagi.
Title：Effects of the immune system on bone regeneration after drill-hole injury.
The 6th Global COE International Symposium
Poster Presentation
Tokyo, 2012 January 23-25
3. ◎Authors：Mikihito Hayashi, Tomoki Nakashima, Hiroshi Takayanagi.
Title：Semaphorin 3A drives bone formation phase in bone remodeling.
4th International Conference on Osteoimmunology：Interactions of the Immune and Skeltal Systems.
Poster Presentation
Corfu, Greece, 2012 June 17 – 22
4. ◎Authors：Tomoki Nakashima, Mikihito Hayashi, Hiroshi Takayanagi.
Title：Osteocyte-derived RANKL in bone metabolism.
4th International Conference on Osteoimmunology：Interactions of the Immune and Skeltal Systems.
Poster Presentation
Corfu, Greece, 2012 June 17 – 22
5. ◎Authors：Takako Negishi-Koga, Eriko Sumiya, Masahiro Shinohara, Hiroshi Takayanagi.
Title：Regulation of bone remodeling by osteoclastic expression of semaphorin 4D.
4th International Conference on Osteoimmunology：Interactions of the Immune and Skeltal Systems.
Poster Presentation
Corfu, Greece, 2012 June 17 – 22
6. ◎Authors：Mikihito Hayashi, Tomoki Nakashima, Hiroshi Takayanagi.
Title：Regulation mechanisms of bone remodeling.
9th Meeting of Bone Biology Forum
Oral Presentation
Shizuoka, 2012 August 25
7. Authors：Tomoki Nakashima, Mikihito Hayashi, Hiroshi Takayanagi.
Title：Osteoprotection by semaphoring 3A.
22nd Annual Scientific Meeting ANZBMS and Asia-Pacific Bone and Mineral Research Meeting.
Oral Presentation
Perth, Australia, 2012 September 3
8. Authors：Tomoki Nakashima, Mikihito Hayashi, Hiroshi Takayanagi.
Title：Osteocyte-derived RANKL in bone remodeling.
34th Annual Meeting of the American Society for Bone and Mineral Research.
Plenary Poster Presentation
Minneapolis USA, 2012 September 12
9. Authors：Tomoki Nakashima, Mikihito Hayashi, Hiroshi Takayanagi.
Title：Osteocyte-derived RANKL in bone remodeling.
34th Annual Meeting of the American Society for Bone and Mineral Research.
Poster Presentation
Minneapolis USA, 2012 September 13
10. ◎Authors：Mikihito Hayashi, Tomoki Nakashima, Hiroshi Takayanagi.
Title：Semaphorin 3A inhibits osteoclastogenesis and promotes osteoblastogenesis synchronously.
34th Annual Meeting of the American Society for Bone and Mineral Research
Poster Presentation

Minneapolis USA, 2012 October 15

11. ◎Authors：Takehito Ono, Kazuo Okamoto, Hiroshi Takayanagi.
Title：Interleukin-17 contributes to bone regeneration after drill-hole injury.
The 7th Global COE International Symposium
Poster Presentation
Tokyo, 2012 November 12-14

11）学会発表（和文）

1. 著者名：古賀貴子
演題名：セマフォリン4Dを介した破骨細胞による骨形成抑制作用
学会名：第6回Bone Research Seminar
東京、平成24年2月17日
2. 著者名：林幹人、中島友紀、高柳広
演題名：骨リモデリング制御機構の解明
学会名：第10回口腔医科学フロンティア
大阪、平成24年3月3日
3. 著者名：中島友紀、高柳広
演題名：RANKLと骨免疫学
学会名：第56回日本リウマチ学会
大阪、平成24年4月28日
4. 著者名：住谷瑛理子、辻香織、古賀貴子、森山啓司、高柳広
演題名：破骨細胞分化の転写制御におけるLRFの分化段階特異的な機能
学会名：第33回日本炎症・再生医学会
福岡、平成24年7月5日
5. 著者名：永井裕介、篠原正浩、高柳広
演題名：クロロキンによる破骨細胞分化抑制
学会名：第33回日本炎症・再生医学会
福岡、平成24年7月5日
6. 著者名：林幹人、中島友紀、高柳広
演題名：Semaphorin 3Aによる骨代謝制御メカニズム
学会名：第33回日本炎症・再生医学会
福岡、平成24年7月5日
7. 著者名：小野岳人、岡本一男、高柳広
演題名：マウス大腿骨骨損傷モデルにおける骨再生に対するIL-17の作用
学会名：第33回日本炎症・再生医学会
福岡、平成24年7月5日
8. 著者名：林幹人、中島友紀、高柳広
演題名：Semaphorin 3Aは骨吸収の抑制と骨形成の促進により、骨の恒常性を維持する
学会名：第30回日本骨代謝学会
東京、平成24年7月19日
9. 著者名：永井裕介、篠原正浩、Al-Bari Md. Adbul Alim、高柳広
演題名：リソソームの酸性化は破骨細胞分化に必要である
学会名：第30回日本骨代謝学会
東京、平成24年7月20日
10. 著者名：林幹人、中島友紀、高柳広
演題名：Sema3Aによる骨リモデリング制御機構の解明
学会名：第15回 骨発生・再生研究会
東京、平成24年11月10日
11. 著者名：林幹人、中島友紀、高柳広
演題名：Semaphorin 3Aによる骨リモデリングの制御
学会名：第6回骨・軟骨フロンティア
東京、平成24年11月17日
12. 著者名：Kazuo Okamoto, Noriko Komatsu, Hiroshi Takayanagi
演題名：Study on the potential of IκBζ as a target for the treatment of inflammatory bone destruction
学会名：第41回日本免疫学会学術集会
横浜、平成24年12月6日
13. 著者名：Eriko Sumiya, Takako Koga, Hiroshi Takayanagi
演題名：Stage-specific functions of LRF in the transcriptional control of osteoclast development
学会名：第41回日本免疫学会学術集会
横浜、平成24年12月5日
14. 著者名：Masatsugu Oh-hora, Noriko Komatsu, Stefan Feske, Shohei Hori, Anjana Rao, Hiroshi Takayanagi
演題名：Agonist-selected T cell development requires strong TCR/calcium signaling
学会名：第41回日本免疫学会学術集会
横浜、平成24年12月5日
15. 著者名：Matteo M Guerrini, Kazuo Okamoto, Tomoki Nakashima, Hiroshi Takayanagi
演題名：RANKL expressed by T lymphocytes is needed for development of experimental autoimmune encephalomyelitis
学会名：第41回日本免疫学会学術集会
横浜、平成24年12月5日

16. 著者名：Kazuo Okamoto , Noriko Komatsu, Hiroshi Takayanagi
演題名：Study on the potential of IκBζ as a target for the treatment of inflammatory bone destruction
学会名：第41回日本免疫学会学術集会
横浜、平成24年12月6日

12）受賞

中島友紀
第30回日本骨代謝学会 学会奨励賞
平成24年7月

岡本一男
平成23年度三浦記念リウマチ学術研究賞（公益財団法人　日本リウマチ財団）
平成23年7月29日

林幹人
4th International Conference on Osteoimmunology Travel Award
平成24年6月

第30回日本骨代謝学会優秀演題賞
平成24年7月

第33 回日本炎症・再生医学会優秀演題賞
平成24年7月

13）外部資金の獲得状況

（独）科学技術振興機構（JST）
戦略的創造研究推進事業（ERATO型研究）
平成21年度発足
研究題目：ERATO　高柳オステオネットワークプロジェクト
代表：高柳広
期間：平成21年度～平成26年度
研究費総額：169,900万円

文部科学省科学研究費補助金　若手研究（A）
研究題目：破骨細胞特異的システムの解明―歯の革新的保存法の確立を目指して
代表：篠原正浩
期間：平成22年度～平成24年度
研究費総額：2,186万円

（独）科学技術振興機構（JST）　戦略的創造研究推進事業（さきがけ）「炎症の慢性化機構の解明と制御」
研究題目：イオンバランス破綻による自己免疫疾患の重症化機構の解明
代表：大洞将嗣
期間：平成23年度～平成25年度
研究費総額：4,000万円

文部科学省科学研究費補助金　若手研究（A）
研究題目：炎症応答と骨破壊の両プロセスを包括して制御できる炎症性骨破壊治療法の確立
代表：岡本一男
期間：平成23年度～平成25年度
研究費総額：2,130万円

文部科学省科学研究費補助金　基盤研究（C）
研究題目：末梢免疫寛容成立におけるカルシウムシグナルの役割の解明
代表：大洞将嗣
期間：平成23年度～平成25年度
研究費総額：410万円

文部科学省科学研究費補助金　挑戦的萌芽研究
研究題目：メタボリックシンドロームにおける破骨細胞の機能解析
代表：篠原正浩
期間：平成23年度～平成24年度
研究費総額：290万円

文部科学省科学研究費補助金　挑戦的萌芽研究
研究題目：細菌感染症におけるIL-17/IL-22産生制御機能の解明
代表：岡本一男
期間：平成23年度～平成24年度
研究費総額：290万円

文部科学省科学研究費補助金　基盤研究（B）
研究題目：骨細胞による骨ミネラリゼーションの制御機構の解明
代表：中島友紀
期間：平成24年度～平成26年度
研究費総額：320万円

文部科学省科学研究費補助金　特別研究員奨励費
研究題目：RANK/RANKLシグナルの新規機能の解明
代表：高柳広
期間：平成22年度～平成23年度
研究費総額：300万円

文部科学省科学研究費補助金　特別研究員奨励費
研究題目：溶骨性疾患と加齢における骨の恒常性におけるB細胞の役割の解明
代表：高柳広
期間：平成23年度～平成24年度
研究費総額：160万円

文部科学省科学研究費補助金　特別研究員奨励費
研究題目：急性免疫反応における破骨細胞・骨芽細胞の意義
代表：寺島明日香
期間：平成23年度～平成25年度
研究費総額：750万円

文部科学省科学研究費補助金　特別研究員奨励費
研究題目：急性免疫反応における破骨細胞・骨芽細胞の意義
代表：寺島明日香
期間：平成23年度～平成25年度
研究費総額：750万円

基礎研究支援プロジェクト　（中外製薬）
研究題目：骨リモデリング制御因子の同定とその機能解析
代表：中島友紀
期間：平成22年度～平成26年度
研究費総額：1,000万円

ブリストル・マイヤーズ関節リウマチ研究助成
（ブリストル・マイヤーズ）
研究題目：関節リウマチに伴う骨破壊の制御機構の解明　滑膜バイオロジーの創成
代表：中島友紀
期間：平成23年度～平成25年度
研究費総額：1,000万円

公益財団法人　興和生命科学振興財団　研究助成
研究題目：骨構成細胞が産生する生理活性物質の探索と機能解明
代表：篠原正浩
期間：平成23年度～平成24年度
研究費総額：100万円

公益財団法人　アステラス病態代謝研究会　研究助成金
研究題目：感染症リスクを提言できる自己免疫疾患治療法の確立
代表：岡本一男
期間：平成23年度～平成24年度
研究費総額：100万円

公益財団法人　日本リウマチ財団
研究題目：自己免疫性Th17細胞を制御できる新規分子標的の探索
代表：岡本一男
期間：平成24年度
研究費総額：100万円

武田科学振興財団 2012年度ビジョナリーリサーチ助成
研究題目：骨リモデリングの制御機構の解明
代表：中島友紀
期間：平成24年度
研究費総額：100万円

公益財団法人　武田科学振興財団　医学系研究奨励（基礎）
研究題目：アルギニンメチル化シグナルによる生体機能制御の証明と解明
代表：古賀貴子
期間：平成24年度～平成25年度
研究費総額：300万円

財団法人　内藤記念科学振興財団
研究題目：アゴニスト選択性腸管上皮間リンパ球の分化制御機構と生理的機能の解明
代表：大洞将嗣
期間：平成24年度～平成25年度
研究費総額：300万円

14）特別講演、招待講演、シンポジウム

1. 高柳広
   International Conference on Progress in Bone and Mineral Research, 2012.11.29, Vienna, Austria
2. 8th InternationalCongress of Spondyloarthropathies Gent, 2012.10.4, Gent, Belgium
3. 第14回日本骨粗鬆症学会、2012.9.27、新潟
4. EMBO Practical Course on Anatomy and Embryology, 2012.9.10, Split, Croatia
5. 1st Asia-Pacific Bone and Mineral Research Meeting with the ANZBMS 22nd Annual Scientific Meeting, 2012.9.4, Perth, Australia
6. 1st Asia-Pacific Bone and Mineral Research Meeting with the ANZBMS 22nd Annual Scientific Meeting, 2012.9.3, Perth, Australia
7. 42th International Sun Valley Workshop, 2012.8.8, Sun Valley, USA
8. 第30回日本骨代謝学会学術集会、2012.7.21、東京
9. 第30回日本骨代謝学会学術集会/第9回ビスフォスフォネートUpdate、2012.7.19、東京
10. 第33回日本炎症・再生医学会、2012.7.6、福岡
11. 第33回日本炎症・再生医学会、2012.7.5、福岡
12. 4th International Conference on Osteoimmunology, 2012.6.21, Corfu, Greece
13. Cold Spring Harbor Asia conferences, 2012.6.12, Suzhou, China

14. 15th International and 14th European Congress of Endocrinology（ICE / ECE 2012）, 2012.5.6, Florence, Italy
15. 第56回日本リウマチ学会総会・学術集会、第21回国際リウマチシンポジウム、2012.4.27、東京
16. 中島友紀
    第56回日本リウマチ学会
    2012年4月28日　東京
17. 第66回 日本口腔科学会学術集会
    2012年5月16日　広島
18. 第12回 日本抗加齢医学会総会
    2012年6月24日　横浜
19. 第54回 日本老年医学会学術集会
    2012年6月29日　東京
20. 第33回 日本炎症・再生医学会
    2012年7月5日　福岡
21. 第30回 日本骨代謝学会
    2012年7月20日　東京
22. 第30回 日本骨代謝学会
    2012年7月21日　東京
23. 第27回 日本整形外科学会基礎学術集会
    2012年10月26日　名古屋
24. 篠原正浩
    第33回日本炎症・再生医学会
    2012年7月5日　福岡
25. 古賀貴子
    第30回日本骨代謝学会学術集会 カレントコンセプト3
    2012年7月20日　東京
26. 岡本一男、高柳広
    日本食品免疫学会2012年度大会
    2012年10月16日　東京

15）主催学会

1. 第4回国際骨免疫学会議、2012年6月17日－22日、ギリシャ
2. 第8回骨免疫ワークショップ
   2012年11月2日、東京

16）新聞、雑誌、TV報道

Mone Zaidi & Jameel Iqbal：Double protection for weakened bones
Nature 485, 47（2012）
http：//www.nature.com/nature/journal/v485/n7396/full/485047a.html

Man Tsuey Tse：SEMA3A strikes a balance in bone homeostasis
Nat Rev Drug Discov. 12, 442（2012）
http：//www.nature.com/nrd/journal/v11/n6/full/nrd3759.html

日刊工業　2012年4月19日
http：//osteoimmunology.com/news/120419_nikkankougyou.pdf

読売新聞　2012年4月23日
http：//osteoimmunology.com/news/120419_yomiuri.pdf

日経産業　2012年4月19日

時事通信　2012年4月19日

朝日新聞　2012年4月19日
http：//osteoimmunology.com/news/120419_asahi.pdf

東京新聞　2012年4月19日

日経バイオテクONLINE　2012年4月19日
https：//bio.nikkeibp.co.jp/article/news/20120417/160636/

マイナビニュース　2012年4月19日
http：//news.mynavi.jp/news/2012/04/19/126/index.html

共同通信　2012年4月19日
http：//www.47news.jp/CN/201204/CN2012041801001508.html

日経新聞　2012年4月19日
http：//osteoimmunology.com/news/120419_nikkei.pdf

日経新聞　2012年10月21日
JST News June 2012「骨と免疫の新しい夜明け」
http：//www.jst.go.jp/pr/jst-news/pdf/2012/2012_06_p03.pdf

ライフサイエンス新着論文レビュー
http：//first.lifesciencedb.jp/archives/4789

17）教室、分野や講座の准教授、講師、助教、特別研究員、ポスドク、指導を受けた大学院生の名前

特任准教授	大洞　将嗣
助教	篠原　正浩（2012年9月まで）
	中島　友紀
	岡本　一男（2012年4月まで）
	春宮　　覚
客員助教	古賀　貴子
特別研究員	末松　綾子

寺島　明日香
Lynette Danks
住谷　恵里子
ポスドク　林　　幹人
永井　祐輔
Matteo Guerrini
高場　啓之
指導を受けた大学院生
○Abdul Alim Al-Bari
○小野　岳人
Warunee Pluemsakunthai

18）GCOE活動についての感想、コメント、改善を望む点

シャペロン教官以外にも、ポスドク研究者の配置を増員できることが望ましい。病理組織作成と解析、ノックアウトマウス作成、トランスクリプトーム・プロテオーム解析、セルソーティング等にあたって、専門の技術補佐員の増員、あるいは共同研究施設と専属の技術員による管理・支援があると有益である。

高柳　広
たかやなぎ・ひろし
東京大学大学院医学系研究科
免疫学講座 教授

1965年生まれ。東京大学医学部卒業、同大学付属病院整形外科等での臨床医の後、同大学大学院医学系研究科博士課程修了。医学博士。同大学医学部助手、東京医科歯科大学教授などを経て、2012年から現職。免疫系による骨代謝制御の研究に従事し、「骨免疫学」分野を開拓。09年からJST ERATO高柳オステオネットワークプロジェクト研究総括。

特集1

骨を中心とした全身の制御メカニズムを解明する

骨と免疫の新しい夜明け

「骨」と「免疫」、別々の機構で制御されているような印象を受ける体の大切な機能が、実は密接な関係を持っている——この10年で切り開かれた「骨免疫学」分野の研究により、骨と全身のかかわりが明かされ始めた。

骨は破壊と形成を繰り返す、代謝が活発な組織

「骨」は体を支える、柱の役割をしている。体の成長と共に骨も大きく、強くなり、骨折しても再生する。普段あまり意識することはないかもしれないが、骨は活発な新陳代謝を繰り返して、約10年から20年で新しく生まれ変わる組織なのだ。そして、このバランスが崩れることで、骨粗鬆症（こつそしょうしょう）や関節リウマチなどの骨の疾患が起こる。

骨の代謝で起こる破壊と形成のプロセスは「骨リモデリング」と呼ばれる。まず骨の表面にある破骨細胞が古くなった骨を溶かし（骨吸収）、その後に骨の表面の骨芽細胞が溶けた部位に新しい骨をつくる（骨形成）。つまり、健康な状態で骨が新陳代謝をするには、破骨細胞と骨芽細胞がバランスよく働くことが必要だ。

「これまでにも破骨細胞を抑制する因子、骨芽細胞を促進する因子はいくつか発見されています。ただ、一つの因子で両方を制御しているものは、これまで見つかっていませんでした」と話すのは、「骨免疫学」という新しい研究分野の世界的なトップランナー、東京大学大学院医学系研究科教授の高柳広さん。骨芽細胞を活性化し、かつ破骨細胞の働きを抑制するという二つの働きを兼ね備えるタンパク質の存在を突き止めた。

一つで二通りの働きをする因子を発見

もともと人体は、骨吸収に応じた量の骨を形成する「骨吸収と骨形成の共役（カップリング）機構」という制御メカニズムを持っている。そのため、骨粗鬆症の治療で使われる“骨の吸収を抑える”薬は、同時に“骨の形成まで抑制”してしまうケースがあった。しかし、高柳さんが見出したタンパク質は、一つで骨吸収をする破骨細胞を減らし、骨形成をする骨芽細胞を増やす。結果として「骨を増やすことができる」因子なのだ。

一つで二通りの働きをする、「骨を作らせる、骨を壊させない」タンパク質は「セマフォリン3A」と呼ばれるものだ。これは、神経細胞が神経回路をつくる過程や、T細胞という免疫細胞の抑制作用にかかわることでも知られているものだった。

体の中で何が起こるか培養細胞だけでは分からない

高柳さんはこのタンパク質を、骨芽細胞が分泌する因子の中から見出した。この因子を見つける実験は、骨芽細胞がつくる多くのタンパク質を丁寧に分離することから始まった。

「分離したタンパク質試料を培養細胞に添加してその作用を調べるのですが、細胞レベルの実験では、体内で果たしている機能の全貌（ぜんぼう）は、なかなかわかりません」

高柳さんたちの研究では、重要な因子を発見しても、生体レベルでの機能の証明が求められる。そのためには、マウスを使った実験が不可欠だ。

「以前は、遺伝子が突然変異を起こした患者さんの症状から、遺伝子の役割を推測するしかありませんでした。それが、人為的に特定の遺伝子を壊した『ノックアウトマウス（遺伝子欠損マウス）』を作成することが可能になったことで、特定の遺伝子の働きを証明できるようになったのです」

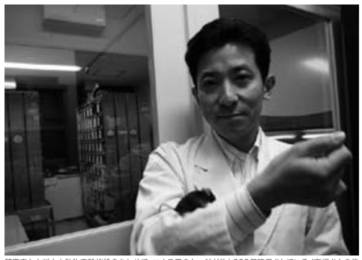

研究室および中央動物実験施設をあわせて、マウス用のケージが約1,000個確保されている（高柳さんの後ろの部屋が飼育室）。研究室で作成した系統や、共同研究で他施設から譲り受けたものを含め、100系統以上のマウスを飼育している。

さまざまな種類の遺伝子を破壊したノックアウトマウスと正常なマウスを比較する必要があるため、実験に使うマウスも1000匹単位になるという。

「研究室では約1000個の飼育ケージを確保しています。1ケージ5匹としても5000匹ほど飼育している計算になりますね。その施設の維持管理、遺伝子の探索とノックアウトマウスの作成と飼育、解析など、やることはたくさんあります」

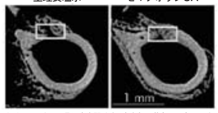

ドリルでマウスの骨に穴を開け（写真上部の黄色い四角で囲まれた領域）、セマフォリン3Aを投与すると、骨の再生が著しく促進された（写真右）。

高柳さんらが、セマフォリン3Aタンパク質をつくる遺伝子を破壊したマウスを調べたところ、正常マウスに比べて破骨細胞の数と骨の吸収が増えていた。だが、一方で骨芽細胞の数と骨形成率も異常に低下しており、骨量も著しく減少していた。更に、正常マウスにセマフォリン3Aを静脈注射すると、骨芽細胞が活性化し、骨量が増加することもわかった。

「培養細胞の実験からセマフォリン3Aが破骨細胞を抑制する作用は、予想していました。しかし、骨芽細胞への作用はマウスを解析することで初めてわかったのです」と骨代謝の専門家である高柳さんも、この結果には驚きの表情だ。

■破骨細胞と骨芽細胞の働き

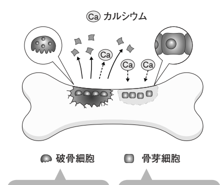

古くなった骨を溶かして破壊する。この時、骨内のカルシウムが溶け出す。

破壊された部位にカルシウムなどを取り入れて新しい骨をつくる。

■セマフォリン3Aの働き

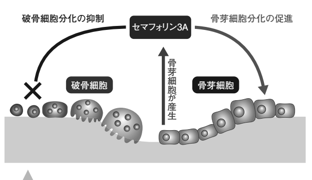

骨芽細胞が産生するタンパク質、セマフォリン3Aが骨芽細胞・破骨細胞の両者に作用して、骨吸収を抑制し、骨形成を促進することで骨が増える。

リウマチを治したくて免疫と骨の関係に行き着いた

大学卒業後の臨床医の時代には整形外科を専攻した高柳さんが、免疫学との学際領域に取り組むようになったのは、なぜだろうか。

「整形外科を専攻したのは、当時お世話になった教授の影響が大きいのです。整形外科は扱う組織が神経や骨、筋肉と非常に広いので、臨床も研究も面白いと話してくれて、魅力を感じました。だんだん自分の興味のある分野に絞っていけるだろうとも思ったのです。それに、整形外科はシリアスな患者さんは少なく、多くが元気になって帰って行く診療科ですから、明るい雰囲気もいいなと思いました」

高柳さんは大学卒業後に7年間、整形外科医として関節リウマチの手術を数多く手がけた。

「関節リウマチでは右膝にメスを入れても次は左膝というように、進行すると、何回も手術を繰り返さなければならないこともあります。手術は対処療法にしかならないので、何とか患者さんに根治してほしいと思うようになりました」

関節リウマチは滑膜（関節を包む関節包の内側の組織）が免疫系に攻撃されて炎症を起こして発症する。外科手術では痛みの原因となる滑膜の切除を行ったり、人工の関節に置換したりする。関節リウマチ患者の関節では、骨が壊れる原因はよくわかっていなかった。そのため、東京都老人医療センター（現・東京都健康長寿医療センター）で医師として勤務していた高柳さんは、関節リウマチにおける破骨細胞の研究に取り組み始めた。

「センターでは、医師が研究員を兼任するシステムがありました。そこで私は、手術で取り出した組織をセンターの隣の研究所で分析し、研究を進めました。良い結果を出すことができたので、大学院で、本格的に基礎研究をしようと考えました」

東京大学大学院医学系研究科に進学した高柳さんは、精力的に関節リウマチの骨破壊と破骨細胞の研究に取り組んだ。

「大学院で、まずは整形外科教室に入りましたが、関節リウマチの原因をさかのぼっていくうちに、免疫学にたどり着きました。そして免疫系と骨を結びつけた研究をしないと、リウマチの根治ができないと考え、後半の2年間は免疫系の調整機能物質、インターフェロンの権威である谷口維紹先生の免疫学教室に移りました。そこで、免疫系の因子と骨代謝制御因子の相互作用について研究しました」

骨代謝は免疫系の因子に絶妙に調整されている

高柳さんが大学院に進んだ翌1998年、日本と米国でそれぞれ、破骨細胞を増やす「破骨細胞分化因子（RANKL）」が発見された。免疫系の異常が、過剰に破骨細胞を分化させることも明らかにされてきた。それはまさに高柳さんが、研究を進めていた核心でもあった。博士課程在学中の2000年、高柳さんの論文が科学誌『Nature』に掲載された。リンパ球の一つであるT細胞が分泌する免疫調整物質、インターフェロン（IFN-γ）には破骨細胞を抑える働きがあるが、関節リウマチにかかると、T細胞がIFN-γを分泌しなくなるため、骨の破壊が進むことを見つけた。更に一方では、T細胞が破骨細胞を分化させる因子RANKLの発現を増やすことも明らかにした。つまり、免疫系に関与する因子が骨の代謝を絶妙に調整していることが示されたのだ。

この高柳さんの研究成果は高く評価され、『Nature』同号の解説記事では「『骨免疫学（Osteoimmunology=オステオイムノロジー）』の幕開け」と紹介された。骨の代謝にかかわる細胞と免疫系を制御する細胞は骨髄でつくられ、多くを共有しているが、それまで互いに別の分野の学問として研究されてきた。それが、この10年ほどで有機的に結びつき、新たな研究領域として確立したのだ。

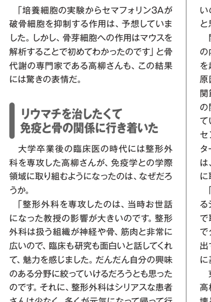

【写真左】研究用の培養細胞をつくるための培養室（クリーンベンチ）での作業風景。培養室内は外部からの埃や微生物などの混入を避け、無菌状態が保たれるようになっている。
【写真下】樹脂で固めたマウスの骨（写真右）を3μm（マイクロは100万分の1）の薄さになるよう、手作業でスライスする。その後、染色した標本を作り、顕微鏡で破骨細胞、骨芽細胞を数えていく地道な作業が続く。

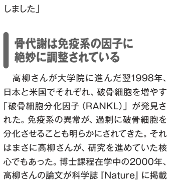

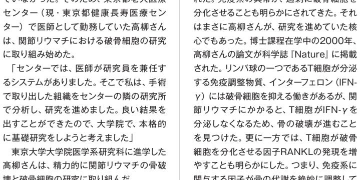

骨が他臓器の働きを制御しているのではないか

「骨免疫学」という研究領域を開いてきた高柳さんは2009年、JST ERATO「高柳オステオネットワークプロジェクト」の研究総括に就任し、パイオニアにしてトップランナーとしてこの分野をリードし続けている。

「通常は人体には、対称・非対称含めて約200個の骨が存在しますが、脊椎動物といわれるように、“骨あっての脊椎動物”なのです。骨は体を支えているだけだととらえがちですが、骨の働きにはもっと深い意味があると考えています」と、高柳さんは骨の役割についてさらなる追求をする覚悟だ。

オステオネットワークの研究には、既成の学問分野を横断した幅広いアプローチが必要となるため、プロジェクトを構成するメンバーの出身も医学部、歯学部はもとより、薬学部、農学部、理学部など実に多彩で、メンバーのほとんどが30代、20代の若手主体の編成だ。プロジェクトは3つのグループから成るが、高柳さんは、とりまとめを各グループリーダーに委ね、若い研究者たちの自主性やアイディアを引き出すようにしているという。また、週に2回はグループ間の情報交換会を行うなど、全体の意思統一を図りながら、メンバーがのびのびと研究に打ち込めるような環境づくりを進めている。

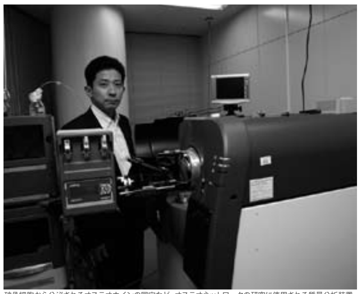

破骨細胞から分泌されるオステオカインの同定など、オステオネットワークの研究に使用される質量分析装置。ピコグラム単位（1グラムの1兆分の1）の分析が可能。

骨免疫学の今後の展望について聞くと、想像以上に大きな展開がありそうな答えが返ってきた。

「骨が免疫系のような制御系統と密接に結びつくことが、だんだんと明らかになっています。この4～5年の間に、骨が生産する物質が他臓器を制御している証拠も発見されてきています。例えば骨細胞が分泌するFGF23というタンパク質は、腎臓の制御に重要な役割を持つことがわかってきました。

骨が“体の柱”という役割だけではなく、いろいろな“内分泌組織”として機能していて、骨がつくりだす因子によって、ほかの臓器の働きが制御されている——そういう視点で見直してみると、いろいろな病気の原因がわかるのではないかと思っています。免疫系だけでなく、さまざまな組織と骨とのネットワークを解明したい、それが、『高柳オステオネットワークプロジェクト』の目的です」

「オステオ」とはギリシア語で「骨」を意味する言葉だ。「オステオネットワークプロジェクト」は、骨による全身の制御メカニズムを解明しようという壮大な計画なのだ。

「かつて、脂肪組織や筋肉の細胞は、内分泌系の組織だと考えられていませんでした。しかし、脂肪組織は『アディポカイン』、筋肉は『マイオカイン』と呼ばれる生理活性物質を分泌しています。このケースにならい、

■オステオネットワーク

骨は単なる運動器の一部ではなく、外界の環境変動やストレスを感受し、骨が分泌する生理活性物質「オステオカイン」と骨免疫の作用により、全身臓器を能動的に制御している。この骨による全身の制御メカニズムを「オステオネットワーク」と呼び、その解明を通じて、骨と他臓器に共通する種々の疾患に対する治療法の基盤を確立することを目指している。

ERATO「高柳オステオネットワークプロジェクト」メンバー。前列左から4番目が高柳さん。その右側から順に「オステオネットワーク解析グループ」リーダー・古賀貴子さん、「オステオサイト・マウスジェネティクスグループ」のリーダー・中島友紀さん、「オステオイムノロジーグループ」リーダー・岡本一男さん。

骨が分泌する生理活性物質は『オステオカイン』と名付けて、その仕組みを明らかにしていこうと考えています。

今後、このプロジェクトでは骨の細胞で発現している全ての遺伝子を網羅的に解析して、骨の代謝だけでなく、ほかの臓器の制御にかかわる因子を探していく予定です」

高柳さんは、まずはいくつかオステオカインを見つけて、その機能や作用機構を証明していくという。オステオカインが明らかにできれば、それを臨床応用していくことが、次のステップとして視野に入ってくるだろう。

オステオカインが次々に明らかになっていく

骨には大きく分けると、「骨芽細胞」、「破骨細胞」と「骨細胞」があるが、その3つの細胞を結びつけている分子はこれまでまったくわかっていなかった。高柳さんらは今回見つけたセマフォリン3Aを含めて、昨年から今年にかけて、細胞の相互作用にかかわる3つの因子を特定することに成功した。

一つは、骨細胞が破骨細胞分化因子RANKLをつくり、骨代謝の指令を出しているということだ。そして、二つ目に、セマフォリン4Dというタンパク質の働きを明らかにしたこと。セマフォリン4Dは破骨細胞がつくりだし、骨芽細胞による骨形成を抑制する因子だった。セマフォリン4Dの働きを抑えることで、骨形成を促進させることにも成功している。この2つの研究成果をどちらも科学誌『Nature Medicine』に発表し、高い評価を受けた。そして三つ目が今回明らかにしたセマフォリン3Aの驚くべき二通りの働きだ。セマフォリン3Aは一つの因子だけで骨吸収の抑制と骨形成の促進を同時に行う機能を持つため、骨量を増やす薬の開発に期待される。また、骨リモデリングのバランスを崩しているマウスではセマフォリン3Aが減少していることがわかったため、疾患診断の指標（バイオマーカー）としても使える可能性がある。

「セマフォリン3A、セマフォリン4Dも骨がつくる因子で、細胞間の相互作用を担っていますので、広い意味で『オステオカイン』の一つといえると思います」

基礎研究で新しい分野をつくってきた高柳さんだが「臨床の現場では、患者さんの求めるものや問題点がはっきり分かります。臨床の経験は、マウスでの研究とは全く違う、重みがあります」と、臨床医時代を振り返る。そして医師らしく「骨を強くし、体を整えるのに一番よいのは、運動ですよ」と笑った。高柳さん自身は学生時代からテニス、スキー、ヨットを楽しみ、忙しい今もスカッシュなどで汗を流すという。

高柳さんは今年5月から、東京大学大学院医学系研究科の教授に就任し、熱意あふれる若手研究者たちを率いて、力強く研究を進めている。骨と免疫の関係から発展を遂げたオステオネットワークの世界は、新たな夜明けを迎えている。

JST 担当者が見た「ERATO 高柳オステオネットワークプロジェクト」
「健康」に対する意識が変わるかもしれない、社会への反響も大きいプロジェクトです。

JST 古屋美和

2009年10月にスタートした「高柳オステオネットワークプロジェクト」は研究期間が中盤に差し掛かった現在、科学誌『Nature』やその姉妹誌などに次々に成果を発表し、国内外から高い評価を受けています。高柳先生とメンバーの皆さんが、医療や創薬の現場で求められる事柄を強く認識し、ぶれない視点で基礎研究にあたっておられることが、一つひとつのデータの出し方にも現れた結果なのではないかと考えています。

こうした順調な成果は、メンバーの皆さんがこのプロジェクトを起点に飛躍する地盤を築かれていることも意味していると思います。ERATO事業は、「人中心」「新たな科学技術の源流を生む」ことを目指していますが、本プロジェクトでそれが実現されることを一担当として願っています。

今後、骨がほかの臓器の代謝調節の一軸として機能していることが明らかになれば、「オステオネットワーク」概念の確立という学術的なインパクトはもとより、社会への反響も大きいと思います。私たちは今まで以上に骨の健康に気遣うようになるでしょうし、健康に関する新しい産業を創出するきっかけになるかもしれません。これからの研究によって、今回の成果のように骨の健康維持にかかわる因子が、更に明らかになることも想定されますので、それらが画期的な創薬ターゲットになることも期待できます。

高柳先生は今年5月から東京大学に移籍されました。プロジェクト事務所と共に、研究環境のセットアップなど、この時期をスムーズに乗り越えられるようサポートしていきたいと思います。

TEXT: 羽柴重文 /PHOTO: 瀬戸正人　7

日本経済新聞　2012年10月21日（日）　17面（サイエンス）

ナゾ謎かがく

骨と免疫、深いかかわり？

「骨免疫学」と呼ばれる新しい医学分野が注目を集めている。細菌などの外敵から体を守る免疫の仕組みと、骨の間には実は深い関係があるらしい。世界的に研究が活発になってきた。

「骨と免疫は独立した別のものと長らく考えられてきたが、見方が大きく変わりつつある」と高柳広・東京大学教授は話す。骨がつくり出す物質が他の臓器をコントロールしている証拠も見つかっている。

腎臓や肝臓にも影響

どうやら骨の役割は体を支える「骨組み」だけではなく、様々な物質を出して身体の機能のバランスを保つ「内分泌組織」の役目も担っているらしい。

関節リウマチは免疫の異常が手足の関節の骨に影響を及ぼし、つらい痛みを生じる。また骨髄には血中の免疫細胞のもとになる幹細胞がたくさんある。骨と免疫の間には浅からぬ縁があっても不思議ではない。しかし医学の世界では、同居してはいるが他人だととらえるのが一般的だった。

認識が変わり始めたのは2000年以降。免疫が働かないマウスで骨の異常が見つかり、骨を作る細胞（骨芽細胞）のたんぱく質が免疫細胞の働きを抑えていた。

さらに驚くことに、骨の細胞が出すたんぱく質が腎臓の働きを制御し、神経細胞が枝（軸索）を伸ばす働きに関わる証拠が見つかった。骨が肝臓など他の臓器に影響を与えているらしい。

甲状腺や膵臓（すいぞう）のランゲルハンス島などは内分泌腺と呼ばれ、多様なホルモン（たんぱく質）を出して体の働きを調整する。骨も知られざる内分泌器官であるかもしれない。

陸上に住む哺乳動物などがしっかりした骨を発達させたのは体を支えるためだ。骨はまた細胞に不可欠なカルシウムの「貯蔵庫」でもある。カルシウムを含む海から離れるには体内にカルシウムをためておく場所が必要だった。

「ひょっとしたら陸上にあがった動物は新たな外敵に対抗する免疫を備える役割を骨に担わせたのかもしれない」と高柳教授は話す。骨がなぜそのような多様な機能を担うのか進化的な意味合いはまだ推測の域を出ないが、骨がいろいろな意味で健康の基盤であることは間違いない。

（編集委員　滝順一）

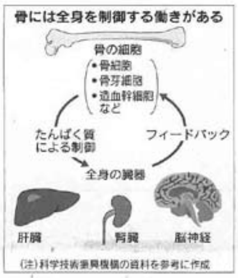

（注）科学技術振興機構の資料を参考に作成

平成24年4月19日　時事通信(net)　平成24年4月19日　プレス共同発表

THE WALL STREET JOURNAL.
ウォール・ストリート・ジャーナル 日本版

骨増やすたんぱく質発見＝破壊と形成、同時に制御―東京医科歯科大

2012年 4月 19日 7:59 JST

骨の破壊抑制と形成促進を同時に行い、骨の増加につなげる働きが「セマフォリン3A」と呼ばれるたんぱく質にあることを東京医科歯科大大学院の高柳広教授（分子情報伝達学）らの研究グループが発見し、19日に英科学誌ネイチャーの電子版に発表した。骨の破壊と形成を同時にコントロールできるたんぱく質の発見は世界初で、骨粗しょう症や関節リウマチなどの新しい治療法開発につながると期待される。

［時事通信社］

平成24年4月19日　東京　28面　平成24年4月19日　プレス共同発表

骨作り促進&保護 タンパク質を発見
骨粗しょう症治療期待

体内で骨を作る細胞を増やす一方、骨を壊す細胞を減らして骨の健康を守るタンパク質を、高柳広東京医科歯科大教授らのチームがマウスの実験で特定し、十八日付の英科学誌ネイチャー電子版に発表した。

骨の新陳代謝の過程で形成と破壊のバランスが崩れると、骨粗しょう症などになる。現在の治療は骨の破壊を抑える薬が中心だが、形成も同時に阻害されてしまうのが問題だった。今回、特定されたタンパク質は人間にもあり、高柳教授は「骨の破壊を減らすとともに形成を増やす新しい治療法の開発につながる」と話している。

チームはマウスの骨を作る細胞から分泌されるタンパク質を解析。そのうち神経細胞の成長などに関わる「セマフォリン3A」というタンパク質が、骨の形成を促進すると同時に、骨を壊す細胞を作りにくくして骨破壊を抑制することを確認した。このタンパク質が働かないようにしたマウスでは、通常と比べて骨を壊す細胞は二倍増加し、骨量が三分の一以下になった。

マウスの大腿骨に小さな穴を開け、このタンパク質を穴周辺に投与して骨の再生度を調べると、投与していない場合と比べて骨量は一・五倍ほど増加した。

平成24年4月19日　朝日　37面　平成24年4月19日　プレス共同発表

骨の減少抑える たんぱく質発見
骨粗鬆症治療に期待
東京医科歯科大

骨の中が空洞化する「骨粗鬆症」など骨量が減る病気について、その減少をくい止めるたんぱく質を、東京医科歯科大の高柳広教授（骨免疫学）らが見つけた。国内に患者が１３００万人いるとされる骨粗鬆症や関節リウマチなど骨の病気への治療の応用が期待される。

骨は、破壊（吸収）と新たな形成のバランスが保たれることで、健康な状態を保っている。このバランスが崩れ、吸収が多くなると骨が空洞化して骨粗鬆症になったり、逆の場合は骨が密になる「大理石骨病」などを引き起こす。現在の骨粗鬆症の治療は、吸収を抑えることが中心で、形成を促す薬はほとんどないという。

高柳教授らは、もともと神経や免疫をコントロールする作用があることが知られていた「セマフォリン３Ａ」（セマ３Ａ）というたんぱく質に、骨の破壊を抑える効果があることを確認した。このたんぱく質を、マウスに静脈注射したところ、吸収の細胞を抑え、形成の細胞が促進され、骨量が適切に増えた。

また、老化するにつれて、骨量が減っているマウスの血中を調べたところ、セマ３Ａの濃度が比例して減っていた。今後、臨床診断の指標になる可能性もあるという。

18日付の英科学誌ネイチャー（電子版）に掲載される。

（石塚広志）

平成24年4月19日　日経産業　11面　平成24年4月19日　プレス共同発表

骨増加促すたんぱく質

東京医歯大が発見　破壊抑制機能も

東京医科歯科大学の高柳広教授らは、骨の成長を促すとともに破壊を抑えて骨の増加につなげる働きを持つたんぱく質を発見し、19日付の英科学誌ネイチャー（電子版）に発表した。このたんぱく質をマウスに投与すると、骨の再生が進んだ。骨粗しょう症や関節リウマチなどの新しい治療薬の開発につながる成果と期待される。

体内では、古い骨を壊す破骨細胞と骨を作る骨芽細胞によって新陳代謝を繰り返し、新しい骨が作られている。年をとるなどしてホルモンのバランスが崩れると、破骨細胞の働きが活発になって骨の破壊が進み、骨粗しょう症などになる。

高柳教授らは、遺伝子を構成するたんぱく質の機能や構造を調べるプロテオーム解析を使い、骨芽細胞と破骨細胞の両方に関係する物質を調べた。骨芽細胞が分泌する「セマフォリン3A」と呼ぶたんぱく質に、骨の成長促進と破壊抑制の両方の働きがあることがわかった。

ドリルで骨に穴をあけたマウスを使って実験したところ、セマフォリン3Aを与えたマウスは骨の再生が速くなった。

骨の成長か破壊かどちらかに関係する物質はこれまでもいくつか見つかっているが、両方に関与するものはなかった。より効果が高い治療薬の開発につながる可能性があると高柳教授らはみている。

平成24年4月19日　日刊工業　17面　平成24年4月19日　プレス共同発表

骨の形成と破壊制御　たんぱく質を特定

東京医科歯科大

東京医科歯科大学大学院医歯学総合研究科の高柳広教授らのグループは、骨の形成と破壊をコントロールして丈夫な骨を作るのに必要なたんぱく質を特定することに成功した。このたんぱく質を骨粗しょう症のマウスに投与したところ、骨の減少を食い止めて再生を促すのを確認した。骨粗しょう症や関節リウマチなど、骨量が減少する病気の新たな治療薬開発に結びつくと期待される。英科学誌ネイチャー電子版に19日掲載される。

このたんぱく質は「セマフォリン3A」と呼ばれ、神経細胞や免疫系の制御に関与していることが知られていたが、骨との関連は不明だった。

骨は新たな骨を形成する「骨芽細胞」と古くなった骨を吸収する「破骨細胞」が、バランスを取ることで正常な骨密度を維持している。どちらかの細胞が減りすぎたり増えすぎたりすると、骨折しやすくなる。グループの研究により、セマフォリン3Aは両細胞のバランスを取る役割を果たしていることが分かった。

従来、骨粗しょう症の治療では破骨細胞の働きを抑制する薬剤が考案されてきたが、相互作用で骨芽細胞も抑制されてしまう課題があった。セマフォリン3Aを指標にした薬剤を開発すれば課題を克服できる可能性があり、グループは5年後をめどに臨床試験に結びつける考え。実用化に向けて高柳教授は「たんぱく質は分解されやすいため、安定して作用する方法を考える必要がある」としている。

2012年（平成24年）4月23日（月曜日）　夕刊　読売新聞　4版　12

たんぱく質を発見

骨の減少抑え成長促進

骨の減少を抑えると同時に成長させるたんぱく質を、東京医科歯科大学の高柳広教授らが初めて突き止めた。骨粗しょう症の治療や診断につながる成果として注目される。

健康な骨は、骨を減らす破骨細胞と、骨を増やす骨芽細胞の働きでバランスが取れている。骨粗しょう症は、何らかの原因で骨の減少量の方が多くなった状態。治療薬は、破骨細胞の働きを抑えるものが中心だが、骨芽細胞の働きも損なわれる性質があるため、大きな効果は望めなかった。

骨粗しょう症治療に期待

高柳教授らは、骨芽細胞が分泌するたんぱく質を分析し、破骨細胞の働きを抑え骨芽細胞の成長も促進する物質として、セマフォリン3A（セマ3A）を見つけた。

これを、正常なマウスに、体重1キロ・グラムあたり1ミリ・グラムの割合で週1回4週間にわたり静脈注射したところ、骨の密度が1・5倍になった。骨芽細胞は3～4割増え、逆に破骨細胞数は約2割減った。

高柳教授は「セマ3Aは体内で分解されやすいので、いかに効果的に働かせるかが課題。5年以内に臨床研究を始められるよう研究を進めたい」としている。

ARTICLE

doi:10.1038/nature11000

Osteoprotection by semaphorin 3A

Mikihito Hayashi[1,2,3], Tomoki Nakashima[1,2,3], Masahiko Taniguchi[4], Tatsuhiko Kodama[5], Atsushi Kumanogoh[6,7] & Hiroshi Takayanagi[1,2,3,8]

The bony skeleton is maintained by local factors that regulate bone-forming osteoblasts and bone-resorbing osteoclasts, in addition to hormonal activity. Osteoprotegerin protects bone by inhibiting osteoclastic bone resorption, but no factor has yet been identified as a local determinant of bone mass that regulates both osteoclasts and osteoblasts. Here we show that semaphorin 3A (Sema3A) exerts an osteoprotective effect by both suppressing osteoclastic bone resorption and increasing osteoblastic bone formation. The binding of Sema3A to neuropilin-1 (Nrp1) inhibited receptor activator of nuclear factor-κB ligand (RANKL)-induced osteoclast differentiation by inhibiting the immunoreceptor tyrosine-based activation motif (ITAM) and RhoA signalling pathways. In addition, Sema3A and Nrp1 binding stimulated osteoblast and inhibited adipocyte differentiation through the canonical Wnt/β-catenin signalling pathway. The osteopenic phenotype in *Sema3a*$^{-/-}$ mice was recapitulated by mice in which the Sema3A-binding site of Nrp1 had been genetically disrupted. Intravenous Sema3A administration in mice increased bone volume and expedited bone regeneration. Thus, Sema3A is a promising new therapeutic agent in bone and joint diseases.

Bone homeostasis has long been thought to be predominantly maintained by the endocrine system by calcium regulating hormones, but increasing evidence indicates that bone is also under the control of factors related to immune and neuronal regulation[1,2]. As an imbalance between bone resorption and formation results in metabolic bone disorders such as osteoporosis[3,4], understanding the balancing mechanisms is important for the development of therapeutic agents. Because bone formation is linked to resorption through coupling factors[5,6], treatment with anti-resorptive agents results in simultaneous suppression of bone formation, with the result that the efficacy is compromised[6–9]. It is thus crucial to identify a molecule that can regulate both resorption and formation synchronously.

Osteoclasts are derived from monocyte/macrophage precursor cells, and their differentiation is regulated by mesenchymal cells, such as osteoblasts, chondrocytes and osteocytes, which express the key osteoclast differentiation factor RANKL[1,10–12]. Osteoblastic cells counterbalance the function of RANKL by producing a soluble decoy receptor for RANKL, osteoprotegerin (Opg), the name of which indicates it is a protector of bone[13]. Here we show that conditioned medium from Opg-deficient mouse calvarial cells contains factors that inhibit osteoclast formation, and one of these factors is the axon guidance molecule Sema3A. Sema3A inhibits osteoclast differentiation and promotes osteoblastic bone formation, and is thus a potent osteoprotective factor produced by osteoblastic cells.

Sema3A mediates anti-osteoclastogenesis in osteoblasts

The conditioned medium of osteoblastic cells was able to inhibit osteoclast differentiation of bone marrow-derived monocyte/macrophage precursor cells (BMMs) stimulated by RANKL in the presence of macrophage colony-stimulating factor (M-CSF) (Fig. 1a). We observed a substantial anti-osteoclastogenic effect in the conditioned medium of calvarial cells lacking the *Tnfrsf11b* gene (encoding Opg in mice) (Fig. 1a), suggesting the presence of one or more other soluble inhibitory factors. To identify the osteoblast-secreted proteins that inhibit osteoclast differentiation, we fractionated the conditioned medium of *Tnfrsf11b*$^{-/-}$ calvarial cells by anion-exchange liquid chromatography (Fig. 1b). We found that fractions 8–10 exerted a potent inhibitory effect on osteoclast differentiation (Fig. 1b). The proteins in fraction 8 were separated by SDS–polyacrylamide gel electrophoresis (SDS–PAGE; Fig. 1c), and the major bands were excised and analysed by liquid chromatography–tandem mass spectrometry (LC–MS/MS). Among the identified proteins (Fig. 1d), we focused on the axon guidance molecule Sema3A[14,15] (Supplementary Fig. 1a), as recent studies have suggested that axon guidance molecules are involved in the interaction between osteoblasts and osteoclasts[16–18]. Previous reports suggest that Sema3A expressed in the skeletal system may have a role in the regulation of innervation and blood vessel invasion and contribute to skeletal patterning[19–21], but the function of Sema3A in the regulation of bone remodelling remains unknown.

Western blot analysis confirmed that Sema3A protein was present in fractions 8 and 9 (Supplementary Fig. 1b), and that the inhibitory effect of fraction 9 is largely mediated by Sema3A, as this effect was abrogated by the addition of soluble Nrp1, which functioned as a Sema3A decoy receptor (Supplementary Fig. 1c). The addition of recombinant Sema3A potently inhibited osteoclast differentiation in a dose-dependent manner when Sema3A was added before RANKL treatment (Fig. 1e). When Sema3A was added after RANKL treatment, the inhibitory effect was not observed (Fig. 1e). *Sema3a* was predominantly expressed in osteoblast lineage cells among various cells examined (Supplementary Fig. 2a), whereas Sema3A was not detected in osteoclasts (Supplementary Fig. 2a–c). The expression of *Sema3a* messenger RNA in isolated osteocytes and osteoblasts was comparable (Supplementary Fig. 2d). *Sema3a* mRNA expression in calvarial cells was higher than that of any other semaphorin family member tested (Supplementary Fig. 2e).

[1]Department of Cell Signaling, Graduate School of Medical and Dental Sciences, Tokyo Medical and Dental University, Yushima 1-5-45, Bunkyo-ku, Tokyo 113-8549, Japan. [2]Japan Science and Technology Agency, Exploratory Research for Advanced Technology Program, Takayanagi Osteonetwork Project, Yushima 1-5-45, Bunkyo-ku, Tokyo 113-8549, Japan. [3]Global Center of Excellence Program, International Research Center for Molecular Science in Tooth and Bone Diseases, Yushima 1-5-45, Bunkyo-ku, Tokyo 113-8549, Japan. [4]Department of Molecular Medical Sciences, Research Institute for Frontier Medicine, Sapporo Medical University School of Medicine, S-1, W-17, Chuo-ku, Sapporo 060-8556, Japan. [5]Laboratory for Systems Biology and Medicine, Research Center for Advanced Science and Technology, Department of Molecular Biology and Medicine, University of Tokyo, Komaba 4-6-1, Meguro-ku, Tokyo 153-8904, Japan. [6]Department of Respiratory Medicine, Allergy and Rheumatic Diseases, Graduate School of Medicine, Osaka University, Yamadaoka 2-2, Suita, Osaka 565-0871, Japan. [7]Department of Immunopathology, Immunology Frontier Research Center, Osaka University, Yamadaoka 3-1, Suita, Osaka 565-0871, Japan. [8]Centre for Orthopaedic Research, School of Surgery, The University of Western Australia, Nedlands, Western Australia 6009, Australia.

RESEARCH ARTICLE

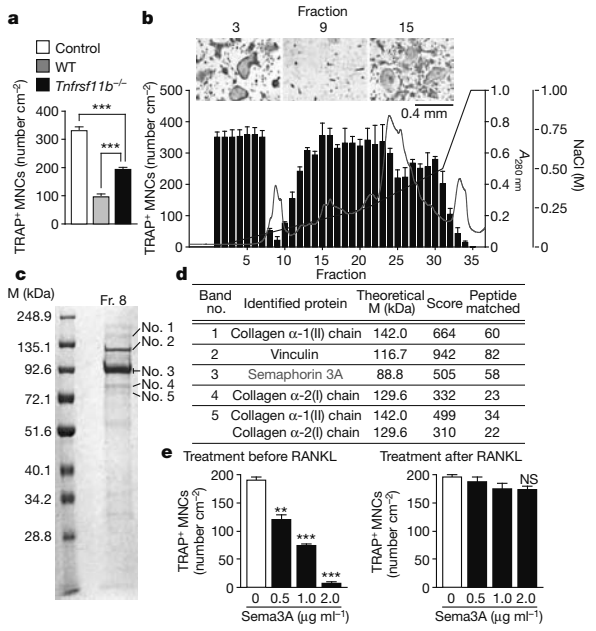

Figure 1 | Identification of Sema3A as an inhibitory factor of osteoclast differentiation. **a**, Effect of wild-type (WT) and Opg-deficient (*Tnfrsf11b*$^{-/-}$) calvarial cell-conditioned medium on osteoclast differentiation. MNC, mononuclear cells. **b**, Fractionation of Opg-deficient calvarial cell-conditioned medium by anion-exchange chromatography, and the effect of each fraction on osteoclast differentiation (black bars). Absorbance at 280 nm is indicated as a red line and the concentration of NaCl as a blue line. Inset shows TRAP staining of osteoclast cultures treated with fractions 3, 9 and 15. **c**, Coomassie brilliant blue-stained SDS–PAGE image of fraction 8. M, molecular mass. **d**, List of the identified proteins (that is, more than 300 on the MASCOT score), their theoretical molecular mass, MASCOT score and the number of non-redundant peptides. **e**, Effect of Sema3A treatment on osteoclast differentiation. Error bars (**a**, **b** and **e**) denote mean ± s.e.m. $^{**}P < 0.01$; $^{***}P < 0.005$; NS, not significant.

Sema3A regulates osteoclast differentiation via Nrp1

Microcomputed tomography along with bone morphometric and radiographic analyses showed that *Sema3a*$^{-/-}$ mice[19] have a severe osteopenic phenotype both in trabecular and cortical bones, accompanied by an increase in the osteoclast number and eroded surface (Fig. 2a, b and Supplementary Fig. 3a–c). There was no difference in the number of osteoclast precursor CD11b$^{low/-}$CD3ε^{-}B220^{-}c-fms^{+}c-kit^{+} cells[22] in the bone marrow of wild-type and *Sema3a*$^{-/-}$ mice (Supplementary Fig. 3d).

When osteoclast formation was analysed in a coculture of bone marrow and calvarial cells, the formation of tartrate-resistant acid phosphatase (TRAP)-positive multinucleated osteoclasts was markedly enhanced in *Sema3a*$^{-/-}$ cells (Fig. 2c and Supplementary Fig. 3e, f). This enhanced osteoclastogenesis was not observed when BMMs were stimulated by RANKL and M-CSF (Supplementary Fig. 3g). In addition, enhanced osteoclastogenesis was observed in the coculture of wild-type bone marrow cells and *Sema3a*$^{-/-}$ calvarial cells, but not in the coculture of *Sema3a*$^{-/-}$ bone marrow cells and wild-type calvarial cells (Fig. 2c and Supplementary Fig. 3e, f). These results indicate that the osteoblastic expression of Sema3A inhibits osteoclastogenesis. The level of RANKL and Opg in the calvarial cells or the serum was not affected by Sema3A deficiency (Supplementary Fig. 3h, i).

Sema3A binds to a receptor complex of the ligand-binding subunit Nrp1 and one of the class A plexins (PlxnA1, PlxnA2, PlxnA3 and PlxnA4), which function as the signal-transducing subunit[23].We found that Nrp1 expression in BMMs was rapidly and markedly suppressed after RANKL stimulation (Fig. 2d). Because Sema3A-induced inhibition of osteoclastogenesis was observed only when Sema3A was added before RANKL stimulation (Fig. 1e), we proposed that Sema3A does not inhibit osteoclastogenesis after RANKL stimulation owing to Nrp1 downregulation.

When Nrp1 was overexpressed by retroviral transfer, Sema3A exerted an inhibitory effect even when Sema3A had been added after RANKL stimulation (Supplementary Fig. 3j). Notably, osteoclastogenesis was inhibited by Nrp1 overexpression only (Supplementary Fig. 3j). When *Nrp1* expression was knocked down by short hairpin RNA (shRNA), the inhibitory effect of Sema3A on osteoclast differentiation was abolished (Supplementary Fig. 3k). Thus, the level of Nrp1 correlates with the inhibitory effect of Sema3A on osteoclastogenesis, suggesting that the Nrp1 downregulation caused by RANKL signalling is important for proper osteoclast differentiation by cancelling the inhibitory effect of Sema3A.

Furthermore, we analysed knockin mice in which the *Nrp1* gene was replaced by mutant *Nrp1* lacking the Sema-binding site (*Nrp1*$^{Sema-}$ mice), as *Nrp1*$^{-/-}$ mice are embryonically lethal and Nrp1 also contains the vascular endothelial growth factor (VEGF)-binding site[24]. Sema3A did not inhibit RANKL-induced osteoclast differentiation in *Nrp1*$^{Sema-}$ cells (Supplementary Fig. 3l), showing that Sema3A inhibits osteoclastogenesis by binding to Nrp1. As expected, *Nrp1*$^{Sema-}$ mice showed an osteopenic phenotype accompanied by enhanced osteoclast differentiation, which was similar to *Sema3a*$^{-/-}$ mice (Fig. 2e, f and Supplementary Fig. 3m–o).

To understand the mechanism of the RANKL-induced inhibition of Nrp1 expression, we examined the involvement of the transcription factors nuclear factor-κB (NF-κB), c-Fos and nuclear factor of activated T cells c1 (NFATc1), which are all activated by RANKL[1]. RANKL-induced downregulation of *Nrp1* expression was abolished by an NF-κB inhibitor, but was not affected by the deficiency of NFATc1 or c-Fos (Supplementary Fig. 4a–c). Chromatin immunoprecipitation analysis showed that NF-κB p65 and, to a lesser extent, p50 were recruited to the proximal NF-κB-binding site of the *Nrp1* promoter after RANKL stimulation (Supplementary Fig. 4d, e). NF-κB p65 and p50 inhibited *Nrp1* promoter activity in a reporter gene assay (Supplementary Fig. 4f). Retroviral overexpression of p65 in BMMs led to Nrp1 downregulation in the absence of RANKL, which was further facilitated by p50 overexpression (Supplementary Fig. 4g). These effects were dependent on histone deacetylases (Supplementary Fig. 4g, h), suggesting that the recruitment of corepressors[25] by RANKL-stimulated NF-κB is involved in Nrp1 downregulation.

Mechanism of anti-osteoclastogenesis by Sema3A

The binding of RANKL to its receptor RANK results in the activation of tumour-necrosis factor (TNF) receptor-associated factor 6 (TRAF6), which stimulates the NF-κB and mitogen-activated protein kinase (MAPK) pathways[1]. RANKL also activates the activator protein 1 (AP-1) transcription factor complex, including c-Fos, which cooperates with NF-κB to induce NFATc1, thus activating the transcription of osteoclast-specific genes[1,26]. The robust induction of NFATc1 is dependent on calcium signalling (costimulatory signalling) stimulated by the ITAM-bearing adaptor molecules DNAX-activation protein 12 (DAP12) and Fc receptor common γ subunit (FcRγ), which associate with immunoglobulin-like receptors such as triggering receptor expressed on myeloid cells 2 (TREM2) and osteoclast-associated receptor (OSCAR)[1,27].

From these observations, the question arises as to how the Sema3A–Nrp1 axis inhibits osteoclastogenic signalling. RANKL-stimulated induction of the osteoclastic genes *Ctsk*, *Acp5* and *Nfatc1* was severely impaired by Sema3A without affecting the expression of *Tnfrsf11a* or *Csf1r* (Fig. 3a). There was no difference in the cell proliferation rate or the percentage of apoptotic cells among the osteoclast precursor cells between the Sema3A-treated and the control cells (Supplementary Fig. 5a, b). RANKL-induced activation

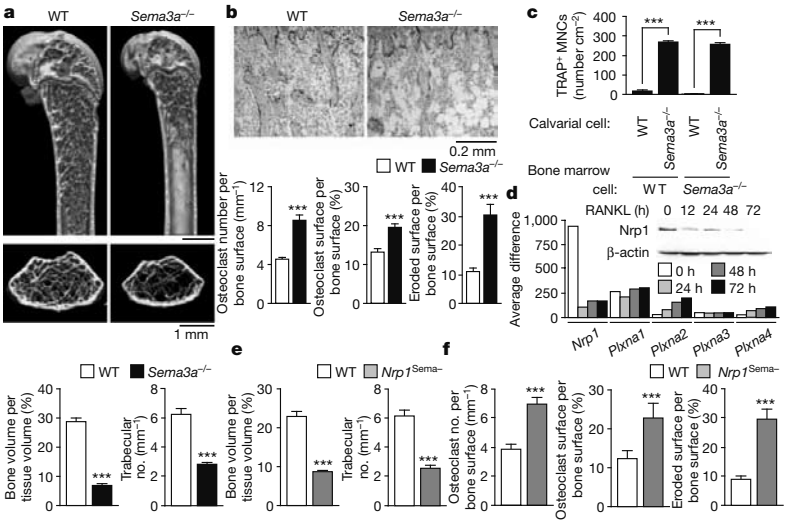

Figure 2 | *Sema3a*$^{-/-}$ and *Nrp1*$^{Sema-}$ mice show a severe low bone mass phenotype. **a**, Microcomputed tomography images of the femurs of 10-week-old *Sema3a*$^{-/-}$ mice and their wild-type littermates ($n = 4–6$). The bone volume and parameters of trabecular bone were determined by microcomputed tomography analysis. **b**, TRAP staining of the proximal tibiae of *Sema3a*$^{-/-}$ mice and their wild-type littermates ($n = 4–6$). Osteoclastic parameters were measured using bone morphometric analysis. **c**, Osteoclast differentiation from wild-type or *Sema3a*$^{-/-}$ bone marrow cells in coculture with wild-type or *Sema3a*$^{-/-}$ calvarial cells at day 4. **d**, GeneChip analysis of the mRNA expression of *Nrp1* and *Plxna1–4* during osteoclast differentiation. Nrp1 protein expression in BMMs stimulated with RANKL was analysed by western blot (inset). **e**, Microcomputed tomography analysis of the femurs of 10-week-old *Nrp1*$^{Sema-}$ mice and their wild-type littermates ($n = 4–5$). **f**, Parameters for osteoclastic bone resorption in the bone morphometric analysis of the proximal tibiae of *Nrp1*$^{Sema-}$ mice and their wild-type littermates ($n = 4–5$). Error bars (**a–c**, **e** and **f**) denote mean ± s.e.m. $^{**}P < 0.01$; $^{***}P < 0.005$.

of the signalling pathways downstream of TRAF6, including the MAPKs (such as ERK, JNK, p38) and inhibitor of κB (IκB) kinases, was comparable in BMMs with or without Sema3A (Supplementary Fig. 5c).

PlxnA1 promotes osteoclast differentiation by activating the ITAM signal through the formation of the PlxnA1–TREM2–DAP12 complex in response to ligands such as Sema6D[17]. However, PlxnA1 is constitutively associated with Nrp1, which mediates Sema3A signalling instead of TREM2−DAP12 signalling[28]. With increasing Nrp1 expression, the amount of TREM2 associated with PlxnA1 decreased and Nrp1 associated with PlxnA1 increased (Fig. 3b).

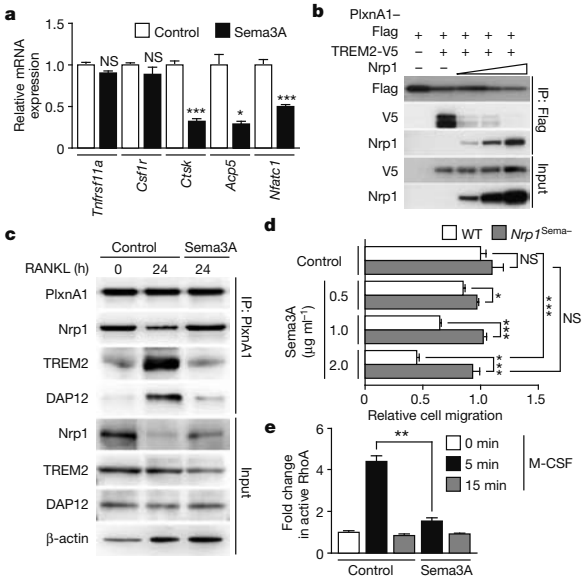

Figure 3 | Inhibition of osteoclast differentiation by Sema3A−Nrp1 signalling. **a**, Effect of Sema3A treatment on osteoclastic gene expression in BMMs treated with RANKL for 2 days. **b**, Effect of Nrp1 expression on the association of PlxnA1 with TREM2. IP, immunoprecipitation. **c**, Effect of Sema3A treatment on the formation of a complex of PlxnA1 with Nrp1 or TREM2/DAP12 in RANKL-treated BMMs. **d**, Transwell assay of the effect of Sema3A on M-CSF-induced migration of BMMs derived from wild-type or *Nrp1*$^{Sema-}$ mice. **e**, Effect of Sema3A treatment on the activation of RhoA in BMMs stimulated with M-CSF. Error bars (**a**, **d** and **e**) denote mean ± s.e.m. $^{*}P < 0.05$; $^{**}P < 0.01$; $^{***}P < 0.005$.

RANKL induced the formation of the PlxnA1–TREM2–DAP12 complex by the downregulation of Nrp1, thereby releasing PlxnA1 from the PlxnA1–Nrp1 complex (Fig. 3c). Sema3A treatment inhibited RANKL-induced formation of the PlxnA1–TREM2–DAP12 complex by inhibiting Nrp1 downregulation and maintaining the PlxnA1–Nrp1 complex (Fig. 3c). The cell surface and intracellular expression of Nrp1 was highly downregulated by RANKL treatment (Supplementary Fig. 5d), but Sema3A treatment induced the internalization of Nrp1, as already reported[29], and protected RANKL-induced Nrp1 downregulation without altering *Nrp1* mRNA expression (Supplementary Fig. 5d, e).

RANKL-induced tyrosine phosphorylation of phospholipase Cγ2 (PLCγ2) and calcium oscillation were both markedly blocked by Sema3A treatment (Supplementary Fig. 5f, g). We observed that osteoclast differentiation in DAP12-deficient (also known as *Tyrobp*-deficient) bone marrow cells was not enhanced even in a coculture with *Sema3a*$^{-/-}$ calvarial cells (Supplementary Fig. 5h), suggesting that Sema3A-induced inhibition is mediated by the modulation of DAP12-induced ITAM signalling. Thus, Nrp1 competes with TREM2 for PlxnA1, thereby functioning as a suppressor of the PlxnA1–TREM2–DAP12-induced costimulatory signal. Sema3A-induced inhibition of osteoclast differentiation was less observed in the presence of Sema6D (Supplementary Fig. 5i).

We examined the effect of Sema3A on the migration of BMMs because the semaphorin–plexin system regulates actin cytoskeletal rearrangement[15,23]. We observed a repulsive effect of Sema3A on M-CSF-induced migration of BMMs (Fig. 3d). By contrast, this repulsive effect was not observed in *Nrp1*$^{Sema-}$ BMMs (Fig. 3d). Because semaphorin–plexin signalling regulates the Rho family of small GTPases[15,23], we examined the effect of Sema3A treatment on M-CSF-induced activation of the RhoA and Rac GTPases. Sema3A treatment abrogated RhoA activation in response to M-CSF (Fig. 3e), but not Rac activation (Supplementary Fig. 5j), suggesting that the inhibition of RhoA activation is involved in the inhibitory effect of Sema3A on the migration of BMMs.

Sema3A regulates osteoblasts through the Wnt pathway

In addition to an osteoclastic phenotype, both *Sema3a*$^{-/-}$ and *Nrp1*$^{Sema-}$ mice were found to have osteoblastic and adipocytic

RESEARCH ARTICLE

phenotypes (Fig. 4a and Supplementary Fig. 6a–c); that is, they had a decreased osteoblast number, a reduced bone formation rate and a markedly increased adipocyte number (Fig. 4b and Supplementary Fig. 6d, e) without any significant difference in the weight of the epididymal white adipose tissue per body weight (Supplementary Fig. 6f, g). Taken together, the severe osteopenic phenotype in *Sema3a*$^{-/-}$ and *Nrp1*$^{\mathrm{Sema-}}$ mice was caused by both a decrease in the osteoblastic bone formation and an increase in osteoclastic bone resorption.

Calvarial cells obtained from *Sema3a*$^{-/-}$ or *Nrp1*$^{\mathrm{Sema-}}$ mice were cultured in an osteogenic medium with or without Sema3A. Alkaline phosphatase activity and bone nodule formation were markedly decreased in *Sema3a*$^{-/-}$ and *Nrp1*$^{\mathrm{Sema-}}$ cells, and Sema3A treatment facilitated the differentiation of *Sema3a*$^{-/-}$ calvarial cells into osteoblastic cells, but not *Nrp1*$^{\mathrm{Sema-}}$ cells (Fig. 4c, d and Supplementary Fig. 6h–k). Neither the cell proliferation rate nor the percentage of apoptotic cells was affected in both types of mutant cells (Supplementary Fig. 6l, m). Adipocyte differentiation was highly increased in both *Sema3a*$^{-/-}$ and *Nrp1*$^{\mathrm{Sema-}}$ cells, and Sema3A treatment blocked the differentiation of wild-type and *Sema3a*$^{-/-}$ cells into adipocytes, but not *Nrp1*$^{\mathrm{Sema-}}$ cells (Fig. 4e and Supplementary Fig. 6n, o). In *Sema3a*$^{-/-}$ cells, the expression of the osteoblast genes *Runx2*, *Sp7* (which encodes osterix), *Alpl* and *Bglap* (encoding osteocalcin) was strongly suppressed (Supplementary Fig. 7a), and the expression of the adipocyte genes *Pparg*, *Cebpa*, *Fabp4* (encoding aP2) and *Lpl* (encoding lipoprotein lipase) was highly increased (Supplementary Fig. 7b). These results indicate that Sema3A activates osteoblast differentiation and inhibits adipocyte differentiation through Nrp1.

Because the mRNA expression levels of the known regulators of mesenchymal cell differentiation[30,31] were comparable in wild-type and *Sema3a*$^{-/-}$ cells (Supplementary Fig. 7c), we performed gene expression profiling of the calvarial cells derived from *Sema3a*$^{-/-}$ mice to obtain insight into the Sema3A-activated molecular pathways in osteoblasts. Gene set enrichment analysis in *Sema3a*$^{-/-}$ cells showed a significant downregulation of the gene sets involved in the Wnt signalling pathway and the Wnt-related signalling pathways (Supplementary Fig. 7d and Supplementary Table 1). We therefore focused on the canonical Wnt pathway, as it is known to promote osteoblast differentiation and inhibit adipocyte differentiation[31–33]. The mRNA expression of most of the transcriptional targets of β-catenin was considerably reduced (Supplementary Fig. 7e), and the Wnt3a-induced nuclear accumulation of β-catenin was suppressed in *Sema3a*$^{-/-}$ calvarial cells (Fig. 5a).

The Sema3A signalling pathway induces activation of the small G protein Rac1 through FARP2 (FERM, RhoGEF and pleckstrin domain protein 2), which is a guanyl-nucleotide exchange factor (GEF) specific for Rac1 (ref. 34). Previous studies suggested a regulatory role of FARP2 in transduction of semaphorin-induced repulsive cues in axons, via Rac1 activation[34]. Because Rac1 promotes the nuclear localization of β-catenin in response to canonical Wnt ligands[35], we examined the activation of Rac proteins and RhoA in *Sema3a*$^{-/-}$ cells. The activation of Rac, but not RhoA, in *Sema3a*$^{-/-}$ calvarial cells in response to Wnt3a treatment was significantly decreased (Fig. 5b and Supplementary Fig. 7f) as compared with that in wild-type control cells. In addition, Sema3A treatment facilitated the nuclear translocation of β-catenin and the activation of Rac in *Sema3a*$^{-/-}$ cells (Fig. 5a, b). The ectopic expression of a dominant negative form of FARP2 (ΔGEF-FARP2)[36] in calvarial cells resulted in the inhibition of osteoblast differentiation, even in the presence of Sema3A (Fig. 5c and Supplementary Fig. 7g). When ΔGEF-FARP2 was overexpressed, reduced nuclear accumulation of β-catenin was observed and Sema3A treatment had no effect on its nuclear localization (Fig. 5d). These results indicate that Sema3A stimulates the canonical Wnt/β-catenin signalling pathway, at least in part, through FARP2-mediated activation of Rac1 during osteoblast differentiation.

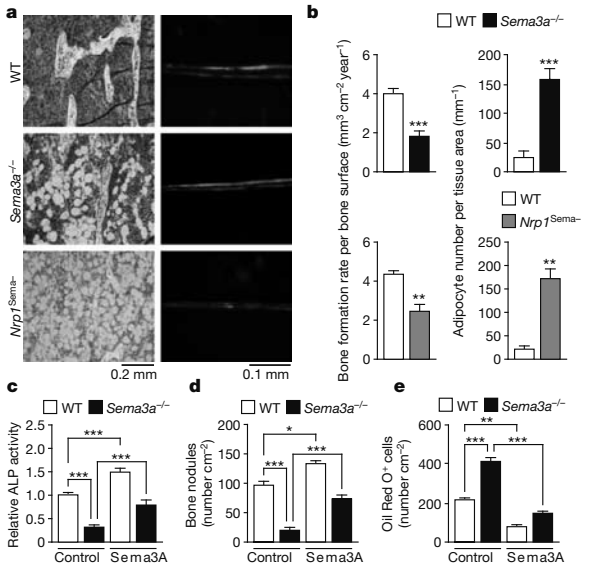

Figure 4 | Impaired osteoblast differentiation and increased adipocyte differentiation in *Sema3a*$^{-/-}$ and *Nrp1*$^{\mathrm{Sema-}}$ mice. **a**, Toluidine blue staining of the proximal tibiae of wild-type, *Sema3a*$^{-/-}$ and *Nrp1*$^{\mathrm{Sema-}}$ mice (left). New bone formation was determined by calcein double labelling (right). **b**, Osteoblastic and adipocytic parameters measured by histomorphometric analysis of wild-type, *Sema3a*$^{-/-}$ and *Nrp1*$^{\mathrm{Sema-}}$ mice ($n = 4$–6). **c**, Alkaline phosphatase (ALP) staining of wild-type and *Sema3a*$^{-/-}$ calvarial cells cultured in osteogenic medium with or without Sema3A. **d**, Bone nodule formation in wild-type and *Sema3a*$^{-/-}$ calvarial cells cultured in osteogenic medium with or without Sema3A. **e**, Adipocyte differentiation in wild-type and *Sema3a*$^{-/-}$ bone marrow stromal cells cultured in adipogenic medium with or without Sema3A. Error bars (**b**–**e**) denote mean ± s.e.m. $*P < 0.05$; $**P < 0.01$; $***P < 0.005$.

Sema3A as an osteoprotective therapeutic agent

To determine the *in vivo* effect of Sema3A administration on bone metabolism, 5-week-old male mice were intravenously injected with recombinant Sema3A or saline once a week. After four weeks of treatment, the trabecular bone volume and trabecular parameters in the distal femur were increased in the Sema3A-treated mice (Fig. 6a and Supplementary Fig. 8a). Bone morphometric analysis showed a decrease in osteoclastic parameters and an increase in osteoblastic parameters (Fig. 6b, c and Supplementary Fig. 8b–e), suggesting that Sema3A exerts a bone-increasing effect by stimulating osteoblastic bone formation and inhibiting osteoclastic bone resorption synchronously. We could not detect any pathological findings in vital organs or any behavioural abnormalities after the Sema3A injection (data not shown). The number of osteoclast precursor cells and osteoprogenitor cells in the bone marrow was not influenced by Sema3A administration (Supplementary Fig. 8f and data not shown), but bone marrow mesenchymal cells derived from Sema3A-treated mice tended to differentiate into osteoblasts instead of adipocytes *in vitro*, although the number of colony forming units was unchanged (Supplementary Fig. 8g, h).

We further investigated the therapeutic potential of Sema3A in a bone regeneration model of cortical bone defects induced by drill hole injury[37]. Microcomputed tomography analysis showed that the regenerated cortical bone volume in Sema3A-treated mice was higher than in saline-treated mice (Fig. 6d and Supplementary Fig. 8i). The significantly increased osteoblast surface and decreased osteoclast surface around the injured region were observed by histomorphometric analysis (Fig. 6e). These results indicate that the local administration of Sema3A into the injured site accelerates bone regeneration, although we cannot rule out the possibility that Sema3A exerted a bone protective effect partly through the regulation of innervation.

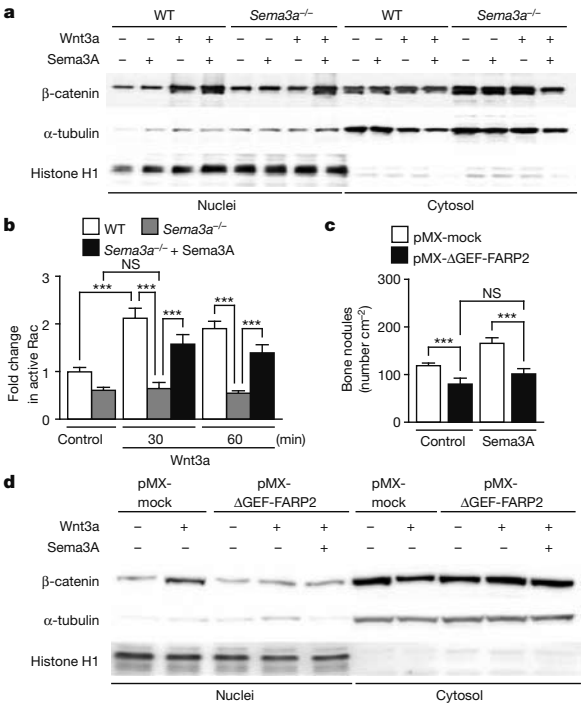

Figure 5 | Regulation of osteoblast differentiation by Sema3A through canonical Wnt signalling. **a**, Analysis of nuclear β-catenin levels in the wild-type and *Sema3a*$^{-/-}$ calvarial cells stimulated by Wnt3a in the presence or absence of Sema3A. Sema3A was simultaneously added with Wnt3a. **b**, Effect of Sema3A treatment on the activation of Rac in the wild-type and *Sema3a*$^{-/-}$ calvarial cells treated with Wnt3a. **c**, Effect of retrovirus-mediated overexpression of ΔGEF-FARP2 on bone nodule formation in calvarial cells cultured in the osteogenic medium in the presence or absence of Sema3A. **d**, Effect of retrovirus-mediated overexpression of ΔGEF-FARP2 on the nuclear localization of β-catenin in calvarial cells treated with Wnt3a in the presence or absence of Sema3A. Error bars (**b**, **c**) denote mean ± s.e.m. ***$P < 0.005$.

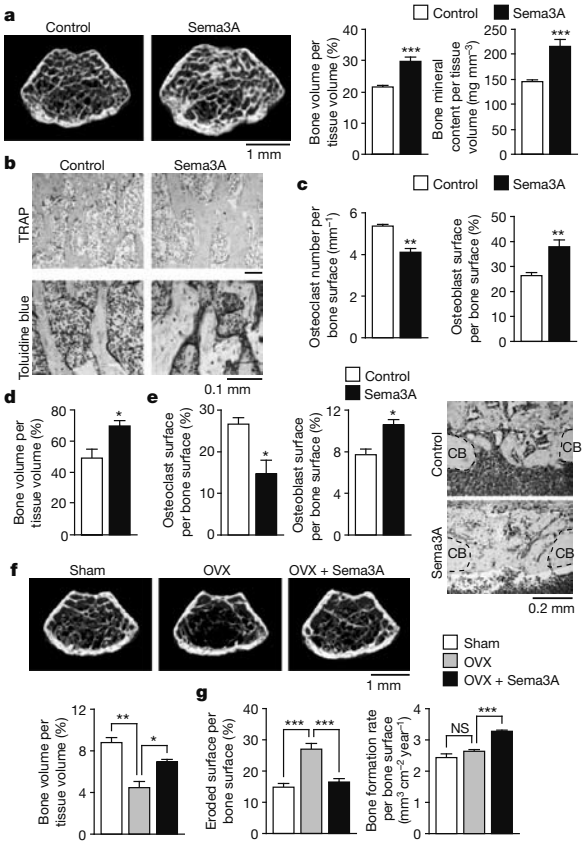

Figure 6 | Sema3A as a potential bone-increasing agent. **a**, Microcomputed tomography analysis of the femurs of 9-week-old wild-type mice treated with Sema3A or saline control ($n = 4–7$). **b**, Histological analysis of the proximal tibiae of wild-type mice treated with Sema3A or saline control. **c**, Parameters for osteoclasts and osteoblasts in the bone morphometric analysis of wild-type mice treated with Sema3A or saline control ($n = 4–7$). **d**, Microcomputed tomography analysis of bone regeneration of femoral cortex after drill-hole injury ($n = 5$). **e**, Histomorphometric analysis of the injured site of the femur (TRAP and haematoxylin staining; $n = 5$). CB, cortical bone. **f**, Microcomputed tomography analysis of the femurs of the sham-operated (Sham), ovariectomized (OVX) and Sema3A-treated OVX mice ($n = 4–5$). **g**, Parameters for osteoclastic bone resorption and osteoblastic bone formation in the bone morphometric analysis of the Sham, OVX and Sema3A-treated OVX mice ($n = 4–5$). Error bars (**a**, **c**–**g**) denote mean ± s.e.m. *$P < 0.05$; **$P < 0.01$; ***$P < 0.005$.

We examined the effect of Sema3A administration on bone loss in an ovariectomized mouse model of postmenopausal osteoporosis. Ovariectomized 9-week-old mice were treated with a weekly intravenous injection of Sema3A starting two days after ovariectomy and continuing for four weeks. Sema3A administration decreased bone loss after ovariectomy both by inhibiting osteoclastic bone resorption and promoting osteoblastic bone formation (Fig. 6f, g and Supplementary Fig. 8j–l). Recombinant human SEMA3A suppressed osteoclastogenesis and promoted osteoblastogenesis in cultured human cells (Supplementary Fig. 9a, b). These results indicate that Sema3A is a promising potential therapeutic target for bone diseases.

Conclusions

This study demonstrates that the Sema3A expressed by osteoblast lineage cells functions as a potent osteoprotective factor by synchronously inhibiting bone resorption and promoting bone formation (Supplementary Fig. 10a–c). Sema3A represents the long sought soluble molecule with the capacity to bring both osteoblasts and osteoclasts into a condition that favours bone mineral increase. Bone remodelling consists of resorption, transition and formation phases, and the transition phase is under the control of classical coupling factors such as insulin-like growth factor and transforming growth factor-β, which link bone resorption with formation[38,39]. Sema3A may have a crucial role in the bone formation phase, in which osteoblasts extensively produce bone, and at the same time restrain osteoclasts from migrating to the formation sites and starting to resorb the newly formed bone. The Sema3A protein level in the serum or bone microenvironment could be an auspicious biomarker for bone turnover, as we observed that the serum level of Sema3A decreased with age in mice (data not shown).

The potent anti-osteoclastogenic function of Sema3A is tightly controlled by Nrp1 expression regulated by RANKL signalling. Unless Nrp1 is downregulated by RANKL, the Sema3A–Nrp1 axis inhibits osteoclast differentiation by sequestering PlxnA1 from TREM2 so as to suppress ITAM signalling, and also inhibits RhoA activation via Nrp1–PlxnA to suppress osteoclast precursor cell migration (Supplementary Fig. 10b). After RANKL reduces Nrp1 expression, PlxnA1 associates with TREM2 and DAP12, which facilitate the ITAM-mediated calcium signalling required for osteoclast differentiation (Supplementary Fig. 10b). Because PlxnA1, PlxnA2 and PlxnA3, but not PlxnA4, are expressed by osteoclast and osteoblast

RESEARCH ARTICLE

lineage cells (data not shown), the relative contribution of these receptor components should be explored in the future.

Therapeutic agents capable of increasing bone formation have essentially been unavailable except for parathyroid hormone or anti-sclerostin antibody[40]. This study may provide a molecular basis for the development of a combined anti-resorptive and bone-increasing agent capable of facilitating bone regeneration.

METHODS SUMMARY

Mice and bone analysis. The generation of *Sema3a*$^{-/-}$, *Nrp1*$^{\mathrm{Sema}-}$, *Fos*$^{-/-}$, *Nfatc1*$^{-/-}$, *Tnfrsf11b*$^{-/-}$ and *Tyrobp*$^{-/-}$ mice was described previously[19,24,41–44]. All mice were maintained under specific pathogen-free conditions. All animal experiments were approved by the Institutional Animal Care and Use Committee of Tokyo Medical and Dental University. Three-dimensional micro-computed tomography analyses and bone morphometric analyses were performed as described[11,14,30,45]. The radiographs were obtained with a high-resolution soft X-ray system (SOFTEX).

Quantitative RT–PCR analysis and GeneChip analysis. Real-time quantitative PCR with reverse transcription (RT–PCR) analysis was performed as described[11,14,30,45]. In brief, total RNA was extracted by ISOGEN (NIPPON GENE) according to the manufacturer's instructions. First-strand complementary DNAs were synthesized using Superscript III reverse transcriptase (Invitrogen). Quantitative RT–PCR analysis was performed with the LightCycler apparatus (Roche Applied Science) using SYBR Green Realtime PCR Master Mix (TOYOBO). All primer sequences are available on request. GeneChip analysis and gene set enrichment analysis were performed as described previously[46].

Full Methods and any associated references are available in the online version of the paper at www.nature.com/nature.

Received 11 November 2011; accepted 27 February 2012.
Published online 18 April 2012.

1. Takayanagi, H. Osteoimmunology: shared mechanisms and crosstalk between the immune and bone systems. *Nature Rev. Immunol.* **7,** 292–304 (2007).
2. Elefteriou, F. Regulation of bone remodeling by the central and peripheral nervous system. *Arch. Biochem. Biophys.* **473,** 231–236 (2008).
3. Seeman, E. & Delmas, P. D. Bone quality–the material and structural basis of bone strength and fragility. *N. Engl. J. Med.* **354,** 2250–2261 (2006).
4. Teitelbaum, S. L. & Ross, F. P. Genetic regulation of osteoclast development and function. *Nature Rev. Genet.* **4,** 638–649 (2003).
5. Martin, T. J. & Sims, N. Osteoclast-derived activity in the coupling of bone formation to resorption. *Trends Mol. Med.* **11,** 76–81 (2005).
6. Lewiecki, E. M. New targets for intervention in the treatment of postmenopausal osteoporosis. *Nature Rev. Rheumatol.* **7,** 631–638 (2011).
7. Rachner, T. D., Khosla, S. & Hofbauer, L. C. Osteoporosis: now and the future. *Lancet* **377,** 1276–1287 (2011).
8. Reid, I. R. *et al.* Effects of denosumab on bone histomorphometry: the FREEDOM and STAND studies. *J. Bone Miner. Res.* **25,** 2256–2265 (2010).
9. Odvina, C. V. *et al.* Severely suppressed bone turnover: a potential complication of alendronate therapy. *J. Clin. Endocrinol. Metab.* **90,** 1294–1301 (2005).
10. Suda, T. *et al.* Modulation of osteoclast differentiation and function by the new members of the tumor necrosis factor receptor and ligand families. *Endocr. Rev.* **20,** 345–357 (1999).
11. Nakashima, T. *et al.* Evidence for osteocyte regulation of bone homeostasis through RANKL expression. *Nature Med.* **17,** 1231–1234 (2011).
12. Xiong, J. *et al.* Matrix-embedded cells control osteoclast formation. *Nature Med.* **17,** 1235–1241 (2011).
13. Simonet, W. S. *et al.* Osteoprotegerin: a novel secreted protein involved in the regulation of bone density. *Cell* **89,** 309–319 (1997).
14. Luo, Y., Raible, D. & Raper, J. A. Collapsin: A protein in brain that induces the collapse and paralysis of neuronal growth cones. *Cell* **75,** 217–227 (1993).
15. Tran, T. S., Kolodkin, A. L. & Bharadwaj, R. Semaphorin regulation of cellular morphology. *Annu. Rev. Cell Dev. Biol.* **23,** 263–292 (2007).
16. Negishi-Koga, T. *et al.* Suppression of bone formation by osteoclastic expression of semaphorin 4D. *Nature Med.* **17,** 1473–1480 (2011).
17. Takegahara, N. *et al.* Plexin-A1 and its interaction with DAP12 in immune responses and bone homeostasis. *Nature Cell Biol.* **8,** 615–622 (2006).
18. Matsuo, K. & Irie, N. Osteoclast-osteoblast communication. *Arch. Biochem. Biophys.* **473,** 201–209 (2008).
19. Taniguchi, M. *et al.* Disruption of *semaphorin III/D* gene causes severe abnormality in peripheral nerve projection. *Neuron* **19,** 519–530 (1997).
20. Gomez, C. *et al.* Expression of Semaphorin-3A and its receptors in endochondral ossification: potential role in skeletal development and innervation. *Dev. Dyn.* **234,** 393–403 (2005).
21. Behar, O., Golden, J. A., Mashimo, H., Schoen, F. J. & Fishman, M. C. Semaphorin III is needed for normal patterning and growth of nerves, bones and heart. *Nature* **383,** 525–528 (1996).
22. Jacquin, C., Gran, D. E., Lee, S. K., Lorenzo, J. A. & Aguila, H. L. Identification of multiple osteoclast precursor populations in murine bone marrow. *J. Bone Miner. Res.* **21,** 67–77 (2006).
23. Neufeld, G. & Kessler, O. The semaphorins: versatile regulators of tumour progression and tumour angiogenesis. *Nature Rev. Cancer* **8,** 632–645 (2008).
24. Gu, C. *et al.* Neuropilin-1 conveys semaphorin and VEGF signaling during neural and cardiovascular development. *Dev. Cell* **5,** 45–57 (2003).
25. Ashburner, B. P., Westerheide, S. D. & Baldwin, A. S. Jr. The p65 (RelA) subunit of NF-κB interacts with the histone deacetylase (HDAC) corepressors HDAC1 and HDAC2 to negatively regulate gene expression. *Mol. Cell. Biol.* **21,** 7065–7077 (2001).
26. Takayanagi, H. *et al.* Induction and activation of the transcription factor NFATc1 (NFAT2) integrate RANKL signaling in terminal differentiation of osteoclasts. *Dev. Cell* **3,** 889–901 (2002).
27. Koga, T. *et al.* Costimulatory signals mediated by the ITAM motif cooperate with RANKL for bone homeostasis. *Nature* **428,** 758–763 (2004).
28. Takahashi, T. & Strittmatter, S. M. Plexina1 autoinhibition by the plexin sema domain. *Neuron* **29,** 429–439 (2001).
29. Narazaki, M. & Tosato, G. Ligand-induced internalization selects use of common receptor neuropilin-1 by VEGF165 and semaphorin3A. *Blood* **107,** 3892–3901 (2006).
30. Nishikawa, K. *et al.* Maf promotes osteoblast differentiation in mice by mediating the age-related switch in mesenchymal cell differentiation. *J. Clin. Invest.* **120,** 3455–3465 (2010).
31. Gimble, J. M., Zvonic, S., Floyd, Z. E., Kassem, M. & Nuttall, M. E. Playing with bone and fat. *J. Cell. Biochem.* **98,** 251–266 (2006).
32. Krishnan, V., Bryant, H. U. & Macdougald, O. A. Regulation of bone mass by Wnt signaling. *J. Clin. Invest.* **116,** 1202–1209 (2006).
33. Takada, I., Kouzmenko, A. P. & Kato, S. Wnt and PPARγ signaling in osteoblastogenesis and adipogenesis. *Nature Rev. Rheumatol.* **5,** 442–447 (2009).
34. Toyofuku, T. *et al.* FARP2 triggers signals for Sema3A-mediated axonal repulsion. *Nature Neurosci.* **8,** 1712–1719 (2005).
35. Wu, X. *et al.* Rac1 activation controls nuclear localization of β-catenin during canonical Wnt signaling. *Cell* **133,** 340–353 (2008).
36. Takegahara, N. *et al.* Integral roles of a guanine nucleotide exchange factor, FARP2, in osteoclast podosome rearrangements. *FASEB J.* **24,** 4782–4792 (2010).
37. Nagashima, M. *et al.* Bisphosphonate (YM529) delays the repair of cortical bone defect after drill-hole injury by reducing terminal differentiation of osteoblasts in the mouse femur. *Bone* **36,** 502–511 (2005).
38. Tang, Y. *et al.* TGF-β1-induced migration of bone mesenchymal stem cells couples bone resorption with formation. *Nature Med.* **15,** 757–765 (2009).
39. Hayden, J. M., Mohan, S. & Baylink, D. J. The insulin-like growth factor system and the coupling of formation to resorption. *Bone* **17,** S93–S98 (1995).
40. Kawai, M., Mödder, U. I., Khosla, S. & Rosen, C. J. Emerging therapeutic opportunities for skeletal restoration. *Nature Rev. Drug Discov.* **10,** 141–156 (2011).
41. Grigoriadis, A. E. *et al.* c-Fos: a key regulator of osteoclast-macrophage lineage determination and bone remodeling. *Science* **266,** 443–448 (1994).
42. Asagiri, M. *et al.* Autoamplification of NFATc1 expression determines its essential role in bone homeostasis. *J. Exp. Med.* **202,** 1261–1269 (2005).
43. Mizuno, A. *et al.* Severe osteoporosis in mice lacking osteoclastogenesis inhibitory factor/osteoprotegerin. *Biochem. Biophys. Res. Commun.* **247,** 610–615 (1998).
44. Kaifu, T. *et al.* Osteopetrosis and thalamic hypomyelinosis with synaptic degeneration in DAP12-deficient mice. *J. Clin. Invest.* **111,** 323–332 (2003).
45. Hayashi, M. *et al.* Ly49Q, an ITIM-bearing NK receptor, positively regulates osteoclast differentiation. *Biochem. Biophys. Res. Commun.* **393,** 432–438 (2010).
46. Subramanian, A. *et al.* Gene set enrichment analysis: a knowledge-based approach for interpreting genome-wide expression profiles. *Proc. Natl Acad. Sci. USA* **102,** 15545–15550 (2005).

Supplementary Information is linked to the online version of the paper at www.nature.com/nature.

Acknowledgements We are grateful to D. D. Ginty and A. L. Kolodkin for providing the *Nrp1*$^{\mathrm{Sema}-}$ knockin mice. We thank Y. Goshima for providing vectors and technical help. We thank A. Yamaguchi, H. Asahara and F. Suto for providing reagents and technical help. We also thank K. Okamoto, T. Negishi-Koga, K. Nishikawa, H. Inoue, T. Suda, T. Ando, Y. Kunisawa, Y. Ogihara and S. Fukuse for discussion and assistance. This work was supported in part by a grant for the Exploratory Research for Advanced Technology Program, the Takayanagi Osteonetwork Project from the Japan Science and Technology Agency; Grant-in-Aid for Young Scientist A from the Japan Society for the Promotion of Science (JSPS); a Grant-in-Aid for Challenging Exploratory Research from the JSPS; grants for the Global Center of Excellence Program from the Ministry of Education, Culture, Sports, Science and Technology of Japan; and grants from the Tokyo Biochemical Research Foundation, the Life Science Foundation of Japan, Takeda Science Foundation, Uehara Memorial Foundation, Naito Foundation, BMKK RA Research Fund and Astellas Foundation for Research on Metabolic Disorders.

Author Contributions M.H. performed most of the experiments, interpreted the results and prepared the manuscript. T.N. performed immunohistochemical experiments and provided advice on project planning and data interpretation and prepared the manuscript. M.T. provided technical help. T.K. conducted the GeneChip analysis. A.K. provided advice on project planning and technical help. H.T. directed, supervised the project and wrote the manuscript.

Author Information Reprints and permissions information is available at www.nature.com/reprints. The authors declare no competing financial interests. Readers are welcome to comment on the online version of this article at www.nature.com/nature. Correspondence and requests for materials should be addressed to H.T. (taka.csi@tmd.ac.jp).

ARTICLE RESEARCH

METHODS

Cell culture. For *in vitro* osteoclast differentiation in the monoculture system, primary bone marrow cells (1×10^5 cells per cm^2) were suspended in culture medium (α-MEM containing penicillin, streptomycin and 10% FBS) supplemented with 10 ng ml^{-1} M-CSF (R&D Systems) for two days to obtain BMMs. The resultant BMMs were further cultured in medium supplemented with 10 ng ml^{-1} M-CSF and 5–50 ng ml^{-1} RANKL (PeproTech) for three days. Culture medium was changed every second day. Where indicated, calvarial cell-conditioned medium with or without soluble Nrp1 (R&D Systems) was added 12 h before the RANKL stimulation. Sema3A-Fc (R&D Systems) was added 12 h before or 12 h after the RANKL stimulation. For Sema6D treatment, BMMs were collected and seeded onto culture plates coated with soluble recombinant Sema6D (R&D Systems), and cultured with 10 ng ml^{-1} M-CSF and 5 ng ml^{-1} RANKL for three days. For the generation of osteoclast *in vitro* in the coculture system, primary bone marrow cells (5×10^4 cells per cm^2) and calvarial cells (5×10^3 cells per cm^2) were cultured in the presence of 10 nM 1α,25-dihydroxyvitamin D3 and 1 μM prostaglandin E2 for 4–6 days. For human osteoclast differentiation, human peripheral blood mononuclear cells were separated from peripheral blood obtained from healthy volunteers by density gradient centrifugation with Lymphoprep (AXIS-SHIELD). Cells (2×10^5 cells per 0.5 ml) were cultured in α-MEM with 10% FBS supplemented with 30 ng ml^{-1} M-CSF for two days. The resultant preosteoclasts were further cultured in medium supplemented with 30 ng ml^{-1} M-CSF and 60 ng ml^{-1} RANKL for four days. Culture medium was changed every second day. The differentiation of osteoclasts was evaluated by TRAP staining. A NF-κB activation inhibitor (6-amino-4-(phenoxyphenylethylamino)quinazline; Calbiochem) was used to inhibit NF-κB activity. The concentration of intracellular calcium was measured as described[27]. For *in vitro* osteoblast differentiation, calvarial cells were isolated from the calvarial bone of newborn mice by enzymatic digestion in α-MEM with 0.1% collagenase and 0.2% dispase, and were cultured with α-MEM with 10% FBS. After two days, cells were reseeded (1×10^4 cells per cm^2) and cultured with osteogenic medium (100 mM ascorbic acid, 5 mM β-glycerophosphate and 10 nM dexamethasone). Culture medium was changed every third day. After seven days, ALP staining and activity measurement were performed, and after 21 days, bone nodule formation was assessed by alizarin red staining. Human mesenchymal stem cells (Lonza) were cultured according to the manufacturer's protocol. To induce adipocyte differentiation *in vitro*, primary bone marrow cells (5×10^5 cells per cm^2) were cultured with α-MEM containing 10% FBS. After 24 h, non-adherent cells were removed and adherent cells were cultured with adipogenic medium (0.5 mM 3-isobutyl-1-methylxanthine, 5 μg ml^{-1} insulin and 1 μM dexamethasone) for 10–14 days. Culture medium was changed every second day. Lipid accumulation in adipocytes was determined with Oil Red O staining. Cell proliferation was determined using a cell proliferation ELISA kit (Roche Applied Science). The percentage of apoptotic cells was determined by TUNEL (TdT-mediated dUTP nick end labelling) staining with the MEBSTAIN apoptosis kit direct (MBL). For colony forming unit (CFU) assays, primary bone marrow cells (2.5×10^5 cells per cm^2) were seeded and cultured with MesenCult basal medium supplemented with mesenchymal stem cell stimulatory supplements (StemCell Technologies). On day 10, the cells were stained with toluidine blue. For CFU-ALP and CFU-osteoblast (CFU-OB) assays, primary bone marrow cells (2.5×10^5 cells per cm^2) were seeded and cultured with MesenCult basal medium and mesenchymal stem cell stimulatory supplements plus 100 mM ascorbic acid, 5 mM β-glycerophosphate and 10 nM dexamethasone. On day 10, CFU-ALP colonies were stained for ALP. Mineral deposition was determined with von Kossa staining of CFU-OB colonies on day 25. Primary osteoblasts and osteocytes were isolated from the long bones of CAG-CAT-EGFP/Dmp1-*Cre* double transgenic mice as described[11].

Purification and identification of inhibitory factor of osteoclast differentiation. Mouse calvarial cells were statically cultured with α-MEM supplemented with 1% FBS. Medium was conditioned for 72 h and filtered to remove non-adherent cells and debris. Conditioned medium was concentrated by ammonium sulphate precipitation (40% saturation), and the pellet was suspended in 10 mM sodium phosphate buffer, pH 7.4, and desalted using a PD-10 column (GE Healthcare). Concentrated conditioned media were then loaded onto a Mono Q 5/50 column (GE Healthcare) in 10 mM sodium phosphate buffer, pH 7.4, and proteins binding to the Mono Q matrix were eluted by a gradient of 0–100% 1 M NaCl and 10 mM sodium phosphate buffer, pH 7.4. Protein concentrations were determined by the absorbance at 280 nm. The effect of the fractionated conditioned media on osteoclast differentiation was examined by directly adding each fraction to RANKL-induced osteoclast differentiation *in vitro*. Fractions 33–35 contained a high concentration of NaCl, which exerts an inhibitory effect on osteoclast differentiation. Proteins of the highly inhibitory fractions were dissolved in SDS–PAGE sample buffer (Nacalai Tesque) and the sample was resolved by SDS–PAGE. Protein bands were visualized by Coomassie brilliant blue staining and all the protein bands were excised by scalpel. The samples were analysed using nano-LC–MS/MS by Japan Bioservice. The data were submitted to the MASCOT program for identification.

Immunohistochemical staining. After fixation in 4% paraformaldehyde, bone tissues were decalcified in 10% EDTA at 4 °C for 2 weeks and embedded in paraffin after dehydration. For immunohistochemical staining, antigen retrieval was carried out with 10 mM citric acid, pH 6.0, at room temperature for 2 h. After quenching of endogenous peroxidase activity by incubation with 3% H_2O_2 in methanol, the sections were incubated with an anti-Sema3A polyclonal antibody (Santa Cruz Biotechnology) in immunoreaction enhancer solution (Can Get Signal immunostain, TOYOBO) at 4 °C for overnight. After washing with PBS, the sections were incubated with peroxidase-conjugated secondary antibody according to the manufacturer's instructions (histofine, Nichirei Bioscience). The signals were visualized with 3,3-diaminobenzidine tetrahydrochloride and H_2O_2. TRAP staining was conducted after the immunostaining. Haematoxylin was used for nuclear counterstaining.

Western blot and immunoprecipitation analyses. Cell lysate or culture supernatant of calvarial cells was subjected to western blot analysis using the specific antibodies for Nrp1 (Calbiochem), β-actin (Sigma-Aldrich), Sema3A, Nrp1, p50, p65, histone H1 (Santa Cruz Biotechnology), phospho-ERK, ERK, phospho-JNK, JNK, phospho-p38, p38, phospho-IKKα/β, IKKα, IKKβ, phospho-PLCγ2, PLCγ2 (Cell Signaling Technology), β-catenin (Millipore) and α-tubulin (MBL). Nuclear proteins were prepared with nuclear extract kit in accordance with the manufacturer's protocol (Active Motif). For immunoprecipitation analysis, cells were solubilized in lysis buffer (1% Nonidet P-40 in 50 mM NaCl, 50 mM Tris-HCl, 5 mM EDTA, 1 mM NaF and 2 mM PMSF), supplemented with complete protease inhibitor cocktail (Roche Applied Science). Immunoprecipitation was performed by incubation with an anti-Flag M2 (Sigma-Aldrich) or anti-PlxnA1 antibody (Santa Cruz Biotechnology) followed by the addition of dynabeads protein G (Invitrogen). Immune complexes were separated by electrophoresis followed by blotting with anti-Flag M2, anti-V5 (Invitrogen), anti-Nrp1, anti-PlxnA1, anti-DAP12 (Santa Cruz Biotechnology) and anti-TREM2 antibodies (R&D Systems).

Flow cytometric analysis. For the analysis of bone marrow-derived osteoclast precursor cells, a single cell suspension of mouse bone marrow cells was stained with anti-CD3ε (145-2C11, eBioscience), anti-B220 (RA3-6B2, eBioscience), anti-CD11b (M1/70, eBioscience), anti-CD115 (AFS98, eBioscience) and anti-CD117 (2B8, eBioscience) antibodies. For intracellular staining of BMMs, anti-CD11b, anti-CD115 and anti-Nrp1 (R&D Systems) were used. Flow cytometric analysis was performed using FACSCantoII with Diva software (BD Biosciences).

ELISA. Concentrations of soluble RANKL and Opg in serum were determined using ELISA kits (R&D Systems), according to the manufacturer's instruction.

Retroviral gene transfer. The retroviral vector pMXs-Nrp1-IRES-EGFP was constructed by inserting DNA fragments encoding *Nrp1* into pMXs-IRES-EGFP. The construction of the retroviral vectors pMX-FARP2-IRES-GFP and pMX-ΔGEF-FARP2-IRES-GFP was described previously[36]. For the construction of the retroviral vectors pSIREN-RetroQ-ZsGreen-shNrp1 and pSIREN-RetroQ-ZsGreen-shControl, RNA targeting regions with a hairpin sequence (*Nrp1* shRNA sense: 5′-GCCCGAATGTTCTCAGAACTACTCGAGTAGTTCTGAGAACATTCGGGCTTTTT-3′; *Nrp1* shRNA antisense: 5′-AAAAAGCCCGAATGTTCTCAGAACTACTCGAGTAGTTCTGAGAACATTCGGGC-3′; control shRNA sense: 5′-GTGCGTTGCTAGTACCAACTTCAAGAGATTTTTTACGCGT-3′; control shRNA antisense: 5′-ACGCGTAAAAAATCTCTTGAAGTTGGTACTAGCAACGCAC-3′) were inserted into RNAi-ready pSIREN-RetroQ-ZsGreen (Clontech). The retrovirus supernatants were obtained by transfecting the retroviral vectors into the Plat-E packaging cell line using FuGENE 6 (Roche Applied Science).

Chromatin immunoprecipitation assay. Chromatin immunoprecipitation assay was performed using the ChIP-IT express chromatin immunoprecipitation kit (Active Motif) according to the manufacturer's instructions. The antibodies used for immunoprecipitation were anti-p50, anti-p65 and normal rabbit IgG (Santa Cruz Biotechnology). The primer sequences were as follows: *Nrp1* region 1, 5′-CATACGTGACCTTGCGCTCT-3′ and 5′-CCTGGCTGGAGATTCAGAGA-3′; *Nrp1* region 2, 5′-ACCTTACCCACCAGCTCCTT-3′ and 5′-ATACGCCACCCACTTACGAG-3′; *Nrp1* region 3, 5′-ATGTGGCTTGGTGAAAGGAG-3′ 5′-TGCTTCTACCTTCGGGTGAT-3′.

Reporter gene assay. The reporter plasmid Nrp1-Luc was constructed by subcloning a 3,259 base pair fragment of the 5′ flanking region of the mouse *Nrp1* gene into the pGL3-basic vector (Promega). The reporter plasmids and the expression plasmids were transfected into NIH3T3 cells using FuGENE 6 (Roche Applied Science). After 36 h, dual luciferase assay was performed according to the manufacturer's protocol (Promega).

Migration assay. BMMs suspended in complete medium were added to the upper chamber of transwell units (Corning). Inserts were placed into the lower chambers

RESEARCH ARTICLE

of transwell units containing M-CSF with or without Sema3A-Fc. After incubation, cells were fixed with 4% paraformaldehyde and stained with 0.5% toluidine blue. The cells on the upper side of the membrane were removed and the cells that had migrated to the lower side of the membrane and chamber were counted.

G-LISA small G protein activation assay. RhoA and Rac GTPase activation were determined using the G-LISA RhoA and Rac absorbance-based assay (Cytoskeleton) according to the manufacturer's instructions. In brief, cell lysates were prepared and normalized. After the addition of antibodies against RhoA or Rac and the incubation with the horseradish peroxidase detection reagent, signals were detected with a spectrophotometer.

***In vivo* treatment with recombinant Sema3A.** Five-week-old C57BL/6 mice were given weekly intravenous injections of 1 mg per kg body weight of Sema3A-Fc or vehicle for four weeks. Three days after the last injection, bone analysis was performed as described earlier.

Bone regeneration model. Skeletal injury was generated as described previously[37]. In brief, C57BL/6 mice were anaesthetized with an intraperitoneal injection of pentobarbital sodium. A 5-mm longitudinal incision was made over the proximal femur and the bone surface was exposed by splitting the muscle. A 0.5-mm hole was made by drilling through the anterior portion of the diaphysis of the bilateral femurs. After four and seven days of surgery, femoral defects were treated with Sema3A-Fc (0.5 mg per kg body weight) by injection into the injury site. Mice were euthanized at day 14 after surgery and bone analyses were performed.

Ovariectomy-induced bone loss. Nine-week-old female mice were ovariectomized or sham operated. More than five mice were examined in each group. Ovariectomized mice were given weekly intravenous injections of 1 mg per kg body weight of Sema3A-Fc or vehicle for four weeks. Three days after the last injection, all of the mice were euthanized and subjected to bone analysis as described earlier.

Statistical analyses. Statistical analyses were performed using the unpaired two-tailed Student's *t* test ($*P < 0.05$; $**P < 0.01$; $***P < 0.001$; NS, not significant, throughout the paper). All data are expressed as the mean ± s.e.m. Results are representative examples of more than three independent experiments.

分子細胞機能学分野

森田 育男

医歯学総合研究科・顎顔面頸部機能再建学系専攻
分子細胞機能学・教授

1）研究の課題名

・新規幹細胞移植技術の歯周組織再生法への応用
Cell-printing and transfer technology applications for periodontal regeneration

歯周疾患は歯周病原性細菌の感染により進行する炎症性疾患であり、本邦では成人の約8割が罹患し、主な歯の喪失原因になっている。したがって、安全で効果的な治療法の開発は社会的見地からも極めて重要な課題である。現在、組織再生治療に誘導組織再生（GTR）法やエナメルタンパクが頻用されていることからも明らかなように、歯根面にシャーピー線維の埋入を伴う新生セメント質を形成することの重要性は広く認識されている。しかしながら、従来法では完全な歯周組織の治癒には至っていない。本研究では、細胞転写技術を応用した新規歯周組織再生法の開発を目的とする。

その結果、歯根膜細胞から単離した間葉系幹細胞を羊膜に転写して、歯周組織欠損モデルに移植したところ、有意にその再生が促進された。

・幹細胞エクソソームを用いた新規組織再生法の開発
Novel regeneration therapy using mesenchymal stem cell derived-exosomes

近年、幹細胞のパラクライン因子が組織修復・維持に関与することが報告されるようになった。一方、タンパク質やmRNA、miRNAを内包した直径100 nm程度の膜小胞、エクソソームの生物学的重要性が注目されている。本研究の最終目的は、細胞移植を伴わない新規組織再生法の確立であるが、研究期間内に前臨床の基礎的検討を行う。具体的には、1）間葉系幹細胞培養上清からのエクソソームの単離法を確立する。2）動物創傷モデルにエクソソームを投与し、創傷治癒促進効果を評価する。3）創傷治癒促進に作用するエクソソーム成分の解析を行う。4）リポソームとエキソソームのfusion治療を行う。その結果、LPSで引き起こした脳損傷モデルマウスに間葉系幹細胞もしくはエキソソームを含む培養液を移植することにより、有意に損傷が抑制された。

2）研究のイラストレーション

幹細胞エクソソームを用いた新規組織再生法の開発

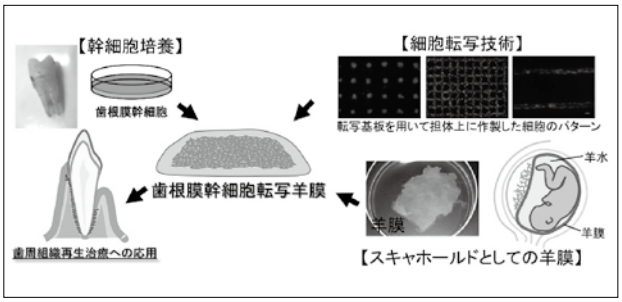

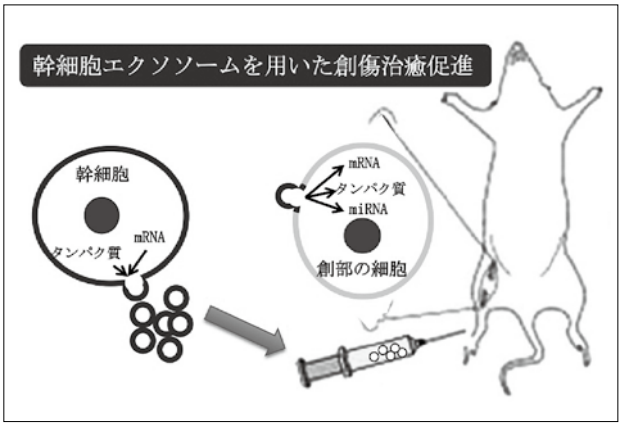

3）発表の研究内容についての英文要約

Periodontal ligament contributes to maintaining homeostasis in periodontal tissues by supplying stem/progenitor cells. It has long been suggested that periodontal ligament stem cells/progenitors are located around blood vessels. Recently mesenchymal stem cells have been isolated and cultured from periodontal ligament in vitro, although the location of the stem cells in periodontal ligament is unclear. The purpose of this study was to test the characteristics of human periodontal ligament stem cells (PDLSC) and examine their similarity to related vascular cell types, such

as pericytes and endothelial cells.
Cultured PDLSC were positive for both mesenchymal stem cell markers and pericyte markers, including CD146, NG2, and CD140b. When pericyte marker expressions was explored in rat periodontal tissue sections, CD146- and NG2-positive signals were observed in the perivascular area of the periodontal ligament. Further, PDLSC located adjacent to endothelial cells and contributed to the stability of the capillary-like structure, when the cells were cultured with human umbilical cord endothelial cells under capillary-like structure forming conditions in vitro. PDLSC possess pericyte-like characteristics and may localize as pericytes in the periodontal ligament. These data provide useful information for stem cell biology in periodontal research and stem cell-based periodontal therapy.

4）本事業に関連して世界的な研究拠点形成に向けて、以下の点で改善・整備等されたこと

A（研究拠点体制）

寄附講座を積極的に本G-COEに組み入れたことで、研究の進捗化が行われた。

B（人材育成）

大学院の研究・教育がスムーズに行われた。

C（国際化）

特任講師が積極的に外国で発表する機会が増え、共同研究先が増加した。

5）GCOE事業を推進するに当たって力を入れた点

若手育成と、若手研究者の本GCOE後の就職先への相談を積極的に行った。

6）英文原著論文

1. ◎ Periodontal Ligament Stem Cells Possess the Characteristics of Pericytes Kengo Iwasaki, D.D.S., Ph.D., Motohiro Komaki, D.D.S., Ph.D. Naoki Yokoyama, Ph.D., Yuichi Tanaka, Ph.D, Atsuko Taki, M.D., Ph.D., Yasuyuki Kimura, D.D.S., Masaki Takeda, ‖ Shigeru Oda, D.D.S., Ph.D., Yuichi Izumi, D.D.S., Ph.D., Ikuo Morita, Ph.D.
   The Journal of Periodontology in press
2. Wang J, Ohno-Matsui K, Morita I.、Cholesterol enhances amyloid β deposition in mouse retina by modulating the activities of A β -regulating enzymes in retinal pigment epithelial cells. Biochem Biophys Res Commun. 424 (4)：704-709, 2012
3. Moriyama M, Ohno-Matsui K, Modegi T, Kondo J, Takahashi Y, Tomita M, Tokoro T, Morita . Quantitative Analyses of High-Resolution 3D MR Images of Highly Myopic Eyes to Determine Their Shapes. Invest Ophthalmol Vis Sci. 53（8）：4510-4518, 2012
4. Li X, Akiyama M, Nakahama K, Koshiishi T, Takeda S, Morita I. Role of intercellular adhesion molecule-2 in osteoclastogenesis. Genes Cells. 17（7）：568-575, 2012.
5. Taki A, Abe M, Komaki M, Oku K, Iseki S, Mizutani S, Morita I. Expression of angiogenesis-related factors and inflammatory cytokines in placenta and umbilical vessels in pregnancies with preeclampsia and chorioamnionitis/funisitis. Congenit Anom ;52（2）：97-103, 2012
6. Wang J, Ohno-Matsui K, Morita I. Elevated amyloid β production in senescent retinal pigment epithelium, a possible mechanism of subretinal deposition of amyloid β in age-related macular degeneration. Biochem Biophys Res Commun. 423（1）：73-78, 2012.
7. ◎ Wayakanon P, Bhattacharjee R, Nakahama K, Morita I. The role of the Cx43 C-terminus in GJ plaque formation and internalization. Biochem Biophys Res Commun. 420（2）：456-61, 2012
8. Nakamura M, Soya T, Hiratai R, Nagai A, Hashimoto K, Morita I, Yamashita K. Endothelial cell migration and morphogenesis on silk fibroin scaffolds containing hydroxyapatite. J Biomed Mater Res A. 100（4）：969-77, 2012

7）総説ならびに著書

1. 森田育男.COX-2と病態.特集　NSAIDsとアミノフェンの基礎と臨床.ペインクリニック.Vol.33, No.2（2012.2）.p209-217.真興交易（株）医書出版部.東京.2012年
2. 森田育男.COX-2PGE2が関与するさまざまな病態.知っておきたいNSAIDsの正しい知識／特集　非ステロイド性抗炎症薬（NSAIDs）に関する正しい知識.内科系総合雑誌Modern Physician.Vol.32, No.11(2012.11).p1334-1339.企画・編集　小川節郎.東京.2012年

著書

1. 森田育男：4.血管のパターニングと再生医療 / 1.はじめに、2.オフセット印刷技術を応用した血管内皮細胞パターニング培養、3.血管内皮細胞の転写と体外血管形成、4.体外で作製した血管内への血流の確認、5.血管再建に用いる細胞の選択、6.他の組織再生への応用.再生医療製品の許認可と組織工学の新しい試み Regulation of Regenerative Medicine Products and New Approaches of Tissue Regeneration / 新材料・新素材シリーズ.（監修：磐田博夫、松岡厚子、岸田晶夫）.125-132頁.シーエムシー出版.東京. 2012年

8）特許取得、特許申請

1. 特許第5057362号
   特許登録日：平成24年8月10日
   発明の名称：リポソーム及びこれを用いた細胞に対する物質注入方法
   発明者：森田育男、秋吉一成、野村慎一郎
   特許権者：国立大学法人東京医科歯科大学、大日本印刷株式会社
   本学整理番号：P04-034P-JP
2. 発明の名称：血小板産生促進因子及びその利用
   出願番号：特願2008-550984
   出願日：2007/10/31
   出願人：国立大学法人東京医科歯科大学、株式会社常磐植物化学研究所
   発明者：佐藤孝浩、森田育男、清水正人、
   妹尾修次郎、渡邊正道、内田勝、小野稔
   ※敬称略
3. 特許番号：特許第5134511号
   登録日：平成24年11月16日
   出願番号：特願2008-299731
   出願日：平成16年10月15日
   発明の名称：人工細胞組織の作成方法、及びそのための基材
   発明者：森田育男、中村真人　他4名

特許申請

1. 発明の名称：眼科疾患の画像解析装置、眼科疾患の画像解析方法及び眼科疾患の画像解析プログラム
   出願番号：特願2011-187872
   共願人：大日本印刷株式会社
   発明者：茂出木敏雄、近藤純一、高橋洋一、森田育男、
   大野京子、森山無価
2. 発明の名称：眼底画像解析装置、眼底画像解析方法及びプログラム
   出願番号：特願2011-226307
   共願人：大日本印刷株式会社
   発明者：茂出木敏雄、近藤純一、高橋洋一、森田育男、
   大野京子、森山無価

9）平成24年度までの自己評価

若手育成委員会委員長として、シャペロン教員、スーパースチューデントの教育、進路指導などに関し、尽力を尽くしてきたが、研究担当理事としての業務が忙しく、100%満足の得られるものではなかった。

10）学会発表（和文）

1. 加藤幸太郎.アシドーシスによる大型破骨細胞形成促進作用の標的と機序の解析.第85回日本薬理学会年会.京都.2012年3月14～16日
2. 森田育男（教授/研究担当理事）.講演.オープニングセッション.包括連携プログラム：クリニカルサミット-”Visualized Medicine ～限界への挑戦”.ソニー（株）先端マテリアル研究所、M&Dタワー20階ソニーオープンラボ.東京.2012年3月28日
3. 森田育男.講演.アラキドン酸カスケードの制御.モーニングセミナー6/眼炎症白熱教室Part Ⅱ.第51回日本白内障学会総会.東京.2012年4月7日
4. 本多泉、滝敦子、岩崎剣吾、小牧基浩、森田育男.ラット子宮内感染モデルを用いた新生児脳室周囲白質軟化症及び慢性肺疾患に対する臍帯由来間質系幹細胞を用いた治療の検討.第33回日本炎症・再生医学会.福岡.2012年7月5～6日
5. 小牧基浩、岩崎剣吾、横山尚毅、森田育男.マウス骨髄細胞は歯周組織欠損へ動員される.第33回日本炎症・再生医学会.福岡.2012年7月5～6日
6. 岩崎剣吾、小牧基浩、滝敦子、本多泉、森田育男.歯根膜幹細胞転写羊膜移植によるラット歯周組織の再生.第33回日本炎症・再生医学会.福岡.2012年7月5～6日
7. 木村康之、小牧基浩、岩崎剣吾、和泉雄一、森田育男.一般口演.マウス歯周組織への骨髄由来細胞の動員について.第77回口腔病学会学術大会.東京.2012年11月30日、12月1日
8. 橋田之彦、中浜健一、原田　清、森田育男.一般口演.骨形成におけるCx43の役割の解明.第77回口腔病学会学術大会.東京.2012年11月30日、12月1日
9. 橋田之彦、清水花織、穐山雅子、加藤幸太郎、中浜健一、原田清、森田育男.骨形成におけるCx43の役割とメカニズムの解明.第85回日本生化学会大会.福岡.2012年12月14～16日
10. 穐山雅子、中浜健一、森田育男.ドコサヘキサエン酸の破骨細胞分化阻害作用に関する遺伝子発現の解析.第85回日本生化学会大会.福岡.2012年12月14～16日

11）学会発表（英文）

1. Safronova O. The mechanism of transcriptional repression via HDAC-dependent deacetylation of p65-subunit of NF-κB in response to hypoxic inflammation. Q4：Advances in Hypoxic Signaling：From Bench to

Bedside. Keystone Symposia conference. Banff, Alberta, Canada, Feb. 12-17, 2012

2. Olga Safronova, 森田育男.The regulatory role of hypoxia on pro-inflammatory cytokine induced NF-KappaB via HDAC-dependent pathways. 第33回日本炎症・再生医学会.福岡.2012年7月5～6日
3. Hatano Y, Nakahama K, Isobe M, Morita I. Tumor associated Osteoclast-like giant cells pro,ote tumor growth and lymphagiogenesis. The 20th Annual Meeting of the Japanese Vascular Biology and Medicine Organization. The 10th Korea-Japan Joint Symposium on Vascular Biology, Tokushima, Japan, December 5-7, 2012

12）外部資金の獲得状況

1. 森田育男：基盤研究（C）（新規） H24～H26
「印刷技術を用いた新規歯周組織再生法」
研究課題番号：24390442-0
2. 森田育男：基盤研究（C）研究分担者 H22～H24（継続）
「核蛋白ピグペンの血管新生促進作用の機序の解明と血管新生制御への応用」
研究課題番号：22501006-1
安部まゆみ：研究代表者
3. 森田育男：基盤研究（A）研究分担者 H22～H24（継続）
「ナノゲルを基盤とした新規ドラッグデリバリーシステムの開発」
研究課題番号：20240047-1
秋吉一成：研究代表者
4. 森田育男：基盤研究（C）研究分担者 H22～H24（継続）
「自己組織を利用した欠損素引き修復と血流回復を目指した新規新生児外科治療戦略」
研究課題番号：20240047-1
久保田俊郎：研究代表者
5. 森田育男：基盤研究（B）研究分担者 H22～H24（継続）
「加齢黄斑変性発症の四次元時空的解明と分子標的治療の確立」
研究課題番号：22390322-1
大野京子：研究代表者
6. 森田育男：萌芽研究 研究分担者 H23～H25（新規）
「アミロイドbを標的とした加齢黄斑変性・緑内障の早期診断・治療に向けた新規戦略法」
研究課題番号：23659808-1
大野京子：研究代表者
7. 穐山雅子：基盤研究（C） H23～H25（継続）
「ドコサヘキサエン酸による破骨細胞分化抑制機序の解明」
研究課題番号：23592729-0
分担研究者：中浜健一23592729-1、森田育男23592729-2
8. 渡邉毅：日本学術振興会特別研究員（DC2）（新規）H24.4.1～H26.3.31
「ASK-p38経路による核内受容体NR4Aファミリーのリン酸化制御と生理機能解析」
研究課題番号：249553-0
9. 森田育男・大日本印刷（株）：共同研究費 平成17年～22年
略称番号：2B040
「ナノテクノロジーを応用した再生医療および薬物導入技術の開発とその応用」 15,000千円
（内訳 研究費13,827,273円〔備品5,000,000円、消耗品6,912,455円〕、光熱水料414,818円）
平成22年～25年：5,000千円
（内訳 直接経費 研究費2,254,545円、間接経費225,455円、共同研究員費2,520,000円、消耗品6,912,455円〕、光熱水料414,818円）
10. 森田育男（大野京子、王紀英、長岡奈都子、森山無価）・ソニー（株）：共同研究費 平成24年～25年
略称番号：2B128
「眼科分野における先端光学イメージ技術応用の研究」
10,000千円
（内訳 直接経費9,090,910円 研究旅費450,000円、消耗品1,777,273円、3,090,910円, 賃金3,500,000円、光熱水料272,727円）
11. 東京医科歯科大学-ソニー（株）包括連携に基づく人材育成プログラム、
大学院特別研究生にかかる研究経費 平成24年～25年
相坂一樹：2,000,000円 略称番号：9B001
小嶋健介：2,000,000円 略称番号：9B002

13）特別講演、招待講演、シンポジウム

Ikuo Morita. Pathogenic mechanism of age-related macular regeneration-Process of choroidal neovscularization. 第33回日本炎症・再生医学会.福岡20.12年7月6日

Ikuo Morita. Invited Speakers. A new technology for tissue regeneration by using cell printing and transfer, “Printing devices for bio and medical applications”, ICPFPE 2012（The 2012 International Conference on Flexible and Printed Electronics）, Tokyo, September 6-8, 2012

14）新聞、雑誌、TV報道

1. 森田育男（東京医科歯科大学　研究担当理事、副学長）、宮坂信之（東京医科歯科大学　医学部付属病院　病院長）、熊谷　修（ソニー株式会社　業務執行役員SVP、先端マテリアル研究所　所長）、安田章夫（ソニー株式会社　先端マテリアル研究所　統括部長）.プレスリリース.「東京医科歯科大学とソニー医療分野での包括連携協定に基づくプログラムを開始」.東京.2012年3月26日
2. 森田育男（東京医科歯科大学理事・副学長（併任）、medU-net会長）.「真の産学官連携」に求められる仕組み～医学系大学産学連携ネットワーク協議会（medU-net）からのご提案.トピックス「2012ライフサイエンス知財フォーラム」を開催.製薬協ニューズレターNo.149、May 2012：10p、編集　日本製薬工業協会　広報委員会、発行　医薬出版センター.2012年.東京

3.森田育男、大野京子　東京医科歯科大学と大日本印刷は共同で日本人に多い「病的近視」の原因が眼球の変形や異常にあることを3D MRI画像解析により解明　プレスリリース
2012年10月11日　東京医科歯科大学　大日本印刷株式会社

15）教室、分野や講座の准教授、講師、助教、特別研究員、ポスドク、指導を受けた大学院生の名前

准教授　　中浜　健一
助　教　　加藤　幸太郎
特任講師（G-COE）：Olga Safronova
特任助教　　穐山　雅子
非常勤講師　藤田　　浩（都立墨東病院・輸血科）
　　長谷（徳島）　貴子
　　安部　まゆみ（上武大学・看護学部）
　　横山　知永子
大学院生
　　○ Praween Wayakanon（～9月）
　　渡辺　　毅
派遣大学院生
　　○ 橋田　之彦（顎顔面外科）
　　清水　花織（インプラント・口腔再生医学）
　　秦野　　雄（循環器制御内科学）
　　本多　　泉（生殖機能協関学）
　　木村　康之（歯周病学）
　　許　　博文（先端倫理医科学開発学）
　　森丘　千夏子（発達病態小児科学）
　　赤澤　恵子（歯周病学）
修士　　沼田　有理（4月～）

Biochemical and Biophysical Research Communications 420 (2012) 456–461

Contents lists available at SciVerse ScienceDirect

Biochemical and Biophysical Research Communications

journal homepage: www.elsevier.com/locate/ybbrc

The role of the Cx43 C-terminus in GJ plaque formation and internalization

Praween Wayakanon [a,b], Rajib Bhattacharjee [a,b], Ken-ichi Nakahama [a,*], Ikuo Morita [a,b]

[a] Department of Cellular Physiological Chemistry, Graduate School, Tokyo Medical and Dental University, 1-5-45 Yushima, Bunkyo-ku, Tokyo 113-8549, Japan
[b] Global Center of Excellence Program, International Research Center for Molecular Science in Tooth and Bone Diseases, Tokyo Medical and Dental University, 1-5-45 Yushima, Bunkyo-ku, Tokyo 113-8549, Japan

ARTICLE INFO

Article history:
Received 2 March 2012
Available online 10 March 2012

Keywords:
Gap junction (GJ)
Connexin 43 (Cx43)
Annular gap junction (AGJ)
C-terminus

ABSTRACT

Connexin 43 (Cx43) is a major gap junction (GJ) protein found in many mammalian cell types. The C-terminal (CT) domain of Cx43 has unique characteristics in terms of amino acid (aa) sequence and its length differs from other connexins. This CT domain can be associated with protein partners to regulate GJ assembly and degradation, which results in the direct control of gap junction intercellular communication (GJIC). However, the essential roles of the CT regions involved in these mechanisms have not been fully elucidated. In this study, we aimed to investigate the specific regions of Cx43CT involved in GJ formation and internalization. Wild type $Cx43_{(382aa)}$ and 10 CT truncated mutants were stably expressed in HeLa cells as GFP or DsRed tagged proteins. First, we found that the deletion of 235–382aa from Cx43 resulted in failure to make GJ and establish GJIC. Second, the Cx43 with 242–382aa CT deletion could form functional GJs and be internalized as annular gap junctions (AGJs). However, the plaques consisting of Cx43 with CT deletions (Δ242–382aa to Δ271–382aa) were longer than the plaques consisting of Cx43 with CT deletions (Δ302–382aa). Third, co-culture experiments of cells expressing wild type $Cx43_{(382)}$ with cells expressing Cx43CT mutants revealed that the directions of GJ internalization were dependent on the length of the respective CT. Moreover, a specific region, 325–342aa residues of Cx43, played an important role in the direction of GJ internalization. These results showed the important roles of the Cx43 C-terminus in GJ expression and its turnover.

1. Introduction

Gap junction (GJ) channels connect the cytoplasms of two apposing cells by docking via a half channel termed a connexon to provide cell–cell communication. Gap junction intercellular communication (GJIC) allows small molecules of less than 1 kDa, including secondary messengers, to pass from one cell to another [1]. Connexons are composed of hexamers of four-transmembrane protein termed connexins (Cxs) [2]. Once transported to the plasma membrane, connexons (hemichannels) routinely assemble in clusters as a double-membrane spanning GJ plaques that are composed of a few to thousands of channels. The size of GJ plaques may vary from a few square nanometers to many square micrometers [3]. The communication via GJ is regulated by the dynamic processes of GJ formation and removal [4]. The removal of GJ from the cell surface involves a unique process. The entire GJ, or a part of it, is endoexocytosed into only one of the two contacting cells [5]. This internalization process generates double-membrane vesicles, termed annular gap junctions (AGJs) or connexosomes. The formation of AGJ vesicles from entire GJs resulted in a rapid reduction in the intercellular communication between two cells [6].

Connexin 43 (Cx43) is a 43 kDa GJ protein widely expressed in many mammalian cell types [7]. It has a short half-life of approximately 1–5 h. Since the turnover of Cx43 is rapid, it has been proposed that Cx43 degradation is important for the regulation of GJIC under pathophysiological conditions [8]. The 17-kDa carboxyl terminal (CT) domain of Cx43 has special features in terms of amino acid sequence and length, which differ from other Cxs [9–11]. It is reported that the Cx43CT domain is extensively phosphorylated by different protein kinases at different motifs containing serine or tyrosine residues [12]. Moreover, this CT domain has been reported to be associated with other proteins to stabilize Cx43 anchoring in plasma membranes [13–15]. Associations of Cx43CT with protein partners have also been proposed to regulate Cx43 assembly and degradation, but the overall functions remain unclear. The aim of this study was to investigate the role of the CT domain of Cx43 in the formation of GJ plaques and in internalization of GJ plaques as an AGJ vesicle. We found that three different amino acid regions in the CT domain of Cx43 played different roles as follows: (1) the region between 235 and 242aa is important for GJ plaque assembly at the plasma membrane; (2) the region between 271 and 302aa is important for sizing of the GJ plaque and AGJ; and (3) the region

* Corresponding author. Fax: +81 3 5803 0212.
E-mail address: nakacell@tmd.ac.jp (K.-i. Nakahama).

0006-291X/$ - see front matter © 2012 Elsevier Inc. All rights reserved.
http://dx.doi.org/10.1016/j.bbrc.2012.03.018

between 325 and 342aa is important for the directionality of GJ internalization. These findings suggest that the formation and internalization of GJ are dependent on the regions of the Cx43 CT domain.

2. Materials and methods

2.1. Cx43-GFP and Cx43-DsRed constructs

DNA fragments coding full-length rat Cx43 (382aa, GenBank ID: NM_012567) and CT truncated mutants [235aa(Δ236–382aa), 242aa(Δ243–382aa), 251aa(Δ252–382aa), 260aa(Δ261–382aa), 271aa(Δ272–382aa), 302aa(Δ303–382aa), 325aa(Δ326–382aa), 342aa(Δ343–382aa), 370aa(Δ371–382aa), and 378aa(Δ379–382aa)] were amplified by a polymerase chain reaction (PCR)-based technique using proofreading DNA polymerase (Pyrobest, Takara, Japan). These DNA fragments were cloned into pEGFP-N3 or a pDsRed monomer (Clonetech, USA). Then, the coding regions of fusion protein were subcloned into a retrovirus expression vector, pQCXIP (Clonetech, USA) (Fig. 1A). To make the deletion mutant Cx43(Δ325–342aa) expressing vector, the Cx43(1–324aa) and Cx43(343–382aa) coding regions were amplified, then these two fragments were ligated via a *Pst*I restriction site (Fig. 3A). All constructs were verified by analysis of restriction enzyme digests and DNA sequencing.

2.2. Cell line and cell culture conditions

Human epitheloid cervix carcinoma cells (HeLa, RIKEN BioResourse Center, Japan) and 293FT cells (Invitrogen, USA) were maintained in Dulbecco's modified Eagle medium (DMEM, Invitrogen, USA) supplemented with 10% fetal bovine serum (FBS) at 37 °C, 100% humidity and 5% CO_2/95% air. Cells were routinely subcultured by trypsinization with 0.05% Trypsin-0.02% EDTA in PBS, and the medium was changed twice a week.

2.3. Establishment of clones expressing the Cx-GFP/DsRed fusion protein

The retrovirus vector and pCL-10A1 (amphotropic vector, Imgenex Corp., USA) were co-transfected to the packaging cell line 293FT using Lipofectamine 2000® (Invitrogen, USA) as described previously [16]. Three days after the transfection, a virus containing conditioned medium was harvested. Then, HeLa cells were infected with the virus containing medium with polybrane (8 μg/ml, Millipore, USA). Three days after infection, Cx43-GFP- or Cx43-DsRed-expressing cells were cultured with 2 μg/ml of puromycin (InvivoGen, USA) containing 10% FBS DMEM for 2 weeks to establish stable clones.

2.4. Immunoblot analysis

Parental HeLa and Cx43 infected cells were harvested on ice in lysis buffer (0.02 M Tris–HCl, 0.137 M NaCl, 0.002 M EDTA, 1% Nonidet P-40 and 10% glycerol, pH 7.6) containing a protease and phosphatase inhibitor cocktail (Sigma, USA). The lysates were then ultrasonicated on ice for 20 s. Total protein concentrations were determined by a Protein Assay kit (Bio-Rad, USA). The protein samples were separated on 8% SDS–polyacrylamide gels, then transferred onto PVDF membranes, and blocked with 5% skim milk (BD transduction, USA) in TBS-T (0.05 M Tris–HCl, 0.150 M NaCl and 0.2% Tween-20, pH7.6). The membranes were incubated with anti-GFP antibody (BD Biosciences, USA) at 1:500 dilution in 5% skim milk in TBS-T at 4 °C overnight. After washing, the membranes were incubated with HRP-conjugated anti-rabbit IgG (GE Healthcare, UK) at 1:1500 dilution at 4 °C for 2 h. The blots were developed using a chemiluminescence method (ECL-plus; GE Healthcare) and were detected by LAS-1000 luminescent image analyzer (Fujifilm, Japan). The blots were reprobed with HRP-conjugated anti-β-actin rabbit polyclonal IgG (MBL, Japan) at 1:500 dilution.

2.5. Cell imagings of Cx43-GFP and -DsRed in living cells

Fluorescence images of GFP- and DsRed-tagged Cx43 were acquired by a LSM 510 META (Carl Zeiss, Germany) confocal microscope. For live cell imaging, cells were placed on a temperature-, CO_2– and humidity-controlled stage. Focus, contrast and brightness settings remained constant during the course of imaging acquisition.

2.6. Quantitative and statistical image analyses

GJ plaque length and AGJ diameter were measured using Zeiss software. Statistical analyses of GJ plaque sizes and AGJ were done in a total of 50 cell-pairs. The experiments were repeated in triplicate. GJ plaques and AGJs were categorized into three groups by size. Then, the ratio of each group was calculated and represented by percentages. Statistical analysis of AGJs internalization directions was also done by counting the number of cells containing internalizing vesicles in a total of 50 cell-pairs in triplicate experiments. The ratio of Cx43-GFP and -DsRed expressing cells containing internalizing AGJs was calculated and represented by percentage values. Data are shown as means ± SEM. Comparisons were made using an independent *t-test* and one-way ANOVA. In all analyses, a p value less than 0.05 was considered statistically significant.

3. Results

3.1. Wild type Cx43 and CT truncated mutants form different sizes of GJ plaques and AGJs

To examine the role of CT in the formation of GJ plaques and AGJs, the wild type Cx43 (382aa) and CT truncated mutants were expressed in non-endogenous connexin-expressing HeLa cells as fusion proteins (with GFP or DsRed) (Fig. 1A). The expression of Cx43-GFP fusion proteins was confirmed by immunoblotting using an antibody against GFP (Fig. 1B). These Cx43 expressing cells showed no different characteristics in terms of cell shape and size compared to parental HeLa cells (data not shown). The wild type $Cx43_{(382aa)}$-GFP and -DsRed were assembled into typical GJ plaques as green and red fluorescent lines at the junction of the infected cells, respectively (arrows in Fig. 1C). The observed GJ plaques from wild type $Cx43_{(382aa)}$-GFP showed variation in length from shorter than 1 μm to a maximum length of 15 μm. Besides GJ plaque formation, wild type $Cx43_{(382aa)}$-GFP formed internalizing AGJ vesicles that originated from a small region or the entire GJ plaque. The AGJs were observed as a circular structure in the cytoplasm. The AGJs from wild type $Cx43_{(382aa)}$-GFP showed variation in diameter from smaller than 1 μm to a maximum of 5 μm (arrow heads in Fig. 1C).

$Cx43_{(235aa)}$-GFP, the shortest CT mutant, did not show any formations of GJ plaque or AGJ (Fig. 1D). On the other hand, $Cx43_{(242aa)}$-GFP, the 7 aa longer CT mutant than $Cx43_{(235aa)}$-GFP could form GJ plaques and AGJ vesicles. This finding suggested an important role of the CT domain 235–242aa of Cx43 in GJ formation at the plasma membrane. Interestingly, GJ plaques and AGJs formed by four mutants ($Cx43_{(242aa)}$-GFP to $Cx43_{(271aa)}$-GFP) were larger than that formed by wild type $Cx43_{(382aa)}$-GFP. The

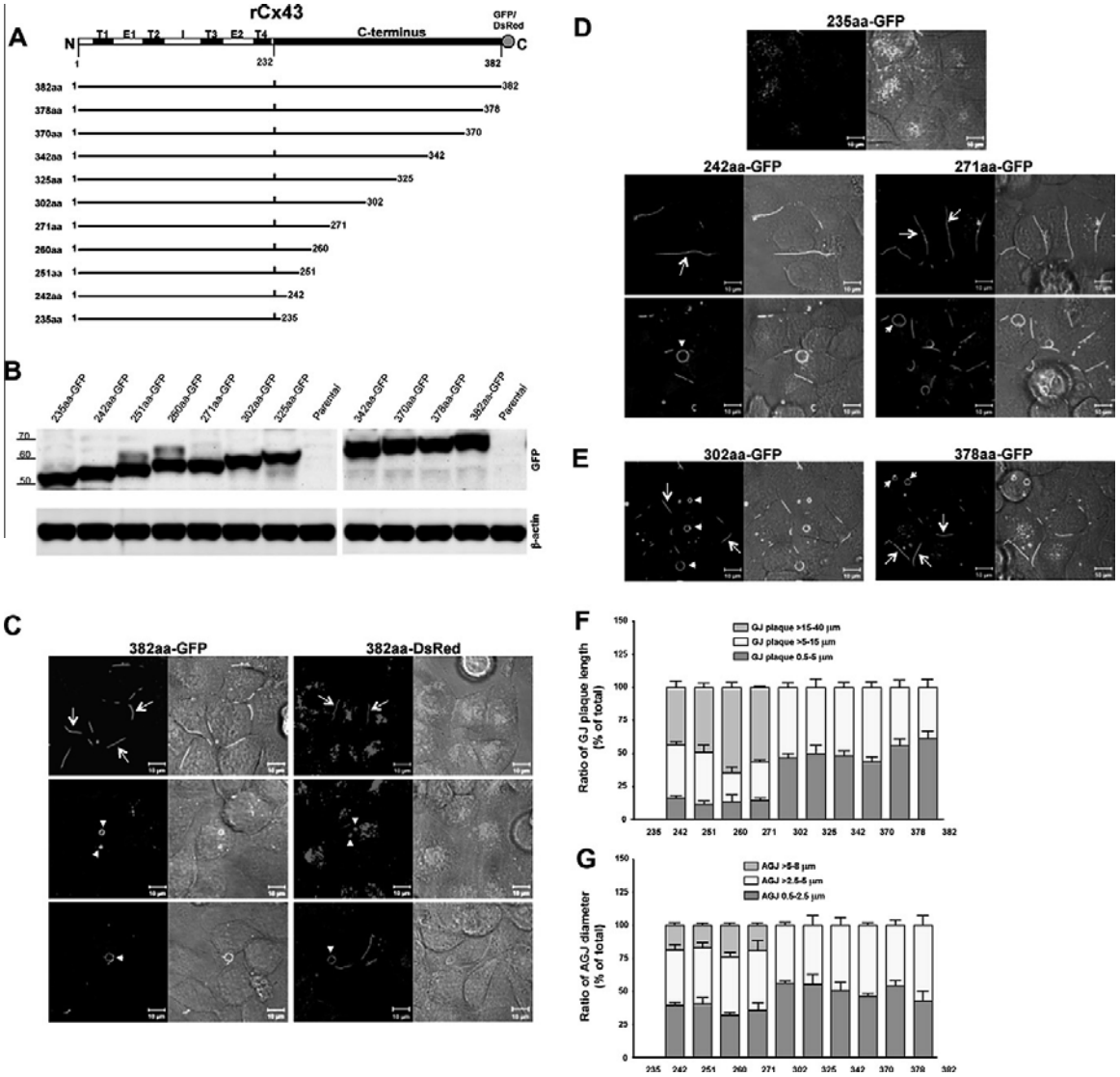

Fig. 1. Formation of GJ plaque and AGJ of wild type Cx43 and CT-truncated mutants. (A) Schematic diagram summarizing a 382aa wild type Cx43 and 10 random truncations of CT. (B) Protein lysates from parental HeLa and cells overexpressing Cx43-GFP were immunoblotted with an anti-GFP antibody. β-actin was used as a protein loading control. (C) Wild type 382aa-GFP (left panel) and 382aa-DsRed (right panel) formed GJ plaques no longer than 15 μm (upper panel, arrows), AGJs 1–3 μm in diameter (middle panel, arrow heads) and large AGJ about 5 μm in diameter (lower panel, arrow head). (D) No GJ plaques could be observed from 235aa-GFP (upper panel). The 242aa- to 271aa-GFP formed large GJ plaques 15–40 μm in length (upper panel, arrows) and AGJs 5–8 μm in diameter (lower panel, arrow heads). (E) 302aa- to 378aa-GFP formed GJ plaques no longer than 15 μm in length (arrows) and AGJs no larger than 5 μm (arrow heads). Schematic diagrams of ratios of (F) GJ plaque length and (G) AGJ diameter in a total of 50 cell-pairs in triplicate experiments. Scale bar = 10 μm.

GJ plaques assembled from these four CT mutants varied in length from shorter than 1 to 40 μm, which is 2.5 times longer than that observed in wild type $Cx43_{(382aa)}$-GFP. These CT mutants also formed large AGJs of about 8 μm in diameter which was 1.6 times larger than that observed in wild type $Cx43_{(382aa)}$-GFP (Fig. 1D, arrow heads). The other five CT mutants ($Cx43_{(302aa)}$-GFP to $Cx43_{(378aa)}$-GFP) formed GJ plaques of up to 15 μm in length and AGJs up to 5 μm in diameter (Fig. 1E, arrows and arrow heads), and these were similar to those observed in wild type $Cx43_{(382aa)}$-GFP. GJ plaques and AGJs were categorized into 3 groups by size (long/large, medium, short/small), and represented as a percentage for each group. About 50% of GJ plaques formed by Cx43CT mutants shorter than 271aa were long, whereas Cx43CT mutants longer than 302aa did not form large GJ plaques (Fig. 1F and 1G). This finding suggests an important role of the amino acid region between 271 and 302aa residues in the C-terminus of Cx43 in the size of GJ plaques and AGJ formations.

Fluorescence recovery after photobleaching (FRAP) experiments showed that all CT mutants, except for $Cx43_{(235aa)}$-GFP, formed functional GJs (Supplementary Fig. 1A).

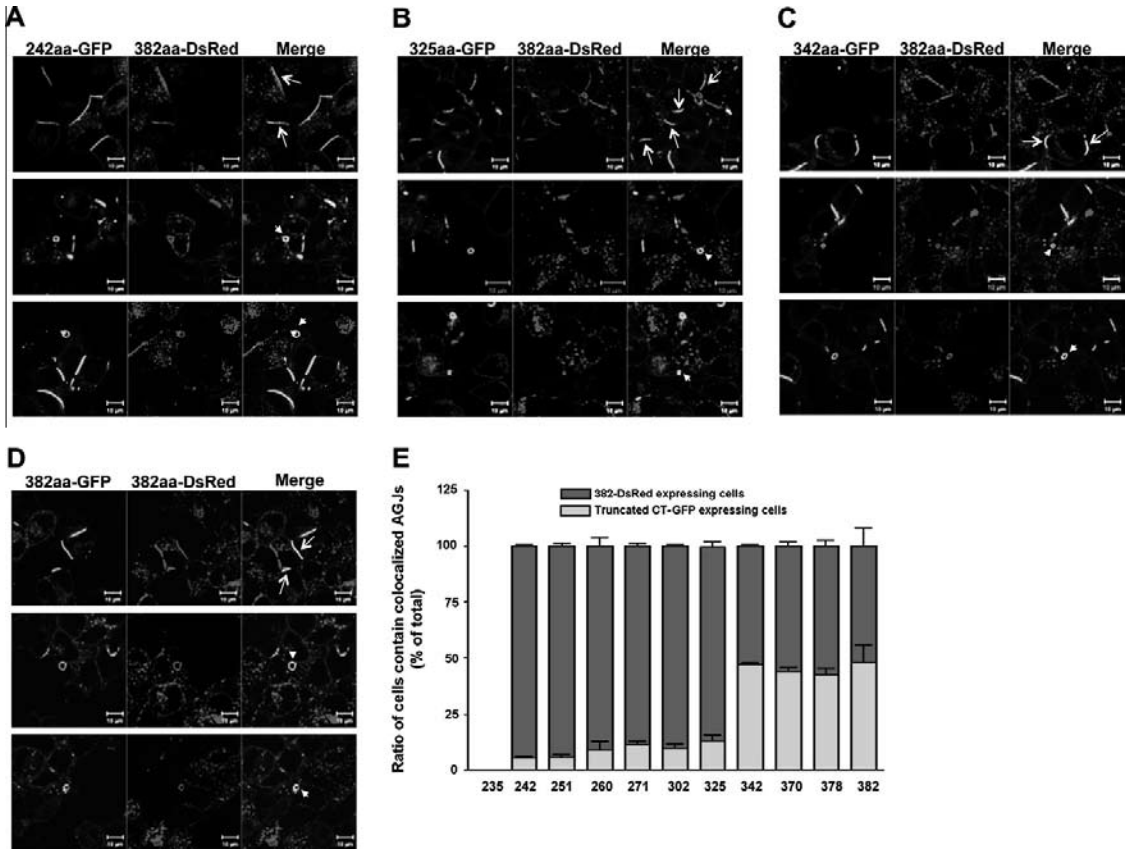

Fig. 2. Directions of AGJ internalization are dependent on the length of the C-terminal domain of Cx43. Colocalized GJ plaques and AGJs between 382aa-DsRed and (A) 242aa-GFP, (B) 325aa-GFP, (C) 342aa-GFP and (D) 382aa-GFP are shown in yellow. Colocalizations of GJ plaque (upper panels, arrows), internalized AGJs into 382aa-DsRed cells (middle panel, arrow heads) and into GFP cells (lower panel, arrow heads). (E) Schematic diagram of the ratio of cells containing colocalized AGJs in a total of 50 cell-pairs in triplicate experiments. Scale bar = 10 μm.

3.2. CT mutants form GJ plaques and AGJs with wild type Cx43 at typical sizes

To investigate the details of Cx43CT's role in GJ plaque size, $Cx43_{(382aa)}$-DsRed-expressing cells were co-cultured with GFP-tagged Cx43CT mutant-expressing cells. All Cx43CT mutants longer than 242aa formed GJ plaques with $Cx43_{(382aa)}$-DsRed as shown in Fig. 2A–C. The length of the GJ plaques and the diameters of AGJs were shorter than 15 μm and smaller than 5 μm respectively, and were similar to those consisting of $Cx43_{(382aa)}$-DsRed and $Cx43_{(382aa)}$-GFP (Fig. 2D). The length of plaque made up of Cx43-$GFP_{(<271aa)}$ was sometimes longer than 15 μm (Fig. 1D and F), and this result suggested that the GJ plaque size and AGJ diameter were restricted not by the connexon of the shorter Cx43-GFP mutant, but by the connexon of $Cx43_{(382aa)}$-DsRed. The function of GJIC among these cells was confirmed by a parachute assay (Supplementary Fig. 1B).

3.3. The Direction of GJ internalization is dependent on the length of Cx43CT

To investigate the role of Cx43CT in the direction of GJ internalization, the cells containing AGJ vesicles between a pair of wild type $Cx43_{(382aa)}$-DsRed and GFP-tagged Cx43CT mutant expressing cells were examined (middle and lower panels in Fig. 2A–D). The ratios of presence of AGJs were randomly examined in a total of 50 cell-pairs and repeated in triplicate experiments (Fig. 2E). A co-culture experiment of $Cx43_{(382aa)}$-DsRed-expressing cells with $Cx43_{(242\ to\ 325aa)}$-GFP expressing cells showed unidirectional internalization of AGJs, that is, AGJs were present in 87–95 percent of wild type $Cx43_{(382aa)}$-DsRed-expressing cells. On the other hand, a co-culture experiment of $Cx43_{(382aa)}$-DsRed-expressing cells with $Cx43_{(342aa\ to\ 382aa)}$-GFP- expressing cells showed bidirectional internalization of AGJs into 52–57 percent of $Cx43_{(382aa)}$-DsRed-expressing cells and 43–48 percent of GFP-expressing cells, respectively. These findings suggest an important role of the region between 325 and 342aa residues of the Cx43 CT domain in the direction of internalization of GJ plaques.

3.4. Deletion of the 325–342aa region confirms the important role of the length of C-terminal domain of Cx43 in the direction of GJ internalization

To investigate whether the region of 18aa between the 325 and 342aa residues of Cx43CT [S^{325}TISNSHAQPFDFPDDNQ^{342}] was important for the direction of GJ plaque internalization, this 18aa region was deleted from the CT of wild type Cx43 and then fused with GFP at the end of CT (Fig. 3A). The expression of $Cx43_{(\Delta 325–342aa)}$-GFP was determined by immublotting using an antibody against GFP (Fig. 3B). The GJ plaque formation and AGJs

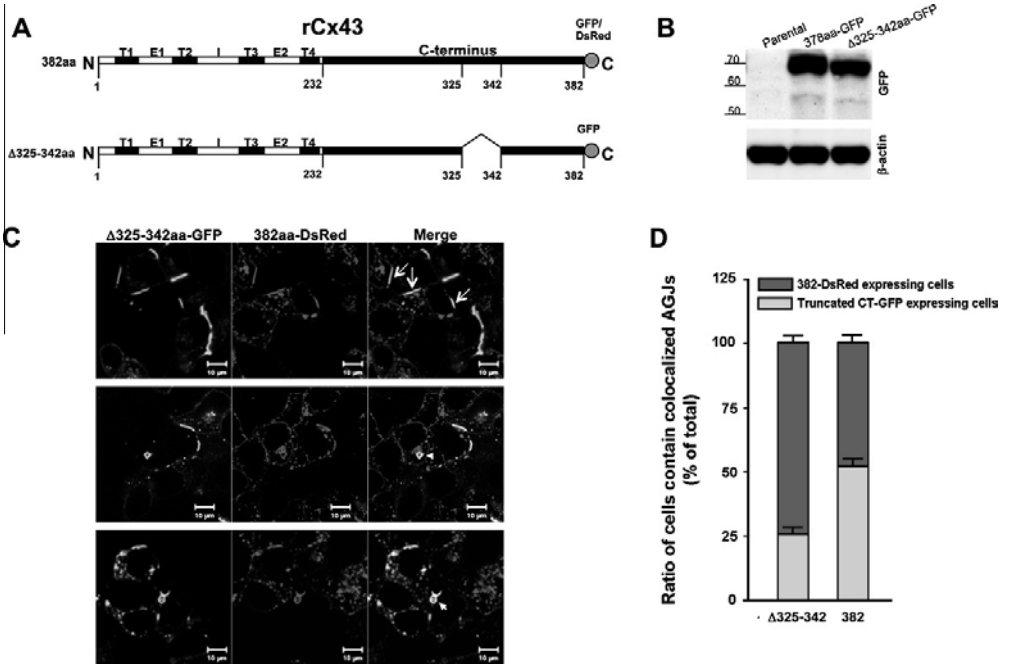

Fig. 3. Deletion of 325–342aa confirms the effect on the direction of AGJ internalization. (A) Schematic diagram summarizing the construction of an 18aa (325–342aa) deletion mutant. (B) Protein lysates from parental HeLa cells, and cells expressing wild type 382aa Cx43-GFP and Δ325–342aa-GFP were immunoblotted with an anti-GFP antibody. β-Actin was used as a protein loading control. (C) Δ325–342aa-GFP cocultured with wild type 382aa-DsRed. Colocalized GJ plaques no longer than 15 μm (upper panel, arrows). Colocalized AGJ no larger than 5 μm internalized into 382aa-DsRed cells (middle panel, arrow head) and into Δ325–342aa-GFP cells (lower panel, arrow head). (D) Schematic diagram of the ratio of cells containing colocalized AGJs in a total of 50 cell-pairs in triplicate experiments. Scale bar = 10 μm.

internalization between $Cx43_{(\Delta 325-342aa)}$-GFP-expressing cells and $Cx43_{(382aa)}$-DsRed-expressing cells were similar to that observed between $Cx43_{(382aa)}$-DsRed-expressing cells and $Cx43_{(242\ to\ 325aa)}$-GFP-expressing cells (Figs. 2E and 3C). That is, the most unidirectional internalization of AGJs into $Cx43_{(382aa)}$-DsRed-expressing cells (middle and lower panels in Fig. 3C). Only 25% of cells expressing $Cx43_{(\Delta 325-342aa)}$-GFP contained AGJs (Fig. 3D). This finding confirmed the important role of the region between 325 and 342aa residues of the Cx43 C-terminal domain in the direction of internalization of GJ.

4. Discussion

In order to determine the role of Cx43CT in GJ formation and internalization, 10 sequentially truncated CT mutants of Cx43 tagged with GFP/DsRed were stably expressed in HeLa cells. This approach aimed to study the formation of GJ plaques and AGJ vesicles originating from different lengths of Cx43CT mutants in living cells by laser scanning confocal microscopy. A previous report showed that the wild type connexins tagged with fluorescence proteins on their CT could be clustered normally into typical GJ plaques [17]. The HeLa cells were used in this study because they do not express endogenous connexins [18]. Moreover, the Cx43-expressing HeLa cells did not show significant differences in cell shape or size compared to typical parental HeLa cells. The wild type $Cx43_{(382aa)}$-GFP or -DeRed formed a GJ plaque as fluorescent lines between 0.5 and 15 μm in length at the membrane junction between two contacting cells. Double-membrane AGJ vesicles between 0.5 and 5 μm in diameter were observed in the cytoplasmic space. The wild type 382aa-GFP and 382aa-DsRed did not show any differences in characteristics in either GJ plaques or AGJs.

Only the shortest mutant of Cx43-GFP, $Cx43_{(235aa)}$-GFP, did not form GJ or GJIC. All other longer mutants from 242aa were assembled into GJ plaques as fluorescent lines at sites of cell–cell apposition. All GJ plaques and AGJs originating from these CT mutants colocalized with caveolin-1 (Cav-1) in an immunostaining experiment (Supplementary Fig. 2). This finding suggested that GJ at the plasma membrane is localized in a lipid raft domain by association with Cav-1. Moreover, it is suggested that the internalization of AGJ is due to caveolae-dependent endocytosis [19]. The FRAP experiment showed that the assembled GJs originating from these CT mutants are functionally efficient (Supplementary Fig. 1). This finding suggested an important role of the amino acid region between 235 and 242aa residues [G^{235}VKDRVKG^{242}] in assembly of GJ plaques at the plasma membrane. This region between 234 and 243aa has been reported previously as a specific tubulin binding domain [20] because Cx43 was reported to be translationally inserted into the endoplasmic reticulum [21] and then transported through the Golgi apparatus [22]. Taken together with our finding, we conclude that region between 235 and 242aa plays an essential role in trafficking of Cx43, along with microtubules, to the cell membrane.

The Cx43CT mutants were classified into two groups according to the size of GJ plaques and AGJs. The first group was composed of four CT mutants from $Cx43_{(242aa)}$-GFP to $Cx43_{(271aa)}$-GFP, that showed GJ plaques between 0.5 and 40 μm in length, and AGJs between 0.5 and 8 μm in diameter. The second group was composed of five truncation mutants from $Cx43_{(302aa)}$-GFP to $Cx43_{(378aa)}$-GFP. They could form GJ plaques no longer than 15 μm and AGJs no larger than 5 μm, sizes similar to GJ and AGJ from wild type $Cx43_{(382aa)}$-GFP. This finding suggested a significant role of the region between 271 and 302aa [C^{271}SSPTAPLSPMSPPGYKLVTGDRNNSSCRNYN^{302}] of Cx43CT in determination of GJ

plaque size and AGJ diameter. These data suggested that this region may be responsible for facilitating the association of Cx43 with protein that plays a role in the endocytic pathway, such as a caveolae-dependent endocytosis [23]. Lacking these 31aa residues may interfere with the internalization of GJ and result in a long GJ plaque remaining at the plasma membrane. The large AGJs may be due to internalization of long GJs. Our finding was supported by recent publications; they reported that the PY motif (xPPxY) of Cx43CT [$P^{283}PGY^{286}$] was associated with Nedd4 [24] and Eps15 [25]. Therefore, Nedd4-mediated ubiquitination of Cx43CT may play a major role in the internalization of GJ plaques in physiological conditions.

One GJ plaque is internalized into only one of the two apposing cells [5]. Therefore, we examined the role of Cx43CT in this unique process of AGJ formation. A significant region of the Cx43 CT domain that is responsible for the direction of internalization was examined by a co-culture experiment with cells expressing GFP-tagged Cx43CT mutants and cells expressing $Cx43_{(382aa)}$-DsRed. When the Cx43CT mutants were smaller than 271aa, the length of GJ plaques formed between the GFP-tagged Cx43CT mutants and the $Cx43_{(382aa)}$-DsRed were shorter than those formed among GFP-tagged Cx43CT mutants. Furthermore, internalization of GJ plaques was observed more in $Cx43_{(382aa)}$-DsRed-expressing cells than in GFP-tagged Cx43CT mutant-expressing cells (unidirectional internalization). Owing to this unidirectional transport of AGJ, the GJ plaque formed between GFP-tagged Cx43CT mutants and the $Cx43_{(382aa)}$-DsRed was of normal size, as observed among $Cx43_{(382aa)}$-DsRed-expressing cells. We also found that the directions of GJ internalization depended on the length of the Cx43CT domain by a co-culture experiment of $Cx43_{(382aa)}$-DsRed-expressing cells with GFP-tagged Cx43CT mutant-expressing cells. The unidirectional internalization of GJ plaques into $Cx43_{(382aa)}$-DsRed-expressing cells was observed when Cx43CT mutants were shorter than 325aa. On the other hand, AGJs originating from Cx43CT mutants longer than 342aa existed almost equally in two apposing cells (bidirectional internalization). This finding suggested the significant role of 18aa residues between 325 and 342aa [S^{325}TISNSHAQPFDFPDDNQ^{342}] of the Cx43CT domain in the direction of GJ internalization. Moreover, we confirmed that this region (325–342aa) was important for directional internalization by a co-culture experiment of $Cx43_{(\Delta 325\text{-}342aa)}$-GFP-expressing cells with $Cx43_{(382aa)}$-DsRed-expressing cells. According to a previous study, phosphorylation sites of casein kinase 1 (CK1) were reported in this region [26]. They suggested that CK1 stimulated Cx43 GJ assembly via serine phosphorylation of Cx43CT. They also observed non-junctional Cx43 accumulation in the plasma membrane by treatment of cells with a CK1 inhibitor; however, the role of CK1 in GJ plaque internalization was not examined. Our data suggest that unidentified protein binding to this region induces active internalization of GJ plaque.

Finally, this study revealed that three important regions in the CT domain of Cx43 may play important roles in GJ formation and internalization. The region between 235 and 242aa residues is important for GJ plaque assembly at the plasma membrane. Moreover, the region between 271 and 302aa residues is important for determining the size of the GJ plaque and AGJ vesicles. Finally, the region between 325 and 342aa residues is important for direction of GJ internalization. These findings will contribute to the molecular understanding of Cx43 turnover.

Acknowledgments

This work was supported by research grant Global COE (Centers of Excellence) Program from the Japan Society for the Promotion of Science, Tokyo, Japan. This work was supported in part by research Grants 21659432 and 20390463 from the Japan Society for Promotion of Science, Tokyo, Japan.

Appendix A. Supplementary data

Supplementary data associated with this article can be found, in the online version, at http://dx.doi.org/10.1016/j.bbrc.2012.03.018.

References

[1] G.S. Goldberg, P.D. Lampe, B.J. Nicholson, Selective transfer of endogenous metabolites through gap junctions composed of different connexins, Nat. Cell Biol. 1 (1999) 457–459.
[2] R. Bruzzone, T.W. White, D.L. Paul, Connections with connexins: the molecular basis of direct intercellular signaling, Eur. J. Biochem. 238 (1996) 1–27.
[3] M.M. Falk, Connexin-specific distribution within gap junctions revealed in living cells, J. Cell Sci. 113 (Pt 22) (2000) 4109–4120.
[4] L.S. Musil, A.C. Le, J.K. VanSlyke, L.M. Roberts, Regulation of connexin degradation as a mechanism to increase gap junction assembly and function, J. Biol. Chem. 275 (2000) 25207–25215.
[5] K. Jordan, R. Chodock, A.R. Hand, D.W. Laird, The origin of annular junctions: a mechanism of gap junction internalization, J. Cell Sci. 114 (2001) 763–773.
[6] B.M. Nickel, B.H. DeFranco, V.L. Gay, S.A. Murray, Clathrin and Cx43 gap junction plaque endoexocytosis, Biochem. Biophys. Res. Commun. 374 (2008) 679–682.
[7] M. Koval, Pathways and control of connexin oligomerization, Trends Cell Biol. 16 (2006) 159–166.
[8] J.E. Saffitz, J.G. Laing, K.A. Yamada, Connexin expression and turnover: implications for cardiac excitability, Circ. Res. 86 (2000) 723–728.
[9] T.W. White, R. Bruzzone, Multiple connexin proteins in single intercellular channels: connexin compatibility and functional consequences, J. Bioenerg. Biomembr. 28 (1996) 339–350.
[10] D.A. Goodenough, J.A. Goliger, D.L. Paul, Connexins, connexons, and intercellular communication, Annu. Rev. Biochem. 65 (1996) 475–502.
[11] A. el Aoumari, C. Fromaget, E. Dupont, H. Reggio, P. Durbec, J.P. Briand, K. Boller, B. Kreitman, D. Gros, Conservation of a cytoplasmic carboxy-terminal domain of connexin 43, a gap junctional protein, in mammal heart and brain, J. Membr. Biol. 115 (1990) 229–240.
[12] P.D. Lampe, A.F. Lau, The effects of connexin phosphorylation on gap junctional communication, Int. J. Biochem. Cell Biol. 36 (2004) 1171–1186.
[13] B.N. Giepmans, W.H. Moolenaar, The gap junction protein connexin43 interacts with the second PDZ domain of the zona occludens-1 protein, Curr. Biol. 8 (1998) 931–934.
[14] A.M. Gumpert, J.S. Varco, S.M. Baker, M. Piehl, M.M. Falk, Double-membrane gap junction internalization requires the clathrin-mediated endocytic machinery, FEBS Lett. 582 (2008) 2887–2892.
[15] W.J. Larsen, H.N. Tung, S.A. Murray, C.A. Swenson, Evidence for the participation of actin microfilaments and bristle coats in the internalization of gap junction membrane, J. Cell Biol. 83 (1979) 576–587.
[16] R. Bhattacharjee, M. Kaneda, K. Nakahama, I. Morita, The steady-state expression of connexin43 is maintained by the PI3K/Akt in osteoblasts, Biochem. Biophys. Res. Commun. 382 (2009) 440–444.
[17] D.W. Laird, K. Jordan, T. Thomas, H. Qin, P. Fistouris, Q. Shao, Comparative analysis and application of fluorescent protein-tagged connexins, Microsc. Res. Tech. 52 (2001) 263–272.
[18] D.F. Hulser, B. Rehkopf, O. Traub, Dispersed and aggregated gap junction channels identified by immunogold labeling of freeze-fractured membranes, Exp. Cell Res. 233 (1997) 240–251.
[19] N. Balasubramanian, D.W. Scott, J.D. Castle, J.E. Casanova, M.A. Schwartz, Arf6 and microtubules in adhesion-dependent trafficking of lipid rafts, Nat. Cell Biol. 9 (2007) 1381–1391.
[20] B.N. Giepmans, I. Verlaan, T. Hengeveld, H. Janssen, J. Calafat, M.M. Falk, W.H. Moolenaar, Gap junction protein connexin-43 interacts directly with microtubules, Curr. Biol. 11 (2001) 1364–1368.
[21] J.T. Zhang, M. Chen, C.I. Foote, B.J. Nicholson, Membrane integration of in vitro-translated gap junctional proteins: co- and post-translational mechanisms, Mol. Biol. Cell 7 (1996) 471–482.
[22] K.L. Puranam, D.W. Laird, J.P. Revel, Trapping an intermediate form of connexin43 in the Golgi, Exp. Cell Res. 206 (1993) 85–92.
[23] A.M. Hommelgaard, K. Roepstorff, F. Vilhardt, M.L. Torgersen, K. Sandvig, B. van Deurs, Caveolae: stable membrane domains with a potential for internalization, Traffic 6 (2005) 720–724.
[24] K. Leykauf, M. Salek, J. Bomke, M. Frech, W.D. Lehmann, M. Durst, A. Alonso, Ubiquitin protein ligase Nedd4 binds to connexin43 by a phosphorylation-modulated process, J. Cell Sci. 119 (2006) 3634–3642.
[25] H. Girao, S. Catarino, P. Pereira, Eps15 interacts with ubiquitinated Cx43 and mediates its internalization, Exp. Cell Res. 315 (2009) 3587–3597.
[26] C.D. Cooper, P.D. Lampe, Casein kinase 1 regulates connexin-43 gap junction assembly, J. Biol. Chem. 277 (2002) 44962–44968.

顎口腔外科学分野

小村　健

医歯学総合研究科・口腔機能再構築学系専攻
顎口腔外科学・教授

1）研究の課題名

1.「EGFRとSGLT1の共発現は口腔扁平上皮癌の組織学的分化度に関連する」

「Coexpression of SGLT1 and EGFR is associated with tumor differentiation in oral squamous cell carcinoma」

（本研究は、東京医科歯科大学大学院医歯学総合研究科顎口腔外科学分野、東京医科歯科大学硬組織疾患ゲノムセンターおよび東京医科歯科大学大学院医歯学総合研究科口腔病理学分野の共同研究である）

EGFRの強発現は 化学療法、放射線療法に抵抗性を示し、浸潤や転移、予後の悪化をもたらすため、化学療法の標的となる。しかしそのキナーゼ活性を標的とした治療薬の奏効率は20%程度である。SGLT1は、グルコースの細胞内移入に関与する分子であるが、EGFRはキナーゼ活性とは無関係にSGLT1を安定化させてグルコースを細胞内に取り入れる。本研究では、口腔扁平上皮癌におけるSGLT1とEGFRの発現を検討し、臨床病理学的特徴との関連を明らかにした。舌扁平上皮癌の切除標本を用いて免疫組織染色で検討したところ、SGLT1とEGFRは、有意に高い関連をもって共発現していた（P = 0.016）。さらに、腫瘍の組織学的分化度が低いほど共発現がみられたことから、SGLT1とEGFRの共発現は腫瘍の分化の過程に関与することが示唆された。

2.「白板症外科的切除後の再発様式：再発と癌化の危険因子」

「Recurrence patterns of oral leukoplakia after curative surgical resection：important factors that predict the risk of recurrence and malignancy」

口腔白板症の治療法は様々存在するが、治療法に関係なくしばしば再発する。本研究の目的は、白板症外科的切除後再発のリスクを低減する因子を明らかにすることである。52症例53病変を対象として、再発率、上皮性異形成程度、病変部位、切除マージンなどについて検討した。再発率は15.1%で、再発した病変部位は歯肉が最も多かった。悪性転化は1例で認められた。再発した病変の切除マージンは3mm未満であった。再発病変の切除マージンには、上皮の異常が認められた。病変の上皮性異形成程度と再発との間に相関は無かった。口腔白板症の外科切除時には、上皮の異常領域を検出してすべて切除することが重要で、さらに適切な切除マージンを設定することにより再発のリスクを低減することができる。

3.「含嗽による剥離細胞中の扁平上皮癌細胞の検出による口腔がん検診法の開発」

「Development of oral cancer screening test by detection of squamous cell carcinoma among exfoliated oral mucosal cells」

口腔がんは早期発見により良好な治療成績が得られるが、病期が進行した状態で受診する患者もいるため、専門医を必要としない簡便な検診法の開発が望まれる。我々は、含嗽による剥離細胞中の癌細胞の検出による簡便な口腔がん検診の実現可能性について検討した。SCCA1をバイオマーカーとして用いた場合、口腔がんおよび前がん病変検出の感度は72.0%で、特異度は73.1%であった。簡便な口腔がん検診実現のためには、さらに高い判別率のバイオマーカーが必要であると考えられた。

4.「口底に発生した神経鞘腫：症例報告と口腔領域神経鞘腫10例の臨床病理学的検討」

「Schwannoma in the floor of the mouth：A case report and clinicopathological studies of 10 cases in the oral region」

神経鞘腫は神経鞘のシュワン細胞由来の良性腫瘍で、口腔領域に発生することは比較的まれである。舌に発生する頻度が最も高く、口底に発生することはまれである。今回、18歳女性の右側口底に発生した神経鞘腫の1例を報告する。さらに、口腔領域に発生した神経鞘腫9例を加え、臨床病理学的考察を加えた。

5.「巨舌症に対する舌縮小術後の感覚変化」

「Sensory changes after tongue reduction for macroglossia」

今回我々は、20歳女性のBeckwith-Wiedemann症候群患者の巨舌症に対して、Harada-Enomoto法による舌縮小術を施行した後の舌の感覚変化について報告する。術前および術後7日目、2か月目に舌感覚検査として静的触覚閾検査、振動覚検査、静的2点識閾別検査、痛覚検査、味覚検査を施行したところ、術後に感覚の悪化はなかった。

6.「母斑基底細胞癌症候群の臨床症状と角化嚢胞性歯原性腫瘍の治療」

「Clinical manifestations and treatment for keratocystic odontogenic tumors associated with nevoid basal cell carcinoma syndrome：a study in 25 Japanese patients」

母斑基底細胞癌症候群（NBCCS）は、腫瘍発生と身体奇形を特徴とする常染色体優性遺伝疾患である。顎骨の角化嚢胞性歯原性腫瘍（KCOT）の発生も、この症候群の特徴の一つである。本研究では、25例の日本人NBCCS患者を対象とし、特徴的な臨床症状の発生率とKCOTの治療と再発について検討した。KCOTは、100%の患者で認め、手掌足底小陥凹は76%で認めた。11例で肋骨の異常を認め、19例で家族集積性を認めた。基底細胞癌の発生と大脳鎌石灰化を認めたのは、比較的少数例であった。当科で一次治療を施行したKCOT 40病変のうち30%で再発が認められ、これらの症例ではKCOTに接する歯を保存的に治療していた。患者のQOLを損なわずにKCOTが再発しない様に治療するための最適な治療法に関しては、検討の余地があると考えられた。

2）研究のイラストレーション

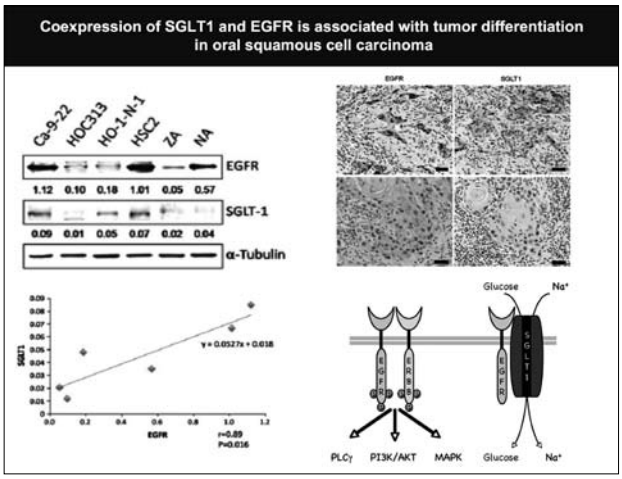

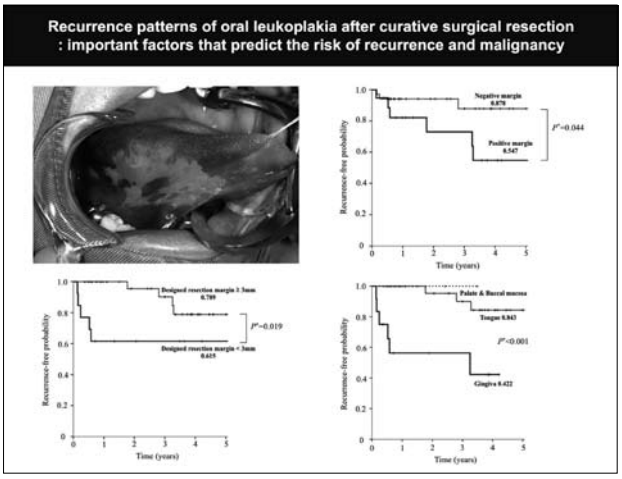

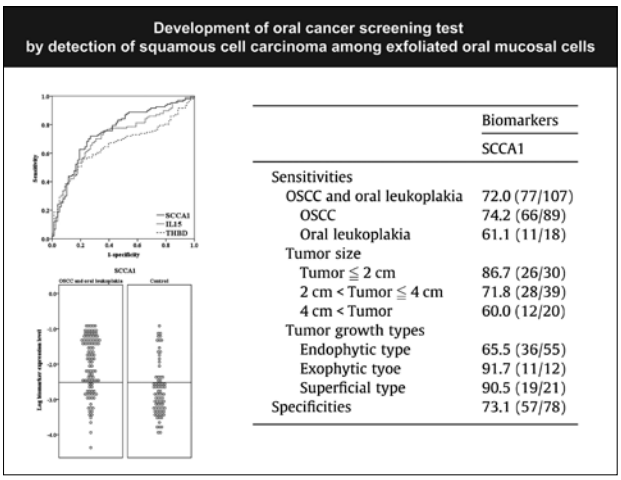

	Biomarkers
	SCCA1
Sensitivities	
OSCC and oral leukoplakia	72.0 (77/107)
OSCC	74.2 (66/89)
Oral leukoplakia	61.1 (11/18)
Tumor size	
Tumor ≦ 2 cm	86.7 (26/30)
2 cm < Tumor ≦ 4 cm	71.8 (28/39)
4 cm < Tumor	60.0 (12/20)
Tumor growth types	
Endophytic type	65.5 (36/55)
Exophytic tyoe	91.7 (11/12)
Superficial type	90.5 (19/21)
Specificities	73.1 (57/78)

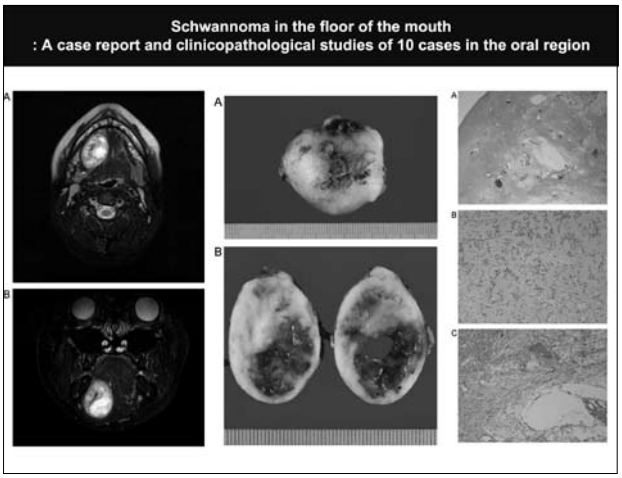

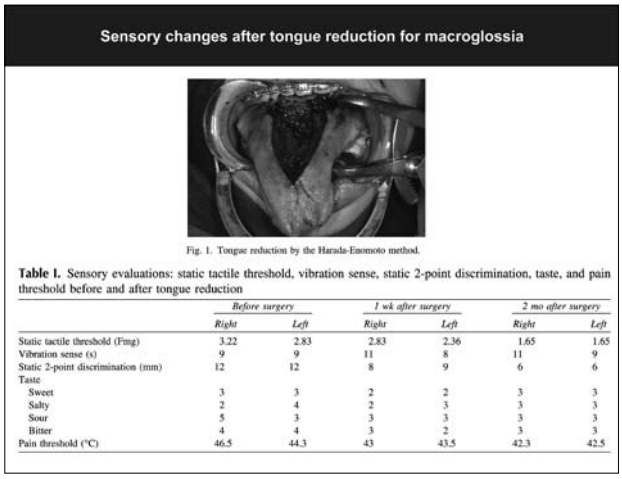
Sensory changes after tongue reduction for macroglossia

Fig. 1. Tongue reduction by the Harada-Enomoto method.

Table I. Sensory evaluations: static tactile threshold, vibration sense, static 2-point discrimination, taste, and pain threshold before and after tongue reduction

	Before surgery		*1 wk after surgery*		*2 mo after surgery*	
	Right	*Left*	*Right*	*Left*	*Right*	*Left*
Static tactile threshold (Fmg)	3.22	2.83	2.83	2.36	1.65	1.65
Vibration sense (s)	9	9	11	8	11	9
Static 2-point discrimination (mm)	12	12	8	9	6	6
Taste						
Sweet	3	3	2	2	3	3
Salty	2	4	2	3	3	3
Sour	5	3	3	3	3	3
Bitter	4	4	3	2	3	3
Pain threshold (°C)	46.5	44.3	43	43.5	42.3	42.5

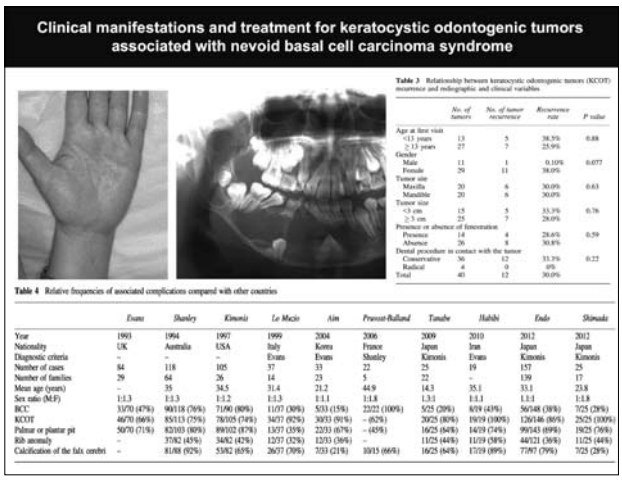
Clinical manifestations and treatment for keratocystic odontogenic tumors associated with nevoid basal cell carcinoma syndrome

Table 3 Relationship between keratocystic odontogenic tumors (KCOT) recurrence and radiographic and clinical variables

	No. of tumors	*No. of tumor recurrence*	*Recurrence rate*	*P value*
Age at first visit				
<13 years	13	5	38.5%	0.88
≥13 years	27	7	25.9%	
Gender				
Male	11	1	0.10%	0.077
Female	29	11	38.0%	
Tumor site				
Maxilla	20	6	30.0%	0.63
Mandible	20	6	30.0%	
Tumor size				
<5 cm	15	5	33.3%	0.76
≥5 cm	25	7	28.0%	
Presence or absence of fenestration				
Presence	14	4	28.6%	0.59
Absence	26	8	30.8%	
Dental procedure in contact with the tumor				
Conservative	36	12	33.3%	0.22
Radical	4	0	0%	
Total	40	12	30.0%	

Table 4 Relative frequencies of associated complications compared with other countries

	Evans	*Shanley*	*Kimmis*	*Le Mucio*	*Aim*	*Provost-Ballard*	*Tanabe*	*Habibi*	*Endo*	*Shimada*
Year	1993	1994	1997	1999	2004	2006	2009	2010	2012	2012
Nationality	UK	Australia	USA	Italy	Korea	France	Japan	Iran	Japan	Japan
Diagnostic criteria	–	–	–	Evans	Evans	Shanley	Kimmis	Evans	Kimmis	Kimmis
Number of cases	84	118	105	37	33	22	25	19	157	25
Number of families	29	64	26	14	23	5	22	–	139	17
Mean age (years)	–	35	34.5	31.4	21.2	44.9	14.3	35.1	33.1	23.8
Sex ratio (M:F)	1:1.3	1:1.3	1:1.2	1:1.3	1:1.1	1:1.8	1.3:1	1:1.1	1.1:1	1:1.8
BCC	31/70 (47%)	90/118 (76%)	71/90 (80%)	11/37 (30%)	5/33 (15%)	22/22 (100%)	5/25 (20%)	8/19 (43%)	56/148 (38%)	7/25 (28%)
KCOT	46/70 (66%)	85/113 (75%)	78/105 (74%)	34/37 (92%)	30/33 (91%)	– (62%)	20/25 (80%)	19/19 (100%)	126/146 (86%)	25/25 (100%)
Palmar or plantar pit	50/70 (71%)	82/103 (80%)	89/102 (87%)	13/37 (35%)	22/33 (67%)	– (45%)	16/25 (64%)	14/19 (74%)	99/143 (69%)	19/25 (76%)
Rib anomaly	–	37/82 (45%)	34/82 (42%)	12/37 (32%)	12/33 (36%)	–	11/25 (44%)	11/19 (58%)	44/121 (36%)	11/25 (44%)
Calcification of the falx cerebri	–	81/88 (92%)	53/82 (65%)	26/37 (70%)	7/33 (21%)	10/15 (66%)	16/25 (64%)	17/19 (89%)	77/97 (79%)	7/25 (28%)

3）発表の研究内容についての英文要約

1.「Coexpression of SGLT1 and EGFR is associated with tumor differentiation in oral squamous cell carcinoma」

Overexpression of epidermal growth factor receptor (EGFR) is associated with resistance to chemotherapy and radiotherapy, advanced tumor stage, invasion, metastasis and poor prognosis in malignant tumors. Sodiumglucose co-transporter 1 (SGLT1) is a membrane protein that mediates the transport of glucose across cellular membranes. EGFR physically associates with and stabilizes SGLT1 to promote glucose uptake into cancer cells through a kinase-independent process. The purpose of this study was to investigate the coexpression of SGLT1 and EGFR and its relationships with clinicopathological features in oral squamous cell carcinoma (OSCC). SGLT1 and EGFR were detected in all OSCC cell lines, and the expression levels of SGLT1 were significantly correlated with those of EGFR. Pearson product–moment correlation coefficient of SGLT1 and EGFR was 0.89 (P = 0.016). The immunohistochemical study using the surgical specimens in 52 patients with tongue SCC also showed a significant correlation between SGLT1 and EGFR. Moreover, SGLT1/EGFR expression was inversely related to tumor differentiation among the 5 clinicopathological factors (P = 0.004). SGLT1/EGFR coexpression might be required in the de-differentiation of OSCC, but further study is needed to clarify the implication of these proteins in the manifestation of malignancy and clinical significance.

2.「Recurrence patterns of oral leukoplakia after curative surgical resection：important factors that predict the risk of recurrence and malignancy」

Oral leukoplakia can be treated using a variety of treatment procedures; however, the lesions recur in many cases irrespective of the treatment procedure used. This study aims to identify the important factors that can lower the risk of recurrence of oral leukoplakia treated by curative surgical resection. The clinical records of 52 oral leukoplakia patients (53 lesions) who underwent curative surgical resection were retrospectively analyzed for the rate of recurrence, clinical outcome, epithelial dysplasia, lesion location, and resection margins. The recurrence rate following curative surgical resection was 15.1%, with the most common site being the gingiva. Malignant transformation occurred in a single patient (1.9%). Minimal resection margins (<3 mm) were observed in many patients with recurrent disease, and recurrence was more likely in cases with positive margins (epithelial abnormalities at the resection margins) than in those with negative margins. There was no significant association between recurrence and the degree of epithelial dysplasia. Our data suggest that surgical resection of oral leukoplakia is curative only if all areas of epithelial abnormalities are identified and resected. Moreover, an adequate resection margin may reduce the risk of recurrence.

3.「Development of oral cancer screening test by detection of squamous cell carcinoma among exfoliated oral mucosal cells」

The early detection of oral cancer improves patient outcomes. However, despite our growing knowledge of oral cancers, patients often present with advanced disease. The development of simple screening methods is desirable to provide an alternative to screening examinations by specialists. Thus, we developed a method of oral cancer detection among exfoliated oral mucosal cells, and we evaluated the feasibility of implementing an oral cancer screening test that is examiner independent. The study population consisted of 185 subjects：89 with oral cancer, 18 with oral leukoplakia, and 78 controls. We used real-time polymerase chain reaction (PCR) to detect the biomarkers. The sensitivities for the detection of oral cancer and oral leukoplakia were 72.0% with SCCA1, and the specificities were 73.1% with SCCA1. Analysis of the sensitivity according to tumor size revealed that sensitivity

was lower for large tumors. When analyzing the sensitivity according to the clinical growth pattern, the sensitivity was observed to be low for endophytic tumors. In conclusion, we developed an oral cancer screening test based on real-time PCR analysis of SCCA1 that is examiner independent, and the sensitivity and specificity were approximately 70%; therefore, we concluded that the performance of this method using a single biomarker was suboptimal.

4.「Schwannoma in the floor of the mouth：A case report and clinicopathological studies of 10 cases in the oral region」

Schwannoma is a benign tumor derived from the Schwann cells of the nerve sheath. This tumor rarely occurs in the oral region. The tongue has been reported the most common oral site; occurrence in the floor of the mouth is rare. In this report, an 18-year-old female patient with schwannoma in the right floor of the mouth is described. We also analyzed 9 additional cases of schwannoma, all of them involving the oral region, and the literature is reviewed regarding clinicopathological features.

5.「Sensory changes after tongue reduction for macroglossia」

We report sensory changes after tongue reduction by the Harada-Enomoto method for macroglossia in a 20-year-old woman with Beckwith-Wiedemann syndrome. Sensory tests were performed before surgery and 1 week and 2 months after surgery. We assessed the static tactile threshold, vibration sense, static 2-point discrimination, pain threshold, and taste. No sensory loss of any category tested was observed after tongue reduction.

6.「Clinical manifestations and treatment for keratocystic odontogenic tumors associated with nevoid basal cell carcinoma syndrome：a study in 25 Japanese patients」

Nevoid basal cell carcinoma syndrome (NBCCS) is an autosomal dominant disorder and is characterized by tumorigenesis and physical deformity. Keratocystic odontogenic tumors (KCOTs) of the jaws are a common manifestation of this syndrome. This study included 25 Japanese patients. The relative frequencies of the major symptoms in these patients were compared with those reported in the literature. We also investigated 11 patients with KCOTs initially treated at Tokyo Medical and Dental University. KCOTs (100%) and palmar and/or plantar pits (n = 19; 76.0%) were the most frequently observed manifestations. Eleven patients had a radiologically confirmed rib anomaly. Nineteen patients had a family history of the syndrome within first-degree relatives. Japanese patients had a relatively low frequency of basal cell carcinoma and falx calcification compared with that reported in other populations. Twelve of the total 40 KCOTs (30.0%) that were followed up for 6 months or more recurred. All recurrent cases had undergone conservative treatment, whereas no recurrences occurred in cases that had undergone radical treatment. Recurrence of KCOTs associated with NBCCS is frequently encountered, and further investigations are required to confirm the optimal treatment that will ensure a complete cure improving the patient's quality of life.

4）本事業に関連して世界的な研究拠点形成に向けて、以下の点で改善・整備等されたこと

A（研究拠点体制）

硬組織領域における教育、研究、臨床について優れた実績を上げるため、平成15年度より開始の21世紀COEプログラム「歯と骨の分子破壊と再構築のフロンティア」において形成した研究基盤をさらに発展させ、一方、特別教育研究経費による「先端硬組織疾患ゲノム・ナノサイエンス統合プロジェクト」との密なる連携を図りつつ、口腔扁平上皮癌などの口腔外科学領域における悪性腫瘍を中心とした硬組織疾患のテーラーメイド医療の実現とともに、トランスレーショナル・リサーチへの発展を視野にいれた研究を展開している。

B（研究教育環境）

教育・研究基盤をさらに発展させ、基礎医・歯学分野から臨床分野までの融合型国際教育研究拠点の強化・拡大を図ることによって、博士課程学生に優れた教育環境・プログラムを提供し、国内外の研究機関とも連携して“国際的創造型科学者”の育成を目指す。

C（人材確保）

基礎医・歯学分野から臨床分野までの様々な情報・技術交流を目指し、学外研究所等との大学院生・教員の相互的な派遣・受け入れの体制を整備し、基礎研究、臨床研究の両分野について先端的かつ十分な知識と技術を持つ人材の確保に取り組んでいる。

D（人材育成）

顎顔面疾患におけるテーラーメイド医療の実現とQOLの向上をも目指したトランスレーショナル・リサーチを推進することによって、基礎医・歯学分野から臨床・応用医学分野までを両立させた“国際的創造型科学者”を養成する。

E（国際化）

国際的な情報交換と技術交流を目指し、タイなどのアジア各国からの留学生を大学院生として受け入れて研究を遂行し、相互の発展に寄与している。

5）GCOE事業を推進するに当たって力を入れた点

臨床情報を具備した口腔扁平上皮癌症例の外科切除試料の系統的な収集と本学のバイオリソースセンターにおける保存を視野に入れつつ、これらの臨床検体を用いた網羅的発現解析によって口腔扁平上皮癌の頸部リンパ節転移診断モデルを構築するとともに、口腔扁平上皮癌細胞株での網羅的ゲノム・エピゲノム解析などにより新規口腔癌抑制遺伝子を単離・同定し、口腔扁平上皮癌における遺伝子変異の同定などについても明らかにすべく研究を推進してきた。また、先端硬組織疾患ゲノム・ナノサイエンス統合プロジェクトとの密接な学内連携のもと、これらのバイオリソースを用いた分子・細胞・組織・個体すべてのレベルにおける分子メカニズムの解明、顎顔面疾患の新たな診断から外科的治療法の開発を目指した系統的研究基盤の整備をすすめている。

6）英文原著論文

1. ◎Hanabata Y, Nakajima Y, Morita KI, Kayamori K, Omura K：Coexpression of SGLT1 and EGFR is associated with tumor differentiation in oral squamous cell carcinoma. Odontology. 100（2）：156-163, 2012.
2. Mochizuki Y, Omura K, Nakamura S, Harada H, Shibuya H, Kurabayashi T：Preoperative predictive model of cervical lymph node metastasis combining fluorine-18 fluorodeoxyglucose positron-emission tomography/computerized tomography findings and clinical factors in patients with oral or oropharyngeal squamous cell carcinoma. Oral Surg Oral Med Oral Pathol Oral Radiol. 113（2）：274-282, 2012.
3. Mochizuki Y, Omura K, Hirai H, Kugimoto T, Osako T, Taguchi T：Chronic mandibular osteomyelitis with suspected underlying synovitis, acne, pustulosis, hyperostosis, and osteitis（SAPHO）syndrome：a case report. J Inflamm Res. 5：29-35, 2012.
4. Sakamoto K, Fujii T, Kawachi H, Miki Y, Omura K, Morita K, Kayamori K, Katsube K, Yamaguchi A：Reduction of NOTCH1 expression pertains to maturation abnormalities of keratinocytes in squamous neoplasms. Lab Invest. 92（5）：688-702, 2012.
5. ◎Kuribayashi Y, Tsushima F, Sato M, Morita KI, Omura K：Recurrence patterns of oral leukoplakia after curative surgical resection：important factors that predict the risk of recurrence and malignancy. J Oral Pathol Med. 41（9）：682-688, 2012.
6. ◎Khanom R, Sakamoto K, Pal SK, Shimada Y, Morita K, Omura K, Miki Y, Yamaguchi A：Expression of basal cell keratin 15 and keratin 19 in oral squamous neoplasms represents diverse pathophysiologies. Histol Histopathol. 27（7）：949-959, 2012.
7. Suzuki M, Hatsuse H, Nagao K, Takayama Y, Kameyama K, Kabasawa Y, Omura K, Yoshida M, Fujii K, Miyashita T：Selective haploinsufficiency of longer isoforms of PTCH1 protein can cause nevoid basal cell carcinoma syndrome. J Hum Genet. 57（7）：422-426, 2012.
8. ◎Kugimoto T, Morita K, Omura K：Development of oral cancer screening test by detection of squamous cell carcinoma among exfoliated oral mucosal cells. Oral Oncol. 48（9）：794-798, 2012.
9. ◎Tsushima F, Sawai T, Kayamori K, Okada N, Omura K. Schwannoma in the floor of the mouth：A case report and clinicopathological studies of 10 cases in the oral region. Journal of Oral and maxillofacial surgery, Medicine, and Pathology. 24：175-179, 2012.
10. Izumo T, Kirita T, Ariji E, Ozeki S, Okada N, Okabe S, Okazaki Y, Omura K, Kusama M, Sato T：General rules for clinical and pathological studies on oral cancer：A synopsis. Jpn J Clin Oncol. 42（11）：1099-1109, 2012.
11. ◎Matsumoto K, Morita KI, Jinno S, Omura K：Sensory changes after tongue reduction for macroglossia. Oral Surg Oral Med Oral Pathol Oral Radiol. 2012 Aug 15. [Epub ahead of print]
12. ◎Shimada Y, Morita KI, Kabasawa Y, Taguchi T, Omura K：Clinical manifestations and treatment for keratocystic odontogenic tumors associated with nevoid basal cell carcinoma syndrome：a study in 25 Japanese patients. J Oral Pathol Med. 2012 Aug 8. [Epub ahead of print]
13. Kabasawa Y, Sato M, Kikuchi T, Sato Y, Takahashi Y, Higuchi Y, Omura K：Analysis and comparison of clinical results of bilateral sagittal split ramus osteotomy performed with the use of monocortical locking plate fixation or bicortical screw fixation. Oral Surg Oral Med Oral Pathol Oral Radiol. 2012 Jul. [Epub ahead of print]
14. Mochizuki Y, Omura K, Nakamura S, Kayamori K, Harada H, Shibuya H：Evaluation of metastatic cervical lymph nodes in patients with oral squamous cell carcinoma using 18F-FDG PET-CT scans and histopathologic correlation. J Surg Rad. in press.
15. Inomata K, Marukawa E, Takahashi Y, Omura K：The effect of covering materials with open wound in alveolar ridge augmentation using beta-tricalcium phosphate：an experimental study in the dog. The International Journal of Oral & Maxillofacial Implants. in press.
16. Takahashi Y, Marukawa E, Omura K：Application of a new material, beta-tricalcium phosphate/collagen composites, to extraction socket preservation：an experimental study in dogs. The International Journal of Oral & Maxillofacial Implants. in press.

7）総説ならびに著書

1. 小村健（共著）：頭頸部癌取扱い規約　第5版　金原出版　2012年6月

8）平成24年度までの自己評価

口腔扁平上皮癌などの口腔外科学領域における悪性腫瘍を中心とした硬組織領域における教育、研究、臨床については世界的にトップレベルの優れた実績を上げ、一方、特別教育研究経費による「先端硬組織疾患ゲノム・ナノサイエンス統合プロジェクト」との密なる連携を図りつつ、テーラーメイド医療の実現をめざしたトランスレーショナル・リサーチが展開できた。

9）和文原著論文

1. 田口貴英, 森田圭一, 島田泰如, 小村健：角化嚢胞性歯原性腫瘍再発に関する臨床的検討．日本口腔腫瘍学会雑誌　24（1）：9-19, 2012.
2. 工藤雅範,小村健,原田浩之,岡田憲彦：上顎洞と鼻腔を広範に占拠した石灰化嚢胞性歯原性腫瘍の1例.日本口腔腫瘍学会誌 24（2）：49-54, 2012.
3. 山本信祐, 島本裕彰, 岡田憲彦,小村健：頬部に生じた多形腺腫由来癌の1例．日本口腔外科学会雑誌 58（6）：395-399, 2012.
4. 高原楠旻,今井英樹,中川聡,角倉可奈子,小村健：関節隆起形成術を適応した片側性陳旧性顎関節脱臼の1例．日本顎関節学会雑誌 24（2）：105-110, 2012.
5. 中川聡, 高原楠旻, 吉本光洋, 小村健：下顎頭に発生した内軟骨種の1例. 日本口腔外科学会雑誌 58（2）：82-86, 2012.
6. 田中香衣, 小村健, 原田浩之, 岡田憲彦：口腔内小唾液腺癌45例の臨床的検討.日本口腔腫瘍学会誌 24（1）：21-27, 2012.
7. 上杉篤史, 丸川恵理子, 丸岡豊, 小村健：三叉神経第Ⅱ・Ⅲ枝領域帯状疱疹後に下顎歯槽骨壊死と歯の脱落が続発したHIV感染者の1例. 日本口腔科学会雑誌　61（3）：275-282, 2012.
8. 吉本光洋：口腔白板症におけるFADDゲノム増幅検出. 口腔病学会雑誌 79（2）：71-81, 2012.
9. 新谷悟, 小村健, 久保田英朗, 金子明寛, 覚道健治, 山下徹郎, 中嶋頼俊, 今井裕, 伊能智明, 山本英雄, 綿貫圭, 平木昭光, 岩永賢二郎, 神部芳則, 坂田秀雄：抜歯後疼痛に対するJNS013（トラマドール塩酸塩/アセトアミノフェン配合錠）の臨床評価 –各配合成分の単独投与との二重盲検比較試験-日本口腔外科学会雑誌 58（3）：110-122, 2012.
10. 島本裕彰, 小村健, 原田浩之：口腔多発扁平上皮癌症例の臨床的検討. 頭頸部癌 38（1）：1-5, 2012.
11. 島本裕彰, 小村健：顎下部の石灰化物. Dental Diamond 37（4）：121-122, 2012.
12. 小村健：学会が求める口腔がん専門医像. 日本口腔腫瘍学会誌　24（2）：35-37, 2012.

10）学会発表（英文）

1. ◎Shimada Y：Genetic etiology of keratocystic odontogenic tumor（KCOT）. The 6th Global COE International Symposium - Molecular Control of Bone Remodeling -. January 23-25, 2012, Tokyo, Japan.
2. ◎Shirakawa J, Ezura1 Y, Notomi1 T, Hayata T, Nakamoto T, Omura K, Noda M：Both the PTH-induced and fluid-flow induced osteoblast proliferation are associated with up-regulation of CyclinD1 expression. The 6th Global COE International Symposium - Molecular Control of Bone Remodeling -. January 23-25, 2012, Tokyo, Japan.　示説
3. ◎Yamamoto S, Inoue J, Bai H, Kawano T, Inazawa J：A transcriptional variant of the LC3A gene is involved in autophagy and frequently inactivated in human cancers. American Association for Cancer Research Annual Meeting 2012. March 31-April 4, 2012, Chicago, USA.　示説
4. Tsushima F, Sakurai J, Omura K：Clinical evaluation of malignant transformation in oral leukoplakia. The 2nd Tri-University Consortium on Oral science and Education. July 27-28, 2012, Beijing, China. 口演
5. ◎Shimada Y, Sakamoto K, Morita KI, Kabasawa Y, Omura K, Yamaguchi A：Role of SUFU and PTCH2 genes in pathogenesis of keratocystic odontogenic tumor. The 2nd Tri-University Consortium on Oral Science and Education. July 27-28, 2012, Beijing, China. 示説
6. Kabasawa Y, Sato M, Kikuchi Y, Sato Y, Takahara Y, Matsushita Y, Kimura A, Omura K：Analysis of facial nerve palsy after orthognathic surgery. XXI Congress of the European association for cranio-maxillofacial surgery. September 11-15, 2012, Dubrovnik, Croatia.口演
7. Marukawa E, Takahashi Y, Hatakeyama I, OmuraK：Application of beta-tricalcium phosphate/collagen composites to　extraction socket preservation：an experimental study in canine maxilla.　AAOMS 94th Annual Meeting, September 10-15, 2012, San Diego, USA.　示説
8. ◎Shimada Y, Sakamoto K, Morita KI, Kabasawa Y, Omura K, Yamaguchi A：Loss of heterozygosity of SUFU or PTCH2 locus associates with keratocystic odontogenic tumor. The 34th American Society for Bone

and Mineral Research（ASBMR）Annual Meeting 2012. October 12-15, 2012, Minneapolis, USA.　示説

9. ◎Shirakawa J, Ezura1 Y, Notomi T, Hayata T, Nakamoto T, Omura K, Noda M：PTH Enhances Mechanical Stress-induced Osteoblast Proliferation in Calvarial Derived Osteoblasts via Up-regulation of CyclinD1 Expression. American Society for Bone and Mineral Research 2012 Annual Meeting. October 12-15, 2012, Minneapolis, USA. 示説
10. Marukawa E, Takahashi Y, Hatakeyama I, Omura K：Evaluation of bone regeneration induced by uncultured bone marrow aspirate concentrate. 10th Asian congress on oral and maxillofacial surgery. November 15-18, 2012. Bali, Indonesia.　口演
11. Kudoh M, Omura K, Harada H, Ishii Y, Matsumoto K, Suzuki K：A case of epidermoid cyst arising in the submandibular region. 10th Asian Congress on Oral and Maxillofacial Surgery. November 15-18, 2012, Bali, Indonesia.　口演

11）学会発表（和文）

1. 釘本琢磨, 森田圭一, 小村健：含嗽による剥離細胞を用いた口腔がん検出法の開発. 第30回日本口腔腫瘍学会総会 2012年1月26-27日　さいたま市
2. 大迫利光, 小村健, 原田浩之, 島本裕彰：口腔扁平上皮癌におけるセンチネルリンパ節生検. 第30回日本口腔腫瘍学会総会 2012年1月26-27日　さいたま市
3. 佐藤潔, 坂本啓, 栢森高,小村健, 山口朗：口腔扁平上皮癌による骨破壊には腫瘍細胞と間質細胞が産生するRANKLが関与する.　第30回日本口腔腫瘍学会総会　2012年1月26-27日　さいたま市
4. 工藤雅範,松本佳奈子,大久保亜耶,石井良昌：緊急治療を要した高齢者急性型突発性血小板減少性紫斑病の1例.　第21回日本有病者歯科医療学会総会　2012年3月16-18日　宇都宮市
5. 上林功樹, 藤巻拓郎, 島田泰如, 中島雄介, 根岸貴志, 市田祐之, 玉城宏一, 横山利幸, 小村健, 村上晶：眼瞼基底細胞癌を発症したGorlin症候群の1例. 第116回日本眼科学会総会 2012年4月5-8日 東京
6. 工藤雅範,石井良昌,津島文彦,根岸綾子,松本佳奈子, 原田浩之,小村健：口唇に発生した多形腺腫の3例. 第66回NPO法人日本口腔科学会学術集会　2012年5月16-18日　広島市
7. 田口貴英, 島本裕彰, 小村健：下顎骨に生じたエナメル上皮線維歯牙腫の一例.　第66回NPO法人日本口腔科学会学術集会 2012年5月17－18日 広島市
8. 尾田誠一郎,丸川恵理子,小村健：当科における外傷歯の臨床的検討.第66回NPO法人日本口腔科学会学術集会　2012年5月17－18日　広島市
9. 平井秀明, 原田浩之, 島本裕章, 富岡寛文, 小村健：免疫抑制剤およびステロイド服用中の口腔領域扁平上皮癌症例の臨床的検討. 第66回NPO法人日本口腔科学会学術集会　2012年5月17－18日　広島市
10. 林孝文, 富岡寛文, 小村健, 柳文修, 浅海淳一, 筑井徹, 吉浦一紀, 南雲達人, 新谷悟, 有地淑子, 有地榮一郎, 湯浅賢治, 楠川仁悟, 野口忠秀, 草間幹夫, 石井純一, 山根正之：舌癌深達度エコー評価基準の策定. 第66回NPO法人日本口腔科学会学術集会　2012年5月17－18日　広島市
11. 富岡寛文, 金親あや乃, 原田浩之, 小村健：毛細血管拡張性運動失調症小児の舌に発生した悪性リンパ腫の1例. 第66回NPO法人日本口腔科学会学術集会　2012年5月17－18日　広島市
12. 望月裕美, 丸川恵理子, 小村健, 原田浩之, 島本裕彰, 高橋幸伸：下顎再建施行患者における術前後の口腔機能変化の検討.　第66回日本口腔科学会総会　2012年5月17－18日　広島市
13. 森田圭一, 根岸綾子, 今泉史子, 小村健：当科における過去11年間の口唇裂・口蓋裂患者に対する手術の検討.　第36回日本口蓋裂学会総会　2012年5月24-25日　京都市
14. 森田圭一, プラディット ルシャタムカヤヌント, 松川祥, 林深, 小崎健一, 稲澤譲治, 小村健：口腔扁平上皮癌のFFPE組織を用いたゲノムコピー数異常解析.　第36回日本頭頸部癌学会　2012年6月7-8日　松江市
15. 島本裕彰, 小村健, 原田浩之, 中島雄介, 富岡寛文, 田中香衣, 金親あや乃, 平井秀明：口腔扁平上皮癌頸部リンパ節転移高度進展例の検討.第36回日本頭頸部癌学会 2012年6月7-8日 松江市
16. 大迫利光, 小村健, 原田浩之, 島本裕彰：口腔扁平上皮癌におけるセンチネルリンパ節生検. 第36回日本頭頸部癌学会 2012年6月7-8日　松江市
17. 原田浩之, 小村健, 中島雄介, 島本裕彰, 富岡寛文, 田中香衣, 釘本琢磨, 大迫利光：口底扁平上皮癌における原発巣再発の臨床的検討. 第36回日本頭頸部癌学会 2012年6月7-8日　松江市
18. 丸川恵理子, 高橋幸伸 , 畠山一朗, 小村健：濃縮非培養自己骨髄細胞とβ-TCPを用いた異所性骨誘導能の検討.第11回日本再生医療学会　6月12-14日　横浜市

19. 佐藤昌,樺沢勇司,高原楠旻,木村敦,佐藤百合子,菊池　剛,樋口佑輔,小村健：顎矯正手術に対する自己血輸血の検討.第22回日本顎変形症学会総会　2012年6月18－19日　福岡市
20. 樺沢勇司,佐藤昌,高原楠旻,菊池剛,佐藤百合子,樋口佑輔,木村敦,小村健：顎矯正手術後に生じた顔面神経麻痺の検討.第22回日本顎変形症学会総会　2012年6月18－19日　福岡市
21. 後藤哲, 稲原英恵, 里見徳久, 佐藤工, 小枝聡子, 長坂浩, 川村仁：当科で行っている変法下顎枝逆L字型骨きり術における術後下唇知覚異常の出現について.第22回日本顎変形症学会総会　2012年6月18－19日　福岡市
22. 須田里香, 今井英樹：巨大な鼻口蓋管嚢胞の2例.第193回日本口腔外科学会関東地方会　2012年6月30日　所沢市
23. 釘本琢磨, 平井秀明, 角倉可奈子, 津島文彦, 島本裕彰, 原田浩之, 小村健：下顎骨内に進展した下顎神経鞘腫の1例.第193回日本口腔外科学会関東地方会　2012年6月30日　所沢市
24. 高原楠旻,今井英樹,中川 聡,角倉可奈子,櫻井仁亨,小村健：当科における間欠的クローズドロックの臨床的検討.第25回日本顎関節学会総会　2012年7月14-15日　札幌市
25. 今井英樹,高原楠旻,角倉可奈子,中川聡,須田里香,櫻井仁亨,塚原宏泰,依田　泰,宮村壽一,小村健：閉口障害の病態分類に関する検討.第25回日本顎関節学会総会　2012年7月14-15日　札幌市
26. 角倉可奈子,今井英樹,高原楠旻,中川聡,小村健：顎関節部に発生したガングリオンの1例.第25回日本顎関節学会総会　2012年7月14－15日　札幌市
27. 中川聡,高原楠旻,角倉可奈子,今井英樹,小村健：急性と慢性に分類した顎関節クローズドロックの臨床的検討.第25回日本顎関節学会総会　2012年7月14－15日　札幌市
28. 佐藤潔,李智媛,飯村忠浩,保田尚孝,伊東昌子,小村健,山口朗：口腔癌による骨破壊では間質細胞と癌細胞の両者が産生するRANKLが重要である.　第30回日本骨代謝学会学術集会　2012年7月19-21日　東京
29. 白川純平, 江面陽一, 中元哲也, 早田匡芳, 納富拓也, 小村健, 野田政樹：PTH及びメカニカルストレスによる骨芽細胞におけるサイクリンD1発現の検討. 第30回日本骨代謝学会学術集会 2012年7月19-21日 東京
30. 丸川恵理子, 小村健, 佐藤昌, 釘本琢磨, 持田薫利：retromandibular transparotid approachによる下顎骨関節突起骨折の治療経験. 第14回日本口腔顎顔面外傷学会総会　2012年7月21日　新潟市
31. 吉住結,中根綾子,庄司仁孝,村田志乃,中久木康一,小川奈美,平井秀明,三串伸哉,寺中智,梅田慈子,栩木紫緒,高島真穂,鈴木瑠璃子,齋藤有美,友利和歌子,高橋ひとみ,関田俊明,原田清,小村健,大渡凡人：口腔腫瘍切除再建後の嚥下機能訓練パス導入による効果～術前における嚥下機能評価の有用性について～.第17回・第18回共催日本摂食・嚥下リハビリテーション学会学術大会　2012年8月31日-9月1日　札幌市
32. 樋口佑輔, 樺沢勇司, 柳下和慶, 小村健：当科における顎骨骨髄炎に対する高気圧酸素療法の検討.　第46回NPO法人日本口腔科学会関東地方会　2012年9月8日 川越市
33. 礒部薫, 生田稔, 向山仁, 小村健：診断に苦慮した特発性非典型的三叉神経痛の3例. 第46回NPO法人日本口腔科学会関東地方会 2012年9月8日 川越市
34. 山本信祐, 井上純, 小村健, 小崎健一, 稲澤譲治：Identification of microRNAs negatively regulating NRF2 pathway. 第71回日本癌学会学術総会　2012年9月19-21日　札幌市
35. 櫻井仁亨,津島文彦,上杉篤史,尾田誠一郎,佐藤昌,原田浩之,小村健：白板症871例の臨床的検討.第22回日本口腔内科学会　2012年9月21日　東京
36. 小井田奈美,櫻井仁亨,渡邊大介,小村健：同種骨髄移植後に生じたサイトメガロウイルス感染を伴った口内炎の1例.第22回日本口腔内科学会　2012年9月21日　東京
37. 丸川恵理子, 高橋幸伸 , 畠山一朗, 小村健:幹細胞・フィブリン含有濃縮骨髄穿刺液を用いた骨誘導能の検討.第57回日本口腔外科学会総会　2012年10月19-21日 横浜市
38. 樺沢勇司, 佐藤昌, 菊池剛, 佐藤百合子, 高原楠旻, 樋口佑輔, 松下善彦, 木村敦, 小村健：下顎枝矢状分割術における骨分割と骨片固定に関連して生じた偶発症の検討. 第57回日本口腔外科学会総会　2012年10月19-21日　横浜市
39. 高原楠旻, 樺沢勇司, 佐藤昌, 樋口佑輔, 木村敦, 松下善彦, 佐藤百合子, 小村健：MRIを用いた下顎枝矢状分割術早期の顎関節への影響についての検討. 第57回日本口腔外科学会総会　2012年10月19-21日　横浜市
40. 原田浩之, 小村健, 中島雄介, 島本裕彰, 富岡寛文, 田

中香衣, 釘本琢磨, 大迫利光：舌扁平上皮癌N0症例の頸部後発転移に関する臨床病理学的検討. 第57回日本口腔外科学会総会　2012年10月19-21日　横浜市

41. 小村健, 原田浩之, 島本裕彰, 富岡寛文, 田中香衣, 平井秀明, 釘本琢磨：445遊離組織移植の成績と合併症. 第57回日本口腔外科学会総会　2012年10月19-21日　横浜市
42. 中島雄介, 原田浩之, 島本裕彰, 富岡寛文, 田中香衣, 平井秀明, 釘本琢磨, 大迫利光, 田口貴英, 小村健：舌扁平上皮癌の生検方法による治療成績の検討. 第57回日本口腔外科学会総会　2012年10月19-21日　横浜市
43. 島本裕彰, 小村健, 田口貴英, 釘本琢磨, 平井秀明, 富岡寛文, 田中香衣, 中島雄介, 原田浩之：80歳以上の高齢者口腔癌症例の検討. 第57回日本口腔外科学会総会　2012年10月19-21日　横浜市
44. 富岡寛文, 小村健, 釘本琢磨, 平井秀明, 望月裕美, 田中香衣, 島本裕彰, 中島雄介, 原田浩之：下顎歯肉扁平上皮癌114例の顎骨浸潤に関する検討. 第57回日本口腔外科学会総会　2012年10月19-21日　横浜市
45. 工藤雅範, 松本佳奈子, 石井良昌, 原田浩之, 小村健：下唇に発生した被角血管腫の2例. 第57回日本口腔外科学会総会 2012年10月19-21日　横浜市
46. 津島文彦, 櫻井仁亨, 佐藤昌, 尾田誠一郎, 小村健：口腔白板症の癌化に対する臨床的検討. 第57回日本口腔外科学会総会　2012年10月19-21日　横浜市
47. 島田泰如, 樺沢勇司, 森田圭一, 小村健, 山口朗：角化嚢胞性歯原性腫瘍の発生とSUFU, PTCH2遺伝子の関連性. 第57回日本口腔外科学会総会 2012年10月19-21日　横浜市
48. 森田圭一, 根岸綾子, 小村健：一期的両側唇裂形成手術のための術前鼻歯槽形成（PNAM）. 第57回日本口腔外科学会総会 2012年10月19-21日　横浜市
49. 澤井俊宏, 熊倉亮, 小村健：同時性に認めた両側耳下腺多形腺腫の1例. 第57回日本口腔外科学会総会 2012年10月19-21日　横浜市
50. 宮崎英隆, 金舞, 中島雄介, 牧口貴哉, 早田隆司, 宇田川雅敏, 樺沢勇司, 小村健, 横尾聡：組織内レーザー照射法による血管病変の治療. 第57回日本口腔外科学会総会 2012年10月19-21日　横浜市
51. 島田泰如, 坂本啓, 樺沢勇司, 森田圭一, 小村健, 山口朗：角化嚢胞性歯原性腫瘍におけるヘッジホッグ関連因子の解析. 日本人類遺伝学会第57回大会 2012年10月25-27日 東京
52. 森田圭一, プラディット ルシャタムカヤヌント, 松川祥, 林深, 小崎健一, 稲澤譲治, 小村健：舌扁平上皮癌後発頸部リンパ節転移症例のFFPE組織を用いたゲノムコピー数異常解析. 第50回日本癌治療学会学術集会 2012年10月25-27日 横浜市
53. 畠山一朗, 丸川恵理子, 高橋幸伸, 小村健：イヌ抜歯窩におけるPPP（platelet poor plasma）, PRF（platelet rich fibrin）, PRP（platelet rich plasma）の効果の違い. 第4回多血小板血漿（PRP）療法研究会 2012年11月25日　豊中市
54. 畠山一朗, 丸川恵理子, 高橋幸伸, 小村健：イヌ抜歯窩治癒過程におけるPPP（platelet poor plasma）, PRP（ platelet rich plasma ）, PRF（ platelet rich fibrin）の効果. 日本バイオマテリアル学会シンポジウム2012 2012年11月26-27日　仙台市
55. 松川祥, 森田圭一, 小村健：口腔扁平上皮癌のプロテオーム解析.　第77回口腔病学会学術大会　2012年11月30日-12月1日　東京
56. 丸川恵理子, 小村健：β-TCP（オスフェリオン®）による顎骨再生部へのインプラント治療. 第16回日本顎顔面インプラント学会 2012年12月1-2日　北九州市
57. 望月裕美, 小村健, 津島文彦, 今泉文子, 高原楠旻, 坂本啓, 出雲俊之：下顎骨正中部に生じた悪性リンパ腫の1例. 第194回日本口腔外科学会関東支部学術集会 2012年12月8日 東京
58. 持田薫利, 田中香衣, 富岡寛文, 丸川恵理子, 小村健：慢性硬化性唾液腺炎の加療を契機に他臓器のIgG4関連疾患が診断・加療された1例. 第194回日本口腔外科学会関東支部学術集会 2012年12月8日 東京
59. 大迫利光, 小村健, 遠山怜, 出雲俊之：12歳女児の下顎部に生じたdesmoid type fibromatosisの1例. 第31回日本口腔腫瘍学会総会 2013年1月24-25日　東京
60. 望月裕美, 小村健, 丸川恵理子, 原田浩之, 島本裕彰, 中島雄介, 富岡寛文, 田中香衣, 平井秀明：下顎区域切除, 半側切除後に下顎再建を施行した患者の術後口腔機能と満足度の検討.　第31回日本口腔腫瘍学会総会 2013年1月24-25日　東京
61. 田口貴英, 中島雄介, 小村健：口腔癌における核内EGFRの発現解析. 第31回日本口腔腫瘍学会総会 2013年1月24日-25日 東京
62. 田中香衣, 小村健, 原田浩之, 中島雄介, 島本裕彰, 富岡寛文, 平井秀明, 望月裕美, 釘本琢磨：下唇・下唇下顎切開による口腔・中咽頭がん切除例の検討. 第31回日本口腔腫瘍学会総会 2013年1月24-25日　東京

63. 平井秀明,小村健,原田浩之,中島雄介,島本裕彰,富岡寛文,田中香衣,釘本琢磨,大迫利光,田口貴英：舌扁平上皮癌症例における頸部リンパ節転移度と予後の検討. 第31回日本口腔腫瘍学会総会　2013年1月24-25日　東京
64. 松川祥,森田圭一,根岸綾子,尾野雅哉,山田哲司,小村健：口腔癌のFFPEサンプルを用いた化学療法感受性予測因子に関するプロテオーム解析.第31回口腔腫瘍学会総会　2013年1月24-25日　東京

12）受賞

1. 佐藤潔, 坂本啓, 栢森高,小村健, 山口朗：口腔扁平上皮癌による骨破壊には腫瘍細胞と間質細胞が産生するRANKLが関与する.　第30回日本口腔腫瘍学会総会優秀ポスター賞　2012年1月26-27日　埼玉
2. 上杉篤史：The tumor suppressive microRNA miR-218 targets the mTOR component Rictor and ihibits AKT phosphorylation in oral cancer. 平成23年度難治疾患研究所発表会優秀論文賞　2012年3月8日　東京
3. 山本信祐：Identification of microRNAs negatively regulating NRF2 pathway. 平成23年度難治疾患研究所発表会ベストディスカッション賞　2012年3月8日　東京
4. 宮崎英隆, 金舞, 中島雄介, 牧口貴哉, 早田隆司, 宇田川雅敏, 樺沢勇司, 小村健, 横尾聡：組織内レーザー照射法による血管病変の治療. 第57回日本口腔外科学会総会 優秀口演発表賞 2012年10月19-21日　横浜市

13）外部資金の獲得状況

1. 日本学術振興会科学研究費補助金・挑戦的萌芽研究
「11q13.3増幅ナビゲーションマイクロダイセクト口腔癌ゲノム構造解析」
研究代表者：小村健
期間：平成24-25年度
平成24年
　直接経費　1,300,000円　　間接経費　390,000円
平成25年
　直接経費　1,100,000円　　間接経費　330,000円
2. 日本学術振興会科学研究費補助金・基盤研究C
「ナノサイズパーティクルを用いた口腔癌レセプターターゲティングDDSの開発」
研究代表者：中島雄介
期間：平成22-24年度
平成22年
　直接経費　1,300,000円　　間接経費　390,000円
平成23年
　直接経費　1,100,000円　　間接経費　330,000円
平成24年
　直接経費　800,000円　　間接経費　240,000円
3. 日本学術振興会科学研究費補助金・基盤研究C
「組織弾性イメージングを用いた舌扁平上皮癌における術前治療効果の判定」
研究代表者：原田浩之
期間：平成23-25年度
平成23年
　直接経費　2,300,000円　　間接経費　690,000円
平成24年
　直接経費　1,700,000円　　間接経費　510,000円
平成25年
　直接経費　100,000円　　間接経費　30,000円
4. 日本学術振興会科学研究費補助金・若手研究B
「自己血漿と骨髄間葉系幹細胞を併用したハイブリッドマテリアルによる骨再生療法の検討」
研究代表者：丸川恵理子
期間：平成23-25年度
平成23年
　直接経費　1,700,000円　　間接経費　510,000円
平成24年
　直接経費　1,400,000円　　間接経費　420,000円
5. 日本学術振興会科学研究費補助金・若手研究B
「11q13.3領域遺伝子増幅と口腔がんストレス応答骨破壊機構」
研究代表者：森田圭一
期間：平成23-24年度
平成23年
　直接経費　1,900,000円　間接経費　570,000円
平成24年
　直接経費　1,400,000円　間接経費　420,000円
6. 日本学術振興会科学研究費補助金・若手研究B
「ゼラチンハイドロゲルを用いたFGF除放による顎骨延長法の改良」
研究代表者：樺沢勇司
期間：平成24-25年度
平成24年
　直接経費　1,900,000円　間接経費　480,000円
平成25年
　直接経費　1,400,000円　間接経費　420,000円

7. 日本学術振興会科学研究費補助金・若手研究B
「パラフィン包埋組織からのプロテオーム解析による新規唾液腺がんマーカーの開発」
研究代表者：根岸綾子
期間：平成24-25年度
平成24年
直接経費　1,600,000円　間接経費　480,000円
平成25年
直接経費　1,600,000円　間接経費　420,000円
8. 日本学術振興会科学研究費補助金・若手研究B
「新規免疫療法の確立を目指した口腔癌患者に誘導されている多能性免疫担当細胞の解析」
研究代表者：田中香衣
期間：平成21-24年度
平成21年
直接経費　700,000円　　間接経費　210,000円
平成22年
直接経費　700,000円　　間接経費　210,000円
平成23年
直接経費　700,000円　　間接経費　210,000円
平成24年
直接経費　800,000円　　間接経費　240,000円
9. 日本学術振興会科学研究費補助金・若手研究B
「口腔白板症の遺伝子異常解析と癌化予測診断への臨床応用」
研究代表者：栗林悠里
期間：平成24-26年度
平成24年
直接経費　2,500,000円　　間接経費　750,000円
平成25年
直接経費　500,000円　　間接経費　150,000円
平成26年
直接経費　300,000円　　間接経費　90,000円
10. 日本学術振興会科学研究費補助金・基盤研究B
「食道扁平上皮癌の新たな治療体系の構築を目指した統合的ゲノム・エピゲノム解析」
研究代表者：河野辰幸　研究分担者：小村健
期間：平成24-26年度
平成24年
直接経費　6,000,000円　（分担：600,000円）
平成25年
直接経費　4,300,000円
平成26年
直接経費　3,700,000円
11. 共同研究費　オリンパス株式会社
「機能性生体材料の顎口腔外科分野での応用検討」
研究代表者：小村健
平成22年1月4日～平成24年9月30日
研究費：7,350,000円　　直接経費　6,681,819円
12. 武田科学振興財団研究助成金
「自己血漿と骨髄間葉系幹細胞を併用したハイブリッドマテリアルによる骨再生療法の検討」
研究代表者　丸川恵理子
2011年7月22日から2年
直接経費　3,000,000円

14）特別講演、招待講演、シンポジウム

1. 小村健：シンポジウム　日本口腔腫瘍学会が求める口腔がん専門医像. 第30回日本口腔腫瘍学会総会 2012年1月26-27日　さいたま市
2. 小村健：BP製剤および抗血栓療法剤投与患者の歯科治療. 医療連携研修会 奈良県歯科医師会　2012年2月9日 奈良市
3. 小村健：口腔扁平上皮がん治療の最前線. 第31回大学院セミナー第5回硬組織疾患ゲノムセンターシンポジウム 遺伝疾患と口腔・食道扁平上皮がん研究の最前線 2012年2月16日 東京
4. 小村健：シンポジウム医歯学融合教育の未来 顎口腔医療を学ぶ意義.　東京医科歯科大学医歯学融合教育開講式 2012年4月19日 東京
5. Omura K：Surgical approach and reconstruction in oral cancer. 6th Seminar of Head Neck and Breast Surgery 2012. May 3, 2012, Bangkok, Thailand.
6. 丸川恵理子：ランチョンセミナー　骨再生療法における platelet-rich plasma（PRP）の効果 platelet-poor plasma（PPP）, platelet-rich fibrin（PRF）との違いについて-　第36回日本口蓋裂学会総会　2012年5月24-25日　京都市
7. 小村健：口腔癌　診断と治療の最前線. 平成24年度島根大学がん医療従事者研修会 2012年8月24日 出雲市
8. 小村健：口腔がんフォーラム　口腔がん治療の実態. 東京都歯科医師会 2012年9月2日 東京
9. 小村健：シンポジウム 口腔がん専門医を中心とした包括的診療体系の構築を目指して「口腔がん専門医制度」の意義と今後の課題. 第57回日本口腔外科学会総会 2012年10月19-21日　横浜市
10. 小村健：シンポジウム 頭頸部がん治療の過去と未来

泰明期治療から拡大切除再建外科への発展 口腔がんに対する拡大切除. 第50回日本癌治療学会学術集会 2012年10月25-27日 横浜市

11. 小村健：シンポジウム 歯槽骨・顎骨および口腔欠損の再建と機能回復の進歩 遊離骨皮弁による下顎骨欠損の再建. 第22回日本歯科医学会総会 2012年11月9-11日　大阪市

15）新聞、雑誌、TV報道

1. 小村健：口内炎は疲労のシグナル. 少年写真新聞 2012年3月18日
2. 小村健：口腔がん.　日本経済新聞　2012年4月27日夕刊
3. 小村健：そこが知りたい!　舌がピリピリと痛むようになり, 食事が一苦労です. ALPHA CLUB　8月号（2012月8月15日発行）
4. 小村健：からだの質問箱　舌にピリピリ感「舌痛症」か. 読売新聞　2012年9月30日
5. 釘本琢磨：インターネット掲載 うがい液で口腔癌の早期発見.（http：//www.m3.com/academy/report/article/147002/）m3.com　2012年1月16日

16）教室、分野や講座の准教授、講師、助教、特別研究員、ポスドク、指導を受けた大学院生の名前

助教授　　原田　浩之
講　師　　中島　雄介
　　櫻井　仁亭
助　教　　樺沢　勇司
　　島本　裕彰
　　丸川　恵理子
　　津島　文彦
　　田中　香衣
　　富岡　寛文
硬組織疾患ゲノムセンター特任講師：森田　圭一
大学院生　大迫　利光
　　○ 島田　泰如
　　畠山　一朗
　　松川　　祥
　　田口　貴英
　　山本　信祐
　　高橋　由貴子
　　○ 白川　順平
　　木村　　敦
プラディット・ルシャタムカヤヌント
高原　楠旻
尾田　誠一郎

第362号（第３種郵便物認可）　ALPHA CLUB　平成24年８月15日　（6）

そこが知りたい！

患者の疑問

舌がピリピリと痛むようになり、食事が一苦労です

胃を全摘して３年たちます。半年前から舌がピリピリと痛み、食事が思うようにとれません。歯科で口腔乾燥症といわれ、保湿薬が処方されましたが改善しません。最近は逆流も頻繁に起こり、また、高血圧で降圧薬も飲んでいますが、舌痛と関連があるのでしょうか。教えてください。（女性・58歳）

回答者

小村　健　先生
東京医科歯科大学大学院
顎口腔外科分野教授

ビタミンB12欠乏による ハンター舌炎の可能性が

舌の痛みには、大きく分けて、舌の外傷、炎症、腫瘍など局所の疾患によるものと、全身疾患との関係から生じるものとがあります。

３年前に胃の全摘手術を受けておられ、舌にピリピリする痛みがあり、口腔乾燥があるとのことから、ビタミンB12の吸収障害によって生じるハンター舌炎の可能性が高いと考えられます。ハンター舌炎では、それほど強くない舌の痛みや、舌の尖端部のピリピリ感、しみる感じ、灼熱感があります。また、乾燥感があり、味覚異常を伴うこともあります。

ハンター舌炎の患者さんの舌では、舌乳頭（舌の表面を覆う小さな突起）が萎縮し、消失して、滑らかになり（平滑舌）、時に発赤を認めます。舌以外にも頬粘膜（口の中の粘膜）や、歯肉、口唇（くちびる）の粘膜に萎縮や発赤を認めることがあります。

胃を全摘すると、ビタミンB12の吸収に必要な内因子というものが胃粘膜で産生されなくなるため、放置しておくとビタミンB12が欠乏して大球性正色素性貧血が生じます。その結果、舌にもさまざまな症状が現れます。

血液検査で貧血の有無、ビタミンB12欠乏の有無を調べてもらうと良いでしょう。貧血やビタミンB12の欠乏が判明すれば、ビタミンB12製剤の投与により舌の症状は比較的早期に改善します。

神経痛に近い舌痛症も考慮

舌の外見上の異常や、血液検査での異常がない場合には、舌痛症が疑われます。舌痛症は舌にヒリヒリ感、ピリピリ感、灼熱感などさまざまな痛みが長期間続く疾患で、口腔乾燥や味覚異常を伴うこともあります。40～50代の女性に多く見られます。明確な原因は未解明ですが、最近では、痛みを伝達する知覚に関わる神経回路の障害が原因とされています。また、不安や抑うつ、恐怖などの精神的なものが原因となることもあります。舌痛症の治療には、抗うつ薬、抗不安薬、漢方薬、口腔用軟膏や亜鉛サプリメントなどの投与や、カウンセリングなどの心理療法も行われます。

また、ご質問者は現在、降圧薬を内服中とのことですが、降圧薬も口腔乾燥症を引き起こすことがあり、場合によっては薬の変更も必要です。また、逆流性食道炎により舌に炎症が生じている可能性もあります。

以上のように、現在の舌の症状は全身疾患との関係から生じている可能性が高いように思われます。まずは貧血の有無、ビタミンB12の欠乏の有無を調べてもらうことをお勧めします。これらに異常がない場合には、舌痛症などが疑われますので、大学病院や大病院の口腔外科を受診し、専門的な診断と治療を受けられることをお勧めします。

★本欄にご質問をお寄せください（無料）

日本経済新聞（夕刊）　2012年（平成24年）4月27日（金曜日）

らいふプラス

口腔がん　自分で月１回チェック

口内炎と似た症状　２週間続けば注意

早期発見が大事

口腔がんのチェック

❶明るいところで鏡を用意。入れ歯があれば外す
❷唇を上や下に引っ張って、唇の内側や前歯の歯肉を見る
❸頭を後ろにそらし、上あごの天井部分を見る
❹左右それぞれの頬を外へ引っ張り、頬の内側や上下の奥歯の歯肉を見る
❺舌を出し、表側だけでなく側面、裏面も見る

注意ポイント

- 粘膜にできた凹凸や潰瘍
- 粘膜が赤くなったり、白くなったりした部分
- 口内炎のような症状が2週間以上続く場合や、サイズが1センチ以上で痛くない場合
- 粘膜の下に固まりや厚みがある
- かみづらい感じ、舌や舌を動かしづらい感じ
- 舌などのしびれやまひ
- 歯肉からの出血
- 首のリンパ節の腫れが3週間以上続く場合

（注）昭和大学歯科病院口腔外科の情報サイト「口腔がん.com」をもとに作成。口腔がんの種類の表も

口腔がんの種類と概要

舌がん	ほとんどは舌の側面や裏側にできる。粘膜の表面に症状（赤くなったり、白くなったり、凹凸や潰瘍ができたりする。以下同じ）が表れ、触ると粘膜の下に固まりや厚みがある
頬粘膜がん	頬の内側の粘膜にできる。かんだり傷つけたりした覚えがないのに症状が表れ、触ると粘膜の下に固まりや厚みがある
歯肉がん	上下の歯肉にでき、粘膜に症状が表れる。歯がぐらぐらしたり、腫れたりすることもある。歯ぐきの裏側にできることも多い
口蓋がん	上あごの天井部分にできる。傷つけた覚えがないのに、症状が表れる
口底がん	下あごの歯ぐきの内側と舌の間の部分にできる。粘膜に症状が表れる。アルコールとの関係が深いといわれる

元気ナビ

17　くらし　日・セット　12版　2012年（平成24年）9月30日（日曜日）

くらし　健康

からだの質問箱

舌にピリピリ感「舌痛症」か

原因に応じた薬物療法が中心

小村　健
東京医科歯科大医学部附属病院口腔外科教授

骨密度検査　手と足で違う結果

背骨の骨折の有無　まず調べて

中村　利孝

少年写真新聞
Juniors' Visual Journal
2012年3月18日発行　第1523号付録
©少年写真新聞社2012年

中学保健ニュース

株式会社 少年写真新聞社 〒102-8232 東京都千代田区九段南4-7-16 市ヶ谷KTビル I
http://www.schoolpress.co.jp/

口内炎は疲労のシグナル

東京医科歯科大学大学院 顎口腔外科学分野
教授　小村　健

口内炎とは

口内炎とは口腔粘膜に炎症が生じている状態をいいます。原因としては、ウイルスや細菌感染、全身抵抗力の低下、アレルギー、自己免疫疾患、外傷などが挙げられていますが、不明なことも多いとされます。

一般的な口内炎としては、アフタ性口内炎、カタル性口内炎、ウイルス性口内炎、口腔カンジダ症があります。

アフタ性口内炎 最も多く見られるものです。原因は不明ですが、睡眠不足や過労、ストレス、不規則な食事など、精神的ならびに肉体的な疲労が誘因となります。若年者に生じやすく、口腔粘膜に直径２～10mm程度の小円形・類円形、周囲に紅暈を伴う潰瘍（アフタ）が１～数個できるものです。重症化すると発語障害や嚥下障害が生じることもあります。通常、１週間程度で自然治癒しますが、症状が強い場合にはステロイド軟膏の塗布を行います。再発することも少なくありませんが（再発性アフタ）、再発を繰り返すアフタ性口内炎は、ベーチェット病という皮膚の結節性紅斑、眼の虹彩毛様体炎・ぶどう膜炎、外陰部潰瘍などを伴う全身性の自己免疫疾患のこともあるので、注意が必要です。また、アフタが難治性で拡大するような場合には、口腔がんなどのほかの疾患との鑑別が必要で、口腔外科や耳鼻科などの受診が必要です。

カタル性口内炎 歯の鋭縁や歯列矯正装置などで口腔粘膜に外傷を生じ、そこに炎症を生じたものです。原因の除去とともにステロイド軟膏の塗布により早期に治癒します。

ウイルス性口内炎 単純疱疹ウイルスなどのウイルス感染が原因です。口唇や口腔粘膜に多数生じた小水疱が破れてびらんや潰瘍を形成し、口臭とともに摂食障害を来すものです。発熱、全身倦怠感、リンパ節腫脹などのかぜ様症状を伴います。安静、栄養補給とともに抗ウイルス剤の投与を行います。

口腔カンジダ症 疲労等による免疫力低下時に、真菌の一種であるカンジダ菌が口腔粘膜表面で繁殖することにより生じるものです。多くは急性偽膜性カンジダ症と呼ばれるもので、口腔粘膜に白苔が生じ、次第に拡大し、時に口腔内全体に広がることもあります。白苔はガーゼなどで剥離可能で、その剥離面にはびらんが形成され出血や接触痛を認めます。慢性に経過すると、粘膜が肥厚し角化が亢進したり（肥厚性カンジダ症）、粘膜の萎縮を来したりすることがあります（萎縮性カンジダ症）。

口内炎の予防

口内炎の予防には、以下のことが推奨されています。1）毎食後、歯磨きやうがいを行い常に口腔内を清潔に保つ、2）疲労、ストレス、睡眠不足を避ける、3）バランスのとれた食生活、特に緑黄色野菜などビタミンB群やCを含む食品を積極的に摂取する。「口腔衛生状態は良好か？」、「疲れてはいないか？」、「睡眠は十分か？」、「ストレスをためていないか？」、「栄養摂取のバランスは良いか？」など、日常生活を見直すことにより口内炎を予防することも可能です。逆に、口内炎に罹患したら生活と健康を見直す良い機会ですので、健康管理に活用することも可能です。

1

Oral Oncology 48 (2012) 794–798

Contents lists available at SciVerse ScienceDirect

Oral Oncology

journal homepage: www.elsevier.com/locate/oraloncology

Development of oral cancer screening test by detection of squamous cell carcinoma among exfoliated oral mucosal cells

Takuma Kugimoto [a], Kei-ichi Morita [b,*], Ken Omura [a,b,c]

[a] Oral and Maxillofacial Surgery, Department of Oral Restitution, Division of Oral Health Sciences, Graduate School of Medical and Dental Sciences, Tokyo Medical and Dental University, Tokyo, Japan
[b] Department of Advanced Molecular Diagnosis and Maxillofacial Surgery, Hard Tissue Genome Research Center, Tokyo Medical and Dental University, Tokyo, Japan
[c] Global Center of Excellence (GCOE) Program, International Research Center for Molecular Science in Tooth and Bone Diseases, Tokyo Medical and Dental University, Tokyo, Japan

ARTICLE INFO

Article history:
Received 5 January 2012
Received in revised form 5 March 2012
Accepted 22 March 2012
Available online 22 April 2012

Keywords:
Oral cancer
Screening test
Exfoliated oral mucosal cells
SCCA1
Real-time PCR

SUMMARY

Objectives: The early detection of oral cancer improves patient outcomes. However, despite our growing knowledge of oral cancers, patients often present with advanced disease. The development of simple screening methods is desirable to provide an alternative to screening examinations by specialists. Thus, we developed a method of oral cancer detection among exfoliated oral mucosal cells, and we evaluated the feasibility of implementing an oral cancer screening test that is examiner independent.
Material and methods: The study population consisted of 185 subjects: 89 with oral cancer, 18 with oral leukoplakia, and 78 controls. We used real-time polymerase chain reaction (PCR) to detect the biomarkers serpin peptidase inhibitor B3 (SCCA1), interleukin 15 (IL-15), and thrombomodulin (THBD).
Results: The sensitivities for the detection of oral cancer and oral leukoplakia were 72.0% (77/107) with SCCA1, 75.7% (81/107) with IL-15, and 56.1% (60/107) with THBD, and the specificities were 73.1% (57/78) with SCCA1, 64.1% (50/78) with IL-15, and 78.2% (61/78) with THBD. Analysis of the sensitivity according to tumor size revealed that sensitivity was lower for large tumors. When analyzing the sensitivity according to the clinical growth pattern, the sensitivity was observed to be low for endophytic tumors.
Conclusion: We developed an oral cancer screening test based on real-time PCR analysis of SCCA1 that is examiner independent, and the sensitivity and specificity were approximately 70%; therefore, we concluded that the performance of this method using a single biomarker was suboptimal.

Introduction

Oral cancer is the most common cancer of the head and neck, and it affects 270,000 people every year worldwide.[1] The number of people affected by oral cancer in Japan was 2100 in 1975 and 6900 in 2005 and is estimated to be 7800 in 2015, representing 1% of all cancers and approximately 40% of head and neck cancers. When adjusted for age, oral cancer is more likely to occur in men, with a male/female ratio of 3:2, and the highest prevalence of oral cancer is in the seventh decade of life. The number of people affected by oral cancer is increasing in proportion with the aging of the population.[2,3]

Although squamous cell carcinoma (SCC) represents approximately 90% of oral malignancies[4], oral cancer presents with various clinical manifestations and is often preceded by precancerous lesions such as leukoplakia and erythroplakia. As for other cancers, the early detection of oral cancer improves patient outcomes.[5] However, despite our growing knowledge of oral cancers, patients often present with advanced disease. Oral cancer often occurs in visible areas, and medical examination can lead to early detection, but many cases require adequate knowledge and experience for an accurate diagnosis. Oral cancer screening performed by oral surgeons in Japan involves inspection and palpation, but such screening is performed less frequently than screening for other cancers and is not widely used.[6,7] Oral cancer screening by specialists is difficult to perform in large patient populations because of difficulty in securing staff and fiscal resources and because of the restricted time available. Cancer screening kits with high detection rates, e.g., those for cervical, gastric or colorectal cancers, are available for patient self-examination.[8–10] Self-examination allows patients to detect malignancy at its early stages. The development of simple screening methods is desirable to provide an alternative to screening examinations by specialists. Thus, we developed a method of oral cancer detection among exfoliated oral mucosal cells, and we evaluated the feasibility of implementing an oral cancer screening test that is examiner independent.

* Corresponding author. Address: Department of Advanced Molecular Diagnosis and Maxillofacial Surgery, Hard Tissue Genome Research Center, Tokyo Medical and Dental University, 1-5-45 Yushima, Bunkyo-ku, Tokyo 113-8549, Japan. Tel.: +81 3 5803 5510; fax: +81 3 5803 0199.
E-mail address: keiichi.m.osur@tmd.ac.jp (K.-i. Morita).

1368-8375/$ - see front matter © 2012 Elsevier Ltd. All rights reserved.
http://dx.doi.org/10.1016/j.oraloncology.2012.03.021

Table 1
Primers for the genes used in real-time polymerase chain reaction.

Gene symbol	Accession number	Product size (bps)	Sense primer	Antisense primer
β-actin	NM_001101.3	155	5′-TGCCCATCTACGAGGGGTATG-3′	5′-CTCCTTAATGTCACGCACGATTTC-3′
SCCA1	NM_006919.2	179	5′-CTTACCTCGGTTCAAAGTGAAG-3′	5′-CTTCTGCTCCCTCCTCTGTAAC-3′
IL15	NM_000585.4	103	5′-ACAAACATCACTCTGCTGCTTAGAC-3′	5′-CTGATCCAAGGTCTGATCATCTTCT-3′
THBD	NM_000361.2	105	5′-AGCACTTGTGTTGTCTGGTGGT-3′	5′-TGTGCACACAGAGATAGCATGAA-3′
18S rRNA	X03205.1	170	5′-GGACCAGAGCGAAAGCATTTG-3′	5′-AGACTTTGGTTTCCCGGAAGC-3′

Materials and methods

Subjects

This study included patients with oral squamous cell carcinoma (OSCC), patients with precancerous lesions, control patients with noncancerous lesions such as periodontal disease, and healthy control volunteers. Informed consent was obtained for participation in this study, which was performed at the Faculty of Dentistry, Tokyo Medical and Dental University, after approval by the local ethics committee. The study population consisted of 189 subjects: 92 with OSCC; 18 with oral leukoplakia, and 79 controls. The age ranges of patients (in years) with OSCC, oral leukoplakia, and controls were 24–89 (median, 63.5), 31–92 (median, 61.5), and 35–88 (median, 57.0), respectively. For detailed patient characteristics, see Tables S1–3 in the Supplementary Data.

Collection of exfoliated oral mucosal cells by oral rinsing

Subjects were provided with 10 mL of phosphate-buffered saline (NaCl 8.0 g/L, KCl 0.2 g/L, Na2HPO4 1.44 g/L, KH2PO4 0.24 g/L) and instructed to gargle thoroughly for 15 s and then spit the solution into a 50 mL test tube. Samples were centrifuged at 500*g* for 5 min at 4 °C. The supernatant was removed by aspiration, and the exfoliated cell pellets were then collected.

Isolation of total RNA and synthesis of cDNA

We added 350 μL of RLT solution from a QIAamp Viral RNA Mini Kit (Qiagen NV, Hilden, Germany) to the exfoliated cell pellets and isolated the total RNA according to the kit's protocol. The cDNA was synthesized using a Transcriptor First Strand cDNA Synthesis Kit (Roche Applied Science, Penzberg, Germany) with oligo(dT) primers.

Real-time polymerase chain reaction (PCR)

We performed PCR using the iQ5™ Real-time PCR Detection system (Bio-Rad Laboratories Inc., Hercules, CA, USA) and the SYBR® Green assay using iQ™ SYBR® Green Supermix (Bio-Rad Laboratories Inc.) to detect the amplicons. PCR was performed in a total volume of 25 μL containing 20 ng of cDNA template and 300 nM primer using 40 cycles of 95 °C for 10 s and 59 °C for 20 s. The housekeeping gene β-actin [accession number (AI): NM_001101.3] was used as an internal control. Serpin peptidase inhibitor B3 (SCCA1; AI: NM_006919.2), interleukin 15 (IL-15; AI: NM_000585.4), and thrombomodulin (THBD; AI: NM_000361.2) were used as biomarkers to detect oral cancer and oral leukoplakia. However, the measured expression levels of β-actin and other biomarkers must be standardized because exfoliated cells show some variability. The causes of this variability include varying degrees of cell degradation and problems with the validity of β-actin as an internal control gene. We used a random primer to measure the expression level of 18S ribosomal RNA (AI: X03205.1) in 24 samples. We then compared the expression level of 18S ribosomal RNA with that of β-actin and obtained a correlation coefficient of 0.761 ($P < 0.0001$). Thus, we concluded that β-actin is a suitable internal control gene. The genes and primers are listed in Table 1. Samples were considered inadequate if the cycle threshold (Ct) value of β-actin was >30 cycles. The expression levels of biomarkers in the adequate samples were calculated by normalizing the biomarker Ct value to the Ct value of β-actin using the following equation:

$$\text{Level of biomarker expression} = 2 - a/2 - b$$

where "*a*" is the biomarker Ct value and "*b*" is the β-actin Ct value. A receiver operating characteristic (ROC) curve was constructed using the biomarker expression levels (Fig. 1), and the cutoff value of each biomarker was determined based on the highest average of the sensitivity and the specificity. Samples were considered positive for biomarkers if the expression level was higher than the cutoff value. To validate the results, we used k-fold cross-validation. The original sample was randomly partitioned into 37 subsamples. Of the 37 subsamples, a single subsample that included five of samples was retained as the validation dataset for testing the model, and the remaining 36 subsamples were used as the training data. A ROC curve was constructed using the training data, and the cutoff value was determined. The five validation samples were classified according to the cutoff value. The cross-validation process was then repeated 37 times, with each of the 37 subsamples used exactly once as the validation dataset. The 37 results were combined to produce a single estimate. In addition, using these results, we performed a discriminant analysis using PASW® Statistics, version 18 (SPSS Inc., Chicago, Illinois, USA).

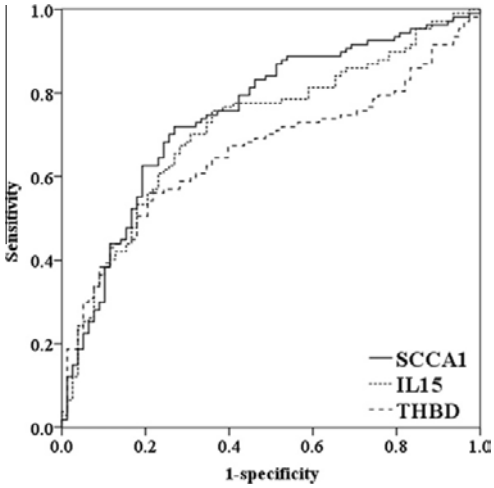

Figure 1 Receiver operator characteristic (ROC) curve for each biomarker.

Results

First, we evaluated the quality of the samples using the Ct value of β-actin. Of the samples from the entire study population, samples from 3 patients with OSCC and a sample from a control were inadequate; no patient with oral leukoplakia provided an inadequate sample. To detect OSCC among exfoliated oral mucosal cells, we evaluated the ability of SCCA1 to serve as a biomarker because this gene is known to be differentially expressed between OSCC and normal mucosa.[11] The scatter plot analysis of expression levels for SCCA1 is shown in Fig. 2. The determined biomarker cutoff value based on the ROC curve is shown by the horizontal line. The diagnostic accuracy for the detection of OSCC and oral leukoplakia was 72.4% (134/185) with SCCA1. The sensitivity for the detection of OSCC and oral leukoplakia was 72.0%, and the specificity was 73.1% (Table 3). To validate these results, we used k-fold cross-validation, and the validated sensitivity was 69.2%, and the validated specificity was 71.8%.

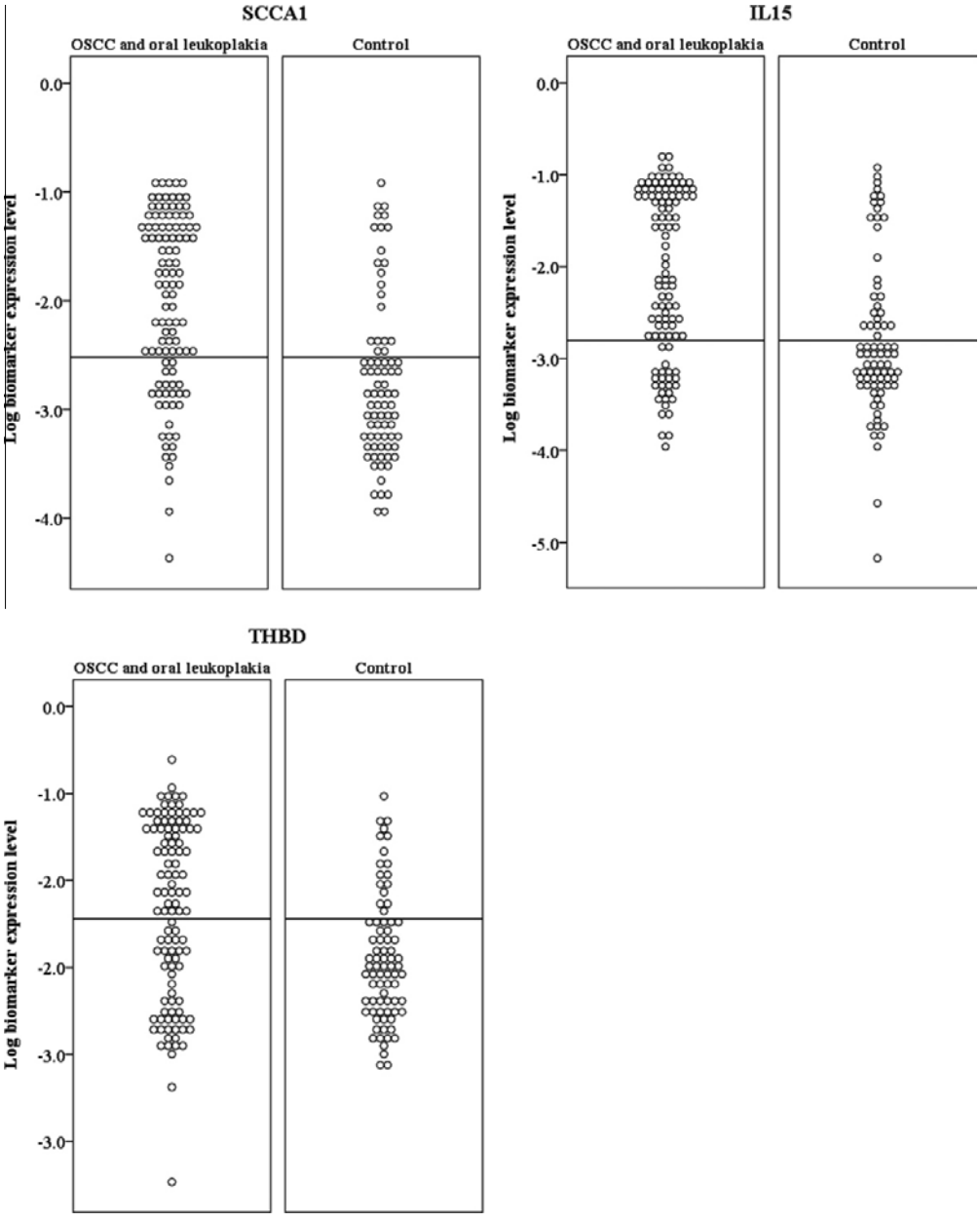

Figure 2 Scatter plot analysis of expression level for each biomarker. Each cycle stands for a unique sample of the expression level of biomarker. The determined biomarker cutoff value is shown by the horizontal line.

Table 2
Receiver operator characteristic (ROC) curve analysis of biomarkers.

Biomarker	Accession number	Description	Area under ROC curve	Cutoff point
SCCA1	NM_006919.2	Squamous cell carcinoma antigen 1	0.753 (95% CI 0.682–0.824)	0.0028
IL15	NM_000585.4	Interleukin 15	0.719 (95% CI 0.645–0.793)	0.00164
THBD	NM_000361.2	Thrombomodulin	0.658 (95% CI 0.582–0.738)	0.0195

Table 3
Sensitivity and specificity for each biomarker.

	Biomarkers		
	SCCA1	IL15	THBD
Sensitivities			
OSCC and oral leukoplakia	72.0 (77/107)	75.7 (81/107)	56.1 (60/107)
OSCC	74.2 (66/89)	78.7 (70/89)	56.2 (50/89)
Oral leukoplakia	61.1 (11/18)	61.1 (11/18)	55.6 (10/18)
Tumor size			
Tumor ≦ 2 cm	86.7 (26/30)	96.7 (29/30)	66.7 (20/30)
2 cm < Tumor ≦ 4 cm	71.8 (28/39)	71.8 (28/39)	56.4 (22/39)
4 cm < Tumor	60.0 (12/20)	65.0 (13/20)	40.0 (8/20)
Tumor growth types			
Endophytic type	65.5 (36/55)	70.9 (39/55)	47.3 (26/55)
Exophytic tyoe	91.7 (11/12)	91.7 (11/12)	83.3 (10/12)
Superficial type	90.5 (19/21)	95.2 (20/21)	66.7 (14/21)
Specificities	73.1 (57/78)	64.1 (50/78)	78.2 (61/78)

There were many false positives; therefore, we investigated the ability of the other biomarkers to decrease the false-positive rate. Although the false-negative rate increased, we performed a preliminary evaluation of several other biomarkers, including IL-15, THBD, DCTD (AI: NM_001012732.1), GSDML (AI: NM_001042471.1), RP5-1022P6 (AI: BE328402.1), C9orf46 (AI: NM_018465.3), LAMC2 (AI: NM_005562.2), MMP9 (AI: NM_004994.2), MMP12 (AI: NM_002426.4), HOXC6 (AI: NM_004503.3), and CTSC (AI: NM_001814.4), that were detected in advanced diseases.[12–16] IL-15 and THBD were selected because of their better diagnostic accuracy in a limited cohort of samples. The scatter plot analysis of the expression levels of IL-15 and THBD is shown in Fig. 2, and the determined biomarker cutoff values based on the ROC curve were 0.00164 and 0.0195, respectively (Table 2). The diagnostic accuracy for the detection of OSCC and oral leukoplakia was 70.8% (131/185) with IL-15 and 65.4% (121/185) with THBD. The sensitivities and specificities are summarized in Table 3. Of the 3 biomarkers, SCCA1 yielded the highest detection rate; however, SCCA1 alone is insufficient for primary screening. Therefore, we investigated the false-positive cases to increase the specificity. ROC curves for IL-15 and THBD were constructed for the SCCA1-positive cases; however, the use of multiple biomarkers did not improve the diagnostic accuracy. We also performed a discriminant analysis using multiple biomarkers, but this analysis also failed to yield higher diagnostic accuracy.

Because of the large number of false negatives, we investigated the causes underlying the high false-negative rate. The sensitivities for the detection of OSCC cases without oral leukoplakia using SCCA1, IL-15, and THBD were 74.2% (66/89), 78.7% (70/89), and 56.2% (50/89), respectively. The sensitivities for the detection of oral leukoplakia alone using SCCA1, IL-15, and THBD were 61.1% (11/18), 61.1% (11/18), and 55.6% (10/18), respectively. When performing the analysis according to tumor size, we observed sensitivities for SCCA1 of 86.7% (26/30) for tumors <2 cm, 71.8% (28/39) for tumors 2–4 cm, and 60% (12/20) for tumors >4 cm. When performing the analysis according to the clinical growth pattern type, we found that the sensitivities of SCCA1 for superficial, exophytic, and endophytic tumors were 90.5% (19/21), 91.7% (11/12), and 65.5% (36/55), respectively (Table 3).

Discussion

The development of highly sensitive oral cancer detection methods using oral rinsing will facilitate the detection of oral cancer by specialists and nonspecialists alike. The advantages of screening based on oral rinsing include simplicity, noninvasiveness, repeatability, lack of examiner subjectivity, and the lack of a requirement for experience or training.

Because the identification of a biomarker with a high detection rate was necessary, we evaluated the ability of three biomarkers. The diagnostic accuracy for the detection of OSCC and oral leukoplakia was 65.4% to 72.4%. SCCA1 alone is insufficient for screening; therefore, we evaluated the use of other biomarkers, alone or in combination with SCCA1, that are known to be expressed in advanced diseases. It is questionable whether these genes would be appropriate for the early detection of oral cancers because the results would be expected to be negative in patients with early-stage (node-negative) lesions, and the use of these genes would be of limited value if they could only be used to detect locally advanced, node-positive disease. Unexpectedly, these biomarkers provided detection rates similar to that of SCCA1 regardless of the stage or tumor size of the cancer. We consider this result to be due to the differences in the type of samples that were isolated from exfoliated cells, swab materials, formalin-fixed tissues, or snap frozen tissues with or without microdissection. To identify the optimal biomarkers for our oral cancer screening test, therefore, we should widely investigate the gene expression profile of exfoliated oral mucosal cells using a DNA microarray or a similar approach.

We investigated the cause of the high false-negative rate. When the screening assay was analyzed from the perspective of pathological features, we found that the sensitivity for oral leukoplakia was lower than that for oral cancer. When we investigated the sensitivity according to tumor size classification, we observed that the sensitivity was lower for large tumors. We consider this result to be high background for normal epithelial cells resulting from necrotic tissues that yield little RNA in advanced large cancers. Other possible causes include the high RNase activities of advanced large cancers due to the high level of expression of RNase, including the catalytic subunit of the RNase H2 complex, RNASEH2A.[17] Analysis based on the clinical growth pattern revealed that the sensitivity was low for endophytic tumors. This low sensitivity is most likely due to the limited exposed area of the tumor, resulting in the collection of tumor cells that are not good condition by oral rinsing.

The incorporation of oral cancer screening into a mass screening program was initially reported by Axéll in Sweden in 1976.[18] According to a report by Sankaranarayanan et al.[19] the incidence of oral cancer was 37.6–43.7 per 100,000 in Kerala, India. Of 96,517 eligible participants in the intervention group in this study, 205 cases (0.2%) of oral cancer were diagnosed. Others have reported that of the individuals screened, 5–15% had oral lesions.[20–22] In Japan, oral cancer screening has been practiced since 1986,[23] and the majority of the screening examinations are performed by local dental associations, oral and maxillofacial surgeons, and hospital dentists or through municipal corporations.[6] Oral cancer screening involves inspection and palpation by a specialist.[7] Reportedly, the detection rates based on oral mucosal screening over 3 years were 0.05% for oral cancer, 0.4% for

leukoplakia, 0.02% for erythroplakia, and 0.6% for lichen planus.[6] If oral cancer screening using our method with SCCA1 as a biomarker were performed on 100,000 people, 120 individuals with oral cancer and/or leukoplakia would be diagnosed as normal, whereas approximately 27,100 patients would require further examination. The positive predictive value is approximately 1%, similar to that of gastric cancer screening.[24]

In addition, intravital staining[25–27], brush biopsy[28–34], salivary analysis[35], exfoliated oral cell analysis[36,37], optical detection methods such as ViziLite® (Zila, Fort Collins, CO, USA)[38] and VELScope (LED Dental, White Rock, British Columbia, Canada)[39–41], and various other methods have been developed, and attempts have been made to use these approaches as auxiliary tools.

Oral cancer screening is essential for the detection of cancer in its early stages, when it is more likely to be successfully treated. We developed an oral cancer screening test based on real-time PCR of SCCA1 that is examiner independent, and the sensitivity and specificity were approximately 70%; therefore, we concluded that the performance of this method using a single biomarker was suboptimal. Future challenges will be the identification of other useful biomarkers to improve the diagnostic accuracy and the development of a more accurate collection method.

Conflict of interest statement

None declared.

Appendix A. Supplementary data

Supplementary data associated with this article can be found, in the online version, at http://dx.doi.org/10.1016/j.oraloncology.2012.03.021.

References

1. Parkin DM, Bray F, Ferlay J, Pisani P. Global cancer statistics, 2002. *CA Cancer J Clin* 2005;**55**:74–108.
2. Japan Society for Head and Neck Cancer Registry Committee. Report of head and neck cancer registry of Japan. Clinical statistics of registered patients, 2002. *Jpn J Head Neck Cancer* 2006;**32**(Suppl.):15–34.
3. Yoshino K. Trends of head and neck cancer – is it on the increase or decrease? 1. Epidemiology of head and neck cancer. *Otolaryngology–Head and Neck Surgery (Tokyo)* 2004;**76**:345–50 [Japanese].
4. Ariyoshi Y, Shimahara M, Omura K, Yamamoto E, Mizuki H, Chiba H, et al. Epidemiology study of malignant tumors in the oral and maxillofacial region: survey of member institutions of the Japanese Society of Oral and Maxillofacial Surgeons, 2002. *Int J Clin Oncol* 2008;**13**:220–8.
5. Cole P, Morrison AS. Basic issues in population screening for cancer. *J Natl Cancer Inst* 1980;**64**:1263–72.
6. Nagao T, Warnakulasuriya S, Ikeda N, Fukano H, Fujiwara K, Miyazaki H. Oral cancer screening as an integral part of general health screening in Tokoname City, Japan. *J Med Screen* 2000;**7**:203–8.
7. Nagao T, Ikeda N, Fukano H, Miyazaki H, Yano M, Warnakulasuriya S. Outcome following a population screening programme for oral cancer and precancer in Japan. *Oral Oncol.* 2000;**36**:340–6.
8. Petry KU, Menton S, Menton M, van Loenen-Frosch F, de Caravalho Gomes H, Holz B, et al. Inclusion of HPV testing in routine cervical cancer screening for women above 29 years in Germany: results for 8466 patients. *Br J Cancer* 2003;**88**:1570–7.
9. Vaira D, Malfertheiner P, Megraud F, Axon ATR, Deltenre M, Gasbarrini G, et al. Noninvasive antigen-based assay for assessing *Helicobacter pylori* eradication:a European multicenter study. *Am J Gastroenterol* 2000;**95**:925–9.
10. Nakama H, Yamamoto M, Kamijo N, Li T, Wei N, Fattah AS, et al. Colonoscopic evaluation of immunochemical fecal occult blood test for detection of colorectal neoplasia. *Hepatogastroenterology* 1999;**46**:228–31.
11. Yoshida Y. Effective biological marker to detect oral squamous cancer cells–expression patterns of CK 10, 17, 19 and SCCA mRNA. *Kokubyo Gakkai Zasshi* 2007;**74**:37–42 [Japanese].
12. Nguyen ST, Hasegawa S, Tsuda H, Tomioka H, Ushijima M, Noda M, et al. Identification of a predictive gene expression signature of cervical lymph node metastasis in oral squamous cell carcinoma. *Cancer Sci* 2007;**98**:740–6.
13. Chen C, Méndez E, Houck J, Fan W, Lohavanichbutr P, Doody D, et al. Gene expression profiling identifies genes predictive of oral squamous cell carcinoma. *Cancer Epidemiol Biomarkers Prev* 2008;**17**:2152–62.
14. Impola U, Uitto VJ, Hietanen J, Hakkinen L, Zhang L, Larjava H, et al. Differential expression of matrilysin-1 (MMP-7), 92 kD gelatinase (MMP-9), and metalloelastase (MMP-12) in oral verrucous and squamous cell cancer. *J Pathol* 2004;**202**:14–22.
15. Hassan NM, Hamada J, Murai T, Seino A, Takahashi Y, Tada M, et al. Aberrant expression of HOX genes in oral dysplasia and squamous cell carcinoma tissues. *Oncol Res* 2006;**16**:217–24.
16. Zhuang Z, Jian P, Longjiang L, Bo H, Wenlin X. Oral cancer cells with different potential of lymphatic metastasis displayed distinct biologic behaviors and gene expression profiles. *J Oral Pathol Med* 2010;**39**:168–75.
17. Flanagan JM, Funes JM, Henderson S, Wild L, Carey N, Boshoff C. Genomics screen in transformed stem cells reveals RNASEH2A, PPAP2C, and ADARB1 as putative anticancer drug targets. *Mol Cancer Ther* 2009;**8**:249–60.
18. Axell T. A prevalence study of oral mucosal lesions in an adult Swedish population. *Odontol Revy Suppl* 1976;**36**:1–103.
19. Sankaranarayanan R, Ramadas K, Thomas G, Muwonge R, Thara S, Mathew B, et al. Trivandrum Oral Cancer Screening Study Group. Effect of screening on oral cancer mortality in Kerala, India: a cluster-randomised controlled trial. *Lancet* 2005;**365**:1927–33.
20. Burzynski NJ, Ferriolo FJ, Butters JM, Sorrell CL. Evaluation of oral cancer screening. *J Cancer Educ* 1997;**12**:95–9.
21. Bouquot JE. Common oral lesions found during a mass screening examination. *J Am Dent Assoc* 1986;**112**:50–7.
22. Malaovalla AM, Silverman S, Mani NJ, Bilimoria KF, Smith LW. Oral cancer in 57,518 industrial workers of Gujarat, India: a prevalence and followup study. *Cancer* 1976;**37**:1882–6.
23. Ikeda N, Downer MC, Ishii T, Fukano H, Nagao T, Inoue K. Annual screening for oral cancer and precancer by invitation to 60-year old residents of a city in Japan. *Community Dent Health* 1995;**12**:133–7.
24. Ohata H, Oka M, Yanaoka K, Shimizu Y, Mukoubayashi C, Mugitani K, et al. Gastric cancer screening of a high-risk population in Japan using serum pepsinogen and barium digital radiography. *Cancer Sci.* 2005;**96**:713–20.
25. Epstein JB, Feldman R, Dolor RJ, Porter SR. The utility of tolonium chloride rinse in the diagnosis of recurrent or second primary cancers in patients with prior upper aerodigestive tract cancer. *Head Neck* 2003;**25**:911–21.
26. Mashberg A. Reevaluation of toluidine blue application as a diagnostic adjunct in the detection of asymptomatic oral squamous cell carcinoma: a continuing prospective study of oral cancer III. *Cancer* 1980;**46**:758–63.
27. Rosenberg D, Cretin S. Use of meta-analysis to evaluate tolonium chloride in oral cancer screening. *Oral Surg Oral Med Oral Pathol* 1989;**67**:621–7.
28. Svirsky JA, Burns JC, Carpenter WM, Cohen DM, Bhattacharyya I, Fantasia JE, et al. Comparison of computer-assisted brush biopsy results with follow up scalpel biopsy and histology. *Gen Dent* 2002;**50**:500–3.
29. Poate TW, Buchanan JA, Hodgson TA, Speight PM, Barrett AW, Moles DR, et al. An audit of the efficacy of the oral brush biopsy technique in a specialist Oral Medicine unit. *Oral Oncol* 2004;**40**:829–34.
30. Potter TJ, Summerlin DJ, Campbell JH. Oral malignancies associated with negative transepithelial brush biopsy. *J Oral Maxillofac Surg* 2003;**61**:674–7.
31. Scheifele C, Schlechte H, Bethke G, Reichart PA. Detection of TP53-mutations in brush biopsies from oral leukoplakias. *Mund Kiefer Gesichtschir* 2002;**6**:410–4 [German].
32. Remmerbach TW, Mathes SN, Weidenbach H, Hemprich A, Bocking A. Noninvasive brush biopsy as an innovative tool for early detection of oral carcinomas. *Mund Keifer Gesichtschir* 2004;**8**:229–36 [German].
33. Maraki D, Becker J, Boecking A. Cytologic and DNA-cytometric very early diagnosis of oral cancer. *J Oral Pathol Med* 2004;**33**:398–404.
34. Remmerbach TW, Weidenbach H, Mullar C, Hemprich A, Pomjanski N, Buckstegge B, et al. Diagnostic value of nucleolar organizer regions (AgNORs) in brush biopsies of suspicious lesions of the oral cavity. *Anal Cell Pathol* 2003;**25**:139–46.
35. Zimmermann BG, Park NJ, Wong DT. Genomic targets in saliva. *Ann N Y Acad Sci* 2007;**1098**:184–91.
36. Spafford MF, Koch WM, Reed AL, Califano JA, Xu LH, Eisenberger CF, et al. Detection of head and neck squamous cell carcinoma among exfoliated oral mucosal cells by microsatellite analysis. *Clin Cancer Res* 2001;**7**:607–12.
37. Rosin MP, Epstein JB, Berean K, Durham S, Hay J, Cheng X, et al. The use of exfoliative cell samples to map clonal genetic alterations in the oral epithelium of high-risk patients. *Cancer Res* 1997;**57**:5258–60.
38. Oh ES, Laskin DM. Efficacy of the VIziLite system in the identification of oral lesions. *J Oral Maxillofac Surg* 2007;**65**:424–6.
39. Mehrotra R, Singh M, Thomas S, Nair P, Pandya S, Nigam NS, et al. A cross-sectional study evaluating chemiluminescence and autofluorescence in the detection of clinically innocuous precancerous and cancerous oral lesions. *J Am Dent Assoc* 2010;**141**:151–6.
40. Awan KH, Morgan PR, Warnakulasuriya S. Evaluation of an autofluorescence based imaging system (VELscope™) in the detection of oral potentially malignant disorders and benign keratosis. *Oral Oncol* 2011;**47**:274–7.
41. Balevi B. Assessing the usefulness of three adjunctive diagnostic devices for oral cancer screening: a probabilistic approach. *Community Dent Oral Epidemiol* 2011;**39**:171–6.

インプラント・口腔再生医学分野

春日井 昇平

医歯学総合研究科・口腔機能再構築学系専攻
インプラント・口腔再生医学・教授

1）研究の課題名

骨造成法の開発
（Development of bone augmentation）

垂直的骨造成を可能にする骨膜挙上法を開発し、そのアイデアをさらに発展させた拡張型GBR（Expansible GBR, E-GBR）を開発した。この手法をさらに発展させることで、現在臨床的に困難な垂直的骨造成を安全に簡便におこなうことが可能になる。移植材を用いない上顎洞挙上法の術式を改良し、その改良した術式の有効性と安全性を臨床的に明らかにした。

歯科インプラントの開発
（Development of dental implant）

インプラント埋入部位の骨の形態がメカニカルストレス分布に及ぼす影響を有限要素法により調べ、インプラント周囲のメカニカルストレスを減らすインプラントデザインを考案し、それを基に新しいインプラントシステムを開発した。我々が開発したハイドロキシアパタイトを薄膜コーティングしたインプラントをイヌの顎骨に埋入し、骨結合後にインプラント周囲炎を惹起してその進行を調べた。その結果、このインプラントは他のインプラントに比較してインプラント周囲炎の進行が遅れたことから、感染に対して抵抗性を示すことが示唆された。これらの実験結果を基に、2-pieceのインプラントシステムを開発し、この新しいインプラントは来年（2013年）に販売される予定である。

2）研究のイラストレーション

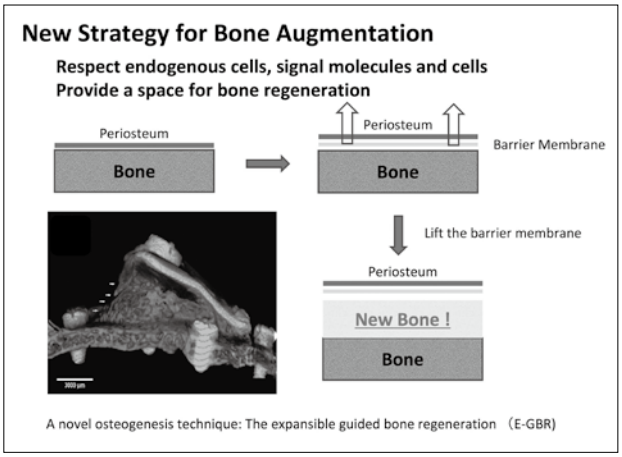

3）発表の研究内容についての英文要約

We developed “periosteal elevation technique” and then further improved this technique. Finally, we developed “expansible GBR（E-GBR）”, which makes vertical bone augmentation effective, simple and less invasive although vertical bone augmentation is currently challenging clinically. We examined effects of bone shape on stress distribution around the implant by finite element analysis and developed a new implant design for decreasing the mechanical stress around the implant. We also demonstrated that thin hydroxyapatite-coated implant, which we developed with a Japanese implant company, was resistant to infection compared to the implant surfaces of other implants. Based on these results, we developed a new two-piece implant system, which will appear in the market in 2013.

4）本事業に関連して世界的な研究拠点形成に向けて、以下の点で改善・整備等されたこと

E（国際化）

海外からの留学生（博士課程大学院生26名中、留学生14名）と、海外研究者（中国から2名、スウェーデンか

ら1名）を受け入れた。当分野において博士の学位を取得した研究者5名が、海外の大学（Harvard University, Gothenburg University, Stuttgart University, Geneva University, Hong Kong University）にポスドクとして採用された。

5）GCOE事業を推進するに当たって力を入れた点

臨床の問題点を抽出し、それを解決するため研究テーマの推進を継続しておこなった。研究室内でのセミナー、研究報告でのディスカッションの活性化、国際学会での発表の奨励、国際交流の促進をおこなった。

6）英文原著論文

1. Madi M, Zakaria O, Kasugai S. Coated vs. uncoated implants：Bone defect configurations. Journal of Oral Implantology in press
2. Madi M, Zakaria O, Noritake K, Fuji M, Kasugai S. Peri-implantitis progression around thin sputtered hydroxyapatite-coated implants：Clinical and radiographic evaluation in dogs. International Journal of Oral and Maxillofacial Implants in press
3. Miyahara T, Dahlin C, Galli S, Parsafar S, Koizumi H, Kasugai S.　A novel dual material mouthguard for patients with dental implants. Dental Traumatology in press
4. Miyahara T, Nyan M, Shimoda A, Yamamoto Y, Kuroda S, Shiota M, Akiyoshi K, Kasugai S. Exploitation of a novel polysaccharide nanogel cross-linking membrane for guided bone regeneration（GBR）. Journal of Tissue Engineering and Regenerative Medicine 6（8）：666-72, 2012
5. Rungsiyanont S, Dhanesuan N, Swasdison S, Kasugai S. Evaluation of biomimetic scaffold of gelatin-hydroxyapatite crosslink as a novel scaffold for tissue engineering：Biocompatibility evaluation with human PDL Fibroblasts, human mesenchymal stromal cells, and primary bone cells. Journal of Biomaterials Applications 27（1）：47-54, 2012
6. Bhargava S, Doi H, Kondo R, Aoki H, Hanawa T, Kasugai S. Effect of sandblasting on the mechanical properties of Y-TZP zirconia. Biomedical and Material Engineering 22（6）：383-98, 2012
7. Umehara K, Iimura T, Sakamoto K, Lin Z, Kasugai S, Igarashi Y, Yamaguchi A. Canine oral mucosal fibroblasts differentiate into osteoblastic cells in response to BMP-2. The Anatomical Redord 295（8）：1327-35, 2012
8. Zakaria O, Madi M, Kasugai S. A novel osteogenesis technique：The expansible guided bone regeneration. Journal of Tissue Engineering：2041731412441194, 2012
9. Zakaria O, Kon K, Kasugai S. Evaluation of a biodegradable novel periosteal distractor. Journal of Biomedical and Material Research Part B - Applied Biomaterials 100（3）：882-9, 2012
10. Zakaria O, Madi M, Kasugai S. Induced osteogenesis using a new periosteal distractor. Journal of Oral Maxillofacial Surgery 70（3）：225-34, 2012
11. Hao J, Kuroda S, Chen K, Noritake K, Rodoriguez R, Pluemsakunthai W, Aoki H, Kasugai S. Bacterial adhesion behavior and bone formation effect of zeledronic acid（ZOL）immobilized sputtered hydroxyapatite implants. Journal of Bio-Integration 2（1）：103-109, 2012
12. Madi M, Zakaria O, Noritake K, Fujii M, Kasugai S. Ligature-induced periimplantitis surrounding thin sputtered HA-coated implants. An experimental study in dogs. Clinical and radiographic evaluations. ournal of Bio-Integration 2（1）：111-117, 2012
13. Date Y, Yokoyama Y, Kondo H, Kuroda S, Ohya K, Ota MS, Iseki S, Kasugai S. Restricted expression of chromatin remodeling associated factor Chd3 during tooth root development. Journal of Periodontal Research 47（2）：180-7, 2012
14. Murakami I, Murakami Y, Clifford DK, Palacci P, Kasugai S. Panoramic implant notation sytem – A mothod to denote implant position and prosthodontic modalities. Journal of Prosthodontic Research 56（1）：65-9, 2012

7）特許取得、特許申請

骨造成器具.国際出願PCT/JP2012/073229（2012.09.11）
特許出願人：国立大学法人東京医科歯科大学
発明者：春日井昇平、オサマ　ザカリア

8）平成24年度までの自己評価

2000年に私が当分野の教授に就任した時点において、我が国のインプラント治療とそれに関連する研究は、欧米に10年から15年遅れていると言われていた。現在、本学歯学部附属病院インプラント外来の臨床と、当分野（インプラント・口腔再生医学分野）の研究は、世界のトップレベルに追い付き、国際的に高い評価を得ている。臨床と研究面でさらに向上を目指すと同時に、この分野で世界をリードする人材を育成したい。

9）学会発表（英文）

1. Kasugai S. How to augment bone effectively, safely and less costly. Bangkok Implant Sympoium 2012　2012.11.28-30 Pullman Hotel, Bangkok, Thailand

2. Bhargava S. Kuroda S, Aoki H, Ohya K, Kasugai S. Osteoblast differentiation on surface modified zirconia - an in vitro study. European Association for Osseointegration 21th Annual Scientific Meeting 2012.10.10-13 Bella Center, Copenhagen, Denmark
3. Miyahara T, Parsafar S, Dahlin C, Pluemsakunthai W, Palmquist A, Akiyoshi K, Thomsen P, Kasugai S. Novel dry type of cholesterolbearing pullulan nanogel crosslinking membrane for guided bone regeneration（GBR）. European Association for Osseointegration 21th Annual Scientific Meeting 2012.10.10-13 Bella Center, Copenhagen, Denmark
4. Yukawa K, Tachikawa N, Akino N, Kon K, Takaya K, Kusomoto Y, Kasugai S. The cell kinetic with porous poly-dllactic acid – anatomical insight. European Association for Osseointegration 21th Annual Scientific Meeting 2012.10.10-13 Bella Center, Copenhagen, Denmark
5. Kon K, Shiota M, Ozeki M, Kasugai S. Alteration of occlusal force in unilateral free-end and intermediate missing cases by implant prosthesis. European Association for Osseointegration 21th Annual Scientific Meeting 2012.10.10-13 Bella Center, Copenhagen, Denmark
6. Kusumoto Y, Kon K, Munakata M, Nakamura T, Tachikawa N, Shiota M, Kasugai S. Clinical outcome of sinus bone augmentation without graft：radiological analysis. European Association for Osseointegration 21th Annual Scientific Meeting 2012.10.10-13 Bella Center, Copenhagen, Denmark
7. Zakaria O, Madi M, Kasugai S. A novel guided bone regeneration technique. European Association for Osseointegration 21th Annual Scientific Meeting 2012.10.10-13 Bella Center, Copenhagen, Denmark
8. Kasugai S. New approach to bone augmentation：Respecting endogenous key players and providing space for regeneration. International Congress of Oral Implantologists（ICOI）, World Congress 2012.9.20-22 World Center Marriot Hotel, Orlando, Florida, USA
9. Kasugai S. New approach to bone augmentation：Respecting endogenous key players and providing space for regeneration. The 15th ICOI Asia Pacific Section Congress 2012.6.23 Intercontinental Hotel, Ho Chi Minh City, Vietnuam
10. Kasugai S. Novel strategy for bone augmentation：Respecting“mother nature”. The 11th Stomatology Confernce of West China 2012.4.20-23 Chengdu Convention Center, Chengdu（成都） China.

10）学会発表（和文）

1. 春日井昇平.薬理学から歯科臨床を考える.Dentistry, Quo Vadis? 2012.12.8-9 青陵会館 東京
2. 春日井昇平.国際インプラント手帳.第16回日本顎顔面インプラント学会学術大会 2012.12-1-2 北九州国際会議場 小倉
3. 佐藤瑞希,宗像源博,古市祥子,立川敬子,春日井昇平.骨密度の計測によるインプラントを用いた顎骨再建に最適な移植骨の検討.第16回日本顎顔面インプラント学会学術大会 2012.12-1-2 北九州国際会議場 小倉
4. 藤井政樹,塩田 真,春日井昇平.吸収性ハイドロキシアパタイトファイバーの骨造成効果の評価.第16回日本顎顔面インプラント学会学術大会 2012.12-1-2 北九州国際会議場 小倉
5. 宗像源博、立川敬子、能村嘉一、湯川健、春日井昇平. ポリ乳酸デバイスをスペースメーキングに用いた移植材を使用しない上顎洞挙上術の臨床検討.第42回日本口腔インプラント学会学術大会 2012.9.21-23 大阪国際会議場 大阪
6. 山本愛、宗像源博、松浦毅士、立川敬子、春日井昇平. ラテラルアプローチによる上顎洞底挙上術同時インプラント埋入をおこなった症例における合併症.第42回日本口腔インプラント学会学術大会 2012.9.21-23 大阪国際会議場 大阪
7. 渕上慧、宗像源博、鈴木章弘、古市祥子、小林裕史、春日井昇平.日本人におけるインプラント周囲炎の発症率に関する臨床的検討.第42回日本口腔インプラント学会学術大会 2012.9.21-23 大阪国際会議場 大阪
8. 井上一彦、塩田真、秋本和宏、加藤良一、春日井昇平.インプラント周囲溝に対する機能水のイリゲーション効果について.第42回日本口腔インプラント学会学術大会 2012.9.21-23 大阪国際会議場 大阪
9. 作山葵、宗像源博、立川敬子、荻野幸治、春日井昇平.サイナスリフト後に上顎洞アスペルギウス症を生じた1症例.第42回日本口腔インプラント学会学術大会 2012.9.21-23 大阪国際会議場 大阪
10. 高尚、塩田真、藤井政樹、佐藤仁、春日井昇平.シンバスタチンを配合したハイドロキシファイバーの骨増生促進.第42回日本口腔インプラント学会学術大会 2012.9.21-23 大阪国際会議場 大阪
11. 渡辺多恵、下尾嘉昭、大口慧士、佐藤大輔、春日井昇平.高安動脈炎患者に対するインプラント治療の一考察.第42回日本口腔インプラント学会学術大会 2012.9.21-23 大阪国際会議場 大阪
12. 楠本雄生、今一裕、立川敬子、宗像源博、春日井昇平.骨補填材を併用しない上顎洞粘膜挙上・同時埋入のX線的検討.第42回日本口腔インプラント学会学

術大会　2012.9.21-23　大阪国際会議場　大阪
13. 湯川健、立川敬子、塩田真、春日井昇平.過去17年間に来院したインプラント治療の既往を持つ新来患者の検討.第42回日本口腔インプラント学会学術大会　2012.9.21-23　大阪国際会議場　大阪
14. 渡邉武、塩田真、今北千春、三田稔、春日井昇平.インプラント外来における新来患者の15年間の動向.第42回日本口腔インプラント学会学術大会　2012.9.21-23　大阪国際会議場　大阪
15. 立川敬子、宗像源博、楠本雄生、原口美穂子、春日井昇平.当院における先進医療「インプラント義歯」の適用症例の検討.第42回日本口腔インプラント学会学術大会　2012.9.21-23　大阪国際会議場　大阪
16. 鶴見和久、宗像源博、湯川健、松浦毅士、春日井昇平.上顎洞底挙上術を併用したインプラント治療の予後.第42回日本口腔インプラント学会学術大会　2012.9.21-23　大阪国際会議場　大阪
17. 藤井政樹、塩田真、今一裕、春日井昇平.吸収性ハイドロキシアパタイトファイバーと非吸収性ハイドロキシアパタイトパーティクルの骨造成の比較.第42回日本口腔インプラント学会学術大会　2012.9.21-23　大阪国際会議場　大阪
18. 下岸将博、古市祥子、黒田真司、宗像源博、春日井昇平.インプラント表面へのフッ素化合物応用が歯病病原性細菌と骨髄細胞に及ぼす影響.第42回日本口腔インプラント学会学術大会　2012.9.21-23　大阪国際会議場　大阪

11）受賞

1. Marwa Madi　FDI Poster Presentation Award 8月29日
2. 渕上慧　第42回日本口腔インプラント学会学術大会最優秀講演賞　2012年9月23日
3. 鶴見和久　第42回日本口腔インプラント学会学術大会最優秀ポスター発表賞　2012年9月23日
4. 藤井政樹　第42回日本口腔インプラント学会学術大会最優秀発表賞　2012年9月23日
5. 宗像源博　クインテッセンス出版株式会社最優秀論文賞　2012年12月

12）外部資金の獲得状況

挑戦的萌芽研究

研究題目：上顎洞挙上のためのX線透過性吸収性材料の開発
代表者：春日井昇平
期間：平成22-24
研究費総額：270万円

挑戦的萌芽研究

研究題目：立体培養脂肪細胞による骨再生へのチャレンジ
代表者：黒田真司
期間：平成23-25
研究費総額：280万円

挑戦的萌芽研究

研究題目：脂肪細胞由来スフェロイドを用いた組織再生の試み
代表者：中田秀美
期間：平成24-26
研究費総額：250万円

若手研究B

研究題目：BP系薬剤のインプラントへの影響ーウサギ骨粗鬆症モデルの組織
代表者：作山葵
期間：平成24-27
研究費総額：320万円

寄付金　株式会社モリタ

研究題目：（奨学交付金）
代表者：春日井昇平
期間：平成24
研究費総額：54万円

寄付金　株式会社ジーシー

研究題目：（奨学交付金）
代表者：春日井昇平
期間：平成24
研究費総額：27万円

寄付金　日中医学協会

研究題目：（奨学交付金）
代表者：春日井昇平
期間：平成24年
研究費総額：30万円

寄付金　Bio-Horizon Co. Ltd.

研究題目：（奨学交付金）
代表者：春日井昇平
期間：平成24-25
研究費総額：160万円

受託研究　文部科学省

研究題目：チーム「ニッポン」マルチサポート　研究開発プロジェクト

代表者：宮川俊平（筑波大学）
期間：平成22-26
研究費総額：30億円

13）特別講演、招待講演、シンポジウム

1. Kasugai S. Novel strategy for bone augmentation：Respecting“mother nature”. The 11th Stomatology Confernce of West China 2012.4.20-23 Chengdu Convention Center, Chengdu（成都）China.
2. 春日井昇平.Successful implant treatment　大学病院のインプラント科に聞こう.東京医科歯科大学歯学同窓会CDEコース　2012.5.20　東京医科歯科大学歯学部特別講堂　東京
3. 春日井昇平.歯を失った場合の治療法　歯科インプラント治療の光と影.神戸薬科大学第38回卒後研修講座「感覚器疾患（眼科・耳鼻科・皮膚科）と口腔歯科の治療最前線」2012.6.2　神戸薬科大学ききょう記念ホール　神戸
4. Kasugai S. New approach to bone augmentation：Respecting endogenous key players and providing space for regeneration. The 15th ICOI Asia Pacific Section Congress 2012.6.23 Intercontinental Hotel, Ho Chi Minh City, Vietnuam
5. 春日井昇平.インプラント治療の長期予後を基礎医学から考える.KYOCERA COLLOQUIM in 2012 2012.7.1 東京ビッグサイト　東京
6. 春日井昇平.インプラント治療における再生医療.中部インプラントアカデミー（CIA）講演会 2012.7.22 ウイング愛知　名古屋
7. 春日井昇平.インプラント治療における再生医療.嵌植義歯研究所講演会　2012.8.26　嵌植義歯研究所、仙台
8. 春日井昇平.骨造成・骨再生のための新しい戦略.プラトンセミナー2012　2012.7.29 日本歯科大学生命歯学部　富士見ホール 東京
9. 春日井昇平.骨造成の新しい戦略：組織の再生能力の尊重と再生のためのスペースの確保.日本歯科先端技術研究所　講演会　2012.9.8　日本歯科先端技術研究所　東京
10. 春日井昇平.骨造成の原則：組織の再生能力の尊重と再生のためのスペースの確保.岩手医科大学 Advanced Educational Course in Implant Dentistry 2012.9.9　岩手医科大学　盛岡
11. Kasugai S. New approach to bone augmentation：Respecting endogenous key players and providing space for regeneration. International Congress of Oral Implantologists（ICOI）, World Congress 2012.9.20-22 World Center Marriot Hotel, Orlando, Florida, USA
12. 春日井昇平.歯科インプラント治療と再生医療.再建歯学研究会講演会　2012.11.4 新宿NSビル　東京
13. 春日井昇平.インプラント治療の問題を考える.渋谷区歯科医師会学術講演会　2012.11.17　渋谷区歯科医師会館　東京
14. Kasugai S. How to augment bone effectively, safely and less costly. Bangkok Implant Sympoium 2012 2012.11.28-30 Pullman Hotel, Bangkok, Thailand
15. 春日井昇平.国際インプラント手帳.第16回日本顎顔面インプラント学会学術大会　2012.12-1-2 北九州国際会議場　小倉
16. 春日井昇平.薬理学から歯科臨床を考える.Dentistry, Quo Vadis? 2012.12.8-9 青陵会館 東京
17. 春日井昇平.簡便で安全で低コストの骨造成のための戦略.Club 22 講演会　2012.12.15　ブローネマルクオッセオインテグレーションセンター　東京
18. 春日井昇平.骨補填材と成長因子.日本臨床口腔科学研究会講演会　2012.12.16　株式会社白鳳東京研修センター　東京

14）教室、分野や講座の准教授、講師、助教、特別研究員、ポスドク、指導を受けた大学院生の名前

准教授	塩田　真
講師	立川　敬子
助教	黒田　真司
	宗像　源博
特任助教	Osama Zakaria
医員	中田　秀美
	作山　葵
	中村　貴弘
	小林　裕史
	鶴見　和久
	赤塚　麻帆
	渕上　慧
	山本　愛
大学院生	高　尚
	下岸　将博

陳　　康
湯川　　健
○ Madi Marwa
山本　麻衣子
高宅　花織
Zayer Lin
于　　淼
○ Pluenmsakunthai Warunee
山下　　優
三田　　稔
楠本　雄生
宮坂　宗充
前田　大樹、濱田　泰治
Kuppusamy Mahaswari
キム　ユキョン
帳　　馗
佐藤　瑞希
柴崎　真樹
松浦　剛士、呉　　松濤
王　　新
Khaing Nyein Soe
Moe Htet

15）GCOE活動についての感想、コメント、改善を望む点

以前より当分野には国内外から優秀な人材が集まっていたが、GCOEによって彼らに国際的な研究者とのディスカッションの機会を提供できたことは、人材育成の面から極めて有効に作用したと実感している。AISSに採用されると外勤（アルバイト）の制限を受けるため、臨床系である当分野の大部分の日本人大学院生がAISSに応募することを躊躇していた。彼らが応募しなかったことが残念であった。

16）その他　研究教育活動について特記する点

国際学会での講演依頼が増え、海外（スウェーデン）の研究助成金の外部評価の依頼があった。臨床と研究レベルで一定の成果を挙げていることが、国際的に評価された結果であると考えている。

JOURNAL OF TISSUE ENGINEERING AND REGENERATIVE MEDICINE
J Tissue Eng Regen Med 2012;**6**: 666–672.
Published online 17 November 2011 in Wiley Online Library (wileyonlinelibrary.com) **DOI:** 10.1002/term.475

RESEARCH ARTICLE

Exploitation of a novel polysaccharide nanogel cross-linking membrane for guided bone regeneration (GBR)

Takayuki Miyahara[1,4]*, Myat Nyan[1,4], Asako Shimoda[2,4], Yuka Yamamoto[2], Shinji Kuroda[1], Makoto Shiota[1], Kazunari Akiyoshi[2,3,4] and Shohei Kasugai[1,4]

[1]*Oral Implantology and Regenerative Dental Medicine, Tokyo Medical and Dental University, Japan*
[2]*Organic Biomaterials Institute of Biomaterials and Bioengineering, Tokyo Medical and Dental University, Japan*
[3]*Department of Polymer Chemistry, Graduate School of Engineering, Kyoto University, Japan*
[4]*Global Centre of Excellence (GCOE) Programme, International Research Centre for Molecular Science in Tooth and Bone Diseases, Tokyo Medical and Dental University, Japan*

Abstract

Cholesterol-bearing pullulan (CHP) nanogel is a synthetic degradable biomaterial for drug delivery with high biocompatibility. Guided bone regeneration (GBR) is a bone augmentation technique in which a membrane is used to create and keep a secluded regenerative space. The purpose of the present study was to evaluate the effects of the novel CHP nanogel membrane in GBR. Thirty-six adult Wistar rats were used and bilaterally symmetrical full-thickness parietal bone defects of 5 mm diameter were created with a bone trephine burr. Each defect was covered with the collagen membrane or the CHP nanogel membrane or untreated without any membrane. The animals were sacrificed at 2, 4 and 8 weeks and analysed radiologically and histologically. Furthermore, after incubating human serum with CHP nanogel or collagen, the amount of PDGF in the serum was measured using ELISA. New bone formation in terms of bone volume was higher in the nanogel group than in the control or collagen groups at 2 and 4 weeks. At 8 weeks, both membrane groups showed higher bone volumes than the control group. Notably, the newly-formed bone in the bone defect in the nanogel group was uniform and histologically indistinguishable from the original bone, whereas in the collagen group the new bone showed an irregular structure that was completely different from the original bone. After incubating with CHP nanogel, the amount of PDGF in the serum decreased significantly. CHP nanogel GBR membrane favourably stimulated bone regeneration, in which a unique characteristic of CHP nanogel, the storage of endogenous growth factors, was likely implicated. Copyright © 2011 John Wiley & Sons, Ltd.

Received 8 February 2011; Revised 14 June 2011; Accepted 5 July 2011

Keywords **guided bone regeneration; biomaterials; bone regeneration; acryloyl group-modified cholesterol-bearing pullulan (CHPOA); morphometric analysis; radiology; membrane; animal experiments**

1. Introduction

Dental rehabilitation of totally or partially edentulous patients with dental implants has become a routine treatment modality in recent decades, with reliable long-term results (Albrektsson *et al*., 1981, 1986; van Steenberghe, 1989; van Steenberghe *et al*., 1990; Lindquist *et al*., 1996; Buser *et al*., 1997; Arvidson *et al*., 1998; Lekholm *et al*., 1999; Brocard *et al*., 2000; Leonhardt *et al*., 2002). However, local conditions of the alveolar ridge, bone volume and bone quality, affect the long-term prognosis. Guided tissue regeneration (GTR) (Nyman *et al*., 1982, 1990) was originally developed for the treatment of periodontal defects and then the same concept was later applied to bone regeneration, which is called guided bone regeneration (GBR) (Dahlin *et al*., 1989). Vertical and horizontal bone augmentation with GBR has been

* *Correspondence to: T. Miyahara, Oral Implantology and Regenerative Dental Medicine, Tokyo Medical and Dental University, 1-5-45 Yushima, Bunkyo-ku, Tokyo 113–8549, Japan. E-mail: miyahara.irm@tmd.ac.jp*

applied to improve alveolar ridge deformities (Buser *et al*., 1993; Simion *et al*., 1996; Urban *et al*., 2009). In GBR procedures, the barrier membrane keeps the bone regeneration space and it also prevents the invasion of fibrous connective tissue, resulting in new bone formation under the membrane.

Several different membranes, including non-resorbable and resorbable membranes, have been developed and clinically used in GBR. Resorbable membranes have been generally preferred because the second surgery for its removal was unnecessary, rendering the procedure less invasive to patients. Biomaterials such as collagen or copolylactic/glycolic acid (PLGA) have been developed as degradable GBR membranes. Since collagen is an animal-derived material, the risk of unknown infection is undeniable and an unfavourable immune response occurs in some patients (Charriere *et al*., 1989; Keefe *et al*., 1992; Lynn *et al*., 2004).

Although PLGA is a completely synthetic material, it will gradually produce acids, inducing inflammatory responses. These disadvantages are not clearly noticed clinically; however, developing more biocompatible synthetic GBR membrane is beneficial.

Hydrophobized polysaccharide, such as cholesterol-bearing pullulan (CHP), is a unique material for drug delivery systems (DDSs) (Akiyoshi *et al*., 1998, 1999, 2002, Akiyoshi, 2006). Cholesterol-bearing pullulan (CHP) self-aggregates to form a monodisperse and stable hydrogel nanoparticle, in which the domains of the associated cholesterol groups of CHP provide cross-linking points in a non-covalent manner (Figure 1). The size and density of the hydrogel nanoparticle can be controlled by changing the degree of substitution of the cholesterol groups of CHP. During that substitution process, it can incorporate growth factors and act as a molecular chaperone. We have reported that delivering prostaglandin E1 with CHP nanogel stimulates wound healing in rats (Kobayashi *et al*., 2009). In this previous study it was surprising to find that CHP nanogel alone enhanced wound healing. Therefore, the barrier membrane containing CHP nanogel may have great potential as a GBR membrane. The purpose of the present study was to evaluate the effectiveness of the novel bioabsorbable CHP nanogel cross-linking membrane as a GBR membrane.

2. Materials and methods

2.1. Collagen membrane

A bioabsorbable membrane made of collagen (Koken Tissue Guide®, Japan) was used. This material was combined with bovine collagen derived from dermis tissue and bovine insoluble collagen derived from tendon (9:1). It was freeze-dried and cross-linked with the addition of hexamethylenediisocyanate (HMDIC). The collagen membranes were cut into circles with a diameter of approximately 6 mm.

2.2. Nanogel cross-linking membrane

CHP was synthesized as reported previously (Akiyoshi *et al*., 1996). Acryloyl group-modified cholesterol-bearing pullulan (CHPOA) nanogel was synthesized by the reaction of 2-(acryloyloxy)-ethyl isocyanate (AOI) and CHP. CHPOA nanogel solution (40.5 μl, 26.7 mg/ml) in Dulbecco's phosphate-buffered saline (PBS; pH 7.4) and 5.4 μl DMSO were mixed and kept at 4 °C for 24 h. This CHPOA nanogel solution and 8.1 μl solution of PEG-SH in PBS (481.8 mg/ml) were mixed at the ratio of thiol groups to acryloyl groups, which was 1:1. Then 13 μl of the mixture was placed between two glass slides coated with Parafilm® for 4 h at 37 °C under humidified conditions, to form a membrane-shaped hydrogel. The diameter and thickness of the nanogel membrane was 6 and 0.4 mm, respectively. The prepared membrane was applied to bone defects of experimental animals within 24 h.

2.3. Animal experiments

The animal experiments in the present study were approved by the Committee of Animal Experiments, Tokyo Medical and Dental University.

2.4. Surgical procedures

Thirty-six adult male Wistar rats, 16 weeks old, were used and divided into three groups. Prior to the experiment, the overall health of each rat was monitored for 2 weeks. The rats were kept in a standard cage (Tokiwa, Japan) in an experimental animal room at 22 ± 3 °C at 40–60% humidity and 1 atm, on 6:00–20:00 light, fed a standard laboratory diet (CE-2 CLEA Japan Inc.) and given sterilized water. The animals were anaesthetized with a combination of ketamine (40 mg/kg)–xylazine (5 mg/kg). In addition, approximately 0.4 ml local anaesthesia with lidocaine–HCl containing epinephrine 1/80 000 (2% Xylocain, Astra Japan Ltd, Fujisawa Pharmaceutical Co. Ltd, Osaka, Japan) was injected at the surgical site. A cutaneous flap was created by making a mid-sagittal incision through the skin, which was raised from the forehead. The periosteum was incised and elevated to expose the calvarial bone on both sides of the midline. Two symmetrical, full-thickness bone defects with outer diameter of 5 mm were created with a bone trephine burr (Tele Components Co., Germany) under continuous saline irrigation. The defects were covered with CHP nanogel cross-linking membrane or collagen membrane or without any membrane. The animals were sacrificed under chloroform anaesthesia at 2, 4 and 8 weeks after the surgery and analysed radiologically and histologically.

2.6. Radiographic evaluation

The calvariae were dissected out and fixed in neutral 10% formalin and then analysed using micro-CT (μCT; InspeXio, Shimadzu Science East Corp., Tokyo, Japan) to measure the bone volume in the defect area.

J Tissue Eng Regen Med 2012;**6**: 666–672.
DOI: 10.1002/term

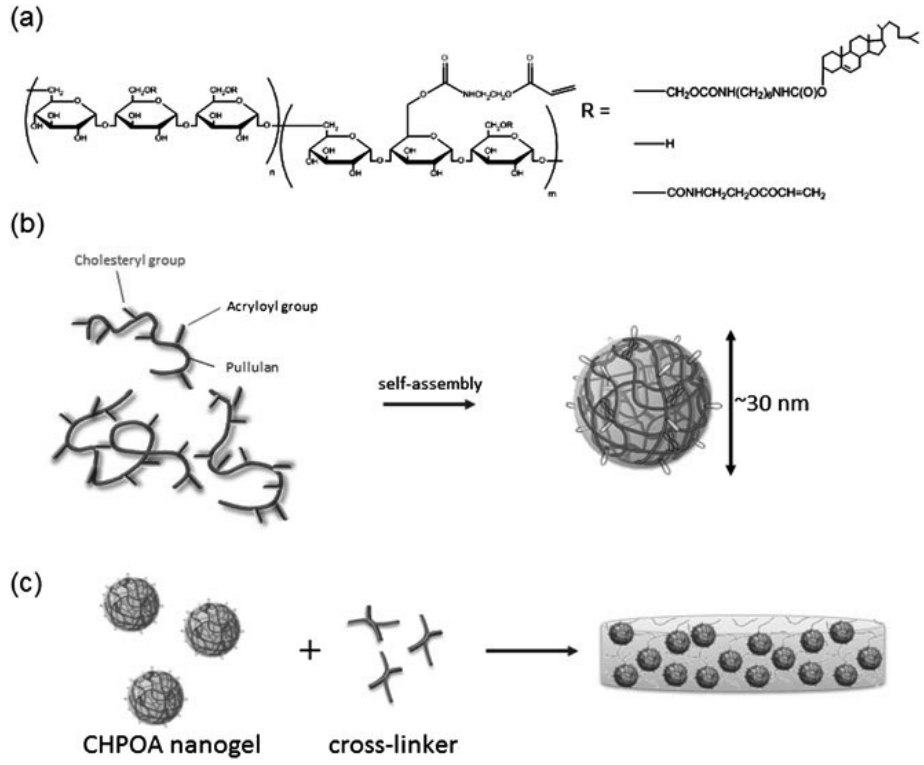

Figure 1. Scheme of acryloyl group-modified cholesterol-bearing pullulan (CHPOA). (A) Chemical structure of CHPOA nanogel. (B) Schematic illustration of CHPOA. (C) Schematic illustration of CHPOA nanogel cross-linking hydrogel (CHPOA–PEGSH)

2.7. Histological analysis

After radiographic analysis the calvariae were decalcified in 5% formic acid for 2 weeks. The specimens were dehydrated in ascending grades of ethanol, embedded in paraffin and sectioned 5 μm thick in the sagittal direction with a microtome. The sections were stained with haematoxylin and eosin (H&E).

2.8. PDGF concentration after incubating serum with materials, ELISA

Whole blood (50 ml) was obtained from the arm vein of a healthy, non-smoker male donor aged 34 years. After being stored overnight in a glass tube at room temperature, serum was prepared. The serum was incubated in three different combinations: serum alone, serum with collagen membrane and serum with nanogel membrane. The diameter of both membranes was 6 mm. These combinations were prepared in Eppendorf-type 1.5 ml vials and incubated for 3 h at room temperature. Then, PDGF-BB concentration in the serum was measured using an ELISA kit (Human PDGF-BB ELISA Kit, Ray Bio®, Ray Biotech Inc., Norcross, GA, USA) according to the manufacturer's instructions.

2.9. Statistical analysis

Data, apart from the ELISA result, were first analysed by one-way ANOVA. When this analysis suggested a significant difference between groups, the data were further analysed by Tukey *post hoc* multiple comparison tests, using SPSS software (v 11.5, SPSS, Chicago, IL, USA). For ELISA assay, statistical evaluation was performed with Student's *t*-tests (SPSS v 11.5). $p < 0.05$ was considered to be statistically significant.

3. Results

3.1. Radiographical images

Post-operative soft tissue healing was similar in all three groups without any membrane exposure in both membrane groups. The radiographical images of all the groups at 2, 4, and 8 weeks are presented in Figure 2. In the control group, newly formed bone could be seen only at the surrounding edge of the defect. In the collagen membrane group, part of the membrane appeared to be calcified, whereas in the CHP nanogel membrane group newly formed bone could be observed in almost the entire defected area. The surface of new bone in the CHP

J Tissue Eng Regen Med 2012;**6**: 666–672.
DOI: 10.1002/term

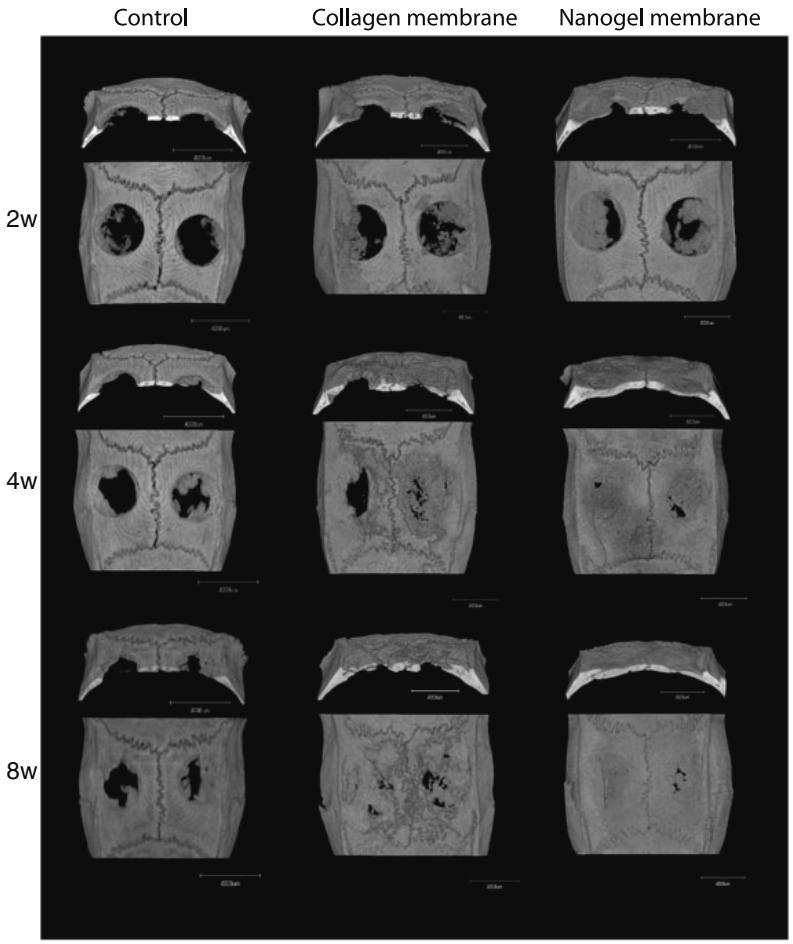

Figure 2. Cross-sectional micro-CT images of the bone defects at 2, 4 and 8 weeks

nanogel group was smooth; however, that in the collagen group was irregular. Volume of the newly formed bone is shown in Figure 3. New bone volume in the defect area in CHP nanogel group was highest at 2 and 4 weeks. At 8 weeks there was no statistical difference of newly-formed bone volume between the collagen and CHP nanogel groups. Newly-formed bone volume in the control group was lowest at the three time points.

3.2. Histological images

Histological images are presented in Figure 4. Corresponding to the radiographical images, new bone formation in CHP nanogel was prominent at 2 and 4 weeks compared with the other two groups. Notably, newly-formed bone in the CHP nanogel group was mature bone containing less connective tissue (Figure 4c, f, i, l),

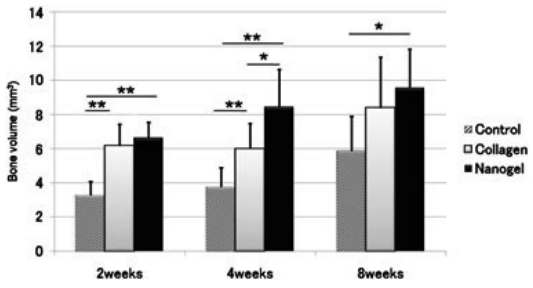

Figure 3. Bone volume in the defects at 2, 4 and 8 weeks. The data were obtained with micro-CT analysis. *$p < 0.05$, **$p < 0.01$

J Tissue Eng Regen Med 2012;**6**: 666–672.
DOI: 10.1002/term

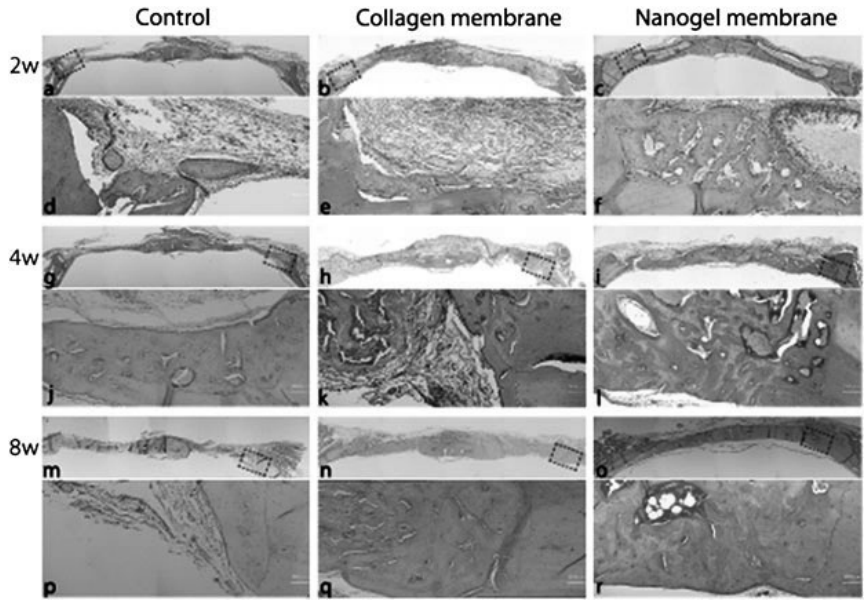

Figure 4. Histological images at 2, 4 and 8 weeks. High-magnification images of the parts of low-magnified images are presented; H&E staining

whereas in the collagen group less mature irregular bone was observed (Figure 4b, e, h, k). In addition, in the CHP nanogel group new bone formation occurred under the membrane, while it was observed both inside and under the membrane in the collagen group.

3.3. PDGF concentration after incubating serum with materials, ELISA

After incubating serum with the membranes, PDGF-BB concentration in the serum was measured. PDGF-BB concentration in the serum was the lowest when the serum was incubated with CHP nanogel membrane (Table 1), suggesting that CHP nanogel membrane trapped PDGF-BB in the material.

4. Discussion

The principle of GBR was originally explored for bone augmentation of the alveolar process in conjunction with oral implant therapy (Dahlin *et al.*, 1988; Buser *et al.*, 1993; Simion *et al.*, 1996; Urban *et al.*, 2009). In GTR and GBR, a membrane is used to keep regenerative space, preventing the invasion of the unfavourable surrounding tissue. The concept of tissue engineering is to provide the three key players to the regenerative site: cells, signal molecules and scaffolds; it is obvious that in both GTR and GBR, cells, signal molecules and scaffolds are endogenous. The progenitor cells are derived from the tissue facing the regenerative site, not from the tissue separated by a membrane. Signal molecules from activated platelets, such as PDGF and TGF-β, initially work for proliferation and differentiation of osteogenic cells. As scaffolds, fibrin initially plays important roles in regeneration. Collagen and other extracellular matrices are produced by the cells in the regenerative space and they work as scaffolds. Thus, GTR and GBR are characterized as encouraging endogenous regenerative ability by providing a space for regeneration.

Table 1. PDGF concentration in the serum after incubating with collagen membrane or CHP nanogel membrane

	Mean ± SD (pg/ml)	
Serum	164.0 ± 5.0	*
Serum + collagen	163.3 ± 4.7	
Serum + nanogel	151.9 ± 6.7	*

*$p < 0.05$, significantly different from one another.

In the present study, a bone defect model of rat calvaria was used to evaluate two types of GBR membrane. Although bone regeneration in the internal bone defect is different from external bone augmentation in GBR, the potential of the material for GBR membrane could be evaluated in the internal bone defect model of the present study. The present bone defect of 5 mm diameter did not heal spontaneously at 8 weeks when the defect was left without a membrane. The proliferation of undesired soft tissues in the bone defect interrupts the proliferation of bone forming cells from the periphery of the defect (Dahlin *et al.*, 1988; Kostopoulos *et al.*, 1994; Hämmerle *et al.*, 1995). Any material with some degree of biocompatibility can work as GTR or GBR membrane. Methyl

J Tissue Eng Regen Med 2012;**6**: 666–672.
DOI: 10.1002/term

cellulose was initially used as a GTR membrane. Polytetrafluoroethylene (PTFE), polyglycolic and polylactic acids (PLGA) and collagen have been clinically applied as GBR membranes (Bunyaratavej and Wang, 2001). Furthermore, other materials, such as chitin/chitosan and alginate, have also been investigated as GBR membranes (Eun-Jung Lee *et al*., 2009). Our previous studies demonstrated the high biocompatibility of CHP nanogel (Kobayashi *et al*., 2009), which is one of the required properties for wound dressing and also for GBR membranes. Compared with the other materials, the uniqueness of CHP nanogel is to trap hydrophobic and hydrophilic molecules inside. Since CHP nanogel contains > 90% of water, the water in the gels would be exchanged for tissue exudates. After incubating in serum for the ELISA assay, the colour of the nanogel changed into yellow, similar to the colour of the serum. PDGF is synthesized mainly by megakaryocytes and is stored in the α-granules of platelets. When platelets are activated, PDGF is released. *In vitro*, PDGF-AA and PDGF-BB enhance the proliferation of multiple types of bone cells, including both osteoblast and osteoclast lineages (Hadjidakis and Androulakis, 2006; Zhang *et al*., 1998). Although long-term exposure to PDGF reduces alkaline phosphatase activity and mineralization (Hsieh and Graves, 1998), application of PDGF stimulates regeneration of periodontal tissue and bone (Nevins *et al*., 2009).

In our previous study, CHP nanogel alone stimulated wound healing in rats (Kobayashi *et al*., 2009) and we speculated that CHP nanogel stored endogenous growth factors in wound exudates. In the present study, the decrease in the amount of PDGF-BB in the serum was small but significant after incubating the serum with CHP nanogel membrane. The result of the ELISA assay indicated that CHP nanogel membrane has an ability to store PDGF-BB. It is also possible that CHP nanogel membrane would store not only PDGF-BB but also other growth factors produced at the regenerative site. In addition to PDGF-BB, TGF-β, VEGF and FGF are also produced in and around the bone defects. It is likely that after storing growth factors at the regenerative site, CHP nanogel membrane would gradually release these growth factors during membrane degradation; in other words, it is reasonable to conclude that CHP nanogel membrane works as signal molecule attractant and reservoir at the regenerative site.

In the present study, both collagen and CHP nanogel membrane stimulated bone regeneration compared to the control, in which no membrane was applied. The amount of newly-formed bone at the early time point and the quality of the bone in the CHP nanogel group were superior to that of the collagen group. The character of the CHP nanogel membrane, storing and releasing endogenous growth factors, could partly explain this difference. In the histological images, bone was formed under the membrane in the CHP nanogel group, whereas it was formed both inside and under the membrane in the collagen group. In the μCT images we also observed the irregular surface of the regenerated bone facing the membrane in the collagen group. It is plausible that the collagen membrane used in the present study worked not only as a barrier membrane of GBR but also as a scaffold for bone regeneration.

CHP nanogel consists of pullulan and cholestesterol. Pullulan is a polysaccharide industrially prepared from starch and its medical application has been approved. CHP nanogel has already been used clinically for delivering insulin (Akiyoshi *et al*., 1998), interleukin 12 (Shimizu *et al*., 2008) and cancer antigen (Kageyama *et al*., 2008); in these studies, CHP nanogel did not exert any adverse effect. Therefore, CHP nanogel is an extremely safe material. The uniqueness of CHP nanogel is that it can incorporate growth factors and acts as a molecular chaperone. Thus, CHP nanogel is an ideal material for delivering growth factors. We have delivered BMP2 with CHP nanogel to the parietal bone of mice and observed new bone formation (Hayashi *et al*., 2009). In addition to growth factors, CHP nanogel can incorporate small biologically active molecules. Using CHP nanogel we have also delivered prostaglandin E agonist and prostaglandin E1 to bone and skin wounds, respectively, and reported the stimulation of bone and skin regeneration (Kobayashi *et al*., 2009; Kamolratanakul *et al*., 2011). The present study demonstrated that CHP nanogel membrane alone stimulated bone regeneration; however, delivering biologically active molecules, such as BMP and prostaglandin E1, with CHP nanogel would be effective and promising in bone regeneration (Hayashi *et al*., 2009). Although CHP nanogel membrane is promising as a GBR membrane, we have to solve the following two points before applying this membrane in GBR clinically. First, the membrane should be stable for a long time at room temperature. In the present study, CHP nanogel membrane was prepared within 24 h before the surgical application. It would be possible to make CHP nanogel membrane durable for a long storage period, because we observed that dried CHP nanogel membrane was also effective in the same bone defect model (authors' unpublished data). Second, enhancement of mechanical strength of the membrane is absolutely required. The present CHP nanongel membrane is strong enough to cover over a relatively small bone defect; however, it is obviously too weak to be applied for vertical or horizontal bone augmentation. Combining CHP nanogel membrane with biodegradable polymer would solve this problem.

5. Conclusion

The present results indicate that novel CHP nanogel cross-linking membrane would be potentially effective as a GBR membrane.

Acknowledgements

We greatly appreciate the help of Dr Tomoko Nagayama, Dr Jia Hao, Dr Reena Rodriguez, Dr Warunee Pluemsakunthai and Dr

J Tissue Eng Regen Med 2012;**6**: 666–672.
DOI: 10.1002/term

Hisham Rojbani with animal experiments and Dr Toshimitsu Yamamoto with histomorphometric analysis. This work was supported by Grants-in-Aid for GCOE Research and for Exploratory Research from the Ministry of Education, Culture, Sports, Science and Technology, Japan (Grant Nos 22791925, 22659355).

References

Albrektsson T, Branemark PI, Hansson HA, *et al*. 1981; Osseointegrated titanium implants. Requirements for ensuring a long-lasting, direct bone-to-implant anchorage in man. *Acta Orthop Scand* **52**: 155–170.

Albrektsson T, Zarb G, Worthington P, *et al*. 1986; The long-term efficacy of currently used dental implants: a review and proposed criteria of success. *Int J Oral Maxillofac Implants* **1**: 11–25.

Arvidson K, Bystedt H, Frykholm A, *et al*. 1998; Five-year prospective follow-up report of the Astra Tech Dental Implant System in the treatment of edentulous mandibles. *Clin Oral Implants Res* **9**: 225–234.

Akiyoshi K, Taniguchi I, Fukui H, *et al*. 1996; Hybrid nanoparticle formed by self-assembly of hydrophobized polysaccharide: stabilization of adriamycin by complexation. *Eur J Pharm Biopharm* **42**: 286–290.

Akiyoshi K, Kobayashi S, Shichibe S, *et al*. 1998; Self-assembled hydrogel nanoparticle of cholesterol-bearing pullulan as a carrier of protein drugs: complexation and stabilization of insulin. *J Control Release* **54**: 313–320.

Akiyoshi K, Sasaki Y, Sunamoto J. 1999; Molecular chaperone-like activity of hydrogel nanoparticles of hydrophobized pullulan: thermal stabilization with refolding of carbonic anhydrase B. *Bioconjug Chem* **10**: 321–324.

Akiyoshi K, Maruichi N, Kohara M, *et al*. 2002; Amphiphilic block copolymer with a molecular recognition site: induction of a novel binding characteristic of amylose by self-assembly of poly(ethylene oxide)-block-amylose in chloroform. *Biomacromolecules* **3**: 280–283.

Akiyoshi K. 2006; Nanogel engineering and chaperone engineering. *Nippon Rinsho* **64**: 215–220.

Buser D, Dula K, Belser U, *et al*. 1993; Localized ridge augmentation using guided bone regeneration. 1. Surgical procedure in the maxilla. *Int J Periodont Restor Dent* **13**: 29–45.

Buser D, Mericske-Stern R, Bernard JP, *et al*. 1997; Long-term evaluation of non-submerged ITI implants. Part 1: 8-year life table analysis of a prospective multi-center study with 2359 implants. *Clin Oral Implant Res* **8**: 161–172.

Brocard D, Barthet P, Baysse E, *et al*. 2000; A multicenter report on 1022 consecutively placed ITI implants: a 7-year longitudinal study. *Int J Oral Maxillofac Implants* **15**: 691–700.

Bunyaratavej P, Wang HL. 2001; Collagen membranes: a review. *J Periodontol* **72**: 215–229.

Charriere G, Bejot M, Schnitzler L, *et al*. 1989; Reactions to a bovine collagen implant. Clinical and immunological study in 705 patients. *J Am Acad Dermatol* **21**: 1203–1208.

Dahlin C, Linde A, Gottlow J, *et al*. 1988; Healing of bone defects by guided tissue regeneration. *Plast Reconstr Surg* **81**: 672–676.

Dahlin C, Sennerby L, Lekholm U, *et al*. 1989; Generation of new bone around titanium implants using a membrane technique: an experimental study in rabbits, *Int J Oral Maxillofac Implants* **4**: 19–25.

Hadjidakis DJ, Androulakis II. 2006; Bone remodeling. *Ann NY Acad Sci* **1092**: 385–396.

Hayashi C, Hasegawa U, Saita Y, *et al*. 2009; Osteoblastic bone formation is induced by using nanogel-crosslinking hydrogel as novel scaffold for bone growth factor. *J Cell Physiol* **220**: 1–7.

Hämmerle CH, Fourmousis I, Winkler JR, *et al*. 1995; Successful bone fill-in late peri-implant defects using guided tissue regeneration: a short communication. *J Periodontol* **66**: 303–308.

Hsieh SC, Graves DT. 1998; Pulse application of platelet-derived growth factor enhances formation of a mineralizing matrix while continuous application is inhibitory. *J Cell Biochem* **69**: 169–180.

Keefe J, Wauk L, Chu S, *et al*. 1992; Clinical use of injectable bovine collagen: a decade of experience. *Clin Mater* **9**: 155–162.

Kostopoulos L, Karring T, Uraguchi R. 1994; Formation of jawbone tuberosities by guided tissue regeneration: an experimental study in the rat. *Clin Oral Implants Res* **5**: 245–253.

Kobayashi H, Katakura O, Morimoto N, *et al*. 2009; Effects of cholesterol-bearing pullulan (CHP)-nanogels in combination with prostaglandin E1 on wound healing. *J Biomed Mater Res B Appl Biomater* **91**: 55–60.

Kageyama S, Kitano S, Hirayama M, *et al*. 2008; Humoral immune responses in patients vaccinated with 1–146 HER2 protein complexed with cholesteryl pullulan nanogel. *Cancer Sci* **99**(3): 601–607.

Kamolratanakul P, Hayata T, Ezura Y, *et al*. 2011; Nanogel-based scaffold delivery of prostaglandin E_2 receptor (EP4) specific agonist in combination with low dosage of growth factor heals critical size bone defect. *Arthritis Rheum* **63**: 1021–1033.

Lindquist LW, Carlsson GE, Jemt T. 1996; A prospective 15-year follow-up study of mandibular fixed prostheses supported by osseointegrated implants. Clinical results and marginal bone loss. *Clin Oral Implants Res* **7**: 329–336.

Lekholm U, Gunne J, Henry P, *et al*. 1999; Survival of the Branemark implant in partially edentulous jaws: a 10-year prospective multicenter study. *Int J Oral Maxillofac Implants* **14**: 639–645.

Leonhardt A, Grondahl K, Bergstrom C, *et al*. 2002; Long-term follow-up of osseointegrated titanium implants using clinical, radiographic and microbiological parameters. *Clin Oral Implants Res* **13**: 127–132.

Lee EJ, Shin DS, Kim HE, *et al*. 2009; Membrane of hybrid chitosan–silica xerogel for guided bone regeneration. *Biomaterials* **30**: 743–750.

Lyn AK, Yannas IV, Bonfield W. 2004; Antigenicity and immunogenicity of collagen. *J Biomed Mater Res B Appl Biomater* **71**: 343–354.

Nyman S, Lindhe J, Karring T, *et al*. 1982; New attachment following surgical treatment of human periodontal disease. *J Clin Periodontol* **9**: 290–296.

Nyman S, Lang NP, Buser D, *et al*. 1990; Bone regeneration adjacent to titanium dental implants using guided tissue regeneration: a report of two cases. *Int J Oral Maxillofac Implants* **5**: 9–14.

Nevins M, Garber D, Hanratty JJ, *et al*. 2009; Human histologic evaluation of anorganic bovine bone mineral combined with recombinant human platelet-derived growth factor BB in maxillary sinus augmentation: case series study. *Int J Periodont Restor Dent* **29**: 583–591.

Simion M, Scarano A, Gionso L, *et al*. 1996; Guided bone regeneration using resorbable and nonresorbable membranes: a comparative histologic study in humans. *Int J Oral Maxillofac Implants* **11**: 735–742.

Shimizu T, Kishida T, Hasegawa U, *et al*. 2008; Nanogel DDS enables sustained release of IL-12 for tumor immunotherapy. *Biochem Biophys Res Commun* **367**: 330–335.

Urban IA, Jovanovic SA, Lozada JL. 2009; Vertical ridge augmentation using guided bone regeneration (GBR) in three clinical scenarios prior to implant placement: a retrospective study of 35 patients 12 to 72 months after loading. *Int J Oral Maxillofac Implants* **24**: 502–510.

van Steenberghe D. 1989; A retrospective multicenter evaluation of the survival rate of osseointegrated fixtures supporting fixed partial prostheses in the treatment of partial edentulism. *J Prosthet Dent* **61**: 217–223.

van Steenberghe D, Lekholm U, Bolender C, *et al*. 1990; Applicability of osseointegrated oral implants in the rehabilitation of partial edentulism: a prospective multicenter study on 558 fixtures. *Int J Oral Maxillofac Implants* **5**: 272–281.

Zhang Z, Chen J, Jin D. 1998; Platelet-derived growth factor (PDGF)-BB stimulates osteoclastic bone resorption directly: the role of receptor beta. *Biochem Biophys Res Commun* **251**: 190–194.

J Tissue Eng Regen Med 2012;**6**: 666–672.
DOI: 10.1002/term

歯髄生物学分野

須田 英明

医歯学総合研究科・口腔機能再構築学系専攻
歯髄生物学・教授

1）研究の課題名

Pulp Biology Field

1. 歯髄・歯肉組織由来の間葉幹細胞による歯髄・歯槽骨再生

【GCOE拠点内における異なる分野のInnovationを確立する研究】

Reconstruction of dental pulp and alveolar bone from mesenchymal stem cells derived from dental pulp and gingiva

ヒトの歯髄および歯肉組織には間葉系幹細胞が存在する。これら間葉系幹細胞を簡便に分離する手法を検討した。間葉系幹細胞を分離する代表的な方法としてコロニー形成法があるが、この手法を用いてヒト歯髄・歯肉組織より幹細胞画分を分離した。さらにその表面マーカー発現を検討した結果、間葉系幹細胞マーカーを強く発現していた。また、脂肪、軟骨、骨分化能を示した。これらの幹細胞を用いての歯髄および歯槽骨再生を検討する目的で、三次元スフェロイド培養を行った。三次元スフェロイド培養と二次元培養を行った歯髄幹細胞における骨芽細胞・象牙芽細胞マーカー発現を検討したところ、三次元スフェロイド培養を行うことによりこれらのマーカー発現が増加することが明らかになった。さらに、硬組織誘導培地中で培養したところ、二次元培養と比較して三次元スフェロイド培養においては、より早く石灰化結節が形成されることが明らかになった。以上より、三次元スフェロイド培養により、硬組織形成性細胞および組織への分化を効率的に行うことが可能なことが明らかになった。

2. MEPEのC末断片は象牙芽細胞の分化を抑制する

Differentiation of odontoblasts is negatively regulated by MEPE via its C-terminal fragment

Matrix extracellular phosphoglycoprotein（ MEPE ）は細胞外マトリックスタンパクの一つで、主に石灰化組織に発現している。本研究の目的はMEPEの歯髄における局在を調べ、さらにその機能について検討することである。生後3日のWistarラット歯髄において、石灰化途上にある象牙芽細胞にMEPEは強く発現していた。象牙芽細胞株OLCにMEPEを強制発現あるいは発現抑制したところ、分化がそれぞれ抑制および促進された。MEPEは細胞内において合成された後、N末とC末に切断されるが、N末はOLCの分化に影響が無かったのに対し、RGD配列を有するC末はOLCの分化を抑制した。MEPEは象牙芽細胞の分化において、象牙質形成あるいはホメオスタシスを保つ上で重要な働きをしていると推察された。

3. MEPEはFurinにより活性化され、歯髄細胞の接着を促進する

MEPE activated by Furin promotes pulpal cell adhesion

Matrix extracellular phosphoglycoprotein（ MEPE ）は骨芽細胞、骨細胞、象牙芽細胞に発現が認められ、骨および象牙質代謝に重要な役割を担っている。このMEPEが活性化されるためには、翻訳後修飾が重要である。本研究は、furinによりMEPEの146R↓147部が切断され、RGD配列を含む切断されたC末が象牙芽細胞の接着に重要なことを本研究は明らかにした。

4. 未分化間葉系のKusaA1細胞の骨芽細胞分化は転写調節制御因子であるRbpjにより促進する

Osteogenic differentiation of mouse mesenchymal progenitor cell, Kusa-A1 is promoted by mammalian transcriptional repressor Rbpj

未分化間葉系の幹細胞は多様な細胞への分化が可能であるが、そのメカニズムはいまだ不明である。我々はNotchの主用な核内メディエーターであるRbpj（ recombination signal-binding protein for immunoglobulin kappa j region）が骨芽細胞分化に関

与していうる事を報告する。Rbpjを強制発現させたKusa-A1細胞は、in vitro、in vivoともに骨芽細胞分化が促進していた。また、RbpjはRunx2およびOse2のプロモーター活性を増加させた。以上の結果より、Rbpjは骨芽細胞分化において重要な働きをしていることが示唆された。

5. 歯髄細胞におけるNotchシグナル関連因子の発現と歯髄細胞分化にともなう発現変動

Expression of Notch signalling-related genes in normal and differentiating rat dental pulp cells

Notchは胎生期のみならず成体においても様々な組織の分化、機能に重要な働きを担っている。Hey1はNotchの重要な転写調節因子であるが、今回、歯髄細胞におけるHey1の発現動態について検討した。Wistarラット歯髄より得られた歯髄細胞を石灰化誘導条件で培養すると、象牙芽細胞特異的なマーカーであるDentin sialophosphoprotein発現が増加する一方、Hey1の発現は抑制された。このことから、Hey1を介するNotchシグナルは歯髄細胞の象牙芽細胞への分化を負の方向へ制御している可能性が示唆された。

6. ラット実験的根尖性歯周炎の進展におけるカテプシンK阻害剤の抑制効果

カテプシンKは破骨細胞に発現し、骨吸収において重要な役割を果たしている。カテプシンK阻害剤であるNC-2300（日本ケミファ）は、新たに開発された関節リウマチの治療薬であり、関節リウマチモデルにおいて、関節の骨破壊ばかりでなく炎症反応も抑制することが報告されている。本研究の目的は、ラットに実験的に誘発した根尖性歯周炎のモデルを用い、根尖性歯周炎の進展におけるNC-2300の抑制効果を検討することである。ラット下顎第一臼歯を露髄後、抜髄し、口腔内に開放することにより根尖性歯周炎を誘発した。露髄開放時よりNC-2300を1日2回経口投与した。21日後に屠殺して下顎臼歯を周囲の顎骨ごと摘出し、左側はマイクロCT撮影により根尖病変の大きさを測定した後、組織学的に検討した。右側は、根尖周囲の病変部を根尖とともに一塊として摘出し、RNA抽出後、リアルタイムPCRにて起炎症性サイトカインの発現量を測定した。マイクロCTによる評価の結果、NC-2300投与群における根尖病変の大きさは、コントロール（非投与）群と比較して有意に小さかった。また、組織学的検討により、コントロール群においては多数の破骨細胞が根尖周囲の歯槽骨上に観察され、活発な骨吸収が行われている像が認められたのに対し、NC-2300群では破骨細胞は認められるものの、その数および密度は有意に少なかった。MHC class II分子発現マクロファージの密度も、NC-2300群ではコントロール群に比べ有意に少なかった。病変中の炎症性サイトカイン発現を比較したところ、NC-2300投与群においてはIL-1 αおよびIL-6の発現が有意に抑制されていた。以上の結果より、NC-2300の投与によって、破骨細胞におけるカテプシンK阻害作用による骨吸収抑制に加えて、炎症性サイトカインの発現が減少することにより破骨細胞形成が抑制され、その結果として根尖周囲の骨吸収が抑制された可能性が示唆された。

7. 歯根膜機械受容神経線維の応答性に対する歯髄の炎症性変化の影響

歯根膜に分布する求心神経は三叉神経の末梢枝であり,解剖学的な神経終末形態は自由神経終末とルフィニ神経終末様神経終末である。特に後者は機械的刺激に対して応答する歯根膜機械受容器としての機能的意義を有している。これまでの研究により,歯髄と歯根膜の両者をその分岐した枝が同時に支配している神経線維が存在することも示されている。他方,象牙質の口腔内への露出による外来刺激や,初期う蝕による細菌学的刺激に対して歯髄が反応し,可逆性歯髄炎の状態に陥る。この状態が適切な処置が施されないままに放置されると,歯髄内には軸策反射によって神経原性炎症が惹起され,ついには根尖孔を介して歯根膜内にも波及することになる。細菌感染などの刺激が歯髄に加わった場合に生ずる不可逆性歯髄炎の場合には,この過程がより顕著に現れるものと考えられる。

ところで,広義の歯髄疾患を対象とした根管治療の過程で,強い自発痛あるいは咬合痛のような臨床症状が消退した後にも,打診に対して軽度の痛みや違和感が残存して,この症状が軽快するのに長期間を要する症例に遭遇することがある。この病態の背景には,歯髄除去療法による根尖孔付近での歯髄神経求心線維の切断,感染根管を有する歯の根尖部での炎症性化学物質による歯根膜求心神経線維への刺激,あるいは根管処置時における根尖孔外への器具突出に伴う刺激に起因する根尖部歯周組織の炎症性変化や神経線維の機械的傷害など,種々の要因が考えられる。しかし,歯髄の初期の病的変化に伴う,歯根膜に分布する神経線維の活動性の変化を神経生理学的に明らかにした研究は,これまでに報告されていない。本研究においては,動物を用いた実験系を構築し,歯髄の

炎症性変化に伴う歯根膜機械受容神経線維の応答性の変化を,単一神経線維の応答性を指標に観察して神経生理学的に検索することを目的とした。

8. マスタードオイル歯髄適用により誘発された感作視床内の神経-免疫系の相互作用

Neuron-immune interactions in the sensitized thalamus induced by mustard oil application to rat molar pulp.

ラット歯髄へのマスタードオイル適用は視床ニューロンの活動性を増強させる,すなわち感作が生じる。ニューロンの活動性の記録,免疫組織化学的分析,並びに分子生物学的分析を,この視床の変化に関係する機構を解明するために実施した。マスタードオイル適用後,視床MD核のニューロンの応答性が増強した。MD核にMK-801を投与すると,一度増強したヌーロン活性は減少した。NMDA型受容器のサブユニット2D、GFAP,並びに抗原提示細胞関連遺伝子のmRNAはマスタードオイルを歯髄適用後10分時において対側視床で亢進した。しかし,拮抗薬の投与後10分時にはこれらは減少した。OX6を発現しているマイクログリア及びGFAPを発現しているアストロサイト数は,マスタードオイル歯髄適用後60分までその数が増加することは無かった。

9. 実験的歯髄病変由来の根分岐部病変の成立に関与するToll-like receptorと抗原提示細胞関連分子の遺伝子発現の増加

Increased gene expression of Toll-like receptors and antigen presenting cell-related molecules in the onset of experimentally induced furcation lesions of endodontic origin in rat molars

歯髄の炎症により惹起された根分岐部の炎症の初期の免疫病理学的機構は未だ十分に解明されていない。抜髄後開放したラット臼歯の分岐部歯根膜内のToll-like recepotors（TLRs）に対する免疫組織化学的および量的遺伝子発現分析を実施した。根分岐部歯根膜内のTLRならびに抗原提示細胞関係分子のmRNA発現レベルは抜髄後開放した臼歯周囲において有意に亢進した。同部位の免疫組織化学ではTLR発現細胞が分岐部直下の歯根膜内に分布していることを明らかにした。

Endodontic Field

10. 歯科用コーンビームCTにおけるモーションアーチファクトの影響

Effect of motion artifact on cone-beam CT images

歯科用コーンビームCT（CBCT）撮影中の患者の体動が画像に与える影響を検討するための研究を行った.実験には1軸移動ステージを用い,撮影中に1度だけ試料を水平方向に移動させ,照射時間37秒でCBCT（ファインキューブ,吉田製作所）撮影した.ブタ下顎骨を試料とした実験では,撮影したCBCT画像を5名の歯科医師が評価した.結果は,試料の移動距離が0.126 mm以下の条件では,対照と有意差が認められなかったが,0.25mm以上の条件では有意に画質が低下した.また,エックス線照射開始6,12,18秒後に移動した群では,対照と比較して有意に画質が低下したが,24,30秒後に移動した群では,対照と統計学的に有意差は認められなかった.このことから今回の実験条件では,被写体の0.25 mm以上の移動によりCBCT画像が劣化した.また,同じ0.25 mm移動を行った場合においても,移動する時期により画質への影響が異なることが示された.次に,形が規格化されたアルミニウム円柱ファントムを用い同様の実験を行った.直径2,3,5 mmのアルミニウム製円柱を試料とし,鉛直に立てた状態でCBCT撮影を行い,軸位断像を観察した.エックス線照射開始18秒後に移動した場合には,移動した試料の大きさ,形態は保持され,移動前と移動後の2つの円が,移動距離分だけ離れた位置に重ね合わせた画像として観察された.エックス線照射開始12,18秒後に移動した場合,断面が2つの円の重なりに近い形態として観察されたが,6,24,30秒後では,外形が1つの円に近い形態であった.対照およびエックス線照射開始18秒後以外の条件では,円の濃度は一様ではなく,部分的に濃淡が認められた.以上の結果からCBCT撮影中の被写体の移動距離および時期がCBCT画像に影響することが結論された.

11. 新規ねじりファイルの相変態挙動と曲げ特性

Phase transformation behavior and bending property of newly twisted nickel–titanium endodontic instruments

近年,NiTiファイルの新しい加工法である,ねじり加工を用いたTwisted File（TF）が開発された.本研究の目的は,TFの相変態挙動と曲げ特性の関連性を調べることである.材料として,先端径0.30 mm,0.06 テーパーのTFと,対照としてK3を用いた.相変態挙動については示差走査熱量測定（DSC）を行い,相変態温度をDSC曲線より算出した.曲げ特性について片持ち梁式曲げ試験法を用い,37 ℃温度条件下で,負荷過程における曲げ荷重を評価した.相変態温度の比較にはStudent’s t-testを,曲げ荷重についてはMann–Whitney U-testを用い,有意水準5 %で統計学的に解析した.その結果,TFの相変態温度はK3より有意に高く,曲げ荷重は弾性領域と超弾性領

域ともにK3より有意に低かった.熱処理をともなったねじり加工は,相変態温度の上昇と,より優れた柔軟性に寄与しているかもしれない.

12. レジン系根管充填用材料の根管封鎖性について
Root canal sealing ability of resin-based root canal sealer

近年様々な種類のレジン系根管充填用シーラーが開発および販売されている.しかしながら,レジン系根管充填用シーラー使用に際して推奨される根管形成方法や根管充填方法についてはいまだ意見が統一されていない.そこで,本研究では各種根管形成および根管充填方法におけるレジン系根管充填用材料の根管封鎖性について比較検討を行った.シングルポイント根管充填およびmatched taperd シングルポイント根管充填を行った被験歯に対して色素浸透試験を行った.その結果,シングルポイント根管充填を行った群では他群と比較して有意に多い色素漏洩を示した.また,水平断面像の観察においては,シングルポイント根管充填を行った群では,全ての断面において最も多いシーラー占有面積を認めた.本研究の結果,レジン系根管充填用シーラーではシーラー占有量の少なくなる充填方法が推奨されることが示唆された.

13. 歯科用レーザー使用時における眼球への安全性
Safety of dental Laser use under microscopes to eyes

本研究の目的はレーザー用防護眼鏡またはフィルターおよび歯科用顕微鏡を介するレーザー光の透過エネルギーを検討することにより、レーザー使用時の眼球への安全性について考察することである。実験にはNd：YAGレーザー、Er：YAGレーザー、半導体レーザーの3種類の歯科用レーザーを用いた。実験1では、各レーザーの導光用ファイバーまたはチップ先端とレーザー用サーモパイル吸収ヘッドとの距離を5cmとし、吸収ヘッドに各種防護眼鏡を固定、パワーメーターで200mJ, 10pps, 10sの条件にて透過エネルギーを測定した（n=3)。防護眼鏡は、Nd：YAGレーザー用、Er：YAGレーザー用、半導体レーザー用、および防塵眼鏡の4種類を使用し、レーザー光の直接照射をコントロールとした。実験2では、実験1で使用した各種防護眼鏡の特性を変えずに平板化し、専用防護フィルターを作成した。レーザー光の透過エネルギーについて、各レーザーにおける眼球に対する最大許容露光量（MPE, IEC60825-1）を基準として比較検討した。その結果、実験1では各レーザーに対する専用防護眼鏡を使用した場合、全てのレーザーにおいて透過エネルギーは0になった。しかし、Nd：YAGレーザー照射時は専用防護眼鏡以外で、また半導体レーザー照射時は専用防護眼鏡およびNd：YAGレーザー用防護眼鏡以外で、透過エネルギーはMPEを超える値となった。実験2では各レーザーに対する専用防護フィルターを使用した場合、全てのレーザーにおいて防護フィルターの位置に関わらず透過エネルギーは0になった。 他の防護眼鏡の使用や裸眼では、MPEを超える透過エネルギーが眼球に到達し、障害が生じる可能性がある。本実験条件下では、顕微鏡下でのレーザー使用の際、専用防護眼鏡の位置が接眼レンズ前でも対物レンズ後でも透過エネルギーが0となり、レーザーは顕微鏡下でも安全に使用できると思われた。したがって、対物レンズに防護フィルターを装着して散乱光を遮断できれば、専用防護眼鏡の代替としうる可能性がある。

14. レーザー照射による象牙質の歪
Dentin strain induced by Laser irradiation

歯科治療において歯根破折が注目されており、象牙質の歪が影響する可能性が考えられている。レーザー照射時における歪に関する報告はほとんどないため、本研究ではEr：YAGレーザーおよびNd：YAGレーザーを注水および非注水に分けて根管内照射を行い、その歪と温度変化について検討した。歪変化はストレインゲージを用いて、また温度変化は熱電対を用いてそれぞれ根尖部に設置して計測した。レーザー照射は1Wの条件で5秒間照射した。今回の結果では注水下Er：YAGレーザー照射群はNd：YAGレーザー群に比較して有意に小さな象牙質の歪および温度変化を示し、両レーザー群ともに注水された群は非注水の群よりも歪変化は小さい結果となった。熱により発生する歪としてはエネルギーを吸収した歯牙組織の熱膨張が考えられる。また注水による冷却は両レーザーに生じる歪を減少させた。

熱の発生は歪変化に対し大きな影響を与えると考えられ、各歯根象牙質の異なる形態や構造や性質や歯根破折に対する耐久性は異なると考えられるものの、より大きな歪は微小歯根破折のより大きな危険性につながると考えられる。レーザーに応じて注水、照射条件等を制御することの必要性が示唆された。

15. 逆根管充填材により誘発される象牙質の歪みと破折に関する研究
Dentin strain and fracture propagation caused by retrofilling materials

歯根端切除術の際には、逆根管充填窩洞を形成し充填

を行う。NTAは現在最も推奨される逆根管充填材であり、その良好な封鎖性は硬化膨張によるものとされている。しかしその反面、膨張により象牙質に歪みが生じ歯根破折が誘発される懸念がある。本研究の目的歯、MTAを用いた逆根管充填により誘発される象牙質のゆがみを測定し、歯根破折の発生を調査することである。30本のヒト抜去前歯に根管形成およびガッタパーチャによる根管充填を行い、根尖部3mmを切除した。注水下あるいは無注水で超音波チップにより逆根管充填窩洞を形成し、Super EBAあるいはMTAにて充填した。根尖1/3に貼付した歪みゲージを用いて、逆根管充填材により生じたひずみを計測した。また、SEMにて破折の有無を観察した。平均最大歪みは、Super EBA と比較し有意にMTAで大きかった。破折は無注水群で散見された。逆根管充填材は、直接的に破折を生じてはいなかったが、逆根管充填窩洞形成により生じた破折線を促進していた。逆根管充填材と象牙壁間の間隙は、MTAで最小だった。本研究結果は、逆根管充填窩洞形成中に適切な冷却がなされないと、逆根管充填剤微小破折の危険性があることを示唆している。

16. 超音波吸引洗浄法の開発

Development of the negative pressure irrigation method

全根管系を機械的に根管形成することは不可能である.臨床的に成功するためには,改良された洗浄法が不可欠である.次亜塩素酸ナトリウム水溶液は,有機質溶解作用および殺菌性が高く最良の根管洗浄剤として良く知られている.次亜塩素酸ナトリウム水溶液を用いての,根尖孔近くの陽圧の洗浄は非常に危険である.最近,次亜塩素酸ナトリウム水溶液の根尖歯周組織への注入による,重篤な障害の症例を多くの学会誌で見ることができる.より良くより安全な洗浄として,陰圧による洗浄が選択されるべきである.我々は新しい陰圧洗浄法として超音波吸引洗浄法（UAT）を開発した.UATでは,吸引針自体が超音波振動し,洗浄効果を上げるとともに吸引針の詰まりを防止することができる.

UATの利点は,

・根尖部根管を洗浄出来る最も安全な方法である.
・デブリ除去効果が様々な洗浄法の中で最も高い.

2）発表の研究内容についての英文要約

1. Reconstruction of alveolar bone from mesenchymal stem cells derived from dental pulp and gingival

Dental pulp tissue, which is mesenchymal in origin, contains dental pulp stem cells（DPSCs）. However, there is no standardized method to isolate DPSCs. Colonies of the dental pulp-derived cells in low seeding condition showed a high expression of mesenchymal stem cell markers, indicating that this method may become one of the standards to isolate DPSCs from dental pulp tissue. Clinical application of DPSCs is one of the hot topics in the endodontic field. To improve their original nature to form hard tissues, we have introduced 3D spheroid culture, which is popularly applied to induce ES cells differentiation. DPSCs cultured in 3D spheroid condition showed a significant up-regulation of odontoblastic/osteoblastic markers expression and alkaline phosphatase activity. Application of 3D spheroid cultured DPSCs to bone defect or pulp cavity is promising in endodontic treatment.

2. Differentiation of odontoblasts is negatively regulated by MEPE via its C-terminal fragment

Matrix extracellular phosphoglycoprotein（MEPE）is an extracellular matrix protein that is mainly expressed in mineralizing tissues, including the dental pulp. The purposes of this study were to clarify the localization of MEPE in the tooth germ and to investigate the roles of MEPE in the differentiation of odontoblasts. The immunohistochemical staining in the tooth germ of the upper first molars of male Wistar rats（postnatal day 3）revealed that MEPE was mainly localized in odontoblasts during dentinogenesis. Stable MEPE-overexpressing and MEPE-knockdown cell lines, which were established in odontoblast-lineage cells（OLCs）, showed lower and higher differentiation capabilities, respectively. Eukaryotic proteins of the N-terminal fragment of MEPE produced in HEK cells had no effect on the differentiation of OLCs, whereas the C-terminal fragment containing an RGD sequence inhibited their differentiation. These results indicated that the C-terminal fragment of MEPE containing an RGD sequence, cleaved in odontoblasts, appeared to be the active form of MEPE, which may play important roles in dentinogenesis and pulpal homeostasis by keeping the odontoblasts in immature condition.

3. MEPE activated by furin promotes pulpal cell adhesion

Matrix extracellular phosphoglycoprotein（MEPE）is predominantly expressed in osteoblasts, osteocytes, and odontoblasts and plays key biological roles in bone and dentin metabolism. Posttranslational modifications are essential for its activation. This study tested the hypothesis that MEPE is activated through proteolytic processing by furin in dental pulp. MEPE was present in three sizes, 1 full-length and 2 cleaved fragments; the cleavage site was 146R ↓ 147. The proprotein convertase family, particularly furin, was a candidate enzyme. Introducing a substitution at

the cleavage
site inhibited hydrolysis, but there was no cleavage of MEPE expressed in furin-deficient LoVo cells. Therefore, furin is a strong candidate for the proteolytic cleavage of MEPE. The C-terminal cleavage product promoted cell adhesion via its RGD
motif. These results indicate that proteolytic processing by furin may activate MEPE during its secretion from odontoblasts and may play important roles in dentinogenesis and pulpal homeostasis.

4. Osteogenic differentiation of mouse mesenchymal progenitor cell, Kusa-A1 is promoted by mammalian transcriptional repressor Rbpj

Pluripotent mesenchymal stem cells possess the ability to differentiate into many cell types, but the precise mechanisms of differentiation are still unclear. Here, we provide evidence that Rbpj (recombination signal-binding protein for immunoglobulin kappa j region) protein, the primary nuclear mediator of Notch, is involved in osteogenesis. Overexpression of Rbpj promoted osteogenic differentiation of mouse Kusa-A1 cells in vitro and in vivo. Transient transfection of an Rbpj expression vector into Kusa-A1 cells
upregulated promoter activities of Runx2 and Ose2. Enhanced osteogenic potentials including high alkaline phosphatase activity, rapid calcium deposition, and increased calcified nodule formation, were observed in established stable Rbpj-overexpressing Kusa-A1 (Kusa-A1/Rbpj) cell line. In vivo mineralization by Kusa-A1/Rbpj was promoted compared to that by Kusa-A1 host cells. Histological findings revealed that expression of Rbpj was primarily observed in osteoblasts. These results suggest that Rbpj may play essential roles in osteoblast differentiation.

5. Expression of Notch signalling-related genes in normal and differentiating rat dental pulp cells

Notch signalling is of fundamental importance to various processes during embryonic development and in adults. The possible role of Hey1, an important Notch signalling component, in odontoblast differentiation was evaluated in this study. Primary cultured dental pulp cells, derived from upper incisors of 5-week-old Wistar rats, were placed in a-modification of Eagle's minimal essential medium supplemented with 10% Fetal Bovine Serum (FBS), and ascorbic acid (AA) and b-glycerophosphate (b-GP), with or without dexamethasone, and cultured on dishes coated with collagen type IA for 7 days.
Conventional and real-time Polymerase Chain Reaction (PCR) was performed to determine the expression of Notch-related genes and dentin sialophosphoprotein as a marker of odontoblast differentiation. Dentin sialophosphoprotein and Hey1 expression was significantly increased and decreased in the presence of AA + b-GP compared with controls, respectively. These findings suggest that Hey1 may be a negative regulator in odontoblast differentiation.

6. Inhibitory effects of the cathepsin K inhibitor on the progress of rat periapical lesions

In this study, we investigated the inhibitory effects of the cathepsin K inhibitor (NC-2300) on the progress of rat periapical lesions. The periapical lesions were induced experimentally in the rat first lower molars, and NC-2300 was administrated orally in the experimental group. In the micro CT and the histological analyses, the size of the periapical lesion and the number and the density of osteoclasts and MHC class II molecules-expressing macrophages in the experimental group were significantly small compared to the control group. The expression of pro-inflammatory cytokines (IL-1 and IL-6) in the experimental group was also significantly suppressed compared to the control group. These results suggest that NC-2300 may inhibit not only the cathepsin K activation in the osteoclasts, but also the osteoclastgenesis which is induced by the inflammatory cytokines, resulting that the bone resorption in the periapical lesion was suppressed.

7. Effects of pulpal inflammation on the activities of periodontal mechanoreceptive afferent fibers

Response properties of periodontal single afferents were investigated in cats with inflammatory irritant-induced pulpitis. A deep dentin cavity was prepared on the right mandibular canine in order to apply an inflammatory agent and small fiber excitant, allyl-isothiocyanate (mustard oil : MO), and single afferents innervating the canine periodontal mechanoreceptor were dissected out from the mandibular nerve bundle by examining impulse responses while applying mechanical stimuli to the tip of the crown. Evoked impulses by mechanical stimuli were increased in number for one hour with MO application to the pulp when compared with those with mineral oil. The mechanoreceptive thresholds of single nerve fibers were decreased after the MO application to the pulp when compared with those with mineral oil. These results suggest that the alteration of responses in the periodontal afferent fiber, or the peripheral sensitization, can be produced by MO-induced pulpal inflammation probably due to the axon reflex mechanism in the furcating branches of nerve fibers innervating both the tooth pulp and periodontal ligament.

8. Neuron-immune interactions in the sensitized thalamus induced by mustard oil application to rat molar pulp.

The application of mustard oil to the rat dental pulp induced neuronal activation or the sensitization in thalamus. The neuronal responsiveness recording, immunohistochemistry,

and molecular biological analysis were performed to address the mechanisms involved in these thalamic changes. After mustard oil application, neuronal responsiveness was increased in the mediodorsal (MD) nucleus. When MK-801 was applied to the MD nucleus, the enhanced responsiveness was decreased. N-methyl D-aspartate receptor subunit 2D, glial fibrillary acidic protein (GFAP), and antigen-presenting cell-related gene mRNAs in the contralateral thalamus were up-regulated at 10 minutes after mustard oil application, but were down-regulated within 10 minutes after the antagonist application. OX6 expressing microglia and GFAP-expressing astrocytes did not increase until 60 minutes after mustard oil application.

9. Increased gene expression of Toll-like receptors and antigen presenting cell-related molecules in the onset of experimentally induced furcation lesions of endodontic origin in rat molars

Early immunopathologic mechanisms behind pulp infection-induced furcal inflammation have not been well understood. The immunohistochemical and quantitative gene expression analysis for toll-like receptors (TLRs) were conducted in the furcal periodontal ligament (PDL) of rat molars subjected to unsealed pulpectomy. Messenger RNA expression levels of TLRs and the antigen presenting cell (APC) -related molecules in the furcal PDL were significantly up-regulated in teeth with unsealed pulpectomy. Immunohistochemistry for unsealed pulpotomized teeth revealed that TLRs-expressing cells were predominantly distributed within the PDL beneath the furcal dentin.

Endodontic Field

10. Effect of motion artifact on cone-beam CT images

We have conducted a study to determine the effect of motion artifact on cone-beam CT images. The specimen was moved horizontally by a motorized x-axis stage. The CBCT images were taken using CBCT (Fine Cube, Yoshida, Japan). The exposure time was 37 seconds. One mandibular jaw of the pig was used in exp. 1. Five dentists individually assessed the CBCT images. Under the conditions of this study, it was revealed that the sample motion of 0.25 mm and over deteriorated visibility of the anatomical structure. Our data indicate that the time of sample moving affects on the image quality. Cylindrical phantom made of aluminum, diameter of 2, 3, 5mm were used and the CBCT axial images were assessed in exp. 2. When the moving timing was 18 seconds after starting X-ray exposure, the shape and size of the samples were well maintained, and two circles in each image showed a moving distance. We conclude that the magnitude and timing of sample movement significantly affects the quality of CBCT images.

11. Phase transformation behavior and bending property of newly twisted nickel–titanium endodontic instruments

Recently, a new manufacturing process was developed to create a nickel–titanium (NiTi) endodontic instrument named the Twisted File (TF). The aim of this study was to investigate the relationship between phase transformation behavior and bending property of NiTi endodontic instruments manufactured by a twisting process. The phase transformation behavior and bending property of Twisted Files (TF; SybronEndo, Orange, CA, USA) and K3 (SybronEndo) with.06 taper and size 30 tip were investigated. K3 was used as control group. Phase transformation behavior was estimated by differential scanning calorimetry (DSC). Transformation temperatures were calculated from the DSC curve. Bending load of the instruments was measured by cantilever-bending test at 37 °C. Student's t-test was used to compare DSC data of the two groups and Mann–Whitney U-test was used to detect the difference of the bending load values between TF and K3 ($P = 0.05$). The phase transformation temperatures of TF were significantly higher ($P < 0.05$) than those of K3. The bending load values were significantly lower for TF than that of K3 ($P < 0.05$), both in the elastic and super-elastic ranges. The new method of manufacturing NiTi instruments by twisting coupled with heat treatment might contribute to the increased phase transformation temperatures and superior flexibility.

12. Root canal sealing ability of resin-based root canal sealer

In recent years obturating sealers has been developed based on dentin adhesion. However, there has no information that which condensation method provides good sealing ability with resin based root canal sealers. The aim of this study was to evaluate factors influencing the sealing ability of resin based root canal sealers. The teeth were prepared and obturated with single condensation method or matched tapered single condensation method using resin based root canal sealers. Then, dye penetration test was done and horizontal sections were made. The images of the horizontal sections were taken by a digital microscope, and sealer occupancy in the root canal was evaluated. The amount of leaked dye in single condensation method group was significantly more than that in the other experimental groups ($p< 0.05$). In the images of horizontal sections, single cone method group showed the highest sealer occupancy at all levels. It was suggested that sealer occupancy may influence the root canal sealing ability of resin based root canal sealers.

13. Safety of dental Laser use under microscopes to eyes

The purpose of this study was to investigate the transmissivity of various types of lasers through the microscope with and without eye protectors. Nd：YAG laser, Er：YAG laser, and diode laser were irradiated to a power meter through laser eye protectors or a microscope. In control experiment, three lasers were irradiated directly or through eye protectors to the power meter positioned at a distance of 5 cm from the fiber tip or the contact tip. In main experiment, the fiber tip was positioned from the objective lens surface of the microscope. The power meter was placed behind the eyepieces. Matched eye protectors for each laser were placed in front of the objective lens or between the eyepieces and the power meter. The results obtained were as follows：No transmitted laser energy was detected when matched eye protectors were used. Mismatched eye protectors were not effective to shut out laser energy, especially for Nd：YAG and diode lasers. Little or no transmitted laser energy was detected through the microscope even when no eye protectors were used. It was concluded that we could use laser devices safely with the dedicated laser eye protectors in clinical situations, although under a microscope.

14. Dentin strain induced by Laser irradiation

The purpose of this study was to investigate the strain and temperature change in dentin induced by laser irradiation of human root canals with or without water cooling. Twenty-eight palatal roots of extracted human maxillary first molars were used. The strain indentin was measured using strain gauges fixed on the apical third of the buccal root surface. The temperature change of the root dentin was monitored using thermocouples embedded into dentin near the apex. The root canal was irradiated with Er：YAG or Nd：YAG laser at an output of 1 W（100 mJ, 10 pps）for 5 s. The tip of the irradiation fiber was located 2.0 mm from the root apex. With water cooling,the mean maximum strain induced by Er：YAG laser was significantly lower than that by Nd：YAG laser（$P< 0.05$）. However, without water cooling, no significant difference between the two lasers（$P> 0.05$）was found. The results suggest that the strain induced by Er：YAG laser irradiation in dentin with water cooling may be minimal, but there still might be a risk of root micro fracture if cooling is not sufficient.

15. Dentin strain and fracture propagation caused by retrofilling materials

The purpose of this study was to investigate the kinetics of dentin strain and fracture propagation caused by retrofilling materials. Thirty roots of extracted human anterior teeth were prepared and laterally condensed with gguttapercha,. Then a 3 mm of the root end was resected. Root-end cavities were prepared using an ultrasonic device（high power setting）with or without water cooling. The cavities were dried and filled with Super EBA or MTA. Strain of dentin caused by the retrofilling materials was measured using strain gauges mounted on the apical third of the root surface., Finally presence or absence of fracture was examined by microscopy and SEM.　The mean maximum strain caused by MTA was significantly larger than that by Super EBA（$p<0.05$）. In Microscopic observation, fractures were found in some samples of the ultrasonic group without water cooling, Although fractures were not caused by retorofilling materials, some fracture lines caused by root-end cavity preparation were propagated by retrofilling materials. In SEM observations, minimal gaps were observed between the retorofilleng material and the dentin wall in MTA group. The results suggest that there might be a risk of micro root fracture propagation by retro -filling materials if cooling is inefficient during root-end preparation.

16. Development of the negative pressure irrigation method

Total root canal systems cannot be mechanically prepared.　For a clinical　success, improved irrigations are inevitable.　Sodium hypochlorite is well known as a best irrigant for its high organic substance dissolving and microorganisms killing actions.　With sodium hypochlorite, positive pressure irrigation near the apical foramen is too dangerous.　Recently, we can find a lot of serious injury cases on journals caused by sodium hypochlorite injection to the surrounding tissue.　For a better and safer irrigation, negative pressure irrigations should be selected.　We could developed a new negative pressure irrigation system, ultrasonic aspiration technique（UAT）. In UAT, aspiration needle itself ultrasonically vibrates. This ultrasonic vibration can enhance irrigation action and prevent needle choke.

The advantages of the UAT are：

- Safest irrigation method that can irrigate apical canals.
- Removal of debris is highest among various irrigation methods.

3）本事業に関連して世界的な研究拠点形成に向けて、以下の点で改善・整備等されたこと

A（研究拠点体制）

グローバルな視点に立って、歯学の中でも歯髄生物学および歯内療法学の発展に寄与できる研究を行うことのできるよう研究の環境整備を進めている。そのため、幅広く研究領域をカバーするとともに、それぞれの領域で先端的な研究を行うことができるよう、専任の指導教官

を配備している。指導教員にはその領域において世界の第一線で活躍できる知識および経験を備えていることが求められる。

B（研究教育環境）

大学院生には、常に臨床と研究の接点を見失うことのないよう、週に最低3コマの診療コマが与えられている。また、専任の指導教官は個別に研究指導を行い、研究遂行上問題が生じた場合にはすぐに対応できる環境が整えられている。

C（人材確保）

大学院を終了した後に教室に残り、研究を続けることができるよう、大学院終了時に医員として大学に残ることが出来るように配慮している。医員は病院職員として臨床業務に携わるが、時間を有効に活用し研究業務に当たることが可能である。

D（人材育成）

研究課題を自ら考えて、それを解明するための実験系を遂行できる人材の育成に力をいれている。そのために、研究の内容について指導者と突っ込んだ話し合いを行い、自らの考えをきちんとまとめることができるよう指導している。

E（国際化）

海外からの留学生も多くいることから、各研究グループのセミナーおよび医局のセミナー用のスライドは原則英語にしている。また、当教室で行う大学院講義はスライド、講義ともに英語で行っている。

4）GCOE事業を推進するに当たって力を入れた点

本事業を推進するにあたり、世界的な研究拠点づくりとのことから海外の研究機関との情報交換および人材交流に力を入れている。アメリカ、カナダ、イギリス、韓国、中国、タイなどの研究機関と現在交流を持っている。

5）英文原著論文

1. Kaneko T, Okiji T, Kaneko R, Suda H, Nor JE,
   Laser- capture microdissection for factor Ⅷ-expressing endothelial cells in cancer tissues,
   Methods Mol Biol 755：395-403, 2011.
2. T. Kaneko, H. Sakaue, T. Okiji, H. Suda,
   Clinical management of dens invaginatus in a maxillary lateral incisor with the aid of cone-beam computed tomography – a case report,
   Dental Traumatology27（6）：478-483, 2011.
3. T. Yoshioka, I. Kikuchi, C. Adorno, H. Suda,
   Periapical bone defects of root filled teeth with persistent lesions evaluated by cone-beamcomputed tomography,
   International Endodontic Journal 44（3）：245-252, 2011.
4. Adorno CG, Yoshioka T, Suda H,
   Crack initiation on the apical root surface caused by three different nickel-titanium rotary files at different working lengths,
   Journal of Endodontics 37（4）：522-5, 2011.
5. Kaneko M, Kaneko T,Kaneko R. Chokechanachaisakul U, Kawamura J, Sunakawa M, Okiji T, Suda H,
   The role of N-methyl-D-aspartate receptor subunits in the rat thalamic mediodorsal nucleus during central sensitization,
   Brain Research 1371：16-22, 2011.
6. ◎Chokechanachaisakul U, Yamanaka Y, Kaneko T,Katsube K,　Kobayashi H, Okiji T, Suda H,
   Gene expression analysis of resident macrophages in lipopolysaccharide-stimulated rat molar pulp,
   Journal of Endodontics 37（9）：1258-1263, 2011.
7. ◎G. Bolortuya, A. Ebihara, S. Ichinose, S. Watanabe, T. Anjo, C. Kokuzawa, H. Saegusa, N. Kawashima and H. Suda,
   Initial fibroblast attachment to Erbium：YAG laser-irradiated dentine,
   International Endodontic Journal 44（12）：1134-1144, 2011.
8. A. Ebihara, Y. Yahata, K. Miyara, K. Nakano, Y. Hayashi and H. Suda,
   Heat treatment of nickel–titanium rotary endodontic instruments：effects on bending properties and shaping abilities,
   International Endodontic Journal 44（9）：843-849, 2011.
9. XM. Hou, Y. Yahata, Y. Hayashi, A. Ebihara, T. Hanawa and H. Suda,
   Phase transformation behaviour and bending property of twisted nickel–titanium endodontic instruments,
   International Endodontic Journal 44（3）：253-258, 2011.
10. ◎H.G. Wang, N. Kawashima, T. Iwata, J. Xu, S. Takahashi, T. Sugiyama, H. Suda,
    MEPE Activated by Furin Promotes Pulpal Cell Adhesion,
    Jouranal of Dental Research 90（4）：529-534, 2011.
11. Li Y, Ikeda H, Suda H,
    Measurement of the Functional Space for Hydrodynamic Fluid　Movement in Rat Dentine Using Fluorescent Microspheres.
    Archives of Oral Biology. in press.
12. Ikeda H, Suda H.
    Functional syncytium through electrical coupling between human odontoblasts.
    J Dental Research. in press.

13. Ikeda H, Suda H.
Facilitatory Effect of AC-Iontophoresis of Lidocaine Hydrochloride on the Permeability of Human Enamel and Dentine in Extracted Teeth.
Archives of Oral Biology. in press.
14. Kaneko T , Chokuchanachaisakul U, Kawamura J, Yamanaka Y, Ito T , Sunakawa M, Suda H, Okiji T.
Upregulation of p38 mitogen-activated protein linase during pulp injuru-induced glial cell/neuronal interaction in the rat thalamus.
J of Endod.　in press.
15. Yoshioka T, Sakaue H, Ishimura H, Ebihara A, Suda H, Sumi Y .
Detection of root surface fractures with swept-source optical coherence tomography（SS-OCT）.
Photomedicine and laser surgery. in press.
16. Kokuzawa C, Ebihara A, Watanabe S, Anjo T, Bolortuya G, Saegusa H, Suda H.
Shaping of the root canal using Er：YAG laser irradiation.
Photomedicine and laser surgery. 30（7）：367-73. 2012.
17. Jamleh A, Kobayashi C, Yahata Y, Ebihara A and Suda H..
Deflecting load of nicel titanium rotary instruments during cyclic fatigue.
Dental Materials Journal. 31（3）：389-93. 2012.
18. Jamleh A, Sadr A , Nomura N, Yahata Y , Ebihara A. Hanawa T, Tagami J. and Suda H. Nano-indentation testing of new and fractured nickel-titanium endodontic instruments.
International Endodontic Journal. 45（5）：462-8. 2012.
19. ◎ Bolortuya G, Ebihara A, Ichinose S, Watanabe S, Anjo T, Kokuzawa C , Saegusa H, Kawashima N, and Suda H.
Effects of Dentin Surface Modifications Treated with Er：YAG and Nd：YAG Laser Irradiation on Fibroblast Cell Adhesion.
Photomedicine and laser surgery. 30（2）：63-70. 2012.
20. Yoshida T, Kumashiro Y, Iwata T, Ishihara J, Umemoto T, Shiratsuchi Y, Kawashima N, Sugiyama T, Yamato M, Okano T.
Requirement of Integrin s3 for Iron Transportation during Enamel Formation.
J Dent Res. in press.
21. Kawashima N.
Characterisation of dental pulp stem cells：A new horizon for tissue regeneration?,
Arch Oral Biol. 57（11）：1439-58. 2012.
22. Sun H, Yang J, Kawashima N, Li Y, Zhang W, Wang P.
A brief comparison of curricula at dental schools in China and Japan.
J Dent Educ. 76（6）：765-73. 2012.
23. ◎ Wei S, Kawashima N, Suzuki N, Xu J, Takahashi S, Zhou M, Koizumi Y, Suda H.
Kinetics of Th17-related cytokine expression in experimentally induced rat periapical lesions. Aust Endod J . in press.
24. ◎ Xu J, Kawashima N, Fujiwara N, Harada H, Ota M, Suda H.
Promotional effects of vasoactive intestinal peptide on the development of rodent Hertwig’s epithelial root sheath.
Congenital Anomalies. 52（3）：162-7. 2012.
25. ◎ Otabe K, Muneta T, Kawashima N, Suda H, Tsuji K, Sekiya I.
Comparison of gingiva, dental pulp, and periodontal ligament cells from the standpoint of mesenchymal stem cell properties.
Cell Medicine. 4. 13-21, 2012.

6）総説ならびに著書

＜著書＞

1. Hideharu Ikeda,（共著者名Hideaki Suda）,
Circulation of the pulp, Seltzer and Bender's Dental Pulp, Quintessence Pub Co, Second Edition, 109-131. 2012.
2. 石黒精、（共著者名 松本宏之　他）、診断と治療社、2012/4/16.
3. 須田英明、歯髄疾患の治療法、歯内治療学、医歯薬出版株式会社、第4版、80-96.
4. 須田英明、歯内療法に用いられる薬物、現代歯科薬理学、医歯薬出版株式会社、第5版、355-369.

＜総説＞

1. 須田英明　ガッタパーチャに代わる新しい根管充填材についてDr.Martin Tropeの講演から
ENDOで臨床を大きく変えよう!歯科治療の根幹
ENDOで天然歯を守る（クインテッセンス出版）1, 4, 2011
2. 須田英明、海老原新　"歯内療法におけるEr：YAGレーザーの臨床歯根端切除"　Er：YAGレーザーの基礎と臨床（第一歯科出版）1, 8, 2011
3. 須田英明　第36章　歯内療法に用いられる薬物
現代歯科薬理学 第5版（医歯薬出版）5, 18, 2011
4. 須田英明　X歯髄疾患の治療法
歯内治療学 第4版（医歯薬出版）4, 1, 2011
5. 八幡祥生、須田英明　基礎と臨床の架け橋として
東京医科歯科大学生体材料工学研究所60周年記念誌、日経BPコンサルティング1, 1, 2011
6. 須田英明、南里嶽仁　連載開始にあたって　歯界展

望（医歯薬出版）, 117（2）, 1, 2011
7. 須田英明、同門会だより「歯髄生物学分野・けんさん会」
8. 須田英明、講演「比較・分析による歯科関連職種における国家試験の在り方の研究から」、第59回全国歯科大学口腔衛生学教授協議会, 2012.8.23.
9. 須田英明、教育理念に合致した取り組みの成果、東京医科歯科大学　ハーバード大学　医学教育提携10年史, 2012.11.
10. 須田英明、歯内療法の役割と展望、日本歯科新聞, 2012.07.03.
11. 須田英明、東京医科歯科大学は今ー理事の視点からー、東京医科歯科大学同窓会, 2012.01.26.
12. 須田英明、編集後記、日本歯科薬物療法学会誌, 31, 1, 2012.04.01.
13. 石川真梨、（共著者名池田英治、須田英明）、漂白剤はメタロプロテアーゼが介在する象牙質コラーゲン分解を増進させるか、FROM INTERNATIONAL JOURNALS、ザ・クインッテッセンス, 31, 7, 202-203, 翻訳, 2012.07.10.
14. 佐藤哲、（共著者名池田英治、須田英明）、根尖孔径とファイル号数がRoot ZXの計測精度に及ぼす影響 in vitro研究として、FROM INTERNATIONAL JOURNALS、ザ・クインッテッセンス, 31, 5, 203-205, 翻訳, 2012.05.10.
15. 宮良香菜、（共著者名須田英明）、総説：最新のNi-Tiロータリーファイル技術と臨床応用、World jouranals of QUINTESSENCE、ザ・クインッテッセンス, 31, 4, 190-203, 翻訳, 2012.04.10.
16. 一戸達也、（共著者名 金子明寛、石河信高、石島弘己、越川憲明、佐藤聡、砂川光宏、妻鹿純一、松島潔、澤木康平）、歯科医薬品Q&A第7回　Q40-Q48、日本歯科医師会雑誌、佐々木広告社, 65, 1039-1044, 2012.
17. 一戸達也、（共著者名 金子明寛、石河信高、石島弘己、越川憲明、佐藤聡、砂川光宏、妻鹿純一、松島潔、澤木康平）、歯科医薬品Q&A第6回　Q31-Q39、日本歯科医師会雑誌、佐々木広告社, 65, 935-941, 2012.
18. 一戸達也、（共著者名 金子明寛、石河信高、石島弘己、越川憲明、佐藤聡、砂川光宏、妻鹿純一、松島潔、澤木康平）、歯科医薬品Q&A第5回　Q26-Q30、日本歯科医師会雑誌、佐々木広告社, 65, 835-839, 2012.
19. 一戸達也、（共著者名 金子明寛、石河信高、石島弘己、越川憲明、佐藤聡、砂川光宏、妻鹿純一、松島潔、澤木康平）、歯科医薬品Q&A第4回　Q19-Q25、日本歯科医師会雑誌、佐々木広告社, 65, 441-444, 2012.
20. 一戸達也、（共著者名 金子明寛、石河信高、石島弘己、越川憲明、佐藤聡、砂川光宏、妻鹿純一、松島潔、澤木康平）、歯科医薬品Q&A第3回　Q14-Q18、日本歯科医師会雑誌、佐々木広告社, 65, 283-287, 2012.
21. 一戸達也、（共著者名 金子明寛、石河信高、石島弘己、越川憲明、佐藤聡、砂川光宏、妻鹿純一、松島潔、澤木康平）、歯科医薬品Q&A第2回　Q1-Q13、日本歯科医師会雑誌、佐々木広告社, 65, 197-200, 2012.
22. 一戸達也、（共著者名 金子明寛、石河信高、石島弘己、越川憲明、佐藤聡、砂川光宏、妻鹿純一、松島潔、澤木康平）、歯科医薬品Q&A 第1-回　Q1-Q7、日本歯科医師会雑誌、佐々木広告社, 65, 95-100, 2012.
23. 海老原新、（共著者名 須田英明）、実践歯学ライブラリー　Ni-Tiファイルの実力　効率的な根管治療を求めて、DENTAL DIAMOND、デンタルダイヤモンド社, 37, 11, 24-27, 2012.8.1.
24. 和達礼子、（共著者名 花岡佑み子）、いまだから見直そう！歯科医院での防災対策 その3　やってみよう！防災対策、デンタルハイジーン、医歯薬出版株式会社, 32, 9, 917-925, 2012.9.20.

7）平成24年度までの自己評価

世界の中心としての研究拠点を構築していくにあたり、各指導教員および大学院生あるいはポスドクが一体となって研究活動に邁進する環境を整備する必要があるが、その整備が十分に行われていない。指導教員は自らの研究を行うと共に指導している大学院生の研究を補助し、さらに臨床、教育、雑務に従事せざるをえず、あまりの多忙に研究に対する熱意が薄れがちである。その一つの解決策として、他分野との共同研究を行うことが考えられる。共同研究を行うことにより、多方面からのアプローチが行えると共に、研究の効率化を進めることも可能となると期待される。

8）和文原著論文

1. 渡辺聡、三枝英敏、安生智朗、海老原新、須田英明
根管照射用チップを用いたEr：YAGレーザー照射による象牙質切削の基礎的検討
日本レーザー歯学会誌20（2）：74-80, 2011
2. 須田英明
わが国における歯内療法の現状と課題
日本歯内療法学会雑誌 32（1）：1-10, 2011
3. 岡野友宏、新井嘉則、伊藤公一、須田英明、西堀雅一、

槇宏太郎、朝田芳信、林孝文
歯科診療における歯科用コーンビームCTの基礎的・臨床的評価
日歯医学会誌, 2011

4. 森田一三、武部純、金村清孝、石橋寛二、須田英明、福田仁一、中垣晴男、末瀬一彦
歯科衛生士国家試験客観式多肢選択試験成績と養成校実技実習成績との相関
日本歯科衛生士教育学会1（1）：16-26, 2011
5. 須田英明
透析患者の象牙質知覚過敏症、う蝕および歯髄疾患
臨床透析27（6）：657-662, 2011
6. 八幡祥生、山内隆守、海老原新、須田英明
複雑な根管を呈する下顎小臼歯の歯内治療 - 歯科用実体顕微鏡とコーンビームCTの有用性 - , 日本歯内療法学会雑誌, 33, 1, 14-19, 2012.
7. 石村瞳、花田隆周、小松恵、吉岡俊彦、八幡祥生、吉岡隆知、須田英明
新型エアスケーラーを用いた根管内水酸化カルシウム材の除去についてーマイクロCTを用いた評価ー, 日歯保存誌, 55, 5, 328-331, 2012.
8. 瀧本晃陽、川島伸之、鈴木規元、小泉悠、山本弥生子、齋藤正寛、原田英光、中島美砂子、須田英明
LPS刺激下における炎症性メディエーター産生に対するMMP-3の影響, 日歯保存誌, 55, 3, 202-10, 2012.

9）学会発表（英文）

1. Gombo B, Ebihara A, Kawashima N, Watanabe S, Anjo T, Saegusa H, Kokuzawa C, Suda H, Evaluation of fibroblast cell adhision to dentin modifications teated with Er：YAG and Nd：YAG laser irradiation, Japanese Society for Laser Dentistry, oral, Osaka, 2011.12.01.
2. Chokechanachaisakul U, Kanreko T, Yamanaka Y, Kaneko R,Sunakawa M, Okiji T, Suda H, Immuno-laser Capture Microdissection of ED2 Expressing Resident Macrophages in Rat Molar Pulp, 第52回日本組織細胞科学会, poster, Ishikawa, 2011.09.24-25.
3. Chokechanachaisakul U, Kanreko T, Yamanaka Y, Sunakawa M, Okiji T, Suda H Immuno-laser Capture Microdissection of Macrophages from Rat Tissue Calture Model, The Japanese Society of Microscopy 2011, Fukuoka, 2011.05.16-18.
4. Suzuki N, Kawashima N, Suda H, Mechanisms of Bone Destruction and its Regulation in the Periapical Lesions, 2011 Autumn Scientific Meeting of KACD（136th）and 13th Joint-Scientific Meeting of KACD-JSCD 2011, poster, Seoul, 2011.11.12.
5. Kawashima N, Takimoto K, Koizumi K, Yamamoto M, Zhou M, Suzuki N, Nakashima M, H Suda, Down-regulation of Inflammatory Mediator Synthesis from macrophages by MMP3, 2011 Autumn Scientific Meeting of KACD（136th）and 13th Joint-Scientific Meeting of KACD-JSCD 2011, poster, Seoul, 2011.11.12.
6. Jamleh A, Sadr A, Nomura N, Yahata Y, Ebihara A, Hanawa T, Tagami J, Suda H, Nanoindentation of NiTi endodontic instruments after cyclic fatigue, 2011 Autumn Scientific Meeting of KACD（136th）and 13th Joint-Scientific Meeting of KACD-JSCD 2011, poster, Seoul, 2011.11.12.
7. Chokechanachaisakul U, Kaneko T, Sunakawa M, Okiji T, Suda H, Artificial Dental Pulp Exposure Injury Up-regulates Mitogen-activated Protain Kinase 13 and 14 in Rat Central Nervous System, 2011 Autumn Scientific Meeting of KACD（136th）and 13th Joint-Scientific Meeting of KACD-JSCD 2011, poster, Seoul, 2011.11.12.
8. Sunakawa M, Suda H, Treatment of Teeth with “Neuropathic Pain” after Endodontic：Treatment. Report of Three Cases, 2011 Autumn Scientific Meeting of KACD（136th）and 13th Joint-Scientific Meeting of KACD-JSCD 2011, oral, Seoul , 2011.11.12.
9. Chokechanachaisakul U, Kaneko T, Yamanaka Y, Kaneko R, Sunakawa M, Okiji T, Suda H, Immune-LCM of Resident Macrophages in Cultured Dental Pulp Tissues, The 10th China-Japan Joint Seminar on Histochemistry and Cytochemistry, poster, Beijing, 2011.10.21-24.
10. Kawashima N, Xu J, Suzuki N, Zhou M, Takimoto K, Koizumi Y, Yamamoto M, Takahashi S, Sugiyama T, Suda H, Mineralization of Odonotoblastic-Lineage Cells Was Accelerated by Enhanced Expression of Mef2c, ESE, poster, Rome, 2011.09.15-17.
11. Takahashi S, Kawashima N, Katsube K, Sugiyama T, Suda H, Shh and Wnt Signaling in Ameloblast Differentiation, ESE, poster, Rome, 2011.09.15-17.
12. Watanabe S, Kokuzawa C, Gomb B, Saegusa H, Ebihara A, Kobayashi C, Suda H, Dentin strain produced by root-end cavity preparation using Er：YAG laser, ESE, oral, Rome, 2011.09.15-17.
13. Ikeda H, Li Y, Suda H, Response to mechanical deformation of human odontoblasts, Symposium on oral neurophysiology and molecular biology, Marseille, 2011.07.26.
14. Kawashima N, Suzuki N, SudaH, Mechanisms of Bone Destruction in the Periapical Lesions and Its Regulation, K, 16th Scientific Meeting of APEC 14th Annual Congress of the IAE, oral, Iran, 2011.04.20-22.
15. Suda H, Diagnosis and management of vertical root fracture, 16th Scientific Meeting of APEC 14th Annual Congress of the IAE, oral, Iran, 2011.04.20-22.
16. Nakano K, Ebihara A, Ishimura H, Suda H , A survey

on cone-beam computed tomography in endodontics, AAE, poster, San Antonio, 2011.04.13-16.
17. Yahata Y, Miyara K, Jamleh AO, Hayashi Y, Ebihara A, Suda H, Change of fatigue property of Ni-Ti rotary instruments through heat treatment, AAE, poster, San Antonio, 2011. 04.13-16.
18. R.Wadachi, H.Suda, Root canal treatment of oculo-fasio-cardio-dental（OFCD）syndrome, AAE, poster, San Antonio, 2011.04.13-16.
19. Li Y, Ikeda H, Suda H, Measurement of Functional Space for Fluid Movement in Dentinal Tubules, IADR/AADR/CADR 89th General Session and Exhibition, poster, San Diego, 2011.03.18.
20. Ikeda H, Suda H, Regulatory Capacity of Volume and Form of Human Odontoblasts, IADR/AADR/CADR 89th General Session and Exhibition, oral, San Diego, 2011.03.18.
21. Chokechanachaisakul U, Yamanaka Y, Kaneko T, Katsube K, Kobayashi H, Okiji T, Suda H, A new method of culturing rat dental pulo tissue, IADR/AADR/CADR 89th General Session and Exhibition, poster, San Diego, 2011.03.16-19.
22. Yamamoto M, Kawashima N, Koizumi Y, Takimoto K, Saito M, Harada H, Suda H, Effects of 3-D Spheroid Culture on Dental Pulp Cells, The 2nd Tri-University Consortium on Oral Science and Education, poster, abstract book, 46, Beijing Friendship Hotel, Beijing, China, 41117
23. Chokuchanachaisakul U, Kaneko T , Sunakawa M , Okiji T , and, Suda H, Immuno-laser capture microdissection analysis of dental pulp macrophages in a whole-tooth culture model, The 14th International Congress of Histochemistry and Cytochemistry（ICHC 2012）, poster, abstract book, Kyoto International Conference Center , Kyoto, Japan, 26-29 Aug 2012
24. Ikeda H, , Fisiología pulpar y consideraciones clinicas -Microcirculación pulpar y estructura vascular, Presión de los tejidos pulpares y regulación del fluido sanguíneo, Odontoblastos y túbulos dentinales, Permeabilidad de la dentina, -, Simposio：Sobre Pulpa Dental- 15to Aniversario De La Carrera De Especializacion En Endodoncia, y 13 Encuentro Internacional del Instituto Salud Bucal, Oral, Universidad Maimonides, Buenos Aires, Argentina, June 16th, 2012
25. Ikeda H, Li Y, Suda H, Space Measurement for The Hydrodynamic Fluid Movement In Rat Dentin, IADR, oral, Iguacu Falls Convention Cente, Iguacu Falls, Brazil, June 23th, 2012
26. Ishimura H, Hanada H, Yoshioka.T , Yahata Y, Yoshioka T, Suda H, Efficacy of sonic and ultrasonic irrigations for removal of calcium hydroxide paste in the root canal：a microtomographic study, AAE, poster, Hynes convension center, Boston, USA, April 21th, 2012.
27. Miyara K, Yahata Y, Hayashi Y, Ebihara A, Hanawa T, Suda H, Mechanical Properties of Nickel-Titanium Endodontic Instrument, PROFILE® VORTEX™, AAE, Poster, Hynes convension center, Boston, USA, April 20th, 2012.
28. Suzuki N, Kawashima N, Suda H, Pathogenesis of bone destruction and its regulation in the periapical lesions, The 2nd Tri-University Consortium on Oral Science and Education, oral, abstract book, Beijing Friendship Hotel, 26, Beijing, China, 41118
29. Yamamoto M, Kawashima N, Koizumi Y, Takimoto K, Saito M, Harada H, Suda H, Effects of 3-D Spheroid Culture on Dental Pulp Cells , IADR, poster, Iguacu Falls, Brazil, June 20th, 2012.
30. ◎ Kawashima N, Mengyu Z, Katsube K, Kudo A, Suda H, Osteoblast differentiation was negatively regulated by periostin, IADR, poster, Iguacu Falls, Brazil, June 20th, 2012.
31. Suzuki N, Kawashima N, Takimoto K, Suda H, Regulation of Periapical Bone Destruction by Cathepsin K Inhibitor, AAE, poster, Hynes convension center, Boston, USA, April 20th, 2012.
32. ◎ Kawashima N, Xu J, Suzuki N, Zhou M, Takimoto K, Koizumi Y, Yamamoto M, Suda H, Involvement of a Myogenic Transcriptional Factor in Odontoblast Differentiation, AAE, poster, Hynes convension center, Boston, USA, April 20th, 2012.
33. ◎ Takimoto K, Kawashima N, Suzuki N, Nakashima M, Suda H, Effects of MMP-3 on Mediator Synthesis and Accumulation of Inflammatory Cells, AAE, poster, Hynes convension center, Boston, USA, April 20th, 2012.

10）学会発表（和文）

1. 吉岡俊彦、白金由紀子、石村瞳、海老原新、須田英明
   OCTを用いた根管の観察
   口腔病学会、口頭、東京、2011.12.10
2. 鶴田潤、須永昌代、川島伸之、木下淳博、須田英明、森尾郁子
   ビデオ会議システムを応用した国際大学院セミナー（TMDU-CU）について
   口腔病学会、口頭、東京、2011.12.10
3. 小松恵、吉岡俊彦、坂上斉、石村瞳、海老原新、須田英明
   歯科用CBCTを用いた根尖病変の三次元的評価
   日本歯科保存学会、口頭、大阪、2011.10.21
4. 石村瞳、小松恵、吉岡俊彦、八幡祥生、吉岡隆知、須田英明
   新型エアスケーラーを用いた根管内水酸化カルシウム材の除去について

日本歯科保存学会、ポスター、大阪、2011.10.21
5. 竹田淳志、池田英治、小林千尋、須田英明
根管長測定可能な学生実習用顎模型の改良
日本歯科保存学会、ポスター、大阪、2011.10.21
6. 池田英治、李穎、須田英明
象牙細管内の動水力学的水圧に対する象牙芽細胞膜の歪みについて
日本歯科保存学会、口頭、大阪、2011.10.21
7. 山本弥生子、川島伸之、須田英明
単層培養法と三次元培養法における歯髄細胞の象牙芽細胞分化について
日本歯科保存学会、ポスター、大阪、2011.10.20
8. 川島伸之、周夢宇、須田英明、工藤 明、勝部憲一
ペリオスチンによる骨芽細胞分化制御
日本歯科保存学会、口頭、大阪、2011.10.20
9. 池田英治、須田英明
交流イオン導入法を用いたヒトエナメル質の物質透過性促進
日本電電気泳動学会総会、口頭、横浜、2011.10.12
10. 小松恵、吉岡俊彦、石村瞳、海老原新、須田英明
歯科用CBCTを用いた根尖病変の三次元的評価
日本歯内療法学会、ポスター、長崎、2011.07.30
11. 吉岡俊彦、石村瞳、海老原新、須田英明
歯根破折歯の非破壊的観察-マイクロフォーカスCTとSS-OCT
日本歯内療法学会、ポスター、長崎、2011.07.30
12. 須田英明、大谷啓一、佐藤田鶴子、伊藤公一、森田章介、中川寛一
歯痛に対する非ステロイド性消炎鎮痛薬（NSAIDs）の鎮痛効果-標準的評価方法の検討
日本歯科薬物療法学会、口頭、幕張、2011.06.25
13 朴錦丹、石村瞳、小林千尋、須田英明、吉岡隆知
新しく開発された根管模型における電気的根管長測定器の測定精度について
日本歯科保存学会、ポスター、舞浜、2011.06.10
14. 辺見浩一、川島伸之、須田英明、鈴木孝尚、山下直也、立花克郎、中島美砂子
低濃度次亜塩素酸溶液にナノバブルを併用した新しい根管洗浄法の開発
日本歯科保存学会、ポスター、舞浜、2011.06.10
15 吉岡俊彦、小松恵、坂上斉、石村瞳、海老原新、島田康史、田上順次、須田英明
OCTの歯根破折線の検出精度について
日本歯科保存学会、口頭、舞浜、2011.06.09
16. 和達礼子、須田英明
瘻孔を有する根尖性歯周炎の患歯の同定におけるComputed Tomographyの有用性
日本歯科保存学会、ポスター、舞浜、2011.06.09
17. 宮良香菜、八幡祥生、海老原新、須田英明、塙隆夫
新型ニッケルチタンファイルPROFILE®
VORTEX™の曲げ特性および相変態挙動
日本歯科保存学会、ポスター、舞浜、2011.06.09
18. 坂上斉、吉岡俊彦、小松恵、石村瞳、海老原新、須田英明
mineral trioxide aggregateおよび接着性材料を用いた根管充填におけるコロナルリーケージの評価
日本歯科保存学会、口頭、舞浜、2011.06.09
19. 瀧本晃陽、川島伸之、小泉悠、山本弥生子、中島美砂子、須田英明
LPS刺激下におけるマクロファージの炎症性メディエーター産生に対するMMP-3の影響
日本炎症・再生医学会、ポスター、京都、2011.06.02
20. 辺見浩一、川島伸之、須田英明、鈴木孝尚、山下直也、立花克郎、中島美砂子
ナノバブルを併用した新しい根管洗浄法に関する基礎的研究
超音波分子診断治療研究会、口頭、福岡、2011.03.05
21. 竹田淳志、須田英明、大林尚人、倉林亨
歯科用コーンビームCTにおけるモーションアーチファクトの影響
日本歯科放射線学会第212回関東地方会、口頭、東京、2011.01.22
22. 小林千尋
Reciprocで根管形成、超音波吸引洗浄法で洗浄、オブチュレーションレーションガッタ+AH Plusで根管充填
第33回日本歯内療法学会学術大会　日経ホール
2012年6月16日
23. 和達礼子
歯根破折の診断の現状と今後
第23回日本歯科医学会総会　インテックス大阪
24. 須田英明
歯内療法の卒前教育について
第33回日本歯内療法学会学術大会　日経ホール
25. 須田英明
Preservation of the Vital Pulp　生活歯髄をまもる
―歯内療法の基本―　2012　PennEndodontic Global Symposium in Japan

ベルサール新宿セントラルパーク

26. 須田英明
歯髄保存の重要性
第10回日本再生歯科医学会学術大会・総会　ニチイ学館神戸ポートアイランドセンター

27. 須田英明
東京医科歯科大学は今―理事の視点から―
東京医科歯科大学歯科同窓会新年会員親睦会2012
東京医科歯科大学

28. 須田英明
予後の良い歯内療法のために
第65回北海道歯科学術大会　札幌パークホテル

29. 須田英明
近赤外線・レーザー等を用いた新たな歯科疾患診断・治療用機器の開発に関する研究
平成24年度長寿医療研究費23-20　国立長寿医療研究センター病院2012.10.25

30. 海老原新
歯科用CTの歯内療法への応用
第137回日本歯科保存学会　広島国際会議場（広島市）2012.11.23

31. 砂川光宏、須田英明
歯内治療に併発した医原性神経障害性疼痛
第22回日本歯科医学会総会　インテックス大阪　大阪　2012年11月9日

32. 沖畠里恵、原澤秀樹、砂川光宏、松本宏之、和泉雄一
本院における注射用抗菌薬の使用実績と特定抗菌薬の適正使用のための提言.
第77回口腔病学会学術大会　東京医科歯科大学　東京　2012.12.1

33. 松本宏之、砂川光宏、和泉雄一、須田英明
職業上の暴露事故について
第22回日本歯科医学界総会　インテックス大阪　大阪　2012年11月10日

34. 森田一三、石村瞳、海老原新、武部純、金村清孝、須田英明、石橋寛二、福田仁一、末瀬一彦、中垣晴男
歯科衛生士国家試験の在り方の研究
日本歯科衛生教育学会　愛知学院大学　名古屋　20121202

35. 末瀬一彦、須田英明、石橋寛二、福田仁一、武部純、金村清孝、中垣晴男、森田一三、海老原新、石村瞳
国内外における比較・分析による歯科技工士国家試験の在り方に関する研究
日本歯科技工士学会　岡山コンベンションセンター　岡山　2012/9/15

36. 海老原新、石村瞳、森田一三、武部純、金村清孝、石橋寛二、福田仁一、中垣晴男、末瀬一彦、須田英明
歯科医師国家試験の在り方の研究　-海外における歯科医師国家試験の現状-
日本歯科医学教育学会　岡山コンベンションセンター　岡山　2012/7/21

37. 瀧本晃陽、和達礼子、須田英明
コーンビームCT撮影が有用であった上顎前歯部の歯内療法
第33回日本歯内療法学会　日経ホール　東京　2012年6月17日

38. 山本大介、鈴木規元、石村瞳、宮良香菜
ニッケルチタンファイルWaveOneを用いたファイル回転方法の違いによる形成時間と切削特性の比較
D4研究体験実習発表会　東京医科歯科大学　東京　2012年9月21日

39 鈴木規元、石村瞳、海老原新、須田英明
先進医療「エックス線CT画像診断に基づく手術用顕微鏡を用いた歯根端切除手術」の治療成績-第2報-
第22回日本歯科医学会総会　インテックス大阪　大阪　2012年11月11日

40 和達礼子、須田英明
臨床研修歯科医による髄食う開拡の傾向
第22回日本歯科医学界総会　インテックス大阪　大阪　2012年11月11日

41. 辺見浩一、新井淳子、川島伸之、市野瀬志津子、鈴木考尚、山下直也、立花克郎、中島美砂子、須田英明
ナノバブル処理を行ったEnterococcus faecalisのSEMによる観察第4回超音波分子診断治療研究会
福岡大学医学部　福岡　2012年3月3日

42. 朴錦丹、宮良香菜、海老原新、須田英明、野村直之、塙隆夫
ニッケルチタンの回転疲労が曲げ特性に及ぼす影響について
第137回日本歯科保存学会　広島国際会議場　広島市　2012年11月23日

43. 宮良香菜、海老原新、須田英明、八幡祥生
ニッケルチタンファイルPROFILE®VORTEX™の湾曲根管模型における切削特性について
第137回日本歯科保存学会　広島国際会議場広島市　2012年11月23日

44. 辺見浩一、川島伸之、市野瀬志津子、立花克郎、中島美砂子、須田英明

ナノバブルを作用させたEnterococcus faecalisの透過型電子顕微鏡を用いた観察
第137回日本歯科保存学会　広島国際会議場　広島市　2012年11月23日

45. 瀧本晃陽、須田英明、川島伸之、鈴木規元、小泉悠、山本弥生子、中島美砂子
実験的ラット歯髄炎における炎症性細胞浸潤に対するMMP-3の影響
第137回日本歯科保存学会　広島国際会議場　広島市　2012年11月23日
46. 小松恵、吉岡俊彦、石村瞳、海老原新、須田英明
根尖部骨欠損の歯科用コーンビームCTを用いた3次元的形態評価
第137回日本歯科保存学会　広島国際会議場　広島市　2012年11月23日
47. 古畑和人、和達礼子、小林千尋、須田英明
Negative Pressure法における根管洗浄液の流れの数値流体力学的解析：吸引針のデザインによる影響
第137回日本歯科保存学会　広島国際会議場　広島市　2012年11月23日
48. 吉岡俊彦、海老原新、須田英明
歯科用コーンビームCTを利用して根管処置を行った2症例
第137回日本歯科保存学会　広島国際会議場　広島市　2012年11月22日
49. 河村隼、金子友厚、山中祐介、伊藤崇史、興地隆史、チョックチャナチャイサクン　ウライワン、須田英明
ラット実験的歯髄炎により生じる視床におけるphospho-p38 MAPKの発現に関する免疫組織学的検索
第137回日本歯科保存学会　広島国際会議場　広島市　2012年11月22日
50. 吉岡俊彦、白金由紀子、小松恵、石村瞳、海老原新、須田英明
OCTを用いた歯髄腔の観察
第136回日本歯科保存学会　沖縄コンベンションセンター　宜野湾市　2012年6月29日
51. 宮良香菜、八幡祥生、海老原新、塙隆夫、須田英明
ニッケルチタン合金線材の繰り返し疲労特性に及ぼす熱処理効果
第136回本歯科保存学会　沖縄コンベンションセンター　宜野湾市　2012年6月29日
52. 渡辺聡、東春生、石澤千鶴子、安生智郎、海老原新、須田英明
Er：YAGレーザー照射による逆根管充填窩洞のスミヤー層除去
第136回日本歯科保存学会　沖縄コンベンションセンター　宜野湾市　2012年6月29日
53. 古畑和人、和達礼子、小林千尋、若林則幸、須田英明
根管内吸引洗浄法における根管洗浄液の挙動分析：数値流体解析による研究
第136回日本歯科保存学会　沖縄コンベンションセンター　宜野湾市2012年6月29日
54. 池田英治、李穎、須田英明：動水力学説の理論的根拠となる象牙細管内腔の逆向きテーパリング
第136回日本歯科保存学会;沖縄コンベンションセンター　宜野湾市　2012年6月29日

11）受賞

1. 西原良治（指導　鈴木規元、石村瞳）.スーパーエンドα、βを用いた根管充填の速度および充填率に関する研究.D4研究体験実習学生発表会　歯学科長賞,2010年9月25日.

12）外部資金の獲得状況

1. 池田英治（分担者 須田英明）, 科学研究費補助金, 基盤研究B, Gap-junctionを介した象牙芽細胞複合体と歯髄神経・循環系との相互作用, 開始年度H20, 終了年度H24, 初年度845万円, 二年度247万円, 三年度247万円, 四年度247万円.
2. 池田英治, 科学研究費補助金, 挑戦的萌芽, 核磁気共鳴映像法（fMRI）と分子生物学的手法を用いたヒト歯髄感覚の明瞭化, 開始年度H24, 終了年度H26, 初年度130万円, 二年度78万円, 三年度65万円.
3. 川島伸之（分担者 勝部憲一, 坂本啓）, 科学研究費補助金, 基盤研究B, 歯髄細胞の分化におけるシグナルネットワークの新しいパラダイムの構築と臨床への展望, 開始年度H22, 終了年度H25, 初年度750万円, 二年度300万円, 三年度250万円.
4. 川島伸之, 科学研究費補助金, 挑戦的萌芽, 歯髄細胞および骨芽細胞の三次元培養におけるシグナルネットワークの解析と臨床的展開, 開始年度H22, 終了年度H25, 初年度50万円, 二年度150万円, 三年度60万円.
5. 渡辺聰, 科学研究費補助金, 若手B, 破折を起こしにくい次代の歯内療法へのレーザー応用の有用性の検討, 開始年度H22, 終了年度H24, 初年度130万円, 二年度90万円, 三年度90万円.
6. 辺見浩一, 科学研究費補助金, 若手B, ナノバブルを応用した新しい根管洗浄システムの開発とその臨床

応用, 開始年度H23, 終了年度H24, 初年度130万円, 二年度90万円.
7. 東春生, 科学研究費補助金, 若手B, サーマルサイクル後の水硬性仮封材の強度、辺縁漏洩への消毒液の影響, 開始年度H23, 終了年度H24, 初年度160万円, 二年度120万円.
8. 須田英明, 厚生労働科学研究費補助金, 地域医療基盤開発推進研究事業, 比較・分析による歯科関連職種における国家試験の在り方, 開始年度H23, 初年度200万円.
9. 須田英明, 寄付金（ネオ製薬工業株式会社）, H23, 100万円.
10. 中島美砂子（分担者 川島伸之）, 長寿医療研究委託費, 歯髄幹細胞を用いた象牙質・歯髄再生医療による う蝕・歯髄疾患等のための治療技術の開発, 開始年度H21, 終了年度H24, 初年度150万円, 二年度120万円, 三年度120万円, 四年度120万円.
11. 中島美砂子（分担者 川島伸之）, 先端医療開発特区補助金, 歯髄幹細胞を用いた象牙質・歯髄再生医療によるう蝕・歯髄疾患等のための治療技術の開発, 開始年度H21, 終了年度H25, 初年度2982万円.
12. 須田英明, 寄付金（デンツプライ三金）, Mechanical properties and shaping ability of new endodontic instrument, Wave One, H24, 初年度30万円.
13. 須田英明, 奨学交付金, H24, 初年度30万円.
14. 河村隼　科学研究費補助金, 研究活動支援, 歯髄炎に伴う神経・免疫相互作用に関する総合的研究, 開始年度H24, 終了年度H25, 初年度110万円, 二年度100万円.

13）特別講演、招待講演、シンポジウム

1. 海老原新、歯科用CTの歯内療法への応用
第137回日本歯科保存学会、シンポジウム、広島国際会議場（広島市）2012.11.23
2. 須田英明、平成24年度長寿医療研究費23-20「近赤外線・レーザー等を用いた新たな歯科疾患診断・治療用機器の開発に関する研究」、シンポジウム
国立長寿医療研究センター病院　2012.10.25
3. 須田英明、予後の良い歯内療法のために、第65回北海道歯科学術大会、招待講演　札幌パークホテル
4. 須田英明、歯髄保存の重要性、第10回日本再生歯科医学会学術大会・総会、シンポジウム　ニチイ学館神戸ポートアイランドセンター
5. 須田英明、Preservation of the Vital Pulp　生活歯髄をまもる―歯内療法の基本―　2012Penn Endodontic Global Symposium in Japan、招待講演　ベルサール新宿セントラルパーク
6. 須田英明、歯内療法の卒前教育について
第33回日本歯内療法学会学術大会、シンポジウム
日経ホール
7. 須田英明, 34th Asia Pacific Dental Congress
The wonderful world -use of lasers in endodontic treatment, 招待講演　Grand Hyatt　Taipei　Taiwan
8. 須田英明, 2012 Spring Scientific Meeting（the 41th）of Korean Academy of Endodontics The 10th JEA-KAE Joint Meeting　Cermony for the 10th Anniversary of JKE-KAE Joint meeting, 招待講演　SETECSeoul　Korea
9. Kawashima N, Suzuki N, SudaH, Mechanisms of Bone Destruction in the Periapical Lesions and Its Regulation, K, 16th Scientific Meeting of APEC 14th Annual Congress of the IAE, oral, Iran, 2011.04.20-22.
10. Suda H, Diagnosis and management of vertical root fracture, 16th Scientific Meeting of APEC 14th Annual Congress of the IAE, oral, Iran, 2011.04.20-22.
11. Suzuki N, Kawashima N, Suda H, Mechanisms of Bone Destruction and its Regulation in the Periapical Lesions, 2011 Autumn Scientific Meeting of KACD（136th）and 13th Joint-Scientific Meeting of KACD-JSCD 2011, poster, Seoul, 2011.11.12.
12. Suda H、香港大学歯学部　香港大学歯学部試験外部評価、香港大学歯学部、香港、中国2011.06.21-24.
13. Suda H, Visual Information for Endodontic Treatmen, 中華牙医学會学術大会、中山医科大学大慶キャンパス、台中、台湾, 2011.08.26-28.

14）新聞、雑誌、TV報道

田口正博, 赤峰昭文、須田英明、久木留廣明、平井順、歯内療法の役割と展望
座談会　日本歯科新聞　2012年7月3日

15）教室、分野や講座の准教授、講師、助教、特別研究員、ポスドク、指導を受けた大学院生の名前

准教授　小林　千尋
砂川　光宏
（クリーンルーム歯科外来兼任）
講師　竹田　淳志、池田　英治
助教　海老原　新、川島　伸之
松本　宏之
（クリーンルーム歯科外来兼任）
和達　礼子、鈴木　規元
渡辺　聡
医員　河村　隼、小泉　悠
石澤　千鶴子、吉岡　俊彦
長谷川　静、佐藤　哲
大学院生　○ 瀧本　晃陽
○ 周　夢宇、李　穎
小松　恵、宮良　香菜
山本　弥生子
Jamleh Ahmed Osama
朴　錦丹、古畑　和人
Salima Arkin
○ 顧　潔、飯野　由子
浦羽　真太郎
大学院研究生　石川　真梨、市川　勝
佐竹　和久
日中笹川医学研究者：丁　江峰
研修登録医　興地　千恵子、戸田　賀世
石塚　智康、永盛　裕二
板谷　敏光、内野　智子
花田　瞳、勝木　崇
泉　亜矢子、熊谷　のりこ
吉橋　典章、稲川　英明
山内　隆守、岩淵　珠代
大出　智佳子、鈴木　純子
若　杉洋平
非常勤講師　興地　隆史、澤田　則宏
寺内　吉継、小澤　雅彦
河西　裕美、福元　康恵
吉川　剛正、石塚　裕子
安生　智郎、菊地　和泉
金子　実弘、大井　智恵
高橋　里美、萩谷　洋子
林　洋介、三枝　英敏
中野　生和子、花田　隆周
東　春生、辺見　浩一
臨床教授　井澤　常泰
客員臨床講師　川津　真紀子
事務補佐員　久保田　美恵

RESEARCH REPORTS
Biological

MEPE Activated by Furin Promotes Pulpal Cell Adhesion

H.G. Wang[1], N. Kawashima[2,3]*, T. Iwata[4], J. Xu[2], S. Takahashi[2], T. Sugiyama[5], and H. Suda[2,3]

[1]Department of Operative Dentistry and Endodontics, School of Stomatology, Fourth Military Medical University, China; [2]Pulp Biology and Endodontics, Graduate School; [3]GCOE Program, International Research Center for Molecular Science in Tooth and Bone Diseases, Tokyo Medical & Dental University, 1–5-45, Bunkyo-ku, Tokyo 113–8549, Japan; [4]Institute of Advanced Biomedical Engineering and Science, Tokyo Women's Medical University, Japan; and [5]Department of Biochemistry, School of Medicine, Akita University, Japan; *corresponding author, kawashima.n.endo@tmd.ac.jp

J Dent Res 90(4):529-534, 2011

ABSTRACT

Matrix extracellular phosphoglycoprotein (MEPE) is predominantly expressed in osteoblasts, osteocytes, and odontoblasts and plays key biological roles in bone and dentin metabolism. Post-translational modifications are essential for its activation. This study tested the hypothesis that MEPE is activated through proteolytic processing by furin in dental pulp. MEPE was present in three sizes, 1 full-length and 2 cleaved fragments; the cleavage site was 146R↓147. The proprotein convertase family, particularly furin, was a candidate enzyme. Introducing a substitution at the cleavage site inhibited hydrolysis, but there was no cleavage of MEPE expressed in furin-deficient LoVo cells. Therefore, furin is a strong candidate for the proteolytic cleavage of MEPE. The C-terminal cleavage product promoted cell adhesion *via* its RGD motif. These results indicate that proteolytic processing by furin may activate MEPE during its secretion from odontoblasts and may play important roles in dentinogenesis and pulpal homeostasis. *Abbreviations*: MEPE, matrix extracellular phosphoglycoprotein; PTM, post-translational modifications; OLC, odontoblast-lineage cells.

KEY WORDS: MEPE, post-translational modifications, proteolytic cleavage, furin, dental pulp cells.

DOI: 10.1177/0022034510391057

Received February 23, 2010; Last revision June 4, 2010; Accepted June 7, 2010

A supplemental appendix to this article is published electronically only at http://jdr.sagepub.com/supplemental.

INTRODUCTION

Matrix extracellular phosphoglycoprotein (MEPE) was first isolated by expression screening of a tumor cDNA library to identify genes up-regulated in the tumors of patients with oncogenic hypophosphatemic osteomalacia (Rowe *et al*., 2000). MEPE seems to be crucially involved in mineralization, but its exact role as a regulator of mineralization and the mechanisms underlying this function remain controversial.

Many studies have revealed the effects of MEPE on mineralization. MEPE expression was markedly increased in fully differentiated osteoblasts (Argiro *et al*., 2001) and promoted regeneration and skeletogenesis of long bones (Lu *et al*., 2004). Furthermore, a synthetic peptide of residues 242–264 of human MEPE called Dentonin or AC-100, which includes the RGD and SGDG motifs, stimulates new bone formation (Hayashibara *et al*., 2004; Nagel *et al*., 2004). This peptide also enhances dental pulp stem cell proliferation *in vitro* (Liu *et al*., 2004) and initiates pulp healing in response to injury (Six *et al*., 2007). In contrast, some have reported that MEPE inhibits mineralization. For example, MEPE was highly expressed in tumor-induced osteomalacia (Rowe *et al*., 2000; Quarles, 2003; Bresler *et al*., 2004) and in Hyp mice, a murine model for X-linked hypophosphatemia (S Liu *et al*., 2005). MEPE expression was observed only in immature odontoblasts, and it was down-regulated during odontoblastic differentiation (MacDougall *et al*., 2002; H Liu *et al*., 2005). A mouse model with targeted deletion of *MEPE* showed increased bone formation and bone mass (Gowen *et al*., 2003).

MEPE shares molecular similarities with several dentin-bone extracellular matrix RGD-containing phosphoglycoproteins, including dentin sialophosphoprotein, osteopontin, dentin matrix protein 1 (DMP1), and bone sialoprotein (Fisher and Fedarko, 2003). These non-collagenous proteins are believed to play key biological roles in the formation and mineralization of bone and/or dentin. Their functions are largely dependent on the nature and extent of post-translational modifications (PTM), including phosphorylation, glycosylation, and proteolytic processing. Proteolytic processing is particularly important in inducing the active forms of various proteins. DMP1 was proteolytically processed by PHEX enzyme or bone morphogenetic protein-1/Tolloid-like proteinases (Qin *et al*., 2003, 2004; Steiglitz *et al*., 2004).

The aims of this study were to evaluate the expression pattern of MEPE in dental pulp, the mechanisms involved in the PTM of MEPE in dental pulp cells and tissues, and the function of proteolytic fragments of MEPE in dentinogenesis.

MATERIALS & METHODS

Construction of Expression Vectors and Mutants, Real-time PCR

The open reading frame of the mouse MEPE cDNA, with or without signal peptides, was subcloned into the eukaryotic expression vector pEF-Dest51 (pEF-mMEPE) or pSecTag2A with a V5His tag (pSecTag2A-V5His-MEPE), respectively. The cDNAs for the mouse MEPE mature peptide, C-terminal fragment (residues 18–146) and N-terminal fragment (residues 147–433), were subcloned into the prokaryotic expression vector pDEST17. MEPE R145G and R146A mutants in the pEF-mMEPE construct and mutant G176A (RGD→RAD) in the pDEST17-mMEPE construct were created by site-directed mutagenesis. MEPE mRNA expression was determined by real-time PCR with specific primers in several cell lines and in primary cells from rat dental pulp, periodontal ligament, and gingiva (Appendix Tables 1 and 2).

Transfection, Transient Expression, and Western Blotting Analysis

Odontoblast-lineage cells (OLC) (Arany *et al*., 2006) and several other types of cells were transfected with the MEPE expression vectors, and the conditioned medium was harvested for SDS-PAGE. Western blotting was performed with the primary antibodies, including anti-V5 (1:5000), anti-mMEPE (LF-156 & LF-155, 1:1000; kind gifts from Dr. L.W. Fisher), and anti-β-actin (1:1000).

Protein Production, Amino Acid Sequencing, Production of Antibody, and Cell Adhesion Assay

The eukaryotic MEPE protein was produced on a large scale by HEK293F cells. Sequencing of the C-terminal fragment was performed by the Edman degradation method. The full-length, C- and N-terminal fragments, and mutant G176A MEPE proteins were expressed in *Escherichia coli*. The full-length protein was used to produce the polyclonal antibody. All the proteins were tested by cell adhesion assay, while collagen I was used as a positive control and BSA as a negative control.

Immunohistochemical Staining

Dental pulp tissues of upper incisors from male Wistar rats (6-wks old) were fixed with 4% paraformaldehyde for 12 hrs at 4ºC. Immunohistochemical staining with anti-mMEPE antibody (LF-155, 1:250) was performed on frozen sections. Immunoreactivity was detected by the ABC method, and the color reaction was developed with DAB. The nucleus was counterstained by methyl green. For immunofluorescence with anti-mMEPE antibody (LF-156, 1:250), Alexa Fluor™ 594 conjugated goat anti-rabbit IgG (1:1000, Invitrogen, Carlsbad, CA, USA) was applied as a secondary antibody, and 4′,6′-diamidino-2-phenylindole (DAPI, 300 nM, Invitrogen) was used for nuclear staining. Based on the literature and our data, LF-156 recognizes full-length, N- and C-terminal fragments of MEPE protein, while LF-155 reacts only against the C-terminal fragment. Adult rat tibia was used as positive control and liver as negative control. All animal experiments were performed in accordance with the Animal Guidelines of Tokyo Medical and Dental University.

Statistical Analysis

All data are represented as means ± standard error. Statistical significance was determined by an unpaired Student's *t* test, and a p value of < 0.05 was considered statistically significant. Additional information on MATERIALS & METHODS can be found in the Appendix.

RESULTS

Cleavage of MEPE in Dental Pulp Tissue

RT-PCR revealed MEPE expression in mouse and rat dental pulp tissues. MEPE was ubiquitously expressed in hard-tissue-forming cells, including osteoblastic cells (Kusa-A1, Kusa-O, and MC3T3E1), chondroblastic cells (ATDC5, Kum5), odontoblast-lineage cells (OLC) and MDPC-23, and ameloblast-lineage cells (ALC) (Fig. 1A). In addition, high and low levels of MEPE expression were observed in rat dental pulp cells and in periodontal ligament cells, respectively. However, MEPE expression was below the detectable level in gingival cells (Appendix Fig. 1). Three forms of MEPE protein, 50, 38, and 25 kDa, were identified in the rat pulp tissue (Fig. 1B). The mature MEPE peptide is a 417-amino-acid secreted peptide with a calculated molecular mass of 44,247 Da. As a result of glycosylation, MEPE in rat dental pulp tissue migrated as an approximately 50-kDa protein in SDS-PAGE under reducing conditions. The 38- and 25-kDa proteins expressed in dental pulp tissue were truncated forms of MEPE, suggesting that MEPE is processed in dental pulp tissue. The similar staining patterns of LF-156 (anti all kinds of fragments of MEPE) and LF-155 (anti C-terminal fragment) suggested that the localization of full-length MEPE and its fragments should be similar (Fig. 1C).

Cleavage of MEPE in Exogenous MEPE-expressing Cells

After transfection of pEF-mMEPE, exogenous expression of the MEPE protein was observed in the cell lysate and the supernatant. Western blotting revealed 3 bands at 58, 45, and 22 kDa in the supernatant and a single band at 55 kDa in the cell lysate. The 58-kDa band, containing a 5-kDa V5-His tag, was full-length MEPE, while the 45-kDa band, containing a 5-kDa V5-His tag, was the C-terminal cleavage product of MEPE. The 28-kDa band, also containing a 5-kDa V5-His tag, was identified as the N-terminal cleavage product of MEPE. This cleavage was widely observed in protein-expression cell lines, and in odontoblastic and osteoblastic cell lines (Figs. 2A, 2B). The size of the full-length MEPE in the supernatant was slightly larger than that in the cell lysate, which may be caused by cell-specific PTM, such as phosphorylation or glycosylation, during secretion. The size of the full-length natural MEPE in the pulp tissues was about 10 kDa less than that of MEPE artificially synthesized with pEF-mMEPE. Most of this size discrepancy was due

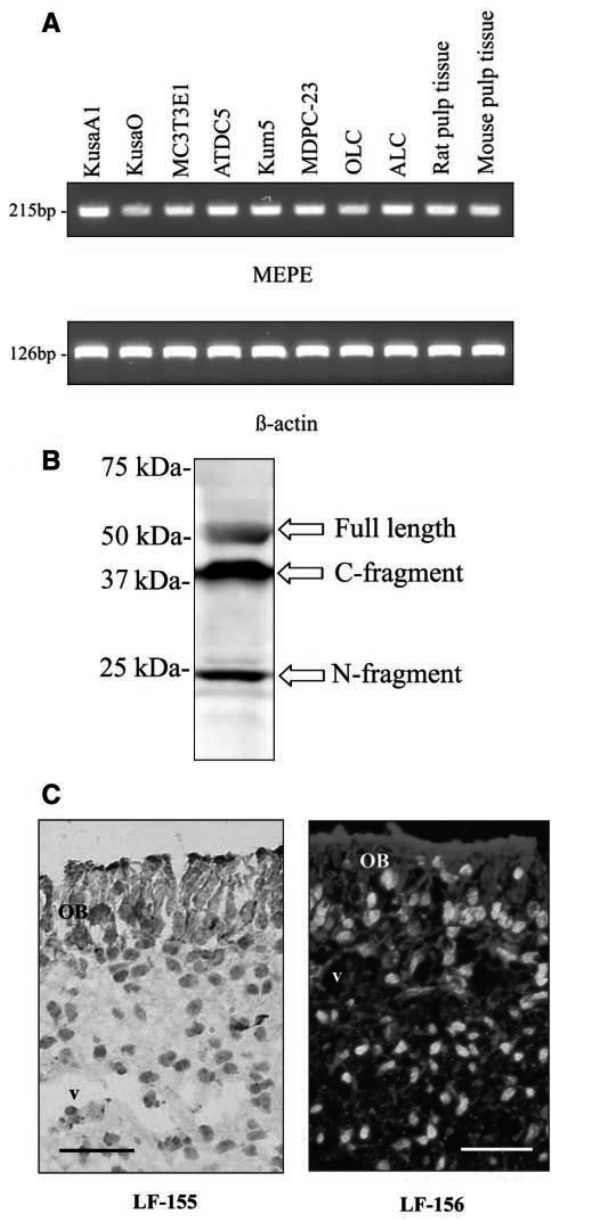

Figure 1. MEPE cleavage in dental pulp tissue. **(A)** MEPE is ubiquitously expressed in osteoblastic (Kusa-A1, Kusa-O, and MC3T3E1), chondroblastic (ATDC5, Kum5), odontoblastic (OLC, MDPC-23), and ameloblastic (ALC) cell lines and in mouse and rat dental pulp tissues. **(B)** Three forms of MEPE protein, 50, 38, and 25 kDa, were identified in rat pulp tissue by Western blotting analysis with anti-MEPE antibody. The 50-kDa protein was the full-length mature peptide, while the lower-molecular-weight proteins were truncated forms of MEPE. **(C)** Detection of MEPE in mature pulp tissue by two types of anti-MEPE antibody, LF-155 and LF-156. The staining pattern with LF-156, which recognizes all fragments of the MEPE protein, was similar to that of LF-155, which recognizes only the C-terminal fragment. The nucleus was counterstained with methyl green or 4′,6′-diamidino-2-phenylindole.

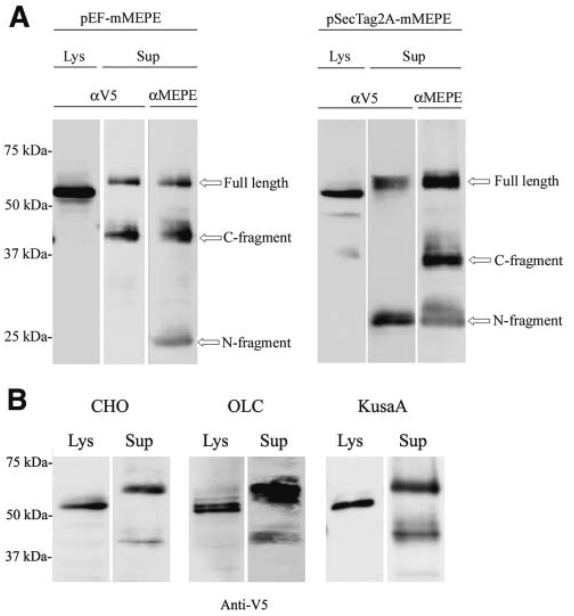

Figure 2. MEPE cleavage in exogenous MEPE-expressing cells. **(A)** Cleavage of MEPE was detected after transient expression in HEK293 cells with either pEF-mMEPE (contains the C-terminal V5-His tag) or pSecTag2A-V5His-MEPE (contains the N-terminal V5-His tag). For pEF-mMEPE, 3 bands at 58, 45, and 22 kDa appeared in the supernatant, and a single band at 55 kDa was observed in the cell lysate. The 58-kDa band, containing a 5-kDa V5-His tag, was full-length MEPE. The 45-kDa band, containing a 5-kDa V5-His tag, was the C-terminal cleavage product of MEPE. For pSecTag2A-V5His-MEPE, the cleaved products were similar, and the 28-kDa band containing the 5-kDa V5-His tag was identified as the N-terminal cleavage product of MEPE. The size of the full-length MEPE in the supernatant was slightly different from that in the lysate, which may be due to post-translational modifications such as phosphorylation or glycosylation, which occurred before secretion of MEPE. **(B)** The cleavage was widely observed in various cell lines. The full-length and C-terminal fragments of MEPE were observed in pEF-mMEPE-transiently transfected CHO cells, and in odontoblastic (OLC) and osteoblastic (Kusa-A1) cell lines. The bar represents 20 μm. OB = odontoblast, v = blood vessel, Lys = lysate, Sup = supernatant, αV5 = anti-V5, αMEPE = anti-MEPE.

to the addition of the 5-kDa V5-His tag to the expression vector, but some PTM may also be responsible for the difference in size of the artificially synthesized MEPE.

Proprotein Convertase is Involved in the Cleavage of MEPE

Amino acid sequencing of the C-terminal fragment (Appendix Fig. 2) revealed the sequence to be ^{147}STHYL, indicating that MEPE was cleaved at the ^{146}R↓^{147}S site. Several proteases, including Arg-C protease, clostripain, trypsin, cathepsin B, and proprotein convertases, may be responsible for the cleavage of MEPE. Arg-C protease, clostripain, and trypsin are serine proteases, while cathepsin B is a cysteine protease. To test these proteases, we added a protease inhibitor cocktail, which inhibits

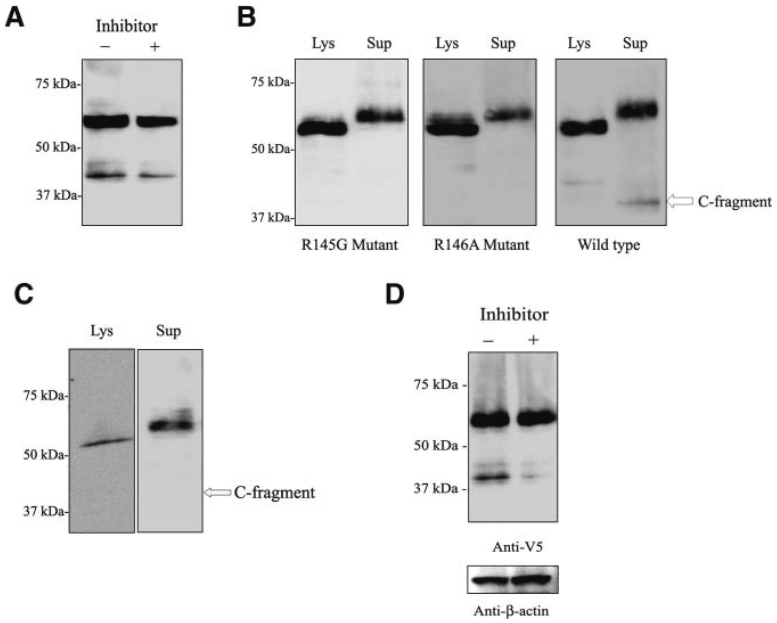

Figure 3. Furin is responsible for the cleavage of MEPE. **(A)** A protease inhibitor cocktail, which inhibits serine, cysteine, and metalloproteases, was added to the culture medium of Cos-7 cells. Protein production was inhibited, but cleavage still occurred, which excluded the 4 candidate proteases, Arg-C proteinase, clostripain, trypsin, and cathepsin B. **(B)** The R145G and R146A mutants were resistant to cleavage. Compared with the wild–type form, the 40-kDa C-terminal fragment was not detected after transfection. **(C)** In LoVo cells (furin-deficit human colon cancer cell line), there was no cleavage of MEPE after transfection and transient expression. **(D)** Cleavage of MEPE was effectively blocked by the furin-specific inhibitor in Cos-7 cells. Lys = lysate, Sup = supernatant.

serine, cysteine, and metalloproteases, to the culture medium for Cos-7 cells. Cleavage was not inhibited, which excluded these 4 proteases (Fig. 3A).

Only the full-length protein was detected in the conditioned medium after transient expression of either the R145G mutant or the R146A mutant, indicating that they were resistant to cleavage (Fig. 3B). ^{145}R and ^{146}R were clearly important for protease activity, which is consistent with the recognition site of proprotein convertases. The rule for recognition by proprotein convertases is (Arg/Lys)-(X)n-Arg (n = 0, 2, 4, or 6). For MEPE, the cleavage occurred at PRARR ↓STHYL for rat MEPE, and RQTRR ↓STHYL for mouse MEPE (n = 0). These results are consistent with the conclusion that proprotein convertases are involved in MEPE cleavage.

The mammalian proprotein convertase family is composed of 7 members, and, based on previous reports (Akamatsu *et al*., 1999, 2000), furin and PACE4 are candidates. In LoVo cells, a human colon carcinoma cell line that lacks enzymatically active furin due to the presence of mutations in both alleles of the furin gene, MEPE was not cleaved after transfection and transient expression (Fig. 3C). Furthermore, cleavage of MEPE was effectively blocked by a furin-specific inhibitor in Cos-7 cells (Fig. 3D). RT-PCR showed that furin was expressed in all of the cell types used in this experiment, except LoVo cells. In contrast, PACE4 expression was detected in all of these cell lines, including LoVo cells (Appendix Fig. 3). Therefore, the expression of furin is consistent with the expression and cleavage of MEPE. These results indicate that furin is responsible for MEPE cleavage.

MEPE-induced Cell Adhesion *via* the RGD Sequence

The full-length eukaryotic protein (F_{HEK}) dose-dependently promoted the attachment of OLCs. Two μg/mL of protein showed activity similar to that of collagen I (Appendix Fig. 4A). In the antibody neutralization test, the antibody to the full-length prokaryotic protein ($F_{E.coli}$) dose-dependently neutralized cell adhesion on plates coated with 100 μL of F_{HEK} at 2 μg/mL. Two μg/mL of this antibody neutralized 100% of cell adhesion. However, the LF-156 antibody raised against a partial sequence of MEPE (CSREKVKGGVEHAGRAG & CSKHTKHTRQTRRSTHGG) showed no effect on the neutralization of protein activity (Fig. 4A). The antibody against full-length MEPE did not abrogate cell binding to collagen I (Appendix Fig. 4B). The C-terminal fragment of prokaryotic protein containing the RGD motif ($C_{E.coli}$) promoted cell adhesion, while the N-terminal fragment of prokaryotic protein ($N_{E.coli}$) did not (Fig. 4B). The G176A mutant (RGD→RAD) of prokaryotic protein ($RAD_{E.coli}$) did not promote cell adhesion, even at 16 μg/mL (Fig. 4C). These results indicate that MEPE promotes cell adhesion *via* the RGD sequence.

DISCUSSION

We revealed that MEPE was synthesized and secreted by odontoblasts, suggesting that MEPE plays roles in dentinogenesis and in the physiology of pulp tissue. In oral tissue, MEPE was highly expressed in dental pulp cells, but its expression was low in periodontal ligament cells and scant in gingival tissues. These results suggest that MEPE tends to be expressed in hard tissues and hard-tissue-related cells, and this indicates MEPE may be involved in the process of mineralization, as either a positive or a negative regulator.

Three forms of MEPE are found in pulp cells and tissues, with significantly different molecular masses: the full-length protein, and N-terminal and C-terminal cleavage products. The small and large MEPE components present in pulp tissues corresponded to the N-terminal and C-terminal fragments, respectively, and they were generated by cleavage between 146R and 147S. We found that the enzyme responsible for the cleavage of

MEPE at this site is furin, which is a ubiquitously expressed proprotein convertase. To date, 7 members of the proprotein convertase family have been identified in mammalian species, namely, furin, PC2, PC1/PC3, PC4, PACE4, PC5/PC6, and LPC/PC7/PC8/SPC7 (Nakayama, 1997). They have been shown to be responsible for the conversion of precursors of peptide hormones, neuropeptides, and many other proteins into their biologically active forms (Nakayama, 1997). For example, furin can initiate BMP activity by direct endoproteolytic cleavage. Cleavage at the upstream site regulates the activity and signaling range of mature BMP-4 (Nakayama, 1997; Cui *et al*., 1998; Degnin *et al*., 2004). In rats, furin is widely expressed at all stages of dentinogenesis, from embryonic day 20.5 to post-natal day 14 (Akamatsu *et al*., 2000). Analysis of our data suggests that furin processes MEPE and that the active C-terminal fragments can be produced *in vitro*. Therefore, furin is a strong candidate enzyme for processing of active fragments of MEPE; however, this study does not exclude the possibility of other MEPE-processing enzymes.

The effects of the matrix are primarily mediated by integrins, a family of cell-surface receptors that attach cells to the matrix and mediate mechanical and chemical signals from the matrix. These signals regulate the activities of cytoplasmic kinases, growth factor receptors, and ion channels, and control the organization of the intracellular actin cytoskeleton (Giancotti and Ruoslahti, 1999). Binding between the RGD and integrins may trigger downstream signaling pathways through mediators such as FAK and ERK to regulate cell adhesion, migration, proliferation, and differentiation (Giancotti and Ruoslahti, 1999; Plow *et al*., 2000; Altroff *et al*., 2001). The cell adhesion test showed that the MEPE protein could induce cell adhesion *via* the RGD motif, which is located in the C-terminal cleavage product. MEPE may form part of the scaffold bridge between osteoblasts or odontoblasts and the extracellular matrix to regulate crystal growth. Therefore, in dental tissue, the C-terminal cleavage product is the active form of MEPE, which can promote cell adhesion through the RGD sequence.

In conclusion, the results of this study indicate that MEPE is cleaved by furin into 2 fragments during its secretion by odontoblasts. The C-terminal cleavage product, *via* the RGD motif, is an active fragment that promotes cell adhesion. Proteolytic processing is required for the activation of MEPE in dental pulp, and may play important roles in dentinogenesis.

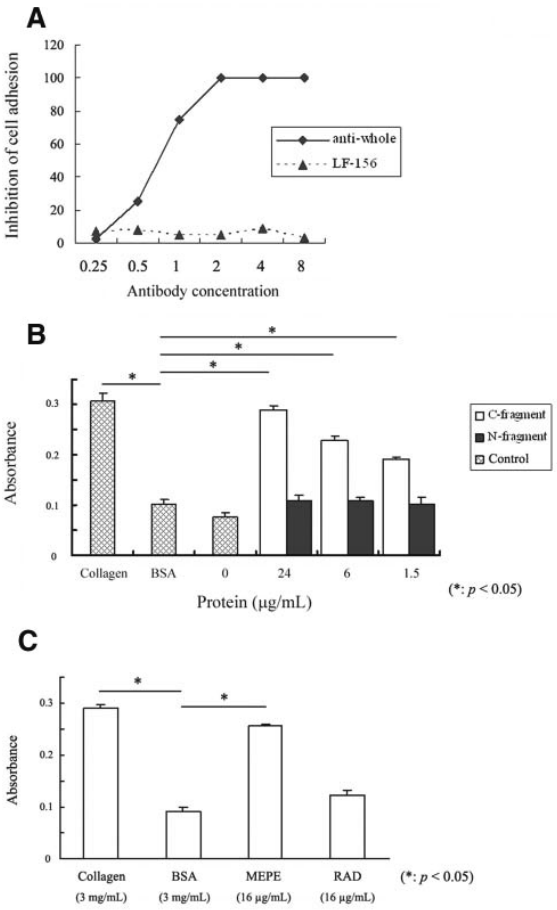

Figure 4. MEPE induces cell adhesion *via* the RGD sequence. **(A)** In the antibody neutralization test, the antibody against the full-length prokaryotic protein ($F_{E.coli}$) dose-dependently neutralized cell adhesion on plates coated with 100 μL of F_{HEK} at 2 μg/mL, and 2 μg/mL of the antibody could neutralize 100% of cell adhesion. However, the LF-156 antibody, which was raised against the partial sequence of MEPE (CSREKVKGGVEHAGRAG & CSKHTKHTRQTRRSTHGG), showed no effect on neutralization of protein activity. **(B)** The C-terminal fragment protein containing the RGD motif produced by *E. coli* ($C_{E.coli}$) promoted cell adhesion, while the N-terminal fragment protein produced by *E. coli* ($N_{E.coli}$) did not. **(C)** The G176A mutant (RGD→RAD) protein produced by *E. coli* ($RAD_{E.coli}$) did not promote cell adhesion at 16 μg/mL. $*p < 0.05$ compared with the control group (BSA).

ACKNOWLEDGMENTS

We greatly appreciate the contributions of Dr. Larry W. Fisher (NIDCR, Bethesda, MD, USA), Professor Wenli Yan (Fourth Military Medical University, China), and Professor James P. Simmer (University of Michigan, Ann Arbor, USA). The work was supported by a Japan-China Sasakawa Medical Fellowship, by Grants-in-Aids from the JSPS (Nos. 22390357 and 22659343 to N.K.; and No. 21791838 to S.T.), and by grants from the NSFC (No. 30901674 to H.W.).

REFERENCES

Akamatsu T, Matsuda Y, Tsumura K, Tada J, Parvin MN, Kanamori N, *et al*. (1999). Subtilisin-like proprotein convertase PACE4 (SPC4) is a candidate processing enzyme of bone morphogenetic proteins during tooth formation. *Dev Dyn* 216:481-488.

Akamatsu T, Matsuda Y, Tsumura K, Tada J, Parvin MN, Wei W, *et al*. (2000). Highly regulated expression of subtilisin-like proprotein convertase PACE4 (SPC4) during dentinogenesis. *Biochem Biophys Res Commun* 272:410-415.

Altroff H, van der Walle CF, Asselin J, Fairless R, Campbell ID, Mardon HJ (2001). The eighth FIII domain of human fibronectin promotes integrin alpha5beta1 binding via stabilization of the ninth FIII domain. *J Biol Chem* 276:38885-38892.

Arany S, Nakata A, Kameda T, Koyota S, Ueno Y, Sugiyama T (2006). Phenotype properties of a novel spontaneously immortalized odontoblast-lineage cell line. *Biochem Biophys Res Commun* 342:718-724.

Argiro L, Desbarats M, Glorieux FH, Ecarot B (2001). MEPE, the gene encoding a tumor-secreted protein in oncogenic hypophosphatemic osteomalacia, is expressed in bone. *Genomics* 74:342-351.

Bresler D, Bruder J, Mohnike K, Fraser WD, Rowe PS (2004). Serum MEPE-ASARM-peptides are elevated in X-linked rickets (HYP): implications for phosphaturia and rickets. *J Endocrinol* 183:R1-R9.

Cui Y, Jean F, Thomas G, Christian JL (1998). BMP-4 is proteolytically activated by furin and/or PC6 during vertebrate embryonic development. *EMBO J* 17:4735-4743.

Degnin C, Jean F, Thomas G, Christian JL (2004). Cleavages within the prodomain direct intracellular trafficking and degradation of mature bone morphogenetic protein-4. *Mol Biol Cell* 15:5012-5020.

Fisher LW, Fedarko NS (2003). Six genes expressed in bones and teeth encode the current members of the SIBLING family of proteins. *Connect Tissue Res* 44(Suppl 1):33-40.

Giancotti FG, Ruoslahti E (1999). Integrin signaling. *Science* 285:1028-1032.

Gowen LC, Petersen DN, Mansolf AL, Qi H, Stock JL, Tkalcevic GT*, et al*. (2003). Targeted disruption of the osteoblast/osteocyte factor 45 gene (OF45) results in increased bone formation and bone mass. *J Biol Chem* 278:1998-2007.

Hayashibara T, Hiraga T, Yi B, Nomizu M, Kumagai Y, Nishimura R*, et al*. (2004). A synthetic peptide fragment of human MEPE stimulates new bone formation *in vitro* and *in vivo*. *J Bone Miner Res* 19:455-462.

Liu H, Li W, Gao C, Kumagai Y, Blacher RW, DenBesten PK (2004). Dentonin, a fragment of MEPE, enhanced dental pulp stem cell proliferation. *J Dent Res* 83:496-499.

Liu H, Li W, Shi S, Habelitz S, Gao C, DenBesten P (2005). MEPE is down-regulated as dental pulp stem cells differentiate. *Arch Oral Biol* 50:923-928.

Liu S, Brown TA, Zhou J, Xiao ZS, Awad H, Guilak F*, et al*. (2005). Role of matrix extracellular phosphoglycoprotein in the pathogenesis of X-linked hypophosphatemia. *J Am Soc Nephrol* 16:1645-1653.

Lu C, Huang S, Miclau T, Helms JA, Colnot C (2004). MEPE is expressed during skeletal development and regeneration. *Histochem Cell Biol* 121:493-499.

MacDougall M, Simmons D, Gu TT, Dong J (2002). MEPE/OF45, a new dentin/bone matrix protein and candidate gene for dentin diseases mapping to chromosome 4q21. *Connect Tissue Res* 43:320-330.

Nagel DE, Khosla S, Sanyal A, Rosen DM, Kumagai Y, Riggs BL (2004). A fragment of the hypophosphatemic factor, MEPE, requires inducible cyclooxygenase-2 to exert potent anabolic effects on normal human marrow osteoblast precursors. *J Cell Biochem* 93:1107-1114.

Nakayama K (1997). Furin: a mammalian subtilisin/Kex2p-like endoprotease involved in processing of a wide variety of precursor proteins. *Biochem J* 327(Pt 3):625-635.

Plow EF, Haas TA, Zhang L, Loftus J, Smith JW (2000). Ligand binding to integrins. *J Biol Chem* 275:21785-21788.

Qin C, Brunn JC, Cook RG, Orkiszewski RS, Malone JP, Veis A*, et al*. (2003). Evidence for the proteolytic processing of dentin matrix protein 1. Identification and characterization of processed fragments and cleavage sites. *J Biol Chem* 278:34700-34708.

Qin C, Baba O, Butler WT (2004). Post-translational modifications of sibling proteins and their roles in osteogenesis and dentinogenesis. *Crit Rev Oral Biol Med* 15:126-136.

Quarles LD (2003). FGF23, PHEX, and MEPE regulation of phosphate homeostasis and skeletal mineralization. *Am J Physiol Endocrinol Metab* 285:E1-E9.

Rowe PS, de Zoysa PA, Dong R, Wang HR, White KE, Econs MJ*, et al*. (2000). MEPE, a new gene expressed in bone marrow and tumors causing osteomalacia. *Genomics* 67:54-68.

Six N, Septier D, Chaussain-Miller C, Blacher R, DenBesten P, Goldberg M (2007). Dentonin, a MEPE fragment, initiates pulp-healing response to injury. *J Dent Res* 86:780-785.

Steiglitz BM, Ayala M, Narayanan K, George A, Greenspan DS (2004). Bone morphogenetic protein-1/Tolloid-like proteinases process dentin matrix protein-1. *J Biol Chem* 279:980-986.

歯周病学分野

和泉 雄一

医歯学総合研究科・生体支持組織学系専攻
歯周病学・教授

1）研究の課題名

新たな歯周治療法の開発と歯周病・全身疾患の関連性およびそのメカニズムに関する研究

Study on the development of novel periodontal therapy and the association between periodontal and systemic diseases and its mechanism.

心臓冠動脈疾患と歯周病との関連性については依然不明な点が多い。今回、マウスに歯周病原細菌のAggregatibacter actinomycetemcomitansを感染させ、心筋肥大症との関連について検索した。その結果、感染群には、心筋肥大、繊維症、動脈硬化が確認された。また、同群にはコントロールに比べてMMP-2の活性が上昇していた。一方、動脈損傷を受けた後の新生動脈内膜の過形成について検索すると、Porphyromonas gingivalis感染群ではその過形成が促進されていた。同様にMMP-2 mRNAの発現が亢進していた。

2型糖尿病と歯周病に罹患している患者に、非外科歯周治療と抗菌剤の局所投与による介入を行うとその血糖コントロールが改善し、血清TNF-αの低下が認められた。しかしながら、重症な歯周病を伴う場合には非外科歯周治療だけではインシュリン抵抗性を改善するまでには至らなかった。

オゾンナノバブル水（NBW3）をフルマウスディスインフェクションと併用し臨床試験を行った。その結果、NBW3併用群では有意に臨床パラメーターの改善が認められた。また、総菌数の減少が確認された。

インプラント周囲炎の治療の一環としてEr：YAGレーザーの治療への可能性について検討した。感染を受けたフィクスチャーに対して感染物を取り除くに適切なレーザー照射条件を探索した。その結果適正条件は30mJ/pulse以下のエネルギー密度で, 30Hzの注水併用で軽く接触照射を行うことが好ましいことが判明した。

2）研究のイラストレーション

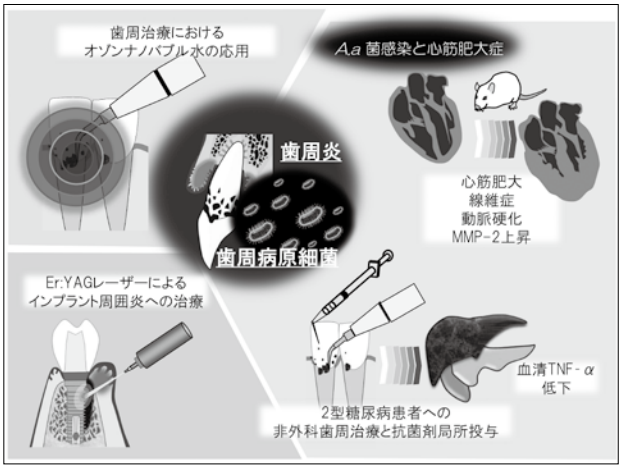

3）発表の研究内容についての英文要約

To analyze the association between periodontal infection and myocardial hypertrophy. Aggregatibacter actinomycetemcomitans-infected mice showed markedly enhanced cardiac hypertrophy, fibrosis and arteriosclerosis 4 weeks after TAC operation. Immunohistochemistry revealed that expression of MMP-2 in the interstitial tissue was enhanced in the infected group suggesting the periodontal pathogen caused a deterioration of pressure overload-induced myocardial hypertrophy through MMP activation.

To examine the effects of non-surgical periodontal treatment incorporating topical antibiotics on glycemic control and serum inflammatory mediators in patients with type 2 diabetes mellitus with periodontitis. A generalized linear model showed significant associations between the change in the HbA1c values at 6 months after periodontal treatment , and the change in the BOP, baseline TNF-α level and the baseline mean PPD. Such treatments might be insufficient for the amelioration of insulin resistance in type 2 diabetic patients with severe periodontitis.

Ozon nano-bubble water（NBW3）seems to be suitable as an adjunct to periodontal treatment owing to its potent antimicrobial effects, high level of safety and long storage

stability. To evaluate the clinical and microbiological effects of NBw3 irrigation to 22 patients who were randomly assigned to one of the two treatment groups：full-mouth mechanical debridement with between tap water or NBW3. Only the NBW3 group showed statistically significant reductions in the mean total number of bacteria in subgingival plaque over the study period with clinically improvement suggesting NBW3 may be a valuable adjunct to periodontal treatment.

4）本事業に関連して世界的な研究拠点形成に向けて、以下の点で改善・整備等されたこと

A（研究拠点体制）

米国UCSFのMark Ryder教授およびタイ国Khon Kaen大学のNawarat W Charoen歯学部長との研究協力体制を継続している。

B（研究教育環境）

大学院講義を英語で実施し、英語に親しむ環境の構築に努めた。

C（人材確保）

8人がAISSに採用された。大学院生を新規に6名受け入れた。

D（人材育成）

新人教育に力を入れ、研究面ではDr. Nawarat W Charoenと研究討議を行い大学院生の指導をお願いした。

E（国際化）

1）The 7th Global COE International Symposium, Molecular Science in Oral-Systemic Medicine –Autumn Seminar–,（2012.11.12-14. 本学）を主催した。

2）The 8th Global COE International Symposium, Molecular Science in Oral-Systemic Medicine –Winter Seminar–,（2013.2.3-4. 本学）を主催した。

3）日本学術振興会の論博事業に参画し、タイからの留学生を受け入れた。

5）GCOE事業を推進するに当たって力を入れた点

若い研究者に出来る限り国際化の意識を植え付けるように努めた。海外での研究発表を積極的に推進している。

6）英文原著論文

1. Almehdi A, Aoki A, Ichinose S, Taniguchi Y, Sasaki KM, Ejiri K, Sawabe M, Chui C, Katagiri S, Izumi Y. Histological and SEM analysis of root cementum following irradiation with Er：YAG and CO_2 lasers. Lasers Med Sci（e-pub May 15th, 2012）.
2. ◎Aoyama N, Suzuki J, Ogawa M, Watanabe R, Kobayashi N, Hanatani T, Yoshida A, Ashigaki N, Izumi Y, Isobe M. Clarithromycin Suppresses the Periodontal Bacteria-Accelerated Abdominal Aortic Aneurysms in Mice. J Periodontal Res. 47（4）：463-469;2012
3. Belal MH, Watanabe H, Ichinose S, Ishikawa I.Effect of PDGF-BB combined with EDTA gel on adhesion and proliferation to the root surface. Odontology 100（2）：206-214, 2012.
4. ◎Bharti P, Katagiri S, Nitta H, Nagasawa T, Kobayashi H, Takeuchi Y, Izumiyama H, Uchiyama I, Inoue S, Izumi Y. Periodontal treatment with topical antibiotics improves glycemic control in association with elevated serum adiponectin in patients with type 2 diabetes mellitus. Obesity Research and Clinical Practice（in press）
5. ◎Chui C, Hiratsuka K, Aoki A, Takeuchi Y, Abiko Y, Izumi Y.Blue LED Inhibits the Growth of Porphyromonas gingivalis by Suppressing the Expression of Genes Associated with DNA Replication and Cell Division. Lasers Surg Med（2012 e-pub Nov 5th.）
6. Hamaya R, Ogawa M, Kobayashi N, Suzuki J, Itai A, Hirata Y, Nagai R, Isobe M. A novel IKK inhibitor prevents progression of restenosis after arterial injury in mice. Int Heart J. 53（2）：133-138, 2012.
7. Hanatani T, Suzuki J, Ogawa M, Aoyama N, Kobayashi N, Hirata Y, Nagai R, Izumi Y, Isobe M. The periodontal pathogen Aggregatibacter actinomycetemcomitans deteriorates ventricular remodeling after myocardial infarction in mice. Int Heart J 53（4）：253-256, 2012.
8. Hayakumo S, Arakawa S, Mano Y, Izumi Y. Clinical and microbiological effects of ozone nano-bubble water irrigation as an adjunct to mechanical subgingival debridement in periodontitis patients in a randomized controlled trial. Clin Oral Investig.（in press）
9. ◎Himeno-Ando A, Izumi Y, Yamaguchi A, Iimura T. Structural differences in the osteocyte network between the calvaria and long bone revealed by three-dimensional fluorescence morphometry, possibly reflecting distinct mechano-adaptations and sensitivities. Biochem Biophys Res Commun 417（2）：765-770, 2012.
10. Katagiri S, Nagasawa T, Kobayashi H, Takamatsu H, Bharti P, Izumiyama H, Uchimura I, Tagami T, Suzuki T, Nanbara H, Taniguchi Y, Hayakumo S, Koyanagi T, Himeno-Ando A, Goto M, Kajio H, Takahashi Y, Izumi Y, Noda M Improvement of glycemic control aft er periodontal treatment by resolving gingival inflammation in type 2 diabetic patients with periodontal disease. J Diabetes Invest 3（4）：402-409, 2012
11. Katagiri S, Nitta H, Nagasawa T, Izumi Y, Kanazawa M,

Matsuo A, Chiba H, Fukui M, Nakamura N, Oseko F, Kanamura N, Inagaki K, Noguchi T, Naruse K, Matsubara T, Miyazaki S, Miyauch T, Ando Y, Hanada N, Inoue S. Effect of glycemic control on periodontitis in type 2 diabetic patients with periodontal disease. J Diabetes Invest（in press）

12. ◎Kobayashi N, Suzuki J, Ogawa M, Aoyama N, Hanatani T, Hirata Y, Nagai R, Izumi Y, Isobe M. Porphyromonas gingivalis accelerates neointimal formation after arterial injury. J Vasc Res. 49（5）：417-424. 2012.
13. Komaki M, Iwasaki K, Arzate H, Narayanan AS, Izumi Y, Morita I. Cementum protein 1（CEMP1）induces a cementoblastic phenotype and reduces osteoblastic differentiation in periodontal ligament cells. Journal of Cellular Physiology 227：649-657,2012
14. Mima A, Hiraoka-Yamomoto J, Li Q, Kitada M, Li C, Geraldes P, Matsumoto M, Mizutani K, Park K, Cahill C, Nishikawa SI, Rask-Madsen C, King GL. Protective Effects of GLP-1 on Glomerular Endothelium and Its Inhibition by PKC β Activation in Diabetes. Diabetes.（Aug 3. [Epub ahead of print] 2012.）
15. Mima A, Kitada M, Geraldes P, Li Q, Matsumoto M, Mizutani K, Qi W, Li C, Leitges M, Rask-Madsen C, King GL. Glomerular VEGF resistance induced by PKC δ /SHP-1 activation and contribution to diabetic nephropathy. The Federation of American Societies for Experimental Biology Journal. 26（7）：2963-74. 2012.
16. Miyazaki H, Oshiro T, Watanabe H, Kakizaki H, Makiguchi T, Kim M, Negishi A, Yokoo S. Ultrasound-guided intralesional laser treatment of voluminous venous malformation in the oral cavity. Int J oral Maxillofac Surg（in press）
17 Nanbara H, Wara-aswapati N, Nagasawa T, Yoshida Y,Yashiro R, Bando Y, Kobayashi H, Khongcharoensuk J,Hormdee D, Pitiphat W, Boch JA, Izumi Y. Modulation of Wnt5a expression by periodontopathic bacteria. PLoS One. 2012;7（4）：e34434. Epub 2012 Apr 2.
18. Rajakaruna GA, Umeda M, Uchida K, Furukawa A, Yuan B, Suzuki Y, Ebe N, Izumi Y, Eishi Y Possible translocation of periodontal pathogene into the lymph nodes draining the oral cavity. J microbiol 50（5）：827-836, 2012
19. ◎Sekinishi A, Suzuki J, Aoyama N, Ogawa M, Watanabe R, Kobayashi N, Hanatani T, Ashigaki N, Hirata Y, Nagai R, Izumi Y, Isobe M. A periodontal pathogen Aggregatibacter actinomycetemcomitans deteriorates pressure overload-induced myocardial hypertrophy in mice. Int Heart J 53（5）：324-330, 2012
20. ◎Takeuchi Y, Nagasawa T, Katagiri S, Kitagawara S, Kobayashi H, Koyanagi T, Izumi Y. Salivary levels of antibacterial peptide（LL-37/hCAP-18）and cotinine in periodontitis patients. J Periodontol 83（6）：766-772, 2012.
21. ◎Taniguchi Y, Aoki A, Mizutani K, Takeuchi Y, Ichinose S, Takasaki AA, Schwarz F, Izumi Y. Optimal Er：YAG laser irradiation parameters for debridement of microstructured fixture surfaces of titanium dental implants. Lasers Med Sci（e-pub Aug 11th, 2012）.

7）総説ならびに著書

総説

1. 和泉雄一. 歯周治療におけるEr：YAGレーザーの応用.日本歯科医師会雑誌, 2012.
2. 須田智也、由利啓子、小田茂. 歯周炎と間違えやすい病変に気づこう　第1回　歯根破折歯科衛生士 2012年1月号P32-35
3. 須田智也、小林宏明、十川裕子、小田茂. 歯周炎と間違えやすい病変に気づこう　第2回　歯内病変 歯科衛生士　2012年3月号P34-38
4. 須田智也、小林宏明、池田実樹子、小田茂. 歯周炎と間違えやすい病変に気づこう　第3回　咬合性外傷　歯科衛生士　2012年4月号　P42―46
5. 谷口陽一、青木章、和泉雄一. Er：YAGレーザーの歯周治療への応用と今後の展望.Medical Photonics No. 9：17-22, 2012.
6. 水谷幸嗣、青木章、谷口陽一、和泉雄一. Er：YAGレーザーによる歯周治療と今後の展望.歯科医療　秋号26（4）：94-101, 2012.

著書

1. Koyanagi T, Takeuchi Y, Taniguchi Y, Izumi Y. Peri-implant disease and bacterial infection. WCOI Year Book 2001 –CD version- 1st Edition, Year Book Committee Publication, World Congress for Oral Implantology, Published in June 25th, Tokyo, Japan, pp26-32, 2012.（Short communication）
2. Taniguchi Y, Aoki A, Koyanagi Y, Takeuchi Y, Izumi Y, Oda S. Current Status of Various Approaches for Treatment of Peri-implant disease. WCOI Year Book 2001 –CD version- 1st Edition, Year Book Committee Publication, World Congress for Oral Implantology, Published in June 25th, Tokyo, Japan, pp33-40, 2012.（Short communication）

3. Yuichi Izumi, Kozue Hasegawa-Nakamura, Kazuyuki Noguchi, Yasushi Furuichi. AT THE FOREFORNT IIIustrated Topics in Dental Research and Clinical Practice Edited by HiromasaYoshie P.27-30 Quintessence publishing Co,Inc発行日：2012年
4. 和泉雄一編、九州インプラント研究会編集 インプラント治療と医療安全 チーム医療としての安全•安心マニュアル;歯周手術時のキュレットの破折 p.60 医学情報社発行日：2012年2月24日
5. 和泉雄一、秋月達也. 歯周治療と患者の全身状態 日歯医学誌102-105、2012 発行：日本歯科医学会 発行日：2012年3月31日
6. 和泉雄一、荒川真一. 歯周病学領域の国際交流 日歯医師誌 105-107,2012 発行：日本歯科医師会 発行日：2012年4月10日
7. 谷口陽一、青木章、和泉雄一. Er：YAGレーザーの歯周治療への応用と今後の展望 Medical Photonics p.17-22 発行：オプトロニクス社 発行日：2012年4月20日
8. 和泉雄一.天野敦雄、岡堅二、村上伸也 監修 ビジュアル：歯周病を科学する p.47-64 クインテッセンス出版株式会社 発行日：2012年5月10日
9. 片桐さやか、和泉雄一. CLINICAL CALCIUM 1 vol.22 No.1 p.49-55、2012 医薬ジャーナル社
10. 和泉雄一. 歯周治療におけるEr：YAGレーザーの応用 日歯医師誌 84-87,2012
11. 和泉雄一. 連載 8020運動の新たな展開を目指して 口腔の機能と全身の健康 社会保険旬報No.2497 p.20-21 発行：社会保険研究所 発行日：2012年6月1日
12. 和泉雄一. 連載 8020運動の新たな展開を目指して 歯周病をめぐる新たな発見 社会保険旬報No.2500 p.24-25 発行：社会保険研究所 発行日：2012年7月1日
13. 和泉雄一、秋月達也. 編集委員;五十嵐順正、岡崎完司、馬場一美、谷田部優 患者に喜ばれるパーシャルデンチャー p.28-31 デンタルダイヤモンド社 発行日：2012年7月1日
14. 和泉雄一、荒川真一編 鴨井久一、芝燁彦 編著 機能水ではじめるヒトと環境に優しい歯科臨床 p.13,22,27-28 砂書房 発行日：2012年9月25日
15. 青木章/和泉雄一 編著 シリーズ@よくわかる歯科用レーザー120%活用術 総ページ数：134ページデンタルダイヤモンド社発行日：2012年10月1日
16. 和泉雄一、青山典生 心血管病と歯周病との関わり 呼吸と循環 第60巻第11号1137-1143、2012年11月15日発行 医学書院
17. 和泉雄一、二階堂雅彦、松井徳雄 編著 成功する歯周組織再生治療 —歯を保存するために— 歯界展望別冊：医歯薬出版株式会社 総ページ数：180ページ 発行日：2012年11月20日
18. 和泉雄一、荒川真一編 伊藤隆利 編集代表 九州インプラント研究会（KIRG）長期経過症例から学ぶ 成功するインプラント治療戦略補綴臨床 別冊 p.128-131医歯薬出版株式会社 発行日：2011年12月25日
19. 青木章、和泉雄一 編著. 歯科用レーザー120%活用術.デンタルダイアモンド社,東京,134 pages,2012.

8）平成24年度までの自己評価

今年度の研究課題についてはほぼ予定通りの進行を示している。また、研究拠点体制作りでは、タイのKhon Kaen大学のNawarat W Charoen歯学部長とのコラボレーションが順調に進んでいる。

9）和文原著論文

1. 塩山秀裕、水谷幸嗣、須田智也、田中敬子、青山典生、藤原、高橋香、秋月達也、竹内康雄、小林宏明、木下淳博、小田茂、和泉雄一、エムドゲイン®ゲルを用いた先進医療「歯周外科治療におけるバイオ・リジェネレーション法」の治療成績.日歯保存誌 55（1）：22-29, 2012.
2. 高森一乗、青木章、加藤純二、永井茂之、吉田格、大浦教一、和賀正明、天谷哲也、田上順次、篠木毅、日本レーザー歯学会第3回歯科用レーザー安全講習会報告-アンケート調査分析ならびに過去2回の講習会との比較.日レ歯誌23（1）：20-26, 2012.

10）学会発表（英文）

1. Aoyama N, Suzuki J, Ogawa M, Watanabe R, Kobayashi N, Hanatani T, Ashigaki N, Sekinishi A, Isobe M, Izumi Y. Porphyromonas gingivalis promotes abdominal aortic aneurysm with increased systemic inflammation. oral presentation. 2013 IADR General Session, March 20-23, 2012. Seattle, USA.
2. Koyanagi T, Takeuchi Y, Maruyama N, Shiba T, Izumi Y. Analysis of microbiota compared peri-implantitis with periodontitis. EURO PERIO 7（Vienna, Austria）

2012.6.6-9
3. Nanbara H, Wara-aswapati N, Yoshida Y, Nagasawa T, Kobayashi H, Izumi Y. Wnt5a expression by Porphyromonasgingivalis LPS via NF- κ B and STAT1. EuroPerio7, Vienna, 2012. 6. 6-9.
4. Mizutani k, Jeong IK, Mima A, Li Q, Park K, Rask-Madsen C, Mooney DJ, King GL. Angiogenic dysfunction by protein kinase C- β induced insulin resistance in diabetic mesenchymal stem cell. The 72nd Scientific Sessions of the American Diabetes Assocation, Philadelphia,USA. 2012.6.9.
5. Mizutani K, Akira Mima A, Kyoungmin Park K, King G. Obesity causes insulin resistance in gingival tissue via PKC activation and oxidative stress. American Acadent of Periodontology 98th Annual Meeting、Los Angels, USA. 2012.9.30.
6. Sawabe M, Aoki A, Komaki M, Iwasaki K, Ogita M, Izumi Y. Gingival healing following Er：YAG laser ablation vs electrosurgery in rats. The 13th congress of the World Federation for lasers Dentistry, Barcelona, April 26-28, 2012.
7. Pavlic V, Aoki A, Vujic-Aleksic V, Izumi Y. Low-level laser therapy in bone repair：a literature review. The 13th congress of the World Federation for lasers Dentistry（WFLD）, Barcelona, April 26-28, 2012.
8. Rosa DSA, Aranha ACC, Eduardo CP, Aoki A. Esthetic Treatment of Gingival Melanin Hyperpigmentation with Er：YAG laser. Fourty-eight months of patient follow-up. The 13th congress of the World Federation for lasers Dentistry（WFLD）, Barcelona, April 27（26-28）, 2012.
9. Tsubokawa M, Aoki A, Taniguchi Y, Sawabe M, Ejiri K, Akizuki T, Oda S, Mizutani K, Sumi Y, Izumi Y. Detection of subgingival calculus using optical coherence tomography. JSP/JACP Poster Session, 98th Annual Meeting American Academy of Periodontology in collaboration with the Japanese Society of Periodontology, Los Angeles, Sep 29- Oct 2, 2012.
10. Taniguchi Y, Aoki A, Sakai K, Mizutani K, Izumi Y. A novel surgical procedure of Er：YAG laser-assisted periodontal regenerative therapy. JSP/JACP Poster Session, 98th Annual Meeting American Academy of Periodontology in collaboration with the Japanese Society of Periodontology, Los Angeles, Sep 29- Oct 2, 2012.
11. Pavlic V, Aoki A, Iwasaki K, Izumi Y. Effect of Er：YAG laser on proliferation of osteoblasts. Congress "Dentistry Today" in BIH with International participation. Teslic, Banja Vrucica, Bosnia and Herzegobina, Oct 19-20, 2012.
12. Matuura T, Akizuki T, Hoshi S, Kinoshita A, Sunaga M, Ikawa T, Imamura R, Kimura M, Kuboki Y, Izumi Y. Periodontal tissue regeneration using random tunnel beta-TCP ceramics in dogs. 98th Annual meeting American academy of periodontology collaboration with the Japanese society of periodontology. 2012. 9. 29. – 10.2. Los Angeles Convention Center. General poster session. p19.
13. Tsubokawa M, Aoki A, Taniguchi Y, Sawabe M, Ejiri K, Akizuki T, Oda S, Mizutani K, Sumi Y, Izumi Y. Detection of subgingival calculus using optical coherence tomography. 98th Annual meeting American academy of periodontology collaboration with the Japanese society of periodontology. 2012. 9.29. – 10.2. Los Angeles Convention Center. General poster session. p22.
14. Tsumanuma Y, Iwata T, Kinoshita A, Washio K, Yoshida T, Yamada A, Ishikawa I, Yamato M, Okano T, Izumi Y. Allogeneic transplantation of periodontal cell sheets in canine horizontal defects. 98th Annual Meeting American Academy of Periodontology in collaboration with Japanese Society of Periodontology. Los Angeles, USA, 2012.9.29-10.2.
15. Ye C, Katagiri S, Bharti P, Kobayashi H, Takeuchi Y, Nagasawa T, Izumi Y. The role of periodontal bacteria onantiphhospholipid syndrome and preterm low birth weight. Japan-China Dental Conference 2012 （2012.4.27, Sichuan, China）
16. Takeuchi Y, Nagasawa T, Katagiri S, Kitagawara S, Kobayashi H, Koyanagi T, Izumi Y. Salivary levels of antibacterial peptide（LL-37/hCAP-18）and cotinine in periodontitis patients. Europerio 7（2012. 6. 6-9, Vienna, Austria）
17. Koyanagi T, Takeuchi Y, Maruyama N, Shiba T, Izumi Y.Analysis of microbiota associated with peri-implantitis. Europerio 7（2012. 6. 6-9, Vienna, Austria）
18. Bharti P, Katagiri1 S, Ye C, Kobayashi H, Takeuchi Y, Nagasawa T, Izumi Y. Expression of CD14, CD16 and CD45 on monocytes from aggressive periodontitis patients. Europerio 7（2012. 6. 6-9, Vienna, Austria）
19. Ye C, Katagiri S, Bharti P, Kobayashi H, Takeuchi Y, Nagasawa T, Izumi Y The role of antibodies against periodontal pathogen on preterm birth. The 98th Annual Meeting of the American Academy of Periodontology（2012.9.29-10.2, Los Angeles, USA
20. Chui C, Aoki A, Hiratsuka K, Takeuchi Y, Sasaki Y, Abiko Y, Izumi Y. Antimicrobial Effect of a-PDT using high power blue LED and red dye agent on Porphyromonas gingival is. The Academy of Laser Dentistry's 20th Annual Conference and Exhibition.（2013.2.7-9, Palm Springs, USA）
21. Watanabe H, Belal MH, Ishikawa I, Izumi Y. PDGF-BB combined with EDTA promotes PDL cell adhesion and proliferation. The 98th Annual Meeting of the American

Academy of Periodontology（2012.9.29-10.2, Los Angeles, USA

22. Watanabe H, Wang H, Ogita M, Izumi Y. Effect of human beta defensin-3 on proliferation of fibroblasts onto periodontal involved root surfaces. EuroPerio7, Vienna, 2012. 6. 6-9.

11）学会発表（和文）

1. 谷口陽一、青木章、市野瀬志津子、竹内康雄、和泉雄一． インプラント体マイクロストラクチャーのデブライドメントへの高ヘルツEr：YAGレーザーの応用―デブライドメントにおける適正出力の検討.口腔先端応用医科学研究会第4回学術会議,日本大学歯学部,東京,2012.1.21-22.
2. 江黒徹、青木章、山内由隆、山口将日、簗瀬武史. インプラント治療におけるEr：YAGレーザーを用いたハードティッシュマネージメント.日本口腔インプラント学会　第31回関東甲信越部学術大会, 東京.2012.2.11-12.
3. 荻田真弓、土田祥央、青木章、佐藤守、澤辺正規、小林宏明、竹内康雄、野村文夫、和泉雄一． 低出力Er：YAGレーザー照射後にヒト歯肉線維芽細胞から産生されるタンパク質のプロテオーム解析.第55回春季日本歯周病学会学術大会,札幌,2012. 5. 18-19.
4. 江尻健一郎、青木章、山口洋子、大島光宏、和泉雄一：低出力半導体レーザー照射が培養ヒト歯肉上皮細胞に及ぼす効果. 第136回日本歯科保存学会春季学術大会.2012.6.28-29, 沖縄.
5. 坪川正樹、青木章、谷口陽一、江尻健一郎、澤辺正規、荻田真弓、野田昌宏、水谷幸嗣、秋月達也、小田茂、角保徳、和泉雄一． 光干渉断層画像診断法（OCT）を用いた歯周組織の観察とその治療への応用.日本歯周病学会　2012秋季学術大会（第55回）.つくば国際会議場,つくば市,2011.9.23.
6. 田中敬子、青木章、竹内康雄、和泉雄一.前歯部の審美性を考慮した慢性歯周炎の一症例.日本歯周病学会　2012秋季学術大会（第55回）.つくば国際会議場,つくば市,2011.9.23.
7. 青木章、坪川正樹、水谷幸嗣、谷口陽一、江尻健一郎、澤辺正規、荻田真弓、秋月達也、小田茂、角保徳、和泉 雄一． 波長走査型光干渉断層画像装置（SS-OCT）の歯周組織診断への応用.第22回日本歯科医学会総会,大阪,2012.11.9-11.
8. Chui C, Aoki A, Takeuchi Y, Sasaki Y, Hiratsuka K, Abiko Y, Izumi Y. Antimicrobial effect of a-PDT using high power blue LED and red dye agent on Porphyromonas gingivalis. 第22回日本歯科医学会総会,大阪,2012.11.9-11.
9. 水谷幸嗣、青木章、和泉雄一． Er：YAGレーザーの歯周治療への応用.第22回日本歯科医学会総会,大阪,2012.11.9-11.
10. 澤辺 正規、青木章、小牧基浩、岩崎剣吾、荻田真弓、和泉雄一． Er：YAGレーザーおよび電気メスによる歯肉処置後の歯周組織の創傷治癒の比較.第137回日本歯科保存学会2012年度秋季学術大会,広島,2012.11.22-23.
11. Chui C, Hiratsuka K, Aoki A, Takeuchi Y, Abiko Y, Izumi Y. Blue LED inhibits the growth of Porphyromonas gingivalis by suppressing the expressions of genes associated with DNA replication and cell division. 第24回日本レーザー歯学会総会・学術大会.神戸,2012.12.1-2.
12. 江尻健一郎、青木章、山口洋子、大島光宏、和泉雄一． 低出力半導体レーザー照射が初代培養ヒト歯肉上皮細胞に及ぼす効果. 第24回日本レーザー歯学会総会・学術大会.神戸,2012.12.1-2.
13. 江尻健一郎、青木章、山口洋子、大島光宏、和泉雄一：最新光歯科治療, 光歯科治療友の会, 東京,2012.7.29.
14. 江尻健一郎、青木 章、山口洋子、大島光宏、和泉雄一：最新光歯科治療, 光歯科治療友の会, 仙台,2012.8.5.
15. 青木章、歯周病のトレンド：歯周病とレーザー.確実に治せる歯周治療へのアプローチ,HDM学術研修会,東京,2012.9.9.
16. 水谷幸嗣、青木章、和泉雄一． Er：YAGレーザーの歯周治療への応用. 第22回日本歯科医学総会.テーブルクリニック、大阪、2012.11.9.
17. 若松美江、藤川佳奈、竹内康雄、小林宏明、片桐さやか、高松秀行、須田智也、田中敬子、塩山秀裕、和泉雄一． ポスター発表;ドーム型歯ブラシのプラーク除去効果　第137回平成24年度秋季学術大会
18. 塩山秀裕、水谷幸嗣、須田智也、田中敬子、青山典生、藤原―高橋香、遠藤亜希子、山脇史寛、楠侑香子、木下淳博、小田茂、和泉雄一． ポスター発表;エムドゲイン®ゲルを用いた先進医療「歯周外科治療におけるバイオ・リジェネレーション法」の臨床評価　第22回日本歯科医学会総会
19. 塩山秀裕． 慢性歯周炎患者に先進医療としてエムドゲイン®ゲルを用いた歯周組織再生療法を適応した一症例.第55回春季日本歯周病学会学術大会

（2012.5.17-19. 札幌）
20. 塩山秀裕、水谷幸嗣、須田智也、青山典生、楠侑香子、木下淳博、荒川真一、小田茂、和泉雄一． 先進医療「歯周外科治療におけるバイオ・リジェネレーション法」の臨床評価.第77回口腔病学会学術大会（2012.11.30-12.1東京）
21. 清水雅美、秋月達也、小田茂、十川裕子、難波佳子、足達淑子、和泉雄一：GCF中のAST量測定キットを用いて歯周組織をモニタリングした1症例,第55回春季日本歯周病学会学術大会,日本歯周病学会誌 vol.54 春季特別号, p.69,176 2012年5月17-19日,5月19日ポスター,札幌
22. 松浦孝典、秋月達也、星崇、井川貴博、木下淳博、須永昌代、木村満利子、久保木芳徳、和泉雄一． ランダムトンネル型β‐TCPを用いた歯周組織再生―イヌ下顎1壁性骨欠損における組織学的評価―, 特定非営利活動法人日本歯科保存学会2012年度春季学術大会（第136回）, 特定非営利活動法人日本歯科保存学会2012年度春季学術大会（第136回）プログラム および講演抄録集, p79, 2012年6月28-29日， 6月29日口演, 宜野湾市 沖縄コンベンションセンター.
23. 星崇、秋月達也、松浦孝典、今村亮祐、小田茂、松井誠、田畑泰彦、和泉雄一． β‐TCP含有ハイドロゲルを用いた歯周組織再生イヌ上顎根分岐部骨欠損における組織学的評価―a pilot study―, 特定非営利活動法人日本歯科保存学会2012年度春季学術大会（第136回）, 特定非営利活動法人日本歯科保存学会2012年度春季学術大会（第136回）プログラム および講演抄録集, p78, 2012年6月28-29日， 6月29日口演, 宜野湾市 沖縄コンベンションセンター.
24. 井川貴博、秋月達也、松浦孝典、星崇、今村亮祐、木下淳博、須永昌代、木村満利子、久保木芳徳、和泉雄一． ランダムトンネル型β‐TCPによるソケットプリザベーション―犬でのパイロットスタディー―． 第55回秋季日本歯周病学会学術大会, 日本歯周病学会会誌. Vol.54, 秋季特別号, p85, 2012年9.22-23日, 9月23日ポスター発表, 茨城県, つくば国際会議場.
25. 葉暢暢、片桐さやか、バルティ パリクシャ、小林宏明、竹内康雄、長澤敏行、和泉雄一. 早産・低体重児出産における歯周病に起因したβ2glycoprotein-Iを認識する抗体の役割 第55回春季日本歯周病学会学術大会（2012.5.17-19. 札幌）
26. 妻沼有香、岩田隆紀、鷲尾薫、葭田敏之、山田梓、大和雅之、石川烈、岡野光夫、和泉雄一． 歯周組織再生における異なる組織由来細胞シートの比較. 第55回春季日本歯周病学会学術大会（2012.5.17-19. 札幌）
27. Kobayashi N, Suzuki J, Ogawa M, Aoyama N, Hanatani T, Ashigaki N, Yoshida A, Hirata Y, Nagai R, Izumi Y, Isobe M. A periodontal pathogen promotes neointimal formation after arterial injury with enhanced expression of matrix metalloproteinase-2 第76回日本循環器学会学術集会（福岡）2012年3月18日poster session
28. 小林宏明、竹内まや、竹内康雄、岩崎剣吾． 年に一度の診察が7年間続いた症例
第55回日本歯周病学会春季学術大会（札幌） 平成24年5月19日発表
29. 須田智也、小林宏明、竹内康雄、秋山俊治、高野琢也、和泉雄一． 超音波スケーリング時におけるスーパーシール®の知覚過敏抑制効果第55回日本歯周病学会秋季学術大会（つくば） 平成24年9月23日発表
30. 早雲彩絵、荒川真一、眞野喜洋、吉仲由之、稲垣好雄、和泉雄一． オゾンナノバブル水の抗菌・抗ウイルス活性. 第13回日本口腔機能水学会学術大会, 東京、2012年3月24日・25日
31. 早雲彩絵、荒川真一、和泉雄一． 第14回日本口腔機能水学会学術大会、札幌、2013年3月23日・24日）
32. Maruyama N, Maruyama F, Takeuchi Y, Koyanagi T, Nakagawa I, Izumi Y. Comparison of the microbiota in peri-implantitis and periodontitis using pyrosequence. 第60回国際歯科研究学会日本部会（JADE）総会・学術大会（新潟） 平成24年12月14-15日発表
33. 津久井明、渡辺久：Er：YAGレーザーによる根面被覆の臨床評価.第24回日本レーザー歯学会総会・学術大会.神戸,2012.12.1-2.
34. 渡辺久． 歯周外科手術へのレーザーの応用―その基礎と臨床.第22回日本歯科医学総会.テーブルクリニック、大阪、2012.11.9.
35. 沼部幸博、渡辺久、和泉雄一、伊藤弘． 歯肉溝滲出液迅速診断キットによる歯周組織のモニタリング.第22回日本歯科医学総会.テーブルクリニック、大阪、2012.11.9.
36. 伊藤弘、関野愉、村樫悦子、井口一美、橋本修一、沼部幸博、佐々木大輔、八重柏隆、國松和司、高井英樹、目澤優、小方頼昌、渡辺久、萩原さつき、和泉雄一、廣島佑香、木戸淳一、永田俊彦． GCFを

用いた歯周病罹患部位の診断と治療効果のモニタリングの有用性―歯周病迅速診断キット開発に向けて―第22回日本歯科医学総会．ポスター、大阪、2012.11.9.

37. 伊藤弘,関野愉、村樫悦子、井口一美、橋本修一、沼部幸博、佐々木大輔、八重柏隆、國松和司、高井英樹、目澤優、小方頼昌、渡辺久、萩原さつき、和泉雄一、廣島佑香、木戸淳一、永田俊彦．歯肉溝滲出液（GCF）を用いた歯周病罹患部位の診断と治療効果のモニタリングの有用性―歯周病迅速診断キット開発に向けて―（第4報）.日本歯周病学会　2012秋季学術大会（第55回）.つくば国際会議場,つくば市,2011.9.23.
38. 伊藤弘、関野愉、村樫悦子、井口一美、橋本修一、沼部幸博、佐々木大輔、八重柏隆、國松和司、高井英樹、目澤優、小方頼昌、渡辺久、萩原さつき、和泉雄一、廣島佑香、木戸淳一、永田俊彦．歯肉溝滲出液（GCF）を用いた歯周病罹患部位の診断と治療効果のモニタリングの有用性―歯周病迅速診断キット開発に向けてー（第5報）.第137回日本歯科保存学会2012年度秋季学術大会,広島,2012.11.22-23.

12）外部資金の獲得状況

1. 和泉雄一（代表）、小林宏明、竹内康雄、片桐さやか（分担）：歯周病由来の自己抗体による早産・低体重児出産への影響、挑戦的萌芽、平成24-25年度、
2. 青木章（代表）、小林宏明、竹内康雄、秋月達也、水谷幸嗣（分担）：光エネルギーを応用した歯周炎およびインプラント周囲炎の革新的治療法・予防法の開発.科学研究費補助金　基盤研究（C）22592308 平成22～24年度.
3. 小林宏明（分担）：医学歯学教育における術者目線3Dムービー作成・供覧・遠隔指導システムの開発と評価、基盤研究（C）、平成24-26年度、代表：須永昌代
4. 小林宏明（分担）：タイムコントロールーサイトカインカクテルによる歯周組織再生療法の開発、基盤研究（C）平成24-26年度、代表：小田茂
5. 秋月達也（代表）：石灰化歯根膜シートと人工ペプチドを使用した歯周組織再生．科学研究費補助金,若手研究（B）23792465　平成23～25年度.
6. 片桐さやか（代表）：糖尿病患者の血管新生緑内障における歯周病由来抗 cardiolipin抗体の役割. 科学研究費補助金,若手研究（B）平成23～24年度.
7. 江部典子（代表）：歯周炎における酸化ストレス条件下でのTrx1とTxnipの役割の解析　科学研究費補助金,研究活動スタート支援 23890058平成23～24年度.
8. 妻沼有香（代表）：日本学術振興会　特別研究員（PD）「歯根膜細胞移植における脈管系ならびに神経組織の再生機序の解明」（平成24～25年度）
9. 山田梓（代表）：日本学術振興会　特別研究員（DC2）「ヒト歯根膜細胞の骨芽細胞分化におけるWNT関連遺伝子発現」（平成23～24年度）
10. 青山典生（代表）：歯周病による大動脈瘤形成促進機序の解明　科学研究費補助金,研究活動スタート支援 平成23～24年度 研究費総額：338万円
11. 早雲彩絵（代表）：新規の機能水が細菌バイオフィルムおよび宿主の免疫系に及ぼす効果の検討　科学研究費補助金、研究活動スタート支援 平成24～25年度 研究費総額：156万円
12. 津野顕子（分担）、伊藤俊之（代表）：抗菌光線力学的療法を用いた新たな口腔ケアの手法の開発と評価 厚生労働省　国際医療研究開発費24指116
13. 藤原香（代表）：コンパニオンアニマルにおける歯周病原細菌の検索と飼い主との相互感染について　奨励研究　研究課題番号：23932008　2012年度：60万円
14. 片桐さやか：一般財団法人　サンスター歯科財団：金田博夫研究助成金　平成24年度ー25年度
15. 和泉雄一：新規ビスフォスフォネート歯周病治療薬の局所投与試験．受託研究.昭和薬品化工株式会社（平成21～24年度）
16. 和泉雄一、渡辺久：歯周病迅速診断キットの開発に向けた歯肉溝滲出液（GCF）成分を用いた歯周病罹患部位の診断と治療効果のモリタリングの有用性に関する研究II. 依託研究　日本歯科医師会（平成23～24年度）

13）特別講演、招待講演、シンポジウム

[招待講演]

1. 和泉雄一：歯周病と糖尿病-その密接な関係、日本産業衛生学会産業歯科保健部会後期研修会、関東地方会例会・関東産業歯科保健部会研修会、(2012.2.4. 東京)
2. 和泉雄一：再生医療の最前線　-歯周外科の限界を探る-　Ⅱ歯周外科治療の現況と展望、第54回福岡県西地区歯科医学会、(2012.2.19. 福岡)
3. 和泉雄一：あなたのお口は大丈夫？　-本当は怖い歯周病の脅威-、三重県歯科医師会公開講座、(2012.2.26. 三重)
4. 和泉雄一：現代歯周治療のスタンダード、平成23年

度三重県歯科医師会学術研修会、(2012.2.26. 三重)
5. 和泉雄一：臨床と基礎の接点　歯周治療における基礎と臨床、平成23年度日本歯科大学大学院生命歯学研究科セミナー、(2012.3.8. 東京)
6. 和泉雄一：天然歯とインプラント、平成24年度九州インプラント研究会、(2012.4.22.熊本)
7. 和泉雄一：歯周治療の進め方と歯周外科治療、2012年度日本インプラント臨床研究会、(2012.6.16. 東京)
8. 和泉雄一：口腔ケアの底ヂカラ、第6回かながわお口の健康フォーラム、(2012.7.1. 神奈川)
9. 和泉雄一：歯周病と循環器疾患の連関、医科歯科連関研究会2012、(2012.7.23. 東京)
10. 和泉雄一：ここまで出来る歯周治療、平成24年度千葉県歯科医師会ブロック別研修会、(2012.7.29. 千葉)
11. Yuichi Izumi：Modern Periodontal Treatment and Periodontal Tissue Regeneration. The 18th Anniversary Faculty of Dentistry, SWU. (2012.8.24. Bangkok)
12. 和泉雄一：歯周病と糖尿病の深い関係、第15回日本臨床腸内微生物学会、(2012.9.1. 東京)
13. Yuichi Izumi：Clinical application of Er：YAG laser in periodontal therapy. The 106th Session of Integrated Presentation of GCOE Program. (2012.9.10. 本学)
14. 和泉雄一：サポーティブペリオドンタルセラピー(SPT)期のリスクマネジメント、シンポジウムⅠ「歯周炎の再発リスクは予測できるか」、第55回秋季日本歯周病学会学術大会、(2012.9.23. 茨城)
15. Yuichi Izumi：Clinical application of Er：YAG laser in periodontal therapy. American Academy of Periodontology, 98th Annual Meeting in Los Angeles, CA, (2012.9.30. Los Angeles, CA)
16. 和泉雄一：歯周治療は歯科の華　-全身とのかかわりから-、東京医科歯科大学歯科同窓会CDE、(2012.10.14. 神戸)
17. 和泉雄一：歯科再生治療最前線、平成24年度九州インプラント研究会、(2012.10.21.熊本)
18. 和泉雄一：口腔ケアの底ヂカラ、群馬県歯科医師会県民公開講座、(2012.10.28. 群馬)
19. 和泉雄一：糖尿病と歯周病の密接な関係、第27回日本糖尿病合併症学会、(2012.11.3. 福岡)
20. 和泉雄一：糖尿病と歯周病の深い関係、第3回千葉糖尿病合併症勉強会、(2012.11.5. 千葉)
21. 和泉雄一：糖尿病の第6の合併症：歯周病、第22回糖尿病診療-最新の動向医師・医療スタッフ向け研修会、(2012.11.18 岡山)
22. 青木章.臨床実践セミナー：Er：YAGレーザーを用いた歯周・インプラント周囲治療.第55回春季日本歯周病学会学術大会,札幌,2012. 5.18-19.
23. 青木章.歯周炎・インプラント周囲炎治療におけるEr：YAGレーザーの効果的応用法.第15回Er：YAGレーザー臨床研究会,東京,2012.8.5.
24. Aoki A. Current Clinical Applications of Er：YAG Laser in Periodontal and Peri-implant Therapy. The 13th congress of the World Federation for Lasers Dentistry (WFLD), Barcelona, April 26-28, 2012.
25. Aoki A. Current Er：YAG laser applications in periodontal and peri-implant therapy. Congress "Dentistry Today" in BIH with International participation. Teslic, Banja Vrucica, Bosnia and Herzegobina, Oct 19-20, 2012.
26. 藤原香：パネルディスカッション歯科part1「歯が折れてしまいました!さあ、どうしよう」犬と猫の破折歯の疫学的特徴　第33回動物臨床医学会年次大会　大阪　2012年11月16-18日
27. 青山典生.パネルディスカッション・心血管疾患発症進展における遺伝・環境的要因「歯周病と心血管疾患の関連　マルファン症候群患者における観察とマウス大動脈瘤モデルでの検討」第60回日本心臓病学会学術集会　金沢、2012年9月16
28. 青山典生.歯周病と循環器疾患の関連を解き明かす「歯周病と循環器疾患の関連を基礎研究から解明する」医科歯科連関研究会2012　東京、2012年7月23日
29. 青山典生.シンポジウム・冠動脈二次予防としての禁煙指導と歯周病治療の取り組み「歯周病菌感染による血管リモデリングの増悪　マクロライドの効果と2次予防の可能性」第21回日本心血管インターベンション治療学会学術集会　新潟、2012年7月14日
30. Aoyama N. Academic Symposium：Clinical Research, "Influence of Periodontal Infection on Circulative Disorders" The 2nd Tri-University Consortium on Oral Science and Education (2012.7.27, Beijing, china)
31. 水谷幸嗣. Er：YAGレーザーによる歯周治療-レーザー治療が歯周組織の治癒に与える影響-. 第24回日本レーザー歯学会総会・学術大会、神戸、2012.12.2.
32. Mizutani K. Brigham and Women's Hospital cardiovascular disease and metabolism seminar

series （2012.4.4 Boston, MA,USA）
33. Mizutani K. Joslin Diabetes Center Tuesday seminar series （2012.2.7. Boston, MA, USA）

［講演会・セミナー主催］

1. 第13回口腔機能水学会学術大会、（2012.3.24-25. 東京）
2. Yuichi Izumi：Tokyo Medical and Dental University, The 7th Global COE International Symposium, Molecular Science in Oral-Systemic Medicine –Autumn Seminar-,（2012.11.12-14. 本学）
3. Yuichi Izumi：Tokyo Medical and Dental University, The 8th Global COE International Symposium, Molecular Science in Oral-Systemic Medicine –Winter Seminar-,（2013.2.3-4. 本学）

14）新聞、雑誌、TV報道

（テレビ出演）

1. 和泉雄一.たけしのエンターテインメント!みんなの家庭の医学 あなたの県は第何位?大発見!全国都道府県別 健康長寿の秘密!O.A.：2012年8月14日
2. 和泉雄一・秋月達也. 健康カプセル!ゲンキの時間 ～臭うほどに要注意!～意外と怖い“歯周病”の真実. 平成24年10月21日OA TBS.

（その他）

1. 和泉雄一.Newton 別冊 体のしくみと病気 症状と病気,その対処法と治療法 p.80-85 株式会社 ニュートンプレス 発行日：2012年5月15日
2. 和泉雄一監修 病に備えるセルフチェック•セルフケア術 歯周病 SALUTE 2012 8/9月号p.7-8 発行：株式会社 星和ビジネスサポート
3. 和泉雄一.特集 意外に知らない健康情報 歯にいい話 健幸手帖 2012年 春 第17号 p.2-5 発行：株式会社 日本医食研究所
4. 和泉雄一.インタビュー 歯周病と早産•低体重児のリスク 月刊 母子保健 2012年6月号 p.1-3 発行日：2012年6月1日
5. 和泉雄一.特集 知っておきたい歯科のこと Asahi medical 2012年2月号 p.16-17 発行日：2012年2月1日
6. 梶村幸市、和泉雄一、菊池重成、中里良次.歯周基本治療における動揺固定の臨床 GC CIRCLE p.4-11 発行：株式会社 GC 発行日：2012年11月10日
7. 和泉雄一.26章 歯周病塚崎朝子 著「いつか罹る病気に備える本 100の病気への不安が軽くなる基礎知識」p.107-110 講談社 発行日 2012年11月20日
8. 和泉雄一.月刊 糖尿病ライフ さかん 12月号 新• 歯科医師からのメッセージ p.22-23 2012 vol.52 No.12 編集• 発行 （社）日本糖尿病協会
9. 和泉雄一.歯周治療におけるEr：YAGレーザーの応用. 平成23年度日歯生涯研修ライブラリー（DVD）シリーズNo.1101～1108 企画;日本歯科医師会 制作;（株）学研教育出版 発行日：2012年3月31日
10. 青木章.暮らしと健康相談室 Question 4.慢性歯周病：膿がたまるたびに切開.レーザー治療は行なえないか? 暮らしと健康,保健同人社,March 2012, 3月号p.76

15）教室、分野や講座の准教授、講師、助教、特別研究員、ポスドク、指導を受けた大学院生の名前

准教授　渡辺　久
講師　萩原　さつき
　　青木　章
助教　荒川　真一（～8月まで）、小林　宏明
　　竹内　康雄、秋月　達也
　　片桐さやか（～4月まで）
　　水谷　幸嗣（7月～）
大学院　○ Aslam AL Mehdi
　　○ GA Rajakaruna
　　○ Bharti Pariksha、高橋　茉莉香
　　妻沼　有香、澤辺　正規
　　○ 山田　梓、小林　奈穂
　　藤原　香、花谷　智哉
　　伊藤　康夫、江尻　健一郎
　　○ Chui Chanthoel、吉田　明日香
　　池田　裕一、木村　康之
　　遠藤　亜希子
　　○ 芦垣　紀彦、丸山　緑子
　　○ 荻田　真弓、津野　顕子
　　芝　多佳彦
　　○ Supreda Suphanantachat
　　○ 葉　暢暢、小沼　邦葉
　　前川　祥吾、松浦　孝典

星　　嵩、赤澤　恵子
遠井　政行、野田　昌宏
始平堂　由佳、御給　美沙
上窪　彩乃、井川　貴博
鬼塚　　理、金子　　誠

（○：AISS）

16）GCOE活動についての感想、コメント、改善を望む点

若手研究者の育成には大いなる成果が認められ、また、国際交流の点でも着実に成果を上げつつある。今後、何らかの形で継続することを希望する。

Lasers Med Sci
DOI 10.1007/s10103-012-1171-7

ORIGINAL ARTICLE

Optimal Er:YAG laser irradiation parameters for debridement of microstructured fixture surfaces of titanium dental implants

Yoichi Taniguchi · Akira Aoki · Koji Mizutani · Yasuo Takeuchi · Shizuko Ichinose · Aristeo Atsushi Takasaki · Frank Schwarz · Yuichi Izumi

Received: 1 February 2012 / Accepted: 16 July 2012

Abstract Er:YAG laser (ErL) irradiation has been reported to be effective for treating peri-implant disease. The present study seeks to evaluate morphological and elemental changes induced on microstructured surfaces of dental endosseous implants by high-pulse-repetition-rate ErL irradiation and to determine the optimal irradiation conditions for debriding contaminated microstructured surfaces. In experiment 1, dual acid-etched microstructured implants were irradiated by ErL (pulse energy, 30–50 mJ/pulse; repetition rate, 30 Hz) with and without water spray and for used and unused contact tips. Experiment 2 compared the ErL treatment with conventional mechanical treatments (metal/plastic curettes and ultrasonic scalers). In experiment 3, five commercially available microstructures were irradiated by ErL light (pulse energy, 30–50 mJ/pulse; pulse repetition rate, 30 Hz) while spraying water. In experiment 4, contaminated microstructured surfaces of three failed implants were debrided by ErL irradiation. After the experiments, all treated surfaces were assessed by stereomicroscopy, scanning electron microscopy (SEM), and/or energy-dispersive X-ray spectroscopy (EDS). The stereomicroscopy, SEM, and EDS results demonstrate that, unlike mechanical treatments, ErL irradiation at 30 mJ/pulse and 30 Hz with water spray induced no color or morphological changes to the microstructures except for the anodized implant surface, which was easily damaged. The optimized irradiation parameters effectively removed calcified deposits from contaminated titanium microstructures without causing substantial thermal damage. ErL irradiation at pulse energies below 30 mJ/pulse (10.6 J/cm^2/pulse) and 30 Hz with water spray in near-contact mode seems to cause no damage and to be effective for debriding microstructured surfaces (except for anodized microstructures).

Keywords Er:YAG laser · High pulse repetition rate · Implant · Peri-implantitis · Titanium · Microstructure

Y. Taniguchi (✉) · A. Aoki (✉) · K. Mizutani · Y. Takeuchi · Y. Izumi
Department of Periodontology, Graduate School of Medical and Dental Sciences, Tokyo Medical and Dental University,
1-5-45 Yushima,
Bunkyo-ku, Tokyo 113-8549, Japan
e-mail: taniperi@tmd.ac.jp
e-mail: aoperi@tmd.ac.jp

S. Ichinose
Instrumental Analysis Research Center for Life Science,
Tokyo Medical and Dental University,
Tokyo, Japan

A. A. Takasaki
Graduation program of Master Course in Clinical Dentistry,
Federal University of Espirito Santo,
Espirito Santo, Brazil

F. Schwarz
Department of Oral Surgery, Heinrich Heine University,
Düsseldorf, Germany

Y. Izumi
Global Center of Excellence (GCOE) Program, International Research Center for Molecular Science in Tooth and Bone Disease, Tokyo Medical and Dental University,
Tokyo, Japan

Introduction

Recently, the increasing occurrence of peri-implant disease has been reported due to the rapid increase of dental implant therapy. The prevalence of peri-implant disease is reported to be as high as 12.4–43.3 % after implant therapy [1–4]. In

Published online: 11 August 2012

peri-implantitis, exposed fixture surfaces of dental implants that lose osseointegration with the supportive bone are contaminated by bacterial biofilms and/or mineralized deposits. To treat peri-implantitis, it is essential to decontaminate the exposed contaminated fixture surfaces [5–8].

To debride fixture surfaces, chemical and mechanical methods have been conventionally employed [5–12]. For mechanical debridement, instruments made from plastic and other non-metals have been developed and applied to avoid damaging titanium surfaces during instrumentation. However, these non-metallic instruments are ineffective and inefficient for removing bacterial plaque and calcium depositions [8, 10]. Air–powder abrasion system can also effectively achieve surface decontamination [9]; however, the system produced microscopically visible alteration [9], and its application in the narrow vertical bone defect is limited. Recently, implant fixtures with various microstructured surfaces have been mainly employed to enhance osseointegration in the short term [13]. Mechanical debridement of microstructured fixture surfaces is much more difficult and less effective for decontamination than of smooth implant surfaces [8, 14, 15]. Thus, there seems to be no instruments suitable for cleaning microstructured fixture surfaces of titanium implants. Consequently, it is important to develop a stable debridement method that does not damage surface microstructures [6].

Recently, application of lasers has been considered for decontamination of fixture surfaces. However, the Nd:YAG laser is contraindicated due to the melting effect of titanium [16] and the CO_2, and diode lasers cannot remove calcified deposits [17]. Among hard lasers, the Er:YAG laser (ErL) has been extensively investigated for applications in periodontal therapy [17–21]. Since the 2.94 μm wavelength of ErL is strongly absorbed by water, this laser is suitable for both soft and hard tissue management [22, 23]. Many in vitro and in vivo periodontal studies have reported the effectiveness of ErL for root surface debridement including removal of sub-gingival calculus and excellent effects of soft and hard tissue ablation with strong bactericidal and detoxification as well as a photobiomodulation effect [14–16, 19, 24–26]. Several clinical studies have found that ErL irradiation is effective for non-surgical and surgical periodontal therapies [21, 27–30]. The beneficial properties of ErL irradiation for periodontal therapy suggest that the ErL has the potential to be applied in the treatment of peri-implantitis, and the ErL is considered promising for peri-implant therapy [11, 19, 20, 31, 32]. However, the optimal ErL irradiation parameters for debridement of microstructured surfaces of titanium implants, particularly at a high pulse repetition rate [33], have not been fully evaluated.

The aims of the present study are as follows: (1) to analyze morphological and elemental changes of microstructured titanium surfaces induced by high-pulse-repetition-rate ErL irradiation for various irradiation conditions; (2) to compare ErL with other conventional treatments; (3) to investigate the effect of ErL on several types of fixture surfaces; and (4) to demonstrate the effectiveness of ErL for removing calcified deposits on the contaminated microstructured fixture surface of explanted implants.

Materials and methods

Samples

Twelve commercially available titanium dental implants [Osseotite® (dual acid etched), Bioment 3i, USA; Tioblast® (blasted with titanium particles), AstraTech AB, Sweden; SLA® (blasted with sodium bicarbonate and acid etched), Straumann AG, Switzerland; RBM® (blasted with calcium phosphate powder) Lifecore Biomedical Inc., USA; TiUnite® (anodized), Nobel Biocare AB, Sweden] were used in vitro experiments.

Three failed implants with calcified deposits on their microstructured surfaces were also used. The implants explanted due to advanced peri-implantitis accompanied with severe bone loss were collected after obtaining informed consent and were stored in saline water prior to use. This study was approved by the Ethics Committee of the Faculty of Dentistry, Tokyo Medical and Dental University (no. 420).

Laser system

The laser system used was an ErL (DELight™, HOYA Conbio Inc., Fremont, CA, USA). This laser has the following characteristics—wavelength, 2.94 μm; output energy, 30–350 mJ/pulse; maximum pulse repetition rate, 30 Hz; pulse duration, 200 μs. This device employs a fiber-optic delivery system. In this experiment, unused and used 80 °-curved quartz contact tips with a diameter of 600 μm were employed. Considering the clinical situation of application, used tips that had rough, degraded contact surfaces were employed [34]. The unused and used tips had transmission rates of approximately 65 % and 50 %, respectively.

A used tip was prepared by roughening the surface of an unused tip. ErL irradiation was performed with an unused tip for 1 min at 52 mJ/pulse (panel setting, 80 mJ/pulse) and 30 Hz to chicken meat in contact mode. After 1 min irradiation, the contact surface was water-sprayed, and the energy output was measured using a power meter (Field Master™, Coherent, Santa Clara, CA, USA). This process of 1 min irradiation followed by energy measurement was repeated approximately ten times until the energy output decreased to 40 mJ/pulse. In this manner, a used tip with a 50 % transmission rate was prepared.

Experiment 1 Investigation of morphological and elemental changes of microstructured titanium surfaces

on ErL irradiation for various irradiation parameters

Six new implants (Osseotite®) were employed. A spot laser irradiation was performed irradiated perpendicularly to the fixture surface in near-contact mode at 1-mm distance using an unused or a used contact tip. For each spot, the ErL was used to irradiate for 10 s at 30, 40, and 50 mJ/pulse [panel setting, 55, 75, and 90 mJ/pulse for unused tips and 60, 80, and 100 mJ/pulse for used tips; energy density (ED) at the tip end—10.6, 14.2, and 17.7 J/cm^2/pulse, respectively] with and without water spray (8 ml/min water, 3.4 l/min air) at 30 Hz. A total of 12 irradiation groups were realized based on combinations of irradiation parameters. For each group, the procedure was independently performed three times.

Experiment 2 Comparison of alteration of microstructured titanium surfaces by ErL and by conventional methods

A metal curette (MC; Scaler Gracey Rigid, Hu-Friedy Co., Chicago, IL), a plastic curette (PC; Implacare®, Hu-Friedy Co., Chicago, IL), and an ultrasonic scaler (US) (Varios 750®, Nakanishi Inc., Kanuma, Japan) with a P20 metal tip (MU) or V-P10 plastic tip (PU) were employed. All treatments were performed in approximately 1×2 mm areas between the threads of an implant (Osseotite®). Mechanical treatments were performed for approximately 30 s. The US was used at a power level of 3 in periodontal (P) mode. The ErL was used to irradiate obliquely (30°angulation) to a surface in near-contact mode with a sweeping motion using a used tip at 40 mJ/pulse (panel, 80 mJ/pulse; ED at tip end, 14.2 J/cm^2/pulse) and 30 Hz with water spray for 20 s, which was sufficiently long to irradiate the whole treatment area.

Experiment 3 Investigation of morphological changes of five microstructured titanium surfaces on ErL irradiation

Five microstructures of commercially available implants (Osseotite®, Tioblast®, TiUnite®, RBM®, and SLA®) were employed. A spot laser irradiation was performed on each microstructured surface in a near-contact mode with 1 mm distance using a used contact chip. For each spot, ErL irradiation was performed for 5 s at 30, 40, and 50 mJ/pulse (panel setting with used tip, 60, 80, and 100 mJ/pulse; ED at tip end, 10.6, 14.2, and 17.7 J/cm^2/pulse) and 30 Hz with water spray and at 50 mJ/pulse without water.

Experiment 4 Debridement of contaminated microstructured surface of explanted titanium implants by ErL

Three explanted implants were employed. Two implants with calculus in a limited area on the sandblasted and acid etched surface received only ErL treatment at 30 mJ/pulse and 30 Hz with water spray. In one remaining implant with possibly titanium plasma spray-treated surface, four contaminated areas with calcified deposits between the threads were selected, and the areas were assigned to ErL treatment at 20 and 30 mJ/pulse (panel, 40 and 60 mJ/pulse; ED, 7.1 and 10.6 J/cm^2/pulse), US treatment, and untreated control. Laser irradiation was performed obliquely (30 °angulation) to the surface in near-contact mode with a sweeping motion using a used contact tip. US treatment with a plastic tip was conducted keeping the tip oblique (30°angulation) to the surface at a power level of 3 in P mode with water spray.

Stereomicroscopy and scanning electron microscopy

In all the experiments, the treated sites were observed by optical stereomicroscopy (VH-7000®, Keyence Corp., NJ, USA) and scanning electron microscopy (SEM; S-4500, Hitachi Ltd., Tokyo, Japan). In the stereomicroscopy, the prepared specimens were observed at a magnification of 200 times in experiments 1, 2, and 3, and 30 times in experiment 4. In the SEM observations, a secondary electron image was obtained at an accelerating voltage of 20 kV and a tilt angle of 50 ° with a magnification of 1,500 and 5,000 times in experiments 1 and 3, and 1,000 times in experiment 2, and 200 times in experiment 4.

Energy-dispersive X-ray spectroscopy (EDS)

Elemental analysis of the treated surfaces was performed for 1,200 s using an energy-dispersive X-ray microanalyzer (EMAX-7000®, Horiba Ltd., Kyoto, Japan) at 20 kV. In experiment 1, the carbon and oxygen contents

on the surface after ErL irradiation with a used tip were assessed. Four points in the center of the irradiation spot were randomly selected and were subjected to spot-scan microanalysis; the data obtained were averaged. In experiment 2, the presence of foreign elements that is not derived from the original composition was investigated. A 100 μm×90-μm area in the center of each treated site was selected and was subjected to area-scan analysis. In the experiment 4, the presence of carbon, oxygen, and foreign elements on the ErL-, US-treated, and non-treated fixture surface of one explanted implant was assessed by area-scan analysis at the center of each treatment area (Table 1).

Statistical analysis

In experiment 1, the mean value and the standard deviation (SD) of the carbon and oxygen contents were calculated. The differences in these measurement results between groups were analyzed by the Kruskal–Wallis test, and the difference relative to the control was evaluated by Steel test.

Results

Experiment 1. Morphological and elemental changes in microstructured titanium surface induced by ErL

Stereomicroscopy and SEM

The contact surface of an unused tip had a smooth mirror-like surface, whereas a used tip surface had a uniform roughness (Fig. 1a).

Irradiation using an unused tip

Surfaces irradiated by ErL at 30 and 40 mJ/pulse with water spray showed no changes, whereas 50 mJ irradiation changed the surface color to a light brown on the Osseotite® surface. When no water spray was applied, all the irradiated sites underwent moderate to severe changes. After 30 mJ irradiation, a brown area with a blue center was observed. After 40 and 50 mJ irradiation, severe color and morphological changes were observed with large blue-gray areas with glossy resolidified particles.

Table 1 Outline of experiments

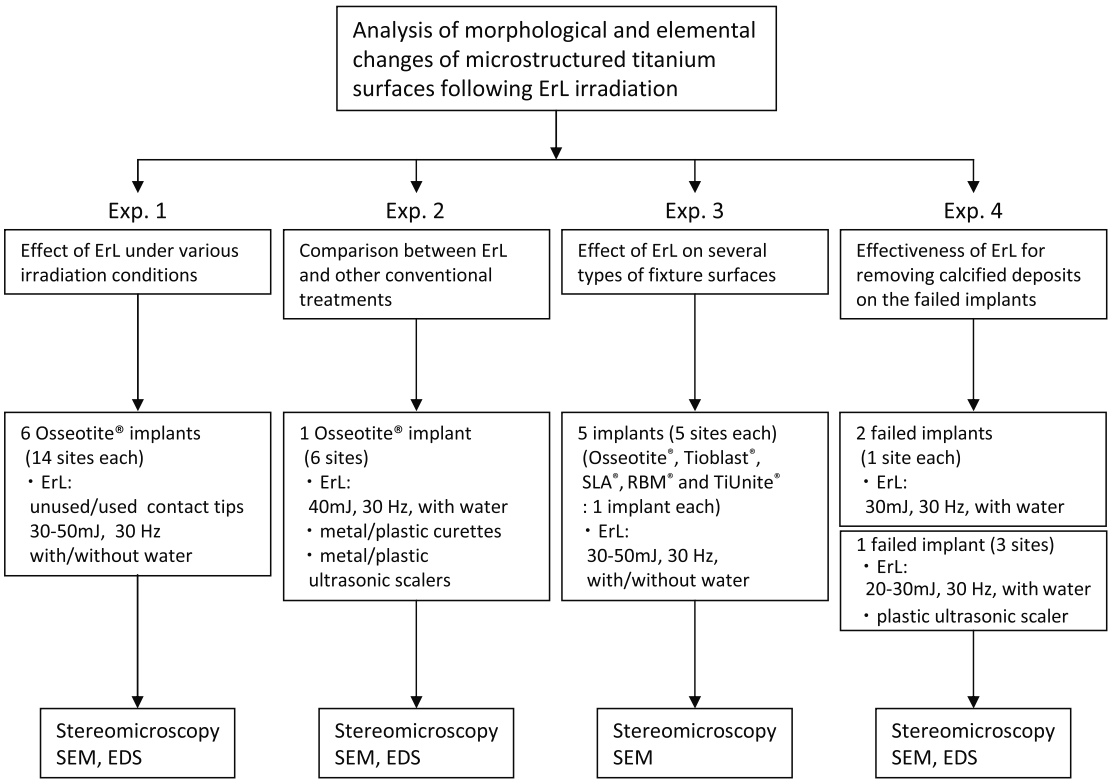

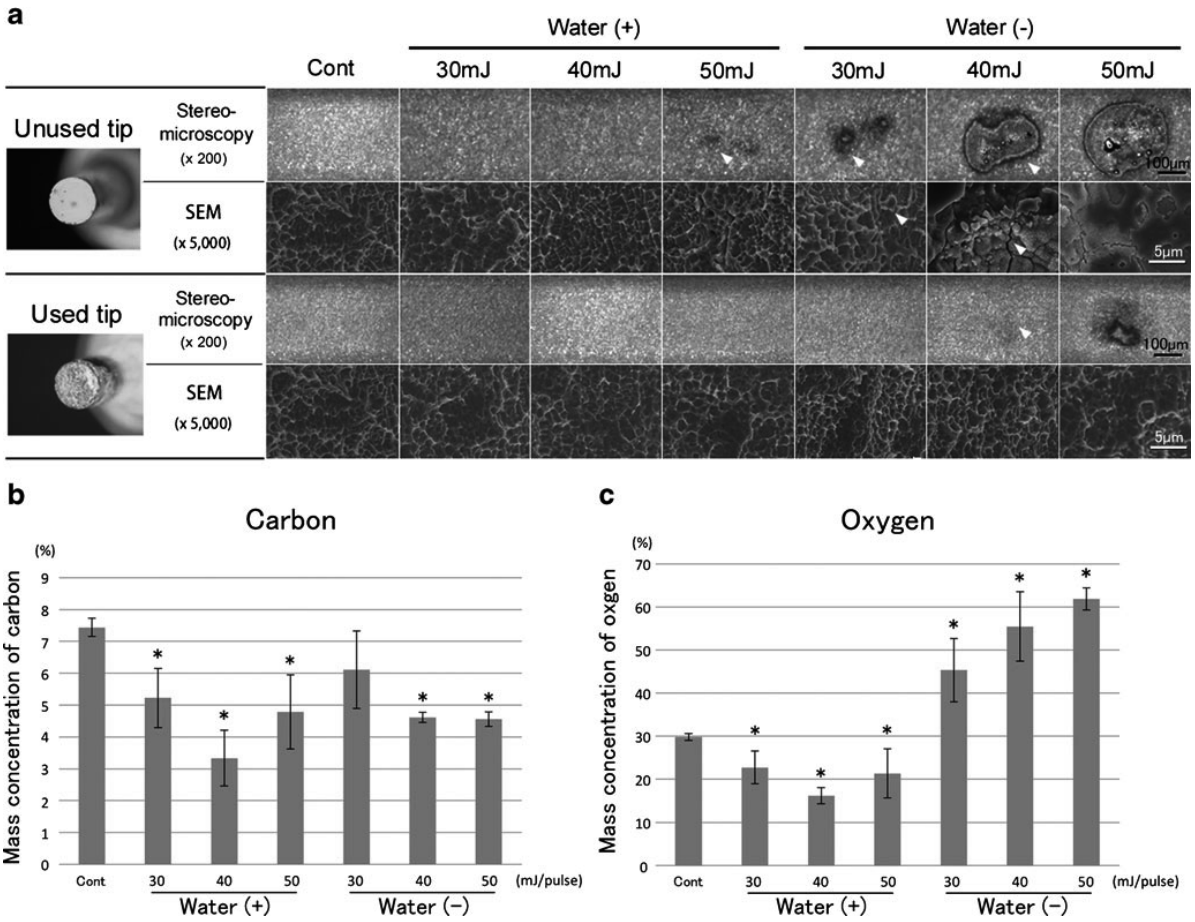

Fig. 1 Stereomicroscopy and SEM images and SEM-EDS analysis of microstructured titanium surface (Osseotite®) after ErL irradiation. **a** Stereomicroscopy and SEM. ErL spot irradiation was performed at 30, 40, and 50 mJ/pulse (energy density at tip end, 10.6, 14.2, and 17.7 J/cm^2/pulse) and 30 Hz in near-contact mode for 10 s with an unused tip and a used tip. When an unused tip was used, irradiation with pulse energies of 30 and 40 mJ/pulse with water spray induced no changes that were visible in stereomicroscopy and SEM observations; however, other irradiation under other conditions produced slight to severe changes. Irradiation with a used tip generally produced less damage than with an unused tip. Except for 40 and 50 mJ/pulse without water spray, no changes were detected by either stereomicroscopy or SEM. *Arrowheads* indicate color change, melting, cracking, or resolidification of the microstructured surface. **b**. SEM-EDS analysis for determining the carbon and oxygen contents of microstructured titanium surfaces (Osseotite®) after ErL spot irradiation with a used tip. The ErL irradiation reduced the carbon content of the microstructured surface except for irradiation using 30 mJ/pulse without water spray. In contrast, irradiation with water spray significantly reduced the oxygen content, while irradiation without water spray significantly increased the oxygen content. Bar indicates mean±SD (n=4). *p<0.05 relative to the non-irradiated control. *Cont*: non-irradiated control; *Water*: water spray

The SEM observations revealed that irradiation with water spray produced no noticeable changes. When water was not applied, 30 mJ irradiation slightly melted the microstructured edges. Forty and 50 mJ produced severe morphological changes with resolidification and microcrack formation occurring after melting (Fig. 1a).

Irradiation with a used tip

Surfaces irradiated using a used tip were generally damaged less than those irradiated using an unused tip. No morphological or color changes were observed for 30, 40, and 50 mJ irradiation with water and 30 mJ irradiation without water. The 40 mJ irradiation without water caused a very slight change that produced a light brown area. Sites irradiated by 50 mJ without water exhibited a moderate change with a blue spot surrounded by a dark brown area. The SEM observations revealed that the microstructure was preserved for irradiation without water spray at all pulse energies except for 50 mJ, which caused the microstructure to partially melt (Fig. 1a).

EDS analysis

ErL irradiation significantly reduced the carbon content of the Osseotite® microstructured surface ($p<0.05$), except for irradiation at 30 mJ without water spray (Fig. 1b). Irradiation with water spray significantly reduced the oxygen content, whereas irradiation without water significantly increased the oxygen ($p<0.05$) (Fig. 1c). The surface that had been irradiated at 40 mJ and 30 Hz with water had the lowest carbon and oxygen contents.

Experiment 2. Comparison of microstructured titanium surfaces after ErL and conventional treatments

Stereomicroscopy and SEM

ErL-irradiated sites exhibited no morphological changes and their morphologies resembled those of the untreated control sample. The MC and MU treatments severely damaged the Osseotite® surface, producing shiny surfaces with scratches and crumples. At the PC-treated site, gray fragments partially covered the surface (Fig. 2a). The PU treatment also crushed the surface and produced a shiny surface.

SEM observations revealed that all the treatments besides ErL irradiation clearly produced morphological changes. The MC, MU, and PU treatments completely removed or crushed the microstructure, and the treated surfaces exhibited linear lines and scales along with titanium wear debris. Residual foreign material (possibly plastic debris) that appeared dark in SEM images was attached to the PC-treated site (Fig. 2a).

EDS analysis

There were no foreign elements besides carbon and oxygen on the titanium surface at ErL and MC treated sites. A large amount of carbon was detected after PC treatment; ferrum was detected after MU treatment, and silica, calcium, and aluminum were detected after PU treatment (Fig. 2b).

Experiment 3. Morphological changes of five microstructured surfaces induced by ErL

Stereomicroscopy and SEM

Thirty and 40 mJ irradiation with water spray produced no change of Osseotite®, Tioblast®, SLA®, and RBM® surfaces, whereas 50 mJ with water produced a slight color change in all these surfaces except for Osseotite®. The 50 mJ without water produced a light brown area and moderate to severe changes on all the irradiated surfaces. With TiUnite®, the microstructured surface layer was always destroyed and scaled at all energies, even when water spray was applied. The periphery of the ablated site had a white flaky structure with a membranous form (Fig. 3).

SEM observations revealed that 40 mJ irradiation with water spray slightly melted the microstructural edges of SLA® and RBM®. The 50 mJ with water slightly melted all the surfaces except for Osseotite®. The 50 mJ without water produced severe morphological changes, such as resolidification and microcrack formation, on all the surfaces (Fig. 3). The TiUnite® microstructure was always removed, resulting in exposure of a fresh rough titanium surface without thermal damage, which was beneath the original microstructure (Fig. 3).

Experiment 4. Debridement of contaminated microstructured surface of explanted implants with ErL

Stereomicroscopy and SEM

All the calcified deposits were easily and efficiently removed by ErL irradiation at 20 and/or 30 mJ and 30 Hz from the contaminated microstructured surfaces of the three explanted implants. Irradiation did not induce any color or morphological changes to the surfaces. The US with a plastic tip could also remove the calculus, but gray fragments (possibly plastic debris) that were lightly attached to the treated surface were observed (Fig. 4a).

The SEM observations revealed that no major thermal damage had occurred at laser-treated site, although slight melting was observed. Some debris and microfragments remained on the fixture surface in areas treated by 20 mJ irradiation and ultrasonic scaling. The surface treated by 30 mJ irradiation generally exhibited less debris and fewer microfragments (Fig. 4b).

EDS analysis

In the US-treated scaled area, a higher titanium content and slightly lower carbon and aluminum contents were observed, while the calcium content was higher than that of the control. A high carbon content was detected in the untreated control area. In the ErL-irradiated area, the carbon content was much lower, and the titanium content was much higher, while the oxygen content was higher than that of control. Calcium was minimally detected. The 30-mJ irradiation gave the lowest carbon content and the highest titanium and oxygen contents (Table 2).

Discussion

In the field of peri-implant disease therapy, recent in vivo studies by Schwarz et al. [31] and Takasaki et al. [32] demonstrated that 10 or 20 Hz ErL irradiation is safe and

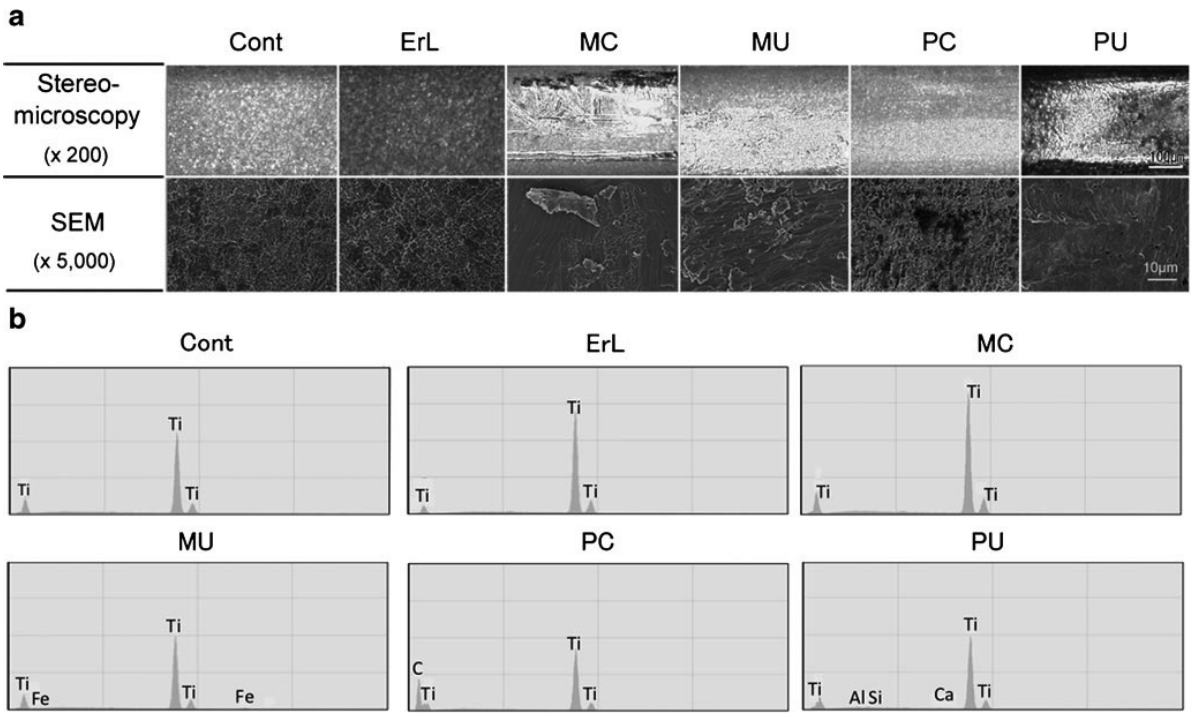

Fig. 2 Stereomicroscopy and SEM images and SEM-EDS analysis of microstructured surface (Osseotite®) after ErL irradiation and other conventional methods. **a** Stereomicroscopy and SEM. For the untreated control (*Cont*), the titanium surface exhibits microirregularity. ErL irradiation (*ErL*) at 40 mJ/pulse (energy density, 14.2 J/cm^2/pulse) and 30 Hz with water-spray in near-contact mode produced no morphological changes. The treatments using a metal curette (*MC*), ultrasonic scaler with a metal tip (*MU*), and with a plastic tip (*PU*) severely damaged the microstructure and produced shiny surfaces with scratches and crumples. The plastic curette (*PC*) treatment deposited gray debris on the treated surface. **b**. SEM-EDS area analysis for detecting foreign elements on the microstructured titanium surface. The *vertical axis* indicates the counting rate, and the *horizontal axis* represents the energy level of character X-rays. The ErL and MC treatments deposited foreign elements besides carbon and oxygen on the titanium surface. The following foreign elements were detected: a carbon content for the PC, ferrum for the MU, and silica, calcium, and aluminum for the PU treatments. *Ti*: titanium; *Fe*: ferrum; *Al*: aluminum; *Si*: silica; *Ca*: calcium

effective for surgical treatment of peri-implantitis in dogs. ErL irradiation seems promising for clinical use in peri-implantitis treatment for removing bacterial plaque and calcified deposits from microstructured implant surfaces as well as removing granulation tissue from bone defects and its application is gradually increasing in clinics.

In the treatment of periodontitis teeth, an energy density and a repetition rate in the approximate ranges of 11–19 J/cm^2/pulse and 10–30 Hz, respectively, are generally employed for removing subgingival calculus [17, 20, 21, 24]. However, these parameters cannot be directly used for titanium implant surfaces since using a high pulse energy risks thermally damaging microstructured titanium surfaces and using a high pulse repetition rate will also give a high surface temperature [24]. Regarding the alteration of the microstructured titanium surface induced by irradiation, Schwarz et al. [12] reported that ErL irradiation (12.7 J/cm^2/pulse, 10 Hz) induced no visible changes on various titanium surfaces. Kreisler et al. [9] reported that ErL irradiation (60 mJ/pulse, 10 Hz) ensures reliable removal of bacterial cytotoxic components from implant surfaces in vitro without altering the surface morphology of microstructured surfaces. Several previous studies have

Fig. 3 Stereomicroscopy and SEM images of five commercially available microstructured titanium implants after ErL irradiation. ErL spot irradiation was performed at 30, 40, and 50 mJ/pulse (energy density, 10.6, 14.2, and 17.7 J/cm^2/pulse) and 30 Hz in near-contact mode for 5 s. Osseotite®, 30, 40, and 50 mJ/pulse with water spray showed no changes in either stereomicroscopy or SEM observations. Tioblast®, 30 and 40 mJ/pulse with water spray showed no changes either stereomicroscopy or SEM observations. SLA® and RBM®, 30 and 40 mJ/pulse with water spray showed no changes in stereomicroscopy observations, but in SEM images, 40 mJ/pulse with water spray showed slight melting. The 50 mJ/pulse without water produced moderate to severe changes on all the surfaces. TiUnite®: anodized surface was always damaged and removed, resulting in exposure of a fresh rough titanium surface below the original microstructure. *Arrowheads* indicate color change, melting, cracking, or resolidification of the microstructured surface. *Low-magnification view of the interface between original microstructured surface (TiUnite®) and the ablated surface. The original surface (**a**) was completely removed and the underlying titanium surface (**b**) was exposed. The border (indicated by *arrowheads*) is sharp and clear without thermal changes such as melting. *Cont*: non-irradiated control; *Water*: water spray

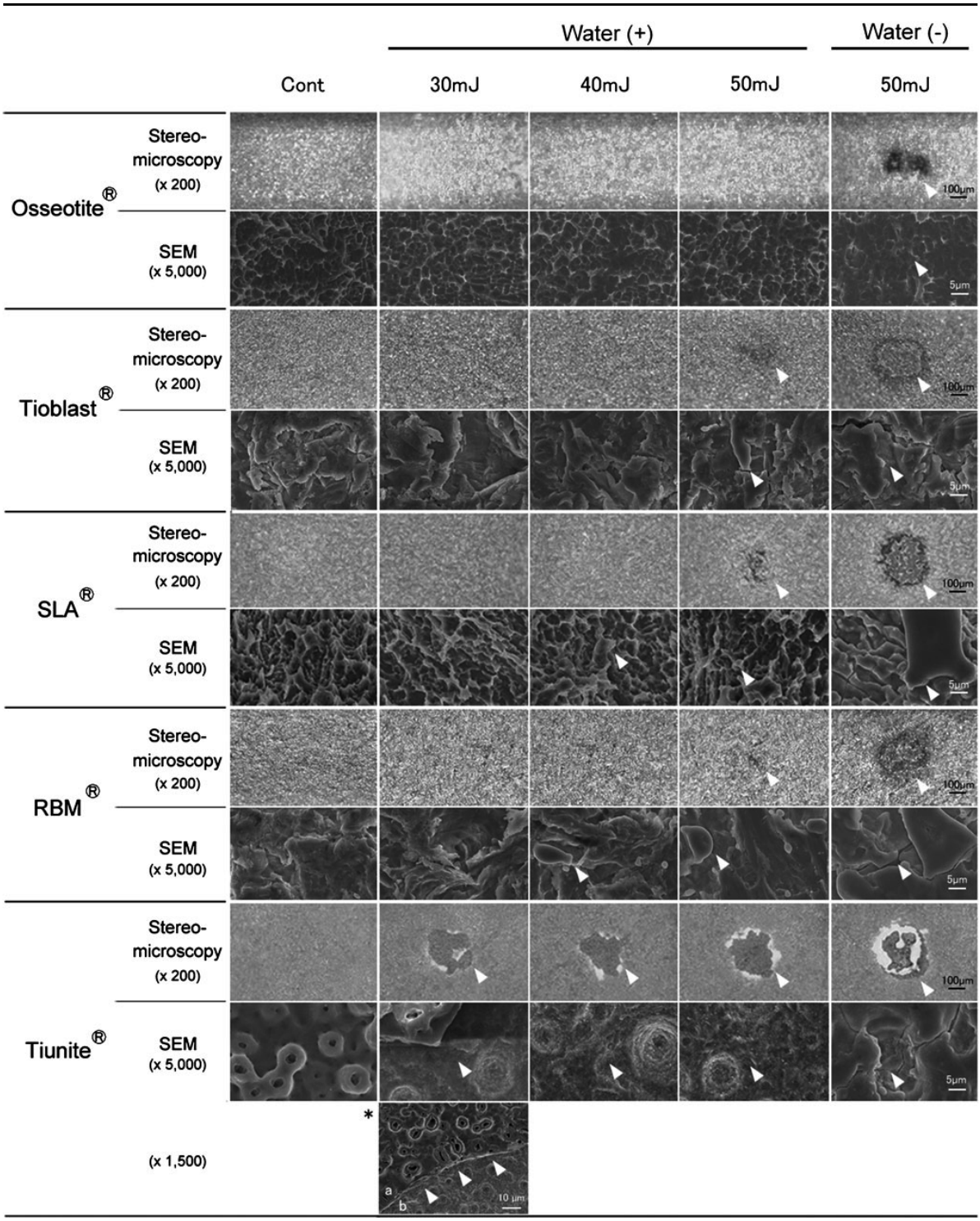

confirmed the effectiveness of the ErL irradiation at 10 Hz. Therefore, in the present study, changes to various microstructured surfaces of titanium implants induced by ErL irradiation at the currently available higher pulse repetition rate of 30 Hz were investigated to determine the optimal irradiation conditions for debridement.

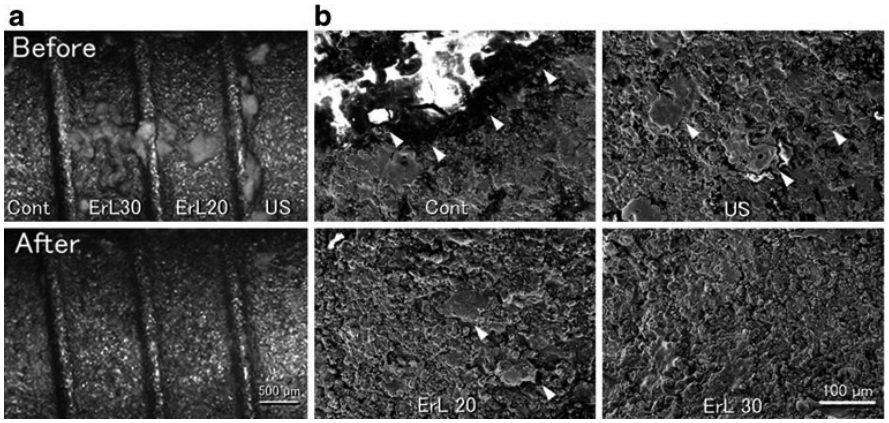

Fig. 4 Stereomicroscopy and SEM images of contaminated microstructured surface of an explanted implant after ErL irradiation and ultrasonic scaling (*US*) with a plastic tip. **a** Stereomicroscopy. Before treatment, calcified deposits were evident on the microstructured surface. ErL irradiation was performed at 20 and 30 mJ/pulse (energy density, 7.1 and 10.6 J/cm^2/pulse) and 30 Hz under water spray in near-contact mode. Calcified deposits were effectively removed without major damage to the microstructured surface in all treated areas. Gray fragments (possibly plastic debris) were observed in the US-treated area (original magnification × 30). **b**. SEM. Untreated control surface exhibits a large dark area and a charged structure; these are due to contamination (*arrowheads*). No major damage was observed in the ErL-irradiated and US-treated area. The US treated area had fragments attached to its surface (*arrowheads*). Compared with ErL irradiation at 20 mJ and US treatment, ErL irradiation at 30 mJ resulted in less residual debris and fewer fragments on the treated surface (original magnification × 200). *Cont*: non-treated control; *US*: ultrasonic scaler; *ErL20*: Er:YAG laser irradiation at 20 mJ/pulse; *ErL30*: Er:YAG laser irradiation at 30 mJ/pulse

First, the effects of ErL on a microstructured implant surface were investigated under various irradiation conditions for Osseotite®. Using 50 mJ/pulse (17.7 J/cm^2/pulse) and 30 Hz for 10 s without water cooling resulted in pronounced melting with severe morphological and color changes. Since titanium has a melting point of 1,668 °C, this observation implies that the ErL was absorbed by the titanium surface and that a very high temperature was probably generated at the irradiated site [35]. However, employing water cooling was effective for reducing heat generated during irradiation and thereby reduced or prevented thermal changes to the titanium microstructure. The energy threshold to prevent observable changes on Osseotite® was found to be below 40 mJ/pulse (14.2 J/cm^2/pulse) under the present experimental conditions.

Table 2 SEM-EDS area analysis of treated surfaces (Fig. 4) of an explanted implant after ErL irradiation and ultrasonic scaling with a plastic tip

	Elements mass concentration (%)				
	C	O	Ti	Al	Ca
Cont	45.5	28.0	25.0	0.3	0.5
US	34.6	26.5	37.7	0.8	0.9
ErL 20 mJ	18.0	36.4	45.1	0.2	0.2
ErL 30 mJ	8.3	39.1	51.8	0.6	0.1

ErL irradiation was performed at 20 and 30 mJ/pulse (energy density, 7.1 and 10.6 J/cm^2 /pulse) and 30 Hz under water spray in near-contact mode. A high carbon content was detected in the untreated control area. The ErL irradiation markedly reduced the carbon content and increased the titanium content. In addition, the irradiation increased the oxygen content. In the ultrasonically scaled area, the titanium content was higher than that of the control, and the carbon content was still high. In addition, both the Al and Ca contents were higher than those of the control area

C: carbon; *O*: oxygen; *Ti*: titanium; *Al*: aluminum; *Ca*: calcium; *Cont*: non-treated control; *US*: ultrasonic scaler; *ErL20 mJ* Er:YAG laser at 20 mJ/pulse; *ErL30 mJ* Er:YAG laser at 30 mJ/pulse

The condition of the contact tip clearly affected the results obtained. For the same pulse energy, used tips tended to produce less damage than unused tips. This difference can be explained by the fact that a used tip has an irregular surface that emits a scattered and defocused beam, resulting in light being emitted with a reduced energy intensity. Care is thus required when using a new tip for a titanium surface in clinical applications.

Interestingly, analysis of the compositional change of titanium surface in experiment 1 revealed that the carbon and oxygen contents decrease on irradiation with water cooling. This implies that ErL removed hydrocarbons, which seem to inhibit osseointegration, from the titanium surface [36]. However, without water cooling, the oxygen content tended to increase, indicating that the titanium implant surface is oxidized. The present results raise the possibility of a novel application of ErL: Optimized irradiation conditions could result in the removal of chemical contamination from titanium microstructures prior to implantation [36].

Unlike ErL irradiation, conventional mechanical instruments damaged microstructured titanium surfaces, resulted in incomplete debridement, and generated additional chemical contamination. These findings are similar to those of

previous studies [36, 37]. In addition, in the case of mechanical debridement or implant-plasty procedure using rotary instruments, particles or fragments of wear debris of titanium are scattered on or penetrate peri-implant tissues. A recent study [38] found that titanium particles directly and indirectly affect osteoblast viability and also induce programmed cell death (apoptosis) in osteoblasts, suggesting that titanium debris are cytotoxic. Additionally, preventing microstructure damage facilitates re-osseointegration [39]. Thus, the ideal procedure for debriding titanium fixtures is to decontaminate an infected surface while avoiding additional chemical contamination and minimizing mechanical and thermal damage to the surface microstructure.

In the present study, morphological changes of five microstructured titanium surfaces induced by 30 Hz ErL irradiation were investigated. Of the microstructures used, Osseotite® was the most resistant to ErL; this is possibly because Osseotite® is made of a titanium alloy whose melting point exceeds that of pure titanium. For 50 mJ irradiation with water cooling, the Osseotite® surface showed no changes, whereas SLA®, Tioblast®, and RBM® surfaces exhibited slight melting. In addition, at 40 mJ with water cooling, slight melting of the microstructural edge was observed for SLA® and RBM® in the SEM observations. Consequently, 30 mJ/pulse (10.6 J/cm^2/pulse) at 30 Hz with water cooling in near contact mode is considered to be generally acceptable for irradiation of Osseotite®, SLA®, Tioblast®, and RBM® surfaces (Fig. 3).

In contrast, the anodized implant surface exhibited a completely different response. The surface was easily damaged and was removed even by 30 mJ irradiation with water cooling. Unlike the other structures that were fabricated by subtraction, the anodized surface consisted of a thick oxide layer containing calcium and phosphate [40, 41]. Based on the SEM observations, the destruction of the microstructure is speculated to be due to complete ablation and/or detachment of the oxidation layer from the underlying titanium surface. Thus, ErL did not preserve the anodized surface. This finding agrees with the results of an in vitro study by Shin et al. [42] who reported peeling of an anodic oxidized surface after ErL irradiation. Yamamoto et al. [43] recently proposed complete removal of the oxidation layer by ErL irradiation (13.0 J/cm^2/pulse) for debridement of the contaminated anodized surfaces, and they reported the successful clinical application of this method for surgical treatment of peri-implantitis. The anodized surface seems to have a specific structure, and its potential poor mechanical properties or structural weakness may threaten the long-term stability of osseointegration on the anodized surfaces [44, 45].

Finally, experiment 4 clearly demonstrated that ErL effectively removes calcified deposits from contaminated microstructured surface (sandblasted and acid etched, and titanium plasma spray-treated surfaces) without noticeably changing the titanium surface. The EDS results reveal that ErL reduces the carbon content which suggested the removal of organic components such as bacterial plaque and increases the titanium content of the treated surfaces relative to those of the untreated control. Due to the variable distributions of the calculus in different areas, a direct comparison could not be made, but a lower calcium content was detected after ErL treatment, although calcium had not been completely removed. Ultrasonic treatment increased the calcium and aluminum contents and reduced the titanium content; this is considered to be due to the attachment of debris from the plastic tip. In addition, contrary to the results of experiment 1, a higher oxygen content was observed after ErL irradiation. This implies that oxidation may occur due to a momentary high temperature generated during calculus ablation. The ErL could effectively remove calculus from the microstructured surface without causing significant thermal damage on a macroscopic level. However, further investigations are required to completely eradicate calcified deposits and to determine slight thermal changes to microstructures induced by irradiation on a microscopic level. Also, it is difficult to irradiate the fixture surface perpendicularly within the intrabony defect with the present device. However, recently a contact tip which enables laser irradiation in the lateral direction has been developed, which is expected to improve the effectiveness of clinical application of ErL for fixture surface debridement.

The present results clearly reveal that the titanium microstructure is affected by thermal effects induced by ErL irradiation. Besides the pulse energy and pulse repetition rate, there are various other important parameters: amount of water spray, tip movement speed, pulse width, and, in particular, the considerably different energy distribution profiles and intensities of the irradiation spot for different laser delivery systems (fiber optic, hollow waveguide, and direct delivery). All these parameters are associated with the concentration or accumulation of heat during irradiation. Further studies are required to clarify the effects of these parameters and to realize safe and reliable clinical application of ErL irradiation for debridement of titanium microstructures and bone defects around implant fixtures.

Conclusion

ErL irradiation at energies below 30 mJ/pulse (ED, 10.6 J/cm^2/pulse) and 30 Hz with water spray in near-contact mode for optic-fiber delivery does not appear to damage the microstructure of titanium fixture surfaces, making it effective for processing all such surfaces with the exception of anodized surface. When using an ErL, a different approach may be required for the anodized implant surface. Care is required when using new tips for irradiating microstructures.

Acknowledgment This study was supported in part by a grant from the Global Center of Excellence Program for International Research Center for Molecular Science in Tooth and Bone Diseases at Tokyo Medical and Dental University and by a Grant-in-Aid for Scientific Research (C) (No. 22592308) to A.A. from the Ministry of Education, Culture, Sports, Science and Technology of Japan. The authors wish to thank Drs. Yasushi Yoda, Kenichiro Ejiri, and Masanori Sawabe of Tokyo Medical and Dental University, Tokyo, Japan for their kind help. The Osseotite® implants were provided by Bioment 3i Japan (Osaka, Japan).

References

1. Subramani K, Jung R, Molenberg A, Hammerle C (2009) Biofilm on dental implants: a review of the literature. Int J Oral Maxillofac Implants 24:616–626
2. Zitzmann NU, Berglundh T (2008) Definition and prevalence of peri-implant diseases. J Clin Periodontol 35:286–291
3. Roos-Jansåker AM, Lindahl C, Renvert H, Renvert S (2006) Nine- to fourteen-year follow-up of implant treatment. Part II: presence of peri-implant lesions. J Clin Periodontol 33:290–295
4. Fransson C, Lekholm U, Jemt T, Berglundh T (2005) Prevalence of subjects with progressive bone loss at implants. Clin Oral Implants Res 16:440–446
5. Lang N, Wilson T, Corbet E (2000) Biological complications with dental implants: their prevention, diagnosis and treatment. Clin Oral Implants Res 11:146–155
6. Claffey N, Clarke E, Polyzois I, Renvert S (2008) Surgical treatment of peri-implantitis. J Clin Periodontol 35:316–332
7. Renvert S, Roos-Jansåker A, Claffey N (2008) Non-surgical treatment of peri-implant mucositis and peri-implantitis: a literature review. J Clin Periodontol 35:305–315
8. Renvert S, Polyzois I, Maguire R (2009) Re-osseointegration on previously contaminated surfaces: a systematic review. Clin Oral Implants Res 20:216–227
9. Kreisler M, Kohnen W, Christoffers A, Götz H, Jansen B, Duschner H, d'Hoedt B (2005) In vitro evaluation of the biocompatibility of contaminated implant surfaces treated with an Er:YAG laser and an air powder system. Clin Oral Implants Res 16:36–43
10. Trejo P, Bonaventura G, Weng D, Caffesse R, Bragger U, Lang N (2006) Effect of mechanical and antiseptic therapy on peri-implant mucositis: an experimental study in monkeys. Clin Oral Implants Res 17:294–304
11. Schwarz F, Sculean A, Rothamel D, Schwenzer K, Georg T, Becker J (2005) Clinical evaluation of an Er:YAG laser for non-surgical treatment of peri-implantitis: a pilot study. Clin Oral Implants Res 16:44–52
12. Schwarz F, Rothamel D, Sculean A, Georg T, Scherbaum W, Becker J (2003) Effects of an Er:YAG laser and the Vector ultrasonic system on the biocompatibility of titanium implants in cultures of human osteoblast-like cells. Clin Oral Implants Res 14:784–792
13. Massaro C, Rotolo P, De Riccardis F, Milella E, Napoli A, Wieland M, Textor M, Spencer N, Brunette D (2002) Comparative investigation of the surface properties of commercial titanium dental implants. Part I: chemical composition. J Mater Sci Mater Med 13:535–548
14. Duarte PM, Reis AF, de Freitas PM, Ota-Tsuzuki C (2009) Bacterial adhesion on smooth and rough titanium surfaces after treatment with different instruments. J Periodontol 80:1824–1832
15. Ando Y, Aoki A, Watanabe H, Ishikawa I (1996) Bactericidal effect of erbium YAG laser on periodontopathic bacteria. Lasers Surg Med 19:190–200
16. Romanos GE, Everts H, Nentwig GH (2000) Effects of diode and Nd:YAG laser irradiation on titanium discs: a scanning electron microscope examination. J Periodontol 71:810–815
17. Aoki A, Sasaki KM, Watanabe H, Ishikawa I (2000) (2004) Lasers in nonsurgical periodontal therapy. Periodontol 36:59–97
18. Aoki A, Ando Y, Watanabe H, Ishikawa I (1994) In vitro studies on laser scaling of subgingival calculus with an erbium:YAG laser. J Periodontol 65:1097–1106
19. Ishikawa I, Aoki A, Takasaki AA, Mizutani K, Sasaki KM, Izumi Y (2009) Application of lasers in periodontics: true innovation or myth? Periodontol 2000 50:90–126
20. Schwarz F, Aoki A, Sculean A, Becker J (2009) The impact of laser application on periodontal and peri-implant wound healing. Periodontol 2000 51:79–108
21. Schwarz F, Aoki A, Becker J, Sculean A (2008) Laser application in non-surgical periodontal therapy: a systematic review. J Clin Periodontol 35:29–44
22. Robertson CW, Williams D (1971) Lambert absorption coefficients of water in the infrared. J Opt Soc Am 61:1316–1320
23. Hale GM, Querry MR (1973) Optical constants of water in the 200-nm to 200-μm wave-length region. Appl Optics 12:555–563
24. Aoki A, Miura M, Akiyama F, Nakagawa N, Tanaka J, Oda S, Watanabe H, Ishikawa I (2000) In vitro evaluation of Er:YAG laser scaling of subgingival calculus in comparison with ultrasonic scaling. J Periodontal Res 35:266–277
25. Aleksic V, Aoki A, Iwasaki K, Takasaki AA, Wang CY, Abiko Y, Ishikawa I, Izumi Y (2010) Low-level Er:YAG laser irradiation enhances osteoblast proliferation through activation of MAPK/ERK. Lasers Med Sci 25:559–569
26. Akiyama F, Aoki A, Miura-Uchiyama M, Sasaki K, Ichinose S, Umeda M, Ishikawa I, Izumi Y (2011) In vitro studies of the ablation mechanism of periodontopathic bacteria and decontamination effect on periodontally diseased root surfaces by erbium: yttrium-aluminum-garnet laser. Lasers Med Sci 26:193–204. Erratum in: Lasers Med Sci 2011; 2026(2012): 2277
27. Schwarz F, Sculean A, Georg T, Reich E (2001) Periodontal treatment with an Er:YAG laser compared to scaling and root planing. A controlled clinical study. J Periodontol 72:361–367
28. Sculean A, Schwarz F, Berakdar M, Romanos GE, Arweiler NB, Becker J (2004) Periodontal treatment with an Er:YAG laser compared to ultrasonic instrumentation: a pilot study. J Periodontol 75:966–973
29. Crespi R, Capparè P, Toscanelli I, Gherlone E, Romanos GE (2007) Effects of Er:YAG laser compared to ultrasonic scaler in periodontal treatment: a 2-year follow-up split-mouth clinical study. J Periodontol 78:1195–1200
30. Gaspirc B, Skaleric U (2007) Clinical evaluation of periodontal surgical treatment with an Er:YAG laser: 5-year results. J Periodontol 78:1864–1871
31. Schwarz F, Jepsen S, Herten M, Sager M, Rothamel D, Becker J (2006) Influence of different treatment approaches on non-submerged and submerged healing of ligature induced peri-implantitis lesions: an experimental study in dogs. J Clin Periodontol 33:584–595
32. Takasaki AA, Aoki A, Mizutani K, Kikuchi S, Oda S, Ishikawa I (2007) Er:YAG laser therapy for peri-implant infection: a histological study. Lasers Med Sci 22:143–157
33. Matsuyama T, Aoki A, Oda S, Yoneyama T, Ishikawa I (2003) Effects of the Er:YAG laser irradiation on titanium implant materials and contaminated implant abutment surfaces. J Clin Laser Med Surg 21:7–17
34. Eguro T, Aoki A, Maeda T, Takasaki A, Hasegawa M, Ogawa M, Suzuki T, Yonemoto K, Ishikawa I, Izumi Y, Katsuumi I (2009) Energy output reduction and surface alteration of quartz and sapphire tips following Er:YAG laser contact irradiation for tooth enamel ablation. Lasers Surg Med 41:595–604

35. Matthew J, Donachie (2000) Titanium: a technical guide. ASM International, Netherlands, pp 1–2
36. Aita H, Att W, Ueno T, Yamada M, Hori N, Iwasa F, Tsukimura N, Ogawa T (2009) Ultraviolet light-mediated photofunctionalization of titanium to promote human mesenchymal stem cell migration, attachment, proliferation and differentiation. Acta Biomater 5: 3247–3257
37. Wang R, Hashimoto K, Fujishima A, Chikuni M, Kojima E, Kitamura A, Shimohigoshi M, Watanabe T (1997) Light-induced amphiphilic surfaces. Nature 31:431–432
38. Pioletti DP, Takei H, Kwon SY, Wood D, Sung KL (1999) The cytotoxic effect of titanium particles phagocytosed by osteoblasts. J Biomed Mater Res 46:399–407
39. Persson L, Araújo M, Berglundh T, Gröndahl K, Lindhe J (1999) Resolution of peri-implantitis following treatment. An experimental study in the dog. Clin Oral Implants Res 10:195–203
40. Fini M, Cigada A, Rondelli G, Chiesa R, Giardino R, Giavaresi G, Nicoli Aldini N, Torricelli P, Vicentini B (1999) In vitro and in vivo behaviour of Ca- and P-enriched anodized titanium. Biomaterials 20:1587–1594
41. Son WW, Zhu X, Shin HI, Ong JL, Kim KH (2003) In vivo histological response to anodized and anodized/hydrothermally treated titanium implants. J Biomed Mater Res B Appl Biomater 66:520–525
42. Shin SI, Min HK, Park BH, Kwon YH, Park JB, Herr Y, Heo SJ, Chung JH (2011) The effect of Er:YAG laser irradiation on the scanning electron microscopic structure and surface roughness of various implant surfaces: an in vitro study. Lasers Med Sci 26:767–776
43. Yamamoto A, Tanabe T, Katagi H, Yamamoto K (2009) Application of Er:YAG laser to peri-implantitis a clinical report. J Jpn Soc Laser Dent 20:81–87
44. Albouy JP, Abrahamsson I, Persson LG, Berglundh T (2008) Spontaneous progression of peri-implantitis at different types of implants. An experimental study in dogs. I: clinical and radiographic observations. Clin Oral Implants Res 19: 997–1002
45. Albouy JP, Abrahamsson I, Persson LG, Berglundh T (2009) Spontaneous progression of ligatured induced peri-implantitis at implants with different surface characteristics. An experimental study in dogs II: histological observations. Clin Oral Implants Res 20:366–371

硬組織病態生化学分野

柳下 正樹

医歯学総合研究科・生体支持組織学系専攻
硬組織病態生化学・教授

1）研究の課題名

ヘパラン硫酸プロテオグライカンと膜ドメインの相互作用に関する研究

Association of heparan sulfate proteoglycans with trypsin-accessible membrane domains

ヘパラン硫酸プロテオグライカンは細胞膜上で各種の受容体と機能的分子複合体を形成しリガンドとの結合、活性ある受容体複合体の発現、細胞膜上での動態（細胞内取り込みによる不活化）を制御している。このような機能的分子複合体に関する詳細な性質を解析するため超遠心/ショ糖密度勾配法を用いて細胞膜分画を調整し細胞膜結合分子、ラフト構造に特徴的分子の局在をもとにヘパラン硫酸プロテオグライカンの分析を行った。結果をPLos Oneに発表した（後記業績欄）。

ヘパリンプロテオグライカンの生合成に関する研究

Biosynthesis of heparin proteoglycan（serglycin）

肥満細胞におけるヘパリンプロテオグライカン（セルグライシン）の生合成過程、特にヘパリン糖鎖のヘパラネースによるプロセッシングに関する実験系の確立を試みた。ヘパリンプロテオグライカンを純粋に生合成する細胞培養系を得ることは事実上困難であった（コンドロイチン硫酸Eを同時に合成する細胞がほとんどであり成分分析上の障害となった）。ヘパリン糖鎖非還元末端の糖鎖構造を解析することによりヘパラネースによるプロセッシングを間接的に分析する方法を実施したところ、硫酸化された特有な構造の存在することが示されこれがヘパリンの生物学的活性を担う構造であることが示唆された。

2）研究のイラストレーション

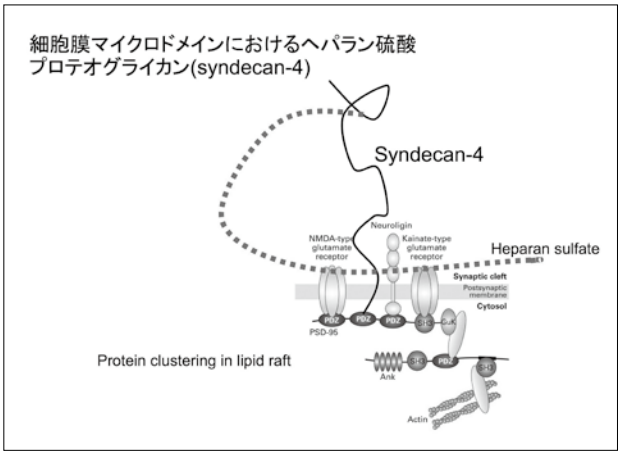

3）発表の研究内容についての英文要約

Association of heparan sulfate proteoglycans with trypsin-accessible membrane domains

We continued our study identifying the presence of a molecular complex on the cell surface involving heparan sulfate proteoglycans, and the role of heparan sulfate chains on the integrity of membrane raft structure. Biochemical properties of heparan sulfate proteoglycans point to the presence of intimate molecular interactions in specialized domains of cell surface and their importance in the cellular signaling mechanisms. Research results, using isolation procedures of plasma membrane and identification of several membrane proteins together with heparan sulfate proteoglycans, indicated that cholesterol-rich, cell surface microdomains constitute one of specialized functional units of the plasma membrane and are associated with a species of cell surface heparan sulfate proteoglycan, syndecan-4. Biological significance of heparan sulfate proteoglycans in specialized membrane domains will be further investigated.

Biosynthesis of heparin proteoglycan（serglycin）

We attempted to establish a cell culture system in which heparin proteoglycan（serglycin）is synthesized.

However, unfortunately, most cell system produced serglycin substituted with both heparin and chondroitin sulfate E. The presence of the latter interfered with the carbohydrate analyses and biosynthetic study of genuine heparin proteoglycan. Then, we took an approach of analyzing nonreducing end terminal sugar structure of heparin to indirectly decipher the activity of heparanase. These analyses revealed series of significant, highly sulfated oligosaccharide structures, which could account for the specific biological activities of heparin.

4）本事業に関連して世界的な研究拠点形成に向けて、以下の点で改善・整備等されたこと

A（研究拠点体制）

アメリカ合衆国、オハイオ州、クリーブランドクリニックにおけるトランスレーショナル研究の実際を体験し、本GCOEにおけるトランスレーショナル研究の改善を試みた。

B（研究教育環境）

GCOE総合講義参加

C（人材確保）

大学院生（AISS）への奨学金授与、大学院生セミナーの開催

D（人材育成）

アメリカ合衆国、オハイオ州、クリーブランドクリニックにおけるトランスレーショナル研究の実際を体験し、本GCOEにおけるトランスレーショナル研究の改善を試みた。

5）GCOE事業を推進するに当たって力を入れた点

アメリカ合衆国、オハイオ州、クリーブランドクリニックにおけるトランスレーショナル研究の実際を体験し、本GCOEにおけるトランスレーショナル研究の改善を試みた。

6）英文原著論文

1. Katarzyna A. Podyma-Inoue, Miki Hara-Yokoyama, Tamayuki Shinomura, Tomoko Kimura and Masaki Yanagishita, Syndecans Reside in Sphyngomyelin-enriched Low-density Fractions of the Plasma membrane Isolated from a Parathyroid Cell Line, PLoS One, (2012) 7：e32351
2. ◎Miki Hara-Yokoyama, Mutsuko Kukimoto-Niino, Kazue Terasawa, Satoru Harumiya, Katarzyna A. Podyma-Inoue, Nobumasa Hino, Kensaku Sakamoto, Satsuki Itoh, Noritaka Hashii, Yoko Hiruta, Nana Kawasaki, Chiemi Mishima-Tsumagari, Yoko Kaitsu, Tomoko Matsumoto, Motoaki Wakiyama, Mikako Shirouzu, Takeshi Kasama, Hiroshi Takayanagi, Naoko Utsunomiya-Tate, Kiyoshi Takatsu, Toshiaki Katada, Yoshio Hirabayashi, Shigeyuki Yokoyama, and Masaki Yanagishita. Tetrameric interaction of the ectoenzyme CD38 on the cell surface enables its catalytic and raft-association activities, Structure 20, 1585-1595（2012）
3. Bodil Fadnes, Anne Husbekk, Gunbjorg Sveing, Oystein Rekdal, Masaki Yanagishita, Svein O. Kolset and Lars Uhlin-Hansen, The proteoglycan repertoire of lymphoid cells, Glycoconjugate J. 29：513-523（2012）

7）平成24年度までの自己評価

海外でのトランスレーショナル研究の実情を体験した、その着実な努力に感銘を受けた。その他の活動内容のうちで私の参加できる主な項目としては大学院生、GCOE教官に対する評価関連の活動および、大学院生に対するセミナーシリーズでの司会であった。これらの活動はGCOE事業全体からすると微力とは思いますが、可能な限り参加させていただきました。

8）学会発表（英文）

1. Katarzyne A. Podyma-Inoue, Miki Yokoyama and Masaki Yanagishita, Association of heparan sulfate proteoglycans with trypsin-accessible membrane domains, Gordon Research Conference on Proteoglycans, July 7-13, 2012, Andover, New Hampshire, U. S. A.
2. Privatananupunt, J., Watari, I., Podyma-Inoue, K. A., Kubono, M., Hattori, I., Honda, K., Ishida, Y., Yanagishita and M. Ono, T., Expression of GIP and its receptor in the rat major salivary glands, September 26-28, 2012, Morioka

9）外部資金の獲得状況

（受託研究）

糖質科学研究所、「グリコサミノグリカンオリゴ糖の生理活性解析と医薬応用」、期間：平成17年 -平成24年、総額：945万円

（受託研究）

ヒアルロン酸研究所、「異なる分子量のヒアルロン酸の大腸細胞株に対する影響」、期間：平成22年 - 平成24年、126万円

10）主催学会

第19回プロテオグライカンフォーラム、「プロテオグライカン、ヒアルロン酸研究の最新トピック」2012年2月11日、東京

11）教室、分野や講座の准教授、講師、助教、特別研究員、ポスドク、指導を受けた大学院生の名前

准教授　　横山　三紀
講師　　粂井　康宏
助教　　井上-Podyma Katarzyna Anna
大学院生　○ Anupama Rajapakshe

Structure
Article

Tetrameric Interaction of the Ectoenzyme CD38 on the Cell Surface Enables Its Catalytic and Raft-Association Activities

Miki Hara-Yokoyama,[1,3,*] Mutsuko Kukimoto-Niino,[5] Kazue Terasawa,[1] Satoru Harumiya,[2] Katarzyna A. Podyma-Inoue,[1] Nobumasa Hino,[5] Kensaku Sakamoto,[5] Satsuki Itoh,[6] Noritaka Hashii,[6] Yoko Hiruta,[6] Nana Kawasaki,[6] Chiemi Mishima-Tsumagari,[5] Yoko Kaitsu,[5] Tomoko Matsumoto,[5] Motoaki Wakiyama,[5] Mikako Shirouzu,[5] Takeshi Kasama,[4] Hiroshi Takayanagi,[2,3,7] Naoko Utsunomiya-Tate,[10] Kiyoshi Takatsu,[11,12] Toshiaki Katada,[8] Yoshio Hirabayashi,[13] Shigeyuki Yokoyama,[5,9] and Masaki Yanagishita[1,3]
[1]Section of Biochemistry
[2]Section of Cell Signaling, Department of Hard Tissue Engineering, Graduate School of Medical and Dental Sciences
[3]The Global Center of Excellence (GCOE) Program, International Research Center for Molecular Sciences in Tooth and Bone Diseases
[4]Instrumental Analysis Research Division, Research Center for Medical and Dental Sciences
Tokyo Medical and Dental University, Tokyo 113-8549, Japan
[5]RIKEN Systems and Structural Biology Center, Yokohama, Kanagawa 230-0045, Japan
[6]Division of Biological Chemistry and Biologicals, National Institute of Health Science, Tokyo 158-8501, Japan
[7]Department of Immunology, Graduate School of Medicine and Faculty of Medicine
[8]Department of Physiological Chemistry, Graduate School of Pharmaceutical Sciences
[9]Department of Biophysics and Biochemistry, Graduate School of Science
University of Tokyo, Tokyo 113-0033, Japan
[10]Research Institute of Pharmaceutical Sciences, Musashino University, Tokyo 202-8585, Japan
[11]Toyama Prefectural Institute for Pharmaceutical Research, 17-1 Naka-Taikoyama, Imizu, Toyama 939-0363, Japan
[12]Department of Immunobiology and Pharmaceutical Genetics, Graduate School of Medicine and Pharmaceutical Science, University of Toyama, 2630 Sugitani, Toyama, Toyama 930-0194, Japan
[13]Brain Science Institute, The Institute of Physical and Chemical Research (RIKEN), Wako, Saitama 351-0198, Japan
*Correspondence: m.yokoyama.bch@tmd.ac.jp
http://dx.doi.org/10.1016/j.str.2012.06.017

SUMMARY

The leukocyte cell-surface antigen CD38 is the major nicotinamide adenide dinucleotide glycohydrolase in mammals, and its ectoenzyme activity is involved in calcium mobilization. CD38 is also a raft-dependent signaling molecule. CD38 forms a tetramer on the cell surface, but the structural basis and the functional significance of tetramerization have remained unexplored. We identified the interfaces contributing to the homophilic interaction of mouse CD38 by site-specific crosslinking on the cell surface with an expanded genetic code, based on a crystallographic analysis. A combination of the three interfaces enables CD38 to tetramerize: one interface involving the juxtamembrane α-helix is responsible for the formation of the core dimer, which is further dimerized via the other two interfaces. This dimerization of dimers is required for the catalytic activity and the localization of CD38 in membrane rafts. The glycosylation prevents further self-association of the tetramer. Accordingly, the tetrameric interaction underlies the multifaceted actions of CD38.

INTRODUCTION

The leukocyte cell-surface antigen CD38 is a glycoprotein, composed of a large extracellular domain, a transmembrane domain, and a short cytoplasmic domain (Jackson and Bell, 1990). The extracellular domain of CD38 contains the catalytic nicotinamide adenide dinucleotide (NAD^+) glycohydrolase (Gelman et al., 1993; Kontani et al., 1993), which is the main NAD^+ glycohydrolase in mammalian cells (Cockayne et al., 1998). The cleavage of the *N*-glycoside linkage of NAD^+ or nicotinamide adenine dinucleotide phosphate ($NADP^+$) generates ADP-ribose/cyclic ADP-ribose from NAD^+ and nicotinic acid adenine dinucleotide phosphate from $NADP^+$ (Malavasi et al., 2008). All of these products are able to trigger intracellular calcium mobilization in an inositol trisphosphate-independent manner, and CD38 thereby plays a role in calcium-mediated signaling (Lee, 1994, 2005). The catalytic activity of CD38 is required in various processes, such as insulin secretion (Kato et al., 1999; Takasawa et al., 1993), intracellular calcium oscillation (Fukushi et al., 2001), neutrophil chemotaxis (Partida-Sánchez et al., 2001), dendritic cell trafficking (Partida-Sánchez et al., 2004), and oxytocin secretion (Jin et al., 2007). CD38 is also involved in the development of diet-induced obesity via the activation of sirtuins, which are NAD^+-dependent deacetylases (Aksoy et al., 2006).

On the other hand, CD38 is concentrated in specialized membrane regions, such as the immunologic synapse (Muñoz et al., 2008) and membrane rafts (Malavasi et al., 2008). CD38 reportedly associates with various supramolecular complexes within membrane rafts in T cells (CD38/CD3/Lck/LAT) (Zubiaur et al., 1997), B cells (CD38/BCR/CD19/CD81) (Deaglio et al., 2003, 2007), natural killer cells (CD38/CD16) (Deaglio et al., 2002), monocytes (CD38/major histocompatibility complex [MHC] Class II/CD9) (Zilber et al., 2005), and mature dendritic

Cell PRESS

Structure
Tetramerization of CD38 on the Cell Surface

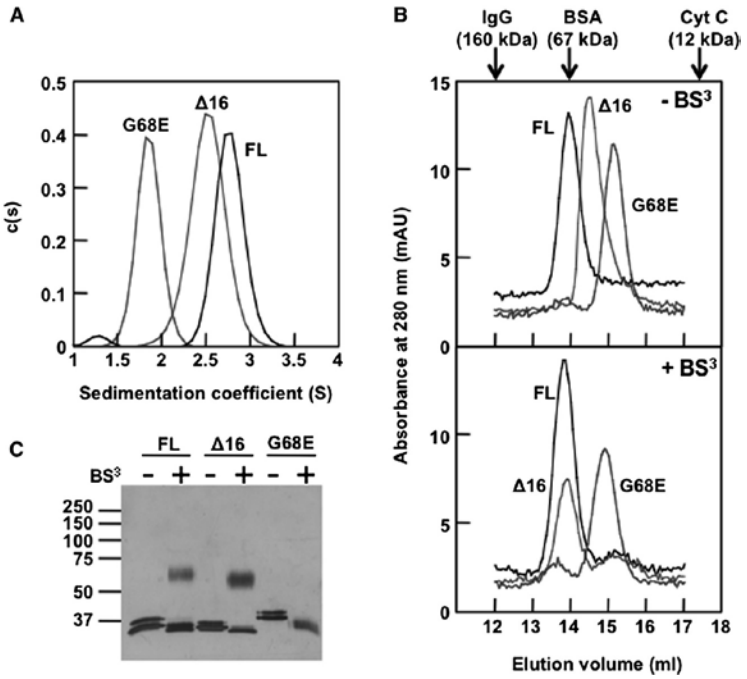

Figure 1. Dimer Structure of the Isolated Extracellular Domain of CD38 in Solution

(A and B) Sedimentation velocity experiments (A) and size-exclusion chromatography (B) were performed with the extracellular domain of CD38, without (full length [FL], black line, FLAG-tag at the N-terminal) or with the C-terminal truncation (Δ16, blue line, FLAG-tag at the N-terminal) or the G68E mutation (red line, FLAGx3-tag at the N-terminal), as described in the Supplemental Experimental Procedures.

(B and C) The extracellular domain of CD38 (0.1 mg/ml) was incubated in the absence and the presence of 200 μM BS^3 at room temperature for 2 hr. The proteins (2 μg each) were then subjected to 9% SDS-PAGE under reducing conditions and silver-stained (C). The presence of two bands without BS^3 is due to high-mannose moieties. See also Figure S1.

cells (CD38/CD83/CD11b/CD81) (Frasca et al., 2006). The association of CD38 with membrane rafts is independent of the catalytic activity of CD38 (Lund et al., 2006, 1999; Manjarrez-Orduño et al., 2007) and may be involved in the initiation of CD38-mediated signaling to trigger cell activation and proliferation.

The overall topology of the extracellular domain of human CD38 (Liu et al., 2005) is similar to those of the other members of the ADP-ribosyl cyclase family, i.e., *Aplysia* ADP-ribosyl cyclase (Prasad et al., 1996) and human bone marrow stromal cell antigen 1 (BST-1/CD157) (Yamamoto-Katayama et al., 2002). However, the three proteins differ from each other in terms of their membrane association. *Aplysia* ADP-ribosyl cyclase is cytosolic, while BST-1 and CD38 are membrane-bound via a glycosylphosphatidylinositol anchor and a transmembrane domain, respectively.

Biochemical and crystallographic analyses revealed that *Aplysia* ADP-ribosyl cyclase and a soluble form of BST-1 exist as dimers (Munshi et al., 1998; Sato et al., 1999). Interestingly, however, the existence of a tetrameric form of human CD38 has been demonstrated (Bruzzone et al., 1998; Franco et al., 1998; Mallone et al., 1998). Consistent with these reports, a high molecular weight form of CD38, corresponding to a tetramer, is induced by retinoic acid in human myeloid (HL-60) leukemia cells (Umar et al., 1996). It was suggested that the oligomerization is relevant to the catalytic activity of CD38 from porcine heart microsomes (Chidambaram et al., 1998). The orientation of the C-terminal α helix (α9) of human CD38 in the crystal is distinct from those of the other two members (Liu et al., 2005), so that the α9 helices would clash if two CD38 molecules formed a dimer in the same manner as the other two members (Figure S3B available online). Thus, CD38 may have a distinct homophilic interaction mode that enables tetramer formation on the cell surface. However, the structural aspects of CD38 assembly and their functional importance have not been elucidated thus far.

In the present study, we investigated the mechanism and the role of CD38 assembly. First, a crystallographic analysis of the extracellular domain of mouse CD38 revealed two interaction modes, whose combination allows the tetramerization of CD38 via a dimer-of-dimers assembly. Second, both interaction modes were actually found for cell-surface CD38 by a site-specific crosslinking experiment using an expanded genetic code. Third, the two interaction modes are both required for the catalytic activity and the targeting of mouse CD38 into membrane rafts. Accordingly, the present study provides the structural basis for the tetramerization of CD38 on the cell surface and demonstrates that the tetramerization of mouse CD38 is crucial for its multifaceted actions.

RESULTS

Novel Homophilic Interaction Modes of Mouse CD38 Deduced from the Crystal Packing of the Extracellular Domain

The full-length extracellular domain of mouse CD38 exists as a homodimer in solution, as revealed by analytical ultracentrifugation and size exclusion chromatography (Figure 1 and Figure S1). However, the homophilic interaction modes of CD38 were not suggested by the previous structural analysis of the full-length extracellular domain of human CD38, since the two molecules in the crystallographic unit lacked an apparent homodimer interface (Liu et al., 2005). In the present study, during the preparation of the extracellular domain of mouse CD38, we noticed that the protein was partially cleaved at F288, causing the truncation of 16 amino acid residues from the C terminus, representing half of the C-terminal α helix (Figure 2A). Thus, the crystal structure of the C-terminal-truncated extracellular domain was solved

Structure
Tetramerization of CD38 on the Cell Surface

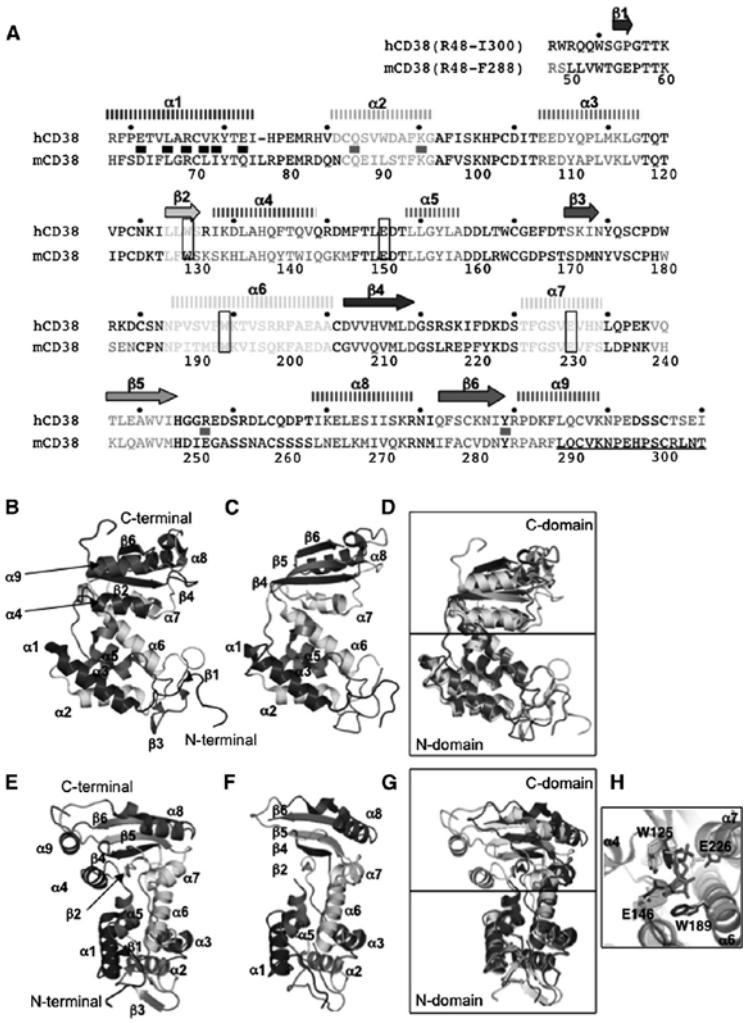

Figure 2. The Crystal Structure of the C-Terminal Truncated Extracellular Domain of Mouse CD38

(A) Sequence alignment between the extracellular domains of the human and mouse CD38 proteins. The truncation in mouse CD38 is underlined. The glycosylation sites were mutated. Catalytically important amino acid residues are boxed. The amino acid residues involving the type I and type II interfaces are indicated by black and pink bars, respectively.

(B, C, E, and F) Structures of the extracellular domain of the full-length human CD38, hCD38 (R48-I300) (B and E) and of the C-terminal truncated mouse CD38, mCD38mut(R48-F288) (C and F).

(D and G) Superimposition of the structures of hCD38(R48-I300) (green) and mCD38mut(R48-F288) (purple).

(H) An expanded view of the active sites. Cyclic inosine diphosphate-ribose is colored orange (2PGJ). See also Figure S2.

(accession code 2EG9; Table 1 and Figure 2) and four types of interfaces (I-IV) were found in the crystal packing (Figure 3).

The extracellular domain of CD38 with the C-terminal truncation also existed as a dimer in solution (Figure 1). The overall structure was not significantly altered by the truncation, based on the circular dichroism spectra (Figure S2). The crystal structure of the full-length extracellular domain of human CD38 (Liu et al., 2005) is divided into the N-domain (β1, α1, α2, α3, α5, β3, and α6) and the C-domain (β2, α4, β4, α7, β5, α8, β6, and α9). As shown in Figure 2, the crystal structure of the C-terminal-truncated extracellular domain of mouse CD38 revealed that the α helices (α1, α2, α3, α5, and α6) of the N-domain all superimposed well on those in the full-length extracellular domain. The two α helices (α7 and α8) and the three-stranded parallel β sheet (β4, β5, and β6) remain intact in the C-domain, and they are only slightly tilted, as compared with those in the full-length extracellular domain.

On the other hand, the α9 helix was entirely disordered, although the amino acid residues corresponding to half of the α9 helix still remained (Figure 2A). In addition, the region corresponding to the α4 helix of the full-length extracellular domain was also disordered (S130–M146) in the C-terminal-truncated form. Thus, the most notable consequence of the C-terminal truncation is the loss of the α9 helix and the fluctuation of the α4 helix.

The α1 helix exists at the type I interface. The α4 helix, which was not fully chain-traced, is actually located at the type III interface (Figure 3H). The edge of the α1 helix is in contact with the loop region between the β5 strand and the α8 helix at the type III interface. Although the type II interface between the α2 helix and the loop region between the β5 strand and the α8 helix by itself is too small to connect two CD38 molecules (Figure 3E), it may contribute to the oligomerization.

Based on the superimposition of the full-length extracellular domain of human CD38, the α4 and α9 helices are both located at the type III interface (Figure 3H). In this situation, the area of the type III interface is calculated to be 1473 Å^2. It is unlikely that the type IV interface exists in the cell-surface CD38, since the glycosylation precludes this interaction, as described below (Figure 6C). The combination of the type I and type II/III interfaces appears to cooperatively function in tetramer formation and is compatible with membrane association (Figure 6).

At the type I interface, hydrophilic interactions (D64•R69/R69•D64 and Q75•Q75) and hydrophobic interaction (D67•I72/I72•D67 and L71•L71) are formed between the α1 helices (Figure 3D). Hydrophilic interactions between Q87 and Y283 and between K94 and E251 are present at the type II interface

Cell PRESS

Structure
Tetramerization of CD38 on the Cell Surface

Table 1. X-Ray Data Collection and Refinement Statistics

Data Collection	
Wavelength (Å)	1.0
Resolution (Å)	50-2.8 (2.90-2.80)
Unique reflections	11912
Redundancy	4.9
Completeness (%)	97.9 (95.5)
I / σ(I)	11.6 (5.2)
R_{sym}[a] (%)	9.8 (22.6)
Refinement	
Resolution (Å)	49.12-2.80
No. of reflections	11873
No. of protein atoms	3390
No. of water molecules	23
R_{work} (%)	26.3
R_{free} (%)[b]	34.0
rmsd bond length (Å)	0.006
rmsd bond angles (°)	1.1

All numbers in parentheses represent last outer shell statistics.
[a] $R_{sym} = \Sigma |I_{avg}-Ii| / \Sigma Ii$, where Ii is the observed intensity and I_{avg} is the average intensity.
[b] R_{free} is calculated for 10% of randomly selected reflections excluded from refinement.

(Figure 3G). These amino acid residues are either conserved or semi-conserved between mouse and human CD38 (Figure 2A). Thus, it is conceivable that the type I and type II interfaces are also possible for human CD38. Actually, an interface similar to type I was previously reported by Shi et al., in the crystal structure of the full-length extracellular domain of human CD38 (1ZVM), as shown in Figure S3C.

In the present study, the full-length extracellular domain of mouse CD38 was not successfully crystallized. For the crystallographic analyses, the glycosylation sites within the proteins were mutated as usual to avoid chemical heterogeneity. The nonglycosylated, full-length mouse CD38 forms a large, amorphous aggregate, probably due to the artificial interface IV, in addition to the three interfaces (types I-III). In contrast, the C-terminal truncation may have facilitated efficient crystal growth by avoiding amorphous aggregation through the weakening of the type III interface.

The Type I Interaction Mode of the Extracellular Domain of CD38 Is Involved in Dimer Formation

The G68E mutation in the α1 helix reduces the stability of the homophilic interaction of mouse CD38, expressed in a murine pro B cell-derived cell line (Ba/F3 cells), after solubilization (Moreno-García et al., 2004). Here, the isolated extracellular domain with the G68E mutation was shown to be present as a monomer in solution by analytical ultracentrifugation and size exclusion chromatography (Figure 1 and Figure S1). According to the crystal structure, the G68E mutation should disrupt the type I interface (Figure 3D). Thus, the results support the interaction between the α1 helices of the extracellular domain of CD38 in solution (the type I interaction mode).

The full-length mouse CD38 on the cell surface was crosslinked by a membrane-impermeable, Lys-reactive chemical crosslinker, BS^3 (Moreno García et al., 2004). Actually, BS^3 treatment of the isolated extracellular domain of CD38 also converted it to a crosslinked dimer, which was abolished by the G68E mutation (Figure 1C). If the BS^3-crosslinking occurs via the type I interaction mode, then the candidate for the crosslinked site is Lys60-Lys60 (Figure S1). However, although trypsin does not cleave CD38 at the Lys residue that reacted with BS^3, efficient cleavage at Lys60 was detected when the tryptic fragments of the crosslinked dimer were analyzed by mass spectroscopy (Figure S1). Thus, it is unlikely that the BS^3-dependent crosslinking occurs via the type I interaction mode.

In the absence of the BS^3-treatment, the extracellular domain of CD38 with the C-terminal truncation eluted after the full-length extracellular domain during size exclusion chromatography, probably due to its smaller size (Figure 1B). However, the extracellular domains with and without the truncation eluted at the same position after the BS^3-dependent crosslinking, suggesting that the exposure of the C-terminal region to the solvent is avoided and the difference in the hydrodynamic property is counteracted by the crosslinking. In addition, the cleavage at Lys145 in the α4 helix was decreased when the crosslinked dimer was analyzed (Figure S1), implying that the BS^3-dependent intermolecular crosslinked via the type III interaction mode. Therefore, the dimer of the extracellular domains of CD38, formed via the type I interaction mode, is further considered to exist in equilibrium to form a tetramer via the type II/III interaction mode, within which the intermolecular BS^3-crosslinking occurs (Figure 3L).

The Homophilic Interaction of CD38 on the Cell Surface

The BS^3-dependent intermolecular crosslinking of cell-surface CD38 was impaired by the G68E mutation and by the C-terminal truncation in A20 cells (Figures 4A and 4B). In addition, the loss of the conserved disulfide bridge, which stabilizes the C-terminal helix (C291A/C300A) (Figure 4C), reduced the intermolecular crosslinking (Figures 4D and 4E). It should be noted that covalently linked CD38 dimers were observed, even in the absence of BS^3, in the cases of the C291A and C300A mutations. Conceivably, the C-terminal helices can contact each other to permit the formation of artificial intermolecular disulfide bridges between Cys300-Cys300 and Cys291-Cys291 when the original disulfide bridge is disrupted and these residues lose their intramolecular partners. These results suggested that the C-terminal helix and the α1 helix are involved in the homophilic interaction of CD38 on the membrane, which supports the type I and type III interaction modes.

To confirm that the type I and type III interaction modes are actually involved in the CD38 assembly on the cell surface, a photo-reactive crosslinker, *p*-benzoyl-L-phenylalanine (*p*Bpa), was separately introduced into CD38 at a defined position, according to the method of Hino et al. (Hino et al., 2005, 2006). Among the 14 variants designed to evaluate the interfaces, three variants, with *p*Bpa in place of V292 in the α9 helix and D64 or I65 in the α1 helix, were sufficiently expressed in Chinese hamster ovary (CHO) cells and subjected to photo-crosslinking (Figure 5A). Crosslinked products with a molecular weight twice as large as that of one CD38 molecule were formed for the CD38 variants with *p*Bpa in place of V292, D64, and I65 (Figure 5B).

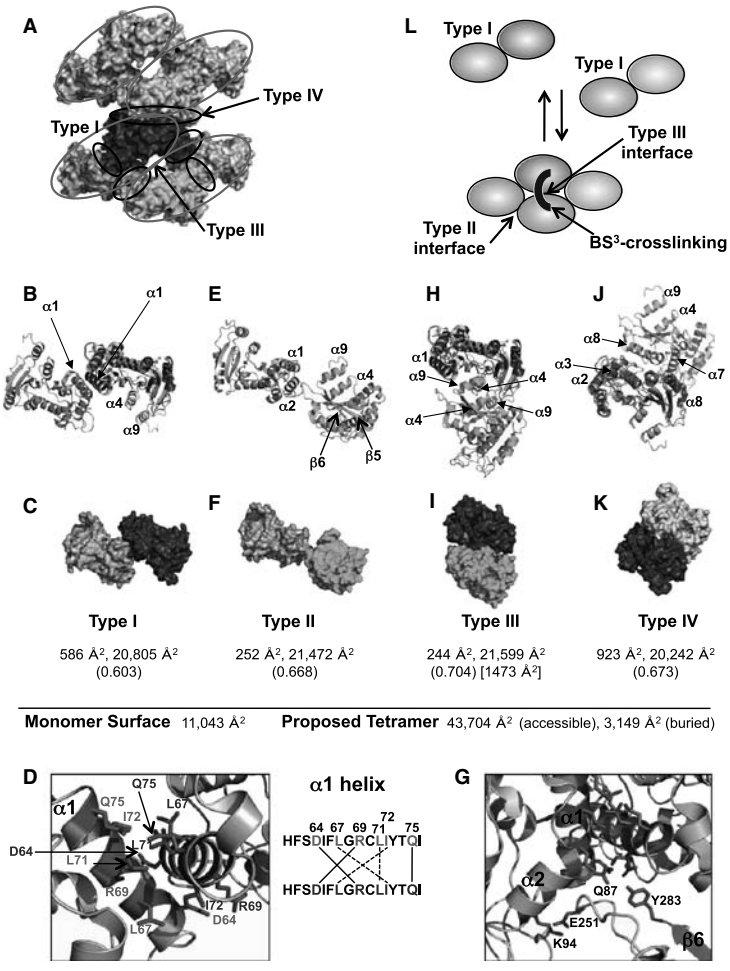

Figure 3. The Interfaces Involved in the Homophilic Interaction of CD38

(A) The crystal packing of mCD38mut(R48-F288) with asymmetric units (red) (2EG9).

(B, E, H, and J) Two molecules of the full-length extracellular domain, hCD38(R48-I300), oriented according to those in mCD38mut(R48-F288) (2EG9), are shown. The monomer structure of mCD38mut(R48-F288) (2EG9) was superimposed (purple).

(C, F, I, and K) The four types of interfaces (I-IV) are depicted with the accessible area and the shape complementarities (in parentheses).

(D and G) Expanded views of the type I and type II interfaces, respectively. Possible electrostatic (solid lines) and hydrophobic (dashed lines) interactions between the two α1 helices are shown in (D).

(L) The proposed dynamic equilibrium of the extracellular domain of CD38 in solution. See also Figure S3.

In order to confirm that the crosslinked products represent homophilic CD38 multimers, FLAG-tagged CD38 and Myc-tagged CD38 were coexpressed in CHO cells. The crosslinked products that were immunoprecipitated with the anti-FLAG antibody reacted with both the anti-FLAG and anti-Myc antibodies (Figures 5C and 5D, respectively). Thus, the results indicated that the crosslinking occurs between CD38 molecules and at least the α9 and α1 helices are near the interface. The detection of the products corresponding to the tetramer (Figures 5C and 5D) suggested that tetramerization of CD38 occurs on the cell surface and that the tetramer appears to be more stable than the isolated extracellular domain in solution.

The Processing of the N-Glycan of CD38 Is Compatible with Tetramerization

During protein synthesis, oligomannose glycans are first processed by α-glucosidases and mannosidases in the endoplasmic reticulum and then are further processed to complex- or hybrid-type oligosaccharides by *N*-acetylglucosaminyltransferase I in the *medial*-Golgi (Figure S5A) (Kato and Kamiya, 2007). An analysis of the site-specific glycan of CD38 unexpectedly revealed that only the oligosaccharides attached to the N213 residue remained as the high-mannose-type (Figure S5B). Within the CD38 tetramer, the N213 residue faces the space between the extracellular domain and the membrane (Figure 6E). This orientation would prevent the access of the processing enzymes. By contrast, the N213 residue is fully accessible to the enzymes when CD38 is present as a dimer or a monomer. Accordingly, the high-mannose-type oligosaccharides of the N213 residue are indicative of the tetramerization of CD38 during the processing of the *N*-glycan.

The Two Interaction Modes Are Crucial for the Catalytic Activity of CD38

Among the ADP-ribosyl cyclase family proteins, the catalytically important residues, W125, E146, W189, and E226 in human CD38, are located at spatially equivalent positions (Liu et al., 2005; Prasad et al., 1996; Yamamoto-Katayama et al., 2002). In the sequence, W125 and E146 are located near the α4 helix (boxed in Figure 2A). As shown in Figure 2H, the positions of W129 and E230 in the C-terminal-truncated extracellular domain of CD38 (shown in purple) were shifted by approximately 3 Å as compared to the corresponding residues, W125 and E226, in the full-length extracellular domain (shown in green). This displacement suggests the importance of the proper interaction between the C-terminal α9 helix and the α4 helix in catalytic-site formation, which is consistent with the

Cell PRESS

Structure
Tetramerization of CD38 on the Cell Surface

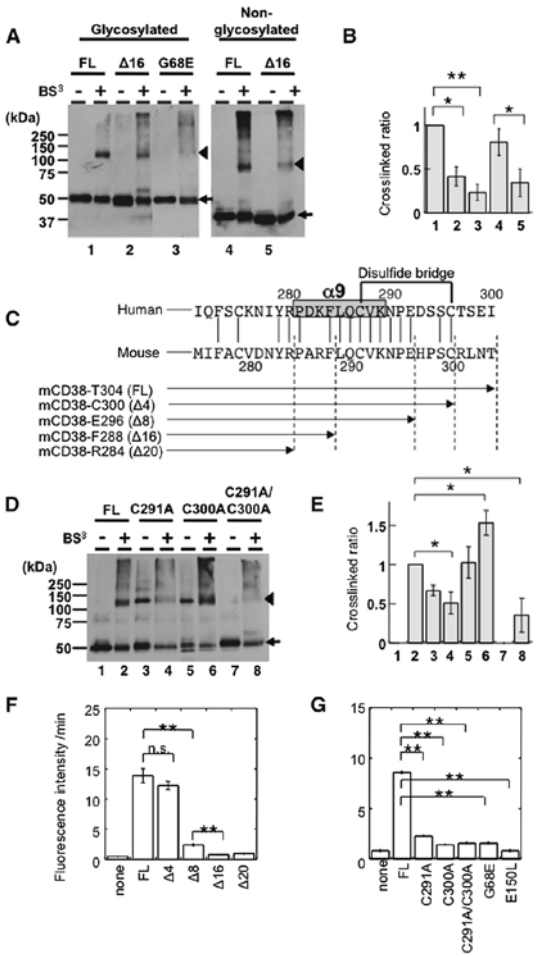

Figure 4. The C-Terminal and Juxtamembrane α Helices Are Both Important for the Homophilic Interaction of CD38 on the Cell Surface and the Catalytic Activity

(A and D) A20 cells (1×10^7 cells/ml) transfected with glycosylated or non-glycosylated FLAG-tagged CD38 in either the FL or truncated form or with the indicated mutations were incubated in the absence or presence of BS^3. The proteins were detected by immunoblotting with a biotin-anti-FLAG pAb, as described in the Supplemental Experimental Procedures. The positions of the crosslinked dimers and the noncrosslinked monomers of CD38 are shown by triangles and arrows, respectively.

(B and E) The crosslinking ratios, which are the intensities of crosslinked dimer to noncrosslinked monomer in Figures 7A and 7D, respectively, are expressed as relative values to that without the truncation. Densitometric analysis was performed using the ImageJ software (http://rsbweb.nih.gov/ij/).

(C) Sequence alignment of the C-terminal regions of human and mouse CD38 and schematic representations of the FLAG-tagged mouse CD38 constructs to probe the roles of the C-terminal α-helix. The two conserved cysteine residues involved in the disulfide bridge (Cys287 and Cys296 in human CD38 and Cys291 and Cys300 in mouse CD38) are also shown.

(F and G) NAD^+ glycohydrolase activities of A20 cells (none) or CD38 transfectants without (FL) and with the C-terminal truncation or the mutations were measured. Significant differences are indicated: ** = $p < 0.01$; n.s. = not significant ($p > 0.05$). Values are means ± SD (n = 3). See also Figure S4.

results previously reported for calcium-loaded CD38 (Liu et al., 2008).

In the case of the isolated extracellular domain, both the C-terminal truncation of 16 amino acid residues and the G68E mutation appreciably decreased the NAD^+ glycohydrolase activity (Figure S4E). In addition, the BS^3-crosslinking and the specific activity of the NAD^+ glycohydrolase were decreased at a lower concentration of the extracellular domain (Figures S4F and S4G), implying that proper assembly is important for the catalytic activity of CD38 in solution.

In A20 cells, the C-terminal truncation of four amino acid residues did not affect the NAD^+ glycohydrolase activity of CD38 (Figure 4F), which is consistent with the fact that the four residues are disordered in the crystal structure of human CD38 (Liu et al., 2005). However, the truncation of eight amino acid residues appreciably reduced the NAD^+ glycohydrolase activity. This may be due to the loss of the disulfide bond between Cys291 and Cys300, which is conserved among the family proteins (Figure 4C), since the mutations affecting the disulfide bond appreciably reduced the catalytic activity (Figure 4G). The truncation of 16 and 20 amino acid residues resulted in the complete loss of the NAD^+ glycohydrolase activity. The cyclase activity was also diminished by the truncation of 16 amino acid residues (Figure S4D). Thus, the C-terminal region involving the type III interaction mode is crucial for the catalytic activity.

The G68E mutation in the α1 helix abolished the NAD^+ glycohydrolase activity of CD38 in A20 cells (Figure 4G). The effect was comparable to that of the mutation of the catalytically important Glu150 to Leu (E150L). A consistent result was previously obtained in Ba/F3 cells (Moreno-García et al., 2004). Since the G68E mutation disrupts the homophilic interaction (Figure 1 and Figure S1) and Gly68 participates in the type I interaction mode (Figure 3), it is suggested that the integrity of the type I interaction mode is necessary for the catalytic activity of CD38 on the cell surface. Accordingly, the two interaction modes are both crucial for the catalytic activity.

The Two Interaction Modes Facilitate the Association of CD38 with Detergent-Resistant Membranes

Biochemical analyses have revealed the specific associations of several membrane proteins with detergent-resistant membranes (DRMs). DRMs are enriched in cholesterol and sphingolipids and can be isolated as low-density fractions from detergent-lysed cells (Brown and Rose, 1992). Although membrane rafts and DRMs should be carefully distinguished (Sonnino, 2008), DRMs can reflect important changes in the distribution of proteins on the membranes.

As shown in Figure 7A, CD38 was recovered in DRMs after A20 cells expressing CD38 were lysed with 1% Brij-58. The amounts of CD38 in DRMs were decreased by the G68E mutation in the α1 helix and by the C-terminal truncation (Figures 7B and 7C). We previously reported that the ligation of CD38 with the agonistic antimouse CD38 antibody, CS/2, increased the association of CD38 with DRMs in mouse splenic B cells (Hara-Yokoyama et al., 2008). The amount of wild-type CD38 in DRMs was further increased by treating A20 cells with CS/2. However, the amount of truncated CD38 in DRMs was not significantly increased by CS/2, although the C-terminal truncation did not reduce the binding of CS/2 to CD38 (Figure S6).

Structure
Tetramerization of CD38 on the Cell Surface

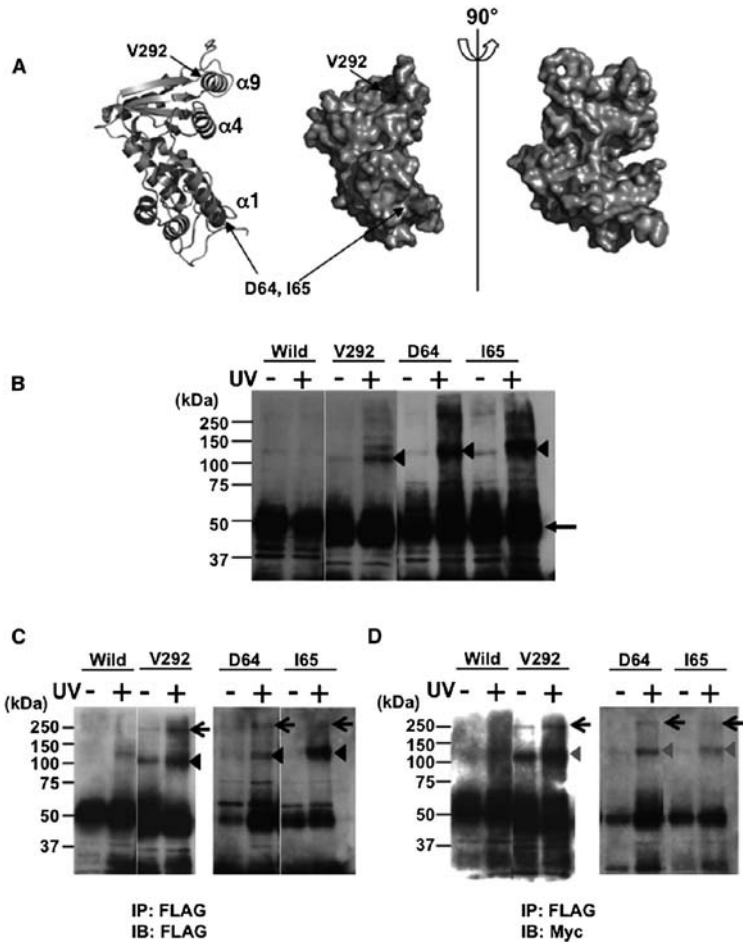

Figure 5. Site-Specific Crosslinking of Cell-Surface CD38

(A) The residues to which the crosslinker was introduced are shown in hCD38(R48-I300) in two perpendicular views.

(B–D) CHO cells were transfected with amber mutants of FLAG-tagged CD38 (B) or with both FLAG-tagged and Myc-tagged CD38 (C and D). Light-dependent crosslinking of CD38 was performed as described in the Experimental Procedures. The reaction was analyzed by immunoblotting with an anti-FLAG antibody (B and C) and an anti-Myc (D) antibody.

These results suggest that the two interaction modes contribute to the association of CD38 with DRMs.

In addition, we examined whether the C-terminal truncation affects the lipid composition of DRMs harboring CD38 (CD38-DRMs) by the immunoprecipitation of CD38 in DRMs. In this context, CD38 has an affinity for sphingolipids, as the catalytic activities of CD38 are inhibited by gangliosides (Hara-Yokoyama et al., 1996, 2001). In the CD38-DRMs, lipids were similarly detected with and without the C-terminal truncation, regardless of the CS/2 stimulation and glycosylation (Figure S6). Accordingly, it is unlikely that the C-terminal truncation alters the lipid composition in CD38-DRMs.

Functional Aspects of N-Glycosylation of CD38

CD38 has four potential N-glycosylation sites (Gao and Mehta, 2007). We compared the wild-type and mutant CD38 proteins, in which the Asn residues were mutated to Asp residues (N104D/N124D/N213D/N223D), to evaluate the role of the *N*-glycosylation. Even in the absence of glycosylation, the C-terminal truncation reduced the BS^3-dependent crosslinking (Figures 4A and 4B) and abolished the catalytic activity (Figure S4). However, the truncation did not alter the amount of nonglycosylated CD38 in DRMs in both the presence and absence of CS/2 (Figures 7D and 7E). Thus, the glycosylated and nonglycosylated CD38 molecules associated with DRMs in different manners. We will discuss this point below from the perspective of the involvement of glycosylation in the regulation of the cell-surface assembly of CD38.

DISCUSSION

In the present study, we demonstrated that the type I and type II/III interaction modes are involved in the assembly of mouse CD38 on the cell surface. The combination of the modes cooperatively stabilizes the tetramer. The type I interaction mode is primarily involved in the core homophilic interaction between the extracellular domains. The core dimer formed via the type I interaction mode is then assembled into the tetramer via the type II/III interaction mode, which provides a structural basis for the previously reported tetramerization. In the case of the extracellular domain, the association/dissociation in the dimer-tetramer equilibrium may be fast, and thus the tetramer was not detectable during analytical ultracentrifugation and size exclusion chromatography. Tetramerization occurs more efficiently with the full-length CD38 on the cell surface than the extracellular domain fragments in solution, probably because the orientation of the extracellular domain is restricted on the cell surface. Since the integrity of both interaction modes was required for the catalytic activity and the raft-association ability of CD38, we conclude that the tetramerization due to the dimer-of-dimers interaction is vital for the functional aspects of CD38 on the cell surface. Furthermore, we discovered the role of glycosylation in the regulation of the homophilic interaction of CD38. Thus, the assembly of CD38 is distinct from those of the other family members, although the structures of the protomers are well conserved among them, except for the orientation of the C-terminal α-helix (Liu et al., 2005).

Cell PRESS

Structure
Tetramerization of CD38 on the Cell Surface

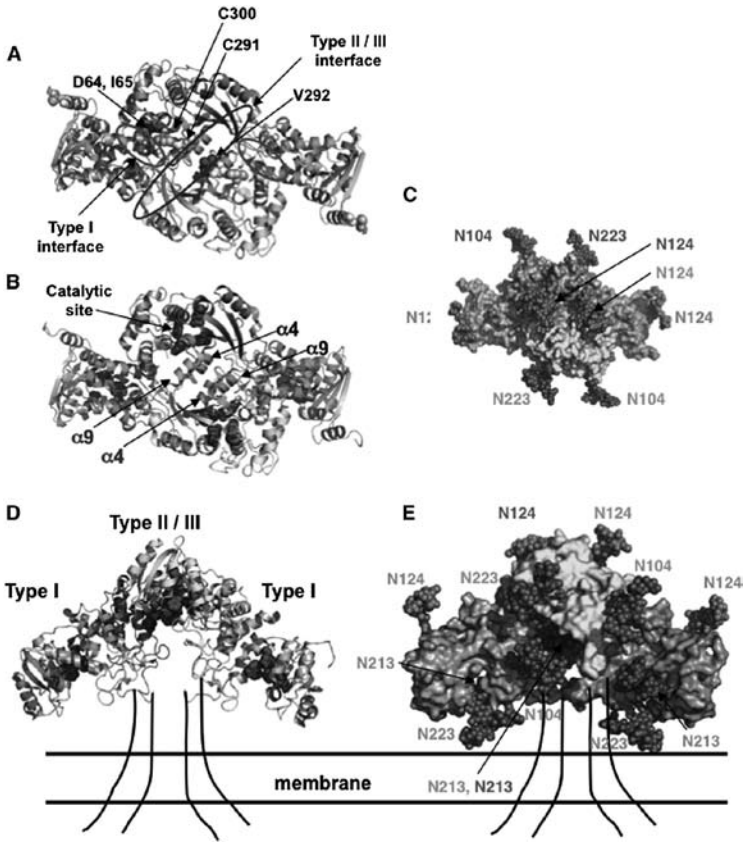

Figure 6. Schematic Representations of the Dimer-of-Dimers Interactions of CD38 on the Cell Surface

The four molecules of hCD38(R48-I300) are assembled by the type I interface (red oval) and by the type II/III interfaces (blue oval), as in mCD38mut(R48-F288) in the crystal (2EG9). The structures in (D and E) are shown in a perpendicular view to those in (A)–(C). The residues corresponding to D64, I65, and V292 of mouse CD38 are depicted in red, and those corresponding to C291 and C300 are yellow and light orange, respectively (A). The catalytically important residues (W125, E146, W189, and E226 in hCD38) are shown in red (B and D). (C and E) The structure of the *N*-linked oligosaccharide moiety from a fat-depleting factor (1ZAG), composed of nine sugar residues, is attached to the residues corresponding to the N-glycosylation sites of mouse CD38 (N104, N124, N213, and N223, respectively). See also Figure S5.

Within the tetramer of CD38, the α9 helix can interact with the α4 helix of the other CD38 molecule at the type III interface to reciprocally stabilize each other's active sites (Figure 6B). In this context, the pair of the α9 and α4 helices is considered to be a molecular device coupling the homophilic interaction to the catalytic site formation. The requirement of the type I interaction mode for the catalytic activity is explained by the stabilization of the type II/III interfaces via tetramerization.

A long-lasting topological problem is how the catalytic activity of the CD38 ectoenzyme is involved in intracellular calcium signaling (Malavasi et al., 2008). The oligomerized CD38 reportedly acts as a channel of cyclic ADP ribose (cADPR) (Franco et al., 1998). Intriguingly, in the tetramer structure, all of the catalytic sites face the space enclosed between the ectoenzyme and the membrane surface (Figure 6D). It would be tempting to determine whether the four transmembrane domains in the tetrameric assembly are the basis for the putative inward channel activity of the produced cADPR.

The clustering of membrane proteins enhances their targeting to membrane rafts (Hammond et al., 2005). The clustering of T cell receptors (TCR), B cell receptors (BCR), and FcεRI, caused by antigen/MHC complexes or oligomeric antigens, facilitates their recruitment to membrane rafts and triggers immune-recognition receptor signaling in T, B, and mast cells, respectively (Gupta and DeFranco, 2007; Jury et al., 2007; Silveira E Souza et al., 2011). The present study suggests that the raft-targeting of CD38 requires its intrinsic clustering on the cell surface rather than the lipid interaction. The C-terminal and juxtamembrane helices of CD38 are required, but the defect due to the C-terminal truncation is not compensated by the ligation with the agonistic antibody. Therefore, the integrity of the two modes of homophilic interactions enabling tetramerization appears to be essential. However, at present, we have not succeeded in detecting the CD38 tetramer clearly after SDS-PAGE. The tetramer is probably stabilized on the membrane and readily dissociates to monomers or dimers in the presence of detergent. A more sophisticated approach, such as single-molecule tracking on live cells, will be required to detect the tetrameric form on the cell surface. Additionally, no partner molecule within membrane rafts that can generally explain the raft-targeting of CD38 has been identified, although the association of CD38 with the Src family protein tyrosine kinase Lck has been reported (Cho et al., 2000). It is conceivable that the identification of the CD38 partner would require experimental conditions that maintain the integrity of the CD38 tetramer.

In contrast to the glycosylated CD38, the effect of the C-terminal truncation on the association of CD38 with DRMs was not observed in the absence of *N*-glycosylation. The absence of the *N*-glycans attached to N104 and N223 is considered to enable the formation of the "type IV" interface (Figure 3K). Actually, BS^3-dependent high-molecular mass aggregates of CD38 were observed in the absence of glycosylation. Similar results were obtained in HeLa and Michigan Cancer Foundation (MCF)-7 cells (Gao and Mehta, 2007). Thus, the *N*-glycans probably regulate the assembly of CD38 on the cell surface by inhibiting the "aggregating" type IV interface.

Structure
Tetramerization of CD38 on the Cell Surface

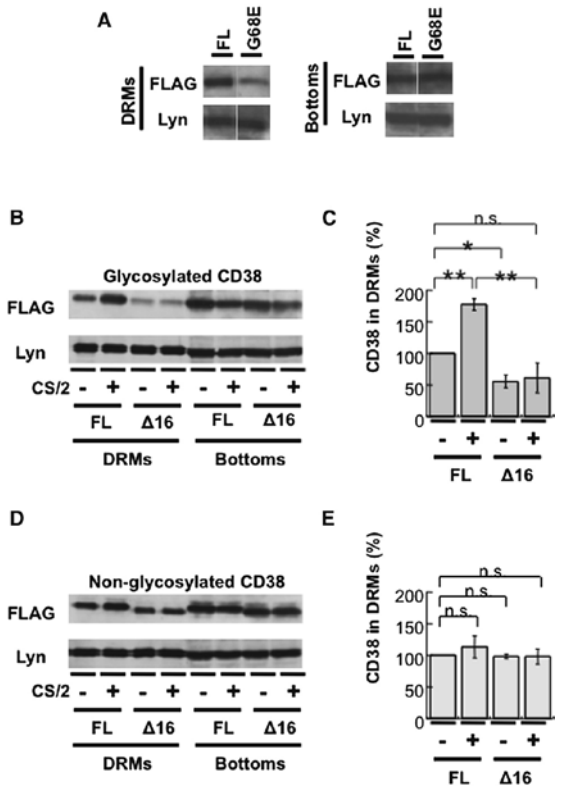

Figure 7. The C-Terminal Region Truncation and the G68E Mutation Decrease the Association of Glycosylated CD38 with DRMs

(A) A20 cells transfected with glycosylated FLAG-tagged CD38 (2×10^8 cells/ml), without (FL) and with the G68E mutation, were lysed in 1% Brij-58 lysis buffer.

(B and D) A20 cells transfected with glycosylated (B) and nonglycosylated (D) FLAG-tagged CD38 (2×10^8 cells/ml) in either the full-length (FL) or truncated form were stimulated with 20 μg/ml CS/2 and then lysed. Lysates were fractionated by sucrose density gradient ultracentrifugation, as described in the Supplemental Experimental Procedures. Proteins in the DRM and bottom fractions were separated by 10% SDS-PAGE and were detected by immunoblotting with a biotinylated anti-FLAG pAb and an anti-Lyn pAb. Essentially, the same results were obtained in an independent experiment.

(C and E) The intensities of the bands in (B and D) were quantified and expressed as the relative values to that without the truncation (FL) in the absence of CS/2. Densitometric analysis of the band intensity was performed using the ImageJ software. Values are means ± SD (n = 3). Significant differences are indicated: ** = $p < 0.01$; * = $p < 0.05$; n.s. = not significant ($p > 0.05$). See also Figure S6.

Recently, the mono *N*-glycosylated forms of bovine CD38 have been revealed as parallel "back-to-back" homodimers (Egea et al., 2012), which would not be allowed in the case of mouse CD38 due to the glycosylation at N124. Thus, the assembly of CD38 might have diversity among species.

From a clinical point of view, CD38 is recognized as a negative prognostic indicator in B cell chronic lymphocytic leukemia patients and in individuals infected with HIV (Malavasi et al., 2008). Based on studies using B cell chronic lymphocytic leukemia cells, CD38 is a potential signaling molecule that regulates cell fate rather than a mere marker (Malavasi et al., 2008). Autoantibodies against CD38 reportedly impaired glucose-induced insulin secretion in a noninsulin-dependent diabetes patient (Ikehata et al., 1998). Considering the functional importance of the cell-surface assembly of mouse CD38 demonstrated here, the assembly of human CD38 should be resolved to develop a new therapeutic strategy, in which the disassembly of CD38 can be manipulated.

EXPERIMENTAL PROCEDURES

Protein Expression and Purification

The extracellular domains of CD38 were transiently expressed as secreted proteins in *Drosophila* S2 cells and purified as described previously (Hara-Yokoyama et al., 2008). Plasmid construction is described in the Supplemental Experimental Procedures. For the crystallization, the four Asn residues were mutated to Asp residues (N104D, N124D, N213D, and N223D).

Crystallization and Data Collection

The crystallization screening of FLAG-mCD38mut(R48-F288) was performed by the sitting-drop vapor diffusion method (protein at 7.4 mg/ml) at 20°C. Diffraction quality crystals were grown by the addition of 0.2 M NDSB-256 (Hampton Research) to the sitting drops, which were equilibrated against a reservoir solution containing 25% polyethylene glycol 1500 (PEG1500). The crystals belonged to the primitive orthorhombic space group $P2_12_12$, with unit cell constants of a = 59.1 Å, b = 176.8 Å, c = 44.6 Å, and contained two CD38 molecules per asymmetric unit. Single crystals were coated with Paratone-N and 10% glycerol, mounted using a nylon loop (Hampton Research), and flash-cooled in the cold stream of the goniometer. The data were collected with a wavelength of 1.0 Å on beamline BL26B2 at SPring-8 (Harima, Japan) and were recorded on a Jupiter210 charge-coupled device detector (Rigaku). The diffraction data were processed with the HKL2000 program (Otwinowski and Minor, 1997).

Structure Determination and Refinement

The structure of FLAG-mCD38mut(R48-F288) was determined by molecular replacement with the program MOLREP (CCP4), using human CD38 (PDBID: 2DF1) as the search model. The model was corrected iteratively using O (Jones et al., 1991), and structure refinement was performed using Crystallography and NMR system (Brünger et al., 1998). Refinement statistics are presented in Table 1. The quality of the model was inspected by the program PROCHECK (Laskowski et al., 1993). Graphic figures were created using the program PyMOL (http://www.pymol.org). The atomic coordinates have been deposited in the Protein Data Bank, with the accession code 2EG9.

Cells

The murine B lymphoma-derived cell line A20 and the CHO cells were maintained in Roswell Park Memorial Institute 1640 medium supplemented with 8% fetal bovine serum and 50 μM 2-mercaptoethanol and in minimum essential medium supplemented with 10% fetal bovine serum, respectively. Both media contained penicillin and streptomycin.

Stable Transfectants

Plasmid construction is described in the Supplemental Experimental Procedures. Transfection of A20 cells was performed using the Nucleofector technology (Amaxa), and puromycin-resistant cells were obtained.

Site-Specific Crosslinking

The CD38 gene in pCEpuro-mCD38-T304 was mutagenized to create an amber codon located at H61, D64, I65, L67, R69, L71, L77, L135, L137, T140, W141, I142, P285, or V292. Each amber mutant CD38 gene (5 μg DNA) was cotransfected into CHO cells (5×10^6 cells) with pc*p*BpaRS ver.1 (5 μg DNA), carrying the bacterial pair of an amber suppressor transfer RNA (tRNA) and an aminoacyl-tRNA synthetase specific to *p*-benzoyl-L-phenylalanine (*p*Bpa) (Hino et al., 2005, 2006), using Lipofectamine 2000 (36 μl). Among

Cell PRESS

Structure
Tetramerization of CD38 on the Cell Surface

the mutants, the protein was sufficiently expressed in the presence of *p*Bpa when the amber codon was introduced at positions D64, I65, and V292 after overnight culture. The cells were then exposed to UV light and lysed with 1% Triton X-100 in buffer A, consisting of 20 mM Tris-HCl, 150 mM NaCl, 10 mM iodoacetamide, 2.5 mM NaF, 2.5 mM sodium pyrophosphate, 10 mM ethylenediaminetetraacetic acid, 10 mM β-glycerophosphate, 1 mM sodium orthovanadate, 1 mM phenylmethylsulfonyl fluoride, 5 μg/ml leupeptin, 10 μg/ml pepstatin, and 10 μg/ml aprotinin, pH 7.5. Cell lysates were incubated for 2 hr at 4°C with a 10 μl slurry of anti-FLAG M2 agarose resin. After the resin was washed, the complexes were eluted with 100 μg/ml FLAGx3 peptide and analyzed by immunoblotting.

Statistical Analysis

Differences between mean values were assessed by the Student's t test. The statistical significance was set at P less than .01 or .05.

SUPPLEMENTAL INFORMATION

Supplemental Information includes six figures and Supplemental Experimental Procedures and can be found with this article online at http://dx.doi.org/10.1016/j.str.2012.06.017.

ACKNOWLEDGMENTS

We thank Mio Inoue, Tomomi Uchikubo-Kamo, and Seisuke Kusano (RIKEN Systems and Structural Biology Center) for the preparation of CD38 proteins, Prof. Chan Fong Chang (National University of Singapore) for valuable discussions, and Prof. Hidetoshi Kobayashi (RIKEN) for providing lysenin and the anti-lysenin antibody. This work was supported by the Targeted Proteins Research Program (TPRP) and Grants-in-Aid for Scientific Research 22592060 (to M.H.), 23650319 (to K.A.P.), and 23659108 (to M.Y.), as well as grants from the Global Center of Excellence (GCOE) Program from the Ministry of Education, Culture, Sports, Science, and Technology, Japan.

Received: January 16, 2012
Revised: June 22, 2012
Accepted: June 30, 2012
Published online: August 2, 2012

REFERENCES

Aksoy, P., Escande, C., White, T.A., Thompson, M., Soares, S., Benech, J.C., and Chini, E.N. (2006). Regulation of SIRT 1 mediated NAD dependent deacetylation: a novel role for the multifunctional enzyme CD38. Biochem. Biophys. Res. Commun. *349*, 353–359.

Brown, D.A., and Rose, J.K. (1992). Sorting of GPI-anchored proteins to glycolipid-enriched membrane subdomains during transport to the apical cell surface. Cell *68*, 533–544.

Brünger, A.T., Adams, P.D., Clore, G.M., DeLano, W.L., Gros, P., Grosse-Kunstleve, R.W., Jiang, J.S., Kuszewski, J., Nilges, M., Pannu, N.S., et al. (1998). Crystallography & NMR system: A new software suite for macromolecular structure determination. Acta Crystallogr. D Biol. Crystallogr. *54*, 905–921.

Bruzzone, S., Guida, L., Franco, L., Zocchi, E., Corte, G., and De Flora, A. (1998). Dimeric and tetrameric forms of catalytically active transmembrane CD38 in transfected HeLa cells. FEBS Lett. *433*, 275–278.

Chidambaram, N., Wong, E.T., and Chang, C.F. (1998). Differential oligomerization of membrane-bound CD38/ADP-ribosyl cyclase in porcine heart microsomes. Biochem. Mol. Biol. Int. *44*, 1225–1233.

Cho, Y.S., Han, M.K., Choi, Y.B., Yun, Y., Shin, J., and Kim, U.H. (2000). Direct interaction of the CD38 cytoplasmic tail and the Lck SH2 domain. Cd38 transduces T cell activation signals through associated Lck. J. Biol. Chem. *275*, 1685–1690.

Cockayne, D.A., Muchamuel, T., Grimaldi, J.C., Muller-Steffner, H., Randall, T.D., Lund, F.E., Murray, R., Schuber, F., and Howard, M.C. (1998). Mice deficient for the ecto-nicotinamide adenine dinucleotide glycohydrolase CD38 exhibit altered humoral immune responses. Blood *92*, 1324–1333.

Deaglio, S., Zubiaur, M., Gregorini, A., Bottarel, F., Ausiello, C.M., Dianzani, U., Sancho, J., and Malavasi, F. (2002). Human CD38 and CD16 are functionally dependent and physically associated in natural killer cells. Blood *99*, 2490–2498.

Deaglio, S., Capobianco, A., Bergui, L., Dürig, J., Morabito, F., Dührsen, U., and Malavasi, F. (2003). CD38 is a signaling molecule in B-cell chronic lymphocytic leukemia cells. Blood *102*, 2146–2155.

Deaglio, S., Vaisitti, T., Billington, R., Bergui, L., Omede', P., Genazzani, A.A., and Malavasi, F. (2007). CD38/CD19: a lipid raft-dependent signaling complex in human B cells. Blood *109*, 5390–5398.

Egea, P.F., Muller-Steffner, H., Kuhn, I., Cakir-Kiefer, C., Oppenheimer, N.J., Stroud, R.M., Kellenberger, E., and Schuber, F. (2012). Insights into the mechanism of bovine CD38/NAD+glycohydrolase from the X-ray structures of its michaelis complex and covalently-trapped intermediates. PLoS ONE *7*, e34918.

Franco, L., Guida, L., Bruzzone, S., Zocchi, E., Usai, C., and De Flora, A. (1998). The transmembrane glycoprotein CD38 is a catalytically active transporter responsible for generation and influx of the second messenger cyclic ADP-ribose across membranes. FASEB J. *12*, 1507–1520.

Frasca, L., Fedele, G., Deaglio, S., Capuano, C., Palazzo, R., Vaisitti, T., Malavasi, F., and Ausiello, C.M. (2006). CD38 orchestrates migration, survival, and Th1 immune response of human mature dendritic cells. Blood *107*, 2392–2399.

Fukushi, Y., Kato, I., Takasawa, S., Sasaki, T., Ong, B.H., Sato, M., Ohsaga, A., Sato, K., Shirato, K., Okamoto, H., and Maruyama, Y. (2001). Identification of cyclic ADP-ribose-dependent mechanisms in pancreatic muscarinic Ca(2+) signaling using CD38 knockout mice. J. Biol. Chem. *276*, 649–655.

Gao, Y., and Mehta, K. (2007). N-linked glycosylation of CD38 is required for its structure stabilization but not for membrane localization. Mol. Cell. Biochem. *295*, 1–7.

Gelman, L., Deterre, P., Gouy, H., Boumsell, L., Debré, P., and Bismuth, G. (1993). The lymphocyte surface antigen CD38 acts as a nicotinamide adenine dinucleotide glycohydrolase in human T lymphocytes. Eur. J. Immunol. *23*, 3361–3364.

Gupta, N., and DeFranco, A.L. (2007). Lipid rafts and B cell signaling. Semin. Cell Dev. Biol. *18*, 616–626.

Hammond, A.T., Heberle, F.A., Baumgart, T., Holowka, D., Baird, B., and Feigenson, G.W. (2005). Crosslinking a lipid raft component triggers liquid ordered-liquid disordered phase separation in model plasma membranes. Proc. Natl. Acad. Sci. USA *102*, 6320–6325.

Hara-Yokoyama, M., Kukimoto, I., Nishina, H., Kontani, K., Hirabayashi, Y., Irie, F., Sugiya, H., Furuyama, S., and Katada, T. (1996). Inhibition of NAD+ glycohydrolase and ADP-ribosyl cyclase activities of leukocyte cell surface antigen CD38 by gangliosides. J. Biol. Chem. *271*, 12951–12955.

Hara-Yokoyama, M., Nagatsuka, Y., Katsumata, O., Irie, F., Kontani, K., Hoshino, S., Katada, T., Ono, Y., Fujita-Yoshigaki, J., Sugiya, H., et al. (2001). Complex gangliosides as cell surface inhibitors for the ecto-NAD+ glycohydrolase of CD38. Biochemistry *40*, 888–895.

Hara-Yokoyama, M., Kimura, T., Kaku, H., Wakiyama, M., Kaitsu, Y., Inoue, M., Kusano, S., Shirouzu, M., Yokoyama, S., Katada, T., et al. (2008). Alteration of enzymatic properties of cell-surface antigen CD38 by agonistic anti-CD38 antibodies that prolong B cell survival and induce activation. Int. Immunopharmacol. *8*, 59–70.

Hino, N., Okazaki, Y., Kobayashi, T., Hayashi, A., Sakamoto, K., and Yokoyama, S. (2005). Protein photo-cross-linking in mammalian cells by site-specific incorporation of a photoreactive amino acid. Nat. Methods *2*, 201–206.

Hino, N., Hayashi, A., Sakamoto, K., and Yokoyama, S. (2006). Site-specific incorporation of non-natural amino acids into proteins in mammalian cells with an expanded genetic code. Nat. Protoc. *1*, 2957–2962.

Ikehata, F., Satoh, J., Nata, K., Tohgo, A., Nakazawa, T., Kato, I., Kobayashi, S., Akiyama, T., Takasawa, S., Toyota, T., and Okamoto, H. (1998). Autoantibodies against CD38 (ADP-ribosyl cyclase/cyclic ADP-ribose

Structure
Tetramerization of CD38 on the Cell Surface

hydrolase) that impair glucose-induced insulin secretion in noninsulin- dependent diabetes patients. J. Clin. Invest. *102*, 395–401.

Jackson, D.G., and Bell, J.I. (1990). Isolation of a cDNA encoding the human CD38 (T10) molecule, a cell surface glycoprotein with an unusual discontinuous pattern of expression during lymphocyte differentiation. J. Immunol. *144*, 2811–2815.

Jin, D., Liu, H.X., Hirai, H., Torashima, T., Nagai, T., Lopatina, O., Shnayder, N.A., Yamada, K., Noda, M., Seike, T., et al. (2007). CD38 is critical for social behaviour by regulating oxytocin secretion. Nature *446*, 41–45.

Jones, T.A., Zou, J.Y., Cowan, S.W., and Kjeldgaard, M. (1991). Improved methods for building protein models in electron density maps and the location of errors in these models. Acta Crystallogr. A *47*, 110–119.

Jury, E.C., Flores-Borja, F., and Kabouridis, P.S. (2007). Lipid rafts in T cell signalling and disease. Semin. Cell Dev. Biol. *18*, 608–615.

Kato, I., Yamamoto, Y., Fujimura, M., Noguchi, N., Takasawa, S., and Okamoto, H. (1999). CD38 disruption impairs glucose-induced increases in cyclic ADP-ribose, [Ca2+]i, and insulin secretion. J. Biol. Chem. *274*, 1869–1872.

Kato, K., and Kamiya, Y. (2007). Structural views of glycoprotein-fate determination in cells. Glycobiology *17*, 1031–1044.

Kontani, K., Nishina, H., Ohoka, Y., Takahashi, K., and Katada, T. (1993). NAD glycohydrolase specifically induced by retinoic acid in human leukemic HL-60 cells. Identification of the NAD glycohydrolase as leukocyte cell surface antigen CD38. J. Biol. Chem. *268*, 16895–16898.

Laskowski, R.A., MacArthur, M.W., Moss, D.S., and Thornton, J.M. (1993). PROCHECK: a program to check the stereochemical quality of protein structures. J. Appl. Cryst. *26*, 283–291.

Lee, H.C. (1994). Cyclic ADP-ribose: a calcium mobilizing metabolite of NAD+. Mol. Cell. Biochem. *138*, 229–235.

Lee, H.C. (2005). Nicotinic acid adenine dinucleotide phosphate (NAADP)-mediated calcium signaling. J. Biol. Chem. *280*, 33693–33696.

Liu, Q., Kriksunov, I.A., Graeff, R., Munshi, C., Lee, H.C., and Hao, Q. (2005). Crystal structure of human CD38 extracellular domain. Structure *13*, 1331–1339.

Liu, Q., Graeff, R., Kriksunov, I.A., Lam, C.M., Lee, H.C., and Hao, Q. (2008). Conformational closure of the catalytic site of human CD38 induced by calcium. Biochemistry *47*, 13966–13973.

Lund, F.E., Muller-Steffner, H.M., Yu, N., Stout, C.D., Schuber, F., and Howard, M.C. (1999). CD38 signaling in B lymphocytes is controlled by its ectodomain but occurs independently of enzymatically generated ADP-ribose or cyclic ADP-ribose. J. Immunol. *162*, 2693–2702.

Lund, F.E., Muller-Steffner, H., Romero-Ramirez, H., Moreno-García, M.E., Partida-Sánchez, S., Makris, M., Oppenheimer, N.J., Santos-Argumedo, L., and Schuber, F. (2006). CD38 induces apoptosis of a murine pro-B leukemic cell line by a tyrosine kinase-dependent but ADP-ribosyl cyclase- and NAD glycohydrolase-independent mechanism. Int. Immunol. *18*, 1029–1042.

Malavasi, F., Deaglio, S., Funaro, A., Ferrero, E., Horenstein, A.L., Ortolan, E., Vaisitti, T., and Aydin, S. (2008). Evolution and function of the ADP ribosyl cyclase/CD38 gene family in physiology and pathology. Physiol. Rev. *88*, 841–886.

Mallone, R., Ferrua, S., Morra, M., Zocchi, E., Mehta, K., Notarangelo, L.D., and Malavasi, F. (1998). Characterization of a CD38-like 78-kilodalton soluble protein released from B cell lines derived from patients with X-linked agammaglobulinemia. J. Clin. Invest. *101*, 2821–2830.

Manjarrez-Orduño, N., Moreno-García, M.E., Fink, K., and Santos-Argumedo, L. (2007). CD38 cross-linking enhances TLR-induced B cell proliferation but decreases IgM plasma cell differentiation. Eur. J. Immunol. *37*, 358–367.

Moreno-García, M.E., Partida-Sánchez, S., Primack, J., Sumoza-Toledo, A., Muller-Steffner, H., Schuber, F., Oppenheimer, N., Lund, F.E., and Santos-Argumedo, L. (2004). CD38 is expressed as noncovalently associated homodimers on the surface of murine B lymphocytes. Eur. J. Biochem. *271*, 1025–1034.

Muñoz, P., Mittelbrunn, M., de la Fuente, H., Pérez-Martínez, M., García-Pérez, A., Ariza-Veguillas, A., Malavasi, F., Zubiaur, M., Sánchez-Madrid, F., and Sancho, J. (2008). Antigen-induced clustering of surface CD38 and recruitment of intracellular CD38 to the immunologic synapse. Blood *111*, 3653–3664.

Munshi, C., Baumann, C., Levitt, D., Bloomfield, V.A., and Lee, H.C. (1998). The homo-dimeric form of ADP-ribosyl cyclase in solution. Biochim. Biophys. Acta *1388*, 428–436.

Otwinowski, Z., and Minor, W. (1997). Processing of X-ray diffraction data collected in oscillation mode. Methods Enzymol. *276*, 307–326.

Partida-Sánchez, S., Cockayne, D.A., Monard, S., Jacobson, E.L., Oppenheimer, N., Garvy, B., Kusser, K., Goodrich, S., Howard, M., Harmsen, A., et al. (2001). Cyclic ADP-ribose production by CD38 regulates intracellular calcium release, extracellular calcium influx and chemotaxis in neutrophils and is required for bacterial clearance in vivo. Nat. Med. *7*, 1209–1216.

Partida-Sánchez, S., Goodrich, S., Kusser, K., Oppenheimer, N., Randall, T.D., and Lund, F.E. (2004). Regulation of dendritic cell trafficking by the ADP-ribosyl cyclase CD38: impact on the development of humoral immunity. Immunity *20*, 279–291.

Prasad, G.S., McRee, D.E., Stura, E.A., Levitt, D.G., Lee, H.C., and Stout, C.D. (1996). Crystal structure of Aplysia ADP ribosyl cyclase, a homologue of the bifunctional ectozyme CD38. Nat. Struct. Biol. *3*, 957–964.

Sato, A., Yamamoto, S., Kajimura, N., Oda, M., Usukura, J., and Jingami, H. (1999). Inhibitor peptide SNP-1 binds to a soluble form of BST-1/CD157 at a 2:2 stoichiometry. Eur. J. Biochem. *264*, 439–445.

Silveira E Souza, A.M., Mazucato, V.M., Jamur, M.C., and Oliver, C. (2011). Lipid rafts in mast cell biology. J. Lipids *2011*, 752906.

Sonnino, S.A.P. (2008). Membrane lipid domains and membrane lipid domain preparations: are they the same thing? Trends Glycosci. Glycotechnol. *20*, 315–340.

Takasawa, S., Nata, K., Yonekura, H., and Okamoto, H. (1993). Cyclic ADP-ribose in insulin secretion from pancreatic beta cells. Science *259*, 370–373.

Umar, S., Malavasi, F., and Mehta, K. (1996). Post-translational modification of CD38 protein into a high molecular weight form alters its catalytic properties. J. Biol. Chem. *271*, 15922–15927.

Yamamoto-Katayama, S., Ariyoshi, M., Ishihara, K., Hirano, T., Jingami, H., and Morikawa, K. (2002). Crystallographic studies on human BST-1/CD157 with ADP-ribosyl cyclase and NAD glycohydrolase activities. J. Mol. Biol. *316*, 711–723.

Zilber, M.T., Setterblad, N., Vasselon, T., Doliger, C., Charron, D., Mooney, N., and Gelin, C. (2005). MHC class II/CD38/CD9: a lipid-raft-dependent signaling complex in human monocytes. Blood *106*, 3074–3081.

Zubiaur, M., Izquierdo, M., Terhorst, C., Malavasi, F., and Sancho, J. (1997). CD38 ligation results in activation of the Raf-1/mitogen-activated protein kinase and the CD3-zeta/zeta-associated protein-70 signaling pathways in Jurkat T lymphocytes. J. Immunol. *159*, 193–205.

口腔病理学分野

山口　朗

医歯学総合研究科・口腔機能再構築学系専攻
口腔病理学・教授

1）研究の課題名

口腔癌顎骨浸潤の分子メカニズムの解明を目指したフロンティア研究拠点

New frontier of molecular mechanism of bone invasion by oral cancer

口腔病理学分野と顎口腔外科分野は、口腔癌の骨浸潤の分子メカニズムの解明を目指して共同研究を行い、口腔癌の産生するIL-6と癌が誘導する間質細胞のIL-6産生が重要な役割を担っていることを明らかにしてきた。今年度は、さらに詳細なメカニズム解明を目指して以下の実験を行った。

a）癌細胞の産生するRANKLと間質細胞の産生するRANKLの作用の区別化：我々が確立したヒト口腔癌をヌードマウス頭蓋部に移植した骨破壊モデルを用いた。口腔癌細胞移植後にヒトRANKL特異的中和抗体またはマウスRANKL特異的中和抗体を投与し、骨破壊の程度を解析した。さらに、両抗体を同時に投与した時の骨破壊も解析した。これらの実験により、口腔扁平上皮癌では、癌細胞と間質細胞の産生するRNAKLの両方が骨破壊で重要であることを明らかにした。

b）ヒト口腔癌細胞（HSC3）から骨吸収能の高いクローンと低いクローンを分離し、両細胞のマイクロアレイ解析により前者のクローンではCXCL2の高いことを明らかにし、口腔扁平上皮癌による骨破壊の過程ではCXCL2が重要な役割を担っていることを明らかにした。

上記研究は、「異なる分野のInnovationの確立する研究」として行われた。

2）研究のイラストレーション

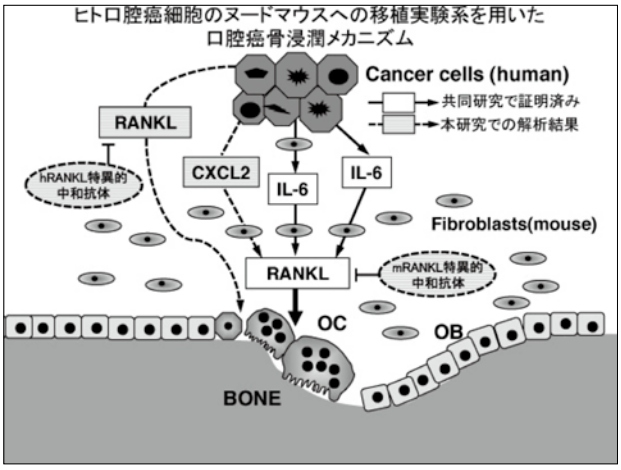

3）発表の研究内容についての英文要約

a）We demonstrated that RANKL-positive fibroblasts and cancer cells were located at sites of bone invasion in human oral cancers. We discriminated the roles of RANKL synthesized by stromal cells and cancer cells in cancer-associated bone resorption by using species-specific RANKL antibodies against murine RANKL and human RANKL, respectively. HSC3-induced bone destruction was greatly inhibited by the administration of anti-mouse RANKL antibody in a xenograft model. HO-1-N-1-induced bone destruction was inhibited by the administration of either anti-mouse or anti-human RANKL antibody. The present study revealed that RANKL produced by both stromal and cancer cells is involved in oral cancer-induced osteoclastic bone resorption.

b）Two clonal cell lines, HSC3-C13 and HSC3-C17, were isolated from the maternal oral cancer cell line, HSC3. Gene expression was compared between HSC3-C13 and HSC3-C17 cells by using microarray analysis, which showed that CXCL2 gene was highly expressed in HSC3-C13 cells as compared to HSC3-C17 cells. Te increase in osteoclast numbers induced by the HSC3-C13-conditioned medium was dose-dependently inhibited

by addition of anti-human CXCL2-neutralizing antibody in a co-culture system. Recombinant CXCL2 increased the expression of Rankl in UAMS-32 cells. These results indicate that CXCL2 is involved in bone destruction induced by oral cancer. This is the first report showing the role of CXCL2 in cancer-associated bone destruction.

4）本事業に関連して世界的な研究拠点形成に向けて、以下の点で改善・整備等されたこと

A（研究拠点体制）

口腔癌による骨破壊のメカニズムは十分に理解されていないために、本研究では骨生物学の基礎研究者、病理専門医および口腔外科専門医の共同で研究を推進し、臨床的な状況を反映した研究拠点を形成した。

B（研究教育環境）

口腔病理学分野および顎口腔外科学分野の大学院生を積極的に研究に参画させ、基礎的、病理学的、口腔外科学的な観点から教育を行った。

C（人材確保）

口腔病理学分野のスタッフと大学院生の他に顎口腔外科学分野、顎顔面口腔外科学分野の大学院生を研究推進の人材として利用した。

D（人材育成）

口腔病理学分野のポスドクには積極的に研究計画の立案をディスカッションし、論文のまとめ方の指導も行った。

E（国際化）

口腔病理学分野の３人の外国人大学院生も研究に参画し、母国に帰国後も本研究に関連した研究の指導者になれるよう指導した。また、口腔病理学分野のポスドクは韓国人のため、彼女が帰国後も十分に研究を推進できるような指導を行った。

5）GCOE事業を推進するに当たって力を入れた点

ヒトの口腔癌の骨破壊に類似した動物モデルの構築とそれを用いた実験結果の臨床応用への展開に重点をおいた。

6）英文原著論文

1. ◎Himeno-Ando A, Izumi Y, Yamaguchi A, Iimura T：Structural differences in the osteocyte network between the calvaria and long bone revealed by three-dimensional fluorescence morphometry, possibly reflecting distinct mechano-adaptations and sensitivities. Biochem Bioph Res Co 417：765-770,2012
2. Sakamoto K, Fujii T, Kawachi H, Miki Y, Omura K, Morita K, Kayamori K, Khanom R, Katsube K, Yamaguchi A：Reduction of NOTCH1 expression pertains to maturation abnormalities of keratinocytes in squamous neoplasms. Lob Invest 92：688-702：2012
3. ◎Khanom R, Sakamoto K, Pal SK, Shimada Y, Morita K-i, Omura K, Miki Y, Yamaguchi A：Expression of basal cell keratin 15 and keratin 19 in oral squamous cell carcinoma represent diverse phthophysiologies. Histol Histopathol 27：949-959,2012
4. Aizawa R, Yamada A, Suzuki D, Iimura T, Kassai H, Harada T, Tsukasaki M, Yamamoto G, Tachikawa T, Nakao K, Yamamoto M, Yamaguchi A, Aiba A, Kamijo R：Cdc42 is required for chondrogenesis and interdigital programmed cell death during limb development. Mech Dev 129：38-50,2012
5. Michikawa C, Uzawa N, Kayamori K, Sonoda I, Ohyama Y, Okada N, Yamaguchi A, Amagasa T：Clinical significance of lymphatic and blood vessel invasion in oral tongue squamous cell carcinomas. Oral Oncol 48：320-324,2012
6. ◎Umehara K, Iimura T, Sakamoto K, Lin Z, Kasugai S, Igarashi Y, Yamaguchi A：Canine oral mucosal fibroblasts differentiate into osteoblastic cellsin response to BMP-2. Anat Rec 295：1327-1335,2012
7. ◎Watanabe T, Tamamura Y, Hoshino A, Makino Y, Nishimura R, Kamioka H, Yoneda T, Amagasa T, Yamaguchi A, Iimura T：Increasing participation of Sclerostin in postnatal bone development revealed by three-dimensional immunofluorescence morphometry. BONE 51：447-458,2012
8. Sakamoto K, Khanom R, Hamagaki M, Yamaguchi A：Ectopic production of hair keratin constitutes Rushton's hyaline bodies in association with hematogenous deposits. J Oral Pathol Med 27：949-959,2012
9. ◎Oue E, Lee JW, Sakamoto K, Iimura T, Aoki K, Kayamori K, Michi Y, Yamashiro M, Yamaguchi A：CXCL2 synthesized by oral squamous cell carcinoma is involved in cancer-associated bone destruction. Biochem Bioph Res Co 424：456-461,2012
10. Nishimura R, Wakabayashi M, Hata K, Matsubara T, Honma H, Wakisaka S, Kiyonari H, Shioi G, Yamaguchi A, Tsumaki N, Akiyama H, Yoneda T：Osterix regulates calcification and degradation of chondrogenic matrices through matrix metalloproteinase（MMP13）expression in association with transcription factor Runx2 during endochondral ossification. J Biol Chem 287：33179-33190,2012
11. ◎Hoshino A, Ueha S, Hanada S, Imai T, Ito M, Yamamoto K, Matsushima K, Yamaguchi A, Iimura T：Roles of chemokine receptor CX3CR1 in maintaining murine bone homeostasis through the regulation of both osteoblasts and osteoclasts. J Cell Sci 258：28826-28837,2012

12. ◎Tanabe R, Haraikawa M, Sogabe N, Sugimoto A, Kawamura Y, Takasugi S, Nagata M, Nakane A, Yamaguchi A, Iimura T, Masae Goseki-Sone：Retention of bone strength by feeding of milk and dairy products in ovariectomized rats; involvement of changes in serum levels of 1alpha, 25（OH）2D3 and FGF23. J Nutr Biochem. 2012 [in press]
13. ◎Makino Y, Takahashi Y, Tanabe R, Tamamura Y, Watanabe T, Haraikawa M, Hamagaki M, Hata K, Kanno J, Yoneda T, Saga Y, Goseki-Sone M, Kaneko K, Yamaguchi A, Iimura T：Spatiotemporal disorder in endochondral ossification during axial skeleton development in the Mesp2-null mouse：A developmental etiology of spondylocostal dysostosis and spondylothoracic dysostosis. BONE（in press）

7）総説ならびに著書

1. Iimura T, Nakane A, Sugiyama M, Sato H, Makino Y, Watanabe T, Takagi Y, Numano R, Yamaguchi A：A fluorescence spotlight on the clockwork development and metabolism of bone. J Bone Miner Metab. 30：254-269,2012
2. 山口朗：種々の脊椎動物における骨細胞ネットワーク、CLINICAL CALCIUM 22：71-76,2012

8）平成24年度までの自己評価

GCOEプログラムに参加することにより、大学院生も積極的に研究を行い、モチベーションが上がったと思う また、異分野との共同研究を推進する契機にもなった。

9）学会発表（英文）

1. Yamaguchi A：Bisphosphonate-related osteonecrosis, updates. 2012 Sino-Japan Dental Conference, Chengdu, Sichaun, China, 2012, April, 27

10）学会発表（和文）

1. Khanom Rumana、坂本啓、山口朗：Expression of keratin（K）15 and K19 in oral squamous neoplasms represents diverse phthophysiologies. 第101回日本病理学会総会、2012年4月26日、東京
2. Samir Pal、坂本啓、山口朗：TSP1 in stroma promotes invasion of oral cancer. 第101回日本病理学会総会、2012年4月26日、東京
3. 坂本啓、山口朗：Rushtonの硝子体の起源、第101回日本病理学会総会、2012年4月26日、東京

11）外部資金の獲得状況

科学研究費補助金、基盤研究A

研究題目：オステオネットワークの維持と破綻：顎顔面骨疾患の病態解明を目指した基盤研究
代表：山口朗
期間：平成22年―平成24年
研究費総額：4810万円

科学研究費補助金、挑戦的萌芽研究

研究題目：オステオネットワーク獲得機構の解明を目指した挑戦的研究代表：山口朗
代表：山口朗
期間：平成22年―平成24年
研究費総額：360万円

科学研究費補助金、特別研究員奨励費用

研究題目：低分子天然化合物を用いた骨形成の治療表的分子の同定
代表：山口朗
期間：平成22年―平成24年
研究費総額：160万円

12）特別講演、招待講演、シンポジウム

1. Yamaguchi A：Bone destruction by oral cancer, The 6th Global COE international Symposium at TMDU, 2012 Jan. 22（Tokyo）
2. 山口朗：口腔癌の骨破壊、第30回日本口腔腫瘍学会、教育講演、2012年1月27日（大宮）
3. 山口朗：オステオネットワークの維持と破壊：顎骨疾患の病態解明と新たな治療法の開発を目指して. 第30回北海道医療大学歯学会、特別講演、2012年3月3日（札幌）
4. 山口朗：顎骨壊死の病態の最新知見、第10回日本歯科骨粗鬆症研究会、シンポジウム「ビスフォスフォネート製剤の長期治療による光と影―顎骨壊死は回避できるのかー」2012年3月18日（大阪）
5. Yamaguchi A：Bisphosphonate-related osteonecrosis, updates. 2012 Sino-Japan Dental Conference, Chengdu, Sichaun, China, 2012, April, 27
6. 山口朗：オステオネットワークの獲得・維持・破綻、米田俊之教授退官記念講演会、大阪大学中之島センター、2012年5月5日（大阪）
7. 山口朗：オステオネットワークの維持と破綻：骨疾患の病態解明を目指して、第27回長崎骨粗鬆症研究会、長崎県医師会館、2012年5月9日（長崎）
8. 山口朗：病理組織学的立場から見たBMA関連顎骨

病変の成因と診断、口腔三学会合同シンポジウム、「Bone-modifying Agents（BMA）関連顎骨病変の病態・診断・治療」、第57回日本口腔外科学会総会・学術大会、パシフィコ横浜会議センター、2012年10月20日

13）主催学会

第23回日本臨床口腔病理学会
平成24年8月29－31日、東京医科歯科大学

14）教室、分野や講座の准教授、講師、助教、特別研究員、ポスドク、指導を受けた大学院生の名前

准教授　　飯村　忠浩
大学院生　○ Pal SK
　　○ Rumana Khanoma

Laboratory Investigation (2012) 92, 688–702

Reduction of NOTCH1 expression pertains to maturation abnormalities of keratinocytes in squamous neoplasms

Kei Sakamoto[1], Takuma Fujii[2], Hiroshi Kawachi[3], Yoshio Miki[4], Ken Omura[5], Kei-ichi Morita[6], Kou Kayamori[7], Ken-ichi Katsube[1] and Akira Yamaguchi[1]

Notch is a transmembrane receptor functioning in the determination of cell fate. Abnormal Notch signaling promotes tumor development, showing either oncogenic or tumor suppressive activity. The uncertainty about the exact role of Notch signaling, partially, stems from inconsistencies in descriptions of Notch expression in human cancers. Here, we clarified basal-cell dominant expression of NOTCH1 in squamous epithelium. NOTCH1 was downregulated in squamous neoplasms of oral mucosa, esophagus and uterine cervix, compared with the normal basal cells, although the expression tended to be retained in cervical lesions. NOTCH1 downregulation was observed even in precancers, and there was little difference between cancers and high-grade precancerous lesions, suggesting its minor contribution to cancer-specific events such as invasion. In culture experiments, reduction of NOTCH1 expression resulted in downregulation of keratin 13 and keratin 15, and upregulation of keratin 17, and *NOTCH1* knockdown cells formed a dysplastic stratified epithelium mimicking a precancerous lesion. The NOTCH1 downregulation and the concomitant alterations of those keratin expressions were confirmed in the squamous neoplasms both by immunohistochemical and cDNA microarray analyses. Our data indicate that reduction of NOTCH1 expression directs the basal cells to cease terminal differentiation and to form an immature epithelium, thereby playing a major role in the histopathogenesis of epithelial dysplasia. Furthermore, downregulation of NOTCH1 expression seems to be an inherent mechanism for switching the epithelium from a normal and mature state to an activated and immature state, suggesting its essential role in maintaining the epithelial integrity.
Laboratory Investigation (2012) **92,** 688–702; doi:10.1038/labinvest.2012.9; published online 13 February 2012

KEYWORDS: epithelial dysplasia; esophagus; Notch1; oral mucosa; squamous cell carcinoma; uterine cervix; keratin

Notch is a transmembrane receptor that regulates cell proliferation and differentiation in various tissues. Notch is constitutively processed and is tethered on the plasma membrane as a heterodimeric protein, and the signal is transduced by the Notch intracellular domain (NICD) produced by ligand-induced cleavage,[1,2] which translocates to the nucleus and directly induces the transcription of downstream targets by forming a transactivation complex with several cofactors.[3] In humans, there are four *Notch* homologs (*NOTCH1*, *2*, *3*, *4*) and they exhibit diverse patterns of expression, suggesting different contributions in each tissue.

The expression of Notch1, Notch2 and Notch3 in mouse skin and hair follicles has been documented,[4–7] and Notch signaling seems to have important roles in the regulation of epidermal differentiation. Conditional knockout of *Notch1* in skin results in epidermal and corneal hyperplasia.[8] Overexpression of constitutively active Notch1 in basal cells leads to hyperplastic epidermis and abnormal hair development.[4,9] In contrast, deletion of *Notch2*, *Notch3* and *Notch4* does not cause significant changes in the epidermis.[6,10,11] These results indicate the significance of Notch1 in epidermal differentiation.

Abnormal Notch signaling can promote tumor development. The first indication that Notch has a role in carcinogenesis was obtained from a mouse mammary tumor virus integration assay in which four genes were identified as candidates that associate with tumor progression, the third of which (int-3) turned out to be a truncated form of *Notch4*.[12]

[1]Section of Oral Pathology, Tokyo Medical and Dental University, Tokyo, Japan; [2]Department of Obstetrics and Gynecology, Keio University School of Medicine, Tokyo, Japan; [3]Section of Human Pathology, Tokyo Medical and Dental University, Tokyo, Japan; [4]Section of Molecular Genetics, Medical Research Institute, Tokyo Medical and Dental University, Tokyo, Japan; [5]Section of Oral and Maxillofacial Surgery, Tokyo Medical and Dental University, Tokyo, Japan; [6]Department of Advanced Molecular Diagnosis and Maxillofacial Surgery, Hard Tissue Genome Research Center, Tokyo Medical and Dental University, Tokyo, Japan and [7]Section of Diagnostic Oral Pathology, Tokyo Medical and Dental University, Tokyo, Japan
Correspondence: Dr K Sakamoto, Section of Oral Pathology, Tokyo Medical and Dental University, Yushima 1-5-45, Tokyo 113-0034, Japan.
E-mail: s-kei.mpa@tmd.ac.jp

Received 29 August 2011; revised 25 November 2011; accepted 15 December 2011

Gain of function mutation of *NOTCH1* was detected in many cases of T-cell acute lymphoblastic leukemia,[13] and this finding gave rise to the concept of treatment by inhibiting the formation of Notch transactivation complex.[14] In cervical cancer, the upregulation of NOTCH1[15,16] and NOTCH2,[16] and an increase in nuclear localization of NICD[17] were documented. On the basis of these observations, activation of Notch signaling is thought to be associated with the development of cervical cancer.[18] However, promotion of carcinogenesis by Notch signal activation seems contradictory to the phenotypes observed in the *Notch1* knockout mouse, which exhibits an increase in the incidence of papilloma and chemical-induced skin cancer,[8] and the transgenic mouse of the pan-Notch inhibitor, dominant-negative *Mastermind-like 1*, which shows dysplasia and SCC of skin.[19] In fact, expression of NOTCH1 is decreased in skin cancer,[20,21] suggesting that *NOTCH1* acts as a tumor suppressor. To solve the discrepancy of the proposed role of Notch, accurate knowledge of its expression is crucial. To assess its contribution in cancer, the Notch expression should be evaluated in comparison with the normal cells from which the cancer cells originated. However, it appears that the expression of Notch in human cancers has not been properly evaluated along this line. Even the localization of Notch proteins in normal adult tissue is unclear, partially, because of the difficulty of detection.

To address this issue, we have engaged in an examination of Notch expression in adult human tissues. In this study, we first demonstrate that NOTCH1 is predominantly expressed in the basal cells of normal squamous epithelium. Then we expand the examination to neoplasms that have originated from squamous epithelium and show that Notch1 expression is downregulated in these lesions. Cell culture experiments indicate that reduction of NOTCH1 expression associates with abnormal differentiation represented by alteration of keratin subtype expression. Our data suggest that aberrant epithelial differentiation in squamous neoplasms is caused by the reduction of NOTCH1 expression, which in turn unveils its essential function in the maintenance of normal epithelial integrity.

MATERIALS AND METHODS

Clinical Specimens

A total of 56 specimens of oral lesions (epithelial dysplasia and squamous cell carcinoma) were collected at the Dental Hospital of Tokyo Medical and Dental University. Pharyngeal cancers were excluded; the case summaries are shown in Supplementary Material 1. A total of 20 specimens of esophageal lesions (squamous cell carcinoma) and normal tissues were collected at Medical Hospital of Tokyo Medical and Dental University; the case summaries are shown in Supplementary Material 2. A total of 57 specimens of uterine cervical lesions (intraepithelial neoplasm and squamous cell carcinoma) were collected at Keio University Hospital; the case summaries are shown in Supplementary Material 3. The tissues were fixed in formalin and embedded in paraffin according to the routine laboratory protocol. HPV genotyping was performed as previously described[22] from the conventional cytology specimens. All experiments were approved by the ethics committees of both universities.

cDNA Microarray Analysis

Oral squamous cell carcinoma (OSCC) cells were taken from surgically excised specimens by laser capture microdissection and were subjected to cDNA microarray analysis, as previously described.[23]

Immunostaining and *In Situ* Hybridization

Immunohistochemical staining was performed using the Sequenza (Thermo Fisher Scientific, MA, USA). For antigen retrieval, the sections were autoclaved in alkaline buffer (10 mM Tris (pH = 9.0) and 1 mM EDTA) at 120 °C for 20 min. The primary antibodies used in this study were anti-Notch1 (EP1238Y, Epitomics, CA, USA); cleaved Notch1 (Val1744; D3B8, Cell Signaling, MA, USA) Notch2 (D67C8, Cell Signaling); Notch3 (D11B8, Cell Signaling); Hes1 (EPR4226, Epitomics); Hey1 (polyclonal, Millipore, MA, USA); keratin 5 (K5; EPR1600Y, Epitomics); K13 (EPR3671, Epitomics); K13 (alternative antibody, KS-1A3, Leica Microsystems, Wetzlar, Germany); K15 (EPR1614Y, Epitomics); K17 (D73C7, Cell Signaling); K17 (alternative antibody, E3, Dako, Glostrup, Denmark); K18 (DC10, Dako); pan-Keratin (AE1/AE3, Dako); Vimentin (SP20, Epitomics); E-cadherin (36/E-Cadherin, BD transduction laboratories, CA, USA); Desmoglein3 (3G133, Santa Cruz, CA, USA); p63 (4A4, Dako); β-tubulin (9F3, Cell Signaling) and β-actin (C-2, Santa Cruz). EnVision Dual Link (Dako) was used as the secondary antibody. Coloration was done in DAB substrate. For immunofluorostaining, Alexa Fluor 488 anti-rabbit IgG (Invitrogen, CA, USA) and DAPI were used. *In situ* hybridization to mouse E18.5 embryos was conducted as previously described.[24] Antibody adsorption test was performed as follows. HEK293 cells were transfected with *Notch1* or *NOTCH3* and were fixed 48 h after transfection. The anti-NOTCH1 or anti-NOTCH3 antibody (diluted 1/500) was applied to the fixed cells, respectively, and incubated for 1 h. The adsorbed supernatants were collected and used for immunohistochemical staining. The immunostaining results were compared with that using the antibody adsorbed to mock-transfected cells.

Protein Extraction from Formalin-Fixed Paraffin-Embedded Specimens

Formalin-fixed paraffin-embedded specimens were sectioned at 10 μm thick and deparaffinized. Tissues were manually dissected under a microscope. The collected tissues were heated at 95 °C for 1 h and then at 60 °C for 4 h in the protein extraction buffer (50 mM Tris (pH = 8.0), 5 mM EDTA, 2% SDS).

Genes

Mouse *Notch1* was provided by Dr J. Nye and constitutive active *Notch1* were previously described.[25] Notch extracellular domain (NECD) was created by ligating the PCR amplified *Notch1* extracellular and transmembrane regions (1M to 1755G) into *pAcGFP1-C2* (Clontech). Human *Notch3* was provided by Dr A. Joutel. *Rbpj* cDNA was provided by the RIKEN BioResource Center (Ibaraki, Japan) courtesy of Dr T. Honjo and cloned into *pCMV-Tag4* (Stratagene, CA, USA), and dominant-negative *Rbpj (R218H)* was created by PCR mutagenesis. Dominant-negative *Dll1* (chick) was previously described.[26] Human *TP63α(TA)* was purchased from Invitrogen. *TP63α(ΔN)* was created as follows. A plasmid (*pBK-CMV-dN*) was made, which contained the sequence corresponding to the *TP63α(ΔN)*-specific N-terminal region by ligating annealed oligoniculeotides into *pBK-CMV* (Stratagene). As the N-terminal *TP63α(TA)*-specific region incidentally coincides to 5′ of MSC1 site, the N-terminal region was deleted from *TP63α(TA)* by MSC1 digestion, and the fragment was ligated into *pBK-CMV-dN*. The resulting plasmid was confirmed by DNA sequencing to carry *TP63α(ΔN)* identical to the wild type. Human *KRT13* and *KRT15* promoters were cloned by PCR from the BAC clone RP11-156A24, and human *KRT17* promoter was cloned from the BAC clone RP13-415G19, both of which were provided by the BACPAC Resources Center (CA, USA). The sequences of the PCR primers used in the cloning procedures will be provided on request. Stealth RNAs for human *NOTCH1* were purchased from Invitrogen. The sequence of the plus strand of the dsRNA is 5′-UCGCAUUGACCAUUCAAACUGGUGG-3′.

Cell Culture Experiments

GE-1, Ca9-22, HeLa and CaSki cells were provided by the RIKEN BioResource Center. HSC-3 and 293 cells were provided by the Japanese Collection of Research Bioresources (Osaka, Japan). Human foreskin (HFS) cells were purchased from Kurabo (Osaka, Japan). Transfections were performed using Lipofectamine 2000 (Invitrogen) or by calcium phosphate method. Cell proliferation was evaluated using a Cell Counting Kit (Dojindo, Kumamoto, Japan). Cells were lysed in RIPA buffer and the concentration of the protein was measured using a BCA Protein Assay Kit (Thermo Fisher Scientific, MA, USA). Western blot analysis and RT-PCR were performed according to standard protocols.[27] Three-dimensional culture was conducted using Millicell Culture Inserts (Millipore). Real-time RT-PCR was performed using a Lightcycler (Roche, Basel, Switzerland). The PCR primer sequences are as follows: hN1-5865F, 5′-CAACATCCAGGACAACATGG-3′; hN1-6093R, 5′-GGACTTGCCCAGGTCATCTA-3′; hN2-7187F, 5′-ATGCTTCCTCAAATGCTGCT-3′; hN2-7513R, 5′-TCATTTCTCTCCCGGATGAC-3′; hN3-7275F, 5′-GTCTGGGACCTCCTTCTTCC-3′; hN3-7628R, 5′-CCAAGGGTGCCTACTTGGTA-3′; hN4-6444F, 5′-TGCAGGCATATGGGATGTAA-3′; hN4-6665R, 5′-CATCCCCACAGTGGAGTTCT-3′; HES1-468F, 5′-GCGGACATTCTGGAATGACA-3′; HES1-594R, 5′-CGTTCATGCACTCGCTGAAG-3′; HEY1-485F, 5′-GATGACCGTGGATCACCTGAA-3′; HEY1-584R, 5′-CCGAAATCCCAAACTCCGATAG-3′; GAPDH-275F, 5′-GCACCGTCAAGGCTGAGAAC-3′; GAPDH-417R, 5′-ATGGTGGTGAAGACGCCAGT-3′.

Luciferase Activity Assay

KRT13, *KRT15* and *KRT17* promoter fragments were cloned as described in the Genes section, and ligated into *pGL4.10.* (Promega, WI, USA). The promoter construct of 0.1 μg, 0.1 μg of the *Notch1* construct and 0.01 μg of the *Renilla* luciferase standardization plasmid were transfected into GE-1 cells on 48-well plates and the luciferase activity was measured 48 h after transfection using a Dual-Luciferase Reporter Assay System (Promega). All transfections were done in triplicate and the experiments were repeated at least twice.

RESULTS

Expression of NOTCH1 in Basal Cells of Squamous Epithelium

In the pilot study, we screened for optimal antibodies that clearly detect an endogenous level of Notch in western blot analysis. The selected antibodies revealed that NOTCH1, NOTCH2 and NOTCH3 were expressed in primary HFS cells and HEK293 cells, whereas NOTCH4 was not detected (data not shown). This result was confirmed by RT-PCR analysis, which revealed expression of *NOTCH1*, *NOTCH2* and *NOTCH3* but not *NOTCH4* (data not shown). These (anti-NOTCH1 and anti-NOTCH3) antibodies reacted with recombinant Notch1 (mouse) and NOTCH3 (human), respectively, which were overexpressed in HEK293 cells as well as with the endogenous proteins, as revealed both by western blot analysis and immunofluorescent staining, validating their specific reactions (Supplementary Material 4A, B). We then examined their immunohistochemical expression in various human adult tissues. Distinct expression of NOTCH1 was observed in the basal cells of squamous epithelium (Figure 1a). This was consistent with the result of *in situ* hybridization, which exhibited basal-cell expression of *Notch1* in an embryonic mouse skin (Figure 1b). The NOTCH1 protein was detected mainly on the plasma membrane, which is consistent with its function as a transmembrane receptor (Figure 1a). Nuclear staining was rarely observed. Antibody adsorption test showed significantly reduced staining when the antibody was absorbed to *Notch1*-transfected cells, validating the usability in immunohistochemical detection (Supplementary Material 4C). Both cornified- and non-cornified squamous epithelia expressed NOTCH1. The expression in the esophagus and vagina appeared weaker than that in the skin and oral mucosa (Figure 1c), suggesting that the epithelium of ectodermal origin (skin, oral mucosa) expresses NOTCH1 more than that of endodermal origin (esophagus, vagina). Basal (myoepithelial) cells in the secretory glands were weakly

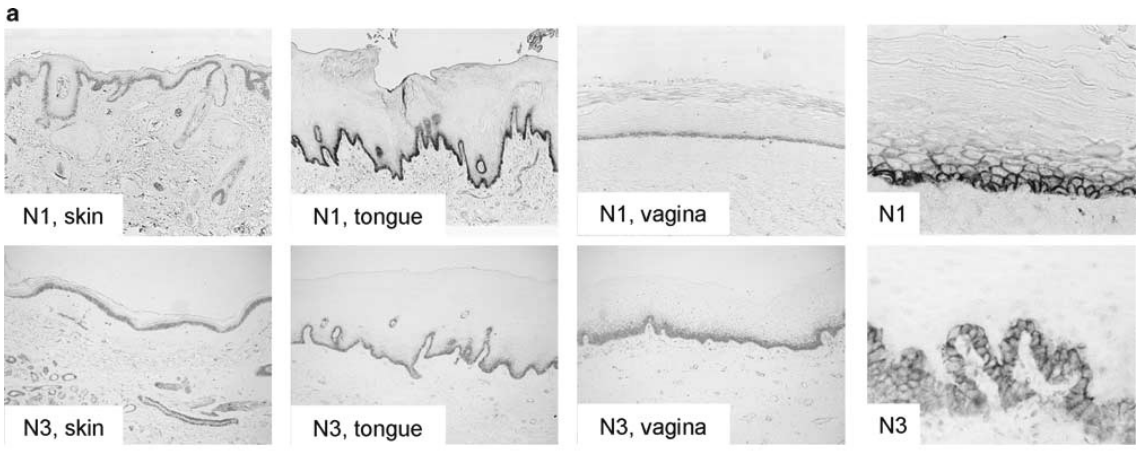

c

Expression of Notch1/Notch3

skin	gingiva	tongue	oral floor	pharynx	esophagous
++/++	++/++	++/++	++/++	+/+	+/+
stomach	intestine	trachea	uterus	vagina	bladder
−/+	−/+	−/+	−/+	+/+	+/+

Figure 1 Expression of NOTCH1 and NOTCH3 in various tissues. (**a**) Immunohistochemical staining of adult human skin, tongue and vagina shows distinct expression in the basal cells. Membrane staining pattern is obvious (right). (**b**) *In situ* hybridization on the skin of mouse E18.5 embryo, using *Notch1* RNA probe. (**c**) Simplified summary of the expression in the epithelium of each tissue.

positive for NOTCH1 (data not shown). In the uterus, the columnar epithelium, including subcolumnar reserve cells, was almost negative for NOTCH1. In the digestive tract, NOTCH1 was detected faintly only in the basal crypts (data not shown). In the subepithelial tissue, NOTCH1 was detected weakly in the vascular endothelial cells (data not shown). NOTCH3 was also expressed in the basal cells of squamous epithelium, showing membranous localization (Figure 1a). The staining pattern of NOTCH3 was a little different from that of NOTCH1, showing weak ubiquitous cytoplasmic staining also in glandular cells (data not shown). This staining in glandular cells seemed nonspecific because it did not decrease when the adsorbed antibody was used, whereas the staining in the basal cells weakened (data not shown). The NOTCH2 antibody was not applicable to immunohistochemical detection, showing no staining in any tissues (data not shown). In summary, NOTCH1 and NOTCH3 were expressed mainly in the basal cells of squamous epithelium.

NOTCH1 Expression Is Downregulated in Squamous Neoplasms

As the anti-NOTCH3 antibody yielded some nonspecific staining that would hamper correct evaluation, we determined to focus on NOTCH1 in this study and expanded our investigations to neoplasms. Because the squamous epithelia were dominant sites of NOTCH1 expression, we chose squamous neoplasms that develop at these sites and investigated whether the expression is upregulated, downregulated or unchanged. For this purpose, we collected surgical specimens of squamous cell carcinoma (cancer). To assess the contribution of NOTCH1 in cancer progression, surgical specimens of intraepithelial neoplasm (precancer) were also collected. To compensate for the organ-specific differences, specimens were collected from three different tissue sources—oral mucosa, esophagus and uterine cervix.

First we examined the NOTCH1 expression in 56 cases of oral epithelial neoplasm, including OSCC and oral intraepithelial neoplasm (OIN). We randomly collected specimens that contained normal epithelium, and the expression was evaluated by the staining intensity in individual tumor cells in comparison with that in normal basal cells within the same specimen. The distinct staining pattern with abrupt changes at the interface between normal epithelium and neoplasm enabled us to adopt this methodology. The expression was scored as being at one of five levels: level 4, upregulated expression compared with the normal basal cells; level 3, expression level similar to the normal basal cells (equivalent to '++' in Figure 1c); level 2, expression level less than the normal basal cells; level 1, stained only faintly

(stained at least more than fibroblasts); or level 0, undetected (equivalent to '−' in Figure 1b). NOTCH1 expression was significantly downregulated in most cases of OSCC and OIN (Figures 2a–d, Supplementary Material 1). The downregulation was observed even in the precancerous lesions with minimum histopathological changes (OIN1) and was apparent in most of the precancerous lesions with moderate histological alterations (OIN2), the lesions with prominent histological alterations (OIN3), and OSCC (Figure 2d). There were no cases showing an increase of NOTCH1 expression. No significant correlation was observed between the level of NOTCH1 expression and the histological variations of OIN or the histological differentiation grade of OSCC. To confirm the immunohistochemical evaluation, we dissected normal tissues and cancers separately from the sections, extracted proteins and conducted western blot analysis. In all, 4 out of 10 cases were informative, all of which showed reduced NOTCH1 expression in cancer, normalized to keratin 5 (Figure 2e). This result is consistent with the immunohistochemical observations. Proteins of sufficient amount and quality were not obtained from the other six specimens, probably due to the fixation period. The downregulation of *NOTCH1* in OSCC was also confirmed by cDNA microarray analysis of 41 OSCC *vs* 7 normal oral epithelia ($P<0.001$), with the average expression in OSCC reduced to 0.43-fold compared with the normal control (Figure 2f). The cDNA microarray showed that *NOTCH2* and *NOTCH3* were also downregulated in OSCC to 0.78-fold and 0.83-fold, respectively (data not shown).

Next, we examined the immunohistochemical expression of NOTCH1 in squamous cell carcinoma of esophagus (ESCC; Supplementary Material 2 and 5). Downregulation was evident in 17 out of 20 cases while weak expression remained. The remaining three cases retained a considerable expression, but there were no cases with NOTCH1 upregulation.

Next, we examined the immunohistochemical expression of NOTCH1 in uterine cervical lesions (Supplementary Material 3, 6). NOTCH1 expression tended to be downregulated in cervical intraepithelial neoplasm (CIN) and cervical squamous cell carcinoma (CSCC). However, more than 50% of the cases retained considerable expression (Supplementary Material 6). More cases showed NOTCH1 downregulation in precancerous lesions with little tendency of differentiation (CIN3 and CSCC), compared with precancerous lesions with some tendency of differentiation (CIN1 or CIN2). No significant difference was observed between CIN3 and CSCC (Supplementary Material 6). There was not a single case showing apparent NOTCH1 upregulation in the individual cancer cells. Indistinct nuclear staining was occasionally observed, but most of the neoplastic cells exhibited a membranous or cytoplasmic staining. No significant correlation was observed between the level of NOTCH1 expression and the type of HPV detected in the lesion (Supplementary Material 3).

In summary, the NOTCH1 expression was downregulated both in precancer and cancer of non-cornified squamous epithelium.

NOTCH1 Regulates the Differentiation of Squamous Epithelium

The fact that NOTCH1 was downregulated not only in cancer but also in precancer suggests that aberrant NOTCH1 expression associates with changes of epithelial properties observed both in precancers and cancers. The essential properties that discriminate cancer from precancer are invasion and resultant metastasis, and our data suggest that the downregulation of NOTCH1 may not contribute to these cancer-specific events. In contrast, dysregulation of differentiation is a common feature observed both in cancer and precancer, appearing as abnormality of cell alignment, stratification and keratinization. Considering that Notch governs cell-to-cell signaling, we hypothesized that reduction of Notch signaling might affect the cell-to-cell-based regulation of epithelial differentiation. To test this hypothesis, we conducted cell culture experiments. First, we examined Notch expression in cell lines derived from cervical cancers (HeLa, CaSki), oral cancers (BHY, Ca9-22, HSC-3) and primary HFS cells. Western blot analysis revealed that both NOTCH1 and NOTCH3 were expressed most abundantly in the normal cells, and variably, but at much lower levels, in the cancer cell lines (Figure 3a), which is a finding consistent with the observation that NOTCH1 expression was downregulated in squamous neoplasms. NOTCH2 was considerably expressed

Figure 2 Expression of NOTCH1 in oral squamous cell carcinoma (OSCC, cancer) and oral intraepithelial neoplasm (OIN, precancer). (**a**) OSCC associated with OIN. Low-magnification view and the highlighted borders of the lesion (A, B). NOTCH1 expression is significantly reduced in OIN (A) and OSCC (B). Clear demarcations of NOTCH1 expression are seen, which coincides with the border of the lesion. Scale bar, 0.5 mm. (**b**) OIN1 (mild epithelial dysplasia). NOTCH1 is significantly downregulated even in this lesion with minimum histological change, and the border of NOTCH1 expression coincides with the border of the lesion. Scale bar, 0.5 mm. (**c**) Papillary-type OSCC. Low-magnification view with the highlighted border of the lesion (C). Downregulation of NOTCH1 is evident. Scale bar, 0.5 mm. (**d**) Numbers of cases (and percentage) with reduction of NOTCH1 expression. G1, well-differentiated; G2, moderately differentiated; G3, poorly differentiated OSCCs. (**e**) Western blot analysis using surgical specimens. Formalin-fixed paraffin-embedded tissues were separately dissected from normal (N) and cancer (C) tissues, and the proteins were extracted. A sufficient amount of protein was obtained from 4 out of 10 cases, in which NOTCH1 expression was reduced in cancer (Case #1 to #4). Keratin 5 (K5) was used for standardization. Case #5 is shown as an example of a non-informative case. (**f**) cDNA microarray analysis of 41 OSCC and 7 normal control epithelia. Vertical axis corresponds to globally normalized signal intensity of *NOTCH1* mRNA expression. *NOTCH1* is significantly downregulated in OSCC compared with normal epithelium (*$P<0.001$). Short bars, expression in each case; long bars, mean; error bars, s.e.

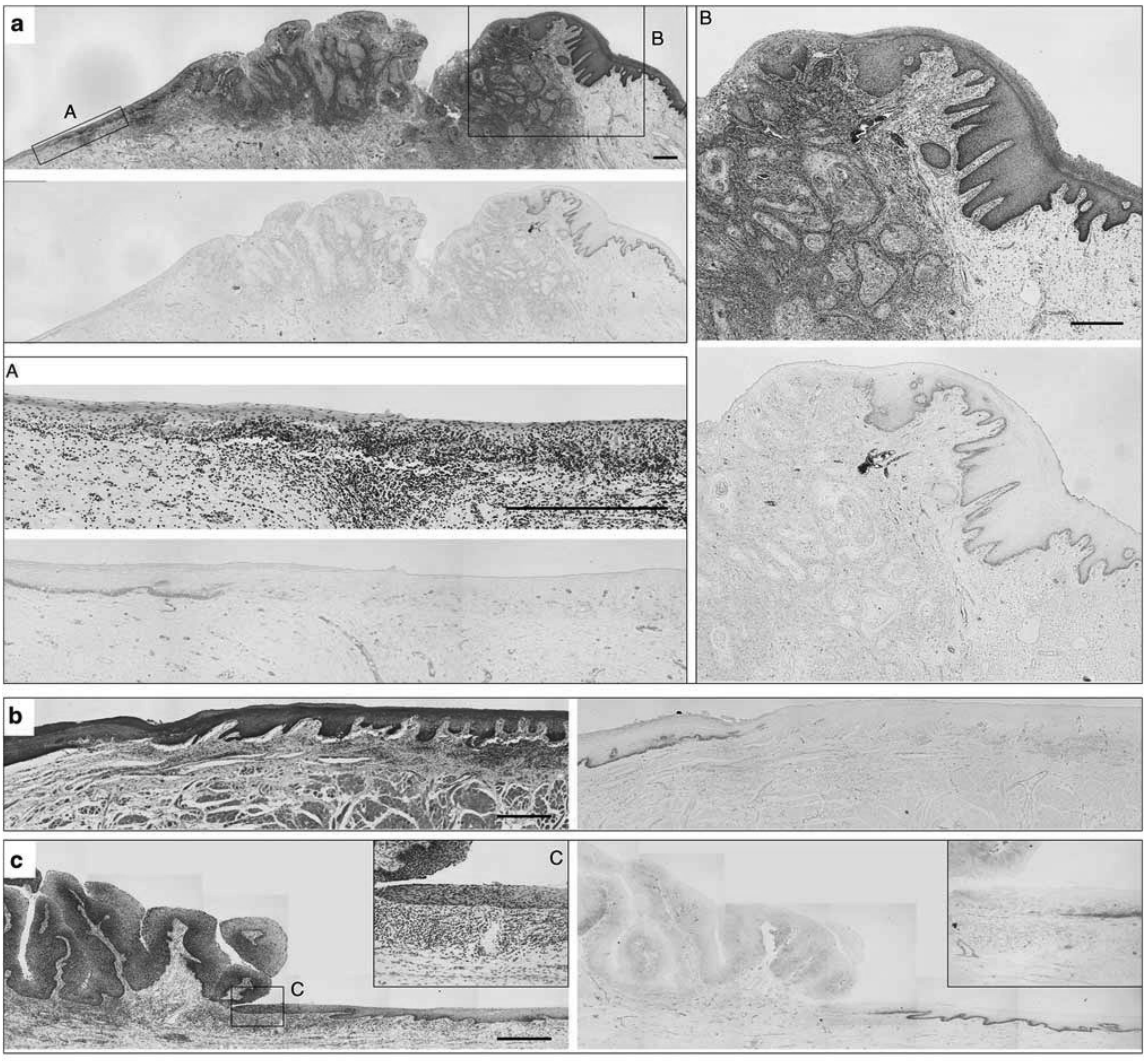

d

OIN		
OIN1	OIN2	OIN3
8/10 (80%)	12/13 (92%)	10/10 (100%)
OSCC		
G1	G2	G3
14/16 (88%)	8/8 (100%)	2/3 (67%)

e

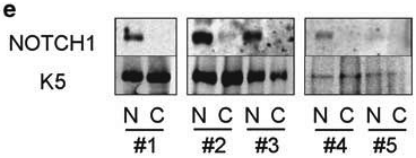

f

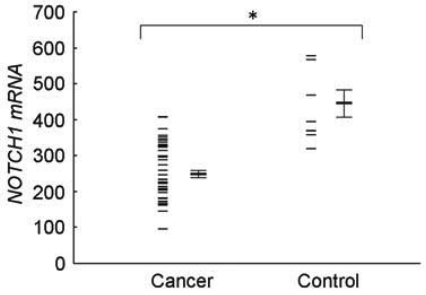

in Ca9-22 and HFS cells, and also in HeLa cells more strongly (Figure 3a). To assess the possible correlation between NOTCH1 and differentiation, we examined the expression of epithelial markers in these cells (Figure 3b). In normal non-cornified squamous epithelium, the basal cells express NOTCH1, K15, K19, CDH1, DSG3 and TP63, whereas K16 and K17 expression is weak, and K18 and vimentin are not expressed (data not shown). HFS cells mimicked this expression pattern. The cancer cell lines showed various expression patterns, reflecting the diversities in differentiation states of each cell line (Figure 3b). When we compared the two cervical cancer cell lines, CaSki expressed more NOTCH1 and exhibited a phenotype more similar to normal epithelium than to HeLa. When we compared the three oral cancer cell lines, Ca9-22 that expressed a significantly higher level of NOTCH1 than BHY and HSC-3 exhibited the phenotype very similar to normal epithelium. When the cells were cultured at a high density, HFS and Ca9-22 cells spontaneously differentiated, showing scattered cells positive for K13, a keratin in terminally differentiated keratinocytes (Figure 3c). The other cancer cells showed little potential to express K13. These results suggest that NOTCH1 expression may associate with differentiation of non-cornified epithelium. Cervical cancer cells, which do not fit into this hypothesis, will be discussed in the Discussion section.

As Ca9-22 mimicked well the phenotype of normal epithelium, and Ca9-22 cells were easily transfected, we thought that they served as a good cell model for assessing differentiation. Accordingly, we examined the effects of Notch signaling in Ca9-22 cells. We treated Ca9-22 cells with gamma-secretase inhibitor (DAPT), which blocks the Notch signaling, and examined K13, K15 and K17 expression after 72 h. These keratins are expressed variably in physiological and pathological conditions, and represent distinct cellular states; K13 represents keratinocytes under terminal differentiation, K15 represents basal cells and K17 represents activated keratinocytes such as those appearing in regenerative epithelium and cancer. DAPT treatment led to reduced expression of a putative downstream target of Notch signaling, HES1, and K13 expression, whereas K15 and K17 levels were largely unchanged (Figure 3d), suggesting that Notch signaling is necessary for terminal differentiation. Next the cells were transfected with various constructs (Figure 3e). Constitutively, active Notch1 (NICD) upregulated HES1 and suppressed K13, suggesting that sustained, high-level Notch signaling inhibits terminal differentiation. Knockdown of *NOTCH1* by siRNA led to a decrease of HEY1, another putative target of Notch signaling, K13 and K15, and an increase of K17. *Rbpjm*, which is a mutant *Rbpj* with a single amino-acid replacement (R218H), and *dnDl*, which is a deletion mutant of *Dll1*, are both known to pose a dominant-negative effect on Notch signaling. Both constructs led to a decrease of HEY1 and an increase of K13. These results indicate that proper expression of NOTCH1 and its signaling are necessary for terminal differentiation, and either the absence of its signaling or its untimely activation results in abnormal differentiation. It should be noted that the phenotype observed in *NOTCH1* knockdown differed from that in the autonomous inhibition of Notch signaling.

We examined the correlation of TP63, a transcription factor that regulates keratinocyte differentiation, with NOTCH1. Among different isoforms, the most abundant TA- and ΔN-isoforms were examined. In uterine cervical cells, TP63(ΔN) acts as a transcriptional repressor of *NOTCH1*, which results in maintenance of self-renewing capacity.[28] In Ca9-22 cells, transfection of *TP63(ΔN)* only slightly decreased NOTCH1 expression and *TP63(TA)* did not have a significant effect on NOTCH1. Both *TP63(TA)* and *TP63(ΔN)* decreased K13 expression (Figure 3f). *NICD* overexpression and *NOTCH1* knockdown both led to downregulation of TP63(ΔN) and K13 (Figure 3g). These results indicate that TP63(ΔN) inhibits differentiation partially by repressing NOTCH1 expression, whereas Notch signaling also mediates TP63(ΔN) expression.

To further investigate the contribution of Notch signaling in regulation of keratin subtype expression, we conducted

Figure 3 NOTCH1 regulates keratin expression. (**a**) Expression of NOTCH1, NOTCH2 and NOTCH3 in cervical cancer cell lines (HeLa, CaSki), oral cancer cell lines (BHY, Ca9-22, HSC-3) and primary human foreskin (HFS) cells, as revealed by western blot. All the antibodies recognize an epitope in the intracellular domain. Most proteins were detected as a furin-cleaved form containing the transmembrane and intracellular domains. A small amount of full-length protein was also detected. Gamma-secretase-cleaved C-terminal fragment (NICD) was not observed in NOTCH1 and NOTCH3 blots. (**b**) Expression of various keratins (K), vimentin (Vim), E-cadherin (Cdh1), desmoglein 3 (Dsg3) and TP63 in various cells, as revealed by western blot. As the full-length NOTCH1 was observed at a much weaker intensity and in proportion to the intensity of the 120 kDa protein, only the 120 kDa protein of NOTCH1 is shown. (**c**) K13 expression in Ca9-22 and HFS cells cultured at a high density. Immunofluorostaining was conducted using the secondary antibody labeled by Alexafluor 488. The nuclei were counterstained by DAPI. K13-expressing cells appear in a scattered manner. HeLa, CaSki, BHY and HSC-3 showed no K13 expression. (**d**) Ca9-22 cells were treated with only DMSO or 2.5 μM DAPT at 80% confluency and were cultured for 72 h. An equal amount of protein was subjected to western blot analysis for keratins (K), HES1, HEY1 and β-tublin (βTub). (**e**) Ca9-22 cells were transfected at 30% confluency with an empty plasmid (Ctrl), NICD, dominant-negative RBPJ (R218H, RBPJm), dominant-negative Dll1 (dnDl) or siRNA for *NOTCH1* (*siN1*) and were cultured for 72 h. (**f**) Ca9-22 cells were transfected with *TP63(TA)* or *TP63(ΔN)* and were incubated for 72 h. Western blot analysis revealed the endogenous expression of TP63 (ΔN), but not TP63 (TA). NOTCH1 was only slightly downregulated by TP63 (ΔN). K13 was downregulated both by TP63 (TA) and TP63 (ΔN). (**g**) Ca9-22 cells were transfected with *NICD* or siRNA for *NOTCH1* and were incubated for 72 h. Both *NICD* and *siN1* downregulated TP63 and K13. (**h**) Luciferase reporter assay for human *KRT13*, *KRT15* and *KRT17* promoters. The promoter construct plus of 0.1 μg and 0.1 μg of the Notch1 construct and 0.01 μg of the *Renilla* luciferase standardization plasmid (*pEF-RL*). Transfections were done into GE-1 cells on 48-well plates and the luciferase activity was measured 48 h after transfection using Dual-Luciferase Reporter Assay System (Promega). The error bars denote standard errors. rlu; relative luciferase unit.

promoter analysis of the keratin genes using GE-1 cells that were established from normal mouse gingival epithelium. We co-transfected the cells with *Notch1*, *NICD* or *NECD*, and the luciferase reporter constructs for *KRT13*, *KRT15* or *KRT17* promoters. NECD is a membrane-tethered Notch1 extracellular domain whose intracellular domain was replaced by AcGFP. Notch1 increased the *KRT13* promoter activity while NICD decreased it. NECD decreased the *KRT15* promoter activity and slightly increased the *KRT17* promoter activity (Figure 3h). These results suggest that NOTCH1-expressing cells have more potential to differentiate, but Notch signaling itself autonomously inhibits differentiation and directs the cell to maintain basal-cell phenotype.

Next we examined the effect of *NOTCH1* knockdown in normal epithelial cells using the primary HFS cells. The knockdown efficiency was more than 90% as revealed by

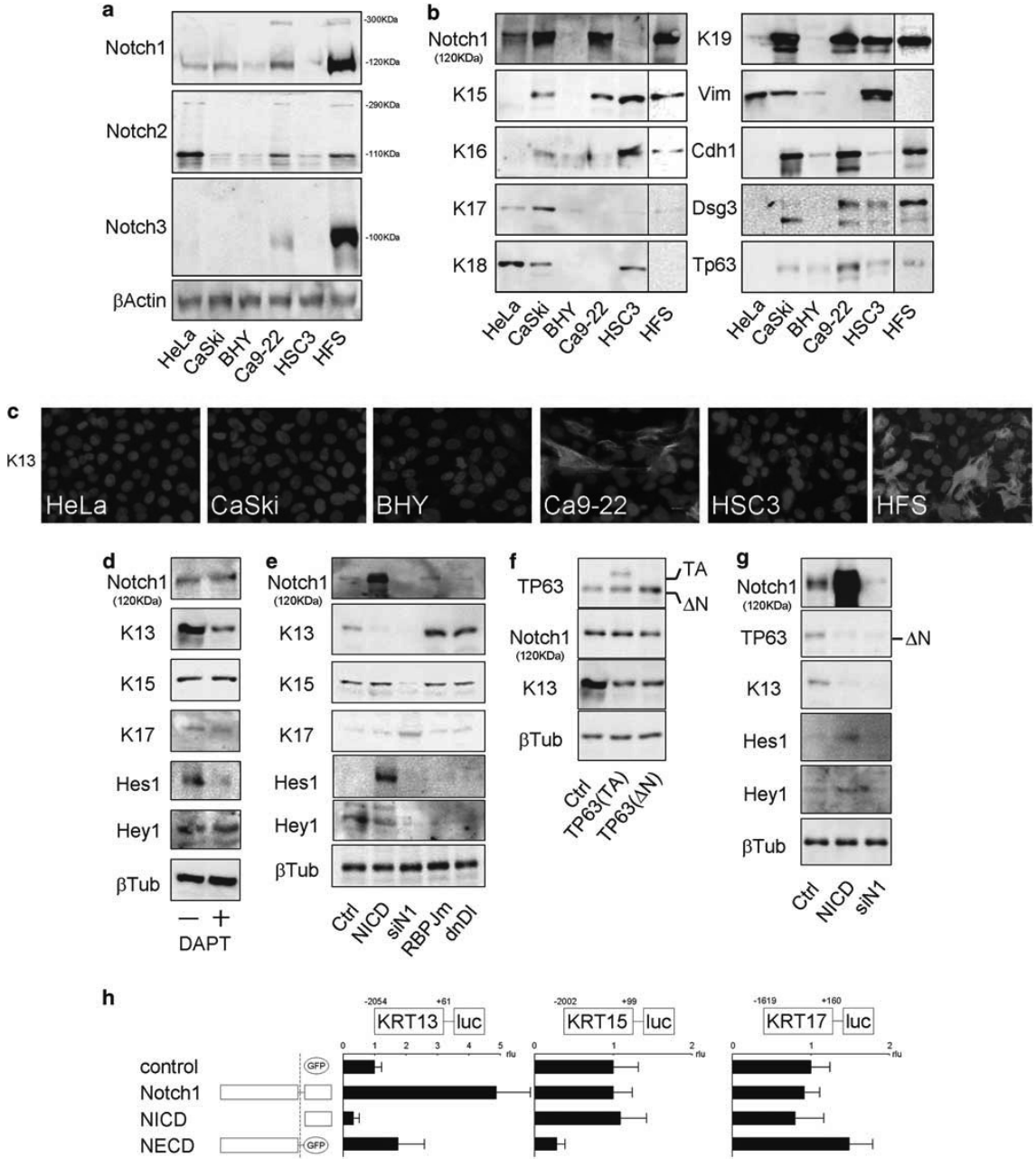

western blot analysis (Figure 4a). *NOTCH1* knockdown significantly suppressed the expression of *HEY1*, whereas *HES1* showed only slight (20%) reduction, as revealed by real-time PCR (Figure 4b, real-time PCR data are not shown). Cell proliferation was not altered by *NOTCH1* knockdown (data not shown). The total amount of keratin protein was unchanged, and vimentin was not induced by *NOTCH1* knockdown (Figure 4c). *NOTCH1* knockdown led to downregulation of K13 and K15, and upregulation of K17. Immunocytostaining using the anti-K13 antibody revealed that *NOTCH1* knockdown resulted in a decrease both of the staining intensity in individual cells and of the number of stained cells (Figure 4d). The expression of CDH1 (E-cadherin), DSG3 (desmoglein 3) and TP63 was not significantly

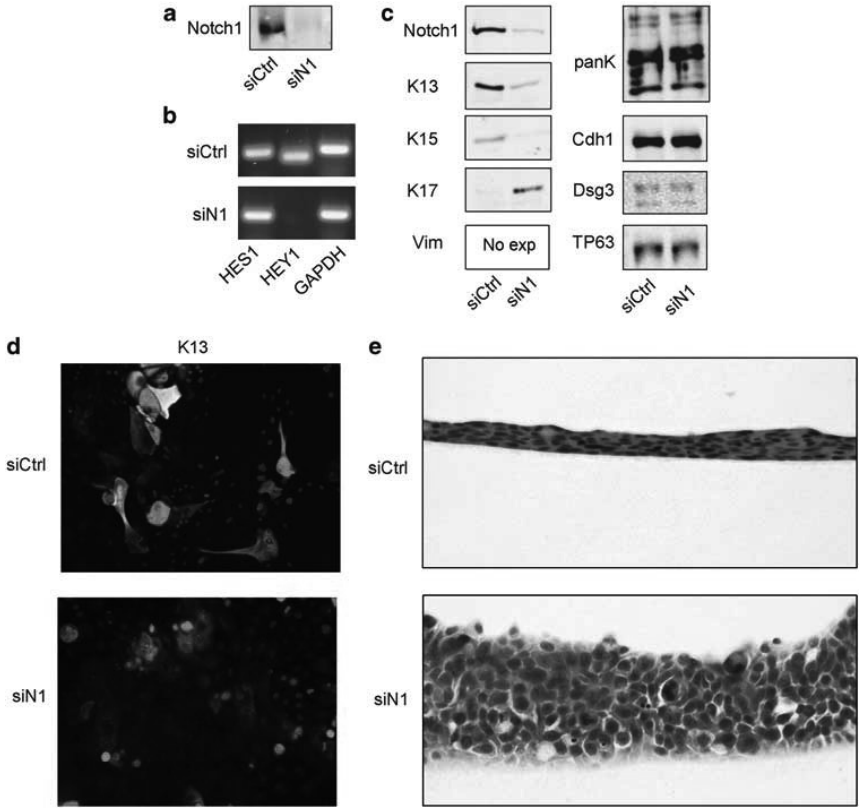

Figure 4 Notch1 knockdown in primary foreskin (HFS) cells results in immature epithelium. (**a**) Efficiency of *NOTCH1* knockdown. HFS cells were transfected with negative control siRNA (*siCtrl*) or siRNA for *NOTCH1* (*siN1*) were incubated for 7 days and subjected to western blot analysis. (**b**) Effect of *NOTCH1* knockdown on the target genes. Real-time RT-PCR revealed that *HEY1* was almost completely suppressed, whereas *HES1* was downregulated only by 20% (data not shown). The post-real-time PCR samples were diluted and amplified for an additional two cycles in order to make them visible on gel electrophoresis. Thus this figure actually shows conventional RT-PCR. (**c**) The effect of *NOTCH1* knockdown on the expression of keratinocyte differentiation markers. K, keratin; Vim, vimentin; panK, pan-keratin; Cdh1, E-cadherin; Dsg3, desmoglein 3; No exp, no expression. (**d**) Expression of K13 in HFS cells transfected with *siCtrl* or *siN1* 7 days after transfection, revealed by immunofluorostaining. The fluorescence intensity in the individual cells and the number of positively stained cells decreased in the siN1-transfected cells. (**e**) Vertical sections of three-dimensionally cultured HFS cell layers, stained with hematoxylin and eosin. Cells were transfected and seeded in Millicell culture inserts and cultured for 10 days.

Figure 5 Immunohistochemical expression of NOTCH1, K13, K15 and K17 in squamous neoplasms. (**a**) In this OIN case, the lesion shows concomitant downregulation of NOTCH1, K13 and K15, with complimentarily induced expression of K17. Scale bar, 0.5 mm. (**b**) In this CIN case showing condylomatous proliferation, the level of NOTCH1 expression in the individual cells is retained, and basaloid cells expressing NOTCH1 and K15 expand in the whole layer. K17 induction is faint. Scale bar, 0.5 mm. (**c**) Schematic summary of the immunohistochemical expression of NOTCH1 and K13 in various squamous neoplasms. Each group of the lesions is plotted by the average scores of NOTCH1 and K13 expression. OIN, oral intraepithelial neoplasm; OSCC, squamous cell carcinoma of the oral cavity; ESCC, squamous cell carcinoma of the esophagus; CIN, cervical intraepithelial neoplasm; CSCC, squamous cell carcinoma of the cervix.

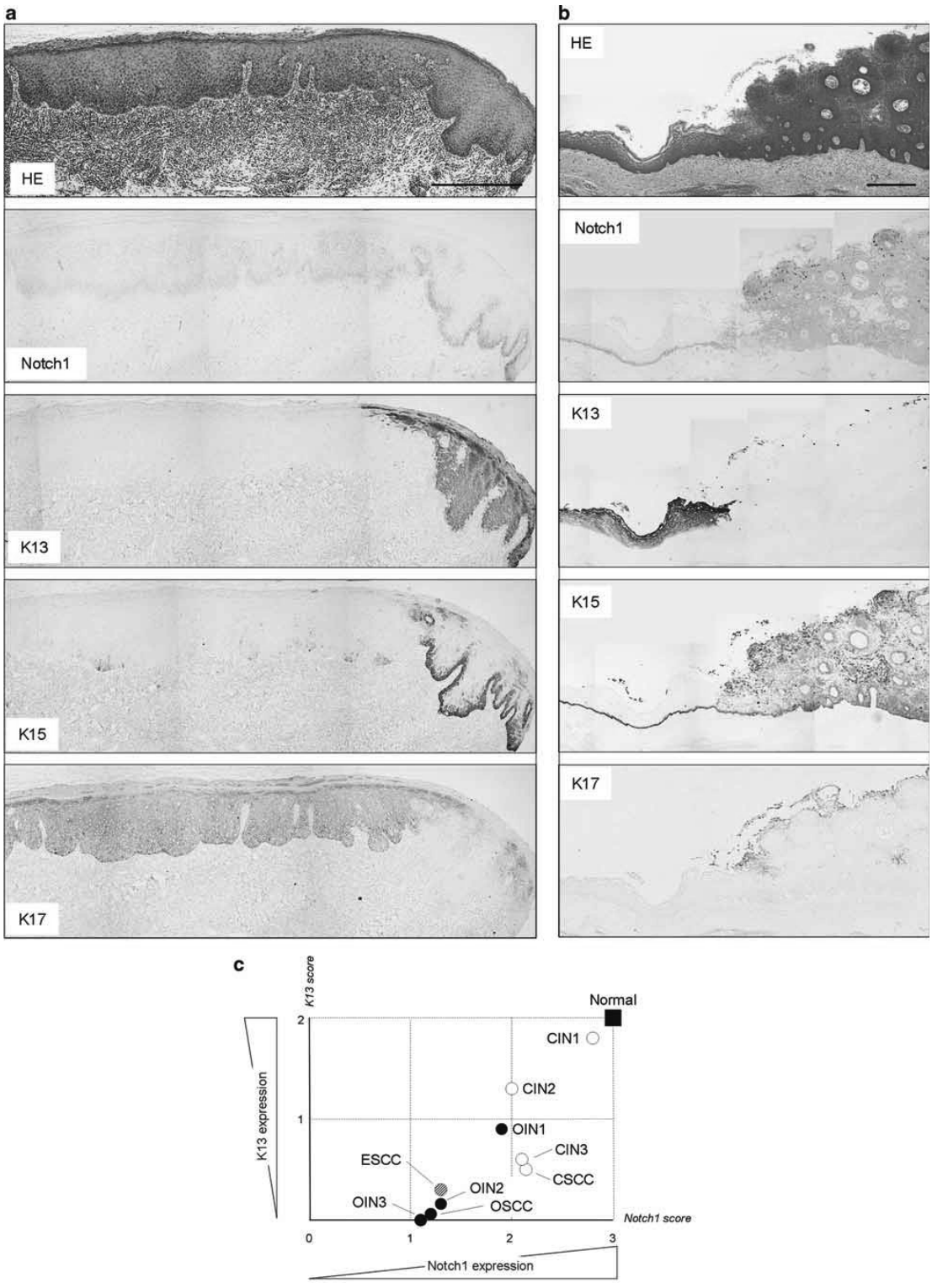
a
HE
Notch1
K13
K15
K17
b
HE
Notch1
K13
K15
K17
c
K13 score
K13 expression
Normal
CIN1
CIN2
OIN1
CIN3
CSCC
ESCC
OIN2
OIN3
OSCC
Notch1 score
Notch1 expression
0
1
2
3

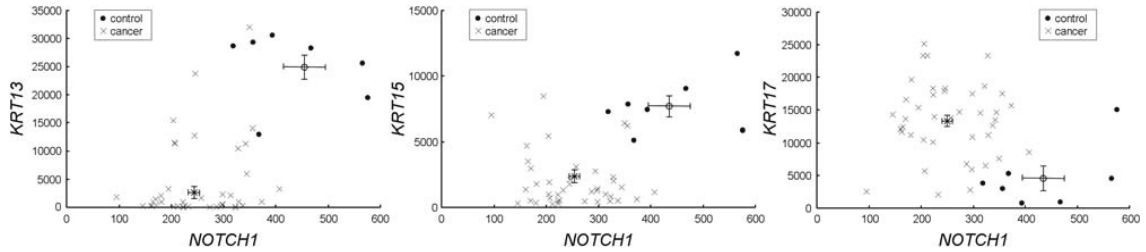

Figure 6 Correlation of *NOTCH1* and *KRT13, KRT15* or *KRT17* expression. cDNA microarray analysis of 41 OSCC and 7 normal controls. Globally normalized hybridization intensity data of each sample were scatterplotted. The filled circles represent normal controls and the crosses represent OSCC cases. The blank circle represents the mean of the normal controls. The large cross represents the mean of OSCC. The error bars represent standard errors.

altered (Figure 4c). In a three-dimensional culture, the *NOTCH1*-knockdown cells formed a stratified epithelium that exhibited a thickened cell layer and a disarray of stratification (Figure 4e), which are reminiscent of the histological features of precancer. These results suggest that reduced NOTCH1 expression results in conversion from a differentiated epithelium to an immature or hyperplastic epithelium represented by K17 expression.

Correlation Between NOTCH1 and Keratin Subtype Expression in Tissue

To validate the results obtained by cell culture experiments, we immunohistochemically examined the keratin expression in cancer and precancer of oral mucosa, esophagus and uterine cervix. NOTCH1 and K13 were concomitantly downregulated along with downregulation of K15 and upregulation of K17 in most oral and esophageal lesions (Figure 5a). In cervical lesions, a similar tendency was observed. However, there were also cases with considerably retained NOTCH1 expression, and NOTCH1-retained lesions showed a different keratin pattern, namely, K15-positive basaloid cell expansion with minimum induction of K17 (Figure 5b). We scored the K13 expression either as being at level 2 (unaffected, almost uniform expression), level 1 (apparent downregulation but patchy expression remaining) or level 0 (almost complete loss of expression), and analyzed the correlation of these three expression levels with the NOTCH1 scores. Loss of K13 expression was observed in accordance with NOTCH1 downregulation (Figure 5c). The average scores of K13 and NOTCH1 decreased in accordance with the grades of OIN and CIN, although the high-grade lesions (OIN2, OIN3, CIN3) showed scores similar to those of OSCC or CSCC (Figure 5c), indicating that these precancers and cancers in each site are essentially the same lesions in the context of NOTCH1 and K13 expression. The cervical lesions, especially low-grade CIN, tended to show more NOTCH1 and K13 expression. Correlation between NOTCH1 expression and keratin expression was further assessed in oral cancers using microarray data. Scatter plots revealed that the downregulation of NOTCH1 in cancer correlated with downregulation of K13 and K15, and upregulation of K17 (Figure 6).

Asymmetric Activation of NOTCH1

In tissue, NOTCH1 was dominantly observed on the cell membrane, and nuclear staining was rarely seen. To gain an insight into when and how NOTCH1 is activated, its cellular localization was further investigated in HFS cells. NOTCH1 was detected on the cell membrane of culture cells, showing accumulation at the cell-cell interface (Figure 7a). No NOTCH1 accumulation was observed on the free surfaces. Western blot analysis, using cleaved NOTCH1-specific antibody, failed to detect activated NOTCH1 (data not shown), probably due to low expression. Still, immunostaining showed distinct nuclear expression of activated NOTCH1, but only in a very few ($<1\%$) cells (Figure 7b). This suggests that NOTCH1 protein is tethered to the cell membrane and is dormant in most cells, and that it is activated only in a limited population or on infrequent occasions. We further assessed nuclear translocation of NOTCH1. As the endogenous level of NOTCH1 expression was not sufficient for clear visualization, we overexpressed *Notch1* by transfection and examined cellular localization of the protein. Again, cells whose nuclei were positive for Notch1 were rare but were definitely observed. Interestingly, nuclear localization of Notch1 was occasionally observed in one of two neighboring cells, which appeared as postmitotic daughter cells (Figure 7c).

DISCUSSION

We demonstrated that NOTCH1 is expressed predominantly in the basal cells of normal squamous epithelium. Contrary to our findings, previous reports had documented the expression in both basal and suprabasal layers of the skin[4,21] and in the uterine cervix,[15,16] as well as in the suprabasal layer of the cornea,[29] but we believe the present study correctly demonstrates the basal-cell dominant NOTCH1 expression in human squamous epithelium and its neoplasms. The most prominent feature that supports the validity of our immunohistochemical examination is the sharp demarcation of NOTCH1 expression that matched to the border between

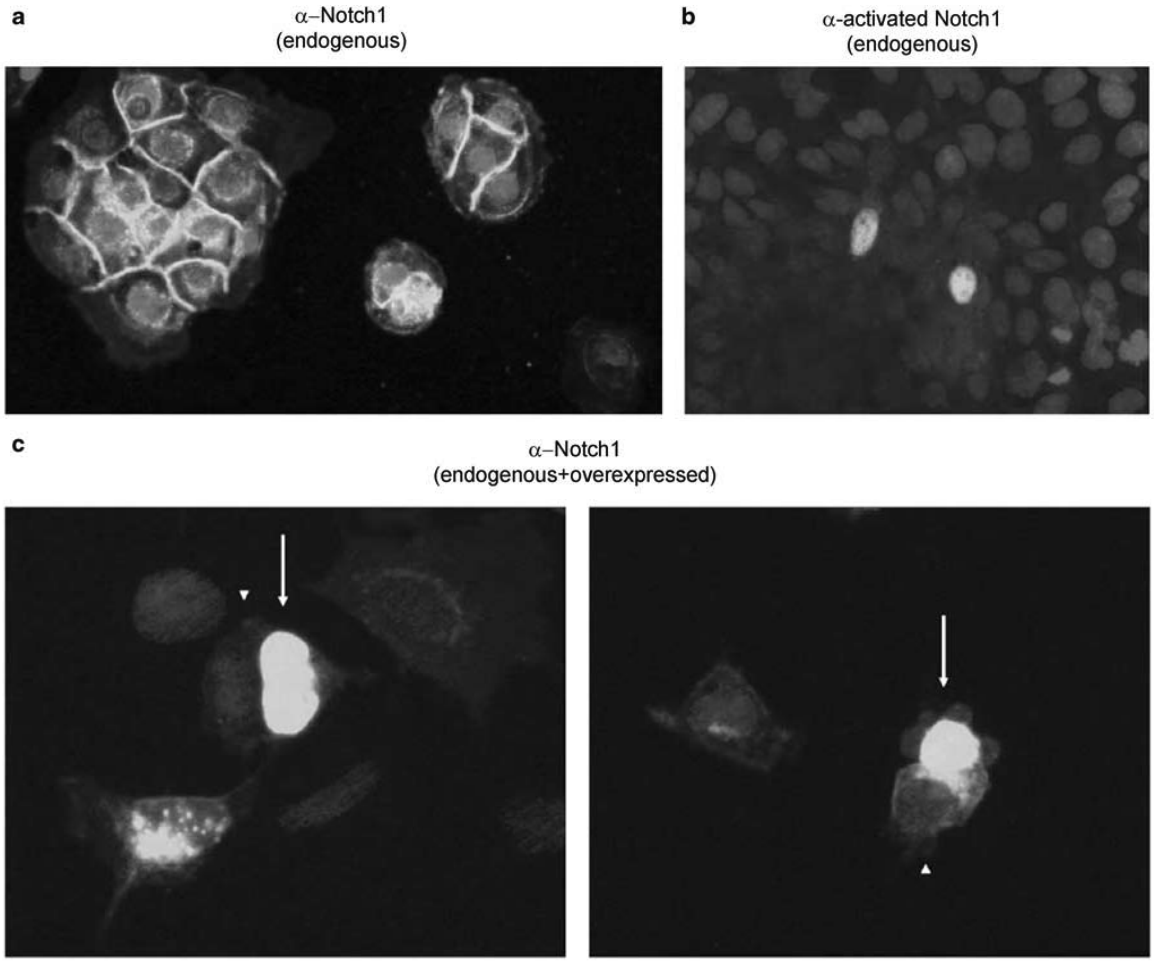

Figure 7 Nuclear translocation of NOTCH1 is rare, and it occasionally occurs asymmetrically in cultured keratinocytes. (**a**) Immunofluorostaining of HFS cells using the anti-NOTCH1 antibody. NOTCH1 protein accumulates at the cell–cell interface. Little protein was detected on the free surface or in the nuclei. (**b**) Immunofluorostaining of HFS cells using the anti-cleaved NOTCH1(Val1744) antibody. This activated form of intracellular domain of NOTCH1 is detected in the nuclei, but only in a very few cells—far $<$1% of the total population. (**c**) Immunofluorostaining of Ca9-22 cells transfected with wild-type mouse Notch1 using the anti-NOTCH1 antibody. The antibody crossreacts with mouse Notch1. Endogenous expression of NOTCH1 is observed as fine membranous or cytoplasmic staining. The transfected cells exhibit much stronger expression, facilitating detection. Nuclear localization of the NOTCH1 is observed in one of two neighboring cells, which appear as postmitotic daughter cells. Arrow: postmitotic cell with nuclear NOTCH1; arrowhead: postmitotic cell without nuclear NOTCH1.

normal and neoplastic epithelia, which would never be observed in nonspecific staining.

Although elevated Notch signaling has been suggested in tumor development,[13,30–32] neither an increase of NOTCH1 expression nor its nuclear translocation was observed in the cases we examined. The cDNA microarray of OSCC showed that neither *NOTCH2* nor *NOTCH3* was upregulated in OSCC, suggesting that quantitative compensation is unlikely. These results indicate that upregulation of Notch-dependent signaling may not make a major contribution to the development and progression of squamous cell carcinoma. Conversely, consistent reduction of NOTCH1 expression in squamous neoplasms was evident. Also, *NOTCH1* has recently been shown to be mutated in 11–15% of head and neck cancer, and about 40% of the mutations were predicted to generate truncated NOTCH1 proteins, whereas no apparent activating mutation was found.[33,34] These results suggest that NOTCH1 may function as a tumor suppressor gene rather than as an oncogene in squamous neoplasms.

We demonstrated that impaired Notch1 signaling led to abnormal differentiation represented by alterations of keratin subtype expression, which was commonly observed not only in cancers but also in precancers. The role of Notch in regulation of squamous epithelium differentiation has also been suggested by studies using cultured cervical[28] and esophageal keratinocytes.[35] Collectively, these results indicate that

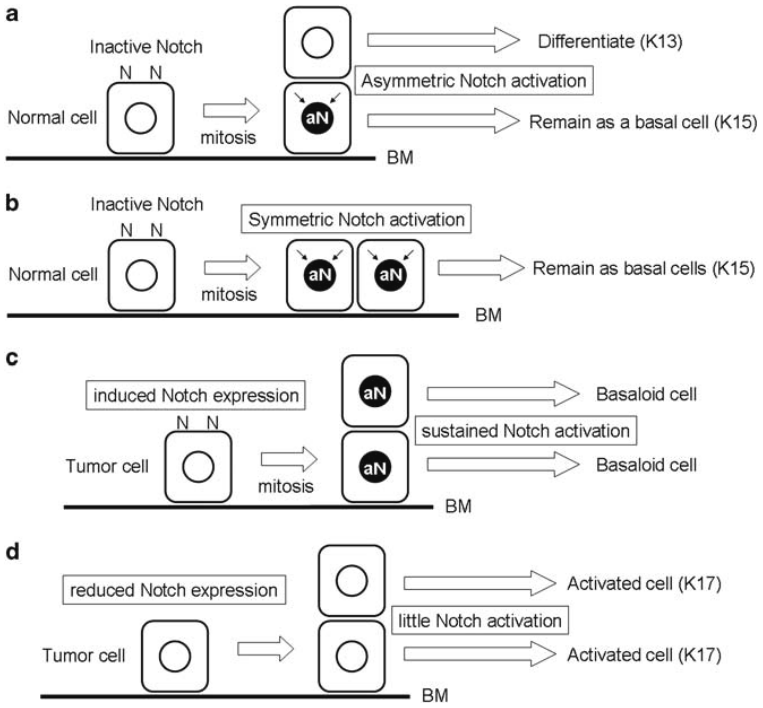

Figure 8 Proposed model of Notch-mediated mechanism of non-cornified squamous epithelium differentiation. (**a**) NOTCH1 is selectively activated in the basal cell (K15 +) when the sister cell divides basoapically, and directs it to remain as a basal cell (K15 +), whereas the apical daughter cell without Notch signal input differentiates (K13 +). (**b**) When the sister cells divide symmetrically, Notch is activated in both cells, which remain as basal cells (K15 +). (**c**) If the asymmetric Notch signaling is impaired and both basal and apical daughter cells undergo Notch activation, both remain as basaloid cells (K15 +). (**d**) The cells with reduced NOTCH1 expression convert to activated cells (K17 +) that lead to a hyperplastic phenotype.

reduced NOTCH1 expression affects the terminal differentiation, thus highlighting the essential role of NOTCH1 in maintaining normal epithelial integrity. In addition, we examined five cases of traumatic ulcer and found that NOTCH1 was downregulated in the regenerative epithelium, accompanied with loss of K13 expression and robust induction of K17 (K.S., unpublished observations). This suggests that the downregulation of NOTCH1 expression level is an inherent mechanism for switching the epithelium from a normal and mature state to an activated and immature state.

Cervical cancers tended to retain NOTCH1 expression compared with oral and esophageal cancers. We evaluated the expression in the cervical cancer cells in comparison with the neighboring vaginal squamous epithelium. However, this evaluation method might be misleading because cervical cancers arise from the reserve cells beneath the columnar epithelium of endocervix,[36] and the vaginal epithelium is not the origin of cervical cancers. As the reserve cells are almost negative for NOTCH1, it can also be said that NOTCH1 expression is increased in cervical cancer compared with its original cell type.

We hypothesized that strong NOTCH1 expression may correlate with a tendency for differentiation toward squamous epithelium. To check this hypothesis, we additionally examined five specimens of squamous metaplasia caused by obstruction of the minor salivary gland duct. As expected, NOTCH1 was significantly induced in ducts, which show ectopic K13 induction and squamous metaplasia (Supplementary Material 7). HPV infection to metaplastic epithelium in the transformation zone initiates progression to CIN or CSCC,[37] and *NOTCH1* is upregulated by HPV E6 and E7 oncoproteins, which are almost uniformly expressed in cervical cancer.[38] Virally induced NOTCH1 expression would tend to be maintained in CIN and CSCC, but would be no more upregulated. In this context, upregulation of NOTCH1 may have an essential role only in generation of metaplastic epithelium.

HPV has been detected only in a minority of OSCC cases, excluding pharyngeal cancer[39] and ESCC.[40] This is probably attributable to the difference in the NOTCH1 expression pattern between oro-esophageal and cervical cancers. The NOTCH1 expression patterns seem to underlie their histopathological differences. Expansion of a basaloid cell population is usually observed in CIN, whereas this finding is exceptional in OIN, whose basaloid cells are usually limited to the lower part of the epithelium. Remaining NOTCH1

expression appears to autonomously direct the cell to maintain the basaloid phenotype.

In our series of cell culture experiments, Notch signaling exhibited seemingly diverse effects. For example, both activation of Notch signaling and downregulation of NOTCH1 expression inhibited differentiation. To better understand such diverse effects, we have developed the following model, which is consistent with the experimental and histopathological findings, and also with the self-organizing nature of stratified epithelium. NOTCH1 is selectively activated in the basal cell when the sister cell divides basoapically, and acts to direct the basal cell to remain as a basal cell, whereas the apical daughter cell without Notch signal input is directed to differentiate (Figure 8a). When the sister cell divides laterally, Notch is activated in both cells, which directs them both to be basal cells (Figure 8b). If asymmetric Notch signaling is impaired, and both basal and apical daughter cells undergo Notch activation, both would remain as basaloid cells (Figure 8c), causing expansion of the basal-cell layer. Cells with reduced NOTCH1 expression convert to activated cells that lead to a hyperplastic phenotype (Figure 8d). In either case, impaired Notch signaling causes an immature epithelium. Although future research is required to confirm this model, it is consistent with the results of genetically engineered mouse experiments.[8,35]

Besides its role as a receptor, Notch is considered to have a function as a modulator of cell adhesion.[7] The NOTCH1 accumulation on the plasma membranes between neighboring cells and the rare observation of the activated form support this notion. Reduced Notch expression may facilitate the cell dissociation and movement that are required for regenerative epithelium and cancer invasion.

Altogether, we assume that NOTCH1 functions in two ways: it mediates the balance between populations of basal cells and differentiated cells in normal epithelium by symmetric and asymmetric activation; and in pathological conditions, such as wound healing, precancer and cancer, its expression is reduced, which converts the cells into an activated and immature state.

Impaired asymmetric cell division affects epidermal Notch signaling and results in defects in stratification and differentiation, suggesting that Notch is an effector of asymmetric cell division.[41] The mechanism of asymmetric Notch activation is unclear. JAG1, one of the canonical ligands, was expressed in the suprabasal layers (K.S., unpublished observations), which suggests that the signal is directionally transmitted from an apical cell to a basal cell because of these localizations of ligand- and receptor-expressing cells. However, JAG1 was also expressed in the basal cells, and the significance of the co-expression of receptors and ligand in the basal cells is yet to be elucidated. Accumulating evidence indicates that the canonical Notch ligands also act as a cell-autonomous repressor of Notch signaling,[26,42–46] suggesting that JAG1 expression in the basal cells may inhibit the signaling. Another possible mechanism of the asymmetric activation is the suppression of Notch signaling by protein degradation mediated by Numb, which is distributed differentially in the daughter cells and governs asymmetric cell division.[47,48]

The transcription of *NOTCH1* gene is suppressed by TP63(ΔN) in cervical keratinocytes,[28] and TP63(ΔN) inhibits differentiation in the oropharyngeal SCC cell line.[49] Our findings using Ca9-22 cells are consistent with these results, suggesting that the interplay between NOTCH1 and TP63(ΔN) in differentiation is common in non-cornified epithelia of various sites. In addition, we found that TP63(ΔN) expression was affected by Notch signaling, suggesting a feedback relationship between these factors. It should be noted that this hypothetical NOTCH1-TP63 interplay does not resemble the expression patterns of these factors in cancer tissues, in which TP63 is uniformly expressed in both basal and suprabasal layers of normal epithelium and cancer (data not shown). Thus, the NOTCH1-TP63 interplay is merely one of many mechanisms that govern the epithelial cell behaviors.

In summary, NOTCH1 is expressed predominantly in the basal cells of squamous epithelium, and it is generally downregulated in squamous neoplasms, even at early stages. Reduction of NOTCH1 expression directs the basal cells to cease terminal differentiation, resulting in an immature epithelium, which may have an essential role in the histopathogenesis of dysplastic features commonly observed in precancerous epithelium. These findings suggest that normal epithelial integrity is autonomously maintained by this evolutionarily conserved cell-to-cell signaling system.

Supplementary Information accompanies the paper on the Laboratory Investigation website (http://www.laboratoryinvestigation.org)

ACKNOWLEDGEMENT

This work was supported by a Grant-in-Aid for Scientific Research (C) (No. 21592320).

DISCLOSURE/CONFLICT OF INTEREST

The authors declare no conflict of interest.

1. Blaumueller CM, Qi H, Zagouras P, *et al.* Intracellular cleavage of Notch leads to a heterodimeric receptor on the plasma membrane. Cell 1997;90:281–291.
2. Logeat F, Bessia C, Brou C, *et al.* The Notch1 receptor is cleaved constitutively by a furin-like convertase. Proc Natl Acad Sci USA 1998;95:8108–8112.
3. Bray SJ. Notch signalling: a simple pathway becomes complex. Nat Rev Mol Cell Biol 2006;7:678–689.
4. Blanpain C, Lowry WE, Pasolli HA, *et al.* Canonical notch signaling functions as a commitment switch in the epidermal lineage. Genes Dev 2006;20:3022–3035.
5. Favier B, Fliniaux I, Thelu J, *et al.* Localisation of members of the notch system and the differentiation of vibrissa hair follicles: receptors, ligands, and fringe modulators. Dev Dyn 2000;218:426–437.
6. Pan Y, Lin MH, Tian X, *et al.* Gamma-secretase functions through Notch signaling to maintain skin appendages but is not required for their patterning or initial morphogenesis. Dev Cell 2004;7:731–743.
7. Watt FM, Estrach S, Ambler CA. Epidermal Notch signalling: differentiation, cancer and adhesion. Curr Opin Cell Biol 2008; 20:171–179.

8. Nicolas M, Wolfer A, Raj K, *et al.* Notch1 functions as a tumor suppressor in mouse skin. Nat Genet 2003;33:416–421.
9. Estrach S, Ambler CA, Lo Celso C, *et al.* Jagged 1 is a beta-catenin target gene required for ectopic hair follicle formation in adult epidermis. Development 2006;133:4427–4438.
10. Krebs LT, Xue Y, Norton CR, *et al.* Notch signaling is essential for vascular morphogenesis in mice. Genes Dev 2000;14:1343–1352.
11. Krebs LT, Xue Y, Norton CR, *et al.* Characterization of Notch3-deficient mice: normal embryonic development and absence of genetic interactions with a Notch1 mutation. Genesis 2003;37:139–143.
12. Robbins J, Blondel BJ, Gallahan D, *et al.* Mouse mammary tumor gene int-3: a member of the notch gene family transforms mammary epithelial cells. J Virol 1992;66:2594–2599.
13. Weng AP, Ferrando AA, Lee W, *et al.* Activating mutations of NOTCH1 in human T cell acute lymphoblastic leukemia. Science 2004; 306:269–271.
14. Moellering RE, Cornejo M, Davis TN, *et al.* Direct inhibition of the NOTCH transcription factor complex. Nature 2009;462:182–188.
15. Veeraraghavalu K, Pett M, Kumar RV, *et al.* Papillomavirus-mediated neoplastic progression is associated with reciprocal changes in JAGGED1 and manic fringe expression linked to notch activation. J Virol 2004;78:8687–8700.
16. Zagouras P, Stifani S, Blaumueller CM, *et al.* Alterations in Notch signaling in neoplastic lesions of the human cervix. Proc Natl Acad Sci USA 1995;92:6414–6418.
17. Daniel B, Rangarajan A, Mukherjee G, *et al.* The link between integration and expression of human papillomavirus type 16 genomes and cellular changes in the evolution of cervical intraepithelial neoplastic lesions. J Gen Virol 1997;78(Pt 5):1095–1101.
18. Maliekal TT, Bajaj J, Giri V, *et al.* The role of Notch signaling in human cervical cancer: implications for solid tumors. Oncogene 2008; 27:5110–5114.
19. Proweller A, Tu L, Lepore JJ, *et al.* Impaired notch signaling promotes *de novo* squamous cell carcinoma formation. Cancer Res 2006; 66:7438–7444.
20. Lefort K, Mandinova A, Ostano P, *et al.* Notch1 is a p53 target gene involved in human keratinocyte tumor suppression through negative regulation of ROCK1/2 and MRCKalpha kinases. Genes Dev 2007; 21:562–577.
21. Panelos J, Tarantini F, Paglierani M, *et al.* Photoexposition discriminates Notch 1 expression in human cutaneous squamous cell carcinoma. Mod Pathol 2008;21:316–325.
22. Yoshikawa H, Kawana T, Kitagawa K, *et al.* Detection and typing of multiple genital human papillomaviruses by DNA amplification with consensus primers. Jpn J Cancer Res 1991;82:524–531.
23. Tomioka H, Morita K, Hasegawa S, *et al.* Gene expression analysis by cDNA microarray in oral squamous cell carcinoma. J Oral Pathol Med 2006;35:206–211.
24. Sakamoto K, Tamamura Y, Katsube K, *et al.* Zfp64 participates in Notch signaling and regulates differentiation in mesenchymal cells. J Cell Sci 2008;121(Pt 10):1613–1623.
25. Minamizato T, Sakamoto K, Liu T, *et al.* CCN3/NOV inhibits BMP-2-induced osteoblast differentiation by interacting with BMP and Notch signaling pathways. Biochem Biophys Res Commun 2007.
26. Sakamoto K, Ohara O, Takagi M, *et al.* Intracellular cell-autonomous association of Notch and its ligands: a novel mechanism of Notch signal modification. Dev Biol 2002;241:313–326.
27. Taylor GP. Current Protocols in Molecular Biology. Wiley, 1987.
28. Yugawa T, Narisawa-Saito M, Yoshimatsu Y, *et al.* DeltaNp63alpha repression of the Notch1 gene supports the proliferative capacity of normal human keratinocytes and cervical cancer cells. Cancer Res 2010;70:4034–4044.
29. Ma A, Boulton M, Zhao B, *et al.* A role for notch signaling in human corneal epithelial cell differentiation and proliferation. Invest Ophthalmol Vis Sci 2007;48:3576–3585.
30. Hu C, Dievart A, Lupien M, *et al.* Overexpression of activated murine Notch1 and Notch3 in transgenic mice blocks mammary gland development and induces mammary tumors. Am J Pathol 2006; 168:973–990.
31. Park JT, Chen X, Trope CG, *et al.* Notch3 overexpression is related to the recurrence of ovarian cancer and confers resistance to carboplatin. Am J Pathol 2010;177:1087–1094.
32. Zhang Z, Wang H, Ikeda S, *et al.* Notch3 in human breast cancer cell lines regulates osteoblast-cancer cell interactions and osteolytic bone metastasis. Am J Pathol 2010;177:1459–1469.
33. Agrawal N, Frederick MJ, Pickering CR, *et al.* Exome sequencing of head and neck squamous cell carcinoma reveals inactivating mutations in NOTCH1. Science 2011;333:1154–1157.
34. Stransky N, Egloff AM, Tward AD, *et al.* The mutational landscape of head and neck squamous cell carcinoma. Science 2011;333:1157–1160.
35. Ohashi S, Natsuizaka M, Yashiro-Ohtani Y, *et al.* NOTCH1 and NOTCH3 coordinate esophageal squamous differentiation through a CSL-dependent transcriptional network. Gastroenterology 2010; 139:2113–2123.
36. Christopherson WM. Dysplasia, carcinoma *in situ*, and microinvasive carcinoma of the uterine cervix. Hum Pathol 1977;8:489–501.
37. Reid R. Genital warts and cervical cancer. II. Is human papillomavirus infection the trigger to cervical carcinogenesis? Gynecol Oncol 1983;15:239–252.
38. Weijzen S, Zlobin A, Braid M, *et al.* HPV16 E6 and E7 oncoproteins regulate Notch-1 expression and cooperate to induce transformation. J Cell Physiol 2003;194:356–362.
39. Machado J, Reis PP, Zhang T, *et al.* Low prevalence of human papillomavirus in oral cavity carcinomas. Head Neck Oncol 2010;2:6.
40. Syrjanen KJ. HPV infections and oesophageal cancer. J Clin Pathol 2002;55:721–728.
41. Williams SE, Beronja S, Pasolli HA, *et al.* Asymmetric cell divisions promote Notch-dependent epidermal differentiation. Nature 2011; 470:353–358.
42. del Alamo D, Schweisguth F. Notch signalling: receptor cis-inhibition to achieve directionality. Curr Biol 2009;19:R683–R684.
43. Klein T, Brennan K, Arias AM. An intrinsic dominant negative activity of serrate that is modulated during wing development in *Drosophila*. Dev Biol 1997;189:123–134.
44. Li Y, Baker NE. The roles of cis-inactivation by Notch ligands and of neuralized during eye and bristle patterning in Drosophila. BMC Dev Biol 2004;4:5.
45. Micchelli CA, Rulifson EJ, Blair SS. The function and regulation of cut expression on the wing margin of Drosophila: Notch, Wingless and a dominant negative role for Delta and Serrate. Development 1997;124:1485–1495.
46. Miller AC, Lyons EL, Herman TG. cis-Inhibition of Notch by endogenous Delta biases the outcome of lateral inhibition. Curr Biol 2009; 19:1378–1383.
47. McGill MA, Dho SE, Weinmaster G, *et al.* Numb regulates post-endocytic trafficking and degradation of Notch1. J Biol Chem 2009; 284:26427–26438.
48. Zhong W, Jiang MM, Weinmaster G, *et al.* Differential expression of mammalian Numb, Numblike and Notch1 suggests distinct roles during mouse cortical neurogenesis. Development 1997;124: 1887–1897.
49. Boldrup L, Coates PJ, Gu X, *et al.* DeltaNp63 isoforms regulate CD44 and keratins 4, 6, 14 and 19 in squamous cell carcinoma of head and neck. J Pathol 2007;213:384–391.

顎顔面矯正学分野

森山 啓司

医歯学総合研究科・顎顔面頚部機能再構築学系専攻
顎顔面矯正学・教授

1）研究の課題名

1. Apert症候群型変異FGFR2とその可溶型は頭蓋冠由来骨芽細胞の骨形成能を相反的に変化させる

Apert syndrome mutant FGFR2 and its soluble form reciprocally alter osteogenesis of primary calvarial osteoblasts

Apert症候群の原因として線維芽細胞増殖因子2型受容体（FGFR2）の細胞外領域の2種類の変異（S252W、P253R）が同定されている。今回、S252Wの骨芽細胞分化への影響を明らかにすることを目的とし、FGFR2IIIc-S252W（FGFR2IIIc-Ap）と細胞内領域を欠落した可溶性変異体（soluble FGFR2IIIc-S252W）を発現するトランスジェニックマウス（各々Ap-Tg、sAp-Tg）を作出し、解析を行った。実験方法として、野生型（WT）、Ap-Tg、sAp-Tg、両者の交配により得られたAp/sAp-Tgの4種のマウスの頭蓋冠骨芽細胞を単離し、細胞数計測による増殖能の解析、ALP活性、alizarin red S染色、リアルタイムPCRによる骨マーカー遺伝子の発現による分化能の検討を行った。またFGFシグナル関連タンパクのリン酸化をWestern blot法で解析した。さらにin vivoにおける骨形成能として、骨芽細胞をβ-TCPと共に免役不全マウス皮下に移植し、8週後の骨組織形成を観察した。その結果、FGFR2IIIc-Apを発現するAp-Tg由来骨芽細胞ではMEK、ERK、p38を介するFGFシグナル経路が活性化し、in vitroでの骨芽細胞の増殖・分化、in vivoでの骨形成を促進するのに対し、sFGFR2III-Apを発現するAp-Tg由来骨芽細胞ではこれらの現象を抑制した。また、FGFR2IIIc-ApとsFGFR2III-Apを共発現させたAp/sAp-Tg由来骨芽細胞はWT由来骨芽細胞に近似した増殖能・分化能を示した。これらの結果から、FGFR2IIIc-ApおよびsFGFR2IIIc-Apは、頭蓋冠縫合部早期癒合症の病態解析や治療法開発に有用な分子と考えられる。

2. 頭蓋冠縫合部の発生におけるHedgehogシグナルの機能解析

Analysis of the role of Hedgehog signaling in the calvaria suture development

頭蓋冠縫合部は、隣接する頭蓋骨を結合する線維性組織であり、頭蓋冠の成長に重要な役割を果たす。頭蓋冠縫合部早期癒合症（Craniosynostosis）は、縫合部が早期に閉鎖する先天性の骨系統疾患であり、重篤な不正咬合を呈する事が多い。GLI3変異は、頭蓋の変形や多指症を主症状とするGreig Cephalopolysyndactyly Syndromeの原因となることが知られている。Gli3欠損マウス（Gli3Xt－J/Xt－J）がラムダ状縫合に早期石灰化を呈することに着目し、Craniosynostosisに対する治療法の開発に向けての基礎的な研究を行ってきた。野生型（Wt）頭蓋冠において、Gli3 mRNAは、ラムダ状縫合および前頭縫合に接するosteogenic frontで限局的に認められた。Gli3Xt－J/Xt－Jラムダ状縫合ではPatched1, Runx2-II, 及びDlx5等の明らかな発現上昇、およびTwist1の発現低下が観察され、骨芽細胞分化の亢進が確認された。BrdU取り込み実験によってGli3Xt－J/Xt－Jでは縫合部中央部の間葉系細胞で有意な細胞増殖亢進が認められた。FGF2除放ビーズをGli3Xt－J/Xt－Jラムダ状縫合に適応したところ、ビーズ周囲にTwist1発現が誘導され、同部位における早期癒合を阻止した。最後に、Gli3/Runx2複合変異マウスを作成したところ、Gli3Xt－J/Xt－J Runx2+/-マウスではラムダ状縫合の開存が全例で認められた。以上より、頭蓋冠縫合部の適切な発生には、Gli3が重要な働きをすることが示唆され、Runx2の機能抑制により、縫合部における早期石灰化が阻止されることが示された。以上の結果は、将来RNAi等を利用したcraniosynostosisに対する非外科的治療法開発へのヒントとなることが期待される。

3. リラクシン含有磁性リポソームを利用した顎顔面領域の縫合部拡大制御法の開発

Development of the strategy for expansion of craniofacial suture with magnetized liposome containing Relaxin

ペプチドホルモンの一種であるリラクシン（RELAXIN;RLN）は哺乳類の出産時に卵巣黄体より血中に分泌され、恥骨結合の弛緩と軟化、子宮頸部の軟化等を惹起する。この作用機序として、RLN2がマトリックスメタロプロテアーゼ（Mmp）の発現を誘導し、Mmpの阻害因子であるTimp1発現を抑制する事で細胞外マトリックスの分解を引き起こす事が報告され、内因性リラクシンは細胞外基質の分解に重要な働きを担うことが示唆される。一方、破骨細胞の分化・成熟に必須のRANKL-OPGシステムを調節することが報告されている。本研究は、リラクシンの骨基質分解促進作用と破骨細胞機能亢進機構作用を頭蓋顎顔面領域の縫合部に生体親和性磁性リポソームを用いて適用し、その局所的骨代謝調節作用を利用することで縫合部の拡大を含めた顎顔面骨格の三次元的位置制御を目指すものである。研究代表者らは、予備実験として、胎生15.5〜18.5日齢ラット胎児における内因性Rxfp1の免疫組織学的検索を行い、主に上皮系組織にその局在を認めた。また、蛍光物質（Cy3）とナノ磁性体内包、リラクシン結合型リポソームを作成し、ラット頭蓋冠（胎生18.5日齢）器官培養系に投与後、磁性ワイヤーを用いてリポソームの局在をコントロールすることに成功している。今後、マウス胎児頭蓋冠由来骨芽細胞様細胞およびマウス胎児口蓋器官培養系においてその安全性と至適条件を決定後、リラクシン磁性リポソームをラット正中口蓋縫合およびラット頭蓋冠矢状縫合部に注入後、矯正用拡大装置にて側方拡大を行う。磁気を帯びたステンレススチール線を装着し、リポソームの作用領域のコントロールを行い、至適条件下で縫合部の拡大を行い、拡大効率に与える影響について検討する。

4. ペリオスチンノックアウトマウスを用いた歯周組織の生物学的特性の解明

Phenotypic and functional analysis of periodontal tissues found in periostin null mice

ペリオスチン（POSTN）は特に骨外膜、歯根膜、心臓弁に特異的に局在する細胞外基質（ECM）タンパクであり、細胞接着、コラーゲン線維形成・架橋形成への関与、線維芽細胞の遊走・活性化促進に重要であると考えられている。POSTNを欠失させたマウス（ノックアウトマウス）を解析した以前の報告では、咬合力に対抗して歯周組織を健全に維持する機能にPOSTNが関与していることが示唆されていた。ところで、歯の移動初期の圧迫側歯根膜には毛細血管の変形による低酸素状態が誘導され、引き続き歯根膜細胞のアポトーシス様細胞死が起こると考えられている。同時に、圧迫側歯根膜では、POSTNの発現が上昇することが報告されている。そこで本研究では、POSTNが低酸素分圧下の歯根膜細胞に誘導されるアポトーシスに対し、どのような役割を果たしているかについて、in vitro、in vivoの両面より検討を行っている。今年度はin vitroにおいてヒト歯根膜細胞（hPDL）に、リコンビナントペリオスチン（rhPOSTN）を添加、POSTN発現ベクターを導入、あるいはPOSTNのsiRNAを導入し、通常酸素分圧下/低酸素分圧下において24-48時間培養後、TUNEL陽性細胞数、低酸素誘導因子1α（HIF1α）等の変化の有無を確認した。その結果、POSTNがHIF1αタンパクを減少させることで、低酸素分圧下におけるhPDLを細胞死から防御していることを示唆するデータを得た。現在、歯の移動時に引き起こされる歯周組織における細胞死とPOSTNの関連について、POSTNノックアウトマウスを用いin vivoにて解析を行なっている。

5. アメロジェニンスプライスアイソフォームの骨・軟骨細胞分化に与える影響

Biological roles of amelogenin splice isoforms on bone and cartilage differentiation

アメロジェニンは、エナメル質に存在する主要なタンパク質であり、エナメル質形成において重要な役割をもつとされている。アメロジェニンはこれまで、エナメル芽細胞に特異的に発現するタンパク質と考えられてきたが、近年の研究では幅広い組織での発現が確認されつつあり、特にM180、LRAPの2つのアメロジェニンアイソフォームは、骨・軟骨組織を含む間葉系細胞において、細胞間のシグナル伝達物質としての役割を担っていると考えられるようになってきた。本研究では、2つのアメロジェニンアイソフォーム、M180とLRAPが、骨・軟骨分化に対してどのような影響をもたらすか検討している。今年度までに、リコンビナントマウスM180およびLRAPタンパクを293-F細胞で作成し株化軟骨細胞（ATDC5）に対する影響を検討した。その結果、ATDC5細胞において、M180とLRAPは、培養14日および28日に、ALP活性と、軟骨基質分泌をそれぞれ有意に増加させた。また、LRAPは軟骨分化誘導後7日以内にRunx2、Col2a1、Aggrecanの遺伝子発現を有意に上昇させ、M180とLRAPは軟骨分化誘導後28

日までにAlkaline phosphatase、Aggrecan、Col10a1、Osteopontinの遺伝子発現を有意に上昇させた。さらに、BrdUアッセイとWntシグナル関連分子の遺伝子発現の分析結果から、ATDC5細胞の増殖は、M180、LRAP添加によって抑制され分化が促進されている結果が得られたが、これらはnon-canonical Wntシグナルを変化させることで引き起こされていることが示唆された。現在は、LRAPを骨に強制発現させたトランスジェニックマウスを作成し、骨におけるアメロジェニンの役割を、in vivoにて解析中である。

6. 象牙質シアロリンタンパク（DSPP）の歯と骨の石灰化における生物学的役割-象牙質マトリクスタンパク1（DMP1）との比較-

Dentin sialophosphoprotein and dentin matrix protein-1：Two highly phosphorylated proteins in mineralized tissues.

象牙質シアロリンタンパク（DSPP）と象牙質マトリクスタンパク1（DMP-1）は高度にリン酸化されたタンパクで small integrin-binding ligand N-linked glycoproteins（SIBLINGs）ファミリーに属し、いずれも歯と骨の発生において重要な役割を持つと考えられている。 また、DSPPとDMP-1は同一染色体上で隣同士に位置し、遺伝子・タンパク質の構造が共に類似しており、N末端とC末端の大きく2つのタンパク質に分解されて機能すると考えられている。本研究では、DSPPタンパクの歯と骨における割について、DMP1の過去の報告と比較しつつ、特に基質石灰化に着目して検討を行なった。本年度は、DSPP遺伝子欠損マウスと、DSPPのN末端側タンパク質であるDSPを歯において強制発現したトランスジェニックマウスを交配し、歯におけるDSPPのC末端側タンパク質であるDPPの機能を検討・報告した。また、DSPPノックアウトマウスの表現型解析において、DSPPは骨における発現量がDMPと比較して少ないため、野生型と比較した際の骨における表現型変化は存在するものの、DMPと比較して僅かであることが示唆された。現在もDSPPノックアウトと他の遺伝子変異マウスと交配を行い、継続して歯と骨の表現系変化をインテグリンシグナルを中心に検討を行なっている。

7. 中顔面部低形成を特徴とする10p11.23 p12.1欠失症候群の2症例

Two cases of deletion at chromosome 10p11.23-p12.1 defines characteristic phenotypes with marked midface retrusion

【目的】新生児の約3%に何らかの先天性奇形が観察され、その約3分の1に顎顔面領域の奇形が発現することが報告されている。また、近年ゲノム異常の多様性が明らかとなってきており、ヒトゲノムの多様性と表現型との連関性が解明されつつある。矯正歯科の分野では、染色体異常を含む40種類の疾患に起因する不正咬合の治療に保険適応が可能となり、個々の先天性疾患の顎態の特徴のさらなる解析や治療方法の確立が望まれている。本報告では、常染色体欠失症候群の2症例を対象に、顎顔面領域の奇形の定量的評価並びに詳細なゲノム解析を行い、表現型とゲノム異常の連関を検討した。【試料】臨床診断がつかず、染色体核型正常である多発奇形を伴う精神発達遅滞（multiple congenital anomalies and mental retardation; MCA/MR）症例のうち、スクリーニングによって見出された2症例を対象とした。【方法】顎顔面領域のセファログラム分析および、ゲノムの評価として、リンパ球から抽出したDNAをアレイCGH法で解析した。さらに検出されたCNV（copy number variation）は、Fluorescence in situ hybridization（FISH）や高解像度オリゴヌクレオチドアレイを用いて詳細に評価を行った。【結果】10p11.23-p12.1領域に反復する欠失を有し、顎顔面領域において共通する奇形を見出した。それぞれの欠失サイズは2.0 Mbおよび2.4 Mbであった。SRO（the shortest region for overlap）は957 kbで、SRO内には4個の遺伝子が存在した。また、2症例に共通して特異な口唇形態ならびに中顔面部の低形成が認められた。【考察】本報告では10p11.23-p12.1領域の欠失症例に対して顎顔面領域の異常を定量的に評価し特徴的な所見を得た。これにはSROに座位している4遺伝子のハプロ不全が2症例の表現型と関与していることが予想された。【結論】類似する顎顔面領域の先天性疾患において、ゲノム異常と表現型の両面から詳細に解析を行った。このことは、本領域の欠失症例のみならず、未だ原因不明の先天性疾患の診断に有意であり、顎顔面領域における奇形の原因検索ならびに治療の一助となりうる。

8. 日本の中学生における不正咬合の発生率とその男女差について～甲州市母子保健縦断調査～

Prevalence and gender comparison of malocclusion among Japanese adolescents：A population-based study.

近年わが国では、不正咬合の割合が増加しており、咬合状態が正常で叢生のない児童の割合は20～30%であるといわれている。しかし、不正咬合の発生率について、矯正歯科医が客観的な基準に基づいて評価したものは少なく、代表性のある集団を対象とした疫学調査により現状を正確に把握することが求められている。また、不正咬合の発生率について欧米では女子が男子より多いとの報告

があるが、我が国ではまだ男女差の検討は少ない。本研究の目的は、日本人の中学生（12-15歳）において、不正咬合の割合とその男女差について検討することである。甲州市立中学校5校に在籍し欠席者を除く全ての生徒（963名：男子53.6%）を対象とした。各校の学校歯科健診時に、訓練された矯正歯科医が矯正治療必要度指標（Index of Orthodontic Treatment Need：以下IOTN）に準じて、Angle分類（臼歯部の前後的な咬合関係）、前歯部および臼歯部のcrossbite（上下の歯のかみ合わせが逆）、上顎および下顎の叢生（歯並びのでこぼこ）、overjet（上下顎前歯の前後的な位置関係）、overbite（前歯の上下的な重なり）、上下顎前歯部正中の不一致、上顎左側中切歯の幅径の診査を行った。男女差の解析は学年、矯正治療歴を調整した多変量ロジスティック解析を用いた。矯正治療を必要とする不正咬合の発生率は、男子40.9%（95% CI：36.6-45.1）、女子46.9%（95% CI：42.2-51.5）であった。女子は男子より、前歯部のcrossbite（adjusted OR, 1.57; 95% CI, 1.08-2.12）、上顎の叢生（adjusted OR, 1.54; 95% CI, 1.09-2.15）、上下顎正中の不一致（adjusted OR, 1.35; 95% CI, 1.03-1.78）、矯正治療を必要とする不正咬合（adjusted OR, 1.32; 95% CI, 1.02-1.71）が多かった。Angle分類、臼歯部のcrossbite、下顎の叢生、overjet、overbite、上顎左側中切歯の幅径に男女差はなかった。日本における不正咬合の頻度は比較的高く、中学生の40%以上が矯正治療を必要とする不正咬合という結果であった。また、女子は男子より不正咬合である割合が高かった。女子において不正咬合の発生率が高くなるメカニズムを明らかにしていくことが、今後の研究で求められる。

9. 細胞増殖因子により軟組織との強い結合力を有するコラーゲン電着固定化チタンの開発

Effects of pH, Potential, and Deposition Time on the Durability of Collagen Electrodeposited to Titanium

矯正用インプラントアンカーの脱落の原因の一つとして、軟組織との界面の微小な間隙からの細菌侵入による感染が挙げられる。これを防ぐためインプラントアンカーに軟組織結合性を付与することにより金属と生体軟組織の結合促進及び結合力強化が必要である。この方法で感染予防が達成できればインプラントアンカーの脱落の可能性を減少できると考えられる。申請者はチタン表面へのコラーゲン電着固定化法の改良など、金属と生体分子を結合する技術の開発を目的とした研究を行ってきた。本研究はこのコラーゲン電着固定化チタンに細胞増殖因子を付加し細胞接着分子を活性化することで、生体内に埋入した際に強固な軟組織への結合力を発揮する新しい金属生体軟組織の結合技術を開発することを目的としている。本研究成果は、感染による脱落の危険性の無い信頼性の高いインプラントアンカーの設計に大きく寄与するものと期待される。

10. 成長期における先天性多数歯欠如（oligodontia）患者の顎顔面形態についての検討

Craniofacial morphology in growing patients with oligodontia

茂木和久、小川卓也、馬場祥行、森山啓司.

Orthodontic-Japanese Edition, 71（3）：187-193.

永久歯胚の先天性欠如は、顎顔面領域にみられる頻度の高い先天異常の一つである。永久歯胚の欠如が多数にわたる場合、咀嚼、発音といった口腔機能に多大な影響を与え、咬合機能獲得のための治療方針立案は非常に困難なものになると考えられる。そこで、歯科矯正治療計画立案の一助とするために、東京医科歯科大学歯学部附属病院矯正歯科外来（顎顔面矯正学分野）に来院した第三大臼歯を除く6歯以上の永久歯胚欠如を呈する先天性多数歯欠如（oligodontia）患者14名（男性5名、女性9名、初診時年齢8.3歳から12.9歳、平均10.0歳）の初診時資料を用い、永久歯胚の欠如様式、成長期における顎顔面形態の特徴に寄与する要因について検討し、以下の結果を得た。歯種別発現頻度は上顎第二小臼歯が最も多く、次いで下顎第二小臼歯、上顎第一小臼歯、下顎第一小臼歯の順であった。一方、上下顎の中切歯、犬歯、第一大臼歯、下顎第二大臼歯が欠如している割合は低かった。顎顔面形態について、上顎骨の後方位、下顎骨の前方位と下顎下縁平面角の減少、および小さな前下顔面高を伴う骨格性下顎前突の傾向を認めた。また、上顎第一大臼歯に関して、同年代の先天性永久歯胚欠如を認めないアングルⅠ級不正咬合30症例と比較して、口蓋平面からの距離が有意に小さく、また有意に前方に位置していた。本検討から成長期の先天性多数歯欠如患者の顎態の特徴には、上顎大臼歯の低位ならびに前方位が関与していると考えられ、上顎大臼歯の挺出による咬合の挙上ならびに下顎の時計方向への回転を促す治療の必要性が示唆された。

11. Oculofaciocardiodental syndromeにおける新規BCOR遺伝子変異の同定

A novel mutation in BCOR in a patient with oculofaciocardiodental syndrome

Oculofaciocardiodental syndrome（OFCD）はX連鎖性優性遺伝形式のまれな遺伝性疾患で、罹患女性において、特異的顔貌、心臓および眼の異常、ならびに長い

歯根を呈する特徴を認める。歯根端が下顎下縁まで達する場合もあり、歯髄処置ならびに矯正治療により歯を移動させる際には注意を要する疾患である。今回、当分野を受診したOFCD患者において、原因遺伝子であるBCOR（encoding BCL-6-interacting corepressor）の変異解析を行い、分子遺伝学的検討を加えたので報告する。永久歯の萌出遅延を主訴に、当分野を受診した初診時年齢10歳9か月の女児を対象とした。発端者以外に家系内に同疾患に罹患している患者を認めない。頬粘膜よりゲノムDNAを抽出し、PCR法とダイレクトシークエンス法でBCOR遺伝子の全翻訳領域とエクソン/イントロン境界の塩基配列を決定した。また、同患者ならびに歯に異常を認めない患者より便宜抜歯された下顎第一小臼歯から歯髄細胞を単離・培養し、培養細胞におけるBCORのmRNAの発現量を半定量的PCR法により検討した。さらに、患者由来の培養歯髄細胞に、シクロヘキシミド（CHX）を添加し、ナンセンス変異依存mRNA分解機構（NMD）の関与の可能性について検討した。当分野を受診したOFCD患者において、BCOR遺伝子にヘテロ接合性の新規変異（c.3668delC）を認め、フレームシフト変異により早期終止コドンを形成した（p.S1223WfsX14）。また、正常コントロールとOFCD由来の培養歯髄細胞におけるBCORのmRNAの発現量に差を認めず、OFCD由来の培養歯髄細胞にCHXを添加しても、mRNAの発現量の変化を認めなかった。本症例において、BCOR遺伝子の新規変異を同定することができた。同患者由来の培養歯髄細胞においては、NMDの関与を伺わせる所見は認められず、他の組織から得られた細胞を用いた解析の必要性が示唆された。

12. 顎顔面領域の発生時におけるヒストンメチル化酵素の役割

The role of histone methyltransferases during craniofacial development

先天性疾患には、遺伝的要因と環境要因との相互作用によって発症する多因子疾患が多数存在する。近年、環境因子がエピゲノムの情報を変えることにより、疾患が引き起こされることが報告されているが、顎顔面領域における先天性疾患とエピゲノムについての報告は少ない。そこで我々は、エピゲノム変化を修飾する酵素であるヒストンメチル化酵素に注目し、顎顔面領域の発生時における役割を解明することにより、先天異常の発症原因の解明、予防法の開発等の臨床応用への基盤となるよう研究を進めている。数種のヒストンメチル化酵素コンディショナルノックアウトマウスの表現型解析を行なっており、その中でもG9aと呼ばれる転写に抑制的に働くヒストンメチル化酵素を神経堤細胞由来の細胞のみにノックアウトした所、骨芽細胞の分化が抑制されていることがわかった。現在は、ターゲット遺伝子の同定およびそれらの遺伝子にG9aがどのようなメカニズムで発現のスイッチを制御しているかを解析中である。

13. ペリオスチンに着目した歯根膜弾性線維の機能解明

Investigation of the function of the elastic system fibers in periodontal ligaments.

弾性線維は様々な組織に存在し、組織に弾力を与えていると言われている。歯根膜中の線維成分では主要な構成要素はコラーゲン線維と弾性線維である。コラーゲン線維は歯槽骨とセメント質を結合するように存在し、咬合力に耐えるように歯を支持する役割があるが、歯根膜の弾性線維の役割は多くの点が不明である。

歯根膜弾性線維の主要構成成分はフィブリリンである。興味深いことにフィブリリン低発現マウス（MgR）の歯根膜ではペリオスチン遺伝子（POSTN）発現が抑制されていた。ペリオスチンは骨外膜と歯根膜に特異的に局在することが知られていたが、最近の研究では胚発生過程、心筋梗塞・がんなど病態、創傷治癒などの治癒や再生過程において機能していることが報告されている。さらにペリオスチンはコラーゲン等の細胞外基質の構成成分と直接相互作用しインテグリンのリガンドとして作用すると報告もされ、ペリオスチンは創傷治癒や細胞増殖・アポトーシスなど組織恒常性の維持に関与していると推測されている。

フィブリリン遺伝子（FBN1）異常であるMarfan症候群患者においては健常者と比べ歯周病の罹患率が高いのと報告があり、歯根膜組織においても組織の恒常性の維持や修復機構の異常とペリオスチン、さらにはフィブリリンになんらかの関連性があることが予想される。本研究の目的はヒトの歯根膜細胞のFBN1の発現を抑制することによってフィブリリンとペリオスチンの関連を詳細に検討し、歯根膜弾性線維の新たなる働きを探索することである。

14. ハイドロキシアパタイトコラーゲン複合体コーティングの最適化

Optimization of HAp/Col coating

【背景】過去1年での成果より,純チタンワイヤーにハイドロキシアパタイト/コラーゲン複合体（HAp/Col）コーティングを行うことによって,4週間で骨と接合する新規矯正用アンカレッジデバイスが実現できる可能性

が示された.HAp/Colが有する破骨細胞やマクロファージに貪食されやすい特性が,線維性組織や辺縁の骨形成に影響を及ぼし,ワイヤーと骨が直接接合したと考えられるが詳細は不明である.【目的】HAp/Colコーティングワイヤーを骨膜下に埋入した後,いつ,どのような細胞によってHAp/Colが吸収され,どのようにワイヤー周囲に新生骨が形成されるかを明らかにし,骨膜下デバイスのコーティングとして最適なHAp/Colの厚さを決定する.【試料および方法】試料は,直径0.5 mm,長さ12 mmの純チタン製ラウンドワイヤーとする.コーティングは,HAp/Colが分散したゾル状の懸濁液にワイヤーを浸漬するディッピング法で行う.コーティングの厚さは,浸漬回数で規定する.厚さの計測は,走査型プローブ顕微鏡で行う.作製した試料を12週齢,雄性SDラットの頭蓋骨骨膜下へ埋入する動物実験を行い,埋入直後,3日後,7日後,14日後,28日後に採材し,評価を行う.評価方法は組織学的観察,μCTによる観察を行う.組織学的観察では,カルセインとテトラサイクリンでのラベリングおよびALP/TRAP染色による観察を行い,新生骨形成速度の評価,破骨細胞および骨芽細胞数の評価を行う.また,シリウスレッド染色で線維性被膜の形成状態を評価する.μCTによる観察では新生骨の骨塩量を評価する.以上より,HAp/Colコーティングワイヤー周囲に新生骨が形成される過程が明らかとなり,骨膜下デバイスのコーティングとして最適なHAp/Colの厚さが決定される.

15. ビーグル犬におけるミニプレート顎間牽引の顎整形効果に関する検討

The orthopedic effects of the intermaxillary traction using miniplates in beagle dogs

近年、成長期に上下顎骨へミニプレートを埋入し、顎間牽引を行う顎矯正治療法Bone anchored maxillary protraction（BAMP）の臨床報告がなされているが、その効果に関する動物実験的検証はなされていない。よって本研究では、BAMPの動物実験モデルを構築し、顎顔面形態の変化について解析を行った。100日齢（-20Day）の雄性ビーグル幼犬10匹を用い、上顎両側後臼歯部と下顎両側前臼歯部にミニプレートを埋入した。120日齢（0Day）から180日齢(60Day）までスプリングにて顎間牽引(初張力：200gf）を行い（牽引群;n=4)、牽引しなかった対照群（n=4）と比較した。また、イヤーロッド付き頭部固定装置を作製し、頭部X線規格写真を経時的に撮影して資料として用いた。解析はPo（Polion）とOr（Orbitale）を通るフランクフルト（FH）平面を基準平面として距離計測と角度計測を行った。-20Dayでは、距離計測、角度計測ともに両群間で有意差を認めなかったが、60Dayでは、距離計測にて、上顎骨は牽引群で有意に大きかったが、下顎骨は有意差を認めなかった。また、角度計測では牽引群においてFH平面に対する上下顎前歯歯軸のなす角はともに有意に小さかった。以上の結果より、BAMPにより上顎骨の前方成長促進および上下顎切歯の歯性補償が生じたと考えられた。以上より、BAMPの動物実験モデルにて上顎骨の前方成長に対する促進効果を認め、BAMPの臨床的有用性を支持する結果が得られた。本研究結果は、今後の顎顔面領域の顎矯正歯科治療法の開発に大きく寄与するものと期待される。

16. 下顎頭軟骨形成メカニズムの生物学的解析

Biological analysis of mechanism for condylar cartilage formation

プロテオグリカン（PG）は重要な細胞外基器質の一つで、一次軟骨においては大型のコンドロイチン硫酸PGであるPG-M/versicanは軟骨形成前の間葉凝集の、またaggrecanは軟骨形成後の主要な細胞外基質成分であると報告されている。一方PG合成阻害剤であるβ-Xylosideは細胞に取り込まれると、そこを基点として異常なコンドロイチン硫酸鎖が合成され、結果として正常なPG分子の合成阻害が生ずることが知られている。本研究ではPG合成阻害が下顎頭軟骨発生過程に及ぼす影響を検討することを目的とし、器官培養系にβ-Xylosideを添加（2.0mM）してその形成過程を観察した。胎生14日齢のICRマウスのメッケル軟骨を含む下顎頭軟骨原基を取り出し、β-Xyloside存在下において6日間無血清培地で器官培養を行った。培養終了後、透明骨格標本からはAlcian blue陽性の組織は認められず、明らかな軟骨形成は認められなかった。組織切片からは軟骨組織は形成されていたが、対照群と比較して大きさは明らかに矮小化していた。形成された軟骨組織内における蛋白、mRNAの発現に関しては著明な差は認めなかった。これらのことよりβ-Xylosideは下顎頭軟骨の形態発生において明らかにその形成を抑制するものの、分化した軟骨組織の性質は維持されることが示唆された。

17. 下顎骨後方移動術が睡眠呼吸機能に及ぼす影響

Effects of mandibular setback surgery on the function of sleep breathing

顎変形症や頭蓋顔面の形成異常等に代表される骨格性不正咬合は患者の社会心理的影響に大きく関与するとともに咀嚼、発音などの機能的問題が生じる。骨格性不正

咬合患者は、矯正治療単独での咬合の改善や顔貌の調和を図ることが困難であり、外科的矯正治療を適応する。特に下顎骨後方移動術は顔貌および咬合状態の劇的な改善、適切な口腔機能の獲得が期待できるが、口腔内容積が減少し、舌房が狭くなることにより睡眠呼吸障害を発症する可能性が指摘される一方、下顎骨後方移動術と睡眠呼吸障害は関連性がないとの報告も散見される。そこで、我々は外科的矯正治療前後での硬組織の大きさと軟組織量との解剖学的バランス（Anatomical Balance）の変化と睡眠時呼吸機能との関連性を解明し、そしてAnatomical Balanceの変化が形態的、機能的に安定した外科的矯正治療の立案の指標となり得るかを検討した。外科的矯正治療前後で下顔面硬組織（LFC）の大きさに対する軟組織（TG）の割合（TG/LFC）を計測したところ、外科的矯正治療前後での統計学的な有意差を認めなかったことから外科的矯正治療適応により成体では何らかの補償機構によりTG/LFCが維持され、睡眠時の生理呼吸機能が保たれている可能性が示唆された。更に我々は簡易型睡眠呼吸計を用いて、下顎骨後方移動術前後での睡眠呼吸機能の変化について解析中である。

18. 下顎枝矢状分割術を施行した骨格性下顎前突症例の長期術後経過からみた咬合安定性の検討

Investigation of long-term stability of occlusion after sagittal split ramus osteotomy for mandibular protrusion

骨格性下顎前突症患者に対する下顎後方移動術に関し、術式や固定法の改善により良好な結果が得られているが、長期経過観察中に臼歯部被蓋の減少により咬合状態が不安定になる症例も散見される。我々は長期術後経過が得られた症例の咬合安定性と歯列弓形態について検討した。下顎枝矢状分割術単独による下顎後方移動術を施行した骨格性下顎前突症患者のうち、術後長期経過した26症例（術後平均8.3年; 2.9〜18.9年、男性13名, 女性13名）を対象とした。初診時（T1）、動的矯正治療終了時（T2）、長期術後経過時（T3）の顎態模型を資料とし、咬合状態の評価にはPAR Indexを用い、T2-T3における咬合状態の変化が無かった安定群（S群）と非安定群（NS群）とに分類した。また、上下顎犬歯尖頭間、小臼歯および大臼歯中心窩間の幅径を計測し、各時点の計測値の変化と各時点間における上下顎の変化量を比較検討した。26症例中、S群は16症例、NS群は10症例であった。T1-T2において、S群では、下顎第二大臼歯部幅径は有意に増加を認め、各大臼歯部において上顎に対し下顎における変化量が有意に大きかった。一方、NS群では各大臼歯部において上下顎の変化量に有意差はなかった。T2-T3において、S群では、幅径は上下顎第一大臼歯部および上顎第二大臼歯部で有意に増加し、下顎第二大臼歯部では増加傾向を認めたが、各大臼歯部において変化量に有意差はなかった。一方、NS群では、幅径は下顎大臼歯部では有意に増加し、第一大臼歯部においては上顎に対し下顎における変化量が有意に大きかった。骨格性下顎前突症患者の長期的咬合変化には動的矯正治療およびその後の下顎大臼歯部の幅径変化が関与している可能性が高く、治療計画立案に際し舌の影響を考慮した口腔内容積確保の重要性が示唆された。

19. 顔面非対称を伴う骨格性下顎前突症例における下顎骨形態の三次元的解析

顔面非対称には様々な要素が関連していると考えられるがその詳細については未だ十分に検討されていない。顔面非対称を伴う顎変形症の分析には正面頭部X線規格写真がよく用いられてきたものの、頭部の位置づけにより影響を受け、骨格的な歪みの正確な把握が困難となる場合があることが問題とされてきた。そこで我々はX線CT撮影により得られた三次元データを解析し、顔面非対称を伴う骨格性下顎前突症例の下顎骨形態の特徴を抽出したので報告する。当分野において外科的矯正治療を施行した顔面非対象を伴う骨格性下顎前突症例12例（FA群）および顔面非対象を伴わない骨格性下顎前突症例12例（NA群）を対象とした。術前に撮影したマルチスライスCTのDICOMデータを用いて顎顔面三次元解析用ソフトウェアにより下顎骨の三次元画像を作成し形態計測を行った。本研究では、下顎頭最上方点と下顎孔窩最下方点を結ぶ線に直交し、かつ下顎頸部最陥凹部を通る平面を設定して、この平面より上方を下顎頭と定義した。得られたデータはFA群とNA群で比較し統計学的に検討した。統計解析にはWilcoxon 符号順位検定、Mann-Whitney順位和検定、Spearman順位相関を用いた。Meの偏位量に関しては初診時に撮影した正面頭部X線規格写真より計測した。FA群において非偏位側と比較して偏位側の下顎頭体積が有意に小さく（$P<0.01$）、Meの偏位量と下顎頭体積の間に相関を認めた（$P<0.05$）。FA群とNA群の二群間で左右下顎頭の体積比に有意に差を認めた（$P<0.01$）。今回試みた三次元的解析より顔面非対称を伴う症例において左右下顎頭形態の差異が顔面非対称の程度に影響を与える一要素となりうる可能性が示唆された。今後は本研究で得られた結果を用いて、骨格的な非対称の原因に応じた術後の予後、顔貌の改善度を評価していきたいと考えている。

20. 上顎前歯部歯槽骨切り術を適応した骨格性下顎後退症患者の側貌軟組織変化

Soft tissue profile changes following anterior segmental maxillary osteotomy in mandibular retrognathia patients.

著明な下顎頭吸収により惹起されたことが疑われる骨格性下顎後退症患者に対して上顎前歯部歯槽骨切り術にて口腔機能の改善を図る機会が近年増加している。顎変形症患者に対する外科的矯正治療においては咬合・咀嚼などの機能の改善とともに,顔貌の改善も重要な治療目標となっている。我々は上顎前歯部歯槽骨切り術を適応した日本人骨格性下顎後退症患者の側貌軟組織変化について検討した。下顎後退群と非後退群の2群に分類し、初診時（T1）と術後約1年時（T2）の側面頭部X線規格写真を用いて、頭蓋冠、前頭蓋底で2時点の透写図を重ね、FH平面に平行でS点を通る直線をX軸とする直交座標を設定し、代表的な軟組織計測点13項目に対して距離計測および軟組織角度分析を行い、統計学的解析を行った。T1からT2にかけてのオトガイ部軟組織の変化量は下顎後退群では非後退群に比べ有意に大きかった。T1からT2にかけて下顎後退群ではオトガイ部軟組織が下方へ移動し、鼻尖角が減少した。非後退群は鼻顔面角が減少し、鼻口唇角が開大した。また、下唇の翻転の程度が減少した。今回の結果から下顎後退群は非後退群と比較して オトガイ部軟組織が下方に移動した。これは、下顎後退群では、口唇閉鎖時に頭蓋に対して前後的位置に問題が少ないと考えられる上唇に合わせ、下唇を伸展させている可能性が考えられ、今後顎態の違いによる上唇、下唇、オトガイ筋の緊張の程度を評価する必要があると考えられた。このように本研究では同じ術式を施行した場合でも、顎態により側貌軟組織形態に与える影響が異なる可能性が示唆された。

21. 当分野の口蓋裂症例における合併症状に関する検討

Examination of associated malformations in cases with isolated cleft palates

口唇裂・口蓋裂は発生頻度の高い先天性疾患のひとつである。その中でも口蓋裂が単独で生じる場合、全身的な合併症状を伴うことが多いとされているが、詳細な検討はいまだ少ない。そこで、当分野に来院した口蓋裂症例に合併する口腔内および全身症状について検討を行ったので報告する。昭和52年から平成23年に当分野を受診した口唇裂、顎裂を伴わない完全口蓋裂患者226名（男性74名、女性152名、平均年齢11歳4か月）を対象とし、初診時調査用紙を用いて合併する1）口腔内および2）全身症状について検討した。結果として、1）永久歯の先天性欠損が54.4%で最も多かった。矮小歯は13.3%にみられ、その多くは上顎側切歯であった。またエナメル質減形成が12.8%でみられ、1歯のみから全歯におよぶものまで様々であった。舌においては舌小帯強直症が16.8%にみられた。2）眼の異常では内眼角贅皮が19.9%と最も多く、次いで両眼隔離が10.2%にみられ、また視力障害が19.5%、白内障も1.8%認めた。耳の異常として、耳介形成異常が14.2%、次いで耳介低位が9.3%にみられ、聴力障害も18.6%認めた。また斜頚や、手足においては指の彎曲がみられた。外胚葉系ではアトピー性皮膚炎や爪の形成不全がみられた。呼吸器系疾患では喘息が7.1%、循環器系疾患では不整脈・心雑音が2.7%、心室中隔欠損が2.2%にみられた。また、精神発達遅滞は7.1%、運動発達遅滞も5.8%にみられた。家族性に口蓋裂を発症している家系が13.7%に認められた。症候性の口蓋裂症例は18.1%にみられ、その中でPierre Robin症候群が4.0%と最も多く、次いでStickler症候群が1.8%であった。口蓋裂に合併する症状を歯科的見地からも詳細に検討することは、他科との連携をとるうえで重要な情報を提供するものと考えられる。

22. 当分野の非症候群性口唇裂・口蓋裂の家系内発生ならびに母体の環境要因に関する臨床統計的調査

Analysis of familial occurrence and maternal environmental factors in non-syndromic cleft lip/ palate

口唇裂・口蓋裂は顎顔面領域に見られる頻度が高い先天性疾患の一つであるが、その発症メカニズムは複雑であると言われている。近年、遺伝−環境相互作用による口唇裂・口蓋裂の発症という点に関心が集まっているが裂型を決定する要因に関する報告は少ない。そこで今回、家系内発生ならびに妊娠中の母体を取り巻く環境について裂型別に統計学的検討を行ったので報告する。2001年4月から2011年3月に当分野を受診した非症候群性の口唇裂（CL）40人、口唇口蓋裂（CLP）114人、口蓋裂（CP）41人、計195人（初診時平均年齢12.5歳）を対象とし、初診時調査用紙を用いて、家系内発生ならびに妊娠中における母体を取りまく環境要因（感染性疾患、服薬、レントゲン撮影、喫煙（父親を含む）、飲酒）について調査した。【結果】発端者の家系内に口唇裂・口蓋裂の発生を認めたものは36例(18.5%)であり、内訳としてCL 9例（22.5%）、CLP 23例（20.2%）、CP 4例（9.8%）であった。また、遺伝的および疫学的に異なると考えられるCL（P）とCPについてchi square testによる比較検討を行ったところ、環境要因ならびに家系内発生において有意差を認めないものの、CL（P）はCPと比較し家系内発生を認める割合が若干高い傾向を示した

(20.9% vs. 14.3%; p=0.12)。裂型を決定する要因についてより詳細に明らかにするためには、遺伝的要因についての解析をさらに進めるとともに、母体を取り巻く環境について一般集団を対象群としながら広範に調査を進めていくことが重要と考えられる。

23. 創内型装置を用いて上顎骨延長法を行った口唇裂・口蓋裂症例における術後変化

Follow-up study on CLP patients treated by maxillary distraction osteogenesis using intra oral distracter

上顎骨の著しい劣成長を伴う口唇裂・口蓋裂症例に対して、創内型装置を用いた上顎骨延長法と下顎骨後方移動術を同時に施行することがある。その際、上顎骨の術後変化を術前の段階である程度予測した上で治療計画を立案することができれば良好な治療結果を得るのに役立つと考えられる。そこで今回創内型装置を用い上顎骨延長法を行った口唇裂・口蓋裂症例の術後1年の上顎骨の変化について検討した。東京医科歯科大学歯学部附属病院において創内型装置(Zurich system)によるLe Fort I型上顎骨延長法を適用した口唇裂・口蓋裂患者7名(男性4名、女性3名、手術時平均年齢23歳0か月)の、術前(T0)、骨延長終了時(T1)、術後1年(T2)における側面頭部X線規格写真を資料とし、上顎骨の変化について検討した。距離分析としては、FH平面を水平基準平面としSellaを原点とするX-Y直交座標系にて、ANSの水平的および垂直的変化量を、角度分析としてSNAの変化量を計測した。統計解析として、分散分析の後に多重比較検定を行った。ANSの水平方向の平均変化量と標準偏差量はT0-T1において6.4±2.1mmで有意な前方移動を認めたが($p<0.05$)、T1-T2においては有意な水平的変化は認めなかった。垂直方向では、T0-T1ならびにT1-T2において有意差を認めなかった。また、SNAのT0-T1における変化量は4.8±1.1°で有意な増加を示したのに対し($p<0.05$)、T1-T2には有意差を認めなかった。創内型装置を用いた上顎骨延長法では、水平ならびに垂直方向における上顎骨の術後変化はごく僅かで、良好な安定性が得られた。一方、創内型装置は創外型装置に比べて設置部位・方向や骨の延長量に制限があるため、個々の症例に応じた装置の選択が必要と考えられた。

24. CLP患者の言語想起時および発音時における言語障害に依存した脳機能

Misarticulation-dependent Brain Activations During Covert/Overt Speech In Cleft-lip-and palate Patients

口唇口蓋裂(CLP)患者は、手術により末梢器官の改善が図られているにも関わらず、構音障害を有する場合が散見される。CLP患者における構音障害の有無と中枢神経機能の関連を知る目的で機能的磁気共鳴画像法(fMRI)を用いて、軟口蓋破裂音(/k/)発音[内言語(言語想起)および外言語(言語発音)]時における脳賦活パタンを解析した。被験者は、健常成人6名と術後成人口唇口蓋裂患者6名(片側性2名および両側性4名、うち両側性の1名のみ軟口蓋音に構音障害あり)であった。その結果、内言語発音時には、CLPの有無にかかわらず言語関連領域が賦活した。一方、外言語発音時には、健常者ならびに構音障害を有しないCLP患者においては運動前野、一次感覚運動野および小脳が賦活したが、構音障害を有するCLP患者においては後帯状回が賦活した。これらの結果から、言語想起時においては、健常者とCLP患者の脳賦活パタンに差異は存在しないが、言語発音時においては、構音障害の有無に依存した中枢神経機能が存在し、構音障害と中枢神経機能が相互に関連していることが示唆された。

25. 側性臼歯部交叉咬合を有する成人骨格性下顎前突症患者における下顎蝶番軸の評価

Mandibular hinge axis in skeletal class III posterior unilateral crossbite patients.

機能的下顎側方偏位を有する小児期の片側性臼歯部交叉咬合(PUXB)は放置した場合、下顎骨および顎関節の形態変化が生じ、成長に伴い骨格性の問題を誘発する原因の一つと考えられている。成人PUXB患者において外科的矯正治療を併用する場合、術前に、顎顔面形態だけでなく下顎運動や下顎蝶番軸を評価することは重要である。しかしながら、成人PUXB患者においては、主に顎顔面領域の形態評価に関する報告が多く、下顎蝶番軸などの機能的評価に関する報告はほとんど認められない。そこで本研究は、骨格性下顎前突症患者におけるPUXBが顎顔面形態および下顎運動に与える影響について評価することを目的とした。PUXBを有する成人骨格性下顎前突症患者(患者群)15名、PUXBを有しない成人骨格性下顎前突症患者(対照群)12名を被験者とした。CADIAX®electronic axiography systemを用いて各被験者の下顎蝶番軸を同定後、下顎蝶番軸の皮膚上に鉛板を貼付した。正面(PA)および軸位(SMV)頭部X線規格写真を撮影し、下顎蝶番軸および顎態の評価を行った。結果、患者群と対照群の比較から、下顎骨体の大きさ、下顎偏位量、下顎大臼歯の頬舌的および近遠心的位置に有意差が認められた。下顎蝶番軸については、PAおよびSMV上の頭蓋基準線に対して、患者群は対照群に対して有意な傾きを示した。PUXBを有する成人骨格性下顎前突症患者において、下

顎蝶番軸の三次元的な位置変化が認められた。このことから、PUXBが下顎蝶番軸の偏位を惹起する原因の一つになることが示唆された。

26. 口腔周囲筋における血流量および筋活動量に関する検討：マルチモダリティ解析

Evaluation of blood flow and electromyographic activity of perioral muscles：Multimodality analysis.

唇部軟組織の機能異常とされる口唇閉鎖不全を伴う、上下顎骨の前後的・垂直的位置関係の不調和が著しい不正咬合においては、矯正歯科治療単独での咬合の改善や顔貌の調和を図ることが困難である。このような場合に併用される筋機能療法のエビデンスには不明な点が多い。そこで、「口唇閉鎖不全患者における口輪筋収縮訓練に伴うオトガイ筋および口輪筋の血流量・筋活動の経時的変化における相互関連を探り、新たな口唇閉鎖不全患者に対する評価法を確立する」ことを本研究の具体的な目的として遂行する。本研究では、その端緒として、健常者群（対照群）、口唇閉鎖不全患者群（実験群）に対し、口唇閉鎖時におけるオトガイ筋・口輪筋の血流量と筋活動を同時計測し、実験群の筋活動に伴う血流動態を対照群と比較検討し評価を行う。続いて、口輪筋収縮訓練時におけるオトガイ筋・口輪筋の血流量と筋活動を同時計測し、健常者群（対照群）、口唇閉鎖不全患者群（実験群）に、2種類の異なる口輪筋収縮訓練課題(低負荷・長時間課題および高負荷・短時間課題)を施行し、その効果に関する機能的評価を行うとともに、顎態および歯列の形態計測による形態的評価を行う。この過程で、対照群と実験群を横断的比較するとともに、実験群において課題の持続効果を縦断的に比較する。

27. 咬みしめに伴う上肢筋の促通とそれに同期した脳賦活パタン

Upper-limb facilitation by teeth clenching and its brain activation pattern

歯科やスポーツ生理学の分野において、随意的な咬みしめに伴って全身運動機能が促通されることが数多く報告されている。そこで我々は、咬みしめが上肢筋筋力に与える影響について非侵襲的脳機能計測法のひとつである機能的磁気共鳴画像法（fMRI）を用いて検討した。個性正常咬合を有する健康成人21名において、行動生理学的実験と神経生理学的実験を行った。前者に関しては、MR室外にて、1）咬みしめ時における最大握力、および2）下顎安静位における最大握力を、それぞれ利き手において測定した。後者に関しては、1.5TのMR装置を用いて1）咬みしめと握りしめを同時に施行（gripping with clenching：GC）、2）咬みしめのみ施行（clenching：C）、3）握りしめのみ施行（gripping without clenching：G）の3条件下でfMRIデータを採得した。握りしめに関連する関心領域を設定し、statistical parametric mapping（SPM）5を用いてBlood oxygenation level dependent（BOLD）信号強度を解析した。咬みしめ時における最大握力は、下顎安静位における最大握力に比べ有意に大きかった。また、握りしめ動作に関連する大脳皮質一次運動野（primary motor cortex：M1）、補足運動野（supplementary motor area：SMA）、および小脳におけるBOLD信号強度は、CG条件下の方がG条件下に比べ有意に大きかった。さらにM1、小脳、被殻に関しては最大握力の増加率とBOLD信号強度の増加率との間に有意な正の相関が認められた。これらの結果から、咬みしめに伴う上肢筋の促通には、M1、SMA、小脳および被殻が関与していることが示唆された。

28. 顔面非対称症例における術前後の顎運動の比較

Mandibular hinge axis in skeletal class III posterior unilateral crossbite patients.

顔面非対称症例では、前方および側方運動時に下顎頭運動距離は偏位側が非偏位側より大きいと言われており、顎顔面形態および軟組織形態の非対称のみならず、機能的にも非対称を呈することが報告されている。

これまで頭蓋顎顔面形態と機能の評価は、2次元における形態的特徴と顎機能の関連性が報告されている。しかしながら、近年ではCTの普及により3次元の形態的評価が可能となり、形態的特徴に関する報告は認められるが、機能的評価を行っている報告はない。顔面非対称症例の骨格形態と顎機能の特徴を検討することは、外科的矯正治療による骨格的非対称の改善の評価や術後の安定性を検討する上でも重要であると考えられる。

そこで、顔面非対称症例における術前後の3次元的顎顔面形態分析および開閉口運動、前方運動、側方運動などの下顎頭運動路の計測を行い、術前の顎顔面形態および顎運動の計測、さらに外科的矯正治療前後における骨格的非対称の改善に伴う機能的変化について比較検討することを本研究の目的とする。

29. 声門破裂音聴取時の聴覚連合野の賦活パタン

Activation Patterns in the Auditory Association Area Involved in Glottal Stop Perception
（Journal of Oral Biosciences, in press）RinaHikita, Jun J Miyamoto, Takashi Ono, Ei-ichi Honda, TohruKurabayashi,Keiji Moriyama

音声は、言語情報や感情情報などを同時に伝えることが

可能な、基本的かつ効率的な情報伝達手段である。しかし、その複雑性ゆえに何らかの言語障害を有する者も少なくない。口唇・口蓋裂（cleft lip and/or palate：CLP）を有する患者は、構音器官の重要な構成要素である口蓋に先天的に器質的障害を有するため、代償性構音（compensatory misarticulations：CMAs）を呈することがある。CMAsは不自然な構音操作により生じるため、流暢さを欠き聞き取りにくいという特徴がある。CLPのCMAsの代表的なものとして声門破裂音（glottal stop：GS）がある。これは構音点が声門に代償的に移行する異常構音であり、慣れない者にとっては聞き取りにくい構音である。「ことばの流暢さ」は、CLP患者の言語治療効果の指標として広く使用されている。しかし、流暢さを欠くCMAsを聴取した場合の、健常被験者における認知機構に関しては、末梢においても中枢においても未だ解明されていない。そこで本研究の目的は、健常成人20人を被験者として、正常構音（normal articulation：NA）聴取時と比較した場合のGS聴取時の認知機構に関して、行動実験ならびに脳機能画像法を用いて解析を行った。結果、NA聴取時と比較して、GS聴取時では構音の識別に時間を要し、また高次聴覚中枢である聴覚連合野が、両側で広くかつ強く賦活することが示された。このことから、NAと比較してGSはより多くの聴覚的注意を要する複雑な音声プロセスであることが示唆された。

30. 当分野を受診したDown症候群患者の歯科臨床的特徴について－頭蓋顎顔面形態，永久歯の先天性欠如歯に関する検討－

Dental characteristics of Down syndrome patients
-Examination of craniofacial skeletal pattern and congenital missing of permanent teeth-

Down症候群（DS）は主に21番染色体過剰によって生じ，特異顔貌，精神発達遅滞，筋緊張低下，低身長などの臨床症状を有し，先天性心疾患などを高率に合併することが知られている，常染色体異常の中で最も頻度の高い疾患の一つである．またDS患者において，下顎前突や叢生などの不正咬合がみられることが知られている．DS患者の歯科矯正治療は平成14年より保険適応となり，矯正歯科を受診する機会は増加しているが，本邦における矯正歯科の観点からの報告は少ない．そこで，今回我々は日本人DS患者の頭蓋顎顔面形態，先天性欠如歯の特徴について検討することを目的とした．

DSは先天奇形や咬合状態の多様性がある疾患で，頭蓋底と上顎骨の大きさは著しく小さく，これまでの報告と類似した結果を得た．また下顎骨の大きさは日本人平均値と近似していた．先天性欠如歯の発症率は健常者と比較し高頻度であった．今回新たに，小さな下顎角が日本人DSにおいて特徴的である可能性が示唆された．DS患者の矯正歯科治療に取り組むにあたり，本疾患の頭蓋顎顔面の特徴をさらに明らかにすることが必要と思われる。

31. 当分野を受診した濃化異骨症2症例の顎顔面形態の特徴

Characteristics of maxillofacial morphology of two pycnodysostosis cases registered in TMDU

濃化異骨症（pycnodysostosis, MIM #265800）は、頭蓋骨の泉門部の開存、指趾末節骨の溶解性欠損、全身性の骨硬化、易骨折性、低身長を特徴とする常染色体劣性遺伝の骨系統疾患であり、cathepsin Kが原因遺伝子として報告されている。平成24年度より本疾患に起因する不正咬合の歯科矯正治療に保険適応がなされるようになったが、発生頻度は極めて低く、顎顔面形態に関する詳細な報告も少ない。今回、我々は当分野を受診した本疾患患者2名について、歯科矯正学的観点から形態的特徴の抽出を行ったので報告する。

〈症例1〉初診時年齢36歳、孤発例の女性。不正咬合を主訴に来院。低身長、手指末節骨先端の溶融性欠損を認め、頻回の骨折の既往があった。〈症例2〉初診時年齢34歳の女性。反対咬合を主訴に来院。低身長、手指末節骨先端の溶融性欠損を認め、症例1と同様に頻回の骨折の既往を認めた。家族歴として同胞に同一疾患を認め、遺伝子検査にて確定診断がなされていた。

顔貌所見では、両症例に共通して前下顔面高が小さい特徴的顔貌を呈していた。口腔内所見では、両症例ともにAngle Class III、上顎に著しい叢生を認め、前歯部反対咬合および過蓋咬合が観察された。Z-scoreを用いた側面頭部X線規格写真分析（症例1, 症例2）では、角度分析においてGonial angle（+6.3, +5.6 ）、Ramus inclination（+6.6, +5.0）がともに著しく大きい値を示し、下顎角の開大と下顎枝の反時計方向の回転を認めた。また距離分析では、ANS-U1（-4.3, -6.7）、Go-Pog（-5.3, -6.3）がともに小さい値を示し、上顎骨の高さならびに下顎骨体長の短小化を認めた。三次元CT画像による顎顔面骨格の所見より、下顎骨において顎角部の平坦化と筋突起の短小化が観察された。

今回の濃化異骨症2症例においては、両者に共通した特徴的な顎顔面形態を認めた。

32. 卒前歯学教育における遺伝医学教育の現状

Status of Genetics Education in Japanese Dental Schools

先天異常疾患はその約70%において頭蓋顔面領域に何らかの奇形を示すといわれている。口唇裂・口蓋裂のように口腔領域に明らかな異常を認めるもの以外でも、歯列や顎骨に何らかの異常が認められ、形態的、機能的障害をきたす先天異常疾患は多く、そのような患者の診断、包括的治療を行っていくうえで、我々歯科の分野において遺伝医学の知識は不可欠であるといえる。また、近年ヒトゲノムの全容が解明され、一般医療の場で個人の遺伝情報が取り扱われる機会も増加し、遺伝情報の個人差に基づく健康維持や医療が現実化しようとしており、遺伝情報は特別な家系だけでなく、健康維持やより良い医療を望むすべての人々に必要な情報になっていくことを鑑みると、歯学教育における遺伝医学教育の重要性は今後更に増していくことが予想される。

H13年に「歯学教育モデル・コア・カリキュラム（コアカリ）-教育内容ガイドライン-」が策定されて以来、コアカリは全ての歯学部学生が卒業時までに共通して修得すべき必須の教育内容とされ、各大学はこのコアカリをもとにシラバス（教育要綱）を作成している。改訂されたH22年度のコアカリにおける遺伝学に関する項目は、大きく分けると「遺伝子の構造と機能および遺伝の基本的機序の理解」、「口唇・口腔・顎顔面領域の先天異常疾患の特徴と病因および診断・治療の基本的概念の理解」の二つである。つまり遺伝学の基礎、顎顔面領域に関連する先天異常疾患の知識に関して学ぶことができる一方で、遺伝情報を臨床の場でどのように収集し、どのように提供していくかという視点での臨床遺伝教育はまだ十分とはいえない。

本学における遺伝医学教育の概要を紹介し、さらに全国歯学部や海外における遺伝医学教育の実態などから、卒前歯学教育における遺伝医学教育の現状をまとめ、今後の遺伝医学教育の普及に役立てる。

33. Noonan Syndrome患者の頭蓋および顎顔面形態に関する検討

Craniofacial and Orthognathics characteristics of Noonan syndrome patients

Noonan症候群（NS）は、低身長、特異顔貌、心疾患、胸郭異常、停留睾丸、精神発達遅滞等の臨床症状を有している先天性疾患である。しかしながら顎顔面形態、口腔内、頭頸部の特徴について詳述した臨床研究は少なく、その詳細は不明である。そこで当分野を受診したNS患者10症例の問診表、顔面写真、手根骨X線写真、歯列模型、口腔内写真、側面頭部X線規格写真を用い、下記の項目について検討し、その特徴を抽出した。①全身的臨床症状および、身長・骨年齢を用いた成長様相の評価、②前歯部被蓋関係の計測およびセファロ分析を用いた顎顔面および頭蓋底形態の評価、③咬合の特徴、歯列弓幅径、口蓋の形態、歯根形成および根尖閉鎖時期の検討による口腔内の評価、④頸椎の頭蓋底への陥入度、頭蓋に対する頸椎・舌骨の位置の計測による頭頸部の評価を行った。当分野のNS10症例においては、①低身長をはじめとする全身的症状が多く認められた。②下顎後退を認めるものの軽度であった。また、前・後頭蓋底の短縮、平坦な頭蓋底が認められた。③上顎歯列弓の狭窄、口蓋後方部が有意に深いこと、歯根形成や根尖閉鎖の遅延が認められた。④NSは、健常者症例に比べて歯突起が有意に陥入し、第三、第四頸椎が有意に高位に位置していた。以上より、NSでは頭蓋および顎顔面に特有な形態を有していることが示唆され、このことはNSの鑑別に有用であると思われる。

34. 鎖骨頭蓋異形成症の3同胞間における過剰歯および歯の萌出様相について

Supernumerary Teeth and Their Eruption State in Three Siblings with Cleidocranial Dysplasia

＜緒言＞鎖骨頭蓋異形成症（CCD）はCBFA1遺伝子を原因遺伝子とする常染色体優性遺伝疾患であり、鎖骨形成不全、頭蓋骨縫合骨化遅延等を特徴とする。口腔内では乳歯晩期残存、永久歯萌出遅延、過剰歯の存在により審美的・機能的問題を伴うことが多い。今回我々はCCDを伴う同胞3名に対する歯科矯正治療を行う機会を得、過剰歯数およびその出現部位、また歯の萌出様相に関して長期的観察を行なったので報告する。＜症例＞父親にCCDの疑いがある同胞3名の第1子（初診時年齢17歳1ヶ月、男性）の埋伏過剰歯数が12本であったのに対し、第2子（初診時年齢15歳11ヶ月、女子）、第3子（初診時年齢12歳4ヶ月、男子）では各々6本であった。また、各患者の過剰歯の出現部位は異なっていた。18歳時における歯の萌出状況では、それぞれに永久歯萌出遅延を認めたが、第1子で最も顕著であった。＜まとめ＞過剰歯数とその出現部位および歯の萌出様相には同胞間に明確な相違が認められた。

2）研究のイラストレーション

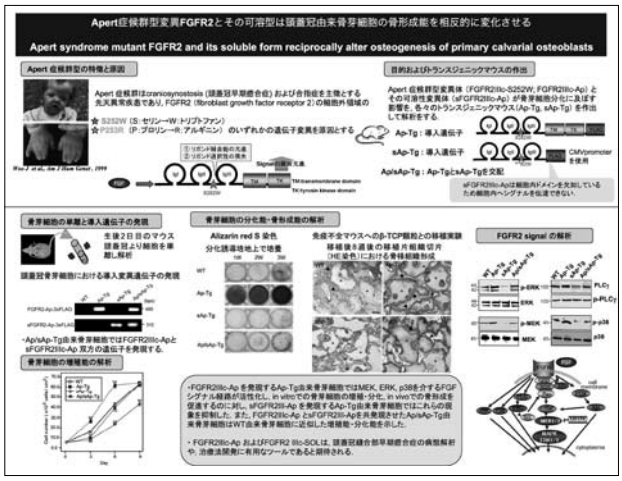

3）発表の研究内容についての英文要約

1. Apert syndrome mutant FGFR2 and its soluble form reciprocally alter osteogenesis of primary calvarial osteoblasts. Suzuki H, Suda N, Shiga M, Kobayashi Y, Nakamura M, Iseki S, Moriyama K. Journal of Cellular Physiology　227 (9)：3267、2012.

Apert syndrome is predominantly caused by mutation of either S252Wor P253W in the fibroblast growth factor receptor (FGFR) 2 gene. In this study, we characterized the effects of S252W mutation using primary calvarial osteoblasts derived from transgenic mice, Ap-Tg and sAp-Tg, that expressed an Apert-type mutant FGFR2 (FGFR2IIIc-S252W; FGFR2IIIc-Ap) , and the soluble form (extracellular domain only) of the mutant FGFR2 (sFGFR2IIIc-Ap) , respectively. Compared to WT-derived osteoblasts, osteoblasts from Ap-Tg mouse showed a higher proliferative activity and enhanced differentiation, while those from sAp-Tg mouse exhibited reduced potential for proliferation and osteogenic differentiation. When transplanted with β-TCP granules into immunodeficient mice, Ap-Tg-derived osteoblasts showed a higher bone forming capacity, whereas sAp-Tg-derived osteoblasts were completely deficient for this phenotype. Phosphorylation of ERK, MEK, PLC γ, and p38 was increased in Ap-Tg-derived osteoblasts, whereas phosphorylation of these signaling molecules was reduced in sAp-Tg-derived osteoblasts. Interestingly, when these experiments were carried out using osteoblasts from the mice generated by crossing Ap-Tg and sAp-Tg (Ap/sAp-Tg) , which co-expressed FGFR2IIIc-Ap and sFGFR2IIIc-Ap, the results were comparable to those obtained from WT-derived osteoblasts. These results indicate that osteoblasts expressing FGFR2IIIc-Ap proliferate and differentiate via highly activated MEK, ERK, and p38 pathways, while these pathways are suppressed in osteoblasts expressing sFGFR2IIIc-Ap.

2. Analysis of the role of Hedgehog signaling in the calvaria suture development

Mutations in the gene encoding the zinc-finger transcription factor GLI-Kruppel family Member 3 (GLI3) have been identified in patients with Grieg cephalopolysyndactyly syndrome in which premature fusion of calvaria suture (craniosynostosis) is an infrequent but important feature. Here we show that Gli3 acts as a repressor in the developing murine calvaria and that Dlx5, Runx2 type II isoform (Runx2-II) and Bmp2 are ectopically expressed in the calvarial mesenchyme which results in aberrant osteoblastic differentiation in Gli3-deficient mouse ($Gli3^{Xt\text{-}J/Xt\text{-}J}$) and resulted in craniosynostosis. At the same time, enhanced activation of phospho-Smad1/5/8 (p-Smad1/5/8) , which is a downstream mediator of canonical Bmp signaling, is observed. Therefore, we generated Gli3; Runx2 compound mutant mice to study the effects of decreasing Runx2 dosage in a $Gli3^{Xt\text{-}J/Xt\text{-}J}$ background. $Gli3^{Xt\text{-}J/Xt\text{-}J}$ $Runx2^{+/-}$ mice have neither craniosynostosis nor additional ossification centers and displayed a normalization of Dlx5, Runx2-II, and p-Smad1/5/8 expression as well as sutural mesenchymal cell proliferation. These findings suggest a novel role for Gli3 in regulating calvarial suture development by controlling canonical Bmp-Smad signaling which integrates a Dlx5/Runx2-II cascade. We propose that targetting Runx2 might provide an attractive way of preventing craniosynostosis in patients.

3. Development of the strategy for expansion of craniofacial suture with magnetized liposome containing Relaxin.

Relaxin is a peptide hormone produced by the corpoea lutea and testis in mammals. This study is focused on the effects of relaxin in osteoclast function and bone degradation in the craniofacial sutures using a biocompatible, nanosized magnetic liposome carrier system to facilitate suture expansion. A preliminary study has been performed to ensure the liability of our experimental design. It comprises the immunohistochemical identification of relaxin receptor 1 (Rxfp1) in E15.5 and E18.5 rat embryos and the in vitro injection of relaxin magnetic liposomes to E18.5 rat embryo sagittal suture tissue cultures using a magnetized stainless steel wire to control liposome location and Cy3 to identify the position of the liposomes by fluorescence microscopy. In addition to these studies, mouse fetus craniofacial suture tissue and osteoblast-like sagittal suture cell cultures will be used to assess the molecular effect of relaxin. After the completion of these in vitro studies the effectiveness of the injection of relaxin magnetic liposomes for facilitation of expansion in rat sagittal and midpalatal sutures will be tested in vivo. After injecting the liposomes to rat sagittal and midpalatal sutures, lateral expansion will be performed with an orthodontic expansion appliance while using a

magnetized stainless steel wire to control the position of liposomes in the exposed tissue.

4. Amelogenin splice isoforms stimulate chondrogenic differentiation of ATDC5 cells. Mitani K, Haruyama N, Hatakeyama J, Igarashi K. Oral Dis. (in press).

Amelogenins are the most abundant matrix proteins in enamel. Among the amelogenin isoforms, full-length amelogenin (M180) and leucine-rich amelogenin peptide (LRAP) are expressed in various tissues and are implicated as signaling molecules in mesenchymal cells. Here, we examined the effects of M180 and LRAP on a chondrogenic cell line, ATDC5, to investigate the role of amelogenins in chondrogenesis. Recombinant mouse M180- or LRAP-protein-containing medium or control medium was mixed with a chondrogenesis-stimulating medium, and changes in the phenotype, gene expression levels and cell proliferation of cultured ATDC5 cells were analyzed. The addition of amelogenins increased alkaline phosphatase activity and glycosaminoglycan secretion at 14 and 21 days of culture, respectively, as compared with the control. Quantitative PCR (Q-PCR) analysis revealed that LRAP increased the gene expression levels of Runx2, Col2a1 and Aggrecan at 7 days of differentiation. Moreover, both M180 and LRAP significantly increased the gene expression levels of ALP, Aggrecan, Col10a1 and osteopontin at 28 days of culture. Bromodeoxyuridine assay and Q-PCR analysis for Wnt signaling indicated that both M180 and LRAP reduced proliferation, but induced the cell differentiation possibly through altered non-canonical Wnt signaling. These results suggest that M180 and LRAP accelerate chondrogenic differentiation and maturation of ATDC5 cells.

5. Dentin sialophosphoprotein and dentin matrix protein-1：Two highly phosphorylated proteins in mineralized tissues. Suzuki S, Haruyama N, Nishimura F, Kulkarni AB. Arch Oral Biol. 57 (9)：1165-75, 2012

Dentin sialophosphoprotein (DSPP) and dentin matrix protein-1 (DMP-1) are highly phosphorylated proteins that belong to the family of small integrin-binding ligand N-linked glycoproteins (SIBLINGs), and are essential for proper development of hard tissues such as teeth and bones. In order to understand how they contribute to tissue organization, DSPP and DMP-1 have been analyzed for over a decade using both in vivo and in vitro techniques. Here, we review the phenotypes of the genetically engineered mouse models of DSPP and DMP-1 and also introduce complementary in vitro studies into the molecular mechanisms underlying these phenotypes. DSPP affects the mineralization of dentin more profoundly than DMP-1. In contrast, DMP-1 significantly affects bone mineralization and importantly controls serum phosphate levels by regulating serum FGF-23 levels, whereas DSPP does not show any systemic effects. DMP-1 activates integrin signaling and is endocytosed into the cytoplasm whereupon it is translocated to the nucleus. In contrast, DSPP only activates integrin-dependent signaling. Thus it is now clear that both DSPP and DMP-1 contribute to hard tissue mineralization and the tissues affected by each are different presumably as a result of their different expression levels.

6. Accuracy of orthodontic miniscrew implantation guided by stereolithographic surgical stent based on cone-beam CT derived 3D images. Qiu L, Haruyama N, Suzuki S, Yamada D, Obayashi N, Kurabayashi T, Moriyama K. Angle Orthod. 82 (2)：284-93, 2012

The purposes of this research were to develop surgical stents for cone-beam computed tomography (CBCT) 3-dimensional (3D) image-based stent-guided orthodontic miniscrew implantation and to evaluate its accuracy. Ten surgical stents were fabricated with stereolithographic appliances (SLAs) according to 3D CBCT image-based virtual implantation plans. Thirty self-drilling miniscrews were implanted at the maxillary or mandibular posterior arches in 3 phantoms; 20 guided by 10 surgical stents in 2 phantoms (stent group) and 10 guided freehand in 1 phantom (freehand group). No root damage was found in the stent group, while 4 of 10 miniscrews contacted with roots in the freehand group. In the stent group, deviations in the mesiodistal and vertical directions were 0.15 ± 0.09 and 0.19 ± 0.19mm at the corona, and 0.28 ± 0.23 and 0.33 ± 0.25mm at the apex, respectively; angular deviations in the mesiodistal and vertical directions were 1.47 ± 0.92° and 2.13 ± 1.48°, respectively. In the freehand group, the corresponding results were 0.48 ± 0.46mm, 0.94 ± 0.87mm, 0.81 ± 0.61mm, 0.78 ± 0.49mm, 7.49 ± 6.09°, and 6.31 ± 3.82°. Significant differences were found in all 6 parameters between the 2 groups (t-test, $P<.05$). These results indicated that the 3D CBCT image-based SLA-fabricated surgical stents can provide a safe and accurate method for miniscrew implantation.

7. Stage-specific functions of leukemia/lymphoma-related factor (LRF) in the transcriptional control of osteoclast development. Tsuji-Takechi K, Negishi-Koga T, Sumiya E, Kukita A, Kato S, Maeda T, Pandolfi PP, Moriyama K, Takayanagi H. Proc Natl Acad Sci USA. 109：2561-6, 2012.

Cell fate determination is tightly regulated by transcriptional activators and repressors. Leukemia/lymphoma-related factor (LRF; encoded by Zbtb7a), known as a POK (POZ/BTB and Krüppel) family transcriptional repressor, is induced during the development of bone-resorbing osteoclasts, but the physiological significance of LRF in bone metabolism and the molecular mechanisms underlying the transcriptional regulation of osteoclastogenesis by LRF have

not been elucidated. Here we show that LRF negatively regulates osteoclast differentiation by repressing nuclear factor of activated T cells c1 (NFATc1) induction in the early phase of osteoclast development, while positively regulating osteoclast-specific genes by functioning as a coactivator of NFATc1 in the bone resorption phase. The stage-specific distinct functions of LRF were demonstrated in two lines of conditional knockout mice in which LRF was deleted in the early or late phase of osteoclast development. Thus, this study shows that LRF plays stage-specific distinct roles in osteoclast differentiation, exemplifying the delicate transcriptional regulation at work in lineage commitment.

8. Deletion at chromosome 10p11.23-p12.1 defines characteristic phenotypes with marked midface retrusion.Okamoto N, Hayashi S, Masui A, Kosaki R, Oguri I, Hasegawa T, Imoto I, Makita Y, Hata A, Moriyama K, Inazawa J. J Hum Genet. 57：191-6, 2012.

Approximately 3% of the live-born infants have major dysmorphic features, and about two-thirds of which are observed in the maxillofacial region; however, in many cases, the etiology of the dysmorphic features remains uncertain. Recently, the genome-wide screening of large patient cohorts with congenital disorders has made it possible to discover genomic aberrations corresponding to the pathogenesis. In our analyses of more than 536 cases of clinically undiagnosed multiple congenital anomalies and mental retardation (MR) by microarray-based comparative genomic hybridization, we detected two non-consanguineous unrelated patients with microdeletions at 10p11.23-p12.1, which overlapped for 957 kb, including four protein-coding genes：ARMC4, MPP7, WAC and BAMBI. As the two patients had similar phenotypes; for example, MR and multiple maxillofacial abnormalities including midface retrusion, wide mouth and large tongue, we assessed the phenotypes in detail to define the common features, using quantitative evaluations of the maxillofacial dysmorphism. The concordance of the genetic and phenotypic alterations is a good evidence of a new syndrome. Although an interstitial deletion of 10p is rare, the current study is the first trial to examine precisely the craniofacial characteristics of patients with a heterozygous deletion at 10p11.23-p12.1, and presents good evidence to diagnose potential patients with the same genetic cause.

9. Prevalence and gender comparison of malocclusion among Japanese adolescents：A population-based study. Komazaki Y, Fujiwara T, Ogawa T, Sato M, Suzuki K, Yamagata Z, Moriyama K. Prevalence and gender comparison of malocclusion among Japanese adolescents：A population-based study. J World Fed Orthod, 1：67-72, 2012.

A lack of studies regarding the prevalence of malocclusion, including gender comparisons, has precluded an efficient dental health policy in Japan. We aimed to describe the prevalence and perform a gender comparison of malocclusion requiring orthodontic treatment in Japan. In addition, we assessed social factors associated with malocclusion. On the basis of the Index of Orthodontic Treatment Need (IOTN), occlusal characteristics of a population-based sample of adolescents aged 12–15 years were evaluated by orthodontists. A questionnaire was used to assess the association between social factors and malocclusion. A total of 821 adolescents participated in this study. The prevalence of malocclusion was 46.5%. Multivariate logistic regression showed that girls were 1.56 times more likely than boys were to develop malocclusion, particularly with anterior crossbite and upper and lower crowding. We found a positive association between headache and malocclusion, especially in lingual crossbite. This population-based study revealed that approximately half of the Japanese adolescents included in this study had malocclusion, which occurred primarily in girls. This study may provide reliable baseline data regarding the orthodontic treatment needs of the Japanese adolescent population.

10. Effects of pH, Potential, and Deposition Time on the Durability of Collagen Electrodeposited to Titanium

Collagen is expected to work as a bonding agent of soft and hard tissues to solid materials. In this study, the electrodeposition of collagen to a titanium (Ti) surface under various conditions, i.e., the pH of the collagen solution, potential, and electrodeposition time, was performed to understand the optimal electrodeposition conditions for the immobilization of collagen to Ti. The effects of these conditions on the thickness and residual ratio of the collagen layer after shaking in water were evaluated by ellipsometry, scanning probe microscopy, and X-ray photoelectron spectroscopy. Collagen molecules were attracted to Ti cathode and immobilized with high durability by combining electrodeposition conditions, pH 5, alternating potential between _1V and +1V vs. SCE with 1 Hz, and 1800 s. The surface of this electrodeposited collagen layer was smooth and uniform maintaining the collagen fibril and natural structure. On the other hand, the collagen layer immobilized by immersion technique in a collagen solution, was rough and irregular. Electrodeposition with alternating potential at pH 5 for 1800 s is a much more appropriate technique to immobilize collagen to Ti than the conventional immersion technique.

11. Craniofacial morphology in growing patients with oligodontia

Tooth agenesis, i.e., the congenital absence of teeth, is a common anomaly of human dentition that compromises facial aesthetics and mastication. Oligodontia, defined as the

congenital absence of 6 or more permanent teeth (excluding the third molars), causes unavoidable dental consequences including malocclusion. Because treatment options for this condition are extremely limited, therapy is complicated and lengthy. In this study, we examined 14 children with oligodontia (5 boys, 9 girls; age, 8.3-12.9 years) to identify characteristic features in the patterns of missing teeth and craniofacial morphology. The most frequently missing teeth were the maxillary second premolars, followed by the mandibular second premolars, maxillary first premolars, and mandibular first premolars. In contrast, the central incisors, canines, first molars, and mandibular second molars were rarely missing. Cephalometric measurements showed maxillary retrognathism and mandibular prognathism with upward-rotated mandibular plane and anterior short face, which represented a skeletal Class III tendency. Furthermore, the upper first molars were most frequently located low and anterior compared with those of control. These results suggest that treatment of oligodontia should include raising the bite by eruption of the upper molar and downward rotation of the mandible because of the craniofacial morphology of children with growing oligodontia.

12. The role of histone methyltransferase during craniofacial development

Congenital anomalies are caused by both genetic and environmental factors. It is recently said that the diseases such as cancers and metabolic diseases were caused by the change of their epigenome that were altered by environmental factors. Since the relationships with congenital anomalies in craniofacial and their epigenome were not well studied, we have been studying the role of histone methyltransferases, which catalyze methyl groups of the genome, to understand the mechanism of how congenital anomalies were developed and to discover the prevention methods for congenital anomalies. To find out the role of histone methyltransferases, conditional KO mice of histone methyltransferases were analyzed for the phenotype. Of those, G9a that were deleted only in neural crest derived cells demonstrated that the differentiation of osteoblasts was inhibited. For looking into more details, we are now trying to find out the downstream target genes and more precise mechanism of G9a to those target genes.

13. Investigation of the function of the elastic system fibers in periodontal ligaments.

The elastic system fibers existed in various organizations and have given the organs elasticity. Periodontal ligaments (PDLs) is composed mainly of collagen fibers, and elastic system fibers. In contrast to collagen, little is known about the role of elastic fibers in PDLs. We examined PDLs of mice under expressing fibrillin (FBN) (mgR mice), which is one of the major proteins of elastic system fibers. The PDLs of homozygous mgR mice showed one-quarter of the elastic system fibers of wild-type mice. Interestingly, gene expression of periostin was also decreased. It is known that periostin is participating in homeostasis of organs, such as wound healing, cell growth, apoptosis. Marfan syndrome is an autosomal dominant disorder of connective tissue, caused by mutations in the FBN. This genetic disorder is frequently accompanied by severe periodontitis, suggesting the crucial function of fibrillin in PDLs. It is expected that homeostasis of organs, the abnormalities of a restoration mechanism, periostin, and also fibrillin have a certain relevance also in PDLs. The purpose of this study is to clarify the relation of fibrillin and periostin in detail and to search for work in elastic system fibers in PDL.

14. Analysis of familial history and maternal environmental factors in nonsyndromic cleft lip/palate

The etiology and the mechanism responsible for occurrence of oral clefts (OCs) remain unclear. The aim of this study was to survey the familial history and maternal environmental factors in different types of OCs at our dental hospital. One hundred ninety-five individuals with non-syndromic CL/P and isolated CP who were registered between 2001 and 2011 at the Section of Maxillofacial Orthognathics, Tokyo Medical and Dental University in Japan were used. The variables registered for the study were parents' environmental exposure factors during pregnancy and family history. Among the 195 patients, 36 patients had positive family history (18.5%), including 9 patients with CP, 23 patients with CLP and 4 patients with CP. Furthermore, patients were classified into two phenotypically and etiologically distinct groups : CL/P and CP. Statistical analysis showed that familial history and maternal environmental factors do not significantly influence type of clefts. However, family history was associated with a higher incidence of CL/P than that of CP (20.8% vs. 9.8%; p=0.12). These results suggest a need for additional genetic studies about factors to determine types of clefts. Further studies that include various maternal environmental factors are also needed to clarify the etiology of OCs by using population-based sample.

15. Optimization of HAp/Col coating

In the last year, we revealed HAp/Col coated Ti wire realized rapid osseointegration. However, the optimum condition of HAp/Col coating is unknown. Now, we are carrying out the animal experiments to find it. Experimental materials are Ti wires with diameter of 0.5 mm and length of 12 mm, with HAp/Col coating of different thickness. Experimental animals are male SD rat, 12-week-old. The periosteal pockets are prepared on the calvaria and the specimens are implanted into the pockets. The bone formation processes around specimens are evaluated 0, 3,

7, 14 and 28 days postoperatively by the observation with μCT and histological analysis.

16. The orthopedic effects of the intermaxillary traction using miniplates in beagle dogs

Recently, bone anchored maxillary protraction (BAMP) with the intermaxillary traction between miniplates was introduced. However, there is no animal experimental evaluation of BAMP. The purpose of this study was to construct the animal model of BAMP, and to analyze the orthopedic effects of the intermaxillary traction. Ten immature male beagles in 100-day-old (-20 Day) were used for this study. Miniplate was placed per jaw quadrant. In 0 Day, the dogs were divided into 2 groups : intermaxillary traction group (Group T, n=5) , and not-traction (control) group (Group C, n=5) . In Group T, the anchor plates were loaded with coil springs (200gf) , continued to 60 Day. The 2 groups were compared by cephalometric analysis, using lateral cephalograms taken by a specially designed cephalostat. Results of the cephalometric analysis, in 60 Day, the depth of the maxillary of the Group T were significantly greater than those of the Group C, and 2 angular measurements (U1-FH, FMIA) were significantly smaller than those of the Group C. These results indicated that the model of BAMP showed the effects of maxillary advancement and dental compensations. This study supported the clinical applications of BAMP.

17. Biological analysis of mechanism for condylar cartilage formation

Large aggregating proteoglycans (PGs) were main extracellular matrices. We examined the effect of β-xyloside which can disturb PG synthesis on condylar cartilage formation using organ culture system. The heads of ICR mice at E14.0 were dissected and anlagen of mandibular condylar cartilage were taken with Meckel's cartilage and put on filters over stainless meshes. Tissues were cultured with BGJB medium with or without β-xyloside (2mM/ml) for 6 days. Then tissues were taken and paraffin sections were cut and analyzed by immunohistochemistry and in situ hybridization for cartilaginous matrix proteins. Condylar cartilage was clearly formed in control groups after 6-days culture, and aggrecan, collagen types I and II were immunohistochemically detected in cartilage matrix and chondrocytes expressed mRNA for these molecules. Meanwhile, condylar cartilage was recognized in experimental groups, but size of cartilage was much smaller than that in control groups, indicating condylar cartilage formation was greatly retarded by β-xyloside. However, cartilaginous matrix proteins detected in control groups were also expressed in experimental groups. Disturbance of PG synthesis by β-xyloside inhibits condylar cartilage formation, but cartilage tissues containing abnormal matrix constituents are never formed.

18. Effects of mandibular setback surgery on the function of sleep breathing

We apply surgical orthodontic treatment to patients with skeletal malocclusion. Although mandibular set-back surgery can be expect to dramatically improvement in facial appearance, occlusion, and appropriate oral function, it is pointed out possibilities of develop sleep disordered breathing due to reduction of the intra-oral volume and narrowing tongue chamber. Therefore, we examine the relationship between change of the Anatomical Balance; the amount of soft tissue and the size of the hard tissue before and after surgical orthodontic treatment and the function of sleep breathing, and whether change of the Anatomical Balance can serve as an indicator of planning of a morphologicaly and functionally stable surgical orthodontic treatment. As a result of measuring the size of soft tissue (TG) , the size of hard tissue in lower face (LFC) , and percentage of TG relative to the LFG (TG / LFC) , hard tissue face down in the before and after surgical orthodontic treatment. This shows it might been suggested TG / LFC is maintained by some comprensation scheme in vivo, and function of sleep breathing is maintained. By using a simplified sleep respirometer, we are being analyzed for changes in the function of sleep breathing before and after surgical orthodontic treatment.

19. Investigation of long-term stability of occlusion after sagittal split ramus osteotomy for mandibular protrusion

The purpose of this study is to investigate whether the changes of dental arch width influence the long-term stability of occlusion in those who have been treated by sagittal split ramus osteotomy (SSRO) to correct mandibular prognathism. Twenty-six patients with mandibular prognathism who underwent SSRO were enrolled in this study. The gnathostatic models taken at first visit (T1) , just before retention (T2) , and at long-term follow-up (T3) were used. PAR Index was used for evaluating the occlusion and the patients were divided into stable group and unstable group depending on the changes of the index scores from T2-T3. Inter-premolars and inter-molars distances in the maxillary and mandibular arches were measured and were compared between the two groups. 16 patients were evaluated as group S and 10 patients were group U. In group U, upper inter-molars were significantly increased between T1-T2. Lower inter-6 and inter-7 were significantly increased between T2-T3. Between T2-T3, Amount of changes in lower inter-6 were significantly larger than upper in group U. There are possibilities that the change of inter-molars distance in the lower arch influence the long-term stability. It is important to ensure the volume of oral cavity that could be affected by tongue function.

20. Soft tissue profile changes following anterior segmental maxillary osteotomy in mandibular retrognathia patients.

The aim of this study is to evaluate soft tissue changes following Anterior segmental maxillary osteotomy (ASMO) in mandibular retrognathia patients.The subjects were divided into two groups：mandibular retrognathia group (MandR group) and maxillary protrusion group (MaxP group). Lateral cephalograms at first visit and approximately twelve months after surgery were traced and superimposed. Linear and angular measurements were statistically evaluated performed regarding 13 representative soft tissue points.The changes of soft tissue at mental region were significantly larger in mandibular retrognathia group as compared to maxillary protrusion group. Nasal and mental region significantly moved downward in MandR group. Nasal tip angle decreased and Collumellar length angle increased in the MandR group. Angle of nasal prominence significantly decreased, while nasolabial angle and inferior labial sulcus angle increased in the MaxP group. The differences of ASMO induced morphological changes at nose, lip, and mental region were found between MandR group and maxillary protrusion group, thus it is necessary to plan a treatment by taking the nature of soft tissue profile changes according to the patients' skeletal patterns into account.

21. Three-dimensional analysis of mandibular morphology in patients with facial asymmetry and mandibular prognathism

The aim of this study is to find out the characteristics of mandibular morphology of the mandibular prognathism patients with facial asymmetry by using three-dimensional computed tomography (3D-CT) data. 26 patients diagnosed as a mandibular prognathism were divided into two groups whether they have a facial asymmetry (FA group, n = 13) or not (NA group, n = 13). DICOM data from multisliced CT were used for 3D analysis. Condyle was defined as a structure superior to the plane that is perpendicularly intersected with the line connecting apex of condyle and the most inferior point of mandibular foramen and that goes through the most depressed point of the neck of mandible. The data were compared in two groups and statistically analyzed. Anterior-posterior cephalograms at initial stage were used for measuring the amount of menton deviation. In FA group, the condylar volume was significantly smaller in deviated side and correlation between the amount of menton deviation and condylar volume was found. Significant difference of volume ratio of both condyles was found between the two groups.

22. Long-term maxillomandibular changes after maxillary distraction osteogenesis in growing children with cleft lip and palate. Honda A, Baba Y, Ogawa T, Suzuki S, Moriyama K. Cleft Palate Craniofac J. (in press)

To evaluate the long-term maxillomandibular changes after maxillary distraction osteogenesis (DOG) in growing children having cleft lip with or without cleft palate (CL ± P). Eight Japanese patients with CL ± P aged 9.3-13.1 years. The maxillary and mandibular positions before (T0), immediately after (T1), and 1, 3, and 5 years after DOG (T2, T3, and T4) measured on cephalograms superimposed at the sella turcica (S) with the Frankfurt horizontal (FH) plane as the horizontal reference. The mean horizontal maxillary advancement was +12.3 mm during T0-T1, but -2.7, -1.1, and -0.1 mm of the post-treatment changes were observed during T1-T2, T2-T3, and T3-T4, respectively. ANS (y) shifted 2.3 mm downward during T0-T1, and further downward changes were observed during T1-T2 and T2-T3 ($P < 0.05$). Pog (x) did not show distinct changes due to individual variance, but Me (y) shifted downward from T1 to T4. SNA significantly decreased during T1-T2 and T2-T3 but not during T3-T4. ANB significantly decreased only during T2-T3, and SNB did not show any distinct change. There was no further maxillary advancement after DOG in the growing children with CL ± P. Therefore, long-term observation and management of occlusion in case of the mandibular growth pattern are important.

23. Post operative stability of maxillary intraoral distraction osteogenesis in cleft lip and palate patients.

Maxillary distraction osteogenesis (DOG) has become an acceptable technique for correction of midfacial deficiency with cleft lip and palate (CLP) patients. If we could estimate maxillary postoperative changes before surgery, we are able to make a treatment plan more precisely. In this study, we assessed skeletal stability of the CLP patients who underwent maxillary intraoral DOG. The study included 7 CLP patients (female, 3; male 4; mean age at operation, 23.0 years) who were treated by Le Fort I osteotomy in combination with intraoral distraction device (Zurich system). Lateral cephalograms before surgery (T0), immediately after surgery (T1), and 1 year after surgery (T2) were used for analysis. Anterior nasal spine (ANS) was employed for horizontal and vertical linear measurements and the SNA angle was used for angular measurement. ANS was significantly advanced horizontally (7.3 ± 2.1 mm) from T0 to T1, though there was no significant horizontal change from T1 to T2. SNA was significantly increased (5.5 ± 1.1°) from T0 to T1 but did not change significantly from T1 to T2. Intraoral devices were limited in installation site and amount of maxillary movement compared to extraoral devices, so that it is necessary to choose the appropriate device according to individual cases.

24. Clinical surveys on associated anomalies in cases with isolated cleft palate

It has been known that isolated cleft palate (CP) is frequently associated with other congenital anomalies. However, the prevalence and types of CP-associated malformations vary among previous studies and it has not been well established whether CP is conclusively related to other birth defects. The aim of this study was to survey the malformations associated with CP at our dental hospital. Two hundred sixty-five cases with CP who were registered between 1977 and 2011 at our dental hospital were used. Data was collected by an inspection and an interview of patients and their parents. Across 278 cases with CP, the incidence rate of recognized syndromes was 14.3%. Among them, Pierre Robin sequence was the most frequently seen condition (2.1%). Thirty-three cases showed familial inheritance of the characteristics. Among non-syndromic cases, the prevalence of associated anomalies in female was about twice as high as those in male. Malformations of eyes were seen the most frequently among any other anomalies (40.1%). The type of almost all familial inheritances was CP. CP seems to be associated with other congenital anomalies in a high prevalence.

25. Misarticulation-dependent Brain Activations During Covert/Overt Speech In Cleft-lip-and palate Patients

Objectives : The speech-related central nervous system (CNS) might be subdivided into motor imaginary and execution for articulatory subsystems. The purpose of this study is to compare the cortical activation for each subsystem between subjects with and without cleft lip and palate (CLP) using functional magnetic resonance imaging (fMRI). Methods : Two unilateral CLP (UCLP), four bilateral CLP (BCLP) and six healthy subjects participated in this study, and only one BCLP subject showed CMA. The subjects were instructed to produce the syllable /ka/ in a normal tone (Overt-task) or generate it in their mind (Covert-task) during fMRI acquisition. Results : In the Covert-task, similar activation patterns were shown in subjects with and without CLP. In the Overt-task, the motor-related areas which were the premotor and primary sensorimotor cortices and the cerebellum were activated in subjects with healty, UCLP, and BCLP without CMA subjects. On the other hand, the posterior cingulate gyrus was activated in the BCLP subject with CMA. Conclusions : It appears that the CNS for motor imaginary of articulation between subjects with and without CLP might be similar. However, the CNS for execution of articulation between subjects with and without CMA might differ irrespective of the presence of CLP.

26. Mandibular hinge axis in skeletal class III posterior unilateral crossbite patients.

Posterior unilateral crossbite (PUXB) may induce skeletal remodeling of the temporomandibular joint, which in turn could lead to permanent mandibular asymmetry. An analysis of mandibular motion found that the center of rotation was located in the condylar head of the mandible. However, few previous studies have evaluated the change in the axis of mandibular hinge movement associated with skeletal asymmetry. Therefore, the purpose of this study was to investigate whether mandibular asymmetry is associated with a change in the mandibular hinge axis in adults with PUXB. Thirty pre-orthodontic patients (PUXB and non-PUXB groups, n = 15 each) participated in the study. The mandibular hinge axis (MHA) was measured by computerized axiography and duplicated on the posteroanterior and submentovertex cephalometric radiographs. Morphological asymmetry was evaluated for both skeletal and dental components and positional deviation of the mandible by cephalometric analysis. Significant differences in both skeletal and dental components were found between the PUXB and non-PUXB groups. The inclination of the MHA toward the mandibular shifted side was greater in the PUXB group than in the non-PUXB group. The present findings suggest that PUXB may cause morphological asymmetry of the mandible and an altered mandibular hinge axis.

27. Evaluation of blood flow and electromyographic activity of perioral muscles : Multimodality analysis.

Although the visual inspection of muscular tension of the mental region and the electromyographic (EMG) activity of the perioral muscles are commonly used to evaluate lip incompetence, it is difficult to make quantitative evaluation using a contactless method. It has been reported that the blood flow (BF) and EMG activity of the extremity muscles increased in parallel with an exercise load. However, the relationship between the change in BF and EMG activity in the orofacial region remains to be elucidated. Therefore, the purpose of this study was to examine the influence of lip-sealing on perioral muscles and establish a new method for evaluation lip incompetence using laser Doppler perfusion imaging.

28. Upper-limb facilitation by teeth clenching and its brain activation pattern

In the field of dentistry and sports physiology, there are many reports that voluntary teeth clenching facilitates human motor function. The purpose of this study was to investigate the facilitatory effect of teeth clenching on upper-limb and its brain activation pattern by using fMRI technique. Twenty-one healthy right-handed subjects participated in this study. The subjects were asked to exert maximal grip force with their right hands. During fMRI scanning, subjects performed the following three tasks; i) gripping with clenching (GC), ii) gripping without clenching (G), iii) only clenching (C). The regions of interests were defined in the activated areas during G

and measured % signal change. The maximal grip force in task-GC was significantly larger than that in task-G. In the primary motor cortex (M1), the supplementary motor area (SMA), and the cerebellum, % signal change in task-GC was significantly stronger than that in task-G. In the M1, cerebellum, and putamen, a significant positive correlation was found between the increasing ratio of the maximal grip force and that of % signal change. The findings suggest that the M1, SMA, cerebellum, and putamen are involved in the upper-limb facilitation by voluntary teeth clenching.

29. Dental and maxillofacial characteristics in six Japanese individuals with ectrodactyly-ectodermal dysplasia-clefting (EEC) syndrome. Okamura E, Suda N, Baba Y, Fukuoka H, Ogawa T, Ohkuma M, Ahiko N, Shiga M, Tsuji M, Moriyama K. Cleft Palate Craniofac J. (in press).

Ectrodactyly-ectodermal dysplasia-clefting (EEC) syndrome is a congenital anomaly characterized by ectodermal dysplasia, ectrodactyly, cleft lip and palate, and lacrimal duct anomalies. Because this syndrome is frequently accompanied by a congenital lack of teeth, narrow palate, and malocclusion, comprehensive orthodontic intervention is required. To highlight the specific dental and maxillofacial characteristics of EEC syndrome, 6 Japanese individuals diagnosed with EEC are described here. Their conditions included ectodermal dysplasia, cleft lip and/or palate, and ectrodactyly. Cephalograms, panoramic X-rays, and dental casts were taken; systemic complications were recorded at the first visit to our dental hospital. All individuals had severe oligodontia with 9 to 18 missing teeth. The missing teeth were mainly maxillary and mandibular incisors and second bicuspids, arranged in a symmetrical manner. Cephalometric analysis showed retruded and short maxilla due to cleft lip and/or palate. Interestingly, all individuals showed a characteristically shaped mandibular symphysis with a retruded point B. It is likely that this unusual symphyseal morphology is due to the lack of mandibular incisors. This study demonstrates the presence of severe oligodontia in the incisal and premolar regions and describes a characteristic maxillary and mandibular structure.

30. Dental characteristics of Down syndrome patients -Examination of craniofacial skeletal pattern and congenital missing of permanent teeth-

Down syndrome (DS), also known as trisomy 21, is the most well-known chromosomal disorder. Many studies report the prevalence of malocclusions that exists among people with DS. More specifically, there is a greater frequency of anterior and posterior crossbites, Class III molar relationships, and crowding in persons with DS. Few reports have investigated dental characteristics of DS in terms of Orthodontics in Japan.

The aims of this study were to investigate the characteristics of craniofacial skeletal pattern and congenitally missing permanent teeth in DS with Japanese. Almost all cases were cranial base lengths, facial height and maxillary liner dimention were smaller. Mandibular ramus and body length was in the mean value. Gonial angle was extreme small. Congenitally missing permanent teeth was observed in 72.7% of patients. DS has a variety of congenital anomalies and occlusions. It was suggested that small gonial angle could be peculiarities in Japanese DS.

31. Characteristics of maxillofacial morphology of two pycnodysostosis cases registered in TMDU

Pycnodysostosis (PDO) is a rare autosomal recessive inherited disease belonging to the group of craniotubular bone dyplasias. The bone metabolism is abnormal due to malfunction of the osteoclasts with a decreased bone remodeling, which usually leads to sclerotic and fragile bones. Genetic research has located mutations in the cathepsin K gene positioned on chromosome 1q21 in patients with PDO. PDO has many general phenotypic characteristics involving the skeleton and most of the affected patients have a history of recurrent fractures of the long bones. The syndrome is also characterized by a number of craniofacial anomalies, hypodontia, malocclusion and malposition of teeth, a grooved palate, obtuse mandibular gonial angles, and generalized micrognathia. We investigate details of characteristics of maxillofacial morphology in two pycnodysostosis patients registered in TMDU.

32. Status of Genetics Education in Japanese Dental Schools

Genomics research is rapidly increasing our understanding of the genetic basis of normal and abnormal growth, development, and disease. Genetic information and technologies are also being applied to develop new diagnostic and treatment strategies. Many diseases with dental, oral, and craniofacial manifestations have a genetic basis. Effective clinical application of genomics to oral medicine will depend on the education of health care professionals, the general public, and policymakers. Dentists must understand genetics to provide accurate information to patients and be able to discuss benefits and limitations of the biological, clinical, and ethical issues related to genomic-based health care. Genetics education in dental schools will significantly impact the integration of genetics into oral medicine. Twenty Japanese dental schools completed a survey in 2011 to assess the status of genetics curricula in dental schools in Japanese. The genetics education currently offered to undergraduate dental students is not standardized, and the content varies considerably among schools. These findings suggest more emphasis on genetics education is needed in Japanese dental schools.

33. Craniofacial and Orthognathics characteristics of Noonan syndrome patients

Noonan syndrome（NS）is characterized by short stature, typical facial dysmorphology, congenital heart disease, chest deformity, cryptorchidism, and intellectual deficit. However, there are only few studies investigating in detail of craniofacial, intraoral and the head and neck morphology. In the present study, the characteristics of 10 cases with NS patients were extracted by using questionnaires, dental models, facial and intraoral photographs, carpal, and cephalometric radiographs. i）Clinical systemic symptoms and growth, ii）Craniofacial morphology, iii）Intraoral characteristic, iv）Degree of skull base invagination and the position of the hyoid bone and cervical spine were evaluated. As results, i）Short stature was commonly found, ii）Mild degree of mandibular retrusion and shortening of anterior and posterior skull base was found, iii）Narrow maxillary arch, high dental palate at posterior part, delayed root formation, and apical closure were found, iv）Odontoid process was significantly invaginated, the third and fourth cervical vertebrae were positioned significantly higher in NS group than in the normal group. These results suggest that they are the typical features of NS and would be useful in differential diagnosis.

34. Supernumerary Teeth and Their Eruption State in Three Siblings with Cleidocranial Dysplasia

【Introduction】Cleidocranial dysplasia（CCD）is an autosomal dominant inheritance caused by mutaions in the CBFA1 gene and characterized by clavicular hypoplasia and retarded skull suture. Prolonged retention of deciduous teeth, delayed eruption of permanent teeth, and supernumerary teeth are often accompanied in oral cavity. As we had provided orthodontic treatment for three siblings with CCD, we conducted a long-term observation in relation to the supernumerary teeth, and the states of teeth eruption.【Case Summary】The oldest（aged 17 years and a month at the first visit, male）among three siblings of a father with suspected CCD had 12 impacted supernumerary teeth, while the second（aged 15 years and 11 months at the first visit, female）and the youngest（aged 12 years and 4 months at the first visit, male）had 6 of those teeth each. In addition, sites of supernumerary teeth in each patient were different from others. In terms of development of the dentition, retarded eruption of permanent teeth was observed in each of them.【Conclusion】Significant variations in number of supernumerary teeth as well as site, state of teeth eruption and the response for orthodontic treatment were recognized among the siblings.

35. Activation Patterns in the Auditory Association Area Involved in Glottal Stop Perception.
Hikita R, Miyamoto J, Ono T, Honda E, Kurabayashi T, Moriyama K. Journal of Oral Biosciences, in press

Some patients with cleft lip and/or palate（CLP）exhibit compensatory misarticulations（CMAs）, which decrease speech fluency and interfere with the intelligibility of the speaker. The glottal stop（GS）is representative of CMAs in CLP patients. GS results from an occlusion or lack of airflow at the level of the glottis. In the context of speech therapy for CLP patients, intelligibility is usually used as an outcome measure. However, little is known about the behavioral and neurobiological mechanisms involved in the perception of speech produced by an individual with CMAs. We aimed to investigate the perception of GS compared with normal articulation（NA）using behavioral and neuroimaging experimentsinsubjects without CMAs. The reaction time for the perception of GS was significantly longer than that for NA. Additionally, the activation area and the percentage signal change in the auditory cortex were largerwhen the subjects listened to GS compared to NA. The auditory association area, which controls the higher-level processing of auditory signals, exhibited more intense bilateral activation in response to GS as compared to NA.Our results suggest that the perception of GS sounds may require more auditory attention and more complex auditory processing than NA sounds in subjects without GS.

4）本事業に関連して世界的な研究拠点形成に向けて、以下の点で改善・整備等されたこと

A（研究拠点体制）

昨年度に引き続き、GCOEの他の事業推進者や硬組織疾患ゲノムセンターならびに、成育医療センターとの連携をさらに強化し、疾患に関わる情報を幅広く得られる基盤を確立した。

B（研究教育環境）

当分野では疾患に即した研究グループ分けが行われており、各グループにおいて、その疾患の原因の解明、検査診断や治療法の改良を目的とした研究が行われている。各大学院生は各研究グループに所属しており、そこで定期的にミーティングを行うなど、グループを基盤とした教育体制の充実化を図っている。また大学院生を含めた新人教育の一環として、先天性疾患（ヌーナン症候群）をテーマにあげ、疾患の成因から臨床的な側面を含めた幅広い内容を求めた発表を課している。

C（人材確保）

本年度、大学院生が5人新たに加わり、各々GCOEのテーマである歯と骨の疾患の分子病態成立のメカニズムの解明を目指した研究だけでなく、当分野の特色である疾患を有する患者の咬合機能の回復のための治療法の開発にも携わっている。

D（人材育成）

GCOEプログラムでは、シャペロン制度やスーパースチューデント制度を創設して、若手研究者の人材の育成に取り組んでいるが、当分野において、本年度6名の大学院生がこの制度を利用している研究に携わっている。当分野の特色である臨床研究と基礎研究の橋渡しが出来る幅広い視野を持った研究者の育成が期待される。

E（国際化）

積極的に海外の学会発表や学術誌に投稿し、成果を発表した。さらに、タイ、ホンジュラス、中国ならびにモンゴルとさまざまな国からの留学生を受け入れている。

5）GCOE事業を推進するに当たって力を入れた点

GCOEのテーマである歯と骨の疾患の分子病態成立のメカニズムを明らかにするには、ヒトから得られる情報を多角的に集積することが非常に大切であると思われる。そこで昨年度に引き続き、成育医療センターとも連携することで、さらに多くの疾患に関わる情報を幅広く得られる基盤を確立した。

また、11月に第7回GCOE国際シンポジウムを主催し、国内外の著名な研究者を招聘し、活発な議論を行える機会を提供した。

6）英文原著論文

1. ◎Tsuji-Takechi K, Negishi-Koga T, Sumiya E, Kukita A, Kato S, Maeda T, Pandolfi PP, Moriyama K, Takayanagi H. Stage-specific functions of leukemia/lymphoma-related factor（LRF）in the transcriptional control of osteoclast development. Proc Natl Acad Sci USA. 109：2561-6, 2012.
2. ◎Okamoto N, Hayashi S, Masui A, Kosaki R, Oguri I, Hasegawa T, Imoto I, Makita Y, Hata A, Moriyama K, Inazawa J. Deletion at chromosome 10p11.23-p12.1 defines characteristic phenotypes with marked midface retrusion. J Hum Genet. 57：191-6, 2012.
3. ◎Suzuki H, Suda N, Shiga M, Kobayashi Y, Nakamura M, Iseki S, Moriyama K. Apert syndrome mutant FGFR2 and its soluble form reciprocally alter osteogenesis of primary calvarial osteoblasts. Journal of Cellular Physiolog. 227（9）：3267, 2012.
4. ◎Suzuki S, Haruyama N, Nishimura F, Kulkarni AB. Dentin sialophosphoprotein and dentin matrix protein-1：Two highly phosphorylated proteins in mineralized tissues. Arch Oral Biol. 57（9）：1165-75, 2012.
5. ◎Qiu L, Haruyama N, Suzuki S, Yamada D, Obayashi N, Kurabayashi T, Moriyama K. Accuracy of orthodontic miniscrew implantation guided by stereolithographic surgical stent based on cone-beam CT derived 3D images. Angle Orthod. 82（2）：284-93, 2012.
6. ◎Komazaki Y, Fujiwara T, Ogawa T, Sato M, Suzuki K, Yamagata Z, Moriyama K. Prevalence and gender comparison of malocclusion among Japanese adolescents：A population-based study. J World Fed Orthod, 1：67-72, 2012.
7. ◎Hikita R, Miyamoto J, Ono T, Honda E, Kurabayashi T, Moriyama K. Activation Patterns in the Auditory Association Area Involved in Glottal Stop Perception. Journal of Oral Biosciences.（in press）
8. ◎Mitani K*, Haruyama N*, Hatakeyama J, Igarashi K. *Authors equally contributed. Amelogenin splice isoforms stimulate chondrogenic differentiation of ATDC5 cells. Oral Dis.（in press）
9. ◎Honda A, Baba Y, Ogawa T, Suzuki S, Moriyama K. Long-term maxillomandibular changes after maxillary distraction osteogenesis in growing children with cleft lip and palate. Cleft Palate Craniofac J.（in press）
10. ◎Okamura E, Suda N, Baba Y, Fukuoka H, Ogawa T, Ohkuma M, Ahiko N, Shiga M, Tsuji M, Moriyama K. Dental and maxillofacial characteristics in six Japanese individuals with ectrodactyly-ectodermal dysplasia-clefting（EEC）syndrome. Cleft Palate Craniofac J.（in press）
11. Watanabe K, Kuroda S, Takahashi T, Kijima T, Torikai K, Moriyama K, Tanaka E. Segmental distraction osteogenesis with modified LeFort II osteotomy for a patient with craniosynostosis. Am J Orthod Dentofacial Orthop. 142（5）：698-709, 2012.
12. Tokugawa Y, Kubota M, Nishimura M, Haruyama N, Igarashi K. Bone regeneration of canine artificial alveolar clefts using bone-marrow-derived mesenchymal stromal cells and β-tricalcium phosphate：A preliminary study. Orthod Waves. 71（2）：51–58, 2012.
13. Tanimoto Y, Veistinen L, Alakurtti K, Takatalo M, Rice DP. Prevention of premature fusion of calvarial suture in GLI-Kruppel family member 3（Gli3）-deficient mice by removing one allele of Runt-related transcription factor 2（Runx2）. J Biol Chem. 15;287（25）：21429-38, 2012.
14. Veistinen L, Takatalo M, Tanimoto Y, Kesper DA, Vortkamp A, Rice DP. Loss-of-Function of Gli3 in Mice Causes Abnormal Frontal Bone Morphology and Premature Synostosis of the Interfrontal Suture. Front Physiol. 3：121, 2012.
15. Shibata S, Fukuoka H, Sato R, Abe T, Suzuki Y. An in situ hybridization study of the insulin-like growth factor system in developing condylar cartilage of the fetal mouse mandible. Eur J Histochem. 23;56（2）, 2012.
16. Suda N, Moriyama K, Ganburged G. Effect of Angiotensin II receptor blocker on experimental periodontitis in a mouse model of Marfan syndrome. Infect Immun.（in press）

7）総説ならびに著書

（著書：英文）

1. Kuroda T, Ohyama K, Motohashi N, Moriyama K. Atlas of orthodontic treatment for patients with birth defect. Needham Press, 1-207, 2012
2. Takeda S, Haga N, Moriyama K. Clinical correlate：cleidocranial dysplasia. 59-63, Mineralized tissues in oral and craniofacial science, WILEY-BLACKWELL, 2012.

（著書：和文）

野田政樹、江面陽一、早田匡芳、納富拓也、中元哲也、渡辺千穂、Smriti Aryal A.C：骨のメカノバイオロジー.細胞工学、Vol.31 No.9、1030-1032、2012.

8）特許取得、特許申請

国内　申請済み

【発明の名称】HAp/Col複合体によって被覆された生体材料

【技術分野】本発明は、生体内に埋植される生体材料に関するものである。

【発明者】菊池正紀、高久田和夫、森山啓司、鈴木聖一、上園将慶

【権利者】NIMS,東京医科歯科大学

【種類】産業財産権　特許（発明）

【番号】特願2012-096056

【出願年月日】2012/04/19

9）平成24年度までの自己評価）

研究面においては、基礎研究の成果と臨床的要素を融合した研究を遂行することが可能であったとともに、公衆衛生の分野にも裾野を広げることで、疾患に関連した情報を幅広く得られる基盤を確立することができた。さらに、各々の大学院生が積極的に海外を含めた学会等で発表するとともに、発表した学術大会で受賞している大学院生も多数見られ、教育面でも充実化が図られた。

10）和文原著論文

1. 冨永直子、川元龍夫、東堀紀尚、福岡裕樹、森山啓司. 開咬を伴う骨格性下顎前突症例に対する下顎枝矢状分割術後の長期安定性について. 日本顎変形症学会誌. 22巻4号（印刷中）
2. 茂木和久、小川卓也、馬場祥行、森山啓司. 成長期における先天性多数歯欠如（oligodontia）患者の顎顔面形態についての検討. Orthodontic Waves-Japanese Edition. 71（3）：187-193, 2012.
3. 丸岡亮、辻美千子、小崎健次郎、森山啓司. 神経線維種症I型患者に歯科矯正治療を行った2治験例、日本レックリングハウゼン病学会雑誌、3（1）：82-85,2012.
4. 山田大輔、東堀紀尚、福岡裕樹、鈴木聖一、川元龍夫、森山啓司. Le Fort I型骨切り術を併用し上下顎移動術を行った骨格性下顎前突症例の外鼻形態変化に対する三次元的検討. 日本顎変形症学会雑誌22（1）：12-19,2012.

11）学会発表（英文）

1. ◎ Watanabe C, Morita M, Ezura Y, Nakamoto T, Hayata T, Notomi T, Yamamoto T, Noda M, Moriyama K. Functional Analysis of Cnot3 in Regulation of Bone Metabolism. The 91st General Session & Exhibition of the International Association for Dental Research, oral presentation, Seattle, March 20-23rd, 2013.
2. ◎ Duarte C, Kobayashi Y, Kawamoto T, Moriyama K. The role of relaxin in proliferation and differentiation of osteoblasts. The 91st General Session & Exhibition of the International Association for Dental Research, poster presentation, Seattle, March 20-23rd, 2013.
3. ◎ Yoshizaki M, Kobayashi Y, Moriyama K. Soluble FGFR2 with Apert mutation inhibits osteoblastic differentiation and proliferation. The 91st General Session & Exhibition of the International Association for Dental Research, poster presentation, Seattle, March 20-23rd, 2013.
4. ◎ Surapornsawasd T, Ogawa T, Shimokawa H, Moriyama K. Oculofaciocardiodental Syndrome：Novel BCOR Mutation and Expression in Dental Cells. The 91st General Session & Exhibition of the International Association for Dental Research, poster presentation, Seattle, March 20-23rd, 2013.
5. ◎ Morita J, Funato N, Komayashi Y, Nakamura M, Moriyama K. Soluble FGFR2 with S252W prevents craniosynostosis of Apert model mouse. The 60th Japanese Association for Dental Research, poster presentation, Nigata, December 14-15, 2012.
6. ◎ Yoshizaki M, Kobayahsi Y, Moriyama K. Soluble FGFR2 with Apert mutation inhibits osteoblastic differentiation and proliferation. The 60th Japanese Association for Dental Research, poster presentation, Nigata, December 14-15, 2012.
7. ◎ Kamata H, Fukuoka H, Shiga M, Higashihori N, Kawamoto T, Moriyama K. Three-dimensional analysis of mandibular morphology in patients with facial asymmetry and mandibular prognathism. The 45th Annual Scientific Congress of Korean Association of Orthodontists. The 45th Annual Scientific Congress of Korean Association of Orthodontists, poster

presentation、Seoul, Korea, November 1-3, 2012.

8. ◎ Suzuki H, Tsuji M, Shiga M, Okamura E, Suzuki S, Moriyama K. Supernumerary Teeth and Their Eruption State in Three Siblings with Cleidocranial Dysplasia. The 45th Annual Scientific Congress of Korean Association of Orthodontists, poster presentation, Seoul, Korea, November 1-3, 2012.
9. ◎ Higashihori N, Nakayama Y, Fukuoka H, Kawamoto T, Moriyama K., Long-term stability of occlusion after sagittal split ramus osteotomy for mandibular prognathism. XIV International Symposium on Dentofacial Development and Function, China, Sep. 20-23, 2012.
10. ◎ Mikami T, Higashihori N, Fukuoka H, Kawamoto T, Moriyama K. Soft tissue profile changes following anterior segmental maxillary osteotomy in mandibular retrognathia patients. The 14th International Symposium on Dentofacial Development and Function. Beijing, China September 19-23, 2012
11. ◎ Kataoka K, Ogawa T, Haruyama N, Kobayahsi Y, Higashihori N, Moriyama K. Post operative stability of maxillary intraoral distraction osteogenesis in cleft lip and palate patients. The 14th International Symposium on Dentofacial Development and Function. Beijing, China September 19-23, 2012
12. ◎ Watanabe C, Ezura Y, Nakamoto T, Hayata T , Notomi T, Moriyama K, Noda M. Analysis of high turnover type bone loss due to haploinsufficiency of Cnot3, a subunit of Ccr4-not complex（mRNA deadenylase）. ANZBMS 2012 Annual Scientific Meeting -1st Asia-Pacific Bone and Mineral Research Meeting with ANZBMS 22nd Annual Scientific Meeting, poster presentation, Perth, September 2-5, 2012
13. ◎ Watanabe C, Morita M, Ezura Y, Nakamoto T, Hayata T , Notomi T, Moriyama K, Yamamoto T, Noda M. Cnot3（Ccr4-not complex subunit3）, a regulator of mRNA stability, regulates bone mass and gene expression related to osteoclast formation. The American Society for Bone and Mineral Research 2012 Annual Meeting, poster presentation, Minneapolis, October 12-15th
14. ◎ Watanabe C, Morita M, Ezura Y, Nakamoto T, Hayata T , Notomi T, Yamamoto T, Noda M, Moriyama K. Functional Analysis of Cnot3 in Regulation of Bone Metabolism. The 60th Japanese Association for Dental Research, oral presentation, Niigata, December 14-15, 2012.
15. ◎Inoue-Arai MS, Ono T, Miyamoto J, Sato-Wakabayashi M, Honda E, Kurabayashi T, Moriyama K. Covert and overt speech in clefts：a functional MRI Study. 90th General Session & Exhibition of the IADR, Poster Presentation, Foz do Iguacu, Brazil, June 20-23, 2012.
16. ◎ Duarte C, Kobayashi Y, Kawamoto T, Moriyama K. Expression Pattern of Relaxin Receptors During Mouse Craniofacial Development. 90th General Session & Exhibition of the IADR, Poster Presentation, Foz do Iguacu, Brazil, June 20-23, 2012.
17. ◎ Dei A, Miyamoto J, Takada J, Ono T, Moriyama K. Evaluation of blood flow and electromyographic activity of perioral muscles. 88th European Orthodontic Society Congress, Poster Presentation, Santiago de Compostela, Spain, June 18-23, 2012.
18. ◎ Uezono M, Takakuda K, Kikuch M, Suzuki S and Moriyama K. The Coating for Enhanced Osseointegration of Subperiosteal Anchorage Device. Conference of STAC6. 1P-B-P67. Poster session, Yokohama, Japan. 17-18 June 2012.

12）学会発表（和文）

1. 佐藤豊、森田圭一、小川卓也、島崎一夫、壬生美智子、立川敬子、小野卓史、森山啓司、谷口尚、小村健、吉増秀實、山城正司.東京医科歯科大学歯学部附属病院における口唇裂・口蓋裂治療チームの現況について. 第36回日本口蓋裂学会総会・学術集会、京都、平成24年5月24-25日
2. 大宅彩、小川卓也、駒﨑裕子、藤原武男、森山啓司. 当分野における非症候群性口唇裂・口蓋裂の家系内発生ならびに母体の環境要因に関する臨床統計的調査. 第36回日本口蓋裂学会総会・学術集会、京都、平成24年5月24-25日
3. 阿彦希、馬場祥行、佐藤麻緒、金沢英恵、志賀百年、森山啓司、金子剛、金田一純子. Hemifacial microsomiaの顎顔面形態および歯の形成に関する検討. 第36回日本口蓋裂学会総会・学術集会、京都、平成24年5月24-25日
4. 片岡恵一、小川卓也、春山直人、小林起穂、阿彦希、大宅彩、東堀紀尚、森山啓司. 創内型装置を用いて上顎骨延長法を行った口唇裂・口蓋裂症例における術後変化. 第36回日本口蓋裂学会総会・学術集会、京都、平成24年5月24-25日
5. 小林正司、齋藤力、飯田順一郎、井上農夫男、後藤滋巳、後藤昌昭、齋藤功、白土雄司、清水典佳、須佐美隆史、高野信夫、原田清、槇宏太郎、森山啓司、日本顎変形症学会顎変形症診療ガイドライン策定委員会. 顎変形症診療ガイドライン策定におけるPatient Questionの収集と分析結果. 第22回日本顎変形症学会総会、福岡、平成24年6月18-19日.
6. 小杉真智子、中久木康一、小川卓也、本田康二、黒原一人、檥武啓幸、細木美佐、友松伸充、小野卓史、

森山啓司、山城正司、原田清. 先天性多数歯欠損の症例に顎矯正手術を適応した3症例. 第22回日本顎変形症学会総会、福岡、平成24年6月18-19日.

7. 三上智彦、福岡裕樹、川元龍夫、森山啓司　上顎前歯部歯槽骨切り術を適応した骨格性下顎後退症患者の側貌軟組織変化.　第22回日本顎変形症学会総会、福岡、平成24年6月18-19日.
8. 鎌田秀樹、福岡裕樹、山田大輔、志賀百年、川元龍夫、森山啓司. 顔面非対称を伴う骨格性下顎前突症例における下顎骨形態の三次元的解析. 第22回日本顎変形症学会総会、福岡、平成24年6月18-19日.
9. 鈴木尋之、辻美千子、志賀百年、岡村絵里花、鈴木聖一、森山啓司. 鎖骨頭蓋異形成症の3同胞間における過剰歯および歯の萌出様相について. 第52回日本先天異常学会学術集会、東京、平成24年7月6－8日.
10. 志賀百年、辻美千子、鈴木尋之、岡村絵里花、鈴木聖一、森山啓司、東京医科歯科大学顎顔面矯正学分野における先天異常疾患患者の来院動向と口腔内の特徴について、第52回日本先天異常学会、東京、2012年7月6-8日
11. 志賀百年、小川卓也、森山啓司. Marfan症候群患者に対する矯正治療の一例、第71回東京矯正歯科学会大会、東京、平成24年7月12日.
12. 渡辺千穂、江面陽一、中元哲也、早田匡芳、納富拓也、森山啓司、野田政樹. 骨量制御の新転写後性分子機構：mRNA deadenylaseであるCcr4-not complex構成因子Cnot3の欠失による高回転型の骨量減少の解析. 第30回日本骨代謝学会、東京、平成24年7月19－21日
13. 鎌田秀樹、福岡裕樹、志賀百年、川元龍夫、鈴木聖一、森山啓司. 顔面非対称症例における下顎骨形態の三次元的解析. 第46回日本口腔科学会関東地方部会、埼玉、平成24年9月8日
14. 福岡裕樹、森山啓司、柴田俊一.　下顎頭軟骨形成に対するβ-xylosideの影響.　第54回歯科基礎医学会総会・学術大会　福島　平成24年9月14日-16日
15. 阿彦希、馬場祥行、佐藤麻緒、金沢英恵、志賀百年、辻美千子、小川卓也、鈴木聖一、金田一純子、森山啓司. Hemifacial microsomiaの顎顔面形態および歯の形成・発育に関する検討. 第71回日本矯正歯科学会大会、盛岡、平成24年9月26-28日.
16. 伊藤洋介、川元龍夫、森山啓司. ビーグル犬におけるミニプレート顎間牽引の顎整形効果に関する検討. 第71回日本矯正歯科学会大会、盛岡、平成24年9月26-28日.
17. 上園将慶、高久田和夫、菊池政紀、鈴木聖一、森山啓司. 骨膜下デバイスにおけるハイドロキシアパタイト-コラーゲン複合体コーティングが骨接合強度に及ぼす効果. 第71回日本矯正歯科学会大会、盛岡、平成24年9月26-28日.
18. 中澤佑紀、鈴木聖一、井上剛、田上順次、森山啓司. セルフエッチングプライマーとリン酸エッチングボンディング材のエナメル質の表層に及ぼす影響. 第71回日本矯正歯科学会大会、盛岡、平成24年9月26-28日.
19. 岡本奈那、林深、稲澤譲治、森山啓司. 中顔面部低形成を特徴とする10p11.23p12.1欠失症候群の2症例. 第71回日本矯正歯科学会大会、盛岡、平成24年9月26-28日.
20. 小川卓也、駒崎裕子、澤田紘美、佐藤智美、寺島多実子、山本俊雄、藤原武男、森山啓司. 乳歯列完成期における不正咬合の発生率ならびに歯の発育異常に関する疫学的検討. 第71回日本矯正歯科学会大会、盛岡、平成24年9月26-28日.
21. スラポンサワッド　タンヤポン、小川卓也、下川仁弥太、森山啓司. Oculofaciocardiodental syndromeにおける新規BCOR遺伝子変異の同定. 第71回日本矯正歯科学会大会、盛岡、平成24年9月26-28日.
22. 藪中友絵、片岡恵一、宮本順、小倉健司、劉世類、志賀百年、辻美千子、森山啓司、Noonan症候群患者に関する検討（第4報）-頭頸部の特徴について-、第71回日本矯正歯科学会大会、盛岡、平成24年9月26-28日.
23. イサリア　エクプラチャヤクン、宮本順、片岡恵一、山本直、梅澤峻之、岡村絵里花、辻美千子、森山啓司、Noonan　症候群患者に関する検討（第3報）-口腔内の特徴について-、第71回日本矯正歯科学会大会、盛岡、平成24年9月26-28日.
24. 植野智子、片岡恵一、宮本順、村本慶子、辻美千子、佐藤麻緒、馬場祥行、金田一純子、森山啓司、Noonan症候群患者に関する検討（第2報）-顎顔面形態の特徴について-、第71回日本矯正歯科学会大会、盛岡、平成24年9月26-28日.
25. 宮本順、片岡恵一、スラポンサワッド　タンヤポン、志賀百年、小川卓也、辻美千子、森山啓司、Noonan症候群患者に関する検討　（第1報）-全身的臨床症状および成長様相について-、第71回日本矯正歯科学会大会、盛岡、平成24年9月26-28日.
26. 中山友美子、川元龍夫、福岡裕樹、東堀紀尚、森山啓

司　下顎枝矢状分割術を施行した骨格性下顎前突症例の長期術後経過からみた咬合安定性の検討　第71回日本矯正歯科学会大会、盛岡、平成24年9月26-28日.

27. アッカラソンサップ パビーナラット、春山直人、松本力、志賀百年、森山啓司. ペリオスチンはヒト歯根膜細胞における低酸素誘導性アポトーシスを抑制する. 第71回日本矯正歯科学会大会、盛岡、平成24年9月26-28日.
28. 阿彦希、馬場祥行、佐藤麻緒、金沢英恵、志賀百年、辻美千子、小川卓也、鈴木聖一、金田一純子、森山啓司. Hemifacial microsomiaの顎顔面形態および歯の形成・発育に関する検討. 第71回日本矯正歯科学会大会、盛岡、平成24年9月26-28日.
29. 岡村絵里花、辻美千子、鈴木尋之、志賀百年、鈴木聖一、森山啓司. 当分野を受診した濃化異骨症2症例の顎顔面形態の特徴. 第71回日本矯正歯科学会大会、盛岡、平成24年9月26-28日.
30. 春山直人：Periostinの歯および歯周組織における新たな役割. 第5回顎顔面の器官発生・形態形成研究会、軽井沢、平成24年11月3-4日.
31. 駒﨑裕子、藤原武男、小川卓也、佐藤美理、鈴木孝太、山縣然太朗、森山啓司.日本の中学生における不正咬合の疫学調査～甲州市母子保健縦断調査～、第22回日本歯科医学会総会、大阪、平成24年11月11日.
32. 金谷和宏、宮本順、川元龍夫、鈴木聖一、森山啓司. 球形樹脂微粒子含有カムを用いた咀嚼効率の研究-正常咬合者と顎変形症者の比較-. 第22回日本歯科医学会総会、大阪、平成24年11月11日.
33. 上園将慶、高久田和夫、菊池正紀、鈴木聖一、森山啓司.HAp/Col コーティンクを用いた新規顎顔面用骨膜下アンカレッシテハイスの開発.第20回顎顔面バイオメカニクス学会大会.東京.平成24年11月27日.
34 駒﨑裕子、藤原武男、小川卓也、佐藤美理、鈴木孝太、山縣然太朗、森山啓司.日本の中学生における不正咬合の疫学調査～甲州市母子保健縦断調査～、第77回口腔病学会学術大会、東京、平成24年12月1日.
35. 上園将慶、高久田和夫、菊池正紀、鈴木聖一、森山啓司.骨膜下テハイスにおける最適なハイトロキシアハタイトコラーケン複合体コーティンクの厚さに関する検討.日本機会学会第25回バイオエンジニアリング講演会.つくば.平成25年1月9-11日.
36. 駒﨑裕子、藤原武男、小川卓也、佐藤美理、鈴木孝太、山縣然太朗、森山啓司.日本の中学生における不正咬合と頭痛との関係について～甲州市母子保健縦断調査～、第23回日本疫学学会学術総会、大阪、平成25年1月24-26日.

13）受賞

1. 片岡恵一、小川卓也、春山直人、小林起穂、阿彦希、大宅彩、東堀紀尚、森山啓司. 創内型装置を用いて上顎骨延長法を行った口唇裂・口蓋裂症例における術後変化. 第36回日本口蓋裂学会総会・学術集会・優秀ポスター賞、京都、平成24年5月24-25日
2. 鎌田秀樹、福岡裕樹、山田大輔、志賀百年、川元龍夫、森山啓司. 顔面非対称を伴う骨格性下顎前突症例における下顎骨形態の三次元的解析. 第22回日本顎変形症学会総会・優秀ポスター賞、福岡、平成24年6月18-19日.
3. 渡辺千穂、江面陽一、中元哲也、早田匡芳、納富拓也、森山啓司、野田政樹. 骨量制御の新転写後性分子機構：mRNA deadenylaseである Ccr4-not complex構成因子Cnot3の欠失による高回転型の骨量減少の解析. 第30回日本骨代謝学会・ANZBMS travel award、東京、平成24年7月19－21日
4. 伊藤洋介、川元龍夫、森山啓司. ビーグル犬におけるミニプレート顎間牽引の顎整形効果に関する検討. 第71回日本矯正歯科学会大会・優秀発表賞、盛岡、平成24年9月26-28日.

14）外部資金の獲得状況

科学研究費補助金、基盤B

研究題目：ゲノム・ナノサイエンスを応用した顎顔面先天異常に対する分子標的治療開発の基盤創成
代表：森山啓司
期間：平成23年―平成25年
研究費総額：1,480万円

科学研究費補助金、挑戦的萌芽

研究題目：リラクシン含有磁気制御型リポソームを応用した新規骨縫合部改造法の開発
代表：森山啓司
期間：平成23年―平成24年
研究費総額：280万円

科学研究費補助金、基盤C

研究題目：生体力学に基づいて材料と形状が最適化された矯正用オンプラントアンカーの開発
代表：鈴木聖一
期間：平成24年―平成26年
研究費総額：410万円

科学研究費補助金、基盤C
研究題目：ペリオスチンに着目した歯根膜弾性線維の機能解析
代表：志賀百年
期間：平成23年―平成25年
研究費総額：390万円

科学研究費補助金　若手（B）
研究題目：象牙質細胞外マトリクスによる骨代謝制御医薬の新規開発
代表：春山直人
期間：平成22年―24年
研究費総額：310万円

科学研究費補助金、若手B
研究題目：眼・顔面・心臓・歯症候群における歯根形成を制御する遺伝子BCORの役割の解明
代表：小川卓也
期間：平成22年―平成24年
研究費総額：300万円

科学研究費補助金、若手B
研究題目：エピゲノムからみた顎顔面領域の先天性疾患～ヒストンメチル化酵素の役割～
代表：東堀紀尚
期間：平成24年―平成25年
研究費総額：429万円

科学研究費補助金、若手B
研究題目：頭蓋冠縫合部早期癒合症に関与する細胞群の同定とその分化制御に関する研究
代表：小林起穂
期間：平成22年―平成24年
研究費総額：330万円

科学研究費補助金、若手研究B
研究題目：ヒト脳機能の咀嚼運動制御の解明：脳機能画像と咀嚼筋活動・咬合力との同時計測の試み
代表：宮本順
期間：平成23年―平成25年
研究費総額：320万円

科学研究費補助金、若手研究B
研究題目：口唇閉鎖不全に対する筋機能療法の効果：マルチモダリティ解析
代表：高田潤一
期間：平成21年―平成24年
研究費総額：300万円

科学研究費補助金　若手（B）
研究題目：解剖学的バランス変化が上部気道開存性・睡眠呼吸機能に与える影響
代表：福岡裕樹
期間：平成24年度―平成27年度
研究費総額：330万

科学研究費補助金、研究活動スタート支援
研究題目：口唇形成術後の瘢痕組織への触覚刺激に伴う一次体性感覚野の賦活パタンの解析
代表：湊亜紀子
期間：平成22年―平成24年
研究費総額：250万

科学研究費補助金、研究活動スタート支援
研究題目：細胞増殖因子により軟組織との強い結合力を有するコラーゲン電着固定化チタンの開発
代表：鎌田秀樹
期間：平成24年―平成25年
研究費総額：250万

科学研究費補助金、研究活動スタート支援
研究題目：FGFシグナル制御によるApert症候群頭蓋冠縫合部早期癒合の治療法開発
代表：鈴木尋之
期間：平成24年―平成25年
研究費総額：230万

特別研究員奨励費
研究題目：骨に固定源を求めた新規矯正用アンカレッジデバイスの開発
代表：上園将慶
期間：平成24年―平成25年
研究費総額：180万円

15）特別講演、招待講演、シンポジウム）

1. Keiji Moriyama： Osteocyte is a key modulator for orthodontic tooth movement induced by mechanical stress. The 112 American Association of Orthodontists, Hawaii, May 7, 2012.
2. Keiji Moriyama：Orthodontic/Orthognathic Treatment of Patients with Mandibular Prognathism. GCOE International General Presentation, TMDU, June 11, 2012.
3. Keiji Moriyama：Clinical Considerations of Nonsurgical and Surgical Orthodontic Treatments for Class III Patients. International Joint Congress of MEAW Technique and Research Foundation, Yokohama, September 15, 2012.
4. Keiji Moriyama：Outcome and stability of surgical

orthodontic treatment for mandibular prognathism with open bite. The 14th International Symposium on Dentofacial Development and Function. Beijing, China, September 20, 2012.

5. Naoto Haruyama：Amelogenins：Multifaceted enamel matrix proteins in hard tissue biology. The 7th Global COE International Symposium, Molecular Science in Oral-Systemic Medicine - Autumn Seminar - at Tokyo Medical & Dental University. Tokyo, Japan. Nov. 13, 2012.
6. Keiji Moriyama：New biological insights of tooth movement in response to mechanical stress. The 7th Global COE International Symposium, Molecular Science in Oral-Systemic Medicine - Autumn Seminar - at Tokyo Medical & Dental University. Tokyo, Japan. Nov. 12, 2012.
7. Keiji Moriyama：Outcome and stability of surgical treatment for mandibular prognathism with long face. The 8th Asian Pacific Orthodontic Conference, New Delhi, December 1, 2012.
8. Michiko Tsuji：Dental problem, 8th International Turner syndrome Conference, Osaka, November 23-25, 2012.
9. 小川卓也：上顎骨延長法を適応した口唇裂・口蓋裂患者の長期予後、第22回日本顎変形症学会総会、福岡、平成24年6月19日.
10. 森山啓司：これからの矯正歯科医療を考える QOL向上をサポートする矯正歯科治療　先天異常患者から学ぶこと. 第71回日本矯正歯科学会大会、盛岡、平成24年9月27日.
11. 春山直人：アメロジェニン：エナメルタンパクの多様な生物学的役割. 東京医科歯科大学 第5回硬組織疾患ゲノムセンターシンポジウム. 東京、平成24年10月31日.
12. 森山啓司：混合歯列期の咬合育成、東京臨床小児歯科研究会、東京国際フォーラム、平成25年1月20日.

16）教室、分野や講座の准教授、講師、助教、特別研究員、ポスドク、指導を受けた大学院生の名前

准教授　　鈴木　聖一
講師　　川元　龍夫
助教　　辻　美千子
　　小川　卓也
　　東堀　紀尚
　　宮本　　順
　　福岡　裕樹
GCOE特任講師：春山　直人
硬組織疾患ゲノムセンター特任助教：小林　起穂
大学院生　　伊藤　洋介、川久保　直美
　　森田　淳平、駒﨑　裕子
　　○ 渡辺　千穂、上園　将慶
　　丸岡　　亮
　　○ 吉崎　正子
　　○ Carolina Duarte
　　Paveenarat Aukkarasongsup
　　梅沢　峻之、小倉　健司
　　村本　慶子、山本　　直、劉　世顕
　　○ Thunyaporn Surapornsawasd
　　八尋　浩平、森下　真紀
　　幸田　直己、池田　安紀津
　　Tsasan Tumurkhuu
外国人特別研究員：井上マリステラ小百合

17）GCOE活動についての感想、コメント、改善を望む点

本年度においても、昨年度に整備したGCOE事業推進者との研究体制をさらに強化することができた。各研究分野でトップを走る他の事業推進者と連携して研究を進めていくことができる環境は、いち早く最先端の情報を得られることでき、今後の研究の展開に大変有意義であると思われた。

ORIGINAL RESEARCH ARTICLE

3267

Journal of Cellular Physiology

Apert Syndrome Mutant FGFR2 and its Soluble Form Reciprocally Alter Osteogenesis of Primary Calvarial Osteoblasts

HIROYUKI SUZUKI,[1,6] NAOTO SUDA,[1,2] MOMOTOSHI SHIGA,[1,6] YUKIHO KOBAYASHI,[1,3] MASATAKA NAKAMURA,[4] SACHIKO ISEKI,[5] AND KEIJI MORIYAMA[1,3,6]*

[1] *Section of Maxillofacial Orthognathics, Department of Maxillofacial Reconstruction and Function, Graduate School of Medical and Dental Sciences, Tokyo Medical and Dental University, Tokyo, Japan*

[2] *Division of Orthodontics, Department of Human Development and Fostering, Meikai University School of Dentistry, Saitama, Japan*

[3] *Hard Tissue Genome Research Center, Tokyo Medical and Dental University, Tokyo, Japan*

[4] *Human Gene Sciences Center, Tokyo Medical and Dental University, Tokyo, Japan*

[5] *Section of Molecular Craniofacial Embryology, Graduate School of Medical and Dental Sciences, Tokyo Medical and Dental University, Tokyo, Japan*

[6] *Global Center of Excellence Program, International Research Center for Molecular Science in Tooth and Bone Diseases, Graduate School of Medical and Dental Sciences, Tokyo Medical and Dental University, Tokyo, Japan*

Apert syndrome is characterized by craniosynostosis and syndactyly, and is predominantly caused by mutation of either S252W or P253W in the fibroblast growth factor receptor (FGFR) 2 gene. In this study, we characterized the effects of one of the mutations (S252W) using primary calvarial osteoblasts derived from transgenic mice, Ap-Tg and sAp-Tg, that expressed an Apert-type mutant FGFR2 (FGFR2IIIc-S252W; FGFR2IIIc-Ap), and the soluble form (extracellular domain only) of the mutant FGFR2 (sFGFR2IIIc-Ap), respectively. Compared to WT-derived osteoblasts, osteoblasts from Ap-Tg mouse showed a higher proliferative activity and enhanced differentiation, while those from sAp-Tg mouse exhibited reduced potential for proliferation and osteogenic differentiation. When transplanted with β-tricalcium phosphate (β-TCP) granules into immunodeficient mice, Ap-Tg-derived osteoblasts showed a higher bone forming capacity, whereas sAp-Tg-derived osteoblasts were completely deficient for this phenotype. Phosphorylation of extracellular signal-regulated kinase (ERK), MEK, PLCγ, and p38 was increased in Ap-Tg-derived osteoblasts, whereas phosphorylation of these signaling molecules was reduced in sAp-Tg-derived osteoblasts. Interestingly, when these experiments were carried out using osteoblasts from the mice generated by crossing Ap-Tg and sAp-Tg (Ap/sAp-Tg), which co-expressed FGFR2IIIc-Ap and sFGFR2IIIc-Ap, the results were comparable to those obtained from WT-derived osteoblasts. Taken together, these results indicate that osteoblasts expressing FGFR2IIIc-Ap proliferate and differentiate via highly activated MEK, ERK, and p38 pathways, while these pathways are suppressed in osteoblasts expressing sFGFR2IIIc-Ap. Our findings also suggest that altered FGFR2IIIc signaling in osteoblasts is mostly responsible for the phenotypes seen in Apert syndrome, therefore these osteoblast cell lines are useful tools for investigating the pathogenesis of Apert syndrome.

J. Cell. Physiol. 227: 3267–3277, 2012.

Fibroblast growth factor receptors (FGFR) 1–4 are members of the tyrosine kinase receptor family, and thus far 22 FGF ligands have been identified. FGFR signaling induces proliferation, migration, differentiation, and survival of many cell types (Ornitz and Itoh, 2001; Eswarakumar et al., 2005). For example, FGF regulates the balance between proliferation and differentiation in osteogenic fronts during cranial suture development (Iseki et al., 1997, 1999; Kim et al., 1998; Rice et al., 2000) and in limb bud morphogenesis (Montero et al., 2001).

Genetic mutations in FGFRs cause several types of syndromic craniosynostosis in an autosomal dominant manner, including Apert (MIM #101200), Beare–Stevenson (MIM #123790), Crouzon (MIM #123500), Jackson–Weiss (MIM #123150), and Pfeiffer (MIM #101600) syndromes (Jabs et al., 1994; Reardon et al., 1994; Rutland et al., 1995; Wilkie et al., 1995; Przylepa et al., 1996). Apert syndrome is characterized by craniosynostosis and severe bony syndactyly of the hands and feet (Cohen and Kreiborg, 1996). It is predominantly caused by missense mutations in FGFR2, which lead to S252W or P253R amino acid substitutions and result in a gain-of-function FGF

Additional Supporting Information may be found in the online version of this article.

Contract grant sponsor: Ministry of Education, Culture, Sports, Science, and Technology of Japan;
Contract grant numbers: 23390471, 18209060, 19406031, 21390546.
Contract grant sponsor: Ministry of Education, Culture, Sports, Science, and Technology of Japan (The Global (21st Century) Center of Excellence (COE) Program, International Research Center for Molecular Science in Tooth and Bone Diseases).

*Correspondence to: Keiji Moriyama, Section of Maxillofacial Orthognathics, Department of Maxillofacial Reconstruction and Function, Graduate School of Medical and Dental Sciences, Tokyo Medical and Dental University 1-5-45 Yushima, Bunkyo-ku, Tokyo 113-8549, Japan. E-mail: k-moriyama.mort@tmd.ac.jp

Manuscript Received: 2 July 2011
Manuscript Accepted: 15 November 2011

Accepted manuscript online in Wiley Online Library (wileyonlinelibrary.com): 21 November 2011
DOI: 10.1002/jcp.24021

signaling. There are two splice variants of FGFR2, FGFR2IIIb, and FGFR2IIIc, which differ in the amino-terminal half of the third immunoglobulin domain (Ig) within the extracellular part of the receptor. The FGF ligand-binding domain comprises the second and third Ig domains, and therefore the FGFR2IIIb and FGFR2IIIc splice variants exhibit differential ligand affinity. Both splice variants are also differentially-expressed within tissues: FGFR2IIIb is preferentially located in the epithelium and binds to FGF7 and 10, whereas FGFR2IIIc is mainly present in the mesenchyme and has a high affinity for FGF2, 4, 6, 8, and 9. Both of the Apert mutations are located within the region linking the second and third Ig domains, which causes both FGFR2IIIb and FGFR2IIIc to show higher affinity and reduced specificity for their ligands (Miki et al., 1992; Ornitz et al., 1996; Anderson et al., 1998).

Multiple signaling cascades have been identified downstream of FGFR2 (Schlessinger, 2000). These pathways include extracellular signal-regulated kinase (ERK) and mitogen-activated protein kinase (MAPK)/ERK kinase (MEK), and are associated with both cell proliferation and differentiation (Ornitz and Itoh, 2001; Raucci et al., 2008). Recent studies suggest that the p38 (Wang et al., 2007) phosphatidylinostol 3-kinase (PI3K)-Akt (Raucci et al., 2008), and phospholipase Cγ (PLCγ)-protein kinase Cα (PKCα) (Debiais et al., 2001; Miraoui et al., 2009), pathways also play roles in FGF signaling.

Our previous study demonstrated that transfection of a mutant type of mesenchyme-specific variant of FGFR2IIIc (FGFR2IIIc-S252W; FGFR2IIIc-Ap) into the osteosarcoma cell line, MG63, enhanced osteoblast differentiation, and that this differentiation was inhibited by the conditioned medium from COS-1 cells transfected with a soluble form of the mutant receptor (sFGFR2IIIc-Ap) that lacked the transmembrane and cytoplasmic domains (Tanimoto et al., 2004). Even though FGFR2-S252W mouse models of Apert syndrome have been generated independently by two groups, and some reports have described the effects of the S252W mutation on osteoblast phenotypes (Mansukhani et al., 2000; Chen et al., 2003; Wang et al., 2005; Yang et al., 2008a; Holmes et al., 2009), the biological function and downstream molecular mechanisms affected by the FGFR2-S252W mutation require further investigation. In the present study, we examined the effect of the S252W mutation in FGFR2IIIc using primary calvarial osteoblasts derived from transgenic mice, rather than transfected cell lines (Tanimoto et al., 2004; Miraoui et al., 2009). We characterized calvarial osteoblasts expressing FGFR2IIIc-Ap and/or sFGFR2IIIc-Ap transgenes by focusing on their proliferative activity and osteogenic differentiation capacity, as well as the downstream FGF signaling pathways involved in osteoblast proliferation and differentiation.

Materials and Methods

Transgenic mice

A 2.4-kbp XbaI/BamHI fragment of the full-length human *FGFR2IIIc* cDNA containing the S252W mutation (*FGFR2IIIc-S252W*; *FGFR2IIIc-Ap*) was cloned into the 3xFLAG CMV13 expression vector (Sigma, St. Louis, MO) as previously described (Tanimoto et al., 2004) (Fig. 1A). Similarly, a 1.1-kbp fragment of the human *FGFR2IIIc-Ap* cDNA lacking the transmembrane and cytoplasmic domains (*sFGFR2IIIc-Ap*) was cloned into the 3xFLAG CMV13 expression vector (Fig. 1A). To generate the founder generation (F_0) of transgenic mice, constructs were purified and microinjected into the pro-nuclei of fertilized eggs from C57BL/6J mice (Japan SLC, Shizuoka, Japan). Among several lines of F_1 mice expressing *FGFR2IIIc-Ap* and *sFGFR2IIIc-Ap*, one line was selected from each type (based on fertility) and these mice were termed Ap-Tg and sAp-Tg (expressing *FGFR2IIIc-Ap* and *sFGFR2IIIc-Ap*), respectively. All mice used in this study were derived from the genetically inbred C57BL/6J background. All experiments were performed in accordance with protocols certified by the Institutional Animal Care and Use Committee of Tokyo Medical and Dental University.

Genotyping of the mice was performed by polymerase chain reaction (PCR) using genomic DNA, specific primers (Forward, 5′-CGCATTGGAGGCTACAAGGTA-3′, corresponding to the extracellular domain of *FGFR2IIIc,* and Reverse, 5′-CTTGTCATCGTCATCCTTGTA-3′, corresponding to FLAG sequence), and KOD plus polymerase (TOYOBO, Osaka, Japan). Genomic DNA was isolated from mouse tails using a DNA Purification Kit (Promega, Madison, WI) according to the manufacturer's instructions. Using the primers listed above, 1,880- and 560-bp fragments were amplified from the genomic DNA of Ap-Tg and sAp-Tg, respectively (Fig. 1B). Mating Ap-Tg and sAp-Tg resulted in offspring carrying both transgenes (Ap/sAp-Tg). Both the 1,880- and 560-bp fragments were also amplified from the genomic DNA of these mice (Fig. 1B).

Isolation and culture of calvarial osteoblasts

Calvarial osteoblasts were isolated from 2-day old mice by digestion with 0.1% collagenase (Wako, Osaka, Japan) and 0.2% dispase (GIBCO, Grand Island, NY). Cells were cultured in α-minimum essential medium (α-MEM; Wako) containing 10% fetal bovine serum (FBS; Japan Bioserum, Hiroshima, Japan) and Antibiotic-Antimycotic (GIBCO) at 37°C under 5% CO_2 and 95% O_2. Cells were isolated from litter mates and cells from the primary or secondary passage were used for the experiments. The culture medium was changed every 3 days.

Mineralization and alkaline phosphatase (ALP) activity in calvarial osteoblasts

After the cultured osteoblasts reached confluence, the medium was changed to a differentiation-inducing medium (α-MEM containing 10% FBS, 50 μg/ml ascorbic acid (Wako), 10 nM dexamethasone (Sigma), and 10 mM β–glycerophosphate (Sigma)). The mineralized matrix within the cultures was stained with Alizarin Red S (AR-S) (Wako) after 1, 2 and 3 weeks. The ALP activity in the cell lysates was measured by the enzymatic conversion of *p*-nitrophenylphosphate to *p*-nitrophenol using a LabAssay™ ALP kit (Wako) according to the manufacturer's instructions. The amount of total protein was measured using the Bradford micro assay (Bio-Rad, Hercules, CA), and the ALP activity was expressed as mmol/mg/15 min. U0126 (20 μM, Cell Signaling, Danvers, MA), U73122 (5 μM, Calbiochem, San Diego, CA), and SB203580 (10 μM, Calbiochem) were added to the culture medium to inhibit MEK (Favata et al., 1998; Raucci et al., 2008), PLCγ (Moenning et al., 2009; Mantha and Jumarie, 2010), and p38 (Huang et al., 2010), respectively. These concentrations were based on those used in previous reports. All experiments were performed in triplicate.

Immunocytostaining of cultured calvarial osteoblasts

Calvarial osteoblasts (2.0×10^4 cells/cm^2) were inoculated onto poly-L-lysine-coated glass (Iwaki, Tokyo, Japan), fixed for 30 min with 4% paraformaldehyde (PFA) in phosphate-buffered saline (PBS), incubated with 1% bovine serum albumin containing Mouse Ig Blocking Reagent (M.O.M. kit; Vector Laboratories, Youngstown, OH), and reacted with a mouse anti-FLAG monoclonal antibody (Sigma) for 1 h. The Mouse Ig Blocking Reagent (M.O.M. kit; Vector Laboratories) was added to block any non-specific binding to mouse cells. Cells were then incubated with rhodamine-conjugated Alexa Fluor 594 goat anti-mouse IgG antibody (Invitrogen, Carlsbad, CA). After washing with PBS, the cell nuclei were stained with 5 μg/ml of 4,6-diamifino-2-phenylindole (DAPI; Sigma) and the fluorescence was observed under a fluorescence microscope (AF6000; Leica, Wetzlar, Germany).

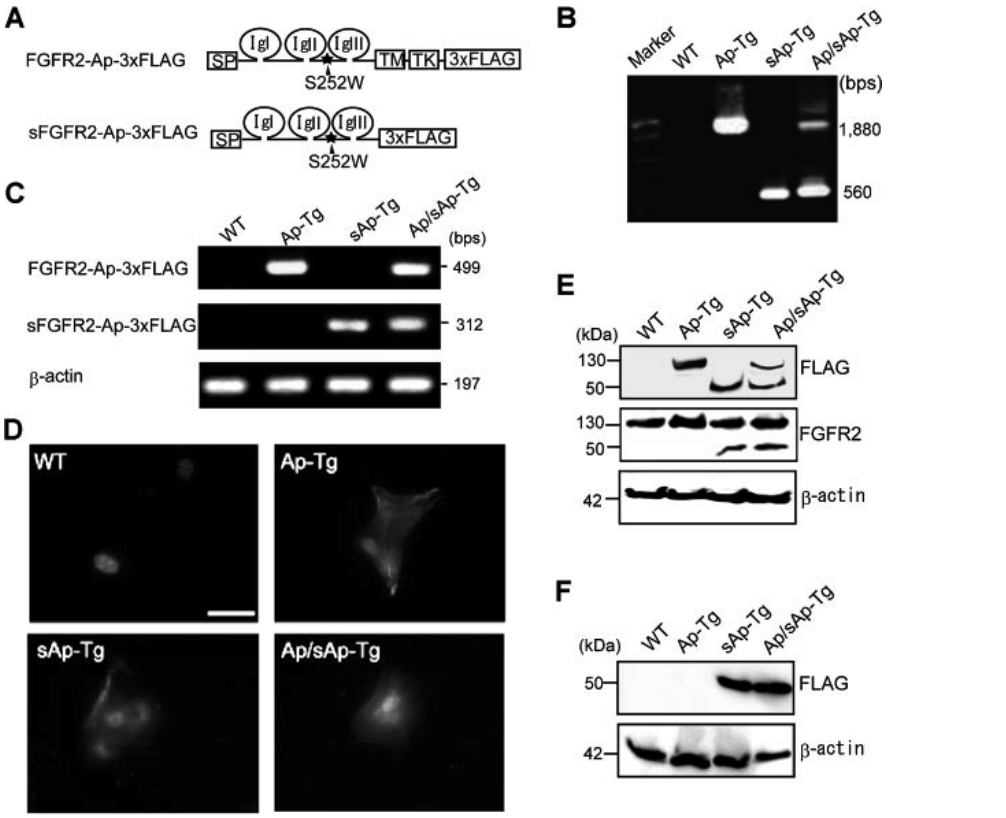

Fig. 1. Constructs and expression of transgenic FGFR2 in calvarial osteoblasts. A: *FGFR2IIIc-Ap-3xFLAG*: 2.4 kbp human *FGFR2IIIc* cDNA containing the S252W mutation and an in-frame 3xFLAG tag; *sFGFR2IIIc-Ap-3xFLAG*: 1.1 kbp human *FGFR2IIIc* cDNA lacking the transmembrane and cytoplasmic domains and containing the S252W mutation and an in-frame 3xFLAG tag. SP, signal peptide; Ig, immunoglobulin-like domain; TM, transmembrane domain; TK, tyrosine kinase domain. The cDNA constructs (driven by the CMV promoter) were microinjected into the pro-nuclei of fertilized eggs. B: PCR products were amplified from genomic DNA of WT mice, transgenic mice expressing *FGFR2IIIc-Ap-3xFLAG* (Ap-Tg) or *sFGFR2IIIc-Ap-3xFLAG* (sAp-Tg), and the offspring of a mating between Ap-Tg and sAp-Tg (Ap/sAp-Tg). PCR products of 1,880- and 560 bp were amplified from Ap-Tg and sAp-Tg DNA, respectively. C: Expression of transgenic FGFR2 in calvarial osteoblasts. The results of RT-PCR for *FGFR2IIIc-Ap-3xFLAG* (upper panel in C), *sFGFR2IIIc-Ap-3xFLAG* (middle panel in C) and *β-actin* (lower panel in C). RT-PCR products of 499 bp and 312 bp were amplified from *FGFR2IIIc-Ap-3xFLAG* and *sFGFR2IIIc-Ap-3xFLAG* samples, respectively. Transgene expression was detected in calvarial cells from Ap-Tg, sAp-Tg and Ap/sAp-Tg mice. D: Immunocytostaining of WT, Ap-Tg, sAp-Tg and Ap/sAp-Tg-derived osteoblasts using an anti-FLAG antibody. E: Western blot analysis of calvarial cell lysates prepared from WT, Ap-Tg, sAp-Tg, and Ap/sAp-Tg-derived osteoblasts using an anti-FLAG antibody and an anti-FGFR2 antibody. The anti-FLAG and anti-FGFR2 antibodies detected transgenic products of 130 and/or 50 kDa in the lysates from transgenic mice. F: Proteins were extracted from culture media conditioned by calvarial osteoblasts. An anti-FLAG antibody detected a 50 kDa protein from medium conditioned by sAp-Tg and Ap/sAp-Tg-derived cells.

RNA preparation, reverse transcription (RT)-PCR and real-time PCR

RNA was isolated from cultured calvarial cells using ISOGEN (Nippon Gene, Tokyo, Japan) according to the manufacturer's instructions. The template cDNA used for subsequent PCR was synthesized from 1 μg of total RNA using the QuantiTect Reverse Transcription Kit (QIAGEN, Hilden, Germany) according to the manufacturer's instructions.

The RT-PCR conditions were as follows: 40 cycles each of 94°C for 1 min, 60°C for 30 sec, and 72°C for 30 sec. KOD plus polymerase (TOYOBO) was used as the enzyme for RT-PCR. The primers used to amplify the transgene *FGFR2IIIc-Ap-3xFLAG* were: forward, 5′-ATCAGAGTGATGTCTGGTCCTTC-3′ (corresponding to the intracellular domain of *FGFR2IIIc* (2692–2714 in NM_000141.1)); and reverse, 5′-CTTGTCATCGTCATCCTTGTAG-3′ (corresponding to the FLAG sequence). For *sFGFR2IIIc-Ap-3xFLAG*, the primers were: forward, 5′-GTGGAAAAGAACGGCAGTAAAT-3′ (corresponding to the extracellular domain of *FGFR2IIIc* (1527–1548 in NM_000141.1)); and reverse, 5′-CTTGTCATCGTCATCCTTGTAGT-3′ (corresponding to the FLAG sequence). Amplified products were separated on 2% agarose gels (Nippon Gene). The primer sequences and their product sizes used to amplify *Runx2* (encoding mouse runx2), *Opn* (encoding mouse osteopontin), *Bglap* (encoding mouse osteocalcin), *Col1α1* (encoding mouse collagen type I alpha 1), *Bsp* (encoding mouse bone sialoprotein), *Bmp2* (encoding mouse bmp2), *Bmp4* (encoding mouse bmp4), *Nog* (encoding mouse noggin), *Msx2* (encoding mouse msx2), *Col2a1* (encoding mouse

collagen type II alpha 1), *Col10a1* (encoding mouse collagen type X alpha 1), *Pparγ2* (encoding mouse peroxisome proliferator-activated receptor γ 2), *aP2* (encoding mouse adipocyte fatty acid protein 2) and β-*actin* (encoding mouse β-actin), are listed in Table 1.

Real-time PCR was performed using TaqMan gene expression assays (Applied Biosystems, Carlsbad, CA) according to the manufacturer's instructions. The primers and TaqMan probes used were as follows: *Bglap* (Mm03413826_mH), *Opn* (Mm01611440_mH), *Runx2* (Mm00501580_m1), *Fgf2* (encoding mouse fgf2) (Mm00627025_g1), *Fgf7* (encoding mouse fgf7) (Mm00627025_g1), and *GAPDH* (encoding mouse GAPDH) (Mm_03302249_g1).

Protein preparation and Western blot analysis

Calvarial osteoblasts were lysed in buffer containing 50 mM Tris-HCl (pH 7.4), 125 mM NaCl, 0.1% Nonident P-40 (NP-40; Sigma), and 1 mM each of EDTA and phenylmethylsulfonyl fluoride, followed by sonication as previously described (Tanimoto et al., 2004; Saito et al., 2005; Shiga et al., 2008). Proteins (20 μg) were loaded onto 10% SDS–PAGE gels and transferred to polyvinylidene difluoride membranes (Amersham Biosciences, Piscataway, NJ). Individual membranes were incubated with the following primary antibodies: anti-FLAG, anti-β-actin (Sigma), anti-FGFR2 (Santa Cruz Biotechnology, Santa Cruz, CA), anti-ERK, anti-p-ERK, anti-MEK, anti-p-MEK, anti-p38, anti-p-p38, anti-PLCγ, anti-p-PLCγ, anti-Src homology and collagen containing protein (Shc), anti-p-Shc, anti-c-Jun N-terminal protein kinase (JNK), anti-p-JNK, anti-Akt or anti-p-Akt (Cell Signaling). After washing, the membranes were probed with an anti-IgG horseradish peroxidase-conjugated secondary antibody (Cell Signaling) and bound antibodies were detected using the enhanced chemiluminescence Western blotting detection reagent (ECL plus Western Blotting Detection System; Amersham Biosciences) according to the manufacturer's instructions. To examine the secretion of sFGFR2IIIc-Ap, the culture medium was concentrated by evaporation and 5 μg of protein was subjected to Western blot analysis with anti-FLAG antibody. All Western blots were performed using equivalent amounts of protein from each cell lysate, and the cell lysates were also probed for β-actin.

Cell adhesion assay

Calvarial osteoblasts were labeled using the PKH26 Red Fluorescent Cell Linker Mini Kit (Sigma) and incubated with β-tricalcium phosphate (β-TCP) granules (Osferion; Olympus, Tokyo, Japan) for 18 h in α-MEM containing 10% FBS as previously described (Shiga et al., 2008). Cells attached to the β-TCP granules were observed under a fluorescence microscope (AF6000; Leica).

In vivo differentiation assay

The osteogenic potential of calvarial osteoblasts was assessed using an in vivo differentiation assay as described previously (Kitagawa et al., 2006; Shiga et al., 2008). Briefly, 1.5×10^6 cells were incubated with 40 mg of β-TCP granules and a fibrin clot (mixture of mouse fibrinogen and thrombin) (Sigma). They were then transplanted subcutaneously into 5-week old male CB-17 *SCID*/*SCID* mice (Nihon Crea, Tokyo, Japan). The mice were sacrificed after 8 weeks and the implanted tissues were collected. The tissues were fixed in a 4% PFA in PBS, decalcified with 10% EDTA in PBS for 1 week, embedded in paraffin, and stained with hematoxylin and eosin (H&E).

To distinguish the origin of the cells in the transplanted tissues, sections were immunostained with an anti-FLAG monoclonal antibody (Sigma), which recognizes transplanted cells but not host-CB-17 *SCID*/*SCID* mouse cells. To avoid non-specific staining by the mouse monoclonal primary antibody, sections were blocked using the M.O.M. kit (Vector Laboratories) as previously described (Shiga et al., 2008). Endogenous peroxidase was quenched by incubating the sections with 0.3% H_2O_2 in PBS for 30 min. A biotinylated anti-mouse IgG secondary antibody (M.O.M. kit; Vector Laboratories) was used as the secondary antibody and the reaction was visualized with a fluorescein avidin conjugate (M.O.M. kit; Vector Laboratories). The sections were then washed with PBS, mounted with Perma Flour Aqueous Mounting Medium (Thermo Fisher Scientific, Waltham, MA), and observed under a

TABLE 1. Mouse oligonucleotide primers used in RT-PCR

Genome sequence mRNA	Oligonucleotide sequence (5′–3′)	Product size (bp)	Index
Runx2	TCTGACACAGCTTTGCCTTTTA GCCTGCAATTTAGAGTTTTGCT	280	3117–3396 in NM_001146038
Opn	GCAAGAAACTCTTCCAAGCAAT ACTAGCAGTGACGGTCTCATCA	169	300–468 in NM_009263.2
Bglap	CGGACAGAGCCTTA CGTGCC CTGCCCGGGTCCGTGG	152	269–420in NM_007541.2
Col1a1	GACAGAGGCATAAAGGGTCATC GCAGGAAGCTGAAGTCATAACC	297	3376–3672 in NM_00742.3
Bsp	GATTCTGAAGAAAACGGGGTCT TCATTCCCCTCAGAATCTTCA	209	151–359 in NM_001040058
Bmp2	ATACAGGAAGCTTTGGGAAACA GAGACACCTGGGTTCTCCTCTA	248	626–873 in NM_007553.2
Bmp4	TTTCCATCACGAAGAACATCTG TCCAGTAGTCGTGTGATGAGGT	246	788–1033 in NM_007544.2
Nog	CTCCGCACAGAGAAACAAGAC GGCATCCGAGATTACTCCAG	150	136–285 in NM_008711.2
Msx2	GGAACTGGAAAAGCTGAAAATG TGCTTTTATGCAAACATCCATC	244	679–922 in NM_013601.2
Col2a1	CTGTAAGAACAGCATCGCCTACCTG CAGGAATTTGGTGTGGACATAGGG	271	Choi et al. (2011)
Col10a1	CGTCTCTGCTTTTACTGTCA CTCACAGAAAATGACCAGGT	300	Choi et al. (2011)
Pparγ2	CTGTAGGGGTGTCGTTCCG TCCTTGGCCCTCTGAGATGAG	530	Garcia et al. (2001)
aP2	GAAGGTCCAAGGGTGTTTTC TCTTCCTTTGGCTCATGCCC	380	Garcia et al. (2001)
β-actin	TGCGTGACATCAAAGAGAAG GATGCCACAGGATTCCATA	197	Shukla et al. (2007)

fluorescence microscope (AF6000; Leica). Ten samples were used for each experiment.

Cell proliferation in monolayer culture

To examine cell proliferation, cells (5.0×10^3 cells/cm^2) were inoculated into six-well dishes (Iwaki) and the number of cells in each well was counted on days 3, 6, and 9 after inoculation. Also, 5-Bromo-2-deoxyuridine (BrdU) incorporation was examined. S phase cells were detected using an in situ cell proliferation kit (Roche Applied Science, Switzerland) according to the manufacturer's instructions. Briefly, cells (1.0×10^4 cells/cm^2) were grown on poly-L-lysine coated glass (Iwaki) for microscopic observation up to 80% confluence. The cells were then incubated for 4 h in the presence of 10 μM BrdU labeling reagent to facilitate the incorporation of BrdU into DNA in place of thymidine. Cells were fixed in 70% ethanol diluted in glycine buffer (50 mM glycine, pH 2.0) for 45 min at room temperature and incubated in 4 M HCl for 20 min at room temperature for DNA denaturation. For immunodetection of the incorporated BrdU, the cells were incubated with fluorescein isothiocyanate-conjugated anti-BrdU monoclonal antibodies for 45 min at 37°C. Cell nuclei were stained with 5 μg/ml of DAPI (Sigma) in PBS for 60 min prior to mounting slides. The fluorescence was visualized using a fluorescence microscope (AF6000; Leica). The frequency of S phase cells was calculated as a ratio of BrdU positive nuclei to total DAPI stained nuclei. All experiments were performed in triplicate wells and glasses.

Chondrogenic and adipogenic differentiation

To determine chondrogenesis and adipogenesis of calvarial cells after 3-weeks of culture in differentiation-inducing medium, cartilaginous extracellular matrix and cytoplasmic lipid droplets were assayed by alcian blue (Sigma) staining and Oil Red O (Muto pure chemicals, Tokyo, Japan) staining, respectively. Staining was performed according to the manufacturers' instructions. The ATDC5 mouse embryonal carcinoma cell line was used as a positive control for chondrogenic differentiation (Yang et al., 2008b), while the TMS-14 murine stromal cell line was used as a positive control for adipogenesis (Garcia et al., 2001).

Statistical analysis

ANOVA and Tukey's post hoc test were used to assess the differences between Ap-Tg, sAp-Tg, Ap/sAp-Tg and WT mice. A P-value < 0.05 was considered significant.

Results

Transgene expression in calvarial osteoblasts

The CMV-driven expression of the *FGFR2IIIc-Ap-3xFLAG*, and *sFGFR2IIIc-Ap-3xFLAG* transgenes in primary calvarial osteoblasts from the transgenic mice was examined by RT-PCR (Fig. 1C). A single 499-bp *FGFR2IIIc-Ap-3xFLAG* fragment was amplified from the calvarial cells derived from Ap-Tg. Similarly, a single 312-bp fragment was amplified from sAp-Tg-derived calvarial cells. Both the 499 and 312-bp fragments were also amplified from Ap/Ap-Tg-derived calvarial cells. In contrast, these transgene-derived fragments were not amplified from calvarial osteoblasts derived from WT mice. Immunocytostaining using the anti-FLAG antibody was performed to localize the transgene products within calvarial osteoblasts isolated from Ap-Tg, sAp-Tg, Ap/sAp-Tg and WT mice (Fig. 1D). Cells from Ap-Tg, sAp-Tg and Ap/sAp-Tg mice showed positive staining, but no staining was seen in cells from WT mice. The FLAG fusion protein was present in the cell membrane and/or cytoplasm of Ap-Tg-, sAp/Tg- and Ap/sAp-Tg-derived osteoblasts. Western blot analysis of cell lysates from the four types of calvarial cells using an anti-FLAG antibody detected transgenic proteins of the expected sizes in Ap-Tg, sAp-Tg and Ap/sAp-Tg (Fig. 1E). This was confirmed using an anti-FGFR2 antibody, and FGFR2 proteins of the expected size were detected in each lysate from the four types of calvarial cells (Fig. 1E). As expected, the sFGFR2IIIc-Ap protein was secreted into the medium of sAp-Tg- and Ap/sAp-Tg-derived cell cultures (Fig. 1F). These results showed that FGFR2IIIc-Ap was localized in the cell membrane and sFGFR2IIIc-Ap was successfully secreted into the culture medium.

Analysis of differentiation and FGFR2 signaling in calvarial osteoblasts

The expression of osteoblast-associated genes was examined in the four types of calvarial cells using RT-PCR and real-time PCR (Fig. 2A). Confluent Ap-Tg-derived cells expressed higher levels of *Runx2*, *Opn*, *Bglap*, *Col1a1*, *Bsp*, and *Bmp2* than WT-derived cells. The expression levels of the genes in sAp-Tg- and Ap/sAp-Tg-derived cells were lower than in Ap-Tg-derived cells, and Ap/sAp-Tg-derived cells showed a similar expression profile to WT-derived cells when evaluated by RT-PCR.

Next, each of the four osteoblast types was cultured in differentiation-inducing medium without addition of exogenous FGFs for 3 weeks after the cells became confluent (Fig. 2B). Real-time PCR indicated that all types of osteoblasts expressed comparable levels of *Fgf2* and *Fgf7*, to which WT FGFR2IIIb and WT FGFR2IIIc preferentially bind, respectively (data not shown). Cells from WT mice showed clear mineralization after 3 weeks in this culture system. In contrast, cells from Ap-Tg mice showed strong mineralization within a week. Cells from sAp-Tg mice did not show positive mineralization staining, and faint mineralization was observed in Ap/sAp-Tg-derived cell culture after 3 weeks (Fig. 2B).

ALP activity was investigated in the four types of calvarial osteoblasts during the course of calcification (Fig. 2C). Ap-Tg-derived calvarial cells showed significantly higher ALP activity (4.3- to 6.2-fold) at all stages examined than WT-derived cells. In contrast, although the levels of ALP activity gradually increased, sAp-Tg-derived cells showed significantly lower ALP activity (0.39- to 0.54-fold) compared to WT-derived cells. The ALP activity in the Ap/sAp-Tg-derived cells was very similar to that of WT-derived cells.

Expression of some of the osteoblast-associated genes was analyzed by real-time PCR (Fig. 2D). This showed a distinct difference between time 0 (when cells became confluent) and after 3 weeks of culture in differentiation-inducing medium. After 3 weeks, the expression of *Runx2*, *Bglap*, and *Opn* was upregulated in all four cell types. Ap-Tg-derived cells showed significantly higher levels of *Runx2* and *Bglap* expression than WT-derived cells, but *Opn* expression was not significantly different between cell types. sAp-Tg-derived cells showed lower levels of *Runx2* and *Bglap* expression than WT-derived cells. The levels in Ap/sAp-Tg-derived cells were comparable to those in WT-derived cells.

To assess the effects of FGFR2IIIc-Ap and sFGFR2IIIc-Ap on cell signaling pathways, the phosphorylation of ERK, MEK, PLCγ, p38, Shc, JNK, and Akt was examined by Western blot analysis when cells became confluent (Fig. 2E). ERK, MEK, PLCγ, and p38 showed the highest levels of phosphorylation in Ap-Tg-derived osteoblasts. However, phosphorylation levels of Shc, JNK, or Akt were not significantly different among the four cell types. Phosphorylation levels of ERK, MEK, PLCγ and p38 were lower in Ap/sAp-Tg-derived cells than in Ap-Tg-derived cells, and were comparable with those in WT-derived cells. In contrast, sAp-Tg-derived cells showed very low levels of phosphorylation of these molecules.

Addition of a MEK inhibitor (U0126), a PLCγ inhibitor (U73122), and a p38 inihibitor (SB203580) suppressed

mineralization of both WT- and Ap-Tg-derived cultures (Fig. 2B). Addition of U0126 and SB203580 prevented mineralization completely, while U73122 showed weak inhibition of mineralization in Ap-Tg-derived cultures. Decreased phosphorylation of MEK, PLCγ and p38 in the presence of their inhibitors was confirmed by Western blot analysis (Fig. 2E).

Osteogenic potential of calvarial osteoblasts in cell transplantation experiments

The osteogenic potential of the four types of calvarial osteoblasts was examined in vivo. Adhesion of the four types of osteoblasts to β-TCP granules, which were used as carriers for transplantation, was first examined before transplantation into

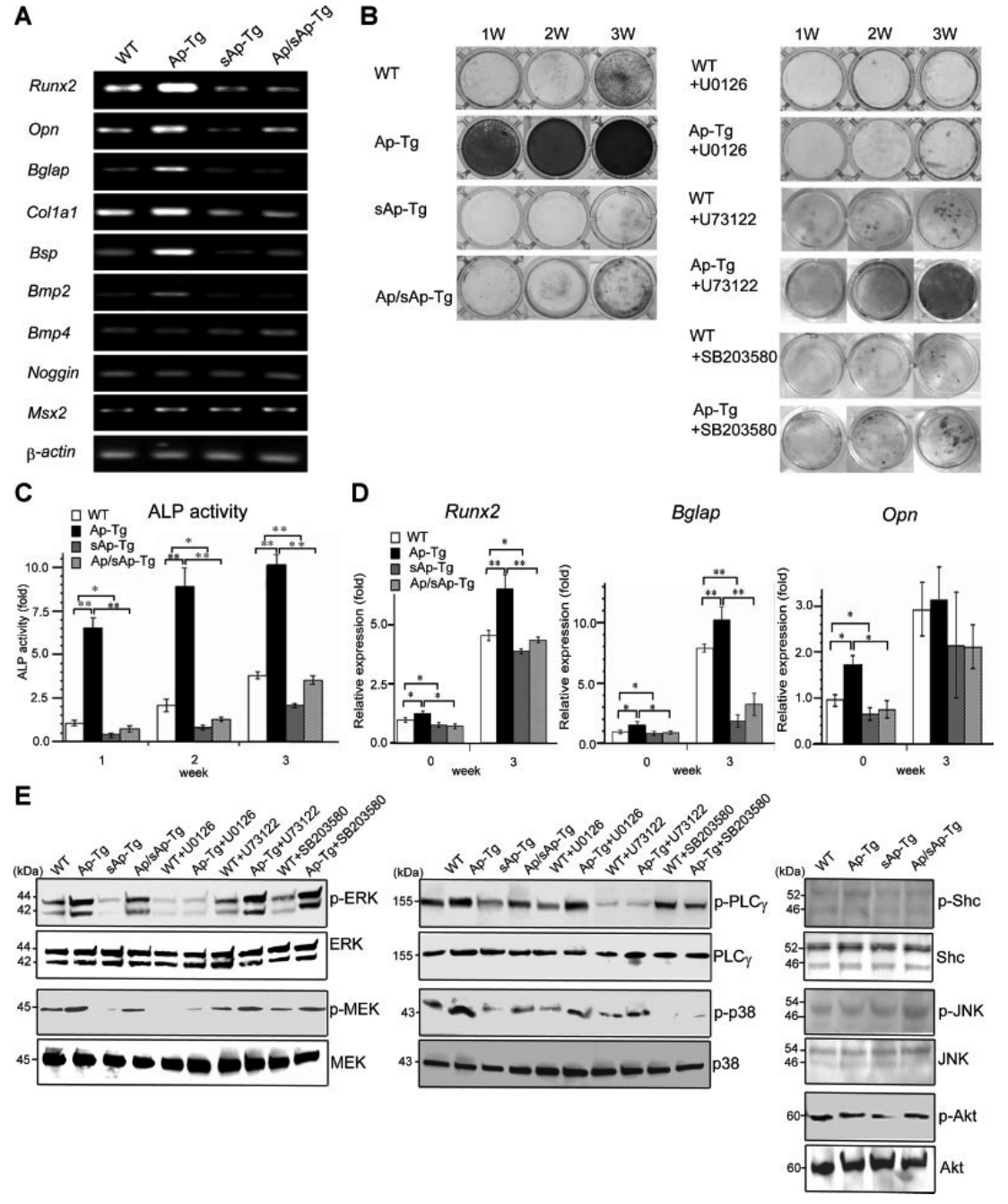

host mice. After labeling the four types of calvarial cells with PKH26, each of them was incubated with β-TCP granules for 18 h and attachment of cells to the β-TCP granules was assessed using a fluorescence microscope (Fig. 3A). All four types showed comparable levels of attachment to the β-TCP granules. No fluorescence was detected with β-TCP granules alone (data not shown).

Next, the survival and presence of the transplanted cells expressing *FGFR2IIIc-Ap* or *sFGFR2IIIc-Ap* in the transplants were examined 8 weeks after transplantation into CB-17 *SCID*/*SCID* mice by immunostaining with an anti-FLAG antibody (Fig. 3B). Clear staining was observed in the transplants with cells from Ap-Tg, sAp-Tg and Ap/sAp-Tg mice, suggesting that the transplanted cells had survived. No positive staining was seen in the transplants with WT-derived cells and mock transplantation of β-TCP granules alone.

Eight weeks after transplantation, histological observation showed that small amounts of bone-like tissue were present in the sections from the transplants with WT-derived cells. When cells from Ap-Tg mice were used for transplantation, the amount of bone-like tissue was substantially increased. Interestingly, the enhanced bone-like tissue formation in the transplants with Ap-Tg-derived cells was dramatically suppressed when Ap/sAp-Tg-derived cells were used for transplantation, with levels similar to those seen with WT-derived cells. Bone formation was never seen with sAp-Tg-derived cells or β-TCP granules alone (Fig. 3C).

Cell proliferation and the effects of FGFR2IIIc-S252W during cell growth

Time course and BrdU incorporation analyses showed that the proliferation rate was highest in osteoblasts derived from Ap-Tg mice, with sAp-Tg-derived osteoblasts being the least active (0.50- to 0.69-times of WT-derived cells in the time course analysis) (Fig. 4A,B). The proliferation of Ap/sAp-Tg-derived osteoblasts was comparable with that of WT-derived osteoblasts. Pharmacological inhibition of MEK and p38, but not PLCγ, significantly reduced the proliferative activity after 3 days in WT- and Ap-Tg-derived cultures (Fig. 4C). Osteoblast-associated gene expression during cell growth was examined after 3 days of culture using real-time PCR (Fig. 4D). The level of *Runx2* expression in Ap-Tg-derived osteoblasts was significantly higher than that in sAp-Tg-derived or WT-derived osteoblasts. The pattern of expression levels of *Opn* between cell types was similar to that of *Runx2*, and a significant difference was observed only between sAp-Tg- and WT-derived cells. The expression of *Bglap* was not significantly different between any of the cell types (data not shown). To determine which signaling pathways were active downstream of FGFR2IIIc-S252W during cell growth, we examined the phosphorylation of ERK, MEK, PLCγ, and p38 after 3 days in culture (Fig. 4E). The phosphorylation of ERK, MEK, and p38 was activated in Ap-Tg-derived osteoblasts more strongly than in WT-derived osteoblasts.

The effects of FGFR2IIIc-S252W and sFGFR2IIIc-S252W on chondrogenic and adipogenic differentiation

We examined whether sAp-Tg-derived osteoblasts that were impaired in their osteogenic capacity could differentiate into other mesenchymal cell lineages such as chondrocytes or adipocytes. Four types of osteoblasts were cultured in differentiation-inducing conditions for 3 weeks, and subsequently analyzed by tissue specific staining and expression study of chondrogenic and adipogenic marker genes. None of the four types of osteoblasts showed synthesis of matrix proteoglycans (a chondrocyte marker) or the presence of lipid droplets (an adipocyte marker) (Supplementary Fig. 1A). In addition, the chondrogenic marker genes, *Col2a1* and *Col10a1*, and the adipogenic marker genes, *Pparγ2* and *aP2*, were also under detection levels by RT-PCR (Supplementary Fig. 1B). Thus, the results indicate that sAp-Tg-derived cells do not have the potential to differentiate into other mesenchymal cell lineages.

Discussion

Our results showed that FGFR2IIIc-Ap accerelated both osteoblast cell proliferation and differentiation. We examined the effects of the S252W mutation on differentiation in non-dividing confluent cells, and on proliferation in actively growing and dividing cells (Figs. 2 and 4). The proliferative activity and differentiation capacity of Ap-Tg-derived calvarial cells was significantly increased compared to WT-derived cells, whereas sAp-Tg-derived cells showed decreased proliferation and differentiation (Figs. 2B and 4A). These observations are consistent with previous studies showing that the S252W mutation led to increased osteoblast proliferation and differentiation (Wang et al., 2005; Yang et al., 2008a; Holmes et al., 2009). In addition, primary calvarial osteoblasts isolated from Ap-Tg mice showed ectopic de novo bone formation in vivo (Fig. 3C). In contrast, proliferative activity in FGFR2IIIc-Ap-transfected MG63 cells or C3H10T1/2 cells was not enhanced (Tanimoto et al., 2004; Miraoui et al., 2009), and C3H10T1/2 cells transfected with FGFR2IIIc-Ap did not induce de novo osteogenesis when transplanted with β-TCP granules (Miraoui et al., 2009). Because C3H10T1/2 cells are mesenchymal cells that display fibroblastic morphology (Tang et al., 2004), and MG63 cells are an osteosarcoma cell line, it is possible that increased proliferation and differentiation, and de novo bone

Fig. 2. Analysis of calvarial osteoblast differentiation and FGFR2 signaling. A: Expression of osteoblast-associated genes in calvarial osteoblasts. Gene expression patterns for *Runx2* (encoding runx2), *Opn* (encoding osteopontin), *Bglap* (encoding osteocalcin), *Col1a1* (encoding collagen type I alpha 1), *Bsp* (encoding bone sialoprotein), *Bmp2* (encoding bmp2), *Bmp4* (encoding bmp4), *Nog* (encoding noggin), *Msx2* (encoding msx2), and *β-actin* (encoding β-actin) were examined by RT-PCR. RNA was extracted from confluent cells cultured in α-MEM containing 10% FBS. B: Mineralization and differentiation of calvarial osteoblasts. Alizarin red staining in WT, Ap-Tg, sAp-Tg, and Ap/sAp-Tg-derived cells cultured with differentiation-inducing medium for 1, 2, or 3 weeks. U0126 (20 μM; an inhibitor of MEK), U73122 (5 μM; an inhibitor of PLCγ), or SB203580 (10 μM; an inhibitor of p38) were added to some WT and Ap-Tg-derived cultures. C: ALP activity in the cells derived from WT, Ap-Tg, sAp-Tg and Ap/sAp-Tg mice cultured in differentiation-inducing medium for 1, 2, or 3 weeks. The data are expressed as mean ± SD (n = 3) and represented as a ratio (fold induction) relative to the value in the 1-week cultures derived from WT mice. Statistical differences between cultures are indicated by asterisks (*$P < 0.05$, **$P < 0.01$). Ap-Tg-derived osteoblasts showed increased ALP activity and sAp-Tg-derived osteoblasts showed decreased ALP activity. The activity of Ap/sAp-derived cells was comparable with that of the WT-derived cells. D: The results of real-time PCR for *Runx2*, *Bglap* and *Opn* in cultures of cells derived from WT, Ap-Tg, sAp-Tg, and Ap/sAp-Tg mice at Week 0 (when cells became confluent) and after 3 weeks of culture in differentiation-inducing medium. The expression of *Runx2*, *Bglap*, and *Opn* was normalized to that of *β-actin*. Data are expressed as mean ± SD (n = 3) and represented as a ratio (fold induction) to the value in WT mice before culture in the cell differentiation medium (Week 0). *$P < 0.05$, **$P < 0.01$. E: The effect of FGFR2IIIc-Ap and sFGFR2IIIc-Ap on FGFR2 signaling. Phosphorylation of signaling molecules functioning downstream of FGFR2 in cell lysates from WT, Ap-Tg, sAp-Tg, and Ap/sAp-Tg mice was examined by Western blot analysis with antibodies against ERK, phosphorylated (p-)ERK, MEK, p-MEK, PLCγ, p-PLCγ, p38, p-p38, Shc, p-Shc, JNK, p-JNK, Akt, and p-Akt. WT- and Ap-Tg-derived cells were treated for 3h with U0126 (20 μM; an inhibitor of MEK), U73122 (5 μM; an inhibitor of PLCγ), or SB203580 (10 μM; an inhibitor of p38) before harvesting.

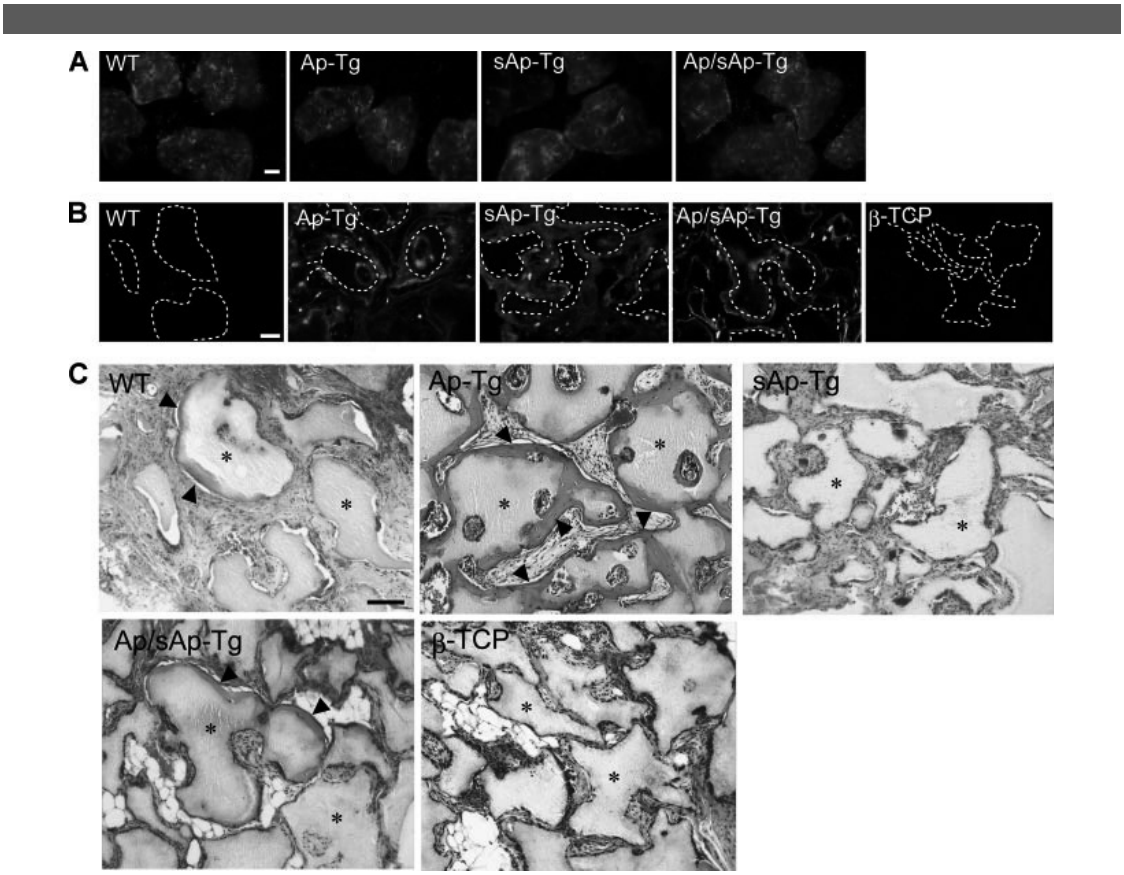

Fig. 3. Osteogenic potential of calvarial osteoblasts in cell transplantation experiments. The in vivo osteogenic potential of WT, Ap-Tg, sAp-Tg, and Ap/sAp-Tg-derived osteoblasts was examined following transplantation. A: Attachment of cells to β-TCP granules after incubation for 18 h. Scale bars = 100 μm. B: Immunostaining of cells transplanted together with β-TCP granules into CB-17 *SCID*/*SCID* mice 8 weeks after transplantation using an anti-FLAG antibody. Positive cells were seen in the transplants containing cells from Ap-Tg, sAp-Tg, and Ap/sAp-Tg (*dotted lines* outline the β-TCP granules). C: H&E stained sections 8 weeks after the transplantation of cells with β-TCP granules into CB-17 *SCID*/*SCID* mice. Ap-Tg-derived cells formed larger amounts of bone-like tissue (*arrowheads*) around the β-TCP granules (*) than those derived from WT, while sAp-Tg-derived cells formed no bone-like tissue. Representative data are shown. Scale bar = 100 μm.

formation, are specific effects of the S252W mutation in osteoblasts.

In our experiment, osteoblasts isolated from the transgenic mice showed positive transgene mRNA expression. However, transgene expression in calvaria tissue in vivo was low, presumably resulting in no appreciable abnormalities in calvaria in the transgenic mice (data not shown). Several other tissues in which the transgene expression was detected by RT-PCR also did not show any particular phenotypes in the transgenic mice (data not shown), which might be due to low levels of the transgene expression to allow phenotype development. It is speculated that the cell isolation process and the culture conditions may have induced epigenetic alternations that allowed transgenes to be expressed (Cao et al., 2000). The FGFR2-S252W knock-in mouse showed impaired phenotypes in many tissues such as skull, long bone, brain, thymus, and lungs (Wang et al., 2005), and osteoblasts from this mouse showed enhanced proliferation and differentiation (Yang et al., 2008a). Our observations of enhanced osteogenic capacity in osteoblasts with the S252W mutation may be related to the skeletal abnormalities of the FGFR2-S252W knock-in mice (Chen et al., 2003; Wang et al., 2005; Martínez-Abadías et al., 2010). The differences between the in vivo phenotypes of the knock-in mice and those of our transgenic mice might be due to the methodological differences of mutant mouse generation and epigenetic regulations.

Heterozygotic abrogation of the mesenchymal isoform FGFR2IIIc causes a splicing switch, and the epithelial isoform FGFR2IIIb is extensively upregulated in developing skull bones to induce the gain-of-function phenotype, craniosynostosis (Hajihosseini et al., 2001). Our data show that FGFR2IIIc-S252W expression influences in vitro osteoblast differentiation and in vivo osteogenesis without the assistance of FGFR2IIIb expression or a dramatic increase in total FGFR2 protein. Therefore, we suggest that our primary calvarial osteoblasts are representative of osteoblasts in Apert syndrome, and altered FGFR2IIIc signaling in osteoblasts is mostly responsible for the human craniosynostosis phenotype.

In this study, we further characterized the S252W mutation by analysis of intracellular signal transduction pathways. Multiple downstream intracellular FGFR2 signaling pathways have been reported (Schlessinger, 2000). Phosphorylation of

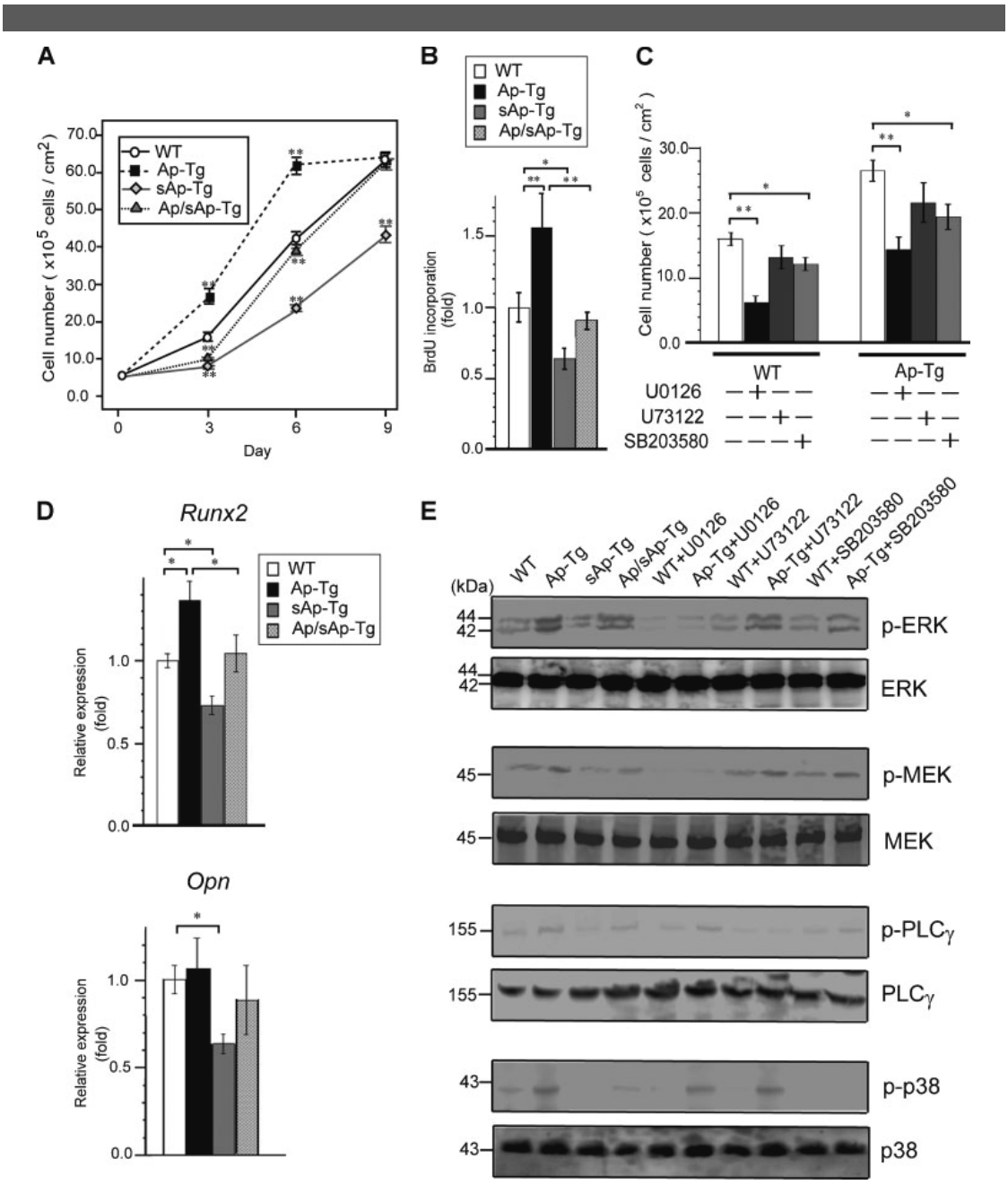

Fig. 4. Proliferation of calvarial osteoblasts and the effects of FGFR2IIIc-S252W during cell growth. A: Time course analysis of cell numbers in cultures of calvarial osteoblasts derived from WT, Ap-Tg, sAp-Tg, and Ap/sAp-Tg. Data are expressed as mean ± SD (n = 3), $^{**}P < 0.01$. Compared to WT-derived cultures, cell proliferation was faster in Ap-Tg-derived cultures and slower in sAp-Tg-derived cultures. B: Proliferative activity of WT, Ap-Tg, sAp-Tg, and Ap/sAp-Tg-derived osteoblasts was determined by the rate of cells incorporating BrdU. The data are expressed as mean ± SD (n = 3) and represented as a ratio (fold induction) relative to the value in WT mice, $^{*}P < 0.05$, $^{**}P < 0.01$. C: The cell number of WT- and Ap-Tg-derived osteoblasts after 3 days in culture with the addition of U0126 (20 μM), U73122 (5 μM), SB203580 (10 μM), or without any inhibitors. Statistical differences compared to untreated cells are indicated by asterisks ($^{*}P < 0.05$, $^{**}P < 0.01$). D: The expression of *Runx2* and *Opn* mRNA in WT, Ap-Tg, sAp-Tg, and Ap/sAp-Tg-derived osteoblasts after 3 days in culture, assessed using real-time PCR. The data are expressed as mean ± SD (n = 3) and represented as a ratio (fold induction) relative to the value in WT mice, $^{*}P < 0.05$, $^{**}P < 0.01$. E: The effect of FGFR2IIIc-Ap on FGFR2 signaling during cell growth. ERK, p-ERK, MEK, p-MEK, PLCγ, p-PLCγ, p38, and p-p38 after 3 days in culture were examined by Western blot analysis. WT- and Ap-Tg-derived cells were pretreated with U0126 (20 μM), U73122 (5 μM), or SB203580 (10 μM).

MEK-ERK, a major pathway regulating cell proliferation and differentiation, is associated with the etiology of Apert syndrome (Shukla et al., 2007). Recently, it was reported that the S252W mutation induced activation of PKCα (Miraoui et al., 2009) or p38 (Holmes et al., 2009) signaling. Our study also suggests the involvement of the PLCγ-PKCα and p38 pathways in accelerating osteogenesis in the mutant cells, although PLCγ does not seem to have much effect. By contrast, sFGFR2IIIc-Ap suppressed these pathways activated by FGFR2IIIc-Ap (Fig. 2E). In our study, pharmacological inhibition of ERK, MEK, and p38 reduced proliferation in Ap-Tg-derived osteoblasts, and their differentiation was blocked by reduced phosphorylation of ERK, MEK and p38 (Figs. 2B,E and 4C,E). Together, these data indicate that ERK, MEK, and p38 mediate signaling via FGFR2IIIc-S252W in primary calvarial osteoblasts. In particular, U0126 downregulated the phosphorylation levels of ERK and MEK, and effectively prevented osteoblast proliferation and differentiation in Ap-Tg-derived cultures. This supports an essential role of MEK-ERK signaling in FGFR2IIIc-Ap expressing osteoblasts. Therefore, the degree to which each of these signaling pathways contributes to osteoblast proliferation and differentiation may be different, and the balance between these contributions may not be altered by the Apert mutation.

It has been suggested that Runx2 DNA binding and transcriptional activity are enhanced by the MEK-ERK (Xiao et al., 2000), PLCγ-PKCα (Kim et al., 2003), and p38 (Greenblatt et al., 2010) pathways. *Runx2* plays an essential role in osteoblast differentiation: overexpression of *Runx2* upregulates the expression of osteoblast-associated genes and promotes osteoblast differentiation, while treatment with *Runx2* antisense oligonucleotides suppresses these effects in vitro (Banerjee et al., 1997; Ducy et al., 1997). Consistent with these observations, our results demonstrated increased phosphorylation of MEK, ERK, PLCγ, and p38, as well as up-regulated *Runx2* expression, in Ap-Tg-derived osteoblasts (Figs. 2D,E and 4D,E).

Mansukhani et al. (2005) showed that the S252W mutation induced a down-regulation of the expression of some Wnt target genes, suggesting inhibitory effects of the mutant FGFR2 on osteoblast differentiation. In their previous work, the FGFR2-S252W (Apert) and FGFR2-C342Y (Crouzon) mutant receptor-expressing cells showed reduced phosphorylation of MAP kinase (Mansukhani et al., 2000). Cross-talk between the FGF signaling pathway and other signals such as Wnt and TGF-β/BMPs has been reported in osteogenesis (Guo and Wang, 2009; Miraoui and Marie, 2010). Therefore, further investigation is required to understand the effect of FGFR2IIIc-Ap on the cross-talk between these signaling pathways.

The characterization of osteoblasts that express *sFGFR2IIIc-Ap* has not been investigated previously. In the present study, sFGFR2IIIc-Ap functioned as a negative regulator for osteoblast activity. Our results clearly show that sFGFR2IIIc-Ap suppresses primary calvarial osteoblast proliferation and differentiation both in vitro and in vivo. Bone formation in vivo by osteoblasts expressing *sFGFR2IIIc-Ap* was completely inhibited, and bone formation by osteoblasts co-expressing *FGFR2IIIc-Ap* and *sFGFR2IIIc-Ap* was comparable to that by WT-derived cells (Fig. 3C). sFGFR2IIIc-Ap expressing osteoblasts non-specifically reduce the phosphorylation levels of the molecules that are activated in FGFR2IIIc-Ap expressing osteoblasts, which may support the idea that the S252W mutation in the *FGFR2* gene results in an increase in the receptor's affinity for ligands and in the loss of ligand specificity (Miki et al., 1992; Ornitz et al., 1996). In our previous study, conditioned media containing sFGFR2IIIc-Ap produced by COS-1 cells showed an inhibitory effect on the differentiation of MG63 cells transfected with FGFR2IIIc-Ap (Tanimoto et al., 2004). sFGFR2IIIc-Ap functions as a decoy receptor (Vorlová et al., 2011) by competing for ligand binding with endogenous FGFR2 and FGFR2IIIc-Ap. Secreted sFGFR2IIIc-Ap could also behave as an extracellular ligand trap for other FGFRs, although this will require further investigation. Taken together, our results suggest that FGFR2IIIc-Ap and sFGFR2IIIc-Ap may be useful tools for understanding the pathological processes involved in syndromic craniosynostosis.

With regard to suture formation, the primordia of the frontal and parietal bones appear in close proximity at the basolateral side of the head, extend upward to the apex of the head, possibly by osteoblast proliferation and migration, and consequently the apical osteogenic fronts meet at the midline and form the midline sutures (Kreiborg and Cohen, 1990; Iseki et al., 1997, 1999; Rice et al., 2000). It is therefore possible that the coronal suture develop during apical growth of the bones between the developing frontal and parietal bones. In the skull of a human Apert patient, the metopic sutures, anterior fontanelles and sagittal sutures are widely patent in many cases, while the coronal suture is prematurely fused (Kreiborg and Cohen, 1990, 1991). It is suggested that the S252W mutation may promote abnormal osteoblast proliferation and premature differentiation locally in lateral osteogenic fronts in the coronal suture area, and this may lead to osteogenesis which results in the fusion of the coronal suture and interrupted upward extension of the developing bone.

Acknowledgments

We thank Dr. Masaki Noda (Tokyo Medical and Dental University) for providing the ATDC5 cell line, and Dr. Kenichi Nakahama (Tokyo Medical and Dental University) for providing the TMS-14 cell line. This study was supported by Grants-in-Aid for Scientific Research (Nos. 18209060, 19406031, 21390546, and the Global (21st Century) Center of Excellence (COE) Program, International Research Center for Molecular Science in Tooth and Bone Diseases) from the Ministry of Education, Culture, Sports, Science, and Technology of Japan.

Literature Cited

Anderson J, Burns HD, Enriquez-Harris P, Wilkie AO, Heath JK. 1998. Apert syndrome mutations in fibroblast growth factor receptor 2 exhibit increased affinity for FGF ligand. Hum Mol Genet 7:1475–1483.

Banerjee C, McCabe LR, Choi J, Hiebert SW, Stein JL, Stein GS, Lian JB. 1997. Runt homology domain proteins in osteoblast differentiation: AML3/CBFA1 is a major component of a bone-specific complex. J Cell Biochem 66:1–8.

Cao YX, Jean JC, Williams MC. 2000. Cytosine methylation of an Sp1 site contributes to organ-specific and cell-specific regulation of expression of the lung epithelial gene t1α. Biochem J 350:883–890.

Chen L, Li D, Li C, Engel A, Deng CX. 2003. A Ser252Trp substitution in mouse fibroblast growth factor receptor 2 (Fgfr2) results in craniosynostosis. Bone 33:169–178.

Choi HJ, Nepal M, Park YR, Lee HK, Oh SR, Soh Y. 2011. Stimulation of chondrogenesis in ATDC5 chondroprogenitor cells and hypertrophy in mouse by Genkwadaphnin. Eur J Pharmacol 655:9–15.

Cohen MM, Jr., Kreiborg S. 1996. Suture formation, premature sutural fusion, and suture default zones in Apert syndrome. Am J Med Genet 62:339–344.

Debiais F, Lemonnier J, Hay E, Delannoy P, Caverzasio J, Marie PJ. 2001. Fibroblast growth factor-2 (FGF-2) increases N-cadherin expression through protein kinase C and Src-kinase pathways in human calvaria osteoblasts. J Cell Biochem 81:68–81.

Ducy P, Zhang R, Geoffroy V, Ridall AL, Karsenty G. 1997. Osf2/Cbfa1: A transcriptional activator of osteoblast differentiation. Cell 89:747–754.

Eswarakumar VP, Lax I, Schlessinger J. 2005. Cellular signaling by fibroblast growth factor receptors. Cytokine Growth Factor Rev 16:139–149.

Favata MF, Horiuchi KY, Manos EJ, Daulerio AJ, Stradley DA, Feeser WS, Van Dyk DE, Pitts WJ, Earl RA, Hobbs F, Copeland RA, Magolda RL, Scherle PA, Trzaskos JM. 1998. Identification of a novel inhibitor of mitogen-activated protein kinase kinase. J Biol Chem 273:18623–18632.

Garcia PV, Morita I, Murota S. 2001. Expression of adipogenesis markers in a murine stromal cell line treated with 15-deoxy delta$^{12, 14}$-prostaglandin J_2, interleukin-11, 9-cis retinoic acid and vitamin K2. Prostaglandins Leukot Essent Fatty Acids 65:215–221.

Greenblatt MB, Shim JH, Zou W, Sitara D, Schweitzer M, Hu D, Lotinun S, Sano Y, Baron R, Park JM, Arthur S, Xie M, Schneider MD, Zhai B, Gygi S, Davis R, Glimcher LH. 2010. The p38 MAPK pathway is essential for skeletogenesis and bone homeostasis in mice. J Clin Invest 120:2457–2473.

Guo X, Wang XF. 2009. Signaling cross-talk between TGF-β/BMP and other pathways. Cell Res 19:71–88.

Hajihosseini MK, Wilson S, De Moerlooze L, Dickson C. 2001. A splicing switch and gain-of-function mutation in FgfR2-IIIc hemizygotes causes Apert/Pfeiffersyndrome-like phenotypes. Proc Natl Acad Sci USA 98:3855–3860.

Holmes G, Rothschild G, Roy UB, Deng CX, Mansukhani A, Basilico C. 2009. Early onset of craniosynostosis in an Apert mouse model reveals critical features of this pathology. Dev Biol 328:273–284.
Huang CY, Lee CY, Chen MY, Tsai HC, Hsu HC, Tang CH. 2010. Adiponectin increases BMP-2 expression in osteoblasts via AdipoR receptor signaling pathway. J Cell Physiol 224:475–483.
Iseki S, Wilkie AO, Heath JK, Ishimaru T, Eto K, Morriss-Kay GM. 1997. Fgfr2 and osteopontin domains in the developing skull vault are mutually exclusive and can be altered by locally applied FGF2. Development 124:3375–3384.
Iseki S, Wilkie AO, Morriss-Kay GM. 1999. Fgfr1 and Fgfr2 have distinct differentiation- and proliferation-related roles in the developing mouse skull vault. Development 126:5611–5620.
Jabs EW, Li X, Scott AF, Meyers G, Chen W, Eccles M, Mao JI, Charnas LR, Jackson CE, Jaye M. 1994. Jackson–Weiss and Crouzon syndromes are allelic with mutations in fibroblast growth factor receptor 2. Nat Genet 8:275–279.
Kim HJ, Rice DP, Kettunen PJ, Thesleff I. 1998. FGF-, BMP- and Shh-mediated signalling pathways in the regulation of cranial suture morphogenesis and calvarial bone development. Development 125:1241–1251.
Kim HJ, Kim JH, Bae SC, Choi JY, Kim HJ, Ryoo HM. 2003. The protein kinase C pathway plays a central role in the fibroblast growth factor-stimulated expression and transactivation activity of Runx2. J Biol Chem 278:319–326.
Kitagawa M, Tahara H, Kitagawa S, Oka H, Kudo Y, Sato S, Ogawa I, Miyaichi M, Takata T. 2006. Characterization of established cementoblast-like cell lines from human cementum-lining cells in vitro and in vivo. Bone 39:1035–1042.
Kreiborg S, Cohen MM, Jr. 1990. Characteristics of the infant Apert skull and its subsequent development. J Craniofac Genet Dev Biol 10:399–410.
Kreiborg S, Cohen MM, Jr. 1991. The infant Apert skull. Neurosurg Clin N Am 2:551–554.
Mansukhani A, Bellosta P, Sahni M, Basilico C. 2000. Signaling by fibroblast growth factors (FGF) and fibroblast growth factor receptor 2 (FGFR2)-activating mutations blocks mineralization and induces apoptosis in osteoblasts. J Cell Biol 149:1297–1308.
Mansukhani A, Ambrosetti D, Holmes G, Cornivelli L, Basilico C. 2005. Sox2 induction by FGF and FGFR2 activating mutations inhibits Wnt signaling and osteoblast differentiation. J Cell Biol 168:1065–1076.
Mantha M, Jumarie C. 2010. Cadmium-induced hormetic effect in differentiated Caco-2cells: ERK and p38 activation without cell proliferation stimulation. J Cell Physiol 224:250–261.
Martínez-Abadías N, Percival C, Aldridge K, Hill CA, Ryan T, Sirivunnabood S, Wang Y, Jabs EW, Richtsmeier JT. 2010. Beyond the closed suture in Apert syndrome mouse models: Evidence of primary effects of FGFR2 signaling on facial shape at birth. Dev Dyn 239:3058–3071.
Miki T, Bottaro DP, Fleming TP, Smith CL, Burgess WH, Chan AM, Aaronson SA. 1992. Determination of ligand-binding specificity by alternative splicing: Two distinct growth factor receptors encoded by a single gene. Proc Natl Acad Sci USA 89:246–250.
Miraoui H, Marie PJ. 2010. Fibroblast growth factor receptor signaling crosstalk in skeletogenesis. Sci Signal 3:1–5.
Miraoui H, Oudina K, Petite H, Tanimoto Y, Moriyama K, Marie PJ. 2009. Fibroblast growth factor receptor 2 promotes osteognic differentiation in mesenchymal cells via extracellular-related kinase and protein kinase C signaling. J Biol Chem 284:4897–4904.
Moenning A, Jäger R, Egert A, Kress W, Wardelmann E, Schorle H. 2009. Sustained platelet-derived growth factor receptor alpha signaling in osteoblasts results in craniosynostosis by overactivating the phospholipase C-gamma pathway. Mol Cell Biol 29:881–891.
Montero JA, Gañan Y, Macias D, Rodriguez-Leon J, Sanz-Ezquerro JJ, Merino R, Chimal-Monroy J, Nieto MA, Hurle JM. 2001. Role of FGFs in the control of programmed cell death during limb development. Development 128:2075–2084.
Ornitz DM, Itoh N. 2001. Fibroblast growth factors. Genome Biol 2:3005.1–3005.12.
Ornitz DM, Xu J, Colvin JS, McEwen DG, MacArthur CA, Coulier F, Gao G, Goldfarb M. 1996. Receptor specificity of the fibroblast growth factor family. J Biol Chem 271:15292–15297.
Przylepa KA, Paznekas W, Zhang M, Golabi M, Bias W, Bamshad MJ, Carey JC, Hall BD, Stevenson R, Orlow S, Cohen MM, Jr., Jabs EW. 1996. Fibroblast growth factor receptor 2 mutations in Beare–Stevenson cutis gyrata syndrome. Nat Genet 13:492–494.
Raucci A, Bellosta P, Grassi R, Basilico C, Mansukani A. 2008. Osteoblast proliferation or differentiation is regulated by relative strength of opposing signaling pathways. J Cell Physiol 215:442–451.
Reardon W, Winter RM, Rutland P, Pulleyn LJ, Jones BM, Malcolm S. 1994. Mutations in the fibroblast growth factor receptor 2 gene cause Crouzon syndrome. Nat Genet 8:98–103.
Rice DP, Åberg T, Chan YS, Tang Z, Kettunen PJ, Pakarinen L, Maxson RE, Jr., Thesleff I. 2000. Integration of FGF and TWIST in calvarial bone and suture development. Development 127:1845–1855.
Rutland P, Pulleyn LJ, Reardon W, Baraitser M, Hayward R, Jones B, Malcolm S, Winter RM, Oldridge M, Slaney SF, Poole MD, Wilkie AO. 1995. Identical mutations in the FGFR2 gene cause both Pfeiffer and Crouzon syndrome phenotypes, Nat Genet 9:173–176.
Saito M, Handa K, Kiyono T, Hattori S, Yokoi T, Tsubakimoto T, Harada H, Noguchi T, Toyoda M, Sato S, Teranaka T. 2005. Immortalization of cementoblast progenitor cells with Bmi-1 and TERT. J Bone Miner Res 20:50–57.
Schlessinger J. 2000. Cell signaling by receptor tyrosine kinases. Cell 103:211–225.
Shiga M, Saito M, Hattori M, Torii C, Kosaki K, Kiyono T, Suda N. 2008. Characteristic phenotype of immortalized periodontal cells isolated from a Marfan syndrome type I patient. Cell Tissue Res 331:461–472.
Shukla V, Coumoul X, Wang RH, Kim HS, Deng CX. 2007. RNA interference and inhibition of MEK-ERK signaling prevent abnormal skeletal phenotypes in a mouse model of craniosynostosis. Nat Genet 39:1145–1150.
Tang QQ, Otto TC, Lane MD. 2004. Commitment of C3H10T1/2 pluripotent stem cells to the adipocyte lineage. Proc Natl Acad Sci USA 101:9607–9611.
Tanimoto Y, Yokozeki M, Hiura K, Matsumoto K, Nakanishi H, Matsumoto T, Marie PJ, Moriyama K. 2004. A soluble form of fibroblast growth factor receptor 2 (FGFR2) with S252W mutation acts as an efficient inhibitor for the enhanced osteoblastic differentiation caused by FGFR2 activation in Apert syndrome. J Biol Chem 279:45926–45934.
Vorlová S, Rocco G, Lefave CV, Jodelka FM, Hess K, Hastings ML, Henke E, Cartegni L. 2011. Induction of antagonistic soluble decoy receptor tyrosine kinases by intronic PolyA activation. Mol Cell 43:927–939.
Wang Y, Xiao R, Yang F, Karim BO, Iacovelli AJ, Cai J, Lerner CP, Richtsmeier JT, Leszl JM, Hill CA, Yu K, Ornitz DM, Elisseeff J, Huso DL, Jabs EW. 2005. Abnormalities in cartilage and bone development in the Apert syndrome $FGFR2^{+/S252W}$ mouse. Development 132:3537–3548.
Wang X, Goh CH, Li B. 2007. p38 mitogen-activated protein kinase regulates osteoblast differentiation through osterix. Endocrinology 148:1629–1637.
Wilkie AO, Slaney SF, Oldridge M, Poole MD, Ashworth GJ, Hockley AD, Hayward RD, David DJ, Pulleyn LJ, Rutland P. 1995. Apert syndrome results from localized mutations of FGFR2 and is allelic with Crouzon syndrome. Nat Genet 9:165–172.
Xiao G, Jiang D, Thomas P, Benson MD, Guan K, Karsenty G, Franceschi RT. 2000. MAPK pathways activate and phosphorylate the osteoblast-specific transcription factor, Cbfa1. J Biol Chem 275:4453–4459.
Yang F, Wang Y, Zhang Z, Hsu B, Jabs EW, Elisseeff JH. 2008a. The study of abnormal bone development in the Apert syndrome $Fgfr2^{+/S252W}$ mouse using a 3D hydrogel culture model. Bone 43:55–63.
Yang L, Clinton JM, Blackburn ML, Zhang Q, Zou J, Zielinska-Kwiatkowska A, Tang BL, Chansky HA. 2008b. Rab23 regulates differentiation of ATDC5 chondroprogenitor cells. J Biol Chem 283:10649–10657.

整形外科学分野

大川　淳

医歯学総合研究科・先端医療開発学専攻
整形外科学・教授

1）研究の課題名

脊柱靱帯骨化に対するRunxの作用に関する研究

Runx2 haploinsufficiency ameliorates the development of Ossification of the Posterior Longitudinal Ligament

後縦靱帯骨化症におけるRunx familyの役割について明らかにするため、OPLLモデルマウスttwマウスとRunx2遺伝子欠損マウスを交配し異所性骨化への影響を検討した。得られた二重変異マウスの骨化部位をμCTを用いて定量し、さらに組織学的に解析した。すると、ttwマウスでみられる異所性骨化は、Runx2 遺伝子のヘテロ欠損ttwマウスで軽減する傾向を認め、また、組織学的にも石灰化部位が減少していた。したがって、ttwマウスでみられる異所性骨化は、Runx2ヘテロ欠損で軽減し、OPLLでみられる異所性骨化にRunx2の関与が示唆された。

（現在進めている研究）

デキサメサゾンはBMPによる骨芽細胞分化、骨形成を促進する

Dexamethasone augment BMP-induced osteogenic differentiation and bone formation

ラット骨髄細胞および筋肉組織由来間葉系細胞（MSC）を10-7Mのデキサメサゾン（DEX）存在下で培養し増殖させると、細胞の増殖速度は低下するが、こうして得られた細胞にBMPを用いて骨芽細胞へ分化誘導すると、骨髄由来、筋肉由来ともに通常の培養液を用いて培養した細胞に比べて、はるかに高いアルカリフォスファターゼやオステオカルシンのmRNAの発現やアルカリフォスファターゼ活性、石灰化能を示すことを確認した。なお、BMPを用いた分化誘導期間中にも継続的にDEXを加えた方が高い骨分化能を示した。DEXにより選択的に分化能の低いMSCの増殖が抑制されたことが、このメカニズムに関与していると考えられた。また、BMPは異所性骨形成を誘導する骨誘導能を有するが、DEXにより、この骨誘導能を促進することができるか検討した。多孔質β-TCPにBMPとDEXを含浸させラット筋肉内に移植したところ、BMPのみを含浸させたものに比較して2倍以上に骨形成量が増加していた。これらの結果より、DEXはMSCを用いた骨再生やBMPを用いた骨再生の両方に有用であることが確認された。

2）研究のイラストレーション

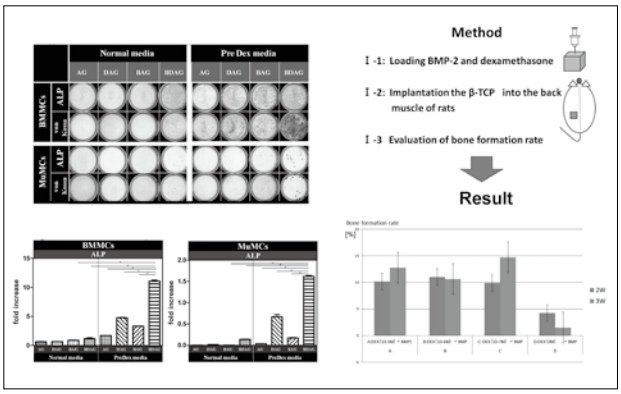

3）発表の研究内容についての英文要約

Runx2 haploinsufficiency ameliorates the development of Ossification of the Posterior Longitudinal Ligament

Ossification of the Posterior Longitudinal Ligament（OPLL）is a disease that is characterized by the ectopic calcification

of the ligament; however, the pathogenesis of OPLL remains to be investigated. We attempted to identify the in vivo role of Runx2, a master regulator of osteoblast differentiation and skeletal mineralization, in the pathogenesis of OPLL. The expression of Runx2 in the ligament was examined using in situ hybridization and immunohistochemistry and by monitoring the activity of a LacZ gene that was inserted into the Runx2 gene locus. To investigate the functional role of Runx2, we studied ENPP1ttw/ttw mice, a mouse model of OPLL, that were crossed with heterozygous Runx2 mice to decrease the expression of Runx2, and we performed histological and quantitative radiological analyses using 3D-micro CT.
Runx2 was expressed in the ligament of wild-type mice. The induction of Runx2 expression preceded the development of ectopic calcification in the OPLL-like region of the ENPP1ttw/ttw mice. Runx2 haploinsufficiency ameliorated the development of ectopic calcification in the ENPP1ttw/ttw mice.
Runx2 is expressed in an OPLL-like region, and its elevation is a prerequisite for developing the complete OPLL-like phenotype in a mouse model of OPLL.

Dexamethasone augment BMP-induced osteogenic differentiation and bone formation

Rat bone marrow derived and muscle tissue derived mesenchymal cells (MSC) proliferated in a culture medium containing 10^{-7}M dexamethasone (DEX) had much higher osteogenic differentiation capability compared to those proliferated in a standard medium, and these were confirmed by mRNA expression of alkaline phosphatase and osteocalcin, alkaline phosphatase activity and mineralization assay. In both cells, proliferation was suppressed by DEX treatment, and the suppression is thought to be one of the mechanisms of the augmentation of the differentiation capability. Dex also augmented BMP induced heterotopic bone formation in rat muscle. In beta-tricalcium phosphate scaffolds containing both BMP and DEX transplanted in rat back muscle, 2 to 2.5-fold larger bone formation was observed compared to those in scaffolds containing BMP alone.

4）本事業に関連して世界的な研究拠点形成に向けて、以下の点で改善・整備等されたこと

A（研究拠点体制）

・ 大学外との連携を図り、また研究環境（設備など）を整備することによって、研究拠点の基礎を立ち上げた（慶應義塾大学）。
・ 企業との連携（HOYA、オリンパス、日本ストライカー、メドトロニックソファモアダネック）により、研究設備の充実を図るとともに、基礎と臨床との橋渡し研究領域を充実させた。
・ 研究専門部門として寄附講座を運営

B（研究教育環境）

・ 週に3回、論文の抄読会や研究報告会を実施することにより、分子生物学、骨・軟骨組織学、骨再生学の研究、教育体制を確立した。
・ 科学研究費補助金やその他研究助成金、企業との共同研究により外部資金を得ることによって、研究環境を整備し得た。

C（人材確保）

・ 寄付講座を開設・運営し、研究に専念できる人材を確保した。
・ 3名の大学院生、2名の大学院研究生を受け入れた

D（人材育成）

・ 9名の大学院生（内留学生3名、他分野大学院生4名）および2名の大学院研究生（留学生2名）に対して、骨・軟骨に関する研究教育、指導を行った。
・ 1名の学部生（医学部医学科）に対し、5か月間、骨・軟骨に関する研究教育、指導を行った。

E（国際化）

・ 5名の留学生（大学院生および大学院研究生）に対して研究指導を行った。
・ 1名の大学院生が留学中である。

5）GCOE事業を推進するに当たって力を入れた点

・ 企業を含む大学内外との連携を強化するなどして、骨・軟骨に関する基礎領域だけでなく、臨床応用を目指した研究にも重点を置いた。
・ 分野内で研究経過・成果に関するdiscussionを重ねるとともに、外部への研究成果の発表の機会を増やすよう努力した。

6）英文原著論文

1. Aini H, Ochi H, Iwata M, Okawa A, Koga D, Okazaki M, Sano A, Asou Y. Procyanidin B3 prevents articular cartilage degeneration and heterotopic cartilage formation in a mouse surgical osteoarthritis model. PLoS One 2012;7（5）：e37728.
2. Enomoto M, Ukegawa D, Sakaki K, Tomizawa S, Arai Y, Kawabata S, Kato T, Yoshii T, Shinomiya K, Okawa A. Increase in paravertebral muscle activity in lumbar kyphosis patients by surface electromyography compared with lumbar spinal canal stenosis patients and healthy volunteers. J Spinal Disord Tech 2012 Aug;25（6）：E167-73.

3. ◎Fujita K, Iwasaki M, Ochi H, Fukuda T, Ma C, Miyamoto T, Takitani K, Negishi-Koga T, Sunamura S, Kodama T, et al. Vitamin E decreases bone mass by stimulating osteoclast fusion. Nat Med 2012 Mar 4;18（4）：589-94.
4. Hirai T, Enomoto M, Machida A, Yamamoto M, Kuwahara H, Tajiri M, Hirai Y, Sotome S, Mizusawa H, Shinomiya K, et al. Intrathecal shRNA-AAV9 inhibits target protein expression in the spinal cord and dorsal root ganglia of adult mice. Hum Gene Ther Methods 2012 Apr;23（2）：119-27.
5. Hirai T, Kato T, Kawabata S, Enomoto M, Tomizawa S, Yoshii T, Sakaki K, Shinomiya K, Okawa A. Adhesive arachnoiditis with extensive syringomyelia and giant arachnoid cyst after spinal and epidural anesthesia：A case report. Spine（Phila Pa 1976）2012 Feb 1;37（3）：E195-8.
6. Hirai T, Kawabata S, Enomoto M, Kato T, Tomizawa S, Sakai K, Yoshii T, Sakaki K, Shinomiya K, Okawa A. Presence of anterior compression of the spinal cord after laminoplasty inhibits upper extremity motor recovery in patients with cervical spondylotic myelopathy. Spine（Phila Pa 1976）2012 Mar 1;37（5）：377-84.
7. Hirai T, Okawa A, Arai Y, Takahashi M, Kawabata S, Kato T, Enomoto M, Tomizawa S, Sakai K, Torigoe I, et al. Middle-term results of a prospective comparative study of anterior decompression with fusion and posterior decompression with laminoplasty for the treatment of cervical spondylotic myelopathy. Spine（Phila Pa 1976）2011 Nov 1;36（23）：1940-7.
8. Ishii S, Kawabata S, Tomizawa S, Tomori M, Sakaki K, Shinomiya K, Sekihara K, Sato T, Adachi Y, Okawa A. Conductive neuromagnetic fields in the lumbar spinal canal. Clin Neurophysiol 2012 Aug;123（8）：1656-61.
9. Itoh H, Hara Y, Tagawa M, Kato T, Ochi H, Koga D, Okawa A, Asou Y. Evaluation of the association between runt-related transcription factor 2 expression and intervertebral disk aging in dogs. Am J Vet Res 2012 Oct;73（10）：1553-9.
10. ◎Iwasaki M, Piao J, Kimura A, Sato S, Inose H, Ochi H, Asou Y, Shinomiya K, Okawa A, Takeda S. Runx2 haploinsufficiency ameliorates the development of ossification of the posterior longitudinal ligament. PLoS One 2012;7（8）：e43372.
11. Koyanagi H, Matsumoto S, Shimoji T, Tanizawa T, Ae K, Shinomiya K, Okawa A, Kawaguchi N. Long-term results from use of pasteurized bone. J Orthop Sci 2012 Sep;17（5）：605-13.
12. Kuroiwa T, Yoshii T, Sakaki K, Inose H, Tomizawa S, Kato T, Kawabata S, Shinomiya K, Okawa A. Vertebral locking lesion following cervical spine fracture in ankylosing spondylitis. Orthopedics 2012 Jun;35（6）：e1005-8.
13. Li W, Enomoto M, Ukegawa M, Hirai T, Sotome S, Wakabayashi Y, Shinomiya K, Okawa A. Subcutaneous injections of platelet-rich plasma into skin flaps modulate proangiogenic gene expression and improve survival rates. Plast Reconstr Surg 2012 Apr;129（4）：858-66.
14. Nimura A, Kato A, Yamaguchi K, Mochizuki T, Okawa A, Sugaya H, Akita K. The superior capsule of the shoulder joint complements the insertion of the rotator cuff. J Shoulder Elbow Surg 2012 Jul;21（7）：867-72.
15. Sakai K, Okawa A, Takahashi M, Arai Y, Kawabata S, Enomoto M, Kato T, Hirai T, Shinomiya K. Five-year follow-up evaluation of surgical treatment for cervical myelopathy caused by ossification of the posterior longitudinal ligament：A prospective comparative study of anterior decompression and fusion with floating method versus laminoplasty. Spine（Phila Pa 1976）2012 Mar 1;37（5）：367-76.
16. Sakaki K, Kawabata S, Ukegawa D, Hirai T, Ishii S, Tomori M, Inose H, Yoshii T, Tomizawa S, Kato T, et al. Warning thresholds on the basis of origin of amplitude changes in transcranial electrical motor-evoked potential monitoring for cervical compression myelopathy. Spine（Phila Pa 1976）2012 Jul 1;37（15）：E913-21.
17. Sawamura C, Matsumoto S, Shimoji T, Ae K, Okawa A. Lymphadenectomy and histologic subtype affect overall survival of soft tissue sarcoma patients with nodal metastases. Clin Orthop Relat Res 2012 Sep 7.
18. Sawamura C, Matsumoto S, Shimoji T, Ae K, Tanizawa T, Gokita T, Koyanagi H, Okawa A. Indications for and surgical complications of rotationplasty. J Orthop Sci 2012 Nov;17（6）：775-81.
19. Taniyama T, Hirai T, Yamada T, Yuasa M, Enomoto M, Yoshii T, Kato T, Kawabata S, Inose H, Okawa A. Modified K-line in MRI predicts insufficient decompression of cervical laminoplasty. Spine（Phila Pa 1976）2012 Sep 13.
20. Yamada T, Yoshii T, Sotome S, Yuasa M, Kato T, Arai Y, Kawabata S, Tomizawa S, Sakaki K, Hirai T, et al. Hybrid grafting using bone marrow aspirate combined with porous beta-tricalcium phosphate and trephine bone for lumbar posterolateral spinal fusion：A prospective, comparative study versus local bone grafting. Spine（Phila Pa 1976）2012 Feb 1;37（3）：E174-9.
21. Yamada T, Yoshii T, Yoshimura H, Suzuki K, Okawa A. Upper limb amputation due to a brachial arterial embolism associated with a superior mesenteric arterial embolism：A case report. BMC Res Notes 2012 Jul 24;5：372.
22. Yamauchi Y, Jinno T, Koga D, Asou Y, Morita S, Okawa A. Comparison of different distal designs of femoral components and their effects on bone remodeling in 1-stage bilateral total hip arthroplasty. J Arthroplasty

2012 Sep;27（8）：1538-43.
23. Yoshii T, Hafeman AE, Esparza JM, Okawa A, Gutierrez G, Guelcher SA. Local injection of lovastatin in biodegradable polyurethane scaffolds enhances bone regeneration in a critical-sized segmental defect in rat femora. J Tissue Eng Regen Med 2012 Jun 20.
24. ◎Yoshii T, Yuasa M, Sotome S, Yamada T, Sakaki K, Hirai T, Taniyama T, Inose H, Kato T, Arai Y, et al. Porous/Dense composite hydroxyapatite for anterior cervical discectomy and fusion. Spine（Phila Pa 1976）2012 Dec 3.

7）総説ならびに著書

1. 加藤剛、大川淳
「【専門医のための疾患・外傷必須診療ガイド】脊椎・脊髄　日常疾患　リウマチ性脊椎炎」 関節外科 135-139　2012年
2. 大川淳
「【腰痛のサイエンス】（第9章）腰痛治療に対するエビデンス　装具療法」 脊椎脊髄ジャーナル　481-485　2012年
3. 川端茂徳、大川淳
「用語解説　電気生理学的検査編　脊髄誘発磁界」 脊椎脊髄ジャーナル　141-143　2012年
4. 王耀東、若林良明、大川淳、黒住健人、新藤正輝、松下隆
「【難治性骨折に対する治療】難治性骨折の治療（各論）　上肢骨折　Transolecranon fracture-dislocation of the elbowの治療戦略」 別冊整形外科　113-120　2012年

8）特許取得、特許申請

西村祐介、四宮謙一、早乙女進一「リン酸カルシウム含有複合多孔体及びその製造方法」特許第4925315号 2012年2月17日

9）平成24年度までの自己評価

本年度は吉井・岩崎・山田の論文が発表されたが、基礎研究に関してやや論文数が少なく、橋渡し研究、臨床研究の論文が多かった。しかし、2005年に特許を取得した多孔質複合材料の認可がおり平成25年4月1から臨床に使用可能となったので、次年度から積極的に臨床研究を進める予定である。

資金面においては、寄附講座の出資元との複数年契約が達成できず、研究者の身分を安定化できていない点も改善の余地があると考えている。

10）和文原著論文

1. 佐々木亨; 神野哲也; 麻生義則; 古賀大介; 小谷野 岳; 高田ちさと; 宗田大; 大川淳; 森田定雄 「術前プロファイリングによる人工股関節全置換術後D-dimer値予測の試み　全例にVTE予防薬は必要か」 Hip Joint, 2012
2. 大川淳; 野村徹; 高橋誠 「手術合併症に対する危険源分析Hazard and Operability Study（HAZOP Study）の経験　人工股関節置換術における神経合併症を対象として」 医療の質・安全学会誌, 2012
3. 小谷野岳; 神野哲也; 麻生義則; 古賀大介; 谷口直史; 高田ちさと; 宗田大; 大川淳; 森田定雄; 山内裕樹 「両側一期的人工股関節全置換術におけるドレーン留置の有用性に関する検討」 Hip Joint, 2012
4. 王耀東; 若林良明; 大川淳; 石突正文; 黒佐義郎 「【難治性骨折に対する治療】難治性骨折の治療（各論）下肢骨折　高齢者に発症する両側大腿骨骨幹部疲労骨折の診断・治療」 別冊整形外科, 2012
5. 若杉琢磨; 黒佐義郎; 若林良明; 大川淳 「骨欠損を伴った陳旧性DIP関節脱臼の1例」 東日本整形災害外科学会雑誌, 2012, 24
6. 請川大; 川端茂徳; 榊経平; 吉井俊貴; 富澤將司; 加藤剛; 榎本光裕; 四宮謙一; 大川淳 「圧迫性脊髄症患者に対する術中脊髄モニタリングにおけるBi-phasic刺激法とMono-phasic刺激法との比較」 脊髄機能診断学, 2012
7. 谷口直史; 神野哲也; 麻生義則; 古賀大介; 山内裕樹; 小谷野岳; 高田ちさと; 森田定雄; 宗田大; 大川淳 「Wedge-taper stemにおける骨性固定の非獲得」 Hip Joint, 2012
8. 高田ちさと; 古賀大介; 神野哲也; 麻生義則; 山内裕樹; 谷口直史; 小谷野岳; 佐々木亨; 森田定雄; 宗田大; 大川淳 「人工股関節全置換術における神経麻痺発生の危険因子の検討」 Hip Joint, 2012

11）学会発表（英文）

1. ◎Tsuyoshi Yamada; Masato Yuasa; Tomokazu Masaoka; Toshitaka Yoshii; Atsushi Okawa; Shinichi Sotome. The effect of the quality of human bone marrow mesenchymal cells（hMSCs）on bone formation. Orthopaedic Research Society 2013 Annual Meeting, San Antonio, Jan 26-29, 2013
2. ◎Masato Yuasa, Tsuyoshi Yamada, Tomokazu Masaoka, Toshitaka Yoshii, Kenichi Shinomiya, Atsushi Okawa, Shinichi Sotome. The Synergistic Effects of

Dexamethasone and BMP-2 on Osteogenesis in vitro and in vivo. Orthopaedic Research Society 2013 Annual Meeting, San Antonio, Jan 26-29, 2013

3. ◎Hirotaka Koyanagi, Shinichi Sotome, Tsuyoshi Yamada, Atsushi Okawa. Massive Bone Reconstruction with Heat-treated Bone Graft loaded Autologous Bone Marrow derived Stromal Cells and β-Tricalcium Phosphate Composites in Canine Models. Orthopaedic Research Society 2013 Annual Meeting, San Antonio, Jan 26-29, 2013

12）学会発表（和文）

1. 早乙女進一、阿江啓介、大川淳、四宮謙一、平野昌弘、石突正文、森岡秀夫; 松本誠一、中村孝志、阿部哲士、別府保男 「多孔質ハイドロキシアパタイト・コラーゲン複合体（HAp/Col）の臨床応用」 第85回日本整形外科学会学術集会　京都　2012年5月17-20日
2. 大川淳 「整形外科後期研修と大学院の位置付け」 第85回日本整形外科学会学術集会　京都　2012年5月17-20日
3. 大川淳、川端茂徳、加藤剛、富沢将司 「整形外科の手術関連有害事象の回避可能性」 第85回日本整形外科学会学術集会　京都　2012年5月17-20日
4. 請川大、川端茂徳、富沢将司、榊経平、猪瀬弘之、吉井俊貴、加藤剛、榎本光裕、大川淳 「脊椎神経鞘腫に対する腫瘍発生神経根糸刺激の筋誘発電位を用いた術中モニタリングの有効性」 第85回日本整形外科学会学術集会　京都　2012年5月17-20日
5. 川端茂徳、富沢将司、榊経平、請川大、加藤剛、榎本光裕、吉井俊貴、猪瀬弘之、大川淳 「測定シーケンス機能付き筋電計とPC用USBフットスイッチを用いた術者のみでできる半自動マルチモダリティー術中脊髄モニタリング」 第85回日本整形外科学会学術集会　京都　2012年5月17-20日
6. 澤村千草、松本誠一、阿江啓介、下地尚、谷澤泰介、五木田茶舞、小柳広高、大川淳 「リンパ節転移のある軟部肉腫患者の長期予後」 第85回日本整形外科学会学術集会　京都　2012年5月17-20日
7. 阿江啓介、下地尚、谷澤泰介、五木田茶舞、澤村千草、小柳広高、真鍋淳、黒田浩司、川口智義、大川淳、松本誠一 「軟部肉腫に対する化学療法と安全な切除縁」 第85回日本整形外科学会学術集会　京都　2012年5月17-20日
8. 坂井顕一郎、進藤重雄、水野広一、大谷和之、前原秀二、草野和生、中井修、大川淳 「頚椎後縦靭帯骨化症に対する前方骨化浮上術の長期成績」 第85回日本整形外科学会学術集会　京都　2012年5月17-20日
9. 古賀大介、神野哲也、麻生義則、谷口直史、高田ちさと、小谷野岳、川端茂徳、森田定雄、宗田大、大川淳 「人工股関節全置換術後の神経合併症に対する術中経頭蓋電気刺激筋誘発電位モニタリングの有用性と限界」 第85回日本整形外科学会学術集会　京都　2012年5月17-20日
10. 富沢将司、川端茂徳、加藤剛、吉井俊貴、大川淳 「頚椎症性脊髄症に対する選択的単一椎弓切除術と広範囲椎弓形成術の治療成績」 第85回日本整形外科学会学術集会　京都　2012年5月17-20日
11. 榊経平、川端茂徳、請川大、富沢将司、大川淳 「頚髄症患者の末梢神経刺激脊髄誘発磁界測定」 第85回日本整形外科学会学術集会　京都　2012年5月17-20日
12. 古賀大介、神野哲也、麻生義則、谷口直史、高田ちさと、小谷野岳、森田定雄、宗田大、大川淳 「術前プロファイリングによる人工股関節全置換術後VTE予防薬の必要度判定」
13. 谷口直史、神野哲也、麻生義則、古賀大介、高田ちさと、小谷野岳、森田定雄、宗田大、大川淳 「Wedge-taper stemにおける骨性固定の非獲得例」 第85回日本整形外科学会学術集会　京都　2012年5月17-20日
14. 高橋誠、田中雄二郎、大川淳 「腰椎椎間板ヘルニア手術のインフォームドコンセント実習の試み」 第85回日本整形外科学会学術集会　京都　2012年5月17-20日
15. 橋本泉智、吉井俊貴、谷山崇、山田剛史、正岡智和、猪瀬弘之、加藤剛、川端茂徳、、榎本光裕、早乙女進一、大川淳 「頚椎前方除圧固定術における緻密質、多孔質緻密質複層ハイドロキシアパタイトの有用性」 第27回日本整形外科学会基礎学術集会　名古屋　2012年10月26-27日
16. 山田剛史、早乙女進一、谷山崇、正岡智和、吉井俊貴、四宮謙一、大川淳 「骨髄由来間葉系細胞（MSC）の質　-骨形成抑制因子の同定-」 第27回日本整形外科学会基礎学術集会　名古屋　2012年10月26-27日
17. 吉井俊貴、早乙女進一、Gautya Sukotto、大川淳 「HMG-CoA還元酵素阻害薬（スタチン）の局所投与、ポリウレタン足場材料を使用した骨再生」 第27回日本整形外科学会基礎学術集会　名古屋　2012年10月26-27日
18. 吉田寛、平井高志、榎本光裕、請川円、早乙女進一、

横田隆徳、大川淳 「後根神経節でのTRPV1発現抑制による神経因性疼痛の制御」 第27回日本整形外科学会基礎学術集会　名古屋　2012年10月26-27日

19. 平井高志、榎本光裕、町田明、請川円、早乙女進一、横田隆徳、四宮謙一、大川淳 「くも膜下腔投与によるshRNA-AAV serotype9は脊髄および後根神経節における内因性標的分子の発現を抑制する」 第27回日本整形外科学会基礎学術集会　名古屋　2012年10月26-27日
20. 正岡智和、早乙女進一、湯浅将人、山田剛史、谷山崇、吉井俊貴、上坂優子、平野昌弘、森田定雄、大川淳 「多孔質ハイドロキシアパタイト・コラーゲン複合体（HAp/Col）移植による骨欠損治療後の骨形成、力学特性の評価」 第27回日本整形外科学会基礎学術集会　名古屋　2012年10月26-27日
21. 谷山崇、早乙女進一、山田剛史、正岡智和、吉井俊貴、上坂優子、平野昌弘、大川淳 「多孔質ハイドロキシアパタイト・コラーゲン複合体（HAp/Col）/BMP-2ハイブリッドの骨軟骨欠損修復に対する有効性の検討」 第27回日本整形外科学会基礎学術集会　名古屋　2012年10月26-27日
22. 朴金瑛、辻邦和、古賀大介、森田定雄、大川淳、竹田秀、麻生義則 「サーチュイン遺伝子Sirt6による軟骨代謝制御」 第27回日本整形外科学会基礎学術集会　名古屋　2012年10月26-27日
23. 岩田宗峻、越智広樹、原康、古賀大介、大川淳、麻生義則 「短期高脂肪食負荷に対するマウス膝関節の初期組織学的反応」 第27回日本整形外科学会基礎学術集会　名古屋　2012年10月26-27日
24. Hailati Aini、越智広樹、岩田宗峻、古賀大介、佐野敦志、大川淳、麻生義則 「マウス変形性膝関節症モデルにおいてプロシアニジンB3は関節軟骨を保護し、異所性骨形成を予防する」 第27回日本整形外科学会基礎学術集会　名古屋　2012年10月26-27日
25. 上坂優子、正岡智和、早乙女進一、平野昌弘、大川淳 「多孔質アパタイト・コラーゲン複合体のウサギ脛骨欠損モデルにおける骨形成・力学的強度の評価」 第32回整形外科バイオマテリアル研究会　東京　2012年12月1日

13）外部資金の獲得状況

1. 研究題目：慢性期損傷脊髄への細胞移植治療の確立とリハビリテーションの併用
   代表：榎本光裕
   期間：平成24年-
   研究費総額：¥1,400,000.-（間接経費¥420,000.-）
2. 科学研究費補助金（基盤研究C）
   研究題目：長寿遺伝子による骨代謝制御機構の解明
   代表：麻生義則
   期間：平成24年度-
   研究費総額：¥1,300,000.-（間接経費¥390,000.-）
3. 若手研究B
   研究題目：軟部肉腫治療の国際比較と再発を防ぐ治療戦略
   代表：澤村千種
   期間：平成24年度-
   研究費総額：¥2,000,000.-（間接経費¥600,000.-）
4. 若手研究B
   研究題目：緻密質、多孔質ポリウレタンを組み合わせた新しい骨欠補填材料の開発
   代表：吉井俊貴
   期間：平成24年-
   研究費総額：1,600,000.-（間接経費¥480,000.-）
5. 若手研究B
   研究題目：miRNAによる骨軟部腫瘍の発生・進展における分子制御機構
   代表：木村文子
   期間：平成23年度-平成25年度
   研究費総額：¥2,200,000.-（間接経費¥660,000.-）
6. 研究活動スタート支援
   研究題目：骨モデリングにおけるマイクロRNAの生理的意義の解明
   代表：猪瀬弘之
   期間：平成23年度-平成24年度
   研究費総額：¥2,500,000.-
7. 共同研究費（キッコーマン株式会社）
   研究題目：関節軟骨代謝に対するプロアントシアニジンとオリゴヒアルロン酸の作用に関する研究
   代表：麻生義則
   期間：平成21年度-平成25年度
   研究費総額：¥3,636,364.-（間接経費¥363,636.-）
8. 委託研究費（独立行政法人科学技術振興機構）
   研究題目：非侵襲脊髄機能イメージング装置の汎用性向上に関する研究
   代表：川端茂徳
   期間：平成24;4.1-H.24.7.31
   研究費総額：¥650,000.-（間接経費¥65,000.-）
9. 助成金（財団法人セコム科学技術振興財団）

研究題目：超伝導磁気センサーを用いた革新的な非侵襲的脊髄機能診断装置の開発。高齢者の転倒・寝たきりを防ぐ「脊髄ドック」を目指して。
代表：川端茂徳
期間：平成24年度
研究費総額：¥10,000,000.-

10. 助成金　一般社団法人　日本損害保険協会
研究題目：ハイドロキシアパタイト・コラーゲン複合体（HAp/Col）をプラスミドベクター担体として使用した遺伝子導入による骨形成促進法の開発
代表：早乙女進一
期間：平成24年-
研究費総額：¥4,950,000.-

11. 助成金　社団法人　農協共済総合研究所
研究題目：ハイドロキシアパタイト・コラーゲン複合体（HAp/Col）とBone Morphogeneticrotein（BMP）を使用した、骨軟骨欠損再生法の開発
代表：早乙女進一
期間：平成24年度
研究費総額：¥1,000,000.-

12. 助成金　（財団法人千代田健康開発事業団）
医学助成金
代表：川端茂徳
期間：平成24年度
研究費総額：¥1,000,000.-

13. 助成金　一般社団法人　日本損害保険協会
研究題目：SIP30遺伝子の制御による脊髄神経伝達効率をターゲットにした治療法の開発
代表：平井高志
期間：平成22年度-24年度
研究費総額：¥2,000,000.-

14. 助成金　日本イーライリリー株式会社
研究題目：合成ステロイドによる筋肉組織由来幹細胞の分化への影響
代表：早乙女進一
期間：平成24年度
研究費総額：¥500,000.-

15. 助成金　日本イーライリリー株式会社
研究題目：交換神経系による関節軟骨代謝制御機構の解明
代表：麻生義則
期間：平成24年度
研究費総額：¥500,000.-

14）特別講演、招待講演、シンポジウム

1. 整形外科の手術関連有害事象の回避可能性　大川淳、川端茂徳、加藤剛、富澤將司　第85回日本整形外科学会学術総会　2012.5.19　国立京都国際会館（京都市）
2. 腰椎疾患の病態と診断のポイント　第119回中部日本整形外科災害外科学会ランチョン講演　2012.10.5　ホテルフジタ福井（福井市）
3. 脊椎脊髄疾患治療の留意点　第10回日本整形外科学会脊椎脊髄病医研修会　2012.8.26　東京コンファレンスセンター品川
4. 骨粗しょう症椎体骨折に対する椎体形成術　長寿科学振興財団文京骨祖セミナー
2013.1.26　鈴木章夫記念講堂

15）教室、分野や講座の准教授、講師、助教、特別研究員、ポスドク、指導を受けた大学院生の名前

教授	大川　淳	
講師	若林　良明	
	川端　茂徳	
	阿江　啓介	
助教	加藤　剛	
	古賀　大介	
	富沢　将司	
	吉井　俊貴	
	澤村　千草	
	猪瀬　弘之	
大学院生	岩崎　牧子、小柳　広高	
	正岡　智和、平井　高志	
	湯浅　将人	
	○ 山田　剛史、請川　大	
	○ 許　レン	
	○ 馬　成山	
	○ 徐　成、請川　円	
	谷山　崇、鏑木　秀俊	
	鈴木　英嗣、角谷　智	

16）GCOE活動についての感想、コメント、改善を望む点

骨と歯の研究は本大学の根幹をなすものであり、当教室としても、今後も積極的に関与・貢献していく方針です。

LETTERS

nature medicine

Vitamin E decreases bone mass by stimulating osteoclast fusion

Koji Fujita[1,2], Makiko Iwasaki[1], Hiroki Ochi[3], Toru Fukuda[3], Chengshan Ma[1,2], Takeshi Miyamoto[4], Kimitaka Takitani[5], Takako Negishi-Koga[6], Satoko Sunamura[3], Tatsuhiko Kodama[7], Hiroshi Takayanagi[6], Hiroshi Tamai[5], Shigeaki Kato[8], Hiroyuki Arai[9], Kenichi Shinomiya[1], Hiroshi Itoh[3], Atsushi Okawa[1] & Shu Takeda[3]

Bone homeostasis is maintained by the balance between osteoblastic bone formation and osteoclastic bone resorption[1–3]. Osteoclasts are multinucleated cells that are formed by mononuclear preosteoclast fusion[1,2,4,5]. Fat-soluble vitamins such as vitamin D are pivotal in maintaining skeletal integrity. However, the role of vitamin E in bone remodeling is unknown. Here, we show that mice deficient in α-tocopherol transfer protein (*Ttpa*$^{-/-}$ mice), a mouse model of genetic vitamin E deficiency[6], have high bone mass as a result of a decrease in bone resorption. Cell-based assays indicated that α-tocopherol stimulated osteoclast fusion, independent of its antioxidant capacity, by inducing the expression of dendritic-cell–specific transmembrane protein, an essential molecule for osteoclast fusion, through activation of mitogen-activated protein kinase 14 (p38) and microphthalmia-associated transcription factor, as well as its direct recruitment to the *Tm7sf4* (a gene encoding DC-STAMP) promoter[7–9]. Indeed, the bone abnormality seen in *Ttpa*$^{-/-}$ mice was rescued by a *Tm7sf4* transgene. Moreover, wild-type mice or rats fed an α-tocopherol–supplemented diet, which contains a comparable amount of α-tocopherol to supplements consumed by many people, lost bone mass. These results show that serum vitamin E is a determinant of bone mass through its regulation of osteoclast fusion.

Bone mass is maintained constant from puberty until menopause by a balance between osteoblastic bone formation and osteoclastic bone resorption, a process called bone remodeling[1–3]. Osteoclasts are multinucleated polykaryons that develop from monocyte-lineage hematopoietic precursors through sequential steps: an initial phase of proliferation and a late phase of differentiation and maturation[1,2,10,11]. Hormones and cytokines have pivotal roles in osteoclast development. Specifically, macrophage colony-stimulating factor (M-CSF) and receptor activator of NF-κB ligand (RANKL) are indispensable for the proliferation of preosteoclasts and the differentiation and maturation of osteoclasts, respectively[1–3,12]. Among the fat-soluble vitamins A, D and K are well known for their ability to affect the skeleton[13,14], however, vitamin E was not examined well in the aspect of bone remodeling.

Vitamin E is a lipid-soluble antioxidant that inhibits lipid peroxidation by scavenging reactive oxygen species and is believed to be protective against arteriosclerotic change and the aging process[15]. Indeed, vitamin E is one of the most popular supplements in the United States; more than 10% of adults in the United States currently take vitamin E daily[16]. Vitamin E, which is a mixture of tocopherols and tocotrienols, is absorbed from food and is transported to the liver, where α-tocopherol transfer protein (α-TTP) mediates the selective transfer of α-tocopherol into lipoproteins[6]. Accordingly, α-tocopherol is the most predominant isoform of vitamin E in the body. Mice deficient in α-TTP (*Ttpa*$^{-/-}$ mice) show ataxia and infertility as a result of reduced serum α-tocopherol concentrations (**Fig. 1a**), which can be rescued by dietary supplementation with α-tocopherol[6,17].

To address the role of vitamin E in bone remodeling, we first studied *Ttpa*$^{-/-}$ mice. The *Ttpa*$^{-/-}$ mice developed a high–bone-mass phenotype in both their vertebrae and long bones as a result of a lower bone resorption compared to wild-type (WT) mice, as evidenced by a lowering of osteoclast surface and deoxypyridinoline, a bone resorption marker (**Fig. 1b–e** and **Supplementary Fig. 1**)[18]. In contrast, the amount of bone formation was unchanged in *Ttpa*$^{-/-}$ mice compared to WT mice. (**Fig. 1d**). This high–bone-mass phenotype was attributed to reduced serum concentrations of vitamin E (**Fig. 1a**) rather than the α-TTP deficiency in the body, as supplementation with α-tocopherol in the diet, which normalized the serum concentrations of α-tocopherol in *Ttpa*$^{-/-}$ mice (**Fig. 1f**), rescued the bone abnormality seen in *Ttpa*$^{-/-}$ mice (**Fig. 1g** and **Supplementary Fig. 2**). In line with this observation, *Ttpa*$^{+/-}$ mice, whose serum concentrations of α-tocopherol are between those of WT and *Ttpa*$^{-/-}$ mice[17], also had an

[1]Department of Orthopedic Surgery, Tokyo Medical and Dental University, Tokyo, Japan. [2]Global Center of Excellence (GCOE) Program, International Research Center for Molecular Science in Tooth and Bone Diseases, Tokyo Medical and Dental University, Tokyo, Japan. [3]Section of Nephrology, Endocrinology and Metabolism, Department of Internal Medicine, School of Medicine, Keio University, Tokyo, Japan. [4]Department of Orthopedic Surgery, School of Medicine, Keio University, Tokyo, Japan. [5]Department of Pediatrics, Osaka Medical College, Osaka, Japan. [6]Department of Cell Signaling, Graduate School of Medical and Dental Sciences, Tokyo Medical and Dental University, Tokyo, Japan. [7]Laboratory for Systems Biology and Medicine, University of Tokyo, Tokyo, Japan. [8]Institute of Molecular and Cellular Biosciences, University of Tokyo, Tokyo, Japan. [9]Department of Health Chemistry, Graduate School of Pharmaceutical Sciences, University of Tokyo, Tokyo, Japan. Correspondence should be addressed to S.T. (shu-tky@umin.ac.jp).

Received 14 July 2011; accepted 1 January 2012; published online 4 March 2012; corrected after print 4 May 2012; doi:10.1038/nm.2659

LETTERS

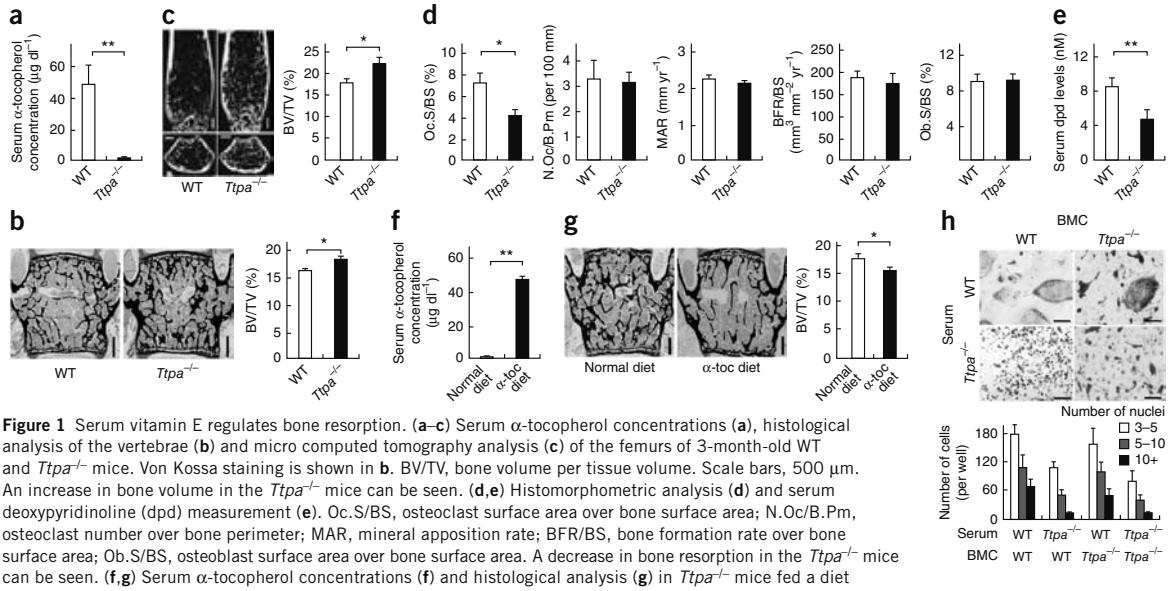

Figure 1 Serum vitamin E regulates bone resorption. (**a**–**c**) Serum α-tocopherol concentrations (**a**), histological analysis of the vertebrae (**b**) and micro computed tomography analysis (**c**) of the femurs of 3-month-old WT and *Ttpa*$^{-/-}$ mice. Von Kossa staining is shown in **b**. BV/TV, bone volume per tissue volume. Scale bars, 500 μm. An increase in bone volume in the *Ttpa*$^{-/-}$ mice can be seen. (**d**,**e**) Histomorphometric analysis (**d**) and serum deoxypyridinoline (dpd) measurement (**e**). Oc.S/BS, osteoclast surface area over bone surface area; N.Oc/B.Pm, osteoclast number over bone perimeter; MAR, mineral apposition rate; BFR/BS, bone formation rate over bone surface area; Ob.S/BS, osteoblast surface area over bone surface area. A decrease in bone resorption in the *Ttpa*$^{-/-}$ mice can be seen. (**f**,**g**) Serum α-tocopherol concentrations (**f**) and histological analysis (**g**) in *Ttpa*$^{-/-}$ mice fed a diet supplemented with α-tocopherol (α-toc diet). Von Kossa staining is shown in **g**. Scale bars, 500 μm. A decrease in bone volume as a result of the α-toc diet can be seen. (**h**) Serum α-tocopherol affects osteoclast differentiation. BMCs from the femurs of WT or *Ttpa*$^{-/-}$ mice were differentiated into osteoclasts in the presence of serum from WT or *Ttpa*$^{-/-}$ mice without addition of FBS. TRAP staining (left) and the number of osteoclasts (right) are shown. Scale bars, 50 μm. A decrease in the number of osteoclasts from WT BMCs with *Ttpa*$^{-/-}$ serum can be seen, whereas *Ttpa*$^{-/-}$ BMCs differentiated into osteoclasts normally with WT serum. $^{*}P < 0.05$, $^{**}P < 0.01$ by Tukey-Kramer testing (**b**) or Student's *t* test (**a**, **c**–**g**). All data are means ± s.e.m.

intermediate bone mass (**Supplementary Fig. 1b**). Moreover, osteoclast development *in vitro* was hampered when WT bone-marrow cells (BMCs) were cultured with the serum from *Ttpa*$^{-/-}$ mice (**Fig. 1h**), and this defect was ameliorated when this serum was supplemented with α-tocopherol or when serum from WT mice was used for the culture (**Fig. 1h** and **Supplementary Fig. 3**). In contrast, *Ttpa*$^{-/-}$ BMCs differentiated into osteoclasts normally when cultured with FBS or serum from WT mice (**Fig. 1h** and **Supplementary Fig. 3**). Thus, serum vitamin E regulates bone mass *in vivo* by affecting bone resorption.

Next, to examine the role of vitamin E in osteoclast development, we treated osteoclasts that were derived from WT BMCs and stimulated by RANKL with α-tocopherol *in vitro*. α-tocopherol stimulated osteoclast differentiation in a dose-dependent manner, as shown by an increase in the number of tartrate-resistant acid phosphatase (TRAP)-positive multinucleated osteoclasts (**Fig. 2a**), whereas the proliferation of osteoclast precursors and the survival of mature osteoclasts were unchanged by treatment with α-tocopherol (**Fig. 2b**,**c**). Osteoblastic differentiation and proliferation were not altered by α-tocopherol treatment (**Fig. 2d** and **Supplementary Fig. 4**), further indicating that vitamin E affects bone mass through osteoclasts rather than osteoblasts. Notably, α-tocopherol not only increased the generation of TRAP-positive multinucleated osteoclasts but also markedly increased the proportion of larger osteoclasts compared to the total osteoclasts (**Fig. 2e**), which indicated that vitamin E stimulated osteoclast maturation. As a result, α-tocopherol increased bone resorption by inducing the formation of additional mature osteoclasts (**Fig. 2f**).

Notably, α-tocopherol treatment administered only during the osteoclast maturation phase significantly increased osteoclast size and the number of nuclei per osteoclast (**Fig. 2e**), whereas α-tocopherol treatment administered at any other period did not have these effects (**Fig. 2e**), further indicating that vitamin E specifically affects late osteoclast maturation (that is, osteoclast fusion). Moreover, vitamin E also stimulated the generation of foreign-body giant cells, which are developed through macrophage fusion (**Fig. 2g**), further suggesting that vitamin E stimulates cell fusion. Indeed, the sizes of the TRAP-positive osteoclasts were smaller in the *Ttpa*$^{-/-}$ mice, which is in agreement with our *in vitro* observations (**Supplementary Fig. 2**). Taken together, the results suggest that vitamin E stimulates osteoclast fusion.

Because vitamin E is well known as an antioxidant[15], we next studied whether the antioxidant properties of vitamin E were indispensable for its ability to stimulate osteoclast fusion. With the exception of α-tocopherol, none of the isoforms of vitamin E, including α-tocotrienol, which is 100-fold stronger in antioxidant activity than α-tocopherol[15], stimulated osteoclast fusion (**Fig. 2h**). Moreover, except for α-tocopherol, none of the antioxidants tested, including ascorbic acid, which is the primary water-soluble antioxidant[19–22], stimulated osteoclast fusion (**Fig. 2i** and **Supplementary Fig. 5**). In line with these observations, hydrogen peroxide did not affect osteoclast fusion when it was present at a concentration that did not affect cell viability (**Supplementary Fig. 5**). Taken together, these results clearly show that, unlike other vitamin E isoforms and antioxidants, α-tocopherol specifically regulates osteoclast fusion independent of its antioxidant activity.

To address the molecular mechanism of the α-tocopherol–specific ability to stimulate osteoclast fusion, we analyzed the molecular markers of osteoclast differentiation after treatment with α-tocopherol. Among the many genes involved in osteoclast differentiation, only the expression of the differentiation marker genes, such as *Trap* and *Ctsk*[1,2,4,12], was increased, whereas the expression of other genes key for osteoclast differentiation, such as *Nfatc1* (nuclear factor of activated T cells c1)[1,2,4,12], was unchanged (**Fig. 3a**). We focused on

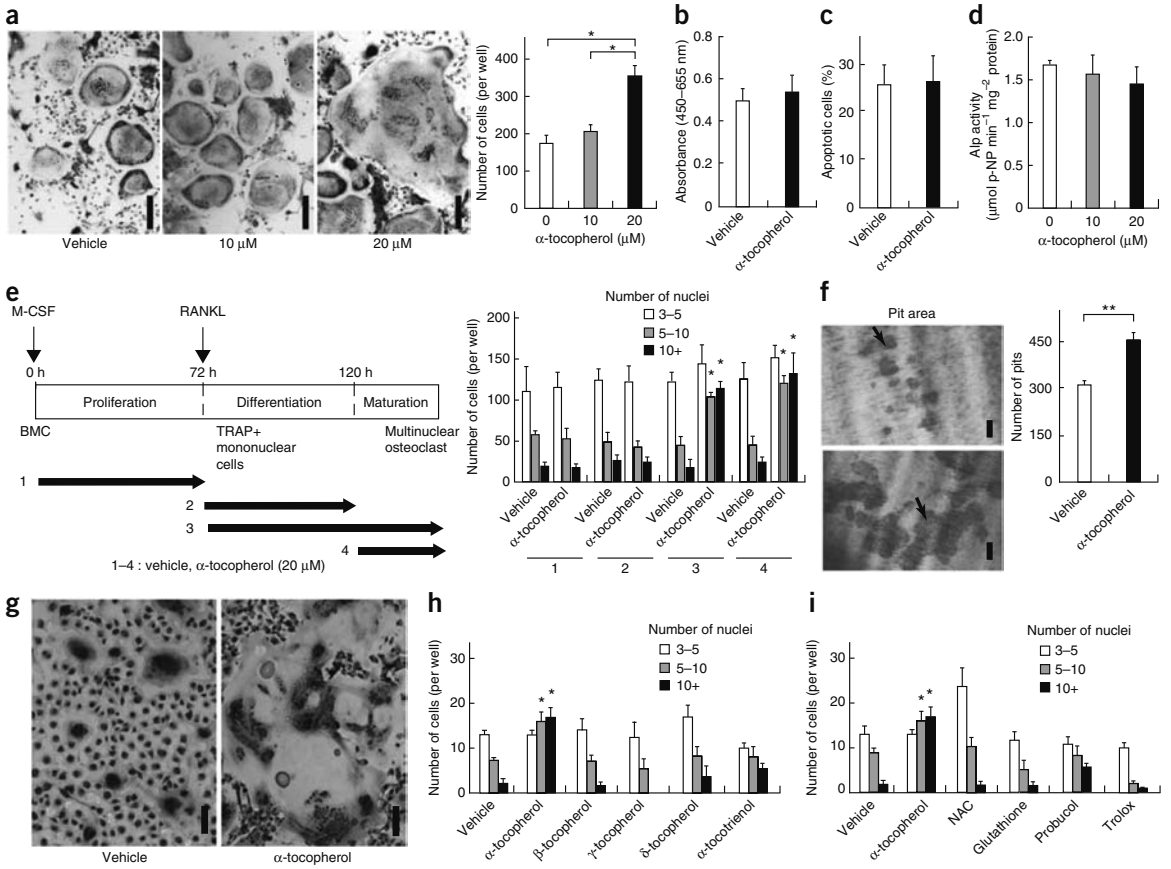

Figure 2 Vitamin E stimulates osteoclast fusion independent of its antioxidant activity. (**a**–**c**) The effect of α-tocopherol on osteoclast differentiation, proliferation and apoptosis. (**a**) BMCs were cultured with M-CSF, RANKL and 10% FBS. TRAP-stained cells (left) and the number of cells with more than three nuclei (right) are shown. An increase in osteoclasts after α-tocopherol treatment can be seen. (**b**) BrdU assay. BMCs were cultured with M-CSF, 10% FBS and α-tocopherol. (**c**) TUNEL assay. BMCs were cultured with M-CSF, RANKL and 10% FBS. (**d**) The effect of α-tocopherol on osteoblasts. An alkaline phosphatase (Alp) assay is shown. p-NP, p-nitrophenol. (**e**) The effect of α-tocopherol on osteoclast fusion. BMCs were cultured with M-CSF and RANKL, and α-tocopherol was added in the proliferation (1), differentiation (2 and 3) or maturation (3 and 4) phase. An increase in the proportion of multinucleated osteoclasts (3 and 4) can be seen. (**f**) The effect of α-tocopherol on bone resorption. A pit formation assay is shown. The eroded area (arrows, left) and the number of pits (right) are shown. BMCs were cultured on dentin with M-CSF and RANKL. α-tocopherol was added later. An increase in bone resorption can be seen. (**g**) Giant-cell progenitors from bone marrow were treated with α-tocopherol. (**h**,**i**) BMCs were cultured with M-CSF and RANKL. Vitamin E isoforms and antioxidants were added later. $*P < 0.05$, $**P < 0.01$ by Tukey-Kramer testing (**a**) or Student's *t* test (**f**,**h**,**i**). Scale bars, 50 μm. All data are means ± s.e.m.

dendritic-cell–specific transmembrane protein (DC-STAMP), a molecule essential for osteoclast fusion, because among the osteoclast-fusion–related genes[4,5], the gene encoding DC-STAMP (*Tmsf4*) was the only one whose expression was induced by α-tocopherol treatment (**Fig. 3a**). Notably, none of the other vitamin E isoforms induced *Tm7sf4* expression (**Fig. 3b**). Conversely, *Tm7sf4* expression was significantly decreased in *Ttpa*$^{-/-}$ mice, whereas expression of other fusion-related genes was unchanged, with the exception of osteoclast stimulatory transmembrane protein, which is another important molecule that is involved in osteoclast fusion (**Fig. 3c**)[23,24]. Next, to clarify the functional role of DC-STAMP in α-tocopherol–induced osteoclast fusion, we performed four sets of gain- and loss-of-function experiments for DC-STAMP. First, overexpression of *Tm7sf4* in RANKL-induced osteoclasts derived from WT mice markedly increased osteoclast fusion even in the absence of α-tocopherol (**Fig. 3d**). Conversely, although knockdown of *Nfatc1* in BMCs derived from WT mice eliminated the appearance of TRAP-positive mononuclear and multinuclear cells, knockdown of *Tm7sf4* only reduced the multinucleation of osteoclasts (that is, osteoclast fusion) (**Fig. 3e** and **Supplementary Fig. 6**), even in the presence of α-tocopherol. Moreover, osteoclast precursors isolated from *Tm7sf4*$^{-/-}$ mice did not differentiate into multinucleated osteoclasts in the presence of α-tocopherol (**Fig. 3f**). Furthermore, *Tm7sf4* transgenic mice[25] rescued the bone abnormality of the *Ttpa*$^{-/-}$ mice, as shown by a decreased bone volume accompanied by an increased bone resorption in the transgenic mice (**Fig. 3g** and **Supplementary Fig. 7**), which is consistent with the hypothesis that vitamin E induces osteoclast fusion through DC-STAMP. Taken together, these results indicate that the induction of DC-STAMP is necessary and sufficient for α-tocopherol to stimulate osteoclast fusion *in vitro* and *in vivo*.

LETTERS

Next, to gain insight into the molecular pathway of the induction of DC-STAMP by α-tocopherol, we examined whether α-tocopherol activates signaling pathways crucial for osteoclast differentiation. Among the pathways we studied, only the p38 pathway was specifically activated by α-tocopherol, as shown by the increase in phosphorylation of p38α, together with mitogen-activated protein kinase kinases 3 and 6 (Mkk3/6), a molecule that is upstream of p38α (**Fig. 4a** and **Supplementary Fig. 8**)[26]. Stimulation of p38α results in the downstream activation of the transcriptional regulator microphthalmia-associated transcription factor (Mitf)[27], an essential molecule for osteoclast maturation and fusion[1], and, indeed, treatment with α-tocopherol increased Mitf phosphorylation (**Fig. 4b**). Moreover, an antibody against Mitf immunoprecipitated the region containing the putative Mitf binding site in the *Tm7sf4* promoter (**Fig. 4c**), showing that Mitf binds to this site *in vivo*. To address the functional role of p38α and Mitf activation in α-tocopherol–induced osteoclast fusion, we knocked down *Tm7sf4* or *Mitf* in osteoclasts derived from WT mice. Knockdown of *Mapk14* (a gene encoding p38) or *Mitf* abolished the stimulatory effect of α-tocopherol on osteoclast fusion (**Fig. 4d**) and *Tm7sf4* induction (**Supplementary Fig. 6**). Conversely, overexpression of *Mapk14* significantly stimulated

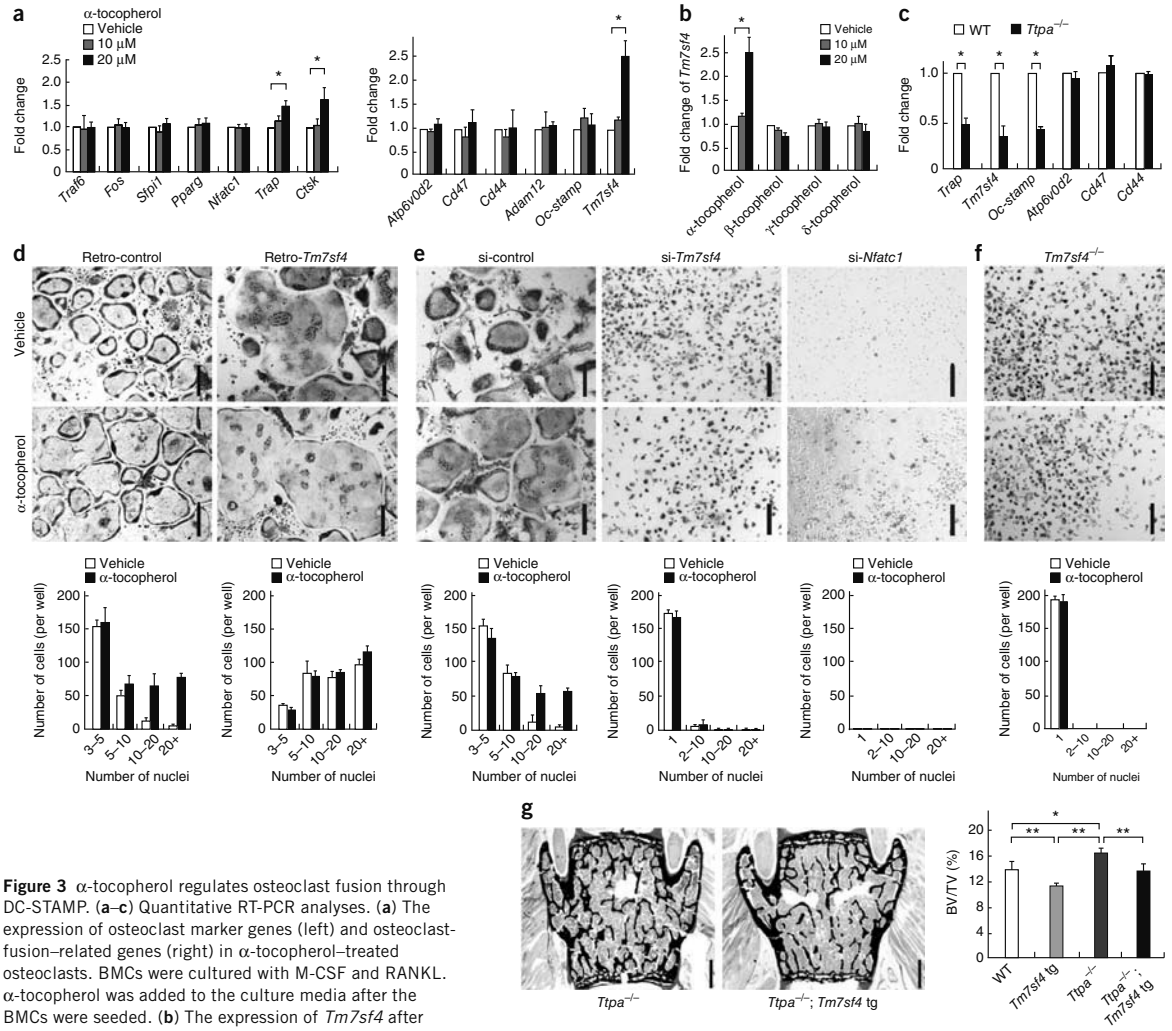

Figure 3 α-tocopherol regulates osteoclast fusion through DC-STAMP. (**a**–**c**) Quantitative RT-PCR analyses. (**a**) The expression of osteoclast marker genes (left) and osteoclast-fusion–related genes (right) in α-tocopherol–treated osteoclasts. BMCs were cultured with M-CSF and RANKL. α-tocopherol was added to the culture media after the BMCs were seeded. (**b**) The expression of *Tm7sf4* after treatment with various isoforms of vitamin E. (**c**) Expression of osteoclast-marker genes in WT and *Ttpa*$^{-/-}$ femurs. A decrease of the expression of *Tm7sf4* among the osteoclast-fusion–related genes can be seen. (**d**–**f**) DC-STAMP is essential for α-tocopherol–induced osteoclast fusion. (**d**) Retroviral overexpression of DC-STAMP. An increase in osteoclast fusion by DC-STAMP in the absence of α-tocopherol can be seen. Retro-*Tm7sf4*, retroviral overexpression of *Tm7sf4*; retro-control, retroviral overexpression of control vector. (**e**,**f**) The effect of α-tocopherol on siRNA-treated BMCs (**e**) and *Tm7sf4*$^{-/-}$ BMCs (**f**). si-control, non-targeting siRNA; si-*Tm7sf4*, siRNA to *Tm7sf4*; si-*Nfatc1*, siRNA to *Nfatc1*. A decrease in osteoclast fusion even in the presence of α-tocopherol can be seen. BMCs from WT (**d**,**e**) and *Tm7sf4*$^{-/-}$ (**f**) mice were cultured with M-CSF and RANKL. α-tocopherol was added to culture media after the BMCs were seeded. Scale bars, 50 μm. (**g**) Histological analysis of the vertebrae from WT, *Tm7sf4* transgenic (*Tm7sf4* tg), *Ttpa*$^{-/-}$ and *Ttpa*$^{-/-}$; *Tm7sf4* tg mice. Scale bars, 500 μm. $^{*}P < 0.05$, $^{**}P < 0.01$ by Tukey-Kramer testing (**a**,**b**,**g**) or Student's *t* test (**c**). All data are means ± s.e.m.

osteoclast fusion in the absence of α-tocopherol (**Fig. 4e**). These results clearly show that α-tocopherol regulates osteoclast fusion through p38α, Mitf and DC-STAMP. Currently, the molecular mechanism by which α-tocopherol induces p38α activation is unknown. A report showing that α-tocopherol succinate, which is a redox-silent analog of α-tocopherol, induces the activation of mitogen-activated protein kinase kinase kinase 5 (Ask-1)[28], which is an upstream protein kinase in the Mkk3/6-p38α pathway, suggests that α-tocopherol may use this same pathway in an antioxidant-independent manner.

Finally, to address the clinical relevance of our observations, we fed WT mice for 8 weeks with a diet containing an amount of α-tocopherol that is comparable to that found in supplements consumed by many people (**Fig. 4f**)[29]. WT mice fed a α-tocopherol–supplemented diet showed a 20% decreased bone mass after 8 weeks, with a concomitant increase in bone resorption and osteoclast size (**Fig. 4g**,**h** and **Supplementary Figs. 2** and **9**). Moreover, WT rats fed the same α-tocopherol–supplemented diet also had a 20% loss of bone mass after 8 weeks (**Fig. 4i** and **Supplementary Fig. 10**), showing that excessive intake of vitamin E is deleterious to maintaining bone mass in rodents. Notably, when WT mice were fed a diet supplemented with δ-tocopherol or antioxidants, we observed no bone loss (**Supplementary Fig. 9**), further indicating that α-tocopherol decreases bone mass independent of its antioxidant activity.

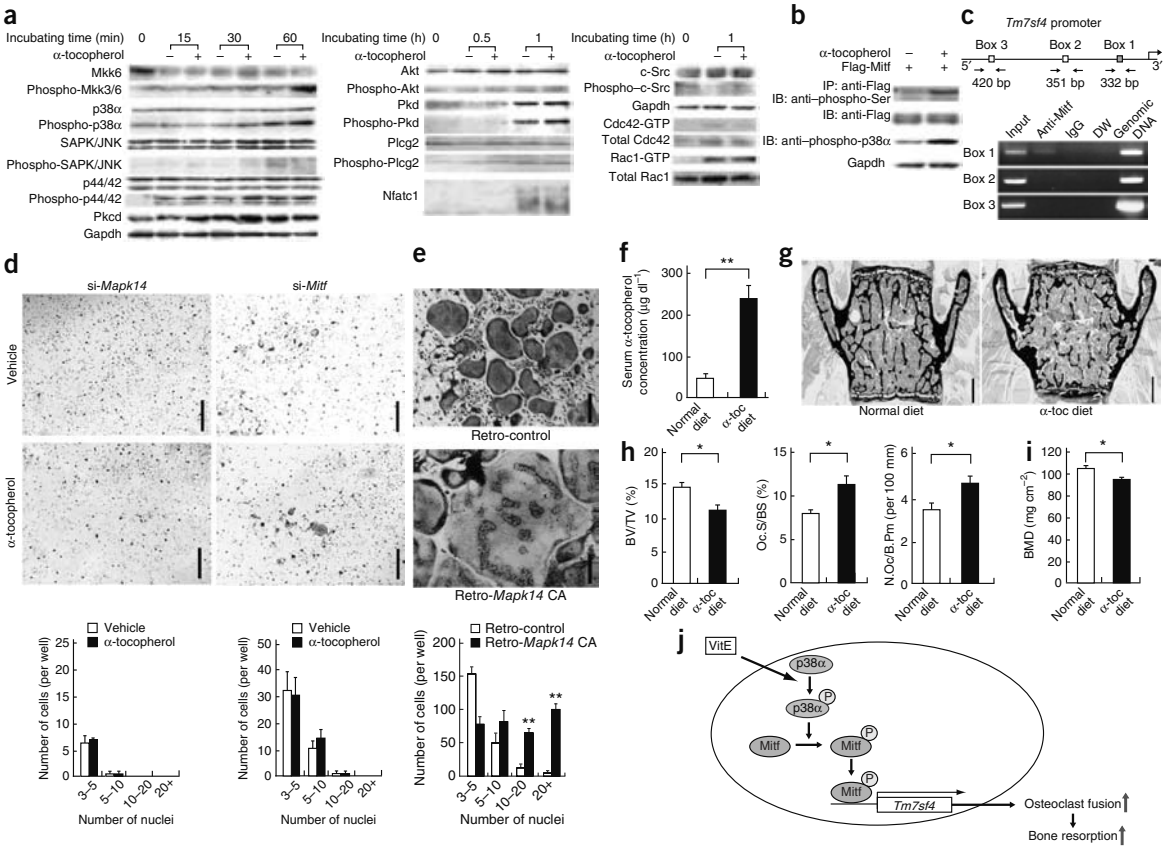

Figure 4 α-tocopherol decreases bone mass through p38α and Mitf. (**a**) Protein analysis of the α-tocopherol–treated osteoclasts. BMCs cultured with M-CSF only (left, middle) or mature osteoclasts that were induced by M-CSF and RANKL (right) were stimulated with α-tocopherol (20 μM) (– or +) and RANKL (middle right). Phospho-, phosphorylated; SAPK/JNK, mitogen-activated protein kinase 9 or mitogen-activated protein kinase 8; p44/42, mitogen-activated protein kinase 3 or cyclin-dependent kinase 20; Pkcd, protein kinase C, δ; Gapdh, glyceraldehyde-3-phosphate dehydrogenase; Akt, thymoma viral proto-oncogene 1; Pkd, protein kinase D; Plcg2, phospholipase C, γ 2; Nfatc1, nuclear factor of activated T cells, cytoplasmic, calcineurin dependent 1; c-Src, Rous sarcoma oncogene. (**b**) Immunoprecipitation analysis. An increase in the phosphorylation of p38α after treatment with α-tocopherol in p38α-expressing HEK293 cells can be seen. (**c**) Chromatin immunoprecipitation assay. Three potential binding sites (boxes 1–3) in the *Tm7sf4* promoter are shown (above). An antibody against Mitf (anti-Mitf) specifically immunoprecipitated the region containing the box 1 site of the *Tm7sf4* promoter. IgG, immunoglobulin G; DW, distilled water. (**d**,**e**) Gene knockdown (**d**) and retroviral overexpression (**e**) in osteoclasts. BMCs derived from WT mice were cultured with M-CSF and RANKL. α-tocopherol was added later. Scale bars, 50 μm. A decrease in osteoclast fusion even in the presence of α-tocopherol in BMCs treated with siRNA to *Mapk14* (si-*Mapk14*) (encoding p38α) or siRNA to *Mitf* (si-*Mitf*) (**d**) and an increase in osteoclast fusion in the absence of α-tocopherol in constitutively active p38α (*Mapk14*CA)-expressing BMCs (**e**) can be seen. (**f**–**h**) Analyses of WT mice and rats fed an α-tocopherol–supplemented diet. Serum α-tocopherol concentrations in these animals (**f**) and histological (**g**) and histomorphometric analyses (**h**). Scale bars, 500 μm. AA decrease in bone mass and an increase in bone resorption after α-tocopherol treatment can be seen. (**i**) Dual-energy X-ray absorptiometry analysis. A decrease in bone mineral density resulting from a α-tocopherol–supplemented diet. (**j**) The proposed mechanism of vitamin E (VitE)-induced osteoclastic fusion. P, phosphorylated. $^{*}P < 0.05$, $^{**}P < 0.01$ by Student's *t* test. All data are means ± s.e.m.

LETTERS

In summary, we show that vitamin E stimulates bone resorption and decreases bone mass by inducing osteoclast fusion (**Fig. 4j**). Moreover, we provide evidence that serum vitamin E is a determinant of bone mass. In contrast with our results, several reports have indicated that vitamin E participates in bone anabolism and that 6-hydroxy-2,5,7,8-tetramethylchroman-2-carboxylic acid (trolox), which is a vitamin E analog, inhibits inflammation-induced osteoclast differentiation[30–33]. In our experiments, trolox mildly inhibited osteoclast differentiation when we added it during the early osteoclast differentiation period (**Supplementary Fig. 11**), but it did not induce osteoclast fusion when we added it during the maturation phase (**Fig. 2i**). Alternatively, differences in the methodologies or the ages of the animals that were used in the previous compared to the present analyses may explain the discrepant results. In addition, several reports have shown the beneficial effects of α-tocopherol on human bone, which probably occur by reducing oxidative stress[21,34,35]. Nevertheless, most of these studies used a small sample size and were not well controlled. Given the widespread use of vitamin E, and especially α-tocopherol, as a supplement in humans, a larger, controlled study that addresses its effects on human bone is warranted.

METHODS

Methods and any associated references are available in the online version of the paper at http://www.nature.com/naturemedicine/.

Note: Supplementary information is available on the Nature Medicine website.

ACKNOWLEDGMENTS

We thank G. Karsenty, R. Baron and S. Tanaka for discussions; Y. Hotta, K. Miyamoto, H. Inose, S. Sato, A. Kimura, R. Xu and C. Xu for technical assistance; and T. Kitamura (Divisions of Cellular Therapy and Hematopoietic Factors, The Institute of Medical Science, The University of Tokyo, Tokyo, Japan) and I. Takada (Department of Microbiology and Immunology, Keio University School of Medicine, Tokyo, Japan) for plasmids. This work was supported by the Funding Program for Next Generation World-Leading Researchers (NEXT Program), grant-in-aid for scientific research from the Japan Society for the Promotion of Science, a grant for Global Center of Excellence Program from the Ministry of Education, Culture, Sports, Science and a Takeda Scientific Foundation grant.

AUTHOR CONTRIBUTIONS

K.F. conducted most of the experiments. M.I., H.O. and C.M. conducted mice analyses. T.F. and S.S. conducted *in vitro* experiments. T.M. provided DC-STAMP–related mice. K.T. and H. Tamai conducted the analyses of vitamin E serum concentrations. T.N.-K. performed western blots. H.A. provided *Ttpa*$^{-/-}$ mice. T.K. and H. Takayanagi conducted gene expression analyses. S.T., K.S., A.O. and H.I. designed the project. S.T. supervised the project and wrote most of the manuscript. S.K. designed the project.

COMPETING FINANCIAL INTERESTS

The authors declare no competing financial interests.

Published online at http://www.nature.com/naturemedicine/.
Reprints and permissions information is available online at http://www.nature.com/reprints/index.html.

1. Teitelbaum, S.L. & Ross, F.P. Genetic regulation of osteoclast development and function. *Nat. Rev. Genet.* **4**, 638–649 (2003).
2. Horne, W.C., Sanjay, A., Bruzzaniti, A. & Baron, R. The role(s) of Src kinase and Cbl proteins in the regulation of osteoclast differentiation and function. *Immunol. Rev.* **208**, 106–125 (2005).
3. Karsenty, G., Kronenberg, H.M. & Settembre, C. Genetic control of bone formation. *Annu. Rev. Cell Dev. Biol.* **25**, 629–648 (2009).
4. Lorenzo, J., Horowitz, M. & Choi, Y. Osteoimmunology: interactions of the bone and immune system. *Endocr. Rev.* **29**, 403–440 (2008).
5. Zou, W. & Teitelbaum, S.L. Integrins, growth factors, and the osteoclast cytoskeleton. *Ann. NY Acad. Sci.* **1192**, 27–31 (2010).
6. Yokota, T. *et al.* Delayed-onset ataxia in mice lacking α-tocopherol transfer protein: model for neuronal degeneration caused by chronic oxidative stress. *Proc. Natl. Acad. Sci. USA* **98**, 15185–15190 (2001).
7. Wagner, E.F. & Nebreda, A.R. Signal integration by JNK and p38 MAPK pathways in cancer development. *Nat. Rev. Cancer* **9**, 537–549 (2009).
8. Weilbaecher, K.N. *et al.* Linkage of M-CSF signaling to Mitf, TFE3, and the osteoclast defect in Mitf(mi/mi) mice. *Mol. Cell* **8**, 749–758 (2001).
9. Yagi, M. *et al.* DC-STAMP is essential for cell-cell fusion in osteoclasts and foreign body giant cells. *J. Exp. Med.* **202**, 345–351 (2005).
10. Vignery, A. Macrophage fusion: the making of osteoclasts and giant cells. *J. Exp. Med.* **202**, 337–340 (2005).
11. Bruzzaniti, A. & Baron, R. Molecular regulation of osteoclast activity. *Rev. Endocr. Metab. Disord.* **7**, 123–139 (2006).
12. Takayanagi, H. Osteoimmunology and the effects of the immune system on bone. *Nat. Rev. Rheumatol.* **5**, 667–676 (2009).
13. Kato, S. *et al.* The function of nuclear receptors in bone tissues. *J. Bone Miner. Metab.* **21**, 323–336 (2003).
14. Cockayne, S. *et al.* Vitamin K and the prevention of fractures: systematic review and meta-analysis of randomized controlled trials. *Arch. Intern. Med.* **166**, 1256–1261 (2006).
15. Azzi, A. *et al.* Specific cellular responses to α-tocopherol. *J. Nutr.* **130**, 1649–1652 (2000).
16. Radimer, K. *et al.* Dietary supplement use by US adults: data from the National Health and Nutrition Examination Survey, 1999–2000. *Am. J. Epidemiol.* **160**, 339–349 (2004).
17. Jishage, K. *et al.* α-tocopherol transfer protein is important for the normal development of placental labyrinthine trophoblasts in mice. *J. Biol. Chem.* **276**, 1669–1672 (2001).
18. Sato, S. *et al.* Central control of bone remodeling by neuromedin U. *Nat. Med.* **13**, 1234–1240 (2007).
19. Le Nihouannen, D., Barralet, J.E., Fong, J.E. & Komarova, S.V. Ascorbic acid accelerates osteoclast formation and death. *Bone* **46**, 1336–1343 (2010).
20. Ragab, A.A., Lavish, S.A., Banks, M.A., Goldberg, V.M. & Greenfield, E.M. Osteoclast differentiation requires ascorbic acid. *J. Bone Miner. Res.* **13**, 970–977 (1998).
21. Ruiz-Ramos, M., Vargas, L.A., Fortoul Van der Goes, T.I., Cervantes-Sandoval, A. & Mendoza-Nunez, V.M. Supplementation of ascorbic acid and α-tocopherol is useful to preventing bone loss linked to oxidative stress in elderly. *J. Nutr. Health Aging* **14**, 467–472 (2010).
22. Tsuneto, M., Yamazaki, H., Yoshino, M., Yamada, T. & Hayashi, S. Ascorbic acid promotes osteoclastogenesis from embryonic stem cells. *Biochem. Biophys. Res. Commun.* **335**, 1239–1246 (2005).
23. Yang, M. *et al.* Osteoclast stimulatory transmembrane protein (OC-STAMP), a novel protein induced by RANKL that promotes osteoclast differentiation. *J. Cell. Physiol.* **215**, 497–505 (2008).
24. Kim, M.H., Park, M., Baek, S.H., Kim, H.J. & Kim, S.H. Molecules and signaling pathways involved in the expression of OC-STAMP during osteoclastogenesis. *Amino Acids* **40**, 1447–1459 (2011).
25. Iwasaki, R. *et al.* Cell fusion in osteoclasts plays a critical role in controlling bone mass and osteoblastic activity. *Biochem. Biophys. Res. Commun.* **377**, 899–904 (2008).
26. Greenblatt, M.B. *et al.* The p38 MAPK pathway is essential for skeletogenesis and bone homeostasis in mice. *J. Clin. Invest.* **120**, 2457–2473 (2010).
27. Steingrimsson, E. *et al.* Mitf and Tfe3, two members of the Mitf-Tfe family of bHLH-Zip transcription factors, have important but functionally redundant roles in osteoclast development. *Proc. Natl. Acad. Sci. USA* **99**, 4477–4482 (2002).
28. Zu, K., Hawthorn, L. & Ip, C. Up-regulation of c-Jun–NH2-kinase pathway contributes to the induction of mitochondria-mediated apoptosis by α-tocopheryl succinate in human prostate cancer cells. *Mol. Cancer Ther.* **4**, 43–50 (2005).
29. Miller, E.R. III *et al.* Meta-analysis: high-dosage vitamin E supplementation may increase all-cause mortality. *Ann. Intern. Med.* **142**, 37–46 (2005).
30. Lee, J.H. *et al.* Trolox prevents osteoclastogenesis by suppressing RANKL expression and signaling. *J. Biol. Chem.* **284**, 13725–13734 (2009).
31. Arjmandi, B. *et al.* Vitamin E improves bone quality in the aged but not in young adult male mice. *J. Nutr. Biochem.* **13**, 543 (2002).
32. Mehat, M.Z., Shuid, A.N., Mohamed, N., Muhammad, N. & Soelaiman, I.N. Beneficial effects of vitamin E isomer supplementation on static and dynamic bone histomorphometry parameters in normal male rats. *J. Bone Miner. Metab.* **28**, 503–509 (2010).
33. Shuid, A.N., Mehat, Z., Mohamed, N., Muhammad, N. & Soelaiman, I.N. Vitamin E exhibits bone anabolic actions in normal male rats. *J. Bone Miner. Metab.* **28**, 149–156 (2010).
34. Chuin, A. *et al.* Effect of antioxidants combined to resistance training on BMD in elderly women: a pilot study. *Osteoporos. Int.* **20**, 1253–1258 (2009).
35. Ostman, B. *et al.* Oxidative stress and bone mineral density in elderly men: antioxidant activity of α-tocopherol. *Free Radic. Biol. Med.* **47**, 668–673 (2009).

ONLINE METHODS

Animals. We purchased the C57BL/6J mice from the Charles River Laboratory and Oriental Yeast, and we purchased the Wister rats from CLEA Japan. *Ttpa*$^{-/-}$, *Tm7sf4*$^{-/-}$ and *Tm7sf4* transgenic mice were previously described[6,9,25]. We crossed *Ttpa*$^{-/-}$ and *Tm7sf4* transgenic mice to obtain *Ttpa*$^{-/-}$; *Tm7sf4* transgenic mice. We fed the mice a diet supplemented with α-tocopherol (600 mg per kg of food; Sigma) from 4–12 weeks of age, and we fed the rats the same diet from 6–14 weeks of age. The α-tocopherol–supplemented diet was made by CLEA Japan. We analyzed seven or eight mice in each group. We maintained all animals under a 12-h light-dark cycle with *ad libitum* access to food and water. All animal experiments were performed with the approval of the Animal Study Committee of Tokyo Medical and Dental University and conformed to the relevant guidelines and laws.

Dual X-ray absorptiometry analyses. We measured the bone mineral density of the femurs of all animals by DCS-600 (ALOKA), as previously described[18]. We examined at least eight mice for each group.

Histological and histomorphometric analyses. We injected mice with calcein (25 mg per kg of body weight; Sigma) and stained the undecalcified sections of the lumbar vertebrae using von Kossa and TRAP, as previously described[18,36]. We performed static and dynamic histomorphometric analyses using the OsteoMeasure Analysis System (OsteoMetrics); the Oc.S/BS and N.Oc/B.pm values were calculated for the slices that stained positive for TRAP. We analyzed seven or eight mice in each group.

Cell culture. *In vitro* osteoclast differentiation was accomplished as previously described[18]. Briefly, BMCs of 6–8-week-old mouse femurs were cultured in minimum essential medium α supplemented with FBS in the presence of human M-CSF (10 ng ml^{-1}; R&D Systems) for 3 d and then differentiated into osteoclasts using human RANKL (50 ng ml^{-1}; PeproTech) and M-CSF for 3 d. The osteoclast culture using mouse serum is decribed in detail in the **Supplementary Methods**. The pit formation assay, BrdU assay and TUNEL assay were performed as previously described[18], and the details are described in the **Supplementary Methods**. The foreign-body giant-cell culture was established as previously described[37]. Briefly, BMCs were collected in DMEM (Sigma) with 10% FBS. Cells were stimulated with interleukin-4 (IL-4) (10 ng ml^{-1}) for 48 h, fixed and stained with May-Grünwald-Giemsa for evaluation. The *in vitro* primary osteoblast culture was established as previously described[38,39] (**Supplemntary Methods**). α-tocopherol was added to the culture media at 20 μM or at the indicated concentrations. Other vitamin E isoforms were added at 20 μM, N-acetylcysteine was added at 2 mM, glutathione was added at 5 mM, probucol was added at 5 μM and trolox was added at 200 μM. We cultured all cells in triplicate or quadruplicate wells and repeated each experiment more than three times. Additional details are given in the **Supplementary Methods**.

Transfection and retroviral infection. A total of 20 nM siRNA (Invitrogen) was transfected into BMCs derived from the femurs of WT mice using HiPerFect (QIAGEN). After transfection, cells were cultured using the same methods as those used for the osteoclast differentiation. Complementary DNA (cDNA) of *Tm7sf4* was cloned from osteoclasts using PCR. The constitutively active form of p38α was obtained from Addgene. Retrovirus was produced by the retroviral vector pMXs-IRES-GFP system, which was based on Moloney murine leukemia virus, as previously described[40]. Briefly, we collected the virus produced by packaging cells after 2 d of transfection. BMCs were infected with the retrovirus for 2 d in the presence of M-CSF. After 2 d of infection, cells were stimulated by RANKL to differentiate into osteoclasts. The details are described in the **Supplementary Methods**.

Quantitative RT-PCR analyses. To acquire RNA from mouse bones, we flushed bone marrow out of the femurs with PBS and used the bones as previously described[18]. RNA was extracted using TRIzol (Invitrogen), and reverse transcription was performed for cDNA synthesis using a High Capacity cDNA Reverse Transcription Kit (Applied Biosystems). We performed quantitative analyses of gene expression using the Mx3000P Real-Time PCR System (Stratagene). We examined the gene expressions in triplicate or quadruplicate individually and repeated each experiment more than three times.

Protein analyses. We collected cell lysate protein using radioimmunoprecipitation assay buffer with a phosphatase inhibitor cocktail (Nacalai) and the Complete Mini protease inhibitor cocktail (Roche). To detect RAS-related C3 botulinum substrate 1 (Rac1) and cell division cycle 42 (Cdc42) expression, we used Active GTPase Pull-Down and Detection kits (Thermo Scientific). For detecting the phosphorylation of Mitf, we used Anti-Flag M2 Affinity beads (Sigma), horseradish peroxidase–conjugated M2 antibody to Flag (1:1,000; Sigma) and antibody to phopshorylated serine (1:1,000; Millipore). Further details are given in the **Supplementary Methods**. We examined the expressions individually and repeated each experiment more than three times.

Chromatin immunoprecipitation (ChIP). We used ChIP-IT Express Chromatin Immunoprecipitation Kits (Active Motif), following the manufacturer's instructions. Briefly, we cultured BMCs from WT mice for 2 d. Cells were crosslinked with 0.4% formaldehyde, and the reaction was stopped by adding glycine. Fixed cells were resuspended in lysis buffer and sonicated for 5 min (with cycles of 30 s on and 30 s off). The supernatant was used immediately for ChIP experiments.

Statistical analyses. We performed statistical analyses using Tukey-Kramer testing for multiple comparisons and Student's *t* tests for two-group comparisons. Values were considered statistically significant at $P < 0.05$. All data are means ± s.e.m. Results are representative of more than four individual experiments.

Additional methods. Detailed methodology is described in the **Supplementary Methods**.

36. Kimura, A. *et al.* Runx1 and Runx2 cooperate during sternal morphogenesis. *Development* **137**, 1159–1167 (2010).
37. McNally, A.K., Macewan, S.R. & Anderson, J.M. Foreign body-type multinucleated giant cell formation requires protein kinase C β, δ, and ζ. *Exp. Mol. Pathol.* **84**, 37–45 (2008).
38. Ducy, P. *et al.* Leptin inhibits bone formation through a hypothalamic relay: a central control of bone mass. *Cell* **100**, 197–207 (2000).
39. Inose, H. *et al.* A microRNA regulatory mechanism of osteoblast differentiation. *Proc. Natl. Acad. Sci. USA* **106**, 20794–20799 (2009).
40. Kitamura, T. *et al.* Retrovirus-mediated gene transfer and expression cloning: powerful tools in functional genomics. *Exp. Hematol.* **31**, 1007–1014 (2003).

doi:10.1038/nm.2659

ERRATA

Erratum: Vitamin E decreases bone mass by stimulating osteoclast fusion

Koji Fujita, Makiko Iwasaki, Hiroki Ochi, Toru Fukuda, Chengshan Ma, Takeshi Miyamoto, Kimitaka Takitani, Takako Negishi-Koga, Satoko Sunamura, Tatsuhiko Kodama, Hiroshi Takayanagi, Hiroshi Tamai, Shigeaki Kato, Hiroyuki Arai, Kenichi Shinomiya, Hiroshi Itoh, Atsushi Okawa & Shu Takeda

Nat. Med. **18, 589–594 (2012); published online 4 March 2012; corrected after print 4 May 2012**

In the version of this article initially published, it was incorrectly stated that the mice were fed a diet supplemented with α-tocopherol at 600 mg per kg of body weight. Instead, the food itself contained 600 mg of α-tocopherol per kg. The error has been corrected in the HTML and PDF versions of the article.

膠原病・リウマチ内科学分野

宮坂 信之

医歯学総合研究科・生体環境応答学系専攻
膠原病・リウマチ内科学・教授

1）研究の課題名

A; 新規関節炎治療法の開発及び作用機序解析

New therapeutic strategy of rheumatoid arthritis; combination therapy of cell cycle regulation and cytokine inhibition

1. 関節リウマチ治療における細胞周期制御・抗炎症併用療法の有効性の検討

関節リウマチ（RA）における滑膜炎には、免疫細胞の浸潤とサイトカイン産生を主体とする炎症相と、滑膜細胞の増殖によるパンヌス形成に代表される増殖相の2つの側面がある。炎症相に注目した抗サイトカイン療法は実臨床でも高い有効性を示したが、免疫抑制などの副作用がある。われわれは増殖相に注目し、CDK4/6阻害による細胞周期制御療法が関節炎の動物モデルに著効することを示してきたが、過量のCDK4/6特異的阻害薬（CDKI）には一過性ながら骨髄抑制作用がある。本研究の目的は、抗サイトカイン療法とCDKI治療の併用によって治療効果が高まり、潜在的な副作用が軽減するか検討することである。方法としては、DBA1/JマウスをⅡ型コラーゲン（CⅡ）とCFAで免疫し、関節炎を発症させ関節炎スコアと組織像、骨破壊像で評価した。CDKIの用量依存性の治療効果と末梢血・骨髄有核細胞数への影響を評価した。抗マウスIL-6受容体抗体（抗IL-6R-Ab）とCDKIの単独療法・併用療法の治療効果を評価し、抗CⅡ抗体価やCⅡ特異的T細胞応答への影響を検討した。治療実験の結果では、低用量のCDKIと抗IL-6R-Abとの併用療法は単独療法より高い有効性を示し、高用量のCDKIと同等の有効性を示した。骨髄抑制作用は高用量CDKIのみでみられた。治療後の血清、脾細胞を用いて検討したCⅡへの免疫応答には影響はみられなかった。本成果は二つの異なる分子標的治療が協調的効果を初めて示すものであり、RAに対するdual targeting therapyによって、副作用を抑えつつ、高い治療効果を得ることができた。

2. 抗マウスTREM-1リガンド抗体作用機序解析及びヒトTREM-1リガンドの同定

Triggering receptor expressed on myeloid cells（TREM）-1は、マクロファージや好中球に発現し、その刺激はToll様受容体刺激による炎症性サイトカインの分泌を増幅させる。一方、TREM-1阻害は感染防御に必要な炎症性サイトカインを温存しつつ炎症を抑制することが示唆されている。我々は重症感染のリスクの少ない抗リウマチ薬の開発を目指し、これまでに、TREM-1の関節リウマチ患者滑膜細胞での発現、及びTREM-1細胞外ドメインIg融合蛋白（TREM-1-Ig）投与によるコラーゲン誘導関節炎（CIA）マウスでの治療効果を報告した。さらに、B細胞上にマウスTREM-1リガンド（TREM-1-L）を同定し、抗TREM-1-L抗体投与によるCIAでの治療効果を検討してきた。しかし、同抗体が刺激性あるいは拮抗性か作用機序は不明であった。また、B細胞に発現するヒトTREM-1-Lは未知であり、TREM-1阻害療法を臨床応用するために、その同定が必要とされている。本研究では抗マウスTREM-1-L抗体のCIAでの作用機序及解明びB細胞上のヒトTREM-1-Lの同定を行った。その結果、in vitroでは、抗TREM-1-L抗体架橋によりTREM-1-L強制発現細胞でのtyrosineのリン酸化はほとんど認められなかった。一方、マクロファージとB細胞の共培養系での抗TREM-1-L抗体の添加ではTNF-α産生は減少した。これらより抗TREM-1-L抗体によるCIA治療効果は拮抗性作用によるものと考えられた。ヒトPBMC cDNAライブラリーからは、発現クローニングによりB細胞に発現するヒトTREM-1-Lを同定した。現在同分子の機能について解析中である。

3. リゾフォスファチジン酸受容体1（LPA1）欠損による関節炎抑制

Lysophosphatidic acid receptor 1（LPA1）is essential for development of arthritis.

リゾフォスファチジン酸（LPA）は生理活性を有す

る脂質メディエーターであり、LPA受容体（$LPA_{1\text{-}6}$）を介して作用する。我々はこれまでに関節リウマチ（RA）滑膜組織でLPA_1発現が上昇し、LPA_1阻害剤がマウスコラーゲン関節炎（CIA）を抑制する事、更にLPA_1阻害により$CD11b^+$細胞の滑膜への遊走及び破骨細胞やTh17細胞分化が抑制される事を見出した。LPA_1の関節炎における機能をより明確にする為、LPA_1遺伝子欠損（KO）マウス、野生型（WT）マウスをII型コラーゲンで免疫しCIA発症を解析したところ、LPA1 KOマウスでは関節炎は全く発症しなかった。また、$CD11b^+$脾細胞をCIAマウスへ移入し、滑膜に浸潤した細胞数を計測したが、LPA_1 KO由来の$CD11b^+$脾細胞は、WTと比較してCIA滑膜組織への浸潤が有意に抑制された。骨髄細胞をRANKL+M-CSFで刺激して破骨細胞分化を解析したところ、LPA_1 KO由来骨髄細胞からの破骨細胞分化は低下していた。さらに$CD4^+$ naïve T細胞をTh1/Th2/Th17分化条件下で培養後、Th分化をFACSを用いて解析した。LPA_1 KO由来T細胞からのTh1, Th2細胞への分化には変化を認めなかったが、Th17細胞分化は抑制された。以上より$LPA\text{-}LPA_1$シグナルは炎症細胞浸潤、破骨細胞分化、Th17分化に関与し、関節炎発症に不可欠である事が示唆された。

4. 関節リウマチの病態形成におけるCCL25/CCR9相互作用の関与

Interaction between CCL25 and CCR9 might play important roles in the pathogenesis of rheumatoid arthritis

CCL25は、CCR9を介してリンパ球や単球/マクロファージに対する走化因子として作用する。CCL25/CCR9相互作用は炎症細胞遊走により関節リウマチ（RA）の病態形成に関与している可能性があると考え、RA滑膜におけるCCL25、CCR9の発現、またその相互作用阻害による関節炎抑制効果を検討した。RA滑膜組織におけるCCL25、CCR9の発現を免疫染色にて解析したところ、CCL25、CCR9ともに、RA滑膜組織において変形性関節症と比較して発現の亢進がみられ、蛍光二重染色にてCCL25はマクロファージ、線維芽細胞様滑膜細胞（FLS）に、CCR9はマクロファージ、樹状細胞、FLSにそれぞれ発現していた。マウスコラーゲン関節炎（CIA）に関節炎発症前よりCCR9阻害薬を投与し、関節炎抑制効果を解析したところ、関節炎スコア、滑膜組織への炎症細胞浸潤、骨破壊の程度が有意に抑制された。関節炎発症後からのCCR9阻害薬投与においても、関節炎スコアの抑制を認めた。また、in vitroにおいて、CCL25刺激はRA由来のFLSからのIL-6、MMP-3産生亢進を誘導した。CCL25刺激により末梢血単球からのIL-6産生亢進もみられ、M-CSF+RANKL併存下での破骨細胞分化も促進された。CCL25/CCR9相互作用はFLSや単球/マクロファージからの炎症性メディエーター産生、破骨細胞誘導などにも関与し、新たな関節炎治療の標的となることが示唆された。

5. Am80によるCandida albicans water-soluble fraction誘導血管炎の抑制効果

Am80 ameliorates murine model of vasculitis via suppression of neutrophil and endothelial cell activation

レチノイドはレチノイン酸受容体に結合し生理活性を示す化合物の総称であり、急性前骨髄球性白血病の治療薬として用いられている。またレチノイドには、Th1、Th17分化を抑制するなどの免疫調節作用が知られている。一方、血管炎症候群に対する治療は副腎皮質ステロイド薬や免疫抑制薬が中心であるが、治療抵抗例や感染症等の副作用が問題となる場合があり、より有効で安全な治療法の開発が求められている。我々は、CAWS（Candida albicans water-soluble fraction）の投与によりマウスの冠動脈に血管炎を惹起するモデルを用いて、合成レチノイドであるAm80による血管炎抑制効果を解析した。Balb/cマウスにCAWSを5日間腹腔内投与し、CAWS投与開始時と同時に、またはCAWS投与開始1週後（血管炎発症後）より、Am80 4 mg/kgを経口投与し、5週間後に冠動脈を観察したところ、ともに病理学的に血管炎の抑制効果を認めた。血管炎の局所には著明な好中球浸潤がみられたため、in vitroで好中球に対するAm80の作用を検討した。Am80はヒト末梢血好中球において、PMA、Pam3CSK4、LPS刺激による活性酸素産生、fMLPに対する遊走、fMLP及びcytochalasin Bによるエラスターゼ放出を抑制し、fMLP及びLPSによるERK、p38のリン酸化を抑制した。またAm80はヒト臍帯静脈内皮細胞からのIL-6、MCP-1産生の抑制作用も認めた。Am80は好中球や血管内皮細胞の活性化抑制により、血管炎を抑制したと考えられた。Am80は血管炎に対する新たな治療法となる可能性が示唆された。

6. リウマチ性疾患における免疫抑制療法の安全性に関する研究

Safety of immunosuppressive treatment in patients with rheumatic diseases

リウマチ性疾患における免疫抑制療法の安全性を評価するため、三つの研究を行った。第一に、「日本における生物学的製剤使用関節リウマチ患者に関する疫学研究（REAL研究）」のデータベースを用いて韓国漢陽大学との

共同研究を行い、日本と韓国の関節リウマチ患者におけるTNF阻害薬の安全性を比較した。その結果、重篤有害事象の発現リスクは日本で相対的に高いことが明らかとなった。第二に、「生物学的製剤使用関節リウマチ患者の長期安全性研究（SECURE研究）」のデータ収集を継続し、生物学的製剤使用患者約19000例のデータベースを作成し、生物学的製剤使用が、RA患者の発癌リスク（固形癌および悪性リンパ腫）を上昇させないという昨年度の結果を確認した。第三に、免疫抑制療法を開始するリウマチ性疾患患者約800名の前向きコホートを用いて、治療開始から1年以内の肺感染症発現リスクを検討し、高齢、喫煙、血清クレアチニン値、初期副腎皮質ステロイド投与量が有意なリスク因子であることを明らかにした。これらの研究に加えて、TNF阻害薬の安全性の経年的変化、抗IL-6受容体抗体であるトシリズマブとTNF阻害薬の安全性の比較などを開始し、来年度も継続する予定である。

B：多発性筋炎・皮膚筋炎（PM/DM）の病態解析と新規治療法開発

Analysis of polymyositis/dermatomyositis pathology and development of new treatments

1. 多発性筋炎・皮膚筋炎における筋力低下に対する治療法の開発

PM/DM患者の筋力低下は、日常生活動作を障害する。このような筋力低下の遷延は、原疾患にステロイド筋症を併発するなどした複合的要因で筋萎縮が進行することが原因と考えられる。そこで我々は、筋萎縮に対する効果が報告されている分岐鎖アミノ酸（BCAA）を用いて、多発性筋炎モデルマウスの筋萎縮と筋力低下に対する有効性を評価した。方法は、我々の開発したC protein誘導型筋炎モデルマウス（CIMマウス）を用い、筋炎治療の第一選択薬であるPrednisolone（PSL）を単剤もしくはBCAAと併用して連日経口投与し、免疫後20日目にgrip testによって前肢筋力を測定した。その結果、CIMマウスでは、組織学的スコア高値に示される筋炎の発症に伴い、筋重量と筋線維断面積の減少ならびに筋力の低下が認められた。21日目の組織学的スコアでは、BCAA併用の有無に関わらずPSLの投与により抑制された。一方で、筋重量と筋線維断面積の低下は、PSL単剤では効果が得られず、BCAAの併用によって予防された。これと対応して、筋力低下においてもPSLは単剤では効果がなく、BCAAの併用によって予防された。このことから、BCAAには筋炎に起因する筋萎縮に対して予防効果があることが示された。

2）研究のイラストレーション

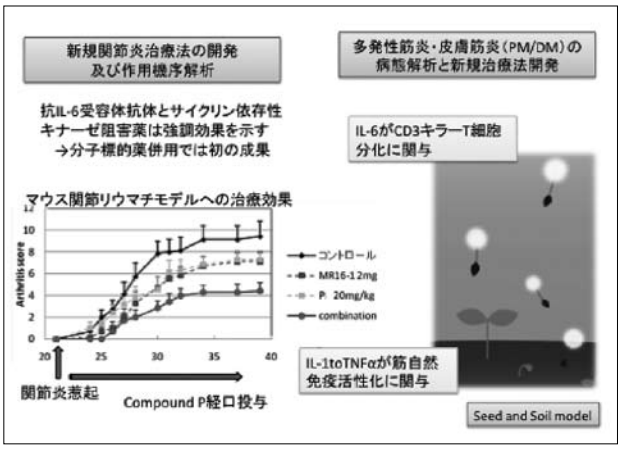

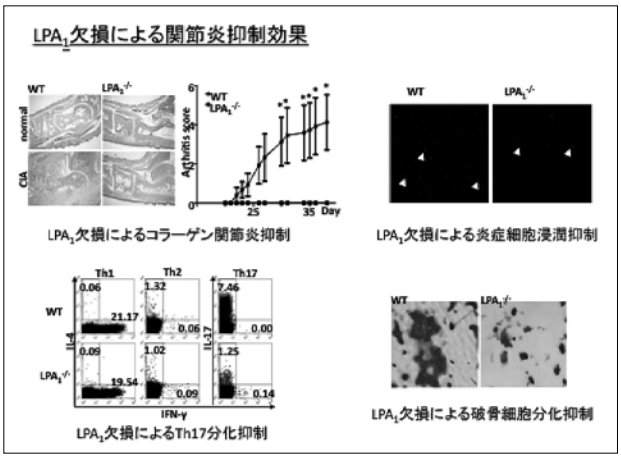

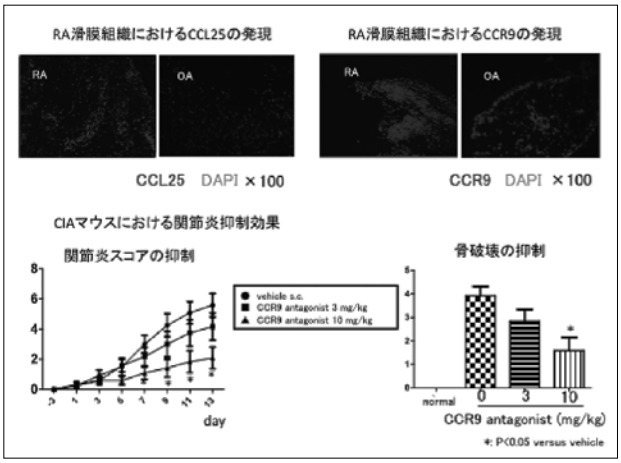

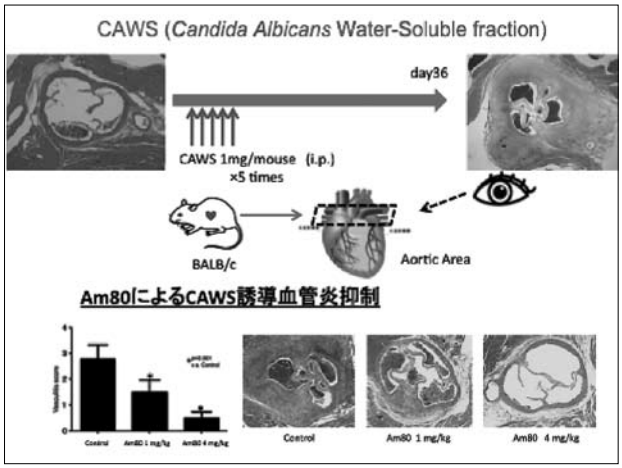

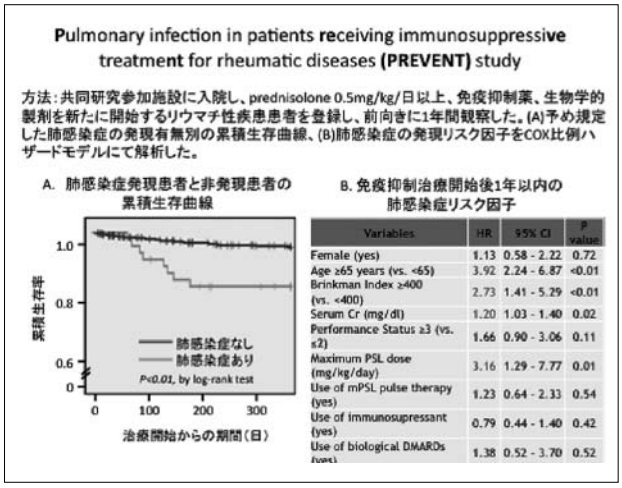

3）発表の研究内容についての英文要約

Arthritis research

1. p16INK4a exerts an anti-inflammatory effect through accelerated IRAK1 degradation in macrophages

Induction of cyclin-dependent kinase (CDK) inhibitor gene p16INK4a into the synovial tissues suppresses rheumatoid arthritis in animal models. The present study was conducted to discern how p16INK4a modulates macrophages, which are the major source of inflammatory cytokines in inflamed synovial tissues. We found that p16INK4a suppresses LPS-induced production of IL-6 but not of TNF-a from macrophages. The results of this study demonstrated that p16INK4a promotes ubiquitin-dependent IRAK1 degradation, impairs AP-1 activation, and suppresses IL-6 production. Thus, p16INK4a senescence gene upregulation inhibits inflammatory cytokine production in macrophages in a different way than in RSF.

2. Identification of murine TREM-1 ligand as a therapeutic target of arthritis

TREM-1 blockade is reported to suppress pathological inflammation with maintaining inflammatory cytokine production for physiological protection against microbes. We identified the TREM-1 ligand molecule and generated blocking anti-TREM-1-ligand monoclonal antibody. Administration of this antibody ameliorated collagen-induced arthritis of mice. The TREM-1 blockade in Rheumatoid Arthritis patients will be a new anti-rheumatic therapy that is less associated with a risk of infection than the current treatments.

3. Identification of crucial microRNA in rheumatoid arthritis

We analyzed the role of 954 kinds of microRNAs in the proliferation and activation of synovial fibroblasts derived from rheumatoid arthritis by using microRNA inhibitor library. We identified the crucial microRNAs in the pathogenesis of rheumatoid arthritis. We are now analyzing the mechanisms of each microRNAs in the pathogenesis of rheumatoid arthritis.

4. Safety of Immunosuppressive treatment in patients with rheumatic diseases

We performed three studies to establish safety of immunosuppressive treatment in patients with rheumatic diseases in Japan. First, we collaborated with Hanyang University in South Korea and implemented a comparative study about safety of treatment with tumor necrosis factor inhibitors (TNFi) in patients with rheumatoid arthritis (RA) between Japan and Korea. Using the registry of Japanese rheumatoid arthritis patients for long-term safety (REAL) database and RESEARCh database of Hanyang University, we demonstrated higher risk for serious adverse events in Japanese patients with RA given TNF inhibitors compared to Korean RA patients. Second, we continued enrollment of patients and collecting data for safety of biologics in clinical use in Japanese patients with rheumatoid arthritis in long-term (SECURE), and enrolled about 19,000 RA patients. We confirmed our finding that use of biological DMARDs did not increase risk for malignancy including solid cancers and malignant lymphoma. Third, we implemented pulmonary infection in patients receiving immunosuppressive treatment for rheumatic diseases (PREVENT) study, a prospective cohort study of 766 patients with rheumatic diseases who started immunosuppressive treatment, and identified risk factors for development of pulmonary infections during the first year of the treatment; older age, smoking, elevated serum creatinine level, and higher initial dose of glucocorticoid. In addition to these studies, we started to investigate 1) changes in safety profiles of TNF inhibitors over time and 2) comparison of safety profiles of TNF inhibitors and tocilizumab, an IL-6 receptor inhibitor.

Myositis research

1. T Lymphocytes and muscle condition act like seeds and soil in a murine polymyositis model

C protein-induced myositis（CIM）we established is similar to polymyositis（PM）in pathology except that it undergoes spontaneous remission. Interestingly, intradermal injection of complete Freund’s adjuvant（CFA）at footpads re-induced myositis. Moreover, myositis was inducible only in the legs treated with CFA. Thus, the regression should be attributable to attenuation of the CFA-induced local immune activation. Requirement of the local immune activation was confirmed by the adoptive transfer model, where T cells from CIM mice provoked myositis only when transferred to recipients treated with CFA or other toll-like receptor（TLR）ligands at the footpads. Anti-cytokine antibody treatment of the transfer model revealed that IL-1 and TNF-α account for the muscle tissues activation. Myositis development requires activation of autoaggressive T cells and conditioning of the muscle tissues.

2. Activation of autoaggressive T cells in PM/DM

Control of autoaggressive T cells is another obvious target in treatment of PM, in which killer T cells are important in the pathology. Instead of suppressing all T cells, we have explored suppressing subset of T cells expressing molecules that are important for killer T cell activity. In vivo and in vitro experiments have shown promising results.

4）GCOE事業を推進するに当たって力を入れた点

From Clinic to Benchを目標に、グローバルスタンダードの臨床研究を行う。

5）英文原著論文

1. Enosawa S, Yamazaki T, Kohsaka H, Tokiwa T. Repopulation of human origin hepatocyte progenitor-like cell line, THLE-5b, in Scid mouse liver under p21-mediated cell growth arresting condition. Cell Transplantation 21（2-3）：447-452, 2012
2. ◎代表論文Sugihara T, Okiyama N, Watanabe N, Miyasaka N and Kohsaka H. IL-1 and TNF-α blockade for treatment of experimental polymyositis. Arthritis Rheum 64（8）：2655-2662, 2012
3. Hasegawa H, Kohsaka H, Takada K, Miyasaka N. Renal involvement in chronic hypertrophic pachymeningitis associated with myeloperoxidase antineutrophil cytoplasmic antibody-positive granulomatosis with polyangiitis. J Rheumatol 39（10）：2053-2055, 2012
4. ◎代表論文Murakami Y, Mizoguchi F, Saito T, Miyasaka N, Kohsaka H. p16INK4a exerts an anti-inflammatory effect through accelerated IRAK1 degradation in macrophages. J Immunol 189（10）：5066–5072, 2012
5. ◎代表論文Okiyama N, Sugihara T, Oida T, Ohata J, Yokozeki H, Miyasaka N, Kohsaka H. T lymphocytes and muscle condition act like seeds and soil in a murine polymyositis model. Arthritis Rheum（in press）
6. Matsubara T, Yamana S, Tohma S, Takeuchi T, Kondo H, Kohsaka H, Ozaki S, Hashimoto H, Miyasaka N, Yamamoto A, Hiraoka M, Abe T. Phase I study in Japanese rheumatoid arthritis patients evaluating the safety, tolerability and efficacy of abatacept Mod Rheumatol（in press）
7. Ohta A, Nagai M, Nishina M, Tomimitsu H, Kohsaka H. Age at onset and gender distribution of systemic lupus erythematosus, polymyositis/dermatomyositis and systemic sclerosis in Japan Mod Rheumatol（in press）
8. Nakasato M, Kohsaka H, Mizutani T, Watanabe G, Taya K, Nagaoka K Pregnancy-associated plasma protein（PAPP）-A expressed in the mammary gland controls epithelial cell proliferation and differentiation. Endocrine（in press）
9. ◎ Matsuo Y, Mizoguchi F, Kohsaka H, Ito E, Eishi Y, Miyasaka N. Tocilizumab-induced immune complex glomerulonephritis in a patient with rheumatoid arthritis. Rheumatol（in press）
10. ◎ Umezawa N, Kohsaka H, Nanki T, Watanabe K, Tanaka M, Shane PY, Miyasaka N. Successful treatment of Eosinophilic granulomatosis with polyangiitis（EGPA; formerly Churg-Strauss syndrome）with rituximab in a case refractory to glucocorticoids, cyclophosphamide, and IVIG. Modern Rheumatol（in press）
11. Fukuda S, Nanki T, Morio T, Hasegawa H, Koike R, Miyasaka N. Recurrent mitral valve regurgitation with neutrophil infiltration in a patient with multiple aseptic abscesses. Mod Rheumatol（in press）
12. Miyabe C, Miyabe Y, Miura NN, Takahashi K, Terashima Y, Toda E, Honda F, Morio T, Yamagata N, Ohno N, Shudo K, Suzuki J, Isobe M, Matsushima K, Tsuboi R, Miyasaka N, Nanki T. Am80, a retinoic acid receptor agonist, ameliorates murine vasculitis through the suppression of neutrophil migration and activation. Arthritis Rheum（in press）
13. Yamazaki H, Nanki T, Harigai M, Miyasaka N. Successful treatment of refractory Takayasu arteritis with tacrolimus. J Rheumatol 39（7）：1487, 2012.
14. ◎Suzuki F, Kubota T, Miyazaki Y, Ishikawa K, Ebisawa M, Hirohata S, Ogura T, Mizusawa H, Imai T, Miyasaka N, Nanki T. Serum level of soluble CX3CL1/fractalkine is elevated in patients with polymyositis and dermatomyositis, which is correlated with disease activity. Arthritis Res Ther 14（2）：R48, 2012.
15. Komano Y, Yagi N, Onoue I, Kaneko K, Miyasaka N, Nanki T. Arthritic joint-targeting small interfering RNA-encapsulated liposome：Implication for treatment

strategy for rheumatoid arthritis. J Pharmacol Exp Ther 340（1）：109, 2012.
16. Takeuchi T, Harigai M, Tanaka Y, Yamanaka H, Ishiguro N, Yamamoto K, Miyasaka N, Koike T, Kanazawa M, Oba T, Yoshinari T, Baker D; the GO-MONO study group. Golimumab monotherapy in Japanese patients with active rheumatoid arthritis despite prior treatment with disease-modifying antirheumatic drugs：results of the phase 2/3, multicentre, randomised, double-blind, placebo-controlled GO-MONO study through 24 weeks.Ann Rheum Dis. in press.
17. Harigai M, Takamura A, Atsumi T, Dohi M, Hirata S, Kameda H, Nagasawa H, Seto Y, Koike T, Miyasaka N. Elevation of KL-6 serum levels in clinical trials of tumor necrosis factor inhibitors in patients with rheumatoid arthritis：a report from the Japan College of Rheumatology Ad Hoc Committee for Safety of Biological DMARDs. Mod Rheumatol. in press.
18. Takamura A, Hirata S, Nagasawa H, Kameda H, Seto Y, Atsumi T, Dohi M, Koike T, Miyasaka N, Harigai M. A retrospective study of serum KL-6 levels during treatment with biological disease-modifying antirheumatic drugs in rheumatoid arthritis patients：a report from the Ad Hoc Committee for Safety of Biological DMARDs of the Japan College of Rheumatology. Mod Rheumatol. in press.
19. Sakai R, Tanaka M, Nanki T, Watanabe K, Yamazaki H, Koike R, Nagasawa H, Amano K, Saito K, Tanaka Y, Ito S, Sumida T, Ihata A, Ishigatsubo Y, Atsumi T, Koike T, Nakajima A, Tamura N, Fujii T, Dobashi H, Tohma S, Sugihara T, Ueki Y, Hashiramoto A, Kawakami A, Hagino N, Miyasaka N, Harigai M; for the REAL Study Group.Drug retention rates and relevant risk factors for drug discontinuation due to adverse events in rheumatoid arthritis patients receiving anticytokine therapy with different target molecules. Ann Rheum Dis 71（11）：1820-6, 2012
20. Sakai R, Komano Y, Tanaka M, Nanki T, Koike R, Nagasawa H, Amano K, Nakajima A, Atsumi T, Koike T, Ihata A, Ishigatsubo Y, Saito K, Tanaka Y, Ito S, Sumida T, Tohma S, Tamura N, Fujii T, Sugihara T, Kawakami A, Hagino N, Ueki Y, Hashiramoto A, Nagasaka K, Miyasaka N, Harigai M; Real Study Group. Time-dependent increased risk for serious infection from continuous use of tumor necrosis factor antagonists over three years in patients with rheumatoid arthritis. Arthritis Care Res 64（8）：1125-34, 2012
21. Tanaka M, Sakai R, Koike R, Komano Y, Nanki T, Sakai F, Sugiyama H, Matsushima H, Kojima T, Ohta S, Ishibe Y, Sawabe T, Ota Y, Ohishi K, Miyazato H, Nonomura Y, Saito K, Tanaka Y, Nagasawa H, Takeuchi T, Nakajima A, Ohtsubo H, Onishi M, Goto Y, Dobashi H, Miyasaka N, Harigai M. Pneumocystis jirovecii pneumonia associated with etanercept treatment in patients with rheumatoid arthritis：a retrospective review of 15 cases and analysis of risk factors. Mod Rheumatol. in press.
22. Harigai M, Takeuchi T, Tanaka Y, Matsubara T, Yamanaka H, Miyasaka N. Discontinuation of adalimumab treatment in rheumatoid arthritis patients after achieving low disease activity. Mod Rheumatol. in press.
23. Kobayashi S, Harigai M, Mozaffarian N, Pangan AL, Sharma S, Brown LS, Miyasaka N. A multicenter, open-label, efficacy, pharmacokinetic, and safety study of adalimumab in Japanese patients with ankylosing spondylitis. Mod Rheumatol 22（4）：589-97, 2012
24. Tanaka Y, Harigai M, Takeuchi T, Yamanaka H, Ishiguro N, Yamamoto K, Miyasaka N, Koike T, Kanazawa M, Oba T, Yoshinari T, Baker D; GO-FORTH Study Group. Golimumab in combination with methotrexate in Japanese patients with active rheumatoid arthritis：results of the GO-FORTH study. Ann Rheum Dis 71（6）：817-24, 2012
25. Watanabe K, Sakai R, Koike R, Sakai F, Sugiyama H, Tanaka M, Komano Y, Akiyama Y, Mimura T, Kaneko M, Tokuda H, Iso T, Motegi M, Ikeda K, Nakajima H, Taki H, Kubota T, Kodama H, Sugii S, Kuroiwa T, Nawata Y, Shiozawa K, Ogata A, Sawada S, Matsukawa Y, Okazaki T, Mukai M, Iwahashi M, Saito K, Tanaka Y, Nanki T, Miyasaka N, Harigai M. Clinical characteristics and risk factors for Pneumocystis jirovecii pneumonia in patients with rheumatoid arthritis receiving adalimumab：a retrospective review and case – control study of 17 patients. Mod Rheumatol. in press.
26. Miyasaka N, Hara M, Koike T, Saito E, Yamada M, Tanaka Y; Additional Members of the GB-0998 Study Group. Effects of intravenous immunoglobulin therapy in Japanese patients with polymyositis and dermatomyositis resistant to corticosteroids：a randomized double-blind placebo-controlled trial. Mod. Rheumatol. 22（3）：382-393, 2012
27. Takeuchi T, Miyasaka N, Tatsuki Y, Yano T, Yoshinari T, Abe T, Koike T. Inhibition of plasma IL-6 in addition to maintenance of an efficacious trough level of infliximab associated with clinical remission in patients with rheumatoid arthritis：analysis of the RISING Study. Ann. Rheum. Dis. 71（9）：1583-5, 2012
28. Takeuchi T, Matsubara T, Nitobe T, Suematsu E, Ohta S, Honjo S, Abe T, Yamamoto A, Miyasaka N; The Japan Abatacept Study Group. Phase II dose-response study of abatacept in Japanese patients with active rheumatoid arthritis with an inadequate response to methotrexate. Mod. Rheumatol. 2012 Jun 9 [Epub ahead of print]

29. Takeuchi T, Miyasaka N, Zang C, Alvarez D, Fletcher T, Wajdula J, Yuasa H, Vlahos B. A phase 3 rancomized, double-blind, multicenter comparative study evaluating the effect of etanercept versus methotrexate on radiographic outcomes, disease activity, and safety in Japanese subjects with active rheumatoid arthritis. Mod. Rheumatol. 2012 Sep 26. [Epub ahead of print]

6）総説ならびに著書

1. 宮坂信之：サイトカインとは 「臨床免疫・アレルギー科」増刊号 57-（21）：2-6, 2012
2. 宮坂信之：MTX投与量成人用量改訂でRA治療はどう変わりますか？ RAVIGATOR臨床医へのRA治療関連アンケート 「Arthritis－運動器疾患と炎症－」10（1）：57-64, 2012
3. 宮坂信之：関節リウマチの治療は可能か？「内科」109（4）：
4. 宮坂信之：関節リウマチ（内科）「今日の治療指針」2013.年版
5. 宮坂信之、立石睦人、阿部香織、片山一朗：座談会/膠原病診療のこつ 特集：最新の膠原病診療－そのパラダイムシフト 「日本医師会雑誌」140（11）：2277-2290, 2012
6. 渡部香織、宮坂信之：関節リウマチ 「medicina」48（11）：502-506, 2012
7. 田中良哉、竹内勤、山中寿、針谷正祥、宮坂信之：2010年関節リウマチ新分類基準とその臨床応用 ACR/EULAR提案のRA診断基準について 「臨床リウマチ」
8. 渡部香織、宮坂信之：ステロイドは感染症を誘発・悪化させるか?
9. 酒井良子、宮坂信之：ホルモン製剤（副腎皮質ホルモン）「臨床栄養」別冊JCNセレクト
10. 座談会：日常診療における関節リウマチ治療薬の選択と使い方.宮坂信之、天野宏一、長坂憲治、中村敦夫特集関節リウマチ診療update—これだけは知っておきたい知識とは？ 内科 109（4）：667-681, 2012
11. 宮坂信之：関節リウマチ治療における光と影 「日本医事新報」
12. 宮坂信之：関節リウマチの治療は変わった! 「週刊朝日臨時増刊号」
13. 宮坂信之：関節リウマチ rheumatoid arthritis.「免疫・アレルギー疾患の分子標的と治療薬事典」田中良哉編集 羊土社
14. 上阪等 サイクリン依存性キナーゼ阻害薬 医学のあゆみ 240（7）, 591-595, 2012
15. 上阪等 滑膜線維芽細胞を標的とした治療法の開発 最新医学67（2）, 281-286, 2012
16. 溝口史高、上阪等 関節リウマチにおけるmiRNAの役割 日本臨床免疫学会会誌 35（1）, 69-74, 2012
17. 岩井秀之、上阪等 新規関節炎治療標的としてのTriggering receptor expressed in myeloid cells-1 阻害 日本臨床免疫学会会誌 35（1）, 81-86, 2012
18. 上阪等 関節リウマチはどのようにおこるのか からだの科学 273：16-19, 2012
19. 上阪等 多発筋炎・皮膚筋炎 マウスモデル Clinical Neuroscience 30（3）：309-312, 2012
20. 上阪等 サイトカインと疾患-炎症性筋疾患- 臨床免疫・アレルギー科 57（suppl. 21）：744-748, 2012
21. 細矢匡、上阪等 CDK阻害薬の発見から臨床応用の可能性まで 炎症と免疫 20（3）：60-65, 2012
22. 上阪等 膠原病内科から見た皮膚筋炎の診断・治療 Visual Dermatology 11（8）：818-821, 2012
23. 上阪等 皮膚筋炎の自己抗体 皮膚科診療 34（9）：822-827, 2012
24. 上阪等 多発性筋炎/皮膚筋炎 感染 炎症 免疫 43（2）, 271-273, 2012
25. 上阪等 臨床免疫学総論 内科学 門脇孝、永井良三総編集 370-371頁 西村書店 2012年7月24日
26. 上阪等 多発性筋炎/皮膚筋炎 最新内科学 内科学 門脇孝、永井良三 総編集 1259-1261頁 西村書店 2012年7月24日
27. 上阪等 三科で診る多発性筋炎・皮膚筋炎 多発性筋炎・皮膚筋炎–その包括的理解 上阪 等 編集 1-5頁 医歯薬出版社 2012年9月20日
28. 上阪等 多発性筋炎・皮膚筋炎 希少疾患/難病の診断・治療と製品開発 817-822頁 技術情報協会 2012年10月31日

7）特許取得、特許申請

① 2012年2月6日 日本国特許出願 特発性炎症性筋疾患の予防または治療剤 （出願番号：特願2012-023521）cf. BCAA
② 2012年3月21日 日本国特許出願 特発性炎症性筋疾患の予防又は治療剤 （出願番号：特願2012-063595）cf. DNAM-1
③ 2012年4月11日 日本国特許出願 TREM-1活性阻害剤 （出願番号：特願2012-90422）

8）平成24年度までの自己評価

関節リウマチの病態及び治療法の開発研究を動物モデル及び患者検体を用いて多角的に行い、グローバルスタンダードに合致する研究成果を挙がることができた。また、関節リウマチの疫学研究、pharmacovigilance研究などについても我が国から世界に向けて情報発信をすることができた。また、筋炎研究においては、主として動物モデルを用いた研究により、病態形成分子機構、新規治療法の開発に貢献をした。

9）和文原著論文

齋藤鉄也、南木敏宏、溝口史高、上阪等、宮坂信之
メトトレキサート肺炎やニューモシスチス肺炎の鑑別を要した関節リウマチの一例　東京内科医会会誌　28(1)：41-44, 2012

10）学会発表（英文）

1. ◎ Hideyuki Iwai, Tadashi Hosoya, Yousuke Murakami, Nobuyuki Miyasaka, Hitoshi Kohsaka. Identification of the TREM-1 ligand as a therapeutic target of arthritis. Keystone Symposium Rheumatoid Arthritis：Molecular and Clinical Insights January 19-24, 2012, Santa Fe
2. ◎ Fumiraka Mizoguchi, Nobuyuki Miyasaka, Hitoshi Kohsaka. MiRNA-31 Controls Cytoskeleton Organization of Osteoclasts by Targeting RhoA. Keystone Symposium Rheumatoid Arthritis：Molecular and Clinical Insights January 19-24, 2012, Santa Fe
3. ◎ Hitoshi Kohsaka, Naoko Okiyama, Naoki Kimura, Nobuyuki Miyasaka. Seed and soil model of autoimmunity-Lessons learned from a new polymyositis model of mice- 21st International Rheumatology Symposium April 26-28, 2012 Tokyo
4. Ran Nakashima, Yoshitaka Imura, Minae Seto, Akihiro Murakami, Yuji Hosono, Kizuku Watanabe, Tomohiro Handa, Michiaki Mishima, Michito Hirakata, Tsutomu Takeuchi, Keishi Fujio, Kazuhiko Yamamoto, Hitoshi Kohsaka, Yoshinari Takasaki, Noriyuki Enomoto, Kingo Chida, Toshihiro Nukiwa and Tsuneyo Mimori. A New Enzyme-Linked Immunosorbent Assay System for Detecting Autoantibodies to Aminoacyl-tRNA Synthetases：Clinical Usefulness in Myositis and Interstitial Pneumonia. American College of Rheumatology 76th National Meeting, Washington DC, Georgia, November 10-14, 2012
5. Jinhyun Kim, Jiyong Choi, Sung Hae Chang, Ki Chul Shin, Sung-Hye Park, Hye Won Kim, Hye Jin Oh, Myeong Jae Yoon, Bong Seung Ku, Eun Young Lee, Eun Bong Lee, Hiroshi Kawachi, Hitoshi Kohsaka and Yeong Wook Song. The Effect of CXCL10 Blockade in C Protein-Induced Myositis. American College of Rheumatology 76th National Meeting, Washington DC, Georgia, November 10-14, 2012

（以上、全てポスター）

6. Miyabe C, Miyabe Y, Miura NN, Takahashi K, Terashima Y, Toda E, Honda F, Morio T, Yamagata N, Ohno N, Shudo K, Suzuki J, Isobe M, Matsushima K, Tsuboi R, Miyasaka N, Nanki T. Am80, a retinoic acid receptor agonist, ameliorates murine vasculitis through the suppression of neutrophil migration and activation. 第76回アメリカリウマチ学会。口頭。Washington DC, USA, 2012年11月
7. Nanki T, Onoue I, Nagasaka K, Hirata S, Hosoya T, Ebisawa M, Sugihara T, Harigai M, Miyasaka N. Anti-IL-6 autoantibody inhibited elevation of serum C-reactive protein level in two patients with severe bacterial infection. ヨーロッパリウマチ学会。示説。Berlin, Germany, 2012年6月
8. Miyabe C, Miyabe Y, Miura NN, Takahashi K, Terashima Y, Morio T, Ohno N, Shudo K, Yamagata N, Suzuki K, Suzuki J, Matsushima K, Tsuboi R, Miyasaka N, Nanki T. Am80 ameliorates murine model of vasculitis via suppression of neutrophil and endothelial cell activation. The Asia Pacific Meeting of Vasculitis and ANCA Workshop 2012.口頭。Tokyo. 2012年3月
9. Yamazaki H, Nanki T, Harigai M, Miyasaka N. Successful treatment of corticosteroid-resistant Takayasu arteritis with tacrolimus. The Asia Pacific Meeting of Vasculitis and ANCA Workshop 2012.示説。Tokyo. 2012年3月
10. Miyabe Y, Miyabe C, Iwai Y, Ebisawa M, Miyasaka M, Miyasaka N, Nanki T. Autotaxin and Lysophosphatidic Acid Receptors：Potential Target Molecules in New Therapies for Rheumatoid Arthritis. Keystone Symposia, Chemokines and Leukocyte Trafficking in Homeostasis and Inflammation.示説。Breckenridge, CO, USA, 2012年1月
11. Sakai R, Tanaka M, Nanki T, Yamazaki H, Watanabe K, Koike R, Miyasaka N, Harigai M, on behalf of the REAL Study Group. Different risk factors are associated with serious infection in rheumatoid arthritis patients with and without pulmonary comorbidities; analyses from the REAL database. The European League Against Rheumatism（EULAR）2012, 示説, Berlin, 2012.06
12. Takeuchi T, Harigai M, Tanaka Y, Yamanaka H, Ishiguro N, Yamamoto K, Kanazawa M, Murakami Y, Yoshinari T, Baker D, Miyasaka N, Koike T. Golimumab, a human anti-TNF monoclonal antibody, administered subcutaneously every four weeks as monotherapy in patients with active rheumatoid arthritis despite DMARD therapy：52-week results of clinical, radiographic and pharmacokinetic assessments. The European League Against Rheumatism（EULAR）

2012, 示説, Berlin, 2012.06

13. Tanaka Y, Harigai M, Takeuchi T,Yamanaka H, Ishiguro N, Yamamoto K, Kanazawa M, Murakami Y, Yoshinari T, Baker D, Miyasaka N, Koike T. 52-week results of clinical, radiographic and pharmacokinetic assessments：golimumab, a human anti-TNF monoclonal antibody, administered subcutaneously every four weeks in patients with active rheumatoid arthritis despite methotrexate therapy. The European League Against Rheumatism（EULAR）2012, 示説, Berlin, 2012.06
14. Sakai R, Cho S, Nanki T, Sung Y, Bae S, Miyasaka N, Harigai M, for the RESEARCh investigators and the REAL Study Group. Drug retention rates and risk factors for discontinuation due to adverse events in patients with rheumatoid arthritis receiving tumor necrosis factor inhibitors：comparison between biologics registries of Japan and Korea. Congress of Asia Pacific League of Associations for Rheumatology Advancing Rheumatology in the Asian Pacific Region（APLAR）, 2012, 示説, Jordan, 2012.09
15. Yamazaki H, Sakai R, Koike R, Miyazaki Y, Tanaka M, Nanki T, Watanabe K, Yasuda S, Kurita T, Kaneko Y, Tanaka Y, Nishioka Y, Takasaki Y, Nagasaka K, Amano K, Tohma S, Dohi M, Sugihara T, Sugiyama H, Kawaguchi Y, Inase N, Ochi S, Hagiyama H, Miyasaka N, Harigai M. How to Assess Risks for Pulmonary Infection in Patients Receiving Immunosuppressive Treatment for Rheumatic Diseases? A Report from a Large-Scale Prospective Cohort Study. American College of Rheumatology（ACR）2012, 示説, Washington, D.C., 2012.11
16. Sugihara T, Ishizaki T, Hosoya T, Iga S, Yokoyama W, Hirano F, Miyasaka N, Harigai M. Treat-to-Target Strategy Aiming At Achievement of Structural and Functional Remission in Patients with Active Elderly-Onset Rheumatoid Arthritis. American College of Rheumatology（ACR）2012, 示説, Washington, D.C., 2012.11
17. Takeuchi T, Harigai M, Tanaka Y, Yamanaka H, Ishiguro N, Yamamoto K, Kanazawa M, Murakami Y, Yoshinari T, Daniel B, Miyasaka N, Koike T. Golimumab, A Human Anti-TNF Monoclonal Antibody, Administered Subcutaneously Every Four Weeks As Monotherapy in Patients with Active Rheumatoid Arthritis Despite Disease Modifying Antirheumatic Drug Therapy：Week 104 Results of Clinical, Radiographic and Safety Assessments. American College of Rheumatology（ACR）2012, 示説, Washington, D.C., 2012.11
18. Tanaka Y, Harigai M, Takeuchi T, Yamanaka H, Ishiguro N, Yamamoto K, Ishii Y, Daniel B, Miyasaka N, Koike T. Prevention of Joint Destruction in Patients with High Disease Activity or High C - reactive protein. American College of Rheumatology（ACR）2012, 示説, Washington, D.C., 2012.11
19. Kawasaki A, Inoue N, Ajimi C, Ito I, Sada K, Kobayashi S, Yamada H, Furukawa H, Tomita M, Sumida T, Tohma S, Miyasaka N, Ozaki S, Hashimoto H, Makino H, Harigai M, Tsuchiya N. Genetic Background of Antineutrophil Cytoplasmic Antibody-Associated Vasculitis in a Japanese Population：Association of STAT4 with Myeloperoxidase Antineutrophil Cytoplasmic Antibody-Positive Vasculitis. American College of Rheumatology（ACR）2012, 示説, Washington, D.C., 2012.11

11）学会発表（和文）

1. 木村直樹、宮坂信之、上阪等
自己免疫性筋炎における再生筋線維の役割　第56回日本リウマチ学会　2012年4月26-28日　東京（シンポジウム）
2. 上阪等、田形勇輔、長谷川久紀、太田晶子、冨滿弘之、宮坂信之
膠原病の難治性病態とアンメットニーズ　第56回日本リウマチ学会　2012年4月26-28日　東京（シンポジウム）
3. 上阪等、岩井秀之、細矢匡、山口悠、宮坂信之
滑膜線維芽細胞を標的とした抗リウマチ療法　第56回日本リウマチ学会　2012年4月26-28日　東京（シンポジウム）
4. 岩井秀之、細矢匡、村上洋介、宮坂信之、上阪等
関節炎治療における新規標的分子としてのTREM-1リガンドの同定　第56回日本リウマチ学会　2012年4月26-28日　東京（シンポジウム）
5. 長谷川久紀、溝口史高、東みゆき、宮坂信之
CD28補助刺激阻害によるCD8T細胞依存性多発性筋炎モデルの治療　第56回日本リウマチ学会　2012年4月26-28日　東京（ワークショップ）
6. 梅澤夏佳、南木敏宏、渡部香織、田中みち、上阪等、宮坂信之
リツキシマブが奏功した治療抵抗性好酸球性肉芽腫性多発血管炎（アレルギー性肉芽腫性血管炎）の一例　第56回日本リウマチ学会　2012年4月26-28日　東京（ワークショップ）
7. 山本晃央、山崎隼人、窪田哲朗、上阪等、宮坂信之
若年性特発性関節炎とクローン病の疑いと診断されていたPAPA症候群の一例　第56回日本リウマチ学会　2012年4月26-28日　東京
8. Fumitaka Mizoguchi, Yusuke Matsuo, Nobuyuki Miyasaka, Hitoshi Kohsaka

Blockade Of Il-20 Suppressed Ovariectomy Induced Bone Loss　第56回日本リウマチ学会　2012年4月26-28日　東京

9. 梅澤夏佳、長谷川久紀、高村聡人、上阪等、宮坂信之
血管炎様の病態を呈した慢性活動性EBウイルス感染症の一例　題53回関東リウマチ研究会　2012年6月23日　東京
10. Hitoshi Kohsaka, Yu Yamaguchi, Tadashi Hosoya, Nobuyuki Miyasaka
Small-molecule cyclin-dependent kinase 4/6 inhibitors for treatment of inflammatory arthropathy.　第33回日本炎症・再生医学会（国際シンポジウム、前掲）　2012年7月5-6日　福岡
11. 岩井秀之、細矢匡、竹中健智、村上洋介、宮坂信之、上阪等
マウスTREM-1リガンドの機能解析,及びヒトTREM-1リガンドの同定 第40回日本臨床免疫学会総会　2012年9月27-29日　東京（ワークショップ）
12. 木村直樹、中里洋子、高村聡人、平田真哉、宮坂信之、上阪等
自己免疫性筋炎における再生筋線維の役割 第40回日本臨床免疫学会総会　2012年9月27-29日　東京
13. 中島麻理、副島誠、三浦圭子、上阪等、宮坂信之
クリオグロブリン血管炎を合併したIgG4関連疾患の一例　第15回東京リウマチ膠原病研究会　2012年10月17日　東京
14. 酒井良子、田中みち、南木敏宏、山崎隼人、渡部香織、小池竜司、宮坂信之、針谷正祥.
REALを用いた関節リウマチ患者における重篤な有害事象に対する肺合併症の影響. 第56回日本リウマチ学会総会・学術集会・第21回国際リウマチシンポジウム、口頭、東京、2012.04
15. 渡部香織、酒井良子、田中みち、駒野有希子、山崎隼人、南木敏宏、小池竜司、宮坂信之、針谷正祥.
TNF阻害薬使用関節リウマチ患者におけるニューモシスチス肺炎. 第56回日本リウマチ学会総会・学術集会・第21回国際リウマチシンポジウム、口頭、東京、2012.04
16. 宮部千恵、宮部斉重、大野尚仁、高橋啓、宮坂信之、南木敏宏。
Am80によるCandida albicans water-soluble fraction誘導血管炎の抑制効果。第56回日本リウマチ学会総会。東京、2012年4月
17. 福田真、高安愛子、横山和佳、宮部千恵、宮部斉重、宮坂信之、南木敏宏。
カンナビノイドによる関節炎抑制作用。第56回日本リウマチ学会総会。東京、2012年4月
18. 宮部斉重、宮部千恵、高安愛子、福田真、横山和佳、宮坂信之、南木敏宏。
オートタキシン/リゾフォスファチジン酸受容体を標的とした関節リウマチの新規治療法開発。第56回日本リウマチ学会総会。東京、2012年4月
19. 横山和佳、金子佳代子、高安愛子、福田真、宮部斉重、宮部千恵、宮坂信之、南木敏宏。
関節リウマチの病態形成におけるCCL25/CCR9相互作用の関与。第56回日本リウマチ学会総会。東京、2012年4月
20. 平野史生、宮部斉重、溝口史高、高田和生、南木敏宏、宮坂信之。
SLEを合併したKlinefelter症候群の1例。第56回日本リウマチ学会総会。東京、2012年4月
21. 髙安愛子、宮部斉重、金子佳代子、宮部千恵、横山和佳、福田真、窪田哲朗、宮坂信之、南木敏宏。
CCL18による関節リウマチ線維芽細胞様滑膜細胞の活性化。第56回日本リウマチ学会総会。東京、2012年4月

12）外部資金の獲得状況

＜文部科研費＞

基盤研究C（主任研究者）　新規　210万円
基盤研究C（主任研究者：南木敏宏）　継続　カンナビノイドによる炎症抑制作用の解明と関節リウマチの新規治療開発（平成23～25年度）10万円
基盤研究C（主任研究者：田中みち）　新規　生物学的製剤及び分子標的薬投与下の重篤感染症、日和見感染症に関する薬剤疫学的研究（平成23～25年度）10万円
萌芽的研究（主任研究者：針谷正祥）　新規　抗好中球細胞質抗体関連血管炎のNETs形成を標的とする新規治療法の開発（平成24～25年度）10万円

＜厚生科研費＞

難治性疾患等克服研究事業（免疫アレルギー疾患等予防・治療研究事業）　指定研究「我が国における関節リウマチ治療の標準化に関する多層的研究」研究代表者：35,880千円（うち間接経費8,280千円）
難治性疾患等克服研究事業（免疫アレルギー疾患等予防・治療研究事業）「関節リウマチの関節破壊の解明と関節破壊ゼロを目指す治療指針の確立に関する

研究」研究分担者：1,600千円
治験推進事業「多発性筋炎・皮膚筋炎に合併する間質性肺炎に対するタクロリムスの臨床試験」の調整・管理に関する研究　研究代表者：2,030千円
厚生労働科学研究費補助金（難治性疾患克服研究事業）免疫疾患におけるT細胞サブセットの機能異常とその修復法の開発[主任研究者：山本一彦]　分担研究者：上阪等　1,000千円

〈戦略的創造研究推進事業CREST〉

慢性炎症に伴う臓器線維化の分子・細胞基盤[研究代表：松島綱治]
主たる共同研究者：上阪等　7,000千円

〈二国間交流事業　韓国との共同研究〉

多発性筋炎の治療標的としての自然免疫細胞の研究
代表：上阪等　1,200千円

〈共同研究〉

多発性筋炎・皮膚筋炎などの難病に対する人免疫グロブリン療法の作用機序の解明　担当：上阪等　1,000千円
マウス筋炎モデル（CIMモデル）を用いた薬効評価研究　担当：上阪等　2,000千円
TREM1及びそのリガンドに対する抗体の作製と評価　担当：上阪等　3,000千円

13）特別講演、招待講演、シンポジウム

1. 宮坂信之：「リウマチ性疾患の過去・現在・未来」第56回日本リウマチ学会会長講演　平成24年4月27日　東京
2. 宮坂信之：「MTX高用量時代を迎えたリウマチ治療」第9回阪神RA研究会　平成24年5月12日　大阪
3. 宮坂信之：「生物学的製剤とMTXの安全性と副作用について」Rheumatology Update 2012　平成24年6月15日　東京
4. 宮坂信之：「関節リウマチ治療における課題と展望」インフリキシマブ関節リウマチ効能追加講演会　平成24年7月21日　東京
5. 宮坂信之：「生物学的製剤の最新の知見」第8回リウマチ関連疾患研究会　平成24年8月28日　埼玉
6. 宮坂信之：「リウマチの過去・現在・未来」社会医療法人かりゆし会ハートライフ病院講演会　平成24年9月25日　沖縄
7. 宮坂信之：「高用量MTXの時代を迎えたリウマチ治療」第3回信州運動器診療フォーラム　平成24年9月29日　松本
8. 宮坂信之：「関節リウマチの過去・現在・未来」産業医科大学内科学講義　平成24年10月19日　北九州
9. 宮坂信之：「リウマチ性疾患の過去・現在・未来」第57回東信医学会特別講演　平成24年10月27日　上田
10. 上阪等　関節リウマチの新しい治療標的　湘南西部BMKK関節リウマチセミナー　平成24年1月18日　海老名
11. 上阪等　多発性筋炎・皮膚筋炎の基礎と臨床　第6回福岡膠原病研究会　平成24年2月4日　福岡
12. 上阪等　リウマチ治療　－現在と未来－　第7回荒川・墨田開成医会病診連携研究会　平成24年2月16日　東京
13. 上阪等　強力なT細胞阻害による免疫疾患治療の新機軸　高知リウマチセミナー　平成24年3月22日　高知
14. Hitoshi Kohsaka Lessons from a new animal model of polymyositis 8th International Congress of Autoimmunity May 9-13, 2012 Granada
15. 上阪等　生物学的製剤による膠原病の早期治療　第42回日本皮膚アレルギー・接触皮膚炎学会総会学術集会　平成24年7月13-15日　軽井沢
16. 上阪等、細矢匡、岩井秀之、宮坂信之　関節リウマチの新規治療法開発　第42回日本皮膚アレルギー・接触皮膚炎学会総会学術集会　平成24年7月13-15日　軽井沢
17. 上阪等　自己免疫疾患におけるT細胞阻害の意義　千葉東葛地区オレンシアセミナー　平成24年9月14日　東京
18. 上阪等　自己免疫疾患のSeed and Soilモデル－T細胞標的治療の意義－　第40回日本臨床免疫学会総会　平成9年9月27-29日　東京

14）主催学会

日本リウマチ学会（東京、2012年4月26～28日）

15）新聞、雑誌、TV報道

PDF参照

16）GCOE総合講義

Rheumatoid arthritis (RA) is a progressive inflammatory disease affecting synovial tissues and other organ resulting in destruction of the joint. RA also shortens life expectancy of the patients by 10 years. However, introduction of biologics with methotrexate caused a pardigm shift in

its treatment. Of note, biologics induce not only clinical remission but also imaging and functional remission. By contrast, serious side effects of biologics have to be focused. Infections of respiratory tract, i.e. bacterial pneumonia and pulmonary tuberculosis are often encounted.
In this lecture, pros and cons of biologics in the treatment of rheumatoid arthritis will be discussed.

17）教室、分野や講座の准教授、講師、助教、特別研究員、ポスドク、指導を受けた大学院生の名前

教授		宮坂　信之
准教授		上阪　　等
GCOE特任講師		岩井　秀之
助教		溝口　史高
助教		高村　聡人
助教		長谷川　久紀
薬害監視学講座		
教授		針谷　正祥
准教授		南木　敏宏
助教		酒井　良子
		渡部　香織
大学院生	○	宮部　斉重
	○	細矢　　匡
	○	木村　直樹
	○	福田　　真
	○	鈴木　晶子
	○	松尾　祐介
	○	横山　和佳
	○	中里　洋子
	○	山崎　隼人
	○	梅澤　夏佳
	○	竹中　健智
	○	齋藤　哲也

夕刊フジ 2012年（平成24年）1月28日 ＜26＞

ニッポン 病院の実力

東京医科歯科大学医学部附属病院 膠原病リウマチで全国トップ

本来、細菌などの外敵に攻撃を仕掛ける免疫機能が、自らの体内組織を攻撃し、関節や筋肉、内臓などに症状を引き起こす「膠原病（こうげんびょう）」には、さまざまな病態がある。その代表格は、患者数が約100万人と最も多い関節リウマチだが、それ以外にも、全身の臓器に炎症を引き起こす全身性エリテマトーデス、筋力低下や皮膚の炎症が特徴の皮膚筋炎など、その多くは国の特定疾患に指定され、早期診断や治療が難しいとされている。

しかし、ここ10年で関節リウマチの治療は劇的に変化した。症状を悪化させる情報伝達物質が特定され、それを狙い撃ちにした生物学的製剤が2003年に承認されたことで、おおよそ50％の人は、進行を止めるだけでなく、早期発見により症状が全く出なくなる人もいる。さらに、かつては50％の生存率と言われた全身性エリテマトーデスは、現在、薬の組み合わせによって生存率が約98％に上がった。

そんな膠原病の診断と治療、さらには最先端の新薬の研究で、全国トップの実力を誇るのが、東京医科歯科大学医学部附属病院膠原病・リウマチ内科だ。

「関節リウマチの患者さんの中には、薬を止めても再発せずに、完全に治ってしまう人も出始めています。しかし、原因が解明されていないため、100％封じ込める方法はまだありません。さらには、患者さんの少ない他の膠原病の薬の開発も、加速させる必要があります。そのためにも努力を私たちは惜しみません」

こう話すのは病院長を兼務する同科の宮坂信之教授（64）＝顔写真。日本リウマチ学会理事長を務め、膠原病の早期発見＆治療などの最先端の研究で、長年けん引し続けている。

新薬研究加速させ最終的には予防も

「膠原病にはたくさんの種類があり、ひとつひとつの病気の患者さんの数が少ないために新薬の開発も遅れがちです。しかし、慢性の病気ゆえに治療ができないと患者さんのQOL（生活の質）はどんどん落ちていきます。それを食い止めるために取り組んできたことが、現在、少しずつ実を結び始めているのです」（宮坂教授）

一般的に、新薬開発の中心は欧米諸国で、日本で承認されるまでに5～10年遅れる「ドラッグラグ」が問題になっている。ドラッグラグの解消のため、同科では積極的に治験などを実施。その結果、症状が出ない「寛解（かんかい）」の状態になる膠原病の患者が増えてきたという。

「今後5年間で、さらに治療は向上するでしょう。最終的には原因を解明し、予防ができるようになれば、と思っています」と宮坂教授。原因解明の微かな光もつかみ、それを大きく広げるために、今も力を注ぎ続けている。（安達純子）

＜データ＞2010年度実績
☆月間外来患者数約2200人
（外来通院患者数の主な内訳）
☆関節リウマチ約1000人
☆全身性エリテマトーデス約200人
☆多発性筋炎／皮膚筋炎約80人
☆シェーグレン症候群約80人
☆病院病床数800床
（住所）〒113―8519東京都文京区湯島1の5の45 ☎03・3813・6111

知っているようで知らない運動器疾患

関節リウマチ

早期発見のために、まずは関節リウマチの正しい知識から

関節リウマチはよく耳にする病名ですが、間違った情報やイメージを持っている人も多く、症状があっても発見が遅れたり、適切な治療を受けずにいる人も多いといいます。
そこで専門医である宮坂信之先生に関節リウマチに関する素朴な疑問を聞いてみました。

Q 関節リウマチはお年寄りの病気というイメージがありますが…。

A 働き盛りの30代から60代の女性に多く発病する病気です。

古くから関節リウマチが神経痛と並んでお年寄りの病気のようにとらえられているのは、病名のわりに実態が知られていないからでしょう。関節リウマチは、体のあちこちの関節に炎症が起こり、腫れて痛み、適切な治療を受けずに進行していくと、関節が破壊され、変形や機能障害を起こす病気です。罹患率は、男女比3：7で、圧倒的に女性に多く、とくに出産後と閉経期（50～60歳前後）の2つの時期に発症のピークがあります。世界的に人口の約1％、日本では数十万人以上が発症していると推測され、患者数の多さからも、この病気が決して他人事ではないことがわかります。まずは多くの人がこの病気に関して正しい知識を持つことが大切です。

Q 原因は何ですか？

A 残念ながら関節リウマチの原因は完全には解明されていません。

関節リウマチは体の中の血管や結合組織に起こる慢性の病気「膠原病」の一つ。難病で、まだその原因が完全には解明されていません。わかっていることは「膠原病」には次の3つの顔があることです。**❶共通して初発症状に関節の痛みがある。❷自分の体に対して免疫反応が起こる。❸体のあちこちに炎症が起こる。**その中の免疫反応（細菌などを防御するシステム）について説明すると、体になんらかの原因によって免疫反応の異常が起き、その結果、関節の毛細血管が増加し、血管内から関節滑膜組織にリンパ球、マクロファージなどの白血球が出てきます。これらの白血球が産生するサイトカイン（TNFαなど）という情報伝達物質が炎症を引き起こし、骨を壊す細胞が活性化され、軟骨や骨の破壊が進んでいくのです。

Q 遺伝する病気ですか？

A 遺伝的要因が多少関与しているといえます。

一卵性双生児の片方に関節リウマチが発症しているケースを調べたところ、もう片方の発症率は25％であることがわかりました。ご存じのように一卵性双生児は遺伝子のコピー人間です。一方、兄弟では発症率は5％。このことから遺伝子の一致率がより高い方が発症しやすいことがわかります。しかしどの遺伝子が悪さをしているのかはわかりません。また、関節リウマチの原因には、喫煙やストレスなど環境的要因も深く関与しているといわれています。しかし、ガンの原因がまだ特定できないように、関節リウマチも病気の原因をまだ特定できないのです。つまり、明確な予防法がないということなのです。

Q 自分でチェックする方法はありますか？

A 関節にこわばりや腫れがあれば病院へ。早期発見がもっとも重要です。

関節リウマチの患者さんの関節の破壊のスピードをみると、発症の1年間の破壊速度が速く、その後ゆるやかに進行していきます（左図参照）。一度破壊されてしまった軟骨や骨は再生しませんから、発症1年以内の早期に発見し治療を開始することがたいへん重要だといえます。そこで、自分自身が関節リウマチを疑う場合、次のことを目安にしてください。**❶朝、手・指などの関節がこわばる。❷疲れる、だるい。❸小さな関節が複数腫れてくる。**関節リウマチのこうした症状は、悪くなったり良くなったりを繰り返すので、つい見逃しやすい。しかし、放っておけば必ず悪化していくので、すぐに受診しましょう。病院では診察と血液検査をすることで、早期から病気を診断し、治療を始めることができます。

6

Q 関節リウマチ治療に温泉や運動などは効果ありますか？

A 病状の進行を止めるのは薬物療法しかありません。

前述したように関節リウマチは、自分に対して免疫反応が起こるために関節炎になるということがわかっています。本来、免疫反応とは、外部から体に入ってきた異物（病原体など）に対し、排除したり、攻撃したりするいわば体に備わった防御反応です。しかし、この病気の場合、外部ではなく自己の成分に対して過剰な免疫反応を示す結果、自己を攻撃、骨や軟骨といった組織の破壊が進んでいくのです。すなわち、温泉や運動といった方法で、この進行を止めることはできません。治療方法は、第一に関節の破壊や痛みを抑えるための薬物療法、大きな関節の破壊が進んだ場合などは人工関節を入れるなどの手術療法、そしてリハビリテーションの3つ。リハビリは、筋力増強・関節の動きの維持と回復にあります。このために理学療法（物理療法・運動療法）、作業療法、装具療法、その他（在宅ケアなど）が行われます。関節リウマチの治療方法は画期的な進歩をしていますので、ぜひ積極的な治療を受けてください。

Moving

取材・文：土居亜子 イラスト：高村あゆみ

Q 一度発症すると、治らないのですか？

A 医学の進歩により、症状のない状態にすることは十分できます。

関節リウマチになると、いずれは車いすや松葉づえが必要になり、日常生活の基本動作や生活の質の低下が起こると当たり前のようにいわれてきました。また、一般的には知られていませんが、関節リウマチの患者さんは寿命が平均して10年短いというデータもあります。しかし、関節リウマチの治療はこの約10年間で飛躍的に進歩しました。日本で有効性の高い「メトトレキサート」や「生物学的製剤」など6つの抗リウマチ薬が次々に承認されたこと、新しい診断基準が確立され早期発見が可能になったこと、さらに、有効性の高い薬の副作用に対する発症予防などの研究も進みました。その結果、痛みや腫れを和らげるケア中心だった治療内容も、より積極的な関節の破壊そのものを防いだり、進行を止めるものへと大きく変化しました。具体的には、痛みや腫れがなく、炎症反応も正常、関節の破壊を抑えることができる「寛解」という状態にすることが十分に可能になりました。薬の服用をやめると再び症状が出る可能性があるので完治とは言えませんが、「寛解」は日常生活に支障をきたすこともほとんどありません。また投薬の必要のない患者さんも少数ですが存在します。今後のさらなる研究により関節リウマチを完治できるようにすることが日本リウマチ学会の目標です。

関節リウマチにおける関節破壊の経時変化
van der Heijde DM. J Rheumatol 1995; 22: 1292-1296より作図

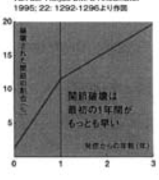

Close up! BJD Japan
運動器の10年・日本協会
参加団体紹介

一般社団法人 日本リウマチ学会

〒105-0001 東京都港区虎ノ門1-1-24 第1オカモトヤビル9F ☎03-5251-5353
URL http://www.ryumachi-jp.com/

日本リウマチ学会は、とくに関節リウマチを代表とする運動器疾患の病因・病態、治療の解明に力を注いでいます。2003年以降に承認された5つの生物学的製剤に関して、厚生労働省から委託を受け、その安全性の検証を行い、極めて有効性が高いことを確認するとともに、副作用である感染症の発症予防、早期発見の重要性を明らかにするなど、世界に向けて新知見を発信しました。また、関節リウマチをはじめ、運動器疾患の早期発見、早期治療、予防体制の確立に向かって、運動器疾患や膠原病などのリウマチ性疾患の診療を専門的に行うことができるリウマチ専門医の育成も行っています。

この人に聞く

宮坂信之さん
みやさか・のぶゆき
一般社団法人日本リウマチ学会理事長／東京医科歯科大学医学部附属病院 病院長／同大学院 膠原病・リウマチ内科学分野 教授

7 vol.3 2012.2.1 Winter

Japan Medicine MONTHLY
CLINICAL & MEDICAL NEWS
株式会社じほう
No.030 7月号 July.2012 6月25日発行

CONTENTS
第48回米国臨床腫瘍学会年次集会（ASCO2012） 10～13
カレントトピック＜関節治療の今を探る＞ 16～17
第85回日本整形外科学会 21
第53回日本神経学会 22
第13回欧州リウマチ学会（EULAR2012） 6～9
生物学的製剤のHead to Headに注目

特集 Bioを使いこなしRAに臨む

エビデンスと実績で最適な診療を実践

東京医科歯科大大学院・宮坂信之氏

関節リウマチ（RA）の治療薬として国内の臨床現場に生物学的製剤（Bio）が登場し、今年で10年目を迎える。その後も相次いで発売され、現在は6製剤。この間に国内のエビデンスと臨床実績を積み重ね、日本に見合った薬物療法の実践を目指してきた。国内でもデータや経験を基にBioを使いこなし、RA診療に臨む時代になったといえる。欧米では近年、診断、治療、寛解に関する基準や手法が新たに提唱され、国内でもそれらを積極的に臨床へ導入する動きがある。ここでも海外の仕組みを丸飲みするのではなく、国内エビデンスによる検証や、日常診療での有効活用の模索が行われている。特集では、Bioを中心に、国内で進展するRAの薬物療法などをリポートする。

Bioをはじめとする薬物療法が、日常診療でRA患者にどのような影響を及ぼしているのかを把握するために、国内では複数のコホート研究が進行する。これらの研究によって、独自のエビデンスが蓄積。実臨床に有益な情報をもたらしている。

その1つ、NinJaコホートからはメトトレキサートの増量傾向や、Bioの選択機会増加を背景に、寛解に至る症例数が大きく伸びていることが分かった。その反面、薬物療法による効果が不十分な患者が多数存在する実態も浮かび上がった。

研究に当たる国立病院機構相模原病院の當間重人氏によると、「疾患活動性の数値が改善しても、ゼロにならない限り、関節破壊や身体機能障害が進んでいく」。新たな薬剤でも十分な効果が得られない患者も少なくないといい、こうした課題の解決につながる研究が、さらに進展することに期待がかかる。

織部リウマチ科内科クリニックの織部元廣氏は実臨床の経験の中で、炎症量と関節破壊のパターンから、Bioを使い分ける手法を見いだした。Bioの広がりとともに個別の研究や取り組みが活性化し、それらの情報共有が進めば、Bio時代の新たな治療戦略を切り開くきっかけになるかもしれない。

国内エビデンスに基づいたGL作成へ

RA診療の"入口"と"出口"に関する新たな基準も、この数年に欧米から提唱された。米国リウマチ学会（ACR）と欧州リウマチ学会（EULAR）は分類基準と寛解基準を発表した。その間をつなぐ治療戦略として、EULARから「Treat to Target（T2T）」という考え方、ACRからは治療勧奨が出された。国内でも世界の潮流に合わせて最新の手法を導入し、日常診療などを通じてさまざまな検証が行われている。

新潟県立リウマチセンターの伊藤聡氏は、DASやCDAI、SDAIといった疾患活動性の評価指標には、足関節の項目が含まれていない点を指摘。これらのスコアが低くても足の痛みを訴える患者では、丁寧な診察が必要と説明する。このほかT2Tを医療者と患者の"共通言語"として活用するメリットも感じている。患者に分かりやすく治療ステップを提示し、患者との信頼関係を構築できれば、治療満足度を向上させる可能性は高い。

ACRの治療勧奨については、発症6カ月未満の早期RA患者でも、疾患活動性が高く予後不良因子があれば、第一選択薬として抗TNF製剤を使えるとした点が大きな特徴だ。ただ豊富なエビデンスに基づき治療の1つの方向性を示すものではあるが、国内の実臨床で全ての患者に同様の治療戦略をとるのは、現実的でない。国内エビデンスや患者の経済的負担を考慮し、最適な活用を検討していく必要がある。

日本リウマチ学会では現在、RAに対するTNF阻害療法施行ガイドラインの改訂作業中で、国内の最新エビデンスも踏まえた方針が間もなく公表される予定。また厚生労働科学研究の一部として、RA診療ガイドラインの作成にも着手しており、今年中にたたき台が完成する見込みだ。主任研究者を務める東京医科歯科大大学院の宮坂信之氏は、国内にはACRの治療勧奨のような戦略を明示できるまでのエビデンスがないと指摘。「日本のエビデンスに基づいて今回の治療勧奨をどう使うのか」を今後の課題に挙げる。

期待高いトファシチニブ 課題への対応がカギ

Bioに続く治療薬として、新規経口JAK阻害薬トファシチニブへの注目度は高い。臨床試験ではACR20改善率のほか、関節破壊の進行抑制や身体機能の改善で、プラセボに対する統計的有意差が認められた。宮坂氏は「Bioに匹敵する有効性が得られ、場合によってはBioより効きが早いかもしれない」と評価する。

一方で、帯状疱疹の発現率が比較的高かったことや、感染症誘発の可能性をデメリットとして提示。さらに発売後には、適正使用への対策が課題になるとの見方を示す。「Bioの次世代薬として有効性を日本で発揮するかどうかはまだ分からず、期待とリスクがある」と話す。

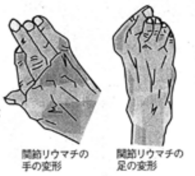

関節リウマチの足の変形

関節リウマチの手の変形

関節を保護する滑膜を攻撃し、炎症や関節の破壊を引き起こします。根本的な原因は不明ですが、からだが作り出す情報伝達物質のTNF（腫瘍壊死因子）やインターロイキン６（ＩＬ－６）が"悪玉"として炎症などの病気の進行に深いかかわりがあることが分かってきました。

リウマチは、関節の破壊が進行すると治療が難しいため、早期発見、早期治療が大事です。関節の破壊は発症してから1年以内に始まるとされていますので、その前に治療を行いましょう。

診断は、診察やX線検査、血液検査で総合的に行われます。確定診断ができない場合は、リウマチの炎症があると増える特殊な抗体を調べる「抗ＣＣＰ抗体検査」で対応します。

リウマチの3つの治療

その1 薬物

薬物の進歩には目覚ましいものがあります。①消炎鎮痛薬、②抗リウマチ薬、③ステロイド薬、④生物学的製剤の4つに大別されます。

これまではピラミッド療法といって、順番に使用していましたが、現在は抗リウマチ薬から使います。これだけで不十分な場合には、生物学的製剤が使われます。

その2 手術

リウマチの炎症が特定の関節だけの場合には、関節に小さな穴をあけて内視鏡を差し込み、炎症を起こしている滑膜を取り除く滑膜切除術を行うことがあります。ただ、痛みを和らげ、症状の進行を抑える効果はありますが、薬物療法が不十分だと再発します。

膝や股関節の変形が進み、体重を支えられなくなった場合は、人工関節置換術も選択肢の一つです。変形した関節を金属やポリエチレンなどの人工関節に置換するものです。膝と股関節の治療成績が優れています。

その3 理学療法

関節は使わないと動かなくなり、拘縮します。それを防ぐためリハビリを行います。「リウマチ体操」と呼

■ 人工関節置換術

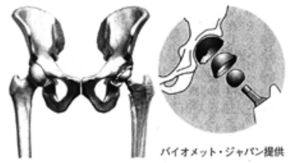

バイオメット・ジャパン提供

おしえて先生 質問なるほドリ

Q.1 リウマチは、なぜ関節が痛くなったりするのですか？

A リウマチは、まず関節を覆う滑膜に炎症が起こります。このとき、サイトカインと呼ばれる物質がかかわり、炎症を増幅させ、滑膜を増殖させたり関節を破壊したりするため痛みが生じます。

Q.2 サイトカインとは何ですか？

A リンパ球が作り出すたんぱく質で、ＴＮＦ（腫瘍壊死因子）やインターロイキン６（ＩＬ－６）に代表され、リウマチの腫れや骨破壊に直接かかわっていることが明らかになっています。そこでサイトカインを標的にした新薬が次々と登場し、サイトカイン療法は治療効果が期待されています。

Q.3 サイトカイン療法とは？

A サイトカイン療法では、インフリキシマブ、エタネルセプト、アダリムマブ、トシリズマブ、アバタセプト、ゴリムマブの６種類の薬が認可されています。いずれも遺伝子組み換えのバイオ技術で生まれた生物学的製剤です。これらを皮下注射や点滴で患者さんに投与します。

医療最前線 Vol.10 リウマチ

関節リウマチに悩まされている人は約100万人いるとされる。日本リウマチ学会理事長の宮坂信之先生は、「リウマチは早期から、積極的に、厳密に炎症をコントロールすることで、関節破壊を阻止し、生命予後の改善を図ることが大切です」と話す。

ライター・秋山晴康／撮影・工藤ケイイチ／監修・MMJ（毎日メディカルジャーナル）

日本リウマチ学会理事長
東京医科歯科大学医学部附属病院病院長
大学院膠原病・リウマチ内科学分野教授
宮坂 信之 先生

みやさか・のぶゆき●1947 年生まれ。東京医科歯科大学医学部卒業。米国カリフォルニア大学、テキサス大学留学。86 年、東京女子医科大学リウマチ痛風センター助教授。89 年、東京医科歯科大学難治疾患研究所教授。95 年、同大学第一内科教授。99 年、同大学大学院膠原病・リウマチ内科学分野教授。2011 年、同大学医学部附属病院病院長併任。日本リウマチ学会理事長

原因がよく分からず予防できないリウマチ

関節リウマチ（以下リウマチ）は関節が病む病気の総称です。その語源は医聖ともいわれるギリシャのヒポクラテスの時代までさかのぼります。

とくに指、手、手首、膝、足、足首などに症状が出やすく、痛みと腫れを繰り返しながら症状が進行していきます。重症になると関節が変形し、動かすことができなくなります。画家ルノワールは47歳のときに発症し、晩年は手に絵筆をくくりつけて描いていました。

リウマチに悩まされる人は、約100万人いるといわれています。どうしてそのようなことが起きるか原因がよく分からないため、予防もできないとされています。男女比は3対7で、女性に多く発症します。その年齢は、30代から60代にわたり、出産後と閉経期の2つのピークがあります。

早期発見と早期治療が大事

リウマチは、外からの病原体を防ぐはずの免疫が、

■ 関節リウマチの構造

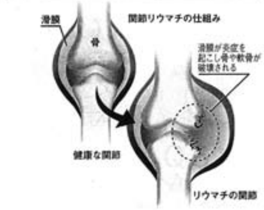

■ リウマチとは？

1．原因不明の多発性、対称性関節炎
2．中年女性に多い
3．軟骨や骨の破壊を特徴とする
4．時に内臓病変を伴う

▶ リウマチ

ばれる特有の体操などで体をほぐすことも大切です。

「寛解」と「治癒」を目指す

リウマチの治療では、薬は使っているけれど、炎症反応が正常な状態で症状がない「寛解」を目指します。薬をやめて、5年たっても再発しない状態を「治癒」といいます。

リウマチは、早期から、積極的に、厳密に炎症をコントロールすることで、関節破壊の阻止を行い、生命予後の改善を図ることが大切です。

リウマチを簡単チェック

リウマチ
- □手がむくみ、腫れぼったい
- □指の関節が痛い
- □疲れやすい
- □体がだるい

上記の項目が気になる方は医療機関にご相談ください

怖い感染症

リウマチが進行すると体力が落ち、感染症にかかりやすくなります。最も怖いのが肺炎です。

肺炎の予防法

- ・インフルエンザワクチンを打つ
- ・肺炎球菌ワクチンを打つ（主治医と相談）
- ・入れ歯を洗い、口腔内を清潔にする
- ・禁煙
- ・糖尿病の人は食事療法と運動を
- ・ステロイド使用量をできるだけ減らす

日常生活の注意点

- ・まずストレスや過労を避けることが大切です。
- ・栄養バランスの良い食事も重要です。薬も決まった量を服薬してください。
- ・リウマチ体操などの適度な運動をすることも必要です。ただし、疲れを翌日に残さないようにしてください。
- ・関節に負担がかかりすぎると症状が悪化するため、補助具なども活用しながら、日常生活での動作、関節に負担をかけないように配慮します。

日本リウマチ学会の取り組み

http://www.ryumachi-jp.com

日本リウマチ学会は、リウマチ性疾患の研究および診療内容の向上を推進することを目的に活動してきました。2009 年、従来の有限責任中間法人から一般社団法人日本リウマチ学会を設立。会員数は 9000 人を超え、学会が認定するリウマチ専門医は 2011 年 8 月現在で 4463 人を数えます。

当学会では、今後もリウマチ学に関する情報発信基地として、学会員および患者団体を含めた一般社会へのリアルタイムな情報の提供と啓発活動に励み、リウマチ性疾患の研究・診療において世界をリードする一翼を担っていきたいと考えます。

●次号は気になる「リハビリ」

第56回日本リウマチ学会総会・学術集会 市民公開講座

企画・制作 読売新聞東京本社広告局 広告

テーマ リウマチに負けない ～ケアからキュアに向けて～

2012年4月29日、東京グランドプリンスホテル新高輪国際館パミールにおいて、市民公開講座が開催されました。
当日は約1,600人の参加者がありました。
座長の東京医科歯科大学大学院医歯学総合研究科膠原病・リウマチ内科学 教授、宮坂信之先生の司会のもと、リウマチ診療の第一線で活躍している先生らによる講演とパネルディスカッションが行われました。

薬の副作用を減らすためには

「飲まなかったことを隠さない、医師との信頼関係を大切に」

東京医科歯科大学大学院 医歯学総合研究科 薬害監視学講座教授 針谷 正祥 先生

あなたのリウマチの治療を成功させるために
1. 薬局でお薬手帳を作って、使った薬の記録を残しましょう
2. 前回の外来からその日までのことを話してください
① リウマチがどうだったか
② 何か体の不調に気がついたか
③ 副作用かもしれないと思うことがあったか
④ 薬はきちんと飲めたか、飲まなかった日があれば何日くらいか
⑤ 他の病院を受診したか
3. 痛みやからだの機能のアンケートには出来るだけ正確にお答えください

監修:針谷正祥 先生

リウマチに使う薬 ―最新情報―

「薬で寛解状態※を維持する ケア（介護）からキュア（治癒）の時代へ」

※リウマチ治療における寛解とは:薬によって、関節炎や関節破壊の起こらない状態を保つこと。

慶應義塾大学医学部 リウマチ内科教授 竹内 勤 先生

生物学的製剤はどのように使うか？
病院で点滴静注を受けます。
インフリキシマブ 標的:TNF
トシリズマブ 標的:IL-6 4週間に1回
アバタセプト 標的:Tcell
通院または自宅で皮下注射を行います。専用の補助具もあります。
エタネルセプト 標的:TNF 週に1回～2回
アダリムマブ 標的:TNF 2週間に1回
ゴリムマブ 標的:TNF 4週間に1回

監修:竹内勤 先生

リウマチと上手につきあうには

「医療関係者会員2,000人も協力。患者も病気の正しい知識と情報を」

日本リウマチ友の会会長 長谷川 三枝子 さん

リウマチ患者に望むこと―特別会員の声―

手術とリハビリ ―もっとよくなるために―

「リハビリは安静と適度な運動、手術はタイミングが大事」

富山大学医学部 整形外科教授 木村 友厚 先生

注意したほうがよい9項目
① 手拭や雑巾をしぼる、蛇口の使用
② 買い物袋をたくさん持つ
③ 重い荷物を持ち上げる
④ 踵の高い先細りの靴
⑤ 床からの立ち上がり
⑥ 正座
⑦ 首に合わない枕
⑧ 膝を深く曲げて寝る
⑨ 長距離歩行
頑張りすぎないことも、関節保護です。適度の手抜きを

監修:木村友厚 先生

Q&A コーナー リウマチ ケア キュア

講座に寄せられた質問に、先生方がお答えしました。

当日は来場者から多数の質問が寄せられました。講座の後半のパネルディスカッションは、その質問に、宮坂座長と4名のパネラーが回答しました。

Q 私はリウマチですが、子どもにリウマチは遺伝しますか？
A 竹内:リウマチは遺伝はしやすい病気ですが、遺伝病ではありません。リウマチの母親から生まれた子どもがリウマチを発症する確率は3%で、一般人口の0.5%よりも高いと言われますが、実際には遺伝的要因は3割、環境的要因が7割と言われます。

Q 長年リウマチの薬を使っていると効かなくなるのですか？
A 針谷:リウマチの薬には、最初から薬に反応しない1次無効と、ある程度まで良くなるが途中で効かなくなる、あるいは悪化してしまう2次無効があります。ただ、2次無効であっても、量の調節、他の薬の追加や切り替えにより対処できるため、1つが効かなくなっても問題はありません。

Q ウォーキングなどを始めたいのですが、どのような種類の運動をどの程度やっていいものでしょうか？
A 木村:ウォーキングなどの有酸素運動は非常にいいと思います。最初はやはり、無理せず10分程度の短時間から少しずつ、関節の痛みが強くならない範囲で始めてください。目安は、次の日に疲れや痛みを持ち越さないのがポイントです。

Q 薬代が高くて負担になっています。なんとか補助を受けられないでしょうか？
A 長谷川:リウマチは難病指定に入らないため、昔は身体障害者手帳を取得し、障害者医療の方で補っている人が大勢いました。一方現在の場合、早期治療で薬が必要な人に対応できる手立てはなく、友の会が継続的に厚生労働省に働きかけているところです。

Q リウマチはなぜ難病指定されないのでしょうか？
A 宮坂:今、国で特別に指定された公費負担の対象となる病気は、まだ治療法が見つからない希少性の高い病気でなければならないという条件があります。通常患者数が1万人以下の病気とされており、人口の0.5～1%の発症率を持つリウマチは当てはまらないことになります。

【主催】第56回日本リウマチ学会総会・学術集会／読売新聞社 【共催】田辺三菱製薬株式会社／中外製薬株式会社／ブリストル・マイヤーズ株式会社／ヤンセンファーマ株式会社／アボット ジャパン株式会社／エーザイ株式会社／武田薬品工業株式会社／ファイザー株式会社
【後援】社団法人日本医師会／社団法人東京都医師会／社団法人日本リウマチ友の会

れる。患者の日常生活への負担や生存率を考えれば腹膜透析のメリットは大きいのだが、日本で腹膜透析を受けているのは透析患者のわずか3％。血液透析は人件費をかけられるため、経営面で医療サイドの都合がいいのだ。患者本位の医療態勢になっていないと、小松医師は嘆く。

腹膜透析を選べるか否かは、病院を選ぶ上で重要なポイントになるだろう。

「もう一つ重視しているのはチーム医療です。慢性腎臓病は、治療が長期間に及ぶこと、生活習慣改善が欠かせないことなどから、患者さん自らが主体的に治療に関わる必要がある。そのため、医師・看護師・栄養士などが連携し、患者さんとともに最善の治療法を選択、進めていくことができる態勢になっていることが必要です。優れた技量・知識・人間性をもつ医師がいたとしても、それを生かし切れない態勢では、いい医療はできません」

「対話力」と「説明力」

●認知症

「私の診療は、ほとんどしゃべっているだけ（笑）。それでも診断はつきます。機械による検査よりも確かですよ」

こう語るメディカルケアクリニック柿の木坂（東京都目黒区）院長の岩田誠医師は、複数の病院や施設で診療を行い、継続的に約300人の認知症患者を抱える、日本で最も認知症を診ている医師の一人だ。

「たとえば私が信頼を置く**小阪憲司**先生のように本人や家族の話によく耳を傾け、病気の進行やケアの仕方について、分かりやすく説明してくれるのがいい医者の条件だと思います。医者の仕事の中で一番大事なことは対話です。話を聞いて、答えを見つける努力を示すことが重要です」

岩田医師は、東日本大震災直後に訪れた高齢者施設で、「地震の時も誰一人怖がらず、平然としていました」という介護士の言葉に疑問を抱き「重症の認知症患者は危機認知能力に欠ける」ことに気付く。震災後、火災などの緊急時における介護現場の避難のあり方に再考を促した。

「学ぶべきは本を読んで一生懸命覚えて勉強することではなく、実際に患者さん自身をよく観察し、そこから大事なことをどうやって引っ張り出すかだと、医学生時代の恩師に教えていただきました」

いい医者を選ぶ際にも、「対話力」を重視するようアドバイスする。

●リウマチ

「リウマチの治療を始めて40年になりますが、この15年間の進歩は劇的でした。これと同じだけのパラダイムシフトは、ほかの病気では起きていません」

東京医科歯科大学医学部附属病院の病院長で、日本リウマチ学会の理事長でもある宮坂信之医師が言うように、かつては松葉杖や車椅子が必要になる疾患の代名詞だったリウマチは、新薬が登場したおかげで、いまや半分は治癒し、治癒しないまでも大半は社会復帰することができる病気になった。

「リウマチ治療は日進月歩で、最新医療を知らずしていい治療はできません。新薬はよく効く反面、感染症を起こしやすくなるといった、両刃の剣的な側面がある。必要な予防策を講じれば済むことですが、そこにはやはり専門性が不可欠です。**竹内勤**先生のように、最新医療に造詣が深く、内科臨床一般についても精通している先生に診てもらうと安心ですね。

また、早期診断・治療に優れているという点で、**田中良哉**先生も素晴らしい医者だと思います」（宮坂医師）

名医が診てもらいたい「名医50」

週現スペシャル

写真上より、岩田医師（認知症）、宮坂医師（リウマチ）、太田医師（骨粗しょう症）、松本医師（スポーツ医学）

専門バカはいらない

●骨粗しょう症

患者数1300万人とも推定される骨粗しょう症だが、実は治療を受けているのはそのうちの30％ほど。

「みなさん骨粗しょう症の怖さを知らな過ぎる。脳血管障害に次いで介護・寝たきり原因の第2位というだけでなく、死亡リスクも8倍から9倍も高くなるんですよ」

と、長年骨粗しょう症に取り組み、骨粗しょう症学会の理事長も務める国際医療福祉大学・山王メディカルセンター（東京都港区）女性医療センター長の太田博明医師は警鐘を鳴らす。

近年、「骨粗しょう症は生活習慣病」との認識が強まり、男性患者の増加も注目されている。単なる老化と見過ごしていると、取り返しの付かないことになりかねない。

太田医師は名医の条件として「トータルヘルスケアができること」を第一に挙げる。骨粗しょう症は動脈硬化や高血圧など、他の生活習慣病を合併している可能性が大きいからだ。

「画一的に診断して、画一的に診療しているようではいけません。患者さんの病態やニーズに応じたオーダーメイド医療が必要です。分かりやすいのは薬の処方です。誰にでも、いつでも、同じ薬を出している医者は、お勧めできませんね」

その点、**白木正孝**先生は患者さんとの対応が抜群です。しなやかで柔軟、どうしてこういう対応ができるのかといつも感心しています。オールラウンドで豊富な医学的知識を有し、なおかつ、「ヒト」を愛している、最強の名医です」

●スポーツ医学

健康ブームを背景に、中高年のスポーツ愛好家は年々増えているが、そこには「加齢」に伴う危険が潜む。張り切ってウェアや道具を揃えたにもかかわらず、早々に膝や腰を痛め、やむを得ずスポーツを諦めてしまうというケースは多い。

「スポーツ医学は単なるケガの治療ではなく、その前後もケアします。運動を続けることを前提にしたリハビリ、個々人の身体の状態に即したトレーニング法の指導や、さまざまな運動療法を行うのです」

慶応義塾大学スポーツ医学総合センターの診療部長、松本秀男医師は解説する。

スポーツ人口が増えたことでスポーツ医学のニーズも高まっているが、いい医者に巡り合う秘訣は何か。

「スポーツをする患者の気持ちは、自分自身も運動をする医者の方がよく分かります。スポーツドクターには運動をする人が多いので、尋ねてみるといいでしょう。私も、サッカーをやっています」（松本医師＝以下同）

松本医師が勧めるのは、日本ハムファイターズのチームドクターの**安田和則**医師だ。大勢のスポーツ選手の膝を手術した実績を持っているため、アスリートの気持ちがよく分かっているという。また、日本ボクシングコミッション・コミッションドクターの**谷諭**医師は、脳へのダメージの治療の第一人者として有名だ。

「我々が行うのは、常にスポーツを再開することを念頭に置いた治療です」

たとえばあなたが、メタボ対策で慣れないジョギングを始め、膝を傷める。あるいは、ゴルフ好きが高じて、腰痛を患う。そんな時、スポーツドクターは安易に「しばらく運動はやめなさい」とは言わない。その時々の患者の体調や状況、そして気持ちを汲み、スポーツを楽しむ気持ちを取り上げない。これこそ、名スポーツドクターの条件だ。

病気になったら、誰もが追い求める「名医」のイメージ。しかし、その条件は病気ごとに違うし、所属する病院にも左右される。各分野の名医たちが総合的に選んだ、本当に頼りになる50人の医師と、その判断基準。これからの医者選びの参考にしてほしい。

（取材・木原洋美）

がんの新薬治療で死亡者も！

約1千万人のB型肝炎の人が再発・劇症化!? 医師も知らない恐ろしい現実

週刊朝日

B型肝炎に感染歴のある人が、がん治療などで新薬を使う療法によってウイルスが増殖、時に死に至るケースがある。医薬品の進歩が難病治療に効果を上げるなか、思わぬ副作用が課題となった形だ。しかし、その事実を多くの医師は知らないという。なぜ、そのようなことが起こるのか。私たちが知っておくべきこととは――。

過去に完治したはずのB型肝炎が、がんやリウマチの治療で免疫力が落ちたことをきっかけに、ウイルスが再び増殖する「再活性化」が全国で報告されている。なかには再活性化によって肝細胞の破壊が急激に進み、劇症肝炎に進展して死に至るケースもある。

厚生労働省の研究班による全国調査では、2004～09年の間にB型肝炎ウイルスの再活性化によって悪性リンパ腫の患者が少なくとも13人死亡、白血病2人、乳がんや多発性骨髄腫でも各1人の死亡例が確認されている。

当時、厚労省研究班の劇症肝炎分科会長で全国調査を担当した鹿児島大学大学院医歯学総合研究科の坪内博仁教授は、その背景についてこう話す。

「B型肝炎ウイルスの再活性化の症例が増えたのは、免疫抑制効果の強い新薬や新しい治療法が登場したためです。特に最近では特定の部位に強い効果を発揮する新薬（生物学的製剤）が開発され、広く使われるようになっています」

しかし、再活性化の問題が知られるようになったのはこの数年で、医師の間でも十分に認識が広まっていない。B型肝炎再活性化に関する厚労省の研究班で代表を務める埼玉医科大学消化器内科・肝臓内科の持田智教授は、現在の状況に危機感を抱いている。

「免疫を抑える薬は、耳鼻科、皮膚科など大部分の診療科で用いられています。B型肝炎の多い日本では、すべての診療科で再活性化に注意しなければなりません。本来は医者が適切に対応すべきですが、現時点では肝臓や血液領域の専門家以外では、このことがあまり理解されていないのが実情です」

かつて「国民病」と呼ばれたB型肝炎は、50歳以上で約2割、日本全国で1千万人以上に感染歴があるといわれている。

B型肝炎の約8割は感染しても自然に完治するため、本人に自覚症状はなく、感染歴があることすら知らないのが一般的だ。完治すれば体内からウイルスは消えるが、ウイルスの遺伝子だけが体内に潜んだ状態で残る。いわば1千万人以上にウイルス再活性化の可能性があるということだ。

劇症化すると全員が死亡

前出の坪内教授のもとにも、過去にB型肝炎ウイルスが再活性化した患者が運ばれてきたことがある。

約7年前、悪性リンパ腫の治療を受けていた九州地方在住の70代の女性が肝臓に異変をきたし、肝臓領域の専門家である坪内教授が担当となった。その患者は、免疫抑制療法を実施する前の検査ではB型肝炎について陰性の結果が出ていたが、坪内教授の再検査では陽性反応が出た。ただちに抗ウイルス剤を投与したものの、次第に黄疸が強くなり、その患者は亡くなった。坪内教授は当時をこう振り返る。

「亡くなった患者さんは悪性リンパ腫で入院治療を受けていたことから、外部からウイルスに感染したとは考えられない状況でした。治療にあたっていた医師も、抗がん剤による肝機能障害が原因だと考えていたようです。それで以前の血液を調べてみると、過去にB型肝炎ウイルスに感染した経験があったのです」

その後、坪内教授は厚労省研究班で劇症肝炎についての調査を実施した。6年間で約450人の症例を集めたところ、冒頭で紹介した17人の死亡者が確認された。注目すべきは死亡率で、再活性化による劇症肝炎では全例で死亡していた。死亡率が高いのは、もともと

写真右はB型肝炎ウイルスの拡大写真（国立感染症研究所提供）。写真左は抗がん剤を混ぜ合わせるミキシング作業の様子（がん研有明病院で）

2011.10.14　28

重い病気の患者が強い免疫抑制療法を受けた後に発症したからだとみられている。

なお、調査は研究班から病院に向けたアンケートが元になっているため、集まった劇症肝炎の症例は全体の2～3割程度にとどまるという。そのため、実際の死者数はもっと多いと推測されている。

では、死に至る危険性のあるウイルスの再活性化を防ぐ手段はあるのだろうか。

持田教授は、昨年1月からB型肝炎の感染歴があり、免疫抑制剤や抗がん剤の投与を受けている症例を対象に調査をしている。8月末までに集まった235人のうち、再活性化した11人を含む計14人からウイルスが検出され、5人は抗ウイルス剤の投与が必要とされる値までウイルス量が増加していた。そこで抗ウイルス剤を投与したところ、肝炎の発症は防げたという。

「血中にウイルスが出現してから肝炎になるまで2～3カ月かかるため、定期的な検査と、早い段階で対処すれば十分対応できます」（持田教授）

この対処法は、坪内教授を中心に持田教授も参画してまとめた再活性化防止のための治療ガイドラインに基づいている。09年に発表されたこのガイドラインでは、免疫抑制療法を実施する前にB型肝炎ウイルスの感染歴を調べ、過去に完治していても、継続して再活性化の兆候について定期検査することを推奨している。

「現在でもこのガイドラインは有効性について検証が進められていますが、これまでの結果では、肝炎の発症が防げることがわかっています」（坪内教授）

再活性化の危険性やその防止策が研究成果で明らかになってきたことで、国も動き始めた。

これまで、ガイドラインに沿って実施された検査は保険適用が認められていなかった。だが、この状況を受けて厚労省は9月に方針を転換、すべての検査で保険適用を認めた。今後は検査態勢のある医療機関で必要な検査のすべてを受けることができるようになった。

日本リウマチ学会理事長の宮坂信之医師（東京医科歯科大学膠原病・リウマチ内科教授）も保険適用の決定を歓迎している。リウマチ治療では免疫抑制を伴う治療法が頻繁にとられるため、学会では以前からガイドラインの有用性を訴えていた。宮坂医師は言う。

「リウマチ治療で劇症肝炎が起こることは10万人に1人以下と極めて低いのですが、学会では注意を呼びかけていました。しかし、これまでは検査が保険診療の対象でなかったのでガイドラインとして発表できませんでした。今後は学会員へ告知していきたい」

医師も知らない新薬治療に伴うB型肝炎の隠れた危険性は、適切な時期に適切な対処をすれば防ぐことができる。しかし、その対処法を知らなければ、今後も不幸な事態は起こりえるだろう。全国の医療関係者に、この事実を周知することが必要である。

本誌・西岡千史

免疫抑制療法によって発症したB型劇症肝炎の死亡例
(2004～08年※B型慢性肝炎患者は除く

年齢	性別	病名
63	男	悪性リンパ腫
64	女	悪性リンパ腫
48	女	悪性リンパ腫
64	男	多発性骨髄腫
61	女	慢性リンパ球性白血病
68	男	悪性リンパ腫
65	女	悪性リンパ腫
67	男	悪性リンパ腫
68	女	乳がん
71	男	悪性リンパ腫
76	女	悪性リンパ腫
63	男	悪性リンパ腫
70	男	悪性リンパ腫
70	男	悪性リンパ腫

坪内博仁教授提供の資料を基に編集部が作成

29　2011.10.14

ARTHRITIS & RHEUMATISM
Vol. 64, No. 8, August 2012, pp 2655–2662
DOI 10.1002/art.34465

Interleukin-1 and Tumor Necrosis Factor α Blockade Treatment of Experimental Polymyositis in Mice

Takahiko Sugihara,[1] Naoko Okiyama,[1] Naoto Watanabe,[2] Nobuyuki Miyasaka,[2] and Hitoshi Kohsaka[1]

Objective. **Histologic studies of the muscles suggest that cytokines are involved in inflammatory myopathy. The therapeutic effects of cytokine blockade are controversial, with anecdotal reports of clinical efficacy. The aim of this study was to discern the significance of interleukin-1 (IL-1) and tumor necrosis factor α (TNFα) as therapeutic targets in polymyositis (PM) by studying their involvement and the effects of their blockade in C protein–induced myositis (CIM), a murine model of PM.**

Methods. **C57BL/6 mice were immunized with recombinant skeletal C protein fragments to induce CIM. The expression of IL-1 and TNFα in the muscles of mice with CIM was detected using immunohistochemical and real-time polymerase chain reaction analyses. After the onset of myositis, the mice with CIM were treated with recombinant IL-1 receptor antagonist (IL-1Ra), anti–IL-1R monoclonal antibody, recombinant TNF receptor (p75)–fusion protein (TNFR-Fc), or anti-TNFα monoclonal antibody. The muscles were examined histologically for the severity of myositis.**

Results. **IL-1α– and TNFα-positive macrophages were observed in the muscle tissue of mice with CIM as early as 7 days after immunization. IL-1α, IL-1β, and TNFα expression in the muscles increased as the severity of myositis peaked, at both the messenger RNA and protein levels. Continuous subcutaneous delivery of IL-1Ra resulted in suppression of established CIM. Intermittent delivery (1-day intervals) of anti–IL-1R monoclonal antibody suppressed myositis, while intermittent delivery of IL-1Ra did not suppress myositis. Treatment with anti-TNFα monoclonal antibody and with TNFR-Fc also reduced the severity of CIM.**

Conclusion. **IL-1 and TNF blockade ameliorated CIM after disease onset and should potentially be a new strategy for the treatment of inflammatory myopathy. As IL-1 blockade, treatment with anti–IL-1R monoclonal antibody appeared more feasible than the other approaches.**

Polymyositis (PM) is a chronic autoimmune inflammatory myopathy affecting striated muscles (1). An accumulated body of evidence supports the notion that the pathology of PM is driven by cytotoxic CD8 T cells (2–7), but the event that initiates the inflammatory processes has not been identified. Currently, patients with PM are treated primarily with nonspecific immunosuppressants, including high-dose corticosteroids, methotrexate, and/or other small-molecule immunosuppressants. Because the administration of therapeutic agents can elicit a wide variety of adverse reactions, treatments that address the specific pathology of PM need to be developed.

In the development of new therapeutic approaches to human diseases, animal models have served as a means with which to identify therapeutic targets and to test the effect of new treatments (8–11). Despite the known limitations, experiments in animals with collagen-induced arthritis (CIA) have facilitated development of new treatments for rheumatoid arthritis (RA). Treatment approaches such as blockade of interleukin-1 (IL-1), tumor necrosis factor α (TNFα), and IL-6 have had an enormous effect in modulating the disease course of RA (12–15).

However, in myositis research, no appropriate

Supported by grants-in-aid from the Ministry of Education, Culture, Sports, Science, and Technology, Japan and from the Ministry of Health, Labor and Welfare, Japan, and by a Global Centers of Excellence Program grant from the Japanese Ministry of Education for the Promotion of Science to the International Research Center for Molecular Science in Tooth and Bone Diseases at Tokyo Medical and Dental University.

[1]Takahiko Sugihara, MD, PhD, Naoko Okiyama MD, PhD, Hitoshi Kohsaka, MD, PhD: Tokyo Medical and Dental University, Tokyo, Japan, and Yokohama Institute, RIKEN, Yokohama, Japan; [2]Naoto Watanabe, MD, Nobuyuki Miyasaka, MD, PhD: Tokyo Medical and Dental University, Tokyo, Japan.

Address correspondence to Hitoshi Kohsaka, MD, PhD, Department of Medicine and Rheumatology, Graduate School of Medical and Dental Sciences, Tokyo Medical and Dental University, 1-5-45 Yushima, Bunkyo-ku, Tokyo 113-8519, Japan. E-mail: kohsaka.rheu@tmd.ac.jp.

Submitted for publication November 17, 2010; accepted in revised form March 1, 2012.

animal model of PM had been available until the murine model of C protein–induced myositis (CIM) was developed (16). Unlike the classic model of experimental autoimmune myositis (EAM), which is induced by repeated immunizations to desferlin gene–mutated mice (SJL/J strain) with crude myosin, CIM can be induced in C57BL/6 (B6) mice by a single immunization with recombinant human fast-type skeletal muscle C protein fragments. Although serum can be used to transfer EAM to naive mice (17), CIM is primarily mediated by cytotoxic CD8 T cells (18). Among the available models, CIM mimics human PM best in terms of pathology (16,18).

Because of the availability of biologic anticytokine reagents for clinical use, these reagents have been anecdotally tested for the treatment of patients with PM and patients with dermatomyositis (DM) who did not respond to conventional treatment (19–21). In this regard, results of animal experiments using anticytokine reagents will represent a rationale for conducting controlled clinical studies in humans. We recently observed that anti–IL-6 receptor (anti–IL-6R) antibodies were effective for the treatment of CIM (22).

In mice with CIM and in the muscles of patients with PM (23,24), both IL-1 and TNFα are expressed by infiltrating mononuclear cells. Previously, we observed that the development of CIM was suppressed in IL-1α/β–null mutant mice but not in TNFα-null mutant mice (16). This observation suggested the differential requirement of inflammatory cytokines for CIM induction. However, it is unclear whether blockade of IL-1 or TNFα after disease onset can suppress CIM. Also, genetically mutated mice may undergo skewed development of the immune system and respond aberrantly to immunogens. In the present study, we examined the therapeutic effects of IL-1 blockade and TNFα blockade in mice with established CIM. In addition, antibodies and soluble decoy molecules were compared for the in vivo effects of IL-1 blockade.

MATERIALS AND METHODS

Induction of CIM. Female B6 mice (Charles River), ages 8–10 weeks, were immunized by intradermal injection of recombinant human fast-type skeletal muscle C protein fragments emulsified in Freund's complete adjuvant (CFA) together with intraperitoneal injection of pertussis toxin (16). All experiments were carried out under specific pathogen–free conditions in accordance with the ethics and safety guidelines for animal experiments of Tokyo Medical and Dental University and RIKEN.

Anticytokine treatment. Murine IL-1R antagonist (IL-1Ra), hamster anti-mouse IL-1R chimeric IgG1 monoclonal antibody (clone M147), and murine recombinant TNF receptor (p75)–fusion protein (TNFR-Fc) were provided by Amgen. Anti-TNFα chimeric (rat and murine) IgG2a monoclonal antibody (clone cV1q) and control chimeric IgG2a monoclonal antibody with unknown antigen specificity (clone cVaM) were provided by Centocor. IL-1Ra was administered continuously with subcutaneously implanted osmotic minipumps (Durect), while the other treatments were administered intraperitoneally 3 times weekly.

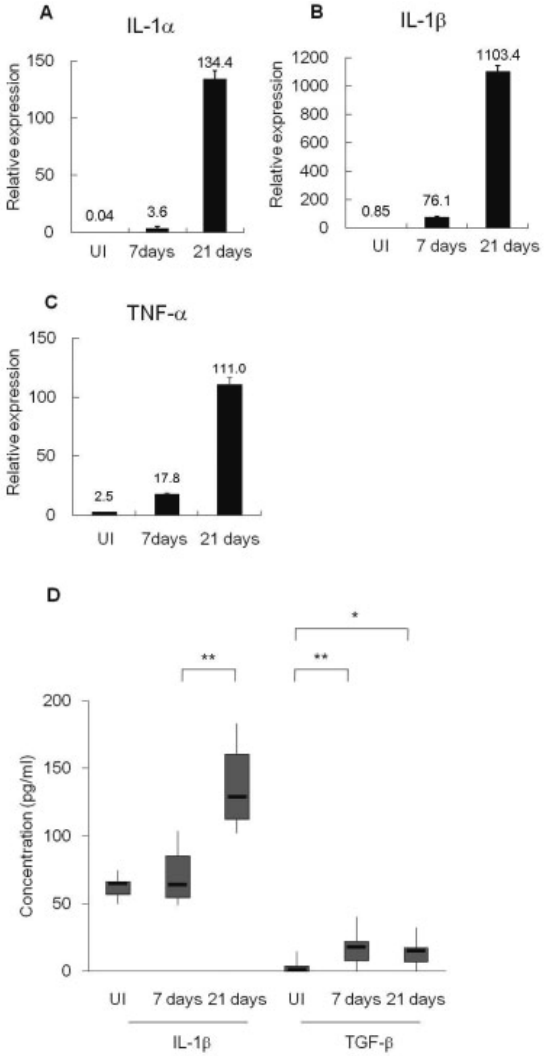

Figure 1. Interleukin-1 (IL-1), tumor necrosis factor α (TNFα), and transforming growth factor β1 (TGFβ1) expression in the muscles of mice with C protein–induced myositis (CIM). **A–C,** Real-time polymerase chain reaction analysis was performed to quantify the expression of IL-1α (**A**), IL-1β (**B**), and TNFα (**C**) mRNA in the muscle tissue of unimmunized (UI) mice and mice with CIM, 7 days and 21 days after immunization. Expression levels are normalized to expression of GAPDH. Bars show the mean ± SD (n = 3 mice). **D,** Enzyme-linked immunosorbent assay of IL-1β and active TGFβ1 was carried out in the muscles of unimmunized mice (n = 6) and mice with CIM (n = 8–10), 7 days and 21 days after immunization. Data are presented as box plots, where the boxes represent the 25th to 75th percentiles, the lines within the boxes represent the median, and the lines outside the boxes represent 0–100%. $* = P < 0.05$; $** = P < 0.01$.

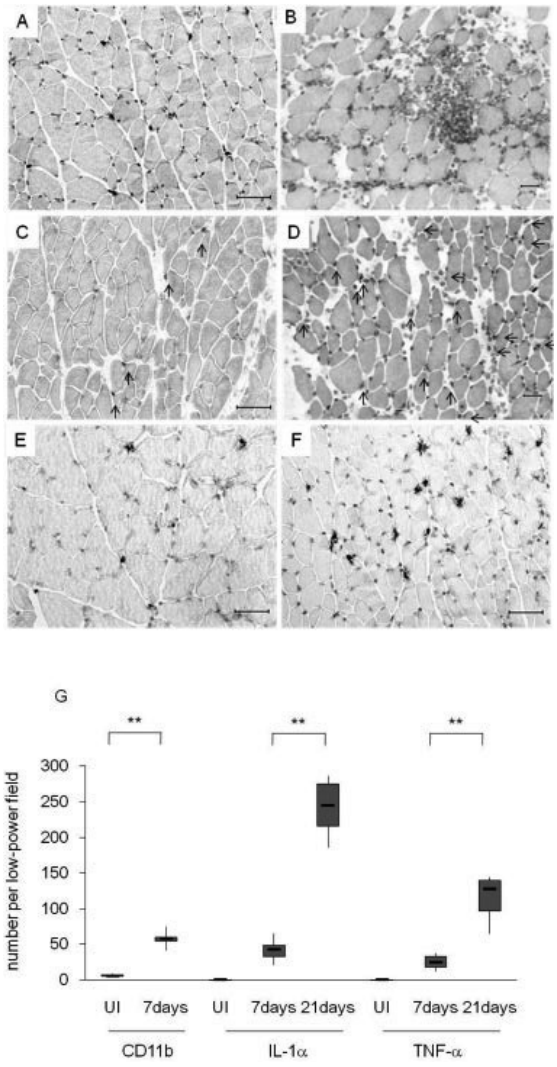

Figure 2. Immunohistochemical analysis of muscle tissue. IL-1α (**A** and **B**), TNFα (**C** and **D**; **arrows** indicate positively stained cells), and CD11b (**E** and **F**) were detected immunohistochemically in muscle sections from unimmunized mice (**E**) and mice with CIM 7 days after immunization (**A**, **C**, and **F**) and 21 days after immunization (**B** and **D**). In these sections, 10 low-power (200×) fields were selected to include myositis lesions, where CD11b-, IL-1α–, and TNFα-positive cells were enumerated (**G**). IL-1– and TNFα-positive cells appeared in the muscles 7 days after immunization with C protein/Freund's complete adjuvant and become more abundant 21 days after immunization. CD11b-positive cells were present in the muscle tissue of unimmunized mice and expressed no detectable inflammatory cytokines. Seven days after immunization, the number of CD11b-positive cells in the muscles increased significantly. The distribution pattern of CD68-positive cells in muscles was the same as the distribution pattern of CD11b-positive cells (data not shown). Bars in **A**, **C**, **E**, and **F** = 50 μm; bars in **B** and **D** = 30 μm. Data in **G** are presented as box plots, where the boxes represent the 25th to 75th percentiles, the lines within the boxes represent the median, and the lines outside the boxes represent 0–100%. ** = $P < 0.01$. See Figure 1 for definitions.

Histologic severity of inflammation. The system for scoring the histologic severity of inflammation in muscles affected by experimental myositis was originally established using a Lewis rat model of myositis (25,26). This system was applied successfully to the evaluation of several treatments of CIM (16,22).

For each mouse, 2 sections of bilateral muscles (hamstrings or quadriceps) were evaluated. Myositis was defined as mononuclear cell infiltration spreading around muscle fibers, including at least 1 necrotic muscle fiber. The histologic score for myositis severity was determined according to the number of muscle fibers associated with cellular infiltration (grade 1 = lesions with <5 muscle fibers involved, grade 2 = lesions involving 5–30 muscle fibers, grade 3 = lesions involving an entire muscle fasciculus, and grade 4 = extensive lesions across muscle fasciculi). When multiple lesions with the same grade were observed in the 2 sections of a muscle block, 0.5 point was added to the grade. The mean score of bilateral muscles was calculated and used as the score for each mouse. The muscle sections were evaluated in a blinded manner by at least 2 independent observers, who reported comparable results.

Quantification of cytokine messenger RNA (mRNA) expression. Total RNA was isolated from hindleg muscle tissue with Isogen reagent (Nippon Gene). Quantitative polymerase chain reaction (PCR) was performed on a PerkinElmer 7700 sequence detector using sets of primers and FAM-labeled TaqMan probes specific for IL-1α, IL-1β, TNFα, and GAPDH complementary DNA (Assays-on-Demand; Applied Biosystems).

Enzyme-linked immunsorbent assay (ELISA) of muscle homogenate. The muscles were homogenized in phosphate buffered saline containing protease inhibitors (cOmplete Mini tablets; Roche Diagnostics) and radioimmunoprecipitation assay buffer (Millipore), 3 times for 20 seconds with homogenizer (Mini-BeadBeater; BioSpec) at 2500 revolutions per minute. The supernatants were collected, and the concentrations of IL-1β and active transforming growth factor β1 (TGFβ1) were measured with Quantikine ELISA kits (R&D Systems) according to the manufacturer's directions.

Immunohistochemical analysis. The expression of CD11b, CD68, IL-1α, and TNFα in muscle sections was examined immunohistochemically, as previously described (16). To quantify the stained cells, 10 low-power (200×) fields in each section were selected to include myositis lesions. The numbers of CD11b-, IL-1α–, and TNFα-positive cells in these fields were then determined.

Statistical analysis. Histology scores and quantitative analysis of immunohistochemical studies were analyzed using the Mann-Whitney U test.

RESULTS

IL-1 and TNFα expression in mice with CIM. In the murine model of CIM, which was induced by immunizing B6 mice with recombinant C protein fragments, necrotic muscle fibers with surrounding mononuclear cell infiltration appeared as early as 7 days and peaked 14–21 days after immunization (16). Real-time quantitative PCR analysis of mRNA in the muscles revealed that IL-1α, IL-1β, and TNFα mRNA were up-regulated 7 days after immunization, with increased expression observed at the peak of inflammation (Figures 1A–C).

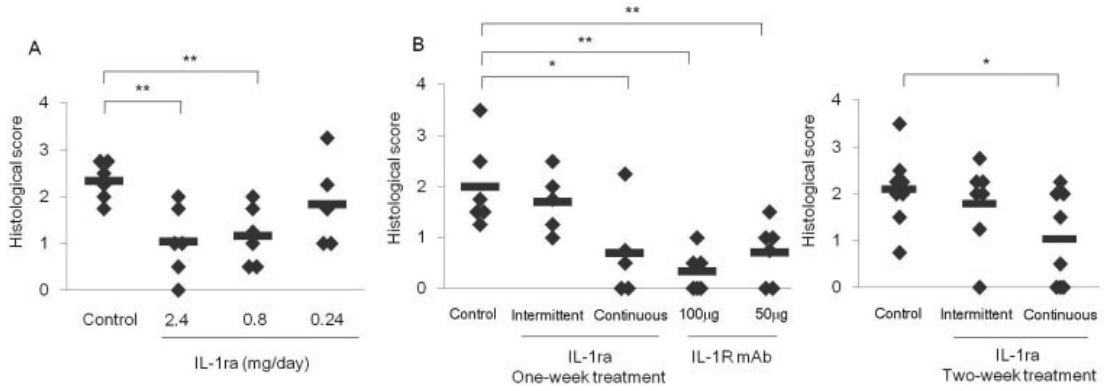

Figure 3. Effect of IL-1 blockade in mice with established CIM. **A,** IL-1 receptor antagonist (IL-1Ra) was administered to mice with CIM by continuous subcutaneous infusion beginning 7 days after immunization with C protein. Bovine serum albumin (2.4 mg/day) was used as a control. The severity of myositis was assessed histologically 14 days after immunization. Each experimental group consisted of 5 or 6 mice. **B,** IL-1Ra (total 7.2 mg) was intraperitoneally injected 7 days, 9 days, and 11 days after immunization (intermittent 1-week treatment). IL-1Ra was injected continuously (0.8 mg/day, total 5.6 mg) with a subcutaneously implanted minipump (continuous 1-week treatment). Anti–IL-1R monoclonal antibody (mAb) was administered intraperitoneally 7 days, 9 days, and 11 days after immunization. Saline was used as a treatment control. The severity of myositis was assessed histologically 14 days after immunization. Each experimental group consisted of 5 or 6 mice. For the 2-week treatment protocol for IL-1Ra, intermittent treatment (total 14.4 mg) and continuous treatment (total 11.2 mg) were started 7 days after immunization, and myositis was assessed histologically 21 days after immunization. Bovine serum albumin (0.8 mg/day) was used as a control. Each experimental group consisted of 7 or 8 mice. Bars represent the mean scores of individual groups. $* = P < 0.05$; $** = P < 0.01$ versus control. See Figure 1 for other definitions.

Similar results were observed at the protein level. ELISA showed that IL-1β expression was significantly increased in the muscles of mice with CIM (Figure 1D). Immunohistochemical studies showed that IL-1– and TNFα-positive cells appeared in the muscles 7 days after the C protein immunization and become more abundant 21 days after immunization (Figures 2A–D and G). In contrast, active TGFβ1 was barely detectable 7 days after immunization and stayed at a constant level even at the peak of inflammation. (Figure 1D).

Resident macrophages were present around nonnecrotic muscle fibers, since CD11b-positive cells were present in the muscle tissue of unimmunized mice (Figures 2E and G). Immunohistochemical studies showed that the resident macrophages expressed no detectable inflammatory cytokines (Figure 2G). Seven days after the C protein/CFA immunization, the number of macrophages in the muscles increased significantly (Figures 2F). Thus, macrophages were recruited and activated to produce inflammatory cytokines in the muscles beginning in the early stage of myositis.

Therapeutic effects of IL-1 blockade on established CIM. IL-1–null mutant mice have been shown to be resistant to CIM induction. In the present study, IL-1 was blocked to discern whether this approach can alleviate the severity of CIM after disease onset. Blockade was carried out using IL-1Ra or anti–IL-1R monoclonal antibodies. Treatment was started 7 days after immunization. IL-1Ra was administered continually (0.24, 0.8, and 2.4 mg/day/mouse) for 7 days with minipumps implanted under the back dermis. The same amount of bovine serum albumin acted as a control. Histologic scoring of the muscles from the treated mice showed that IL-1Ra successfully suppressed CIM, in a dose-dependent manner (Figure 3A).

Although continuous administration of IL-1Ra was effective, this mode of infusion would not be practical for the treatment of patients. Thus, we next treated the mice with CIM intermittently (7, 9, and 11 days after immunization) and examined the muscles 3 days after treatment completion. Although a total of 7.2 mg of IL-1Ra was administered, intermittent administration of IL-1Ra failed to ameliorate the disease (Figure 3B). Continuous administration of IL-1Ra (0.8 mg/day), starting on the same day as the intermittent injections, was effective. The advantage of continuous treatment over intermittent treatment was maintained in a 2-week treatment protocol (Figure 3B).

Generally, monoclonal antibodies bind more stably to cell surface receptors than do soluble forms of the corresponding ligands. Indeed, when recombinant TNF receptor (p75)–fusion protein (TNFR-Fc) (100 μg/day and 50 μg/day) was injected intraperitoneally according to the same 1-week intermittent administration

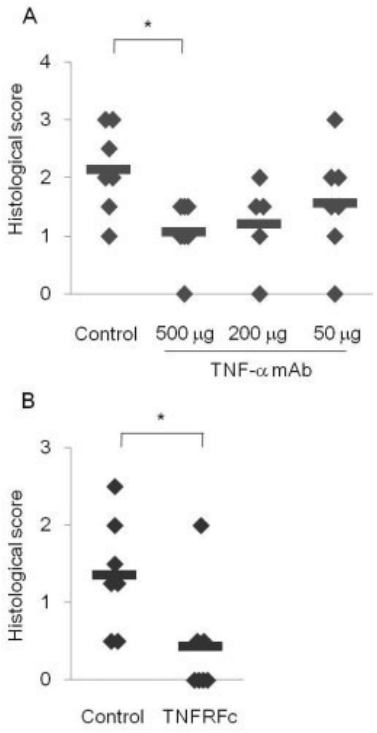

Figure 4. Effect of TNFα blockade on established CIM. **A,** Anti-TNFα monoclonal antibodies (50 μg, 200 μg, and 500 μg) and control antibodies (500 μg) were administered intraperitoneally 3 times weekly for 2 weeks, starting 7 days after immunization with C protein. **B,** Murine recombinant TNF receptor (p75)–fusion protein (TNFR-Fc) (100 μg) and bovine serum albumin (100 μg) were administered as described in **A**. Myositis was assessed histologically 21 days after immunization. Each experimental group consisted of 7 mice. Bars represent the mean scores of each group. $* = P < 0.05$ versus control. See Figure 1 for other definitions.

protocol, treatment with both doses ameliorated CIM (Figure 3B).

Therapeutic effects of TNFα blockade on ongoing CIM. Mice with CIM were also treated with TNFα-blocking reagents, including anti-TNFα monoclonal antibody and TNFR-Fc. Different doses of the anti-TNFα monoclonal antibody (50 μg, 200 μg, and 500 μg) and TNFR-Fc (100 μg) were administered 3 times weekly for 2 weeks, starting 7 days after immunization. The muscles of the treated mice were assessed 3 days after treatment completion. The histologic scores of the mice treated with either type TNFα (500 μg) or TNFR-Fc were significantly lower than those of the control mice (Figures 4A and B).

DISCUSSION

The expression of IL-1 and TNFα in the muscles of mice with CIM was observed beginning in the early phase of disease (day 7) and increased as the severity of inflammation peaked. Blockade of either cytokine after disease onset suppressed CIM. These results suggest that both IL-1 and TNFα are potential therapeutic targets in the treatment of PM.

Both IL-1 blockade and TNFα blockade reduced the severity of CIM. Previous histologic studies of the muscles of patients with PM showed that IL-1 expression by mononuclear cells accompanied up-regulation of class I major histocompatibility complex (MHC) molecules on the muscle fibers (27), and that IL-1R expression on muscle fibers was most pronounced in the vicinity of IL-1–expressing cells (28). TNFα-positive mononuclear cells have also been observed in the muscles of patients with PM (24). Like IL-1, TNFα increased class I MHC expression on human myoblasts in vitro (29,30). Also, TNF can damage muscle fiber directly (31). These findings suggest that IL-1 and TNFα expression of activated macrophages in muscles may contribute to both up-regulation of class I MHC molecules on muscle fibers and direct muscle damage.

IL-1 is involved in antigen-specific T cell differentiation. T cell proliferative responses to type II collagen were impaired in IL-1α/β–double-null mutant mice immunized with type II collagen for induction of CIA, which is also a model of induced autoimmune disease. In vitro experiments suggested that dendritic cells cannot activate T cells fully if they are not activated by IL-1 (32–34). Recently, it was shown that IL-1, together with TGFβ and IL-6, is involved in the differentiation of Th17 cells (35). In addition, IL-1 promoted Th17 cell differentiation in mice with experimental autoimmune encephalomyelitis (EAE) (36) and also in IL-1Ra–deficient mice with destructive arthritis (37). However, IL-17A was dispensable in the development of CIM (22). Actually, CD3 cells from the inguinal lymph nodes of mice with CIM that had or had not received IL-1Ra treatment proliferated equally in response to C protein–pulsed dendritic cells (data not shown). Thus, we did not see attenuation of pathogenic T cell responses in the IL-1Ra–treated mice.

The therapeutic effects of cytokine blockade could not be tested until CIM had developed. The classic EAM model not only is mediated by CD4 humoral immune responses (17) but also requires continual administration of CFA throughout the disease course. This makes it difficult to discern whether any treatment blocked the adjuvant effects of CFA or the pathologic

processes of myositis per se. In contrast, CIM can be induced with a single immunization and can be treated after disease onset. However, it is still difficult to initiate treatment at the very peak of the disease, because regression occurs spontaneously.

We performed ELISA of active TGFβ as an antiinflammatory cytokine. Previous studies showed that TGFβ was expressed in the muscles of patients with PM (23) and suggested that TGFβ from macrophages may contribute to muscle regeneration after muscle injury (38). This is consistent with the marginal elevation of TGFβ expression observed in the muscles of mice with CIM.

Because a major clinical manifestation of myositis is muscle weakness, rotarod testing was used to measure muscle function as the clinical outcome in our previous study (16). We actually used the same rotarod test in the anti-TNFα antibody treatment experiment and observed that the mean running time of the treated mice was longer than that of control mice. However, the difference did not reach statistical significance. According to our experience, the rotarod test is not as sensitive as histologic analyses, because mice become accustomed to the device and thus are able to avoid falling off, and the efforts of mice are inconsistent. We have used different techniques to measure muscle weakness in mice with CIM, including measurement of walking time, walking distance, and rearing time in open-field tests but have not yet identified an appropriate technique for use in mice with CIM.

In a clinical trial of the treatment of multiple sclerosis, TNF inhibitors occasionally exacerbated the disease (39). In accordance with this finding, TNF-null mice developed severe EAE (40). TNF inhibitors sometimes induce a lupus-like syndrome in the clinical setting (41). In an animal model, TNF-null (NZB $\times$ NZW)F_1 mice developed lupus nephritis (42), and injection of high doses of TNF delayed disease onset (43). In contrast, TNF inhibitors were proven to be useful in the treatment of both RA and CIA (8,12). Nevertheless, TNFα-null mice are fully susceptible to CIA (44). The current study showed that TNFα inhibitors are effective in treating a murine model of PM, although TNFα-null mice are fully susceptible to CIM induction. Thus, this is the second instance in which the inducibility of autoimmune diseases is different between TNFα-null mice and mice treated with TNFα inhibitors. It has been proposed that increased numbers of memory CD4 T cells and augmented interferon-γ production from CD4 T cells are responsible for exacerbated disease activity of CIA in TNFα-null mice (44). Although CD4 T cells and IL-17–producing lymphocytes play a critical role in CIA (45), both are dispensable for muscle injury in CIM. The genetic absence of TNFα appears to have extensive effects on the effector function of lymphocytes. The efficacy of TNF inhibitors in the treatment of PM and DM is controversial (19–21). According to anecdotal case reports, myositis occurred in patients with RA even after initiation of treatment with TNF inhibitors (46,47). It would be of particular interest to know the clinical effects of TNF inhibitors in patients with myositis.

In the US, IL-1Ra (anakinra) has been approved for the treatment of RA. Because its terminal half-life ranges from 4 hours to 6 hours, IL-1Ra should be injected subcutaneously every day. The discrepant efficacy of IL-1Ra and anti–IL-1R monoclonal antibody in the present studies may be explained by differences in the half-life as well as the affinity to IL-1R.

DM is another inflammatory myopathy that is driven by autoimmunity. It has been proposed that PM is mediated by cytotoxic CD8 T cells, while DM is mediated by humoral responses. However, the accumulated body of evidence suggests that PM and DM are similar in terms of muscle pathology as well as responses to various treatments (48). Sontheimer proposed that both PM and DM are within a single disease spectrum (49). With the CIM model, we believe that by using the CIM model in this study, we provide support for clinical trials of IL-1 and TNF blockade to treat PM and DM.

ACKNOWLEDGMENTS

We thank Drs. Wayne Tsuji and Takashi Nakae for their critical advice and Eri Yoshimoto for her technical assistance.

AUTHOR CONTRIBUTIONS

All authors were involved in drafting the article or revising it critically for important intellectual content, and all authors approved the final version to be published. Dr. Kohsaka had full access to all of the data in the study and takes responsibility for the integrity of the data and the accuracy of the data analysis.

Study conception and design. Sugihara, Okiyama, Miyasaka, Kohsaka.

Acquisition of data. Sugihara, Okiyama, Watanabe, Miyasaka, Kohsaka.

Analysis and interpretation of data. Sugihara, Okiyama, Watanabe, Miyasaka, Kohsaka.

REFERENCES

1. Dalakas MC, Hohlfeld R. Polymyositis and dermatomyositis. Lancet 2003;362:971–82.
2. Arahata K, Engel AG. Monoclonal antibody analysis of mononuclear cells in myopathies. I: quantitation of subsets according to diagnosis and sites of accumulation and demonstration and counts of muscle fibers invaded by T cells. Ann Neurol 1984;16:193–208.
3. Engel AG, Arahata K. Monoclonal antibody analysis of mononuclear cells in myopathies. II: phenotypes of autoinvasive cells in

polymyositis and inclusion body myositis. Ann Neurol 1984;16: 209–15.
4. Goebels N, Michaelis D, Engelhardt M, Huber S, Bender A, Pongratz D, et al. Differential expression of perforin in muscle-infiltrating T cells in polymyositis and dermatomyositis. J Clin Invest 1996;97:2905–10.
5. Emslie-Smith AM, Arahata K, Engel AG. Major histocompatibility complex class I antigen expression, immunolocalization of interferon subtypes, and T cell-mediated cytotoxicity in myopathies. Hum Pathol 1989;20:224–31.
6. Bender A, Ernst N, Iglesias A, Dornmair K, Wekerle H, Hohlfeld R. T cell receptor repertoire in polymyositis: clonal expansion of autoaggressive $CD8^+$ T cells. J Exp Med 1995;181:1863–8.
7. Nishio J, Suzuki M, Miyasaka N, Kohsaka H. Clonal biases of peripheral CD8 T cell repertoire directly reflect local inflammation in polymyositis. J Immunol 2001;167:4051–8.
8. Williams RO, Feldmann M, Maini RN. Anti-tumor necrosis factor ameliorates joint disease in murine collagen-induced arthritis. Proc Natl Acad Sci U S A 1992;89:9784–8.
9. Taniguchi K, Kohsaka H, Inoue N, Terada Y, Ito H, Hirokawa K, et al. Induction of the p16INK4a senescence gene as a new therapeutic strategy for the treatment of rheumatoid arthritis. Nat Med 1999;7:760–7.
10. Sekine C, Sugihara T, Miyake S, Hirai H, Yoshida M, Miyasaka N, et al. Successful treatment of animal models of rheumatoid arthritis with small-molecule cyclin-dependent kinase inhibitors. J Immunol 2008;180:1954–61.
11. Takagi N, Mihara M, Moriya Y, Nishimoto N, Yoshizaki K, Kishimoto T, et al. Blockage of interleukin-6 receptor ameliorates joint disease in murine collagen-induced arthritis. Arthritis Rheum 1998;41:2117–21.
12. Lipsky PE, van der Heijde DM, St Clair EW, Furst DE, Breedveld FC, Kalden JR, et al, for the Anti–Tumor Necrosis Factor Trial in Rheumatoid Arthritis with Concomitant Therapy Study Group. Infliximab and methotrexate in the treatment of rheumatoid arthritis. N Engl J Med 2000;343:1594–602.
13. Klareskog L, van der Heijde D, de Jager JP, Gough A, Kalden J, Malaise M, et al. Therapeutic effect of the combination of etanercept and methotrexate compared with each treatment alone in patients with rheumatoid arthritis: double-blind randomised controlled trial. Lancet 2004;363:675–81.
14. Jiang Y, Genant HK, Watt I, Cobby M, Bresnihan B, Aitchison R, et al. A multicenter, double-blind, dose-ranging, randomized, placebo-controlled study of recombinant human interleukin-1 receptor antagonist in patients with rheumatoid arthritis: radiologic progression and correlation of Genant and Larsen scores. Arthritis Rheum 2000;43:1001–9.
15. Smolen JS, Beaulieu A, Rubbert-Roth A, Ramos-Remus C, Rovensky J, Alecock E, et al, for the OPTION Investigators. Effect of interleukin-6 receptor inhibition with tocilizumab in patients with rheumatoid arthritis (OPTION study): a double-blind, placebo-controlled, randomised trial. Lancet 2008;371: 987–97.
16. Sugihara T, Sekine C, Nakae T, Kohyama K, Harigai M, Iwakura Y, et al. A new murine model to define the critical pathologic and therapeutic mediators of polymyositis. Arthritis Rheum 2007;56: 1304–14.
17. Matsubara S, Shima T, Takamori M. Experimental allergic myositis in SJL/J mice immunized with rabbit myosin B fraction: immunohistochemical analysis and transfer. Acta Neuropathol 1993;85:138–44.
18. Sugihara T, Okiyama N, Suzuki M, Kohyama K, Matsumoto Y, Miyasaka N, et al. Definitive engagement of cytotoxic CD8 T cells in C-protein induced myositis, a murine model of polymyositis. Arthritis Rheum 2010;62:3088–92.
19. Efthimiou P, Schwartzman S, Kagen LJ. Possible role for tumour necrosis factor inhibitors in the treatment of resistant dermatomyositis and polymyositis: a retrospective study of eight patients. Ann Rheum Dis 2006;65:1233–6.
20. Dastmalchi M, Grundtman C, Alexanderson H, Mavragani CP, Einarsdottir H, Helmers SB, et al. A high incidence of disease flares in an open pilot study of infliximab in patients with refractory inflammatory myopathies. Ann Rheum Dis 2008;67: 1670–7.
21. The Muscle Study Group. A randomized, pilot trial of etanercept in dermatomyositis. Ann Neurol 2011;70:427–36.
22. Okiyama N, Sugihara T, Iwakura Y, Yokozeki H, Miyasaka N, Hitoshi Kohsaka. Therapeutic effects of interleukin-6 blockade in a murine model of polymyositis that does not require interleukin-17A. Arthritis Rheum 2009;60:2505–12.
23. Lundberg I, Ulfgren AK, Nyberg P, Andersson U, Klareskog L. Cytokine production in muscle tissue of patients with idiopathic inflammatory myopathies. Arthritis Rheum 1997;40:865–74.
24. Kuru S, Inukai A, Liang Y, Doyu M, Takano A, Sobue G. Tumor necrosis factor-α expression in muscles of polymyositis and dermatomyositis. Acta Neuropathol 2000;99:585–8.
25. Kojima T, Tanuma N, Aikawa Y, Shin T, Sasaki A, Matsumoto Y. Myosin-induced autoimmune polymyositis in the rat. J Neurol Sci 1997;151:141–8.
26. Kohyama K, Matsumoto Y. C protein in the skeletal muscle induces severe autoimmune polymyositis in Lewis rats. J Neuroimmunol 1999;98:130–5.
27. Lundberg I, Kratz AK, Alexanderson H, Patarroyo M. Decreased expression of interleukin-1α, interleukin-1β, and cell adhesion molecules in muscle tissue following corticosteroid treatment in patients with polymyositis and dermatomyositis. Arthritis Rheum 2000;43:336–48.
28. Grundtman C, Salomonsson S, Dorph C, Bruton J, Andersson U, Lundberg IE. Immunolocalization of interleukin-1 receptors in the sarcolemma and nuclei of skeletal muscle in patients with idiopathic inflammatory myopathies. Arthritis Rheum 2007;56: 674–87.
29. Nagaraju K, Raben N, Merritt G, Loeffler L, Kirk K, Plotz P. A variety of cytokines and immunologically relevant surface molecules are expressed by normal human skeletal muscle cells under proinflammatory stimuli. Clin Exp Immunol 1998;113:407–14.
30. Chevrel G, Granet C, Miossec P. Contribution of tumour necrosis factor α and interleukin (IL) 1β to IL6 production, NF-κB nuclear translocation, and class I MHC expression in muscle cells: in vitro regulation with specific cytokine inhibitors. Ann Rheum Dis 2005;64:1257–62.
31. Guttridge DC, Mayo MW, Madrid LV, Wang CY, Baldwin AS Jr. NF-κB-induced loss of MyoD messenger RNA: possible role in muscle decay and cachexia. Science 2000;289:2363–6.
32. Nakae S, Asano M, Horai R, Sakaguchi N, Iwakura Y. IL-1 enhances T cell-dependent antibody production through induction of CD40 ligand and OX40 on T cells. J Immunol 2001;167:90–7.
33. Saijo S, Asano M, Horai R, Yamamoto H, Iwakura Y. Suppression of autoimmune arthritis in interleukin-1–deficient mice in which T cell activation is impaired due to low levels of CD40 ligand and OX40 expression on T cells. Arthritis Rheum 2002;46:533–44.
34. Eriksson U, Kurrer MO, Sonderegger I, Iezzi G, Tafuri A, Hunziker L, et al. Activation of dendritic cells through the interleukin 1 receptor 1 is critical for the induction of autoimmune myocarditis. J Exp Med 2003;197:323–31.
35. Miossec P, Korn T, Kuchroo VK. Interleukin-17 and type 17 helper T cells. N Engl J Med 2009;361:888–98.
36. Sutton C, Brereton C, Keogh B, Mills K, Lavelle EC. A crucial role for interleukin (IL)-1 in the induction of IL-17-producing T cells that mediate autoimmune encephalomyelitis. J Exp Med 2006;203: 1685–91.
37. Nakae S, Saijo S, Horai R, Sudo K, Mori S, Iwakura Y. IL-17 production from activated T cells is required for the spontaneous development of destructive arthritis in mice deficient in IL-1 receptor antagonist. Proc Natl Acad Sci U S A 2003;100:5986–90.
38. Arnold L, Henry A, Poron F, Baba-Amer Y, van Rooijen N, Plonquet A, et al. Inflammatory monocytes recruited after skeletal

muscle injury switch into antiinflammatory macrophages to support myogenesis. J Exp Med 2007;204:1057–69.
39. The Lenercept Multiple Sclerosis Study Group and The University of British Columbia MS/MRI Analysis Group. TNF neutralization in MS: results of a randomized, placebo-controlled multicenter study. Neurology 1999;53:457–65.
40. Liu J, Marino MW, Wong G, Grail D, Dunn A, Bettadapura J, et al. TNF is a potent anti-inflammatory cytokine in autoimmune-mediated demyelination. Nat Med 1998;4:78–83.
41. Soforo E, Baumgartner M, Francis L, Allam F, Phillips PE, Perl A. Induction of systemic lupus erythematosus with tumor necrosis factor blockers. J Rheumatol 2010;37:204–5.
42. Kontoyiannis D, Kollias G. Accelerated autoimmunity and lupus nephritis in NZB mice with an engineered heterozygous deficiency in tumor necrosis factor. Eur J Immunol 2000;30:2038–47.
43. Jacob CO, McDevitt HO. Tumour necrosis factor-α in murine autoimmune 'lupus' nephritis. Nature 1988;331:356–8.
44. Campbell IK, O'Donnell K, Lawlor KE, Wicks IP. Severe inflammatory arthritis and lymphadenopathy in the absence of TNF. J Clin Invest 2001;107:1519–27.
45. Nakae S, Nambu A, Sudo K, Iwakura Y. Suppression of immune induction of collagen-induced arthritis in IL-17-deficient mice. J Immunol 2003;171:6173–7.
46. Hall HA, Zimmermann B. Evolution of dermatomyositis during therapy with a tumor necrosis factor α inhibitor. Arthritis Rheum 2006;55:982–4.
47. Ishikawa Y, Yukawa N, Ohmura K, Hosono Y, Imura Y, Kawabata D, et al. Etanercept-induced anti-Jo-1-antibody-positive polymyositis in a patient with rheumatoid arthritis: a case report and review of the literature. Clin Rheumatol 2010;29:563–6.
48. Kohsaka H. Current insights in polymyositis and dermatomyositis. Clin Exp Neuroimmunol 2010;1:22–32.
49. Sontheimer RD. Cutaneous features of classic dermatomyositis and amyopathic dermatomyositis. Curr Opin Rheumatol 1999;11:475–82.

運動器外科学分野
軟骨再生学分野

宗田　大

医歯学総合研究科・生体支持組織学系専攻
運動器外科学・教授

1）研究の課題名

（1）前十字靱帯（ACL）損傷膝の問題の解決

Solution of ACL injured knee related problems

スポーツ膝傷害の代表である前十字靱帯（ACL）損傷とその治療法の発展を長年の教室テーマとして取り組んでいる。内側ハムストリング腱を移植腱として用いる2重束再建術を開発し、臨床的に取り組んできた。本年は昨年に引き続き2束の初期張力計測器を用いた術中計測の影響について報告した（1、2）。また近年注目されているACL損傷後の遺残組織を残す手術術式の意義について、遺残量が示す術前、術後因子を臨床成績の検討から明らかにした（3）。さらにACL遺残組織を完全に温存する新しい術式を開始しその意義を今後解析する予定である。

ACL損傷を放置すると外傷性関節症を発症する。発症素因について患者の検体を用いたマイクロアレイ解析により、重要な遺伝子を明らかにし関節症治療に結びつける取り組みを引き続き行っている。また術直後からの関節内へのヒアルロン酸投与の影響について前向き研究を行っている。

1. Koga H, Muneta T, et al. Arthroscopy 2012（accepted）
2. Koga H, Muneta T, et al. Am J Sports Med. 2012 40（3）: 615-23
3. Muneta T, et al. Knee Surg Sports Traumatol Arthrosc. 2012 Apr 28. [Epub ahead of print]

（2）その他のスポーツ損傷に対する臨床的取組み

Solution of Problems in Orthopaedic Sports Injuries besides ACL injury related surgery

運動器外科学ではスポーツの下肢損傷に対して積極的な治療や介入研究、解剖学的な基礎研究を行っている。解剖学的検討としては前十字靭帯と関節内で共同して機能する後十字靭帯の詳細は肉眼的解剖を完成した（4）。またスポーツ患者にも多発し、世界的にも先駆的に行ってきた内側膝蓋大腿靭帯の解剖学的検討をまとめた（5）。下腿部のスポーツ障害として数多くみられるシンスプリントに対して大学院生が主体となり神奈川県の高校陸上競技選手を対象に行った介入研究が雑誌掲載された（6）。膝蓋腱炎もスポーツ障害として代表的な障害であるが、10数年にわたる臨床研究のまとめが雑誌掲載された（7）。新しい治療法として今後とも多方面の検討が必要である。

4. Hatsushika D, Muneta T, et al. Knee Surg Sports Traumatol Arthrosc. 2012 Sep. 29 [Epub ahead of print]
5. Mochizuki T, Muneta T, et al. Knee Surg Sports Traumatol Arthrosc. 2012 Apr 11. [Epub ahead of print]
6. Muneta T, et al. J Orthop Sci. 2012 17（4）: 425-31

（3）人工膝関節置換術の進歩への取り組み

Development of new design total knee arthroplasty and its related clinical researches

運動器外科学は主に下肢関節疾患の治療を扱っているが、手術として確立している人工膝関節や人工股関節の成績向上の臨床的意義は大きい。人工膝関節のデザイン上後十字靱帯（PCL）を温存するか否かで、コンセプトが異なり、両者の優劣は得られていない。我々は両膝同時置換例で無作為に双方の使い分け、左右の成績の検討を行いPCLを切除するデザインの成績が良好であることを報告した（7）。また人工膝関節のより正常な動きとポリエチレン摩耗を軽減させるために脛骨インサートに回旋自由度などを与えるモバイルベアリングタイプのデザインが検討されているが、透視画像を使用したイメージマッチング法を用いてその有用性を検討した（8）。

2010.12より当教室で開発した新しい人工膝関節の臨床使用が可能になり、東京医科歯科大学で使用を開始して2年が経過した。安全性や機能についてほかの機種と遜色ない成績を上げているが、今後のさらなるデザインの向上や術式の改良の必要性があり、多方面の検討を行っている。

7. Watanabe T, Muneta T, et al. Clin Biomech（Bristol, Avon）2012 27（9）: 924-8
8. Yagishita K, Muneta T, et al. J Arthroplasty 2012 27（3）: 368-74.

(4) 骨、軟骨の形成、ホメオスタシスおよび造血微小環境の制御における骨形成因子BMPの生理機能の解析

Roles of BMPs in postnatal bone and joint homeostasis

骨形成因子（BMP）ファミリーの中でBMP2, 4, 7は、胎生期の骨格ならびに生後の骨組織にオーバーラップして発現が観察される分子である。私たちは、コンディショナルノックアウトマウスの解析から、BMP2は生後の骨のホメオスタシスにおいて必須の分子であり、その欠損により、骨折後の骨修復の過程が完全に阻害されることを明らかとしてきた（Tsuji et al., Nature Genetics, 2006）。これに対して、BMP4及びBMP7のコンディショナルノックアウトマウスでは、X線による解析では、明らかな骨折は確認できず、骨折後の組織修復過程も明らかな遅延は観察されなかった。生後の骨組織で発現しているBMPの中でBMP2のみが重要な生理機能を持っている理由は未だ不明である。一方、BMP4、BMP7を同時に欠損したマウスにおいては、胎生期の骨形成は生じるが、生後の骨形成に重篤な障害が生じることが明らかとなった。このことは、BMP4、BMP7の分子機能は互いに補完しあう関係にあることを示唆している。本研究では、BMP2, 4, 7の機能的分担をより詳細に検討することで、それぞれの骨、軟骨のホメオスタシスにおける生理機能を明らかとしていくことを目的としている。本年度は、関節軟骨のホメオスタシスにおけるBMP7の生理機能の解析を行った。

BMP7（Bone Morphogenetic Protein 7）は、60A サブグループに属するTGFbetaファミリー分子であり、硬組織の発生に機能している事が示されている。これまでの報告から、BMP7は、in vitroにおいて間葉系幹細胞の軟骨分化を促進する事、リコンビナントBMP7蛋白の関節内投与により関節炎と関節軟骨の変性が抑制される事が示されている事から、発生だけでなく、生後の関節のホメオスタシスにも機能している事が予想されている。しかしながら、BMP7のノックアウトマウスは、腎機能不全により生後直ちに死亡してしまうため、これまで成体の関節におけるBMP7の生理機能の解析は行われてこなかった。そこで、四肢特異的BMP7欠損マウス（BMP7c/c;Prx1：：cre）を作製し、BMP7欠損下で関節軟骨の表現型の詳細な検討を行ったところ、4週齢までは、BMP7欠損マウスにおける関節軟骨の変性は確認されなかったが、加齢に伴いBMP7欠損マウスの関節軟骨では、コントロールマウスに比して、著明な退行変性が観察された。加えて、BMP7欠損マウスでは、半月板の損傷（断裂）が顕著に観察された。以上の事は、生後の関節軟骨および半月板の構造、機能の維持にBMP7の活性が必須である事を示唆している。

発表抄録　Abula, K., et al. J Bone Miner Res 27（s1）, S263, 2012

(5) 関節症発症及び病態の進行の分子メカニズムの解析および非侵襲性のマウス関節症モデルの確立

Identification and characterization of the genes in the pathogenesis of osteoarthritis and a new model of osteoarthritis by forced running in mice

変形性関節症は多因子病でありその発症ならびに変性の進行には様々な要因が考えられている。閉経期におけるエストロゲン欠乏はOA進行に重要な要素であると考えられているがその影響はいまだ明らかにされていない。今回マウスにおいて閉経期のモデルである子宮摘出と関節内に侵襲を加えることのない強制走行を組み合わせる方法で関節軟骨の退行変性の進行の検討を行った。

卵巣摘出群では全例子宮標本の重量がコントロール群と比較し有意に軽く、子宮の萎縮が認められ、卵巣摘出が適切に行なわれたことを確認した。関節軟骨の組織像では、正常コントロールと比較し、卵巣摘出群及び強制走行群では有意な差を認めなかった。しかし卵巣摘出して強制走行させた群では、正常コントロールと比較し有意に軟骨基質の染色性が低下した。またこれらは、半月板の変性を伴っていた。私たちはこれまでラットに強制歩行させると、関節軟骨が早期に変性し、軟骨変性に対する薬剤の関節内投与の効果を検討するのによいモデルであることを報告した。しかしマウスは強制歩行のみでは軟骨変性が得られず、重量を含めた種の違いが影響したと推察される。今回卵巣摘出と強制走行を組み合わせることにより、関節内に侵襲を加えることなく軟骨変性を起こさせることが可能であった。このことは変形性関節症の発症にmechanical stressだけでなくhormonal effectが強く関わっていることを示唆すると考えられた。

(6) 間葉幹細胞による再生医療の開発

Repair of intraarticular tissue injury by synovial mesenchymal stem cells

骨髄液や滑膜などの間葉系組織中には、体外でよく増殖し、多分化能を有する「間葉系幹細胞」が存在する。私たちは膝の関節液中に間葉系幹細胞が少量存在し、前十字靭帯損傷、軟骨損傷、半月板損傷、変形性関節症を呈すると関節液中の間葉系幹細胞が増加することを明らかにした。遺伝子プロファイルの解析によると、関節液中の間葉系幹細胞は滑膜由来のものに類似する。膝関節

内の組織損傷・障害を生じると、間葉系幹細胞が滑膜から関節液中に動因され、組織修復に寄与する機構の存在が予測される。私たちはこれまでの基礎研究の成果を踏まえ、滑膜の間葉系幹細胞を体外で自己血清を使用して増殖させ、人工素材を使用せずに、関節鏡視下で、軟骨欠損部に移植する、関節軟骨の再生医療をすでに開始している。また、滑膜間葉系幹細胞を用いた半月板治療も計画している。本年度の業績は下記の通りである。

① ブタの軟骨損傷を作成し、滑膜間葉系幹細胞浮遊液を10分間静置することにより軟骨再生が促進される過程を、関節鏡、組織、MRIで解析した。
（Arthroscopic, histological and MRI analyses of cartilage repair after a minimally invasive method of transplantation of allogeneic synovial mesenchymal stromal cells into cartilage defects in pigs. Nakamura et al. Cytotherapy. 2012）

② 滑膜間葉系幹細胞を集合体にすると軟骨分化能が増加し軟骨欠損部への移植が容易であることをin vitro及びin vivoで示した。
（Properties and usefulness of aggregates of synovial mesenchymal stem cells as a source for cartilage regeneration.
Suzuki et al. Arthritis Res Ther. 2012）

③ 変形性膝関節症のレントゲン重症度に応じて関節液中の間葉系幹細胞が増加することを明らかにした。
（Human mesenchymal stem cells in synovial fluid increase in the knee with degenerated cartilage and osteoarthritis. Sekiya et al. J Orthop Res. 2012）

④ ラット半月板円柱状欠損モデルで滑膜間葉系幹細胞の関節内注射が半月板再生を促進することを示した。
（Implantation of allogenic synovial stem cells promotes meniscal regeneration in a rabbit meniscal defect model. Horie et al. J Bone Joint Surg Am. 2012）

⑤ ラット半月板欠損モデルにヒト間葉系幹細胞を投与するモデルの解析で、間葉系幹細胞がBMP2等の栄養因子を産生することを明らかにした。
（Intra-articular injection of human mesenchymal stem cells（MSCs）promote rat meniscal regeneration by being activated to express Indian hedgehog that enhances expression of type II collagen. Horie et al. Osteoarthritis Cartilage. 2012）

⑥ マウスの滑膜から間葉系幹細胞を採取する方法を確立した。
（Isolation and characterization of multipotential mesenchymal cells from the mouse synovium. Futami et al. PLoS One. 2012）

⑦ 滑膜から間葉系幹細胞を採取する手法を用いて、歯肉、歯髄、歯根膜から間葉系幹細胞を採取し、特性を比較し、歯肉由来のものが収量が高く、骨分化能が高いことを明らかにした。
（Comparison of Gingiva, Dental Pulp, and Periodontal Ligament Cells From the Standpoint of Mesenchymal Stem Cell Properties. Otabe et al. Cell Medicine 2012）

2）研究のイラストレーション

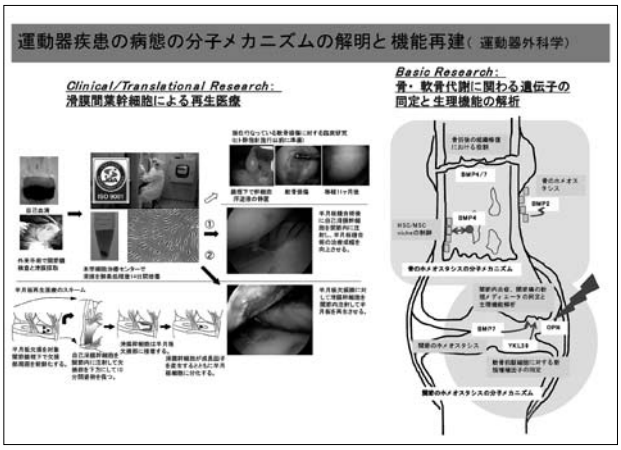

3）発表の研究内容についての英文要約

1. Futami, I., Ishijima, M., Kaneko, H., Tsuji, K., Ichikawa-Tomikawa, N., Sadatsuki, R., Muneta, T., Arikawa-Hirasawa, E., Sekiya, I., and Kaneko, K.（2012）. Isolation and characterization of multipotential mesenchymal cells from the mouse synovium. PLoS One 7, e45517.

The human synovium contains mesenchymal stem cells（MSCs）, which are multipotential non-hematopoietic progenitor cells that can differentiate into a variety of mesenchymal lineages and they may therefore be a candidate cell source for tissue repair. However, the molecular mechanisms by which this can occur are still largely unknown. Mouse primary cell culture enables us to investigate the molecular mechanisms underlying various phenomena because it allows for relatively easy gene manipulation, which is indispensable for the molecular analysis. However, mouse synovial mesenchymal cells（SMCs）have not been established, although rabbit, cow, and rat SMCs are available, in addition to human MSCs. The aim of this study was to establish methods to harvest the synovium and to isolate and culture primary SMCs from mice. As the mouse SMCs were not able to be harvested and isolated using the same protocol for human, rat and rabbit SMCs, the protocol for humans was modified for SMCs from the Balb/c mouse knee joint. The mouse SMCs obtained showed superior proliferative potential, growth kinetics and colony formation compared to cells derived

from muscle and bone marrow. They expressed PDGFRa and Sca-1 detected by flow cytometry, and showed an osteogenic, adipogenic and chondrogenic potential similar or superior to the cells derived from muscle and bone marrow by demonstrating in vitro osteogenesis, adipogenesis and chondrogenesis. In conclusion, we established a primary mouse synovial cell culture method. The cells derived from the mouse synovium demonstrated both the ability to proliferate and multipotentiality similar or superior to the cells derived from muscle and bone marrow.

2. **Horie, M., Choi, H., Lee, R.H., Reger, R.L., Ylostalo, J., Muneta, T., Sekiya, I., and Prockop, D.J. (2012). Intra-articular injection of human mesenchymal stem cells (MSCs) promote rat meniscal regeneration by being activated to express Indian hedgehog that enhances expression of type II collagen. Osteoarthritis Cartilage 20, 1197-1207.**

Meniscal regeneration was previously shown to enhance by injection of mesenchymal stem/stromal cells (MSCs) but the mode of action of the MSCs was not established. The aim of this study was to define how injection of MSCs enhances meniscal regeneration. For the purpose of this study, a hemi-meniscectomy model in rats was used. Rat-MSCs (rMSCs) or human-MSCs (hMSCs) were injected into the right knee joint after the surgery, and PBS was injected into the left. The groups were compared macroscopically and histologically at 2, 4, and 8 weeks. The changes in transcription in both human and rat genes were assayed by species-specific microarrays and real-time RT-PCRs. Although the number of hMSCs decreased with time, hMSCs enhanced meniscal regeneration in a manner similar to rMSCs. hMSCs injection increased expression of rat type II collagen (rat-Col II), and inhibited osteoarthritis progression. The small fraction of hMSCs was activated to express high levels of a series of genes including Indian hedgehog (Ihh), parathyroid hormone-like hormone (PTHLH), and bone morphogenetic protein 2 (BMP2). The presence of hMSCs triggered the subsequent expression of rat-Col II. An antagonist of hedgehog signaling inhibited the expression of rat-Col II and an agonist increased expression of rat-Col II in the absence of hMSCs. Despite rapid reduction in cell numbers, intra-articular injected hMSCs were activated to express Ihh, PTHLH, and BMP2 and contributed to meniscal regeneration. The hedgehog signaling was essential in enhancing the expression of rat-Col II, but several other factors provided by the hMSCs probably contributed to the repair.

3. **Koga, H., Muneta, T., Yagishita, K., Ju, Y.J., and Sekiya, I. (2012a). Surgical management of grade 3 medial knee injuries combined with cruciate ligament injuries. Knee Surg Sports Traumatol Arthrosc 20, 88-94.**

Although various surgical procedures have attempted to restore valgus stability in medial knee injuries, so far none has achieved satisfactory results. The purpose of this study was to assess clinical outcome for patients with grade 3 valgus instability who were treated according to our surgical management strategy. For this purpose, eighteen patients with both acute and chronic grade 3 medial knee injuries, all of which had combined cruciate ligament injuries, were treated with a proximal advancement of both the superficial medial collateral ligament (MCL) and posterior oblique ligament together with underlying deep MCL and joint capsule, in conjunction with cruciate ligament reconstructions in chronic phase. Augmentation with doubled semitendinosus tendon was added in 7 patients whose medial knee stability had been considered to be insufficient with only the proximal advancement procedure. They were evaluated preoperatively and at final follow-up.
Manual valgus laxities at 0° and 30°, as well as side-to-side difference in medial joint opening in stress radiograph, were significantly improved at final follow-up. The Lysholm knee scale was also significantly improved. Median values of the subjective evaluations of the patients' satisfaction, stability and sports performance level measured with visual analogue scale at final follow-up were 82 (60-100), 94 (71-100) and 88 (60-100), respectively.
Clinical outcomes of our surgical management strategy were reasonable in terms of restoring medial knee stability. This treatment protocol can help determine the surgical management of grade 3 medial knee injuries combined with cruciate ligament injuries.

4. **Koga, H., Muneta, T., Yagishita, K., Ju, Y.J., and Sekiya, I. (2012b). The effect of graft fixation angles on anteroposterior and rotational knee laxity in double-bundle anterior cruciate ligament reconstruction : evaluation using computerized navigation. Am J Sports Med 40, 615-623.**

One of the main differences affecting outcome between single-bundle and double-bundle anterior cruciate ligament (ACL) reconstructions may be graft fixation angles and initial force settings; however, there has been little research to investigate these effects in either technique.
Eleven patients who underwent double-bundle ACL reconstruction were included in this study. The anteromedial bundle (AMB) and the posterolateral bundle (PLB) were provisionally fixed to a graft tensioning system during surgery. The graft fixation settings were as follows: (1) AMB only at 20° (A20), (2) PLB only at 20° (P20), (3) AMB at 20° and PLB at 0° (A20P0), (4) AMB at 20° and PLB at 20° (A20P20), and (5) AMB at 20° and PLB at 45° (A20P45). All the grafts were tensioned at a constant stress level. Anterior tibial translation (ATT), internal rotation (IR), and external rotation (ER) at 30°

and 90° of knee flexion applied with manual maximum load were measured before graft insertion and in each setting using a navigation system. A pivot-shift test was also evaluated manually with modified International Knee Documentation Committee criteria in each setting.A20 was less constrained than A20P20 and A20P45 in ATT at 30° and less constrained than A20P45 in IR at 30° . P20 was less constrained than any other settings in ATT at 30° and less constrained than A20P45 in IR at 30° . A20P0 was less constrained than A20P45 in IR at 30° and in ER at 30° . Grade 1 pivot-shift phenomenon persisted in 8 cases in P20, in 4 cases in A20, and in 3 cases in A20P0, whereas no case showed a positive pivot-shift result in A20P20 and A20P45. In this in vivo laboratory model, double-bundle ACL reconstruction with fixation of AMB at 20° and PLB at 20° or 45° restored better stability than single AMB or single PLB reconstruction in which the graft was of smaller size.

5. **Kokabu, S., Gamer, L., Cox, K., Lowery, J., Tsuji, K., Raz, R., Economides, A., Katagiri, T., and Rosen, V. (2012) . BMP3 suppresses osteoblast differentiation of bone marrow stromal cells via interaction with Acvr2b. Mol Endocrinol 26, 87-94.**

Enhancing bone morphogenetic protein (BMP) signaling increases bone formation in a variety of settings that target bone repair. However, the role of BMP in the maintenance of adult bone mass is not well understood. Targeted disruption of BMP3 in mice results in increased trabecular bone formation, whereas transgenic overexpression of BMP3 in skeletal cells leads to spontaneous fracture, consistent with BMP3 having a negative role in bone mass regulation. Here we investigate the importance of BMP3 as a mediator of BMP signaling in the adult skeleton. We find that osteoblasts (OBL) and osteocytes are the source of BMP3 in adult bone. Using in vitro cultures of primary bone marrow stromal cells, we show that overexpression of BMP3 suppresses OBL differentiation, whereas loss of BMP3 increases colony-forming unit fibroblasts and colony-forming unit OBL. The ability of BMP3 to affect OBL differentiation is due to its interaction with activin receptor type 2b (Acvr2b) because knockdown of endogenous Acvr2b in bone marrow stromal cells reduces the suppressive effect of BMP3 on OBL differentiation. These findings best fit a model in which BMP3, produced by mature bone cells, acts to reduce BMP signaling through Acvr2b in skeletal progenitor cells, limiting their differentiation to mature OBL. Our data further support the idea that endogenous BMPs have a physiological role in regulating adult bone mass.

6. **Muneta, T., Koga, H., Ju, Y.J., Horie, M., Nakamura, T., and Sekiya, I. (2012a) . Remnant volume of anterior cruciate ligament correlates preoperative patients' status and postoperative outcome. Knee Surg Sports Traumatol Arthrosc.**

A cohort study was conducted to evaluate the correlation of anterior cruciate ligament (ACL) remnant volume with preoperative status and postoperative outcome of the patients after a remnant-preserving double-bundle (DB) ACL reconstruction.
Eighty-eight patients of 105 unilateral DB anatomic ACL reconstructions performed between 2006 and 2008 were followed up for 24 months or more. They were evaluated with regard to preoperative knee laxity data under anaesthesia. Postoperative outcome was evaluated based on knee extension and flexion strength, manual laxity tests, KT measurements, etc. Overall knee condition and sports performance were evaluated with Lysholm knee score and subjective rating scale. Overall correlation of the remnant volume with the preoperative and postoperative evaluation was assessed. Then, the patients were divided into three subgroups based on the remnant volume (remnant volume : ≦30, 35-55 and ≦60 %) . The evaluation was performed and analysed statistically among the three subgroups. Generally, preoperative laxity tests showed a weak correlation with the ACL remnant volume. Postoperative knee stability also indicated a weak correlation with the ACL remnant volume. Statistical analyses revealed that there were significant differences among the three groups regarding age at surgery, preoperative period, number of giving-way and preoperative KT measurements. Postoperatively, there were significant differences in Lachman test, KT measurements, Lysholm knee scale, subjective and sports performance recovery scores. As the clinical relevance, the study suggests that the remnant volume will be important as a background of preoperative condition and a predictor of operative outcome for each patient and that a remnant preserving surgery may not be simply better than a non-preserving technique with regard to subjective evaluation and sports performance recovery. The preoperative condition of patients with ACL injury was different depending upon the remnant volume. The remnant volume was also weakly correlated with the postoperative outcome regarding objective stability and subjective recovery.

7. **Muneta, T., Koga, H., Ju, Y.J., Mochizuki, T., and Sekiya, I. (2012b) . Hyaluronan injection therapy for athletic patients with patellar tendinopathy. J Orthop Sci 17, 425-431.**

Patellar tendinopathy produces activity-related pain and focal tenderness at the attachment of the patellar tendon at the lower pole of the patella. It frequently causes a reduction in athletic ability. An injection of hyaluronan was found to be useful for patellar tendinopathy, provided the indication is appropriate, based on the authors' pilot cases.

The purpose of this study was to summarize the clinical experience of and to describe the appropriate indication for this injection therapy.
Fifty patients were treated from January 1999 to December 2006. The observation period averaged 25.7 months (range 6-88). All patients were graded stage 2 or 3 by Blazina's classification. Each treatment was counted separately for 9 patients (10 knees) who had more than one treatment period with 3 months or more between the injections. There were 4 bilaterally injected patients. Patellar tendinopathy was classified into 4 types according to the degree of tenderness and the regions that are tender. Hyaluronan was injected into the interface between the patellar tendon and the infrapatellar fat pad at the proximal insertion, or into the region of maximum tenderness.
The total number of injections was 135, and there were an average of 2.0 injections per case (range 1-11). Following treatment, 54 % of the cases were rated in excellent condition, as they were able to return to their previous athletic activities with little difficulty, while 40 % of the cases were rated in good condition-these patients were able to return to their previous sporting activities with some degree of limitation.
In conclusion, hyaluronan injection therapy for athletic patients with patellar tendinopathy is an optional but effective treatment.

8. **Nakamura, T., Sekiya, I., Muneta, T., Hatsushika, D., Horie, M., Tsuji, K., Kawarasaki, T., Watanabe, A., Hishikawa, S., Fujimoto, Y., et al. (2012). Arthroscopic, histological and MRI analyses of cartilage repair after a minimally invasive method of transplantation of allogeneic synovial mesenchymal stromal cells into cartilage defects in pigs. Cytotherapy 14, 327-338.**

Transplantation of synovial mesenchymal stromal cells (MSCs) may induce repair of cartilage defects. We transplanted synovial MSCs into cartilage defects using a simple method and investigated its usefulness and repair process in a pig model.
The chondrogenic potential of the porcine MSCs was compared in vitro. Cartilage defects were created in both knees of seven pigs, and divided into MSCs treated and non-treated control knees. Synovial MSCs were injected into the defect, and the knee was kept immobilized for 10 min before wound closure. To visualize the actual delivery and adhesion of the cells, fluorescence-labeled synovial MSCs from transgenic green fluorescent protein (GFP) pig were injected into the defect in a subgroup of two pigs. In these two animals, the wounds were closed before MSCs were injected and observed for 10 min under arthroscopic control. The defects were analyzed sequentially arthroscopically, histologically and by magnetic resonance imaging (MRI) for 3 months.
Synovial MSCs had a higher chondrogenic potential in vitro than the other MSCs examined. Arthroscopic observations showed adhesion of synovial MSCs and membrane formation on the cartilage defects before cartilage repair. Quantification analyses for arthroscopy, histology and MRI revealed a better outcome in the MSC-treated knees than in the non-treated control knees.
In conclusion, leaving a synovial MSC suspension in cartilage defects for 10 min made it possible for cells to adhere in the defect in a porcine cartilage defect model. The cartilage defect was first covered with membrane, then the cartilage matrix emerged after transplantation of synovial MSCs.

9. **Sekiya, I., Ojima, M., Suzuki, S., Yamaga, M., Horie, M., Koga, H., Tsuji, K., Miyaguchi, K., Ogishima, S., Tanaka, H., et al. (2012). Human mesenchymal stem cells in synovial fluid increase in the knee with degenerated cartilage and osteoarthritis. J Orthop Res 30, 943-949.**

We investigated whether mesenchymal stem cells (MSCs) in synovial fluid (SF) increased in the knee with degenerated cartilage and osteoarthritis. SF was obtained from the knee joints of 22 patients with anterior cruciate ligament (ACL) injury during ACL reconstruction, and cartilage degeneration was evaluated arthroscopically. SF was also obtained from the knee joints of 6 healthy volunteers, 20 patients with mild osteoarthritis, and 26 patients with severe osteoarthritis, in which the grading was evaluated radiographically. The cell component in the SF was cultured for analyses. Synovium (SYN) and bone marrow (BM) were also harvested during total knee arthroplasties. The MSC number in SF was correlated with the cartilage degeneration score evaluated by arthroscopy. The MSC number in the SF was hardly noticed in normal volunteers, but it increased in accordance with the grading of osteoarthritis. Though no significant differences were observed regarding surface epitopes, or differentiation potentials, the morphology and gene profiles in SF MSCs were more similar to those in SYN MSCs than in BM MSCs. We listed 20 genes which were expressed higher in both SYN MSCs and SF MSCs than in BM MSCs, and 3 genes were confirmed by quantitative RT-PCR. MSCs in SF increased along with degenerated cartilage and osteoarthritis.

10. **Suzuki, S., Muneta, T., Tsuji, K., Ichinose, S., Makino, H., Umezawa, A., and Sekiya, I. (2012). Properties and usefulness of aggregates of synovial mesenchymal stem cells as a source for cartilage regeneration. Arthritis Res Ther 14, R136.**

Transplantation of mesenchymal stem cells (MSCs) derived from synovium is a promising therapy for cartilage regeneration. For clinical application, improvement of

handling operation, enhancement of chondrogenic potential, and increase of MSCs adhesion efficiency are needed to achieve a more successful cartilage regeneration with a limited number of MSCs without scaffold. The use of aggregated MSCs may be one of the solutions. Here, we investigated the handling, properties and effectiveness of aggregated MSCs for cartilage regeneration.
Human and rabbit synovial MSCs were aggregated using the hanging drop technique. The gene expression changes after aggregation of synovial MSCs were analyzed by microarray and real time RT-PCR analyses. In vitro and in vivo chondrogenic potential of aggregates of synovial MSCs was examined.
Aggregates of MSCs cultured for three days became visible, approximately 1 mm in diameter and solid and durable by manipulation; most of the cells were viable. Microarray analysis revealed up-regulation of chondrogenesis-related, anti-inflammatory and anti-apoptotic genes in aggregates of MSCs. In vitro studies showed higher amounts of cartilage matrix synthesis in pellets derived from aggregates of MSCs compared to pellets derived from MSCs cultured in a monolayer. In in vivo studies in rabbits, aggregates of MSCs could adhere promptly on the osteochondral defects by surface tension, and stay without any loss. Transplantation of aggregates of MSCs at relatively low density achieved successful cartilage regeneration. Contrary to our expectation, transplantation of aggregates of MSCs at high density failed to regenerate cartilage due to cell death and nutrient deprivation of aggregates of MSCs.
In conclusion, aggregated synovial MSCs were a useful source for cartilage regeneration considering such factors as easy preparation, higher chondrogenic potential and efficient attachment.

11. Yagi, S., Muneta, T., and Sekiya, I. (2012). Incidence and risk factors for medial tibial stress syndrome and tibial stress fracture in high school runners. Knee Surg Sports Traumatol Arthrosc.

Medial tibial stress syndrome (MTSS) and tibial stress fracture (SF) are common lower leg disorders in runners. A prospective study was done to identify the incidence of MTSS and SF in high school runners and to determine risk factors. A total of 230 runners participating in high school running teams were evaluated. All runners aged 15 years as first grade of high school were involved in the study. They were followed up for 3 years. The measured items included height, weight, body mass index (BMI), range of hip and ankle motion, straight leg raising (SLR), intercondylar and intermalleolar interval, Q-angle, navicular drop test, hip abductor strength and physical conditioning. Each runner was followed for 3 years to report occurrence of MTSS and SF.
A total number of 102 MTSS (0.29 athlete exposures) and 21 SF (0.06 athlete exposures) were identified. In females, BMI significantly increased the risk of MTSS after adjustment for the other variables in this study (adjusted odds ratio, 0.51; 95 % confidence interval, 0.31-0.86). Increased internal rotation of the hip significantly increased the risk of MTSS (adjusted odds ratio, 0.91; 95 % confidence interval, 0.85-0.99). In males, limited SLR also significantly increased the risk of SF with adjustment for the other variables in this study (adjusted odds ratio, 1.38; 95 % confidence interval, 1.04-1.83).
A significant relationship was found between BMI, internal hip rotation angle and MTSS in females, and between limited SLR and SF in males.

12. Yagishita, K., Muneta, T., Ju, Y.J., Morito, T., Yamazaki, J., and Sekiya, I. (2012). High-flex posterior cruciate-retaining vs posterior cruciate-substituting designs in simultaneous bilateral total knee arthroplasty : a prospective, randomized study. J Arthroplasty 27, 368-374.

The superiority between the posterior cruciate-retaining and the posterior cruciate-substituting designs still remains controversial. We performed a prospective, randomized control study for evaluation of the superiority of these designs. This study investigated 58 knees in 29 patients with simultaneous bilateral total knee arthroplasty, in which the high-flex CR design was randomly implanted in one knee and the high-flex PS design was implanted in the other knee. The follow-up duration averaged 5.0 years, with a minimum duration of 3 years. Postoperatively, Knee Score and pain points in Knee Score resulted in no significant differences between the 2 designs. However, postoperative arc of range of motion, patient satisfaction, and posterior knee pain at passive flexion in the PS design were significantly superior to that of the CR design.

13. Yamaga, M., Tsuji, K., Miyatake, K., Yamada, J., Abula, K., Ju, Y., Sekiya, I., and Muneta, T. (2012). Osteopontin level in synovial fluid is associated with the severity of joint pain and cartilage degradation after anterior cruciate ligament rupture. PLoS ONE In Press.

To explore the molecular function of Osteopontin (OPN) in the pathogenesis of human OA, we compared the expression levels of OPN in synovial fluid with clinical parameters such as arthroscopic observation of cartilage damage and joint pain after joint injury.
Synovial fluid was obtained from patients who underwent anterior cruciate ligament (ACL) reconstruction surgery from 2009 through 2011 in our university hospital. The amounts of intact OPN (OPN Full) and it's N-terminal fragment (OPN N-half) in synovial fluid from each patient were quantified by ELISA and compared with clinical parameters such as severity of articular cartilage damage (TMDU cartilage score) and severity of joint pain (Visual

Analogue Scale and Lysholm score）.
Within a month after ACL rupture, both OPN Full and N-half levels in patient synovial fluid were positively correlated with the severity of joint pain. In contrast, patients with ACL injuries greater than one month ago felt less pain if they had higher amounts of OPN N-half in synovial fluid. OPN Full levels were positively correlated with articular cartilage damage in lateral tibial plateau. Our data suggest that OPN Full and N-half have distinct functions in articular cartilage homeostasis and in human joint pain.

4）本事業に関連して世界的な研究拠点形成に向けて、以下の点で改善・整備等されたこと

A（研究拠点体制）

間葉幹細胞を用いた新規治療：教室のメインテーマとしての滑膜幹細胞の細胞移植術の対象を軟骨欠損から、もう一つの関節機能の維持に重要な半月板損傷まで拡大するため、半月板損傷モデルを用いた各種動物に対する実験的検討を行っている。大動物を用いた臨床前研究は臨床実施をするための大切な基盤的研究である。本学動物実験施設において、富士マイクラで開発したマイクロミニピッグを用いた実験を継続的に可能にすべく施設の改良を行い軌道に乗せた。また性能の良い修復法を検討し、microsphere法を次のステップ候補として研究しまた適切なサイズや細胞数について引き続き検討を進めている。また半月板損傷に対する細胞移植術の併用手技を開発し、臨床応用を実施している。現在東京医科歯科大学医学部倫理審査委員会で承認された方法により自主研究を進めている形式であるが、国の承認を得るべく「ヒト幹指針」の来年早期の取得にむけて年内の申請に向けて準備中である。

滑膜幹細胞の臨床応用を米国の施設とも共同して臨床応用を進める計画が進んでいる。研究の対象を広げるために最終的な治療対象である変形性関節症の進展の研究をマウスの実験モデルの開発から着手し、数種類のモデルの開発・解析を進めている。

各種BMPの機能解析と新規治療法の開発：各種BMPを発生過程さらに生後の必要な時期にノックアウト、ノックダウンする技術を駆使して研究をしてきた研究者をGCOEの国際シャペロン教官として教室に得た。M・Dタワーに教室が移転し、ノックアウトマウスの飼育スペースも確保され、BMP4, BMP7のコンディショナルノックアウトマウスの作成に成功した。現在解析中である。Harvard大学との共同研究も引き続いて行われている。形成外科との共同研究で皮膚の治癒過程におけるBMPの解析を行うため新しいコンディショナルノックアウトマウスも入手している。

膝前十字靱帯損傷治療などの主要関節手術の成績改善：高い臨床治療実績、長年のACL研究、解剖学的研究に基づいた新しい再建手術を開発し実践している。また関節機能のための半月板の保存は非常に大切である。新しい術式を開発し、積極的に半月板温存を図っている。新しく開発した人工膝関節手術の向上のための臨床研究や人工股関節機種の臨床的検討や開発も世界規模で進めている。

B（研究教育環境）

M・Dタワーへの引っ越しにより研究面積が3倍増し、新しい動物実験設備も完備、遺伝子組み換え実験室も整った。GCOE事業担当分野間の共同研究も継続している。教育スタッフの増員により大学院生各人に対する個別教育の密度や時間が増した。平成22年10月に再生医療ハイウェープログラムに滑膜幹細胞を用いた半月板再生が採択され、10年のグラントを得たため、実験施設の改築、フローサイトメトリーの購入などを実現し、研究手法が多様化した。複数の研究テーマを扱うことを大学院生のルーチンにし大学院生の研究が活発化している。

C（人材確保）

国際シャペロンの分野への採用により研究の幅が広がり、教育の充実化が図られた。毎年3,4人の大学院生を受け入れ、国外からの留学生も慎重な選択のもとに受け入れている。また他大学からの研究委託や学内の共同研究が進んでいる。グラントを用いた研究者の雇用も常に念頭に置いている。

D（人材育成）

週3回の早朝カンファランスと勉強会により、研究基盤として最新研究に遅れないように留意している。海外の著名な研究者や新進の研究者に積極的に依頼し、セミナーを適時開催している。グラント獲得により、海外からの招聘セミナーや個別指導の機会が倍増している。国際シャペロンの分野への採用により教育の充実化が図られた。

E（国際化）

国際シャペロンとの関係からHarvard大学歯学部との2つの共同研究プロジェクトを立ち上げた。滑膜幹細胞を用いた関節軟骨細胞治療の臨床研究が米国テキサス州の病院と進みつつある。ベルギーとの情報の交換も進んでいる。

本年も大学院4年目で米国留学し、米国スクリプス研究所との共同研究が進行中である。引き続き複数の大学院卒業生が留学を希望し、準備を行っている。

5）GCOE事業を推進するに当たって力を入れた点

GCOEにより新たに教室に加わった国際シャペロン教官による各種改変マウスを駆使したBMP研究の推進。シャペロン教官による大学院生の個別教育の充実。滑膜幹細胞を用いた治療法の臨床応用の推進と間葉幹細胞研究の対象の広域化。国際的な共同研究の推進。事業者間の共同研究の立ち上げ。

6）英文原著論文

1. ◎Otabe K, Muneta T, Kawashima N, Suda H, Tsuji K, Sekiya I.
   Comparison of Gingiva, Dental Pulp, and Periodontal Ligament Cells From the Standpoint of Mesenchymal Stem Cell Properties.
   Cell Medicine 4（1）： 13-21, 2012
2. Hatsushika D, Nimura A, Mochizuki T, Yamaguchi K, Muneta T, Akita K.
   Attachments of separate small bundles of human posterior cruciate ligament：an anatomic study
   Knee Surgery, Sports Traumatology, Arthroscopy（in press）
3. ◎Nakamura T, Sekiya I, Muneta T, Hatsushika D, Horie M, Tsuji K, Kawarasaki T, Watanabe A, Hishikawa S, Fujimoto Y, Tanaka H, Kobayashi E.
   Arthroscopic, histological and MRI analyses of cartilage repair after a minimally invasive method of transplantation of allogeneic synovial mesenchymal stromal cells into cartilage defects in pigs.
   Cytotherapy. 14（3）：327-338, 2012.
4. Horie M, Driscoll MD, Sampson HW, Sekiya I, Caroom CT, Prockop DJ, Thomas DB.
   Implantation of allogenic synovial stem cells promotes meniscal regeneration in a rabbit meniscal defect model.
   J Bone Joint Surg Am. 18;94（8）：701-12, 2012.Apr.
5. Horie M, Choi H, Lee RH, Reger RL, Ylostalo J, Muneta T, Sekiya I, Prockop DJ.
   Intra-articular injection of human mesenchymal stem cells（MSCs）promote rat meniscal regeneration by being activated to express Indian hedgehog that enhances expression of type II collagen.
   Osteoarthritis Cartilage. 20（10）：1197-207, 2012.Oct.
6. Tsukada S, Hoshino A, Cho S, Ikeda H.
   Intraoperative soft tissue tension and postoperative range of motion in posterior stabilized total knee arthroplasty.
   Arch Orthop Trauma Surg. Published online; 02 November, 2012（in press）
7. Akiyama H, Hoshino A, Iida H, et al.
   A pilot project for the Japan arthroplasty register.
   J Orhop Sci. 17（4）：358-369, 2012.
8. Muneta T, Koga H, Ju YJ, Mochizuki T, Sekiya I.
   Hyaluronan injection therapy for athletic patients with patellar tendinopathy.
   J Orthop Sci. 17（4）：425-31, 2012.Jul.
9. Muneta T, Koga H, Ju YJ, Horie M, Nakamura T, Sekiya I.
   Remnant volume of anterior cruciate ligament correlates preoperative patients' status and postoperative outcome.
   Knee Surg Sports Traumatol Arthrosc, 2012 Apr 28.
   [Epub ahead of print]
10. Mochizuki T, Nimura A, Tateishi T, Yamaguchi K, Muneta T, Akita K.
    Anatomic study of the attachment of the medial patellofemoral ligament and its characteristic relationships to the vastus intermedius.
    Knee Surg Sports Traumatol Arthrosc.（in press）
11. Hatsushika D, Nimura A, Mochizuki T, Yamaguchi K, Muneta T, Akita K.
    Attachments of separate small bundles of human posterior cruciate ligament：an anatomic study.
    Knee Surg Sports Traumatol Arthrosc.（in press）
12. Kato A, Nimura A, Yamaguchi K, Mochizuki T, Sugaya H, Akita K.
    An anatomical study of the transverse part of the infraspinatus muscle that is closely related with the supraspinatus muscle.
    Surg Radiol Anat. 34：257-265, 2012.
13. Nimura A, Kato A, Yamaguchi K, Mochizuki T, Okawa A, Sugaya H, Akita K.
    The superior capsule of the shoulder joint complements the insertion of the rotator cuff. J Shoulder Elbow Surg. 21：867-872, 2012.
14. ◎Sekiya I, Ojima M, Suzuki S, Yamaga M, Horie M, Koga H, Tsuji K, Miyaguchi K, Ogishima S, Tanaka H, Muneta T.
    Human mesenchymal stem cells in synovial fluid increase in the knee with degenerated cartilage and osteoarthritis.
    J Orthop Res. 30（6）：943-9, 2012.
    Yamauchi Y, Jinno T, Koga D, Asou Y, Morita S, Okawa A.
    Comparison of Different Distal Designs of Femoral Components and Their Effects on Bone Remodeling in 1-Stage Bilateral Total Hip Arthroplasty.
    J Arthroplasty（8）：1538-43, 2012.Sep.27.
15. ◎Suzuki S, Muneta T, Tsuji K, Ichinose S, Makino H, Umezawa A, Sekiya I.
    Properties and usefulness of aggregates of synovial mesenchymal stem cells as a source for cartilage regeneration.
    Arthritis Res Ther.;14（3）：R136, 2012.
16. Koga H, Muneta T, Yagishita K, Ju YJ, Sekiya I.
    Surgical management of grade 3 medial knee injuries combined with cruciate ligament injuries.
    Knee Surg Sports Traumatol Arthrosc 20（1）：88-94,

2012.
17. Koga H, Muneta T, Yagishita K, Ju YJ, Sekiya I.
The effect of graft fixation angles on anteroposterior and rotational knee laxity in double-bundle anterior cruciate ligament reconstruction：evaluation using computerized navigation.
Am J Sports Med 40（3）：615-623, 2012.
18. Koga H, Muneta T, Yagishita K, Watanabe T, Mochizuki T, Horie M, Nakamura T, Okawa A, Sekiya I.
Arthroscopic Centralization of an Extruded Lateral Meniscus：a Technical Note. Arthroscopy Techniques（in press）.
19. Koga H, Muneta T, Yagishita K, Ju YJ, Mochizuki T, Horie M, Nakamura T, Okawa A, Sekiya I.
Effect of Posterolateral Bundle Graft Fixation Angles on Graft Tension Curves and Load Sharing in Double-bundle Anterior Cruciate Ligament Reconstruction Using a Transtibial Drilling Technique.
Arthroscopy（in press）.
20. ◎Yamaga M, Tsuji K, Miyatake K, Yamada J, Abula K, Ju YJ, Sekiya I, Muneta T. Osteopontin level in synovial fluid is associated with the severity of joint pain and cartilage degradation after anterior cruciate ligament rupture.
PLoS ONE In Press.
21. ◎Kokabu S, Gamer L, Cox K, Lowery J, Tsuji K, Raz R, Economides A, Katagiri T, Rosen V.
BMP3 suppresses osteoblast differentiation of bone marrow stromal cells via interaction with Acvr2b.
Mol Endocrinol 26, 87-94, 2012.
22. ◎Futami I, Ishijima M, Kaneko H, Tsuji K, Ichikawa-Tomikawa, N., Sadatsuki R, Muneta T, Arikawa-Hirasawa, E, Sekiya I, Kaneko K.
Isolation and characterization of multipotential mesenchymal cells from the mouse synovium.
PLoS One 7, e45517, 2012.
23. Watanabe T, Ishizuki M, Muneta T, Banks SA.
Knee Kinematics in Anterior Cruciate Ligament-Substituting Arthroplasty With or Without the Posterior Cruciate Ligament.
J Arthroplasty.（in print）
24. Watanabe T, Ishizuki M, Muneta T, Banks SA.
Matched comparison of kinematics in knees with mild and severe varus deformity using fixed- and mobile-bearing total knee arthroplasty.
Clin Biomech. 27（9）：924-8, 2012.

7）総説ならびに著書

1. 池田浩夫
Ⅲ. 部位別のガイドライン　足・足関節部の疾患
中足骨疲労骨折の診断・治療指針、
運動器診療　最新ガイドライン、総合医学社、742-743、2012
2. 荻内隆司
JOSKAS　疾患啓蒙パンフレット　運動器疾患とスポーツ外傷・障害 Vol.1
膝蓋腱炎（patellar tendonitis）、
JOSKAS広報委員会作成　（中外製薬協賛）、2012.07
3. 荻内隆司
2013 今日の治療指針　私はこう治療している
Today's Therapy Vol.55
分担執筆　ジャンパー膝、医学書院、2013.01（印刷中）
4. 星野明穂
中～大欠損膝に対するTKA手術. OS Now Instruction
膝関節の難治性病態に対する手術、 メジカルビュー社
Vol.24、51-61、2012
5. 宗田大
前十字靭帯再建術
整形外科看護2012臨時増刊、165-17、2012
6. 宗田大
膝蓋大腿関節痛による痛み
運動器の痛みプライマリケア　膝・大腿部の痛み、
南江堂、290-300、2012.6.1
7. 宗田大
変形性関節症の慢性疼痛発生機序
運動器の慢性疼痛―治療新戦略
整形外科、Vol.63（8）（2012 7増刊）、746-49、2012
8. 望月智之
肩腱板損傷の病態・リスクと治療.
上肢急性外傷のリハビリテーションとリコンディショニング、31-38、2012
9. 望月智之、二村昭元、秋田恵一
診断・治療に必要な機能解剖. 肩と肘のスポーツ障害
診断と治療にテクニック、1-7、2012
10. 関矢一郎
滑膜由来の幹細胞による再生医療
Bone Joint Nerve、159-165、Vol. 2 No.1 、2012
11. 関矢一郎
滑膜間葉幹細胞の役割と低侵襲な軟骨再生への応用
整形外科、228 Vol.63 No.3 、2012
12. 関矢一郎
関節と体性幹細胞　滑膜間葉系幹細胞による軟骨再生
BIO Clinica、27巻9号、830-834、2012.08
13. 関矢一郎
滑膜間葉幹細胞を使った軟骨再生
朝倉書店 「再生医療叢書 第6巻　骨格系」

山中伸弥・中内啓光 編 、2012
14. 関矢一郎
軟骨治療の進歩：滑膜幹細胞による軟骨再生
日本医師会雑誌、1739 第141巻8号、2012
15. 神野哲也
ストレスシールディング
特集：THAの合併症対策
関節外科、31（2）：72-81、2012
16. 神野哲也
大腿骨頚部・転子部骨折に対する最新の整形外科的治療
特集：再考 大腿骨頚部/転子部骨折の理学療法
理学療法、29（6）：611-620、2012
17. 神野哲也
股関節の痛み―変形性股関節症の治療がよくわかる
別冊NHKきょうの健康、杉山 肇（監修）、NHK出版 （編集）、2012
8. 神野哲也（監修）、相澤純也、中丸宏二、（編集・ビジュアル実践リハ）
整形外科リハビリテーション　カラー写真でわかるリハの根拠と手技のコツ
羊土社、2012
19. 古賀英之、宗田大、関矢一郎
膝十字靱帯損傷に合併した3度膝内側側副靱帯損傷に対するつり上げ修復法
Bone Joint Nerve、2（1）：185-189、2012
20. 古賀英之
Model-based Image-matching法とACL受傷メカニズムの解析
臨床スポーツ医学、29（7）：695-702、2012
21. 古賀英之
Model-based image-matching techniqueを用いた動作解析
リハビリテーション医学、49（6）：270-274、2012
22. 渡邊敏、関矢一郎、宗田大
高齢者の自立を支える人工膝関節置換術
クリニカルカルシウム、22（4）：103-9、2012

8）平成24年度までの自己評価

GCOEの国際シャペロンが教室に加わったことにより基礎的研究と教育の密度が増し、新しい研究が芽生えつつある。教室も活気を増した。新棟に引っ越し研究環境も改善した。しかし本年度の基礎研究論文数は少なく、来年度の飛躍が待たれる。

一方10年のグラントを得て、研究費がふんだんに用いることができる環境になったことは非常に大きな収穫だった。これをもとに研究の質をあげ大動物研究を増加させる計画が実現しつつある。臨床面での滑膜幹細胞を用いた軟骨治療に対する一層の改善と発展が求められる。

9）和文原著論文

1. ◎山田淳、神野哲也、長谷川清一郎、土屋正光
ハンソンピンを用いた大腿骨頭すべり症の治療経験
臨床雑誌　整形外科、Vol63 No.4：313-318、2012
2. 堀江雅史、宗田大、関矢一郎
膝滑膜由来の幹細胞を用いた半月板の再生治療
デンタルダイヤモンド、2012、4月号
3. 中川裕介、浅野浩司、中村香織、小森博達、宗田大
踵骨関節内骨折に対する外側小皮切による顆粒状β-TCPを使用した観血的整復固定術の治療成績
骨折、34（2）：446-450、2012.
4. 鈴木志郎、関矢一郎、宗田大
軟骨再生の細胞源としての滑膜間葉系幹細胞集合体の特性と有用性
整形・災害外科、55（10）：1243-1248,2012.

10）学会発表（英文）

1. ◎Kahaer A, Muneta T, Yamaga M, Miyatake M, Yamada J, MatsukuraY, Sekiya I Tsuji K.
BMP7 is prerequisite for postnatal joint homeostasis
The 6th Global COE International Symposium. Poster, Tokyo, Japan, 2012.1.23
2. Koga H, Muneta T, Sekiya I.
Effect of graft fixation angles on knee kinematics, graft tension curves and load sharing in double-bundle anterior cruciate ligament reconstruction.
International Symposium on Ligaments & Tendons - XII, Oral, San Francisco, LA, 2012.2.3.
3. ◎Otabe K, Sekiya I, Kawashima N,Tsuji K, Muneta T.
Properties of mesenchymal stem cells derived from removed teeth.
2012 Orthopaedic Research Society（ORS）, Annual Meeting, San Francisco, 2012.2.4-7.
4. ◎Hatsushika D, Sekiya I, Horie M, Takeshi Muneta T.
Intraarticular injection of synovial stem cells promotes meniscal regeneration in rabbit massive meniscal defect
2012 Orthopaedic Research Society（ORS）, Annual Meeting, Oral, Sanfrancisco, 2012.2.6.
5. ◎Miyatake K, Yamaga M,Sekiya I ,Muneta T,Tsuji K.
Human chitinase 3-like protein 2（YKL39）is a novel secreted protein which supports cell proliferation and chondrocytic differentiation of ATDC5

2012 Orthopaedic Research Society（ORS）, Poster, San Francisco, 2012.2.4.

6. Watanabe T, Ishizuki M, Muneta T, Dunbar N, Iorgulescu A, Banks SA.
Knee Kinematics in ACL Substituting Arthroplasty With or Without PCL
2012 Orthopaedic Research Society（ORS）, Podium, San Francisco, 2012.2.7.
7. Watanabe T, Ishizuki M, Muneta T, Dunbar N, Iorgulescu A, Banks SA.
Kinematic comparison of fixed-and mobile-bearing total knee arthroplasty in vivo
2012 Orthopaedic Research Society（ORS）, Poster, San Francisco, 2012.2.4-5
8. Watanabe T, Kreuzer S, Leffers K, Conditt M, Jones J, Dunbar N, Iorgulescu A, Banks SA.
Is Cruciate-Ligament Functionality Retained in Partial and Multicompartmental Knee Arthroplasty?
2012 Orthopaedic Research Society（ORS）, Poster, San Francisco, 2012.2.4-5.
9. ◎J Yamada. K Miyatake, M Yamaga,I Sekiya, T Muneta, K Tsuji.
Follistatin alleviates articular cartilage degradation induced by carrageenan.
2012 Orthopaedic Research Society（ORS）, Poster, San Francisco ,2012.2.4.
10. Ozeki N, Sekiya I, Otabe K, Katagiri H, Okuno M, Tsuji K, Saito T, Muneta T.
BMP-7 treated Achilles tendon transplantation for meniscal defect in a rat model
2012 Orthopaedic Research Society（ORS）,Annual Meeting, San Francisco,
2012.2.4-2.7.
11. Horie M, Choi H, Sekiya I, Muneta T, Prockop D J.
Xenografts of Human Mesenchymal Stromal Cells（MSCs）Improve Repair of Rat Meniscus by Being Activated to Express Indian Hedgehog that Enhances Expression of Rat Type II Collagen.
2012 Orthopaedic Research Society（ORS）,Annual Meeting,Oral presentation,San Francisco, 2012.2.5.
12. ◎Suzuki S, Muneta T, Tsuji K, Sekiya I.
Properties and effectiveness of aggregated synovial mesenchymal stem cells for cartilage regeneration.
2012 Orthopaedic Research Society（ORS）, Poster, San Francisco, 2012.2.4-7.
13. Koga H, Muneta T, Sekiya I.
Effect of Graft Fixation Angles on Knee Kinematics in Double-bundle Anterior Cruciate Ligament Reconstruction.
58th Annual Meeting of the Orthopaedic Research Society, Oral, San Francisco, LA, USA, 2012.2.4-7.
14. Muneta T,
Articular Cartilage Wear and its Background：Serum Glucosamine Content, Cartilage Hardness and Thickness in ACL Injured Knees.
ACL Study Group Meeting in Jackson Hole, WM, 2012.2.14.
15. ◎Kahaer A, Muneta T, Yamaga M, Miyatake K, Yamada J, Matsukura Y, Sekiya I, Tsuji K.
BMP7 is prerequisite for postnatal joint homeostasis
The 25th Annual Meeting of The Japanese Society of Cartilage Metabolism. Poster, Nagoya, Japan, 2012.3.9.
16. Koga H, Ogasawara I.
Investigation of non-contact ACL injury mechanism through estimating knee joint moment using a model-based image-matching technique.
ACL Research Retreat VI, Oral, Greensboro, NC, USA, 2012.3.22-24.
17. Mochizuki T.
The epidemiology of shoulder dislocation in Japan top-league rugby compared with high school rugby -How can we prevent shoulder dislocation in rugby football?-.
The 9th International Symposium for Orthopaedic Sports Medicine, Oral presentaion; Keelung, Taiwan, 2012.3.24.
18. Mochizuki T.
Anatomic and histologic analysis of the articular capsule on the greater tuberosity.
The 9th International Symposium for Orthopaedic Sports Medicine,Oral presentaion; Keelung, Taiwan, 2012.3.24.
19. Mochizuki T.
Anatomic evaluation of the footprint of the supraspinatus and infraspinatus -whati is the anatomic repair of the rotator cuff tear?-.
The 9th International Symposium for Orthopaedic Sports Medicine,Oral presentaion; Keelung, Taiwan, 2012.3.24.
20. ◎Tsuji K, Yamada J, Miyatake K, Abula K, Matsukura Y, Sekiya I, Muneta,T.
Follistatin alleviates synovitis and articular cartilage degradation induced by carrageenan in mice
World Congress on Osteoarthritis, Barcelona's International Convention Centre, Barcelona, Spain,2012. 4. 26-29.
21. ◎Miyatake K, Tsuji K, Yamada M, Kahaer A, Matsukura Y, Sekiya I, Muneta T.
Articular cartilage degradation induced by extensive treadmill exercise is greatly exacerbated by estrogen depletion in mice.
2012 Osteoarthritis Research Society International（OARSI）, Poster, Barcelona , Spain,2012.4.26.
22. ◎Suzuki S, Muneta T, Tsuji K, Sekiya I.
Properties and usefulness of aggregates of synovial mesenchymal stem cells as a source for cartilage regeneration.

2012 Osteoarthritis Research Society International（OARSI）, Poster, Barcelona , Spain 2012.4.26-29.

23. Ozeki N, Sekiya I, Saito T, Muneta T.
Transplantation of Achilles tendon treated with BMP-7 promoted meniscus regeneration in a rat massive meniscus defect model.
World Congress on Osteoarthritis, Barcerona, Spain, 2012.4.26-29.
24. Ozeki N, Sekiya I, Saito T, Muneta T.
Transplantation of Achilles tendon treated with BMP-7 promoted meniscus regeneration in a rat massive meniscus defect model.
11th World Congress of the international cartilage repair society, Montreal, Canada, 2012.5.12-15.
25. Horie M, Driscoll M, Sampson W, Sekiya I, Caroom C, Prockop D J, Thomas D.
Implantation of Allogenic Synovial Stem Cells Promotes Meniscal Regeneration in a Rabbit
World Congress of the International Cartilage Repair Society（ICRS）2012, Montereal, Canada, 2012.5.12.
26. Jinno T, Koga D, Asou Y, Morita S, Hasegawa S, Matsubara M, Okawa A, Muneta T
Progressive bone atrophy around a stem with a proximal coating of arc-deposited titanium and hydroxyapatite.
The 85th Annual Meeting of the Japanese Orthopaedic Association, Oral, Kyoto, Japan, 2012.5.19.
27. Watanabe T, Ishizuki M, Muneta T, Banks SA.
Matched comparison of fixed- and mobile-bearing TKA kinematics in vivo
The 85th Annual Meeting of the Japanese Orthopaedic Association, Oral, Kyoto, Japan, 2012.5.17-20.
28. ◎Kahaer A, Muneta T,Yamaga M, Miyatake K, Yamada J, Matsukura Y, Sekiya I, Tsuji K.
Endogenous BMP7 activity is prerequisite for postnatal joint homeostasis
The American Society for Bone and Mineral Research's 2012 Annual Meeting. Poster, Minneapolis, US, 2012.10.13.
29. ◎Kahaer A, Muneta T, Yamaga M, Miyatake K, Yamada J, YMatsukura Y, Sekiya I, Tsuji K.
Endogenous BMP7 activity is prerequisite for postnatal joint homeostasis
The 27th Annual Research Meeting of The Japanese Orthopedic Association. Oral, Nagoya, Japan, 2012.10.27.
30. Mochizuki T.
Anatomic analysis of the rotator cuff and it vascularity.
The 1st Congress of the Asian Association of Clinical Anatomists, Oral presentation,
Busan, Korea, 2012.11.3-4.
31. ◎Hatsushika D, Sekiya I, Nakamura T, Horie M, Koga H, Tsuji K,Muneta T.
Porcine massive meniscal defect is regenerated by intraarticular injections of synovial stem cells
2013 Orthopaedic Research Society（ORS）,Annual Meeting,Oral,SanAntonio, 2013.1.29
32. ◎Miyatake K, Tsuji, K, Yamada J, Matsukura Y, Kahaer A, Arai Y, Sekiya I,Muneta T.
Articular cartilage degeneration and synovitis observed in the ovariectomized mice are greatly exacerbated by forced running.
2013 Orthopaedic Research Society（ORS）, poster, Henry B Gonzalez Convention Center, San Antonio, 2013.1.26.
33. ◎Yamada J,Tsuji K, Miyatake K, Matsukura Y,Kahar A,Arai Y,Sekiya I, Muneta T.
Forced running（60km in 6wks）reverses bone and articular cartilage degeneration induced by ovariectomy in C57Bl/6 mice.
2013 Orthopaedic Research Society（ORS）, Poster, Henry B Gonzalez Convention Center, San Antonio,2013.1.26.
34. ◎Matsukura Y, Sekiya I, Tsuji K, Muneta T.
Mesenchymal stem cells in synovial fluid increase after meniscus injury.
2013 Orthopedic Research Society（ORS）, Annual Meeting, Henry B Gonzalez Convention Center, San Antonio, TX, USA, 2013.1.26-29.
35. ◎Ozeki N, Sekiya I, Tsuji K, Katagiri H, Okuno M, Nakagawa Y, Saito T, Muneta T.
Weekly intraarticular injections of synovial mesenchymal stem cells delay cartilage degeneration in a rat anterior cruciate ligament transection model
2013 Orthopedic Research Society（ORS）, Annual Meeting, Henry B Gonzalez Convention Center, San Antonio, TX, USA, 2013.1.26-29.
36. Intraoperative Joint Gap Affects Postoperative Knee Kinematics in Posterior-Stabilized Total Knee Arthroplasty
Watanabe T, Muneta T, Sekiya I, Banks S, Koga H, Horie M, Nakamura T, Banks S.
2013 Orthopaedic Research Society（ORS）, Poster, Henry B Gonzalez Convention Center, San Antonio, USA, 2013.1.26-29.

11）学会発表（和文）

1. 宗田大、関矢一郎、柳下和慶、朱寧進、古賀英之、堀江雅史、中村智祐
新しいプライマリー症例用PS型人工膝関節の紹介と短期成績
第42回日本人工関節学会、沖縄、2012.2.25
2. 朱寧進、関矢一郎、柳下和慶、古賀英之、堀江雅史、中村智祐、大川淳、宗田大
人工膝関節全置換術における大腿骨コンポーネント

設置前後のギャップ変化と大腿骨骨切り量との関係
第42回日本人工関節学会、沖縄、2012.2.24-25.

3. 浅野浩司
Para patellar approach と Under vastus approach による人工膝関節置換術の短期成績の比較
第42回日本人工関節学会、沖縄、2012.2.24.

4. 相澤純也、増田正、神野哲也、柳下和慶、小山貴之、中丸宏二、森田定雄
健常成人における3つの異なる上腕肢位での肩関節自動回旋角度の比較
第42回日本人工関節学会、沖縄、2012.02.24-25.

5. 高橋徹、星野明穂、池田浩夫、塩田幹夫、仲津留恵日、尾辻正樹、小松秀郎、塚田幸行、島谷雅之、吉村英哉
強直膝に対し伸展機構を温存し可動域を獲得したTKAの1例
第42回日本人工関節学会,ポスター発表、沖縄、2012.2.24.

6. ◎宮武和正、辻邦和、山田淳、Kahaer Abula、松倉遊、関矢一郎、宗田大
変形性関節症（OA）発症における卵巣摘出と強制走行の影響
第25回日本軟骨代謝学会、ポスター発表、名古屋、2012.3.9

7. ◎山田淳、辻邦和、宮武和正、Kahaer Abula、松倉遊、関矢一郎、宗田大
Carrageenan誘導性の関節炎においてFollistatinは軟骨の退行変性を抑制する
第25回日本軟骨代謝学会、口演発表、名古屋、2012.3.9.

8. 鈴木志郎、関矢一郎、辻邦和、宗田大
滑膜間葉幹細胞集合体による軟骨再生
第25回日本軟骨代謝学会、口演発表、名古屋、2012.3.9-10.

9. 宇尾基弘、神野哲也、大川淳
人工股関節関節液中のTi, Co のXAFS による状態分析
第29回PFシンポジウム、2012.3.15-16.

10. 高橋晃、朱寧進、関矢一郎、大川淳、宗田大
人工膝関節全置換術後に手指壊死を来たした1例
第52回関東整形外科災害外科学会、横浜、2012.3.22-23.

11. 関矢一郎
変形性関節症膝の関節液中に存在する間葉系幹細胞
第85回日本整形外科学会学術総会、京都、2012.5.20.

12. 中村智祐、関矢一郎、柳下和慶、朱　寧進、古賀英之、堀江雅史、大川淳、宗田大
2重束前十字靭帯再建術における術中固定時の張力パターンが術後成績に及ぼす影響
第85回日本整形外科学会、京都、2012.5.17.

13. 堀江雅史、関矢一郎、望月智之、朱　寧進、古賀英之、中村智佑、大川淳、宗田大
2重束ACL再建術における大腿骨孔位置計測のための新しい術後レントゲン評価法（modified quadrant method）：その有用性と再現性について
第85回日本整形外科学会学術総会、京都、2012.5.19.

14. 望月智之、二村昭元、立石智彦、山口久美子、宗田大、大川淳、秋田恵一
内側膝蓋大腿靭帯付着部の解剖学的検討-中間広筋および内側広筋との関係について-第85回日本整形外科学会学術総会、京都、2012.5.17-20.

15. 神野哲也、古賀大介、正岡智和、高田ちさと、山内裕樹、大川淳、森田定雄
人工股関節置換術における股関節回旋可動域：進入法別の術中・術後比較
第49回　日本リハビリテーション医学会、福岡、2012.5.31-6.2.

16. 堀江雅史、中村智祐、古賀英之、望月智之、Darwin J Prockop、関矢一郎、宗田大
滑膜間葉幹細胞の局所投与は半月板の再生を促進する-ウサギ半月板無血行野部分欠損モデルを用いた検討
第4回日本関節鏡・膝・スポーツ整形外科学会（JOSKAS）、沖縄、2012.7.20.

17. 朱寧進、宗田大、関矢一郎、柳下和慶、古賀英之、堀江雅史、中村智祐、大川淳
PS型人工膝関節全置換術において術前の上顆軸撮影で術中の大腿骨後顆骨切り前の屈曲ギャップの内外側不均衡は推測できるか
第4回日本関節鏡・膝・スポーツ整形外科学会（JOSKAS）、沖縄、2011.7.17-19.

18. 白澤進一
診断、治療に難渋したTKA術後発症のヘパリン起因性血小板減少症（HIT）の1例
第4回日本関節鏡・膝・スポーツ整形外科学会（JOSKAS）ポスター発表、沖縄、2012.7.19.

19. 荻内隆司、山本利春、笠原政志、有馬三郎
前十字靭帯再建術後の学内におけるアスレチックリハビリテーションの評価
第4回日本関節鏡・膝・スポーツ整形外科学会（JOSKAS）沖縄、ポスター発表、2012.7.19.

20. 望月智之、二村昭元、藤代瞳、山口久美子、宗田大、秋田恵一
腱板の大結節停止部における血管分布の解剖学的解析
第4回日本関節鏡･膝･スポーツ整形外科学会(JOSKAS)、沖縄、2012.7.19-21.
21. 望月智之、藤代瞳、二村昭元、安田和則、宗田大、秋田恵一
膝伸展位および屈曲位におけるACL大腿骨付着形態の解剖学的研究
第4回日本関節鏡・膝・スポーツ整形外科学会(JOSKAS)、沖縄、2012.7.19-21.
22. 中川裕介、浅野浩司、立石智彦
陳旧性坐骨結節剥離骨折に手術を施行した一例
第4回日本関節鏡・膝・スポーツ整形外科学会(JOSKAS)、ポスター発表、沖縄、2012.7.19.
23. 古賀英之、結城新、関矢一郎、柳下和慶、渡邊敏文、望月智之、堀江雅史、中村智祐、大川淳、宗田大
7段階評価法を用いたpivot shift testのより詳細な評価の試み
第4回日本関節鏡・膝・スポーツ整形外科学会(JOSKAS)、展示発表、沖縄、2012.7.19-21.
24. 浅野浩司、島谷雅之
Opening wedge high tibial osteotomyの手術前後の軟骨変化について
第4回日本関節鏡・膝・スポーツ整形外科学会(JOSKAS)、沖縄、2012.7.20.
25. 渡邊敏文、宗田大、Scott Banks
後方安定型人工膝関節全置換術の関節ギャップは術後可動域に影響する
第4回日本関節鏡・膝・スポーツ整形外科学会(JOSKAS)、沖縄、2012.7.19-21.
26. 高橋徹、池田浩夫、吉村英哉、島谷雅之、塚田幸行、小松秀郎、仲津留恵日、尾辻正樹、塩田幹夫、仁賀定雄
前十字靭帯損傷に合併した内側半月板損傷の自然経過に関するMRIを用いた検討
第4回日本関節鏡・膝・スポーツ整形外科学会(JOSKAS)、口演発表、沖縄、2012.7.20.
27. 大関信武、関矢一郎、辻邦和、片桐洋樹、小田邊浩二、奥野真起子、齋藤知行、宗田大
ラット膝前十字靭帯損傷モデルにおける滑膜由来間葉系幹細胞の関節内毎週投与による軟骨変性抑制効果
第31回日本運動器移植・再生医学研究会、弘前、2012
28. ◎初鹿大祐、関矢一郎、堀江雅史、古賀英之、辻邦和、大川淳、宗田大
ピッグ半月板広範囲切除モデルで滑膜間葉系幹細胞の関節内投与は関節軟骨変性を抑制する
第27回日本整形外科基礎学術集会、口演発表、名古屋、2012.10.27.
29. ◎初鹿大祐、関矢一郎、堀江雅史、古賀英之、辻邦和、大川淳、宗田大
滑膜間葉系幹細胞の関節内投与は家兎広範囲半月板切除後の半月板再生を促進する
第27回日本整形外科基礎学術集会、ポスター発表、名古屋、2012.10.26.
30. ◎宮武和正、辻邦和、山田淳、松倉　遊、Kahaer Abula、大川淳、関矢一郎、宗田大
変形性関節症（OA）発症における卵巣摘除と強制走行の影響
第27回日本整形外科基礎学術集会、ポスター発表、名古屋、2012.10.26.
31. ◎山田淳、辻邦和、宮武和正、松倉遊、Kahaer Abula、新井嘉則、大川淳、関矢一郎、宗田大
C57Bl/6マウスにおいて6週60kmの走行負荷は卵巣摘除後の関節軟骨退行変性を抑制する
第27回日本整形外科学会基礎学術総会、口演発表、名古屋、2012.10.27.
32. 大関信武、関矢一郎、辻邦和、片桐洋樹、小田邊浩二、奥野真起子、齋藤知行、大川淳、宗田大
BMP-7は腱細胞を軟骨細胞に形質転換させる
第27回日本整形外科学会基礎学術集会、名古屋、2012.10.26-27.
33. 大関信武、関矢一郎、辻邦和、片桐洋樹、小田邊浩二、奥野真起子、齋藤知行、大川淳、宗田大
アキレス腱の半月板移植における細胞動態
第27回日本整形外科学会基礎学術集会、名古屋、2012.10.26-27.
34. 望月智之、二村昭元、大川淳、宗田大、秋田恵一
腱板大結節停止部における血管分布の解剖学的研究
-micro CTを用いた三次元的解析-
第27回日本整形外科学会基礎学術集会、名古屋、2012.10.26-27.
35. 松倉遊、関矢一郎、辻邦和、大川淳、宗田大
半月板損傷後に関節液中に間葉系幹細胞は増加する
第27回日本整形外科基礎学術学会,ポスター発表、名古屋、2012.10.27.
36. 中川裕介、関矢一郎、辻邦和、市野瀬志津子、袴塚康治、

大川淳、宗田大
β-TCPミクロン顆粒は間葉系幹細胞に貪食され石灰化を促進する
第27回日本整形外科学会基礎学術集会、ポスター発表、名古屋、2012.10.27.

37. 堀江雅史、中村智佑、古賀英之、望月智之、Darwin J Prockop、関矢一郎、宗田大
関節内投与した骨髄由来の間葉系幹細胞はIndian Hedgehogシグナルが活性化し半月板再生に寄与する
第27回日本整形外科学会基礎学術集会、名古屋、2012.10.26.
38. 鈴木志郎、関矢一郎、辻邦和、大川淳、宗田大
軟骨再生における滑膜間葉系幹細胞集合体の使用：その特性と有用性
第27回日本整形外科学会基礎学術総会、口演発表、名古屋、2012.10.26-27.
39. 古賀英之、宗田大、柳下和慶、渡邊敏文、望月智之、堀江雅史、中村智祐、大川淳、関矢一郎
2重束ACL再建術における移植腱固定角度が制動性および張力に与える影響
第27回日本整形外科学会基礎学術集会、口演発表、名古屋、2012.10.26-27.
40. 結城新、宗田大、関矢一郎、大川淳、古賀英之
Model-based image-matching techniqueを用いたpivot shift testの解析
第27回日本整形外科学会基礎学術集会、名古屋、2012.10.27.
41. 渡邊敏文、石突正文、宗田大、関矢一郎、大川淳、Scott Banks
前十字靱帯置換型人工膝関節において後十字靱帯がキネマティクスに及ぼす影響
第27回日本整形外科基礎学会、2012.10.26-27.
42. 古賀英之、小笠原一生、宗田大
Model-based image-matching techniqueを用いた膝モーメントの推定によるACL損傷メカニズムの解明
第23回日本臨床スポーツ医学会学術集会、口演発表、横浜、2012.11.3-4.
43. 祢津雅彦、有馬三郎、八亀康次、金成仙太郎、濱崎亜希子、荻内隆司、満園良一
バレーボール選手におけるジャンパー膝の痛みと超音波像との関係について
第23回日本臨床スポーツ医学会、ポスター発表、横浜、2011.11.3.
44. 笠原政志、山本利春、荻内隆司、
新入生大学生野球選手のコンディショニングの実態
～傷害予防を目的とした運動機能評価から～
第23回日本臨床スポーツ医学会、ポスター発表、横浜、2011.11.4.
45. 中村智祐、関矢一郎、柳下和慶、渡邊敏文、古賀英之、堀江雅史、宗田大
2重束前十字靭帯再建術における術中固定時の張力パターンと術後成績・大腿骨孔位置の関係
第40回日本関節病学会、鹿児島、2012.11.8.
46. 結城新、宗田大、関矢一郎、大川淳、古賀英之
Model-based image-matching techniqueを用いたpivot shift testの解析
臨床バイオメカニクス学会、千葉、2012.11.10.
47. ◎山田淳、辻邦和、宮武和正、松倉遊、KahaerAbula、関矢一郎、宗田大
変形性膝関節症に対する三次元歩行解析の有用性について
48.　第5回日本運動器疼痛学会、ポスター発表、東京、2012.11.17.
49. 関矢一郎
変性半月板に対する細胞治療
第29回膝関節フォーラム、口演発表、東京、2012.12.1.
50. 高橋徹、星野明穂、池田浩夫、日山鐘浩、洪洋熹、仲津留恵日、尾辻正樹、小松秀郎、吉村英哉、朱寧進
PS型人工膝関節置換術における脛骨component設置後傾角と術後可動域の関係の検討
第43回日本人工関節学会、口演発表、京都、2013.2.22.
51. 渡邊敏文、宗田大、関矢一郎、古賀英之、中村智祐、堀江雅史、Scott Banks
PS型TKAにおいて術中関節ギャップが術後膝キネマティクスに与える影響
第43回日本人工関節学会、口演発表、京都、2013.2.22.

12）受賞

2012年度お茶の水会医科同窓会研究奨励賞

Arthritis Res Ther. 2010;12（6）：R206. Epub 2010 Nov 5.
“ Intradiscal transplantation of synovial mesenchymal stem cells prevents intervertebral disc degeneration through suppression of matrix metalloproteinase-related genes in nucleus pulposus cells in rabbits.”
Miyamoto T, Muneta T, Tabuchi T, Matsumoto K, Saito H, Tsuji K, Sekiya I.

13）外部資金の獲得状況

文部科学省委託　国家基幹研究開発推進事業

「再生医療の実現化プロジェクト　再生医療の実現化ハイウェイ」
研究課題：「滑膜幹細胞による膝半月板再生」
代表：関矢一郎
期間：平成23年―平成33年
研究総額：10億円

厚生労働科学研究費　再生医療実用化研究事業

研究課題：「幹細胞による次世代の低侵撃軟骨再生治療の開発と臨床応用」
代表：関矢一郎
期間：平成23年―平成25年
研究総額：1億6千万円

科学研究費補助金、 基盤C

研究題目：「人工関節全置換術後の動態解析および日本人膝の形態学的検討」
代表：関矢一郎
期間：平成24年―平成26年
研究費総額：420万円

科学研究費補助金、基盤研究C

研究題目：「骨形成因子BMPシグナルによる造血微小環境のホメオスタシスの制御」
代表：辻邦和
期間：平成22年度―平成24年度
研究費総額：405万円

科学研究費補助金、基盤研究C

研究題目：「変形性膝関節症における疼痛の分子メカニズムの解析」
代表：朱寧進
期間：平成22年度―平成24年度
研究費総額：382万円

科学研究費補助金、基盤研究C

研究題目：「変形性関節症の発症機構解明の為の新規動物モデルの確立と間接組織の初期病変の解析」
代表：神野哲也
期間：平成23年度―平成25年度
研究費総額：450万円

14）特別講演、招待講演、シンポジウム

1. 宗田大
膝痛のメカニズムと治療法の選択
第122回北海道整形災害外科学会、北海道、2012.1.28.
2. 古賀英之
ACL損傷-ビデオ映像を用いた損傷メカニズムの解明-.
スポーツ傷害フォーラム、大阪、2012.1.28.
3. 宗田大
変形性膝関節症の治療とエビデンス
OA講演会、和歌山、2012.2.2.
4. 関矢一郎
滑膜間葉系幹細胞による関節軟骨・半月板再生 基礎から臨床まで
第44回再生医療カンファランス、東京大学、2012.2.16.
5. 関矢一郎
滑膜間葉系幹細胞集合体の特性と軟骨再生への応用
第10回JCBJD研究講演会、六本木、2012.2.18.
6. 神野哲也、古賀大介、麻生義則、小谷野岳,高田ちさと,森田定雄、大川淳,宗田大
前方および後方進入による人工股関節置換術における術前後の股関節回旋可動域.
第42回日本人工関節学会、パネルディスカッション、沖縄、2012.2.24.
7. Hideyuki Koga
A new hypothesis for ACL injury mechanisms -based on video analysis using model-based image-matching technique.
Sports Injury Prevention Forum, Tokyo, Japan, 2012.2.26
8. 関矢一郎
滑膜幹細胞による半月板再生
再生医療の実現化ハイウェイ キックオフシンポジウム、御茶ノ水、2012.2.28.
9. 関矢一郎
滑膜由来の幹細胞による軟骨・半月板再生
埼玉県整形外科医会、大、2012.3.2.
10. 関矢一郎
滑膜幹細胞の視点から関節疾患の病態と治療を考える
東京医科歯科大学整形外科開業医会　銀座　2012.3.3.
11. 関矢一郎
滑膜幹細胞による膝半月板再生
再生医療の実現化ハイウェイ　公開シンポジウム、有楽町、2012.3.4.
12. ◎Kunikazu Tsuji
Osteopontin level in synovial fluid is associated with the severity of joint pain and cartilage degradation after anterior cruciate ligament rupture
久光製薬　海外特別招待講演会　～ノルスパンテー

プ発売記念～
東京ガーデンパレス、2012. 3. 7.

13. Ichiro Skiya
Synovium as a reservoir of mesenchymal stem cells to contribute to intraarticular tissue repairs
9th International Symposium for Orthopaedic Sports Medicine. Taiwan 2012.3.23.

14. Ichiro Skiya
Cartilage regeneration by synovial mesenchymal stem cells
9th International Symposium for Orthopaedic Sports Medicine, Taiwan, 2012.3.23.

15. Ichiro Skiya
Mesenchymal stem cells derived from synovium promote meniscus healing
9th International Symposium for Orthopaedic Sports Medicine, Taiwan, 2012.3.23.

16. 宗田大
「ひざの痛みとうまくつきあう～痛みの軽減から人工関節手術まで～」
市民公開講座、有楽町朝日ホール、2012.3.31.

17. 関矢一郎
滑膜由来の間葉系幹細胞による軟骨・半月板再生
東京歯科大学、千葉、2012.4.18.

18. 古賀英之
非接触性ACL損傷の受傷メカニズム
第10回東京スポーツ整形外科研修会、東京、2012.4.21.

19. 宗田大
膝・足関節の痛みの病態と治療
第4回東海ロコモサイトソマコ研究会、名古屋、2012.5.12.

20. 神野哲也、古賀大介、小谷野岳、高田ちさと、麻生義則、森田定雄、大川淳、宗田大
脱臼しない人工股関節全置換術のための手術アプローチの選択と工夫
第85回日本整形外科学会学術総会、パネルディスカッション、京都、2012.5.18.

21. ◎辻邦和
硬組織のホメオスタシスにおける骨形成因子BMPの生理機能の解析
第2回硬組織疾患ゲノムセンターセミナー、東京医科歯科大学, 2012.5.30

22. 関矢一郎
滑膜間葉系幹細胞による低侵襲軟骨再生医療ミニブタを用いた検討
自治医科大学ビッグシンポジウム、秋葉原、2012.6.11.

23. 関矢一郎
滑膜幹細胞による関節軟骨・半月板再生　基礎から臨床まで
日本再生医療学会　ランチョンセミナー、横浜、2012.6.13.

24. ◎Kunikazu Tsuji
Role of Endogenous BMP-7 in Articular Cartilage Homeostasis
International Conference on Bone Morphogenetic Proteins,
Granlibakken Conference Center, Lake Tahoe, CA, USA, 2012.6.19-23.

25. Ichiro Skiya
Mesenchymal stem cells derived form synovium; their properties and clinical applications for cartilage regeneration
International Conference on BMPs,Lake Tahoe,2012.6.23.

26. 宗田大
遺残組織温存ACL再建術の意義と展望
大和運動器疾患セミナー、奈良、2012.6.22.

27. Ozeki N, Sekiya I, Saito T, Muneta T
BMP-7 treated Achilles tendon transplantation for meniscal defect in a rat model
9th International conference on bone morphogenetic protein, Tahoe, USA, 2012.6.19-23（Invited speaker）

28. 渡邊敏文
人工膝関節置換術後のキネマティクス
第12回　膝と歩む会、講演、東京、2012.7.2

29. 関矢一郎
関節軟骨に対する再生医療
日本老年医学会シンポジウム 、有楽町、2012.6.29

30. 宗田大
ロコモティブシンドロームと膝関節
筑後臨床整形外科医会学術講演会、久留米、2012.7.6

31. 宗田大
内側ハムストリング腱を用いた2重束再再建術の成績と最近の工夫。パネルディスカッションACL再再建術：術式の工夫と成績
第4回日本関節鏡・膝・スポーツ整形外科学会（JOSKAS）、沖縄、2012.7.19.

32. 宗田大
膝講義 PCL再建術。
第4回日本関節鏡・膝・スポーツ整形外科学会（JOSKAS） セミナー、沖縄、2012.7.22.
33. 堀江雅史、宗田大、関矢一郎
滑膜間葉系幹細胞移植による半月板再生
骨代謝学会、シンポジウム、東京、2012.7.19.
34. 関矢一郎
滑膜間葉系幹細胞の特性と関節軟骨・半月板再生への応用
京都大学大学院医学研究科「再生医療・臓器再建医学コース」、滋賀、2012.8.4.
35. 荻内隆司
剣道指導における傷害予防・応急処置.
教員免許状更新講習　選択講座、千葉、2012.8.17
36. 関矢一郎
滑膜幹細胞の観点から膝疾患の病態と治療を考える
第21回近整会夏季研修会、大阪、2012.8.25
37. 宗田大
膝のスポーツ障害
第30回日本スポーツ整形外科医学会、ランチョンセミナー、横浜、2012. 9. 14.
38. 望月智之, 二村昭元, 吉村英哉.
ラグビーという競技特性を考慮した外傷性肩関節脱臼の予防と治療.
第38回日本整形外科スポーツ医学会学術集会, 横浜、2012.9.14-15.
39. 関矢一郎
滑膜幹細胞による低侵襲軟骨再生医療
第38回日本整形外科スポーツ医学会学術集会シンポジウム、横浜、2012.9.15.
40. 古賀英之
膝前十字靱帯損傷の受傷メカニズム
東日本整形災害外科学会、高崎、2012.9.22.
41. 関矢一郎
滑膜幹細胞を用いた軟骨・半月板再生
東京医科歯科大学 - ソニー株式会社 包括連携プログラム
第1 回 クリニカルサミット、東京、2012.9.28
42. 望月智之
ラグビーにおける肩関節脱臼の特徴
第39回日本肩関節学会、東京、2012.10.5-6.
43. 宗田大
外来における四肢の痛みの診方と私の治療アプローチ
第9回痛みの治療研究会、大阪、2012.10.20.
44. 関矢一郎
滑膜幹細胞による半月板再生の現状
第22回大阪スポーツ傷害研究会、大阪、2012.10.20.
45. 関矢一郎
BMPの継続的関節内注射による変形性膝関節症の予防
日本整形外科基礎学術集会シンポジウム、名古屋、2012.10.26
46. 大関信武、関矢一郎、辻邦和、片桐洋樹、小田邊浩二、奥野真起子、齋藤知行、大川淳、宗田大
BMP-7を投与したアキレス腱移植による半月板再生
第27回日本整形外科学会基礎学術集会（シンポジウム）、名古屋、2012.10.26-27
47. 神野哲也
臼蓋形成不全症の骨形態と病態
第27回日本整形外科学会基礎学術集会、シンポジウム、名古屋、2012.10.27.
48. 荻内隆司
下肢のスポーツ傷害～足関節捻挫に隠れた病態の診断と治療～
第2回堺市臨床整形外科医会学術講演会、大阪、2012.10.27.
49. 古賀英之
IOC Advanced Team Physician Course報告
第2回チームドクター&トレーナーミーティング、横浜、2012.11.2.
50. 関矢一郎
滑膜幹細胞による半月板再生　―基礎から臨床へ-
第40回日本関節病学会、鹿児島、2012.11.8.
51. 神野哲也、古賀大介、麻生義則、森田定雄、長谷川清一郎、松原正明、大川淳、宗田大
セメントレス髄腔占拠型ストレートステム周囲の骨リモデリング
第40回日本関節病学会、パネルディスカッション、鹿児島、2012.11.8
52. Takeshi Muneta
ICL1 – Double bundle ACL reconstruction Controversies & future directions in DB ACL reconstruction.
Jaipur, India, CASM,2012.11.9.
53. Takeshi Muneta
ACL Symposium Case based interactive discussion on diagnostic dilemmas, surgical techniques, controversies in ACL surgery, bundle specific ACL

reconstructions, paediatric ACL injuries, ACL tears with medial compartment osteoarthritis, failed ACL and revision ACL.
Jaipur, India, CASM ,2012.11.9.

54. Takeshi Muneta
Patellofemoral Joint. MPFL reconstruction – indications, technique, results.
Jaipur, India, CASM ,2012.11.9.

55. Takeshi Muneta
Articular Cartilage. Cartilage repair – future directions.
Jaipur, India, CASM ,2012.11.9

56. 古賀英之
Model-based image-matching technique を用いた動作解析
臨床バイオメカニクス学会、千葉、2012.11.9

57. 関矢一郎
滑膜由来間葉系幹細胞と軟骨・半月板再生
第16回循環器再生医療研究会、東京、2012.11.17.

58. 関矢一郎
滑膜幹細胞による軟骨・半月板再生
産業医科大学、北九州、2012.11.21.

59. 古賀英之
前十字靱帯損傷の受傷メカニズムについて
熊谷市医師会健康スポーツ医会、熊谷、2012.11.26.

60. 古賀英之
変性半月板に対する対応：逸脱外側半月板の対応
膝関節フォーラム、東京、2012.12.1.

61. 神野哲也
Porous Tantalum の基礎と Cup 使用経験
第39回日本股関節学会、モーニングセミナー・日整会教育研修講演、新潟、2012.12.8

62. 神野哲也、古賀大介、森田定雄、長谷川清一郎、松原正明、麻生 義則、大川淳、宗田大
長期経過から見た髄腔占拠型ストレートステムの利点と問題点
第43回日本人工関節学会、シンポジウム、新潟、2013.2.22-23.

15）主催学会

1. 第27回運動器外科セミナー
日時：2012年3月12日（月）10：00～20：00
場所：東京医科歯科大学　MDタワー10階　共用セミナー室8
特別講演　18：00～19：00
「Engineering lubrication in articular cartilage」
Dr. A. Hari Reddi
Adjunct Professor, UC Davis School of Medicine

2. 第1回東京医科歯科大学再生医療の実現化研究会
再生医療の実現化ハイウェイ・キック・オフ・シンポジウム
日時：平成24年3月19日　金曜日　17時～
場所：MDタワー2階　鈴木記念講堂　大講堂
『iPS細胞研究の進展』
京都大学iPS細胞研究所　所長山中伸弥先生

3. 第2回東京医科歯科大学再生医療の実現化研究会
日時：平成24年6月1日　金曜日　18時～
場所：MDタワー2階　共用講義室1（階段講義室）
「iPS細胞を用いた網膜細胞移植医療」
理化学研究所　発生・再生科学総合研究センター
網膜再生医療研究開発プロジェクト　高橋政代　先生

4. 第12回　膝と歩む会
日時：2012年7月2日（金）午後18：00～21：00
場所：東京

5. 第28回運動器外科セミナー
日時：2012年 9月7日（金）17：00～19：00
場所：東京医科歯科大学　MDタワー9階　大学院講義室4
特別講演　18：00～19：00
「フローサイトメーターを用いた間葉系幹細胞の予期的分離と機能的解析」
馬渕洋　先生
東京医科歯科大学　分子生命情報解析学

6. 第29回運動器外科セミナー
日時：2012年9月14日（金）16：30～17：30
場所：東京医科歯科大学　M&Dタワー11階　大学院講義室
特別講演　16：30～17：30
「Lessons from adult stem/progenitor cells（MSCs）that teach us how to repair tissues」
Dr. Darwin Prockop
Adjunct Professor, Texas A&M Health Science Center, USA

7. 第39回日本肩関節学会
第9回肩の運動機能研究会（会長　望月智之）
日時：2012年10月5日（金）-6日（土）
場所：京王プラザホテル

8. 大学院特別講義

日時：2012年10月12日（金）18：00〜
場所：MDタワー2階　共用講義室1（階段講義室）
「iPS細胞技術が可能にする新しい医療」
中内啓光先生
東京大学医科学研究所・幹細胞治療研究センター長
ERATO中内幹細胞制御プロジェクト

9. 第30回運動器外科セミナー
日時：2012年11月29日（木）9：30〜17：30
場所：東京医科歯科大学　M&Dタワー11階　大学院講義室
特別講演　17：00〜18：00
「Macroscopic and histopathologic analysis of human knee menisci in aging and osteoarthritis」
Dr. Martin K. Lotz
Adjunct Professor, Inflammatory and Infectious Disease Center
Sanford-Burnham Medical Research Institute, La Jolla, California
10. 第31回運動器外科セミナー
日時：2013年1月11日（木）　9：30〜17：30
場所：東京医科歯科大学
特別講演　17：00〜18：00
Dr.Oscar Lee
11. 第3回東京医科歯科大学再生医療の実現化研究会
日時：平成25年1月16日　水曜日　18時〜
場所：MDタワー2階　共用講義室　1（階段講義室）
「iPS細胞を用いた心臓の再生と心臓病の病態解明
慶応義塾大学医学部循環器内科教授　福田恵一先生
12. 第32回運動器外科セミナー
日時：2013年1月21日（月）9：30〜17：30
場所：東京医科歯科大
特別講演　17：00〜18：00
Dr.Im Gunil
13. 第9回お茶の水間接症研修会
日時：2013年2月8日（金）午後18：00〜21：00
場所：東京医科歯科大学

16）新聞、雑誌、TV報道

1. 日経産業新聞
先端技術：再生医療ハイウェイ
掲載日：2012年2月22日
2. 番組名：ワールドビジネスサテライト
「再生医療最前線」
製作著作：テレビ朝日
放送日：6月21日
3. 番組名：「Channel Japan」
http：//www.ch-japan.com/ja/
製作著作：日本経済新聞社・TBS
媒体　CNBCアジア、インド（TV18）・台湾（非凡電視台）
※経済専門チャンネル国内ではUSTREAMにて配信
放送日：8月5日
4. 公益財団法人テルモ　フクロウ博士の森の教室
生命の不思議を考える
第15回膝軟骨と半月板の再生
http：//www.terumozaidan.or.jp/labo/class/0 1/interview0

17）GCOE総合講義

宗田大
サマリー
種々の動物関節症（OA）モデルによって示唆される新らしい治療戦略　2012.11.19

われわれは種々の動物を用いて、新しい関節症の治療法を検討しようとしている。マウスのモデルはノックアウトマウスを検討できることから重要だと考えられるが、手術を用いないランニング負荷によるOAモデルはその種によっても影響が異なり、なかなか良いモデルの確立が難しい。ラットのOAモデルは作成は困難でない。ACL切除モデルはOAの進行を完全に防ぐことは不可能であり、これは多くの手術侵襲モデルの問題点と考えられる。その点モノヨードアセテートを関節内注入するモデルは関節症モデルとして有用性が高い可能性がある。至適な投与量を検討している。当科で開発した半月板半切モデルはラット、ラビット、ミニピッグで実施しており、コントロール側でも自然治癒傾向とOAの進行が観察されるため、治療法の有用性を判断する良いモデルである。本モデルを用いて滑膜幹細胞投与の有用性を幅広く検討している。

18）教室、分野や講座の准教授、講師、助教、特別研究員、ポスドク、指導を受けた大学院生の名前

運動器外科	教授	宗田　大
軟骨再生学	教授	関矢　一郎
GCOE	講師	辻　邦和
運動器外科	講師	神野　哲也
〃	助教	古賀　英之
軟骨再生学	助教	渡邊　敏文

間接機能再建学	准教授	望月　智之
運動器外科	医員	堀江　雅史
〃	医員	中村　智祐
〃	大学院生	小田邉　浩二（留学中）
〃	〃	片桐　洋樹
〃	〃	初鹿　大祐
〃	〃	宮武　和正
〃	〃	山田　　淳
〃	〃	結城　　新
〃	〃	中川　祐介
〃	〃	松倉　　遊
〃	〃	アブラ・カハル
〃	〃	宇土　美於
〃	〃	近藤　伸平
〃	〃	斎藤　龍佑
〃	〃	柳澤　克昭
〃	〃	井上　牧子
〃	〃	田口　翔子
〃	非常勤講師	山本　晴康
〃	〃	松原　正明
〃	〃	朱　　寧進
〃	〃	森戸　俊行
運動器外科	非常勤講師	八木　茂典
〃	〃	荻内　隆司
〃	〃	立石　智彦

19）GCOE活動についての感想、コメント、改善を望む点

GCOEによる研究の活発化や業績の評価は高い。しかし活動を通じて感じるのは、海外特にアジアからの熱心な研究者を教育実践しているという実感で、日本の本学の若い研究者の活動が目立たない。臨床分野の一事業担当者としてみるとGCOEのメリットはあまり大きいとはいえない。メリットに対する報告書作成に必要な労力、拘束時間は少ないとはいえない。

20）その他　研究教育活動について特記する点

海外からの著名な研究者を定期的に招聘し、英語によるプレゼンテーション、討論、講演を行っている。本年も3名の講師を招聘した。年明けにも2名の研究者が訪れることになっている。また留学経験者の話やトラベリングフェローの経験を聞く機会を設け、留学に対する前向きな姿勢を養うことに努力している。

日経産業新聞
2012年(平成24年)
2月22日
水曜日

先端技術

フロンティア。知恵を絞る

文科省・厚労省・経産省
再生医療ハイウェイ ㊦

普及へ指針改定不可欠

「2012年内に膝の半月板損傷の臨床研究スタートを目指す。参加を希望する患者も10人集まった」と意気込むのは東京医科歯科大学の関矢一郎教授。膝の内側を囲んでいる滑膜とよばれる組織に存在する体性幹細胞を使って、半月板を再生しようという研究だ。既にブタなど大動物で安全性と効果を確認し、1月には学内の倫理委員会で承認された。

「再生医療ハイウェイ」の課題では最も早い実用化が見込まれ、患者からの期待も高い。事故やスポーツなどで半月板を損傷する人は年間6万人。臨床研究に関する指針（ヒト幹指針）」に基づいて申請し、認められる必要がある。関矢教授らは3月中にも申請したいと考えだ。

こういった臨床研究を始めるには、学内倫理委員会に続き、厚生労働省のヒト幹指針の見直しを始めた。ポイントの一つに将来の産業化を見据えた指針に備蓄し、多数の患者に提供していくことを検討しなくてはいけない。そこで焦点となっているのは細胞ソースの個人情報と匿名性の問題だ。

不特定多数に提供することになった場合、どの愚者に誰のどの細胞を使ったかをいつでも遡れるようにした方がいいかどうか、治療後に提供細胞にウイルス感染があることが分かった場合にどう

東京医科歯科大の関矢教授らは膝の半月板再生を目指す

げられる。現行の指針が前提とするのは「ある1つの細胞集団を1人の患者に移植する、オーダーメード医療」（医政局再生医療研究推進室）。

一方、厚労省はこのヒト幹指針の見直しを始め医療として広く一般に普及する産業化を目指す場合は、ある細胞を大量に備えるかなどの議論が始まっている。細胞は提供者の遺伝情報が詰まっているだけに、悪用される危険性も考慮しないといけないからだ。

また、細胞をバンクなどの形式で長期保存したり、様々な細胞に加工したりするにあたって、安全性の検証項目の見直しも検討課題。現行指針では医療応用を認めていない胚性幹細胞（ES細胞）を使った臨床研究も「ハイウェイ」では5～7年以内に国立成育医療研究センターで始める計画。計画倒れにしないためにも指針の改定は待ったなしの状態だ。

臨床研究の後は先進医療として特定の医療機関だけで実施する方法と大規模な臨床試験（治験）を実施し、保険収載を目指す方法がある。治験は薬事法に基づく申請をしなくてはいけないが、現行制度には薬か医療機器かという分類で、細胞を使った再生医療製品に特化した制度はない。

ある再生医療研究者は「欧米規制当局は最終的な細胞製品の安全性が確認できれば了承する。ところが日本は、その細胞がどんな由来か、どんなふうに育てたかなど薬同様に一つ一つの段階で壁を設けようとしており、膨大な規制の壁ができ産業化はほど遠い」と憤る。

製薬や医療機器企業などで作る再生医療イノベーションフォーラム（会長は富士フイルムの戸田雄三常務執行役員）は昨年12月、厚労省あてに「再生医療の（生きた細胞を扱うなど）特殊性を踏まえた審査対応を」との要望を提出する動きを見せている。

海外では再生医療が実用化段階に来ている。

日本は日本発の新型万能細胞（iPS細胞）による再生医療を強力に推進。ES細胞以上の安全性と有効性を示し先行する欧米に対抗できるかどうか関心が高まる。安易であってはいけないが、迅速な規制整備と先端技術による治療への国民理解を求める活動も必要ではないか。

（吉野真由美）

記者の目

欧米企業に対抗 国民理解も必要

米バイオベンチャー、アドバンスト・セル・テクノロジー社が1月、網膜の難病でES細胞を使った治療に成功したと発表した。米ファイザーは近くES細胞由来の網膜で治験を始めるほか、仏でもES細胞による心不全治療で治験準備中だ。

Suzuki *et al. Arthritis Research & Therapy* 2012, **14**:R136
http://arthritis-research.com/content/14/3/R136

arthritis research&therapy

RESEARCH ARTICLE Open Access

Properties and usefulness of aggregates of synovial mesenchymal stem cells as a source for cartilage regeneration

Shiro Suzuki[1], Takeshi Muneta[1,2], Kunikazu Tsuji[2], Shizuko Ichinose[3], Hatsune Makino[4], Akihiro Umezawa[4] and Ichiro Sekiya[5*]

Abstract

Introduction: Transplantation of mesenchymal stem cells (MSCs) derived from synovium is a promising therapy for cartilage regeneration. For clinical application, improvement of handling operation, enhancement of chondrogenic potential, and increase of MSCs adhesion efficiency are needed to achieve a more successful cartilage regeneration with a limited number of MSCs without scaffold. The use of aggregated MSCs may be one of the solutions. Here, we investigated the handling, properties and effectiveness of aggregated MSCs for cartilage regeneration.

Methods: Human and rabbit synovial MSCs were aggregated using the hanging drop technique. The gene expression changes after aggregation of synovial MSCs were analyzed by microarray and real time RT-PCR analyses. *In vitro* and *in vivo* chondrogenic potential of aggregates of synovial MSCs was examined.

Results: Aggregates of MSCs cultured for three days became visible, approximately 1 mm in diameter and solid and durable by manipulation; most of the cells were viable. Microarray analysis revealed up-regulation of chondrogenesis-related, anti-inflammatory and anti-apoptotic genes in aggregates of MSCs. *In vitro* studies showed higher amounts of cartilage matrix synthesis in pellets derived from aggregates of MSCs compared to pellets derived from MSCs cultured in a monolayer. In *in vivo* studies in rabbits, aggregates of MSCs could adhere promptly on the osteochondral defects by surface tension, and stay without any loss. Transplantation of aggregates of MSCs at relatively low density achieved successful cartilage regeneration. Contrary to our expectation, transplantation of aggregates of MSCs at high density failed to regenerate cartilage due to cell death and nutrient deprivation of aggregates of MSCs.

Conclusions: Aggregated synovial MSCs were a useful source for cartilage regeneration considering such factors as easy preparation, higher chondrogenic potential and efficient attachment.

Introduction

Synovial mesenchymal stem cells (MSCs) are an attractive cell source for cartilage regeneration because of their high expansion and chondrogenic potentials [1-5]. We previously reported that more than 60% of synovial mesenchymal stem cells placed on osteochondral defects adhered to the defect within 10 minutes and promoted cartilage regeneration [6,7]. With this local adherent technique, we can transplant synovial MSCs without scaffold. One of the disadvantages in this method is that the cell component in the suspension is invisible to the naked eye.

One of the solutions for this problem is to make aggregates of synovial MSCs [8-10]. This could enable MSCs not only to be visible but also to be heavier. Consequently, aggregates of MSCs will sink faster in the suspension medium than dispersed MSCs. The use of aggregates of MSCs may help to avoid loss of MSCs from targeted cartilage defects and improve the procedures of transplantation of synovial MSCs. However, there are still concerns; properties of synovial MSCs will be altered when synovial MSCs are aggregated. We do not know

* Correspondence: sekiya.orj@tmd.ac.jp
[5]Section of Cartilage Regeneration, Graduate School, Tokyo Medical and Dental University, 1-5-45 Yushima, Bunkyo-ku, Tokyo 113-8519, Japan
Full list of author information is available at the end of the article

whether aggregates of MSCs adhere on the cartilage defect as we expect it will, and the proper number of aggregates is unclear.

In this study, properties of aggregates of human synovial MSCs were analyzed from the standpoints of morphology, gene profile and *in vitro* chondrogenic potential. Also, the effect of transplantation of aggregates of synovial MSCs was investigated in a rabbit cartilage defect model in terms of aggregate number, cell behavior and influential factors in the *in vivo* chondrogenesis of aggregates of synovial MSCs. Finally, we demonstrated the usefulness of aggregates of synovial MSCs as a source for cartilage regeneration therapy.

Materials and methods

Isolation and culture of human synovial MSCs

This study was approved by an institutional review board of Tokyo Medical and Dental University (No.1030), and informed consent was obtained from all subjects. Human synovium was harvested from donors during anterior cruciate ligament reconstruction surgery for ligament injury and digested in a 3 mg/ml collagenase D solution (Roche Diagnostics, Mannheim, Germany) in α-minimal essential medium (αMEM) (Invitrogen, Carlsbad, CA, USA) at 37°C. After three hours, digested cells were filtered through a 70 μm nylon filter (Becton, Dickinson and Company, Franklin Lakes, NJ, USA), and the remaining tissues were discarded. The digested cells were plated in a 150 cm^2 culture dish (Nalge Nunc International, Rochester, NY, USA) in complete culture medium (CCM): αMEM containing 10% fetal bovine serum (FBS; Invitrogen), 100 units/ml penicillin (Invitrogen), 100 μg/ml streptomycin (Invitrogen), and 250 ng/ml amphotericin B (Invitrogen) and incubated at 37°C with 5% humidified CO_2. The medium was changed to remove nonadherent cells one day later and cultured for 14 days as passage 0, then replated at 100 cells/cm^2 in a 150 cm^2 culture dish, cultured for 14 days and cryopreserved as passage 1. To expand the cells, a frozen vial of the cells was thawed, plated in 60 cm^2 culture dishes, and incubated for four days in the recovery plate. These cells were replated at 100 cells/cm^2 in a 150 cm^2 culture dish (passage 3), and cultured for an additional 14 days. These passage 3 cells were harvested and used in this study.

Isolation and culture of rabbit synovial MSCs

This study was approved by the Animal Experimentation Committee of Tokyo Medical and Dental University (No.0120296A). Wild type skeletally mature Japanese White Rabbit and GFP transgenic rabbits [11,12] were anesthetized with an intramuscular injection of 25 mg/kg ketamine hydrochloride and with an intravenous injection of 45 mg/kg sodium pentobarbital and 150 μg/kg medetomidine hydrochloride. Synovium was harvested aseptically from knee joints of the rabbits, and digested in a 3 mg/ml collagenase type V in aMEM for three hours at 37°C. The digested cells were plated at 5×10^4 cells/cm^2 in a 150 cm^2 culture dish in CCM and incubated at 37°C with 5% humidified CO_2. The medium was changed to remove nonadherent cells one day later and cultured for seven days as passage 0. The cells were then trypsinized, harvested and resuspended to be used for further assays. The cells that were transplanted in animals to be sacrificed at Day 0 and Day 14 were labeled for cell tracking by the fluorescent lipophilic tracer DiI (Molecular Probes, Eugene, OR, USA). For labeling, synovial MSCs were resuspended at 1×10^6 cells/ml in αMEM without FBS and a DiI was added at a final concentration of 5 μl/ml. After incubation for 20 minutes at 37°C with 5% humidified CO_2, the cells were centrifuged at 450 *g* for 5 minutes and washed twice with phosphate-buffered saline (PBS) and the cells were then resuspended in CCM and cultured in hanging drops. We already reported that these cells had characteristics of MSCs [3,6,7,11].

Preparation of aggregates of synovial MSCs

A total of 2.5×10^5 synovial MSCs were trypsinized, harvested and resuspended in 35 μl of CCM, plated on an inverted culture dish lid. The lid was inverted and placed on a culture dish containing PBS. The cells were cultured at 37°C with 5% humidified CO_2 for three days in hanging drops.

Histology of aggregates of human synovial MSCs

Aggregates of human synovial MSCs were fixed with 2.5% glutaraldehyde in 0.1 M PBS for two hours. The aggregates were washed overnight at 4°C in the same buffer and post-fixed with 1% OsO4 buffered with 0.1 M PBS for two hours. The aggregates were dehydrated in a graded series of ethanol and embedded in Epon 812. Semi-thin (1 μm) sections for light microscopy were collected on glass slides and stained for 30 seconds with toluidine blue.

In vitro chondrogenic differentiation assay

A total of 2.5×10^5 human synovial MSCs cultured as a monolayer were pelleted by trypsinization and centrifugation. The pellets or aggregate of human synovial MSCs cultured for three days in hanging drops were cultured in 400 μl chondrogenic medium consisting of high-glucose Dulbecco's modified Eagle's medium (Invitrogen) supplemented with 1,000 ng/ml *BMP-7* (Stryker Biotech, Boston, MA, USA), 10 ng/ml transforming growth factor-β3 (R&D Systems, Minneapolis, MN, USA), 100 nM dexamethasone (Sigma-Aldrich Corp., St. Louis, MO, USA), 50 μg/ml ascorbate-2-phosphate, 40 μg/ml proline, 100 μg/ml pyruvate, and 1:100 diluted ITS+Premix (6.25 μg/ml insulin, 6.25 μg/ml transferrin, 6.25 ng/ml selenious acid, 1.25 mg/ml bovine serum

albumin, and 5.35 mg/ml linoleic acid; BD Biosciences Discovery Labware, Bedford, MA, USA). The medium was changed every 3 to 4 days for 21 days.

Histology of pellets of human synovial MSCs

The pellets were embedded in paraffin, cut into 5-μm sections and stained with 1% Toluidine Blue. For immunohistochemistry, sections were treated with 0.4 mg/ml proteinase K (DAKO, Carpinteria, CA, USA) in Tris-HCl and normal horse serum after deparaffinization. Primary antibodies for type II collagen (Daiichi Fine Chemical, Toyama, Japan) and a secondary antibody of biotinylated horse anti-mouse IgG (Vector Laboratories, Burlingame, CA, USA) were employed. Immunostaining was detected with VECTASTAIN ABC reagent (Vector Laboratories) followed by 3,3'-diaminobenzidine staining.

Real-time RT PCR analysis

Total RNA was extracted from human synovial MSCs in a monolayer culture, aggregates of human synovial MSCs cultured for 1, 2 and 3 days, and the pellets cultured for 7, 14 and 21 days using QIAzol (Qiagen, Hiden, Germany) and the RNeasy mini kit (Qiagen). cDNA was synthesized with oligo-dT primer from total RNA using the Transcriptor High Fidelity cDNA Synthesis kit (Roche Diagnostics) according to the manufacturer's protocol. Reverse transcription (RT) was performed by 30 minutes incubation at 55°C followed by 5 minutes incubation at 85°C. Real-time PCR was performed in a LightCycler 480 instrument (Roche Diagnostics). Primer sequences and TaqMan probes are listed in Table 1. After an initial denaturation step (95°C for 10 minutes), amplification was performed for 40 cycles (95°C for 15 seconds, 60°C for 60 seconds). Relative amounts of mRNA were calculated and standardized as previously described [13,14].

DNA microarray analysis

Total RNA was extracted from human synovial MSCs in a monolayer culture, aggregates of human synovial MSCs cultured for three days. Human Genome U133 Plus 2.0 Array (GeneChip; Affymetrix, Santa Clara, CA, USA) containing the oligonucleotide probe set for more than 47,000 transcripts was used. The fluorescence intensity of each probe was quantified by using the GeneChip Analysis Suite 5.0 (Affymetrix). Gene expression data were normalized in Robust MultiChip Analysis (RMA). To analyze the data, we used hierarchical clustering using TIGR MultiExperiment Viewer (MeV) [15]. The microarray data have been deposited to the public database (GEO accession# GSE 31980).

In vivo transplantation

Under anesthesia, the left knee joint was approached through a medial parapatellar incision, and the patella was dislocated laterally. Full-thickness osteochondral defects (5 mm × 5 mm wide, 1.5 mm deep) were created in the trochlear groove of the femur. A total of 5, 10, 20, 40 and 80 aggregates of autologous rabbit synovial MSCs (2.5×10^5 cells/aggregate) or 25 and 100 smaller aggregates of autologous rabbit synovial MSCs (1.0×10^5 cells/aggregate) suspended in PBS were transplanted to the defect. To trace the transplanted cells, DiI-labeled aggregates of autologous rabbit synovial MSCs and aggregates of allogenic synovial MSCs derived from GFP transgenic rabbit were transplanted to the defect. For the control group, the defect was left empty. All rabbits were returned to their cages after the operation and were allowed to move freely. Animals were sacrificed with an overdose of sodium pentobarbital at 1, 2, and 4 days and at 12 weeks after the operation (n = 5 at each time).

Table 1 Real time-RT PCR primer sequences

Primer name		Sequences	Probe No.
β-actin	forward	5'-ATTGGCAATGAGCGGTTC-3'	11
	reverse	5'-TGAAGGTAGTTTCGTGGATGC-3'	
BMP2	forward	5'-CGGACTGCGGTCTCCTAA-3'	49
	reverse	5'-GGAAGCAGCAACGCTAGAAG-3'	
SOX5	forward	5'-TCTGTCCCAGCAGCGTTAG-3'	41
	reverse	5'-TGACAGCATCATGGTCATTTAAG-3'	
SOX6	forward	5'-GCTTCTGGACTCAGCCCTTTA-3'	50
	reverse	5'-GGCCCTTTAGCCTTTGGTTA-3'	
SOX9	forward	5'-GTACCCGCACTTGCACAAC-3'	61
	reverse	5'-TCGCTCTCGTTCAGAAGTCTC-3'	
TSG6	forward	5'-CCAGATGACATCATCAGTACAGG-3'	78
	reverse	5'-CATTGCAACATATTTGATTTGGA-3'	
STC1	forward	5'-CCCAATCACTTCTCCAACAGA-3'	40
	reverse	5'-TGCTGACTGTGTCTTCATCACA-3'	
COL2A1	forward	5'-GTGTCAGGGCCAGGATGT-3'	75
	reverse	5'-TCCCAGTGTCACAGACACAGAT-3'	
AGGRECAN	forward	5'-CTGGAAGTCGTGGTGAAAGG-3'	21
	reverse	5'-TCGAGGGTGTAGCGTGTAGA-3'	

Macroscopic examination

The cartilage defects were examined macroscopically for color, integrity and smoothness. Osteoarthritic changes and synovitis of the knee were also investigated. Digital images were taken using an Olympus MVX10 (Olympus, Tokyo, Japan).

Histological examination and fluorescent microscopic examination

The dissected distal femurs were immediately fixed in a 4% paraformaldehyde (PFA) solution. The specimens were decalcified in 4% ethylenediamine tetraacetic acid solution, dehydrated with a gradient ethanol series and

embedded in paraffin blocks. Sagittal sections 5 μm thick were obtained from the center of each defect and were stained with toluidine blue and Safranin O. For fluorescent microscopic examination and terminal deoxynucleotidyl transferase dUTP nick end labeling (TUNEL) staining, the fixed specimens were incubated at 4°C for three hours in 5%, 10%, 15% and 20% sucrose solution, respectively. After incubation, the fixed specimens were mounted on a holder. Then 30% optimal cutting temperature (OCT) (Sakura Finetek, Tokyo, Japan) in sucrose solution was added gently into the holder. The holder was frozen in hexan chilled by dry ice and stored at -80°C. Cryosections (10 μm) were prepared with an ultracut S microtome (Reichert, Wien, Austria) and a Microm HM560 cryostat.

Histological score

Histological sections of the repaired tissue were analyzed using a grading system consisting of five categories (cell morphology, morphology, matrix staining, surface regularity, cartilage thickness and integration of donor with host), which were modified from the repaired cartilage score described by Wakitani and colleagues [16], so that overly thick, regenerated cartilage could not be overestimated [6]. The scoring was performed in a blinded manner by two observers and there was no significant interobserver difference. The ratio of the safranin-O positive area over the defect was evaluated. Zeiss AxioVison software (Carl Zeiss, Oberkochen, Germany) was used for measurement of defects and safranin-O positive areas.

In vitro viability assay

Aggregates of rabbit synovial MSCs were plated at 1 or 40 aggregates/well in 96-well plates (Nunc) in CCM, and incubated at 37°C with 5% humidified CO_2 for seven days without medium change. Aggregates were fixed in 4% PFA for TUNEL staining.

TUNEL staining

For TUNEL staining, an apoptosis *in situ* detection kit (Wako Pure Chemical Industries, Ltd, Osaka, Japan) was used. The frozen semi-thin sections were incubated with terminal deoxynucleotidyl transferase for 10 minutes at 37°C in a moist chamber. The sections were washed with 0.1 M PBS for 15 minutes. Peroxidase-conjugated antibody was then applied to the specimens at 37°C for 10 minutes in a moist chamber. The sections were developed with 3,3-diaminobenizidine and counterstained with methyl green.

Statistical analysis

Comparisons between two groups were analyzed using the Mann-Whitney U test. Comparisons between multi groups were analyzed using the Kruskal-Wallis test and the Steel test. A *P*-value of < 0.05 was considered statistically significant.

Results

Appearance of aggregates of human synovial MSCs

Human synovial MSCs were aggregated using the hanging drop technique (Figure 1A). Three days after being cultured in the drop (Figure 1B), the aggregate, consisting of 250,000 MSCs, became approximately 1 mm in diameter (Figure 1C). The aggregate was not easily broken by manipulation. Sagittal sections of the aggregates showed heart-shape as a whole (Figure 1Da). The superficial layer was composed of spindle cells parallel to the surface, whereas the deep layer was comprised of round cells both at top and bottom of the aggregate (Figure 1Db, c). Though cells positive for TUNEL staining were observed, the number was only approximately under 5% (Figure 1Dd).

Transcriptome profile of aggregates of human synovial MSCs

To examine the sequential changes of gene expression profiles during aggregation of human synovial MSCs, microarray analyses were performed. The differences of gene profile between before and after aggregation exceeded those among donor variances (Figure 2A). The number of genes up-regulated more than five-fold was 621. The number of genes up-regulated more than 100-fold was 10, and these genes were related to hypoxia (integrin, alpha 2 (*ITGA2*), stanniocalcin 1 (*STC1*), chemokine (C-X-C motif) receptor 4 (*CXCR4*)), nutrient (*BMP2*, proprotein convertase subtilisin/kexin type 1 (*PCSK1*), secreted phosphoprotein 1 (*SPP1*), *ITGA2*, *STC1*), extracellular region (*MMP1*, *MMP3*), and cell adhesion (*SPP1*, *ITGA2*) (Table 2). The most up-regulated gene was *BMP2*, increased to 273 folds (Table 2). *STC1* was also highly up-regulated in aggregates of synovial MSCs. The number of genes down-regulated less than one-fifth was 409, and the ontology for the genes was related to cell cycle. The microarray data are available at the public database (GEO accession# GSE 31980).

To further investigate gene expressions during aggregation of human synovial MSCs, real time RT-PCR analyses were additionally used for chondrogenesis-related genes (SRY (sex determining region Y)-box (*SOX)5, -6, -9*, and *BMP2*) and anti-inflammatory genes (TNFα inducible gene 6 (*TSG-6*), and *STC-1*) in four donors. In most cases, expressions for these genes increased sequentially (Figure 2B).

In vitro chondrogenesis of aggregates of human synovial MSCs

In vitro chondrogenic ability of human synovial MSCs after hanging drop culture was compared to that of MSCs after monolayer culture (Figure 3A). Aggregates

Suzuki *et al. Arthritis Research & Therapy* 2012, **14**:R136
http://arthritis-research.com/content/14/3/R136

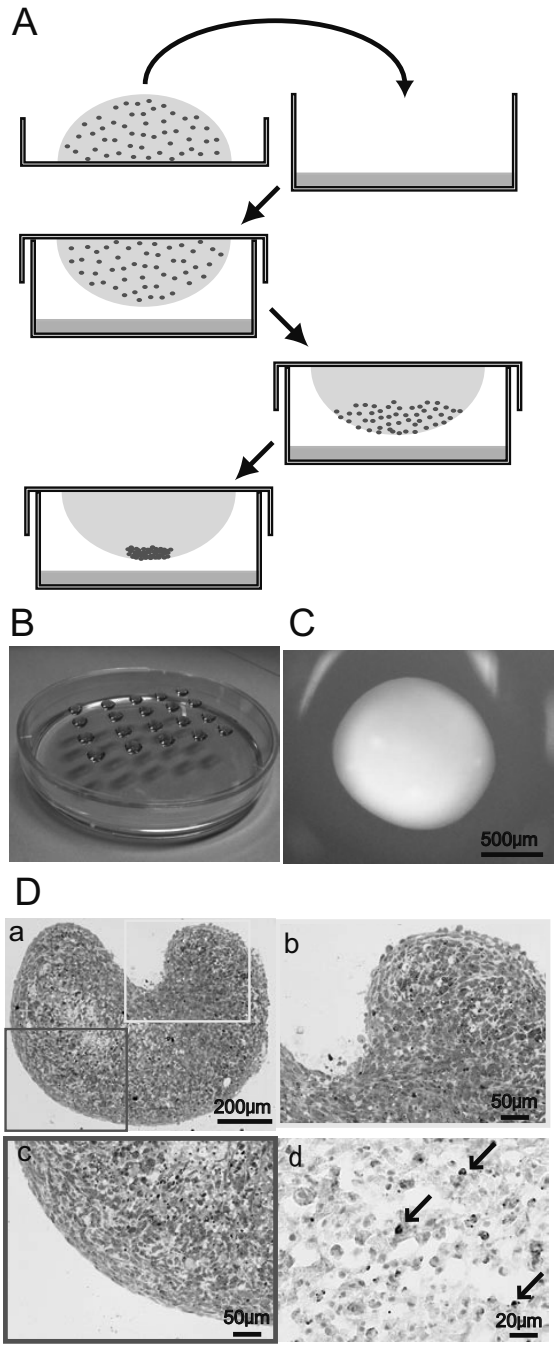

Figure 1 Preparation and appearance of aggregates of human synovial MSCs. **(A)**: Scheme of preparation of aggregates using hanging drop technique. **(B):** Drops hanging on the cover of 15 cm dish. **(C):** Macroscopic image of aggregate consisted of 250,000 MSCs, three days after cultured in hanging drop. **(D):** Sagittal sections of aggregates stained with toluidine blue (a, b, c) and TUNEL (d). TUNEL positive cells are indicated with arrows.

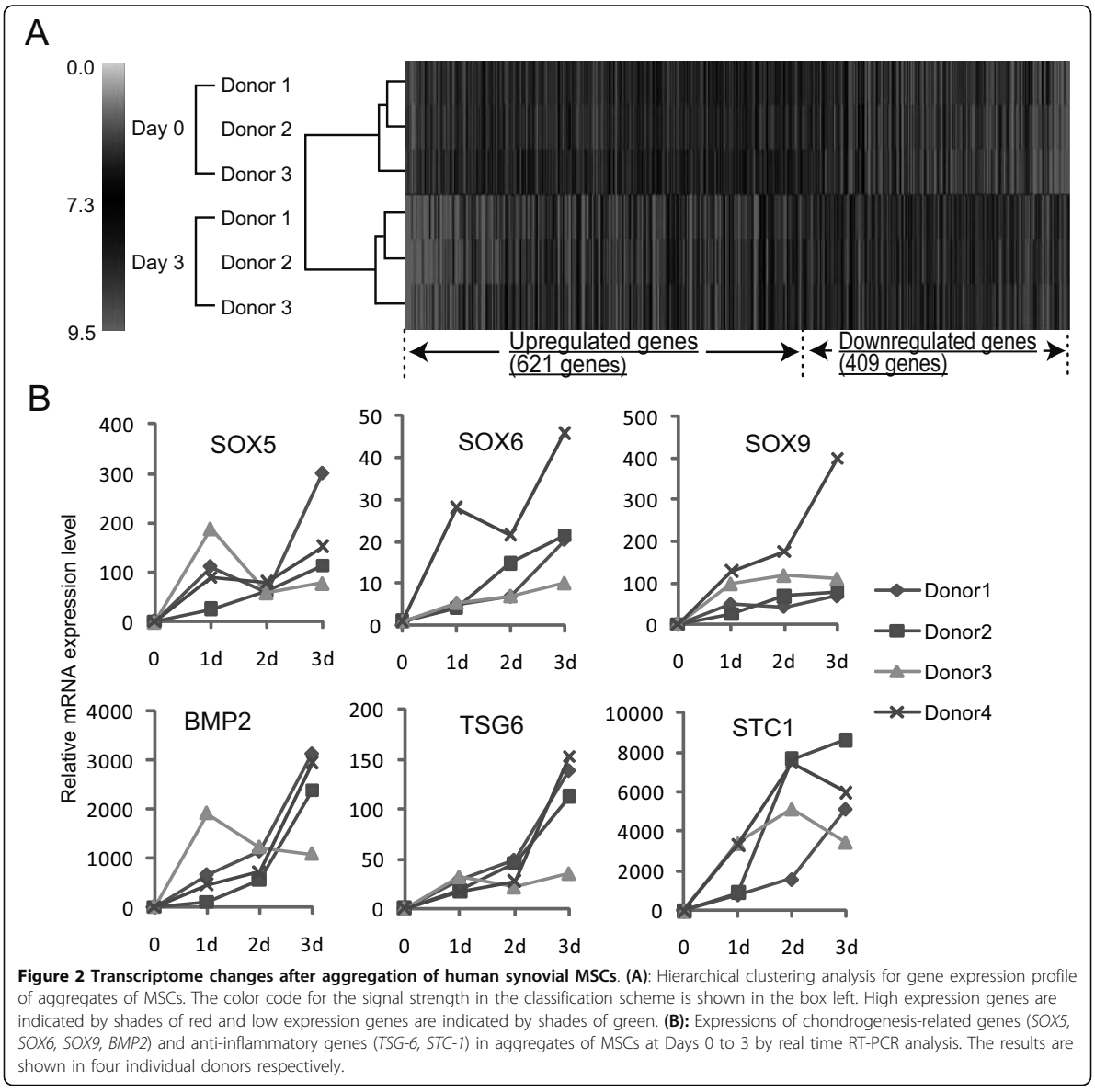

Figure 2 Transcriptome changes after aggregation of human synovial MSCs. **(A)**: Hierarchical clustering analysis for gene expression profile of aggregates of MSCs. The color code for the signal strength in the classification scheme is shown in the box left. High expression genes are indicated by shades of red and low expression genes are indicated by shades of green. **(B):** Expressions of chondrogenesis-related genes (*SOX5, SOX6, SOX9, BMP2*) and anti-inflammatory genes (*TSG-6, STC-1*) in aggregates of MSCs at Days 0 to 3 by real time RT-PCR analysis. The results are shown in four individual donors respectively.

of MSCs differentiated into chondrocytes as well (Figure 3B). The wet weight of pellets derived from MSCs after hanging drop culture was heavier than that of pellets derived from MSCs after monolayer culture in all four donors at 14 or 21 days (Figure 3C). Real time RT-PCR analysis showed higher expression levels of collagen *(COL)2A1*, aggrecan and *SOX9* for pellets derived from MSCs after hanging drop culture compared to MSCs after monolayer culture at 14 and 21 days (Figure 3D). Cartilage extracellular matrix synthesis and accumulation of type II collagen were confirmed by histological analysis stained with toluidine blue and immunohistochemical analysis (Figure 3E).

In vivo analysis for cartilage regeneration by transplantation of aggregates of synovial MSCs in rabbits

To examine whether transplantation of aggregates of synovial MSCs promotes cartilage regeneration, *in vivo* study was performed in rabbits. To further investigate the optimal number of aggregates consisting of 250,000 MSCs, 0 to 80 aggregates were transplanted into the defect.

Table 2 The top 10 upregulated genes in aggregates of MSCs

No.	Genebank No.	Gene name	Symbol	fold change
1	AA583044	bone morphogenetic protein 2	***BMP2***	273
2	NM_002421	matrix metalloproteinase 1	***MMP1***	205
3	NM_000439	proprotein convertase subtilisin/kexin type 1	***PCSK1***	179
4	M86849	gap junction protein, beta 2	***GJB2***	170
5	M83248	secreted phosphoprotein 1 (osteopontin)	***SPP1***	156
6	L27624	tissue factor pathway inhibitor 2	***TFPI2***	137
7	NM_002422	matrix metalloproteinase 3	***MMP3***	136
8	N95414	integrin, alpha 2 (CD49B)	***ITGA2***	129
9	AW003173	stanniocalcin 1	***STC1***	124
10	AJ224869	chemokine (C-X-C motif) receptor 4	***CXCR4***	101

The top 10 genes which increased higher in aggregates of MSCs cultured in hanging drops for three days compared with MSCs in a monolayer culture. Values are the means among three individual donors.

At 0 days, in the case of 40 and 80 transplanted aggregates, the osteochondral defects were filled with aggregates labeled with DiI macroscopically (Figure 4A).

At four weeks, in the case of 5 and 10 transplanted aggregates, the osteochondral defect was mostly covered with a thick cartilage matrix (Figure 4B, C). In the case of 20 and 40 transplanted aggregates, the defect was partially covered with cartilage matrix. In the case of 80 transplanted aggregates, the defect was filled with only fibrous tissue, which appeared to be similar to the control (Figure 4B).

At 12 weeks, in the case of 10 transplanted aggregates, the border between cartilage and bone moved up, and thickness of the regenerated cartilage became similar to the neighboring cartilage (Figure 4B, D). In the case of 5 and 20 transplanted aggregates, the bone defect was repaired, but the cartilage defect was filled partially with cartilage matrix. In the case of 40 and 80 transplanted aggregates, the osteochondral defect was poorly repaired, similar to the control (Figure 4B). Histological score was the best and the safranin-O positive area ratio was highest in the case of 10 transplanted aggregates both at 4 and 12 weeks (Figure 4E, F).

To trace MSCs, 10 aggregates of GFP positive MSCs were transplanted into the defect. At Day 1, no GFP positive aggregates could be observed in the knee joint except the defects with a fluorescent stereomicroscope. Histologically, aggregates changed their forms but have not fused yet (Figure 5A). At four weeks, the defect was filled with cartilage matrix and the GFP positive cells were still observed both at the bottom and the center of the regenerated cartilage (Figure 5B). Regenerated cartilage consisted of both GFP positive cells and GFP negative cells.

Influences of cell number per aggregate and of aggregate number for transplantation

Cell number per aggregate as well as aggregate number may be a factor affecting properties of the aggregates. To answer this question, 25 or 100 aggregates, in which an aggregate consisted of 100,000 MSCs, were transplanted into the osteochondral defect.

At four weeks, in the case of 25 transplanted aggregates, the defect was fully filled with cartilage matrix (Figure 6A), in which the result was different from the case of 20 or more aggregates, in which an aggregate consisted of 250,000 MSCs. In the case of 100 transplanted aggregates, the defect was filled with fibrous tissue, and the histological score was inferior and the safranin-O positive area ratio was smaller. (Figure 6B, C).

Influences of aggregate number on viability of MSCs

To clarify why transplantation of aggregates over a certain number resulted in poor outcome, viability of cells was first examined by TUNEL staining. Compared to the case of 10 transplanted aggregates, much more TUNEL positive cells could be observed in the case of 80 transplanted aggregates (Figure 6D).

Another factor might be a nutrient deprivation and *in vitro* analyses using aggregates of rabbit synovial MSCs were performed. Seven days after 1 or 40 aggregates were cultured in a well of 96-well plates, the medium color changed to yellow in the case of 40 aggregates, while the color remained red in the case of only 1 aggregate (Figure 6E). TUNEL positive cells were much higher in the case of 40 aggregates than in the case of only 1 aggregate.

Discussion

In this study, to form aggregates of synovial MSCs, the hanging drop technique was used [8-10]. This is a simple method; expensive or specific tools are not required. Three days after cultured in the drop, the aggregate, consisting of 250,000 MSCs, became approximately 1 mm in diameter, large enough to be visible and solid enough to aspirate with a pipette. Aggregates of MSCs sank faster in the suspension medium than dispersed

Suzuki *et al. Arthritis Research & Therapy* 2012, **14**:R136
http://arthritis-research.com/content/14/3/R136

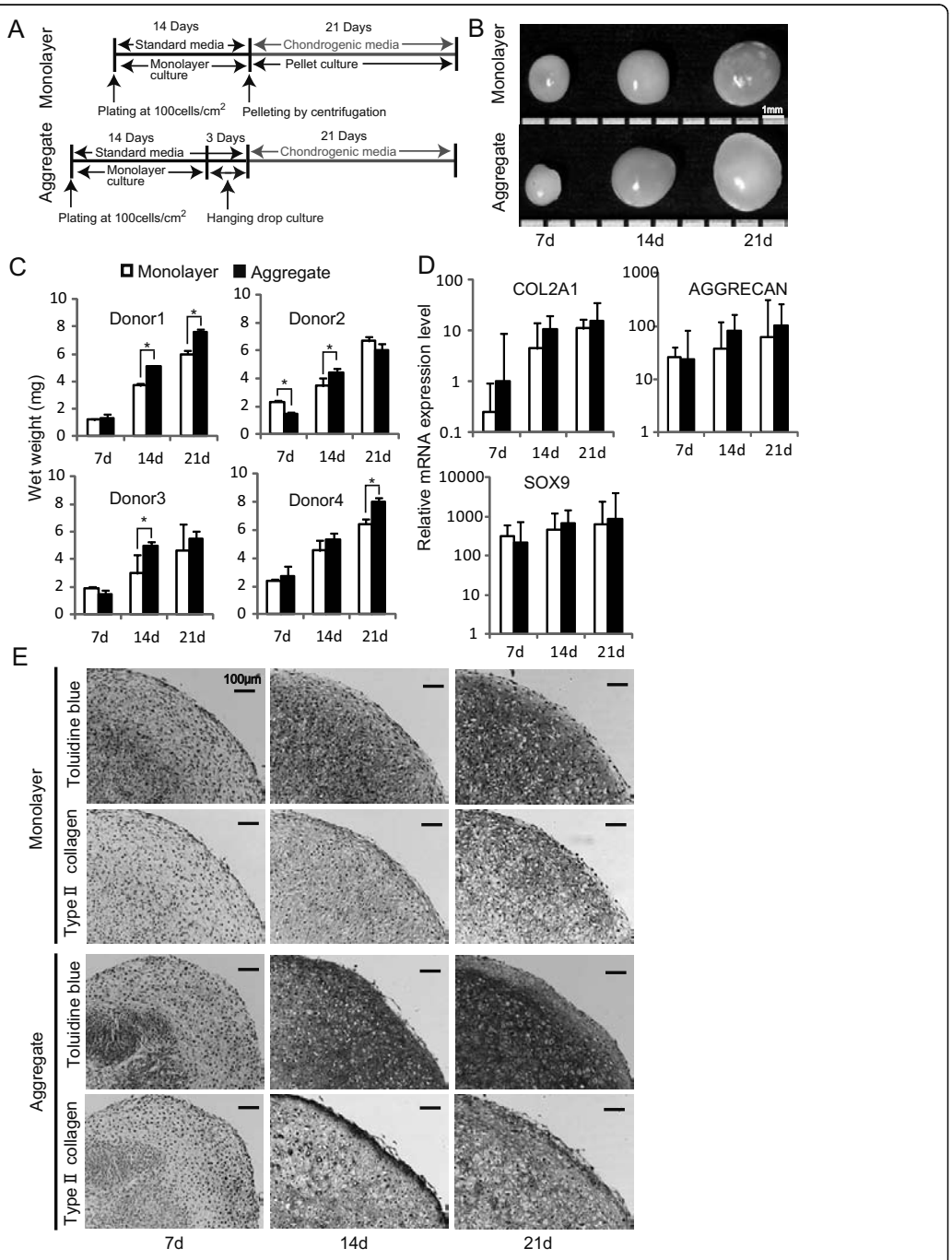

Figure 3 ***In vitro*** **chondrogenic ability of human synovial MSCs after hanging drop culture (A): Scheme for the analyses**. **(B):** Macroscopic images of pellets derived from aggregates of MSCs and those of pellets derived from MSCs in a monolayer culture. **(C):** Wet weight in four individual donors. Values are the means with standard deviation (SD) ($P < 0.05$ by the Mann-Whitney U test). **(D):** Expressions of chondrogenesis-related genes by RT-PCR analyses. Values are the means with SD among four donors. The fold changes of *SOX9* and *AGGRECAN* expression levels were shown when the gene expression levels at Day 0 were normalized as 1. The fold changes of *COL2A1* expression levels were shown when the gene expression levels in MSCs in monolayer at Day 7 were normalized as 1 because *COL2A1* expression level at Day 0 was undetectable. **(E):** Histological sections of pellets stained with toluidine blue and immunohistochemical analysis for type II collagen.

Suzuki *et al. Arthritis Research & Therapy* 2012, **14**:R136
http://arthritis-research.com/content/14/3/R136

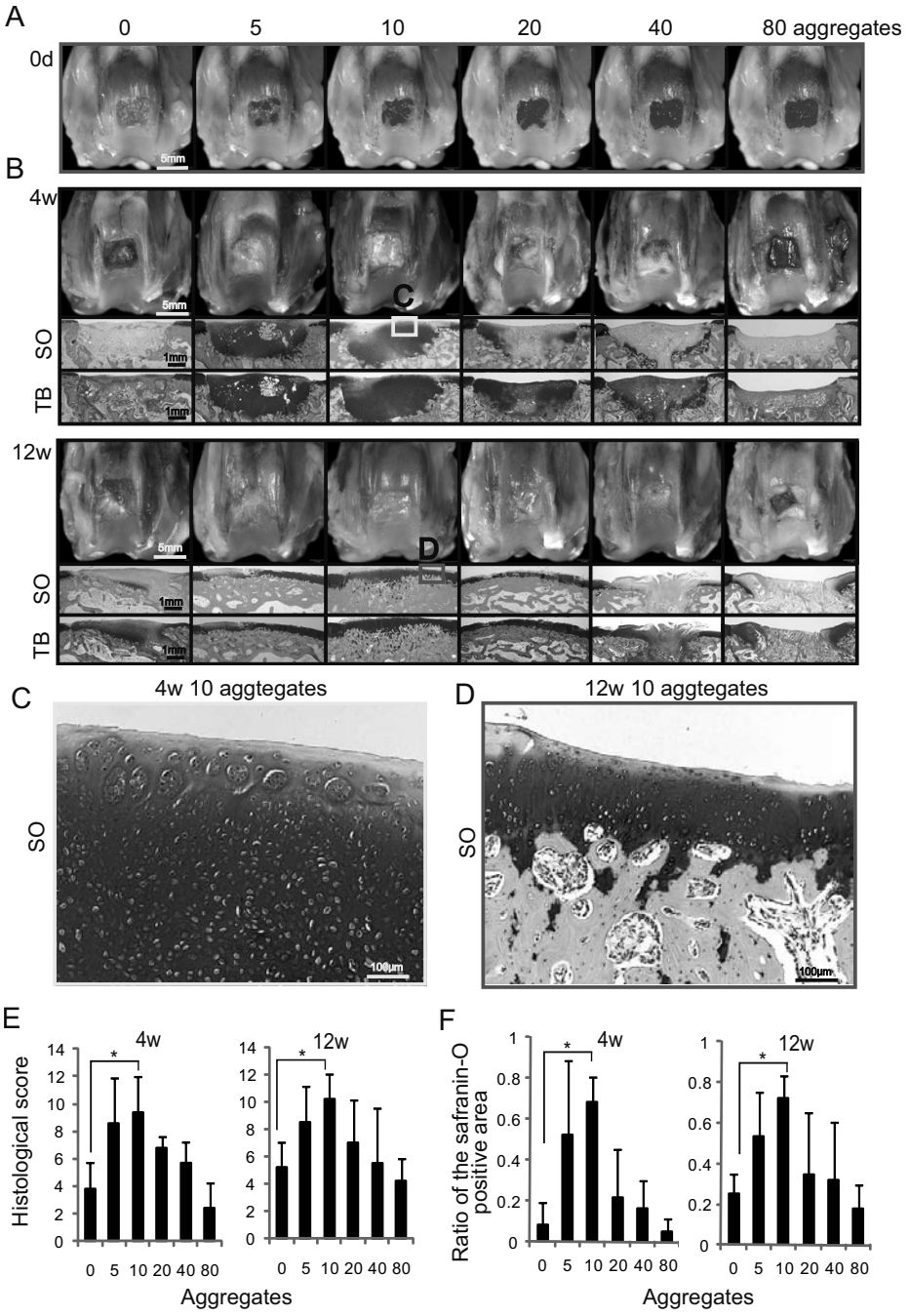

Figure 4 Cartilage regeneration by transplantation of aggregates of synovial MSCs in rabbits. **(A)**: Macroscopic observation of osteochondral defects one minute after transplantation of indicated number of aggregates of MSCs. The aggregate consisted of 250,000 MSCs, labeled with DiI for visualization. **(B):** Macroscopic and histological observation. For histologies, sagittal sections were stained with safranin-O (SO) and toluidine blue (TB). **(C, D):** Magnified histology of the indicated area. **(E):** Histological score. Values are the means with SD. (n = 5; P < 0.05 by the Kruskal-Wallis test and the Steel test). **(F):** Ratio of the safranin-O positive area to the defect area. Values are the means with SD. (n = 5; P < 0.05 by the Kruskal-Wallis test and the Steel test).

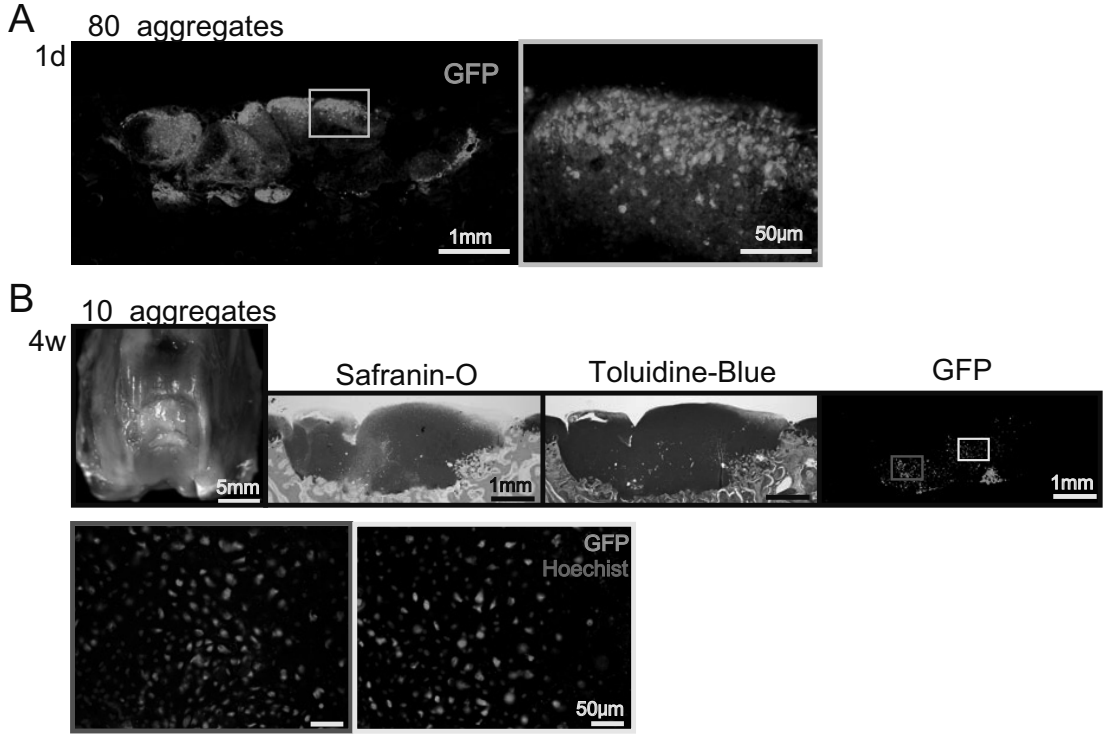

Figure 5 Transplantation of 10 aggregates of synovial MSCs derived from a GFP rabbit. **(A)**: Sagittal sections of osteochondral defect under fluorescence for GFP at one day. **(B):** Macroscopic and histological observation four weeks after transplantation. Nuclei were shown as blue in higher magnified pictures.

MSCs and helped to avoid loss of MSCs from targeted cartilage defect. The use of aggregates was practically convenient for transplantation of MSCs.

In the previous report, the number of apoptotic or necrotic cells was greater in aggregates prepared with 100,000 or 250,000 human bone marrow MSCs, which was examined by flow cytometry, measuring propidium iodide uptake and annexin V labeling [10]. We examined the viability of aggregates of MSCs by TUNEL staining and confirmed that cells positive for TUNEL staining were observed; the number was small compared to the previous report. This difference may have been due to the difference of methods. Microarray analysis showed up-regulation of genes with ontology for regulation of cell death. The microarray data are available at the public database (GEO accession# GSE 31980). These results suggest that aggregation of 250,000 MSCs affect the viability of cells. However, we thought that aggregates of MSCs could be used as a source for cartilage regeneration because most cells which are cultured in drops for three days are viable.

Aggregation of synovial MSCs changed the gene expression profile dramatically without any special tools or chemical factors. This is possibly due to environmental changes, including cell-to-cell contact, hypoxic condition and low nutrient condition. Aggregation of human synovial MSCs increased expressions of several chondrogenesis-related genes and the most up-regulated gene was BMP2, which was also up-regulated in bone marrow MSCs [8,10].

In this study, we compared *in vitro* chondrogenesis potential of synovial MSCs after hanging drop culture with that of MSCs after monolayer culture. We used 1,000 ng/ml *BMP7* for *in vitro* chondrogenic differentiation assay. We previously examined the dose effect of BMP6 between 0 to 500 ng/ml for *in vitro* chondrogenesis of bone marrow MSCs. Cartilage pellets increased in size along with the concentration of *BMP6*, and a maximal effect was at 500 ng/ml [17]. Our preliminary experiments showed that 1,000 ng/ml *BMP6* induced larger cartilage pellets than 500 ng/ml *BMP6* in bone marrow and synovial MSCs. We obtained similar results with *BMP7*. Real time RT-PCR analysis showed higher expression levels of *COL2A1*, aggrecan and *SOX9* for pellets derived from MSC-aggregates after hanging drop culture compared to those of MSCs in a monolayer culture.

Suzuki *et al. Arthritis Research & Therapy* 2012, **14**:R136
http://arthritis-research.com/content/14/3/R136

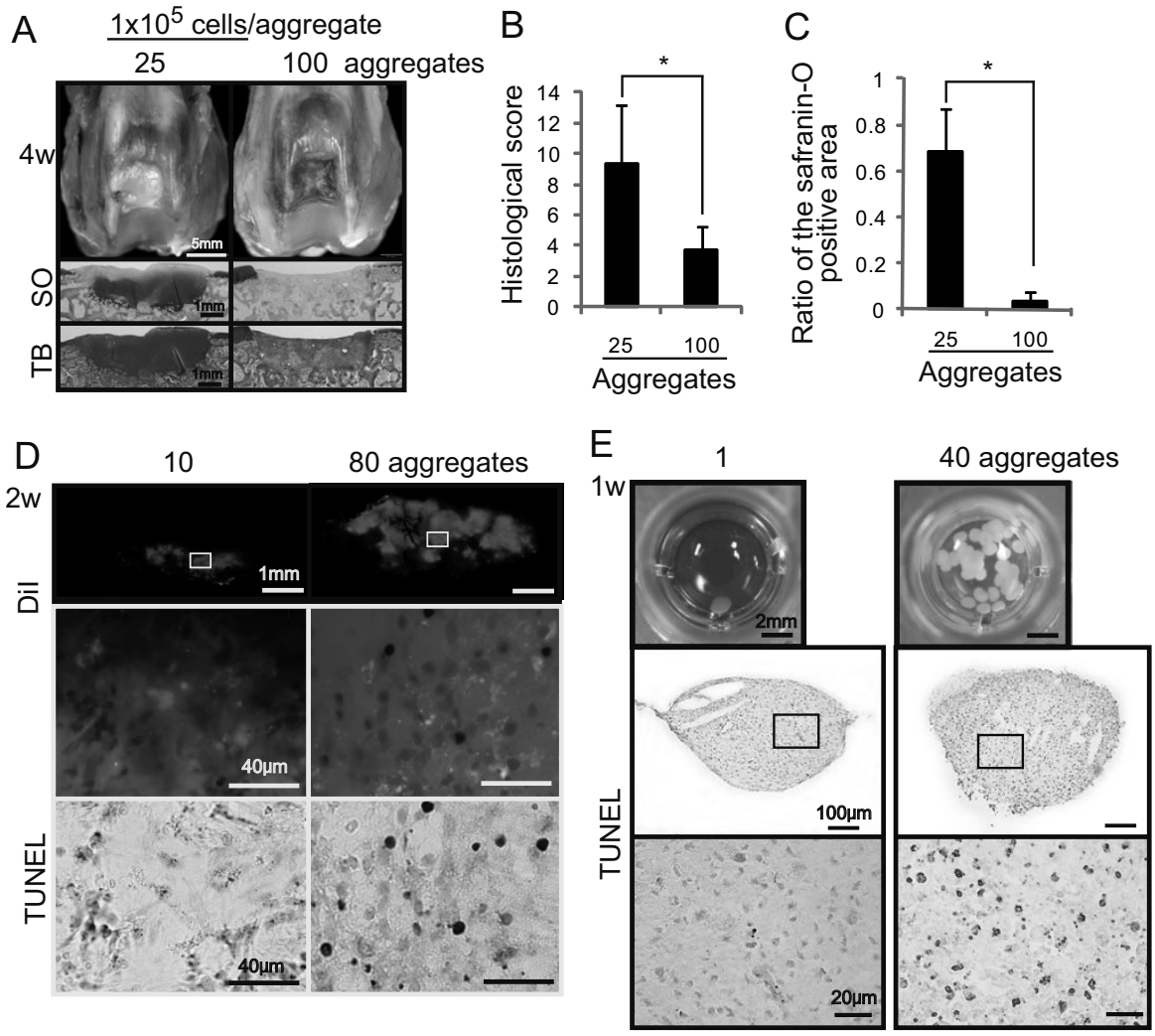

Figure 6 Influences of cell number per an aggregate and of aggregate number for transplantation. **(A)**: Macroscopic and histological observation four weeks after transplantation of 25 or 100 aggregates in which an aggregate consisted of 100,000 MSCs. **(B):** Histological score. Values are the means with SD ($n = 4$; $P < 0.05$ by the Mann-Whitney U test). **(C):** Ratio of the safranin-O positive area to the defect area. Values are the means with SD. ($n = 4$; $P < 0.05$ by the Mann-Whitney U test). **(D):** Histological observation two weeks after transplantation of 10 and 80 aggregates in which an aggregate consisted of 250,000 MSCs labeled with DiI. Sagittal sections under fluorescence and the serial sections stained with TUNEL were shown. **(E):** *In vitro* analyses of aggregates of rabbit synovial MSCs. One or 40 aggregates, in which an aggregate consisted of 250,000 MSCs, were cultured in a well of 96-well plates. Macroscopic images for the wells and sagittal sections of the aggregates stained with TUNEL were shown.

Furthermore, the wet weight of pellets derived from MSC-aggregates after hanging drop culture was heavier than that of pellets derived MSCs in a monolayer culture. These indicate that chondrogenic potential increased in aggregates of MSCs after hanging drop culture.

In this study, we used an osteochondral defect model of rabbits, which have a higher, self-renewal capacity than bigger animals and humans. Therefore, the results obtained here should be critically evaluated. However, we prepared negative controls, which healed poorly at 4 and 12 weeks. We previously confirmed that the osteochondral defect created in the trochlear groove of the femur, similar to this study, was not repaired without any treatments 24 weeks after surgery [6]. These findings indicate that this rabbit model is useful to evaluate the effects of the treatments for cartilage regeneration.

For *in vivo* analysis of cartilage regeneration by transplantation of aggregates of synovial MSCs in rabbits,

successful cartilage regeneration was observed in the cases of a relatively small number of transplanted aggregates of MSCs, and the worst results were observed when the highest number of aggregates of MSCs was transplanted. These results were not what we expected, because we previously reported that better cartilage regeneration was obtained when higher cell densities of MSCs were embedded in collagen gel [3].

Why were poor results obtained when more than a certain number of aggregates were transplanted? We listed three possible reasons. First, nutrition to maintain transplanted MSCs was depleted and the environment around transplanted MSCs worsened when too many aggregates were transplanted. As shown in Figure 6E, in the case of 40 aggregates that were cultured for seven days in a well of 96-well plates, medium color changed to yellow. This means that adjustment of pH could not be controlled. Second, TUNEL positive cells increased when too many aggregates were transplanted. The number of TUNEL positive cells was higher when too many aggregates were transplanted (Figure 6D) than before transplantation (Figure 1D) and after a suitable number of aggregates were transplanted (Figure 6D). Third, transplantation of too many aggregates prevented chondro-progenitor cells from moving to the osteochondral defect from bone marrow and from synovial fluid.

We confirmed that transplanted aggregates of synovial MSCs were directly differentiated into chondrocytes by transplanting MSCs derived from GFP transgenic rabbit. This result suggests that aggregates of synovial MSCs were involved in the reparative process. However, as shown in Figure 5B, in the case of aggregates of GFP positive MSCs being transplanted, regenerated cartilage consisted of both GFP positive cells and GFP negative cells. MSCs existed in synovial fluid [18] and these MSCs contributed to the repair of cartilage injury [6,19]. These results suggest that some host MSCs were also involved in the reparative process. In addition, host MSCs may have been involved in the anti-inflammatory process. In our rabbit osteochondral defect model, inflammation like a synovitis was not severe even in the control group. Therefore, we could not confirm the anti-inflammatory effect of MSCs. It would be interesting to investigate the anti-inflammatory effect of transplantation of aggregates of synovial MSCs and host MSCs in other arthritis models.

As previously reported, in bone marrow MSCs [10], aggregates of human synovial MSCs expressed anti-inflammatory genes *TSG6* and *STC1*. *TSG6* is secreted by synoviocytes, mononuclear cells and chondrocytes under inflammatory conditions and has an anti-inflammatory effect. Overexpression of *TSG6* or administration of recombinant *TSG6* inhibited inflammation and joint destruction in a murine collagen induced arthritis model [20-23]. *STC1* is reported to have an anti-apoptotic effect as well as an anti-inflammatory effect [24,25]. However, their roles in joint homeostasis are unknown.

In this study, transplantation of low numbers of aggregates, in other words, low density of aggregates to the volume of the cartilage defect, showed better regeneration (Figures 4 and 6). This is favorable for clinical application. We have performed clinical trials of autologous human synovial MSCs transplantation for cartilage defects. In the experiences of 12 patients, approximately 50 million synovial MSCs at passage 0 were transplanted for approximately 280 mm^2 cartilage defects (unpublished data). In a rabbit model, we transplanted synovial MSC-aggregates into the osteochondral defects without any loss of cells, and 10 MSC-aggregates (2.5×10^6 cells) per 25 mm^2 defects were needed for better cartilage regeneration. According to these data, we can prepare a sufficient amount of human synovial MSCs at passage 0.

In this study, we did not use scaffolds for transplantation of aggregates of synovial MSCs. We were able to adhere aggregates of synovial MSCs on the osteochondral defect without scaffolds; however, the use of scaffolds or materials to improve survival of transplanted cells is attractive. One of the methods is the use of a fibrin glue, which has an effect of improving survival of transplanted cells [26]. In addition, cell transplantation of MSCs with a fibrin glue can probably be performed under arthroscopic surgery. Further studies are needed to improve cell transplantation procedures.

Conclusion

Aggregated synovial MSCs were a useful source for cartilage regeneration considering such factors as easy preparation, higher chondrogenic potential and efficient attachment.

Abbreviations

αMEM: α-minimal essential medium; *BMP*: bone morphogenetic protein; CCM: complete culture medium; *COL*: collagen; *CXCR4*: chemokine (C-X-C motif) receptor 4; EDTA: ethylenediaminetetraacetate; FBS: fetal bovine serum; GFP: green fluorescent protein; *GJB2*: gap junction protein, beta 2; *ITGA2*: integrin, alpha 2; MeV: MultiExperiment Viewer; MMP: matrix metalloproteinase; MSC: mesenchymal stem cell; OCT: optimal cutting temperature; PBS: phosphate-buffered saline; *PCSK1*: proprotein convertase subtilisin/kexin type 1; PFA: paraformaldehyde; RMA: Robust MultiChip Analysis; RT: reverse transcription; SD: standard deviation; SO: safranin-O; *SOX*: SRY (sex determining region Y)-box; *SPP1*: secreted phosphoprotein 1; *STC1*: stanniocalcin 1; TB: toluidine blue; *TFPI2*: tissue factor pathway inhibitor 2; *TNF*: tumor necrosis factor; *TSG6*: TNFα inducible gene 6; TUNEL: terminal deoxynucleotidyl transferase dUTP nick end labeling.

Acknowledgements

This study was supported by "the Project for Realization of Regenerative Medicine" and "the Global Center of Excellence (GCOE) Program" by the Ministry of Education, Culture, Sports, Science and Technology (MEXT), Japan to IS, grants from the Japanese Ministry of Education Global Center of Excellence Program, International Research Center for Molecular Science in

Tooth and Bone Diseases to TM, and from a Health and Labor Sciences Research Grant, Research on Regenerative Medicine for Clinical Application to IS. Recombinant human *BMP-7* was distributed by Stryker Biotech. We thank Miyoko Ojima for her expert help with histology and Izumi Nakagawa for management of our laboratory.

Author details
[1]Section of Orthopedic Surgery, Graduate School, Tokyo Medical and Dental University, 1-5-45 Yushima, Bunkyo-ku, Tokyo 113-8519, Japan. [2]Global Center of Excellence Program, International Research Center for Molecular Science in Tooth and Bone Diseases, Tokyo Medical and Dental University, 1-5-45 Yushima, Bunkyo-ku, Tokyo 113-8519, Japan. [3]Instrumental Analysis Research Center, Tokyo Medical and Dental University, 1-5-45 Yushima, Bunkyo-ku, Tokyo 113-8519, Japan. [4]Department of Reproductive Biology, National Research Institute for Child Health and Development, 2-10-1 Okura, Setagaya-ku, Tokyo 157-8535, Japan. [5]Section of Cartilage Regeneration, Graduate School, Tokyo Medical and Dental University, 1-5-45 Yushima, Bunkyo-ku, Tokyo 113-8519, Japan.

Authors' contributions
SS participated in the design of the study, carried out the animal experiments, analyzed the results and drafted the manuscript. TM participated in the design of the study and provided the administrative and financial support. KT participated in the design of the study. SI helped with histological analysis. HM and AU carried out the microarray analysis and participated in the evaluation of the results. IS participated in the design of the study, provided the financial support and completed the final manuscript. All authors read and approved the final manuscript.

Competing interests
The authors declare that they have no competing interests.

Received: 24 November 2011 Revised: 30 April 2012
Accepted: 7 June 2012 Published: 7 June 2012

References

1. Sakaguchi Y, Sekiya I, Yagishita K, Muneta T: **Comparison of human stem cells derived from various mesenchymal tissues: superiority of synovium as a cell source.** *Arthritis Rheum* 2005, **52**:2521-2529.
2. Shirasawa S, Sekiya I, Sakaguchi Y, Yagishita K, Ichinose S, Muneta T: ***In vitro* chondrogenesis of human synovium-derived mesenchymal stem cells: optimal condition and comparison with bone marrow-derived cells.** *J Cell Biochem* 2006, **97**:84-97.
3. Koga H, Muneta T, Nagase T, Nimura A, Ju YJ, Mochizuki T, Sekiya I: **Comparison of mesenchymal tissues-derived stem cells for *in vivo* chondrogenesis: suitable conditions for cell therapy of cartilage defects in rabbit.** *Cell Tissue Res* 2008, **333**:207-215.
4. Nimura A, Muneta T, Koga H, Mochizuki T, Suzuki K, Makino H, Umezawa A, Sekiya I: **Increased proliferation of human synovial mesenchymal stem cells with autologous human serum: comparisons with bone marrow mesenchymal stem cells and with fetal bovine serum.** *Arthritis Rheum* 2008, **58**:501-510.
5. Koga H, Engebretsen L, Brinchmann JE, Muneta T, Sekiya I: **Mesenchymal stem cell-based therapy for cartilage repair: a review.** *Knee Surg Sports Traumatol Arthrosc* 2009, **17**:1289-1297.
6. Koga H, Shimaya M, Muneta T, Nimura A, Morito T, Hayashi M, Suzuki S, Ju YJ, Mochizuki T, Sekiya I: **Local adherent technique for transplanting mesenchymal stem cells as a potential treatment of cartilage defect.** *Arthritis Res Ther* 2008, **10**:R84.
7. Shimaya M, Muneta T, Ichinose S, Tsuji K, Sekiya I: **Magnesium enhances adherence and cartilage formation of synovial mesenchymal stem cells through integrins.** *Osteoarthritis Cartilage* 2010, **18**:1300-1309.
8. Potapova IA, Gaudette GR, Brink PR, Robinson RB, Rosen MR, Cohen IS, Doronin SV: **Mesenchymal stem cells support migration, extracellular matrix invasion, proliferation, and survival of endothelial cells *in vitro*.** *Stem Cells* 2007, **25**:1761-1768.
9. Potapova IA, Brink PR, Cohen IS, Doronin SV: **Culturing of human mesenchymal stem cells as three-dimensional aggregates induces functional expression of CXCR4 that regulates adhesion to endothelial cells.** *J Biol Chem* 2008, **283**:13100-13107.
10. Bartosh TJ, Ylostalo JH, Mohammadipoor A, Bazhanov N, Coble K, Claypool K, Lee RH, Choi H, Prockop DJ: **Aggregation of human mesenchymal stromal cells (MSCs) into 3D spheroids enhances their antiinflammatory properties.** *Proc Natl Acad Sci USA* 2010, **107**:13724-13729.
11. Miyamoto T, Muneta T, Tabuchi T, Matsumoto K, Saito H, Tsuji K, Sekiya I: **Intradiscal transplantation of synovial mesenchymal stem cells prevents intervertebral disc degeneration through suppression of matrix metalloproteinase-related genes in nucleus pulposus cells in rabbits.** *Arthritis Res Ther* 2010, **12**:R206.
12. Takahashi R, Kuramochi T, Aoyagi K, Hashimoto S, Miyoshi I, Kasai N, Hakamata Y, Kobayashi E, Ueda M: **Establishment and characterization of CAG/EGFP transgenic rabbit line.** *Transgenic Res* 2007, **16**:115-120.
13. Niikura T, Hak DJ, Reddi AH: **Global gene profiling reveals a downregulation of BMP gene expression in experimental atrophic nonunions compared to standard healing fractures.** *J Orthop Res* 2006, **24**:1463-1471.
14. Willems E, Leyns L, Vandesompele J: **Standardization of real-time PCR gene expression data from independent biological replicates.** *Anal Biochem* 2008, **379**:127-129.
15. Saeed AI, Bhagabati NK, Braisted JC, Liang W, Sharov V, Howe EA, Li J, Thiagarajan M, White JA, Quackenbush J: **TM4 microarray software suite.** *Methods Enzymol* 2006, **411**:134-193.
16. Wakitani S, Goto T, Pineda SJ, Young RG, Mansour JM, Caplan AI, Goldberg VM: **Mesenchymal cell-based repair of large, full-thickness defects of articular cartilage.** *J Bone Joint Surg Am* 1994, **76**:579-592.
17. Sekiya I, Colter DC, Prockop DJ: **BMP-6 enhances chondrogenesis in a subpopulation of human marrow stromal cells.** *Biochem Biophys Res Commun* 2001, **284**:411-418.
18. Morito T, Muneta T, Hara K, Ju YJ, Mochizuki T, Makino H, Umezawa A, Sekiya I: **Synovial fluid-derived mesenchymal stem cells increase after intra-articular ligament injury in humans.** *Rheumatology (Oxford)* 2008, **47**:1137-1143.
19. Koga H, Muneta T, Ju YJ, Nagase T, Nimura A, Mochizuki T, Ichinose S, von der Mark K, Sekiya I: **Synovial stem cells are regionally specified according to local microenvironments after implantation for cartilage regeneration.** *Stem Cells* 2007, **25**:689-696.
20. Wisniewski HG, Hua JC, Poppers DM, Naime D, Vilcek J, Cronstein BN: **TNF/IL-1-inducible protein TSG-6 potentiates plasmin inhibition by inter-alpha-inhibitor and exerts a strong anti-inflammatory effect *in vivo*.** *J Immunol* 1996, **156**:1609-1615.
21. Maier R, Wisniewski HG, Vilcek J, Lotz M: **TSG-6 expression in human articular chondrocytes. Possible implications in joint inflammation and cartilage degradation.** *Arthritis Rheum* 1996, **39**:552-559.
22. Mindrescu C, Dias AA, Olszewski RJ, Klein MJ, Reis LF, Wisniewski HG: **Reduced susceptibility to collagen-induced arthritis in DBA/1J mice expressing the TSG-6 transgene.** *Arthritis Rheum* 2002, **46**:2453-2464.
23. Mindrescu C, Thorbecke GJ, Klein MJ, Vilcek J, Wisniewski HG: **Amelioration of collagen-induced arthritis in DBA/1J mice by recombinant TSG-6, a tumor necrosis factor/interleukin-1-inducible protein.** *Arthritis Rheum* 2000, **43**:2668-2677.
24. Block GJ, Ohkouchi S, Fung F, Frenkel J, Gregory C, Pochampally R, DiMattia G, Sullivan DE, Prockop DJ: **Multipotent stromal cells are activated to reduce apoptosis in part by upregulation and secretion of stanniocalcin-1.** *Stem Cells* 2009, **27**:670-681.
25. Huang L, Garcia G, Lou Y, Zhou Q, Truong LD, DiMattia G, Lan XR, Lan HY, Wang Y, Sheikh-Hamad D: **Anti-inflammatory and renal protective actions of stanniocalcin-1 in a model of anti-glomerular basement membrane glomerulonephritis.** *Am J Pathol* 2009, **174**:1368-1378.
26. Guo HD, Wang HJ, Tan YZ, Wu JH: **Transplantation of marrow-derived cardiac stem cells carried in fibrin improves cardiac function after myocardial infarction.** *Tissue Eng Part A* 2011, **17**:45-58.

doi:10.1186/ar3869
Cite this article as: Suzuki *et al.*: Properties and usefulness of aggregates of synovial mesenchymal stem cells as a source for cartilage regeneration. *Arthritis Research & Therapy* 2012 **14**:R136.

分子細胞遺伝学分野

稲澤 譲治

難治疾患研究所
分子細胞遺伝学・教授

1）研究の課題名

Integrative genomics and epigenomics for personalized medicine in cancer and genetic disorders

癌と遺伝子疾患の個別化医療に向けたゲノム・エピゲノム解析研究

（小村健教授、森山啓司教授との共同イノベーション研究である）

2）研究のイラストレーション

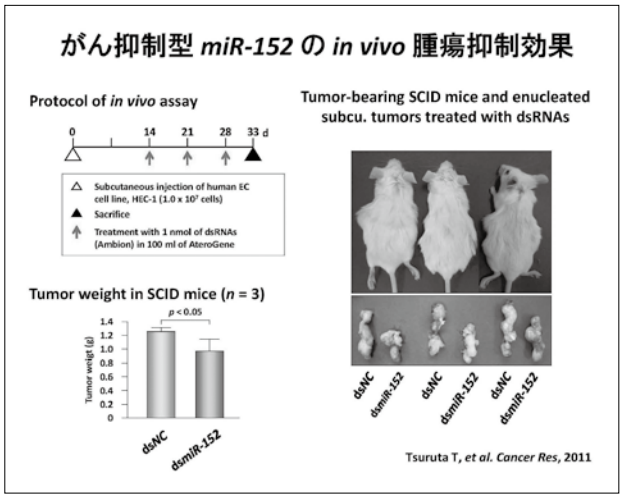

3）発表の研究内容についての英文要約

Innovative techniques for genomic and epigenomic alterations underlying the pathogenesis in cancer and genetic diseases have been established and using those techniques numerous disease-related genes or disease-related genomic alterations have been successfully identified during the course of the research program. In particular, we identified a number of candidate genes including tumor suppressor micro RNAs epigenetically silenced by DNA methylation. Furthermore, we constructed a consortium with 23 medical institutes and hospitals in Japan, and recruited 646 patients with clinically uncharacterized multiple congenital disorders and/or mental retardation (MCA/MR), whose karyotypes were normal according to conventional cytogenetics. Three-stage screening was performed using three different types of microarrays, and the first screening using a targeted array detected pathogenic copy number variation (CNV) in 69 of 646 cases (10.7%), whereas the second screening showed pCNV in 64 cases showed pCNV. Furthermore we performed sequence analyses of breakpoints involved de novo pCNVs in 23 patients with MCA/MR. Among them, fourteen cases showed microhomology-mediated break-induced replication (MMBIR), six showed non-homologous end joining (NHEJ), and three showed non-allelic homologous recombination (NAHR).We could reveal precise mechanisms in CNV formation patients with MCA/MR.

4）本事業に関連して世界的な研究拠点形成に向けて、以下の点で改善・整備等されたこと

病態不明の顎顔面奇形を伴う先天異常症の潜在的ゲノムコピー数異常解析を集学的に実施して、新しい病態関連ゲノム異常の探索を実施した。X染色体連鎖精神発達遅滞症の解析と併せ総数800症例を超える解析を終了しデータベースを構築した。さらに日本人健常者のCNV解析を実施して日本人CNVデータベースを構築し公開した。23例の先天異常症に検出したde novo pathogeneic CNVのゲノムコピー数異常切断点のシークエンス解析を行い、CNV生成機構を明らかにした。 日本人健常者の100家系トリオ（両親と子）のCNV解析を行いdatabaseを構築し、MCG CNV databaseとして公開した。本databaseには日本人のCNV、UPDの位置、サイズ、頻度、親子間でのCNV比較、de novoCNV情報が格納されており病的CNVを診断する時のreference情報を提供している。また、口腔扁平上皮がん（OSCC）において癌関連遺伝子マイクロRNAの探索を行い、DNAメチル化により遺伝し機能を消失する癌抑制遺伝子型マイクロRNAとしてmiR-218を同定した。miR-218はRictorを標的として、Rictor/mTOR/AKTパスウェ

イを負に制御している。口腔がんではしばしばDNAメチル化によりmiR-218が遺伝子サイレンシングを受けることにより、Rictor/mTOR/AKTパスウェイの活性化が惹起され、これにより細胞増殖等が誘導される可能性が示唆された。がん抑制miRNAの補充療法は新たながん治療法として期待さているが、その臨床応用には有効な投与法やデリバリーの開発が今後の大きな課題であり、ナノテクノロジー

A（研究拠点体制）

1. 難治性硬組織疾患の病態オミックス先端研究拠点（Advanced Omics Research for Intractable Hard-Tissue Diseases）オミックス解析の成果とナノサイエンス技術の統合化を図り、成果に基づく難治性硬組織疾患トランスレーショナルリサーチを推進し、当該疾患の克服に向けたオミックス医科学の実現、ならびに教育・人材育成の充実・強化を目指したオミックス研究の先端拠点を構築する。
   【参加教授】野田政樹、小村健、森山啓司、宮坂信之、三木義男、稲澤譲治
   【分担研究者】江面陽一、小崎健一、津田均、森田圭一、上阪等、佐々木善浩、林深
   【研究協力】秋吉一成（京大・院工・教授）
2. 口腔がんの国際共同研究拠点：タイ王国チュラロンコン大学Atiphan Pimkamkam博士と「口腔癌のゲノム・エピゲノム解析」に関する国際共同研究体制を構築
3. 先天異常症の病態解明・診断法開発研究拠点：国内23医療機関（大学病院・国立成育医療センターなど）とコンソーシアムを形成し先天異常症の新規診断法開発と病因性CNV探索研究体制を構築

B（研究教育環境）

・毎月曜日セミナーにて国際一流誌原著論文、総説論文の抄読会を実施。
・毎土曜日研究進捗状況報告会を実施
・各研究者は半年に一度、Research in progress報告を行い研究進捗の確認・助言
・癌ゲノムサイエンス研究会を毎年2回定例開催

C（人材確保）

大学院特別研究学生

D（人材育成）

1. 平成24年度は以下の24名の大学院生が在籍して研究を実施している。そのうち7名は歯科医師（下線）である。坂本宙子、村松智輝、古田繭子、鶴田智彦、倉沢泰浩、上杉篤史、小野宏晃、岡本奈那、遠藤寛則、宮脇豊、原園陽介、山本信祐、永田啓明、岩舘怜子、長縄光代、Nuylan Michelle Loyola、Daniela Tiaki Uehara、李慧、與子田一輝、藤原直人、谷中淑光、Sujata Sakha、森下真紀、髙橋寛吉
2. 古田繭子が東京医科歯科大学グローバルCOE（GCOE）スーパースチューデント（SS）研究発表で優秀賞「Excellent Award」を受賞した。
3. 林深特任講師の原著論文が掲載誌Journal of Human Genetics の表紙で紹介された。
4. 井上純助教が川野小児医学奨学財団の研究助成に採択された。
5. 村松智輝が平成23年度東京医科歯科大学大学院学生研究奨励賞を受賞した。
6. ヒトゲノム多様性データベース「MCG CNV Database」にSNPアレイによる解析データを追加公開した。http：//www.cghtmd.jp/CNVDatabase/top!changeJaLocale
7. 古田繭子が東京医科歯科大学グローバルCOE（GCOE）プログラム研究発表で「Excellent Presentation-Special Award-」を受賞した。
8. 原園陽介が財団法人金原一郎記念医学医療振興財団第26回研究交流助成に採択された。
9. 鶴田智彦が平成23年度日本産科婦人科学会「優秀論文賞婦人科腫瘍学部門」を受賞した。
10. 小崎健一准教授が公益財団法人大阪癌研究会平成24年度一般学術研究助成に採択された。

E（国際化）

1. 古田繭子が文部科学省科学研究費新学術領域研究がん研究分野の特性等を踏まえた支援活動・平成23年度日仏がんワークショップの公募に採択されフランスに派遣された。
2. 3名の国費外国人留学生、Nuylan Michelle Loyola（フィリピン）、Daniela Tiaki Uehara（ブラジル）、Sujata Sakha（ネパール）が在籍している。

5）GCOE事業を推進するに当たって力を入れた点

基礎研究成果が医療貢献するよう研究成果の出口「トランスレーショナルリサーチ」、「個別化医療」をキーワードに、具体的かつ明確に設定してこれを達成するよう努力した。

6）英文原著論文

1. Endo H, Kozaki K, Furuta M, Uzawa N, Pimkhaokham A, Amagasa T, Inazawa J. Potency of tumor-suppressive miR-596 targeting LGALS3BP for epigenetic marker and therapeutic agent in oral cancer. Carcinogenesis（in press）
2. Takanashi J, Okamoto N, Yamamoto Y, Hayashi S, Arai H, Takahashi Y, Maruyama K, Mizuno S, Shimakawa S, Ono H, Oyanagi R, Kubo S, Barkovich AJ, Inazawa J：Clinical and radiological features of Japanese patients with a severe phenotype due to CASK mutations. Am J Med Genet A. 158A：3112-8. 2012
3. Gaffney CJ, Oka T, Mazack V, Hilman D, Gat U, Muramatsu T, Inazawa J, Golden A, Carey DJ, Farooq A, Tromp G, Sudol M：Identification, basic characterization and evolutionary analysis of differentially spliced mRNA isoforms of human YAP1 gene. Gene. 509：215-22. 2012
4. Dobashi Y, Kimura M, Matsubara H, Endo S, Inazawa J, Ooi A：Molecular alterations in AKT and its protein activation in human lung carcinomas. Hum Pathol. 43：2229-40. 2012
5. ◎Miyawaki Y, Kawachi H, Ooi A, Eishi Y, Kawano T, Inazawa J, Imoto I：Genomic copy-number alterations of MYC and FHIT genes are associated with survival in esophageal squamous-cell carcinoma. Cancer Sci. 103：1558-66. 2012
6. ◎Matsumura S, Imoto I, Kozaki K, Matsui T, Muramatsu T, Furuta M, Tanaka S, Sakamoto M, Arii S, Inazawa J：Integrative array-based approach identifies MZB1 as a frequently methylated putative tumor-suppressor in hepatocellular carcinoma. Clin Cancer Res. 18：3541-3551. 2012
7. ◎Honda S, Hayashi S, Nakane T, Imoto I, Kurosawa K, Mizuno S, Okamoto N, Kato M, Yoshihashi H, Kubota T, Nakagawa E, Goto Y, Inazawa J：The incidence of hypoplasia corpus callosum in patients with dup（X）（q28）involving MECP2 is associated with the location of distal breakpoints. Am J Med Genet A. 158A：1292-303. 2012
8. Akamatsu S, Takata R, Haiman CA, Takahashi A, Inoue T, Kubo M, Furihata M, Kamatani N, Inazawa J, Chen GK, Le Marchand L, Kolonel LN, Katoh T, Yamano Y, Yamakado M, Takahashi H, Yamada H, Egawa S, Fujioka T, Henderson BE, Habuchi T, Ogawa O, Nakamura Y, Nakagawa H：Common variants at 11q12, 10q26 and 3p11.2 are associated with prostate cancer susceptibility in Japanese. Nat Genet. 44：426-9. 2012
9. Yamamoto S, Tsuda H, Honda K, Takano M, Tamai S, Imoto I, Inazawa J, Yamada T, Matsubara O：ACTN4 gene amplification and actinin-4 protein overexpression drive tumour development and histological progression in a high-grade subset of ovarian clear-cell adenocarcinomas. Histopathology. 60：1073-1083. 2012
10. ◎Kozaki K, Inazawa J：Tumor-suppressive microRNAs silenced by tumor-specific DNA hypermethylation in cancer cells. Cancer Sci. 103：837-45. 2012
11. ◎Ono H, Imoto I, Kozaki K, Tsuda H, Matsui T, Kurasawa Y, Muramatsu T, Sugihara K, Inazawa J：SIX1 promotes epithelial-mesenchymal transition in colorectal cancer through ZEB1 activation. Oncogene. 31：4923-34. 2012
12. Maeda M, Mitsui J, Soong B, Takahashi Y, Ishiura H, Hayashi S, Shirota Y, Ichikawa Y, Matsumoto H, Arai M, Okamoto T, Miyama S, Shimizu J, Inazawa J, Goto J, Tsuji S：Increased gene dosage of myelin protein zero causes Charcot-Marie-Tooth disease. Ann Neurol. 71：84-92. 2012
13. ◎Okamoto N, Hayashi S, Masui A, Kosaki R, Oguri I, Hasegawa T, Imoto I, Makita Y, Hata A, Moriyama K, Inazawa J：Deletion at chromosome 10p11.23-p12.1 defines characteristic phenotypes with marked midface retrusion. J Hum Genet. 57：191-6. 2012
14. ◎Bai H, Inoue J, Kawano T, Inazawa J：A transcriptional variant of the LC3A gene is involved in autophagy and frequently inactivated in human cancers. Oncogene. 31：4397-408. 2012
15. Ooi A, Inokuchi M, Harada S, Inazawa J, Tajiri R, Sawada-Kitamura S, Ikeda H, Kawashima H, Dobashi Y：Gene amplification of ESR1 in breast cancers - Fact or fiction? A fluorescence in situ hybridization and multiplex ligation-dependent probe amplification study. J Pathol. 227：8-16. 2012
16. ◎Honda S, Satomura S, Hayashi S, Imoto I, Nakagawa E, Goto Y, Inazawa J：Concomitant microduplications of MECP2 and ATRX in male patients with severe mental retardation. J Hum Genet. 57：73-7.2012
17. ◎Kurasawa Y, Kozaki K, Pimkhaokham A, Muramatsu T, Ono H, Ishihara T, Uzawa N, Imoto I, Amagasa T, Inazawa J：Stabilization of phenotypic plasticity through mesenchymal-specific DNA hypermethylation in cancer cells. Oncogene. 31：1963-74. 2012

7）総説ならびに著書

1. （分担）小崎健一、古田繭子、井本逸勢、稲澤譲治：肝細胞癌の早期診断：画像と分子マーカー.株式会社アークメディア（東京）.pp241-249（9P）,2012/3/16（265P）

8）特許取得、特許申請

［特許取得］

1. 発明の名称：癌の検出方法および抑制方法. 稲澤譲治、井本逸勢、于衛、富士フイルム株式会社. 特許第4867018号、出願年月日：2006/3/22、登録年月日：

2011/11/25
2. 発明の名称：癌抑制剤. 稲澤譲治、井本逸勢、和泉 宏幸、横井左奈、富士フイルム株式会社. 特許第5002749号、出願年月日：2006/3/22、登録年月日：2012/6/1
3. 発明の名称：食道癌の検出方法. 稲澤譲治、井本逸勢、田中浩司、津田均、株式会社ビー・エム・エル. 特許第5044837号、出願年月日：2006/11/8、登録年月日：2012/7/27
4. 発明の名称：癌の検出方法および癌抑制剤. 稲澤譲治、小崎健一、井本逸勢、富士フイルム株式会社. 特許第5116026号、出願年月日：2008/1/23、登録年月日：2012/10/26

［海外特許］

1. ［米国］「核酸マイクロアレイの異常スポットを検出する方法」、金原秀行・吉田淳哉・氏原大・稲澤譲治・井本逸勢、国立大学法人東京医科歯科大学・富士写真フィルム株式会社、2010.5.26、12/787,953 特願2009-128162
2. ［EP］「核酸マイクロアレイの異常スポットを検出する方法」、金原秀行・吉田淳哉・氏原大・稲澤譲治・井本逸勢、国立大学法人東京医科歯科大学・富士写真フィルム株式会社、2010.5.27、10164051.4 特願2009-128162
3. ［CN］「核酸マイクロアレイの異常スポットを検出する方法」、金原秀行・吉田淳哉・氏原大・稲澤譲治・井本逸勢、国立大学法人東京医科歯科大学・富士写真フィルム株式会社、2010.5.27、201010193364.8 特願2009-128162
4. ［EP］発明の名称：癌抑制剤.稲澤譲治、井本逸勢、和泉宏幸、横井左奈、富士フイルム株式会社.登録番号：1837399（独：60 2007 015 313.1）、出願年月日：2007/3/22、登録年月日：2011/6/22
5. ［EP］発明の名称：癌の検出方法および癌抑制剤.稲澤譲治、小崎健一、井本逸勢、富士フイルム株式会社. 登録番号：2088208（独：60 2009 001 116.2）、出願年月日：2009/1/23、登録年月日：2011/4/27
6. ［US］発明の名称：口腔扁平上皮癌の検出方法.稲澤譲治、井本逸勢、中村恵理奈、津田均、富士フイルム株式会社.登録番号：8143003、出願年月日：2009/4/27、登録年月日：2012/3/27
7. ［EP］発明の名称：卵巣癌の検出方法、及び抑制方法.稲澤譲治、井本逸勢、菊池良子、富士フイルム株式会社.登録番号：1997910 （独：60 2008 017 939.7）、出願年月日：2008/5/30、登録年月日：2012/8/15
8. ［US］発明の名称：癌の検出方法および癌抑制剤.稲澤譲治、小崎健一、井本逸勢、富士フイルム株式会社..登録番号：8183223、出願年月日：2010/12/9、登録年月日：2012/5/22
9. ［US］発明の名称：神経芽腫の検出方法.稲澤譲治、井本逸勢、井上純、富士フイルム株式会社..登録番号：8216785、出願年月日：2009/9/28、登録年月日：2012/7/10
10. ［US］発明の名称：卵巣癌の検出方法、及び抑制方法.稲澤譲治、井本逸勢、菊池良子、富士フイルム株式会社..登録番号：8318431、出願年月日：2008/5/28、登録年月日：2012/11/27

9）平成24年度までの自己評価

我が国において、はじめて集学的な通常の染色体検査で衣装を検出することのない先天異常症を対象に646例において集学的なゲノム異常スクリーニングを実施した。その結果、約24%の症例に病因性のある微細染色体コピー数異常（copy number variation, CNV）を検出した。これらの中で、顎顔面形成不全症ならびに軽度精神発達遅滞を共通の表現形とする10p11.23-p12.1 欠失の独立した2症例や、さらに、小頭症、小脳脳幹部低形成を症状とする疾患群にCASK遺伝子の重複を見出すなど、幾つかの新しい疾患単位となる病態を同定した点において特筆すべき成果が上がった。また、体系的な癌抑制型マイクロRNAのスクリーニング法を確立し、複数の新規癌抑制型マイクロRNAとその標的分子を明らかにした。これら癌抑制型マイクロRNAミミック核酸を動物個体への導入することで腫瘍抑制効果が確認されたことから癌治療の応用に期待ができる。

10）学会発表（英文）

国際シンポジウム

1. Inazawa J：Exploring of tumor suppressor micro RNAs silenced by DNA methylation. Tokyo Medical and Dental University The 6th Global COE International Symposium. Tokyo, Japan. 23-25/January/2012
2. Inazawa J：Identification of tumor-suppressor micro-RNAs silenced by DNA hypermethylation in cancer. 2012 Seoul National University Cancer Research Institute Symposium. Seoul National University Kwanak Campus, Culture Center, Seoul, South Korea. 16-19/May/2012

3. Inazawa J：Exploring of tumor suppressive micro-RNAs silenced by tumor-specific DNA hypermethylation in cancer. The 22nd HCS/the 4th JARI Joint International Symposium. Hiroshima, Japan. 30/August/2012

国際学会

1. Hayashi S, Naganawa M, D.T.Uehara, Inazawa J：Investigation of the parental origin and genomic mechanisms involved in de novo pathogenic CNVs in congenital disorders. The American Society of Human Genetics 62th annual meeting. San Francisco, U.S.A. 6-10/November/2012

11）学会発表（和文）

1. 稲澤譲治：新世代ゲノム解析技術によって浮上するがんのバックシートドライバー.第16回日本がん分子標的治療学会.西日本総合展示場.福岡.2012年6月29日
2. 原園陽介、小崎健一、村松智輝、河野辰幸、原田清、稲澤譲治：E-cadherinの発現変化を指標とした機能的スクリーニングによるMET誘導生microRNAの探索. 第71回日本癌学会学術総会. さっぽろ芸文館. 北海道. 2012年9月19日
3. 古田繭子、小崎健一、田中真二、有井滋樹、井本逸勢、稲澤譲治：Argonute2免疫沈降と統合的情報解析による肝細胞癌抑制性miRNAクラスターの標的遺伝子群の同定. 第71回日本癌学会学術総会. さっぽろ芸文館. 北海道. 2012年9月20日
4. 山本信祐、井上純、小村健、小崎健一、稲澤譲治：NRF2 pathwayを負に制御するmicroRNAの同定. 第71回日本癌学会学術総会. さっぽろ芸文館. 北海道. 2012年9月20日
5. 宮脇豊、河内洋、江石義信、大井章史、河野辰幸、稲澤譲治、井本逸勢：食道扁平上皮癌の術後予後因子として遺伝子MYCおよびFHITにおけるゲノムコピー数異常の意義. 第71回日本癌学会学術総会. 札幌市教育文化会館. 北海道. 2012年9月20日
6. 永田啓明、小崎健一、谷本幸介、古田繭子、井元清哉、宮野悟、市川大輔、大辻英吾、稲澤譲治：食道扁平上皮癌におけるDNAメチル化関連遺伝子の統合的スクリーニング. 第71回日本癌学会学術総会. 札幌教育文化会館. 北海道. 2012年9月20日
7. 村松智輝、小崎健一、井元清哉、山口類、宮野悟、稲澤譲治：ヒト口腔癌細胞株を用いた癌転移分子メカニズムの解析. 第71回日本癌学会学術総会. ロイトン札幌. 北海道. 2012年9月21日
8. 林深、長縄光代、Daniela Tiaki Uehara、稲澤譲治：高解像度アレイを用いたpathogenic CNV を付加的に修飾する微細CNVの探索. 日本人類遺伝学会第57回大会.京王プラザホテル.東京.2012年10月27日
9. 西山直隆、新井恵吏、長塩亮、藤元博行、細田文恵、柴田龍弘、横井左奈、井本逸勢、稲澤譲治、金井弥栄：尿路上皮がんにおけるゲノム構造異常：臨床病理学的意義ならびにDNAメチル化異常との関係. 第71回日本癌学会学術総会.ロイトン札幌. 北海道. 2012年9月20日
10. 細田文恵、十時泰、新井康仁、津田均、井本逸勢、稲澤譲治、大木操、柴田龍弘：乳がん原発巣とリンパ節転移巣における遺伝的変異の解析. 第71回日本癌学会学術総会.ロイトン札幌. 北海道. 2012年9月21日
11. Daniela Tiaki Uehara、林深、長縄光代、井本逸勢、蒔田芳男、羽田明、稲澤譲治：原因不明の先天異常疾患に対するSNPアレイを用いたゲノム異常探索. 日本人類遺伝学会第57回大会.京王プラザホテル.東京.2012年10月25日
12. 林深、本田尚三、里村茂子、井本逸勢、中川栄二、後藤雄一、稲澤譲治：重度精神遅滞を呈する男児例に同時に見られたMECP2,ATRXの重複. 日本人類遺伝学会第57回大会.京王プラザホテル.東京.2012年10月26日
13. 長縄光代、林深、Daniela Tiaki Uehara、稲澤譲治：先天異常疾患におけるpathogenic CNVの生成機構と由来する両親アリルの探索. 日本人類遺伝学会第57回大会.京王プラザホテル.東京.2012年10月25日

12）受賞

1. 春木茂男が「Frequent silencing of protocadherin 17, a candidate tumour suppressor for esophageal squamous-cell carcinoma.（Carcinogenesis. 31：1027-36. 2010発表）」の研究成果で平成22年度東京医科歯科大学　田中道子賞を受賞した。
2. 古田繭子が東京医科歯科大学グローバルCOE（GCOE）プログラム研究発表で「Excellent Presentation-Special Award-」を受賞した。
3. 鶴田智彦（現・永寿総合病院産婦人科勤務）が平成23年度日本産科婦人科学会「優秀論文賞婦人科腫瘍学部門」を受賞した。

13）外部資金の獲得状況

1. 文科省「次世代がん研究戦略推進プロジェクト」次世代がん研究シーズ戦略的育成プログラム（研究代表者・稲澤譲治）「食道扁平上皮癌の新規治療標的分子と診断バイオマーカーの同定」22,500千円（平成24年度）
2. 文科省科研費補助金（研究代表者・稲澤譲治）　新学術領域研究「がんの統合的ゲノム・エピゲノム解析と治療標的分子シーズの探索」41,100千円（平成24年度）
3. 文科省科学技術試験研究委託事業（研究代表者・稲澤譲治）「ゲノム網羅的解析情報を基盤とするオーダーメイドがん医療（大腸がんの個別化医療を目指した新規胃がん関連遺伝子の探索と同定）」3,300千円（平成24年度）
4. 独）日本学術振興会科学研究費補助金（研究代表者・稲澤）基盤研究A「がんのゲノム・エピゲノム解析に基づく個性診断法の開発」10,100千円（平成24年度）
5. 厚労科研・第3次対がん総合戦略（横田班）「網羅的なゲノム異常解析と詳細な臨床情報に基づく、ヒトがんの多様な多段階発がん過程の分子基盤の解明とその臨床応用に関する研究」分担者・稲澤譲治、3,000千円（平成24年度）
6. 厚労科研・障害者対策総合研究事業（研究代表者・林深）「原因不明の精神遅滞の病態解明を目指した統合的ゲノム解析」分担者・稲澤譲治、1,000千円（平成24年度）
7. 厚労科研・第3次対がん総合戦略（研究代表者・井上純）「オートファジー活性を指標とした癌個別化医療の分子基盤に関する研究」分担者・稲澤譲治、1,000千円（平成24年度）
8. 独）日本学術振興会科学研究費補助金（研究代表者・小崎健一）基盤研究B「癌抑制遺伝子型microRNAの統合的スクリーニングと核酸医薬への応用」分担者・稲澤譲治、500千円（平成24年度）
9. 独）日本学術振興会科学研究費補助金（研究代表者・河野辰幸）基盤研究B「食道扁平上皮癌の新たな治療体型の構築を目指した統合的ゲノム・エピゲノム解析」分担者・稲澤譲治、600千円（平成24年度）
10. 文科省科研費補助金（研究代表者・宮野悟）新学術領域研究「領域の研究方針の策定」分担者・稲澤譲治、100千円（平成24年度）

14）特別講演、招待講演、シンポジウム

1. Inazawa J：Exploring of tumor suppressor micro RNAs silenced by DNA methylation. Tokyo Medical and Dental University The 6th Global COE International Symposium. Tokyo, Japan. 23-25/ January/2012
2. Inazawa J：Identification of tumor-suppressor micro-RNAs silenced by DNA hypermethylation in cancer. 2012 Seoul National University Cancer Research Institute Symposium. Seoul National University Kwanak Campus, Culture Center, Seoul, South Korea. 16-19/ May/2012
3. Inazawa J：Exploring of tumor suppressive micro-RNAs silenced by tumor-specific DNA hypermethylation in cancer. The 22nd HCS/the 4th JARI Joint International Symposium. Hiroshima, Japan. 30/August/2012
4. 稲澤譲治：がんにおけるリソソーム分解系の障害.第21回日本Cell Death学会学術集会.名古屋大学医学部付属病院中央診療棟3階講堂.愛知.2012年7月28日
5. 井上純、稲澤譲治：ヒト癌におけるオートファジー関連遺伝子の異常.第71回日本癌学会学術総会. さっぽろ芸文館. 北海道. 2012年9月19日
6. 小崎健一、遠藤寛則、稲澤譲治：がんDNAメチル異常を指標とした癌抑制遺伝子型microRNAの探索.第71回日本癌学会学術総会. 札幌市教育文化会館. 北海道. 2012年9月20日
7. 原園陽介、小崎健一、村松智輝、遠藤寛則、河野辰幸、原田清、稲澤譲治：Exploration of EMT-suppressive microRNA using function-based screening with expression analysis of CDH1 in cancer cells. 平成24年度文部科学省科学研究費補助金・新学術領域研究「がん研究分野の特性等を踏まえた支援活動」.がん若手研究者ワークショップ.蓼科グランドホテル滝の湯.長野.2012年9月5日
8. 横井左奈、稲澤譲治：がんのゲノム医学入門.日本人類遺伝学会第57回大会.京王プラザホテル.東京.2012年10月25日
9. 稲澤譲治：疾患バイオリソースバンクが今後の医薬品・医療機器の開発に与えるインパクト.平成24年度医療イノベーション推進人材養成プログラム.東京医科歯科大学.学際生命科学東京コンソーシアム主催.平成24年12月4日
10. 稲澤譲治：新世代ゲノム解析技術によって浮上する

がんのバックシートドライバー. 第5回岐阜大学先端創薬医療シンポジウム・岐阜大学RNA創薬研究会合同シンポジウム～RNA創薬への掛け橋～. TKP品川カンファレンスセンター. 東京. 2012年12月7日

15）主催学会

1. 第22回 癌ゲノムサイエンス研究会. 東京医歯大学. 2012年2月23日
2. 第23回 癌ゲノムサイエンス研究会. 東京医歯大学. 2012年6月21日

16）教室、分野や講座の准教授、講師、助教、特別研究員、ポスドク、指導を受けた大学院生の名前

教授　稲澤　譲治
准教授　小崎　健一
助教　井上　純
硬組織疾患ゲノムセンター特任講師：林　深
ゲノム解析室助教 谷本　幸介
大学院博士課程
○ 村松　智輝
○ 古田　繭子、鶴田　智彦
坂本　宙子、松村　聡
倉沢　泰浩、上杉　篤史
小野　宏晃、岡本　奈那
遠藤　寛則、宮脇　豊
原園　陽介、山本　信祐
永田　啓明、岩舘　怜子
○ Nuylan Michelle Loyola
○Daniela Tiaki Uehara
李　慧、藤原　直人
谷中　淑光、Sujata Sakha
○ 森下　真紀
大学院修士課程　長縄　光代、與子田　一輝
大学院特別研究学生
小西　博貴、髙橋　寛吉
與子田　一輝

Human Cancer Biology

Clinical Cancer Research

Integrative Array-Based Approach Identifies MZB1 as a Frequently Methylated Putative Tumor Suppressor in Hepatocellular Carcinoma

Satoshi Matsumura[1,5], Issei Imoto[1,7], Ken-ichi Kozaki[1], Takeshi Matsui[2], Tomoki Muramatsu[1,3], Mayuko Furuta[1,3], Shinji Tanaka[5], Michiie Sakamoto[6], Shigeki Arii[5], and Johji Inazawa[1,3,4]

Abstract

Purpose: The aim of this study was the identification of novel tumor suppressor genes (TSG) silenced by DNA hypermethylation in hepatocellular carcinoma (HCC).

Experimental Design: We conducted integrative array-based approach for genome-wide screening of methylation targets using a methylated DNA immunoprecipitation-CpG island microarray and expression array in three universal hepatoma cell lines and normal liver tissue. Through detailed expression and functional analyses using hepatoma cell lines and primary HCC samples, we isolated novel TSGs for HCC.

Results: A total of 642 genes were identified as methylated in three hepatoma cell lines but unmethylated in normal liver tissue, whereas 204 genes on autosomes were identified as genes unexpressed but restored after treatment with 5-aza-2′-deoxycytidine in these cell lines and expressed in normal tissue. Through the integration of results of the two-array analyses and further validation analyses of expression and methylation status in 17 cell lines and 30 primary tumors of hepatoma, we identified *MZB1*, *marginal zone B and B1 cell-specific protein*, encoding an endoplasmic reticulum protein, as a putative TSG frequently methylated within its CpG island in hepatoma. Among 162 patients with primary HCC, silencing of MZB1 protein was significantly and independently associated with a worse outcome. Restoration of MZB1 expression in hepatoma cells reduced cell proliferation *in vitro* and *in vivo* through G_1-arrest.

Conclusions: These results suggest that methylation-mediated silencing of MZB1 expression leads to loss of its tumor-suppressive activity, which may be a factor in the hepatocarcinogenesis, and is a useful prognosticator in HCC. *Clin Cancer Res; 18(13); 3541–51. ©2012 AACR.*

Introduction

Hepatocellular carcinoma (HCC), one of the most common malignancies worldwide, is associated with hepatitis virus infections, dietary aflatoxin, chronic alcohol/tobacco consumption, and cirrhosis. Genomic alterations, such as the gain or loss of chromosomal regions and specific gene mutations, have been frequently noted in hepatocarcinogenesis (1). Furthermore, epigenetic abnormalities, such as DNA methylation and chromosome remodeling, may also promote tumorigenesis (2, 3). DNA hypermethylation of promoter CpG islands leads to the inactivation of tumor suppressor genes (TSG) and critical cancer-related genes in human cancers including HCC (4, 5). DNA methylation changes have been reported to be specific to the cancerous tissue making it possible to distinguish HCC and surrounding nontumorous tissues (6). Indeed, abnormal DNA methylation of several TSGs, such as *RASSF1A*, *CDKN2A*, *CRABP1*, *GSTP1*, *CHRNA3*, *DOK1*, *SFRP1*, *GAAD45a*, and *CDKN2B*, is reported to be associated with HCC, and hypermethylation of specific genes, such as *CHFR* and *SYK* is detected in advanced stages of HCC (6). However, the number of reported methylation-target genes is far fewer for HCC than for colon cancer or gastric cancer (7). Therefore, further identification of remaining targets for methylation may clarify the specific molecular events involved in HCC progression, enabling the prevention, diagnosis, and treatment of HCC to be approached as potential clinical applications of DNA methylation signature at a molecular level.

To discover novel methylation-target sequences with high specificity and sensitivity in a genome-wide manner, large-scale screening methods, which have the potential to

Authors' Affiliations: [1]Department of Molecular Cytogenetics, [2]Medical Top Track Program, Medical Research Institute and School of Biomedical Science, [3]Global Center of Excellence Program for International Research Center for Molecular Science in Tooth and Bone Diseases, [4]Department of Genome Medicine, Hard Tissue Genome Research Center, and [5]Department of Hepato-Biliary-Pancreatic Surgery, Graduate School of Medicine, Tokyo Medical and Dental University; [6]Department of Pathology, School of Medicine, Keio University, Tokyo; and [7]Department of Human Genetics, Institute of Health Biosciences, The University of Tokushima Graduate School, Kuramoto-cho, Tokushima, Japan

Note: Supplementary data for this article are available at Clinical Cancer Research Online (http://clincancerres.aacrjournals.org/).

Corresponding Author: Johji Inazawa, Department of Molecular Cytogenetics, Medical Research Institute, Tokyo Medical and Dental University, 1-5-45 Yushima, Bunkyo-ku, Tokyo 113-8510, Japan. Phone: 81-3-5803-5820; Fax: 81-3-5803-0244; E-mail: johinaz.cgen@mri.tmd.ac.jp

doi: 10.1158/1078-0432.CCR-11-1007

Translational Relevance

Although hepatocellular carcinoma (HCC) is one of the most common malignancies worldwide, the molecular mechanisms underlying hepatocarcinogenesis remain unclear. Epigenetic abnormalities, such as DNA methylation, may promote tumorigenesis as well as genomic alterations in hepatocarcinogenesis. To discover novel methylation-target sequences with high specificity and sensitivity in a genome-wide manner, we conducted expression array analyses as well as methylated-DNA immunoprecipitation in combination with an oligonucleotide array, which allows for rapid and efficient genome-wide assessment of DNA methylation, resulting in the identification of *marginal zone B and B1 cell-specific protein (MZB1)* as a tumor suppressor gene silenced by DNA hypermethylation in hepatoma. Among 162 patients with primary HCC, silencing of MZB1 protein was significantly and independently associated with a worse outcome. Moreover, restoration of MZB1 expression in hepatoma cells reduced cell proliferation *in vitro* and *in vivo* through G_1 arrest. Our findings provide a novel insight into the prevention, diagnosis, and treatment of HCC.

find novel methylation targets in a whole range of cancers, have been developed. A combination of 3 types of pretreatments, such as enzyme digestion, affinity enrichment, or sodium bisulfite, was followed by different analytical steps, such as gel-, array-, or next-generation sequencing-based analysis (8). Among them, methylated-DNA immunoprecipitation (MeDIP; ref. 9) in combination with an oligonucleotide array or next-generation sequencing allows for rapid and efficient genome-wide assessment of DNA methylation, although these methodologies generally result in a list of several hundred candidate genes. Although an analysis of possible promoters or dense CpG islands is used to narrow down the number of candidate genes, the list is still too long. Pharmacologic unmasking expression microarray approaches are also used widely to identify methylation targets (10), although they are also prone to give false-positive genes that are indirect methylation targets themselves and not considered to be a reliable gauge of DNA methylation at a given locus.

To identify genes that are downregulated because of DNA hypermethylation and to concentrate those genes most frequently involved in HCC, we applied the following integrative array-based approach to 3 hepatoma cell lines: (i) MeDIP in combination with CpG island-array (MeDIP-chip) analysis to identify genes methylated in a cancer-specific manner, (ii) expression microarray analysis to identify genes downregulated in a cancer-specific manner and reactivated upon treatment with 5-aza-2′deoxycytidine (5-aza-dCyd), and (iii) a combination of data from both approaches. Through further examination of a subset of obtained candidates, we identified marginal zone B and B1 cell-specific protein (MZB1), also known as proapoptotic caspase adaptor protein (PACAP), pERp1, or MGC29506 (11), whose inactivation is related with a worse prognosis in primary tumors as a possible TSG for HCC.

Materials and Methods

Cell lines and primary tumor samples

A total of 17 hepatoma cell lines including 15 HCC lines (cHc4, Hep3B, Hep-Kano, Hep-TABATA, HLE, HLF, huH-1, HuH-7, JHH-1, JHH-4, JHH-5, JHH-7, Li-7, PLC/PRF/5, and SK-HEP-1) and 2 hepatoblastoma lines (HepG2 and HUH-6) were used (12). All 162 primary HCC samples were obtained during surgery from patients with HCCs treated at Tokyo Medical and Dental University (Tokyo, Japan) between 2000 and 2005. Relevant clinical and survival data were available for all patients (Table 1). The median follow-up period for the surviving patients was 19 months (ranging from 1 to 103 months). Samples from 17 of these patients with HCC were immediately frozen in liquid nitrogen and stored at −80°C until required for DNA and RNA analyses. Normal liver tissues were obtained from surgical samples in 2 patients (cases C20 and C40) with colon cancer metastasis. Written consent was obtained after approval by the local ethics committee.

MeDIP-chip analysis

The DNA methylation profiles were analyzed by MeDIP using anti-5-methylcytidine antibody (Eurogentec) followed by the Human 244K CpG island microarray (Agilent), which contains 237,220 probes, covering 27,800 CpG islands (97.5% of UCSC annotated CpG islands), according to the manufacturer's instructions. Image analysis with data extraction was done using Feature Extraction Software, version 9.0 (Agilent Technologies). The analytic procedure used for the results of the MeDIP-chip assay was described in the Supplementary Experimental Procedure.[1]

Gene expression array

Gene expression was profiled using a 4 × 44K Human Whole Genome Ver. 2.0 gene expression array (Agilent Technologies) according to the manufacturer's instructions. Total RNAs extracted from hepatoma cell lines and from these cells treated with 10 μmol/L 5-aza-dCyd for 5 days were used for conventional and pharmacologic unmasking analyses, respectively. Two normal livers (C20 and C40) were used as controls. All samples were analyzed twice. Image analysis with data extraction and the data analysis were conducted using Feature Extraction Software, version 9.0 and GeneSpring GX10 software (Agilent Technologies), respectively.[1]

Real-time reverse transcription PCR

To analyze the restored expression of genes, the cell lines were cultured with 1 to 10 μmol/L 5-aza-dCyd for 5 days. Levels of mRNA expression were measured with ABI PRISM

[1]The entire microarray data set is available at http://www.ncbi.nlm.nih.gov/geo/info/linking.html under the data series accession no. GSE35313.

Table 1. Association between clinicopathologic characteristics and MZB1 expression

		MZB1 immunoreactivity		
	n	**Negative (%)**	**Positive (%)**	***P*** [a]
Total	162	84 (51.9)	78 (48.1)	
Gender				
Male	122	66 (54.1)	56 (45.9)	0.4139
Female	40	18 (45.0)	22 (55.0)	
Age, y				
Mean		65.7	65.7	
>65	98	49 (50.0)	49 (50.0)	0.5594
<65	64	35 (54.7)	29 (45.3)	
Virus				
HCV(+)	79	39 (49.4)	40 (50.6)	0.2742
HBV(+)	38	25 (65.8)	13 (34.2)	
HCV(−), HBV(−)	45	20 (44.4)	25 (55.6)	
AFP, ng/mL[b]		5,390 ± 22,968	2,819 ± 13,373	0.3982
PIVKA-II, mAU/mL[b]		7,252 ± 43,097	6,767 ± 25,669	0.9325
Aspartate aminotransferase, IU/L[b]		48.6 ± 25.3	54.7 ± 34.2	0.1982
Alanine aminotransferase, IU/L[b]		42.8 ± 32.6	53.7 ± 34.8	**0.0418**
Platelet (%)[b]		84.1 ± 13.1	85.9 ± 13.6	0.3862
Total bilirubin, mg/dL[b]		0.86 ± 0.44	0.86 ± 0.40	0.9795
Albumin, g/dL[b]		3.9 ± 0.5	3.9 ± 0.4	0.6972
Child–Pugh score[b]		5.4 ± 0.6	5.3 ± 0.7	0.8199
Tumor size, cm[b]		4.6 ± 2.8	4.5 ± 3.1	0.8411
Tumor number				
Single	105	50 (47.6)	55 (52.4)	0.1940
Multiple	57	34 (59.6)	23 (40.4)	
Histopathologic grading				
Well-differentiated	43	24 (55.8)	19 (44.2)	0.4560
Moderately differentiated	90	43 (47.8)	47 (52.2)	
Poorly differentiated	29	17 (58.6)	12 (41.4)	
Portal vein invasion				
Absent	92	40 (43.5)	52 (56.5)	**0.0222**
Present	70	44 (62.9)	26 (37.1)	
Surgical margin				
Absent	139	73 (52.5)	66 (47.5)	0.8478
Present	23	11 (47.8)	12 (52.2)	
Background liver parenchyma				
Normal liver	10	2 (20.0)	8 (80.0)	0.0696
Chronic hepatitis	78	39 (50.0)	39 (50.0)	
Liver cirrhosis	74	43 (58.1)	31 (41.9)	
Tumor stage				
I	13	3 (23.1)	10 (76.9)	**0.0207**
II	57	25 (43.9)	32 (56.1)	
III	58	33 (56.9)	25 (43.1)	
IVA	34	23 (67.6)	11 (32.4)	

NOTE: Statistically significant values are in boldface type.
Abbreviations: HBV, hepatitis B virus; HCV, hepatitis C virus.
[a]*P* values are from χ^2, Fisher exact, or Student *t* test and were statistically significant at <0.05.
[b]Mean ± SD.

7500 sequence detection System (Applied Biosystems) using TaqMan Gene Expression Assays (Hs01048042_m1 for *ANGPT2*, Hs00174937_m1 for *CCK*, Hs00405322_m1 for *DERL3*, Hs00417143_m1 for *RADIL*, Hs00191390_m1 for *KCNK6*, Hs00219458_m1 for *L1TD1*, Hs00414907_m1 for *MZB1*, Hs00386153_m1 for *FAR1*, Hs00382235_m1 for *OCIAD2*, Hs00257935_m1 for *PBX4*, and Hs00610060_m1 for *SFRP1*; Applied Biosystems)

according to the manufacturer's instructions. Gene expression values are given as ratios between the genes of interest and an internal reference gene (Hs99999903_m1 for *ACTB*; Applied Biosystems) that provides an internal normalization factor, and subsequently normalized with the value in the controls (relative expression level). The assay was conducted twice for each sample.

Methylation analysis

Sodium bisulfite-treated genomic DNA was subjected to PCR using primer sets to amplify regions of interest (Supplementary Table S1). For the combined bisulfite restriction analysis (COBRA), PCR products were digested with *Bst*U1, *Taq*1, or *Hha*1 and electrophoresed (13). The intensity of methylated alleles as a percentage on the ethidium bromide-stained gels was calculated, and a methylation density cutoff point of 20% was considered significant as described elsewhere (14). For bisulfite genomic sequencing (BGS), PCR products were subcloned and sequenced.

Immunohistochemistry

Indirect immunohistochemistry was conducted with formalin-fixed, paraffin-embedded tissue sections using an automated immunostainer (Benchmark XT; Ventana Medical Systems) with heat-induced epitope retrieval, anti-MZB1 (1:50; 11454-1-AP; Protein Tech), anti-PCNA (1:1,000; #2586; Cell Signaling Technology), or anti-Ki-67 antibodies (1:100; M7240; Dako). The slides were counterstained with Mayer's hematoxylin, and analyzed under a light microscope by 2 pathologists blinded to clinical characteristics and outcomes. Twenty representative fields per slide were examined, and the percentage of the total cell population that expressed MZB1 was evaluated for each case at $\times$200 magnification. Expression of MZB1 protein was graded as either positive ($\geq$10% of tumor cells showing immunopositivity) or negative ($\pm$10% of tumor cells showing immunopositivity or no staining). Plasma cells and bile duct epithelial cells were used as positive and negative controls, respectively.

Western blotting

Western blotting was conducted as described elsewhere (12). Anti-FLAG-tag and anti-β-actin antibodies were purchased from Sigma-Aldrich, and the anti-cleaved caspase-3 antibody (#9661) was purchased from Cell Signaling Technology.

Fluorescent immunocytochemistry

The plasmid expressing C-terminally FLAG-tagged MZB1 (pCMV-3Tag3A-MZB1) was obtained by cloning the full coding sequence of MZB1 in-frame along with the 3xFLAG-epitope into the pCMV-3Tag3A vector (Stratagene). Cells were fixed in 10% trichloroacetic acid, permeabilized with 0.2% Triton X-100, and treated with blocking solution (1% bovine serum albumin in PBS). After incubation with the primary antibodies (anti-MZB1, 1:100 and/or anti-Calnexin, 1:100) for 1 hour, the bound antibody was visualized using a Cy3-conjugated or fluorescein isothiocyanate (FITC)-conjugated secondary antibody (1:1,000). After being mounted with DAPI (4′,6′-diamidino-2-phenylindole) to stain nuclei, the cells were observed under a fluorescence microscope (BZ-8100; Keyence).

***In vitro* and *in vivo* growth assay**

Colony formation assays using cells transiently introduced with pCMV-3Tag3A-MZB1 or the empty vector (pCMV-3Tag3A-mock) was conducted as described elsewhere (15). The expression of MZB1 protein was confirmed 48 hours after transfection by Western blotting and fluorescent immunocytochemistry.

Stable MZB1 transfectants and control counterparts were obtained by introducing pCMV-3Tag3A-MZB1 or pCMV-3Tag3A-mock into cells with G418 selection, and 2.5×10^4 cells were seeded in 24-well plates. The numbers of viable cells were assessed 24 to 72 hours after seeding by the water-soluble tetrazolium salt assay. The cell cycle was evaluated 48 hours after seeding by a fluorescence-activated cell sorting (FACS) as described elsewhere (15).

The *in vivo* tumor-suppressive ability of MZB1 was investigated by conducting tumor xenograft experiments. Six-week-old female severe combined immunodeficient (SCID) mice were injected subcutaneously in the lower back with MZB1-expressing or control mock-transfected cells (4×10^7). All procedures involving animals were approved by and conformed to the guidelines of our Institutional Animal Care and Use Committee. Tumor formation in SCID mice was monitored daily and the recipient mice were sacrificed for tumor weight evaluation and protein expression analyses 5 weeks postinjection.

Statistical analysis

The χ^2 or Fisher's exact test was used to test for differences between groups. Kaplan–Meier method and log-rank test were used for the survival analyses. Univariate and multivariate survival analyses were conducted using the likelihood ratio test of the stratified Cox proportional-hazards model. Differences between subgroups were tested with the Student *t* test. For multiple group comparisons, ANOVA followed by Scheffé *post-hoc* test was used. Differences were assessed with a 2-sided test, and considered significant at the $P < 0.05$ level.

Results

Screening in the MeDIP-chip analysis

For the screening of aberrantly methylated genes by MeDIP-chip analysis, we used a CpG island microarray, in which 11,229 genes harbor CpG islands upstream or within, with the algorithm shown in the Supplementary Experimental Procedure and Supplementary Fig. S1. Among 11,229 genes, CpG islands of 2,476 genes were unmethylated in normal liver tissue (case C20) but methylated in at least 1 of 3 hepatoma cell lines (Hep3B,

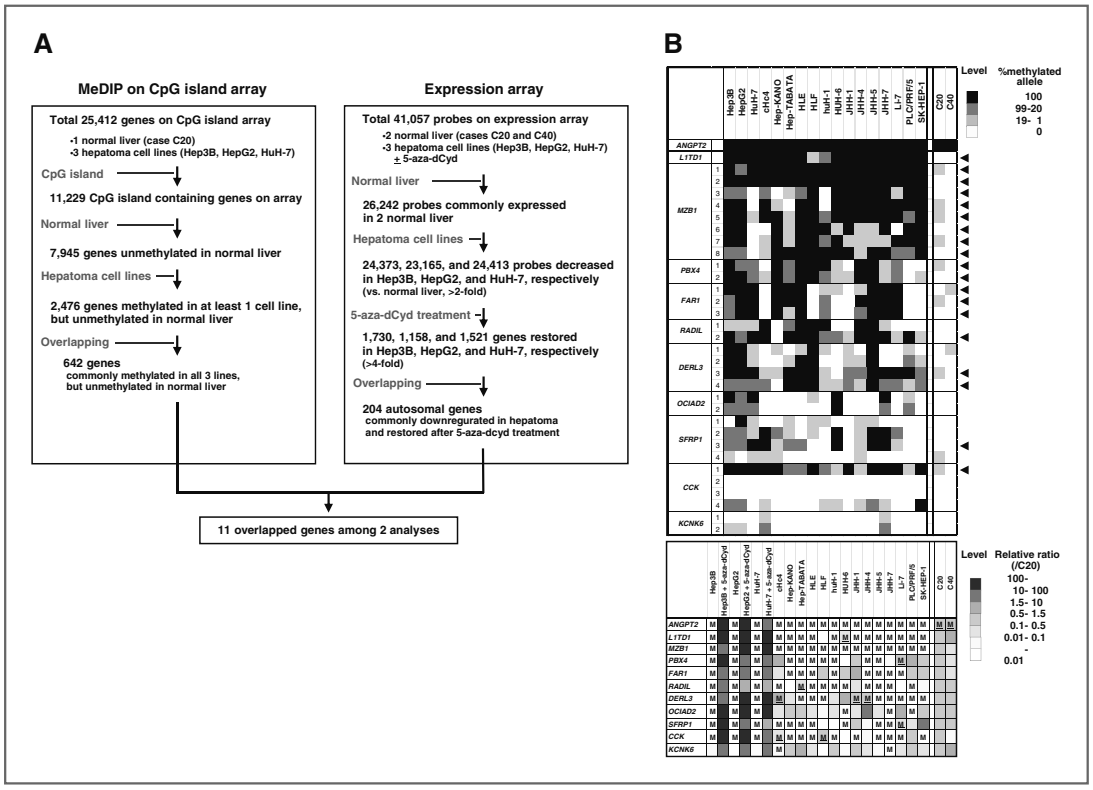

Figure 1. Identification of 11 genes as possible methylation targets. A, left top, overview of the screening approach using MeDIP-chip analyses in 3 hepatoma cell lines (Hep3B, HepG2, and HuH-7) and control normal liver tissue (case C20); right top, overview of the screening approach using duplicate expression array analyses in the same 3 hepatoma cell lines without and with 5-aza-dCyd treatment and 2 normal liver tissues (cases C20 and C40); bottom, by combining results obtained from 2 different genome-wide array-based screening methods, 11 genes overlapped between 2 approaches as possible genes, which are consistently silenced by tumor-specific CpG island methylation. B, top, summary of DNA methylation status of CpG islands around 11 selected candidates in 17 hepatoma cell lines and normal liver tissue determined by COBRA. Each box indicates restricted status by enzymes (% methylated allele). A methylation density cutoff point of 20% was considered significant (13). Arrowheads indicate regions in which more than 50% (>9 of 17) of cell lines showed tumor-specific hypermethylation compared with normal liver tissue; bottom, profiles of expression of 11 candidates determined by real-time RT-PCR in 17 hepatoma cell lines. Three (Hep3B, HepG2, and HuH-7) of 17 lines were treated with 5-aza-dCyd. Ratio relative to normal liver tissue (C20) is shown by a 7-gradient pattern. "M's" indicates that genes showed hypermethylation (see C, top) in each cell line: nonunderlined and underlined "M's" indicate silenced (<0.01 compared with C20) and retained gene expression, respectively.

HepG2, and HuH-7). Because CpG islands of 642 of those 2,476 genes were methylated in all 3 cell lines (Fig. 1A), we selected them as candidates consistently hypermethylated in hepatomas.

Screening in the expression array analysis

In expression array analysis done in a duplicate manner, we used only reproducible probes (the coefficient of variation, CV <50%) in each set of experiments to evaluate obtained values. We focused on genes satisfying 2 criteria: (a) genes whose expression was observed in normal liver tissue but repressed in hepatoma cells, and (b) genes whose expression was restored after treatment with 5-aza-dCyd in hepatoma cells. Among genes expressed in normal liver tissue (C20 and C40), the expression of 1,730, 1,158, and 1,521 genes was silenced but restored by 5-aza-dCyd in Hep3B, HepG2, and HuH-7 cells, respectively. Among them, 204 genes on autosomes commonly satisfied criteria in all 3 lines (Fig. 1A), indicating 204 genes to be candidates consistently silenced through methylation in hepatocarcinogenesis.

Integration and validation of results in two microarray-based analyses

On the basis of the MeDIP-chip and expression array analyses, 11 genes were selected as overlapping genes in 2 different genome-wide array-based screening methods, suggesting them to be pharmacologically unmasked, tumor-specific methylation targets in all 3 hepatoma cell lines (Fig. 1A and Supplementary Table S2). Because these genes seem to be silenced in a tumor-specific manner, they are also candidates for TSG in hepatocarcinogenesis.

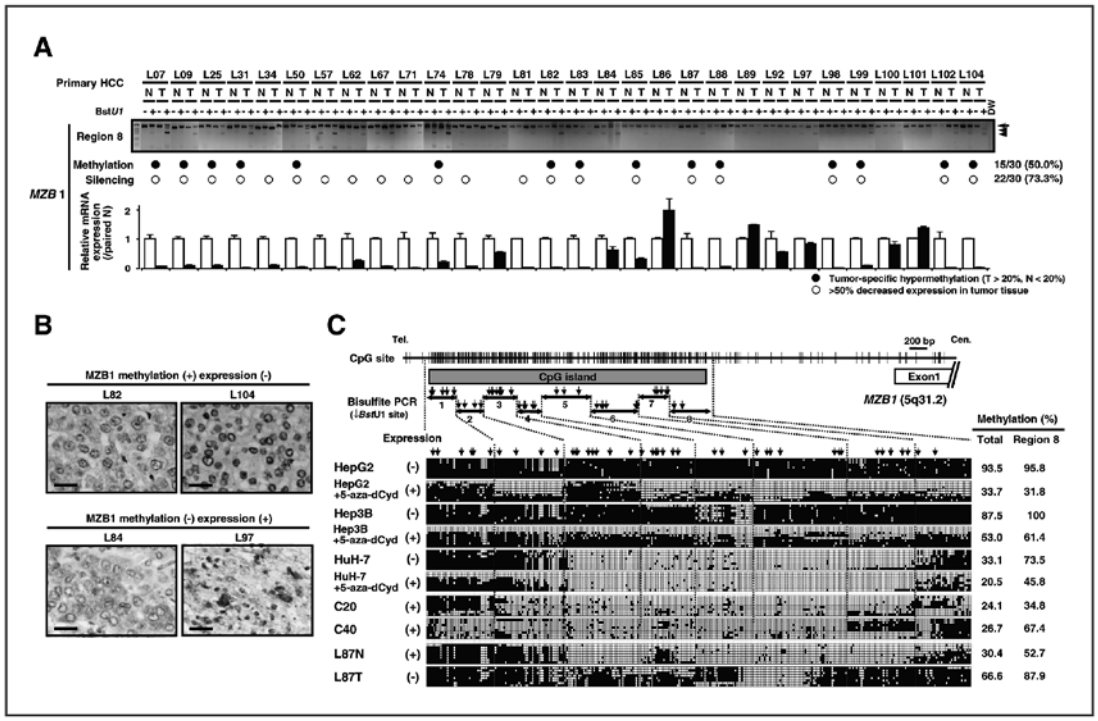

Figure 2. Correlation of methylation and expression status of MZB1 in primary HCCs. A, representative results of the methylation status of region 8 within the *MZB1* CpG island determined by COBRA (top) and the relative level of *MZB1* mRNA expression determined by real-time RT-PCR (bottom) in primary HCC tumors (T) and corresponding noncancerous liver tissues (N). Arrowheads, fragments specifically restricted at sites recognized as methylated CpGs; arrow, undigested fragments indicating unmethylated CpGs. A methylation density of cutoff point of 20% was considered significant (14). Closed and open circles indicate samples with tumor-specific methylation (positive in tumor but negative in corresponding nontumorous tissue) and those with the reduced mRNA expression (>50% decreased expression) in tumor tissue compared with paired nontumorous tissue, respectively. B, representative results of immunohistochemical analysis of MZB1 protein expression in primary HCCs indicate that methylation status of *MZB1* is inversely correlated with its mRNA and protein expression. Bars, 20 μm. Magnifications are ×200. C, top, a schematic map of the CpG-rich region around the CpG island and exon 1 of *MZB1*. Vertical ticks, CpG sites on the expanded axis. Gray box, CpG island. Horizontal closed arrows, the regions examined in the COBRA and BGS. Downward arrows, restriction sites (*Bst*U1) for the COBRA. Bottom, representative results of BGS of the *MZB1* CpG island in 3 hepatoma cell lines without and with 5-aza-dCyd, 2 normal livers (C20 and C40), and a paired representative case (cases L87) examined in the COBRA. Open and filled squares represent unmethylated and methylated CpG sites, respectively, and each row represents a single clone. Restriction sites are indicated by downward arrows.

We then determined the status of methylation and expression for all 11 candidates through COBRA and real-time reverse transcription PCR (RT-PCR), respectively, in a panel of 17 hepatoma cell lines and 2 normal liver tissues (Fig. 1B). Among them, *ANGPT2* was highly methylated in both the hepatoma cells and normal liver tissue. Among the other 10 genes, 8 genes (*L1TD1*, *MZB1*, *PBX4*, *FAR1*, *RADIL*, *DERL3*, *SFRP1*, and *CCK*) harbored at least 1 hypermethylated region in >50% of hepatoma cell lines compared with normal liver tissue, whereas *OCIAD2* and *KCNK6* were infrequently methylated in the hepatoma lines. Among those 8 genes, only *MZB1* and *FAR1* were downregulated (<0.1 relative to normal liver) in all cell lines with their hypermethylation, whereas the other 6 genes were expressed even in cell lines with their hypermethylation, suggesting *MZB1* and *FAR1* to be possible methylation targets for gene silencing in hepatoma cells, although the expression of all 11 genes was more or less restored by 1 to 10 μmol/L of 5-aza-dCyd treatment in each of the 3 cell lines (Supplementary Fig. S2).

MZB1 is frequently silenced through CpG island methylation in primary tumors

We next determined the methylation and expression status of *MZB1* and *FAR1* in 17 paired tumorous and nontumorous tissues from primary HCCs (cases L81-L104; Fig. 2A and Supplementary Fig. S3). Tumor-specific *MZB1* (region 8) and *FAR1* (region 3) hypermethylation was observed in 9 (52.9%) and 8 (47.1%) cases, respectively. In those cases with hypermethylation, tumor-specific downregulation of *MZB1* and *FAR1* expression was observed in 9/9 (100%) and 5/8 (62.5%) cases, respectively, suggesting *MZB1* to be the most probable candidate for a gene silenced through tumor-specific methylation. In additional 13 cases (Fig. 2A, cases L07-L79), tumor-specific *MZB1* hypermethylation was observed in 6 (46.2%) cases

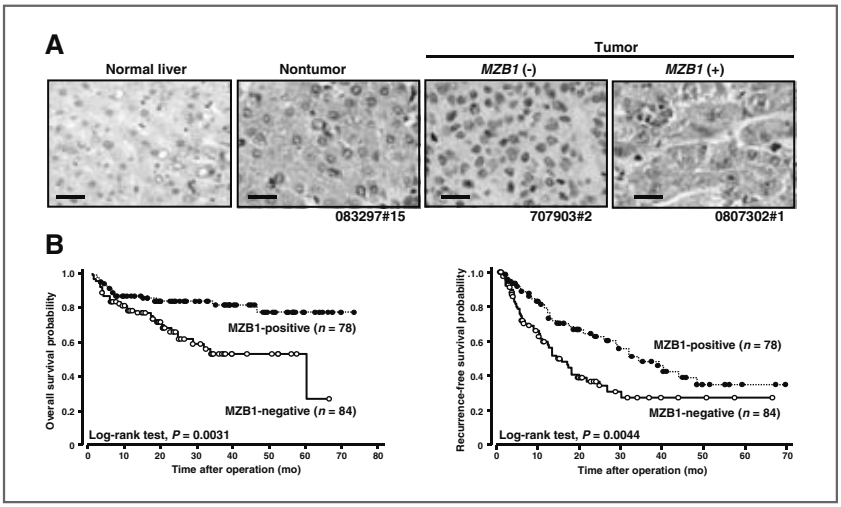

Figure 3. A, representative results of immunohistochemical staining of MZB1 protein in normal liver tissue, nontumorous liver tissue, and tumorous tissues in HCCs. Both normal and nontumorous hepatocytes showed MZB1 immunopositivity, whereas tumor cells showed either negative or positive immunoreactivity. Bars, 25 μm. Magnifications are ×200. B, Kaplan–Meier curves for overall survival (left) and recurrence-free survival (right) rates of 162 patients with primary HCCs. Negative MZB1 immunoreactivity of tumor cells was significantly associated with worse overall and recurrence-free survivals ($P = 0.0031$ and 0.0044, respectively; log-rank test).

and all of those cases also showed tumor-specific downregulation of this gene. Among 12 cases available for immunohistochemical staining of MZB1 protein, MZB1 was expressed in nontumorous tissues and the methylation status and protein expression status of MZB1 matched in 8 tumorous tissues (Fig. 2B).

To clarify the methylation status of the CpG island of *MZB1*, we conducted BGS in cell lines and tumorous and nontumorous tissues of HCC as well as normal liver tissue. CpG sites within the CpG island tended to be differentially methylated among the cell lines and primary samples: MZB1-nonexpressing cell lines except HuH-7 and primary tumors showed a highly methylated pattern within the CpG island, whereas MZB1-expressing normal liver tissue and nontumorous tissue of HCC case showed partially methylated (Fig. 2C). Although total %methylation of CpG sites within the CpG island of HuH-7 cells is higher than but close to those in MZB1-expressiong samples, dense methylation without unmethylated allele was observed in specific regions within CpG island in HuH-7 cells. In addition, we confirmed that treatment with 5-aza-dCyd partially restored methylation within the CpG island of *MZB1* in HepG2, Hep3B, and HuH-7 cells, whose expression of MZB1 was restored after the same treatment (Fig. 1B), suggesting that methylation within the CpG island upstream to *MZB1* occurs in cell lines and primary tumors of hepatoma and at least partly contributes to the silencing of its expression of the mRNA and protein level. Notably, 5-aza-dCyd-treated hepatoma cells and C20 showed similar methylation level of the *MZB1* CpG island (Fig. 2C), whereas 5-aza-dCyd-treated hepatoma cells showed much higher MZB1 expression level compared with C20 (Fig. 1B), suggesting that 5-aza-dCyd treatment indirectly activates transcription of MZB1 through demethylation of transcription factors/cofactors for MZB1, which might downregulated in normal hepatocytes or other mechanisms.

Immunohistochemical staining of MZB1 in primary HCCs

To determine clinicopathologic significance of the MZB1downregulation in primary HCCs, we conducted an immunohistochemical analysis of the MZB1 in 162 primary cases (Fig. 3 and Table 1). In the tumorous regions, 78 (48.1%) showed immunoreactivity to MZB1 (positive in Table 1), whereas 84 (51.9%) did not (negative in Table 1). In the nontumorous regions, on the other hand, 135 (83.3%) showed immunoreactivity to MZB1, whereas 27 (16.7%) did not. Negative MZB1 immunoreactivity was more frequent in cases with portal invasion ($P = 0.0222$) and in higher tumor stages ($P = 0.0207$). However, the MZB1 protein expression in each tumor was not associated with other characteristics.

In Kaplan–Meier survival curves, univariate analyses of overall and nonrecurrent survival with log-rank tests showed a significant association between negative MZB1 immunoreactivity and a poor survival rate of patients ($P = 0.0031$ and 0.0044, respectively; Fig. 3B). In the Cox proportional hazard regression model (Table 2), univariate analyses showed that negative MZB1 immunoreactivity, α-fetoprotein (AFP), tumor size, tumor number, portal vein invasion, background liver parenchyma, and tumor stage were significantly associated with overall survival. Multivariate analysis using a stepwise

Table 2. Cox proportional hazard regression analysis for overall survival

	Univariate		Multivariate[a]
Factor	**HR (95% CI)**	***P*[a]**	***P*[b]**
Gender			
Male vs. female	0.990 (0.509–1.925)	0.9764	X
Age, y			
>65 vs. <65	0.957 (0.527–1.738)	0.8859	X
AFP			
>200 vs. <200 ng/mL	2.202 (1.214–3.995)	**0.0094**	X
Tumor size			
>3 vs. <3 cm	3.548 (1.498–8.401)	**0.0040**	**0.0319**
Tumor number			
Multiple vs. single	2.531 (1.406–4.554)	**0.0019**	X
Histopathologic grading			
Poor-moderate vs. well	2.312 (1.074–4.975)	0.0321	X
Portal vein invasion			
Present vs. absent	2.309 (1.136–3.716)	**0.0173**	X
Surgical margin			
Present vs. absent	1.948 (0.963–3.940)	0.0637	X
Background liver parenchyma			
LC vs. CH + NL	1.825 (1.009–3.300)	**0.0468**	X
Stage			
III + IVA vs. I + II	3.466 (1.710–7.024)	**0.0006**	**0.0301**
MZB1 expression[c]			
Negative vs. positive	2.532 (1.338–4.791)	**0.0043**	**0.0234**

NOTE: Statistically significant values are in boldface type.
Abbreviations: CH, chronic hepatitis; LC, liver cirrhosis; NL, normal liver.
[a]Forward and backward stepwise analyses were used for multivariate analysis.
[b]*P* values are from 2-sided tests and were statistically significant at <0.05.
[c]MZB1 expression was evaluated by immunohistochemical analysis as described in Materials and Methods.

Cox regression procedure revealed that MZB1 immunoreactivity, tumor size, and tumor stage were independently selected as predictive factors for overall survival in both forward and backward procedures ($P = 0.0234$, 0.0319, and 0.0301, respectively).

MZB1 reexpression suppresses proliferation and tumor formation of cancer cells *in vitro* and *in vivo*

To investigate the biologic significance of MZB1 in hepatocarcinogenesis, MZB1 expression was transiently or stably restored in hepatoma cells lacking MZB1 expression. We then measured the proliferation and tumor formation of those cells in comparison with the control counterparts transduced with an empty vector *in vitro* and *in vivo*.

In colony-formation assays using transiently transfected cells, the occupancy of the stained area of colonies produced by MZB1-transfected HLE cells (Fig. 4A), which show *MZB1* hypermethylation pattern (Supplementary Fig. S4), and other hepatoma cells (data not shown) decreased compared with those of control counterparts. In an *in vitro* proliferation assay using stably transfected cells, cells expressing MZB1 protein, which was predominantly colocalized with an endoplasmic reticulum (ER) marker in the cytoplasm, grew slightly but significantly slower than the control cells (Fig. 4B). In a FACS analysis to examine the mode of action of MZB1 in the cell cycle, an accumulation of cells in G_0–G_1 phase and a decrease in S and G_2–M phase cells but no increase in sub-G_1 phase cells was observed among MZB1-transfected cells compared with mock-transfected counterparts (Fig. 4C), suggesting that MZB1 contributes to the arrest of hepatoma cells at the G_1-S checkpoint without inducing apoptosis. Indeed, a similar expression pattern of cleaved caspase 3, one of markers of apoptosis, was observed between stable MZB1 transfectants and control counterparts even after treatment with CDDP for induction of apoptosis (Fig. 4C). Subcutaneous tumor growth experiments using stable transfectants showed that restored expression of MZB1 in hepatoma cells correlated with reduced tumor volume and weight *in vivo* probably because of a decrease in cell proliferation shown by lower PCNA and Ki-67 positivities in MZB1-transfected cells (Fig. 4D). In resected tumors, no induction of apoptosis detected by

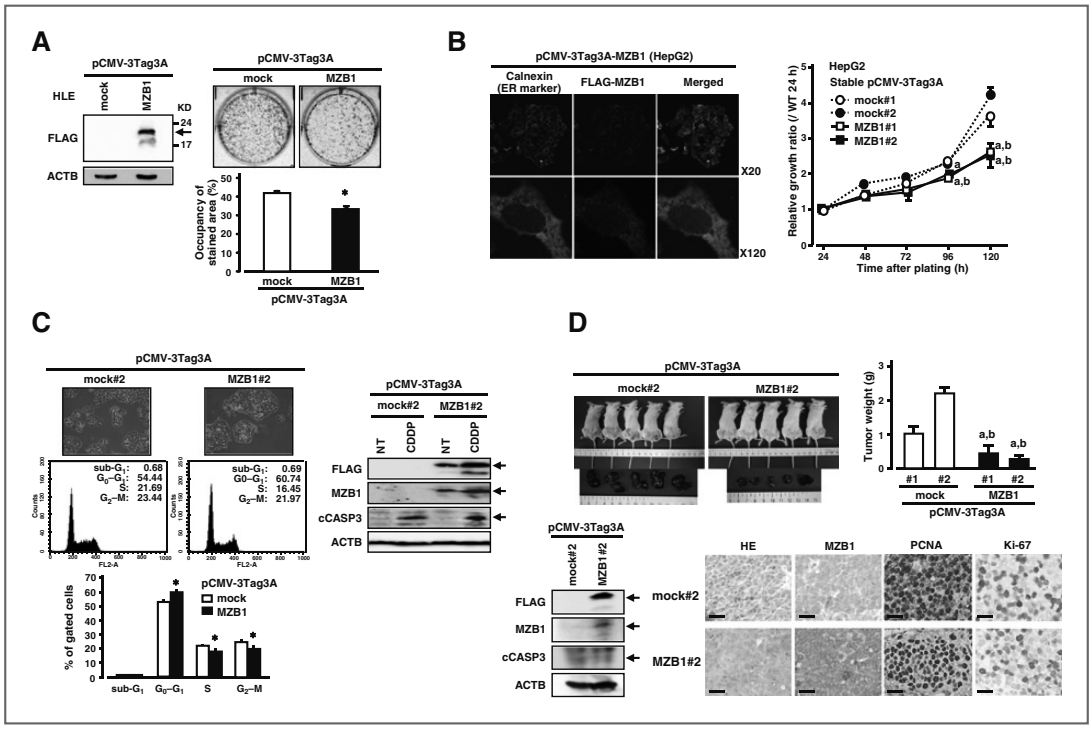

Figure 4. Tumor-suppressive effects of restoration of MZB1 expression in hepatoma cells *in vitro* and *in vivo*. A, HLE cells lacking MZB1 expression were transiently transfected with pCMV-3Tag3A-MZB1 or pCMV-3Tag3A-mock and selected with G418 for 2 weeks. MZB1 expression was confirmed by immunoblotting using 10 μg of protein extract and anti-MZB1 antibody (left). The drug-resistant colonies formed by the MZB1-transfected cells were more numerous than those formed by control counterparts (top right). Occupancy of the stained colony area was calculated (bottom right). Columns, means of 3 separate experiments, each conducted in triplicate; bars, SD (histogram). *, $P < 0.05$ versus mock control (Student *t* test). Similar results were obtained in the Hep3B and SK-HEP-1 cell lines (data not shown). B, stable HepG2 transfectants were established by transfection of pCMV-3Tag3A-MZB1 or pCMV-3Tag3A-mock with G418 selection. Immunofluorescence cytochemistry showed almost all pCMV-3Tag3A-MZB1–transfected cells to express FLAG-tagged MZB1 predominantly with an endoplasmic reticulum (ER) marker (calnexin, left). After plating into 24-well plates (2.5×10^4 cells per well), the proliferative activity of stably MZB1-transfected cells was found to be less than that of the control counterparts. Results of relative growth ratio are shown with the mean ± SD for 3 separate experiments, each done in triplicate (right). Differences were analyzed by 1-way ANOVA with subsequent Scheffé tests: a and b, $P < 0.05$ versus mock #1 and #2, respectively. C, top left, representative results of the population in each phase of the cell cycle in stable transfectants described in (B) assessed by FACS. Bottom left, columns, means of 3 separate clones, each conducted in triplicate; bars, SD (histogram). *, $P < 0.05$ versus mock control (Student *t* test). Right, representative results of immunoblotting of MZB1 protein and cleaved caspase-3 (cCASP3), one of apoptotic markers, without (no treatment, NT) or with cisplatinum (CDDP, 20 μmol/L) treatment for 48 hours. D, representative results of tumors formed in SCID mice following injection of stably MZB1-transfected cells. MZB1-transfected HepG2 cells or mock-transfected cells (4×10^7) were injected into the right and left dorsal flanks. SCID mice were sacrificed for tumor weight evaluation 5 weeks postinjection (top left). Results of tumor weight are shown with the mean ± SD for 3 separate experiments, each done in triplicate (top right). Differences were analyzed as described in (B). Bottom left, representative results of immunohistochemical analysis of MZB1 as well as PCNA and Ki-67, markers for cell proliferation, in resected tumors. A positive MZB1 immunoreactivity was detected in MZB1-transfetced cells but not in mock-transfected counterparts, and both PCNA and Ki-67 immunoreactivities were less frequently observed in MZB1-transfetced cells compared with mock-transfected counterparts. Bars, 25 μm. Magnifications are ×200. Bottom right, representative results of immunoblotting of MZB1 protein and cCASP3 in resected tumors.

cleaved caspase 3 expression in MZB1-transfetced cells was observed compared with mock-transfected counterparts *in vivo* (Fig. 4D).

Discussion

Epigenetic silencing of TSGs plays an important role in the carcinogenesis (16), including hepatomagenesis (5–7). Although many studies have reported aberrant hypermethylation of genes in HCC, e.g. *CDH1*, *RASSF1A*, *GSTP*, *SOCS1*, *SFRP1*, and *PTEN* identified as TSGs silenced by hypermethylation, most of these studies were limited to the analysis of a single or a few genes (5–7, 17). Because the number of methylation-target TSGs identified to date is far fewer for HCC than for other cancers possibly because of fewer attempts to conduct genome-wide analysis (18), there remain many genes hypermethylated in HCC. With advancements in microarray technology, the number of genes found to be hypermethylated in HCC in a cancer-specific manner is

expected to increase (8, 19). Although the functional consequence of promoter hypermethylation is transcriptional silencing of the associated gene, this assumption often goes untested, as few have concurrently investigated both methylation and expression (6, 7). On the basis of these hypotheses and background, we conducted genome-wide screening of methylation-target TSGs using a combination of 2 microarray-based approaches: MeDIP-chip analysis in hepatoma cell lines and expression array analysis for genes pharmacologically unmasked in the same lines. As a result of this approach, several genes were newly identified as candidate methylation targets, and among them MZB1 was showed to be the most possible TSG, which is silenced through methylation and contributes to the hepatocarcinogenesis.

Among 11 genes we identified through genome-global screening of methylation-mediated silenced genes in hepatoma cells, 10 were newly identified candidates and only SFRP1 was known as possible methylation-target TSG in HCC (20, 21). The remarkable reduction in the number of candidate genes and lack of various known HCC-related methylation targets within candidates may be because of a small number of commonly methylated and/or silenced genes among the 3 cell lines used in this study. Indeed, several frequently methylated genes, such as SLIT2, PTGS2 (COX2), and HHIP, for which methylation data are available in all 3 hepatoma cell lines, showed different methylation patterns among the cell lines (22–24). These variations may come from the different backgrounds of the 3 cell lines, such as hepatitis B virus infection in Hep3B and no hepatitis virus infection in the other 2 lines, because hypermethylated genes in HCC tumors are known to exhibit remarkably distinct patterns depending on associated risk factors (25, 26). Therefore, it is suggested that the candidate genes identified and validated in the present study may contribute to functional pathways shared among different subtypes of HCC regardless of associated risk factors, and this might be the reason why MZB1 protein expression status was not statistically associated with the status of hepatitis virus infection and background liver parenchyma in our analysis.

One of striking findings of our immunohistochemical analysis of MZB1 using a panel of primary tumor samples of HCC was that immunoreactivity to the MZB1 protein in each sample was significantly associated with a worse clinical outcome even after stratification with other clinicopathologic characteristics. This result indicates that MZB1 might be useful as an independent prognosticator in patients with HCC, although MZB1 immunoreactivity in each case was significantly associated with portal invasion and in tumor stages. Because MZB1 seems to be downregulated in a cancer-specific manner in HCC and its expression is observed in most normal human tissues (11), it will be interesting whether MZB1 works as a TSG in specific tissues including liver or in various tissues.

MZB1 was first identified as a caspase-2–binding molecule through a yeast 2–hybrid system using a human B lymphocyte cDNA library, which was conducted to determine the mechanism of activation of caspase-2 in apoptosis of B cells triggered by ligation of the antigen receptor (11). Although MZB1 was shown to bind caspase-2 and -9 *in vitro* and *in vivo* and be triggered upon the transient transfection of human kidney cells and Rat-1 fibroblasts and stable transfection of human B cell lines (11), the precise mechanisms by which it exerts proapoptotic activity remain unclear because of the absence of structural hallmarks besides a CXXC thioredoxin motif and no homology with other molecules in apoptotic pathways. Recently, it was shown that MZB1 occurs in the luminal ER and affects multiple cellular processes, such as (a) the oxidative folding and assembly and secretion of immunoglobulin in plasma cells (27, 28) and (b) the regulation of Ca^{2+} homeostasis and ER Ca^{2+} stores, integrin-mediated adhesion, and antibody secretion in marginal zone B cells of the spleen and innate-like B cells (B1 cells, ref. 29). Because those processes are associated with the functional differentiation of B cells, it is possible that the MZB1-induced assembly of several target proteins including integrin may contribute to the antiproliferative effect of MZB1 on hepatoma cells without induction of apoptosis observed in this study. The expression of this gene is observed not only in the B-cell lineage including plasma cells, marginal zone B cells, or B1 cells (27–29), but also in most normal human tissues except the placenta constitutively even in the absence of an apoptotic stimulus (11), suggesting MZB1 to affect various biologic processes in different tissues possibly through interaction with various proteins and/or the targeting of various molecules. Indeed, MZB1 protein was reported to be downregulated in intestinal-type gastric cancer, although the clinicopathologic and biologic significance was not analyzed (30), suggesting MZB1 to act as a TSG at least in some tissues including stomach and liver tissue. Further examination will be required to clarify the mechanisms of the antiproliferative effect of MZB1.

Disclosure of Potential Conflicts of Interest

No potential conflicts of interest were disclosed.

Authors' Contributions

Conception and design: S. Matsumura, I. Imoto, J. Inazawa
Development of methodology: S. Matsumura, I. Imoto, T. Matsui, J. Inazawa
Acquisition of data: S. Matsumura, M. Furuta, S. Tanaka
Analysis and interpretation of data: S. Matsumura, I. Imoto, K. Kozaki, J. Inazawa
Writing, review, and/or revision of the manuscript: S. Matsumura, I. Imoto, J. Inazawa
Administrative, technical, or material support: I. Imoto, T. Muramatsu, M. Sakamoto, J. Inazawa
Study supervision: I. Imoto, T. Matsui, S. Arii, J. Inazawa

Acknowledgments

The authors thank Ayako Takahashi, Rumi Mori, and Ayumi Shioya for technical assistance.

Grant Support

This study was supported in part by Grant-in-Aid for Scientific Research (A) and (C), and Scientific Research on Priority Areas and Innovative Areas,

and a Global Center of Excellence (GCOE) Program for International Research Center for Molecular Science in Tooth and Bone Diseases from the Ministry of Education, Culture, Sports, Science, and Technology, Japan; a Health and Labour Sciences Research Grant by the Ministry of Health, Labour and Welfare, Japan; a grant from the New Energy and Industrial Technology Development Organization (NEDO).

The costs of publication of this article were defrayed in part by the payment of page charges. This article must therefore be hereby marked *advertisement* in accordance with 18 U.S.C. Section 1734 solely to indicate this fact.

Received April 28, 2011; revised April 17, 2012; accepted April 27, 2012; published OnlineFirst May 9, 2012.

References

1. Herath NI, Leggett BA, MacDonald GA. Review of genetic and epigenetic alterations in hepatocarcinogenesis. J Gastroenterol Hepatol 2006;21:15–21.
2. De Zhu J. The altered DNA methylation pattern and its implications in liver cancer. Cell Res 2005;15:272–80.
3. Kondo Y, Shen L, Suzuki S, Kurokawa T, Masuko K, Tanaka Y, et al. Alterations of DNA methylation and histone modifications contribute to gene silencing in hepatocellular carcinomas. Hepatol Res 2007;37:974–83.
4. Gao W, Kondo Y, Shen L, Shimizu Y, Sano T, Yamao K, et al. Variable DNA methylation patterns associated with progression of disease in hepatocellular carcinomas. Carcinogenesis 2008;29:1901–10.
5. Tischoff I, Tannapfe A. DNA methylation in hepatocellular carcinoma. World J Gastroenterol 2008;14:1741–8.
6. Herceg Z, Paliwal A. Epigenetic mechanisms in hepatocellular carcinoma: how environmental factors influence the epigenome. Mutat Res 2011;727:55–61.
7. Shin SH, Kim B, Jang JJ, Suh KS, Kang GH. Identification of novel methylation markers in hepatocellular carcinoma using a methylation array. J Korean Med Sci 2010;258:1152–9.
8. Laird PW. Principles and challenges of genome-wide DNA methylation analysis. Nat Rev Genet 2010;11:191–203.
9. Weber M, Davies JJ, Wittig D, Oakeley EJ, Haase M, Lam WL, et al. Chromosome-wide and promoter-specific analyses identify sites of differential DNA methylation in normal and transformed human cells. Nat Genet 2005;37:853–62.
10. Yamashita K, Upadhyay S, Osada M, Hoque MO, Xiao Y, Mori M, et al. Pharmacologic unmasking of epigenetically silenced tumor suppressor genes in esophageal squamous cell carcinoma. Cancer Cell 2002;2:485–95.
11. Bonfoco E, Li E, Kolbinger F, Cooper NR. Characterization of a novel proapoptotic caspase-2- and caspase-9-binding protein. J Biol Chem 2001;276:29242–50.
12. Furuta M, Kozaki KI, Tanaka S, Arii S, Imoto I, Inazawa J. miR-124 and miR-203 are epigenetically silenced tumor-suppressive microRNAs in hepatocellular carcinoma. Carcinogenesis 2009;31:766–76.
13. Xiong Z, Laird PW. COBRA: a sensitive and quantitative DNA methylation assay. Nucleic Acids Res 1997;25:2532–4.
14. Sonoda I, Imoto I, Inoue J, Shibata T, Shimada Y, Chin K, et al. Frequent silencing of low density lipoprotein receptor-related protein 1B (LRP1B) expression by genetic and epigenetic mechanisms in esophageal squamous cell carcinoma. Cancer Res 2004;64:3741–7.
15. Muramatsu T, Imoto I, Matsui T, Kozaki KI, Haruki S, Sudol M, et al. YAP is a candidate oncogene for esophageal squamous-cell carcinoma. Carcinogenesis 2011;32:389–98.
16. Baylin SB, Herman JG. DNA hypermethylation in tumorigenesis: epigenetics joins genetics. Trends Genet 2000;16:168–74.
17. Calvisi DF, Ladu S, Gorden A, Farina M, Lee JS, Conner EA, et al. Mechanistic and prognostic significance of aberrant methylation in the molecular pathogenesis of human hepatocellular carcinoma. J Clin Invest 2007;117:2713–22.
18. Schuebel KE, Chen W, Cope L, Glockner SC, Suzuki H, Yi JM, et al. Comparing the DNA hypermethylome with gene mutations in human colorectal cancer. PLoS Genet 2007;3:1709–23.
19. Schones DE, Zhao K. Genome-wide approaches to studying chromatin modifications. Nat Rev Genet 2008;9:179–91.
20. Shih YL, Shyu RY, Hsieh CB, Lai HC, Liu KY, Chu TY, et al. Promoter methylation of the secreted frizzled-related protein 1 gene SFRP1 is frequent in hepatocellular carcinoma. Cancer 2006;107:579–90.
21. Huang J, Zhang YL, Teng XM, Lin Y, Zheng DL, Yang PY, et al. Down-regulation of SFRP1 as a putative tumor suppressor gene can contribute to human hepatocellular carcinoma. BMC Cancer 2007;7:126.
22. Jin J, You H, Yu B, Deng Y, Tang N, Yao G, et al. Epigenetic inactivation of SLIT2 in human hepatocellular carcinomas. Biochem Biophys Res Commun 2009;379:86–91.
23. Murata H, Tsuji S, Tsujii M, Sakaguchi Y, Fu HY, Kawano S, et al. Promoter hypermethylation silences cyclooxygenase-2 (Cox-2) and regulates growth of human hepatocellular carcinoma cells. Lab Invest 2004;84:1050–9.
24. Tada M, Kanai F, Tanaka Y, Tateishi K, Ohta M, Asaoka Y, et al. Down-regulation of hedgehog-interacting protein through genetic and epigenetic alterations in human hepatocellular carcinoma. Clin Cancer Res 2008;14:3768–76.
25. Deng YB, Nagae G, Midorikawa Y, Yagi K, Tsutsumi S, Yamamoto S, et al. Identification of genes preferentially methylated in hepatitis C virus-related hepatocellular carcinoma. Cancer Sci 2010;101:1501–10.
26. Lambert MP, Paliwal A, Vaissière T, Chemin I, Zoulim F, Tommasino M, et al. Aberrant DNA methylation distinguishes hepatocellular carcinoma associated with HBV and HCV infection and alcohol intake. J Hepatol 2011;54:705–15.
27. Shimizu Y, Meunier L, Hendershot LM. pERp1 is significantly up-regulated during plasma cell differentiation and contributes to the oxidative folding of immunoglobulin. Proc Natl Acad Sci U S A 2009;106:17013–8.
28. van Anken E, Pena F, Hafkemeijer N, Christis C, Romijn EP, Grauschopf U, et al. Efficient IgM assembly and secretion require the plasma cell induced endoplasmic reticulum protein pERp1. Proc Natl Acad Sci U S A 2009;106:17019–24.
29. Flach H, Rosenbaum M, Duchniewicz M, Kim S, Zhang SL, Cahalan MD, et al. Mzb1 protein regulates calcium homeostasis, antibody secretion, and integrin activation in innate-like B cells. Immunity 2010;33:723–35.
30. Katoh M, Katoh M. MGC29506 gene, frequently down-regulated in intestinal-type gastric cancer, encodes secreted-type protein with conserved cysteine residues. Int J Oncol 2003;23:235–41.

分子遺伝分野

三木 義男
難治疾患研究所
分子遺伝・教授

1）研究の課題名

① 骨肉腫におけるP53によって誘導されるアポトーシス関連遺伝子の解析（Discovery of pro-apoptotic genes induced by p53 in osteosarcoma）

P53の遺伝子変化は骨肉腫を含め、がんの主な原因だと考えられている。我々が骨肉腫細胞をMicroarrayとChIP sequenceで分析して比較することでP53のSer46のリン酸化で誘発されるプロアプトーシス遺伝子の研究開発を行っている。これまでに、Microarray分析とChIP sequence分析で得られた結果によりisoform of paralemmin protein（IPP）を取り出すことに成功した。そこで、IPP蛋白質のアポトーシスを誘発するメカニズムを調べることで骨肉腫等の癌発生に関する研究を行っている。これまでは、IPPはcAMP経路や細胞核にある蛋白質に作用することでアポトーシスを誘発することが確認した。具体的には、IPPがDNAのダメージに対してwt-P53のみに（変異P53等を除く）制御され、アプトーシスを誘発することが確認された。

② ヒト乳癌骨転移における切断型BRCA2機能の解明（ Cleavage BRCA2 function in human breast cancer of bone metastases）

遺伝性乳癌の原因遺伝子産物であるBRCA2タンパク質は、核内でのDNA損傷部位や、間期における中心体、細胞質分裂時におけるMid-bodyへの局在が観察されるなど、細胞周期を通じて様々な局面に登場するが、そのすべての機能が明らかにされているわけではない。我々はヒト乳癌細胞株に対してBRCA2抗体によるイムノブロットを行った場合、野生型BRCA2（分子量：384kDa）の他に分子量240kDaに相当するバンドが検出されることを見出した。これは、BRCA2が細胞膜結合型マトリクスメタロプロテアーゼMT1-MMPによって切断されたもので、MT1-MMP阻害剤によって抑制された。さらにMT1-MMPと合成ペプチドを用いた質量分析による詳細な切断部位の同定を行った結果、BRCA2の2135番目のアスパラギンと2136番目のロイシンとの間で切断されることが判明した。次いで、この切断型BRCA2の抗体作成に成功し、免疫染色を行った。N末端から240kまでの切断型BRCA2（BRCA2-N）は、細胞周期を通じて細胞質に局在し、240kからC末端までの切断型BRCA2（BRCA2-C）は、核内にドット状に局在した。しかし、この局在は野生型BRCA2-FLAGのドット状の局在とは異なっていた。このことから切断型BRCA2は、野生型BRCA2とは異なる機能を有する可能性が示唆され、切断型BRCA2のパートナータンパク質の同定は、タンパク質レベルでのBRCA2の異常と乳癌の発症メカニズムや骨転移との関連性を解明する研究に重要であると考えている。

2）研究のイラストレーション

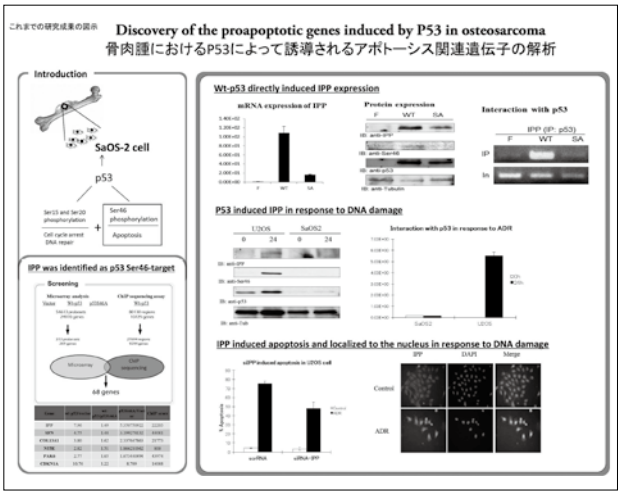

3）発表の研究内容についての英文要約

① The genetic alterations in p53 are one of the most frequently mutated tumor suppressor gene in human cancer including osteosarcoma. The tumor suppressor gene p53 regulates apoptosis in response to DNA

damage. Notably, the phosphorylation at serine-46 (Ser46) of p53 is essential to promote pro-apoptotic genes. However, little is known about pro-apoptotic genes induced by Ser46 phosphorylation.
In our research we achieved to investigate pro-apoptotic genes induced by p53 in Ser46 specific manner using microarray analysis and chromatin immunoprecipitation (ChIP) sequencing assay in osteosarcoma cells. Comparison of two assays resulted in the isoform of paralemmin protein (IPP) was strongly elicited from the phosphorylation of Ser46. The clarification study showed that the upregulation of IPP in only wild type p53 transfected cells but not in mutant p53 samples (p53S46A). Furthermore, the expression of candidate gene was induced by p53 in response to DNA damage. TUNEL assay showed that the inhibition of IPP using siRNA reduced apoptosis by 25 percent. Immunohistochemistry assay indicated that the IPP localization mainly in the cytoplasm but moved to the nucleus in response to DNA damage. Our future study will be focused on the investigation of functional analysis of IPP in relation with p53.

② Cleavage BRCA2 function in human breast cancer of bone metastases
Breast cancer susceptibility gene2 (BRCA2) plays an important role in DNA repair, transcription, and cell proliferation. The human BRCA2 is a large protein that consists of 3418 amino acids and is composed of multiple domains to interact with several proteins. Here, we focus on the function of cleavage BRCA2 in the breast cancer and bone metastasis. The matrix metalloproteinases (MMPs) can promote cancer progression by increasing cancer-cell growth, migration, invasion, metastasis and angiogenesis. We found that membrane-type MMP (MT1-MMP) cleaves the BRCA2 protein. One cleavage BRCA2 is near N terminal (CN') with NES domain, the other cleavage BRCA2 is near C terminal (CC') with NLS domain. We hypothesize that wild BRCA2 is not only in the cytoplasm but also on the cell membrane and is cleaved by membrane-type MMPs to promote tumor invasion and angiogenesis. In order to prove our hypothesis we will create a parallel set of FLAG-fusion proteins containing the N and C terminals of BRCA2. We want to figure out whether each part of BRCA2 is able to stimulate tumor stromal cells.

4）本事業に関連して世界的な研究拠点形成に向けて、以下の点で改善・整備等されたこと

A（研究拠点体制）

研究室におけるスペースの確保、機器の整備および補充、研究推進のためのスケジュール等を作成し研究室内部の体制の整備を継続するとともに、整形外科、口腔外科等の臨床グループと立案した共同研究計画を進めるなど、総合的に研究拠点体制の継続に努めた。

B（研究教育環境）

ジャーナルクラブ、研究進捗ミーティング、GCOEセミナー等研究教育環境の整備を継続した。

C（人材確保）

大学院生2名がGCOE研究を遂行した。

D（人材育成）

新たに入学する大学院生を含め上記体制で人材育成に努めている。

E（国際化）

GCOEプログラムの中で国際セミナーへの参加、海外招聘研究者との議論等を通して国際化を図った。

5）GCOE事業を推進するに当たって力を入れた点

GCOE推進研究者間で立案した共同研究計画を積極的に進め、特に臨床グループとの共同研究で患者臨床検体を用いたゲノム研究推進体制の構築及びその継続に努めた。

6）英文原著論文

1. Elgazzar, S., Zembutsu, H., Takahashi, A., Kubo, M., Aki, F., Hirata, K., Takatsuka, Y., Okazaki, M., Ohsumi, S., Yamakawa, T., Sasa, M., Katagiri, T., Miki, Y. and Nakamura, Y. A genome-wide association study identifies a genetic variant in the SIAH2 locus associated with hormonal receptor-positive breast cancer in Japanese. J Hum Genet, in press.
2. Iyevleva, A.G., Kuligina, E., Mitiushkina, N.V., Togo, A.V., Miki, Y. and Imyanitov, E.N. High level of miR-21, miR-10b, and miR-31 expression in bilateral vs. unilateral breast carcinomas. Breast Cancer Res Treat, 131, 1049-59, 2012.
3. Khanom, R., Sakamoto, K., Pal, S.K., Shimada, Y., Morita, K., Omura, K., Miki, Y. and Yamaguchi, A. Expression of basal cell keratin 15 and keratin 19 in oral squamous neoplasms represents diverse pathophysiologies. Histol Histopathol, 27, 949-59, 2012.
4. Sakamoto, K., Fujii, T., Kawachi, H., Miki, Y., Omura, K., Morita, K., Kayamori, K., Katsube, K. and Yamaguchi, A. Reduction of NOTCH1 expression pertains to maturation abnormalities of keratinocytes in squamous neoplasms. Lab Invest, 92, 688-702, 2012.
5. Satoh, Y., Sugai, S., Uehara, H., Mun, M., Sakao, Y., Okumura, S., Nakagawa, K., Ishikawa, Y., Miki, Y. and Miyata, S. Clinical Impact of Intraoperative Detection of Carcinoembryonic Antigen mRNA in Pleural Lavage Specimens from Nonsmall Cell Lung Cancer Patients.

Thorac Cardiovasc Surg, 2012.
6. Suzuki, K., Dashzeveg, N., Lu, Z.G., Taira, N., Miki, Y. and Yoshida, K. Programmed cell death 6, a novel p53-responsive gene, targets to the nucleus in the apoptotic response to DNA damage. Cancer Sci, 103, 1788-94, 2012.
7. Taira, N., Mimoto, R., Kurata, M., Yamaguchi, T., Kitagawa, M., Miki, Y. and Yoshida, K. DYRK2 priming phosphorylation of c-Jun and c-Myc modulates cell cycle progression in human cancer cells. J Clin Invest, 122, 859-72, 2012
8. Wang, L., Tsutsumi, S., Kawaguchi, T., Nagasaki, K., Tatsuno, K., Yamamoto, S., Sang, F., Sonoda, K., Sugawara, M., Saiura, A., Hirono, S., Yamaue, H., Miki, Y., Isomura, M., Totoki, Y., Nagae, G., Isagawa, T., Ueda, H., Murayama-Hosokawa, S., Shibata, T., Sakamoto, H., Kanai, Y., Kaneda, A., Noda, T. and Aburatani, H. Whole-exome sequencing of human pancreatic cancers and characterization of genomic instability caused by MLH1 haploinsufficiency and complete deficiency. Genome Res, 22, 208-19, 2012.

7）総説ならびに著書

1. 斉藤広子、三木義男；乳癌の検査・診断　乳癌の分子生物学的検査　遺伝性乳癌スクリーニングの課題（遺伝子診断を含めて）.日本臨床　70巻増刊7乳癌,480-486,（2012）
2. 斉藤広子、三木義男；乳癌治療戦略を目指した基礎研究　遺伝子診断の基礎　遺伝子発現プロファイリング研究.日本臨床　70巻増刊7乳癌,227-231,（2012）
3. 斉藤広子、三木　義男；乳癌の分子生物学と発癌機序　発癌機序　乳癌の発癌機序　概論（分子機構、多段階発癌機序を含めて）.日本臨床　70巻増刊7乳癌,92-96,（2012）
4. 須貝幸子、三木義男；分子標的薬の個別化医療.薬事54巻6号,919-923,（2012）
5. 三木義男；BRCA1とBRCA2遺伝子産物の機能　基礎から臨床.癌と化学療法　39巻4号,498-501,（2012）
6. 斉藤広子、三木義男；治療につながる診断の新規技術と分子生物学の進歩　合成致死とBRCA1/2.最新医学　67巻6月増刊,1403-1414,（2012）
7. 三木義男；BRCA遺伝子と個別化治療.がん分子標的治療　10巻1号,13-18,（2012）

8）平成24年度までの自己評価

GCOEプログラムに参加し、骨軟部腫瘍（骨肉腫、軟骨肉腫、歯肉癌など）を中心に、ゲノム科学を応用した研究を進めてきた。一方、骨肉腫におけるp53 Ser46のリン酸化により活性化されるプロアポトーシス分子として、paralemminタンパクファミリーの同定に成功した。今度は、臨床系グループとの共同研究体制を維持し臨床検体収拾システムを作製、順次癌組織の収集を促進し遺伝子発現プロファイル解析を進める。また、教育等には大きく貢献できたと判断している。

9）学会発表（英文）

1. ◎Nurmaa Dashzeveg., et al, Discovery of pro-apoptotic genes induced by p53 in osteosarcoma, Fourth Annual Retreat camp-GCOE, Jan.22-23, 2012, Japan
2. Nurmaa Dashzeveg., et al, Discovery of pro-apoptotic genes induced by tumor suppressor p53, 103rd Annual Meeting of American Association of Cancer Research, Mar.31-Apr.4.2012, Chicago, USA
3. ◎Nurmaa Dashzeveg., et al, Discovery of the pro-apoptotic genes induced by tumor suppressor p53, Student Research Day of Harvard School of Dental Medicine, Apr.10.2012, Boston, USA
4. Nurmaa Dashzeveg., et al, Discovery of the pro-apoptotic genes induced by the tumor suppressor p53, The Joint Symposium of the 7th International Symposium of the Institute Network and the 4th IDAC Symposium, the 2nd Symposium for the Usage / Research Center of Aging, June 14-15, Tohoku University, Sendai, Japan
5. Nurmaa Daszheveg., et al, The comprehensive search of p53 target genes that promote apoptosis, The 71th Annual Meeting of the Japanese Cancer Association, Sep.19-21, 2012, Sapporo, Japan
6. Miyaguchi K, Guo T, Miki Y and Nakanishi A. Phosphorylation of BRCA2 by Akt is involved in BRCA2-14-3-3 γ interaction related to centrosome dynamics. 15th International Congress on Hormonal Steroids and Hormones & Cancer, poster presentation, Kanazawa, Japan, November 16, 2012

10）学会発表（和文）

1. 大石陽子、三ツ木秀征、中井麻木、石田文孝、大西 清、三浦妙太、三木義男；乳癌新規予後予測因子Stathmin1の検討.第20回日本乳癌学会学術総会、熊本市、2012年6月28-30日
2. 三木義男、中西啓；BRCA2の新規機能と合成致死理論に基づく新規乳癌治療法開発の可能性.第20回日本乳癌学会学術総会、熊本市、2012年6月28-30日
3. 中村清吾、高橋將人、戸崎光宏、中山貴寛、野水整、三木義男、村上茂、村上好恵、青木大輔、新井正美、有賀智之、岩瀬拓士、大住省三、繁永礼奈、清水忠夫、西村誠一郎、馬場信一、阪埜浩司、平沢晃、藤森実、

森美樹、山内英子、四元淳子；2010年度日本乳癌学会班研究課題最終報告 「我が国における遺伝性乳癌・卵巣癌（BRCA陽性患者）及び未発症陽性者のデータベース構築及び対策に関する研究」.第20回日本乳癌学会学術総会、熊本市、2012年6月28-30日

4. 佐藤友理、瀧景子、須貝幸子、小松美樹、三木義男、新井 正美；先進医療としてのRET遺伝子診断への取り組み.第18回日本家族性腫瘍学会学術集会、大阪市、2012年6月15日-16日
5. 瀧景子、佐藤友理、菅野康吉、三木義男、新井正美；APC遺伝子変異が同定できない家族性大腸腺腫症症例に対するAPC体細胞モザイクおよびMUTYH遺伝子変異の解析.第18回日本家族性腫瘍学会学術集会、大阪市、2012年6月15日-16日
6. 三木義男、中西 啓；遺伝性乳がん卵巣がんの現状 問題点と展望 遺伝性乳がん原因遺伝子BRCA2の新規機能と新たな治療法開発の試み.第18回日本家族性腫瘍学会学術集会、大阪市、2012年6月15日-16日
7. 平直江、三本麗、倉田盛人、北川昌伸、三木義男、吉田清嗣；三木義男；Dysregulation of c-Jun/c-Myc expression by depletion of DYRK2 triggers tumorigenesis DYRK2の発現欠失によるc-Jun/c-Mycの制御異常は細胞の腫瘍化を引き起こす.第71回日本癌学会学術総会、札幌市、2012年9月19日-21日
8. 三本麗、山口乃里子、平直江、鷹橋浩幸、三木義男、吉田清嗣；DYRK2 phosphorylates Snail and regulates the invasion and metastasis in breast cancer DYRK2はSnailをリン酸化し乳がんの浸潤・転移を制御する.第71回日本癌学会学術総会、札幌市、2012年9月19日-21日
9. 古田玲子、利安隆史、佐藤由紀子、山本智理子、秋山太、石川雄一、新橋渉、川端一嘉、竹島信宏、須貝幸子、三木義男、北川知行；Ectopic chromosome around centrosome（ ECAC ）in metaphase cells of oropharyngeal carcinoma as a marker of HPV-association HPV関連中咽頭がんの指標となる分裂中期細胞核の中心体近傍異所性染色体.第71回日本癌学会学術総会、札幌市、2012年9月19日-21日
10. 宮口健、郭甜甜、三木義男、中西啓；Phosphorylation of BRCA2 by Akt is involved in BRCA2-1 4-3-3 gamma interaction related to centrosome dynamics 中心体制御に関わるBRCA2 - 14-3-3γ複合体形成にはAktによるBRCA2のリン酸化が関与する.第71回日本癌学会学術総会、札幌市、2012年9月19日-21日
11. 木村仁美、中西啓、三木義男；Proteasome activity affects cancerous centrosome hypertrophy プロテアソームの活性は癌細胞における中心体の肥大化に影響する.第71回日本癌学会学術総会、札幌市、2012年9月19日-21日
12. DASHZEVEG NURMAA、木村純子、平直江、三木義男、吉田清嗣；The comprehensive search of p53 target genes that promote apoptosis .第71回日本癌学会学術総会、札幌市、2012年9月19日-21日
13. 高岡美帆、斉藤広子、中西啓、三木義男；BRCA2 contributes success of cytokinesis through regulation of non-muscle myosin IIC ATPase activity 乳癌原因遺伝子産物 BRCA2 は II型ミオシンIIC の ATPase 活性の制御を通して細胞質分裂に働く第71回日本癌学会学術総会、札幌市、2012年9月19日-21日.
14. サディヤ、斉 広子、中西啓、三木義男；Analysis of a centrosome localization signal（ CLS ）in BRCA2 BRCA2由来中心体局在化シグナル（CLS）の機能解析.第71回日本癌学会学術総会、札幌市、2012年9月19日-21日
15. 石場俊之、中西啓、高木洋子、笠原舞、杉本斉、永原誠、中川剛士、佐藤隆宣、杉原健一、三木義男；The correlation of decorin and periostin indicated by the proteomics of phyllodes 葉状腫瘍のプロテオーム解析から導いたdecorinとperiostinの関連性.第71回日本癌学会学術総会、札幌市、2012年9月19日-21日

11）外部資金の獲得状況

1. 新学術領域研究、公募研究
   研究題目：乳癌の分子サブタイプ分類と個別化抗癌剤治療の開発
   代表：三木義男
   期間：平成23-24年
   研究費総額：1600万円
   科学研究費補助金、挑戦的萌芽研究
   研究題目：MT1-MMPの中心体制御を介した新規がん形質転換機構の解明
   代表：三木義男
   期間：平成23-24年
   研究費総額：280万円
2. 科学研究費補助金、基盤C
   研究題目：細胞アレイによる卵巣癌抗癌剤効果予測システムの構築と分子標的薬の探索
   代表：津田浩史

期間：平成22-23年
研究費総額：234万円

3. 文部科学省科学技術試験研究・委託業務
研究題目：ゲノム網羅的解析情報を基盤とするオーダーメイドがん医療
代表：稲澤譲治
期間：平成20年～平成23年
研究費総額：2,000万円

4. 文部科学省科学技術試験研究・委託業務
研究題目：分子プロファイリングによる新規標的同定を通じた難治がん治療法開発
代表：三木義男
期間：平成23年
研究費総額：1,400万円

5. 厚生労働科学研究費補助金（第3次対がん総合戦略研究事業）
研究題目：難治性乳癌の克服に向けた画期的治療法の開発基盤推進研究
代表：三木義男
期間：平成24年
研究費総額：2,550万円

12）特別講演、招待講演、シンポジウム

1. 三木義男;Whole exon sequencingとトランスレーショナルリサーチ、第二回乳がん分子標的治療セミナー、特別講演、東京、2012年6月23日
2. 三木 義男、中西啓;Hereditary breast/ovarian cancer -New development of the molecular diagnosis and treatment- 遺伝性乳がん・卵巣がん症候群 - 分子診断・治療の新たな展開 -. 第71回日本癌学会学術総会、シンポジウム、札幌市、2012年9月19日-21日

13）教室、分野や講座の准教授、講師、助教、特別研究員、ポスドク、指導を受けた大学院生の名前

准教授　吉田　清嗣（H24年3月まで）
特任講師　中西　　啓
助教　竹中　克也
特任助教　平　　直江（H24年3月まで）
D4　高岡　美帆
○ D3　Wali Nadila
（瓦力 娜迪拉）
○ D2　Dashzeveg Nurmaa
（ダシュゼウェゲ　ヌルマ）
D1　加賀美　裕也
D1　王　　均輝
M2　木村　仁美
M2　滝沢　涼子
M2　中澤　和也
M2　山本　武徳
M2　和田　匠太
M1　手代木　翔太

14）GCOE活動についての感想、コメント、改善を望む点

GCOEプログラムに参加した学生の教育、研究推進は大きな前進が認められ、このような活動が財政的支援とともに継続されることを強く希望する。

Research article

DYRK2 priming phosphorylation of c-Jun and c-Myc modulates cell cycle progression in human cancer cells

Naoe Taira,[1,2] Rei Mimoto,[1,3] Morito Kurata,[2] Tomoko Yamaguchi,[1] Masanobu Kitagawa,[2] Yoshio Miki,[1] and Kiyotsugu Yoshida[1]

[1]Department of Molecular Genetics, Medical Research Institute, Tokyo Medical and Dental University, Tokyo, Japan. [2]Department of Comprehensive Pathology, Aging and Developmental Sciences, Graduate School, Tokyo Medical and Dental University, Tokyo, Japan. [3]Department of Surgery, The Jikei University School of Medicine, Tokyo, Japan.

Dysregulation of the G_1/S transition in the cell cycle contributes to tumor development. The oncogenic transcription factors c-Jun and c-Myc are indispensable regulators at this transition, and their aberrant expression is associated with many malignancies. Degradation of c-Jun/c-Myc is a critical process for the G_1/S transition, which is initiated upon phosphorylation by glycogen synthase kinase 3 β (GSK3β). However, a specific kinase or kinases responsible for priming phosphorylation events that precede this GSK3β modification has not been definitively identified. Here, we found that the dual-specificity tyrosine phosphorylation–regulated kinase DYRK2 functions as a priming kinase of c-Jun and c-Myc. Knockdown of DYRK2 in human cancer cells shortened the G_1 phase and accelerated cell proliferation due to escape of c-Jun and c-Myc from ubiquitination-mediated degradation. In concert with these results, silencing DYRK2 increased cell proliferation in human cancer cells, and this promotion was completely impeded by codeprivation of c-Jun or c-Myc in vivo. We also found marked attenuation of DYRK2 expression in multiple human tumor samples. Downregulation of DYRK2 correlated with high levels of unphosphorylated c-Jun and c-Myc and, importantly, with invasiveness of human breast cancers. These results reveal that DYRK2 regulates tumor progression through modulation of c-Jun and c-Myc.

Introduction

The c-Jun and c-Myc transcription factors are critical promoters of cellular proliferation. Dysregulated expression and activation of these oncogenes are frequently observed in most human cancers. Control of their expression is thus vital to maintaining regulated cell proliferation in normal cells. Indeed, expressions of c-Jun and c-Myc are tightly governed at transcriptional, posttranscriptional, translational, and posttranslational levels (1, 2). These proteins rapidly accumulate when quiescent cells are stimulated into the cell cycle. This transient increase and subsequent decline in their protein levels potentiate the transition from the G_1 phase into the S phase (G_1/S transition) with progression through the cell cycle and continued proliferation (2, 3). The clearance of these oncoproteins in continuously cycling cells and the maintenance of low levels in quiescent cells are controlled by ubiquitin-mediated proteolysis (4, 5). In many cases, proteins that are targeted for degradation by the ubiquitin-proteasome pathway are first marked by phosphorylation of specific residues, allowing for their recognition by the ubiquitination machinery. Notably, previous studies have demonstrated that c-Jun and c-Myc are polyubiquitinated in a glycogen synthase kinase 3β–dependent (GSK3β-dependent) fashion by an Skp–cullin–F-box protein ligase complex containing Fbw7 (6). GSK3β is a serine/threonine protein kinase that operates in the G_1 phase to receive input from several signaling pathways (7). Growth factor–dependent inactivation of GSK3β promotes cell cycle entry by stabilizing proteins such as c-Jun and c-Myc (8–10). In this context, dysregulation of GSK3β has been implicated in tumorigenesis and cancer progression (11). GSK3 phosphorylates many of its substrates via a "priming phosphorylation" mechanism, recognizing the canonical phosphorylation motif S/TXXXpS/T (12). This motif contains the phospho-accepting Ser or Thr that is separated by 3 residues from phospho-Ser or phospho-Thr. A different kinase capable of the priming phosphorylation must first phosphorylate the substrate at the P+4 position, before GSK3 can phosphorylate the P0 residue. In this regard, priming kinases play critical roles in the regulation of molecular and biological activities for c-Jun and c-Myc. Degradation of c-Myc protein is controlled by ordered phosphorylation at 2 specific sites near the N terminus of the protein: Ser62 for a priming phosphorylation and Thr58 for the GSK3β phosphorylation. Surprisingly, Ser62 kinase or kinases remain inconsistent in spite of biological importance. Although both ERK and cdc2 kinase specifically phosphorylate Ser62 in vitro and cellular phosphorylation of Thr58/Ser62 is stimulated by mitogens, in vivo experiments do not support a role for these kinases in the phosphorylation of c-Myc (13, 14). Likewise, c-Jun is destroyed after sequential phosphorylation at Ser243 and Thr239 (10). Phosphorylation of Thr239 is catalyzed by GSK3β. However, as seen for c-Myc, a priming kinase or kinases phosphorylating Ser243 are as yet unidentified. Previously, GSK3 was reported to be capable of phosphorylation at both Thr239 and Ser243; a subsequent study concluded that GSK3 can phosphorylate at Thr239, and not Ser243 (15, 16). The results also demonstrated that Ser243 kinase or kinases are distinct from the MAPK superfamily, including ERK, JNK, and p38MAPK (16). While they implied the possibility that dual specificity tyrosine phosphorylation–regulated kinases (DYRKs) are capable of phosphorylating Ser243 in vitro, no data have been provided (16). These studies collectively suggest that priming kinases themselves for GSK3β in Fbw7-mediated degradation of c-Jun and c-Myc remains uncertain.

Authorship note: Yoshio Miki and Kiyotsugu Yoshida share senior authorship.
Conflict of interest: The authors have declared that no conflict of interest exists.
Citation for this article: *J Clin Invest.* 2012;122(3):859–872. doi:10.1172/JCI60818.

research article

DYRK2 is a member of an evolutionarily conserved family of DYRKs that autophosphorylate a critical tyrosine in their activation loop, but function only as serine/threonine kinases toward their substrates (17). Until recently, the functional role for DYRK2 in cells has been largely obscure. A recent report indicated that DYRK2 functions as a scaffold for an E3 ligase complex and controls mitotic transition (18). Another study demonstrated that DYRK2 contributes to proteasomal degradation of the transcription factor GLI2 (19). These findings shed light on a role for DYRK2 in protein proteolysis. Our recent study revealed an unexpected role for DYRK2 in the regulation of the p53 tumor suppressor (20). We found that DYRK2 translocated from the cytoplasm to the nucleus in response to DNA damage. Subsequently, ataxia telangiectasia mutated (ATM) activated DYRK2, allowing it to phosphorylate p53 at Ser46, which is a crucial modification for induction of apoptosis. In this context, DYRK2 plays an indispensable role on the determination of cell fate in response to DNA damage. However, to our knowledge, there has been no physiological substrate identified for DYRK2 in cells besides p53.

Here, we demonstrate that DYRK2 is identified as a priming kinase responsible for phosphorylation of c-Jun/c-Myc. Importantly, priming phosphorylation by DYRK2 is a prerequisite for GSK3β phosphorylation to the G_1/S transition. Moreover, silencing of DYRK2 contributes to accelerated proliferation by stabilizing c-Jun/c-Myc in vitro and in vivo. These findings thus support a coordinate regulation of c-Jun/c-Myc by DYRK2.

Results

DYRK2 affects cell proliferation by controlling the expression of c-Jun and c-Myc. To examine the role of DYRK2 on cell proliferation, HeLa cells were transfected with 2 different siRNAs targeting DYRK2 (20). Colony formation assays revealed that depletion of DYRK2 elevated cell growth (Figure 1A). Similar results were obtained in U2OS cells (Supplemental Figure 1A; supplemental material available online with this article; doi:10.1172/JCI60818DS1), indicating the independence of the p53 tumor suppressor. To confirm these results, we evaluated the growth rate of cells in the presence or absence of DYRK2 siRNAs by trypan blue dye exclusion assays. Analysis of the growth curves demonstrated that, in HeLa cells silenced for DYRK2, the exponential growth was markedly elevated compared with that in mocked cells. (Figure 1B). Comparable results were obtained in U2OS cells (Supplemental Figure 1B). To extend these findings, we explored cell cycle analysis by flow cytometry. Depletion of DYRK2 did not induce apoptosis, but led to a decrease in the percentage of cells in the G_1 phase of the cell cycle and a concomitant increase in the number of cells in the S and G_2/M phases (Figure 1C and Supplemental Figure 1C). We used the growth curves determined by trypan blue dye exclusion assays to estimate doubling times and combined both pieces of information to calculate the length of each phase of the cell cycle. The results demonstrated that knocking down DYRK2 leads to a significant reduction in length of the G_1 phase of the cell cycle (Figure 1D and Supplemental Figure 1D). These findings indicated that DYRK2 regulates cell cycle progression at the G_1 phase. In order to identify potential effectors that might cause this phenotype, we compared the expression status of cell cycle–associated genes between control cells and DYRK2-depleted cells. Toward this end, we found with surprise that silencing DYRK2 substantially augments the expression of c-Jun and c-Myc (Figure 1E and Supplemental Figure 1E), both of which affect cell proliferation by controlling the G_1/S transition. To determine whether the increase in c-Jun and c-Myc depends on kinase activity of DYRK2, we prepared GFP-tagged plasmids expressing DYRK2 WT or the kinase-dead (KR) DYRK2 mutant, both of which are resistant to silencing by DYRK2 siRNA. Introduction of the resistant DYRK2 WT (designated GFP-rDYRK2 WT) in DYRK2-depleted cells abrogated the augmentation of c-Jun and c-Myc (Supplemental Figure 1F). In contrast, transduction of the resistant DYRK2-KR (GFP-rDYRK2-KR) had no remarkable effect on their expression levels (Supplemental Figure 1F), clearly demonstrating that the increase of these transcription factors requires kinase activity of DYRK2. To determine whether upregulation of *c-Jun* and *c-Myc* expression is regulated at transcriptional levels, we analyzed mRNA by RT-PCR. The demonstration that there is no significant increase of mRNA in cells silenced for DYRK2 (Figure 1E and Supplemental Figure 1E) indicates that the expression of these genes must be controlled at posttranslational levels.

DYRK2 phosphorylates c-Jun and c-Myc, which is required for subsequent GSK3β phosphorylation. In order to define mechanisms in which DYRK2 contributes to the expression of c-Jun and c-Myc, we attempted to identify the potential phosphorylation sites in c-Jun and c-Myc. During this process, we eventually focused on Ser243 for c-Jun and Ser62 for c-Myc, both of which have been considered "priming phosphorylation" residues, since surrounding amino acid sequences of serine coincide with consensus phosphorylation sites of DYRK kinases (P-X-S/T-P) (Figure 2A and ref. 21). These colinear motifs, including serine, are highly conserved through evolution (10). More importantly, accumulating studies have revealed that phosphorylation at these residues is tightly integrated with appropriate control of their stability at the G_1 phase (6). To determine whether DYRK2 can specifically phosphorylate these serine residues, recombinant DYRK2 was incubated with purified c-$Jun_{210–310}$ or c-$Myc_{1–100}$. The finding that kinase-active DYRK2 phosphorylated GST–c-$Jun_{210–310}$-WT by detection with an anti–phospho–c-Jun(Ser243) antibody demonstrated that DYRK2 is a Ser243 kinase in vitro (Figure 2B). Similar phosphorylation was obtained with coincubation of DYRK2 and the GST–c-$Jun_{210–310}$–T239A mutant in which Thr239 is substituted with Ala (Figure 2B). Notably, coincubation of DYRK2 with the GST–c-$Jun_{210–310}$–S243A mutant or the GST–c-$Jun_{210–310}$–T239A/S243A mutant completely abrogated reaction with the anti–phospho–c-Jun(Ser243) antibody (Figure 2B), indicating the specificity of this antibody against phospho-Ser243. We also performed in vitro kinase assays to explore DYRK2 phosphorylation of c-Myc at Ser62 by using anti–phospho–c-Myc(Ser62). As shown for c-Jun, DYRK2 specifically phosphorylated c-Myc at Ser62 in vitro (Figure 2B). To extend these findings to cellular DYRK2, 293T cells were transfected with Flag vector, Flag-DYRK2 WT, or the catalytically inactive Flag-DYRK2-KR mutant (20). Cell lysates were immunoprecipitated with anti-Flag followed by in vitro kinase assays using GST–c-$Jun_{210–310}$ as the substrate. Expression of DYRK2 WT was associated with substantial phosphorylation of c-Jun at Ser243 (Supplemental Figure 2A). In contrast, Ser243 phosphorylation was completely abrogated by expression of the dominant negative DYRK2 mutant (Supplemental Figure 2A). Similar results were obtained in phosphorylation of c-Myc at Ser62 (Supplemental Figure 2A). These findings collectively support a role for DYRK2 as a kinase for the priming phosphorylation of c-Jun and c-Myc in vitro. To assess whether DYRK2 phosphorylates c-Jun and c-Myc in cells, 293T cells were cotransfected with Flag–c-Jun or Flag–c-Myc and GFP vector, GFP-DYRK2 WT, or the GFP-DYRK2-KR mutant. Immunoprecipitates with anti-Flag were analyzed by immunoblotting with the phospho-specific antibodies. Expression of DYRK2 WT enhanced phosphorylation of c-Jun at Ser243 (Figure 2C). Moreover, there was little if any induction of Ser243 phosphorylation in cells ectopically expressed with the dominant negative DYRK2, suggest-

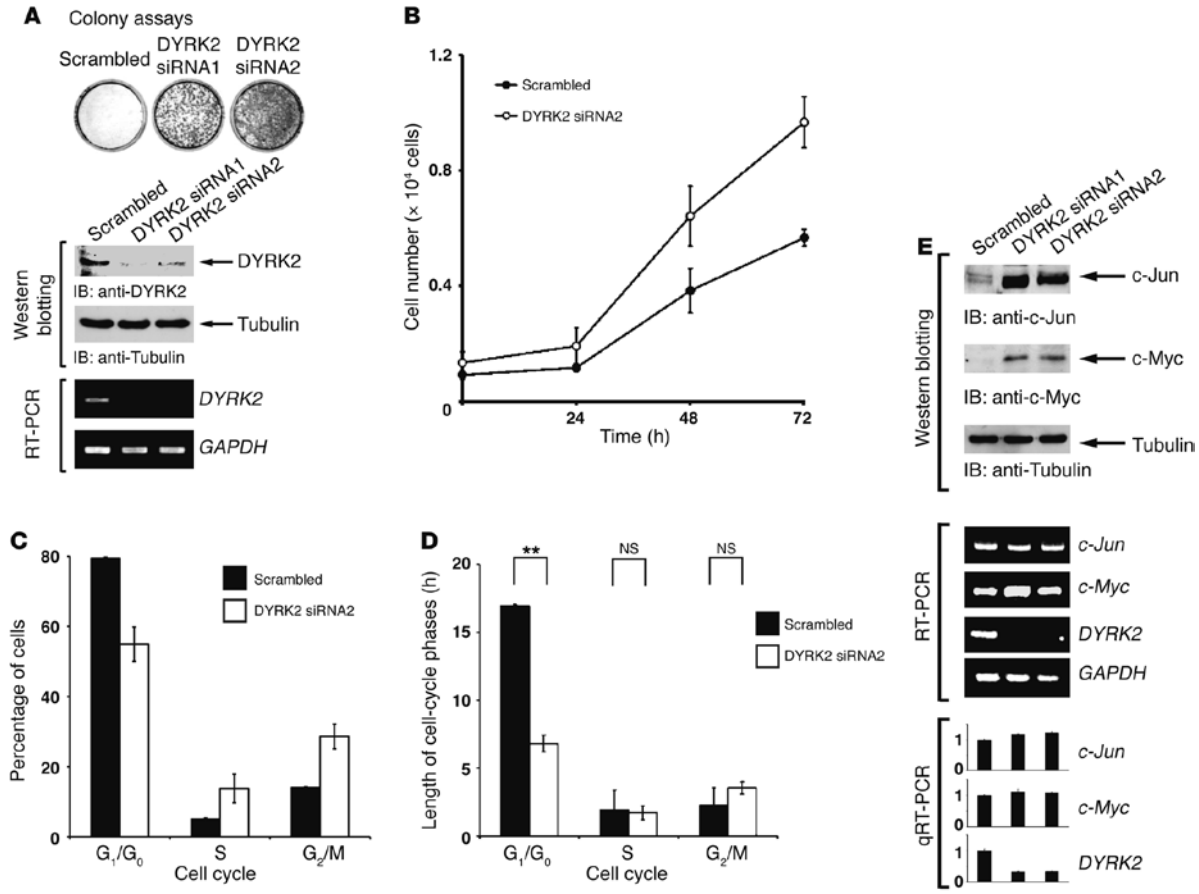

Figure 1

Silencing of DYRK2 results in hyperproliferation by upregulation of c-Jun and c-Myc. (**A**) HeLa cells were transfected with scrambled siRNA or DYRK2-specific siRNAs. After transfection, colony formation assays were performed. Cell lysates were immunoblotted with anti-DYRK2 or anti-tubulin. Total RNAs were analyzed by RT-PCR using *DYRK2*-specific or *GAPDH*-specific primers. (**B**) HeLa cells were transfected with scrambled siRNA or DYRK2 siRNA, and cell growth was analyzed by trypan blue exclusion assay. (**C** and **D**) HeLa cells were transfected with scrambled siRNA or DYRK2 siRNA. After transfection, cells were stained with propidium iodide and the cell cycle was analyzed using flow cytometry. $^{**}P < 0.01$. (**E**) HeLa cells were transfected and analyzed by immunoblotting (IB) with anti–c-Jun (top panel), anti–c-Myc (2nd panel), or anti-tubulin (3rd panel). Total RNAs were analyzed with *c-Jun*–specific (4th and 8th panels), *c-Myc*–specific (5th and 9th panels), *DYRK2*-specific (6th and 10th panels), or *GAPDH*-specific (7th panel) primers. The result of quantitative RT-PCR was normalized for the level of *GAPDH* and represents the relative fold induction compared with control sample. The data were evaluated from 3 independent experiments, each performed in triplicate. Data represent mean ± SD. qRT-PCR, quantitative RT-PCR.

ing that kinase activity is required for DYRK2 phosphorylation of c-Jun at Ser243 (Figure 2C). Comparable findings were obtained in phosphorylation of c-Myc at Ser62 (Figure 2C). We previously demonstrated that DYRK2 is virtually localized in the cytoplasm and the nucleus; however, nuclear DYRK2 is constitutively degraded by the ubiquitination-proteasome machinery (22). Conversely, upon exposure to genotoxic stress, DYRK2 escaped from ubiquitination and was thereby stabilized in the nucleus. In this regard, to confirm that DYRK2 phosphorylates c-Jun and c-Myc in the cytoplasm, we examined phosphorylation of c-Jun and c-Myc by expressing the GFP-DYRK2-(KKR→NNN) mutant, in which key amino acids of nuclear localization signal were mutated with asparagine; thus, this mutant is localized exclusively in the cytoplasm (22). The GFP-DYRK2-(KKR→NNN) mutant phosphorylated c-Jun at Ser243 to levels equivalent to those of DYRK2 WT (Supplemental Figure 2B). Similar results were obtained in phosphorylation of c-Myc at Ser62 (Supplemental Figure 2B). These data suggest DYRK2 phosphorylation of c-Jun and c-Myc in the cytoplasm. We also found that DYRK2 interacts with c-Jun/c-Myc in cells (Supplemental Figure 2, B and C) and that the binding of DYRK2 to c-Myc is abrogated after exit from the G_1 phase (Supplemental Figure 2D). To further define the prerequisite role for DYRK2 in subsequent GSK3β phosphorylation, GST–c-$Jun_{210–310}$–WT or –S243A mutant was incubated with purified GSK3β in the presence or absence of recombinant DYRK2. Incubation of GST–c-$Jun_{210–310}$–WT with GSK3β did not increase the reactivity of c-Jun with anti–phospho–c-Jun(Thr239) antibody (Figure 2D). However, prior phosphorylation of c-Jun by DYRK2 significantly enhanced the ability of GSK3β to phosphorylate c-Jun at Thr239 in vitro (Figure 2D).

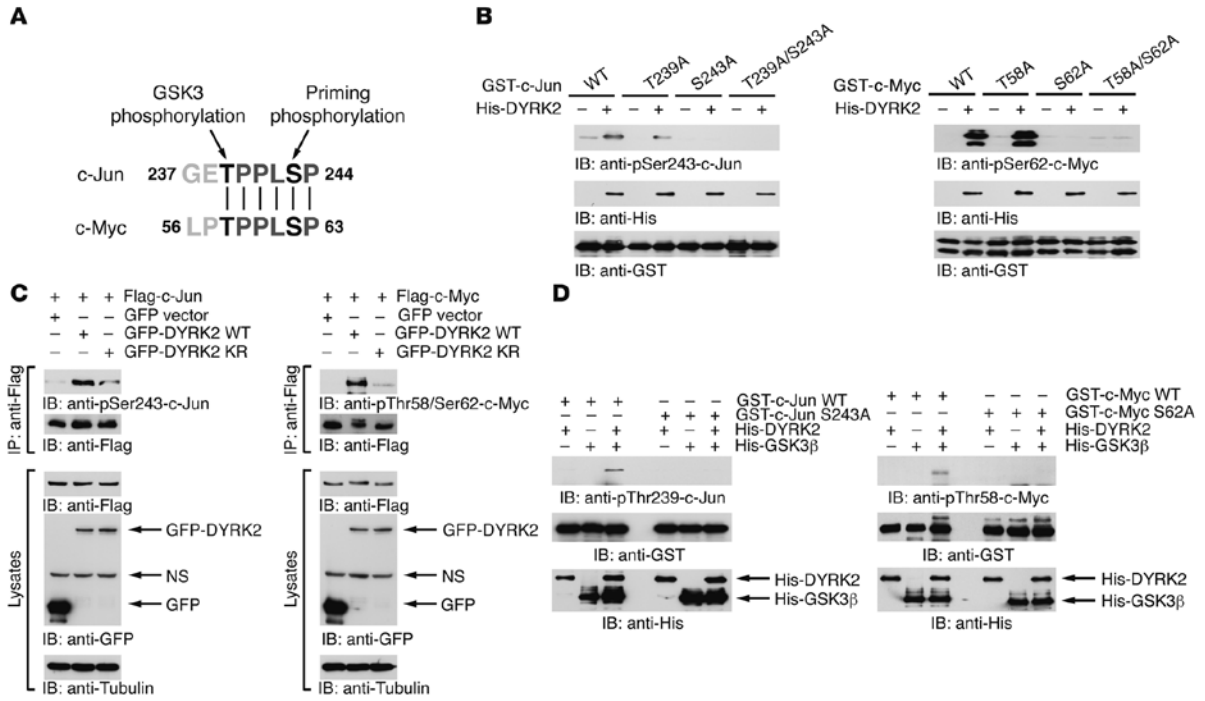

Figure 2

DYRK2 phosphorylates c-Jun and c-Myc at the priming phosphorylation residues. (**A**) Sequence alignments around phosphorylation residues of c-Myc and c-Jun. (**B**) Recombinant DYRK2 was incubated with GST–c-Jun$_{210–310}$ or GST–c-Myc$_{1–100}$ in the presence of ATP. Reactants were analyzed by immunoblotting with anti–phospho–c-Jun(Ser243) (left upper panel), anti–phospho–c-Myc(Ser62) (right upper panel), anti-His (middle panels), or anti-GST (lower panels). (**C**) 293T cells were cotransfected with GFP vector, GFP-DYRK2 WT, or GFP-DYRK2-KR and Flag-tagged c-Jun (Flag–c-Jun) or c-Myc (Flag–c-Myc). Lysates were immunoprecipitated with anti-Flag agarose. Immunoprecipitates were then subjected to immunoblot analysis with anti–phospho–c-Jun(Ser243) (left top panel), anti–phospho–c-Myc(Thr58/Ser62) (right top panel), or anti-Flag (2nd panels). Lysates were also subjected to immunoblot analysis with anti-Flag (3rd panels), anti-GFP (4th panels), or anti-tubulin (bottom panels). (**D**) Recombinant DYRK2 and/or His-GSK3β were incubated with GST–c-Jun$_{210–310}$ or GST–c-Myc$_{1–100}$. Reaction products were analyzed with the indicated antibodies.

More importantly, incubation of the GST–c-Jun–S243A mutant with DYRK2 did not facilitate Thr239 phosphorylation by GSK3β (Figure 2D). Equivalent findings were obtained in phosphorylation of c-Myc at Thr58 (Figure 2D). These results demonstrated an indispensable role for DYRK2 on a priming function for GSK3β phosphorylation.

Abrogation of DYRK2 stabilizes c-Jun and c-Myc. Accumulating studies have revealed that GSK3β phosphorylates and destabilizes c-Jun and c-Myc (12). In this context, we observed that phosphorylation by GSK3β requires prior phosphorylation by DYRK2, suggesting its indispensable involvement in the stability of c-Jun and c-Myc. To determine the direct role for DYRK2 on the half-life of c-Jun and c-Myc, U2OS cells were treated with an inhibitor of protein synthesis, cycloheximide (CHX). As expected, expression of c-Jun was unstable following treatment with CHX (Figure 3A). In sharp contrast, depletion of DYRK2 stabilized c-Jun even after inhibition of protein synthesis (Figure 3A). Comparable findings were obtained with c-Myc stability (Figure 3A). Previous studies have demonstrated that turnover of c-Jun and c-Myc is regulated by the ubiquitin-proteasome pathway. In this regard, to determine whether abrogation of DYRK2 impairs ubiquitination of c-Jun and c-Myc, U2OS cells were transfected with scrambled siRNA or DYRK2 siRNA in the presence of the proteasome inhibitor MG-132. Analysis with antiubiquitin demonstrated that constitutive ubiquitination of c-Jun and c-Myc was prevented in cells silenced for DYRK2 (Figure 3B). Moreover, ectopic expression of DYRK2 WT, but not the dominant negative DYRK2-KR mutant, increased ubiquitination of c-Myc (Supplemental Figure 3A). Intriguingly, however, ectopic expression of GSK3β or DYRK2 alone was insufficient to downregulate c-Jun/c-Myc (Supplemental Figure 3B). Cotransfection of GSK3β with DYRK2 robustly attenuated c-Jun/c-Myc expression (Supplemental Figure 3B). Destabilization of c-Jun/c-Myc was completely rescued by treatment of cells with MG-132 (Supplemental Figure 3B), suggesting that c-Jun and c-Myc were ubiquitinated and degraded in the proteasome following phosphorylation by DYRK2 and GSK3β. To further define an indispensable role for GSK3β on c-Jun/c-Myc ubiquitination, U2OS cells were transfected with HA vector, HA-GSK3β, or Flag-DYRK2 WT in the presence of MG-132. Coexpression of DYRK2 and GSK3β substantially enhanced ubiquitination of c-Jun/c-Myc compared with GSK3β or DYRK2 expression alone (Supplemental Figure 3, C and D), suggesting that dual phosphorylations by DYRK2 and GSK3β require full ubiquitination of c-Jun/c-Myc. Phosphorylated c-Jun/c-Myc are eventually ubiquitinated by Fbw7 for degradation (6). In this regard, we examined the effect of Fbw7 on DYRK2-mediated turnover of c-Jun/c-Myc. As previously shown, knockdown of DYRK2 increased expres-

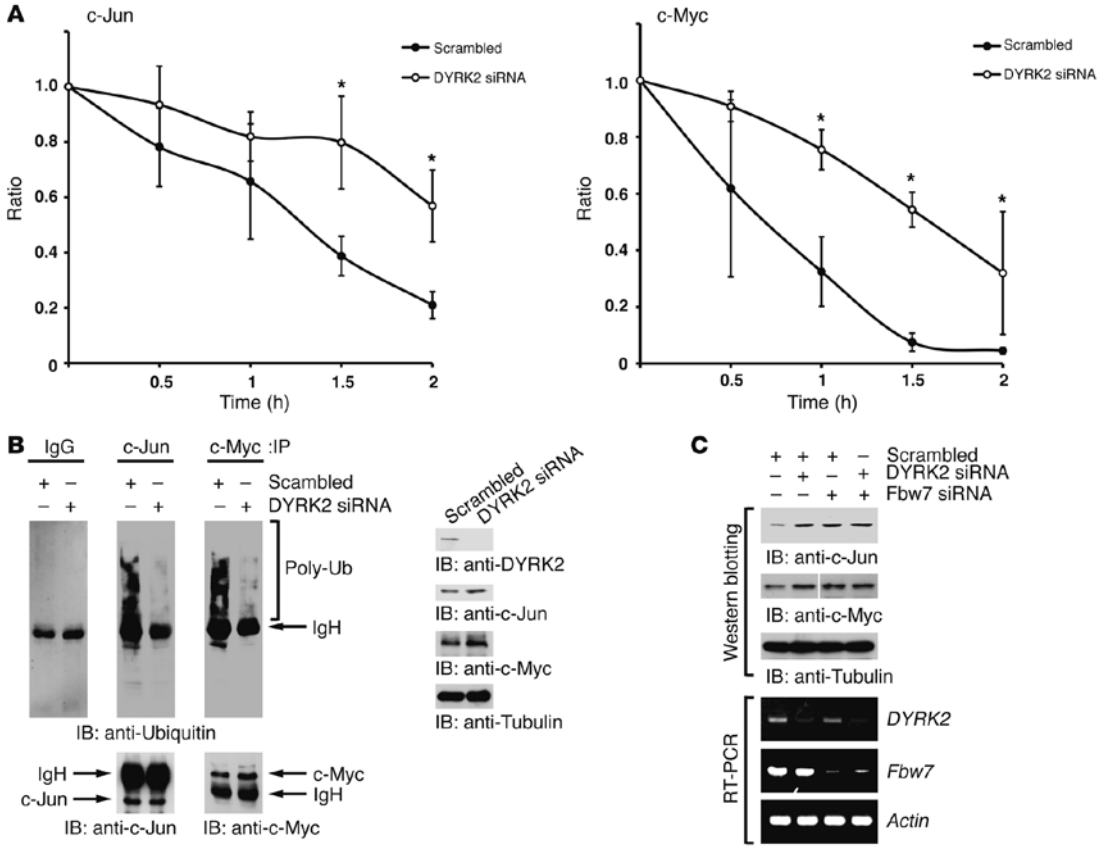

Figure 3

DYRK2 regulates c-Jun and c-Myc stability. (**A**) U2OS cells were transfected with scrambled siRNA or DYRK2 siRNA. After transfection, cells were incubated with 40 μg/ml CHX for the indicated times. Lysates were analyzed by immunoblotting with anti–c-Jun, anti–c-Myc, or anti-tubulin. The signals for c-Jun (left) or c-Myc (right) were scanned to compare the amount in control (time 0). *$P < 0.05$. Data represent mean ± SD. (**B**) U2OS cells were transfected with scrambled siRNA or DYRK2 siRNA and incubated with 10 μM MG-132 for 4 hours. Lysates were immunoprecipitated with rabbit IgG, anti–c-Jun, or anti–c-Myc followed by immunoblotting with anti-ubiquitin, anti–c-Jun, or anti–c-Myc. Lysates were also analyzed by immunoblotting with indicated antibodies (right panels). (**C**) U2OS cells were transfected with scrambled siRNA, DYRK2 siRNA, or Fbw7 siRNA. Lysates were immunoblotted with anti–c-Jun, anti–c-Myc, or anti-tubulin. The lanes separated by the white line were run on the same gel, but were noncontiguous. Total RNAs were analyzed by RT-PCR using *DYRK2*-specific, *Fbw7*-specific, or *actin*-specific primers.

sion of c-Jun/c-Myc (Figure 3C). Strikingly, depletion of Fbw7 elevated c-Jun/c-Myc expression regardless of DYRK2, to levels similar to those with DYRK2 depletion alone (Figure 3C). These findings clearly indicate that DYRK2 functions upstream of Fbw7. To determine the stability of the c-Jun/c-Myc mutant proteins in the priming sites, 293T cells were cotransfected with the Flag–c-Jun S243A mutant and scrambled siRNA or DYRK2 siRNA. Immunoblot analysis of anti-Flag revealed that the stability of the c-Jun S243A mutant remained constant regardless of DYRK2 status (Supplemental Figure 3E). Comparable results were obtained with the c-Myc S62A mutant (Supplemental Figure 3E). These findings suggest that mutations for the corresponding DYRK2 priming sites in c-Jun/c-Myc confer resistance to being phosphorylated by DYRK2/GSK3, followed by degradation. Taken together, these results collectively support a model in which sequential phosphorylation by DYRK2 followed by GSK3β destabilizes c-Jun and c-Myc to induce the Fbw7-mediated ubiquitination and subsequent proteasomal degradation.

Silencing DYRK2 accelerates the G_1/S transition. The findings that DYRK2 controls destruction of c-Jun and c-Myc provided us with the further notion that DYRK2 affects the G_1/S transition coupled with c-Jun and c-Myc. c-Jun expression was increased at 1–2 hours and then markedly declined in control cells (Figure 4A). In contrast, in cells silenced for DYRK2, expression of c-Jun was constant from 1 to 8 hours (Figure 4A). Serum refeeding into serum-starved cells was also associated with a transient augmentation and subsequent decline of c-Myc expression (Figure 4A). In contrast, deprivation of DYRK2 abrogated downregulation of c-Myc expression (Figure 4A). We also assessed the phosphorylation status of endogenous c-Myc. The priming phosphorylation of endogenous c-Myc at Ser62 was detectable at 4 to 8 hours after serum stimulation (Figure 4A). In contrast, Ser62 phosphorylation was completely revoked in cells silenced for DYRK2, suggesting that endogenous DYRK2 is responsible for Ser62 phosphorylation. Phosphorylation of c-Myc at Thr58 by GSK3β occurred at 8 hours, thus indicating that this modification

research article

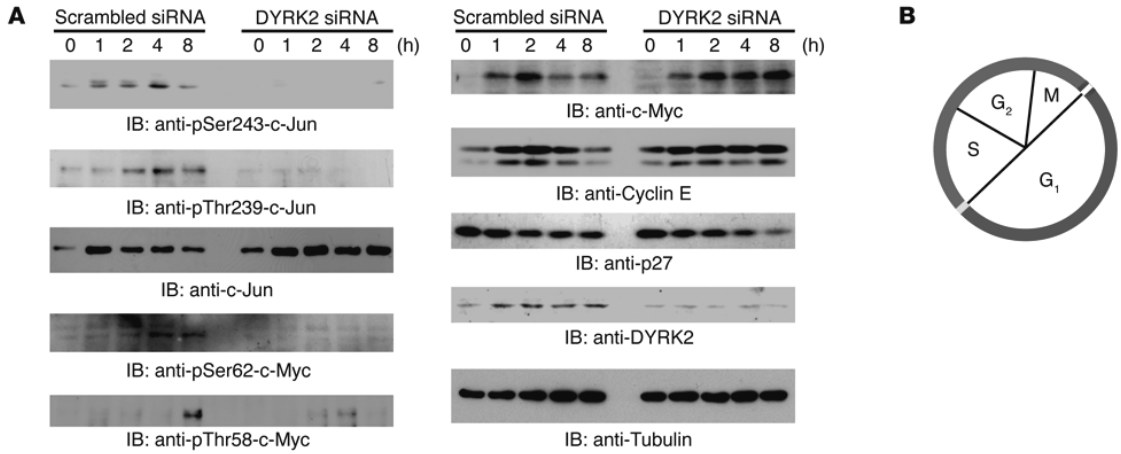

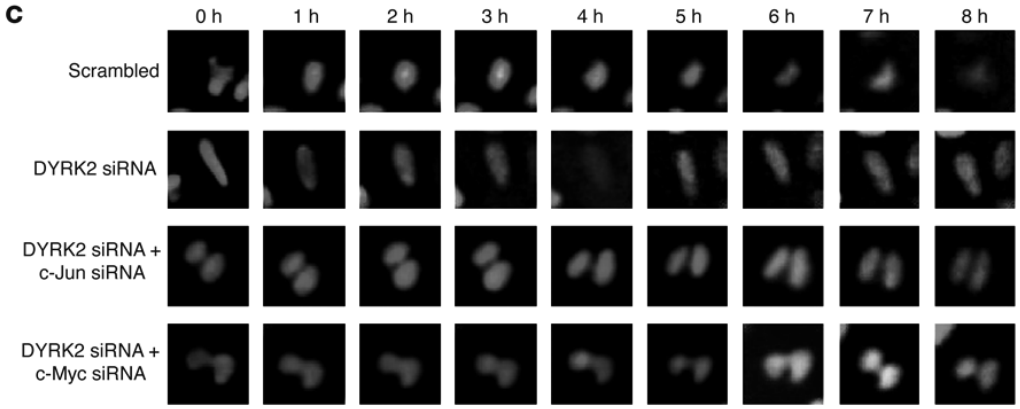

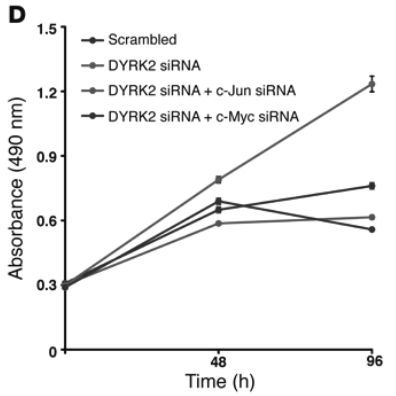

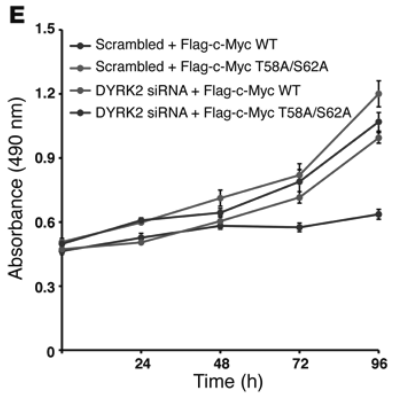

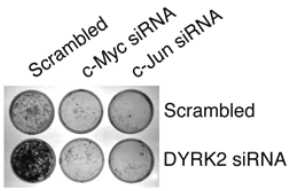

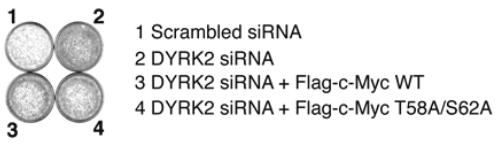

Figure 4
The G_1/S transition is accelerated in DYRK2-depleted cells. (**A**) U2OS cells were transfected with scrambled siRNAs or DYRK2 siRNAs, followed by serum starvation and stimulation for the indicated amount of time. Lysates were subjected to immunoblot analysis with the indicated antibodies. (**B**) Schematic depiction of Fucci system. (**C**) Fucci-expressing HeLa cells were transfected with scrambled siRNA or DYRK2 siRNA. Culture medium was changed to DMEM containing 0.25% serum. After refeeding with serum, cells were subjected to time-lapse fluorescence microscopy. (**D**) U2OS cells were transfected with scrambled siRNA, DYRK2 siRNA, c-Jun–specific siRNA, or c-Myc–specific siRNA. After transfection, cells were subjected to the MTS assay (upper panel) or the colony formation assay (lower panel). (**E**) U2OS cells were cotransfected with scrambled siRNA or DYRK2 siRNA and Flag–c-Myc WT or Flag–c-Myc T58A/S62A. After transfection, cells were subjected to the MTS assay (upper panel) or the colony formation assay (lower panel). Data represent mean ± SD.

follows Ser62 phosphorylation by DYRK2 (Figure 4A). Importantly, the finding that depletion of DYRK2 impaired Thr58 phosphorylation demonstrated that DYRK2-mediated priming phosphorylation is a prerequisite for subsequent phosphorylation of c-Myc by GSK3β. Similar characteristics, albeit occurring prior to the phosphorylation of c-Myc, were observed in endogenous c-Jun phosphorylation (Figure 4A). Coincident with the expression levels of c-Jun or c-Myc, their target gene controlling the G_1/S transition, cyclin E, exhibited enhanced and prolonged expression in cells silenced for DYRK2 (Figure 4A). As expected, degradation of G_1/S cyclin/cdk inhibitor p27Kip1 by cyclin E/cdk2 phosphorylation was promoted in DYRK2-depleted cells (Figure 4A). To visualize the cell cycle progression, we utilized fluorescent, ubiquitination-based cell cycle indicator, (Fucci) technology, which can distinguish cells in the G_1 phase from those in the S/G_2/M phases (Figure 4B and ref. 23). Fucci-expressing HeLa cells were serum starved for synchronization prior to transfection with siRNAs. Cells were then stimulated with serum under time-lapse imaging using computer-assisted fluorescence microscopy. As expected, cell nuclei were visualized in red, indicating that cells were in the G_1 phase. In control cells, the G_1/S transition was around 8 hours after serum refeeding (Figure 4C). In contrast, onset of the S phase was at 4 hours after serum stimulation in DYRK2-depleted cells (Figure 4C). Intriguingly, depletion of c-Jun/c-Myc rescued aberrant S phase entry in cells silenced for DYRK2 (Figure 4C). These findings indicated that impairment of DYRK2 is associated with accelerated progression of the G_1 phase. Serum-starved cells entered the S phase around 8 hours following serum stimulation. In contrast, depletion of DYRK2 accelerated the onset of S phase at 4 hours. To extend these findings, we analyzed the growth rate of U2OS cells by MTS assays. As shown previously (Figure 1B and Supplemental Figure 1B), knocking down DYRK2 alone accelerated cell growth. In contrast, deprivation of c-Jun/c-Myc normalized dysregulated cell growth elicited by DYRK2 depletion (Figure 4D). Similar results were obtained in colony formation assays with U2OS cells (Figure 4D) and HeLa cells (Supplemental Figure 4G). To determine whether priming phosphorylation of c-Myc affects proliferation of cells, we carried out MTS assays. Ectopic expression of the c-Myc T58A/S62A mutant, but not c-Myc–WT, accelerated proliferation of U2OS cells (Figure 4E). Moreover, DYRK2 silencing elevated cell growth regardless of c-Myc phosphorylation status, suggesting that abrogation of c-Myc priming phosphorylation by DYRK2 is associated with induction of aberrant cell growth (Figure 4E). Similar findings were obtained in colony formation assays (Figure 4E). Taken together, these results indicate that DYRK2 governs proper progression from G_1 to S phase by controlling c-Jun and c-Myc via priming phosphorylation.

DYRK2 depletion enhances tumor growth. To determine whether abrogation of DYRK2 expression affects tumor cell growth, scrambled siRNA or DYRK2 siRNA was cotransfected together with GFP vector or DYRK2 variants into HeLa cells (Supplemental Figure 4A). Analysis of colony formation assays revealed that knockdown of DYRK2 was associated with aberrant proliferation (Supplemental Figure 4B). Significantly, this dysregulation of cell growth was overcome by ectopic expression of rDYRK2 WT, but not rDYRK2-KR (Supplemental Figure 4B). Comparable results were obtained in U2OS cells (Supplemental Figure 4, A and B). To extend these findings in vivo, transduced HeLa cells were injected subcutaneously into the flanks of nude mice. In concert with in vitro data from colony formation assays, impairment of DYRK2 in HeLa cells was associated with a significant acceleration of tumor growth (Supplemental Figure 4, C and D). Moreover, elevated tumor growth by endogenous DYRK2 silencing was markedly attenuated in exogenous expression of rDYRK2 WT, but not rDYRK2-KR (Supplemental Figure 4, C and D). These results indicate that DYRK2 controls tumor progression in a kinase activity–dependent manner. We assessed the expression levels of DYRK2 in enucleated tumors from HeLa xenografts. Both analyses of RT-PCR and immunostaining indicated that DYRK2 expression was attenuated in tumors (Supplemental Figure 4, E and F). These results provide evidence that transient transfection of DYRK2 siRNA into HeLa cells sustained knockdown efficiency in vivo by an unknown mechanism. In this context, a previous study reported that depletion of ILK expression prior to introduction of cells by siRNAs into the mouse xenograft model resulted in striking and sustained in vivo effects on tumor growth and apoptotic and angiogenic characteristics (24), implying a more permanent alteration by siRNA transfection of cells in vivo. To extend and confirm findings with transient siRNA transfection, we established stably DYRK2-depleted cells. MCF-7 cells were transfected with pSuper vector or pSuper DYRK2 shRNAs. Knockdown of DYRK2 was confirmed by RT-PCR (Figure 5, A and B) and immunoblotting (Figure 5B). Interestingly, the protein expression of c-Jun, c-Myc, and cyclin E were all upregulated in MCF-7 cells stably silenced for DYRK2 (Figure 5B). Importantly, transcripts of *c-Jun* and *c-Myc* remained unchanged, whereas transcript of *cyclin E* was markedly elevated in DYRK2-depleted cells (Figure 5B). These findings suggest that stable deprivation of DYRK2 hinders consistent degradation of c-Jun/c-Myc to augment their transcriptional target in the G_1/S cyclin, cyclin E. In concert with the data obtained using siRNA transfection (Figure 1B and Supplemental Figure 1B), stable knockdown of DYRK2 strikingly elevated cell growth (Figure 5C). In addition, as previously shown in the transient transfection studies (Figure 1A, Supplemental Figure 1A, and Supplemental Figure 4B), colony formation assays revealed that stable knockdown of DYRK2 was associated with aberrant proliferation (Figure 5D). We further conducted in vivo tumorigenicity experiments with MCF-7 cells stably silenced for DYRK2. No marked tumor growth has been observed in mice injected with mocked MCF-7 cells (Figure 5, E and F). In stark contrast, similarly shown in xenograft studies with HeLa cells transiently transfected with DYRK2 siRNA (Supplemental Figure 4C), stable depletion of DYRK2 significantly accelerated tumor growth (Figure 5, E and F). As shown in HeLa xenografts (Supplemental Figure 4F), immunohistochemical analysis at sacrifice demonstrated that depletion of DYRK2 xenografts displayed dramatically elevated expression of c-Jun/c-Myc compared with controls, supporting the conclusion

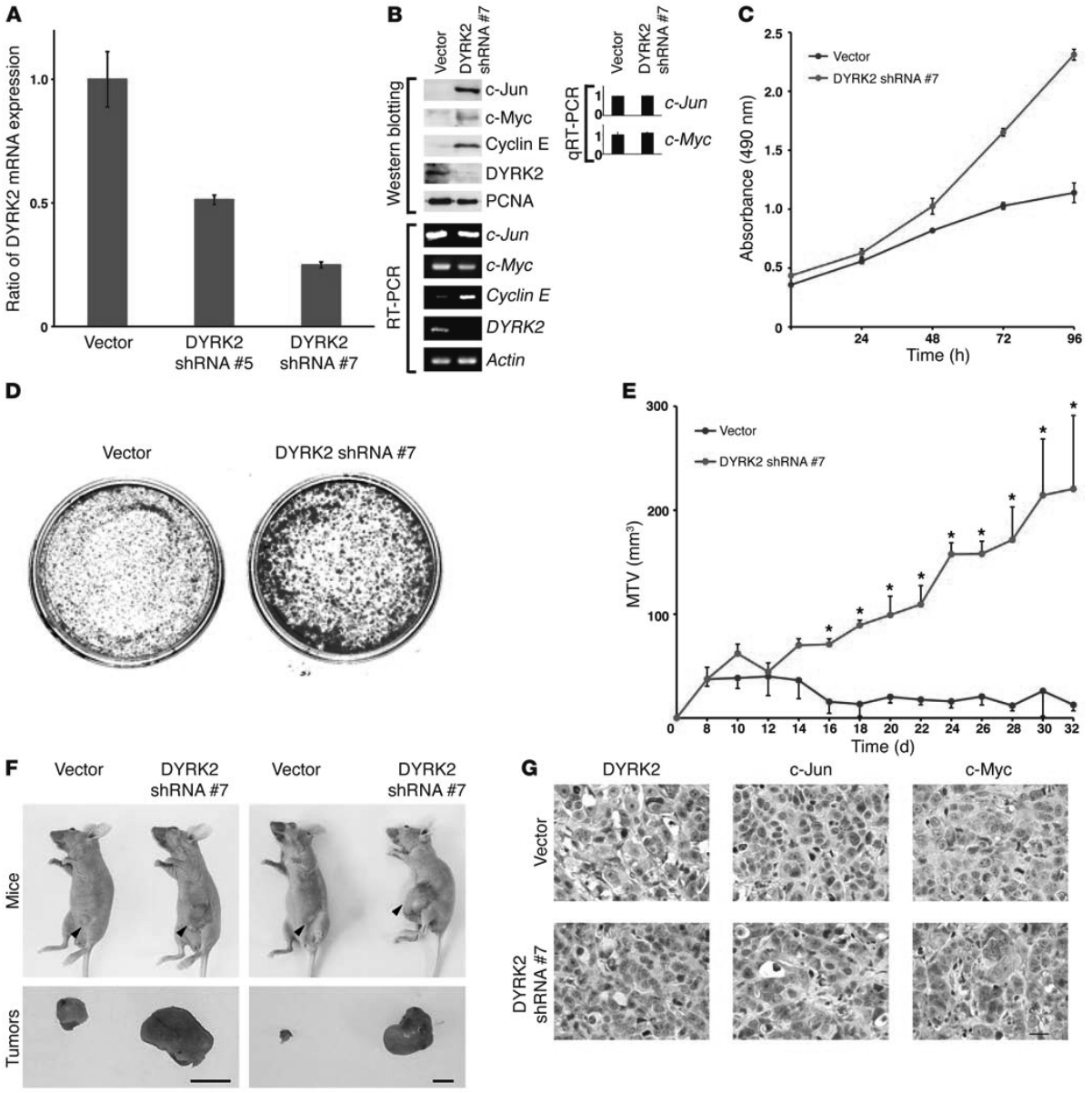

Figure 5

Stable knockdown of DYRK2 elevates tumor growth in vitro and in vivo. (**A**) MCF-7 cells were transfected with pSuper vector or pSuper-DYRK2 shRNA. To isolate stable shRNA-expressing cells, transfected cells were selected with puromycin. Knockdown efficiency of DYRK2 was monitored by quantitative RT-PCR. (**B**) Lysates form MCF-7 cells stably expressing vector (vector) or pSuper DYRK2 shRNA (DYRK2 shRNA #7) were analyzed by immunoblotting with indicated antibodies. Total RNAs were analyzed by RT-PCR. The result of quantitative RT-PCR was normalized for the level of *Actin* and represents the relative fold induction compared with control sample. The data were evaluated from 3 independent experiments, each performed in triplicate. (**C** and **D**) Cell growth was analyzed by the MTS assay (**C**) or the colony formation assay (**D**). (**E** and **F**) Transduced MCF-7 cells with 50% matrigel were inoculated into the opening of the lactiferous duct in the abdominal mammary gland in BALB/c nu/nu mice implanted with 17β-estradiol tablets. Tumor size was measured using calipers (n = 3). Data (maximum tumor volume [MTV]) indicate mean ± SD (**E**). *P < 0.05. Representative pictures of tumor-bearing nude mice (upper panels) and tumors (lower panels), which were taken 10 weeks after inoculation (**F**). Arrowheads indicate inoculated tumors. Scale bar: 10 mm. (**G**) Enucleated tumors were subjected to immunostaining with anti-DYRK2, anti–c-Jun, or anti–c-Myc. Scale bar: 50 μm.

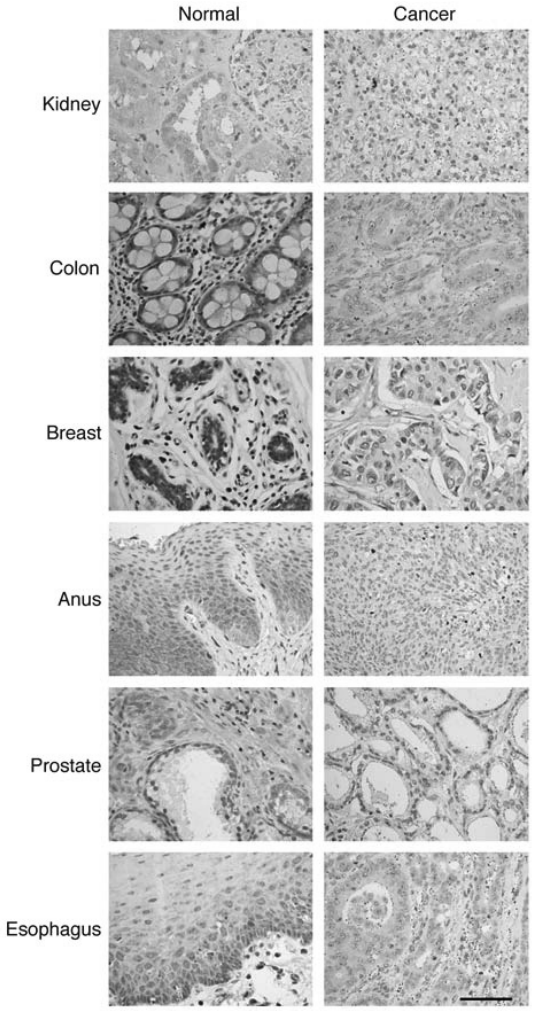

Figure 6
Downregulation of DYRK2 in various human tumor tissues. Immunohistochemical staining of anti-DYRK2 was performed using multiple cancerous and corresponding normal tissue microarrays. Scale bar: 200 μm.

that DYRK2 is a negative regulator of c-Jun/c-Myc stability (Figure 5G). These findings demonstrate that knockdown of DYRK2 confers aberrant growth of various carcinoma cells in in vivo tumor models. To further assess whether DYRK2 abrogation–induced tumor cell proliferation requires c-Myc and c-Jun, scrambled siRNA or DYRK2 siRNA was cotransfected together with c-Myc siRNA or c-Jun siRNA into HeLa cells. Analysis of colony formation assays revealed that, as shown previously, depletion of DYRK2 conferred accelerated proliferation (Supplemental Figure 4G). Moreover, this dysregulation of cell growth was completely overcome by codeprivation of c-Myc or c-Jun. Consistent results were obtained in U2OS cells (Figure 4D). These data suggest that regulation of cell growth by DYRK2 depends upon c-Myc or c-Jun. To strengthen these findings in vivo, transfected HeLa cells were injected subcutaneously into the flanks of nude mice. Coincident with the data obtained from colony formation assays, codepletion of c-Myc or c-Jun completely cancelled facilitation of tumor growth driven by silencing of DYRK2 alone (Supplemental Figure 4, H and I; also see Supplemental Figure 4C). Taken together, these findings indicate that DYRK2 contributes to growth of carcinoma cells in in vivo tumor models.

DYRK2 expression is reduced or abolished in multiple human tumor tissues. To assess the physiological relevance of our results to the biology of human cancers, we investigated DYRK2 expression using tissue microarrays derived from distinct human tumor tissues. Analysis of immunohistochemistry with anti-DYRK2 revealed that DYRK2 expression was positive and intact in all normal tissues (Figure 6). In contrast, DYRK2 was markedly attenuated or abolished in tumor samples originating from tissues such as breast, colon, esophagus, anus, prostate, kidney, and hypopharynx (Figure 6 and data not shown). These findings thus provide a potential correlation between downregulation of DYRK2 expression and carcinogenesis or tumor progression.

Downregulation of DYRK2 correlates with the invasiveness of human breast cancers. To further define a biological role for DYRK2 in carcinogenesis or tumor progression, we focused on human breast cancers, since aberrant activation of c-Jun and c-Myc affects progression of breast cancers (25, 26). To initially examine protein levels of DYRK2 in human breast cancers, we obtained samples of breast cancerous tissues and concomitant normal tissues from 20 patients with various stages of breast cancers. The ratios of DYRK2-positive cells were scored to categorize its expression levels into 4 grades, which were defined as follows: negative, 0; weak, greater than 0 to 1/3; moderate, greater than 1/3 to 2/3; and strong, greater than 2/3 to 1 (Supplemental Figure 5). In all normal tissues, DYRK2 was highly expressed to levels classified into moderate or strong, both of which were clustered as a high group (Table 1). Similar findings were obtained in noninvasive breast cancer tissues (Table 1). In contrast, in 6 out of 11 invasive breast cancer tissues, DYRK2 expression was significantly decreased to levels classified into weak or negative, both of which were categorized as a low group (Table 1 and Figure 7A). These results suggest the possibility that downregulation of DYRK2 contributes to the invasive potential of human breast cancers. We further examined the expression of c-Jun, c-Myc, and cyclin E in the invasive ductal breast cancer tissues. Positive expression was significantly higher in tissues in the low DYRK2 group compared with those in the high DYRK2 group (Table 2). This finding thus indicated that the accumulation of c-Jun, c-Myc, and cyclin E is inversely correlated with the expression level of DYRK2. Since DYRK2 phosphorylation of c-Jun and c-Myc targets them for degradation, we explored a potential correlation between expression levels of DYRK2 and phosphorylation levels of c-Jun and c-Myc in the invasive ductal breast cancer tissues. In samples from the high group of DYRK2, more than 50% of cells stained positive for phospho–c-Jun at Ser243 or phospho–c-Myc at Ser62 (Table 3 and Figure 7B). In stark contrast, the percentages of cells with phosphorylated c-Jun or c-Myc were significantly attenuated in samples from the low group of DYRK2 (Table 3 and Figure 7B). These findings support a model in which downregulation of DYRK2 stabilizes c-Jun and c-Myc to accelerate tumor progression and invasion (Figure 8).

Discussion

We report here for what we believe is the first time that DYRK2 functions as a priming kinase of GSK3β for destroying c-Jun or c-Myc at the G_1/S transition. Previous studies have demonstrated that c-Jun and c-Myc are coordinately regulated by GSK3β and

Table 1
Expression levels of DYRK2 in normal breast tissues and noninvasive and invasive breast ductal carcinomas

	Negative	Weak	Moderate	Strong	High DYRK2 (%)
Normal (n = 20)	0	0	4	16	100
Noninvasive (n = 9)	0	0	0	9	100
Invasive (n = 11)	1	5	4	1	45.45

Expression levels of DYRK2 were classified into 4 grades (see Supplemental Figure 5).

the ubiquitin ligase Fbw7 (6). Growth stimulation in the early G_1 phase induces Akt that phosphorylates and inactivates GSK3β (27). Conversely, Akt activity markedly diminishes in the late G_1 phase, which triggers reactivation of GSK3β. In this model, GSK3β phosphorylation of c-Jun and c-Myc requires priming phosphorylation at Ser residues. Indeed, identification of priming kinases has been studied; however, little is known about physiological kinases. Moreover, to our knowledge, there is no report demonstrating that a single kinase contributes to priming phosphorylation of both c-Jun and c-Myc. Intriguingly, c-Jun and c-Myc were simultaneously destroyed at the late G_1 phase. Given the fact that these oncogenes are regulated by the common kinase GSK3β and the common ubiquitin ligase Fbw7, it is conceivable that there should be a common priming kinase. In this context, the present study delineates DYRK2 kinase as a candidate. We further demonstrate indispensable prephosphorylation by DYRK2 in GSK3β-mediated degradation of c-Jun and c-Myc. In this regard, previous studies have shown that GSK3β activity inversely reflects expression levels of c-Jun and c-Myc in the G_1 phase (10). Nonetheless, deprivation of DYRK2 rendered GSK3β unable to phosphorylate c-Jun and c-Myc, regardless of GSK3β activity. Collectively, these data suggest that sequential phosphorylation of DYRK2 followed by GSK3β constitutes a fail-safe mechanism that accurately regulates the degradation of these proteins.

While accumulating studies have ensured a requirement of priming phosphorylation for GSK3β-mediated destruction, biological roles for priming phosphorylation on c-Jun or c-Myc are controversial. A previous study showed that Ser62 phosphorylation stabilizes c-Myc (28). In contrast, other studies demonstrated that abrogation of Ser243 phosphorylation by mutation or dephosphorylation stabilizes c-Jun, resulting in an increase in c-Jun–induced gene expression (10, 29). These findings thus indicate opposite roles for priming phosphorylation: stabilization for c-Myc and destabilization for c-Jun. We are unable to distinctly explain this apparent inconsistency. In any case, however, priming phosphorylations of c-Jun and c-Myc are eventually triggered for Fbw7-mediated proteolysis. It should be noted that the study conducted by Sears et al. (28) was based on the overexpression of the c-Myc S62A mutant in quiescent cells. In this context, it could not exclude the possibility that conformational changes elicited by S62A mutation might render c-Myc more susceptible to being destroyed by Fbw7 or undefined ubiquitin ligases. Obviously, further studies are needed to clarify this issue. Instead, at least in the G_1/S transition in proliferating cells, our data clearly demonstrate that loss of phosphorylation by DYRK2 allows c-Jun and c-Myc to escape from ubiquitin-mediated destruction. It is thus likely that DYRK2 phosphorylation of c-Jun and c-Myc is a licensing event that allows GSK3β to phosphorylate them, thus targeting them for degradation. Significantly, elevated and stable expression of c-Jun and c-Myc induced by stably knocking down DYRK2 exhibited dysregulation of transactivation targets, especially those controlling the G_1/S transition, such as cyclin E. As a consequence, we observed accelerated proliferation, presumably due to premature progression through the G_1 phase (Figure 1). In concert with these in vitro data, we revealed that downregulation of DYRK2 potentiates facilitation of tumor growth in xenograft models (Figure 5E and Supplemental Figure 4C). Strikingly, this growth advantage was completely abrogated by codeprivation with c-Jun or c-Myc in vivo (Supplemental Figure 4H). Taken together, our findings support a model in which DYRK2 controls cell proliferation via c-Jun and c-Myc.

As found for c-Jun and c-Myc, GSK3β phosphorylation recruits ubiquitin ligases for degradation of substrates, such as cdc25A, Mcl-1, PRLr, and cyclin D (30–34). However, in contrast to c-Jun and c-Myc, these substrates are modified by distinct ubiquitin ligases despite coordinate phosphorylation by GSK3β. While each of the priming kinases themselves remain unclear, we speculate that a priming phosphorylation, rather than GSK3 phosphorylation, determines the specificity for the ubiquitin ligase. In this regard, it is plausible that the recruitment of Fbw7 could predominately stipulate priming phosphorylation by DYRK2.

Dysregulated expression of c-Myc/c-Jun exerts significant roles on cell cycle progression. A reduction in c-Myc levels results in a length-

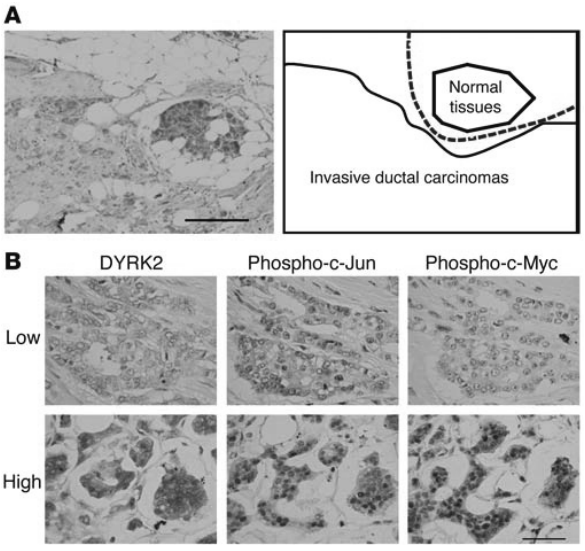

Figure 7
DYRK2 inactivation is associated with the impairment of c-Jun/c-Myc phosphorylation and with aggressiveness of human breast cancers. (**A**) Representative immunohistochemical staining of DYRK2 protein in the breast cancer specimen (left panel). Scale bar: 500 μm. Schematic depiction for the boundary of the normal tissues and invasive breast ductal carcinomas shown in the left panel (right panel). (**B**) Mutual analysis for the expression level of DYRK2 and the phosphorylation status of c-Jun/c-Myc in invasive human breast cancers. Representative immunohistochemical staining of anti-DYRK2, anti–phospho–c-Jun(Ser243), and anti–phospho–c-Myc(Ser62) are shown. Scale bar: 150 μm.

Table 2
Mutual analysis for the expression levels of DYRK2 and c-Jun, c-Myc, or cyclin E in invasive human breast cancers by immunohistochemistry

	Expression level of DYRK2[A]		
	High	Low	*P* value[B]
c-Jun	64.68	85.35	<0.001
c-Myc	67.93	88.93	<0.001
Cyclin E	11.19	38.61	<0.001

Data represent the percentage of cancer cells positive for immunoreactivity from invasive human breast cancers (n = 11). [A]Expression levels of DYRK2 were evaluated and categorized into 2 groups, the high-expression group (including moderate and strong categories) and the low-expression group (including negative and weak categories). [B]*P* values were calculated using Mann-Whitney *U* test.

ened G_1 phase, with concomitant delayed expression of cyclin E, whereas ectopic expression of c-Myc leads to a shortened G_1 phase mainly due to cyclin E overexpression (35–37). Furthermore, accumulating studies have demonstrated that overexpression of cyclin E shortens the G_1 phase and accelerates the G_1/S transition (38–41), indicating that cyclin E expression directly precedes the transition from the G_1 to the S phase. Indeed, the cyclin E/cdk2 phosphorylation of p27Kip1 triggers its degradation to induce an exit from the G_1 phase (42). This evidence supports our findings that sustained expression of c-Jun/c-Myc by DYRK2 knockdown accelerates G_1/S transition attributable to elevated expression of cyclin E accompanied with expedited degradation of p27/Kip1 (Figure 4A). Importantly, a shortened G_1 phase is one of the prominent characteristics in cancer progression. This may at least in part be explained by our results showing that impaired DYRK2 correlates with the invasiveness of breast cancers. A recent study demonstrated that DYRK2 phosphorylates katanin p60 for its degradation and controls mitotic transition in HeLa cells (18). Similarly, our findings revealed relative increments of the G_2/M phase in HeLa cells depleted for DYRK2. However, calculated duration of the G_2/M phase in DYRK2-deprived cells was comparable with that in mocked cells. Instead, duration of the G_1 phase was markedly reduced in DYRK2-depleted HeLa cells (Figure 1D). Based on our findings, we thus concluded that DYRK2 controls the cell cycle at the G_1 phase, whereas we cannot exclude the possibility that DYRK2 plays a role in mitosis. Indeed, the length of the G_2/M phase was (not statistically significant but) still substantially augmented in cells silenced for DYRK2 (Figure 1D and Supplemental Figure 1D). These findings suggest the possibility that DYRK2 regulates the cell cycle at G_1/S and/or G_2/M transitions by distinct mechanisms.

Dysregulated expression of c-Myc/c-Jun also exerts critical influences on cancer progression. For example, high c-Myc expression by missense mutations in many human hematopoietic malignancies has been correlated with a poor prognosis (43). Intriguingly, the majority of the mutations reside within the aminoterminal transactivation domain of c-Myc including Thr58 and Ser62 in Burkitt's lymphoma (44). Importantly, somatic mutations of c-Myc at Thr58 and Ser62 and their flanking amino acids confer increased oncogenic activity in Burkitt's lymphoma (45), suggesting that phosphorylation of these sites leads to downregulation of c-Myc growth-promoting activity. Consistent with this is the finding that v-myc oncogenes frequently contain mutations in these phosphorylation sites (46, 47). Similar findings were observed with oncogenic v-Jun, in which the priming phosphorylation residue coinciding with c-Jun Ser243 is mutated to Phe (48). In contrast, another study demonstrated that normal mammary epithelial cells exhibited low c-Myc Ser62 phosphorylation, whereas invasive adenocarcinoma showed high Ser62 phosphorylation together with high c-Myc levels (49). It is conceivable that if GSK3β is inactivated, phospho-Ser62 is upregulated but phospho-Thr58 is downregulated; thus, c-Myc is accumulated, which is frequently observed in breast cancers (50). Notably, we found that impairment of priming phosphorylation in c-Myc and c-Jun by silencing DYRK2 increased cell proliferation as well as tumor growth. Collectively, lack of priming phosphorylation in c-Myc or c-Jun would be suspected for contribution to cancer development. In this context, our findings that robust correlation between DYRK2 inactivation and impaired phosphorylation of c-Jun and c-Myc in advanced human breast cancers imply that dysregulation of DYRK2 could trigger enhanced migration and invasion of tumors. In agreement with this model, accumulation of unphosphorylated c-Jun or c-Myc contributes to tumor progression. In this context, besides c-Jun and c-Myc, substrates for DYRK2 are largely unknown. It is thus possible that DYRK2 may phosphorylate unknown targets that are associated with cell proliferation or tumor progression. Considering this and given the previous findings that DYRK2 phosphorylates p53 at Ser46 to induce apoptosis in response to DNA damage (20), we are now investigating the hypothesis that DYRK2 exerts suppressive function for tumor development.

Until now, dysregulation of DYRK2 expression in human cancer has also been uncertain. DYRK2 is harbored at the locus on the chromosome 12q15 region, which is frequently amplified in various cancers. Importantly, MDM2 is mapped to the same locus, suggesting the possibility that DYRK2 and MDM2 exhibit genetic linkage on expression (51). Despite the amplification of copy number at 12q15, to our knowledge, no study has been carried out to assess DYRK2 expression at the protein levels. In contrast, accumulating reports employed upregulation of MDM2 expression at the protein levels in various tumor tissues. In this regard, our recent findings indicate that DYRK2 is constitutively degraded by an MDM2-mediated ubiquitination and proteasome machinery (22). It is thus conceivable that overexpressed MDM2 is associated with attenuation or abrogation of DYRK2 expression at the protein level even if the *DYRK2* gene is amplified due to the 12q15 amplicon.

In conclusion, the present study demonstrates that DYRK2 controls cell cycle progression at the G_1/S phase via phosphorylation of c-Jun and c-Myc. DYRK2 inactivation contributes to cell prolifera-

Table 3
Mutual analysis for the expression level of DYRK2 and the phosphorylation status of c-Jun/c-Myc in invasive human breast cancers

	Expression level of DYRK2[A]		
	High	Low	*P* value[B]
Phospho–c-Jun	58.17	20.38	<0.001
Phospho–c-Myc	55.04	21.42	<0.001

Data represent the percentage of cancer cells positive for nuclear immunoreactivity with anti–phospho–c-Jun(Ser243) or anti–phospho–c-Myc(Ser62) from invasive human breast cancers (n = 11). [A]Expression levels of DYRK2 were evaluated and categorized into 2 groups, the high-expression group (including moderate and strong categories) and the low-expression group (including negative and weak categories). [B]*P* values were calculated using Mann-Whitney *U* test.

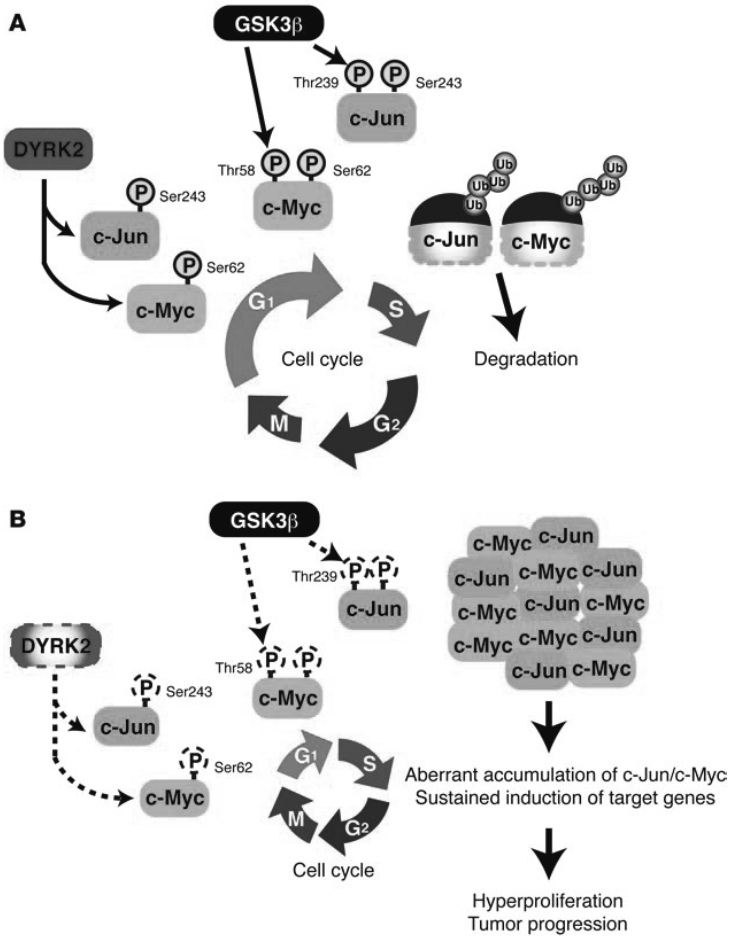

Figure 8
The model of DYRK2-mediated cell cycle regulation. (**A**) At the late G_1 phase, c-Myc and c-Jun are phosphorylated by DYRK2, which serves as a priming site for binding of GSK3β. GSK3β then obtains the license to phosphorylate (P) c-Jun and c-Myc via recognition of priming phosphorylation. Phosphorylated c-Jun and c-Myc bind to the ubiquitin ligase for their degradation. (**B**) In the absence of DYRK2, GSK3β is unable to phosphorylate c-Jun and c-Myc. Unphosphorylated c-Jun and c-Myc escape from the ubiquitin-mediated proteasomal degradation. Accumulation of c-Jun and c-Myc induces their target genes, such as cyclin E.

tion and tumor progression. We therefore propose that dissecting both DYRK2 expression and c-Jun/c-Myc phosphorylation could be valuable for the prognosis of invasiveness in tumors. Our results also emphasize the use of DYRK2 as a potential target of therapeutic intervention for advanced cancers, which may be achieved by restoring its expression and function.

Methods

Cell culture and treatment. U2OS (human osteosarcoma) cells were cultured in RPMI 1640 medium supplemented with 10% heat-inactivated fetal bovine serum, 100 units/ml penicillin, 100 μg/ml streptomycin, and 2 mM L-glutamine. 293T (human embryonal kidney), HeLa (human cervical carcinoma), and MCF-7 (human mammary carcinoma) cells were grown in DMEM containing 10% heat-inactivated fetal bovine serum, 100 units/ml penicillin, 100 μg/ml streptomycin, and 2 mM L-glutamine. Fucci-expressing HeLa cells were provided by Riken Cell Bank. Cells were treated with 40 μg/ml CHX (Merck).

Plasmid construction. Flag-tagged and GFP-tagged DYRK2 was constructed as described previously (20). c-Myc cDNA was cloned into the pcDNA3-Flag vector (52, 53). Flag-tagged c-Jun was a gift from S. Kitajima (Tokyo Medical and Dental University) (54). GSK3β cDNA was cloned into the pcDNA3-HA vector. Various mutations were introduced by site-directed mutagenesis. siRNA-resistant forms of DYRK2 were generated by introducing silent mutations in the targeting regions for DYRK2 siRNA.

Cell transfection. Plasmids were transfected using FuGENE 6 (Roche). DYRK2-specific siRNAs (QIAGEN, Invitrogen), c-Jun siRNA (Invitrogen), c-Myc siRNA (Invitrogen), Fbw7 siRNA (Nippon EGT), and negative control siRNAs (QIAGEN) were used. Transfection of siRNAs was performed using Lipofectamine 2000 and Lipofectamine RNAi MAX (Invitrogen). To isolate stable transfectants, MCF-7 cells were transfected with pSuper vector (Oligoengine) or pSuper DYRK2 shRNA in the presence of puromycin.

Immunoblotting and immunoprecipitation. Cells were washed twice in chilled PBS and resuspended in lysis buffer (50 mM Tris-HCl, pH 7.6, 150 mM NaCl, 10 mM NaF, 1 mM Na_3VO_4, 1 mM PMSF, 1 mM DTT, 10 μg/ml aprotinin, 1 μg/ml leupeptin, 1 μg/ml pepstatin A, and 1% NP-40). Cell extracts were centrifuged for 5 minutes at 4°C. Supernatants were separated by SDS-PAGE and transferred to nitrocellulose membranes. The membranes were incubated with anti–c-Jun (Santa Cruz Biotechnology Inc.), anti–phospho–c-Jun(Ser243) (Abcam), anti–phospho–c-Jun(Thr239) (Abcam), anti–c-Myc (Santa Cruz Biotechnology Inc.), anti–phospho–c-Myc(Thr58/Ser62) (Cell Signaling Technology), anti–phospho–c-Myc(Ser62) (MBL), anti–phospho–c-Myc(Thr58) (Abcam), anti-tubulin (Sigma-Aldrich), anti–cyclin E (Santa Cruz Biotechnology Inc.), anti-ubiquitin (Santa Cruz Biotechnology Inc.), anti-DYRK2 (Santa Cruz Biotechnology Inc.), anti-Flag (Sigma-Aldrich), anti-GFP (Nacalai Tesque), anti-PCNA (Santa Cruz Biotechnology Inc.), or anti-GST (Nacalai Tesque). Immune complexes were incubated with secondary antibodies and visualized by chemiluminescence (PerkinElmer). For endogenous c-Myc immunoprecipitation, cell lysates were incubated with anti–c-Myc (Santa Cruz Biotechnology Inc.) for 2 hours at 4°C and the beads were incubated with protein G–sepharose (Invitrogen). The beads were washed 3 times with the lysis buffer and boiled for 5 minutes. For immunoprecipitation of Flag-tagged proteins, lysates were incubated with anti-Flag agarose (Sigma-Aldrich). Immunoprecipitates were eluted with the Flag peptide (Sigma-Aldrich) as needed.

Cell growth assay. The number of viable cells was counted by trypan blue dye exclusion using a hemocytometer. For MTS assay, cells were seeded in 96-well plates and transfected as described (55). MTS assays were performed using CellTiter 96 AQ One Solution Cell Proliferation Assay Kit (Promega). The absorbance was measured at 490 nm with the use of a multilabel counter (PerkinElmer). Doubling time for cells was calculated as described (56). The length of each phase of the cell cycle was calculated as a product of the doubling time and the percentage of cells in a given phase, as measured by FACS analysis.

In vitro kinase assay. Recombinant His-DYRK2 and GST-GSK3β were obtained from Millipore and Invitrogen, respectively. Flag-DYRK2 was immunoprecipitated with anti-Flag agarose (Sigma-Aldrich) from 293T cells transfected with Flag-DYRK2. Immunoprecipitates were washed 3 times with lysis buffer and then with kinase buffer (20 mM HEPES, pH 7.0, 10 mM $MgCl_2$, 0.1 mM Na_3VO_4, and 2 mM DTT). As substrates, GST–c-Jun (amino acid residues 210–310) and GST–c-Myc (amino acid residues 1–100) were purified from *E. coli* cultures with GST-sepharose beads (GE Healthcare). Immunoprecipitates, GST-GSK3β, or His-DYRK2 was incubated in kinase buffer with substrates and ATP for 20 minutes at 30°C (57). Samples were boiled for 5 minutes and analyzed by SDS-PAGE.

RT-PCR analysis. Isolation of total RNA from cells or tumor tissues was performed using TRIsure (Nippon Genetics) according to the manufacturer's instructions. 500 ng of total RNA was amplified using the SuperScript III One-Step RT-PCR System with Platinum Taq Kit (Invitrogen). The reaction for RT-PCR was as follows: cDNA synthesis at 55°C for 30 minutes, denaturation at 94°C for 2 minutes, followed by 30 cycles at 94°C for 15 seconds, 55°C for 30 seconds, and 68°C for 30 seconds, with a final extension at 68°C for 5 minutes. PCR products were separated by 2% agarose gels. For quantitative RT-PCR analysis, total RNA was reverse transcribed into cDNA using a PrimeScript 1st strand cDNA Synthesis Kit (Takara) following the manufacturer's protocol. The PCR reaction was performed by using KAPA SYBR FAST ABI Prism 2X qPCR Master Mix (Nippon Genetics) according to the instruction manual. Primer sequences are described as follows: c-Jun, 5′-TGACTGCAAAGATGGAAACG-3′ and 5′-CAGGGTCATGCTCTGTTTCA-3′; c-Myc, 5′-TCAAGAGGCGAACACACAAC-3′ and 5′-GGCCTTTTCATTGTTTTCCA-3′; DYRK2, 5′-GGGGAGAAAACGTCAGTGAA-3′ and 5′-TCTGCGCCAAATTAGTCCTC-3′; cyclin E, 5′-ATCCTCCAAAGTTGCACCAG-3′ and 5′-AGGGGACTTAAACGCCACTT-3′; GAPDH, 5′-TCAAGGCTGAGAACGGGAAG-3′ and 5′-ATGGTGGTGAAGACGCCAGT-3′; and actin, 5′-GTGGCCGAGGACTTTGATTG-3′ and 5′-TGGAVTTGGGAGAGGCTGG-3′.

Colony formation assay. Cells were washed with chilled PBS and fixed with 70% ethanol for 30 minutes at –20°C. After fixation, cells were stained using Giemsa Solution (Wako) for 10 minutes at room temperature. The cells were then washed with PBS twice.

Cell cycle analysis. Cells were washed with chilled PBS and resuspended with PBS. Cells were incubated with RNase and propidium iodide for 30 minutes at 37°C. Data from the flow cytometry were acquired and analyzed using CytoSoft software (Guava Technologies).

Imaging of Fucci-expressing cells. Fucci-expressing HeLa cells (23) were transfected with scrambled siRNA or DYRK2-specific siRNA. Serum-starved cells were released by stimulation with serum, and the time-lapse images were acquired at 20-minute intervals using a fluorescence microscope (BioZero BZ-8000; Keyence) equipped with a phase difference lens (Nikon). For fluorescence imaging, the halogen lamp was used with excitation (BP520-540HQ) and emission (BP555-600HQ) filters. Image acquisition and analysis were performed using analyzer software (BZ-H1TL; Keyence).

In vivo tumorigenicity studies. Seven-week-old nude mice (BALB/c, nu/nu, SLC) were housed under pathogen-free conditions. HeLa cells (1×10^7) were subcutaneously injected with a 26-gauge needle. For MCF-7 cell–derived xenografts, mice were implanted with the E2 pellet (Innovative Research of America) and inoculated with 5×10^6 cells suspended in matrigel (BD Biosciences) into the abdominal mammary gland. Tumor size was monitored every 2 days using calipers. Frozen or paraffin-embedded tumor samples were immunostained with anti-DYRK2, anti–c-Jun, or anti–c-Myc.

Immunohistochemistry. Tissue microarrays were purchased from Provitro. Immunostaining was detected by the avidin–biotin–peroxidase method according to the manufacturer's instructions (Vectastain ABC Kit; Vector Laboratories). For antigen retrieval, slides were microwaved for 20 minutes in sodium citrate buffer. After blocking endogenous peroxidase, the sections were incubated with normal serum and then incubated at 4°C overnight with anti-DYRK2 (Abgent), anti–c-Jun (Santa Cruz Biotechnology Inc.), anti–c-Myc (Santa Cruz Biotechnology Inc.), anti–cyclin E (Santa Cruz Biotechnology Inc.), anti–phospho–c-Jun(Ser243) (Abcam), and anti–phospho–c-Myc(Thr58/Ser62) (Cell Signaling Technology). Evaluation of the staining has been performed by pathologists using a light microscope. Scoring was based on examining all tumor cells on the slide. The evaluations were recorded as the proportion of positive cells in each of 4 proportion categories that were denoted as negative, weak, moderate, and strong. The categories were also divided into 2 groups, consisting of high-expression groups (including moderate and strong categories) and low-expression groups (including negative and weak categories). For phospho–c-Jun and phospho–c-Myc staining, only the nuclear staining was taken into consideration. For the evaluation, 3 fields at a magnification of ×400 were captured randomly from each slide, and the results are represented as the percentage of positive staining. In cases with carcinoma in situ and invasive carcinoma in the same specimen, only the invasive component was counted.

Statistics. Statistical analysis was performed with 2-tailed *t* tests. Data represent the mean ± SD. The Mann-Whitney *U* test was also used to compare frequencies in the contingency tables. $P < 0.05$ was considered statistically significant.

Study approval. Animal experiments were approved by the Animal Research Committee of Tokyo Medical and Dental University and were performed in accordance with established guidelines. The use of tissue specimens was reviewed and approved by the ethical committee of Tokyo Medical and Dental University. The samples were retrospectively acquired from the surgical pathology archives of Tokyo Medical and Dental University and did not directly involve human subjects; the study was considered no more than minimal risk. In accordance with Ethical Guidelines for Clinical Studies from the Ministry of Health, Labour and Welfare, Japan, informed consent has been obtained via disclosing information, along with specification that coded or anonymous leftover material is used for research and patients have been offered the option to opt out.

Acknowledgments

We thank Masabumi Shibuya, Tsuyoshi Osawa, Masashi Muramatsu, and Miori Inoue for technical assistance. We also thank Shigetaka Kitajima for c-Jun cDNA. This work was supported by grants from the Ministry of Education, Science and Culture of Japan (to N. Taira, Y. Miki, and K. Yoshida), the Yasuda Memorial Foundation (to N. Taira), the Uehara Memorial Foundation (to K. Yoshida), the Takeda Science Foundation (to K. Yoshida), the Sankyo Foundation of Life Science (to K. Yoshida), the Sato Memorial Foundation for Cancer Research (to K. Yoshida), the Ichiro Kanehara Foundation (to K. Yoshida), the Terumo Life Science Foundation (to K. Yoshida), the Foundation for Promotion of Cancer Research (to K. Yoshida), and the Kobayashi Foundation for Cancer Research (to K. Yoshida).

Received for publication September 1, 2011, and accepted in revised form December 21, 2011.

Address correspondence to: Kiyotsugu Yoshida, Department of Molecular Genetics, Medical Research Institute, Tokyo Medical and Dental University, 1-5-45 Yushima, Bunkyo-ku, Tokyo, 113-8510, Japan. Phone: 81.3.5803.5826; Fax: 81.3.5803.0242; E-mail: yos.mgen@mri.tmd.ac.jp.

research article

1. Hann SR. Role of post-translational modifications in regulating c-Myc proteolysis, transcriptional activity and biological function. *Semin Cancer Biol*. 2006;16(4):288–302.
2. Shaulian E, Karin M. AP-1 as a regulator of cell life and death. *Nat Cell Biol*. 2002;4(5):E131–E136.
3. Pelengaris S, Khan M, Evan G. c-MYC: more than just a matter of life and death. *Nat Rev Cancer*. 2002; 2(10):764–776.
4. DeSalle LM, Pagano M. Regulation of the G_1 to S transition by the ubiquitin pathway. *FEBS Lett*. 2001; 490(3):179–189.
5. Krek W. Proteolysis and the G_1-S transition: the SCF connection. *Curr Opin Genet Dev*. 1998;8(1):36–42.
6. Welcker M, Clurman BE. FBW7 ubiquitin ligase: a tumour suppressor at the crossroads of cell division, growth and differentiation. *Nat Rev Cancer*. 2008; 8(2):83–93.
7. Cohen P, Frame S. The renaissance of GSK3. *Nat Rev Mol Cell Biol*. 2001;2(10):769–776.
8. Cross DA, Alessi DR, Cohen P, Andjelkovich M, Hemmings BA. Inhibition of glycogen synthase kinase-3 by insulin mediated by protein kinase B. *Nature*. 1995;378(6559):785–789.
9. Doble BW, Woodgett JR. GSK-3: tricks of the trade for a multi-tasking kinase. *J Cell Sci*. 2003; 116(pt 7):1175–1186.
10. Wei W, Jin J, Schlisio S, Harper JW, Kaelin WG Jr. The v-Jun point mutation allows c-Jun to escape GSK3-dependent recognition and destruction by the Fbw7 ubiquitin ligase. *Cancer Cell*. 2005;8(1):25–33.
11. Luo J. Glycogen synthase kinase 3beta (GSK3beta) in tumorigenesis and cancer chemotherapy. *Cancer Lett*. 2009;273(2):194–200.
12. Frame S, Cohen P. GSK3 takes centre stage more than 20 years after its discovery. *Biochem J*. 2001; 359(pt 1):1–16.
13. Lutterbach B, Hann SR. Hierarchical phosphorylation at N-terminal transformation-sensitive sites in c-Myc protein is regulated by mitogens and in mitosis. *Mol Cell Biol*. 1994;14(8):5510–5522.
14. Lutterbach B, Hann SR. c-Myc transactivation domain-associated kinases: questionable role for map kinases in c-Myc phosphorylation. *J Cell Biochem*. 1999;72(4):483–491.
15. Boyle WJ, et al. Activation of protein kinase C decreases phosphorylation of c-Jun at sites that negatively regulate its DNA-binding activity. *Cell*. 1991;64(3):573–584.
16. Morton S, Davis RJ, McLaren A, Cohen P. A reinvestigation of the multisite phosphorylation of the transcription factor c-Jun. *EMBO J*. 2003; 22(15):3876–3886.
17. Yoshida K. Role for DYRK family kinases on regulation of apoptosis. *Biochem Pharmacol*. 2008; 76(11):1389–1394.
18. Maddika S, Chen J. Protein kinase DYRK2 is a scaffold that facilitates assembly of an E3 ligase. *Nat Cell Biol*. 2009;11(4):409–419.
19. Varjosalo M, et al. Application of active and kinase-deficient kinome collection for identification of kinases regulating hedgehog signaling. *Cell*. 2008; 133(3):537–548.
20. Taira N, Nihira K, Yamaguchi T, Miki Y, Yoshida K. DYRK2 is targeted to the nucleus and controls p53 via Ser46 phosphorylation in the apoptotic response to DNA damage. *Mol Cell*. 2007; 25(5):725–738.
21. Himpel S, Tegge W, Frank R, Leder S, Joost HG, Becker W. Specificity determinants of substrate recognition by the protein kinase DYRK1A. *J Biol Chem*. 2000;275(4):2431–2438.
22. Taira N, Yamamoto H, Yamaguchi T, Miki Y, Yoshida K. ATM augments nuclear stabilization of DYRK2 by inhibiting MDM2 in the apoptotic response to DNA damage. *J Biol Chem*. 2010; 285(7):4909–4919.
23. Sakaue-Sawano A, et al. Visualizing spatiotemporal dynamics of multicellular cell-cycle progression. *Cell*. 2008;132(3):487–498.
24. Durbin AD, Somers GR, Forrester M, Pienkowska M, Hannigan GE, Malkin D. JNK1 determines the oncogenic or tumor-suppressive activity of the integrin-linked kinase in human rhabdomyosarcoma. *J Clin Invest*. 2009;119(6):1558–1570.
25. Chen Y, Olopade OI. MYC in breast tumor progression. *Expert Rev Anticancer Ther*. 2008; 8(10):1689–1698.
26. Gee JM, Barroso AF, Ellis IO, Robertson JF, Nicholson RI. Biological and clinical associations of c-jun activation in human breast cancer. *Int J Cancer*. 2000;89(2):177–186.
27. Grimes CA, Jope RS. The multifaceted roles of glycogen synthase kinase 3beta in cellular signaling. *Prog Neurobiol*. 2001;65(4):391–426.
28. Sears R, Nuckolls F, Haura E, Taya Y, Tamai K, Nevins JR. Multiple Ras-dependent phosphorylation pathways regulate Myc protein stability. *Genes Dev*. 2000;14(19):2501–2514.
29. Huang CC, et al. Calcineurin-mediated dephosphorylation of c-Jun Ser-243 is required for c-Jun protein stability and cell transformation. *Oncogene*. 2008;27(17):2422–2429.
30. Kang T, et al. GSK-3 beta targets Cdc25A for ubiquitin-mediated proteolysis, and GSK-3 beta inactivation correlates with Cdc25A overproduction in human cancers. *Cancer Cell*. 2008;13(1):36–47.
31. Ding Q, et al. Degradation of Mcl-1 by beta-TrCP mediates glycogen synthase kinase 3-induced tumor suppression and chemosensitization. *Mol Cell Biol*. 2007;27(11):4006–4017.
32. Maurer U, Charvet C, Wagman AS, Dejardin E, Green DR. Glycogen synthase kinase-3 regulates mitochondrial outer membrane permeabilization and apoptosis by destabilization of MCL-1. *Mol Cell*. 2006;21(6):749–760.
33. Plotnikov A, et al. Oncogene-mediated inhibition of glycogen synthase kinase 3 beta impairs degradation of prolactin receptor. *Cancer Res*. 2008; 68(5):1354–1361.
34. Diehl JA, Cheng M, Roussel MF, Sherr CJ. Glycogen synthase kinase-3beta regulates cyclin D1 proteolysis and subcellular localization. *Genes Dev*. 1998;12(22):3499–3511.
35. Hanson KD, Shichiri M, Follansbee MR, Sedivy JM. Effects of c-myc expression on cell cycle progression. *Mol Cell Biol*. 1994;14(9):5748–5755.
36. Jansen-Durr P, et al. Differential modulation of cyclin gene expression by MYC. *Proc Natl Acad Sci U S A*. 1993;90(8):3685–3689.
37. Karn J, Watson JV, Lowe AD, Green SM, Vedeckis W. Regulation of cell cycle duration by c-myc levels. *Oncogene*. 1989;4(6):773–787.
38. Ohtsubo M, Theodoras AM, Schumacher J, Roberts JM, Pagano M. Human cyclin E, a nuclear protein essential for the G_1-to-S phase transition. *Mol Cell Biol*. 1995;15(5):2612–2624.
39. Perez-Roger I, Solomon DL, Sewing A, Land H. Myc activation of cyclin E/Cdk2 kinase involves induction of cyclin E gene transcription and inhibition of p27(Kip1) binding to newly formed complexes. *Oncogene*. 1997;14(20):2373–2381.
40. Resnitzky D, Gossen M, Bujard H, Reed SI. Acceleration of the G_1/S phase transition by expression of cyclins D1 and E with an inducible system. *Mol Cell Biol*. 1994;14(3):1669–1679.
41. Richardson H, O'Keefe LV, Marty T, Saint R. Ectopic cyclin E expression induces premature entry into S phase and disrupts pattern formation in the Drosophila eye imaginal disc. *Development*. 1995; 121(10):3371–3379.
42. Sheaff RJ, Groudine M, Gordon M, Roberts JM, Clurman BE. Cyclin E-CDK2 is a regulator of p27Kip1. *Genes Dev*. 1997;11(11):1464–1478.
43. Nesbit CE, Tersak JM, Prochownik EV. MYC oncogenes and human neoplastic disease. *Oncogene*. 1999; 18(19):3004–3016.
44. Bhatia K, Huppi K, Spangler G, Siwarski D, Iyer R, Magrath I. Point mutations in the c-Myc transactivation domain are common in Burkitt's lymphoma and mouse plasmacytomas. *Nat Genet*. 1993; 5(1):56–61.
45. Smith-Sorensen B, Hijmans EM, Beijersbergen RL, Bernards R. Functional analysis of Burkitt's lymphoma mutant c-Myc proteins. *J Biol Chem*. 1996; 271(10):5513–5518.
46. Frykberg L, Graf T, Vennstrom B. The transforming activity of the chicken c-myc gene can be potentiated by mutations. *Oncogene*. 1987;1(4):415–422.
47. Symonds G, Hartshorn A, Kennewell A, O'Mara MA, Bruskin A, Bishop JM. Transformation of murine myelomonocytic cells by myc: point mutations in v-myc contribute synergistically to transforming potential. *Oncogene*. 1989;4(3):285–294.
48. Maki Y, Bos TJ, Davis C, Starbuck M, Vogt PK. Avian sarcoma virus 17 carries the jun oncogene. *Proc Natl Acad Sci U S A*. 1987;84(9):2848–2852.
49. Zhang X, et al. Mechanistic insight into Myc stabilization in breast cancer involving aberrant Axin1 expression [published online ahead of print August 1, 2011]. *Proc Natl Acad Sci U S A*. doi:10.1073/pnas.1100764108.
50. Armanious H, Deschenes J, Gelebart P, Ghosh S, Mackey J, Lai R. Clinical and biological significance of GSK-3beta inactivation in breast cancer-an immunohistochemical study. *Hum Pathol*. 2010;41(12):1657–1663.
51. Italiano A, et al. HMGA2 is the partner of MDM2 in well-differentiated and dedifferentiated liposarcomas whereas CDK4 belongs to a distinct inconsistent amplicon. *Int J Cancer*. 2008; 122(10):2233–2241.
52. Liu H, Lu ZG, Miki Y, Yoshida K. Protein kinase C delta induces transcription of the TP53 tumor suppressor gene by controlling death-promoting factor Btf in the apoptotic response to DNA damage. *Mol Cell Biol*. 2007;27(24):8480–8491.
53. Yoshida K, Yamaguchi T, Shinagawa H, Taira N, Nakayama KI, Miki Y. Protein kinase C delta activates topoisomerase IIalpha to induce apoptotic cell death in response to DNA damage. *Mol Cell Biol*. 2006;26(9):3414–3431.
54. Cai Y, et al. Homocysteine-responsive ATF3 gene expression in human vascular endothelial cells: activation of c-Jun NH(2)-terminal kinase and promoter response element. *Blood*. 2000;96(6):2140–2148.
55. Kimura J, Nguyen ST, Liu H, Taira N, Miki Y, Yoshida K. A functional genome-wide RNAi screen identifies TAF1 as a regulator for apoptosis in response to genotoxic stress. *Nucleic Acids Res*. 2008; 36(16):5250–5259.
56. Lujambio A, et al. CpG island hypermethylation-associated silencing of non-coding RNAs transcribed from ultraconserved regions in human cancer. *Oncogene*. 2010;29(48):6390–6401.
57. Yoshida K, Yamaguchi T, Natsume T, Kufe D, Miki Y. JNK phosphorylation of 14-3-3 proteins regulates nuclear targeting of c-Abl in the apoptotic response to DNA damage. *Nat Cell Biol*. 2005;7(3):278–285.

エピジェネティクス分野

石野 史敏

難治疾患研究所
エピジェネティクス・教授

1）研究の課題名

1. レトロトランスポゾン由来の哺乳類特異的遺伝子群の個体発生・生殖機構における役割

Functions of mammalian-specific retrotransposon-derived genes in mammalian development and reproduction

哺乳類を構成する真獣類、有袋類、単孔類の3つのグループのなかで、胎生の生殖機構を採用している前二者にのみ存在しているレトロトランスポゾン由来の内在性遺伝子の機能の体系的解析を進めている。以前にPeg10（Ono et al. Genomics 2001, Nat Genet 2006）およびPeg11/Rtl1（Sekita et al. Nat Genet 2008）が胎盤形成や機能に必須の役割をはたすことを報告してきた。そこで、真獣類、有袋類のゲノムに存在するLTR型レトロトランスポゾンに由来する遺伝子群について現在までの知見を総説としてまとめ、これらがどのように内在遺伝子化したのかを、遺伝子の中立説とダーウィンの進化論をもとに考察した（Kaneko-Ishino and Ishino, Frontiers Microbiol 2012, Kaneko-Ishino and Ishino, Evolutionary Biology in press）。また、真獣類に存在するPeg10, Peg11/Rtl1と同じsushi-ichiレトロトランスポゾンに由来する9個のSirh family（sushi-ichi retrotransposon homologues）遺伝子の機能について、東海大学の金児−石野研と共同で一連のノックアウトマウスの解析を進めている。

2. 体細胞クローンマウスにおけるエピジェネティクス異常の改善

Improvement of epigenetic status of mouse somatic clones.

体細胞クローン技術はiPS細胞作製技術とならんで将来の再生医療を大きく変える可能性を秘めている。これまで理化学研究所バイオリソースセンターの小倉淳郎室長のグループとの共同研究で、低成功率の原因が性染色体であるX染色体の全域に渡る遺伝子発現低下にあることを明らかにした（Inoue et al. Science 2010, Inoue et al. PNAS 2011）。今回、これらの成功率の改善には、体細胞クローンマウスにみられていたエピジェネティックな遺伝子発現異常が大幅に改善されていることを理研発生再生総合研究所の若山照彦博士のグループとの共同研究で明らかにした（Kohda et al. Cellular Reprogramming 2012）。

3. 哺乳類の初期発生過程における雌雄前核間におけるepigenetic asymmetry

Epigenetic asymmetry between female- and male-derived genomes in early mammalian development.

昨年、ヒトにおける不妊治療の一つとして広く用いられている顕微授精技術（ICSI：intracaytoplasmic sperm injection）の影響をマウスをモデルに解析した。体外受精（IVF：in vitro fertilization）では全く影響が見られないのに対し、ISCIでは全発現遺伝子の5%に発現量の増減が確認されることを報告した（Kohda et al. BBRC 2011）。この原因が受精直後におきる雌雄ゲノムのDNA修飾の違いによる可能性について、エピジェネティクスの立場から議論をした（Kohda and Ishino, Phil Trans B 2012）。

2）研究のイラストレーション

図：受精直後における雌雄ゲノムのエピジェネティックアシンメトリー

説明：精子と卵子の受精後、受精卵が2細胞に分裂をするまでの間に、ゲノムのエピジェネティックな状態は大きく変化する。ゲノム中のDNAのメチル化シトシンはヒドロキシメチルシトシンへと酸化修飾を受けるが、雌雄ゲノムでこの過程は大きく異なる（上段）。またZygotic activationとよばれる新規の遺伝子発現のタイミングも異なる（中段のd）。卵に蓄積しているmaternal RNAの分解もこの過程で起きる（下段）。人工授精などの生殖医療は、この時期に受精卵を体外で培養し、操作を加えているため、この時期のエピジェネティック制御は非常に重要な問題となっている。

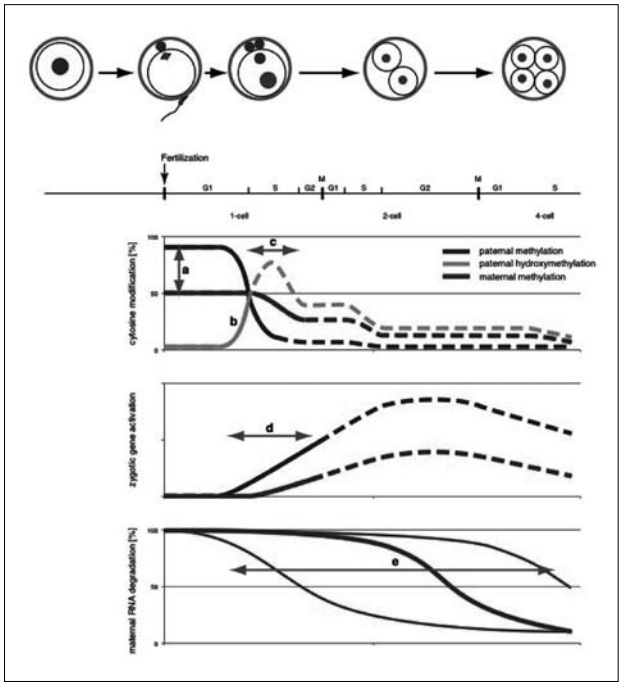

3）発表の研究内容についての英文要約

1. Gene expression profile normalization in cloned mice by trichostatin A treatment

Cloning mammals by somatic cell nuclear transfer (SCNT) has become an established procedure, but the success rate remains low and gene expression abnormalities are also observed. In addition, SCNT pups exhibited an abnormal gene expression profile with a high degree of heterogeneity among individuals. Recently, we reported that somatic clones treated with trichostatin A (TSA) exhibited a significantly improved success rate, probably due to its effects on chromatin remodeling and histone modification in early embryos. Here we show that the TSA treatment also improves the long-term consistency of genome-wide gene expression regulation : the total number of genes commonly exhibiting up- or down-regulation in the TSA clone pups decreased to half of the conventional SCNT pups, and the variation among individuals observed in the SCNT pups was also reduced to the level of the pups produced by the intracytoplasmic sperm injection (ICSI) method. Interestingly, the total gene expression profile of the TSA clones came to resemble that of the ICSI pups.

2. Evolution of Viviparity and Genomic Imprinting in Mammals by Retrotransposons

PEG10 and PEG11/RTL1 are paternally expressed imprinted genes which play an essential role in mammalian development via the formation and maintenance of the placenta, an organ unique to viviparous mammals, respectively. The former is present only in therians and the latter is a eutherian-specific gene. Interestingly, these genes are derived from sushi-ichi- related LTR retrotransposons. Thus, PEG10 and PEG11/RTL1 are very good examples of Darwinian evolution and also provide strong evidence of macroevolution, that is, natural selection at work beyond the individual species. Retrotransposon domestication is a new mode of evolution. Although it seems quite likely that this happens rarely, it is clear that once it, in fact, did occur, its impact was profound. We propose that DNA methylation was involved in this mechanism in an essential way and that the process took place in the placenta in a manner similar to the nearly neutral theory of molecular evolution, working together with Darwinian evolution.

3. The role of genes domesticated from LTR retrotransposons and retroviruses in mammals.

The acquisition of multiple genes from long terminal repeat (LTR) retrotransposons occurred in mammals. Genes belonging to a sushi-ichi-related retrotranspon homologues (SIRH) family emerged around the time of the establishment of two viviparous mammalian groups, marsupials and eutherians. These genes encode proteins that are homologous to a retrotransposon Gag capsid protein and sometimes also have a Pol-like region. We previously demonstrated that PEG10 (SIRH1) and PEG11/RTL1 (SIRH2) play essential but different roles in placental development. PEG10 is conserved in both the marsupials and the eutherians, while PEG11/RTL1 is a eutherian-specific gene, suggesting that these two domesticated genes were deeply involved in the evolution of mammals via the establishment of the viviparous reproduction system. In this review, we introduce the roles of PEG10 and PEG11/RTL1 in mammalian development and evolution, and summarize the other genes domesticated from LTR retrotransposons and endogenous retroviruses (ERVs) in mammals. We also point out the importance of DNA methylation in inactivating and neutralizing the integrated retrotransposons and ERVs in the process of domestication.

4. Embryo manipulation via assisted reproductive technology and epigenetic asymmetry in mammalian early development

The early stage of mammalian development from fertilization to implan- tation is a period when global and differential changes in the epigenetic landscape occur in paternally and maternally derived genomes, respectively. The sperm and egg DNA methylation profiles are very different from each other, and just after fertilization, only the paternally derived genome is sub- jected to genome-wide hydroxylation of 5-methylcytosine, resulting in an epigenetic asymmetry in parentally derived genomes. Although most of these differences are not present by the

blastocyst stage, presumably due to passive demethylation, the maintenance of genomic imprinting memory and X chromosome inactivation in this stage are of critical importance for post-implantation development. Zygotic gene activation from paternally or maternally derived genomes also starts around the two-cell stage, presum- ably in a different manner in each of them. It is during this period that embryo manipulation, including assisted reproductive technology, is nor- mally performed; so it is critically important to determine whether embryo manipulation procedures increase developmental risks by disturb- ing subsequent gene expression during the embryonic and/or neonatal development stages. In this review, we discuss the effects of various embryo manipulation procedures applied at the fertilization stage in relation to the epigenetic asymmetry in pre-implantation development. In particular, we focus on the effects of intracytoplasmic sperm injection that can result in long-lasting transcriptome disturbances, at least in mice.

4）本事業に関連して世界的な研究拠点形成に向けて、以下の点で改善・整備等されたこと

A（研究拠点体制）

拠点を形成することで関連研究を行う他の研究室での研究内容をより深く理解し、共同研究などを通じて自分の研究に新たな展開を盛り込む事が可能になった。

B（研究教育環境）

独立した研究者をめざす優秀なポスドク（GCOE特任講師）が研究室におり頑張っている姿をみせることは、大学院生に自分の将来を考える上で重要なロールモデルとなっている。英語での総合プレゼンテーションも参加したメンバーに対しての教育効果は高いと考えている。

C（人材確保）

将来性の高い研究者をGCOE特任講師として採用できた。さきがけ研究にも選ばれており、若い大学院生に良い影響をあたえている。

D（人材育成）

採用したGCOE特任講師には、施設、機器などの利用に便宜をはかり、自身の研究に専念してもらえる環境を提供している。また、将来、独立して研究室を運営できるよう、研究の将来構想や学生の指導法や研究室運営の仕方などについても相談にのっている。

E（国際化）

博士課程の大学院生には、国際共同研究で1－3ヶ月海外に滞在して研究できる機会を与えている。相手国からも大学院生を受け入れており、大学院生のときから海外の研究者との交流をもたせている。本拠点には外国人大学院生が多くいるため、国際化はスムーズに展開できるようになると考えている。

5）GCOE事業を推進するに当たって力を入れた点

指導している大学院生にとって自分の研究者としての将来を考える上で良い経験を得られる環境を作ること。流行に流されない息の長い仕事の重要性を覚えるのも、大学の研究者として必要なことであると考えている。また、大学院生のそれぞれの個性を伸ばすため、個別の研究指導をすることは当然として、研究者としての経歴にはいろいろな選択肢が存在することを理解させる事は重要である。本制度GCOEのポスドク、研究所独自のテニュアトラックのポスドク、大型研究費によるポスドクなどが、研究所内にいることで、大学の正規の助教ポストだけでなく自分の将来の選択の幅を知ることが可能になった。

6）英文原著論文

1. Kohda, T., Kishigami, S., Kaneko-Ishino, T., Wakayama T. and Ishino F. Gene expression profile normalization in cloned mice by trichostatin A treatment. Cellular Reprogramming 14（1）, 45-55（2012）.
2. Kaneko-Ishino, T. and Ishino, F. The role of genes domesticated from LTR retrotransposons and retroviruses in mammals. Frontiers Microbiol 3, Article 262（2012）.
3. Ishino, F., Shinkai, Y. and Whitelaw, E. Mammalian epigenetics in biology and medicine. In Mammalian Epigenetics in Biology and Medicine（eds. Ishino, F., Shinkai, Y. and Whitelaw, E.）, Royal Society Publishing, Phillos Trans R Soc Lond B Biol Sci, 368（1609）：20120386（2012）.
4. Kohda, T. and Ishino, F. Embryo manipulation via assisted reproductive technology and epigenetic asymmetry in mammalian early development. In Mammalian Epigenetics in Biology and Medicine（eds. Ishino, F., Shinkai, Y. and Whitelaw, E.）, Royal Society Publishing, Phillos Trans R Soc Lond B Biol Sci, 368（1609）：20120353（2012）.

7）総説ならびに著書

1. Kaneko-Ishino, T. and Ishino, F. Evolution of viviparity and genomic imprinting in mammals by retrotransposons. In Evolutionary Biology：Mechanisms and Trends, Chapter 15（ed. Pontarotti, P.）, Springer-Verlag Berlin Heidelberg（in press）.
2. Lee, J., Kohda, T. and Ishino, F. Nuclear transfer with

germ cells -Germ cell cloning contributes to current understanding of genomic imprinting in mammals- In Principles of Cloning 2nd Edition（ed. Cibelli, J）, Elsevier（in press）.

8）平成24年度までの自己評価

哺乳類の個体発生に影響をあたえたレトロトランスポゾン由来の遺伝子群の機能解析は、ノックアウトマウス解析からの新たな発見に加えて、タンパク質の機能という生化学的レベル、行動に関係する脳機能、ホルモン調節という生理学のレベルまで研究が発展してきている。哺乳類特異的エピジェネティクスの医学研究への展開として、再生医療における細胞リプログラミングの研究やICSIなどの発生工学技術における遺伝子発現解析を行っているが、さらに対象をヒトとして社会に還元できる知識の生産を目指している。

9）学会発表（英文）

1. Fumitoshi Ishino, Ryuichi Ono, Sunsuke Suzuki, Yoichi Sekita, Mie Naruse, Takashi Kohda and Tomoko Kaneko-Ishino. Contribution of Retrotransposons to Evolution of Genomic Imprinting and Placentation in Mammals. The 8th Okazaki Bioloby Conference "Speciation and Adaptation II - Environment and Epigenetics -" March 18-23（Okazaki, Aichi）
2. Takashi Kohda, Narumi Ogonuki, Kimiko Inoue, Tamio Furuse, Hideki Kaneda, Tomohiro Suzuki, Tomoko Kaneko-Ishino, Teruhiko Wakayama, Shigeharu Wakana, Atsuo Ogura and Fumitoshi Ishino. Epigenetic Regulation of Somatic Cell Cloning and Embryo Manipulation. The 8th Okazaki Bioloby Conference "Speciation and Adaptation II - Environment and Epigenetics -" March18-23（Okazaki, Aichi）.

10）学会発表（和文）

1. 幸田尚、高木清考、及川真美、越後貫成美、井上貴美子、金児—石野知子、小倉淳郎、石野史敏：顕微授精によって最初に誘導される遺伝子発現調節の変化、ワークショップ「有性生殖におけるゲノム・遺伝子相関」第35回日本分子生物学会年会、2012年12月11-14日（福岡国際会議場、福岡）。
2. 小野竜一、成瀬美衣、北澤萌恵、金児—石野知子、石野史敏：哺乳類特異的レトロトランスポゾン獲得による胎生進化、ワークショップ「分化・再生からゲノム進化まで — その多様なメカニズム」第35回日本分子生物学会年会、2012年12月11-14日（福岡国際会議場、福岡）。
3. 成瀬美衣、小野竜一、日野敏昭、赤塚明、中村健司、横山峯介、石野史敏、金児—石野知子：哺乳類で新しく獲得された遺伝子Sirh7と哺乳類の胎盤進化、ワークショップ「発生と進化に関わるトランスポゾン由来のDNA」 第35回日本分子生物学会年会、2012年12月11-14日（福岡国際会議場、福岡）。
4. 相馬未来、十時泰、松本和也、藤原祥高、豊田敦、榊佳之、岡部勝、石野史敏、小林慎：マウス着床前胚において雌のみで発現するsmall RNAの探索、ワークショップ「脊椎動物の初期発生研究における新たな展開」 第35回日本分子生物学会年会、2012年12月11-14日（福岡国際会議場、福岡）。
5. 岩崎佐和、幸田尚、鈴木俊介、小野竜一、Helen Clark、Geoff Shaw、Mailyn B Renfree、金児 — 石野知子、石野史敏：真獣類および有袋類特異的なレトロトランスポゾン由来の遺伝子群PNAMファミリーとインプリンティングの解析、第35回日本分子生物学会年会、2012年12月11-14日（福岡国際会議場、福岡）。
6. 入江将仁、成瀬美衣、幸田尚、小野竜一、若菜茂晴、石野史敏、金児—石野知子　Sushi-ishiレトロトランスポゾン由来の遺伝子Sirh3の機能解析、 第35回日本分子生物学会年会、2012年12月11-14日（福岡国際会議場、福岡）。
7. 石井雅之、小野竜一、黒木陽子、豊田敦、藤山秋佐夫、金児—石野知子、石野史敏：なぜトランスポゾン由来の真獣類特異的遺伝子群Sirh4, Sirh5, Sirh6は複数コピーで存在するのか？第35回日本分子生物学会年会、2012年12月11-14日（福岡国際会議場、福岡）。
8. 小野由美子、入江将仁、朝倉（渡辺）久子、幸田尚、石野史敏、金児—石野知子　低栄養が胎仔期に与える遺伝子発現への影響、第35回日本分子生物学会年会、2012年12月11-14日（福岡国際会議場、福岡）。
9. 山口佑季、李知英、幸田尚、金児－石野知子、石野史敏：Ex vivo、in vitro培養法による始原生殖細胞のDMR脱メチル化の解析、第35回日本分子生物学会年会、2012年12月11-14日（福岡国際会議場、福岡）。
10. 北澤萌恵、遠藤大輔、関田洋一、小野竜一、金児−石野知子、石野史敏：真獣類特異的遺伝子Peg11の胎盤における役割と成長への影響、第35回日本分子生物学会年会、2012年12月11-14日(福岡国際会議場、福岡)。
11. 及川真実、井上貴美子、的場章悟、志浦寛相、越後貫成美、水谷英二、阿部訓也、石野史敏、小倉淳郎：核移植技術によるXist遺伝子のインプリント確立の解析、第35回日本分子生物学会年会、2012年12月

11-14日（福岡国際会議場、福岡）。
12. 西本正純、片野幸、山岸敏之、菱田友昭、加門正義、鍋島曜子、鍋島陽一、桂有加子、颯田葉子、Janaine Deakin, Jennifer Graves、黒木陽子、小野竜一、石野史敏、加藤英政、奥田晶彦：真獣類特異的遺伝子UTF1は胎盤の増殖を促進する、第35回日本分子生物学会年会、2012年12月11-14日（福岡国際会議場、福岡）。
13. 高橋沙央里、李知英、幸田尚、若山照彦、金児－石野知子、石野史敏　マウスにおける雌性単為発生胚由来1倍体ES細胞の樹立と特性解析、第35回日本分子生物学会年会、2012年12月11-14日（福岡国際会議場、福岡）。

11）外部資金の獲得状況

1. 科学研究費基盤研究（S）
研究課題「哺乳類特異的ゲノム機能の解析」代表
研究期間　平成23年度～平成27年度（5年間）
総額　165,200千円　平成24年度分32,800千円
2. 科学研究費基盤研究（S）
研究課題「マウスを用いたゲノム高度可塑化因子の同定とその応用」分担（代表 小倉淳郎）
研究期間　平成23年度～平成27年度（5年間）
分担金：平成24年度分3,000千円
3. 日本学術振興会　日豪二国間共同研究
研究課題「有袋類におけるゲノムインプリンティングの進化」
研究期間　平成23年度～平成24年度（2年間）
平成24年度分　2,450千円

12）特別講演、招待講演、シンポジウム

1. 石野史敏：ゲノムインプリンティングから見えてくるもの　―哺乳類の個体発生と進化―　日本分子生物学会第12回春季シンポジウム　トランスレ―ショナル分子生物学　～新世代への知の継承～、2012年4月25日-26日（石和温泉、山梨）。
2. Fumitoshi Ishino：Role of mammalian-specific retrotransposon-derived genes in mammalian reproductive system, The 2nd SKLRB Symposia in Reproductive Biology, May 6-10, 2012, Beijing Friendship Hotel（Beiling, China）.
3. Fumitoshi Ishino and Tomoko Kaneko-Ishino：Contribution of LTR retrotransposons to evolution of mammals：a novel view from comparative genomics, 11th Surugadai Symposium, July 31, 2012（TMDU, Tokyo, Japan）.
4. Fumitoshi Ishino：Functions of mammalian-specific SIRH family genes- LTR retrotransposon-derived genes in mammalian reproducion system-, Fujihara Seminar 2012, A New Horizon of Retroposon Research, July 31-August 3, 2012（Shiran-Kaikan, Kyoto, Japan）.
5. Fumitoshi Ishino：Evolution of Genomic Imprinting, Viviparity and Placentation in Mammals Suggest Critical Contribution of LTR-Retrotransposons and/or Exogenous DNAs, Quantitative Evolutionary and Comparative Genomics 2012, August 6-10, 2012（Okinawa Inst Sci Tech, Okinawa, Japan）.
6. 石野史敏：ゲノム情報から哺乳類の進化を読み解く　第11回知の拠点セミナー「ゲノム情報の読み取りから難治疾患に挑む」、2012年8月24日（京都大学東京オフィス、品川インターシティ、東京）。
7. 石野史敏　LTRレトロトランスポゾン由来の新規獲得遺伝子とその哺乳類特異的機能について、第2回Tokyo Vertebrate Morphology Meeting, 2012年12月1日（東京慈恵医大、東京）。

13）新聞、雑誌、TV報道

読売新聞朝刊　2012年9月2日　「わかるサイエンス」

14）GCOE総合講義

生物進化を説明するためには、ダーウィンの自然選択説にメンデルの遺伝法則を取り込んだネオダーウィニズムだけではなく、木村資生の中立説やそれを発展させた太田朋子のほぼ中立説を総合した観点が必要になる。また、ゲノム進化がこれらの基にあることも当然、考えに入れるべきである。これらの組み合せにより、環境の変化やDNA変異という2つの偶然に支配されながらもDNAレベルから表現型のレベルの進化までを統一した解釈が可能になる。本講義では、哺乳類を例にとって、哺乳類のゲノム進化と哺乳類特異的機能の獲得がどのように起こったのか、新しい進化機構であるイグザプテーション（Exaptation）について解説した。哺乳類のゲノムの半分以上がレトロトランスポゾン由来のDNA配列で埋まっている。これらはゲノム中のゴミと考えられてきたが、そのなかには哺乳類にとって必須の機能をはたすように変化した遺伝子群が存在している。LTRレトロトランスポゾンの一種であるスシイチレトロトランスポゾン由来のPEG10、PEG11/RTL1が哺乳類特異的臓器である

胎盤の形成と維持に必須な遺伝子となっている例を紹介し、どのようにしてこれらレトロトランスポゾンが新規遺伝子として獲得されたかを考えた場合、ほぼ中立説に従った過程でゲノムに固定され、変異を重ねる間に有益な機能を獲得した場合、自然選択により正の淘汰を受けた可能性が考えられる。哺乳類の中でも、有袋類と真獣類は胎生という共通点をもつが、胎盤構造や生殖戦略の違いは、これら新規遺伝子の獲得の違いで説明できる可能性も指摘した。

15）教室、分野や講座の准教授、講師、助教、特別研究員、ポスドク、指導を受けた大学院生の名前

准教授		幸田	尚
助教		小野	竜一
非常勤講師		小林	慎
GCOE特任講師		李	知英
特任助教		成瀬	美衣
大学院生	D3 ○	山口	祐季
	D2	及川	真実
	D2	高橋	沙央里
	D2	相馬	未来
	D1	高木	清考
	M2	北澤	萌絵
	M1	川尻	成俊

16）GCOE活動についての感想、コメント、改善を望む点

英語での講義が、日本人大学院生の負担になっているように思うが、これらには積極的に関わって行くべきであり、このプロジェクトにおいて英語でのプレゼンテーションの演習など学生にとって良い環境が整えられてきたと感じている。若手研究者支援としての国際シャペロン（特任講師）の将来のキャリアー設計については、今後充分考えて行く必要があると考えている。

（第3種郵便物認可）　2012年(平成24年)9月2日（日曜日）　読売新聞

日わかるサイエンス

遺伝子に共通ルール

石野史敏教授

19世紀の科学者ダーウィンのおかげで、生物は進化で種類が広がったと知ることができた。我々はゲノム（全遺伝情報）を調べることで、当時以上に進化について確信を持てる。遺伝子が、4種類の塩基の組み合わせでたんぱく質を作る際、大腸菌でも動物でも共通のルールに従っている。

論理的には、生物すべてが同じものから分かれたとしか考えられない。

遺伝子により次世代に様々な形質が伝わるが、哺乳類には両親が必要だ。例えば父親由来のPeg10という遺伝子は胎盤形成に重要で、これがないと胎児が育たない。ゲノムを調べると、Peg10は1億6000万～1億8600万年前に哺乳類が獲得したことがわかる。

Peg10は、細胞内で動き回る遺伝物質レトロトランスポゾン由来だ。レトロトランスポゾンは、ゲノムの中で入る場所が悪いと、必要な遺伝子の働きを封じて病気を引き起こすなど有害な側面がある。

一方、進化の過程で有利な形質として残り、大事な役割を果たすこともある。非常にまれながら、Peg10のようなことが起こって胎盤が生まれ、我々がいる。ゲノムを調べると、我々は偶然の産物だとわかる。

知の拠点セミナー

東京医科歯科大学難治疾患研究所

「ゲノム情報の読み取りから難治疾患に挑む」

frontiers in
MICROBIOLOGY

REVIEW ARTICLE
published: 27 July 2012
doi: 10.3389/fmicb.2012.00262

The role of genes domesticated from LTR retrotransposons and retroviruses in mammals

Tomoko Kaneko-Ishino[1]* and Fumitoshi Ishino[2]

[1] School of Health Sciences, Tokai University, Isehara, Kanagawa, Japan
[2] Medical Research Institute, Tokyo Medical and Dental University, Tokyo, Japan

Edited by:
Yukihito Ishizaka, National Center for Global Health and Medicine, Japan

Reviewed by:
Matthew Lorincz, University of British Columbia, Canada
Kenji Ichiyanagi, Kyushu University, Japan

****Correspondence:***
Tomoko Kaneko-Ishino, School of Health Sciences, Tokai University, Bohseidai, Isehara, Kanagawa 259-1193, Japan.
e-mail: tkanekoi@is.icc.u-tokai.ac.jp

The acquisition of multiple genes from long terminal repeat (LTR) retrotransposons occurred in mammals. Genes belonging to a sushi-ichi-related retrotransposon homologs (*SIRH*) family emerged around the time of the establishment of two viviparous mammalian groups, marsupials and eutherians. These genes encode proteins that are homologous to a retrotransposon Gag capsid protein and sometimes also have a Pol-like region. We previously demonstrated that *PEG10* (*SIRH1*) and *PEG11/RTL1* (*SIRH2*) play essential but different roles in placental development. *PEG10* is conserved in both the marsupials and the eutherians, while *PEG11/RTL1* is a eutherian-specific gene, suggesting that these two domesticated genes were deeply involved in the evolution of mammals via the establishment of the viviparous reproduction system. In this review, we introduce the roles of *PEG10* and *PEG11/RTL1* in mammalian development and evolution, and summarize the other genes domesticated from LTR retrotransposons and endogenous retroviruses (ERVs) in mammals. We also point out the importance of DNA methylation in inactivating and neutralizing the integrated retrotransposons and ERVs in the process of domestication.

Keywords: domesticated genes, LTR retrotransposons and ERVs, mammals, development and evolution

INTRODUCTION

Domestication (exaptation, co-option) is an extended mode of restricting the retrotransposons, endogenous retroviruses (ERVs), and DNA transposons that are integrated into host genomes. It has been proposed that host organisms make use of such transposable DNA elements as a genetic resource of genes for novel purposes (Brosius and Gould, 1992; Smit, 1999). Telomerase, which maintains the telomere end repeats in chromosomes in eukaryotes, and two *recombination activating genes* (*RAG1* and *RAG2*) that are essential for producing the vast diversity of immunoglobulin types by V(D)J recombination in vertebrates, are good examples. The former was derived from a reverse transcriptase of a long terminal repeat (LTR) retrotransposon or retrovirus (Nakamura and Cech, 1998) and the latter from a transposase of a DNA transposon (Agrawal et al., 1998; Hiom et al., 1998). Mammalian centromere-associated protein B (CENP-B) facilitates centromere formation and is a DNA-binding protein derived from a transposase of the *pogo*-like DNA transposon family (Tudor et al., 1992; Casola et al., 2008). Although it bears considerable similarity to three fission yeast proteins, ARS-binding protein (Abp1), CENP-B homologs 1 and 2 (Cbh1 and Cbh2), which also exhibit centromere binding, it was recently reported that the origin of mammalian CENP-B is different from that of the three fission yeast proteins. That is, they are all derived from distinct *pogo*-like DNA transposons, indicating that convergent domestication occurred in the mammalian and fission yeast lineages. In plants, the Arabidopsis *far-red elongated hypocotyls 3* (*FHY3*) and *far-red-impaired response* (*FAR1*) genes are derived from an ancient Mutator-like transposase, a kind of DNA transposons. They encode transcription factors essential for the light response via phytochrome A signaling (Lisch et al., 2001; Hudson et al., 2003; Lin et al., 2007). From these data, it is clear that the domestication of transposable elements had a profound effect on quite a large numbers of animals and plants during the course of biological evolution, even though only few cases are currently known.

The retrotransposons, ERVs, and their remnant DNA sequences occupy approximately 40% of the mammalian genome and they have long been thought to be either "selfish" genes or useless "junk." Is it thus the case that domestication events are very rare in mammals? Are there any domesticated genes which are present in a mammalian-, therian-, and eutherian-specific manner? Alternatively, are there domesticated genes which have been conserved in a more restricted manner, i.e., as species- and strain-specific genes? If so, it would be highly probable that they have contributed to mammalian evolution in various ways and to different degrees.

The recent availability of mammalian genome sequence information enabled us to identify dozens of novel domesticated genes from LTR retrotransposons/ERVs. In 2000, human *SYNCYTIN* (*ERVWE1*) was identified as the first candidate domesticated gene derived from ERVs in mammals (Blond et al., 2000; Mi et al., 2000). As shown in **Figure 1**, it derives from an *envelope* (*Env*) gene of a human-specific endogenous retrovirus, HERV-W, and was suggested by *in vitro* study to mediate placental cytotrophoblast fusion so as to produce syncytiotrophoblast cells in human placental morphogenesis. Interestingly, humans have two *SYNCYTIN* genes, but they are primate-specific genes (Blaise et al., 2003). Similar genes (also called *Syncytin*) were also discovered in several mammalian lineages that were independently acquired from *Env* genes from different ERVs (Dupressoir et al., 2005; Heidmann et al., 2009).

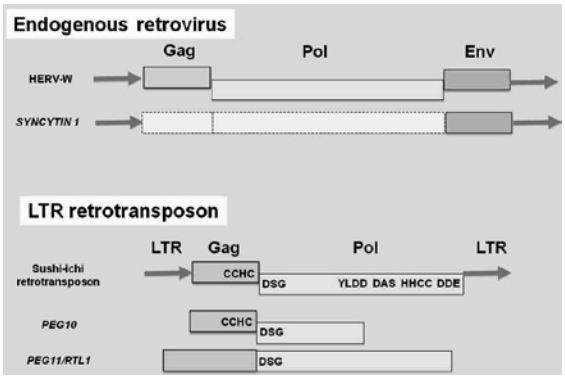

FIGURE 1 | Endogenous retrovirus, LTR retrotransposon and their domesticated genes. *Top*: an endogenous retrovirus, HERV-W, and *SYNCYTIN 1*. *SYNCYTIN 1* retains LTRs at both ends and the *Env* gene, while the *Gag* and Pol genes do not support ORFs corresponding functional proteins because of stop mutations. *Bottom*: an LTR retrotransposon, sushi-ichi, and the domesticated *PEG10* and *PEG11/RTL1* genes. Both *PEG10* and *PEG11/RTL1* have lost LTRs while entire regions exhibit significant homologies to the Gag and Pol genes remaining in some of the retrotransposon domains. The −1 frameshift mechanism is conserved in *PEG10*. LTR, long terminal repeat; Gag, group-specific antigen; Pol, polymerase; Env, envelope; CCHC, RNA-binding motif; DSG, protease active site; YYDD, reverse transcriptase; DAS, RNase highly conserved motif; HHCC, integrase DNA binding motif; DDE, strongly conserved integrase.

Finally, mouse *SyncytinA* and *B* have been to be essential placental genes using knockout mice (Dupressoir et al., 2009, 2011).

In 2001, the first and second candidate domesticated genes from a sushi-ichi-related LTR retrotransposon were identified as *paternally expressed 10* (*PEG10*; Ono et al., 2001) and *paternally expressed 11/retrotransposon-like 1* (*PEG11/RTL1*; Charlier et al., 2001). They encode proteins homologous to a retrotransposon Gag and a Pol protein, respectively (**Figure 1**). Combined with definitive genetic studies using knockout mice, *PEG10* and *PEG11/RTL1* have been shown to be essential for mammalian development via placenta formation and the subsequent maintenance of its placental function, respectively (Ono et al., 2006; Sekita et al., 2008). As *PEG10* is conserved in all the eutherian and marsupial species, it is a therian-specific gene (Suzuki et al., 2007), while *PEG11/RTL1* is eutherian-specific (Edwards et al., 2008). All these findings demonstrated that these two domesticated genes are essential in the current mammalian developmental system and indicate that they have been critically involved in the establishment and diversification of viviparous mammals. In other words, these domesticated genes could be major players in the macroevolution of mammals (Kaneko-Ishino and Ishino, 2010).

The concept of macroevolution by such domesticated genes from the LTR retrotransposons/ERVs and the DNA transposons, as well as rewiring gene regulatory networks by non-LTR retrotransposons (Kuwabara et al., 2009; Lynch et al., 2011; Schmidt et al., 2012) is a subject of interest not only to biologists, but also to those in the general public who are interested in biological evolution and the origin of human beings. It is of special interest because it implies the existence of a unique long-term relationship between the transposable elements and the emergence of mammals.

In this review, we introduce the essential role played by *PEG10* and *PEG11/RTL1* in mammalian development via placenta formation, and summarize the current understanding of domesticated genes from the LTR retrotransposons/ERVs, especially those in the mammalian lineages. We also discuss the critically important role of DNA methylation in the process of retrotransposon domestication.

PEG10 AND *PEG11/RTL1* IN MAMMALIAN DEVELOPMENT AND EVOLUTION

PEG10 and *PEG11/RTL1* were identified as paternally expressed genes in the course of an investigation on genomic imprinting (Charlier et al., 2001; Ono et al., 2001). Genomic imprinting is a mammalian-specific epigenetic mechanism regulating the parent-of-origin expression of a subset of specific genes. For these imprinted genes, the two parental alleles are not equivalent: some of the genes are transcribed only from maternally transmitted alleles (maternally expressed genes, *MEGs*) and the others are transcribed only from paternally transmitted alleles (paternally expressed genes, *PEGs*; Kaneko-Ishino et al., 2006). Then, genomic imprinting plays an essential role in mammalian development, growth, and behavior via the activity of certain critically important imprinted genes. In mice, there are more than 10 imprinted regions which have been identified, consisting of both *PEGs* and *MEGs*. Among them, a proximal region of chromosome 6 is known to cause early embryonic lethality upon maternal duplication, while maternal duplication of a distal region of chromosome 12 causes late embryonic/neonatal lethality associated with growth retardation (Cattanach and Beechey, 1990; see also Genomic imprinting map: http://www.har.mgu.ac.uk/research/genomic_imprinting/). Mouse *Peg10* and *Peg11/Rtl1* are the major genes responsible for the lethal phenotypes observed in these imprinted regions, respectively (Ono et al., 2006; Sekita et al., 2008). Using knockout mice, we demonstrated that *Peg10* and *Peg11/Rtl1* play essential roles in early placenta formation and maintenance of the placenta in the mid-to-late stages of gestation, respectively. No labyrinth or spongiotrophoblast formation was observed in the placenta of *Peg10* knockout mice. The labyrinth layer is a central part of the mouse placenta in which feto-maternal interactions take place. A large portion of the fetal capillaries exist in the labyrinth layer and allow an exchange of nutrients and gases between maternal and fetal blood cells (**Figure 2**). Mouse embryos require nutrient supply from the placenta starting on day 9.5 of gestation, therefore, *Peg10* KO embryos do not survive beyond this stage.

PEG10 encodes two open reading frames exhibiting the highest homology to the Gag and Pol proteins of the sushi-ichi retrotransposon, respectively, and produce two types of proteins, one derived from ORF1 and the other from both ORF1 and 2 (Ono et al., 2001; Volff et al., 2001; **Figure 1**). The PEG10 protein retains a CCHC RNA-binding motif in the Gag protein and there is a DSG protease domain in the Pol protein. The −1 frameshift mechanism which produces a Gag–Pol fusion

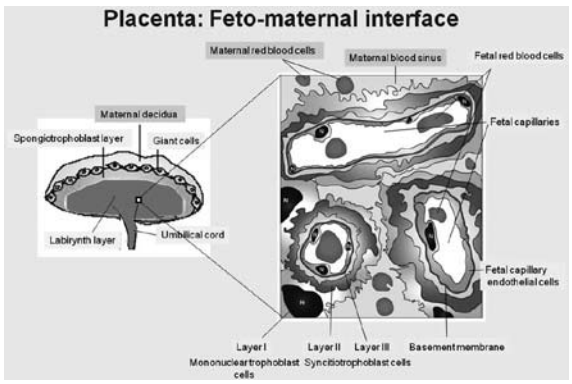

FIGURE 2 | Mouse mature placenta. *Left*: mouse placenta is composed of labyrinth, spongiotrophoblast, and giant cell layers. *Right*: magnified view of the labyrinth layer. In the labyrinth layers, fetal capillaries are surrounded by three layers of trophoblast cells and are bathed in maternal blood, functioning as a site of nutrient and gas exchange between the fetal and maternal blood.

protein that is unique to LTR retrotransposons and ERVs is conserved in *PEG10*, providing strong evidence for its origin from an LTR retrotransposon (Ono et al., 2001; Shigemoto et al., 2001; Manktelow et al., 2005). The biochemical function of the PEG10 protein has yet to be elucidated. However, it was reported that *PEG10* is highly expressed in a great majority of hepatocellular carcinomas and confers oncogenic activity. Furthermore, the PEG10 protein is reportedly associated with a member of the "seven in absentia homolog" family (SIAH1 protein) that acts as a mediator of apoptosis. Overexpression of PEG10 decreased the cell death mediated by SIAH1, suggesting that PEG10 has a growth promoting function related to apoptosis in somatic cells (Okabe et al., 2003).

The genomic record shows that *PEG10* is conserved in the eutherian and marsupial mammals among the vertebrates (Suzuki et al., 2007). As the placenta is an organ unique to the viviparous reproduction system in these two mammalian groups, it is clearly evident that this gene domesticated from the LTR retrotransposon contributed to the establishment of the current developmental systems of viviparous mammalian groups as a positively selected gene (Suzuki et al., 2007; Kaneko-Ishino and Ishino, 2010). Thus, *PEG10* is a very good example of Darwinian evolution and natural selection at work in a macroevolutionary process beyond the individual species which led to the establishment of a subclass of mammals, the therians (**Figure 3**).

The PEG11/RTL1 protein also possesses homology to both the Gag and Pol proteins, including the DSG protease domain in the latter, although no frameshift is required in this case (Charlier et al., 2001). The amino acid sequence homology between the PEG10 and PEG11/RTL1 proteins is approximately 20–30%, indicating their different functions. Mouse *Peg11/Rtl1* knockout clearly showed that *Peg11/Rtl1* has both a different role from *Peg10* and is essential for the maintenance of placental function in the mid-to-late fetal stages (Sekita et al., 2008). *Peg11/Rtl1* is expressed in endothelial cells (of extraembryonic mesoderm lineage) of the fetal capillaries in the labyrinth layer, in contrast with *Peg10*, which is expressed in the labyrinth and spongiotrophoblast cells (of extraembryonic endoderm lineage; **Figure 2**). As mentioned above, the fetal capillary is the place where feto-maternal interaction occurs. The loss of *Peg11/Rtl1* causes clogging in many of the fetal capillaries in the labyrinth layer because of the phagocytosis of endothelial cells carried out by the surrounding trophoblast cells. The Peg11/Rtl1 protein may protect endothelial cells against placental trophoblast cells, which have a highly invasive and hence dangerous nature, although its biochemical function awaits demonstration. It should be noted that the loss and overexpression of *PEG11/RTL1* are thought to attribute to the etiology of two different human imprinted diseases, maternal and paternal disomies of human chromosome 14 (matUPD14 and patUPD14), where *PEG11/RTL1* is located, respectively (Kagami et al., 2008). In these cases, *PEG11/RTL1* plays a major role, not only in placental function, but also in fetal and postnatal growth.

PEG11/RTL1 is conserved in all eutherian mammals but is absent from marsupial mammals, and is, therefore, a eutherian-specific gene (Edwards et al., 2008). Marsupials use a choriovitelline placenta (yolk sac placenta), which is different from the eutherian chorioallantoic placenta and give birth to their young after a very short gestation period compared to the eutherians (Renfree, 2010). PEG11/RTL1 function is necessary for the latter to complete their longer gestational period. Therefore, it is probable that *PEG11/RTL1* has a role in the reproduction system of eutherians, which have the chorioallantoic placenta and that it thus contributed to the diversification of these two viviparous mammalian groups. We can say that *PEG11/RTL1* provides another good example of macroevolution in mammals (i.e., the establishment of an infraclass of mammals, the eutherians) by domesticated genes from LTR retrotransposons (Kaneko-Ishino and Ishino, 2010; **Figure 3**).

OTHER *SIRH* FAMILY GENES DERIVING FROM THE SUSHI-ICHI-RELATED RETROTRANSPOSON

PEG10 and *PEG11/RTL1* belong to a sushi-ichi-related retrotransposon homolog (*SIRH*) family consisting of 12 genes, including these two genes as *SIRH1* and *SIRH2*, respectively (**Figure 2**; Ono et al., 2006). It is also called the mammalian-specific retrotransposon transcripts (*MART*; Brandt et al., 2005a,b) or *SUSHI* family (Youngson et al., 2005). The *SIRH1–11* genes are conserved in the eutherian species but no marsupial orthologs have been found, yet nevertheless, *SIRH12* is derived from a marsupial-specific insertion event (Ono et al., 2011; **Figure 3**). Among the *SIRH* family genes, *PEG10* (*SIRH1*), *PEG11/RTL1* (*SIRH2*), and *SIRH9* share homology to both the Gag and Pol proteins, while all the others bear homology only to the Gag protein, but encode proteins of more than 100 amino acid sequences (Brandt et al., 2005a,b; Youngson et al., 2005; Campillos et al., 2006; Ono et al., 2006).

SIRH12 is present in the tammar wallaby, an Australian marsupial species, but its amino acid sequence is degenerated in the gray short-tailed opossum, a South American marsupial species, suggesting that it is only functional in the former (Ono et al., 2011). No ortholog has been reported in any eutherian species

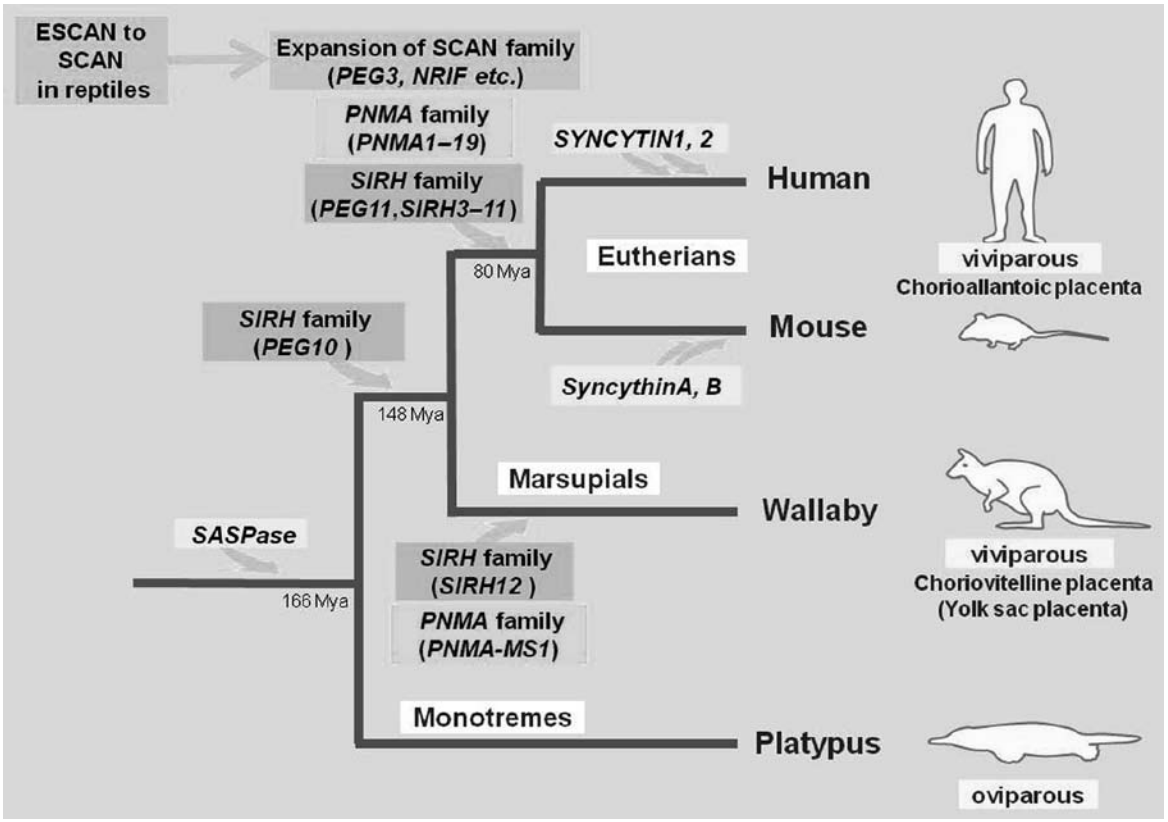

FIGURE 3 | Domestication from LTR retrotransposons and ERVs in mammals. The acquisition of *SASPase* occurred in a common mammalian ancestor. *PEG10* was domesticated in a common therian ancestor while *PEG11/RTL1*, *SIRH3–11*, and *PNMA1–19* were domesticated in a common eutherian ancestor with subsequent loss of some of the *PNMA* genes in rodents. The ESCAN domain was domesticated in lower vertebrates and its transition to the SCAN domain took place by combining with the zinc finger and/or KRAB motifs which had already occurred in certain reptiles. In any event, the expansion of SCAN family is obvious in the eutherians. *SIRH12* and *PNMA-MS1* are derived from marsupial-specific domestication events. The *SYNCYTINs* were independently recruited in several different mammalian lineages. The eutherians and marsupials are viviparous, having chorioallantoic and choriovitelline placentas (yolk sac placentas), respectively. Both *PEG10* and *PEG11/RTL1* are essential for the proper formation of efficient chorioallantoic placentas.

in the corresponding region between the *ectodermal-neural cortex* (*ENC1*) and *rho-guanine nucleotide exchange factor* (*RGNEF*) genes where wallaby *SIRH12* and opossum pseudo *SIRH12* are located in the marsupial genome. These findings demonstrate that the *SIRH* family of genes appeared mainly around the establishment of the therian mammals, one (*PEG10*) before and all the others after the split of the marsupials and eutherians (**Figure 3**). Consequently, the eutherians and the marsupials have a different set of *SIRH* family genes except for *PEG10*. It is likely that *SIRH3–11* and *SIRH12* also have roles in the eutherian and marsupial developmental and reproductive systems as well as *PEG10* and *PEG11*. As they are expressed in the brain, ovary, and testis as well as the placenta, they may be related to ovulation, gestation, delivery, and/or maternal nursing behaviors, including lactation, as well as placenta formation. Their respective functions are now under investigation using knockout mice.

PNMA-FAMILY GENES FROM THE Gypsy12_DR-RELATED LTR RETROTRANSPOSON

A paraneoplastic Ma antigen (*PNMA*) family is another large family consisting of eutherian- and marsupial-specific genes (Schüller et al., 2005; Iwasaki et al., in preparation; **Figure 3**). *PNMA*-family genes (*PNMA1–3*) were first identified as genes encoding neuronal auto-antigens using sera from human patients with paraneoplastic neurological syndromes (Voltz et al., 1999; Rosenfeld et al., 2001). By comprehensive search of a protein database, Schüller et al. (2005) identified additional human *PNMA* genes, *MOAP1/PNMA4*, *PNMA5*, and *PNMA6*, among which *PNMA6* has no mouse ortholog. Campillos et al. (2006) performed a genome-wide search for *PNMA* genes and identified a total 15 genes and 1 pseudogene in humans. They also showed that all of the *PNMA* genes were related to a Gypsy12_DR-related Gag protein group of the Ty3/Gypsy LTR retrotransposons isolated from zebrafish (*Danio rerio*) and that there was no Gypsy12_DR-derived

sequences in birds. Recently, Iwasaki and colleagues identified novel *PNMA* genes by a re-examination of the entire mouse and human entire genome sequences and the *PNMA*-family genes found thus far number 15 and 19 in mice and humans, respectively; all of these genes have Gag-like proteins, but none are homologous to the Pol protein. The difference in number may be due to the rodent-specific deletion of the *PNMA6A–6D* genes on X chromosome (Schüller et al., 2005; Iwasaki et al., in preparation).

No knockout mouse studies on *PNMA* genes have been reported, but there are reports indicating that these genes are involved in important biological pathways and related to human diseases. *PNMA4*-deficient cells exhibit aggressive anchorage-independent growth, suggesting that *PNMA4* has an important role in regulating apoptosis signaling in a strict temporal manner in mammalian cells, because the PNMA4/MOAP-1 protein is short-lived and constitutively degraded by the ubiquitin–proteasome system (Lee et al., 2009).

Cho et al. (2008a, 2011) reported *PNMA10* to be a candidate gene for X-linked mental retardation (*XLMR*) in humans. In mice, *Pnma10/Zcchc12* is expressed in the embryonic ventral forebrain in a cholinergic–neuron-specific manner (Cho et al., 2011), and is known to act as a transcriptional co-activator for bone morphogenic protein (BMP) signaling by binding to the SMAD family of proteins (Cho et al., 2008b). Therefore, it is likely that *PNMA10* is related to the evolution of brain function in mammals.

Recently, *Pnma14/CCDC8* was suggested to be one of the genes responsible for 3-M syndrome (Hanson et al., 2011a,b). 3-M syndrome is an autosomal-recessive disease characterized by severe postnatal growth restriction, leading to a significantly diminished stature. *CULLIN7* (*CUL7*) and *Obsculin-like 1* (*OBSL1*) are both related to the transcription of *insulin-like growth factor-binding protein* (*IGFBP*) genes and have been identified as two of the genes involved in 3-M syndrome (Huber et al., 2005; Hanson et al., 2009). Importantly, the OBSL1 protein interacts with both the PNMA14/CCDC8 and CUL7 proteins, indicating that this protein complex is responsible for the growth retardation observed in 3-M patients. These findings suggest that *PNMA* genes play an important role in the eutherian development and growth that are impacted by human diseases.

We have recently identified two marsupial-specific *PNMA* genes, *PNMA-MS1* and *-MS2* (Iwasaki et al., in preparation; **Figure 3**). *PNMA-MS1* exists in the same genome location in both the Australian (tammar wallaby) and South American (gray short-tailed opossum) marsupial species, but no orthologs exist in the eutherians, suggesting that they are derived from a marsupial-specific domestication event similar to that of *SIRH12*. *PNMA-MS2* was only found in the opossum because there is a gap in the corresponding region of the wallaby genome sequence. However, it is clear that no ortholog exists in any eutherian species. Thus, it is also clear that *PNMA*-family genes were independently domesticated in the eutherian and the marsupial lineages, and may have certain eutherian- and marsupial-specific functions, respectively.

THE RETROVIRAL-LIKE ASPARTIC PROTEASE SASPase IS CONSERVED IN MAMMALS

Skin aspartic protease (SASPase), which is known a retroviral-like aspartic protease (Bernard et al., 2005), plays a key role in determining the texture of skin by modulating the degree of hydration via the processing of profilaggrin (Matsui et al., 2006, 2011; Barker et al., 2007). *SASPase* is a single gene conserved in the eutherians, marsupials, and presumably the monotremes (Matsui, personal communication), and thus is a mammalian-specific gene (**Figure 3**). The profilaggrin protein comprises a tandem array of filaggrin monomers and the SASPase is its specific protease which produces the filaggrin monomer (Matsui et al., 2011). The *Filaggrin* gene has recently been identified to be etiologically responsible for atopic dermatitis (Barker et al., 2007). Interestingly, both SASPase and profilaggrin are unique to mammals and expressed exclusively in the stratified epithelia in skin. Therefore, it is highly likely that they contributed to the establishment of the mammalian-specific skin barrier system. Aberrant *SASPase* expression in transgenic mice reportedly leads to impaired skin regeneration and skin remodeling after cutaneous injury or chemically induced hyperplasia (Hildenbrand et al., 2010), and *SASPase*-deficient mice exhibit fine wrinkles on the sides of the adult body (Matsui et al., 2006).

SCAN-FAMILY GENES RAPIDLY EXPANDED IN THE COURSE OF EUTHERIAN EVOLUTION

The SCAN-family is not a mammalian-specific gene family because its ancestral form exists in non-mammalian vertebrates, but nevertheless, an enormous expansion occurred in the eutherian species (**Figure 3**). The SCAN motif consists of only a C-terminal portion of the Gag capsid (CA) protein and, in mammals, it always accompanied by multiple C2H2 zinc finger motifs and/or Krüppel-associated box (KRAB) domains neither of which is of retrotransposon origin. It is suggested that the former part was already domesticated at or near the root of the tetrapod animal branch from a full-length CA gene derived from a Gmr1-like retrotransposon. This is called the extended SCAN (ESCAN) domain and that either it or its truncated SCAN motif combined with the zinc finger and/or KRAB motifs in the Anolis lizard (Emerson and Thomas, 2011). Approximately, 60 and 40 genes are known in humans and mice, respectively, and some of them are involved in development and differentiation as transcription factors, such as *ZNF202*, *ZNF197*, *ZNF444*, *ZNF274* (*neurotrophin receptor interacting factor*, *NRIF*), *Zfp496* (*NSD1-interacting zinc finger protein 1*, *Nizp1*) and *Zfp263* (*NT2*; Edelstein and Collins, 2005).

Therefore, it is highly likely that some of the *SCAN*-family genes are related to certain eutherian-specific functions. One example is *paternally expressed gene 3* (*PEG3*; Kuroiwa et al., 1996) that was reported to be essential for maternal nursing behavior as well as promoting embryonic growth (Li et al., 1999). The *PEG3* protein has very unique structural features among C2H2 zinc finger proteins, such as amino acid sequences for 11 C2H2 zinc finger motifs and a wider spacing of these motifs. The C2H2 zinc finger proteins comprise the largest class of eukaryotic transcription factors, yet no other C2H2 zinc finger proteins have such features (Kuroiwa et al., 1996). *PEG3* is widely expressed during fetal development of mice, and strongly in adult neurons and skeletal muscle. The *Peg3* KO offspring are approximately 20% smaller at birth, with markedly reduced nursing behavior and a reduced number of oxytocin-positive neurons in the hypothalamus of *Peg3* KO females (Li et al., 1999). Human *PEG3* has

tumor-suppressing activity in glioma cell lines by its capacity to inhibit Wnt signaling, and the loss of its expression is reportedly observed in gliomas (Kohda et al., 2001; Maekawa et al., 2004; Jiang et al., 2010).

INDEPENDENT DOMESTICATION EVENTS OF THE *SYNCYTINs* IN DIFFERENT LINEAGES IN EUTHERIANS

As mentioned in Section "Introduction," *SYNCYTIN* was first discovered in humans (Blond et al., 2000; Mi et al., 2000). Although there are many *Env*-related DNA sequences in the human genome, only two exhibit fusogenic activity in cell fusion assays and now these are called *SYNCYTIN1* and *2* (Blaise et al., 2003). They are derived from different human-specific ERVs, HERV-W, and HERV-FRD, and became integrated into a primate lineage 25 and >40 MYA, respectively (**Figure 3**). Recent studies demonstrated that similar genes exist in an order- or family-specific manner in several mammalian lineages, i.e., producing syncytiotrophoblast cells by cell fusion in the placenta. Mice also have two *Syncytin* genes, *SyncytinA* and *B*, derived from Muridae family-specific integrations of HERV-F/H-related ERV(s) approximately 20 MYA (Dupressoir et al., 2005; **Figure 3**), and rabbits (*Oryctolagus cuniculus*) have another *SYNCYTIN-Ory1* from Leporidae family-specific integration of a different type-D retrovirus 12–30 MYA (Heidmann et al., 2009). Therefore, at least three independent domestication events have been confirmed in the eutherians, indicating that domestication from ERVs which were actively functioning during the time of mammalian radiation.

SyncytinA knockout mice exhibit mid-fetal lethality because of the structural abnormality of the placenta (Dupressoir et al., 2009), and double knockout of both *SyncytinA* and *B* causes an even more severe phenotype, early embryonic lethality (Dupressoir et al., 2011). Among the eutherians, placental morphology and functions are quite substantially diverged. Therefore, it is very interesting that the *SYNCYTINs* from the ERVs appear to have important roles in the placenta that they play in an order- or family-specific manner, while *PEG10* and *PEG11/RTL1* from the LTR retrotransposons are conserved in the therians and eutherians, respectively, and presumably have contributed to the establishment of the basic structure of viviparous reproductive systems in the current eutherian species.

RESISTANCE TO VIRAL INFECTION BY DOMESTICATED VIRAL GENES

ERVs have long been thought to confer resistance to infection by exogenous retroviruses. Well-known examples are *Friend virus susceptibility 1* and *4* (*Fv1* and *Fv4*) and *resistance to mink cell focus-forming (MCF) virus* (*Rmcf*) genes, which exhibit resistance to murine leukemia viruses (MuLVs) in mice (Pincus et al., 1971; Suzuki, 1975; Hartley et al., 1983). *Fv1* is derived from the Gag region of an ancient MERV-L element (Best et al., 1996; Bénit et al., 1997), whereas *Fv4* and *Rmcf* consist of intact *Env* genes, the expression of which prevents infection via receptor interference (Ikeda et al., 1985; Lyu and Kozak, 1996; Taylor et al., 2001; Jung et al., 2002). Endogenous betaretroviruses (enJSRVs) in sheep are another example (Dunlap et al., 2005). The ovine genome possesses approximately 20 copies of enJSRVs that are highly related to two exogenous oncogenic viruses, Jaagsiekte sheep retrovirus (JSRV) and enzootic nasal tumor virus. It has been proposed that the enJSRVs *Env* genes are beneficial to the host and help protect of the uterus from viral infection and act as regulators of placental morphogenesis and function. They exist as species- or strain-specific genes, meaning that they are derived from recent domestication events compared to the *SIRH*-, *PNMA*-, and SCAN-family genes as well as the *SASPase* gene.

Therefore, it is clear that the domestication from LTR retrotransposons and ERVs has a very long history, dating from around the time of the establishment of vertebrates, on through the establishment and diversification of mammals and ultimately to the radiation of each mammalian species. Koala retrovirus (KoRV) has recently been reported to cause leukemia, lymphoma, and immunosuppression in the Australian Koala population (Tarlinton et al., 2006, 2008; Stoye, 2006). Interestingly, KoRV is currently undergoing endogenization and it is likely that it entered the koala genome within the last 200 years. Therefore, retrotransposon endogenization may be a fairly ordinary process in the long course of evolution, and novel genes may continue to appear by this mechanism in the future.

GENE DUPLICATION OF DOMESTICATED GENES

Although dozens of domesticated genes have been found in mammals, this does not necessarily mean that independent domestication events have happened as often as the number of domesticated genes. Certain domesticated genes have apparently been produced by the gene duplication of an originally domesticated gene, such as in the SCAN family of genes. The SCAN domain was domesticated long before the emergence of mammals in the lower vertebrates (ESCAN) and then a new combination of this domain and zinc finger and/or KRAB motifs produced the SCAN-family gene prototype in a reptile, and its expansion occurred during radiation of the eutherians (Emerson and Thomas, 2011; **Figure 3**).

SIRH4, *5*, and *6* as well as *PNMA6A*, *6B*, *6C*, and *6D*, are other clear examples of gene duplication. The domestication of the original gene must have occurred in the ancestral eutherian mammals, but these clusters were produced by gene duplication because they encode very nearly the same coding frames. It is interesting to elucidate whether they are in the process of diversifying into genes with different functions or there is some as yet unknown reason for them to multiply and increase their copy numbers in this way. Nevertheless, as discussed above, at least two independent domestication events occurred in the eutherians and the marsupials in the *SIRH* and *PNMA* families, and at least four independent domestications have been confirmed in three different eutherian lineages in the case of the *SYNCYTINs* (**Figure 3**).

THE ESSENTIAL ROLE OF DNA METHYLATION IN THE DOMESTICATION PROCESS

Retrotransposons are potentially harmful to host organisms because their integration not only causes genetic diseases by disrupting essential genes, but also induces chromosomal deletion as well as recombination by DNA homologous recombination between the two of them. Their integration could also disturb transcription of neighboring genes. Thus, host organisms must

prevent any further propagation that would result in an accumulation of new insertion events by regulating their transcription. How are they critically silenced and yet stably inherited from generation to generation in a manner similar to endogenous DNA sequences in the host genome?

Mammals have adopted certain defense mechanisms against them, such as DNA methylation and histone modifications (Rowe and Trono, 2011). The integrated retrotransposons are usually heavily DNA methylated and transcriptionally silenced in almost all somatic cells. They have the character of being neutral genes in the mammalian genome. According to the neutral theory of molecular evolution proposed by Kimura (1968, 1983), such neutral mutations are fixed in a population by the mechanism of random drift. Ohta (2002) proposed in her "nearly neutral theory" as an extension of neutral evolution that less harmful mutations could become fixed in a population if the population size were sufficiently small). We previously proposed the hypothesis that in the course of retrotransposon domestication the neutral or nearly neutral evolution preceded Darwinian evolution and helped supply novel genes for novel purposes from the integrated retrotransposons (Kaneko-Ishino et al., 2006; Kaneko-Ishino and Ishino, 2010). In brief, we assume that either neutral or nearly neutral evolution played essential background roles by both inactivating and neutralizing integrated retrotransposons. Subsequently, their gradual conversion from silenced harmful genes to slightly advantageous genes took place as the result of multiple mutations. A loss of such silencing, at least in a subset of tissues, was ultimately required for the "new gene" to have a certain function. Darwinian forces then came into play, and by natural selection certain of these genes became more usefully functional and thus advantageous for the host organisms. It should be noted that in extraembryonic organs, such as the yolk sac and placenta in mammals, the DNA methylation levels are lower than those in other embryonic and adult tissues. Therefore, a leaky expression of retrotransposons and retroviruses constantly occurs. In this situation, the integrated retrotransposons and their subsequent mutated forms would be less harmful. However, in the case of advantageous mutations, a swift transition from the state of nearly neutral evolution to that of Darwinian evolution would take place. In this regard, the extraembryonic tissues might have been a site of retrotransposon domestication during the course of mammalian evolution, which is consistent with the fact that the domesticated *PEG10*, *PEG11/RTL1*, and *SYNCYTIN* genes play essential roles in the placenta (Kaneko-Ishino and Ishino, 2010).

In this hypothetical scenario, various epigenetic mechanisms, such as DNA methylation and/or histone modification, might have played a critical role. In mammals, DNMT1 is the essential maintenance DNA methyltransferase and the loss of its activity causes early embryonic lethality associated with overexpression of IAP retrovirus (Li et al., 1992; Walsh et al., 1998). The two *de novo* DNA methyltransferase DNMT3A and DNMT3B are also essential for mammalian development, and the loss of their activities causes lethality in the postnatal and embryonic period in mice, respectively (Okano et al., 1999). Overexpression of IAP retrovirus was also observed in *Dnmt3a* and *3b* double knockout mice, although to a lesser degree than *Dnmt1* KO mice (Okano et al., 1999). DNMT3L does not have DNA methyltransferase activity itself, but has an essential function of producing a different DNA methylation status in female- and male-derived genomic DNA in the process of establishing the genomic imprinting memories associated with *DNMT3A* (Bourc'his et al., 2001; Hata et al., 2002). It is known that this complex is also essential for retrotransposon methylation in the paternal germ line (Bourc'his et al., 2001; Bourc'his and Bestor, 2004). The coincident emergence of *DNMT3L* in the therian mammals is highly suggestive, both for the origin of the genomic imprinting mechanism as well as the abundance of LTR retrotransposons/ERVs, each of which is specific to the therian genome (Yokomine et al., 2006). It should be noted that H3K9 methyltransferase ERG-associated protein with SET domain (ESET, also called SETDB1) coupled with KRAB-associated protein 1 (KAP1, also called TRIM28) and zinc finger protein ZFP806 is required for H3K9 trimethylation as well as the repression of the retrotransposons and ERVs in undifferentiated mouse ES cells (Wolf and Goff, 2007, 2009; Matsui et al., 2010). Such a DNA methylation-independent pathway may be necessary, because DNA methylation is dynamically reprogrammed during the early embryonic period in mammals.

Finally, we would like to consider how the mammalian viviparous reproductive system originally started using the retrotransposon-derived *PEG10* gene. If this new reproductive system first happened in a single individual, was it possible for such an individual to survive and propagate his or her offspring? It is worth mentioning that the nearly neutral theory of molecular evolution can also explain how new species originated not from a single individual, but rather from a population subset (Kimura, 1983). Preadaptive mutations were already distributed in a neutral manner. Adaptive functions emerged under the selective pressures of a new environment. This suggests the neutral evolution process could also play a role as an "evolutionary capacitor," as predicted in the case of heat shock protein (Hsp) 90, where genotypic variations in other genes are masked and therefore are accumulated without causing any evident phenotypic changes in the chaperone activity of Hsp90 *per se* (Rutherford and Lindquist, 1998; Bergman and Siegel, 2003). However, this original scenario has recently come under challenge because Hsp90 also acts as a suppressor of retrotransposons and its mutation induces retrotransposon transposition, thus causing a number of secondary mutations (Specchia et al., 2010; Gangaraju et al., 2011).

DNA methylation is commonly observed in a wide range of organisms, from bacteria to plants and animals, although certain model organisms do in fact lack this feature. We propose that changes in DNA methylation in genome regulation systems gave rise to the great diversity of the organisms across the earth. In particular, as mammals developed their particularly specialized DNA methylation system, mammalian evolution was advanced by a series of retrotransposon domestication events. Retrotransposons serve as a double-edged sword in development and evolution, i.e., either harmful or beneficial depending on which time scale is used. The domestication of retrotransposons seems likely to be a very rare event, but once it has taken place, its impact is profound, which is especially the case in mammalian evolution. That may provide the *raison d'etre* for the LTR retrotransposons in the mammalian genome.

ACKNOWLEDGMENTS

We thank all the collaborators and all the laboratory members, especially, Ryuichi Ono, Yoichi Sekita, Shunsuke Suzuki, and Takashi Kohda for analyzing *Peg10* and *Peg11* KO mice and marsupial *PEG10* and Marilyn Renfree and Jeniffer Graves for several marsupial researches. The work has long been supported by a number of grants, Grants-in-Aid for Scientific Research (S) from the Ministry of Education, Culture, Sports, Science, and Technology (MEXT) of Japan, Funding Program for Next Generation World-Leading Researchers (NEXT Program; to Tomoko Kaneko-Ishino), Bilateral Program on Joint Research Project (to Fumitoshi Ishino), and Creative Science Research (to Fumitoshi Ishino and Tomoko Kaneko-Ishino) from the Japan Society for the Promotion of Science (JSPS), Asahi Glass Foundation (to Tomoko Kaneko-Ishino) and Mitsubishi foundation (to Fumitoshi Ishino). Pacific Edit reviewed the manuscript prior to submission.

REFERENCES

Agrawal, A., Eastman, Q. M., and Schatz, D. G. (1998). Transposition mediated by RAG1 and RAG2 and its implications for the evolution of the immune system. *Nature* 394, 744–751.

Barker, J. N., Palmer, C. N., Zhao, Y., Liao, H., Hull, P. R., Lee, S. P., Allen, M. H., Meggitt, S. J., Reynolds, N. J., Trembath, R. C., and McLean, W. H. (2007). Null mutations in the filaggrin gene (FLG) determine major susceptibility to early-onset atopic dermatitis that persists into adulthood. *J. Invest. Dermatol.* 127, 564–567.

Bénit, L., De Parseval, N., Casella, J. F., Callebaut, I., Cordonnier, A., and Heidmann, T. (1997). Cloning of a new murine endogenous retrovirus, MuERV-L, with strong similarity to the human HERV-L element and with a gag coding sequence closely related to the *Fv1* restriction gene. *J. Virol.* 71, 5652–5657.

Bergman, A., and Siegel, M. L. (2003). Evolutionary capacitance as a general feature of complex gene networks. *Nature* 424, 549–552.

Bernard, D., Méhul, B., Thomas-Collignon, A., Delattre, C., Donovan, M., and Schmidt, R. (2005). Identification and characterization of a novel retroviral-like aspartic protease specifically expressed in human epidermis. *J. Invest. Dermatol.* 125, 278–287.

Best, S., Le Tissier, P., Towers, G., and Stoye, J. P. (1996). Positional cloning of the mouse retrovirus restriction gene *Fv1*. *Nature* 382, 826–829.

Blaise, S., de Parseval, N., Bénit, L., and Heidmann, T. (2003). Genomewide screening for fusogenic human endogenous retrovirus envelopes identifies syncytin 2, a gene conserved on primate evolution. *Proc. Natl. Acad. Sci. U.S.A.* 100, 13013–13018.

Blond, J.-L., Lavillette, D., Cheynet, V., Bouton, O., Oriol, G., Chapel-Fernandes, S., Mandrand, B., Mallet, F., and Cosset, F. L. (2000). An envelope glycoprotein of the human endogenous retrovirus HERV-W is expressed in the human placenta and fuses cells expressing the type D mammalian retrovirus receptor. *J. Virol.* 74, 3321–3329.

Bourc'his, D., and Bestor, T. H. (2004). Transposon silencing and imprint establishment in mammalian germ cells. *Cold Spring Harb. Symp. Quant. Biol.* 69, 381–388.

Bourc'his, D., Xu, G. L., Lin, C. S., Bollman, B., and Bestor, T. H. (2001). Dnmt3L and the establishment of maternal genomic imprinting. *Science* 294, 2536–2539.

Brandt, J., Veith, A. M., and Volff, J. N. (2005a). A family of neofunctionalized Ty3/gypsy retrotransposon genes in mammalian genomes. *Cytogenet. Genome Res.* 110, 307–317.

Brandt, J., Schrauth, S., Veith, A. M., Froschauer, A., Haneke, T., Schultheis, C., Gessler, M., Leimeister, C., and Volff, J. N. (2005b). Transposable elements as a source of genetic innovation: expression and evolution of a family of retrotransposon-derived neogenes in mammals. *Gene* 345, 101–111.

Brosius, J., and Gould, S. J. (1992). On "genomenclature": a comprehensive (and respectful) taxonomy for pseudogenes and other "junk DNA". *Proc. Natl. Acad. Sci. U.S.A.* 89, 10706–10710.

Campillos, M., Doerks, T., Shah, P. K., and Bork, P. (2006). Computational characterization of multiple Gag-like human proteins. *Trends Genet.* 22, 585–589.

Casola, C., Hucks, D., and Feschotte, C. (2008). Convergent domestication of pogo-like transposases into centromere-binding proteins in fission yeast and mammals. *Mol. Biol. Evol.* 25, 29–41.

Cattanach, B. M., and Beechey, C. V. (1990). Autosomal and X-chromosome imprinting. *Dev. Suppl.* 1990, 63–72.

Charlier, C., Segers, K., Wagenaar, D., Karim, L., Berghmans, S., Jaillon, O., Shay, T., Weissenbach, J., Cockett, N., Gyapay, G., and Georges, M. (2001). Human–ovine comparative sequencing of a 250-kb imprinted domain encompassing the callipyge (clpg) locus and identification of six imprinted transcripts: *DLK1*, *DAT*, *GTL2*, *PEG11*, *antiPEG11*, and *MEG8*. *Genome Res.* 11, 850–862.

Cho, G., Bhat, S. S., Gao, J., Collins, J. S., Rogers, R. C., Simensen, R. J., Schwartz, C. E., Golden, J. A., and Srivastava, A. K. (2008a). Evidence that SIZN1 is a candidate X-linked mental retardation gene. *Am. J. Med. Genet. A* 146A, 2644–2650.

Cho, G., Lim, Y., Zand, D., and Golden, J. A. (2008b). Sizn1 is a novel protein that functions as a transcriptional coactivator of bone morphogenic protein signaling. *Mol. Cell. Biol.* 28, 1565–1572.

Cho, G., Lim, Y., and Golden, J. A. (2011). XLMR candidate mouse gene, Zcchc12 (Sizn1) is a novel marker of Cajal–Retzius cells. *Gene Expr. Patterns* 11, 216–220.

Dunlap, K. A., Palmarini, M., Adelson, D. L., and Spencer, T. E. (2005). Sheep endogenous betaretroviruses (enJSRVs) and the hyaluronidase 2 (HYAL2) receptor in the ovine uterus and conceptus. *Biol. Reprod.* 73, 271–279.

Dupressoir, A., Marceau, G., Vernochet, C., Bénit, L., Kanellopoulos, C., Sapin, V., and Heidmann, T. (2005). Syncytin-A and syncytin-B, two fusogenic placenta-specific murine envelope genes of retroviral origin conserved in Muridae. *Proc. Natl. Acad. Sci. U.S.A.* 102, 725–730.

Dupressoir, A., Vernochet, C., Bawa, O., Harper, F., Pierron, G., Opolon, P., and Heidmann, T. (2009). Syncytin-A knockout mice demonstrate the critical role in placentation of a fusogenic, endogenous retrovirus-derived, envelope gene. *Proc. Natl. Acad. Sci. U.S.A.* 106, 12127–12132.

Dupressoir, A., Vernochet, C., Harper, F., Guégan, J., Dessen, P., Pierron, G., and Heidmann, T. (2011). A pair of co-opted retroviral envelope syncytin genes is required for formation of the two-layered murine placental syncytiotrophoblast. *Proc. Natl. Acad. Sci. U.S.A.* 108, 1164–1173.

Edelstein, L. C., and Collins, T. (2005). The SCAN domain family of zinc finger transcription factors. *Gene* 359 1–17.

Edwards, C. A., Mungall, A. J., Matthews, L., Ryder, E., Gray, D. J., Pask, A. J., Shaw, G., Graves, J. A., Rogers, J., SAVOIR Consortium, Dunham, I., Renfree, M. B., and Ferguson-Smith, A. C. (2008). The evolution of the *DLK1-DIO3* imprinted domain in mammals. *PLoS Biol.* 6, e135. doi: 10.1371/journal.pbio.0060135

Emerson, R. O., and Thomas, J. H. (2011). Gypsy and the birth of the SCAN domain. *J. Virol.* 85, 12043–12053.

Gangaraju, V. K., Yin, H., Weiner, M. M., Wang, J., Huang, X. A., and Lin, H. (2011). Drosophila Piwi functions in Hsp90-mediated suppression of phenotypic variation. *Nat. Genet.* 43, 153–158.

Hanson, D., Murray, P. G., O'Sullivan, J., Urquhart, J., Daly, S., Bhaskar, S. S., Biesecker, L. G., Skae, M., Smith, C., Cole, T., Kirk, J., Chandler, K., Kingston, H., Donnai, D., Clayton, P. E., and Black, G. C. (2011a). Exome sequencing identifies CCDC8 mutations in 3-M syndrome, suggesting that CCDC8 contributes in a pathway with CUL7 and OBSL1 to control human growth. *Am. J. Hum. Genet.* 89, 148–153.

Hanson, D., Murray, P. G., Black, G. C., and Clayton, P. E. (2011b). The genetics of 3-m syndrome: unravelling a potential new regulatory growth pathway. *Horm. Res. Paediatr.* 76, 369–378.

Hanson, D., Murray, P. G., Sud, A., Temtamy, S. A., Aglan, M., Superti-Furga, A., Holder, S. E., Urquhart, J., Hilton, E., Manson, F. D., Scambler, P., Black, G. C., and Clayton, P. E. (2009). The primordial growth disorder 3-M syndrome connects ubiquitination to the cytoskeletal adaptor OBSL1. *Am. J. Hum. Genet.* 84, 801–806.

Hartley, J. W., Yetter, R. A., and Morse, H. C. III. (1983). A mouse gene on chromosome 5 that restricts infectivity of mink cell focus-forming recombinant murine leukemia viruses. *J. Exp. Med.* 158, 16–24.

Hata, K., Okano, M., Lei, H., and Li, E. (2002). Dnmt3L cooperates with the Dnmt3 family of de novo DNA methyltransferase to establish maternal imprints in mice. *Development* 129, 1983–1993.

Heidmann, O., Vernochet, C., Dupressoir, A., and Heidmann, T. (2009). Identification of an endogenous retroviral envelope gene with fusogenic activity and placenta-specific expression in the rabbit: a new "*syncytin*" in a third order of mammals. *Retrovirology* 6, 107.

Hildenbrand, M., Rhiemeier, V., Hartenstein, B., Lahrmann, B., Grabe, N., Angel, P., and Hess, J. (2010). Impaired skin regeneration and remodeling after cutaneous injury and chemically induced hyperplasia in taps-transgenic mice. *J. Invest. Dermatol.* 130, 1922–1930.

Hiom, K., Mele, M., and Gellert, M. (1998). DNA transposition by the RAG1 and RAG2 proteins: a possible source of oncogenic translocations. *Cell* 94, 463–470.

Huber, C., Dias-Santagata, D., Glaser, A., O'Sullivan, J., Brauner, R., Wu, K., Xu, X., Pearce, K., Wang, R., Uzielli, M. L., Dagoneau, N., Chemaitilly, W., Superti-Furga, A., Dos Santos, H., Mégarbané, A., Morin, G., Gillessen-Kaesbach, G., Hennekam, R., Van der Burgt, I., Black, G. C., Clayton, P. E., Read, A., Le Merrer, M., Scambler, P. J., Munnich, A., Pan, Z. Q., Winter, R., and Cormier-Daire, V. (2005). Identification of mutations in CUL7 in 3-M syndrome. *Nat. Genet.* 37, 1119–1124.

Hudson, M. E., Lisch, D. R., and Quail, P. H. (2003). The *FHY3* and *FAR1* genes encode transposase-related proteins involved in regulation of gene expression by the phytochrome A-signaling pathway. *Plant J.* 34, 453–471.

Ikeda, H., Laigret, F., Martin, M. A., and Repaske, R. (1985). Characterization of a molecularly cloned retroviral sequence associated with Fv-4 resistance. *J. Virol.* 55, 768–777.

Jiang, X., Yu, Y., Yang, H. W., Agar, N. Y., Frado, L., and Johnson, M. D. (2010). The imprinted gene *PEG3* inhibits Wnt signaling and regulates glioma growth. *J. Biol. Chem.* 285, 8472–8480.

Jung, Y. T., Lyu, M. S., Buckler-White, A., and Kozak, C. A. (2002). Characterization of a polytropic murine leukemia virus proviral sequence associated with the virus resistance gene *Rmcf* of DBA/2 mice. *J. Virol.* 76, 8218–8224.

Kagami, M., Sekita, Y., Nishimura, G., Irie, M., Kato, F., Okada, M., Yamamori, S., Kishimoto, H., Nakayama, M., Tanaka, Y., Matsuoka, K., Takahashi, T., Noguchi, M., Tanaka, Y., Masumoto, K., Utsunomiya, T., Kouzan, H., Komatsu, Y., Ohashi, H., Kurosawa, K., Kosaki, K., Ferguson-Smith, A. C., Ishino, F., and Ogata, T. (2008). Deletions and epimutations affecting the human 14q32.2 imprinted region in individuals with paternal and maternal upd(14)-like phenotypes. *Nat. Genet.* 40, 237–242.

Kaneko-Ishino, T., and Ishino, F. (2010). Retrotransposon silencing by DNA methylation contributed to the evolution of placentation and genomic imprinting in mammals. *Dev. Growth Differ.* 52, 533–543.

Kaneko-Ishino, T., Kohda, T., Ono, R., and Ishino, F. (2006). Complementation hypothesis: the necessity of a monoallelic gene expression mechanism in mammalian development. *Cytogenet. Genome Res.* 113, 24–30.

Kimura, M. (1968). Evolutionary rate at the molecular level. *Nature* 217, 624–626.

Kimura, M. (1983). *The Neutral Theory of Molecular Evolution.* Cambridge: Cambridge University Press, 305–327.

Kohda, T., Asai, A., Kuroiwa, Y., Kobayashi, S., Aisaka, K., Nagashima, G., Yoshida, M. C., Kondo, Y., Kagiyama, N., Kirino, T., Kaneko-Ishino, T., and Ishino, F. (2001). Tumour suppressor activity of human imprinted gene *PEG3* in a glioma cell line. *Genes Cells* 6, 237–247.

Kuroiwa, Y., Kaneko-Ishino, T., Kagitani, F., Kohda, T., Li, L-L., Tada, M., Suzuki, R., Yokoyama, M., Shiroishi, T., Wakana, S., Barton, S. C., Ishino, F., and Surani, M. A. (1996). *Peg3* imprinted gene on proximal chromosome 7 encodes for a zinc finger protein. *Nat. Genet.* 12, 186–190.

Kuwabara, T., Hsieh, J., Muotri, A., Yeo, G., Warashina, M., Lie, D. C., Moore, L., Nakashima, K., Asashima, M., and Gage, F. H. (2009). Wnt-mediated activation of NeuroD1 and retro-elements during adult neurogenesis. *Nat. Neurosci.* 12, 1097–1105.

Lee, S. S., Fu, N. Y., Sukumaran, S. K., Wan, K. F., Wan, Q., and Yu, V. C. (2009). TRIM39 is a MOAP-1-binding protein that stabilizes MOAP-1 through inhibition of its poly-ubiquitination process. *Exp. Cell Res.* 315, 1313–1325.

Li, E., Bestor, T. H., and Jaenisch, R. (1992). Targeted mutation of the DNA methyltransferase gene results in embryonic lethality. *Cell* 69, 915–926.

Li, L., Keverne, E. B., Aparicio, S. A., Ishino, F., Barton, S. C., and Surani, M. A. (1999). Regulation of maternal behavior and offspring growth by paternally expressed *Peg3*. *Science* 284, 330–333.

Lin, R., Ding, L., Casola, C., Ripoll, D. R., Feschotte, C., and Wang, H. (2007). Transposase-derived transcription factors regulate light signaling in *Arabidopsis*. *Science* 318, 1302–1305.

Lisch, D. R., Freeling, M., Langham, R. J., and Choy, M. Y. (2001). Mutator transposase is widespread in the grasses. *Plant Physiol.* 125, 1293–1303.

Lynch, V. J., Leclerc, R. D., May, G., and Wagner, G. P. (2011). Transposon-mediated rewiring of gene regulatory networks contributed to the evolution of pregnancy in mammals. *Nat. Genet.* 43, 1154–1159.

Lyu, M. S., and Kozak, C. A. (1996). Genetic basis for resistance to polytropic murine leukemia viruses in the wild mouse species *Mus castaneus*. *J. Virol.* 70, 830–833.

Maekawa, S., Itaba, N., Otsuka. S., Kamitani, H., Watanabe, T., Tahimic, C. G., Nanba, E., and Oshimura, M. (2004). Coordinate downregulation of a novel imprinted transcript *ITUP1* with *PEG3* in glioma cell lines. *DNA Res.* 11, 37–49.

Manktelow, E., Shigemoto, K., and Brierley, I. (2005). Characterization of the frameshift signal of Edr, a mammalian example of programmed -1 ribosomal frameshifting. *Nucleic Acids Res.* 33, 1553–1563.

Matsui, T., Kinoshita-Ida, Y., Hayashi-Kisumi, F., Hata, M., Matsubara, K., Chiba, M., Katahira-Tayama, S., Morita, K., Miyachi, Y., and Tsukita, S. (2006). Mouse homologue of skin-specific retroviral-like aspartic protease involved in wrinkle formation. *J. Biol. Chem.* 281, 27512–27525.

Matsui, T., Leung, D., Miyashita, H., Maksakova, I. A., Miyachi, H., Kimura, H., Tachibana, M., Lorincz, M. C., and Shinkai, Y. (2010). Proviral silencing in embryonic stem cells requires the histone methyltransferase ESET. *Nature* 464, 927–931.

Matsui, T., Miyamoto, K., Kubo, A., Kawasaki, H., Ebihara, T., Hata, K., Tanahashi, S., Ichinose, S., Imoto, I., Inazawa, J., Kudoh, J., and Amagai, M. (2011). SASPase regulates stratum corneum hydration through profilaggrin-to-filaggrin processing. *EMBO Mol. Med.* 3, 1–14.

Mi, S., Lee, X., Li, X.-P., Veldman, G. M., Finnerty, H., Racie, L., LaVallie, E., Tang, X.-Y., Edouard, P., Howes, S., Keith, J. C. Jr., and McCoy, J. M. (2000). Syncytin is a captive retroviral envelope protein involved in human placental morphogenesis. *Nature* 403, 785–789.

Nakamura, T. M., and Cech, T. R. (1998). Reversing time: origin of telomerase. *Cell* 92, 587–590.

Ohta, T. (2002). Near-neutrality in evolution of genes and gene regulation. *Proc. Natl. Acad. Sci. U.S.A.* 99, 16134–16137.

Okabe, H., Satoh, S., Furukawa, Y., Kato, T., Hasegawa, S., Nakajima, Y., Yamaoka, Y., and Nakamura, Y. (2003). Involvement of PEG10 in human hepatocellular carcinogenesis through interaction with SIAH1. *Cancer Res.* 63, 3043–3048.

Okano, M., Bell, D. W., Haber, D. A., and Li, E. (1999). DNA methyltransferases Dnmt3a and Dnmt3b are essential for *de novo* methylation and mammalian development. *Cell* 99, 247–257.

Ono, R., Kobayashi, S., Wagatsuma, H., Aisaka, K., Kohda, T., Kaneko-Ishino, T., and Ishino, F. (2001). A retrotransposon-derived gene, *PEG10*, is a novel imprinted gene located on human chromosome 7q21. *Genomics* 73, 232–237.

Ono, R., Kuroki, Y., Naruse, M., Ishii, M., Iwasaki, S., Toyoda, A., Fujiyama, A., Shaw, G., Renfree, M. B., Kaneko-Ishino, T., and Ishino, F. (2011). Identification of *SIRH12*, a retrotransposon-derived gene specific to marsupial mammals. *DNA Res.* 18, 211–219.

Ono, R., Nakamura, K., Inoue, K., Naruse, M., Usami, T., Wakisaka-Saito, N., Hino, T., Suzuki-Migishima, R., Ogonuki, N., Miki, H., Kohda, T., Ogura, A., Yokoyama, M., Kaneko-Ishino, T., and Ishino, F. (2006). Deletion of *Peg10,* an imprinted gene acquired from a retrotransposon, causes early embryonic lethality. *Nat. Genet.* 38, 101–106.

Pincus, T., Hartley, J. W., and Rowe, W. P. (1971). A major genetic locus affecting resistance to infection with murine leukemia viruses. I. Tissue culture studies of naturally occurring viruses. *J. Exp. Med.* 133, 1219–1233.

Renfree, M. B. (2010). Marsupials: placental mammals with a difference. *Placenta* 31(Suppl.), 24, S21–S26.

Rosenfeld, M. R., Eichen, J. G., Wade, D. F., Posner, J. B., and Dalmau, J. (2001). Molecular and clinical diversity in paraneoplastic immunity to Ma proteins. *Ann. Neurol.* 50, 339–348.

Rowe, H. M., and Trono, D. (2011). Dynamic control of endogenous retroviruses during development. *Virology* 411, 273–287.

Rutherford, S. L., and Lindquist, S. (1998). Hsp90 as a capacitor for morphological evolution. *Nature* 396, 335–342.

Schmidt, D., Schwalie, P. C., Wilson, M. D., Ballester, B., Gonçalves, A., Kutter, C., Brown, G. D., Marshall, A., Flicek, P., and Odom, D. T. (2012). Waves of retrotransposon expansion remodel genome organization and CTCF binding in multiple mammalian lineages. *Cell* 148, 335–348.

Schüller, M., Jenne, D., and Voltz, R. (2005). The human PNMA family: novel neuronal proteins implicated in paraneoplastic neurological disease. *J. Neuroimmunol.* 169, 172–176.

Sekita, Y., Wagatsuma, H., Nakamura, K., Ono, R., Kagami, M., Wakisaka, N., Hino, T., Suzuki-Migishima, R., Kohda, T., Ogura, A., Ogata, T., Yokoyama, M., Kaneko-Ishino, T., and Ishino, F. (2008). Role of retrotransposon-derived imprinted gene, *Rtl1*, in the feto-maternal interface of mouse placenta. *Nat. Genet.* 40, 243–248.

Shigemoto, K., Brennan, J., Walls, E., Watson, C. J., Stott, D., Rigby, P. W., and Reith, A. D. (2001). Identification and characterisation of a developmentally regulated mammalian gene that utilises −1 programmed ribosomal frameshifting. *Nucleic Acids Res.* 29, 4079–4788.

Smit, A. F. (1999). Interspersed repeats and other mementos of transposable elements in mammalian genomes. *Curr. Opin. Genet. Dev.* 9, 657–663.

Specchia, V., Piacentini, L., Tritto, P., Fanti, L., D'Alessandro, R., Palumbo, G., Pimpinelli, S., and Bozzetti, M. P. (2010). Hsp90 prevents phenotypic variation by suppressing the mutagenic activity of transposons. *Nature* 463, 662–665.

Stoye, J. P. (2006). Koala retrovirus: a genome invasion in real time. *Genome Biol.* 7, 241.

Suzuki, S. (1975). Fv-4: a new gene affecting the splenomegaly induction by Friend leukemia virus. *Jpn. J. Exp. Med.* 45, 473–478.

Suzuki, S., Ono, R., Narita, T., Pask, A. J., Shaw, G., Wang, C., Kohda, T., Alsop, A. E., Graves, M. J. A., Kohara, Y., Ishino, F., Renfree, M. B., and Kaneko-Ishino, T. (2007). Retrotransposon silencing by DNA methylation can drive mammalian genomic imprinting. *PLoS Genet.* 3, e55. doi: 10.1371/journal.pgen.0030055

Tarlinton, R., Meers, J., and Young, P. (2008). Biology and evolution of the endogenous koala retrovirus. *Cell. Mol. Life. Sci.* 65, 3413–3421.

Tarlinton, R. E., Meers, J., and Young, P. R. (2006). Retroviral invasion of the koala genome. *Nature* 442, 79–81.

Taylor, G. M., Gao, Y., and Sanders, D. A. (2001). Fv-4: identification of the defect in Env and the mechanism of resistance to ecotropic murine leukemia virus. *J. Virol.* 75, 11244–11248.

Tudor, M., Lobocka, M., Goodell, M., Pettitt, J., and O'Hare, K. (1992). The pogo transposable element family of *Drosophila melanogaster*. *Mol. Gen. Genet.* 232, 126–134.

Volff, J., Körting, C., and Schartl, M. (2001). Ty3/Gypsy retrotransposon fossils in mammalian genomes: did they evolve into new cellular functions? *Mol. Biol. Evol.* 18, 266–270.

Voltz, R., Gultekin, S. H., Rosenfeld, M. R., Gerstner, E., Eichen, J., Posner, J. B., and Dalmau, J. (1999). A serologic marker of paraneoplastic limbic and brain-stem encephalitis in patients with testicular cancer. *N. Engl. J. Med.* 340, 1788–1795.

Walsh, C. P., Chaillet, J. R., and Bestor, T. H. (1998). Transcription of IAP endogenous retroviruses is constrained by cytosine methylation. *Nat. Genet.* 20, 116–117.

Wolf, D., and Goff, S. P. (2007). TRIM28 mediates primer binding site-targeted silencing of murine leukemia virus in embryonic cells. *Cell* 131, 46–57.

Wolf, D., and Goff, S. P. (2009). Embryonic stem cells use ZFP809 to silence retroviral DNAs. *Nature* 458, 1201–1204.

Yokomine, T., Hata, K., Tsudzuki, M., and Sasaki, H. (2006). Evolution of the vertebrate DNMT3 gene family: a possible link between existence of *DNMT3L* and genomic imprinting. *Cytogenet. Genome Res.* 113, 75–80.

Youngson, N. A., Kocialkowski, S., Peel, N., and Ferguson-Smith, A. C. (2005). A small family of sushi-class retrotransposon-derived genes in mammals and their relation to genomic imprinting. *J. Mol. Evol.* 61, 481–490.

Conflict of Interest Statement: The authors declare that the research was conducted in the absence of any commercial or financial relationships that could be construed as a potential conflict of interest.

Received: 08 April 2012; paper pending published: 20 April 2012; accepted: 04 July 2012; published online: 27 July 2012.

Citation: Kaneko-Ishino T and Ishino F (2012) The role of genes domesticated from LTR retrotransposons and retroviruses in mammals. Front. Microbio. ***3****:262. doi: 10.3389/fmicb.2012.00262*

This article was submitted to Frontiers in Virology, a specialty of Frontiers in Microbiology.

分子細胞生物学分野

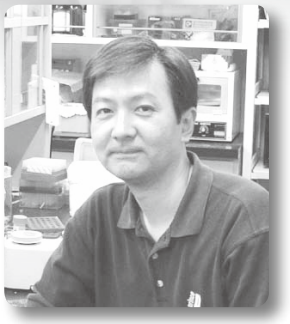

澁谷 浩司

医歯学総合研究科・器官システム制御学系専攻
分子細胞生物学・教授

1）研究の課題名

WNKシグナル伝達経路の解析

セリン/スレオニンキナーゼWNK（with no lysine（K））ファミリーは、線虫・ショウジョウバエからほ乳類に至るまで保存されており、WNK1及びWNK4は偽性低アルドステロン症II型（PHAII）の原因遺伝子として同定されている。

ショウジョウバエのWNK（DWNK）及びその下流因子の相同因子であるFrayが、ほ乳類のWNK及びOSR1と同様の相互作用を持つかを調べたところ、DWNK及びFrayも培養細胞中で相互作用し、DWNKはFrayをリン酸化していた。また、DWNK及びFray、ほ乳類のWNK1及びOSR1の異所発現系用いて、翅後部に異所的に発現させたところ、全ての発現系においてwing veinと呼ばれる翅の支持組織の異所的形成という表現型が観察された。以上のことから、WNK→OSR1というシグナル伝達経路は、ショウジョウバエでも保存されている経路であることが予測された。当研究室による、マウスや線虫における結果と合わせて考えると、WNKシグナル伝達経路は進化的に広く保存されていると考えられる。

DWNK変異体のモザイク解析、及び、Dominant Negativeとして機能するキナーゼ不活性型DWNKを腹部で異所発現させると、腹部形成不全という表現型が観察された。Awh遺伝子の突然変異体が同様の表現型を示すことから、AwhとDWNKとの遺伝的相互作用が予想された。キナーゼ不活性型DWNKとAwhを腹部で異所的に共発現させると、キナーゼ不活性型DWNKによる表現型が回復したこと、さらにDWNK変異体の表現型がAwhの異所発現により回復したことから、AwhがDWNKの下流で機能する因子であることが予測された。また、胚期において、DWNK変異体では、腹部原基でのAwhの発現が消失していた。以上の結果から、AwhはDWNKの下流で機能している遺伝子であると考えられた。

2）研究のイラストレーション

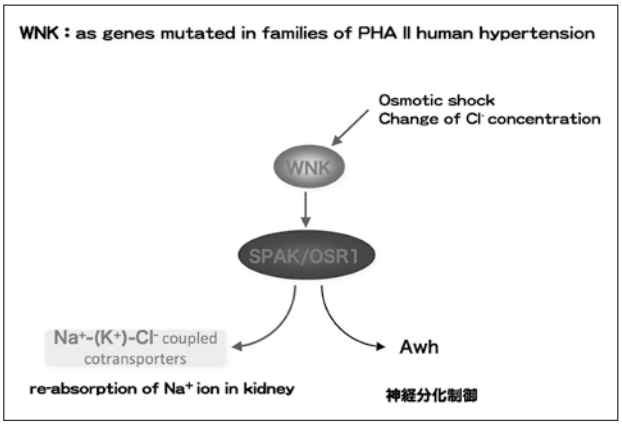

3）GCOE事業を推進するに当たって力を入れた点

将来の優秀な研究者に成るべく大学院生の育成

4）平成24年度までの自己評価

残念ながら研究の進行が停滞し、2012年の論文発表はなかった。しかしながら、現在、投稿中の論文が2報あり、1年以内には成果を発表できるものと思われる。

5）学会発表（和文）

1. A new downstream molecule, Awh is involved in the WNK signaling.
   Atsushi Sato, Hiroshi Shibuya
2. 第35回日本分子生物学会年会2012年12月13日、福岡。

6）外部資金の獲得状況

科学研究費補助金、基盤B
研究題目：WNKシグナルによる発生制御機構の解明
代表：澁谷浩司
期間：平成23年―平成25年
研究費総額：1520万円

7）教室、分野や講座の准教授、講師、助教、特別研究員、ポスドク、指導を受けた大学院生の名前

准教授　　後藤　利保

助教　　佐藤　　淳

大学院生　清水　幹容、大熊　祐一

分子代謝医学分野

小川 佳宏

医歯学総合研究科・器官システム制御学系専攻
分子代謝医学・教授

1）研究の課題名

1. 糖尿病血管障害における内皮PGC-1alphaの役割の解明

Role of endothelial PGC-1alpha in diabetic vascular dysfunction

糖尿病に随伴する血管内皮機能不全は、下肢虚血をはじめとする糖尿病合併症の主たる要因である。しかし、代謝異常と内皮機能障害を結ぶ細胞内メカニズムには不明な点が多い。転写コアクチベータPGC-1alphaは、種々の細胞において強力なエネルギー代謝調節分子として作用し、糖尿病の発症機序においても肝臓からの糖新生亢進や骨格筋におけるインスリン感受性の減弱に大きな役割を果たすが、PGC-1alphaの血管細胞における意義は不明である。我々は、培養内皮細胞、糖尿病マウス、糖尿病患者のすべてのレベルにおいて、高血糖により内皮PGC-1alphaの発現上昇が認められることを明らかにした。培養内皮細胞においてPGC-1alphaの発現レベルを強制的に上昇させるとVEGF、スフィンゴシン1リン酸によるRac/Akt/eNOS経路の活性化が抑制され、細胞遊走およびvasculogenesisが阻害された。マウスの全身の血管内皮にPGC-1alphaを強制発現させると、傷害血管の再内皮化の抑制、皮膚創傷治癒の遅延、下肢虚血モデルにおける血管新生の減弱、すなわち糖尿病性血管障害に類似する表現型を呈した。一方、マウスの血管内皮においてPGC-1alphaを欠失させると、Ⅰ型およびⅡ型糖尿病による血管障害が顕著に抑制された。以上の結果から、高血糖により誘導される内皮PGC-1alphaが、糖尿病性血管障害の成因に中心的な役割を果たすことが示された。

2. マウス新生仔の肝臓における脂肪合成酵素GPAT1のDNAメチル化による遺伝子発現制御

Role of DNA methylation in the regulation of lipogenic glycerol-3-phosphate acyltransferase 1 gene expression in the mouse neonatal liver

胎児期や新生児期の栄養環境が成人期に発症する生活習慣病の易罹患性に影響を与えることが示唆されており、分子基盤としてエピジェネティクス制御の関与が示唆される。我々は既に新生仔～離乳期のマウス肝臓において、中性脂肪合成律速酵素GPAT1が遺伝子プロモーターのDNAメチル化低下を伴い発現増加することを見出した。今回メチル化の機能的意義を解析した。培養細胞を用い、GPAT1の遺伝子プロモーターのDNAメチル化がSREBP-1cのリクルートと中性脂肪合成に与える影響を解析した。GPAT1プロモーターのDNAメチル化はSREBP-1cのリクルートとGPAT1の遺伝子発現、さらに中性脂肪合成を低下させた。このことから、メチル化が中性脂肪合成を制御する可能性が示唆された。可塑性の高い胎児期・新生児期の代謝臓器におけるエピジェネティクス制御の役割を解明することにより、胎児期・新生児期の栄養環境が成人期の生活習慣病発症を左右する機序を知る手掛かりを得ることが期待される。

2）研究のイラストレーション

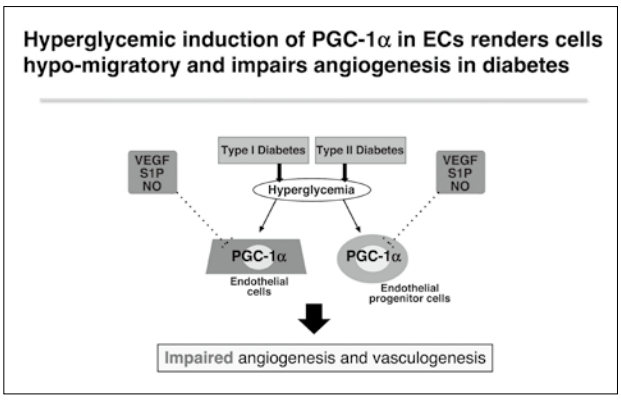

3）発表の研究内容についての英文要約

1. Role of endothelial PGC-1alpha in diabetic vascular dysfunction

Endothelial dysfunction is a central hallmark of diabetes. The transcriptional coactivator PGC-1alpha is a powerful

regulator of metabolism in numerous cell types, but its role in endothelial cells remains poorly understood. We show here that hyperglycemia induces the expression of PGC-1alpha in endothelial cells in cell culture and in vivo, and that PGC-1alpha powerfully blocks endothelial migration in cell culture and vasculogenesis in vivo. Conversely, VEGF and other pro-angiogenic stimuli rapidly down-regulate PGC-1alpha, and deletion of PGC-1alpha phenocopies the pro-migratory effect of VEGF. Mechanistically, PGC-1alpha blunts activation of Rac/Akt/eNOS signaling in response to VEGF or sphingosine 1-phosphate（S1P）, established activators of endothelial cells, while leaving the ERK arm intact. Transgenic overexpression of PGC-1alpha in endothelial cells in mice mimics multiple diabetic phenotypes, including aberrant re-endothelialization in response to carotid injury, blunted wound healing, and reduced blood flow recovery in response to hindlimb ischemia. Conversely, deletion of PGC-1alpha in endothelial cells rescues wound healing dysfunction in high-fat fed animals, and rescues blood flow recovery in type I and II diabetic animals with hindlimb ischemia. PGC-1alpha thus potently inhibits endothelial function and angiogenesis, and induction of PGC-1alpha by hyperglycemia contributes to multiple aspects of vascular dysfunction in diabetes.

2. Role of DNA methylation in the regulation of lipogenic glycerol-3-phosphate acyltransferase 1 gene expression in the mouse neonatal liver

The liver is a major organ of lipid metabolism, which is markedly changed in response to physiological nutritional demand; however, the regulation of hepatic lipogenic gene expression in early life is largely unknown. Here, we show that expression of glycerol-3-phosphate acyltransferase 1（GPAT1; Gpam）, a rate-limiting enzyme of triglyceride biosynthesis, is regulated in the mouse liver by DNA methylation, an epigenetic modification involved in the regulation of a diverse range of biological processes in mammals. In the neonatal liver, DNA methylation of the Gpam promoter, which is likely to be induced by Dnmt3b, inhibited recruitment of the lipogenic transcription factor SREBP-1c, whereas in the adult decreased DNA methylation resulted in active chromatin conformation, allowing recruitment of SREBP-1c. Maternal overnutrition causes decreased Gpam promoter methylation with increased GPAT1 expression and triglyceride content in the pup liver, suggesting that environmental factors such as nutritional conditions can affect DNA methylation in the liver. This study is the first detailed analysis of the DNA-methylation dependent regulation of the triglyceride biosynthesis gene Gpam, thereby providing new insight into the molecular mechanism underlying the epigenetic regulation of metabolic genes, and thus metabolic diseases.

4）本事業に関連して世界的な研究拠点形成に向けて、以下の点で改善・整備等されたこと

A（研究教育環境）

研究教育に力を入れて若手研究者が国内学会で受賞者が出た。うち一人は企業研究者（社会人大学院生）であり、産学連携の基礎を作ることができた。

5）GCOE事業を推進するに当たって力を入れた点

若手研究者の育成に力を入れ、国内学会にて複数の受賞者が出た。

6）英文原著論文

1. Y. Watanabe, T. Nakamura, S. Ishikawa, S. Fujisaka, I. Usui, K. Tsuneyama, Y. Ichihara, T. Wada, Y. Hirata, T. Suganami, H. Izaki, S. Akira, K. Miyake, H. Kanayama, M. Shimabukuro, M. Sata, T. Sasaoka, Y. Ogawa, K. Tobe, K. Takatsu, and Y. Nagai. The Radioprotective 105/MD-1 complex contributes to diet-induced obesity and adipose tissue inflammation. Diabetes 61：1199-1209, 2012.
2. ◎T. Ehara, Y. Kamei, M. Takahashi, Y. Xunmei, S. Kanai, E. Tamura, M. Tanaka, T. Yamazaki, O. Ezaki, T. Suganami, M. Okano, and Y. Ogawa. Role of DNA methylation in the regulation of lipogenic gene expression in the neonatal mouse liver. Diabetes 61：2442-2450, 2012.
3. N. Satoh-Asahara, A. Shimatsu, Y. Sasaki, H. Nakaoka, A. Himeno, M. Tochiya, S. Kono, T. Takaya, H. Wada, T. Suganami, K. Hasegawa, and Y. Ogawa. Highly purified eicosapentaenoic acid increases interleukin-10 levels of peripheral blood monocytes in obese patients with dyslipidemia. Diabetes Care 35：2631-2639, 2012.
4. S. Yogosawa, S. Mizutani, Y. Ogawa, and T. Izumi. Activin receptor-like kinase 7 suppresses lipolysis to accumulate fat in obesity through downregulation of peroxisome proliferator-activated receptor γ and C/EBP α. Diabetes In press.
5. F. Maekawa, S. Shimba, S. Takumi, T. Sano, T. Suzuki, J. Bao, M. Ohwada, T. Ehara, Y. Ogawa, and K. Nohara. Diurnal expression of Dnmt3b mRNA in mouse liver is regulated by feeding and hepatic clockwork. Epigenetics 7：1046-1056, 2012.

7）総説ならびに著書

1. T. Suganami, M. Tanaka, and Y. Ogawa. Adipose tissue inflammation and ectopic lipid accumulation. Endocr. J. 59：849-857, 2012.
2. 亀井康富、小川佳宏：「エピゲノムと糖尿病」：最新

医学　第67巻　第1号　27-31　2012
3. 山本貴信、菅波孝祥、小川佳宏：「脂肪細胞とRAS -肥満-」：Angiotensin Research Vol.9 No.1 17-24 2012
4. 蜂屋瑠見、菅波孝祥、小川佳宏：「肥満症の危険因子発生における脂肪組織の役割」：RharmaMedica Vol.30 No.1　19-22　2012
5. 岩崎順博、菅波孝祥、小川佳宏：「肥満における脂肪組織の慢性炎症とインスリン抵抗性」：糖尿病学イラストレイテッド　98-107　2012
6. 飯降直男、三原正朋、小川佳宏：「インクレチン関連薬を使いこなすQ1」 治療　5　Vol.94　942-944　2012　南山堂
7. 足立淳一郎、三原正朋、小川佳宏：「インクレチン関連薬を使いこなすQ2」 治療　5　Vol.94　945-947　2012　南山堂
8. 池田賢司、菅波孝祥、小川佳宏：「種々の脂肪酸の受容体と細胞応答」 内分泌・糖尿病・代謝内科　34（4）307-312　2012
9. 田中都、菅波孝祥、小川佳宏：「肥満と炎症」 Current Therapy　30（6）88　2012
10. 岩崎順博、菅波孝祥、小川佳宏：「インクレチンと脂肪組織炎症」 医学のあゆみ別刷　Vol.241 No.7 517-521　2012..5
11. 吉本貴宣、小川佳裕：「脂肪組織からアディポサイトカインを介した代謝情報ネットワークと高血圧」 血管医学　Vol.13 No.3 27-33　2012　メディカルビュー社
12. 亀井康富、田中都、菅波孝祥、小川佳裕「飢餓応答の分子機構と中枢性摂食異常症」最新医学第67巻第9号　88（2020）-92（2024）2012　最新医学社
13. 岩崎順博、菅波孝祥、小川佳宏：「TLR,GPCRと動脈硬化」 動脈硬化予防 Vol.11 No.3 24-30 2012　メジカルビュー社
14. 神山隆治、小川佳裕「オーバービューー高血圧、糖尿病における慢性炎症とRASの意義―Angiotensin Research Vol.9 No.4 1（187）-6（192）先端医学社　2012/10/04
15. 西條美佐、菅波孝祥、小川佳宏：「生活習慣病と癌の共通基盤病態としての慢性炎症」 内分泌・糖尿病・代謝内科　Vol.35 No.3 195-201 2012　科学評論社

8）平成24年度までの自己評価

最終年度まで若手育成を中心に継続的に活動できたものと考えている。研究成果をより良い形で論文化できるようにしたい。

9）学会発表（英文）

◎Naoki Sawada, Aihua Jiang, Fumihiko Takizawa, Kevin Croce, Andre Manika, Yevgenia Tesmenitsky, Kyu-Tae Kang, Joyce Bischoff, Hermann Kalwa, Thomas Michel, Yasutomi Kamei, Laura Benjamin, Masataka Sata, Yoshihiro Ogawa, Zolt Arany
Endothelial PGC-1alpha Mediates Vascular Dysfunction In Diabetes
American Heart Association Scientific Sessions 2012.
口頭
Los Angeles, California, USA.
November 3-7, 2012.

10）学会発表（和文）

1. 大橋琢也、川堀健一、山口実菜、三原正朋、杉山徹、泉山肇、吉本貴宣、内村功、伴大輔、有井滋樹、明石巧：「膵全摘出後に持続皮下インスリン注入療法を導入し奏功したMEN1型の1例」 第49回日本糖尿病学会関東甲信越地方会　2012年1月　東京
2. 赤座至、弘重栄美子、岩嶋富美子、吉本貴宣、内村功：「膵全摘後早期に抗インスリン抗体陽性化し低血糖が頻発した1例　第49回日本糖尿病学会関東甲信越地方会　2012年1月　東京
3. 宮地康高、柴久美子、佐藤文紀、川堀健一、宮腰夏輝、永田友香、櫻田麻耶、西田賢司、辻野元祥、小川佳宏：「2型糖尿病の経過中血糖悪化および肝障害を契機に診断された自己免疫性膵炎の1例」 第49回日本糖尿病学会関東甲信越地方会　2012年1月　東京
4. 川堀健一、柴久美子、宮越夏輝、宮地康高、永田友香、櫻田麻耶、佐藤文紀、西田賢司、辻野元祥、小川佳宏：「エキセナチドを追加投与し血糖値が改善し、日内変動を抑制し得た1例」 第49回日本糖尿病学会関東甲信越地方会　2012年1月　東京
5. 柴久美子、佐藤文紀、川堀健一、宮地康高、宮腰夏輝、永田友香、櫻田麻耶、西田賢司、辻野元祥、小川佳宏：「リラグルチド導入にてインスリン療法から離脱し得た2型糖尿病の2症例-CGMでの検討-」 第49回日本糖尿病学会関東甲信越地方会　2012年1月　東京
6. 西尾勇一郎、山口実菜、谷祐至、鈴木志保、有泉洋介、杉山美帆、飯降直男、足立淳一郎、三原正朋、杉山徹、泉山肇、吉本貴宣、岸本誠司、平田結喜緒：「Ca刺激試験で微小甲状腺髄様癌（MTC）の存在を確認したMEN2Aの一例」 第21回臨床内分泌代謝Up date 2012年1月　浜松
7. 足立淳一郎、川堀健一、山口実菜、大橋琢也、杉山美帆、飯降直男、三原正朋、杉山徹、泉山肇、吉本

貴宣、高橋直人、岸根有美、猪狩亨、平田結喜緒：「上顎にBrown腫瘍を合併した原発性副甲状腺機能亢進症の一例」 第21回臨床内分泌代謝Up date 2012年1月 浜松

8. 小宮力、大橋琢也、落合高徳、小林大輔、澤井瑞貴、畠山里枝、西尾勇一郎、飯降直男、足立淳一郎、三原正朋、杉山徹、泉山肇、吉本貴宣、有井滋樹、平田結喜緒：「SRSが局在診断に有用であった十二指腸原発ガストリノーマ」 第21回臨床内分泌代謝Up date 2012年1月 浜松
9. 長谷川裕美、岩嶋富美子、西澤麻依子、鈴木紗加、宇根直子、長沼朋佳、吉橋廣一、熊谷廣太郎、岡田洋一、堀内敏行、平田結喜緒：「多発性硬化症にMRIで下垂体前葉・茎の腫大を認めた若年女性例」第21回臨床内分泌代謝Up date 2012年1月 浜松
10. 大橋忠将、山内健、柴久美子、辻本和峰、粕谷綾子、小澤直子、平田結喜緒：「甲状腺中毒症を契機に診断に至った視床下部性副腎不全の1例」 第21回臨床内分泌代謝Up date 2012年1月 浜松
11. 赤座至、岩嶋富美子、木田道也、杉山美帆、吉本貴宣：「小児期より移行した成人成長ホルモン分泌不全症（GHD）の一例」 第21回臨床内分泌代謝Up date 2012年1月 浜松
12. 畠山里枝、足立淳一郎、小宮力、西尾勇一郎、大橋琢也、飯降直男、三原正朋、杉山徹、泉山肇、吉本貴宣、内村功、落合高徳、有井滋樹、竹本暁、小川佳宏：「肝 adrenal rest tumorとの鑑別が困難であった肝浸潤を伴った両側副腎腫瘍の一例」 第12回日本内分泌学会関東甲信越支部学術集会 2012年3月 さいたま市
13. 上田恵利、小宮力、畠山里枝、西尾勇一郎、大橋琢也、飯降直男、足立淳一郎、三原正朋、杉山徹、泉山肇、吉本貴宣、山田正三、井下尚子、小川佳宏：原発性胆汁性肝硬変を合併した先端巨大症の1例 第12回日本内分泌学会関東甲信越支部学術集会 2012年3月 さいたま市
14. 三原正朋、宇根直子、畠山里枝、澤井瑞貴、小宮力、西尾勇一郎、大橋琢也、山口実菜、杉山美帆、飯降直男、足立淳一郎、杉山徹、泉山肇、吉本貴宣、内村功、平田結喜緒、小川佳宏：「褐色細胞腫における耐糖能異常とカテコラミン分泌異常との関連性に関する臨床的解析」 第85回日本内分泌学会学術総会 2012年4月 名古屋
15. 大橋琢也、吉本貴宣、山口実菜、三原正朋、杉山徹、泉山肇、平田結喜緒、内村功、小川佳宏：「原発性アルドステロン症に対する手術・薬物治療による高血圧・心腎機能への効果」 第85回日本内分泌学会学術総会 2012年4月 名古屋
16. 早川恵理、宇根直子、杉山徹、吉本貴宣、泉山肇、木原和徳、小川佳宏、平田結喜緒：「褐色細胞腫における血中クロモグロニンA（CgA）濃度測定の臨床的意義の検討 第85回日本内分泌学会学術総会 2012年4月 名古屋
17. 岩崎順博、菅波孝祥、蜂屋瑠見、白川伊吹、西條美佐、亀井康富、小川佳宏：「飽和脂肪酸による炎症性サイトカイン転写誘導において転写因子ATF4が果たす役割の検討」 第85回日本内分泌学会学術総会 2012年4月 名古屋
18. 岩崎順博、菅波孝祥、蜂屋瑠見、白川伊吹、西條美佐、亀井康富、小川佳宏：「小胞体ストレス応答性転写因子ATF4による炎症性サイトカイン転写誘導機構の検討」 第55回日本糖尿病学会年次学術集会 2012年5月 横浜市
19. 與五沢里美、水谷伸、小川佳宏、泉哲郎：「糖尿病・肥満モデルマウスにおける脂肪蓄積に関与する遺伝子の解析」 第55回日本糖尿病学会年次学術集会 2012年5月 横浜市
20. 佐藤文紀、柴久美子、川堀健一、宮地康高、永田友香、黒澤由貴子、櫻田麻耶、西田賢司、辻野元祥、小川佳宏：「コントロール困難な2型糖尿病患者に対する、インスリンとシタグリプチンの併用療法の検討」第55回日本糖尿病学会年次学術集会 2012年5月 横浜市
21. 宮地康高、佐藤文紀、柴久美子、川堀健一、宮越夏輝、永田友香、黒澤由貴子、櫻田麻耶、西田賢司、辻野元祥、小川佳宏：「持続血糖モニター（CGM）を用いた2型糖尿病患者におけるエキセナチド導入例の検討 第55回日本糖尿病学会年次学術集会 2012年5月 横浜市
22. 川堀健一、柴久美子、宮地康高、永田友香、佐藤文紀、黒澤由貴子、櫻田麻耶、西田賢司、辻野元祥、小川佳宏：「2型糖尿病患者におけるDPP-4阻害薬からリラグルチドへの変更による効果」 第55回日本糖尿病学会年次学術集会 2012年5月 横浜市
23. 辻野元祥、佐藤文紀、宮地康高、永田友香、柴久美子、川堀健一、黒澤由貴子、櫻田麻耶、西田賢司、小川佳宏：「2型糖尿病患者におけるメトホルミン投与量増量による臨床効果の検討」 第55回日本糖尿病学会年次学術集会 2012年5月 横浜市

24. 黒澤由貴子、柴久美子、川堀健一、宮地康高、永田友香、佐藤文紀、櫻田麻耶、西田賢司、辻野元祥、小川佳宏：「劇症1型糖尿病の発症急性期に前立腺膿瘍を併発した一例」 第55回日本糖尿病学会年次学術集会 2012年5月 横浜市
25. 柴久美子、川堀健一、宮地康高、永田友香、佐藤文紀、黒澤由貴子、櫻田麻耶、西田賢司、辻野元祥、小川佳宏：「2型糖尿病患者における頚動脈エコーおよび冠動脈MDCTを用いた無症候性冠動脈疾患スクリーニングの検討 第55回日本糖尿病学会年次学術集会 2012年5月 横浜市
26. 永田友香、辻野元祥、西田賢司、櫻田麻耶、佐藤文紀、黒澤由貴子、柴久美子、宮地康高、川堀健一、小川佳宏：「気腫性腎盂腎炎を合併した未治療2型糖尿病の1例」 第55回日本糖尿病学会年次学術集会 2012年5月 横浜市
27. 江藤達弥、亀井康富、高橋真由美、袁勲梅、金井紗綾香、田村江梨奈、田中都、山崎聖美、三浦進司、江崎浩、菅波孝祥、岡野正樹、小川佳宏：「マウス新生仔の肝臓における脂肪合成酵素GPATIのDNAメチル化による遺伝子発現制御」 第33回日本肥満学会 2012年10月 京都市
28. 岩崎順博、菅波孝祥、蜂屋瑠見、白川伊吹、濱口美穂、亀井康富、小川佳宏：「代謝ストレス応答性転写因子ATF4による炎症性サイトカイン産生調節機構」 第33回日本肥満学会 2012年10月 京都市
29. 田中都、菅波孝祥、池田賢司、小宮力、白川伊吹、越智梢、青江誠一郎、亀井康富、小川佳宏：「肥満の脂肪組織における新規病原体センサー・Mincleの意義」 第33回日本肥満学会 2012年10月 京都市
30. 亀井康富、服部真季、笠原知美、杉田聡、金井紗綾香、岡淳一郎、三浦進司、江崎浩、菅波孝祥、北村忠弘、小川佳宏：「飢餓時の骨格筋でフォークヘッド型転写因子FOXO1はアミノ酸代謝を調節する」 第33回日本肥満学会 2012年10月 京都市

11）受賞

亀井康富　日本肥満学会学術奨励賞
「肥満・生活習慣病における核内受容体・転写共役因子の病態生理的意義の解明」

江原達弥　日本肥満学会若手研究奨励賞
「マウス新生仔の肝臓における脂肪合成酵素GPAT1のDNAメチル化による遺伝子発現制御」

12）外部資金の獲得状況

1. 科学研究費補助金・基盤研究（B）（一般）
DNAメチル化に着目したメタボリックメモリーの分子機構の解明と医学応用
平成23年－平成25年　代表　小川佳宏
14,300千円
2. 厚生労働科学研究費補助金・難治性疾患克服研究事業
中枢性摂食異常症に関する調査研究
平成24年－平成25年　代表　小川佳宏
9,231千円
3. 上原記念生命科学財団特定研究助成金
NASHの病態解明と革新的医療の創生
平成24年－平成25年　代表　小川佳宏
9,000千円
4. 厚生労働科学研究費補助金・肝炎等克服緊急対策研究事業
肝硬変症に対する細胞療法の臨床的確立とメカニズム解明
平成24年－平成26年　代表　坂井田功
7,500千円
5. 厚生労働科学研究費補助金・成育疾患克服等次世代育成基盤研究事業
母子コホート研究による成育疾患の病態解明に関する研究
平成22年－平成24年　代表　堀川玲子
3,650千円
6. 科学研究費補助金・挑戦的萌芽研究
「生理的炎症」の概念の確立と機能的意義の解明
平成24年－平成24年　代表　小川佳宏
2,900千円
7. 平成24年度日本糖尿病財団研究助成
研究題目：「糖尿病に伴う血管新生不全における責任分子群の同定とその血管再生医療への応用」
代表：澤田直樹
期間：平成24年－平成25年
研究費総額：100万円
8. 臨床薬理研究振興財団　平成24年度（第37回）研究奨励金
研究題目：「糖尿病における血管再生不全の機序解明と下肢虚血潰瘍に対する新たな遺伝子・細胞治療法の開発」
代表：澤田直樹
期間：平成24年－平成25年
研究費総額：200万円

9. 科学研究費補助金、基盤C
研究題目：「転写コアクチベータPGC-1αによる血管内皮遊走・血管新生制御機構」
代表：澤田直樹
期間：平成22年－平成24年
研究費総額：455万円
10. 科学研究費補助金、新学術領域研究
研究題目：「血管内皮による神経再生作用の賦活化におけるRac1 GTPaseの意義の検討」
代表：澤田直樹
期間：平成23年－平成24年
研究費総額：1,248万円

13）特別講演、招待講演、シンポジウム

1. 小川佳宏：「慢性炎症と生活習慣病」 第46回糖尿病学の進歩　2012年3月　岩手
2. Yoshihiro Ogawa：「Chronic Inflammation and Ectopic Fat Accumulation in the Metabolic Syndrome」: The 2012 Spring Conference of the Korean Association of Immunologists 2012年4月 Korea
3. 小川佳宏：「メタボリックシンドロームと自然炎症」: 第49回日本臨床分子医学会学術集会　2012年4月 京都
4. 菅波孝祥、小川佳宏：「脂肪組織炎症における飽和脂肪酸の意義」 第85回日本内分泌学会学術総会 2012年4月　名古屋
5. 鈴木（堀田）眞理、堀川玲子、小川佳宏：「中性脂肪摂食異常症の全国疫学調査―東京都の高校生におけるパイロット研究―　第85回日本内分泌学会学術総会　2012年4月　名古屋
6. 菅波孝祥、小川佳宏：「慢性炎症とインスリン抵抗性」第55回日本糖尿病学会年次学術集会　2012年5月 横浜市
7. Yoshihiro Ogawa & Takayashi Suganami：「Chronic inflammation and ectopic fat accumulation in the metabolic syndrome」20th International Symposium on Molecular Cell Biology of Macrophages 2012 2012年6月　Tokyo
8. 菅波孝祥、小川佳宏：「脂肪組織の慢性炎症と飽和脂肪酸」 第33回日本炎症・再生医学会　2012年7月 福岡市
9. 小川佳宏：「生活習慣病と自然炎症」 日本食品免疫学会第8回学術大会　2012..10　東京
10. 菅波孝祥、小川佳宏：「肥満脂肪組織と慢性炎症」第16回日本心血管内分泌代謝学会学術総会　2012.11 東京
11. Yoshihiro Ogawa;「Adipose tissue remodeling as homeostatic inflammation」: The 12th Biennial International Endotoxin & Innate Immunity Society（IEIIS）meeting, The Homeostatic Inflammation International Symposium 2012年10月　東京

14）新聞、雑誌、TV報道

1. 2012年9月27日
朝日新聞
2. 2012年4月28日（土）PM8：00 ～ PM8：45
ここが聞きたい! 名医にQ「ひざの痛み　あなたの疑問に答えます!」（NHK Eテレ）
http：//www.nhk.or.jp/kenko/drq/archives/2012/04/0428.html
3. 2012年4月21日（土）PM8：00 ～ PM8：45
ここが聞きたい! 名医にQ「ダイエットがカギ! ひざ痛徹底対策」（NHK Eテレ）
http：//www.nhk.or.jp/kenko/drq/archives/2012/04/0421.html

15）GCOE総合講義

炎症は内外のストレスに対する生体防御反応であり、この適応反応が破綻すると様々な病態・疾患を発症する。一方、微生物感染に代表される急性炎症と同様に、メタボリックシンドロームや生活習慣病の病態に炎症性サイトカインや免疫細胞が関与することが知られているが、炎症反応が慢性化する臓器では経時的に多彩な機能的かつ形態的変化がもたらされるため（組織リモデリング）、慢性炎症の全体像には不明な点が多い。ストレス応答として各臓器の機能を担う実質細胞とマクロファージなどの間質細胞の相互作用により誘導される軽度な炎症反応が、健常時の可逆的な定常状態を逸脱して慢性化することにより、組織リモデリングを経て不可逆な臓器の機能不全に至る可能性がある。

メタボリックシンドロームの概念は、内臓脂肪型肥満を背景として耐糖能異常、脂質異常症、血圧上昇が同時に発症し、全身臓器の機能不全として糖尿病、高血圧症、非アルコール性脂肪肝炎、慢性腎臓病、動脈硬化症などの生活習慣病に至る流れを指摘したものである。近年、メタボリックシンドロームや多くの生活習慣病の発症・進展において持続的な炎症反応（慢性炎症）の病態生理

的意義が注目されている。即ち、メタボリックシンドロームは、内臓脂肪組織局所における脂肪細胞とマクロファージの相互作用により遷延化した炎症反応（慢性炎症）により脂肪分解が亢進して過剰の遊離脂肪酸が放出され、複雑かつ巧妙な臓器代謝ネットワークの破綻により全身臓器に異所性脂肪が蓄積して臓器機能不全が波及・拡大化していく過程と理解できる。

本講義では、メタボリックシンドロームから生活習慣病を発症する過程において、臓器代謝ネットワークの破綻により内臓脂肪組織局所から全身臓器に波及・拡大する慢性炎症と異所性脂肪の病態生理的意義について概説した。

16）教室、分野や講座の准教授、講師、助教、特別研究員、ポスドク、指導を受けた大学院生の名前

亀井　康富、菅波　孝祥
吉本　貴宣、泉山　肇
澤田　直樹、杉山　徹
三原　正朋、南　勲
加藤　真子、田中　都
伊藤　美智子、袁　勲梅
高橋　真由美、白川　伊吹
蜂屋　瑠見、西條　美佐
木田　道也、渡邉（浅野）貴子
池田　賢司、滝沢　文彦
江原　達弥、津田　直人
岩崎　順博、加藤　秀昭
狩野　理延、笠原　知美
田村　江梨奈、畑澤　幸乃

ORIGINAL ARTICLE

Role of DNA Methylation in the Regulation of Lipogenic Glycerol-3-Phosphate Acyltransferase 1 Gene Expression in the Mouse Neonatal Liver

Tatsuya Ehara,[1,2] Yasutomi Kamei,[1,3] Mayumi Takahashi,[1] Xunmei Yuan,[1] Sayaka Kanai,[1] Erina Tamura,[1] Miyako Tanaka,[1,3] Tomomi Yamazaki,[4] Shinji Miura,[4] Osamu Ezaki,[4] Takayoshi Suganami,[1] Masaki Okano,[5] and Yoshihiro Ogawa[1,6,7]

The liver is a major organ of lipid metabolism, which is markedly changed in response to physiological nutritional demand; however, the regulation of hepatic lipogenic gene expression in early life is largely unknown. In this study, we show that expression of glycerol-3-phosphate acyltransferase 1 (GPAT1; *Gpam*), a rate-limiting enzyme of triglyceride biosynthesis, is regulated in the mouse liver by DNA methylation, an epigenetic modification involved in the regulation of a diverse range of biological processes in mammals. In the neonatal liver, DNA methylation of the *Gpam* promoter, which is likely to be induced by Dnmt3b, inhibited recruitment of the lipogenic transcription factor sterol regulatory element–binding protein-1c (SREBP-1c), whereas in the adult, decreased DNA methylation resulted in active chromatin conformation, allowing recruitment of SREBP-1c. Maternal overnutrition causes decreased *Gpam* promoter methylation with increased GPAT1 expression and triglyceride content in the pup liver, suggesting that environmental factors such as nutritional conditions can affect DNA methylation in the liver. This study is the first detailed analysis of the DNA-methylation–dependent regulation of the triglyceride biosynthesis gene *Gpam*, thereby providing new insight into the molecular mechanism underlying the epigenetic regulation of metabolic genes and thus metabolic diseases. ***Diabetes*** **61:2442–2450, 2012**

The liver is a major organ of lipid metabolism, which is physiologically changed during organ maturation (1,2). The rate of hepatic de novo lipogenesis (i.e., triglyceride [TG] biosynthesis) is very low during the suckling period, when fat intake is high from milk, but it rises with the onset of weaning, when glucose is used as a source of energy (1). Thus, hepatic gene expression may change markedly before and after weaning, which could be regulated in response to nutritional demand.

TG is the major storage form of energy in animals. TG biosynthesis begins with the acylation of glycerol-3-phosphate by glycerol-3-phosphate acyltransferase 1 (GPAT1; *Gpam*) to form lysophosphatidic acid; this is the rate-limiting step in the hepatic TG biosynthesis pathway (3). In the acylation process, fatty acids produced by stearoyl CoA desaturase 1 (SCD1; *Scd1*) and fatty acid synthase (FAS; *Fasn*) are used as acyl donors. Among the lipogenic enzymes, GPAT1 plays an important role in the regulation of hepatic TG biosynthesis (4,5). The lipogenic genes such as *Gpam*, *Scd1*, and *Fasn* are activated by sterol regulatory element–binding protein-1c (SREBP-1c), which is a transcription factor and master regulator of lipogenesis. Indeed, their promoter regions contain the SREBP-responsive elements (SREs) (6–8). Aberrant lipogenic gene regulation can contribute to fatty liver, which is associated with obesity, type 2 diabetes, and insulin resistance (9). However, the molecular mechanism involved in the regulation of lipogenic genes during early life remains largely unclear.

The methylation of cytosine residues in DNA is a major epigenetic modification, and its role is well studied in organ development and cell differentiation (10–12). In most instances, DNA methylation of the promoter regions causes suppression of gene expression (13). In mammals, three CpG DNA methyltransferases (Dnmt)—Dnmt1, Dnmt3a, and Dnmt3b—coordinately regulate DNA methylation in the genome. Dnmt1 promotes DNA methylation after DNA replication and plays a major role in the maintenance of methylation (14). Dnmt3a and Dnmt3b are required for the initiation of de novo DNA methylation (10).

DNA methylation may be affected by environmental factors, thereby regulating a variety of metabolic processes and diseases (15–18). Although the fetal and neonatal periods, which are highly plastic to environmental changes, should be under the epigenetic control, the role of DNA methylation in early life has not fully been addressed. This study is the first demonstration that the DNA methylation status of the *Gpam* promoter and its mRNA expression are inversely correlated during mouse liver maturation. This study highlights the role of DNA methylation in the regulation of lipogenic genes, thereby providing new insight into the molecular mechanism underlying epigenetic regulation of metabolic diseases.

RESEARCH DESIGN AND METHODS

Animals and the experiment with high-fat/high-sucrose diet–fed dams. Pregnant female C57BL/6 mice were obtained from Japan SLC (Hamamatsu, Japan). The mice were fed ad libitum a standard rodent chow, CRF1 (Charles River Japan, Tokyo, Japan). Offspring at the indicated ages were used for tissue

From the [1]Department of Molecular Medicine and Metabolism, Medical Research Institute, Tokyo Medical and Dental University, Tokyo, Japan; the [2]Functional Food Research Department, Food Science and Technology Institute, Morinaga Milk Industry Co., Ltd., Kanagawa, Japan; the [3]Department of Organ Network and Metabolism, Medical Research Institute, Tokyo Medical and Dental University, Tokyo, Japan; the [4]Nutritional Science Program, National Institute of Health and Nutrition, Tokyo, Japan; the [5]Laboratory for Mammalian Epigenetic Studies, Center for Developmental Biology, RIKEN, Kobe, Japan; the [6]Department of Molecular Endocrinology and Metabolism, Graduate School of Medical and Dental Sciences, Tokyo Medical and Dental University, Tokyo, Japan; and the [7]Global Center of Excellence Program, International Research Center for Molecular Science in Tooth and Bone Diseases, Medical Research Institute, Tokyo Medical and Dental University, Tokyo, Japan.

Corresponding author: Yoshihiro Ogawa, ogawa.mem@tmd.ac.jp.

Received 4 January 2012 and accepted 19 April 2012.

DOI: 10.2337/db11-1834

This article contains Supplementary Data online at http://diabetes.diabetesjournals.org/lookup/suppl/doi:10.2337/db11-1834/-/DC1.

T.E. and Y.K. contributed equally to this work.

sampling. They were weaned at 25 days of age and thereafter fed CRF1 throughout the experiment.

The experiment with high-fat/high-sucrose (HF/HS) diet–fed dams was performed as follows. Six-week-old male and female C57BL/6 mice (Japan SLC) were crossed, and pregnant dams were used. Two weeks before the beginning of mating and throughout the experiment, dams were fed ad libitum either CRF1 (standard) or HF/HS diet (D12079B; Research Diets, New Brunswick, NJ). Schematic experimental design is shown in Supplementary Fig. 1. Five-day-old offspring were used for analysis. All animal experiments were approved by Institutional Animal Care and Use Committee of Tokyo Medical and Dental University (approval identification number 0090041).

Quantitative real-time PCR analysis. Gene expression levels were measured as described (19). The primers used are shown in Supplementary Table 1.

Western blot analysis. The nuclear fraction of cell lysate was prepared using a ProteoJET Cytoplasmic and Nuclear Protein Extraction Kit (Fermentas, Glen Burnie, MD). Mitochondrial fraction of the liver was prepared as described (4). Western blot analysis was performed as described previously (19). Anti-GPAT1 (sc-161674; Santa Cruz Biotechnology, Santa Cruz, CA), anti-SCD1 (ab19862; Abcam, Cambridge, MA), anti-FAS (sc-48357; Santa Cruz Biotechnology), anti–SREBP-1 (ab3259; Abcam), anti-CoxIV (ab14774; Abcam), anti–α-tubulin (T9026; Sigma-Aldrich, St. Louis, MO), anti-Lamin a/c (sc-20681; Santa Cruz Biotechnology), anti-Dnmt3b (IMG184A; Imgenex, San Diego, CA), or histone H1 (sc-10806; Santa Cruz Biotechnology) was used as the primary antibody.

Bisulfite DNA methylation analysis. Sodium bisulfite treatment of genomic DNA was performed with a BisulFast DNA modification kit (Toyobo, Tokyo, Japan) according to the manufacturer's instructions. Sequential PCR amplification of the genes of interest was performed using specific primers (Supplementary Table 2). The PCR profile was as described in Supplementary Table 2. The amplified fragments were ligated into the vector pGEM-T-easy (Promega KK, Tokyo, Japan) and sequenced. At least 16 bacterial colonies were picked up per PCR amplification. A web-based tool, quantification tool for methylation analysis, was used for bisulfite sequencing analysis of CpG methylation (http://quma.cdb.riken.jp/) (20).

Quantification of DNA methylation of the *Gpam* promoter. DNA digestion with methylation-sensitive *Hpa*II and quantitative real-time PCR were performed as described previously (21), with the following primers: forward primer 5′-CCCTAAAACTGGCTCCGGA-3′ and reverse primer 5′-CAGCCAATCGAAAGCTTCAGA-3′. The forward primer contains the *Hpa*II site of *Gpam* promoter (underlined).

Primary culture of mouse hepatocytes. Primary hepatocytes were isolated as described previously (22,23).

Preparation of recombinant adenovirus. The full-length mouse Dnmt3b1 cDNA was subcloned into the pShuttle vector provided in the BD Adeno-X Expression System (BD Biosciences, Franklin Lakes, NJ). BD Adeno-X enhanced green fluorescent protein (GFP) was used as a control (Ad-GFP; BD Biosciences). Ad–SREBP-1c (active-nuclear form) (24) was kindly provided from Dr. Hitoshi Shimano (Tsukuba University). Each recombinant adenovirus (Ad-Dnmt3b, Ad-SREBP-1c, or Ad-GFP) was added to the medium of primary cultured hepatocytes (1.8×10^7 infection-forming units in 500 μL).

TG/diacylglycerol synthesis in isolated liver and primary hepatocytes. The liver was dissected from tendon to tendon and placed in modified Krebs-Henseleit buffer containing 4% fatty acid-free bovine serum albumin (Sigma-Aldrich), 5 mmol/L glucose, and 0.5 mmol/L palmitate, giving a palmitate-to-bovine serum albumin molar ratio of 1:1. After a 30-min preincubation period, liver strips were transferred to vials containing 0.5 μCi/mL [1-^{14}C]palmitate (GE Healthcare Life Sciences, Buckinghamshire, U.K.) for 60 min. For primary hepatocytes, cells were incubated with [1-^{14}C]palmitate in medium for 6 h. From the liver or cells, lipids were extracted with chloroform/methanol (2:1) and resolved by thin-layer chromatography (hexane/ethyl ether/acetic acid = 60:40:3) followed by photoimaging detection.

Transfection and luciferase assay with methylated plasmids. A luciferase gene construct containing the *Gpam* promoter fragment (from −489 to +79, taking the first nucleotide of exon 1 as +1) was prepared. For in vitro DNA methylation, the construct was digested with *Asp*718/*Xho*I, and a fragment containing the *Gpam* promoter (−489 to +79) was purified, which was followed by treatment with *Sss*I (CpG methylase) as described previously (17). Methylation was confirmed by digestion with a methylation-sensitive restriction enzyme, *Hpa*II. The luciferase assay was performed as described in (19,24).

Chromatin immunoprecipitation analysis. Chromatin immunoprecipitation (ChIP) was performed using an assay kit (Upstate, Temecula, CA) (25). The lysate was incubated with DynaBeads protein G-conjugated (Life Technologies, Carlsbad, CA) anti–SREBP-1c (sc-8984X; Santa Cruz Biotechnology), anti-Dnmt1 (sc-20701; Santa Cruz Biotechnology), anti-Dnmt3a (ab2850; Abcam), anti-Dnmt3b (ab2851; Abcam), anti-trimethyl-histone H3 (Lys4) (#07-473; Upstate), anti-acetyl-histone H3 (Lys9) (#06-911; Millipore, Temecula, CA), anti-dimethyl-histone H3 (Lys9) (#9753; Cell Signaling Technology, Danvers, MA) antibody, or rabbit normal IgG (sc-2027; Santa Cruz Biotechnology). The ChIP-enriched DNA samples were analyzed by quantitative PCR. PCR primers were designed to locate SREs of the *Gpam* or *Scd1* promoter (Supplementary Table 3).

Liver TG analysis. The liver TG levels were measured by enzymatic colorimetry as described (19).

Statistical analysis. Statistical analysis was performed using Student *t* test and ANOVA followed by Scheffe test. Data were expressed as the mean ± SE. A P value of <0.05 was considered statistically significant.

RESULTS

Lipogenic gene and SREBP-1c mRNA expression in the neonatal and adult livers. We examined lipogenic gene expression in the neonatal and adult livers before and after weaning. The GPAT1 mRNA was only slightly expressed in the neonatal liver (days 0, 5, and 9), but markedly increased (~40-fold) in the adult liver (10 weeks of age). Similar to GPAT1, both SCD1 and FAS mRNA levels, as well as protein levels of GPAT1, SCD1, and FAS, and GPAT-mediated TG/diacylglycerol (DG) biosynthesis were increased in the adult liver relative to the neonatal liver (Fig. 1*A* and Supplementary Fig. 2). There is a GPAT1 splicing-variant (GPAT1-variant) with an alternative first noncoding exon (GenBank accession number: NM_008149) using an alternative promoter that is ~30 kb downstream from the *Gpam* promoter containing SREs, thus producing the identical coding GPAT1 protein. In this study, its mRNA expression showed a relatively small increase (approximately threefold) from neonates (day 0) to adults (Fig. 1*A*).

SREBP-1c mRNA was weakly expressed in the neonatal liver (day 0) and increased markedly (~100-fold) in the adult liver (10 weeks of age). At day 9, approximately half the level seen in the adults was observed (Fig. 1*A*). SREBP-1c protein level was very low on day 0 and modestly and markedly increased on day 9 and in adults, respectively (Fig. 1*A*). Namely, on day 9, SREBP-1c was expressed but its target genes were not; they showed delayed expression than SREBP-1c, suggesting that the activity of SREBP-1c is regulated posttranslationally.

DNA methylation of lipogenic gene promoters in neonatal and adult livers. The *Gpam* promoter region contains three SREs (Fig. 1*B*) (6). Bisulfite analysis revealed high DNA methylation levels of the *Gpam* promoter containing SREs in the neonatal liver (day 0) (Fig. 1*C*). By contrast, less DNA methylation levels were observed in the adult liver (Fig. 1*C*). We also confirmed the differential DNA methylation of the *Gpam* promoter in the neonatal and adult livers, based upon digestion with a methylation-sensitive enzyme, *Hpa*II, for which the recognition site locates between the first and second SREs (Fig. 1*B*), and a subsequent quantitative real-time PCR analysis. Consistent with the data of bisulfite analysis, DNA methylation levels were high in the neonatal liver (day 0 and 5; ~60%, day 9; ~55%) relative to the adult liver (~15%) (Fig. 1*D*). By contrast, appreciable DNA methylation of the *Scd1* and *Fasn* promoters, containing SREs, was not observed in both the neonatal (day 0) and adult (10 weeks of age) livers (Fig. 1*E*).

In a CpG island of the alternative promoter of the *Gpam*, there was also no significant DNA methylation in the neonatal (day 0) and adult (10 weeks of age) livers (Fig. 1*E*). In contrast, DNA methylation levels were high in the repetitive element of intracisternal A particle (IAP) (26), one of the markers of global DNA methylation, in both the neonatal and adult livers (Fig. 1*E*). It is therefore likely that DNA methylation differs in certain regions of the genome between neonatal and adult livers.

DNA methylation of the *Gpam* promoters in the adult skeletal muscle. In contrast to the liver, high DNA methylation levels in the *Gpam* promoter were observed in

DNA METHYLATION OF THE *Gpam* PROMOTER IN LIVER

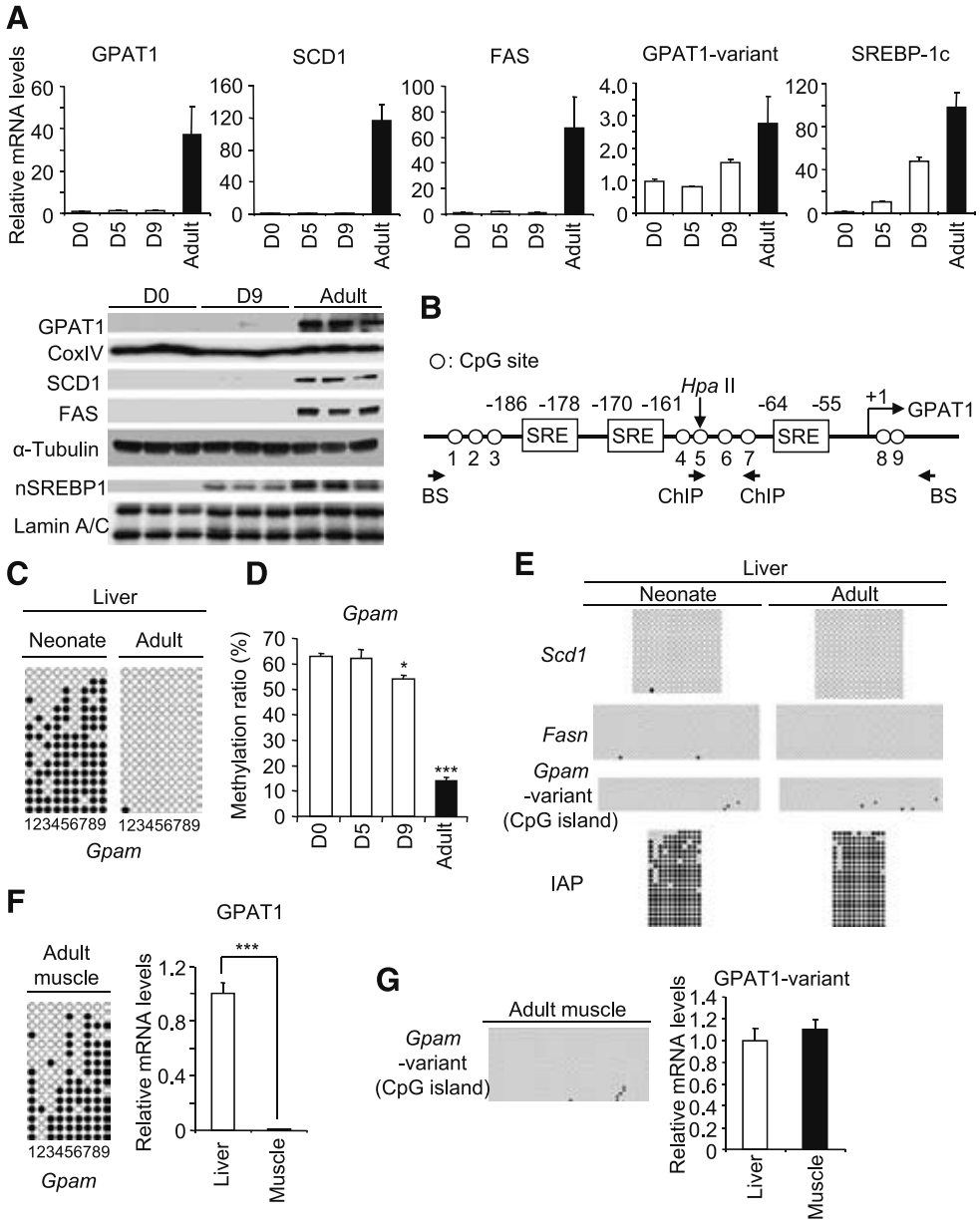

FIG. 1. Lipogenic gene expression and DNA methylation in the neonatal and adult mice livers. *A*: Relative lipogenic gene and SREBP-1c mRNA levels in the neonatal (days after birth: 0, 5, and 9) and adult livers (after weaning, 10 weeks of age), examined by quantitative real-time PCR. Values for day 0 were set at 1. Western blot analysis of GPAT1, SCD1, FAS, and nuclear form of SREBP-1 (nSREBP1) in neonatal (days 0 and 9) and adult livers (10 weeks of age). For GPAT1, mitochondrial fraction was used. For FAS/SCD1 and SREBP-1, cytoplasmic and nuclear fractions were used, respectively. α-Tubulin and Lamin a/c are cytoplasmic and nuclear markers, respectively, used for loading controls. *B*: Schematic representation of the *Gpam* promoter region. The *Gpam* promoter contains three SREs (−186 to −178, −170 to −161, and −64 to −55, transcription start site counted as +1). Each circle denotes a CpG site, numbered 1–9. The *Hpa*II site is indicated (arrow). Position of PCR primers for bisulfite PCR analysis (BS) and ChIP analysis are indicated. *C*: Bisulfite analysis of the *Gpam* promoter. PCR primers used in bisulfite analysis for the *Gpam* promoter are shown in *B*. Filled circles are methylated and open circles are unmethylated CpGs. The numbers beneath are as shown in *B*. The *left panel* is a neonatal liver sample (day 0), and the *right panel* is an adult liver sample (10 weeks of age). Representative results of three independent animals of each group with similar results are shown. *D*: DNA methylation of the *Gpam* promoter, estimated by *Hpa*II digestion followed by quantitative real-time PCR. Genomic DNA treated with *BamH*I alone was prepared as an uncut control (i.e., a fully methylated control [100%]) and diluted as a standard dilution series. *$P < 0.05$, ***$P < 0.001$ compared with D0 sample; $n = 3$. *E*: Bisulfite analysis of the *Scd1* and *Fasn* promoters and the alternative *Gpam* promoter, containing CpG island, and IAP in the neonatal and adult liver. Representative results of three independent animals of each group with similar results are shown. *F*: Bisulfite analysis and quantitative real-time PCR mRNA analysis of the *Gpam* promoter in the adult skeletal muscle (10 weeks of age). Values for the liver were set at 1. $n = 3$. For bisulfite analysis, a typical result from three independent experiments with similar results is shown. ***$P < 0.001$. *G*: Bisulfite analysis of the alternative *Gpam* promoter in the adult skeletal muscle and relative GPAT1-variant mRNA levels in the adult liver and skeletal muscle. $n = 3$. CoxIV, cytochrome oxidase IV, a mitochondrial marker.

the skeletal muscle of adult mice, where its mRNA expression was very low (Fig. 1*F*). DNA methylation levels of the alternative *Gpam* promoter were low in the skeletal muscle and liver, and GPAT1-variant expression levels were similar between the skeletal muscle and liver (Fig. 1*G*). These observations, taken together, suggest that DNA methylation of the *Gpam* promoter, containing SREs, and its mRNA expression are inversely correlated in the skeletal muscle.

DNA methylation of the *Gpam* promoter in primary culture of neonatal mouse hepatocytes. We next examined DNA methylation of the *Gpam* promoter in primary culture of neonatal mouse hepatocytes. In this study, the gene expression of albumin, a marker of mature hepatocytes, increased during the course of culture, suggesting the maturation of primary hepatocytes (Fig. 2*A*). The DNA methylation levels of the *Gpam* promoter was high at 0 h but gradually decreased at 48 and 96 h, and GPAT1 mRNA levels were low at 0 h and increased at 48 and 96 h (Fig. 2*B*). By contrast, DNA methylation levels of IAP remained high at both 0 and 96 h (Fig. 2*B*), suggesting that decreased methylation is not likely due to total demethylation of the whole genome. These observations also suggest an inverse correlation between DNA methylation of the *Gpam* promoter and its mRNA expression in primary culture of neonatal mouse hepatocytes.

Reporter activity from the *Gpam* promoter with in vitro DNA methylation. In an in vitro reporter assay, we examined whether DNA methylation of the *Gpam* promoter affects the SREBP-1c–induced transcriptional activity. Cotransfection of the *Gpam* promoter-Luc without DNA methylation and SREBP-1c expression plasmid in HEK293 cells caused increased reporter activity from the *Gpam* promoter (Fig. 2*C*). By contrast, upon methylation of the *Gpam* promoter, Luc activity was not increased above the basal level even in the presence of the SREBP-1c expression plasmid (Fig. 2*C*).

Adenovirus-mediated SREBP-1c overexpression and ChIP analysis of the *Gpam* promoter in neonatal and adult primary hepatocytes. To address whether DNA methylation of the *Gpam* promoter is critical for SREBP-1c–dependent GPAT1 expression, we overexpressed SREBP-1c in neonatal (high DNA methylation) and adult (low DNA methylation levels in the *Gpam* promoter) primary hepatocytes through the adenoviral technique. We observed similarly high expression of nuclear form of SREBP-1c protein in neonatal and adult primary hepatocytes (Fig. 2*D*). In this experiment, we observed less expression of GPAT1 with lower recruitment of SREBP-1 to the *Gpam* promoter in the neonatal primary hepatocytes relative to adult primary hepatocytes (Fig. 2*D*). The data indicated that GPAT1 expression is low even in the presence of considerable SREBP-1c expression, suggesting that DNA methylation of the *Gpam* promoter is critical for SREBP-1c–dependent GPAT1 expression.

ChIP analysis of the *Gpam* promoter in neonatal and adult liver. Dnmt1, -3a, and -3b mRNA expression was detected in the neonatal and adult livers, although the

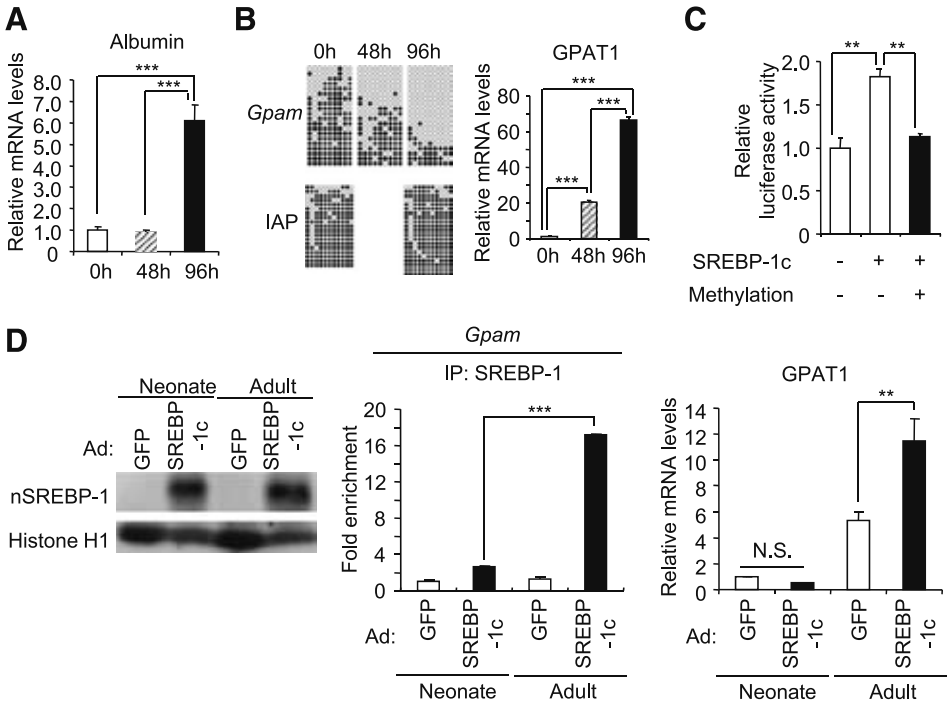

FIG. 2. In vitro analysis of DNA methylation and SREBP-1 recruitment of the *Gpam* promoter. mRNA expression levels of albumin (*A*) and DNA methylation and mRNA expression levels (*B*) of the *Gpam* in neonatal primary hepatocytes, cultured at 0, 48, and 96 h. The *upper panels* are the results of the *Gpam* promoter and lower panels are those of IAP. ***$P < 0.001$. *C*: In vitro methylation reporter assay. Relative luciferase activities are shown. Values without DNA methylation and in the absence of SREBP-1c expression vector are set at 1. **$P < 0.01$; $n = 4$. *D*: *Left*: Western blot analysis of primary hepatocytes from day 0 (neonate) and 10 weeks (adult) of age, overexpressing SREBP-1c and control GFP. *Middle*: ChIP analysis; recruitment of SREBP-1c to the *Gpam* promoter in those cells. *Right*: Quantitative real-time PCR analysis of GPAT1 mRNA. Values for the neonatal hepatocytes with GFP were set at 1. **$P < 0.01$, ***$P < 0.001$; $n = 3$.

hepatic Dnmt1 mRNA levels were lower in the adult liver than in the neonatal liver (Fig. 3*A*). Therefore, we performed ChIP analysis to compare the recruitment of SREBP-1 and Dnmts to the *Gpam* promoter between the neonatal and adult livers. In this study, SREBP-1 was not recruited to the *Gpam* promoter in the neonatal liver (day 0 after birth), although it was clearly recruited in the adult liver (Fig. 3*B*). Importantly, Dnmt3b was strongly recruited to the *Gpam* promoter in the neonatal liver, but not in the adult liver (Fig. 3*B*). Dnmt3a was also recruited, although weakly, to the *Gpam* promoter in the neonatal liver, but not in the adult liver (Fig. 3*B*). We also found that levels of histone H3 lysine-4-trimethylation (H3K4me3) and lysine-9-acetylation (H3K9Ac), two transcriptionally active histone codes, are increased and those of the repressive histone H3 lysine-9-di-methylation (H3K9me2) are decreased at the *Gpam* promoter in the adult liver relative to the neonatal liver (Fig. 3*B*). The recruitment of Dnmt3a and Dnmt3b to the *Scd1* promoter did not differ significantly between the neonatal and adult livers (Fig. 3*C*). In this study, we observed that the recruitment of SREBP-1 and level of H3K9Ac are increased and that of H3K9me2 is decreased at the *Scd1* promoter in the adult liver relative to the neonatal liver (Fig. 3*C*).

DNA methylation of the *Gpam* promoter and GPAT-mediated TG/DG synthesis in primary hepatocytes with Dnmt3b overexpression. With adenoviral transduction of Dnmt3b, which was strongly recruited to the *Gpam* promoter

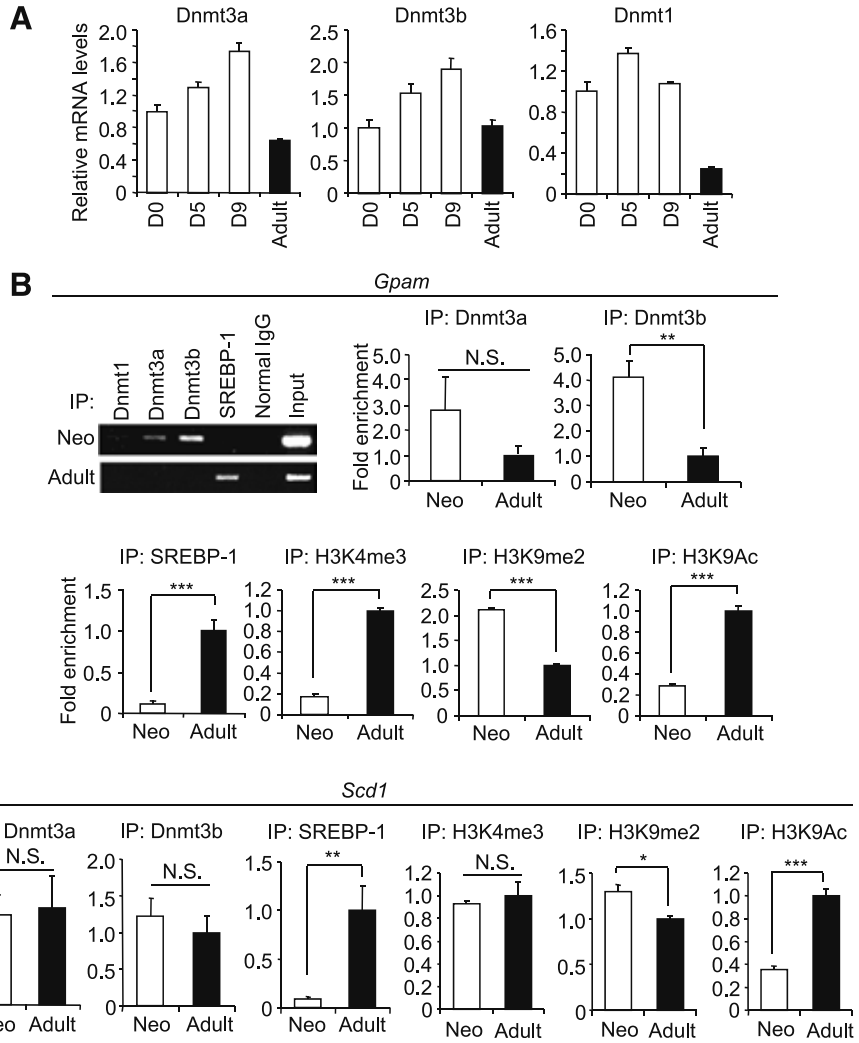

FIG. 3. Recruitment of SREBP-1c and Dnmts to the *Gpam* and *Scd1* promoters containing SREs, with changes in histone modification. *A*: Relative Dnmts mRNA levels in the neonatal (days after birth: 0, 5, and 9) and adult livers (10 weeks of age) examined by quantitative real-time PCR. Values for day 0 were set at 1. *n* = 3 to 4. *B*: ChIP analysis. Neonatal (day 0) and adult (10 weeks) livers were used for ChIP analysis with the indicated antibodies. Amplified PCR primers are as shown in Fig. 1*B*. The *top left panel* is a representative gel electrophoresis photo. Input is a PCR product from the aliquot of liver lysate before immunoprecipitation (IP). The graphs demonstrate quantitative PCR analysis. The graph of Dnmt1 is not shown because signals from the neonatal and adult livers are lower than the negative control IgG signals. *C*: ChIP analysis in the *Scd1* promoter in the samples used in *B*. Values of adult sample are set at 1. **P* < 0.05, ***P* < 0.01, ****P* < 0.001, *n* = 3 to 4.

in the neonatal liver (Fig. 3*B*), we next examined DNA methylation of the *Gpam* promoter, its mRNA expression, and TG/DG synthesis in primary hepatocytes, which were obtained from adult mice with low DNA methylation levels of the *Gpam* promoter. In this study, we confirmed Dnmt3b overexpression causes significant Dnmt3b protein expression (Fig. 4*A*). We found increased DNA methylation of the *Gpam* promoter (Fig. 4*B*), but not *Scd1* and *Fasn* promoters (Fig. 4*C*), in Dnmt3b-expressing hepatocytes relative to control GFP-expressing hepatocytes. The GPAT1 mRNA levels were markedly lower in hepatocytes with Dnmt3b overexpression than those with control GFP (Fig. 4*D*). In the *Gpam* promoter (Fig. 4*E*), but not the *Scd1* promoter (Fig. 4*F*), SREBP-1 was less recruited in Dnmt3b-expressing hepatocytes than in control GFP-expressing hepatocytes. In addition, TG/DG synthesis and TG contents were lower in Dnmt3b-expressing hepatocytes than in GFP-expressing hepatocytes (Fig. 4*G*). These data suggest that increased DNA methylation suppresses SREBP-1 recruitment in the *Gpam* promoter, decreased GPAT1 expression, and TG/DG synthesis.

DNA methylation of the *Gpam* promoter in the neonatal offspring liver of the HF/HS diet–fed dams. We next examined whether the observed DNA methylation of the *Gpam* promoter is affected by environmental factors in vivo. A high-fat or high-calorie diet fed to female animals during gestation and lactation has been reported to increase lipogenic gene expression and TG levels in the liver of offspring (27). In this study, we fed a high-calorie, lipogenic HF/HS diet to dams and examined DNA methylation of the *Gpam* promoter in the offspring. In pups of the HF/HS diet–fed dams, DNA methylation levels of the *Gpam* promoter were lower, and GPAT1 mRNA levels and SREBP-1 recruitment, but not SREBP-1c mRNA levels, were higher than those in the pups of standard diet–fed dams (Fig. 5*A*–*D*). In this study, hepatic TG levels increased in the pups of the HF/HS diet–fed dams relative to those of the standard diet–fed dams (Fig. 5*E*).

DISCUSSION

The DNA methylation status has been considered to be relatively stable except during embryogenesis and carcinogenesis. However, recent studies showed that DNA methylation can be modulated in normal tissues even after birth (28). In this study, we show that expression of *Gpam*, which encodes a rate-limiting enzyme for TG biosynthesis, increases in the liver during weaning in response to the physiologic demand of TG biosynthesis. This may be related to the dynamic change in the DNA methylation status of the *Gpam* promoter during liver maturation. In the neonatal liver, the *Gpam* promoter region, containing three SREs, shows high DNA methylation levels with low *Gpam* expression, whereas in the adult liver, it shows low DNA methylation levels with high *Gpam* expression. Importantly, SREBP-1c is recruited to the promoter in the adult liver but not in the neonatal liver. In this study, in vitro analysis revealed that DNA methylation of the *Gpam* promoter can suppress the

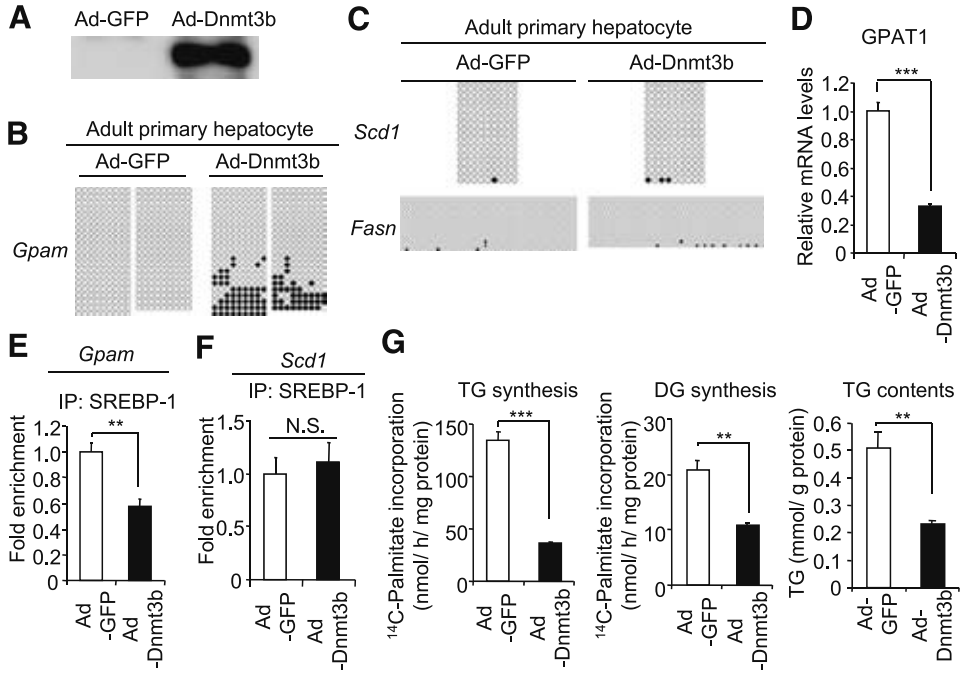

FIG. 4. DNA methylation level of the *Gpam* promoter and GPAT-mediated TG/DG synthesis in the adult primary hepatocytes overexpressing Dnmt3b. *A*: Protein expression levels of Dnmt3b in adult primary hepatocytes overexpressing Dnmt3b and control GFP. Endogenous Dnmt3b protein expression is known to be high in early embryo and embryonic stem cells, but very low in adult tissues (33) and was not detected in this experiment using adult primary hepatocyte samples. *B*: DNA methylation level of the *Gpam* promoter in adult primary hepatocytes overexpressing Dnmt3b and control GFP. Results of two independent dishes from each group are shown. *C*: DNA methylation level of the *Scd1* and *Fasn* promoters. *D*: Expression of GPAT1 mRNA levels and recruitment of SREBP-1 to the *Gpam* (*E*) and *Scd1* (*F*) promoters. Values of GFP cells are set at 1. *G*: TG/DG synthesis levels and TG contents. **$P < 0.01$, ***$P < 0.001$. $n = 3$.

DNA METHYLATION OF THE *Gpam* PROMOTER IN LIVER

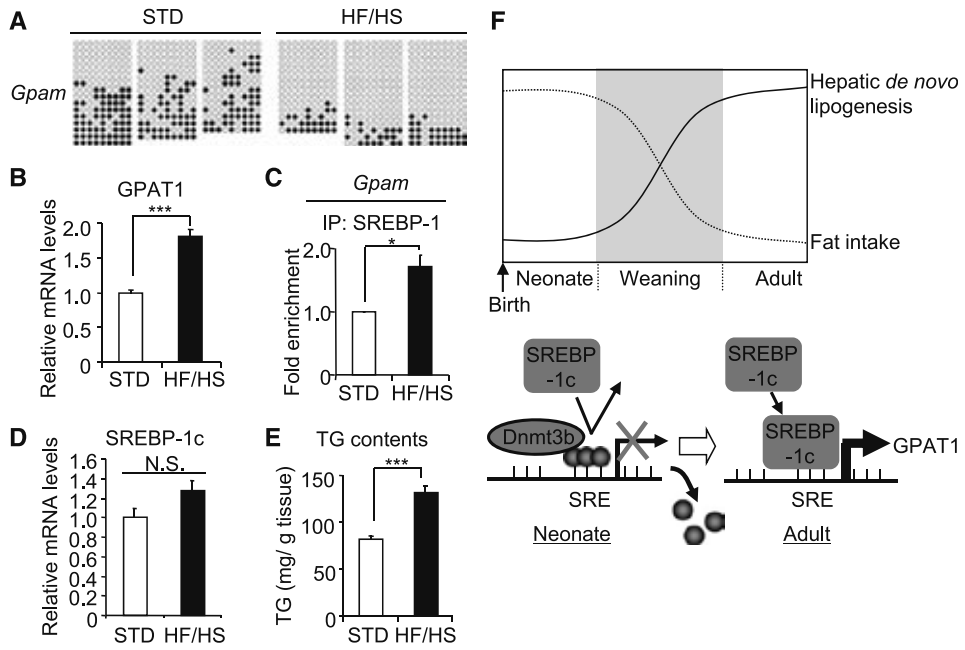

FIG. 5. DNA methylation of the *Gpam* promoter and its mRNA expression in pups of dams fed an HF/HS diet during gestation and lactation. *A*: DNA methylation of the *Gpam* promoter in pups (day 5) of the HF/HS or standard (STD) diet–fed dams. Representative bisulfite sequencing data from three animals in each group. Relative GPAT1 mRNA levels (*B*), recruitment of SREBP-1 to the *Gpam* promoter (*C*), and relative SREBP-1c mRNA levels (*D*) in pups of the HF/HS and STD diet–fed dams. *E*: Liver TG levels of neonatal liver (day 5). Open bar, STD-fed dams; filled bar, HF/HS diet-fed dams. *$P < 0.05$, ***$P < 0.001$; $n = 7$ (open bars), $n = 4$ (filled bars). *F*: Schematic model of the DNA methylation-mediated regulation of *Gpam* expression in the neonatal and adult livers. The graph shows the time course of the dietary fat content and rate of hepatic de novo lipogenesis before and after weaning. In the neonatal liver, the *Gpam* promoter may be highly methylated at least in part by Dnmt3b, when SREBP-1c cannot make access to the promoter. In the adult liver, the *Gpam* promoter is less methylated, with SREBP-1c being recruited to the promoter, thereby activating GPAT1 mRNA expression. Environmental factors, such as nutritional state, may change the DNA methylation status. Closed circle denotes methyl group.

SREBP-1c–mediated transcriptional activation. Less SREBP-1 recruitment in the *Gpam* promoter in Dnmt3b-overexpressing hepatocytes suggests that DNA methylation of the *Gpam* promoter inhibited SREBP-1c recruitment. These observations, taken together, suggest the role of DNA methylation in the suppressed *Gpam* expression in the neonatal liver even in the presence of SREBP-1c. This above discussion is consistent with a previous observation that the extent of hepatic de novo lipogenesis in the neonatal liver is lower than that in the adult liver (1). Consistent with the decreased DNA methylation, transcriptionally active H3K4me3 and H3K9Ac are increased, whereas repressive H3K9me2 is decreased at the *Gpam* promoter in the adult liver. It is conceivable that in the neonatal liver, DNA methylation of the *Gpam* promoter plays roles in the formation and/or maintenance of transcriptionally repressive chromatin conformation, thereby inhibiting the recruitment of SREBP-1c. In contrast, in the adult liver, decreased DNA methylation and increased active histone modifications may lead to the recruitment of SREBP-1c to the *Gpam* promoter.

The mechanism underlying the altered DNA methylation of the genome has not been thoroughly investigated. In this study, we found that Dnmt3b, which is implicated in de novo DNA methylation, is strongly recruited to the *Gpam* promoter in the neonatal liver but not in the adult liver. Dnmt3b overexpression markedly increases DNA methylation levels of the *Gpam* promoter in primary adult hepatocytes. Dnmt3b plays important roles in embryogenesis (10). It has been recently reported to be involved in colon cancer (29) and hormonal gene regulation in renal tubular cells (30). Therefore, it is likely that the decreased recruitment of Dnmt3b plays a role in the decreased DNA methylation of the *Gpam* promoter, and additional mechanism(s) for DNA demethylation may be involved in the process.

The H3K4 methylation level is reported to be reciprocal with the DNA methylation level, and H3K4me2/3 and DNA methylation occur mutually exclusively (11,31). In the region of H3K4me2/3, the DNA methylation levels are generally low. Alternatively, Dnmt3 may preferentially bind to genomic DNA without H3K4 methylation. In this study, the H3K4me3 level in the *Gpam* promoter was low in the neonatal liver and high in adult liver, whereas the H3K4me3 level in the *Scd1* promoter was similar in neonatal and adult livers. Thus, it is possible that histone modification is involved in the regulation of specificity of DNA methylation in *Gpam* and *Scd1* promoters. In addition, because GPAT1 contributes to the transfer of fatty acid to glycerol, whereas SCD1 and FAS are involved in fatty acid biosynthesis (3), the differential positioning of GPAT1, SCD1, and FAS in the TG biosynthesis pathway may explain the different mechanisms of their gene expression. Further studies are required to elucidate how *Scd1* and *Fasn* transcription is regulated in the neonatal liver.

In this study, we also found that GPAT1 mRNA levels are much lower in the adult skeletal muscle than those in the adult liver, although SREBP-1c is highly expressed in

both tissues (19). This is consistent with a previous report that the GPAT1 enzymatic activity in the skeletal muscle is much lower than that in the liver (32). The low expression of *Gpam* in the adult skeletal muscle may be because the high DNA methylation of the *Gpam* promoter suppresses the SREBP-1c–mediated transcriptional activation. Therefore, it is conceivable that DNA methylation of the *Gpam* promoter is involved in the SREBP-1c–dependent tissue-specific regulation of *Gpam* expression. In contrast, the expression of the GPAT1-variant transcript from the alternative promoter without SRE in the neonatal liver is roughly comparable to that in the adult liver. This is consistent with our observation that the alternative promoter is unmethylated in both the neonatal and adult livers, thereby suggesting the role for DNA methylation in the promoter-specific regulation of *Gpam* in the liver.

The change in hepatic gene expression before and after weaning could be regulated in response to nutritional demand. Indeed, we demonstrated that the lipogenic HF/HS diet fed to female mice during pregnancy and lactation results in decreased DNA methylation of the *Gpam* promoter in the liver of offspring, suggesting that the DNA methylation status can be modulated, at least in part, by the nutritional factors. Thus, the change in DNA methylation of the *Gpam* promoter is likely to be affected by the fetal and neonatal environments, such as nutrition, and/or be a programmed process of liver maturation.

Whether DNA methylation would affect hepatic de novo lipogenesis later in life is an important issue to be addressed. Previous reports showed that maternal overnutrition in animals contributes to the development of nonalcoholic fatty liver disease in adult offspring (27), suggesting that hepatic lipid metabolism is nutritionally affected early in life. In this study, maternal overnutrition caused decreased *Gpam* promoter methylation with increased GPAT1 expression and TG level in the liver of the offspring; however, the possibility cannot be excluded that increased lipid flux from dam, as well as increased de novo TG biosynthesis, might have affected the liver TG content of offspring. Further studies are required to understand whether DNA methylation can affect hepatic de novo lipogenesis and susceptibility to fatty liver-related diseases in later life.

In conclusion, this study is the first demonstration of reciprocal change in DNA methylation of the *Gpam* promoter and its mRNA expression in the mouse liver before and after weaning (Fig. 5*F*). Our data suggest that in the neonatal liver, DNA methylation of the *Gpam* promoter containing SREs, which is likely to be induced by Dnmt3b, inhibits the recruitment of SREBP-1c, whereas in the adult liver, the decreased DNA methylation may result in active chromatin conformational change, thereby allowing the recruitment of SREBP-1c. This is the first detailed analysis of the DNA methylation-dependent regulation of TG biosynthesis gene in the liver, thereby leading to the better understanding of the molecular mechanism underlying the epigenetic regulation of metabolic genes and thus metabolic diseases.

ACKNOWLEDGMENTS

This work was supported in part by Grants-in-Aid for Scientific Research from the Ministry of Education, Culture, Sports, Science and Technology of Japan and the Ministry of Health, Labour and Welfare of Japan and research grants from "To promote basic research by research personnel in private-sector business (Japan Science and Technology Agency)," Mitsukoshi Health and Welfare Foundation, The Danone Institute of Japan Foundation, Nestle Nutrition Council, Novo Nordisk Study Award for Growth and Development, Ono Medical Research Foundation, and The Morinaga Foundation for Health and Nutrition. No other potential conflicts of interest relevant to this article were reported.

T.E., Y.K., and Y.O. designed the research. T.E., Y.K., M.Tak., X.Y., S.K., E.T., M.Tan., T.Y., and S.M. performed research. T.S. and M.O. analyzed data. O.E. and M.O. contributed new reagents and analytic tools. Y.K. and Y.O. wrote the manuscript. All authors contributed to the discussion. Y.O. is the guarantor of this work and, as such, had full access to all the data in the study and takes responsibility for the integrity of the data and the accuracy of the data analysis.

The authors thank Dr. Hitoshi Shimano (Tsukuba University, Japan) for the kind gift of Ad-SREBP-1c and Drs. Jun Inoue and Ryuichiro Sato (University of Tokyo, Japan) for advice on SREBP-1c Western blotting. The authors also thank Dr. Shigeomi Shimizu (Tokyo Medical and Dental University, Japan) for advice on mitochondrial preparation, Drs. Eriko Misawa and Miyuki Tanaka (Morinaga Milk Industry Co. Ltd., Kanagawa, Japan) for assistance in TG synthesis measurement, Kozue Ochi (Tokyo Medical and Dental University, Tokyo Japan) for technical assistance, and Hiroko Takahashi (Tokyo Medical and Dental University) for secretarial assistance.

REFERENCES

1. Perez-Castillo A, Schwartz HL, Oppenheimer JH. Rat hepatic mRNA-S14 and lipogenic enzymes during weaning: role of S14 in lipogenesis. Am J Physiol 1987;253:E536–E542
2. Decaux JF, Ferré P, Robin D, Robin P, Girard J. Decreased hepatic fatty acid oxidation at weaning in the rat is not linked to a variation of malonyl-CoA concentration. J Biol Chem 1988;263:3284–3289
3. Wendel AA, Lewin TM, Coleman RA. Glycerol-3-phosphate acyltransferases: rate limiting enzymes of triacylglycerol biosynthesis. Biochim Biophys Acta 2009;1791:501–506
4. Lindén D, William-Olsson L, Ahnmark A, et al. Liver-directed overexpression of mitochondrial glycerol-3-phosphate acyltransferase results in hepatic steatosis, increased triacylglycerol secretion and reduced fatty acid oxidation. FASEB J 2006;20:434–443
5. Hammond LE, Gallagher PA, Wang S, et al. Mitochondrial glycerol-3-phosphate acyltransferase-deficient mice have reduced weight and liver triacylglycerol content and altered glycerolipid fatty acid composition. Mol Cell Biol 2002;22:8204–8214
6. Ericsson J, Jackson SM, Kim JB, Spiegelman BM, Edwards PA. Identification of glycerol-3-phosphate acyltransferase as an adipocyte determination and differentiation factor 1- and sterol regulatory element-binding protein-responsive gene. J Biol Chem 1997;272:7298–7305
7. Tabor DE, Kim JB, Spiegelman BM, Edwards PA. Identification of conserved cis-elements and transcription factors required for sterol-regulated transcription of stearoyl-CoA desaturase 1 and 2. J Biol Chem 1999;274:20603–20610
8. Wong RH, Chang I, Hudak CS, Hyun S, Kwan HY, Sul HS. A role of DNA-PK for the metabolic gene regulation in response to insulin. Cell 2009;136:1056–1072
9. Stefan N, Kantartzis K, Häring HU. Causes and metabolic consequences of Fatty liver. Endocr Rev 2008;29:939–960
10. Okano M, Bell DW, Haber DA, Li E. DNA methyltransferases Dnmt3a and Dnmt3b are essential for de novo methylation and mammalian development. Cell 1999;99:247–257
11. Weber M, Hellmann I, Stadler MB, et al. Distribution, silencing potential and evolutionary impact of promoter DNA methylation in the human genome. Nat Genet 2007;39:457–466
12. Mikkelsen TS, Xu Z, Zhang X, et al. Comparative epigenomic analysis of murine and human adipogenesis. Cell 2010;143:156–169
13. Maunakea AK, Nagarajan RP, Bilenky M, et al. Conserved role of intragenic DNA methylation in regulating alternative promoters. Nature 2010;466:253–257

14. Sharif J, Muto M, Takebayashi S, et al. The SRA protein Np95 mediates epigenetic inheritance by recruiting Dnmt1 to methylated DNA. Nature 2007;450:908–912
15. Barrès R, Osler ME, Yan J, et al. Non-CpG methylation of the *PGC-1α* promoter through DNMT3B controls mitochondrial density. Cell Metab 2009;10:189–198
16. Gluckman PD, Hanson MA, Buklijas T, Low FM, Beedle AS. Epigenetic mechanisms that underpin metabolic and cardiovascular diseases. Nat Rev Endocrinol 2009;5:401–408
17. Fujiki K, Kano F, Shiota K, Murata M. Expression of the peroxisome proliferator activated receptor gamma gene is repressed by DNA methylation in visceral adipose tissue of mouse models of diabetes. BMC Biol 2009;7:38
18. Kamei Y, Suganami T, Ehara T, et al. Increased expression of DNA methyltransferase 3a in obese adipose tissue: studies with transgenic mice. Obesity (Silver Spring) 2010;18:314–321
19. Kamei Y, Miura S, Suganami T, et al. Regulation of SREBP1c gene expression in skeletal muscle: role of retinoid X receptor/liver X receptor and forkhead-O1 transcription factor. Endocrinology 2008;149:2293–2305
20. Kumaki Y, Oda M, Okano M. QUMA: quantification tool for methylation analysis. Nucleic Acids Res 2008;36(Web Server issue):W170–W175
21. Fuso A, Scarpa S, Grandoni F, Strom R, Lucarelli M. A reassessment of semiquantitative analytical procedures for DNA methylation: comparison of bisulfite- and HpaII polymerase-chain-reaction-based methods. Anal Biochem 2006;350:24–31
22. Honkakoski P, Moore R, Gynther J, Negishi M. Characterization of phenobarbital-inducible mouse Cyp2b10 gene transcription in primary hepatocytes. J Biol Chem 1996;271:9746–9753
23. Hayhurst GP, Strick-Marchand H, Mulet C, et al. Morphogenetic competence of HNF4 α-deficient mouse hepatic cells. J Hepatol 2008;49:384–395
24. Kumadaki S, Matsuzaka T, Kato T, et al. Mouse Elovl-6 promoter is an SREBP target. Biochem Biophys Res Commun 2008;368:261–266
25. Suganami T, Yuan X, Shimoda Y, et al. Activating transcription factor 3 constitutes a negative feedback mechanism that attenuates saturated Fatty acid/toll-like receptor 4 signaling and macrophage activation in obese adipose tissue. Circ Res 2009;105:25–32
26. Kato Y, Kaneda M, Hata K, et al. Role of the Dnmt3 family in de novo methylation of imprinted and repetitive sequences during male germ cell development in the mouse. Hum Mol Genet 2007;16:2272–2280
27. Bruce KD, Cagampang FR, Argenton M, et al. Maternal high-fat feeding primes steatohepatitis in adult mice offspring, involving mitochondrial dysfunction and altered lipogenesis gene expression. Hepatology 2009;50:1796–1808
28. Waterland RA, Kellermayer R, Rached MT, et al. Epigenomic profiling indicates a role for DNA methylation in early postnatal liver development. Hum Mol Genet 2009;18:3026–3038
29. Steine EJ, Ehrich M, Bell GW, et al. Genes methylated by DNA methyltransferase 3b are similar in mouse intestine and human colon cancer. J Clin Invest 2011;121:1748–1752
30. Kim MS, Kondo T, Takada I, et al. DNA demethylation in hormone-induced transcriptional derepression. Nature 2009;461:1007–1012
31. Ooi SK, Qiu C, Bernstein E, et al. DNMT3L connects unmethylated lysine 4 of histone H3 to *de novo* methylation of DNA. Nature 2007;448:714–717
32. Lewin TM, Granger DA, Kim JH, Coleman RA. Regulation of mitochondrial *sn*-glycerol-3-phosphate acyltransferase activity: response to feeding status is unique in various rat tissues and is discordant with protein expression. Arch Biochem Biophys 2001;396:119–127
33. Chen T, Ueda Y, Xie S, Li E. A novel Dnmt3a isoform produced from an alternative promoter localizes to euchromatin and its expression correlates with active *de novo* methylation. J Biol Chem 2002;277:38746–38754

細胞生理学分野

水島　昇

医歯学総合研究科・器官システム制御学系専攻
細胞生理学・教授

1）研究の課題名

オートファジーは、オートファゴソーム形成などの複雑な膜動態を伴う細胞内分解系である。オートファゴソーム形成には約20のオートファジー関連因子（Atg）が必要である。これらのAtg因子の網羅的解析を行っており、これまでの遺伝学的解析に加え、本年度は生細胞観察による時間的相互関係を解析している。

一方、これらのAtg因子はほぼすべての真核生物でよく保存されているが、原虫類ではその一部しか存在しない。それらはまったくランダムではなく、Atg8システムというAtg3, Atg4, Atg7, Atg8からなる共有結合系は常に保存されている。今回、ヒトマラリア原虫であるPlasmodium falciparumのAtg8を赤内型ステージで調べたところ、Atg8はアピコプラストという、アピコンプレックス門に特異的な細胞内小器官に局在することを見いだした。オートファゴソーム様構造体は検出されなかった。アピコプラストは4重膜からなる光合成能を持たない小器官であり、マラリアの生育に必須である。今回の研究は、マラリアはAtg因子の一部をアピコプラストの生合成かなんらかの機能に利用していることを示唆しており、Atg因子の分子機能を知る上で重要な情報になると考えられる。

オートファゴソーム形成の分子機構の研究が進む一方で、オートファゴソームの成熟過程やオートファゴソームとリソソームの融合メカニズムの多くは未だに不明である。リソソームは細胞内の分解専門の小器官であり、他の小器官と融合するとその内容成分を分解することができる。そのため、リソソームと他の小器官との融合は厳密に制御されなければならない。リソソームの細胞内ターゲットとしてよく知られているのは、後期エンドソームとオートファゴソームである。しかし、後期エンドソームとリソソームとの融合機構はよく知られているのに対し、オートファゴソームとリソソームとの融合のメカニズムはまだほとんど不明である。今回、シンタキシン17（Stx17）というSNARE分子の1種がオートファゴソームに局在化することが、オートファゴソームとリソソームとの融合に必要であることを発見した。Stx17はオートファゴソームの形成中間体には存在しないが、完成したオートファゴソームの外膜に結合する。Stx17は他のSNAREであるSNAP-29、VAMP8と結合し、これらのいずれを欠損しても、オートファゴソームはリソソームと融合できなくなる。Stx17はカルボキシル末端に二つの膜貫通部位を有しており、それぞれが「グリシンジッパー」と呼ばれるユニークな配列をもつ。Stx17は大部分がサイトゾルに可溶化状態で存在するが、この二つの膜貫通部位がヘアピン状に折れ曲がるとオートファゴソーム膜に挿入されることが示唆された。今回の結果は、オートファゴソームが、リソソームとの結合に必要なSNARE分子をどのように獲得しているかについて全く新しいモデルを提唱した。

2）研究のイラストレーション

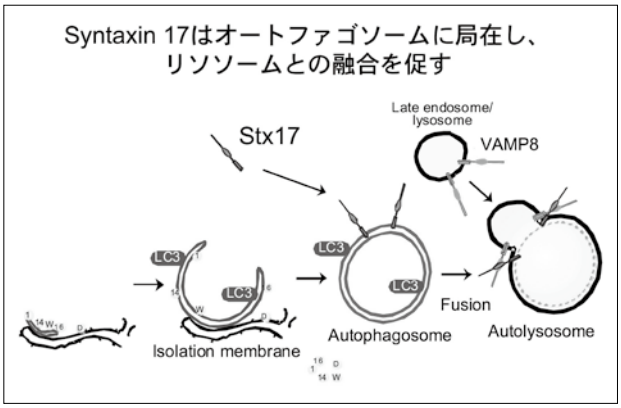

3）発表の研究内容についての英文要約

Autophagy is an intracellular degradation process, through which cytosolic materials are delivered to the lysosome. Although Atg proteins are highly conserved in eukaryotes, protozoa possess only a partial set of Atg proteins. Nonetheless, almost all protozoa have the complete factors belonging to the Atg8 conjugation system, namely, Atg3, Atg4, Atg7, and Atg8. We found that

Plasmodium falciparum Atg8 localizes to the apicoplast, a four membrane-bound non-photosynthetic plastid. These data suggest that, although Plasmodium parasites have lost most Atg proteins during evolution, they use the Atg8 conjugation system for the unique organelle, the apicoplast.

The lysosome is a degradative organelle, and its fusion with other organelles is strictly regulated. In contrast to fusion with the late endosome, the mechanisms underlying autophagosome–lysosome fusion remain unknown. We identified syntaxin 17 (Stx17) as the autophagosomal SNARE required for fusion with the endosome/lysosome. Stx17 localizes to the outer membrane of completed autophagosomes, but not to the isolation membrane (unclosed intermediate structures) ; for this reason, the lysosome does not fuse with the isolation membrane. Stx17 interacts with SNAP-29 and the endosomal/lysosomal SNARE VAMP8. These findings reveal a novel mechanism by which the SNARE protein is available to the completed autophagosome.

4）本事業に関連して世界的な研究拠点形成に向けて、以下の点で改善・整備等されたこと

A（研究拠点体制）

第6回Autophagy Research Seminarを開催。

B（人材確保）

非常勤講師1名（2012年8月～)、特任助教2名（～2012年7月）を採用。

C（人材育成）

特任助教2名が海外留学。大学院生1名が日本学術振興会DC1を獲得。

D（国際化）

The 6th International Symposium on Autophagy（オートファジーに関する国際学会：開催地は沖縄）で、シンポジウム組織委員会のメンバーとして開催をサポート。

5）GCOE事業を推進するに当たって力を入れた点

1. インド人大学院生2名（うち1名は2012年3月卒業)、ベトナム人大学院生1、中国人留学生1名を引き続き指導し、国際性を維持。
2. インド人大学院生1名が　第9期AISS学生に選ばれ、2012年10月から2013年3月までの半年間の研究支援を獲得。

6）英文原著論文

1. Itakura, E., Kishi-Itakura, C., Mizushima, N. The hairpin-type tail-anchored SNARE syntaxin 17 targets to autophagosomes for fusion with endosomes/lysosomes. Cell in press
2. Lin, T.C., Chen, Y.R., Kensicki, E., Li, A.Y., Kong, M., Li, Y., Mohney, R.P., Shen, H.M., Stiles, B., Mizushima, N., Lin, L.I., Ann, D.K. Autophagy：Resetting glutamine-dependent metabolism and oxygen consumption. Autophagy 8：1477-93（2012）
3. Kitamura, K., Kishi-Itakura, C., Tsuboi, T., Sato, S., Kita, K., Ohta, N., Mizushima, N. Autophagy-Related Atg8 Localizes to the Apicoplast of the Human Malaria Parasite Plasmodium falciparum. PLoS One 7：e42977（2012）
4. Liu, S., Hartleben, B., Kretz, O., Wiech, T., Igarashi, P., Mizushima, N., Walz, G., Huber, T.B. Autophagy plays a critical role in kidney tubule maintenance, aging and ischemia-reperfusion injury. Autophagy 8：826-837（2012）.
5. Itakura, E., Kishi-Itakura, C., Koyama-Honda, I., Mizushima, N. Structures containing Atg9A and the ULK1 complex independently target depolarized mitochondria at initial stages of Parkin-mediated mitophagy. J. Cell Sci. 125：1488-1499（2012）.
6. Velikkakath, A.K.G, Nishimura, T., Oita, E., Ishihara, O., Mizushima, N. Mammalian Atg2 proteins are essential for autophagosome formation and important for regulation of size and distribution of lipid droplets. Mol. Biol. Cell 23：896-909（2012）.

7）総説ならびに著書

1. Klionsky, D.J., Mizushima, N., et al. Guidelines for the use and interpretation of assays for monitoring autophagy. Autophagy 8：445-544（2012）.
2. Shpilka, T., Mizushima, N., Elazar, Z. Ubiquitin-like proteins and autophagy at a glance. J. Cell Sci. 125：2343-2348（2012）.

8）平成24年度までの自己評価

オートファジーメカニズム研究と生理学的研究の双方は順調に進んでいる。オートファゴソームとリソソームに関する重要な発見があった。

9）学会発表（英文）

1. Hideaki Morishita, Michael L. Robinson, Noboru Mizushima　Autophagy-deficient lens develop age-related cataract　Keystone Symposium on Aging and Diseases of Aging　示説　Tokyo　2012.10.22-27
2. Hideaki Morishita, Michael L. Robinson, Noboru Mizushima　Autophagy-deficient lens develop age-related cataract　The 6th International Symposium on Autophagy 2012　示説　Okinawa　2012.10.28-11.1
3. Taki Nishimura, Takeshi Kaizuka, Ken Cadwell,

Sahani Mayurbhai Himatbhai, Tatsuya Saitoh, Shizuo Akira, Herbert W. Virgin, Noboru Mizushima　FIP200 regulates the isolation membrane targeting of Atg16L1 The 6th International Symposium on Autophagy 2012 示説　Okinawa　2012.10.28-11.

4. Ikuko Koyama-Honda, Eisuke Itakura, Takahiro K. Fujiwara and Noboru Mizushima　Temporal relationships among mammalian Atg proteins for recruitment to the autophagic structures　The 6th International Symposium on Autophagy 2012 示説　Okinawa　2012.10.28-11.1

10）学会発表（和文）

1. 森下英晃、岸千絵子、水島昇
   水晶体オルガネラ分解過程におけるリソソームの関与　第38回水晶体研究会　口頭　東京　2012.1.7-8
2. 西村多喜、水島昇
   オートファジー関連因子による小胞体膜の膜動態制御機構の解析　第117回　日本解剖学会総会・全国学術集会　シンポジウム　甲府　2012.3.26-28
3. 久万亜紀子、吉井紗織、板倉英祐、原太一、設楽浩志、江石義信、水島昇
   Analysis of Atg5-deficient mice rescued with Atg5 expression in the brain　第35回日本分子生物学会年会　ワークショップ　福岡　2012.12.11-14
4. Miyuki Sato, Taichi Hara, Satoshi Tsukamoto, Noboru Mizushima and Ken Sato
   Fertilization-triggered autophagy degrades paternal mitochondria in C. elegans early embryos　第85回日本生化学会大会　シンポジウム　福岡　2012.12.14-16
5. 内藤貴子、久万亜紀子、水島昇
   マウス生体内でのオートファジー制御におけるインスリンとアミノ酸の寄与　Contribution of insulin and amino acids to autophagy regulation in vivo.　第85回日本生化学会大会　口頭および示説　福岡　2012.12.14-16
6. Pham Nguyen Quy, Akiko Kuma, Philippe Pierre, and Noboru Mizushima
   プロテアソーム依存的mTORC1の活性化は脱神経に伴うオートファジーの抑制と骨格筋のリモデリングに重要である　Proteasome-dependent activation of mTORC1　第85回日本生化学会大会　口頭および示説　福岡　2012.12.14-16
7. 森下英晃、江口賢史、木村洋貴、佐々木純子、酒巻有里子、Michael L. Robinson、佐々木雄彦、水島昇
   Autophagy-related 5（Atg5）and Pik3C3（Vps34）are not essential for the programmed organelle degradation, but important for the quality control and development of the lens, respectively　第85回日本生化学会大会　示説　福岡　2012.12.14-16

11）外部資金の獲得状況

最先端・次世代研究開発支援プログラム
研究題目：オートファジーの分子機構と生理機能に関する分野横断型研究
代表：水島昇
期間：平成22―25年
研究費総額：13900万円

12）特別講演、招待講演、シンポジウム

1. Noboru Mizushima
   Autophagy regulation in cells and whole organisms 2012 Senri Life Science International Symposium. "Cutting-edge of Autophagy Study"　2012.1.20　大阪
2. Noboru Mizushima
   Physiological role of autophagy and its regulation mechanism The 6th Global COE international symposium "Molecular control of bone remodeling"　2012.1.24　東京
3. 水島昇
   オートファジーの生理的役割　第11回リウマチ性疾患研究会　2012.1.28　東京
4. Noboru Mizushima
   Autophagy in cells and whole organisms
   Gordon Research Conference "Autophagy in stress, development and disease"　2012.3.11-16　Ventura, CA USA
5. Noboru Mizushima
   Regulation of Autophagosome formation in cells and mice　Special Symposium on Autophagy in Health and Disease　2012.3.16　Arcadia, CA USA
6. Noboru Mizushima
   Physiological role of autophagy and its regulation mechanism　2012 Asia-Pacific Diabetes and Obesity Meeting　2012.4.20-21　Seoul, Korea
7. 水島昇
   Molecular mechanism of autophagosome formation and maturation　第64回日本細胞生物学会年会　2012.5.28-30　神戸

8. 水島昇
オートファジーの生理的役割　第17回東京肝臓シンポジウム　2012.6.18　東京
9. 水島昇
オートファジーの分子機構、病態生理との関連 “未来へのバイオ技術”勉強会「オートファジー研究-基礎から疾患に挑戦する」2012.7.5　東京
10. 水島昇
オートファジーの生理的役割と選択的基質分解　第18回成人病の病因・病態の解明に関する研究会　2012.7.7-8　大阪
11. 水島昇
オートファジー：細胞質からリソソームへ　第8回日本ファブリー病フォーラム　2012.7.22　東京
12. Noboru Mizushima
Autophagosome formation site and recruitment of selective substrates　14th International Congress of Histochemistry and Cytochemistry　2012.8.27　Kyoto
13. 水島昇
Autophagosome formation site and recruitment of selective substrates　20th Euroconference on Apoptosis　2012.9.14-17　Rome, Italy
14. Noboru Mizushima
Physiological role of autophagy and its molecular mechanism　Mitochondrial Interest Group Rome　2012.9.17　名古屋
15. Noboru Mizushima
Physiological role of autophagy and its regulation mechanism　11th Biennial Meeting of the Asia-Pacific Society for Neurochemistry（APSN）　2012.10.1　Kobe
16. Noboru Mizushima
Autophagy：Its Regulation Mechanism and Selective Substrates　Keystone Symposium on Aging and Diseases of Aging　2012.10.22-27 Tokyo
17. Noboru Mizushima
Molecular mechanism of autophagosome formation　The 6th International Symposium on Autophagy 2012　2012.10.28-11.1　Okinawa
18. 水島昇
哺乳類オートファジーの代謝生理的役割と分子メカニズム　第28回京都賞記念ワークショップ「オートファジーの50年」　2012.11.12　京都
19. Noboru Mizushima
Molecular mechanism of autophagosome formation and maturation　第85回日本生化学会大会　2012.12.14-16　福岡

13）主催学会

第3回オートファジーリサーチセミナー
2012.5.15-17　掛川

14）新聞、雑誌、TV報道

1. 文化放送　くにまるジャパン　ラジオ白熱教室　『“細胞が自分を食べる”オートファジーの謎』2012.4.9
（Cell誌掲載論文に関するプレスリリースを2012.12.7に行う予定です）

15）教室、分野や講座の准教授、講師、助教、特別研究員、ポスドク、指導を受けた大学院生の名前

助教		久万　亜紀子
助教		田中　　敦
助教		西村　多喜
特任助教（～7月）		岸　千絵子
特任助教（～7月）		板倉　英祐
非常勤講師（8月～）		本田　郁子
		（～7月　学振特別研究員）
大学院生	D4	渡邉（浅野）　貴子
	MD-PhD4	北村　　圭
	D4	Velikkakath,Anoop Kumar Gopi
		（2012年3月卒業）
	D4	Sahani, Mayurbhai Himatbhai
	D4	森下　英晃
	D4	Pham Nguyen, Quy
	D4	内藤　貴子
	D3	貝塚　剛志
	D3	山本　　篤
	D2	Jiang, Peidu
	M1	田村　律人

Please cite this article in press as: Itakura et al., The Hairpin-type Tail-Anchored SNARE Syntaxin 17 Targets to Autophagosomes for Fusion with Endosomes/Lysosomes, Cell (2012), http://dx.doi.org/10.1016/j.cell.2012.11.001

Cell

The Hairpin-type Tail-Anchored SNARE Syntaxin 17 Targets to Autophagosomes for Fusion with Endosomes/Lysosomes

Eisuke Itakura,[1,2] Chieko Kishi-Itakura,[1] and Noboru Mizushima[1,3,*]
[1]Department of Physiology and Cell Biology, Tokyo Medical and Dental University, Tokyo 113-8519, Japan
[2]Present address: MRC Laboratory of Molecular Biology, Hills Road, Cambridge CB2 0QH, UK
[3]Present address: Department of Biochemistry and Molecular Biology, Graduate School and Faculty of Medicine, The University of Tokyo, Tokyo 113-0033, Japan
*Correspondence: nmizu@m.u-tokyo.ac.jp
http://dx.doi.org/10.1016/j.cell.2012.11.001

SUMMARY

The lysosome is a degradative organelle, and its fusion with other organelles is strictly regulated. In contrast to fusion with the late endosome, the mechanisms underlying autophagosome-lysosome fusion remain unknown. Here, we identify syntaxin 17 (Stx17) as the autophagosomal SNARE required for fusion with the endosome/lysosome. Stx17 localizes to the outer membrane of completed autophagosomes but not to the isolation membrane (unclosed intermediate structures); for this reason, the lysosome does not fuse with the isolation membrane. Stx17 interacts with SNAP-29 and the endosomal/lysosomal SNARE VAMP8. Depletion of Stx17 causes accumulation of autophagosomes without degradation. Stx17 has a unique C-terminal hairpin structure mediated by two tandem transmembrane domains containing glycine zipper-like motifs, which is essential for its association with the autophagosomal membrane. These findings reveal a mechanism by which the SNARE protein is available to the completed autophagosome.

INTRODUCTION

The lysosome is an organelle that is specialized for degradation. When the lysosome fuses with other cellular compartments, lysosomal hydrolases degrade materials inside the target compartments. Because this is a destructive process, lysosomal fusion must be strictly regulated. The autophagosome and late endosome are the two major organelles that can fuse with the lysosome.

The autophagosome is a unique organelle that mediates macroautophagy (simply referred to as autophagy hereafter). At the initial step, an isolation membrane (also known as a phagophore) is generated directly from or in close proximity to the endoplasmic reticulum (ER) and surrounds a small portion of the cytoplasm to become a double-membrane organelle, the autophagosome (Mizushima et al., 2011; Tooze and Yoshimori, 2010). Formation of the autophagosome is regulated by the hierarchical function of a number of autophagy-related (Atg) proteins. All these Atg proteins except LC3 detach from completed autophagosomes (Fujita et al., 2008; Itakura and Mizushima, 2010). Next, at least some of the autophagosomes fuse with endosomes, which generates a hybrid organelle, the amphisome (Berg et al., 1998). At the final step, the amphisome or autophagosome directly fuses with the lysosome to form the autolysosome, and autophagosomal contents are degraded together with the inner autophagosomal membrane. Autophagy has a critical role in many physiological processes, such as cellular quality control, stress responses, and development (Deretic and Levine, 2009; Levine and Kroemer, 2008; Levine et al., 2011; Mizushima and Komatsu, 2011; White et al., 2010).

How the autophagosome fuses with the lysosome has not been fully characterized. Specific membrane fusion is generally achieved by SNARE complexes (Hong, 2005; Jahn and Scheller, 2006). Upon membrane fusion, the SNARE complex forms parallel four-helix bundles consisting of the Qa-, Qb-, Qc-, and R-SNAREs. Fusion between the late endosome and lysosome uses syntaxin 7 (Stx7) (Qa), Vti1b (Qb), and Stx8 (Qc) on the late endosome and VAMP7 (R) on the lysosome (Pryor et al., 2004). Regarding the autophagy pathway, it has been suggested that Vam3 (Qa) (Darsow et al., 1997; Ohashi and Munro, 2010), Vam7 (Qc) (Ohashi and Munro, 2010; Sato et al., 1998), Ykt6 (R) (Dilcher et al., 2001; Klionsky, 2005), and Vti1 (Qb) (Fischer von Mollard and Stevens, 1999; Ishihara et al., 2001) are involved in autophagosome-vacuole fusion in yeast, and VAMP7 (R) (Fader et al., 2009), VAMP8 (R), and Vti1b (Qb) (Furuta et al., 2010) in mammals. However, these studies have not identified specific SNARE protein(s) on the autophagosomal membrane. SNAREs such as mammalian Stx5 (Renna et al., 2011) and VAMP7 (Moreau et al., 2011), and yeast Sec22, Ykt6, Tlg2, Sex9, and Sso1 (Nair et al., 2011) are also involved in autophagy steps other than the autophagosome-vacuole fusion step. Thus, autophagosomal SNARE remains to be identified.

Almost all SNAREs are tail-anchored proteins, which have a single transmembrane domain (TMD) at the extreme C terminus (Borgese and Fasana, 2011; Hegde and Keenan, 2011). The N-terminal fragments of tail-anchored proteins are exposed to

Please cite this article in press as: Itakura et al., The Hairpin-type Tail-Anchored SNARE Syntaxin 17 Targets to Autophagosomes for Fusion with Endosomes/Lysosomes, Cell (2012), http://dx.doi.org/10.1016/j.cell.2012.11.001

Cell

the cytosol. Whereas conventional transmembrane proteins are cotranslationally inserted into the ER membranes, membrane insertion of tail-anchored proteins is posttranslational, because their TMD is still inside the ribosomes when protein translation is completed and cannot be recognized by the signal recognition particle (Borgese and Fasana, 2011; Hegde and Keenan, 2011). In mammals, target membranes of tail-anchored proteins thus far identified are those of the ER, mitochondria, and peroxisomes (Borgese et al., 2007; Rabu et al., 2009). Selective targeting is achieved by the length of the TMD and charged residues in the C-terminal flanking regions. Although tail-anchored proteins also exist in many cellular compartments including the plasma membrane, endosome, and nuclear envelope, they are first inserted into the ER membrane and then transported to their final destinations (Borgese and Fasana, 2011). Therefore, how the autophagosome acquires SNARE(s) is unknown.

One possibility is that the SNARE proteins, which are required for lysosome fusion, are provided upon fusion with the endosome (Noda et al., 2009). However, it remains unclear whether all autophagosomes fuse with the endosomes prior to lysosomal fusion. In addition, this cannot explain why autophagosomes can fuse with endosomes. Another question that we should answer is why the lysosome can fuse with the autophagosome only after sequestration of the cytoplasm has been completed. If the lysosome fuses with the elongating isolation membrane (unclosed autophagosome), it cannot accomplish cytoplasmic degradation.

In the present study, we identified the autophagosomal SNARE, Stx17. Depletion of Stx17 causes accumulation of autophagosomes without any feature of degradation. Upon autophagy induction, Stx17 is recruited to the outer membrane of completed autophagosomes but not to the isolation membrane. Furthermore, we show that Stx17 has a unique hairpin structure formed by two TMDs containing glycine zipper-like motifs, and this structure is essential for its selective targeting to the outer autophagosomal membrane.

RESULTS

Stx17 Translocates to the Autophagosome during Starvation

To identify SNARE proteins that are involved in the fusion between the autophagosome and endosome/lysosome, we focused on the ER SNAREs Stx17 and Stx18 (Hong, 2005), because autophagosomes are considered to be generated from (or on) the ER (Mizushima et al., 2011; Tooze and Yoshimori, 2010) and we initially speculated that the autophagosomal SNARE may be supplied from the ER. Under growing conditions, green fluorescent protein (GFP)-Stx17 showed reticular and tubular structures, and did not colocalize with the autophagosomal marker LC3 (Figures 1A and 1B). The reticular and tubular structures represented the ER and mitochondria (Figure 1C). Under starvation conditions, many LC3 punctate or ring-like structures were formed, which represented autophagosomes or related membranes (Kabeya et al., 2000; Klionsky et al., 2008a; Mizushima et al., 2010). Most, but not all, of these LC3 structures colocalized with Stx17, which also formed punctate and ring structures under starvation conditions (Figures 1A and 1B). By contrast, GFP-Stx18 only localized to reticular structures and did not colocalize with LC3 even under starvation conditions (Figure 1A). These data suggest that Stx17, but not Stx18, is recruited to autophagic membranes.

SNARE proteins reside not only in the original membrane on which they mediate fusion, but also in other membranes after fusion or during recycling (Jahn and Scheller, 2006). To rule out the possibility that Stx17 localizes to the autophagosome as a secondary result of prior membrane fusion, we generated two truncated mutants: GFP-Stx17ΔTM-b5, in which the two TMDs of Stx17 were replaced by the TMD of ER cytochrome b5, and GFP-Stx17TM, in which the entire N-terminal region upstream of the TMDs (including the SNARE domain) was deleted. GFP-Stx17ΔTM-b5 only localized to reticular structures and did not form puncta in starved cells. By contrast, GFP-Stx17TM formed punctate structures, which were colocalized with LC3 (Figure 1D). Thus, autophagosomal localization of Stx17 is not a result of its SNARE-mediated membrane fusion, and the C-terminal region including the TMDs is sufficient for autophagosomal localization of Stx17.

Stx17 Is Required for Fusion between the Autophagosome and Endosome/Lysosome

The localization of Stx17 on the autophagosome prompted us to analyze whether Stx17 is required for autophagosome-lysosome fusion. When autophagosome-lysosome fusion and/or lysosomal degradation were blocked by treatment with the vacuolar ATPase inhibitor bafilomycin A_1 in control siRNA-treated cells, the level of LC3-II (a membrane form) was increased (Figure 2A) (Klionsky et al., 2008b). This suggests the accumulation of autophagosomes. Knockdown of Stx17 causes accumulation of LC3-II even under growing conditions to a level comparable to that in bafilomycin A_1-treated control (siLuc) cells under starvation conditions (Figure 2A). This level was not further increased by bafilomycin A_1 treatment, suggesting that autophagic flux is blocked in Stx17 small interfering RNA (siRNA)-treated cells. Expression of siRNA-resistant Stx17, but not Stx17 without the SNARE domain, suppressed the accumulation of LC3-II caused by Stx17 knockdown, confirming that autophagy inhibition is not an off-target effect (Figure 2A). These biochemical data suggest that Stx17 functions at a late step of autophagy.

In contrast to control siRNA-treated cells, many GFP-LC3 puncta accumulated in Stx17 knockdown cells even under growing conditions (Figure 2B). Punctate structures of upstream autophagic factors such as ULK1 and DFCP1 did not accumulate in Stx17 knockdown cells, suggesting that autophagosomes, but not isolation membranes/omegasomes, accumulated (Figure S1A available online). These GFP-LC3 puncta did not colocalize with late endosomal and lysosomal markers (Figure 2C). This suggests that fusion between the autophagosome and endosome/lysosome is blocked, rather than degradation of GFP-LC3 in the amphisome or lysosome is impaired. Consistent with this suggestion, electron microscopy showed accumulation of autophagosomes in Stx17 knockdown cells (Figure 2D). Of note, these accumulated autophagosomes contained intact cytoplasmic material without any features of degradation. This was different from the situation in control cells in which both autophagosomes and autolysosomes could be easily detected

Please cite this article in press as: Itakura et al., The Hairpin-type Tail-Anchored SNARE Syntaxin 17 Targets to Autophagosomes for Fusion with Endosomes/Lysosomes, Cell (2012), http://dx.doi.org/10.1016/j.cell.2012.11.001

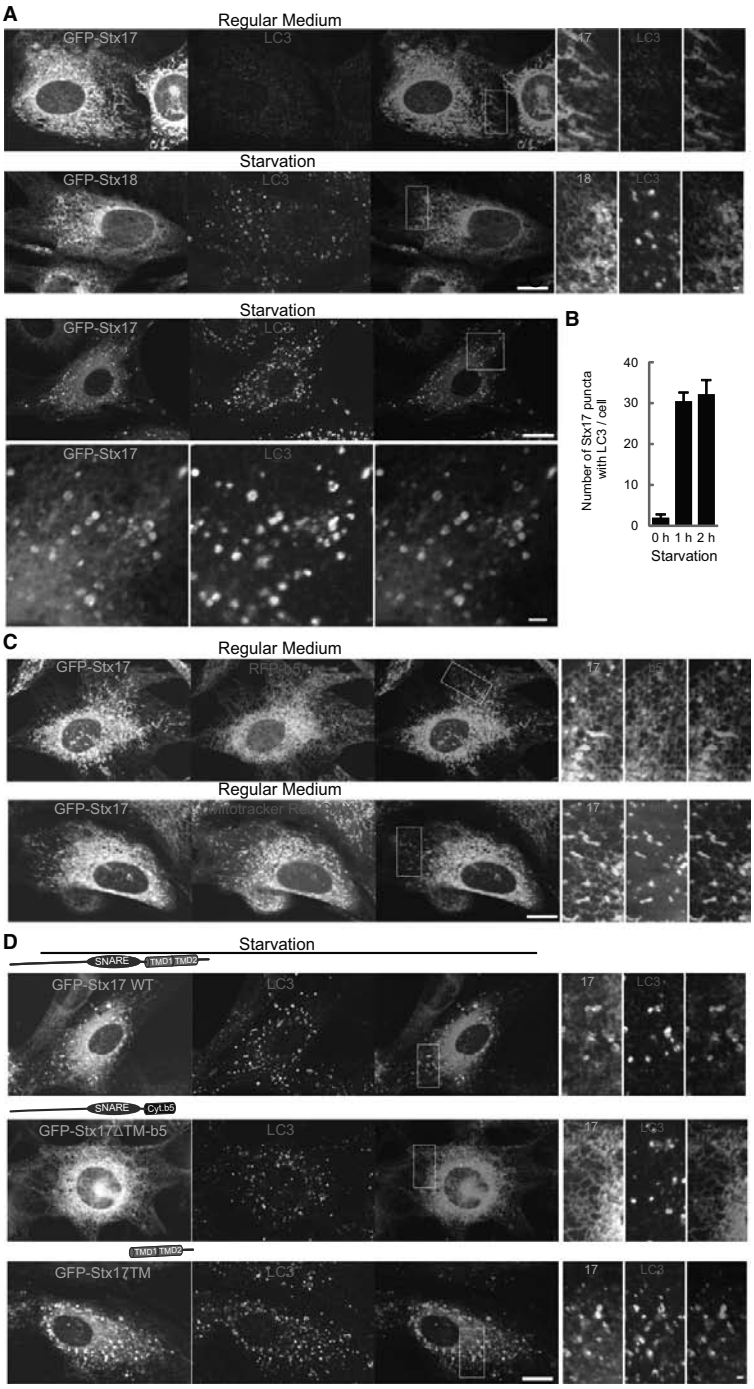

Figure 1. Stx17 Translocates to the Autophagosome under Starvation Conditions

(A) MEFs stably expressing GFP-Stx17 or GFP-Stx18 were cultured in regular medium or starvation medium for 2 hr. Cells were stained with anti-LC3 antibodies and analyzed by immunofluorescence microscopy.

(B) Quantification of the number of punctate structures positive for both Stx17 and LC3 per cell at the indicated times after starvation. Data represent mean ± SEM of ten images.

(C) MEFs stably expressing GFP-Stx17 with or without RFP-cytochrome b5 (an ER marker) were cultured in the presence or absence of 50 nM Mitotracker Red CMXRos and analyzed by immunofluorescence microscopy. Signal color is indicated by color of typeface.

(D) MEFs stably expressing GFP-Stx17 WT, GFP-Stx17ΔTM-b5, or GFP-Stx17TM were cultured in starvation medium for 2 hr and analyzed by immunofluorescence microscopy using anti-LC3 antibody.

Bars: 10 μm (white) and 1 μm (yellow).

See also Table S1.

Please cite this article in press as: Itakura et al., The Hairpin-type Tail-Anchored SNARE Syntaxin 17 Targets to Autophagosomes for Fusion with Endosomes/Lysosomes, Cell (2012), http://dx.doi.org/10.1016/j.cell.2012.11.001

Cell

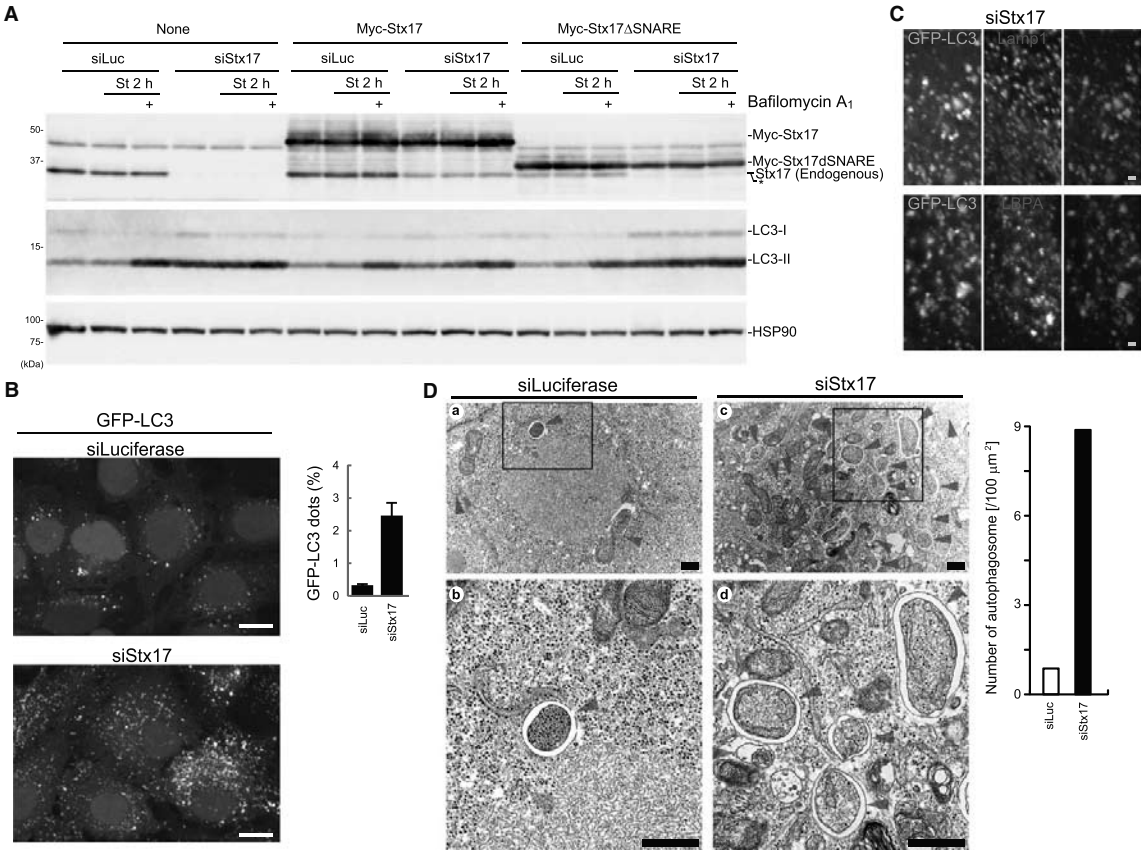

Figure 2. Stx17 Is Required for Fusion between the Autophagosome and Late Endosome/Lysosome

(A) HeLa cells stably expressing siRNA-resistant Myc-Stx17 or Myc-Stx17ΔSNARE (deleted amino acids 162–224) were treated with siRNA oligonucleotides against luciferase or Stx17. Cells were cultured in regular or starvation medium for 2 hr with or without 100 nM bafilomycin A_1 and analyzed by immunoblotting using the indicated antibodies. An asterisk indicates degradation products of transfected Myc-Stx17.

(B) HeLa cells stably expressing GFP-LC3 were treated with siRNA oligonucleotides against luciferase or Stx17. Cells were cultured in regular medium and analyzed by immunofluorescence microscopy. The ratio of the total area of GFP-LC3 dots to the total cellular area is shown as a percentage in the graph. Data represent mean ± SEM of ten images. Scale bars, 10 μm.

(C) HeLa cells stably expressing GFP-LC3 were treated with Stx17 siRNA oligonucleotides. Cells cultured in regular growing medium were analyzed by immunofluorescence microscopy using anti-Lamp1 (lysosome) and anti-LBPA (late endosome) antibodies. Scale bars, 1 μm.

(D) HeLa cells treated with siLuciferase or siStx17 were cultured in starvation medium for 1 hr followed by conventional electron microscopic analysis. Autophagosomes are indicated by arrowheads. Scale bars, 500 nm. Quantification of the number of autophagosomes from at least 25 randomly selected areas is shown in the graph.

See also Figure S1.

even though the number of autophagic structures was smaller (Figure 2D). From these results, we conclude that Stx17 is required for fusion between the autophagosome and endosome/lysosome.

Next, we explored cofactors of Stx17 in the autophagosome-lysosome fusion step. Because Stx17 belongs to the Qa-SNARE family (Hong, 2005), we hypothesized that Stx17 might interact with an R-SNARE on the membranes of endosomes and/or lysosomes. VAMP7 and VAMP8 are lysosomal R-SNAREs and form a complex with Stx7 (Qa-SNARE), Vti1b (Qb-SNARE), and Stx8 (Qc-SNARE) (Jahn and Scheller, 2006). Our immunoprecipitation analyses demonstrated that Stx17 interacts with VAMP7, VAMP8, and Vti1b (Figure S2A). Endogenous Stx17 and VAMP8 were precipitated with FLAG-VAMP8 and FLAG-Stx17, respectively (Figures 3A and 3B). We also detected an endogenous interaction between Stx17 and VAMP8, which was enhanced under starvation conditions (Figure 3C).

Knockdown of VAMP8 induced accumulation of LC3-II and GFP-LC3 puncta, and impaired autophagic flux (Figures S2B and S2C), which was consistent with previous reports (Furuta

Please cite this article in press as: Itakura et al., The Hairpin-type Tail-Anchored SNARE Syntaxin 17 Targets to Autophagosomes for Fusion with Endosomes/Lysosomes, Cell (2012), http://dx.doi.org/10.1016/j.cell.2012.11.001

et al., 2010). VAMP8 was mainly localized to the late endosome and lysosome, and only partially colocalized with LC3 even during starvation (Figure S2D). In contrast, knockdown of Vti1b or VAMP7 showed virtually no or very weak effects on the behavior of LC3-II (Figure S2E) and did not induce GFP-LC3 puncta accumulation (our unpublished data). If Vti1b functions together with Stx17, Vti1b should be present on LC3-positive autophagosomes. However, Vti1b mainly localized to late endosomes/lysosomes, but not to autophagosomes (Figure S2D). These results suggest that autophagosomal Stx17 functions with endosomal/lysosomal VAMP8 at the fusion step.

We next tried to identify Qb and Qc SNARE proteins that function together with Stx17 at the autophagosomal fusion step. Interaction between Stx17 and SNAP-29 (Qbc SNARE) was previously reported, although its precise role remains unknown (Sato et al., 2011; Steegmaier et al., 1998). We confirmed that SNAP-29 was immunoprecipitated with Stx17 dependently on the SNARE domain in Stx17 (Figure 3D). Of note, overexpression of Stx17 enhanced interaction between SNAP-29 and VAMP8 (Figure 3D, lanes 5 and 6). Overexpression of SNAP-29 also enhanced interaction between Stx17 and VAMP8 (Figure 3E). Furthermore, we detected endogenous interaction between SNAP-29 and Stx17 (Figure 3F). In SNAP-29 knockdown cells, the LC3-II form accumulated and autophagic flux was inhibited (Figure 3G). GFP-LC3 puncta also accumulated in SNAP-29 knockdown cells under growing conditions (Figure 3H). Finally, GFP-SNAP-29 efficiently colocalized with Stx17-positive LC3 structures in starved cells (Figure 3I). This colocalization rate was much higher than that between Stx17 and Vti1b under the same condition. These data suggest that Stx17, SNAP-29, and VAMP8 form a SNARE complex, which is required for the autophagosomal fusion step.

Knockdown of Stx7 also blocked autophagic flux (Figures S2E and S2F). However, Stx7 primarily exist on lysosomes, but not autophagosomes (Figure S2D). Thus, it is unlikely that Stx7 functions as a second autophagosomal Qa-SNARE. LC3-II accumulation in Stx7-depleted cells might be a result of a defect in lysosomal function.

Stx17 Is Recruited to the Completed Autophagosome but Not to Intermediate Autophagic Structures

Because LC3 can be present on the isolation membrane (unclosed autophagosome or autophagosome intermediates), completed (closed) autophagosome, amphisome (the autophagosome fused with the endosome), and autolysosome (the autophagosome/endosome fused with the lysosome), we next determined which structures Stx17 localized to. GFP-Stx17 only rarely colocalized with lysobisphosphatidic acid (LBPA) (Kobayashi et al., 1998) or Lamp1, which are the markers for the late endosome or lysosome, respectively (Figure S3). Furthermore, full-length Stx17 and Stx17TM (Figure 1C) did not colocalize with Atg16L1, an isolation membrane marker (Figure 4A). Approximately 20% and 60% of the LC3 puncta colocalized with Atg16L1 and Stx17, respectively, but these two populations were distinct and there was virtually no overlapping between Stx17 and Atg16L1 (Figure 4B). We confirmed that LC3, but none of the upstream Atg factors that are present only on the isolation membrane (ULK1, WIPI-1, and Atg14), colocalized with Stx17TM (Figures 4C and 4D). DFCP1, which is present on the omegasome, an ER-derived structure scaffolding autophagosome formation, also showed no colocalization with Stx17TM (Figures 4C and 4D). Furthermore, intermediate autophagic structures (unclosed autophagosomes) accumulated in Atg5 knockout (KO) and Atg3 KO cells due to a defect in a late step of autophagosome formation (Itakura and Mizushima, 2010; Sou et al., 2008), but these structures were not colocalized with Stx17TM (Figure 4E).

We further investigated the recruitment of Stx17 to the autophagosome by time-lapse microscopy. Although SECFP-Stx17TM was not detected on Venus-DFCP1-positive omegasomes, SECFP-Stx17TM puncta emerged from the same area where Venus-DFCP1 puncta had disappeared (Figure 4F; Movie S1). To confirm that this is indeed a continuous event, we performed live imaging using SECFP-Stx17TM and Venus-LC3. LC3 is recruited to the isolation membrane during autophagosome formation (Mizushima et al., 2001). Several minutes after the appearance of the LC3 signal, it reached a plateau, after which the Stx17 signal gradually appeared on the same structures (Figure 4F; Movie S2). If Stx17 is recruited to completed autophagosomes, Stx17 should not have access to the inner autophagosomal membrane. Indeed, immunoelectron microscopy of GFP-Stx17 showed that Stx17 specifically existed on the outer autophagosomal membrane but not on the inner membrane (Figure 4G). These results suggest that, in contrast to our initial expectation, Stx17 directly localizes to completed autophagosomes, not through intermediate structures.

TMDs of Stx17 Are Sufficient for Localization to the Autophagosome

We next questioned how Stx17 localizes to completed autophagosomes. Flanking charges at the C terminus are important for selective targeting of tail-anchored proteins to the ER and mitochondria (Borgese et al., 2003). Indeed, there are several charged residues in the C-terminal flanking region of Stx17 (Figure 5A). Localization to mitochondria and reticular structures was defective in truncation mutants of the C-Terminal region (GFP-Stx17Δ1 and Δ2) (Figure 5B). However, these mutants still localized to autophagosomes (Figures 5C and 5D), suggesting that the charged resides may be important for targeting to mitochondria and the ER, but not to the autophagosome.

Stx17 is an unusual tail-anchored protein among the SNARE proteins, because it possesses two TMDs (Steegmaier et al., 1998). Hydrophobicity of these TMDs, especially that of TMD2, is relatively low, indicating that one of them may not function as a true TMD. However, deletion of either TMD suppressed targeting to all membranes including autophagosomes (TMΔTM1 and TMΔTM2 in Figures 5C and 5D). These results suggest that both TMDs are sufficient and necessary for Stx17 targeting to the autophagosome. The findings also indicate that localization of Stx17 to the ER and mitochondria is not necessary for its localization to the autophagosome in vivo.

The TMDs of Stx17 Form a Hairpin-like Structure with Its C Terminus in the Cytosol

Conventional SNARE proteins contain a single TMD with their C terminus in the luminal side. If the two TMDs in Stx17 are

Please cite this article in press as: Itakura et al., The Hairpin-type Tail-Anchored SNARE Syntaxin 17 Targets to Autophagosomes for Fusion with Endosomes/Lysosomes, Cell (2012), http://dx.doi.org/10.1016/j.cell.2012.11.001

Cell

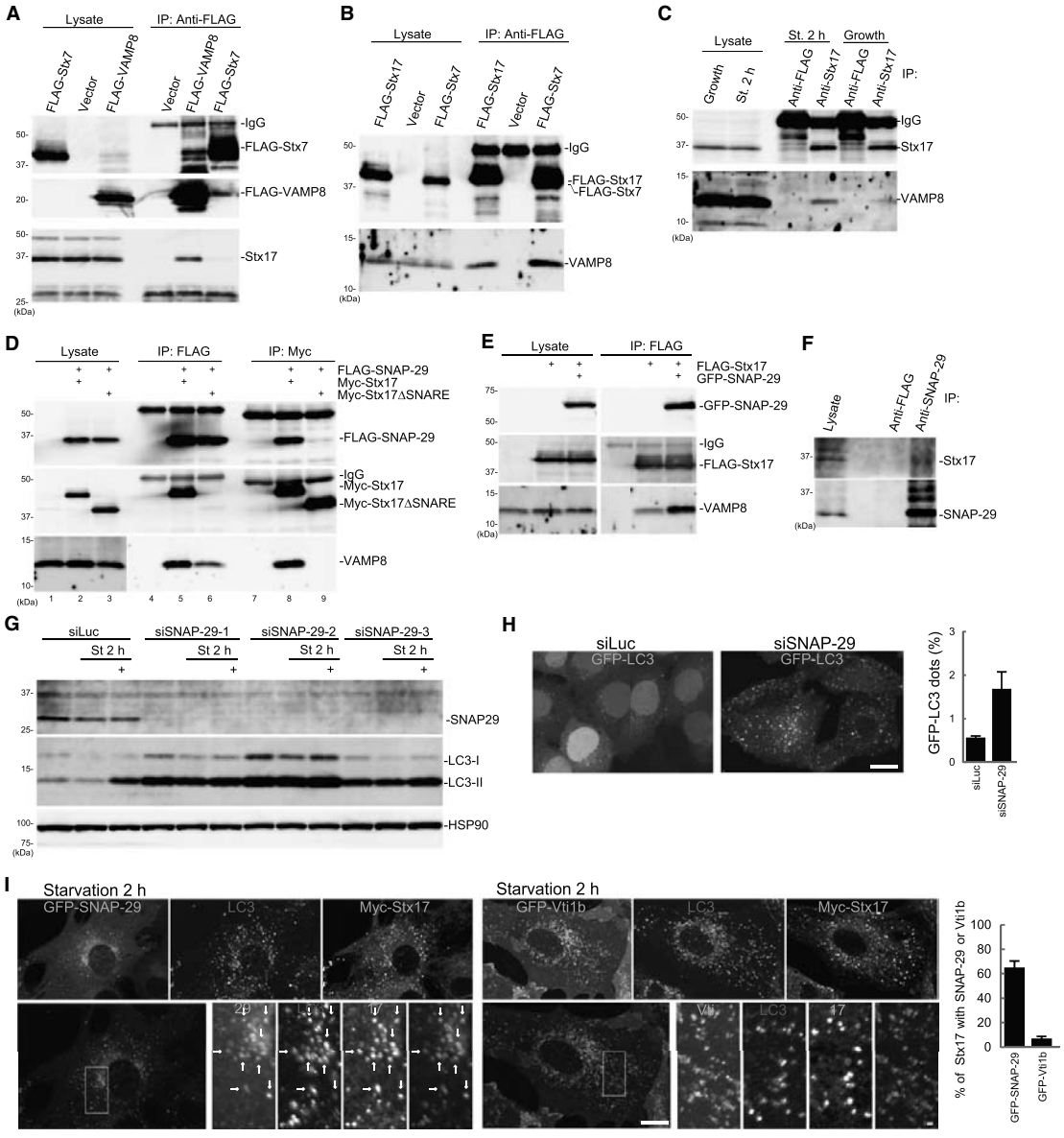

Figure 3. Stx17 Functions Together with VAMP8 and SNAP-29

(A and B) HEK293T cells were transfected with empty vector, FLAG-Stx7, FLAG-VAMP8, or FLAG-Stx17. Two days later, cells were lysed, and immunoprecipitated with anti-FLAG antibody.

(C) MEFs were cultured in regular or starvation medium for 2 hr, followed by immunoprecipitation using anti-FLAG and anti-Stx17 antibodies.

(D) HEK293T cells were transfected with empty vector, FLAG-SNAP-29 with or without Myc-Stx17 or Myc-Stx17ΔSNARE. Two days later, cells were lysed, and immunoprecipitated with indicated antibodies.

(E) HEK293T cells were transfected with empty vector, FLAG-Stx17 with or without GFP-SNAP-29 and analyzed as in (D).

(F) MEFs were cultured in starvation medium for 2 hr, followed by immunoprecipitation using anti-FLAG and anti-SNAP-29 antibodies.

(G) HeLa cells were treated with siRNA oligonucleotides against luciferase or SNAP-29. Autophagic flux assay was performed as in Figure 2A.

(H) HeLa cells stably expressing GFP-LC3 were treated with siRNA oligonucleotides against luciferase or SNAP-29-2. Cells were cultured in regular medium and analyzed by immunofluorescence microscopy. The ratio of the total area of GFP-LC3 dots to the total cellular area is shown as a percentage in the graph. Data represent mean ± SEM of ten images. Scale bars, 10 μm.

Please cite this article in press as: Itakura et al., The Hairpin-type Tail-Anchored SNARE Syntaxin 17 Targets to Autophagosomes for Fusion with Endosomes/Lysosomes, Cell (2012), http://dx.doi.org/10.1016/j.cell.2012.11.001

inserted into the membrane, they should form a hairpin-like structure, exposing the C terminus to the cytosol. Artificial addition of the glycosylation site of opsin is often used to determine the topology and ER targeting of tail-anchored proteins (Pedrazzini et al., 2000). Indeed, addition of the glycosylation site to the C terminus of ER cytochrome b5 caused its glycosylation as its mobility in SDS-PAGE was increased by treatment with Endo H, a deglycosylation enzyme (Figure 6A). However, glycosylation was not observed in Stx17TM-Gly, which has the opsin glycosylation site at its C terminus, suggesting that the C terminus of Stx17 is not in the lumen of the ER and both N and C termini are cytosolic.

Stx17 has a KKXX sequence at the C terminus, which could function as a canonical ER retrieval signal and is recognized by the COPI complex in the cytosol (Popoff et al., 2011). We thus replaced the C-terminal KKCS by AACS and determined its effect on localization of Stx17. GFP-Stx17TM localized to the ER but not to the Golgi. By contrast, a significant amount of GFP-Stx17TM-AACS localized to the Golgi (Figure 6B). This result suggests that the C-terminal KKCS sequence in Stx17 is a functional ER-retrieval signal facing the cytosol. Deletion mutants of C-terminal KKCS also localized to the Golgi (Stx17TMΔ3 in Figure 5). Taken together these findings suggest that the two TMDs of Stx17 form a hairpin-like structure (Figure 6C).

The Glycine Zipper-like Motifs in the TMDs Are Essential for Stx17 to Localize to the Autophagosome

As mentioned above, hydrophobicity of the Stx17 TMDs is not as high as that of other SNARE proteins (Figure S4). Indeed, half of the endogenous Stx17 and exogenous GFP-Stx17 was present in the supernatant fraction, whereas typical membrane proteins such as calnexin, mitochondrial complex III core 1 subunit, and GFP-Stx18 were mainly fractionated into the high-speed (100,000 × *g*) pellet (Figure 7A). This suggests that a significant amount of Stx17 exists in the cytosol, which is unusual for a protein possessing TMDs.

We also found that glycine residues are enriched in both TMDs in Stx17. These domains contain repeated GXXXG motifs (Figure 7B). Indeed, it was previously suggested that TMD1 of Stx17 contains a potential glycine zipper motif (GXXXGXXXG), which has glycine residues spaced every four positions (Kim et al., 2005). We found perfect glycine zipper motifs not only in TMD1 but also in TMD2 of human Stx17 (Figure 7B). These glycine zipper-like motifs are evolutionarily conserved in Stx17 homologs (Figure 7B), but are not found in other syntaxin family proteins (Figure S4). Generally, the GXXXG motif or glycine zipper motif enables close packing of transmembrane helixes (Brosig and Langosch, 1998; Curran and Engelman, 2003; Kim et al., 2005; Russ and Engelman, 2000). We hypothesized that these glycine zipper-like motifs would contribute to the tight hairpin-like structure of the Stx17 TMDs (Figure 7C). In addition, as hydrophobic amino acids are located on the other sides of both TMDs, interaction mediated by the glycine zipper motifs would expose the hydrophobic faces outside.

We therefore generated two types of Stx17 mutants in which G244 and G248, or G264 and G268, were substituted with leucine to disrupt the glycine zipper-like packing interface (Figure 7D). These mutants localized to the ER and mitochondria as efficiently as the wild-type (WT) (Figures 1C and 7E), indicating that the close packing structure is not required for targeting to the ER and mitochondria. However, translocation to the autophagosome was severely defective in these two mutants (Figure 7F). Colocalization of LC3 with these mutants was significantly decreased. These data suggest that the glycine zipper-like motifs of the TMDs of Stx17, which would mediate the close packing interaction, are required for autophagosomal localization of Stx17.

We further performed rescue experiments using HeLa cells stably expressing GFP-Stx17 with the glycine zipper mutations. As shown in Figure 2, expression of GFP-Stx17 WT suppressed the LC3-II accumulation caused by knockdown of Stx17. By contrast, expression of GFP-Stx17 G244/248L or G264/268L did not effectively suppress the LC3-II accumulation (Figure 7G). In addition, mutations in all four glycine residues did not restore LC3-II accumulation. These data suggest that the glycine zipper-like motifs in Stx17 mediate the unique architecture of its TMDs, which is essential for targeting of Stx17 to the autophagosome.

DISCUSSION

In the present study, we identified the autophagosomal Qa-SNARE Stx17, which is essential for fusion between the outer autophagosomal membrane and the endosomal/lysosomal membrane. In contrast to other SNARE proteins, Stx17 has two tandem TMDs. We suggest that the unique hairpin-like structure of the TMDs, which is mediated by the glycine zipper-like motifs, is sufficient and critical for its targeting to the outer autophagosomal membrane. We propose the following model (Figure 7H). Early Atg proteins initiate isolation membrane formation on or near the ER causing elongation of the membrane on the omegasome. Immediately after or before closure, Atg proteins (except LC3) dissociate from the autophagosomal membrane. Then, Stx17 translocates to the outer membrane of the completed autophagosome. Although the degree of hydrophobicity of the Stx17 TMDs is not high, the packed hairpin-like structure causes exposure of the hydrophobic residues. This unique structure is important for localization of Stx17 to the autophagosome. Finally, Stx17, SNAP-29, and endosomal/lysosomal membrane VAMP8 mediate fusion between these structures, leading to degradation of the enclosed materials. A striking observation is that the isolation membranes do not contain Stx17, which is important for achieving autophagic degradation of the cytoplasm. If the isolation membranes possess the fusion machinery, the lysosome would easily fuse

(I) MEFs stably coexpressing GFP-SNAP-29 and Myc-Stx17 (left), or GFP-Vti1b and Myc-Stx17 (right) were cultured in starvation medium for 2 hr. Cells were stained with anti-LC3 and anti-Myc antibodies and analyzed by immunofluorescence microscopy. The structures positive for SNAP29, Stx17, and LC3 are indicated by arrows. Data represent mean ± SEM of ten images. Scale bars, 10 μm (white) and 1 μm (yellow).
See also Figure S2.

Please cite this article in press as: Itakura et al., The Hairpin-type Tail-Anchored SNARE Syntaxin 17 Targets to Autophagosomes for Fusion with Endosomes/Lysosomes, Cell (2012), http://dx.doi.org/10.1016/j.cell.2012.11.001

Cell

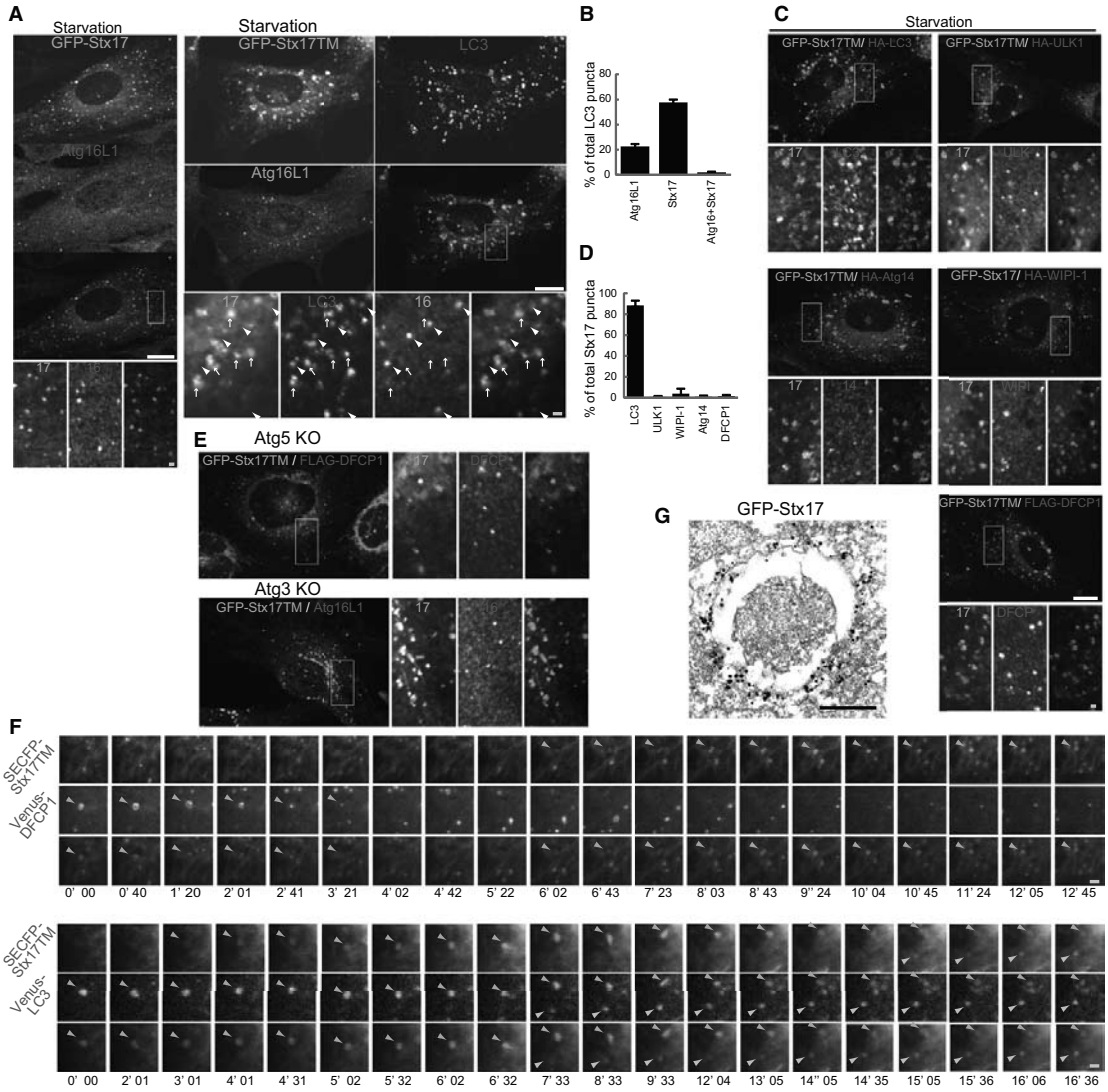

Figure 4. Stx17 Is Present on the Outer Membrane of Completed Autophagosomes

(A and B) MEFs stably expressing GFP-Stx17 or GFP-Stx17TM were starved for 2 hr and analyzed by immunofluorescence microscopy using anti-LC3 and anti-Atg16L1 antibodies. The Stx17- and LC3-positive and Atg16L1- and LC3-positive puncta are indicated by arrows and arrowheads, respectively. Stx17 or Atg16L1 positivity (%) of the LC3 puncta under starvation conditions is shown. Data represent mean ± SEM of ten images.

(C and D) MEFs stably coexpressing GFP-Stx17TM and one of HA-LC3, HA-ULK1, HA-WIPI-1, HA-Atg14, or FLAG-DFCP1 were cultured in starvation medium for 2 hr and analyzed by immunofluorescence microscopy using anti-HA and anti-FLAG antibodies. HA-LC3, HA-ULK1, HA-WIPI-1, HA-Atg14, or FLAG-DFCP1 positivity (%) of the Stx17 puncta under starvation conditions is shown. Data represent mean ± SEM of ten images.

(E) Atg5 KO and Atg 3 KO MEFs stably expressing GFP-Stx17TM with or without FLAG-DFCP1 were cultured in starvation medium for 2 hr and analyzed by immunofluorescence microscopy using anti-FLAG and anti-atg16L1 antibodies.

(F) Selected frames from time-lapse movies of MEFs cultured in starvation medium stably coexpressing SECFP-Stx17TM and either Venus-DFCP1 (upper panel) or Venus-LC3 (bottom panel). The cells were imaged from around 60 min after starvation. Localization of SECFP-Stx17TM and Venus-DFCP1 or LC3 is indicated by blue arrowheads. Another newly generated SECFP-Stx17 and Venus-LC3 structure is indicated by yellow arrowheads (bottom panel). See Movies S1 and S2 for whole images.

(G) MEFs stably expressing GFP-Stx17 were cultured in starvation medium for 2 hr and analyzed by immunoelectron microscopy using anti-GFP antibody.

(A–G) Signal color is indicated by color of typeface. Scale bars, 10 μm (white); 1 μm (yellow) (A, C, E, and F); 200 nm (black) (G).

See also Figure S3.

Please cite this article in press as: Itakura et al., The Hairpin-type Tail-Anchored SNARE Syntaxin 17 Targets to Autophagosomes for Fusion with Endosomes/Lysosomes, Cell (2012), http://dx.doi.org/10.1016/j.cell.2012.11.001

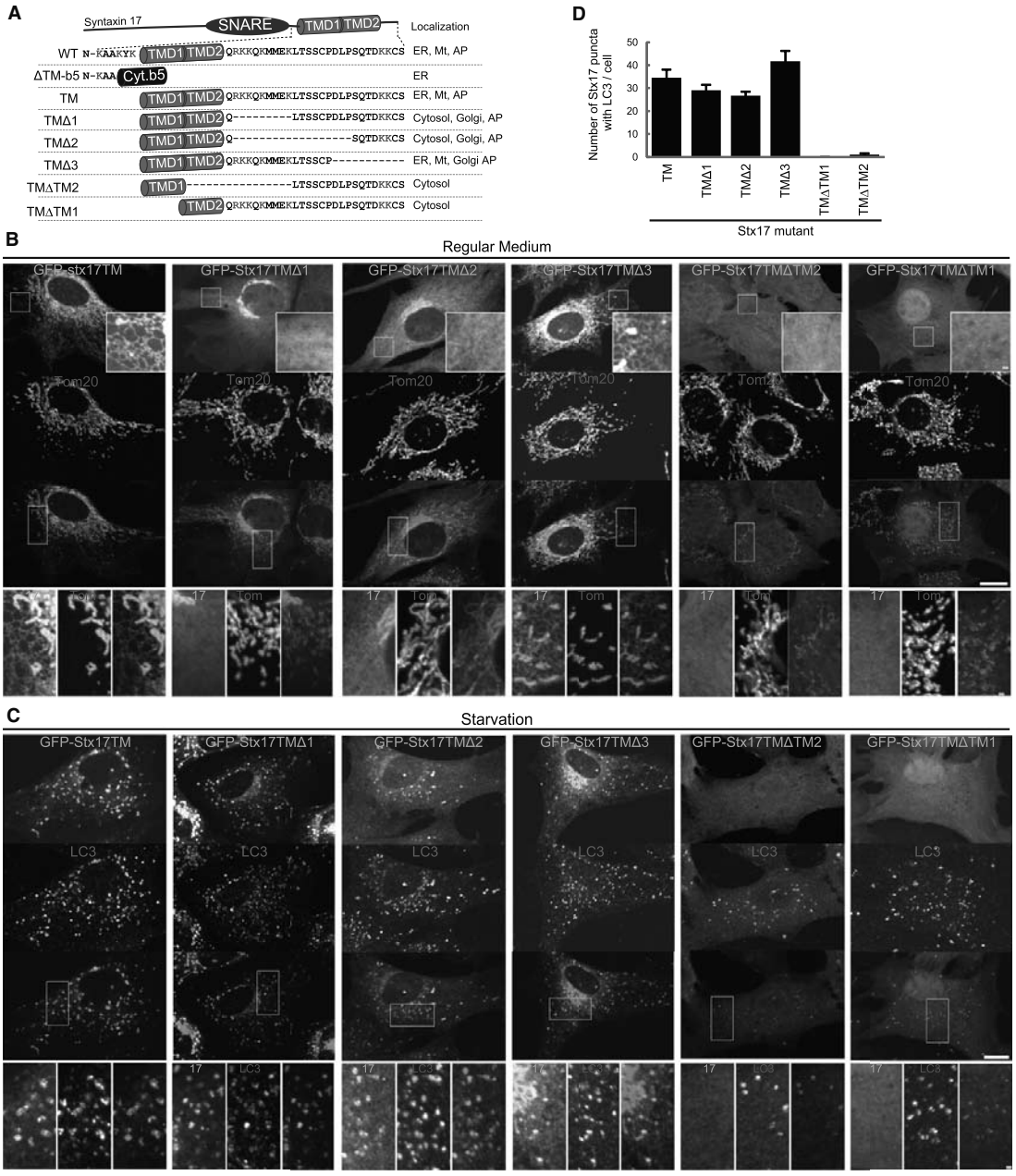

Figure 5. The Two Tandem TMDs in Stx17 Are Sufficient for Autophagosomal Localization

(A) Schematic representation of Stx17 and its deletion mutants. The positively charged residues are shown in red. Their localization patterns observed in immunofluorescence experiments (B and C) are shown.

(B–D) MEFs stably expressing GFP-Stx17TMΔ1, GFP-Stx17TMΔ2, GFP-Stx17TMΔ3, GFP-Stx17TMΔTM2, or GFP-Stx17 TMΔTM1 were cultured in regular (B) or starvation (C) medium for 2 hr and analyzed by immunofluorescence microscopy using anti-Tom20 and anti-LC3 antibodies. Signal color is indicated by color of typeface. Bars: 10 μm (white) and 1 μm (yellow). Quantification of the number of punctate structures positive for both Stx17 and LC3 per cell under starvation conditions (D). Data represent mean ± SEM of ten images.

See also Table S1.

Please cite this article in press as: Itakura et al., The Hairpin-type Tail-Anchored SNARE Syntaxin 17 Targets to Autophagosomes for Fusion with Endosomes/Lysosomes, Cell (2012), http://dx.doi.org/10.1016/j.cell.2012.11.001

Cell

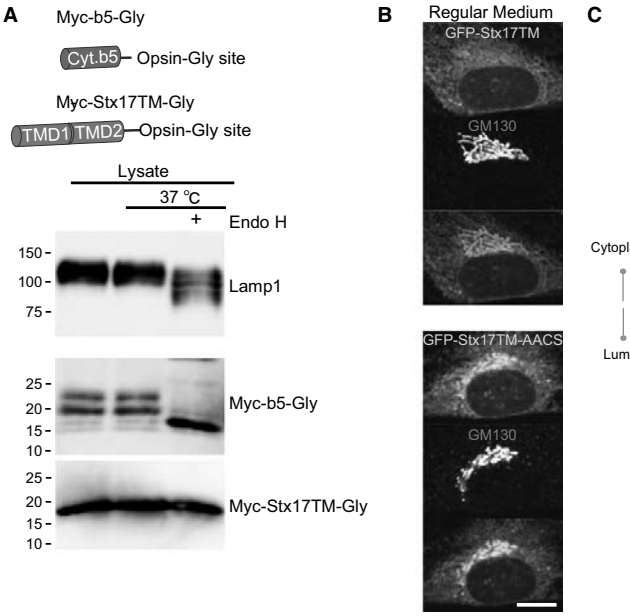

Figure 6. TMDs of Stx17 Forms Hairpin-like Structure

(A) Lysates from MEFs stably expressing the opsin glycosylation site-added Myc-cytochrome b5 (Myc-b5-Gly) or Myc-Stx17TM (Myc-Stx17TM-Gly) were treated with or without endoglycosidase H and analyzed by immunoblotting using anti-Myc and anti-Lamp1 antibodies.

(B) MEFs stably expressing GFP-Stx17TM or GFP-Stx17TM-AACS mutant cultured in regular medium were analyzed by immunofluorescence microscopy using anti-GM130 antibody. Signal color is indicated by color of typeface. Scale bars, 10 μm.

(C) Model of hairpin-like TMDs of Stx17. C terminus of Stx17 is exposed to the cytosol.

with them even prior to completion of autophagosome closure. Thus, the late recruitment of Stx17 to the autophagosome can prevent premature fusion with the lysosome.

Our finding that Stx17 is available to the autophagosome not through the isolation membrane raises the question where Stx17 does come from. One possibility is that autophagosomes acquire Stx17 directly from the cytosol. Indeed, approximately half of the available Stx17 is present in the cytosolic pool, which can be used immediately upon induction of autophagy (Figure 7A). Another, but less likely, possibility is that Stx17 in the ER or mitochondria translocates to the autophagosome. In this case, completed autophagosomes should still have direct connections with the ER/mitochondria (although it is generally believed that they are detached from the ER), or an unknown source of vesicles containing Stx17 that bud off from the ER/mitochondria and fuse with the completed autophagosomes. Further experiments will be needed to clarify this issue.

How Stx17 can localize to completed autophagosomes but not to the isolation membrane is also unknown. Among the known Atg proteins, only LC3 and its related proteins are present on the completed autophagosome. However, we could not detect an interaction between LC3 family proteins and Stx17 (our unpublished data). Furthermore, recruitment of LC3 to the autophagosome occurs much earlier than that of Stx17 (Figure 4). Thus, it is unlikely that the LC3 family is a receptor for Stx17. There may be unidentified protein(s) that serve as a receptor for Stx17. Another possibility is that the presence of upstream Atg proteins or phosphatidylinositol 3-phosphate may inhibit Stx17 recruitment. More details of the autophagosomal contents will be required to understand the specific recruitment of Stx17.

Because Stx17 efficiently binds the R-SNARE VAMP8 (Figure 2) and VAMP8 is required for autophagosome-lysosome fusion (Figure S2) (Furuta et al., 2010), it is likely that VAMP8 is a partner SNARE on the lysosomal membrane. Although knockdown of VAMP7 did not cause accumulation of LC3-II (Figure S2E), we do not completely rule out the possible involvement of VAMP7 as an alternative R-SNARE for the autophagosome-lysosome fusion. Since it was suggested that VAMP7 functions during autophagosome formation (Moreau et al., 2011), knockdown of VAMP7 may inhibit both synthesis and consumption of LC3-II. It was also reported that Vti1b plays a role in the autophagosome-lysosome fusion step (Atlashkin et al., 2003; Furuta et al., 2010). However, we observed that Vti1b mainly localized to the endosome but not the autophagosome (Figure S2D). As Vti1b KO mice showed accumulation of both intact (AVi) and degrading (AVd) autophagic vacuoles (Atlashkin et al., 2003), Vti1b likely functions at a later step than Stx17.

Regarding Qb- and Qc-SNAREs, Stx17 and VAMP8 were shown to bind with SNAP-29, which has both Qb- and Qc-SNARE motifs (Steegmaier et al., 1998; Weng et al., 2007), which we confirmed in this study. Indeed, SNAP-29 is recruited to the Stx17-positive LC3 structures (Figure 3I) and knockdown of SNAP-29 causes autophagosome accumulation (Figure 3G). This is consistent with the fact that silencing of SNAP-29 in *Caenorhabditis elegans* also increases the number of autophagosome-like structures in the intestine (Sato et al., 2011). As SNAP-29 possesses neither a TMD nor a palmitoylation site (Steegmaier et al., 1998), recruitment of Stx17 to autophagosomes may be sufficient for recruitment of cytosolic SNAP-29 to form a Qabc-SNARE complex.

It should be noted that Stx17 is not conserved in yeast. It has been suggested that autophagosome-vacuole fusion in yeast requires the SNAREs Vam3 (Qa) (Darsow et al., 1997), Vti1 (Qb) (Fischer von Mollard and Stevens, 1999; Ishihara et al., 2001), Vam7 (Qc) (Ohashi and Munro, 2010; Sato et al., 1998), and Ykt6 (R) (Dilcher et al., 2001; Klionsky, 2005). None of these SNAREs has a glycine zipper motif or hairpin-like structure. On the contrary, Vam3 is not conserved in mammals. Thus, yeast seems to have a different set of SNARE proteins for

Please cite this article in press as: Itakura et al., The Hairpin-type Tail-Anchored SNARE Syntaxin 17 Targets to Autophagosomes for Fusion with Endosomes/Lysosomes, Cell (2012), http://dx.doi.org/10.1016/j.cell.2012.11.001

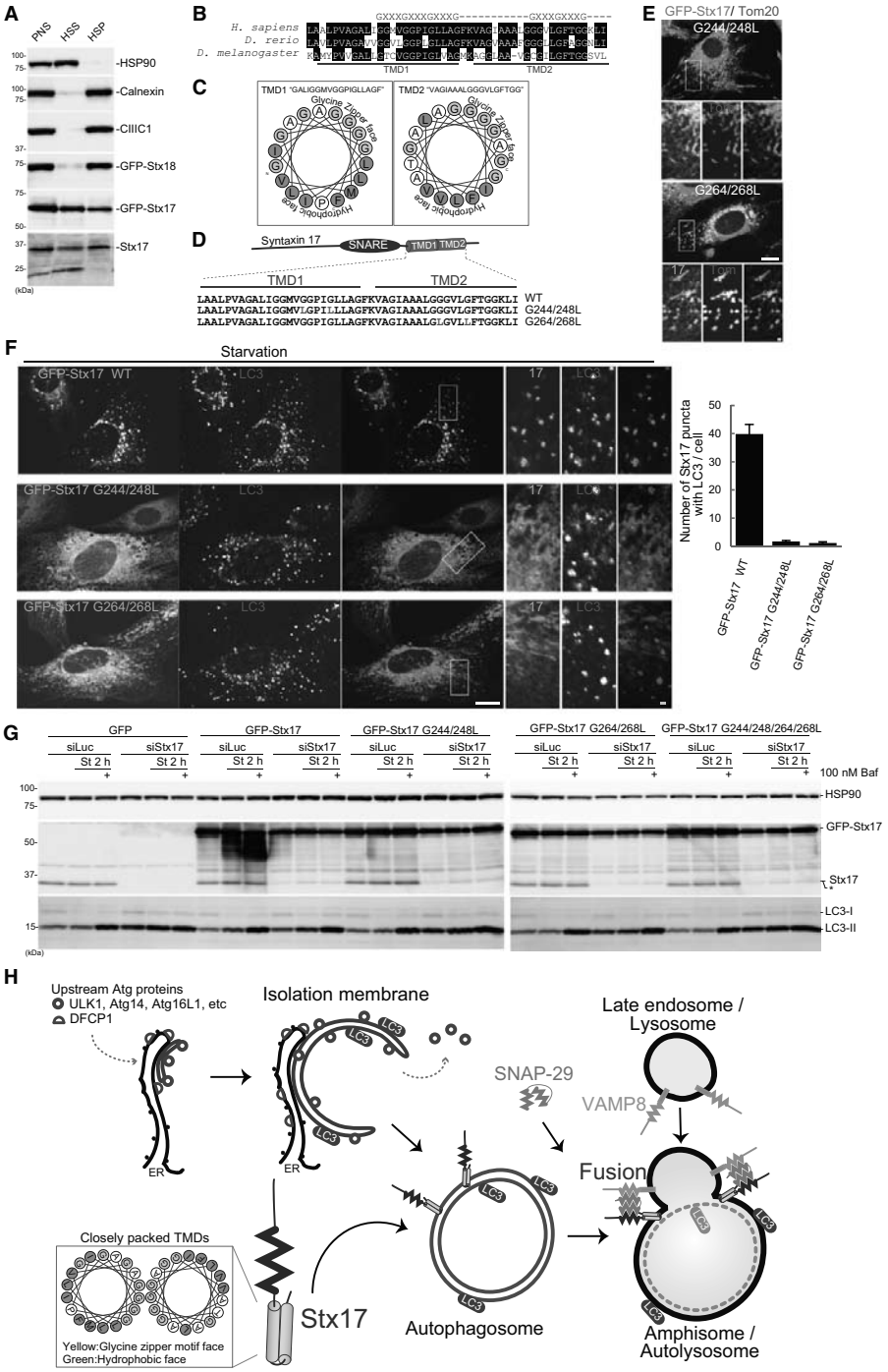

Please cite this article in press as: Itakura et al., The Hairpin-type Tail-Anchored SNARE Syntaxin 17 Targets to Autophagosomes for Fusion with Endosomes/Lysosomes, Cell (2012), http://dx.doi.org/10.1016/j.cell.2012.11.001

Cell

autophagosome-vacuole fusion. Although the mechanism by which SNAREs are provided to yeast autophagosomes remains unknown, a different mechanism may prevent premature fusion of autophagosome intermediates.

Localization of GFP-Stx17 to mitochondria is somewhat unexpected. It was reported that another mitochondrial tail-anchored protein (mitochondrial membrane cytochrome b5; Mito^{cb5}TM) translocates from mitochondria to the autophagosome (Hailey et al., 2010), raising the possibility that autophagosomal Stx17 also translocates from mitochondria. However, the case of Stx17 is completely different; whereas Mito^{cb5}TM seems to translocate to the autophagosome through the isolation membrane, Stx17 is not present on the isolation membrane (Figure 4). Stx17 mutants lacking the C-terminal positive-charged residues can localize to autophagosomes but not to mitochondria (Figure 5). Thus, mitochondrial localization is not essential for autophagosomal targeting of Stx17.

EXPERIMENTAL PROCEDURES

Cell Culture

HeLa cells, human embryonic kidney (HEK) 293T cells, and mouse embryonic fibroblasts (MEFs) were cultured in Dulbecco's modified Eagle's medium (DMEM) supplemented with 10% fetal bovine serum, 50 μg/ml penicillin, and streptomycin (regular medium) in a 5% CO_2 incubator. Atg3 KO (Sou et al., 2008) and Atg5 KO MEFs (Kuma et al., 2004) were generated previously. For starvation treatment, cells were washed with PBS and incubated in amino acid-free DMEM without serum (starvation medium). The oligonucleotide sequences for siRNA experiments are described in Extended Experimental Procedures.

Retroviral Infections and Generation of Stable Cell Lines

Plasmids used in this study are described in Extended Experimental Procedures. Stable cell lines were generated using a retroviral expression system as previously described (Hara et al., 2008; Kitamura et al., 2003). Briefly, Plat E cells (kindly provided by T. Kitamura, The University of Tokyo) were transiently transfected with retroviral vectors using FuGENE HD reagent (Roche Applied Science). After culture for 72 hr, the growth medium containing retrovirus was collected. MEFs were incubated with the collected virus-containing medium with 8 μg/ml polybrene for 24 hr. Uninfected cells were removed by puromycin (Sigma) selection.

Immunocytochemistry

Cells grown on coverslips were washed with PBS and fixed in 4% paraformaldehyde in PBS for 10 min at 4°C. Fixed cells were permeabilized with 50 μg/ml digitonin in PBS for 5 min, blocked with 3% bovine serum albumin in PBS for 30 min, and incubated with primary antibodies for 1 hr. Antibodies used in this study are described in Extended Experimental Procedures. After washing, cells were incubated with Alexa Fluor 488-conjugated goat anti-rat, anti-rabbit, or anti-mouse IgG, Alexa Fluor 564-conjugated goat anti-rabbit or anti-mouse IgG, or Alexa Fluor 660-conjugated goat anti-rabbit IgG secondary antibodies (Invitrogen) for 30 min. Images were acquired on a confocal laser microscope (FV1000D IX81, Olympus) using a 60 × oil-immersion objective lens with a numerical aperture (NA) of 1.42 and a 1.5 × zoom, and captured with Fluoview software (Olympus). The image size was set at 1,024 × 1,024 pixels.

Live-Cell Imaging

Live-cell fluorescence imaging was performed with a microscope (Olympus, IX81) with a 60 × PlanAPO oil-immersion lens (NA 1.42) and a CCD camera (CoolSNAP HQ^2, Photometrics). Cells were placed on a glass bottom dish 1 day before observation. During live imaging, the culture dish was mounted in a chamber (TOKAI HIT) to maintain incubation conditions at 37°C and 5% CO_2. Two-color time-lapse images were acquired at 10 s intervals. The external devices (shutters, filter wheels, stage, and camera) were controlled and image data were processed by MetaMorph version 7.0 (Molecular Devices Japan).

Immunoprecipitation and Immunoblotting

Cell lysates were prepared in a lysis buffer (50 mM Tris-HCl [pH 7.5], 150 mM NaCl, 1 mM EDTA, 1% Triton X-100, 1 mM phenylmethanesulfonyl fluoride [PMSF], 1 mM Na_3VO_4, and protease inhibitor cocktail [complete EDTA-free protease inhibitor, Roche]). The lysates were clarified by centrifugation at 15,000 rpm and were subjected to immunoprecipitation using specific antibodies in combination with protein G-Sepharose (Amersham Biosciences). Precipitated immunocomplexes were washed five times in a washing buffer (50 mM Tris-HCl [pH 7.5], 150 mM NaCl, 1 mM EDTA, and 1% Triton X-100) and boiled in sample buffer. Samples were subsequently separated by SDS-PAGE and transferred to Immobilon-P polyvinylidene diflouride membranes (Millipore). Immunoblot analysis was performed with the indicated antibodies and visualized with Super Signal West Pico Chemiluminescent substrate (Pierce).

Electron Microscopy

MEFs were cultured on collagen-coated plastic coverslips. They were fixed in 2.5% glutaraldehyde in 0.1 M sodium phosphate buffer (pH 7.4) for 2 hr. The cells were washed in the same buffer three times, postfixed in 1% osmium

Figure 7. Glycine Zipper-like Motif Is Essential for Stx17 Localization to the Autophagosome

(A) MEF homogenates were centrifuged at 1,000 × *g* to generate a postnuclear supernatant (PNS). The PNS was then centrifuged at 100,000 × *g* to obtain high-speed supernatant (HSS) and high-speed pellet (HSP), and analyzed by immunoblotting using antibodies against HSP90, calnexin, the core 1 subunit of complex III (CIIIC1), GFP, and Stx17.

(B) Amino acid alignment of TMDs of *Homo sapiens* Stx17 (accession number P56962), *Danio rerio* Stx17 (accession number Q5U3U5), and *Drosophila melanogaster* Stx17 (accession number Q9VZC9). Identical residues are indicated with filled boxes. Glycine zipper-like motifs are shown above.

(C) Helical wheel plots of Stx17 TMD1 and TMD2 generated using HeliQuest (http://heliquest.ipmc.cnrs.fr). Glycine residues are shown in yellow, hydrophobic resides in green, and others in white.

(D) Schematic representation of Stx17 TMD mutants. Glycine 244 and 248, or 264 and 268 are replaced by leucine as shown in red.

(E) MEFs stably expressing GFP-Stx17 G244/248L or G264/268L were analyzed by immunofluorescence microscopy using anti-Tom20 antibody.

(F) MEFs stably expressing GFP-Stx17 WT, GFP-Stx17 G244/248L, or G264/268L were cultured in starvation medium for 2 hr and analyzed by immunofluorescence microscopy using anti-LC3 antibodies. Stx17 positivity (%) of the LC3 puncta is shown. Data represent mean ± SEM of ten images. Signal color is indicated by color of typeface. Bars: 10 μm (white) and 1 μm (yellow).

(G) HeLa cells stably expressing GFP, siRNA-resistant GFP-Stx17, GFP-Stx17 G244/248L, GFP-Stx17 G264/268L, or GFP-Stx17 G244/248/264/268L were treated with siRNA oligonucleotides against luciferase or Stx17. Cells were cultured in regular or starvation medium for 2 hr with or without 100 nM bafilomycin A_1 and analyzed by immunoblotting using the indicated antibodies. An asterisk indicates degradation products of transfected GFP-Stx17.

(H) Model of Stx17 translocation to completed autophagosome. Early Atg proteins generate the isolation membrane on or close to the ER membrane. Immediately after or before completion, almost all Atg proteins dissociate from the membrane and only LC3 remains on the autophagosomal membrane. Then, Stx17, which likely has closely packed TMDs through the glycine zipper-like motifs, translocates to the outer autophagosomal membrane. The outer autophagosomal membrane fuses with the late endosomal/lysosomal membrane; this process is mediated by interaction between Stx17, SNAP-29, and VAMP8.

See also Figure S4.

Please cite this article in press as: Itakura et al., The Hairpin-type Tail-Anchored SNARE Syntaxin 17 Targets to Autophagosomes for Fusion with Endosomes/Lysosomes, Cell (2012), http://dx.doi.org/10.1016/j.cell.2012.11.001

tetroxide in 0.1 M phosphate buffer for 1 hr, dehydrated, and embedded in Epon 812 (Hara et al., 2008). Ultrathin sections were stained with uranyl acetate and lead citrate and observed using a Hitach H-7100 electron microscope.

For immunoelectron microscopy analysis, cells were fixed with 4% paraformaldehyde in 0.1 M sodium phosphate buffer (pH 7.4) for 2 hr at room temperature. The pre-embedding silver enhancement immunogold method was used as previously described (Yoshimori et al., 2000).

SUPPLEMENTAL INFORMATION

Supplemental Information includes Extended Experimental Procedures, four figures, one table, and two movies and can be found with this article online at http://dx.doi.org/10.1016/j.cell.2012.11.001.

ACKNOWLEDGMENTS

We thank Taki Nishimura (Tokyo Medical and Dental University) for help with RNAi experiments, Masaaki Komatsu (Tokyo Metropolitan Institute of Medical Science) for providing Atg3 KO MEFs, and Toshio Kitamura (The University of Tokyo) and Shoji Yamaoka (Tokyo Medical and Dental University) for the retroviral vectors and Plat-E cells, and Atsushi Miyawaki (RIKEN) for providing Venus and SECFP. We also thank Ramanujan S. Hegde and Sichen Shao (MRC Laboratory of Molecular Biology) for critical reading of this manuscript and helpful discussions. This work was supported by the Funding Program for Next Generation World-Leading Researchers, and the Takeda Science Foundation (to N.M.) and grants for a research fellowship of the Japan Society for the Promotion of Science for Young Scientists (to E.I.).

Received: June 4, 2012
Revised: August 20, 2012
Accepted: October 16, 2012
Published: December 6, 2012

REFERENCES

Atlashkin, V., Kreykenbohm, V., Eskelinen, E.L., Wenzel, D., Fayyazi, A., and Fischer von Mollard, G. (2003). Deletion of the SNARE vti1b in mice results in the loss of a single SNARE partner, syntaxin 8. Mol. Cell. Biol. *23*, 5198–5207.

Berg, T.O., Fengsrud, M., Strømhaug, P.E., Berg, T., and Seglen, P.O. (1998). Isolation and characterization of rat liver amphisomes. Evidence for fusion of autophagosomes with both early and late endosomes. J. Biol. Chem. *273*, 21883–21892.

Borgese, N., and Fasana, E. (2011). Targeting pathways of C-tail-anchored proteins. Biochim. Biophys. Acta *1808*, 937–946.

Borgese, N., Colombo, S., and Pedrazzini, E. (2003). The tale of tail-anchored proteins: coming from the cytosol and looking for a membrane. J. Cell Biol. *161*, 1013–1019.

Borgese, N., Brambillasca, S., and Colombo, S. (2007). How tails guide tail-anchored proteins to their destinations. Curr. Opin. Cell Biol. *19*, 368–375.

Brosig, B., and Langosch, D. (1998). The dimerization motif of the glycophorin A transmembrane segment in membranes: importance of glycine residues. Protein Sci. *7*, 1052–1056.

Curran, A.R., and Engelman, D.M. (2003). Sequence motifs, polar interactions and conformational changes in helical membrane proteins. Curr. Opin. Struct. Biol. *13*, 412–417.

Darsow, T., Rieder, S.E., and Emr, S.D. (1997). A multispecificity syntaxin homologue, Vam3p, essential for autophagic and biosynthetic protein transport to the vacuole. J. Cell Biol. *138*, 517–529.

Deretic, V., and Levine, B. (2009). Autophagy, immunity, and microbial adaptations. Cell Host Microbe *5*, 527–549.

Dilcher, M., Köhler, B., and von Mollard, G.F. (2001). Genetic interactions with the yeast Q-SNARE VTI1 reveal novel functions for the R-SNARE YKT6. J. Biol. Chem. *276*, 34537–34544.

Fader, C.M., Sánchez, D.G., Mestre, M.B., and Colombo, M.I. (2009). TI-VAMP/VAMP7 and VAMP3/cellubrevin: two v-SNARE proteins involved in specific steps of the autophagy/multivesicular body pathways. Biochim. Biophys. Acta *1793*, 1901–1916.

Fischer von Mollard, G., and Stevens, T.H. (1999). The Saccharomyces cerevisiae v-SNARE Vti1p is required for multiple membrane transport pathways to the vacuole. Mol. Biol. Cell *10*, 1719–1732.

Fujita, N., Hayashi-Nishino, M., Fukumoto, H., Omori, H., Yamamoto, A., Noda, T., and Yoshimori, T. (2008). An Atg4B mutant hampers the lipidation of LC3 paralogues and causes defects in autophagosome closure. Mol. Biol. Cell *19*, 4651–4659.

Furuta, N., Fujita, N., Noda, T., Yoshimori, T., and Amano, A. (2010). Combinational soluble N-ethylmaleimide-sensitive factor attachment protein receptor proteins VAMP8 and Vti1b mediate fusion of antimicrobial and canonical autophagosomes with lysosomes. Mol. Biol. Cell *21*, 1001–1010.

Hailey, D.W., Rambold, A.S., Satpute-Krishnan, P., Mitra, K., Sougrat, R., Kim, P.K., and Lippincott-Schwartz, J. (2010). Mitochondria supply membranes for autophagosome biogenesis during starvation. Cell *141*, 656–667.

Hara, T., Takamura, A., Kishi, C., Iemura, S., Natsume, T., Guan, J.L., and Mizushima, N. (2008). FIP200, a ULK-interacting protein, is required for autophagosome formation in mammalian cells. J. Cell Biol. *181*, 497–510.

Hegde, R.S., and Keenan, R.J. (2011). Tail-anchored membrane protein insertion into the endoplasmic reticulum. Nat. Rev. Mol. Cell Biol. *12*, 787–798.

Hong, W. (2005). SNAREs and traffic. Biochim. Biophys. Acta *1744*, 120–144.

Ishihara, N., Hamasaki, M., Yokota, S., Suzuki, K., Kamada, Y., Kihara, A., Yoshimori, T., Noda, T., and Ohsumi, Y. (2001). Autophagosome requires specific early Sec proteins for its formation and NSF/SNARE for vacuolar fusion. Mol. Biol. Cell *12*, 3690–3702.

Itakura, E., and Mizushima, N. (2010). Characterization of autophagosome formation site by a hierarchical analysis of mammalian Atg proteins. Autophagy *6*, 764–776.

Jahn, R., and Scheller, R.H. (2006). SNAREs—engines for membrane fusion. Nat. Rev. Mol. Cell Biol. *7*, 631–643.

Kabeya, Y., Mizushima, N., Ueno, T., Yamamoto, A., Kirisako, T., Noda, T., Kominami, E., Ohsumi, Y., and Yoshimori, T. (2000). LC3, a mammalian homologue of yeast Apg8p, is localized in autophagosome membranes after processing. EMBO J. *19*, 5720–5728.

Kim, S., Jeon, T.J., Oberai, A., Yang, D., Schmidt, J.J., and Bowie, J.U. (2005). Transmembrane glycine zippers: physiological and pathological roles in membrane proteins. Proc. Natl. Acad. Sci. USA *102*, 14278–14283.

Kitamura, T., Koshino, Y., Shibata, F., Oki, T., Nakajima, H., Nosaka, T., and Kumagai, H. (2003). Retrovirus-mediated gene transfer and expression cloning: powerful tools in functional genomics. Exp. Hematol. *31*, 1007–1014.

Klionsky, D.J. (2005). The molecular machinery of autophagy: unanswered questions. J. Cell Sci. *118*, 7–18.

Klionsky, D.J., Abeliovich, H., Agostinis, P., Agrawal, D.K., Aliev, G., Askew, D.S., Baba, M., Baehrecke, E.H., Bahr, B.A., Ballabio, A., et al. (2008a). Guidelines for the use and interpretation of assays for monitoring autophagy in higher eukaryotes. Autophagy *4*, 151–175.

Klionsky, D.J., Elazar, Z., Seglen, P.O., and Rubinsztein, D.C. (2008b). Does bafilomycin A1 block the fusion of autophagosomes with lysosomes? Autophagy *4*, 849–950.

Kobayashi, T., Stang, E., Fang, K.S., de Moerloose, P., Parton, R.G., and Gruenberg, J. (1998). A lipid associated with the antiphospholipid syndrome regulates endosome structure and function. Nature *392*, 193–197.

Kuma, A., Hatano, M., Matsui, M., Yamamoto, A., Nakaya, H., Yoshimori, T., Ohsumi, Y., Tokuhisa, T., and Mizushima, N. (2004). The role of autophagy during the early neonatal starvation period. Nature *432*, 1032–1036.

Levine, B., and Kroemer, G. (2008). Autophagy in the pathogenesis of disease. Cell *132*, 27–42.

Levine, B., Mizushima, N., and Virgin, H.W. (2011). Autophagy in immunity and inflammation. Nature *469*, 323–335.

Please cite this article in press as: Itakura et al., The Hairpin-type Tail-Anchored SNARE Syntaxin 17 Targets to Autophagosomes for Fusion with Endosomes/Lysosomes, Cell (2012), http://dx.doi.org/10.1016/j.cell.2012.11.001

Cell

Mizushima, N., and Komatsu, M. (2011). Autophagy: renovation of cells and tissues. Cell *147*, 728–741.

Mizushima, N., Yamamoto, A., Hatano, M., Kobayashi, Y., Kabeya, Y., Suzuki, K., Tokuhisa, T., Ohsumi, Y., and Yoshimori, T. (2001). Dissection of autophagosome formation using Apg5-deficient mouse embryonic stem cells. J. Cell Biol. *152*, 657–668.

Mizushima, N., Yoshimori, T., and Levine, B. (2010). Methods in mammalian autophagy research. Cell *140*, 313–326.

Mizushima, N., Yoshimori, T., and Ohsumi, Y. (2011). The role of Atg proteins in autophagosome formation. Annu. Rev. Cell Dev. Biol. *27*, 107–132.

Moreau, K., Ravikumar, B., Renna, M., Puri, C., and Rubinsztein, D.C. (2011). Autophagosome precursor maturation requires homotypic fusion. Cell *146*, 303–317.

Nair, U., Jotwani, A., Geng, J., Gammoh, N., Richerson, D., Yen, W.L., Griffith, J., Nag, S., Wang, K., Moss, T., et al. (2011). SNARE proteins are required for macroautophagy. Cell *146*, 290–302.

Noda, T., Fujita, N., and Yoshimori, T. (2009). The late stages of autophagy: how does the end begin? Cell Death Differ. *16*, 984–990.

Ohashi, Y., and Munro, S. (2010). Membrane delivery to the yeast autophagosome from the Golgi-endosomal system. Mol. Biol. Cell *21*, 3998–4008.

Pedrazzini, E., Villa, A., Longhi, R., Bulbarelli, A., and Borgese, N. (2000). Mechanism of residence of cytochrome b(5), a tail-anchored protein, in the endoplasmic reticulum. J. Cell Biol. *148*, 899–914.

Popoff, V., Adolf, F., Brügger, B., and Wieland, F. (2011). COPI budding within the Golgi stack. Cold Spring Harb. Perspect. Biol. *3*, a005231.

Pryor, P.R., Mullock, B.M., Bright, N.A., Lindsay, M.R., Gray, S.R., Richardson, S.C., Stewart, A., James, D.E., Piper, R.C., and Luzio, J.P. (2004). Combinatorial SNARE complexes with VAMP7 or VAMP8 define different late endocytic fusion events. EMBO Rep. *5*, 590–595.

Rabu, C., Schmid, V., Schwappach, B., and High, S. (2009). Biogenesis of tail-anchored proteins: the beginning for the end? J. Cell Sci. *122*, 3605–3612.

Renna, M., Schaffner, C., Winslow, A.R., Menzies, F.M., Peden, A.A., Floto, R.A., and Rubinsztein, D.C. (2011). Autophagic substrate clearance requires activity of the syntaxin-5 SNARE complex. J. Cell Sci. *124*, 469–482.

Russ, W.P., and Engelman, D.M. (2000). The GxxxG motif: a framework for transmembrane helix-helix association. J. Mol. Biol. *296*, 911–919.

Sato, T.K., Darsow, T., and Emr, S.D. (1998). Vam7p, a SNAP-25-like molecule, and Vam3p, a syntaxin homolog, function together in yeast vacuolar protein trafficking. Mol. Cell. Biol. *18*, 5308–5319.

Sato, M., Saegusa, K., Sato, K., Hara, T., Harada, A., and Sato, K. (2011). Caenorhabditis elegans SNAP-29 is required for organellar integrity of the endomembrane system and general exocytosis in intestinal epithelial cells. Mol. Biol. Cell *22*, 2579–2587.

Sou, Y.S., Waguri, S., Iwata, J., Ueno, T., Fujimura, T., Hara, T., Sawada, N., Yamada, A., Mizushima, N., Uchiyama, Y., et al. (2008). The Atg8 conjugation system is indispensable for proper development of autophagic isolation membranes in mice. Mol. Biol. Cell *19*, 4762–4775.

Steegmaier, M., Yang, B., Yoo, J.S., Huang, B., Shen, M., Yu, S., Luo, Y., and Scheller, R.H. (1998). Three novel proteins of the syntaxin/SNAP-25 family. J. Biol. Chem. *273*, 34171–34179.

Tooze, S.A., and Yoshimori, T. (2010). The origin of the autophagosomal membrane. Nat. Cell Biol. *12*, 831–835.

Weng, N., Thomas, D.D., and Groblewski, G.E. (2007). Pancreatic acinar cells express vesicle-associated membrane protein 2- and 8-specific populations of zymogen granules with distinct and overlapping roles in secretion. J. Biol. Chem. *282*, 9635–9645.

White, E., Karp, C., Strohecker, A.M., Guo, Y., and Mathew, R. (2010). Role of autophagy in suppression of inflammation and cancer. Curr. Opin. Cell Biol. *22*, 212–217.

Yoshimori, T., Yamagata, F., Yamamoto, A., Mizushima, N., Kabeya, Y., Nara, A., Miwako, I., Ohashi, M., Ohsumi, M., and Ohsumi, Y. (2000). The mouse SKD1, a homologue of yeast Vps4p, is required for normal endosomal trafficking and morphology in mammalian cells. Mol. Biol. Cell *11*, 747–763.

Cell

Supplemental Information

EXTENDED EXPERIMENTAL PROCEDURES

Plasmids

Full-length cDNAs encoding human Stx17, Stx7, Stx18, VAMP8, SNAP-29, and Vti1b were amplified by PCR from total cDNA of HeLa cells. An IMAGE Consortium cDNA clone encoding mouse DFCP1 (GenBank accession number CB526501) was obtained from Invitrogen. A cDNA clone encoding mouse Vamp7 (Clone 3601755) was obtained from Open Biosystems. To generate the pMRXIP-GFP-Stx17, pMRXIP-GFP-Stx18, pMRXIP-GFP-VAMP8, pMRXIP-GFP-Vti1b, and pMRXIP-FLAG-DFCP1 plasmids, cDNAs were cloned into pMRXIP (provided by S. Yamaoka, Tokyo Medical and Dental University, Tokyo, Japan) together with enhanced green fluorescence protein (EGFP) or 3xFLAG. Deletion and point mutants of Stx17 were made by inverse PCR; the amino acid sequences are shown in Table S1. Venus and super enhanced cyan fluorescent protein (SECFP) were provided by A. Miyawaki (RIKEN). The following plasmids have been previously described: pMXs-IP-GFP-LC3 and pMXs-IP-HA-ULK1 (Hara et al., 2008) and pMXs-puro-mRFP-b5, pMXs-puro-HA-Atg14, and pMXs-puro HA-WIPI-1 (Itakura and Mizushima, 2010). An siRNA-resistant Stx17 silent mutant was created by substituting five nucleotides in the Stx17 siRNA-targeting region (A519G, C522G, A525G, A528G, and A537G).

Antibodies

Rat monoclonal anti-GFP antibodies (GF090R) for immunocytochemistry were purchased from NacalaiTesque. Rabbit polyclonal anti-GFP antibodies for immunoblotting were purchased from MBL. The rabbit polyclonal antibodies against LC3 (LC3#1) for immunoblotting (Hosokawa et al., 2006) and Atg16L1 (Mizushima et al., 2003) have been described previously. Mouse monoclonal anti-LC3 antibody (Clone: LC3 1703) for immunocytochemistry was purchased from COSMO BIO. Mouse monoclonal anti-HA (16B12) and anti-Myc (9E10) antibodies were purchased from Covance Research Products. Mouse monoclonal anti-FLAG (M2), anti-β-actin, and rabbit polyclonal anti-Stx17 and anti-VAMP8 antibodies were purchased from Sigma. Rabbit polyclonal anti-Tom20 antibodies were purchased from Santa Cruz. Mouse monoclonal anti-GM130, anti-HSP90, and anti-Vti1b antibodies were purchased from BD Bioscience. Rabbit polyclonal anti-calnexin antibodies were purchased from Stressgen. Rabbit polyclonal anti-Lamp1 antibodies were provided by Y. Tanaka (Kyushu University, Fukuoka, Japan). Mouse monoclonal anti-core 1 subunit of complex III antibody was purchased from Invitrogen. Rabbit polyclonal anti-SNAP-29 antibodies were purchased from Synaptic Systems. Mouse monoclonal anti-VAMP7 antibody was purchased from CovalAb.

RNA Interference

Stealth RNAi oligonucleotides were used for siRNA experiments (Invitrogen). The sequences used were as follows: human Stx17siRNA antisense, 5′-AATTAAGTCCGCTTCTAAGGTTTCC-3′, sense, 5′-GGAAACCTTAGAAGCGGACTTAATT-3′; luciferase siRNA antisense, 5′-AATTAAGTCCGCTTCTAAGGTTTCC-3′, sense, 5′-CGCGGTCGGTAAAGTTGTTCCATTT-3′, human SNAP-29-1 siRNA antisense, 5′-TATCATCCAGCTTTCTAAGGTTTGG-3′, sense, 5′- CCAAACCTTAGAAAGCTGGATGATA-3′, human SNAP-29-2 siRNA antisense, 5′-GGCTGACAACCAAAGTGGACAAGTT-3′, sense, 5′-AACTTGTCCACTTTGGTTGTCAGCC-3′, human SNAP-29-3 siRNA antisense, 5′-CCACACCTTCGAGCCTATCACCAGA −3′, sense, 5′-TCTGGTGATAGGCTCGAAGGTGTGG-3′, human Vti1b-1 siRNA antisense, 5′-TATGCCATATTTCATGTCTCCTCGG-3′, sense, 5′- CCGAGGAGACATGAAATATGGCATA −3′, human Vti1b-2 siRNA antisense, 5′- TTCAGTGCCCTGCAGAAGCATTGCC −3′, sense, 5′- GGCAATGCTTCTGCAGGGCACTGAA −3′, human Vti1b-3 siRNA antisense, 5′- TTCACTTGTGTTTACCAGTCTACTC −3′, sense, 5′- GAGTAGACTGGTAAACACAAGTGAA −3′, human VAMP7-1 siRNA antisense, 5′- ATAATTGCCATGTGAGTACGTTAGT −3′, sense, 5′- ACTAACGTACTCACATGGCAATTAT A-3′, human VAMP7-2 siRNA antisense, 5′- TTCTGACCATGATTCCTTTCAGTTC −3′, sense, 5′- GAACTGAAAGGAATCATGGTCAG AA −3′, human VAMP7-3 siRNA antisense, 5′- ATTCCAATCTTTCTCCTCGCTGAGC −3′, sense, 5′- GCTCAGCGAGGAGAAAGA TTGGAAT −3′, human Stx7-1 siRNA antisense, 5′- ATAATCTGCTGCCCTTGACAGCTGC −3′, sense, 5′- GCAGCTGTCAAGGGCAG CAGATTAT −3′, human Stx7-2 siRNA antisense, 5′- TGATGAGACTGATAATCGCAACTCC −3′, sense, 5′- GGAGTTGCGATTATCA GTCTCATCA 3′, human Stx7-3 siRNA antisense, 5′- TCAAGTTGCCTGATAGAAGATTCTC −3′, sense, 5′- GAGAATCTTCTATCAGG CAACTTGA −3′. The siRNA oligonucleotides for human VAMP 8 (HSS112731) were reported previously (Furuta et al., 2010). The Stealth RNAi oligonucleotides were transfected into cells using Lipofectamine RNAi MAX (Invitrogen) according to the manufacturer's instructions. After 2 days, the cells were again transfected with the same siRNA and cultured for an additional 4 days before analysis.

Cell Fractionation

MEFs were cultured and harvested using 0.5% trypsin-EDTA. Cells were resuspended in regular medium. To prevent nonspecific protein binding to plastic tubes, 2-methacryloyloxyethyl phosphorylcholine polymer-coated tubes were used. Cell pellets were resuspended in homogenization buffer (HB; 20 mM HEPES (pH 7.4), 0.22 M mannitol, 0.07 M sucrose, 0.5 mM EDTA, 0.5 mM PMSF, 10 μg/ml soybean trypsin inhibitor, and complete protease inhibitors mixture), and were passaged 20 times through a 27 gauge needle. Postnuclear supernatant (PNS) was prepared by two consecutive centrifugation steps at 1,000 × *g*. The PNS was subsequently centrifuged at 100,000 × *g* for 30 min to generate high-speed supernatant (HSS) and high-speed pellet (HSP) fractions. The resulting HSP was washed in HB, centrifuged at 100,000 × *g*, and resuspended in HB.

Cell

Reverse Transcriptase PCR and Real-Time PCR

Total RNA was extracted from cells using Isogen (Nippon Gene) according to the manufacturer's instruction. Trace contamination of DNA was removed by DNase digestion (Promega). cDNA was synthesized from 2 μg of total RNA using ReverTra Ace (Toyobo). Real-time PCR was performed on a Thermal Cycler Dice (Takara) using SYBR premix EX Taq (Takara). Human Stx7 forward, 5′- GTTCAGCAAGCAAATCAGCA −3′; reverse, 5′- CGCAACTCCAATGACAAGG −3′. Human GAPDH forward, 5′- GCCAAGGTCAT CCATGACAACT −3′; reverse, 5′- GAGGGGCCATCCACAGTCTT −3′. Amplicon expression in each sample was normalized to its GAPDH mRNA content.

SUPPLEMENTAL REFERENCES

Furuta, N., Fujita, N., Noda, T., Yoshimori, T., and Amano, A. (2010). Combinational soluble N-ethylmaleimide-sensitive factor attachment protein receptor proteins VAMP8 and Vti1b mediate fusion of antimicrobial and canonical autophagosomes with lysosomes. Mol. Biol. Cell *21*, 1001–1010.

Hara, T., Takamura, A., Kishi, C., Iemura, S., Natsume, T., Guan, J.L., and Mizushima, N. (2008). FIP200, a ULK-interacting protein, is required for autophagosome formation in mammalian cells. J. Cell Biol. *181*, 497–510.

Hosokawa, N., Hara, Y., and Mizushima, N. (2006). Generation of cell lines with tetracycline-regulated autophagy and a role for autophagy in controlling cell size. FEBS Lett. *580*, 2623–2629.

Itakura, E., and Mizushima, N. (2010). Characterization of autophagosome formation site by a hierarchical analysis of mammalian Atg proteins. Autophagy *6*, 764–776.

Mizushima, N., Kuma, A., Kobayashi, Y., Yamamoto, A., Matsubae, M., Takao, T., Natsume, T., Ohsumi, Y., and Yoshimori, T. (2003). Mouse Apg16L, a novel WD-repeat protein, targets to the autophagic isolation membrane with the Apg12-Apg5 conjugate. J. Cell Sci. *116*, 1679–1688.

Cell

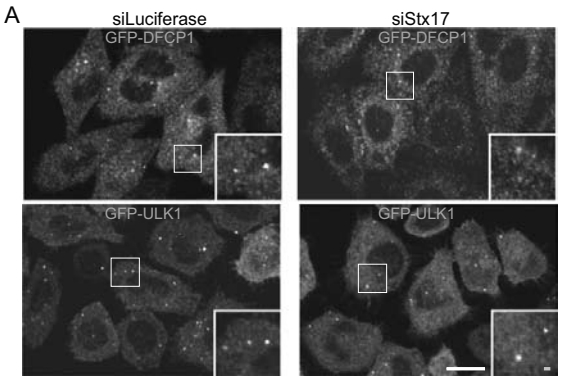

Figure S1. Depletion of Stx17 Does Not Cause Accumulation of Isolation Membranes/Omegasomes, Related to Figure 2
HeLa cells stably expressing GFP-DFCP1 or GFP- ULK1 were treated with siRNA oligonucleotides against luciferase or Stx17. Cells were cultured in starvation medium for 1 hr and analyzed by immunofluorescence microscopy. Scale bars, 10 μm (white) and 1 μm (yellow).

Cell

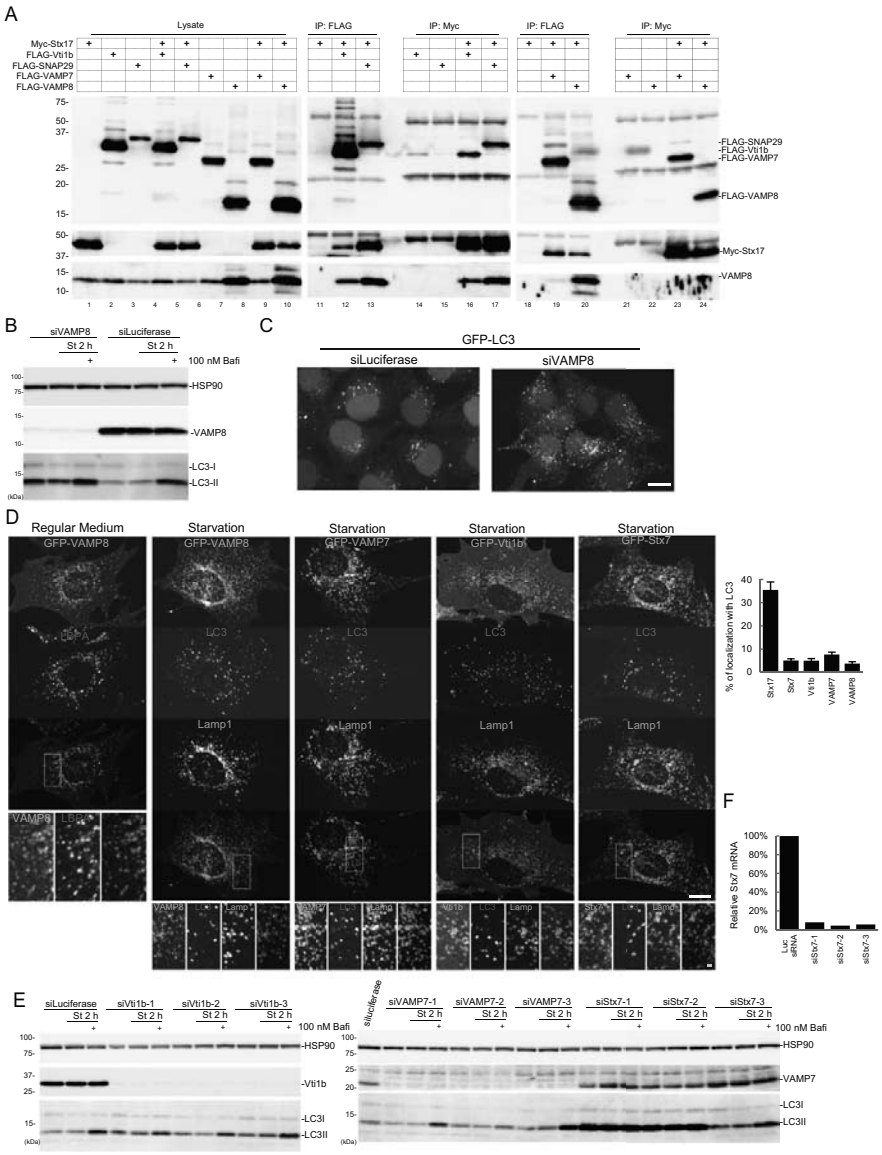

Figure S2. Stx17 Interaction and Localization of Lysosomal SNAREs, Related to Figure 3

(A) HEK293T cells were transfected with indicated plasmids. Two days later, cells were lysed, and immunoprecipitated with indicated antibodies.

(B) HeLa cells were treated with siRNA oligonucleotides against luciferase or VAMP8. Cells were cultured in regular or starvation medium for 2 hr with or without 100 nM bafilomycin A_1 and analyzed by immunoblotting using the indicated antibodies.

(C) HeLa cells stably expressing GFP-LC3 were treated with siRNA oligonucleotides against luciferase or VAMP8. Cells were cultured in regular medium and analyzed by immunofluorescence microscopy.

(D) MEFs stably expressing indicated GFP-fused proteins were cultured in regular medium or starvation medium for 2 hr. Cells were stained with anti-LBPA (a late endosome marker), anti-Lamp1, and anti-LC3 antibodies and analyzed by immunofluorescence microscopy. Quantification of the number of punctate structures positive for LC3 per cell in starvation (right panel). Data represent mean ± SEM of ten images.

(E) HeLa cells were treated with siRNA oligonucleotides against three different regions of the indicated targets. Cells were cultured in regular or starvation medium for 2 hr with or without 100 nM bafilomycin A_1 and analyzed by immunoblotting using the indicated antibodies.

(F) HeLa cells were treated with siRNA oligonucleotides against luciferase or Stx7. The mRNA level was measured by real-time PCR.

Scale bars, 10 μm (white) and 1 μm (yellow).

Cell

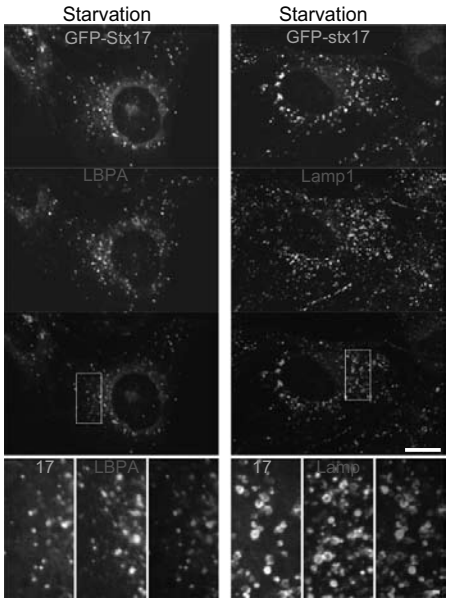

Figure S3. GFP-Stx17 Does Not Localize to the Late Endosome/Lysosome, Related to Figure 4
MEFs stably expressing GFP-Stx17 were cultured in starvation medium for 2 hr. Cells were stained with anti-LBPA or anti-Lamp1 antibodies and analyzed by immunofluorescence microscopy. Scale bars, 10 μm (white) and 1 μm (yellow).

Cell

Stx1	IMIIICCVILGIVIASTVGGI
Stx2	WIIIAVSVVLVAIIALIIGLSVG
Stx3	LIIIIVLVVVLLGILALIIGLSVGL
Stx4	VLIAICVSITVVLLAVIIGVTVV
Stx5	WLMVKIFLILIVFFIIFVVFL
Stx6	WCAIAILFAVLLVVLILFLVL
Stx7	CIIILILVIGVAIISLIIWGL
Stx8	SASCGMIMVILLLLVAIVVVAVW
Stx10	WCAIAVLVGVLLLVLILLFSL
Stx12	MCILVLVLSVIILILGLIIWLV
Stx16	MLVILILFVIIIVLIVVLVGV
Stx18	AGFRVWILFFLVMCSFSLLFL
Stx17TMD1	LAALPVAGALIGGMVGGPIGLLAG
Stx17TMD2	VAGIAAALGGGVLGFTGGKLI

Figure S4. Glycine Residues Are Enriched in TMDs of Stx17, Related to Figure 7
Amino acid sequences of TMDs of syntaxin family proteins. Glycine residues are shown in red.

細菌感染制御学分野

中川 一路

医歯学総合研究科・口腔機能再構築学系専攻
細菌感染制御学・教授

1）研究の課題名

① 細胞内侵入性細菌の認識機構と細胞内分解機構の解析

Molecular analysis of recognition system and inflammation responses against bacterial infection.

病原性細菌の病原性の発揮は、宿主組織への付着により生体組織に定着することから開始する。そのため、生体を広く覆う上皮や粘膜といった組織は、これらの菌の侵入を感知する最前線の組織であり、かつ重要な防御組織となっている。近年、多くの細菌種がこのような上皮組織の細胞内に侵入することが知られているが、その動態はほとんど明らかとされていない。本年度は、細胞内に侵入するA群レンサ球菌の動態を、特にエンドソームでの菌の動態を、細胞内の小胞輸送に関わるRabタンパク質について解析を行った。その結果、A群レンサ球菌の細胞内侵入に関わり、通常の飢餓状態で誘導されるオートファジーとは異なり、Rab9AとRab23が関与していることが明らかとした。Rab9Aは、近年報告された代替性オートファジーに必須な因子であることから、さらにAtg5遺伝子破壊細胞を用いて生体防御におけるRab9Aの動態をさらに詳細に解析した。その結果、Atg5遺伝子破壊細胞内においてもRab9A陽性の小胞内にA群レンサ球菌が認められた。この小胞は、電子顕微鏡の観察から通常のオートファゴソームで見られるような多重膜構造は持たないが、リソソームとの融合は認められたことから細胞内の菌体の排除に機能していることが示唆された。以上の結果よりA群レンサ球菌の細胞内からの排除には、通常のAtg5依存性のオートファジーだけでなく、Rab9Aによって制御される代替性オートファジーも機能していることが明らかとなった。

② 比較ゲノム解析に基づく病原性細菌の外来性遺伝子獲得機構と進化の解析

Comparative genomics for bacterial gene acquisition and evolution systems.

病原性細菌は生体の防御機構に対抗するため、ゲノムの再構成や、外来性遺伝子の取り込みなど様々な方法を用いて進化してきたと考えられる。そこで細菌の個別ゲノムの完全塩基配列解析、高速シーケンサーを用いた多株ゲノム比較解析および発現機能解析などを行った。まず、細菌ゲノムの完全配列では、歯周病原性細菌であるP. gingivalis TDC60株、Streptococcus pyogenes JRS4株、ATCC14918、ATCC14918株の3株、う触病原性細菌であるStreptococcus mutans LJ23株のゲノムを決定した。また、多株比較ゲノム解析では、S. pyogenesの90株の比較ゲノム解析、Vibrio cholerae 60株の比較ゲノム解析、P. gingivalis　40株の比較ゲノム解析、Tannerella forsythia 40株の比較ゲノム解析、S. suisの13株の比較ゲノム解析を行った。また、高速シーケンサーの利点を生かして、現在日本で使用されているBCG株の品質管理を目的として、日本のBCG研究所に保管されている株、過去に東南アジアに分与された株、現在の日本で市販されているBCG株などの比較ゲノム解析を行い、結核菌における遺伝子変異部位を同定することができた。この技術については、現在東京医科歯科大学、岡山大学、日本BCG研究所と共同で特許書類を作成して本学の知財に提出している。さらに、原因菌がわからないような感染性の疾患に対応するため、Metagenomics解析も立ち上げ、現在本学の顎顔面外科学、歯周病学、矯正学の歯系臨床分野、また耳鼻咽喉科や眼科の医系臨床系分野との研究を進めている。

2）研究のイラストレーション

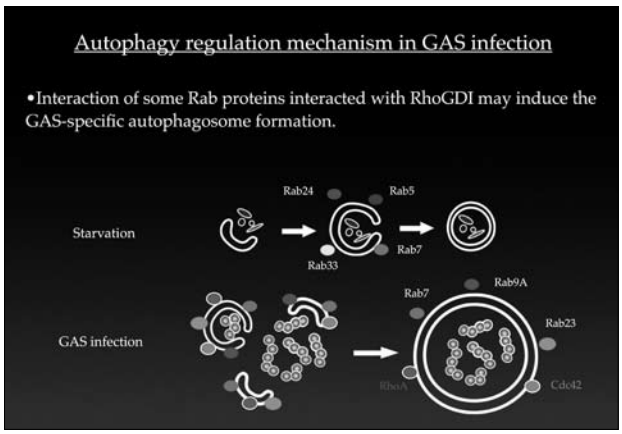

3）発表の研究内容についての英文要約

Autophagy mediates the degradation of cytoplasmic contents in the lysosome and plays a significant role in immunity. Here we identified the small GTPases Rab9A and Rab23 as novel autophagy regulators during Group A streptococcus (GAS) infection. Rab9A was recruited to GAS-containing autophagosome-like vacuoles (GcAVs) after autophagosomal maturation and its activity was required for GcAV enlargement and eventual lysosomal fusion. GcAV enlargement seemed to be related with homotypic fusion of GcAVs by Rab9A. Rab23 was recruited to GAS-capturing forming autophagosomes. Knockdown of Rab23 expression decreased both LC3- and Atg5-positive GAS and caused the accumulation of LC3-positive structures that did not associate with intracellular GAS. It was suggested, therefore, that Rab23 is required for GcAV formation and is involved in GAS targeting of autophagic vacuoles. Furthermore, knockdown of Rab9A or Rab23 expression impaired the degradation of intracellular GAS. Therefore, our data reveal that the Rab9A and Rab23 GTPases play a crucial role in autophagy of GAS. However, neither Rab9A nor Rab23 were localized to starvation-induced autophagosomes. Not only Rab9A but also Rab23 was dispensable for starvation-induced autophagosome formation. These findings demonstrate that specific Rab proteins function at distinct steps during autophagy in response to GAS infection.

4）本事業に関連して世界的な研究拠点形成に向けて、以下の点で改善・整備等されたこと

A（研究拠点体制）

東京医科歯科大学で微生物ゲノム解析が可能な設備として、高速シーケンサーRoche GSjuniorに加え、Illumina MiSeqが分野内に設置された。またそれに伴い微生物ゲノム専門のゲノム解析が可能な設備として、Unix計算サーバーを研究室内に5台設置し、研究室内で微生物ゲノムの完全配列の決定、多株比較ゲノム解析が可能となった。

B（研究教育環境）

研究教育環境については、本分野内での細胞機能解析システム（共焦点レーザー顕微鏡、FACS, リアルタイム蛍光観察システム）および次世代型高速シーケンサー（Roche GSjunioおよびIllumina MiSeq）が導入されたことにより、分野内で微生物ゲノムの全配列決定、細菌叢解析などが可能となった。

C（人材確保）

人材確保については、高速シーケンサーの運用・稼働のため、ウェット・ドライ双方の研究が可能な人材として、東京工業大学出身の修士学生、また大阪大学微生物病研究所よりH24年3月より野澤孝志助教を採用した。

D（人材育成）

人材育成については、高速シーケンサーの運用・稼働のため、現在分野に所属するポスドク・大学院生でも運用可能になるように教育を行っている。現在では、高速シーケンサーの運用可能なスタッフ3名、大学院生3名となっている。また、臨床系分野での貴重なサンプルを高速シーケンサー解析するための人材の育成に力をいれ、現在5名の臨床系分野の大学院生の指導も行なっている。

E（国際化）

大学院生としてインドよりTejaswini Kulkarniが大学院生として入学し、本分野での外国人留学生は3名となった。タイ国NIHとの共同研究としてを更に推し進め、Vibrio choleraeの多株比較ゲノム解析、S. suisの多株ゲノム比較解析を行い、S. suisについては、現在論文投稿中である。

5）GCOE事業を推進するに当たって力を入れた点

本分野は、大量のゲノム情報を扱うためのプラットフォームを確定することが、本事業での任務であると捉えているため、本年度はそのためのアプリケーションの開発・運営指導体制の確立を行ってきた。高速シーケンサーであるIllumina GIIxは、高速シーケンサーとしては現段階では世界的な標準となっているが、その性能上、短いDNA配列（約150bp）を大量に取得するため、ゲノム配列を決定するというよりもSNP解析やde novoでの配列確定に使われているのが現状である。本分野として通常のサンガー法と次世代型シーケンサーの中間的な性能をもつRoche GS juniorを、またサンプル数が少ない場合にも数Gbのデータ取得が可能となるMiSeqを分

野内に導入し、数少ないサンプルにも対応できるようなシステムを構築した。また、このゲノム解析システムを利用することで、個別ゲノム解析だけでなく、メタゲノム解析を本年度は立ち上げることに成功し、本事業での支援を得て、インプラント歯周炎の原因菌の同定や、難治性顎骨骨髄炎の起炎菌の同定などを行なっている。

6）英文原著論文

1. Aoki A, Shibata Y, Okano S, Maruyama F, Amano A, Nakagawa I, Abiko Y. Transition metal ions induce carnosinase activity in PepD-homologous protein from Porphyromonas gingivalis. Microb Pathog. 52（1）：17-24.（2012）
2. Okada K, Roobthaisong A, Nakagawa I, Hamada S, Chantaroj S. Genotypic and PFGE/MLVA analyses of Vibrio cholerae O1：geographical spread and temporal changes during the 2007-2010 cholera outbreaks in Thailand. PLoS One. 7（1）：e30863.（2012）
3. Aikawa C,, Furukawa N, Watanabe T, Minegishi K, Furukawa A, Eishi Y, Oshima K, Kurokawa K, Hattori M, Nakano K, Maruyama F, Nakagawa I, Ooshima T. Complete Genome Sequence of the serotype k Streptococcus mutans LJ23. J Bacteriol. 194:2754.（2012）
4. Nozawa T, Aikawa C, Goda A, Maruyama F, Hamada S, Nakagawa I. The small GTPases Rab9A and Rab23 function at distinct steps in autophagy during Group A Streptococcus infection. Cell. Microbiol. 14（8）：1149-1165.（2012）
5. Ogawa M, Sugita S, Shimizu N, Watanabe K, Nakagawa I, Mochizuki M. Broad-range real-time PCR assay for detection of bacterial DNA in ocular smaples from infectious endophatalmitis. Jpn J Ophthalmol. 2012 Aug 31. In Press.
6. Jorquera M, Saavedra N, Maruyama F, Richardson A, Crowley D, Catrilaf R, Henriquez E, Mora M. Phytate addition to soil induces changes in the abundance and expression of Bacillus ß–propeller phytase genes in the rhizosphere. FEMS Microbiol. Ecol.（2013）In press
7. Minegishi K, Aikawa C, Furukawa A, Watanabe T, Nakano T, Ogura Y, Ohtubo Y,Kurokawa K, Hayashi T, Maruyama F, Nakagawa I, Eishi Y. Complete Genome Sequence of Propionibacterium acnes Isolate from sarcoidosis patient." J Bacteriol.（2013）in press.

7）平成24年度までの自己評価

平成22年5月より本GCOEに参加させていただき、高速シーケンサーを実稼働させた。多量の核酸サンプルを高精度に扱うスタッフの育成と、多量の情報処理を行うバイオインフォマティクスのウェットとドライ双方のスタッフの育成を行い、平成24年度では,細胞生物学的な解析や個別ゲノムだけでなく微生物全ゲノム解析を5株で終了し、そのうち2株については論文として発表することができた。現在解析を行っているものも5株あり引き続きその解析をおこなっていく。また、臨床系分野との共同でのメタゲノム解析も順調に解析が進み、現在2本の論文の投稿中、また3本を投稿準備中である。

8）学会発表（英文）

1. Paveenkittiporn W, Nozawa T, Dejsirilert S, Baggett K, Hamada S
   "Unique distribution of emm types and superantigen gene profiles of group A streptococci isolated in Thailand"
   15th International Congress on Infectious Diseases（ICID）, 2012年6月13日-16日,（タイ・バンコク）
2. Takayasu Watanabe, Nayuta Furukawa, Takashi Nozawa, Chihiro Aikawa, Bijaya Haobam, Akiko Endo, Fumito Maruyama, Ichiro Nakagawa
   "Elucidation of diversification mechanism of periodontogenic bacterium Porphyromonas gingivalis by analyzing genomic and diversity features"
   asm2012（アメリカ微生物学会総会）, 2012年6月16日-19日,（アメリカ・サンフランシスコ）
3. Chihiro Aikawa, Takashi Nozawa, Takayasu Watanabe, Akira Goda, Takashi Ode, Fumito Maruyama, Ichiro Nakagawa
   "Discovery of Streptococcus pyogenes genes contributing to evasion of autophagic degradation system"
   第11回あわじしま感染症・免疫フォーラム, 2012年9月11-14日, 淡路夢舞台国際会議場（兵庫県）
4. Takashi Nozawa, Chihiro Aikawa, Akira Goda, Fumito Maruyama, Ichiro Nakagawa
   "The small GTPases Rab9A and Rab23 function at distinct steps in autophagy during Group A Streptococcus infection"
   第11回あわじしま感染症・免疫フォーラム, 2012年9月11-14日, 淡路夢舞台国際会議場（兵庫県）

9）学会発表（和文）

1. 野澤孝志、細見晋吾、相川知宏、丸山史人、中川一路
   "ファージとその防御機構に着目したA群レンサ球菌ゲノムの種内多様性"
   第2回NGS現場の回研究会, 2012年5月23日-25日, ホテル阪急エキスポパーク（大阪府）
2. 渡辺孝康、遠藤亜希子、野澤孝志、相川知宏、丸山史人、中川一路
   "可動性遺伝因子による歯周病原性細菌の種内多様性

創出"
第6回細菌学若手コロッセウム, 2012年8月8日-10日, 八王子セミナーハウス（東京都）

3. 遠藤亜希子、渡辺孝康、細見晋吾、野澤孝志、相川知宏、荒川真一、梅田誠、丸山史人、中川一路、和泉雄一
"多株ゲノム解析により見えたTannerella forsythiaの生存戦略"
第54回歯科基礎医学会学術大会・総会, 2012年9月14-16日, 奥羽大学（福島県）
4. 渡辺孝康、野澤孝志、相川知宏、遠藤亜希子、丸山史人、中川一路
"可動性因子が生み出すPorphyromonas gingivalis種内多様性機構の解明"
第54回歯科基礎医学会学術大会・総会, 2012年9月14-16日, 奥羽大学（福島県）
5. 野澤孝志、相川知宏、郷田瑛、丸山史人、中川一路
"Rabタンパク質によるA群レンサ球菌感染誘導オートファジーの制御機構"
第54回歯科基礎医学会学術大会・総会, 2012年9月14-16日, 奥羽大学（福島県）
6. 細見晋吾、渡辺孝康、相川知宏、野澤孝志、丸山史人、中川一路
"ファージとその防御機構に着目したA群レンサ球菌ゲノムの多様化機構"
日本ゲノム微生物学会若手の会研究会, 2011年9月27-28日, ろうきん研修所富士センター（静岡県）
7. 遠藤亜希子、渡辺孝康、細見晋吾、野澤孝志、相川知宏、荒川真一、梅田誠、丸山史人、和泉雄一、中川一路
"比較ゲノム解析とCRISPR解析から見えたTannerella forsythiaの生存戦略"
日本ゲノム微生物学会若手の会研究会, 2011年9月27-28日, ろうきん研修所富士センター（静岡県）
8. 渡辺孝康、野澤孝志、相川知宏、遠藤亜希子、丸山史人、中川一路
"可動性因子が生み出すPorphyromonas gingivalis種内多様性機構の解明"
日本ゲノム微生物学会若手の会研究会, 2011年9月27-28日, ろうきん研修所富士センター（静岡県）
9. 遠藤亜希子、渡辺孝康、細見晋吾、野澤孝志、相川知宏、荒川真一、梅田誠、丸山史人、和泉雄一、中川一路
"全ゲノム解析と多株比較ゲノム解析により見えたTannerella forsythiaの生存戦略"
細菌学会関東支部会, 2012年10月10-12日, ホテル日航東京（東京）
10. 郷田瑛、細見晋吾、渡辺孝康、野澤孝志、相川知宏、丸山史人、道泰之、原田清、中川一路
"顎骨骨髄炎における細菌叢の高解像度解析"
細菌学会関東支部会, 2012年10月10-12日, ホテル日航東京（東京）
11. 遠藤亜希子、渡辺孝康、細見晋吾、相川知宏、野澤孝志、荒川真一、丸山史人、中川一路、和泉雄一
"多株比較ゲノム解析による歯周病原細菌Tannerella forsythiaの進化機構"
第86回日本細菌学会総会, 2013年3月18-20日, 幕張メッセ国際会議場（千葉県）
12. 郷田瑛、丸山史人、野澤孝志、相川知宏、渡辺孝康、中川一路
"顎骨骨髄炎の細菌叢を規定する因子とコア・マイクロバイオーム"
第86回日本細菌学会総会, 2013年3月18-20日, 幕張メッセ国際会議場（千葉県）
13. 渡辺孝康、野澤孝志、相川知宏、丸山史人、中川一路
"遺伝的組換えとCRISPRによる相反的な細菌種内多様性制御"
第86回日本細菌学会総会, 2013年3月18-20日, 幕張メッセ国際会議場（千葉県）
14. 相川知宏、野澤孝志、郷田瑛、丸山史人、中川一路
"オートファジー回避に関与するA群レンサ球菌遺伝子の同定"
第86回日本細菌学会総会, 2013年3月18-20日, 幕張メッセ国際会議場（千葉県）
15. 野澤孝志、相川知宏、郷田瑛、丸山史人、中川一路
"A群レンサ球菌によるオートファジーを制御するRabタンパク質群"
第86回日本細菌学会総会, 2013年3月18-20日, 幕張メッセ国際会議場（千葉県）
16. 丸山史人、渡辺孝康、相川知宏、野澤孝志、中川一路
"ファージとその防御機構に着目したA群レンサ球菌ゲノム多様化機構の解明"
第86回日本細菌学会総会, 2013年3月18-20日, 幕張メッセ国際会議場（千葉県）

10）外部資金の獲得状況

1. 最先端次世代研究開発支援プログラム
「病原性細菌のゲノム情報を応用した細菌感染特異的オートファジー誘導による感染防御法の開発」
中川一路 期間：平成22年―平成24年 研究費総額：13,500万円

2. 科学研究費補助金、基盤C 研究題目：高解像度細菌叢解析による口腔微生物環境の恒常性維持メカニズムの解明 代表：丸山史人 期間：平成22年―平成24年 研究費総額：500万円

11）主催学会

日本細菌学会若手の会、2012年8月9～11日、八王子セミナーハウス

12）教室、分野や講座の准教授、講師、助教、特別研究員、ポスドク、指導を受けた大学院生の名前

准教授　　丸山　史人
助教　　野澤　孝志（平成24年3月1日より）
日本学術振興会特別研究員：相川　知宏
大学院生　　渡辺　孝康（博士課程4年）
○ Bijaya Haobam（博士課程3年）
Amonrattana Roobthaisong
（博士課程2年）：平成23年9月入学(国費)
細見　晋吾（修士課程2年）

13）GCOE活動についての感想、コメント、改善を望む点

次世代型シーケンサーを用いた解析が、ようやく本分野内で完結できるようになった。これは、計算サーバーを5台導入できたことが非常に大きい。また、バイオインフォマティクスについても分野内での教育が順調に推移し、かなり高度な解析も可能となってきた。

Cellular Microbiology (2012) **14**(8), 1149–1165

doi:10.1111/j.1462-5822.2012.01792.x
First published online 17 April 2012

The small GTPases Rab9A and Rab23 function at distinct steps in autophagy during Group A Streptococcus infection

Takashi Nozawa,[1,2] Chihiro Aikawa,[1] Akira Goda,[1] Fumito Maruyama,[1] Shigeyuki Hamada[2] and Ichiro Nakagawa[1]*

[1]*Section of Bacterial Pathogenesis, Graduate School of Medical and Dental Sciences, Tokyo Medical and Dental University, 1-5-45, Yushima, Bunkyo-ku, Tokyo 113-8510, Japan.*

[2]*Thailand-Japan Research Collaboration Center on Emerging and Re-emerging Infections (RCC-ERI), Nonthaburi, Thailand.*

Summary

Autophagy mediates the degradation of cytoplasmic contents in the lysosome and plays a significant role in immunity. Here we identified the small GTPases Rab9A and Rab23 as novel autophagy regulators during Group A streptococcus (GAS) infection. Rab9A was recruited to GAS-containing autophagosome-like vacuoles (GcAVs) after autophagosomal maturation and its activity was required for GcAV enlargement and eventual lysosomal fusion. GcAV enlargement appeared to be related to homotypic fusion of GcAVs with Rab9A. Rab23 was recruited to GAS-capturing forming autophagosomes. Knockdown of Rab23 expression decreased both LC3- and Atg5-positive GAS formation and caused the accumulation of LC3-positive structures that did not associate with intracellular GAS. It was suggested, therefore, that Rab23 is required for GcAV formation and is involved in GAS targeting of autophagic vacuoles. Furthermore, knockdown of Rab9A or Rab23 expression impaired the degradation of intracellular GAS. Therefore, our data reveal that the Rab9A and Rab23 GTPases play crucial roles in autophagy of GAS. However, neither Rab9A nor Rab23 were localized to starvation-induced autophagosomes. Not only Rab9A but also Rab23 was dispensable for starvation-induced autophagosome formation. These findings demonstrate that specific Rab proteins function at distinct steps during autophagy in response to GAS infection.

Received 6 December, 2011; revised 2 March, 2012; accepted 15 March, 2012. *For correspondence. E-mail ichiro-n.bac@tmd.ac.jp; Tel. (+81) 3 5803 5455; Fax (+81) 3 5803 5455.

Introduction

Autophagy is a fundamental cellular homeostatic mechanism in which cytoplasmic constituents are engulfed by a characteristic double-membrane autophagosome, which eventually has its contents degraded in vacuoles or lysosomes. Autophagy was originally considered as a non-selective degradation system in response to starvation. But it is now clear that autophagy can selectively degrade substrates such as damaged mitochondria, excess peroxisomes, aggregated proteins or damaged endoplasmic reticulums. In addition to cytoplasmic organelles, invading pathogens such as *Salmonella enterica serovar typhimurium*, *Listeria monocytogenes*, *Shigella flexineri* and *Streptococcus pyogenes* also can be targets of autophagy in a selective manner (Levine *et al*., 2011). However, the precise membrane dynamics and the regulatory mechanisms involved are not fully understood.

The Rab guanosine triphosphatase (GTPase) family is a key regulator of intracellular membrane trafficking and several Rab proteins were reported to be involved in autophagy regulation (Chua *et al*., 2011). Rab1 is required for the biogenesis of the pre-autophagosomal isolation membrane (Huang *et al*., 2011), Rab5 is involved in autophagosome formation, while Rab7 facilitates the fusion of autophagosomes with lysosomes (Gutierrez *et al*., 2004; Jager *et al*., 2004; Ravikumar *et al*., 2008). Moreover, Rab24 is localized in autophagosomes and functions in the autophagic pathway (Munafo and Colombo, 2002), Rab33B interacts with Atg16L and modulates autophagosome formation (Itoh *et al*., 2008). However, most of this information is limited to starvation-induced autophagy and the role of other Rab proteins in autophagy in mammalian cells has not been explored.

Autophagy is now recognized as one of the key immune systems involved in bacterial infections in association with other immune functions such as inflammation and antigen presentation. We have previously demonstrated that intracellular *S. pyogenes* (Group A streptococcus; GAS) is

captured by LC3-positive autophagosome-like vacuoles and degraded upon fusion of these compartments with lysosomes in non-phagocytic cells (Nakagawa *et al.*, 2004). We found that the diameter of GAS-containing autophagosome-like vacuoles (GcAVs) can be as large as 10 μm compared with 0.5–1.0 μm for non-selective autophagosomes, and further demonstrated that Rab7 is required for GcAV formation (Sakurai *et al.*, 2010). Furthermore, GcAV enlargement is due to Rab7-dependent fusion of small isolation membranes (Yamaguchi *et al.*, 2009). However, Rab7 is not required for the formation of starvation-induced autophagosomes but is required for the autophagosome–lysosome fusion step. Together, these findings suggest that there are distinct and specific autophagy regulatory systems adapted for bacterial infection. We hypothesized that other Rab proteins also serve as regulators of antibacterial autophagy during GAS infection because GcAVs showed morphological differences compared with the canonical autophagosomes. In this study, we examined the GcAV localization of various Rab proteins and identified some Rab proteins that regulate GcAV biogenesis and maturation. Specifically, we show that Rab9A and Rab23 play important roles in the autophagic process during GAS infection.

Results

Rab9A and Rab23 are localized in GcAVs

In order to identify Rab proteins that are associated with autophagy during GAS infection, we expressed various EmGFP-fused Rab proteins and examined whether EmGFP-Rab proteins become localized in GcAVs of GAS-infected HeLa cells. To observe GcAVs, we coexpressed mCherry-fused LC3, a marker of autophagosomes. The colocalization of each Rab protein with GcAVs was assessed from 1 to 4 h after infection, the duration of GcAV formation process (Nakagawa *et al.*, 2004). As shown in Fig. 1, we observed that EmGFP-Rab9A and EmGFP-Rab23 efficiently associated with GcAVs. Interestingly, EmGFP-Rab5, -Rab24 and -Rab33B, that were reported to colocalize with starvation-induced autophagosomes, were not found in GcAVs at all time points we examined (Figs 1A and S1). Although Rab11, which is associated with recycling endosomes, is also involved in the fusion between autophagic vacuoles and multivesicular bodies in K562 cells and colocalizes with LC3 (Fader and Colombo, 2006; Fader *et al.*, 2008), EmGFP-Rab11 was also not associated with GcAVs (Figs 1A and S1). Colocalization of EmGFP-Rab5, Rab11, Rab24 and Rab33B with starvation-induced autophagosomes was also observed in our experiments (data not shown). EmGFP-Rab9A and -Rab23 were preferentially found on GcAVs at the late (3–4 h after infection) and the early stages (1–3 h after infection) respectively (Fig. 1B and C). Rab9A and Rab23 respectively were shown to regulate endosome to Golgi trafficking and endocytic pathways (Riederer *et al.*, 1994; Evans *et al.*, 2003). However, localization of these Rab proteins to LC3-positive vacuoles is a novel observation.

Forming autophagosomes contain Rab23 but not Rab9A

The process of GcAV formation can be divided into three stages: isolation membrane (forming autophagosomes), autophagosome and autolysosome formation. To identify the GcAV stage(s) that Rab9A and Rab23 are involved in, we used Atg5 and LAMP1. Atg5 is an isolation membrane marker and LAMP1 is a marker for lysosomal membranes. In our previous study, LC3 was shown to be a consistent marker for GcAVs (Nakagawa *et al.*, 2004). Atg5 was mainly localized in GAS-associated LC3-positive membrane structures that are not yet closed (Fig. S2A), and fully enclosed GcAVs did not contain Atg5 (Fig. S2B). We investigated the time-course of colocalization of GcAVs markers, LC3, Atg5 and LAMP1. Atg5-positive GcAVs were found only during the early phases of autophagy (Fig. S2C), whereas LAMP1-positive GcAVs increased with time and most of the GAS-containing LAMP1-positive membrane structures showed EmGFP-LC3 signals (Fig. S2D). These results also indicate that LC3 is a constant marker of GcAVs, Atg5-positive GcAVs are forming autophagosomes, and LAMP1-positive GcAVs are autolysosomes. In addition, the number of Atg5-associated GAS significantly increased in Atg4B C74A-overexpressing cells (Fig. S3A and B). Because overexpression of Atg4B C74A is known to cause defects in autophagosome closure (Fujita *et al.*, 2008), Atg5-positive membrane structures can be considered to be forming autophagosomes that are not fully closed. As shown in Fig. 2A, we could not observe EmGFP-Rab9A in Atg5-positive structures, suggesting that Rab9A did not localize to forming autophagosome of GcAVs. On the other hand, EmGFP-Rab23 colocalized with Atg5-positive ($Atg5^+$) GcAVs immediately after infection (Fig. 2B). Subsequently, EmGFP-Rab23 was also found in Atg5-negative ($Atg5^-$) GcAVs 3 h after infection (Fig. 2B), indicating that Rab23 resides not only in forming autophagosomes but also in autophagosomes of GcAVs. To confirm these findings, we examined the time-course of GcAV development. As shown (Fig. 2C), most of the GcAVs were Rab23-positive/Atg5-positive ($Rab23^+/Atg5^+$) 1 h after infection but this gradually decreased with time, whereas the rate of Rab23-positive/Atg5-negative ($Rab23^+/Atg5^-$) GcAVs increased. This result also indicated that Rab23

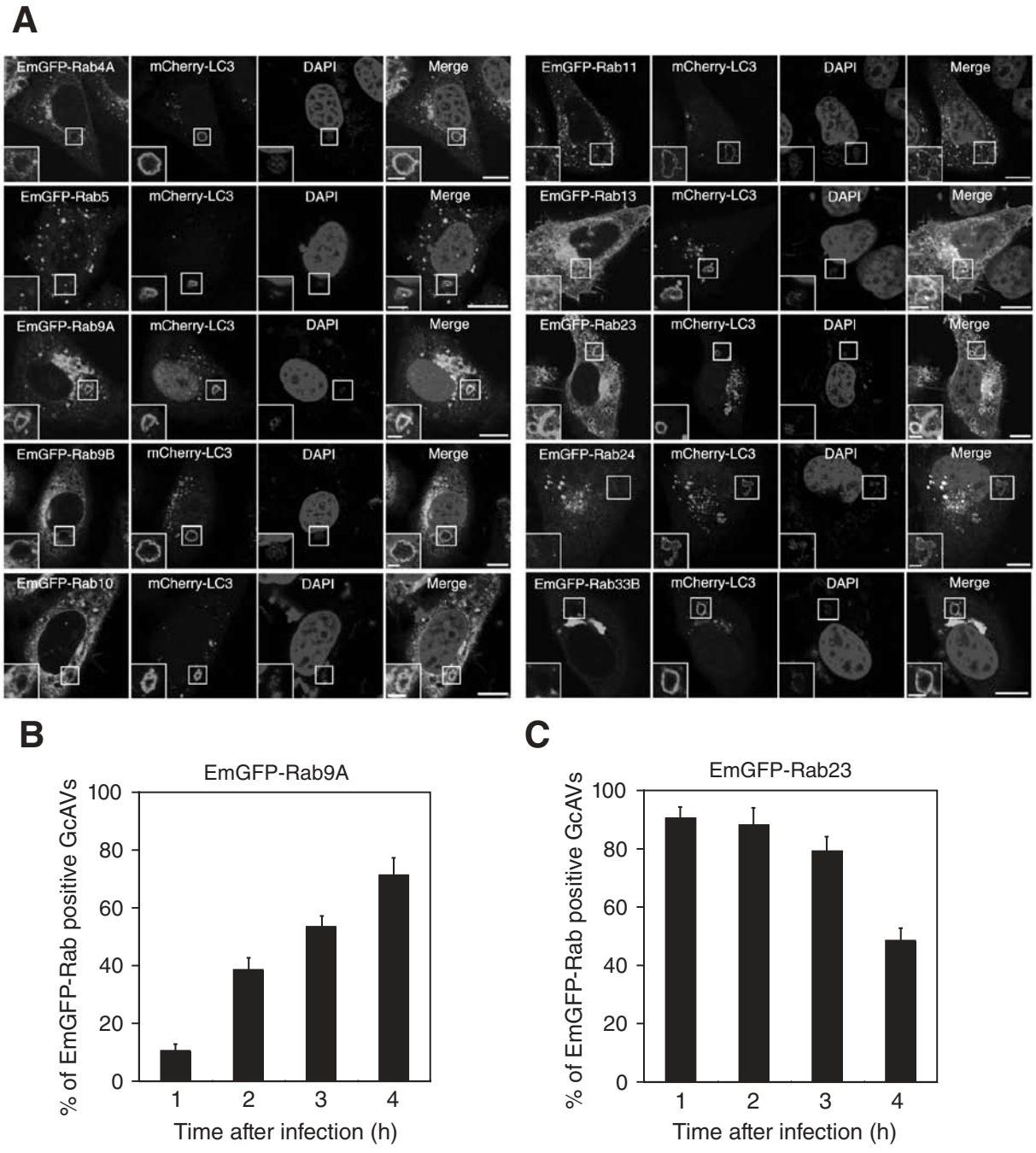

Fig. 1. Colocalization of LC3 and Rab proteins during GAS infection.
A. Confocal microscopic images of GAS (blue)-containing autophagic vacuoles (red) and Rab proteins (green). HeLa cells expressing mCherry-LC3 and EmGFP-Rab proteins (Rab4A, Rab5, Rab9A, Rab9B, Rab10, Rab11, Rab13, Rab23, Rab24, Rab33B) were infected with GAS for 3 h at an moi 100. After 1 h infection with GAS, infected cells were further incubated for 2 h with antibiotics to kill extracellular GAS. Cellular and bacterial DNA were stained with DAPI. Insets show higher magnification of the boxed areas. Bars, 10 μm for the main panel and 3 μm for the inset.
B and C. Colocalization efficiencies of Rab9A or Rab23 with GcAVs. HeLa cells expressing mCherry-LC3 and EmGFP-Rab9A or -Rab23 were incubated with GAS for the indicated times. Cells were then fixed with 4% PFA for 30 min. Colocalization efficiencies of GcAVs and EmGFP-Rab proteins were calculated as the percentage of total number of GcAVs. Data shown represent results of > 40 GcAVs and each percentage represents the mean value ± SD from three independent experiments.

 Cellular Microbiology, **14**, 1149–1165

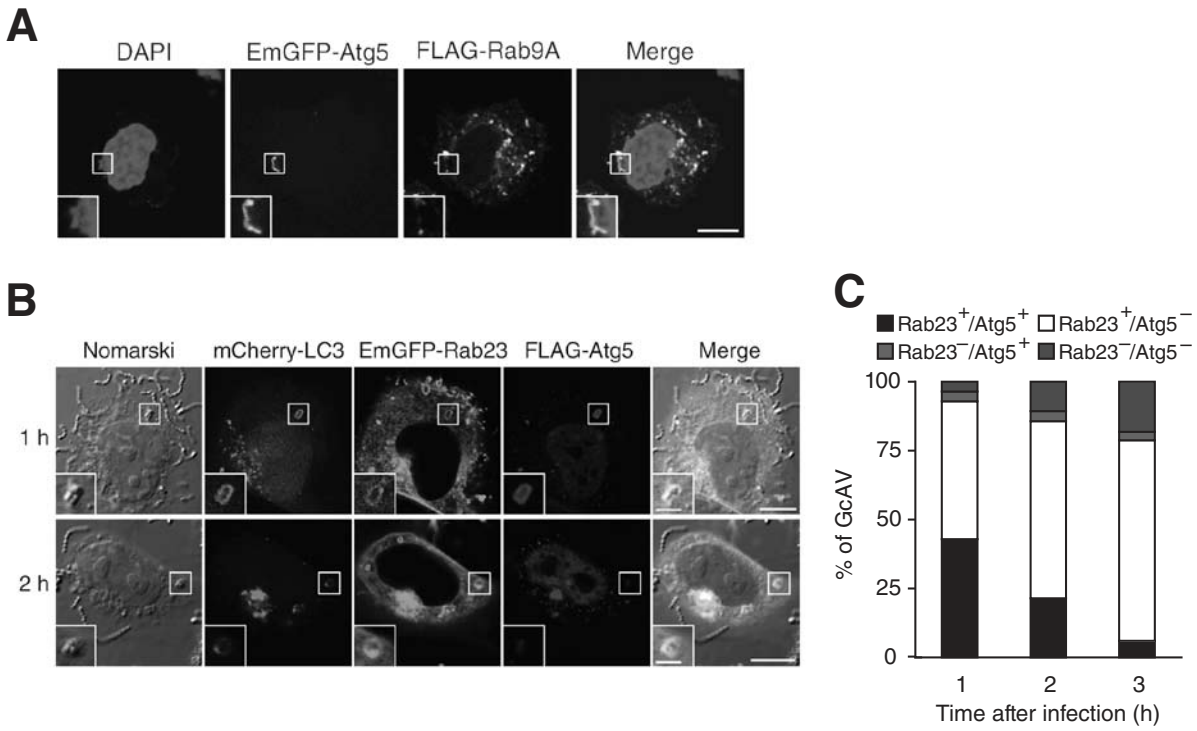

Fig. 2. Localization analysis of Rab9A and Rab23 with developing autophagosomes of GcAVs.
A. Confocal microscopic images of Atg5 (green)-positive GAS-capturing isolation membrane structures with Rab9A (gray). HeLa cells transiently expressing FLAG-Rab9A and EmGFP-Atg5, an isolation membrane marker, were infected with GAS at an moi 100. After infection for the indicated times, cells were fixed and DNA was stained with DAPI. Insets show higher magnification of the boxed areas. Bars, 10 μm for the main panel and 3 μm for the inset.
B. Confocal microscopic images of Atg5 (blue)-positive GcAVs (red) isolation membranes. HeLa cells expressing mCherry-LC3, EmGFP-Rab23 and FLAG-Atg5, an isolation membrane marker, were infected with GAS at a moi 100. After infection for the indicated times, cells were fixed and DNA was stained with DAPI. Insets show higher magnification of the boxed areas. Bars, 10 μm for the main panel and 3 μm for the inset.
C. Time-course of colocalization efficiencies of GcAVs with Atg5 and Rab23. Colocalization efficiencies of GcAVs with Rab23 and Atg5 were determined by confocal microscopic images as in (B). Rab23- and Atg5-positive GcAVs are shown in black, Rab23-positive and Atg5-negative GcAVs in white, Rab23-negative and Atg5-positive GcAVs in grey and Rab23- and Atg5-negative GcAVs in red. Data shown represent the results for > 50 GcAVs.

could localize to both forming autophagosomes and autophagosomes.

Matured autophagosomes and autolysosomes contain both Rab9A and Rab23

Because EmGFP-Rab9A was not found in Atg5-positive membrane structures, Rab9A is suggested to be a constituent of autophagosomes or autolysosomes. We next examined the time-course of EmGFP-Rab9A and LAMP1 colocalizations with GcAVs. EmGFP-Rab9A clearly colocalized with both LAMP1-negative and -positive GcAVs at 3 h (Fig. 3A and B), suggesting that Rab9A could localize with both autophagosomes and autolysosomes. These results are consistent with the results of Fig. 1B, demonstrating that Rab9A is found in GcAVs at a later stage of autophagy.

To follow the fate of Rab23 in autophagosomes of GcAVs, we examined the colocalization of EmGFP-Rab23 with mCherry-LC3 and LAMP1. At 2 h, the majority of GcAVs were Rab23-positive/LAMP1-negative (Rab23$^+$/LAMP1$^-$) and Rab23-positive/LAMP1-positive (Rab23$^+$/LAMP1$^+$) at 3 h (Fig. 3C and D). After that, Rab23-negative/LAMP1-positive (Rab23$^-$/LAMP1$^+$) GcAVs were increasingly detected (Fig. 3C and D). These results suggested that Rab23 is localized in autolysosomes as well as to autophagosomes and Rab23 disappeared from GcAVs during the later stages of autophagy.

Rab23 is required for GcAV formation

To clarify the roles of Rab9A and Rab23 in autophagy of GAS, we investigated the effects of knockdown of Rab9A and Rab23 expression on autophagy. To this end, we

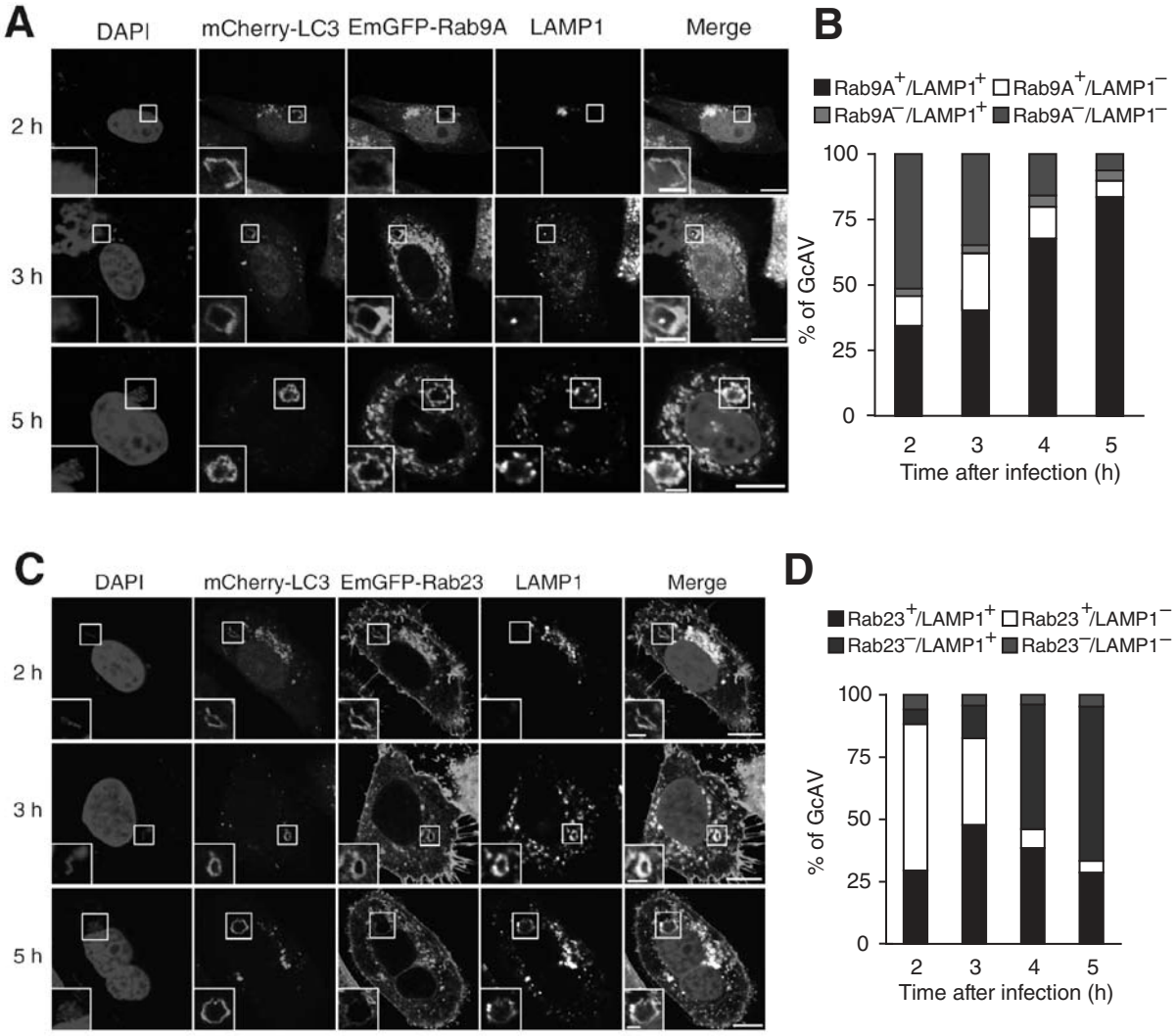

Fig. 3. Localization analysis of Rab9A and Rab23 in mature GcAVs.
A. Confocal microscopic images of GcAVs (red) associated with Rab9A (green) and lysosomes (gray). HeLa cells expressing mCherry-LC3 and EmGFP-Rab9A were infected with GAS at a moi 100. After infection for the indicated times, cells were fixed and stained with an antibody to LAMP1. Cellular and bacterial DNA were stained with DAPI. Insets show higher magnification of the boxed areas. Bars, 10 μm for the main panel and 3 μm for the inset.
B. Time-course of colocalization efficiencies of GcAVs with Rab9A and LAMP1. Colocalization efficiencies of GcAVs with Rab9A and LAMP1 were determined by confocal microscopic images as in A. Rab9A- and LAMP1-positive GcAVs are shown in black, Rab9A-positive and LAMP1-negative GcAVs in white, Rab9A-negative and LAMP1-positive GcAVs in grey and Rab9A- and LAMP1-negative GcAVs in red. Data shown represent the results for > 50 GcAVs.
C. Confocal microscopic images of LAMP1 (gray)-positive GcAVs (red) autolysosomes, with Rab23. HeLa cells expressing mCherry-LC3 and EmGFP-Rab23 were infected with GAS at a moi 100. After infection for the indicated times, cells were fixed and stained with anti-LAMP1 antibodies. Cellular and bacterial DNA were stained with DAPI. Insets show higher magnification of the boxed areas. Bars, 10 μm for the main panel and 3 μm for the inset.
D. Time-course of colocalization efficiencies of GcAVs with Rab23 and LAMP1. Colocalization efficiencies of GcAVs with Rab23 and LAMP1 were determined by confocal microscopic images as in (C). Rab23- and LAMP1-positive GcAVs are shown in black, Rab23-positive and LAMP1-negative GcAVs in white, Rab23-negative and LAMP1-positive GcAVs in grey and Rab23- and LAMP1-negative GcAVs in red. Data shown represent the results for > 50 GcAVs.

 Cellular Microbiology, **14**, 1149–1165

Fig. 4. Rab23 is required for GcAV formation.
A. Effects of knockdown of Rab9A and Rab23 expression. HeLa cells were transfected with FLAG-Rab9A or Rab23 expression vectors and miR vectors for the control, Rab9A and Rab23 respectively. After 48 h of transfection, expression of Rab9A and Rab23 was analysed by Western blotting using anti-FLAG antibodies.
B. Knockdown of Rab9A and Rab23 expression did not affect the invasion of GAS. HeLa cells transfected with each miR-knockdown vectors were infected with GAS at a moi 100. After 1 h of infection, cells were washed with PBS and further incubated for 1 h with DMEM/10% FCS with antibiotics to kill the extracellular bacteria. Cells were disrupted with distilled water and serial dilutions of cellular extracts were plated on THY agar plates. Efficiencies of GAS invasion are presented as the ratio of 'intracellular live GAS after 1 h incubation with antibiotics-containing medium' to 'intracellular and adherent GAS at 1 h'.
C. Confocal microscopic images of GcAVs (green) in Rab9A- or Rab23-knockdown cells. HeLa cells transfected with EmGFP-LC3 and miR-knockdown vectors for the control, Rab9A or Rab23 were infected with GAS at a moi 100 and fixed at 4 h. Cellular and bacterial DNA were stained with DAPI. Arrowheads indicate GcAVs. Bars, 10 μm.
D. Effect of Rab9A- and Rab23-knockdown on GcAV formation efficiency. Cells were transfected and infected as described in (C). The rate of GcAV-positive cell formation was calculated as the ratio of GcAV-positive cells to GAS-infected cells from confocal microscopic images. Data shown represent the results for > 200 infected cells and each percentage represents the mean ± SD from three independent experiments. $^{**}P < 0.01$.
E. Overexpression of Rab23 WT, Rab23 Q68L and Rab23 S23N did not affect the invasion of GAS. HeLa cells expressing FLAG-Rab23, FLAG-Rab23 Q68L or FLAG-Rab23 S23N were infected with GAS and the efficiency of GAS invasion was determined as described in (B).
F. GcAV formation requires Rab23 GTPase activity. HeLa cells expressing FLAG-Rab23 WT, FLAG-Rab23 Q68L or FLAG-Rab23 S23N were infected and fixed as described in (C). GcAV formation efficiency was calculated as described in (D).

used a miR-RNAi system to knockdown Rab protein expression in HeLa cells. The effects of knockdown were confirmed by Western blotting (Fig. 4A). Knockdown of Rab9A did not affect Rab9B levels (Fig. S4). We first examined the effects of Rab9A- and Rab23-knockdown on GAS invasion. The number of invaded GAS was not altered by knockdown of Rab9A and Rab23 expression (Fig. 4B). Next, to determine whether Rab9A and Rab23 are required for GcAV formation, HeLa cells expressing EmGFP-LC3 were transfected with either Rab protein knockdown vector and were infected with GAS. As shown in Fig. 4C and D, the efficiency of formation of GcAV-harbouring cells was not affected by knockdown of Rab9A expression. On the other hand, it was reduced more than 50% by knockdown of Rab23 expression (Fig. 4C and D). These results implied that Rab23, but not Rab9A, is involved in GcAV formation. However, recent studies suggested that the LC3 recruitment system is independent of the isolation membrane formation system (Kageyama *et al*., 2011). There is a possibility, therefore, that Rab23-knockdown attenuated the recruitment of LC3 to GAS-associated forming autophagosomes. We then examined the effects of Rab23-knockdown on the formation of autophagosomes (Atg5-positive membrane structures). The number of Atg5-associated GAS also decreased following knockdown of Rab23 expression (Fig. S5A and B), indicating that Rab23-knockdown inhibited GcAV formation. Furthermore, to determine whether the impairment of GcAV formation by Rab23-knockdown resulted from the loss of the GTP-bound form of Rab23, we used Rab23 Q68L or Rab23 S23N that are constitutively GTP or GDP bound forms. These act in a dominant-active or dominant-negative manner respectively. Overexpression of Rab23 wild-type (WT), Rab23 Q68L or Rab23 S23N did not affect GAS invasion (Fig. 4E). Overexpression of Rab23 WT or Rab23 Q68L did not substantially affect GcAV formation, whereas that of Rab23 S23N significantly diminished GcAV formation efficiency (Figs 4F and S6). These results demonstrated that GcAV formation requires Rab23 GTPase activity. To further confirm this finding, we transfected purified Rab23 WT into Rab23-knockdown cells. Protein transfection of Rab23 WT increased the rate of GcAV-harbouring cells, indicating that Rab23-knockdown was rescued by transfected Rab23 protein (Fig. S7).

Although only a few GcAVs were observed in Rab23-knockdown cells and Rab23 S23N-expressing cells, these Rab23-non-functional cells harboured multiple LC3-positive dots (Figs 4C and S6). We compared the number of LC3-positive dots in the control and Rab23A-knockdown cells. As shown in Fig. 5A and B, although only a few LC3-positive dots were observed in control and Rab23-knockdown cells under non-infection conditions, GAS infection increased LC3-positive dots and the number in Rab23-knockdown cells was significantly higher than that in control cells. It was therefore demonstrated that LC3-positive dot formation was induced by GAS infection and these LC3-positive structures that do not associate with intracellular GAS accumulated in Rab23-knockdown cells. Moreover, a portion of these LC3-positive dots colocalized with Atg5 (Fig. 5B). Taken together, these observations suggested that Rab23 is involved in delivering LC3-positive structures around GAS for GAS-capturing autophagosomes formation.

To confirm the induction of LC3-positive structures in Rab23-knockdown cells during GAS infection, we examined the accumulation of lipid-conjugated forms of LC3 (LC3-II) with bafilomycin A1 (Baf A1). Because bafilomycin A1 blocks autophagosomes–lysosome fusion and inhibits LC3-II degradation, differences in LC3-II levels in response to particular component knockdowns in the presence or absence of bafilomycin A1 reflect changes in autophagic vacuole formation or degradation (Mizushima

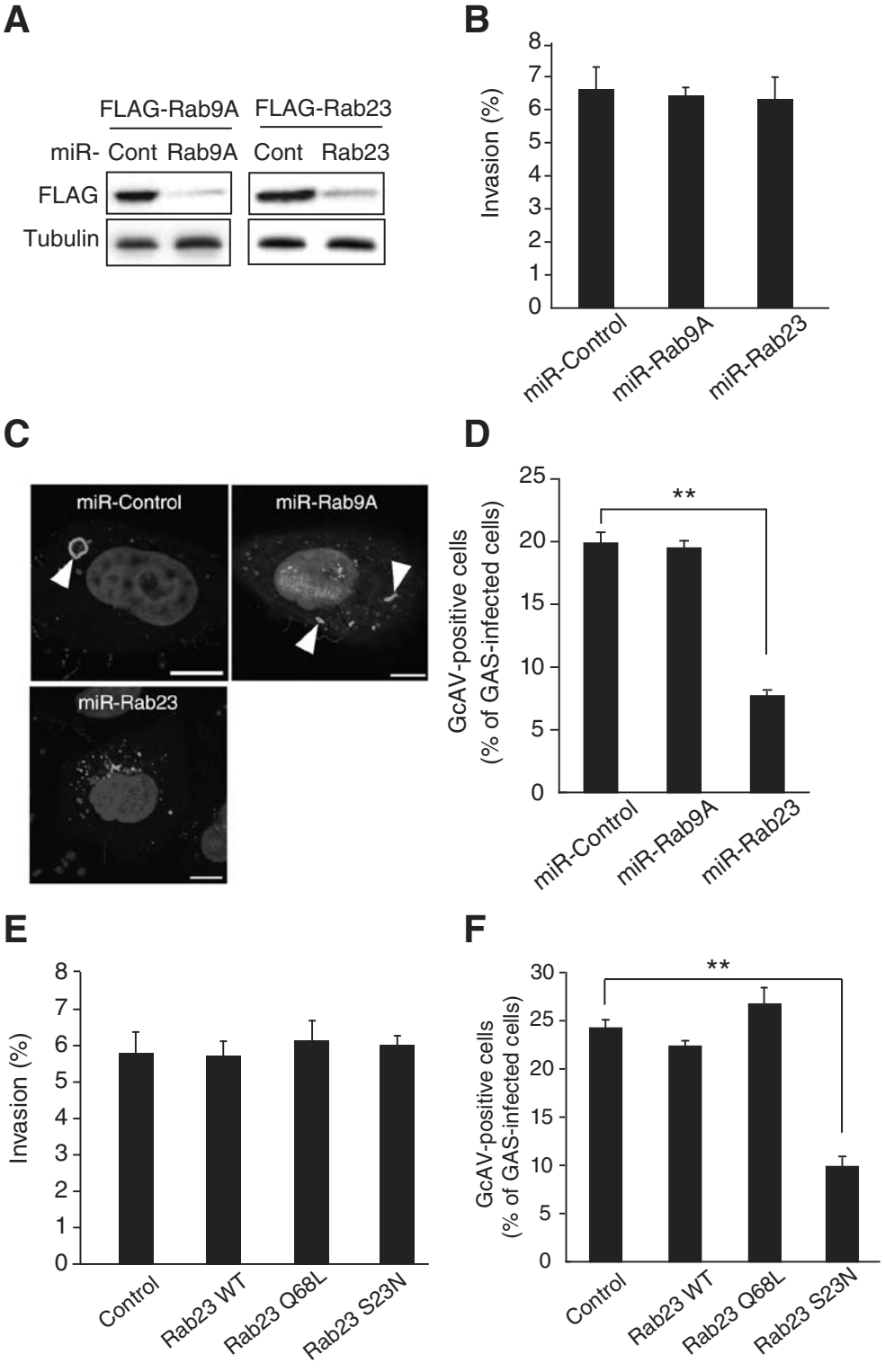

 Cellular Microbiology, **14**, 1149–1165

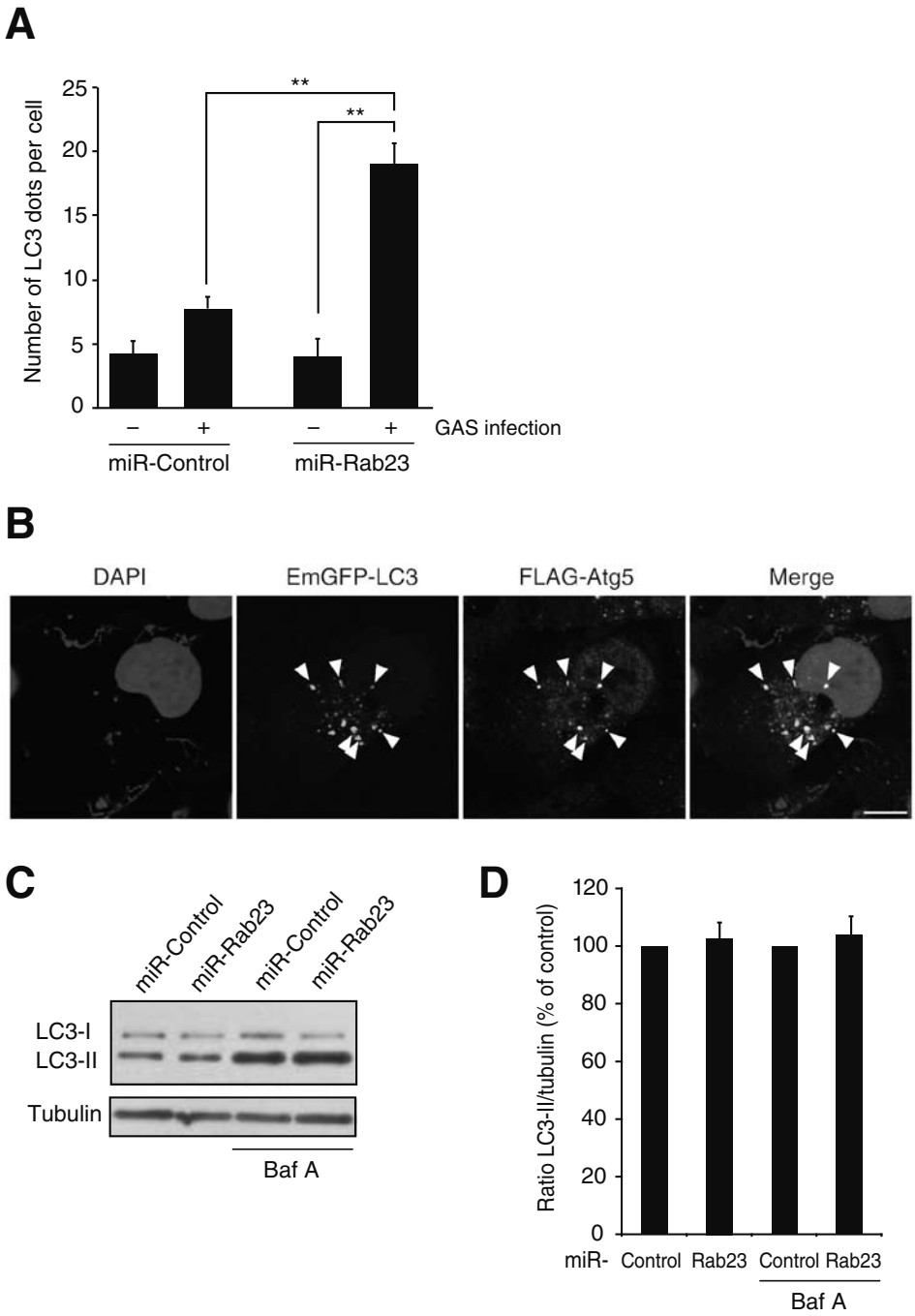

Fig. 5. GAS infection causes LC3-positive structure accumulation in Rab23-knockdown cells.
A. Quantification of LC3-positive dots in GAS-infected Rab23-knockdown cells. HeLa cells transfected with miR-knockdown vectors as controls or Rab23 were infected with GAS for 2 h. The number of LC3 dots was quantified from the confocal microscopic images using ImageJ software. Data shown represent the results for > 30 GcAVs and each percentage represents the mean value ± SD from three independent experiments.
B. Confocal microscopic images of LC3-positive structures in GAS-infected Rab23-knockdown cells. HeLa cells transfected with EmGFP-LC3, FLAG-Atg5 and the miR-knockdown vector for Rab23 were infected with GAS at a moi 100 for 2 h. After fixation, cellular and bacterial DNA were stained with DAPI. Bars, 10 μm.
C. HeLa cells transfected with miR-control or miR-Rab23 were infected with GAS at a moi 100 for 3 h with bafilomycin A1 (Baf A1) or DMSO.
D. Means ± SD of the percentage of LC3-II/tubulin ratio from three independent experiments are shown.

 Cellular Microbiology, **14**, 1149–1165

et al., 2010). Knockdown of Rab23 did not change LC3-II levels in the presence or absence of Baf A1 (Fig. 5C and D), suggesting that Rab23 is not involved in LC3-positive structure formation in GAS infected cells. Therefore, it was shown that Rab23 is not involved in the induction of LC3-positive structure formation but is essential for directing developing autophagosomes to GAS.

Rab9A regulates GcAV enlargement and lysosomal fusion

Although the number of GcAV-harbouring cells was not changed by Rab9A-knockdown, GcAVs found in Rab9A-knockdown cells appeared to be smaller than those in control cells (Fig. 4C). Therefore, we hypothesized that Rab9A is involved in the enlargement of GcAVs for more efficient elimination of invading GAS. To test this, we measured the areas of GcAVs observed in control and Rab9A-knockdown cells at 4 h after infection, and compared the sizes of GcAVs in each cell. We found that the average size of GcAVs observed in Rab9A-knockdown cells was significantly smaller than that of control cells (Fig. 6A and B). Additionally, GcAVs found in Rab9A wild-type or Rab9A Q66L (constitutive active form)-overexpressing cells were larger than that in control cells (Fig. 6A and B). Overexpression of Rab9A S21N (constitutive negative form) also inhibited the enlargement of GcAVs. These results indicated that Rab9A GTPase activity is involved in GcAV enlargement.

It was reported that Rab7 facilitates homotypic fusion of GcAVs to form larger structures. In order to examine whether Rab9A also promotes the fusion between GcAVs, we counted the number of GcAVs per cell in control or Rab9A-knockdown cells. Knockdown of Rab9A expression increased the number of GcAVs (Fig. 6C), suggesting that Rab9A is involved in the homotypic fusion of small GcAVs.

We next tested the effects of the knockdown of Rab9A expression on the lysosomal fusion of GcAVs. More than 80% of GcAVs in control cells clearly merged with LAMP1 at 4 h, whereas LAMP-positive GcAVs decreased to less than 40% in Rab9A-knockdown cells (Fig. 6D and E). These results indicate that Rab9A is involved not only in the GcAV enlargement through the fusion between small GcAVs but also in the lysosomal fusion of GcAVs.

Rab9A and Rab23 are involved in the elimination of intracellular GAS by autophagy

To further examine the involvement of Rab9A and Rab23 in autophagy during GAS infection, we examined the effects of Rab9A- and Rab23-knockdown on the killing of GAS by autophagy. HeLa cells transfected with each knockdown vector were infected with GAS and the number of surviving intracellular GAS was counted using a colony forming assay. In control cells, the rate of survival of GAS rapidly decreased with time (Fig. 7A), which is consistent with previous reports. However, the decrease in the GAS survival rate was suppressed by Rab9A-knockdown and almost completely suppressed by Rab23-knockdown (Fig. 7A). These results indicated that the elimination of intracellular surviving GAS was inhibited by knockdown of Rab9A or Rab23. Autophagy degrades the substrates using lysosomal components. To examine whether the suppression of GAS elimination is due to the impairment of autophagy, we utilized lysosomal protease inhibitors. As shown in Fig. 7B, decreases in GAS survival rates were not observed following treatment with lysosomal protease inhibitors (E64d and leupeptin), suggesting that the killing of GAS was caused by autophagy. Taken together, these results establish the functional requirements for Rab9A and Rab23 in the degradation of GAS by autophagy.

Rab9A and Rab23 are not required for starvation-induced autophagosome formation

To examine whether Rab9A and Rab23 are also involved in starvation-induced autophagy, we examined colocalization of EmGFP-Rab9A and EmGFP-Rab23 with autophagosomes under starvation conditions. Both EmGFP-Rab9A and EmGFP-Rab23 did not show efficient colocalization with autophagosomes (Fig. 8A). Nishida *et al*. (2009) previously reported that Rab9A is not involved in starvation-induced autophagy. We then determined whether Rab23 is required for autophagosome formation under starvation conditions. As shown (Fig. 8B), similar numbers of autophagosomes were observed in both control and Rab23-knockdown cells. Moreover, we examined starvation-induced autophagosome formation by studying LC3-II accumulation on Western blots. Knockdown of Rab23 showed no significant effects on LC3-II level in the presence or absence of Baf A1, indicating that Rab23 is also dispensable for starvation-induced autophagosome formation and subsequent processes.

Discussion

In this study we identified Rab9A and Rab23 as specific regulators of autophagy during GAS infection. In contrast, Rab5, Rab11, Rab24 and Rab33B, which are involved in starvation-induced autophagy, did not show localization in infected GcAVs. Previous reports demonstrated that functioning of Rab7 in an early step of autophagy is also specific to autophagy during GAS infection (Yamaguchi *et al*., 2009). Therefore, it has been established that although antibacterial autophagy (xenophagy)

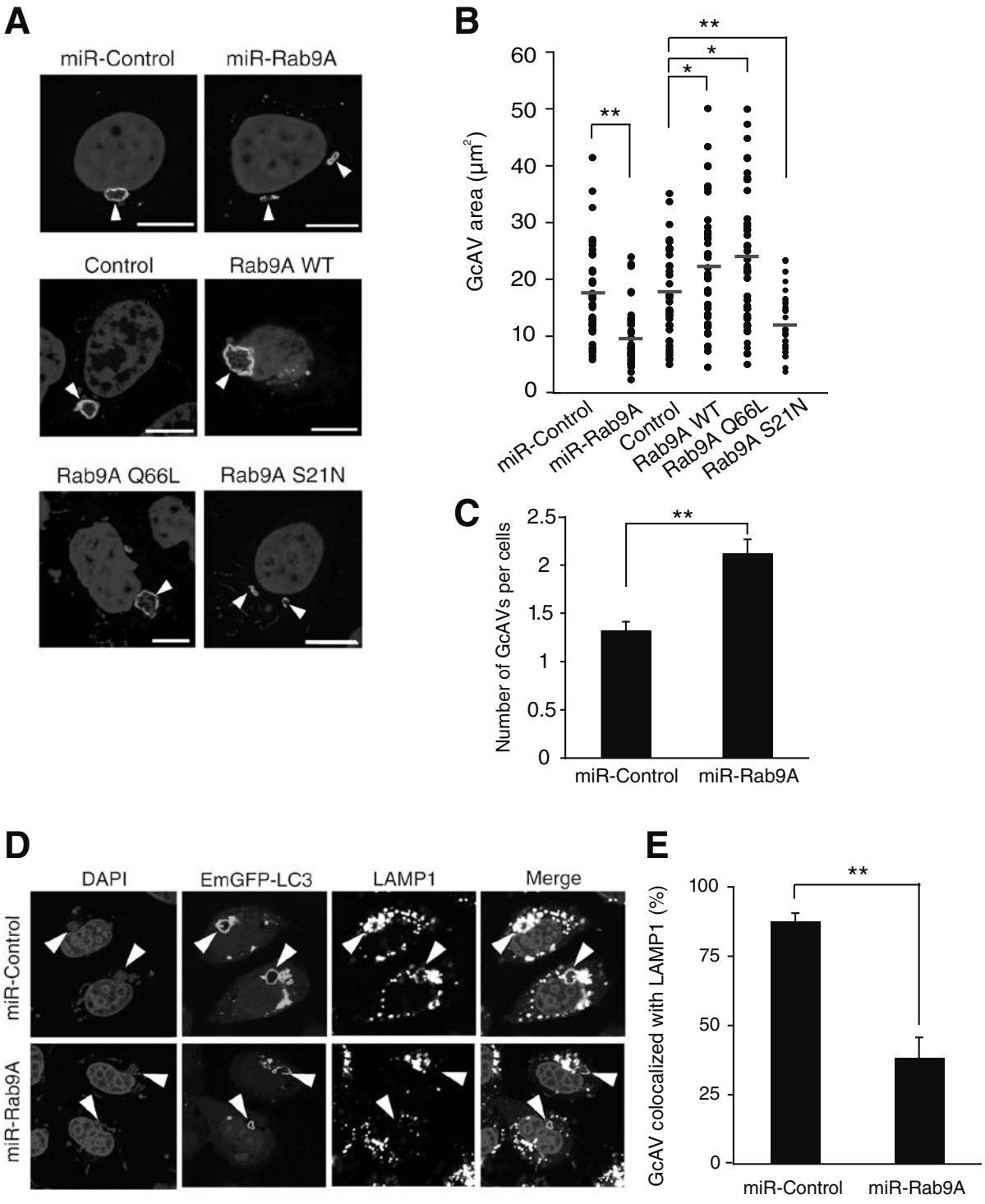
A
miR-Control
miR-Rab9A
Control
Rab9A WT
Rab9A Q66L
Rab9A S21N
B
GcAV area (μm²)
60
50
40
30
20
10
0
**
*
*
**
miR-Control
miR-Rab9A
Control
Rab9A WT
Rab9A Q66L
Rab9A S21N
C
Number of GcAVs per cells
2.5
2
1.5
1
0.5
0
**
miR-Control
miR-Rab9A
D
DAPI
EmGFP-LC3
LAMP1
Merge
miR-Control
miR-Rab9A
E
GcAV colocalized with LAMP1 (%)
100
75
50
25
0
**
miR-Control
miR-Rab9A

Fig. 6. Rab9A is involved in the enlargement of GcAVs and lysosomal fusion.
A. Confocal microscopic images of GcAVs (green) in Rab9A-knockdown or -overexpression cells. HeLa cells transfected with EmGFP-LC3, Rab9A WT, Rab9A Q66L, Rab9A S21N or miR-knockdown vectors as well as Rab9A or expression vectors as controls were infected with GAS at a moi 100 and fixed at 5 h after infection. Cellular and bacterial DNA were stained with DAPI. Arrowheads indicate the GcAVs. Bars, 10 μm.
B. The size of the GcAVs affected by Rab9A activity. HeLa cells were transfected and infected as in (A). The GcAV areas were measured by Image-J software. $n = 40$ GcAVs. Red lines indicate means. $^{*}P < 0.05$. $^{**}P < 0.01$.
C. Quantification of total number of GcAVs per cell in control or Rab9A-knockdown cells. HeLa cells were transfected and infected as in (A). Data shown represent the results for > 50 GcAV-harbouring cells and each percentage represents the mean ± SD from three independent experiments. $^{**}P < 0.01$.
D. Confocal microscopic images of GcAVs (green) with LAMP1 (gray) in Rab9A-knockdown cells. HeLa cells transfected with EmGFP-LC3 and miR-knockdown vectors as well as Rab9A as a control were infected with GAS at a moi 100 and fixed at 4 h after infection. Cellular and bacterial DNA were stained with DAPI. Arrowheads indicate the GcAVs. Bars, 10 μm.
E. Lysosomal fusion of GcAVs requires Rab9A. Cells were transfected and infected as described in (D). The rate of LAMP1-positive GcAV formation was calculated as the ratio of LAMP1-positive GcAVs to total GcAVs from confocal microscopic images. Data shown represent the results for > 50 GcAVs and each percentage represents the mean ± SD from three independent experiments. $^{**}P < 0.01$.

has common fundamental mechanisms with starvation-induced autophagy, e.g. dependence on Atg5 and involvement of SNARE proteins (Furuta *et al.*, 2010), the regulatory Rab proteins involved in antibacterial autophagy are largely distinct from those playing a role in starvation-induced autophagy. In addition, this difference in Rab proteins may be responsible for the morphologic and functional differences observed for antibacterial and starvation-induced autophagy.

One of the key differences between antibacterial autophagy and starvation-induced autophagy is the specificity of the process, and it is likely that some GAS-recognition molecules are involved in this distinction. Moreover, our present results indicate the possibility that Rab23 is involved in this recognition step. Rab23 is recruited to developing autophagosomes of GcAVs and knockdown of Rab23 decreased the number of Atg5-associated GAS and GcAVs, suggesting that Rab23 is required for GcAV formation. However, knockdown of Rab23 did not changed LC3-II levels, and a large number of LC3-positive structures that did not associate with GAS were observed in Rab23-knockdown or Rab23 S23N-overexpressing cells in response to GAS infection. In addition, these LC3-positive dots colocalized with Atg5. Therefore, we postulate that Rab23 is involved in the interaction between GcAV precursor-like structures, which are likely forming autophagosomes, and intracellular GAS (Fig. 9). This scenario is similar to what we have recently found with GcAV formation influenced by Rab7. It may be worth studying the interdependence between Rab7 and Rab23. Because of this potential role in autophagy during GAS infection, Rab23 may not be necessary for starvation-induced autophagy. Rab23 has been well described as a negative regulator of the signalling of Sonic hedgehog, a secreted morphogen that controls the development of multiple organs during embryogenesis (Evans *et al.*, 2003; 2005; Eggenschwiler *et al.*, 2006; Wang *et al.*, 2006; Huang *et al.*, 2009). Although Rab23 was considered to play a major role in embryogenesis, it was also found to be expressed in multiple adult tissues (Guo *et al.*, 2006; Wang *et al.*, 2006), implying that Rab23 has postnatal functions in various cells. Indeed, Rab23 was reported to play a role in the development of focal segmental glomerulosclerosis (Huang *et al.*, 2009).

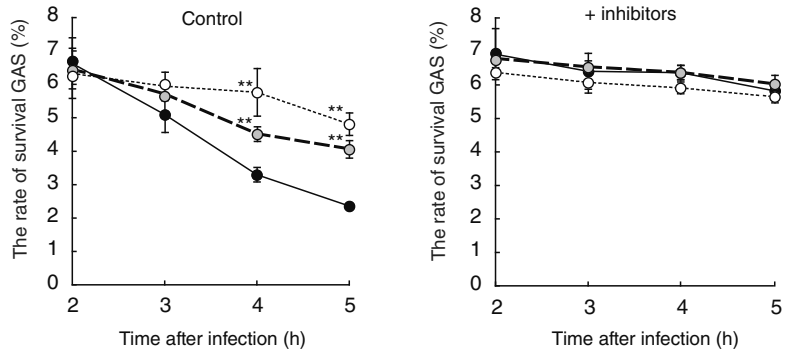

Fig. 7. Rab9A and Rab23 are involved in the elimination of intracellular GAS by autophagy. HeLa cells were transfected with miR-knockdown vectors (black circle/black line), or Rab9A (gray circle/dashed line), Rab23 (open circle/dotted line) as the controls. After 48 h of transfection, HeLa cells were infected with GAS for 1 h with or without lysosomal enzyme inhibitors (10 μM E64d and 1 mg ml^{-1} leupeptin). The number of intracellular surviving GAS was determined by a bacterial viability assay and presented as the ratio of 'intracellular live GAS at the indicated time' to 'intracellular and adherent GAS at 1 h'. Data shown as the mean ± SE from three independent experiments. $^{**}P < 0.01$.

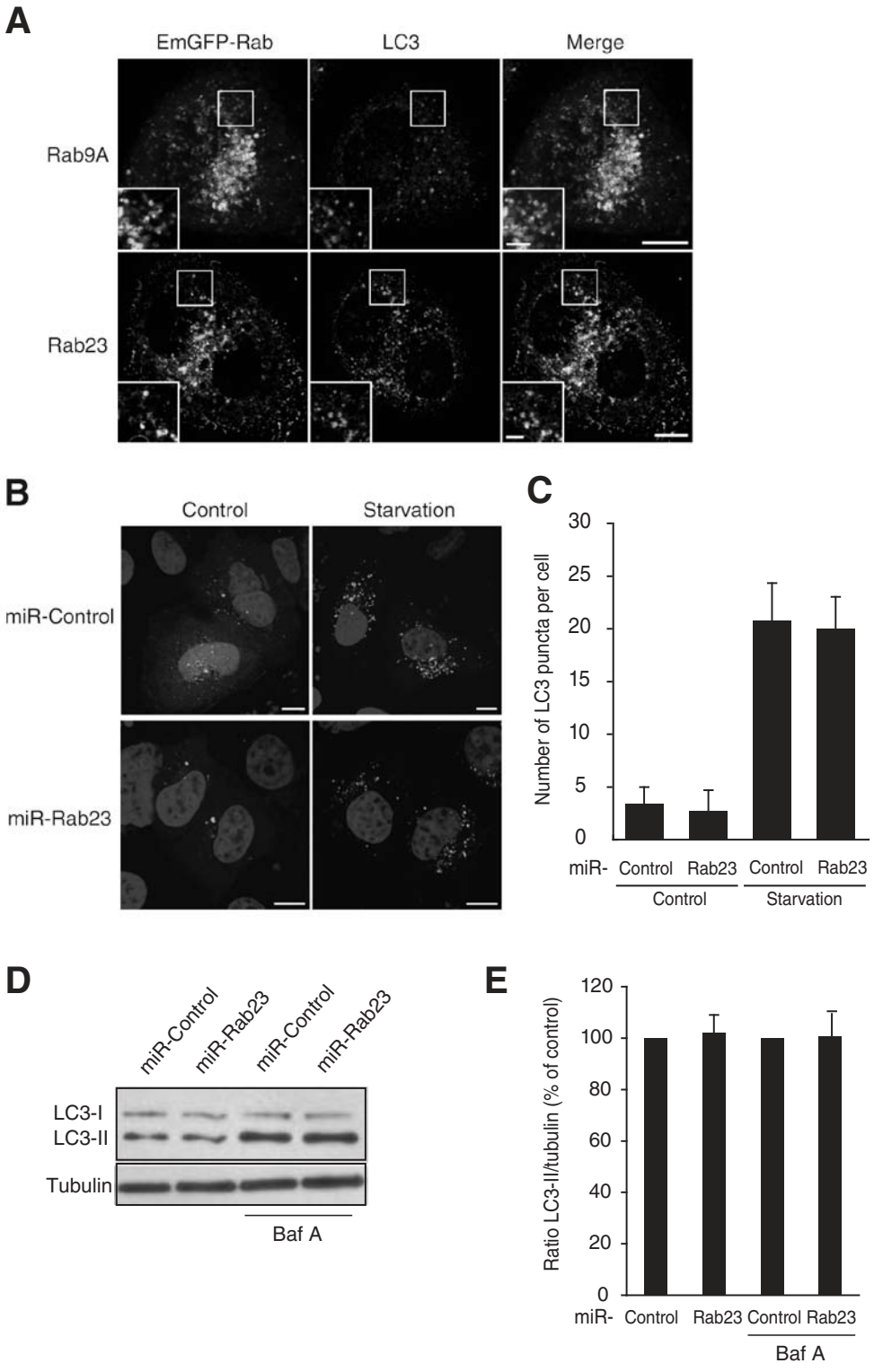

Fig. 8. Rab23 is not necessary for starvation-induced autophagy.
A. HeLa cells expressing EmGFP-Rab9A or Rab23 (cyan) were incubated in HBSS for 2 h to induce starvation-induced autophagosome formation. Cells were stained with an antibody to LC3 (magenta). Insets show higher magnification of the boxed areas. Bars, 10 μm for the main panel and 3 μm for the inset.
B. Confocal microscopic images of autophagosomes (green) in the control or Rab23-knockdown cells. HeLa cells expressing EmGFP-LC3 were transfected with miR-knockdown vectors or Rab23 as a control and incubated in DMEM (control) or HBSS (starvation conditions) for 2 h.
C. The number of starvation-induced autophagosomes is independent of Rab23. The number of autophagosomes per cells was quantified from confocal microscopic images using ImageJ software. $n = 20$ cells. $^{**}P < 0.01$.
D. HeLa cells transfected with miR-control or miR-Rab23 were infected under starvation condition with bafilomycin A1 (Baf A1) or DMSO.
E. Means ± SD of the percentage of LC3-II/tubulin ratio from three independent experiments are shown.

Moreover, Rab23 is also suggested to be involved in phagosome–lysosome fusion (Smith *et al*., 2007). In this study, although we demonstrated that Rab23 plays a role in an early step in autophagy, Rab23 may also be involved in the later stages of autophagy. Rab GTPase proteins interact with their specific effectors and these effectors also specifically function at each step (Stenmark, 2009). However, only a few effectors of Rab23 have been identified up to now (Wang *et al*., 2006). Thus, it would be interesting to identify the effector(s) of Rab23 to understand the role(s) of Rab23 in various cells.

The other characteristic of GcAVs distinct from the cells involved in starvation-induced autophagy is their relatively large size. Previous reports showed that this enlargement of GcAVs is caused by fusion of isolation membranes through Rab7 (Yamaguchi *et al*., 2009). In this study, we demonstrated that Rab9A is also involved in the enlargement of GcAVs probably through the fusion between small GcAVs and GcAV expansion can occur even at the later stages of autophagy (Fig. 9). Rab9A was recruited to GcAVs after autophagosomal maturation and knockdown of Rab9A or overexpression of Rab9A S21N significantly decreased the size of GcAVs, whereas knockdown of Rab9A increased the number of GcAV per cell. Therefore, it was demonstrated that GcAVs can expand even after autophagosomal maturation by Rab9A GTPase activity and suggested the homotypic fusion of small GcAVs by Rab9A. However, it should be noted that these smaller GcAVs in Rab9A-knockdown cells are larger than starvation-induced autophagosomes. Rab9A is also involved in trafficking from late endosomes to the trans-Golgi (Carroll *et al*., 2001; Barbero *et al*., 2002). Interestingly, there is a report that Rab9A plays a role in generating Atg5-independent alternative macroautophagy (Nishida *et al*., 2009). According to this report, alternative autophagosomes appear to be generated in a Rab9A's GTPase activity-dependent manner by the fusion of isolation membranes with vesicles derived from the trans-Golgi and endosomes. Because GcAV formation is Atg5-dependent and GcAVs are LC3-positive vacuoles, GcAVs are apparently different from alternative autophagosomes. However, GcAVs may also utilize vesicles derived from the trans-Golgi and endosomes as a source of GcAV membranes in a Rab9A-dependent manner. In this regard, a previous study also has suggested the possibility that GcAVs may fuse with endosomes and acquire

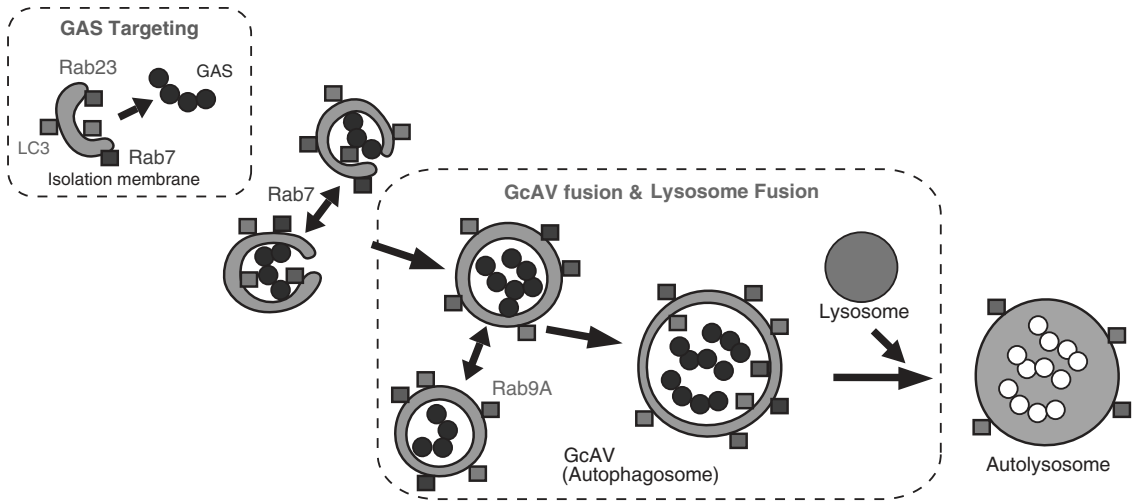

Fig. 9. Proposed model for Rab association in autophagy during GAS infection. Model showing Rab protein functions at each step of GcAV formation. Rab23 regulates the targeting of developing autophagosomes to invading GAS and GcAV formation, whereas Rab9A facilitates homotypic fusion between GcAVs as well as lysosomal fusion.

 Cellular Microbiology, **14**, 1149–1165

endosome SNAREs by this fusion (Furuta *et al*., 2010). Because GcAVs require large amounts of membrane components to form its enormous vacuoles, GcAVs may use this additional autophagosome formation system.

In this study, it was demonstrated that GcAVs harbour different Rab proteins with canonical autophagosomes. Although we examined the localization of 10 Rab proteins, approximately 70 types of Rabs have now been identified in humans. Therefore, other Rabs also would be involved in GcAV regulation. Moreover, future studies such as identification of effectors of Rabs on GcAV would be important for understanding of the GcAV development process.

In summary, we identified two novel GcAV-regulating Rab proteins, Rab9A and Rab23. These Rab proteins were not observed in starvation-induced autophagosomes. We demonstrated that Rab9A is involved in GcAV enlargement through homotypic fusion of small GcAVs and in lysosomal fusion and Rab23 is required for GcAV formation (Fig. 9). Autophagy involves highly conserved cellular machinery and has various physiological roles and can play a role in immunity against intracellular pathogens. Our findings suggest that autophagy uses different Rab proteins for its distinct stages of development. Further studies of autophagy during GAS infection will help us to understand in greater detail the interactions between host cells and pathogens.

Experimental procedures

GAS strains

GAS strain JRS4 ($M6^+$ $F1^+$) was grown in Todd-Hewitt broth (BD Diagnostic Systems, Sparks, MD) supplemented with 0.2% yeast extract (THY) as described previously (Nakagawa *et al*., 2004).

Cell cultures and transfection

HeLa cells were maintained in Dulbecco's modified Eagle's medium (DMEM; Nalacai Tesque) supplemented with 10% fetal bovine serum (FBS; JRH Biosciences) and 50 μg ml^{-1} gentamicin (Sigma-Aldrich) in a 5% CO_2 incubator at 37°C. Plasmid transfection was performed with polyethylenimine (Polyscience). Protein transfection was performed using Xfect transfection reagents as recommended by the manufacturer (Clontech Laboratories). For starvation, cells were cultured in Hanks' balanced salt solution (HBSS; Nacalai Tesque) medium for 2 h.

Plasmids

Gateway (Invitrogen) cloning technology was used to create the designated vectors. Human Rab proteins cDNA were amplified with PCR from human PBMC cDNA libraries by using primer pairs shown in Table S1. The PCR products were cloned into pENTR/D-TOPO vectors using the pENTR Directional TOPO cloning kit (Invitrogen) and subcloned into pcDNA6.2/N-EmGFP-DEST. Underlined sequences of the primers were recognition sites for TOPO cloning. Rab23 constitutive active and negative mutants (Rab23 Q68L and Rab23 S23N) were constructed by introducing a point mutation using primer pairs shown in Table S1. The BLOCK-iT Pol II miR RNAi expression vector kit (Invitrogen) was used to knock down Rab9A and Rab23 expression. We designated the targeting sequences for Rab9A as 5′-ATTCACAACTTCCAGAACT-3′ (GenBank Accession No. NM_004251.3) and Rab23 as 5′-ATATGGAACGCCATAAAGA-3′ (GenBank Accession No. NM_016277.3). The miRNA sequence double-strands were ligated to pcDNA-6.2-GW/miR (Invitrogen) or pcDNA-6.2-GW/EmGFP-miR (Invitrogen) according to the supplier's instructions. pcDNA6.2-GW/miR-neg (Invitrogen) was used as a miRNA-Control. These plasmids were transfected into HeLa cells as described above.

Western blotting

Western blotting was performed as described previously (Nakagawa *et al*., 2001). HeLa cells transfected with plasmids were lysed in Triton lysis buffer [1% Triton X-100, 150 mM NaCl, 50 mM HEPES (pH 7.4)]. Cellular lysates (30–40 μg protein) were subjected to immunoblot analysis. Mouse monoclonal anti-FLAG (Sigma-Aldrich), anti-LC3 (MBL), mouse polyclonal anti-Rab9B (Abcam), and rabbit monoclocal anti-GFP (Nacalai Tesque), anti-α-tubulin (Sigma-Aldrich) antibodies were used as primary antibodies, and the secondary antibodies were HRP-conjugated anti-mouse or anti-rabbit IgG (Jackson Immunoresearch). Blots were visualized using ECL-Plus reagent (GE Health Sciences).

GAS infection

Infection of GAS was performed as described previously. In brief, bacteria were added to cell cultures at a moi 100 without antibiotics for 1 h, the infected cells washed with PBS and antibiotics (100 μg ml^{-1} gentamicin and 100 U ml^{-1} penicillin G) were added for an appropriate period to kill extracellular bacteria.

Fluorescence microscopy

For immunostaining, the cells were washed with phosphate-buffered saline (PBS), fixed with 4% paraformaldehyde in PBS for 30 min, and permeabilized with 0.1% Triton in PBS for 10 min. After being washed with PBS, the cells were incubated in blocking solution for 1 h and subsequently with primary antibodies diluted 1:400 with blocking solution at room temperature for 1 h. Mouse monoclonal anti-LAMP1 antibodies (Santa Cruz Biotechnology) and mouse monoclonal anti-FLAG antibodies (Sigma-Aldrich) were used as primary antibodies. After being washed with PBS, the cells were then probed with secondary antibodies (anti-mouse IgG) conjugated with AlexaFluo 488, 594 (Invitrogen), or Cy5 (Jackson Immuno Research) diluted 1:200 with blocking solution. To label bacterial and cellular DNA, cells were stained with DAPI (Nacalai Tesque) in blocking solution. All fluorescence micrographs were confocal images acquired with a FV1000 laser-scanning microscope (Olympus).

Protein preparation

Rab23 proteins were expressed in *Escherichia coli* cells. pGEX-6P-1 plasmids encoding Rab23 were transformed into the *E. coli*

DH10B strains, and cells were cultured in LB medium. Expression of each protein was induced by the addition of IPTG (final concentration 1 mM) to the medium. After induction, cells were disrupted by sonication in lysis buffer (1% Triton X-100 in PBS). Lysates were applied to a glutathione-Sepharose 4B (GE Healthcare) column. The column was washed with PBS and GST-Rab23 was eluted with 10 mM glutathione in 50 mM Tris-HCl (pH 7.5).

Measurement of GcAV formation efficiency and GcAV area

For quantification of GcAV formation efficiency, samples for fluorescence microscopy prepared as described above were examined using confocal microscopy. The rate of GcAV formation was expressed as the ratio of GcAV-bearing cells to GAS-infected cells. More than 200 cells were analysed in each assay. For measurement of GcAV area, more than 30 GcAV images were analysed in each experiment using ImageJ software (http://rsb.info.nih.gov/ij/).

Bacterial viability assay

HeLa cells (2×10^4 cells/well) were cultured in 24-well culture plates. Transfection of miR-RNA vectors was performed 48 h before infection. Cells were infected as described above. After an appropriate incubation time, cells were lysed in sterile distilled water and serial dilutions of lysates were plated on THY agar plates. The number of viable intracellular GAS was determined by colony counting and presented as the ratio of 'intracellular live GAS at the indicated time' to 'total intracellular and adherent GAS at 1 h', with ± SE for three independent experiments.

Acknowledgements

This work was supported by Grants-in-Aids for Scientific Research (#21390487 and #22592032), and by the Japanese Ministry of Education, Global Center of Excellence (GCOE) Program, 'International Research Center for Molecular Science in Tooth and Bone Diseases' and by a funding program for Next Generation World-Leading Researchers (LS041), Japan Society for the Promotion of Science.

References

Barbero, P., Bittova, L., and Pfeffer, S.R. (2002) Visualization of Rab9-mediated vesicle transport from endosomes to the trans-Golgi in living cells. *J Cell Biol* **156:** 511–518.

Carroll, K.S., Hanna, J., Simon, I., Krise, J., Barbero, P., and Pfeffer, S.R. (2001) Role of Rab9 GTPase in facilitating receptor recruitment by TIP47. *Science* **292:** 1373–1376.

Chua, C.E., Gan, B.Q., and Tang, B.L. (2011) Involvement of members of the Rab family and related small GTPases in autophagosome formation and maturation. *Cell Mol Life Sci* **68:** 3349–3358.

Eggenschwiler, J.T., Bulgakov, O.V., Qin, J., Li, T., and Anderson, K.V. (2006) Mouse Rab23 regulates hedgehog signaling from smoothened to Gli proteins. *Dev Biol* **290:** 1–12.

Evans, T.M., Ferguson, C., Wainwright, B.J., Parton, R.G., and Wicking, C. (2003) Rab23, a negative regulator of hedgehog signaling, localizes to the plasma membrane and the endocytic pathway. *Traffic* **4:** 869–884.

Evans, T.M., Simpson, F., Parton, R.G., and Wicking, C. (2005) Characterization of Rab23, a negative regulator of sonic hedgehog signaling. *Methods Enzymol* **403:** 759–777.

Fader, C.M., and Colombo, M.I. (2006) Multivesicular bodies and autophagy in erythrocyte maturation. *Autophagy* **2:** 122–125.

Fader, C.M., Sanchez, D., Furlan, M., and Colombo, M.I. (2008) Induction of autophagy promotes fusion of multivesicular bodies with autophagic vacuoles in k562 cells. *Traffic* **9:** 230–250.

Fujita, N., Hayashi-Nishino, M., Fukumoto, H., Omori, H., Yamamoto, A., Noda, T., and Yoshimori, T. (2008) An Atg4B mutant hampers the lipidation of LC3 paralogues and causes defects in autophagosome closure. *Mol Biol Cell* **19:** 4651–4659.

Furuta, N., Fujita, N., Noda, T., Yoshimori, T., and Amano, A. (2010) Combinational soluble N-ethylmaleimide-sensitive factor attachment protein receptor proteins VAMP8 and Vti1b mediate fusion of antimicrobial and canonical autophagosomes with lysosomes. *Mol Biol Cell* **21:** 1001–1010.

Guo, A., Wang, T., Ng, E.L., Aulia, S., Chong, K.H., Teng, F.Y., *et al.* (2006) Open brain gene product Rab23: expression pattern in the adult mouse brain and functional characterization. *J Neurosci Res* **83:** 1118–1127.

Gutierrez, M.G., Munafo, D.B., Beron, W., and Colombo, M.I. (2004) Rab7 is required for the normal progression of the autophagic pathway in mammalian cells. *J Cell Sci* **117:** 2687–2697.

Huang, J., Birmingham, C.L., Shahnazari, S., Shiu, J., Zheng, Y.T., Smith, A.C., *et al.* (2011) Antibacterial autophagy occurs at PI(3)P-enriched domains of the endoplasmic reticulum and requires Rab1 GTPase. *Autophagy* **7:** 17–26.

Huang, T.H., Shui, H.A., Ka, S.M., Tang, B.L., Chao, T.K., Chen, J.S., *et al.* (2009) Rab 23 is expressed in the glomerulus and plays a role in the development of focal segmental glomerulosclerosis. *Nephrol Dial Transplant* **24:** 743–754.

Itoh, T., Fujita, N., Kanno, E., Yamamoto, A., Yoshimori, T., and Fukuda, M. (2008) Golgi-resident small GTPase Rab33B interacts with Atg16L and modulates autophagosome formation. *Mol Biol Cell* **19:** 2916–2925.

Jager, S., Bucci, C., Tanida, I., Ueno, T., Kominami, E., Saftig, P., and Eskelinen, E.L. (2004) Role for Rab7 in maturation of late autophagic vacuoles. *J Cell Sci* **117:** 4837–4848.

Kageyama, S., Omori, H., Saitoh, T., Sone, T., Guan, J.L., Akira, S., *et al.* (2011) The LC3 recruitment mechanism is separate from Atg9L1-dependent membrane formation in the autophagic response against Salmonella. *Mol Biol Cell* **22:** 2290–2300.

Levine, B., Mizushima, N., and Virgin, H.W. (2011) Autophagy in immunity and inflammation. *Nature* **469:** 323–335.

Mizushima, N., Yoshimori, T., and Levine, B. (2010) Methods in mammalian autophagy research. *Cell* **140:** 313–326.

Munafo, D.B., and Colombo, M.I. (2002) Induction of autophagy causes dramatic changes in the subcellular distribution of GFP-Rab24. *Traffic* **3:** 472–482.

Nakagawa, I., Nakata, M., Kawabata, S., and Hamada, S. (2001) Cytochrome c-mediated caspase-9 activation triggers apoptosis in *Streptococcus pyogenes*-infected epithelial cells. *Cell Microbiol* **3:** 395–405.

Nakagawa, I., Amano, A., Mizushima, N., Yamamoto, A., Yamaguchi, H., Kamimoto, T., *et al.* (2004) Autophagy defends cells against invading group A Streptococcus. *Science* **306:** 1037–1040.

Nishida, Y., Arakawa, S., Fujitani, K., Yamaguchi, H., Mizuta, T., Kanaseki, T., *et al.* (2009) Discovery of Atg5/Atg7-independent alternative macroautophagy. *Nature* **461:** 654–658.

Ravikumar, B., Imarisio, S., Sarkar, S., O'Kane, C.J., and Rubinsztein, D.C. (2008) Rab5 modulates aggregation and toxicity of mutant huntingtin through macroautophagy in cell and fly models of Huntington disease. *J Cell Sci* **121:** 1649–1660.

Riederer, M.A., Soldati, T., Shapiro, A.D., Lin, J., and Pfeffer, S.R. (1994) Lysosome biogenesis requires Rab9 function and receptor recycling from endosomes to the trans-Golgi network. *J Cell Biol* **125:** 573–582.

Sakurai, A., Maruyama, F., Funao, J., Nozawa, T., Aikawa, C., Okahashi, N., *et al.* (2010) Specific behavior of intracellular *Streptococcus pyogenes* that has undergone autophagic degradation is associated with bacterial streptolysin O and host small G proteins Rab5 and Rab7. *J Biol Chem* **285:** 22666–22675.

Smith, A.C., Heo, W.D., Braun, V., Jiang, X., Macrae, C., Casanova, J.E., *et al.* (2007) A network of Rab GTPases controls phagosome maturation and is modulated by *Salmonella enterica* serovar Typhimurium. *J Cell Biol* **176:** 263–268.

Stenmark, H. (2009) Rab GTPases as coordinators of vesicle traffic. *Nat Rev Mol Cell Biol* **10:** 513–525.

Wang, Y., Ng, E.L., and Tang, B.L. (2006) Rab23: what exactly does it traffic? *Traffic* **7:** 746–750.

Yamaguchi, H., Nakagawa, I., Yamamoto, A., Amano, A., Noda, T., and Yoshimori, T. (2009) An initial step of GAS-containing autophagosome-like vacuoles formation requires Rab7. *PLoS Pathog* **5:** e1000670.

Supporting information

Additional Supporting Information may be found in the online version of this article:

Fig. S1. Time-course of colocalization between EmGFP-Rab proteins and GcAVs. HeLa cells expressing mCherry-LC3 and EmGFP-Rab proteins (Rab4A, Rab5, Rab9B, Rab10, Rab11, Rab13, Rab24, Rab33B) were infected with GAS at an moi 100 for the indicated times. Cells were fixed and DNA was stained with DAPI for confocal microscopic analysis. Colocalization efficiencies were calculated as the percentage of total number of GcAVs. Data shown represent results of > 40 GcAVs and each percentage represents the mean value ± SD from three independent experiments.

Fig. S2. Localization of GcAV markers.

A and B. Confocal microscopic images of serial sections of GcAVs. HeLa cells expressing EmGFP-LC3 (green) and FLAG-Atg5 (red) were infected with GAS at an moi 100 for 2 h (A) or 3 h (B). After fixation, DNA was stained with DAPI.

C. Time-course of colocalization of LC3 with Atg5 on GcAVs. Colocalization efficiencies were determined from confocal microscopic images. LC3-positive and Atg5-negative GAS are shown in black, LC3- and Atg5-positive GAS in grey, LC3-negative and Atg5-positive GAS in white. Data shown represent the results for > 30 GAS associated with either marker.

D. Time-course of colocalization of LC3 with LAMP1 on GcAVs. Colocalization efficiencies were determined from confocal microscopic images. LC3-positive and LAMP1-negative GAS are shown in black, LC3- and LAMP1-positive GAS in grey, LC3-negative and LAMP1-positive GAS in white. Data shown represent the results for > 30 GAS associated with either marker.

Fig. S3. Atg4B C74A increase Atg5-associated GAS.

A. Confocal microscopic images of Atg5 (green)-positive GAS (blue). HeLa cells expressing EmGFP-Atg5 were infected with GAS at an moi 100 for 3 h. After fixation, cellular and bacterial DNA were stained with DAPI. Bars, 10 μm.

B. Quantification of Atg5-associated GAS. Percentages of Atg5-associated GAS-harbouring cells were determined from confocal microscopic images shown in A. Data shown represent results of > 100 GAS-infected cells and each percentage represents the mean value ± SD from three independent experiments.

Fig. S4. Effect of Rab9A-knockdown on Rab9B levels.

A. HeLa cells were transfected with EmGFP-Rab9B expression vectors and miR vectors for the control and Rab9A. After 48 h of transfection, expression of Rab9B was analysed by Western blotting using anti-GFP antibodies.

B. HeLa cells were transfected with miR vectors for the control and Rab9A. After 48 h of transfection, expression of Rab9B was analysed by Western blotting using anti-Rab9B antibodies.

Fig. S5. Knockdown of Rab23 decrease Atg5-associated GAS.

A. Confocal microscopic images of Atg5 (green)-positive GAS (blue). HeLa cells expressing EmGFP-Atg5 were infected with GAS at an moi 100 for 2 h. After fixation, cellular and bacterial DNA were stained with DAPI. Bars, 10 μm.

B. Quantification of Atg5-positive GAS. Percentages of Atg5-associated GAS-harbouring cells were determined from confocal microscopic images shown in (A). Data shown represent results of > 100 GAS-infected cells and each percentage represents the mean value ± SD from three independent experiments.

Fig. S6. Overexpression of Rab23 S23N inhibits GcAV formation but not starvation-induced autophagosome formation. Confocal microscopic images of starvation-induced autophagosomes and GcAVs. HeLa cells were transfected with EmGFP-LC3 and mCherry-Rab23 S23N and incubated in HBSS or infected with GAS for 2 h. After fixation, cellular and bacterial DNA were stained with DAPI. mCherry-Rab23 S23N (red)-expressing cells show starvation-induced autophagosomes but not GcAVs.

Fig. S7. Protein transfection of Rab23 rescued knockdown of Rab23 expression.

A. GST-Rab23 produced in *E. coli* and purified using Glutathione Sepharose 4B.

B. Quantification of GcAV-harbouring Rab23-knockdown cells. HeLa cells transfected with miR-Rab23 vectors for 48 h were transfected with purified GST or GST-Rab23 for 2 h and infected

with GAS at a moi 100 for 4 h. The rate of GcAV-positive cell formation was calculated as the ratio of GcAV-positive cells to GAS-infected cells from confocal microscopic images. Data shown represent the results for > 100 infected cells and each percentage represents the mean ± SD from three independent experiments. $^{**}P < 0.01$.

Table S1. Primers used in this study.

Please note: Wiley-Blackwell are not responsible for the content or functionality of any supporting materials supplied by the authors. Any queries (other than missing material) should be directed to the corresponding author for the article.

有機材料学分野

秋吉 一成

生体材料工学研究所
素材研究部門・非常勤講師

1）英文原著論文

1. A. Shimoda, Y. Yamamoto, S. Sawada, K. Akiyoshi, Biodegradable Nanogel-integrated Hydrogels for Sustained Protein Delivery, Macromol. Research, 20, 266-270（2012）
2. Y.Sasaki, K. Akiyoshi, Self-assembled Nanogel Engineering for Advanced Biomedical Technology, Chem. Lett. 41, 202-208（2012）
3. Y. Sekine, K. Abe, A. Shimizu, Y. Sasaki, S. Sawada, K. Akiyoshi, Shear flow-induced nanotubulation of surface-immobilized liposomes, RSC Advances, 2, 2682-2684（2012）
4. G. Kashiwazaki, T. Bando, T. Yoshidome, S. Masui, T. Takagaki, K. Hashiya, G. Pandian, J. Yasuoka, K. Akiyoshi, H. Sugiyama, Synthesis and Biological Properties of Highly Sequence-Specific Alkylating N-Methylpyrrole-N-Methylimidazole（PI）Polyamide Conjugates, J. Medicinal Chemistry, 55, 2057-2066（2012）.
5. T. Nakai, T. Hirakura, Y. Sakurai, T. Shimoboji, M. Ishigai, K. Akiyoshi, Injectable Hydrogel for Sustained Protein Release by Salt-Induced Association of Hyaluronic Acid Nanogel, Macromol. Bioscience, 12, 475-483（2012）
6. Y. Kishia, T. Higuchia, S. Phoon, Y. Sakamakia, K. Kamiya, G. Riemekasten, K. Akiyoshi, M. Weigert, T. Tsubata, Apoptotic marginal zone deletion of anti-Sm/ribonucleoprotein B cells, Proc. Natl. Acad. Sci. USA, 109, 7811-7816（2012）
7. A. Shimoda, S. Sawadad, A. Kano, A. Maruyama, A. Moquin, F. M. Winnik, K. Akiyoshi, Dual crosslinked hydrogel nanoparticles by nanogel bottom-up method for sustained-release delivery, Colloids and Surfaces B：Biointerfaces, 99, 38-44（2012）
8. T. Miyahara, M. Nyan, A. Shimoda, Y. Yamamoto, S. Kuroda, M. Shiota, K. Akiyoshi, S. Kasugai, Exploitation of a novel polysaccharide　nanogel cross-linking membrane for guided bone regeneration（GBR）, J. Tissue Engineering and Regererative Medicine, 6, 666-672（2012）
9. M. Fujioka-Kobayashi, M. S. Ota, A. Shimoda, K. Nakahama, K. Akiyoshi, Y. Miyamoto, S. Iseki, Cholesteryl group- and acryloyl group-bearing pullulan nanogel to deliver BMP2 and FGF18 for bone tissue engineering, Biomaterials, 33, 7613-7620（2012）
10. Y. Sasaki, K. Akiyoshi, Nanogel Engineering by associating polymers for biomedical applications, Hydrogel Micro and Nanoparticles, First Edition. Edited by L. Andrew Lyon and Michael Joseph Serpe. Wiley-VCH, 187-207（2012）.
11. M. Takeo, T. Mori, T. Niidome, S. Sawada, K. Akiyoshi, Y. Katayama, A polyion complex nanogel, J. Collod. Interf. Sci., 390（1）, 78-84（2013）

2）和文原著論文

1. 佐々木善浩、秋吉一成
   生体膜トンネルナノチューブ－その生物学的機能と材料科学への展開、化学、167, 68-69（2012）
2. 佐々木善浩、秋吉一成
   ナノバイオ、自己組織化と機能材料、最先端材料システム、One Point 3、高分子学会、113-122（2012）
3. 向井貞篤、秋吉一成
   ナノゲル工学による新規バイオ材料の設計と医療応用、PHARM TECH JAPAN, 28, 125（2721）-131（2727）（2012）

Colloids and Surfaces B: Biointerfaces 99 (2012) 38–44

Contents lists available at SciVerse ScienceDirect

Colloids and Surfaces B: Biointerfaces

journal homepage: www.elsevier.com/locate/colsurfb

Dual crosslinked hydrogel nanoparticles by nanogel bottom-up method for sustained-release delivery

Asako Shimoda[a], Shin-ichi Sawada[d], Arihiro Kano[b], Atsushi Maruyama[b], Alexandre Moquin[c], Françoise M. Winnik[c], Kazunari Akiyoshi[a,d,*]

[a] Institute of Biomaterials and Bioengineering, Tokyo Medical and Dental University, 2-3-10 Kanda-Surugadai, Chiyoda-ku, Tokyo 101-0062, Japan
[b] Institute for Materials Chemistry and Engineering, Kyushu University, 744 Motooka, Nishi-ku, Fukuoka 819-0395, Japan
[c] Faculty of Pharmacy and Department of Chemistry, Universite de Montreal, CP 6128 Succursale Centre Ville, Montreal QC H3C 3J7, Canada
[d] Department of Polymer Chemistry, Graduate School of Engineering, Kyoto University, Katsura, Nishikyo-ku, Kyoto, 615-8510, Japan

ARTICLE INFO

Article history:
Available online 19 September 2011

Keywords:
Nanogel
Polysaccharide
Sustained drug delivery
Hydrogel
Biodegradable
Asymmetrical flow field-flow fractionation

ABSTRACT

Polysaccharide–PEG hybrid nanogels (CHPOA–PEGSH) crosslinked by both covalent ester bonds and physical interactions were prepared by the reaction of a thiol-modified poly(ethylene glycol) (PEGSH) with acryloyl-modified cholesterol-bearing pullulan (CHPOA). Experimental parameters, including CHPOA concentration, the degree of acryloyl substitution of CHPOA, and the initial amounts of CHPOA and PEGSH, were modified in order to assess their effect on the size of the nanogels (50–150 nm) and on their degradation kinetics, monitored by dynamic light scattering (DLS) and asymmetrical flow field-flow fractionation (AF4) chromatography. Rhodamine-labeled nanogels were injected intravenously into mice and their concentration in blood was determined by a fluorescence assay as a function of post-injection time. The elimination half-life ($t_{1/2}$) of CHPOA–PEGSH nanoparticles was about 15-fold longer (18 h) than that of CHP nanogels (1.2 h). The half-life enhancement of CHPOA–PEGSH was attributed to the presence of the crosslinker PEG chains, which prevent non-specific protein adsorption, and to the slow hydrolysis kinetics of the crosslinking esters in the biological milieu. The hybrid CHPOA–PEGSH nanogels are expected to be useful as injectable nanocarriers for drugs and proteins, in view of their low surface fouling and slow hydrolysis rate.

1. Introduction

Nanometer-sized polymer hydrogel particles (nanogels) have recently received much attention for biomedical applications such as drug delivery systems [1–4]. Chemically crosslinked nanogels are usually prepared by nanoemulsion polymerization or by chemical crosslinking of the hydrophilic or hydrophobic polymer chains in polymer micelles [5–7]. We reported a new method of preparation of physically crosslinked nanogels formed by amphiphilic derivatives of the neutral polysaccharide pullulan, such as pullulans bearing low levels of cholesteryl groups (CHP), upon simple self-assembly in dilute aqueous solution [8]. The nanogels were shown to prevent the massive aggregation of proteins that typically occurs upon rapid removal of urea from solution of unfolded proteins. The enhanced yield of correct protein folding was ascribed to the hydrophobic binding of CHP with proteins, which in turn slows down the kinetics of protein aggregation [9,10].

In this fashion, CHP nanogels have been used to encapsulate in a transient fashion proteins, such as insulin [11], interleukin-12 (IL-12) [12], antigen proteins for cancer vaccine [13,14], and nasal vaccine [15]. Recombinant murine IL-12 (rmIL-12) was successfully incorporated in CHP nanogel simply by incubating rmIL-12 with nanogels. Subcutaneous injection into mice of CHP/rmIL-12/nanogel complexes resulted in a prolonged elevation of rmIL-12 concentration in the serum. However, the kinetics of drug level in serum was the same following intravenous or intraperitoneal injections of CHP/rmIL-12 nanogels as those recorded upon injection of a rmIL-12 solution used as a control. This observation was taken as an indication of the poor stability of CHP nanogels in the bloodstream, presumably due to the fact that nanogels are held together exclusively by physical forces without any covalent crosslinkers. Consequently, they rapidly release their cargo in blood following displacement of the therapeutic protein by plasma proteins.

To overcome the instability of physically crosslinked nanogel in vivo, we devised a means to strengthen nanogels by chemical crosslinking of the nanogels with polyethylene glycol (PEG)

* Corresponding author at: Department of Polymer Chemistry, Graduate School of Engineering, Kyoto University, Katsura, Nishikyo-ku, Kyoto, 615-8510, Japan. Tel.: +81 75 383 2589; fax: +81 75 383 2590.
E-mail address: akiyoshi@bio.polym.kyoto-u.ac.jp (K. Akiyoshi).

0927-7765/$ – see front matter © 2011 Elsevier B.V. All rights reserved.
doi:10.1016/j.colsurfb.2011.09.025

derivatives and coating the surface of nanogels with PEG. Acryloyl group-modified CHP nanogels were crosslinked by thiol group-modified four-armed polyethylene glycol (PEGSH) in water, thus forming nanogel-assembly like "raspberry-like" nanoparticles [16]. In the previous article, we reported the stability and sustained release of the nanogels assemblies upon subcutaneous injection in mice. We assess here the stability of PEG-crosslinked nanogels in blood serum and blood both in vitro and in vivo, following intravenous injection in mice. The nanogels assemblies were analyzed by asymmetrical flow field-flow fractionation with combined multiangle light scattering and dynamic light scattering detection coupled to UV–vis absorption detection, to assess, respectively, the concentration and the hydrodynamic size of the nanogels.

2. Experimental

2.1. Materials

Water was deionized using a Milli-Q water purification system (Millipore, Bedford, MA). Pentaerythritol tetra(mercaptoethyl) polyoxyethylene (PEGSH, Mw = 1.0×10^4 g mol^{-1}) was purchased from NOF Co. (Tokyo, Japan). Di-*n*-butyltin (IV) dilaurate (DBTDL), cysteine hydrochloride monohydrate, and 5,5′-dithio-*bis*-(2-nitrobenzoic acid) (DTNB) were purchased from Wako Pure Chemical Industries, Ltd. (Osaka, Japan). Fetal bovine serum (FBS) and minimum essential medium (MEM) were obtained from Invitrogen (Carlsbad, CA). 2-(Acryloyloxy) ethyl isocyanate (AOI) was purchased from Showa Denko Co (Tokyo, Japan). The cholesteryl pullulan nanogel sample (CHP, 1.2 cholesteryl groups per 100 glucose units) was synthesized as previously reported [17].

2.2. Dynamic light scattering (DLS)

The hydrodynamic diameters of the nanogels were determined by dynamic light scattering (DLS; Zetasizer Nano; Malvern, UK). The scattering angle was kept at 137° and the wavelength was set at 633 nm. The CHPOA nanogel concentration ranged from 1.0 to 5.0 mg mL^{-1}.

2.3. Asymmetrical flow field-flow fractionation (AF4)

Asymmetric flow field-flow fractionation was performed using an AF4 system (AFx2000MT, Postnova Analytics, Landsberg, Germany) combined with an UV/vis detector (SPD-20A, Postnova Analytics), a multiangle light scattering detector (MALS, Dawn 8+, Wyatt Technology), and a dynamic light scattering detector (Wyatt-QELS, Wyatt Technology). The channel had a thickness of 350 μm and was fitted with a regenerated cellulose membrane (10 kDa cut off, Z-MEM-AQU-631, RC, Postnova Analytics). The carrier medium was prefiltered (0.1 μm) phosphate buffered saline (pH 7.4). The sample was injected with a flow rate of 0.2 mL/min, followed by a 4 min-focusing with a cross-flow rate of 1.8 mL/min and a detector flow rate of 0.52 mL/min. Following a 1 min transition, a three-step cross-flow rate gradient was initiated for the elution mode. The starting cross-flow rate (1.8 mL/min) was kept constant for 8 min. It was decreased linearly to 0 mL/min within 10 min, and kept constant at 0 mL/min for 15 min to allow elution of the nanogels or assemblies of nanogels. The detector flow rate was kept at 0.52 mL/min throughout. The detection of the eluted nanogels was performed sequentially by UV absorbance at 556 nm (ε_{556} = 1411 mmol g^{-1} cm^{-1}, determined using a calibration curve), fluorescence with λ_{ex} 468 nm and λ_{em} 581 nm, multiangle light scattering (MALS) and DLS. Each fractogram presented is representative of a triplicate sample.

2.4. Synthesis of the nanogels

The CHPOA nanogels having 5, 19 or 23 acryloyl groups per 100 glucose units were prepared starting from a CHP sample (1.0 g, 6.2 mmol of anhydrous glucose units) dried under vacuum for 2 days at 70 °C before use. The CHP was dissolved under nitrogen in 50 mL of anhydrous dimethyl sulfoxide (50 mL, DMSO) at 45 °C. DBTDL (53, 201 or 242 μL; 90, 340 or 410 μmol) and AOI (42, 155 or 181 μL; 0.3, 1.2 or 1.4 mmol) were added to the CHP solution. The resulting mixture was kept in the dark for 24 h at 45 °C. The reaction mixture was subjected to repeated precipitations into ether/ethanol solution (ether >80% v/v). The isolated solid material was suspended in DMSO, dialyzed against deionized water, and isolated by lyophilization. The degree of substitution of acryloyl groups was determined from the ^{1}H NMR (500 MHz, DMSO-d6/D_2O: δ (ppm) 0.6–2.4 (cholesterol); 3.1–4.0 (glucose 2H, 3H, 4H, 5H, 6H); 4.7 (glucose 1H (1 → 6)); 4.9–5.1 (glucose 1H (1 → 4)); 5.9–6.3 (olefinic protons of the acryloyl group −CH=CH_2−). Rhodamine-labeled CHPOA (CHPOA–Rh) nanogels were synthesized as reported previously [18]. The degree of labeling was determined by UV/vis analysis at 556 nm (UV-1650PC, Shimadzu, Japan).

2.5. Preparation of CHPOA–PEGSH nanoparticles

To prepare CHPOA–PEGSH nanoparticles, samples of CHPOA nanogel (8 mg) in a PBS buffer (1 mL, pH 7.4) were treated with PEGSH in amounts such that the acryloyl group:thiol group molar ratios were 1:1, 2:1 and 4:1. The mixtures were kept at 37 °C for 24 h. Micrographs of CHPOA nanogels and CHPOA–PEGSH nanoparticles were obtained by freeze–fracture TEM (FF-TEM, JEM-1011, JEOL, Tokyo, Japan) at an accelerating voltage 100 kV. The sample was prepared using the aqueous solution of CHPOA nanogel or CHPOA–PEGSH nanoparticles containing 30% glycerol. The concentration of nanogel was 4 mg mL^{-1}, and the acryloyl:thiol molar ratio was 2:1 or 4:1. CHPOA–PEGSH nanogels were isolated in the dry form by lyophilization after 24 h incubation in PBS. Freeze-dried samples were resuspended in deionized water.

The thiol content of CHPOA–PEGSH nanoparticles was determined using Ellman's reagent [19]. CHPOA–PEGSH (4.0 mg mL^{-1}, obtained from acryloyl group:thiol group molar ratios of 1:1, 2:1 and 4:1) were dissolved in PBS. The nanoparticle solution (250 μL) was added to a mixture of the reaction buffer (2.5 mL, 0.1 M sodium phosphate, pH 8.0, containing 1 mM EDTA) and of Ellman's reagent solution (50 μL, 4.0 mg Ellman's Reagent in 1 mL reaction buffer). The mixture was kept at room temperature for 15 min prior to analysis. The SH concentration of the solutions was determined from their absorbance at 412 nm using a calibration curve obtained from cysteine–HCl. The degradation of CHPOA–PEGSH nanoparticles was monitored by ^{1}H NMR spectroscopy for samples incubated in PBS containing D_2O for 24 h at 37 °C. The level of nanoparticle degradation was estimated from the increase in the signal at 2.36 ppm, attributed to the protons in the Fig. S2 [20]. The stability of the nanogels in serum was monitored using 500 μL of CHPOA nanogels or CHPOA–PEGSH nanoparticles (acryloyl:thiol = 1:1, 2:1 or 4:1) solutions in MEM (2.0 mg mL^{-1}, 500 μL). The mixtures were incubated at 37 °C with 5% (v/v) FBS for different times. The resulting solution was analyzed by DLS in order to determine the hydrodynamic sizes of the nanoparticles.

2.6. Blood clearance measurements

The animal experiments were carried out under the guidance of the Animal Care and Use Committee, Kyushu, University. Seven-week-old Balb/c mice purchased from Kyudo Co., Ltd. (Tosu, Japan) were treated with suspensions of CHP–Rh or CHPOA–Rh–PEGSH

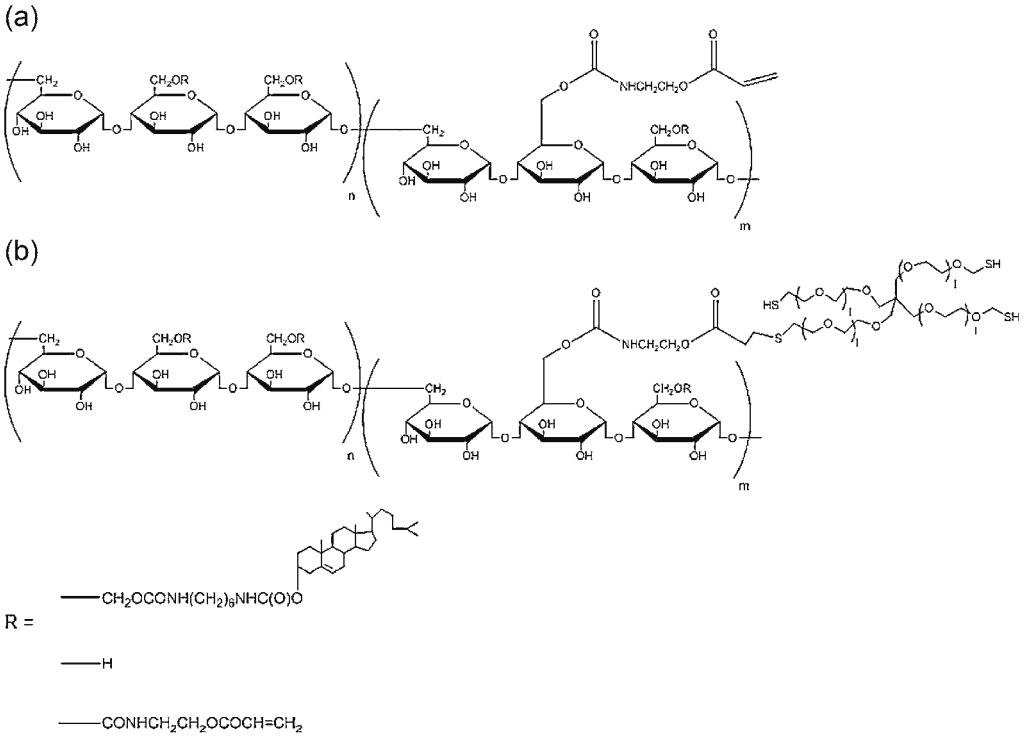

Fig. 1. Chemical structures of (a) CHPOA nanogel and (b) CHPOA–PEGSH nanoparticle.

(acryloyl:thiol = 2:1 or 4:1) in PBS (100 μL 4 mg mL^{-1}) by injection into a tail vein. At various time intervals, blood was collected with a hematocrit tube from the orbital sinus. The blood samples were mixed with a solution of EDTA (1.0 μL, 0.5 M) in PBS and centrifuged for 5 min at 10,000 rpm. The supernatant was diluted with PBS. The fluorescence intensity of the supernatant was determined upon excitation at 550 nm using a Wallac ARVOSX 1420 Multilabel Counter. The total blood volume was calculated as 0.08 mL g^{-1} body weight. The pharmacokinetic parameters were analyzed with a non-compartmental model using WinNonlin (4.0 software; Pharsight Corporation, Mountain View, CA).

3. Results and discussion

3.1. Synthesis and crosslinking of acryloyl CHP nanogels (CHPOA)

The synthesis of CHPOA is outlined in Fig. 1. It involves the reaction of 2-(acryloyloxy) ethyl isocyanate with hydroxyl groups of CHP using di-*n*-butyl-tin (IV) dilaurate as a catalyst. The reaction takes place under mild conditions and provides excellent control over the degree of modification of the nanogels. ^{1}H NMR spectroscopy analysis of CHPOA samples in DMSO-d6/D_2O confirmed that the level of acryloyl group incorporation was nearly identical to the initial feed (Fig. S1). In previous studies [16], acryloyl CHP nanogels were obtained by esterification of CHP hydroxyl groups with acrylic acid in the presence of N,N-dicyclohexylcarbodiimide (DCC). Although, the transformation took place, the esterification yield was low, leading to difficulties in adjusting the level of acryloyl group incorporation. Moreover, the urea that is formed as a by-product of the synthesis, could not be removed readily. The new synthesis reported here, which overcomes these difficulties, is a significant improvement over other synthetic routes.

Three batches of CHPOA were prepared, setting the initial ratio of AOI per glucose unit to 5, 19 or 23. The modified CHP samples were purified thoroughly to remove the catalyst prior to further transformation. Their hydrodynamic diameter measured by dynamic light scattering for suspensions (1.0 mg mL^{-1}) in PBS at pH 7.4, decreased as follows, with increasing OA incorporation: CHPOA5, 53.7 ± 1.8 nm; CHPOA19, 43.3 ± 1.0 nm; and CHPOA23, 30.6 ± 0.4 nm. Asymmetrical flow field-flow fractionation analysis of the CHPOA samples confirmed that the mean molecular weight (Mw) of single CHPOA23 nanogels was 9.7×10^5 g mol^{-1}, as determined from fractograms monitored by MALS (Fig. 2). Hence, the number of CHPOA molecules per nanogel was 8–9. This value is larger that the number of CHP molecules (4–5) associated in CHP nanogels nanoparticle consisting of approximately 4–5 CHP molecules [21]. The increase of the number of associated CHPOA molecules and the enhanced size of CHPOA nanogels, compared to CHP nanogels, may be attributed to the presence of the hydrophobic acryloyl groups.

Several experimental parameters affecting the outcome of the Michael addition of PEGSH to the acryloyl groups of CHPOA were examined in order to provide guidelines to control the properties of the resulting crosslinked CHPOA–PEGSH nanogels. First, reactions were conducted with solutions of increasing CHPOA concentration (1.0–10 mg mL^{-1}), keeping the acryloyl:thiol molar ratio set at 1:1. All syntheses were carried out at 37 °C for 24 h. The size of the nanogels was monitored by DLS analysis of aliquots taken from the mixture at specific times during the reaction. It increased rapidly over the first two hours and leveled off to a constant value after 24 h. The ultimate sizes of the crosslinked nanogels, as well as the size distribution, depend on the initial CHPOA concentration. For instance crosslinking of CHPOA23 led to nanogels with hydrodynamic diameters of 53.5 ± 0.1 nm (1 mg mL^{-1}) and 142.7 ± 3.7 nm (5 mg mL^{-1}) and polydispersity indices (PDI) of 0.163 (1 mg mL^{-1})

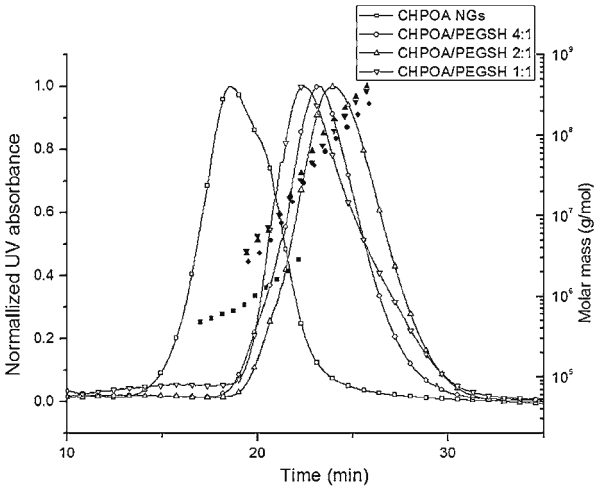

Fig. 2. AF4 fractograms of CHPOA–rhodamine and CHPOA–PEGSH-rhodamine raspberry like nanogels. The lines and the unconnected dots represent, respectively, the normalized UV absorbance at 556 nm and the molar masses of the nanogels as function of the elution time. The separation is based on the diffusion coefficient of the particles.

and 0.463 (5 mg mL^{-1}). Further increase in size and PDI of the crosslinked nanogels was observed when the CHPOA concentration exceeded 5 mg mL^{-1}. Viscous gels formed when the initial CHPOA was 10 mg mL^{-1} or higher, signaling the occurrence of second-order micro/macro gelation due to the crosslinking of preformed raspberry nanogels (Fig. 3).

Second, we set the initial CHPOA concentration at 4 mg mL^{-1} and assessed the effect of the acryloyl/thiol molar ratio on the outcome of the crosslinking reaction. This set of measurements was carried out starting from CHPOA23. The acryloyl:thiol molar ratios were 1:1, 2:1, and 4:1. The resulting nanogels were

Table 1
The diameter of CHPOA–PEGSH nanoparticles.

Molar ratio (acryloyl:thiol)	Diameter (nm)	PdI
1:1	108.7 ± 1.7	0.291 ± 0.013
2:1	117.5 ± 1.5	0.290 ± 0.002
4:1	78.0 ± 0.8	0.244 ± 0.001

Nanogel concentration: 4 mg mL^{-1}

Table 2
The diameter of CHPOA–PEGSH nanoparticles before and after freeze-dry.

Sample	Before	After
	Diameter (nm)	Diameter (nm)
CHPOA23–PEGSH 1:1	113.0 ± 4.3	Gel
CHPOA23–PEGSH 2:1	121.7 ± 4.5	Gel
CHPOA23–PEGSH 4:1	87.3 ± 7.4	71.1 ± 2.9

Nanogel concentration: 4 mg mL^{-1}

analyzed by DLS and by a colorimetric assay with Ellman's reagent for quantitative determination of the unreacted thiol groups. The hydrodynamic diameter of the nanogels ranged from 80 to 120 nm with increasing acryloyl:thiol molar ratio (Table 1), while the free thiol ratios in the CHPOA23–PEGSH nanoparticles were 34.5 ± 2.5%, 8.2 ± 2.3%, and 1.6 ± 1.9% of the total thiol concentration, respectively, with initial acryloyl/thiol ratios of 1:1, 2:1 and 4:1. The residual amounts of acryloyl groups of nanogel after the reaction with PEGSH were estimated by using ^{1}H NMR. The percentage of the residual acryloyl groups in the CHPOA23-PEGSH nanoparticles were 0%, 58%, and 68%, with initial acryloyl/thiol ratios of 1:1, 2:1 and 4:1, respectively. The residual thiol groups and acryloyl groups bound to the nanogels will be useful to prepare functional nanoparticles carrying ligands such as peptides or antibodies. We observed however that when nanoparticles bearing more than ~8% SH were freeze-dried, rehydration resulted in irreversible gelation via disulfide formation. In contrast the nanoparticles with ~2% free SH or less readily redispersed in deionized water after freeze drying (Table 2).

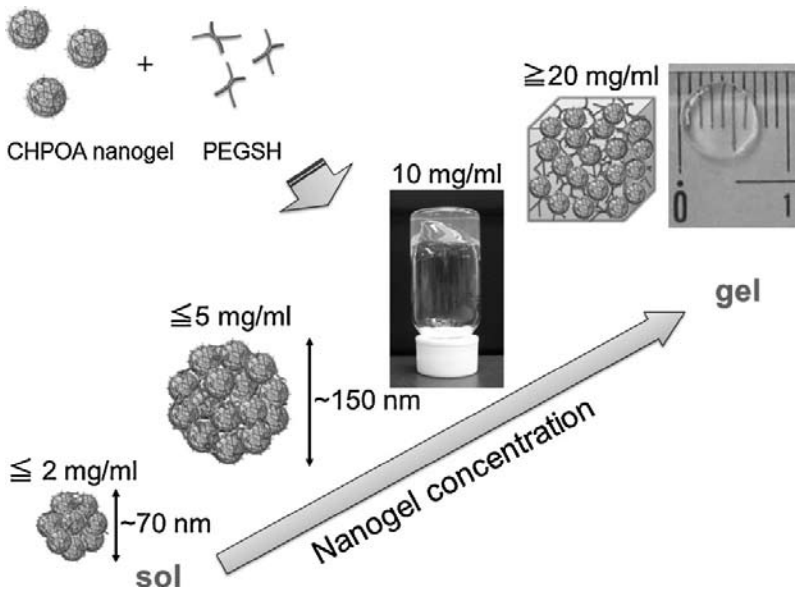

Fig. 3. Hierarchical structure of CHPOA–PEGSH hydrogel. Under dilute conditions, CHPOA–PEGSH forms nanoparticles around 150 nm in diameter. Under higher concentrations, CHPOA–PEGSH forms macrogels. Nanogel crosslinked nanoparticles can be used for injectable materials, and macrogels can be used as scaffolds for tissue engineering.

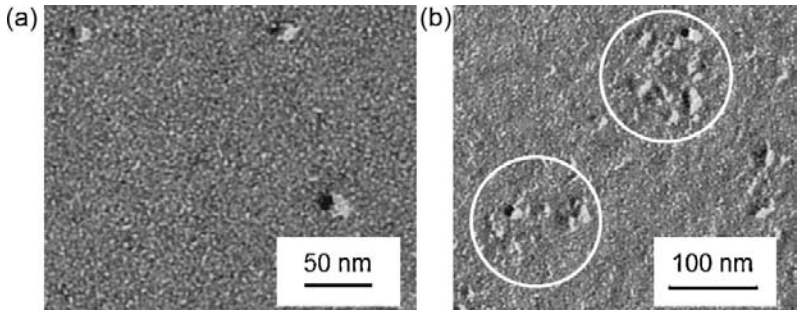

Fig. 4. TEM images of (a) CHPOA nanogels and (b) CHPOA–PEGSH nanoparticles. The nanogel concentration was 4 mg mL^{-1}. The molar ratio of acryloyl/thiol was 2:1.

Crosslinked nanogels obtained from CHPOA23 (4 mg mL^{-1}) and PEGSH (acryloyl/thiol molar ratios 4:1, 2:1 and 1:1) were analyzed by AF4 (Table S1). The fractograms of each sample presented a broad band eluting at longer times, compared to the initial nanogels. This increase in elution time, together with the absence of signal at shorter times, confirm that crosslinking of isolated nanogels occurred with high yield. The size distribution of the crosslinked nanogel was significantly broader than that of the starting CHPOA23 nanogels, revealing some level of heterogeneity in their composition. Under these reaction conditions, both inter- and intra-nanogel crosslinking can occur. When the acryloyl/thiol molar ratio is 1:1, i.e. the CHPOA concentration is high relative to the PEGSH concentration, inter-nanogel crosslinking reactions are most efficient, leading to relatively large crosslinked nanogels. In contrast, when the reaction is carried under conditions of higher PEGSH concentration (acryloyl/thiol is 4:1), intra-nanogel crosslinking reaction predominate, due to dilute conditions of PEGSH. As a result, the size of the resulting particles was smaller than that in the case of acryloyl/thiol = 1:1. The size of the nanoparticle is determined by the balance of concentration of nanogel and PEGSH as a crosslinker.

3.2. Structure of the crosslinked nanogels

The "raspberry-like" morphology of the crosslinked nanogels was confirmed by transmission electron microscopy imaging of freeze-fractured specimens of CHPOA23–PEGSH embedded in frozen 30% glycerol. Micrographs of a CHPOA23–PEGSH (acryloyl/thiol: 2/1) sample and of the original nanogel are presented in Fig. 4. Clusters of closely associated individual nanogels are seen readily in Fig. 4b, corresponding to the crosslinked sample. In contrast (Fig. 4a), the micrograph of the initial nanogel features only well separated nanogels, with no sign of clustering or aggregation.

To confirm the covalent nature of the inter-nanogel crosslinking we carried out a physico-chemical test, which consisted in treating samples of CHPOA–PEGSH suspensions with methyl-β-cyclodextrin, (Me-β-CD) a complexing agent of cholesterol. Treatment of CHP suspensions with Me-β-CD triggers the unraveling of the nanogels as a consequence of the disruption of the hydrophobic cholesteryl clusters due to preferential interaction of isolated cholesteryl groups with Me-β-CD. In contrast, the addition of Me-β-CD to a suspension of CHPOA–PEGSH nanogels resulted in the swelling of the nanoparticles, by a factor of ~20–30% in volume (Table 3). The increase in size of the nanoparticles reflects the increase in the size of the nanogel units (building blocks) as a result of the destruction of the physical crosslinking points by complexation of cholesteryl groups and Me-β-CD, coupled with the fact that disintegrated nanogels have to remain part of the larger object as a result of the chemical crosslinking, unaffected by the addition of Me-β-CD. A pictorial representation of the swelling mechanism is given in Fig. 5. Me-β-CD-loaded nanoparticles are currently investigated building blocks in the construction of cyclodextrin-based supramolecular nano-architectures [22–24]. The complex formed between Me-β-CD and CHPOA–PEGSH may be of use as new supramolecular materials such as artificial chaperones.

Table 3
The diameter change of CHPOA–PEGSH nanoparticles before and after Me-β-CD addition.

Sample	Acryloyl:Thiol	Before	After
		Diameter (nm)	Diameter (nm)
CHPOA23–PEGSH	1:1	108.7 ± 1.7	131.5 ± 0.5
	2:1	117.5 ± 1.5	143.5 ± 4.5
	4:1	78.0 ± 0.8	86.0 ± 0.4

Nanogel concentration: 4 mg mL^{-1}

3.3. Degradation of crosslinked nanogels under physiological conditions

As seen in Fig. 1, the synthetic route selected involves the formation of an ester function linking pullulan chains to the PEGSH crosslinker. This functional group was chosen specifically in view of its ability to undergo hydrolysis at pH 7.4, hence allowing slow disruption of the crosslinked nanogel network and reversal to isolated units. To confirm that hydrolysis of the ester group takes place within the nanogel construct, CHPOA–PEGSH of various composition were exposed to a pH 7.4 phosphate buffer at 37 °C for over 1 month. During this incubation time, they were analyzed repeatedly by ^{1}H NMR spectroscopy in order to detect changes in the intensity of the signal at 2.36 ppm, attributed to the ester hydrolysis (Fig. S2). The percent hydrolysis recovered from this ^{1}H NMR analysis was plotted as a function of time for three different CHPOA–PEGSH nanoparticles (Fig. 6a). Hydrolysis reached levels of ~25–50% after 10 days and gradually leveled off.

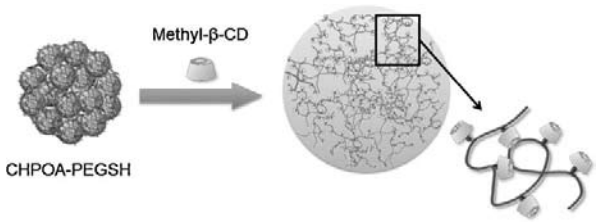

Fig. 5. Methyl-β-CD responding swelling behavior.

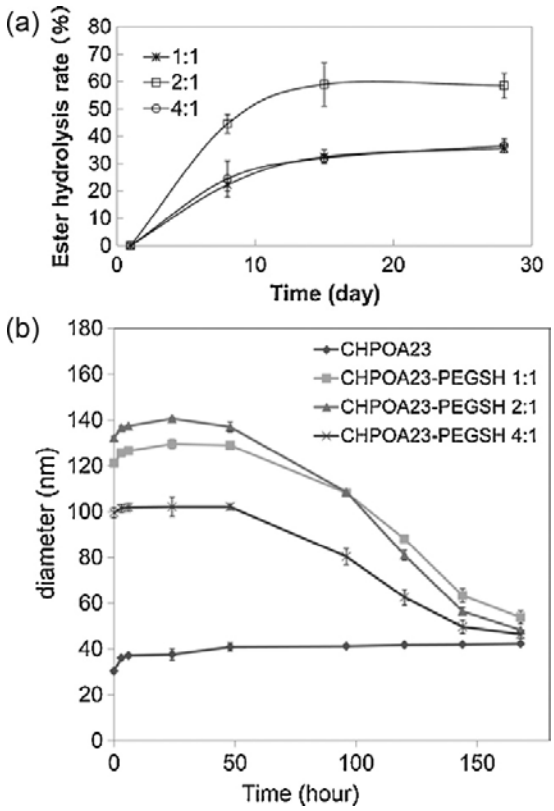

Fig. 6. (a) The ester hydrolysis of CHPOA–PEGSH nanoparticles. Final nanogel concentration was 4 mg mL^{-1}, the molar ratio of acryloyl/thiol was 1:1, 2:1 and 4:1. The data represent mean ± standard deviation (SD), $n = 3$. (b) Stability of CHPOA nanogel (♦) and CHPOA–PEGSH nanoparticles (acryloyl:thiol = 1:1 (■), 2:1(▲) and 4:1 (×)) in the presence of 5% FBS. The data represent mean ± standard deviation (SD), $n = 3$.

We monitored also the fate of crosslinked nanogels incubated in serum at 37 °C. The extent of ester hydrolysis could not be measured by ^{1}H NMR, due to the complexity of the incubation medium. Instead, we recorded by DLS the changes in the hydrodynamic size of the nanoparticles as a function of incubation time (Fig. 6b). The hydrodynamic diameters were constant for 2 days, then, they decreased with time reaching the value of the diameter of the initial nanogel (~40 nm) after 1 week. These results suggest that the hydrolysis of the ester bonds between the CHPOA nanogel and PEGSH was catalyzed by serum esterases [25,26], resulting in the gradual release of nanogels from the crosslinked constructs.

3.4. Blood clearance of crosslinked nanogels following intravenous injection in mice

Suspensions of rhodamine-labeled CHP nanogels and CHPOA–PEGSH nanogels in PBS were injected intravenously in mice followed by blood sampling and analysis after regular time periods, in order to determine the concentration of rhodamine-labeled nanoparticles in blood. The results of the experiments performed with CHP nanogel and two types of crosslinked nanogels are plotted in Fig. 7 as the percent of the injected nanogel concentration remaining in the blood as a function of post-injection time. CHP nanogels were eliminated from the blood within 6 h, whereas the CHPOA–PEGSH nanogels had a significantly longer circulation time: approximately 40–50% of the nanoparticles remained in circulation 6 h following injection and, after 24 h, 20–30% of the

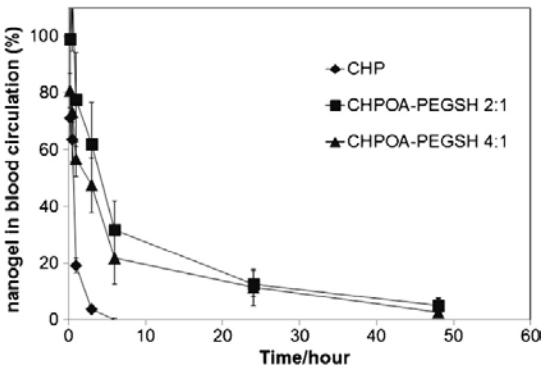

Fig. 7. Blood circulation of CHP nanogel (♦) and CHPOA–PEGSH (acryloyl:thiol = 2:1 (■), 4:1 (▲)). The data represent mean ± standard deviation (SD), $n = 4$.

nanoparticles remained in the blood. A pharmacokinetic analysis of the data revealed that the half-life ($t_{1/2}$) of CHPOA–PEGSH nanoparticles (2:1, 18.0 h; 4:1, 15.5 h) was about 15-fold greater than that of CHP nanogels (1.2 h).

The long circulation in blood is one of the most important issues to achieve effective cancer chemotherapy in intravenous drug delivery system. The superior performance of CHPOA–PEGSH nanogels, compared to CHP nanogels, can be attributed to several effects acting in concert: (1) structural stabilization provided by the covalent crosslinks; (2) prevention of non-specific protein adsorption by the PEG fragments associated with the chemical crosslinkers [27–29]; and (3) controlled release of individual nanogel by sustained hydrolysis of the ester bond between the PEG crosslinker and the glucose units of the nanogel.

4. Conclusion

We designed nanoparticles comprising assemblies of CHPOA nanogel particles and thiol-modified polyethylene glycol. The size of the nanogel assemblies was controlled in the range 50–150 nm by varying the nanogel concentration, degree of substitution of acryloyl groups of CHPOA nanogels and acryloyl:thiol molar ratio. The elimination half-life ($t_{1/2}$) of CHPOA–PEGSH nanoparticles was much longer than that of CHP nanogels. Thus, the nanoparticles can be utilized as injectable nanocarriers capable of controlled release of proteins such as cytokines over relatively long periods. We are able to select various self-assembled nanogels as building blocks and prepare multi-functional naoparticles. The bottom-up nanogel fabrication method opens up a new field for creating tailor-made functional hydrogel materials.

Acknowledgements

This work was supported by a Grant-in-Aid for Scientific Research from the Ministry of Education, Culture, Sports, Science and Technology (No. 20240047 and 22114009). This work was performed under the Cooperative Research Program of Network Joint Research Center for Materials and Devices (Institute for Materials Chemistry and Engineering, Kyushu University).

Appendix A. Supplementary data

Supplementary data associated with this article can be found, in the online version, at doi:10.1016/j.colsurfb.2011.09.025.

References

[1] J.P. Rao, K.E. Geckeler, Prog. Polym. Sci. 36 (2011) 887.
[2] A.V. Kabanov, S.V. Vinogradov, Angew. Chem. Int. Ed. 48 (2009) 5418.
[3] A. Fernández-Barbero, I.J. Suárez, B. Sierra-Martín, A. Fernández-Nieves, F.J. de Las Nieves, M. Marquez, J. Rubio-Retama, E. López-Cabarcos, Adv. Colloid Interface Sci. 147–148 (2009) 88.
[4] Y. Sasaki, K. Akiyoshi, Chem. Rec. 10 (2010) 366.
[5] K. Nagahama, T. Ouchi, Y. Ohya, Macromol. Biosci. 8 (2008) 1044.
[6] M. Oishi, Y. Nagasaki, React. Funct. Polym. 67 (2007) 1311.
[7] E.S. Lee, D. Kim, Y.S. Youn, K.T. Oh, Y.H. Bae, Angew. Chem. Int. Ed. Engl. 47 (2008) 2418.
[8] K. Akiyoshi, S. Deguchi, T. Tajima, T. Nishikawa, J. Sunamoto, Macromolecules 30 (1997) 857.
[9] Y. Nomura, M. Ikeda, N. Yamaguchi, Y. Aoyama, K. Akiyoshi, FEBS Lett. 553 (2003) 271.
[10] N. Morimoto, T. Endo, Y. Iwasaki, K. Akiyoshi, Biomacromolecules 6 (2005) 1829.
[11] K. Akiyoshi, S. Kobayashi, S. Shichibe, D. Mix, M. Baudys, S.W. Kim, J. Sunamoto, J. Control. Release 54 (1998) 313.
[12] T. Shimizu, T. Kishida, U. Hasegawa, Y. Ueda, J. Imanishi, H. Yamagishi, K. Akiyoshi, E. Otsuji, O. Mazda, Biochem. Biophys. Res. Commun. 367 (2008) 330.
[13] Y. Ikuta, N. Katayama, L. Wang, T. Okugawa, Y. Takahashi, M. Schmitt, X. Gu, M. Watanabe, K. Akiyoshi, H. Nakamura, K. Kuribayashi, J. Sunamoto, H. Shiku, Blood 99 (2002) 3717.
[14] S. Kageyama, S. Kitano, M. Hirayama, Y. Nagata, H. Imai, T. Shiraishi, K. Akiyoshi, A.M. Scott, R. Murphy, E.W. Hoffman, L.J. Old, N. Katayama, H. Shiku, Cancer Sci. 99 (2008) 601.
[15] T. Nochi, Y. Yuki, H. Takahashi, S. Sawada, M. Mejima, T. Kohda, N. Harada, I.G. Kong, A. Sato, N. Kataoka, D. Tokuhara, S. Kurokawa, Y. Takahashi, H. Tsukada, S. Kozaki, K. Akiyoshi, H. Kiyono, Nat. Mater. 9 (2010) 572.
[16] U. Hasegawa, S. Sawada, T. Shimizu, T. Kishida, E. Otsuji, O. Mazda, K. Akiyoshi, J. Control. Release 140 (2009) 312.
[17] K. Akiyoshi, S. Deguchi, N. Moriguchi, S. Yamaguchi, J. Sunamoto, Macromolecules 26 (1993) 3062.
[18] H. Ayame, N. Morimoto, K. Akiyoshi, Bioconjug. Chem. 19 (2008) 882.
[19] I. Bravo-Osuna, D. Teutonico, S. Arpicco, C. Vauthier, G. Ponchel, Int. J. Pharm. 340 (2007) 173.
[20] A.E. Rydholm, K.S. Anseth, C.N. Bowman, Acta Biomater. 3 (2007) 449.
[21] K. Kuroda, K. Fujimoto, J. Sunamoto, K. Akiyoshi, Langmuir 18 (2002) 3780.
[22] R. Villalonga, R. Cao, A. Fragoso, Chem. Rev. 107 (2007) 3088.
[23] M.E. Davis, Mol. Pharm. 6 (2009) 659.
[24] F. Manakker, T. Vermonden, C.F. Nostrum, W.E. Hennink, Biomacromolecules 10 (2009) 3157.
[25] H. Xu, Y. Deng, D. Chen, W. Hong, Y. Lu, X. Dong, J. Control. Release 130 (2008) 238.
[26] B. Li, M. Sedlacek, I. Manohaban, R. Boopathy, E.G. Duysen, P. Masson, O. Lockridge, Biochem. Pharmacol. 7 (2005) 1673.
[27] R.L.C. Wang, H.J. Kreuzer, M.M. Grunze, J. Phys. Chem. B 101 (1997) 9767.
[28] D.L. Elbert, J.A. Hubbell, Chem. Biol. 5 (1998) 177.
[29] M.A. Cooper, Nat. Rev. Drug Discov. 1 (2002) 515.

形質発現制御学分野

萩原 正敏

疾患生命科学研究部
高次生命制御研究部門・非常勤講師

1）英文原著論文

1. Ohno G, Ono K, Togo M, Watanabe Y, Ono S, Hagiwara M, Kuroyanagi H
（2012）Muscle-specific splicing factors ASD-2 and SUP-12 cooperatively
switch alternative pre-mRNA processing patterns of the ADF/cofilin
gene in C. elegans. PloSGenet 8（10）e1002991.
2. Saitoh N, Sakamoto C, Hagiwara M, Agredano-Moreno LT,
Jimenez-Garcia LF, Nakao M.（2012）The distribution of phosphorylated
SR proteins and alternative splicing are regulated by RANBP2. Mol Biol Cell.
23（6）：1115-28.
3. Kusano-Kitazume A, Sakamoto N, Okuno Y, Sekine-Osajima Y, Nakagawa
M, Kakinuma S, Kiyohashi K, Nitta S, Murakawa M, Azuma S,
Nishimura-Sakurai Y, Hagiwara M, Watanabe M.（2012）Identification of
novel
N-（morpholine-4-carbonyloxy）amidine compounds as potent inhibitors
against hepatitis C virus replication.　Antimicrob Agents Chemother,
56（3）：1315-23.

2）特許取得、特許申請

1. 発明の名称：抗ウイルス組成物
①発明者：萩原正敏、奥野友紀子、細谷孝充、小野木博、吉田優
②日本出願日：2012年3月15日（特願2012-58340）
③出願人：国立大学法人京都大学、国立大学法人東京医科歯科大学、株式会社キノファーマ
④発明の内容の概略：宿主細胞の蛋白質リン 酸化酵素を阻害し抗ウイルス活性を示す新規化合物に関する特許。
2. 発明の名称：スクリーニング方法、タンパク質の不安定性及び/又は安定性を誘導する物質、及び、タンパク質の活性評価
①発明者：萩原正敏、喜井勲、細谷孝充、隅田有人、吉田優
②日本出願日：2012年6月6日（特願2012-129094）
③出願人：国立大学法人京都大学、国立大学法人東京医科歯科大学

OPEN ACCESS Freely available online

PLOS | GENETICS

Muscle-Specific Splicing Factors ASD-2 and SUP-12 Cooperatively Switch Alternative Pre-mRNA Processing Patterns of the ADF/Cofilin Gene in *Caenorhabditis elegans*

Genta Ohno[1,2,3], Kanako Ono[4], Marina Togo[1], Yohei Watanabe[1], Shoichiro Ono[4], Masatoshi Hagiwara[1,2,5], Hidehito Kuroyanagi[1,2,6]*

1 Laboratory of Gene Expression, Graduate School of Biomedical Science, Tokyo Medical and Dental University, Tokyo, Japan, **2** Department of Functional Genomics, Medical Research Institute, Tokyo Medical and Dental University, Tokyo, Japan, **3** Research Fellowship for Young Scientists, Japan Society for the Promotion of Science (JSPS), Tokyo, Japan, **4** Department of Pathology, Emory University, Atlanta, Georgia, United States of America, **5** Graduate School of Medicine, Kyoto University, Kyoto, Japan, **6** Precursory Research for Embryonic Science and Technology (PRESTO), Japan Science and Technology Agency (JST), Kawaguchi, Saitama, Japan

Abstract

Pre–mRNAs are often processed in complex patterns in tissue-specific manners to produce a variety of protein isoforms from single genes. However, mechanisms orchestrating the processing of the entire transcript are not well understood. Muscle-specific alternative pre–mRNA processing of the *unc-60* gene in *Caenorhabditis elegans*, encoding two tissue-specific isoforms of ADF/cofilin with distinct biochemical properties in regulating actin organization, provides an excellent *in vivo* model of complex and tissue-specific pre–mRNA processing; it consists of a single first exon and two separate series of downstream exons. Here we visualize the complex muscle-specific processing pattern of the *unc-60* pre–mRNA with asymmetric fluorescence reporter minigenes. By disrupting juxtaposed CUAAC repeats and UGUGUG stretch in intron 1A, we demonstrate that these elements are required for retaining intron 1A, as well as for switching the processing patterns of the entire pre–mRNA from non-muscle-type to muscle-type. Mutations in genes encoding muscle-specific RNA–binding proteins ASD-2 and SUP-12 turned the colour of the *unc-60* reporter worms. ASD-2 and SUP-12 proteins specifically and cooperatively bind to CUAAC repeats and UGUGUG stretch in intron 1A, respectively, to form a ternary complex *in vitro*. Immunohistochemical staining and RT–PCR analyses demonstrate that ASD-2 and SUP-12 are also required for switching the processing patterns of the endogenous *unc-60* pre-mRNA from UNC-60A to UNC-60B in muscles. Furthermore, systematic analyses of partially spliced RNAs reveal the actual orders of intron removal for distinct mRNA isoforms. Taken together, our results demonstrate that muscle-specific splicing factors ASD-2 and SUP-12 cooperatively promote muscle-specific processing of the *unc-60* gene, and provide insight into the mechanisms of complex pre-mRNA processing; combinatorial regulation of a single splice site by two tissue-specific splicing regulators determines the binary fate of the entire transcript.

Citation: Ohno G, Ono K, Togo M, Watanabe Y, Ono S, et al. (2012) Muscle-Specific Splicing Factors ASD-2 and SUP-12 Cooperatively Switch Alternative Pre-mRNA Processing Patterns of the ADF/Cofilin Gene in *Caenorhabditis elegans*. PLoS Genet 8(10): e1002991. doi:10.1371/journal.pgen.1002991

Editor: Douglas L. Black, University of California Los Angeles, United States of America

Received April 27, 2012; **Accepted** August 10, 2012; **Published** October 11, 2012

Funding: We acknowledge support from grants from the Ministry of Education, Culture, Sports, Science, and Technology (MEXT) and from Japan Science and Technology Agency (JST) to HK and MH, and a grant from the National Institute of Health (R01 AR48615) to SO. GO was supported by Japan Society for the Promotion of Science (JSPS), including JSPS Research Fellowships for Young Scientists. The funders had no role in study design, data collection and analysis, decision to publish, or preparation of the manuscript.

Competing Interests: The authors have declared that no competing interests exist.

* E-mail: kuroyana.end@tmd.ac.jp

Introduction

Alternative pre-mRNA processing is a major way to produce a number of different mRNAs and proteins from one gene [1,2]. Recent transcriptome analyses by deep sequencing estimated that more than 90% of human multi-exon genes undergo alternative processing and most alternative processing events are regulated in tissue-specific manners [3,4]. These alternative pre-mRNA processing events are classified into seven elementary events: cassette exons, mutually exclusive exons, alternative 5′ splice sites, alternative 3′ splice sites, intron retention, alternative first exons and alternative polyadenylation sites [5,6]. A variety of tissue-specific splicing factors and RNA secondary structures have been shown to regulate these elementary events in the minigene context or by knockdown and/or knockout experiments [7,8,9]. However, pre-mRNA processing in multicellular organisms is often complex due to various combinations of the elementary events and the molecular mechanisms by which tissue-specific factors regulate such complex alternative processing of the entire gene *in vivo* remain to be elucidated.

Muscle is one of tissues in which many genes undergo tissue-specific pre-mRNA processing [3,4]. A number of muscle-specific protein isoforms are expressed by alternative pre-mRNA splicing and play adapted roles depending on the specific properties of muscle fiber types [10,11,12]. For instance, tissue-specific splicing generates functionally distinct isoforms of tropomyosin [13] and troponin T [14]. Global analyses of splicing patterns during development of heart and skeletal muscle revealed that splicing

Author Summary

Muscle is a specialized organ with specialized contractile apparatuses. A number of genes encoding contractile apparatus-related proteins undergo muscle-specific pre–mRNA processing. However, the molecular mechanisms and consequences of muscle-specific alternative pre–mRNA processing remain largely unknown. In this study, we reveal regulation mechanisms of pre–mRNA processing of the *unc-60* gene locus, encoding two tissue-specific isoforms of ADF/cofilin in *C. elegans*. The *unc-60A* and *unc-60B* genes share only the first exon, and UNC-60B protein is specifically expressed in muscle. We visualize the tissue-specific processing patterns of the *unc-60* pre–mRNA with green and red fluorescent proteins in living worms. We provide genetic, biochemical, and immunohistochemical evidence that muscle-specific RNA–binding proteins ASD-2 and SUP-12 cooperatively bind to specific motifs in intron 1A to retain intron 1A, which leads to skipping of exon 2A through 5A and splicing between exon 1 and 2B. Consistently, disruption of the splicing factors leads to expression of UNC-60A in muscle and suppresses paralysis of an *unc-60B*-specific mutant. Our study raises a model of step-by-step execution of complex co-transcriptional pre–mRNA processing and provides insight into the fate decision of the entire transcript.

transitions of these genes occur at specific times [15,16]. Bioinformatics analyses have revealed candidate *cis*-elements regulating muscle-specific splicing patterns [16,17,18]. In addition, several *trans*-acting splicing factors are known to regulate muscle-specific alternative splicing. These include muscleblind-like (MBNL) [19], RBFOX family [20], CUGBP and ETR-3 like factor (CELF) family [21], polypyrimidine tract binding protein (PTB) [22] and hnRNP H [23]. However, how multiple splicing factors coordinate regulation of specific splicing events is poorly understood.

Alternative processing of the *uncoordinated* (*unc*)*-60* gene in *Caenorhabditis elegans* provides an excellent model of muscle-specific and complex pre-mRNA processing of genes related to contractile apparatuses. The *unc-60* gene encodes two homologous proteins, UNC-60A and UNC-60B [24], which are members of the actin depolymerising factor (ADF)/cofilin family of actin-binding proteins that promote rapid turnover of the actin cytoskeleton [25]. The *unc-60* gene consists of a common first exon and two separate series of downstream exons, exons 2A through 5A for UNC-60A and exons 2B through 5B for UNC-60B (Figure 1A). Alternative choices of exons 2A–5A or exons 2B–5B result in tissue-specific expression patterns of the two ADF/cofilin isoforms: UNC-60A protein is expressed in most embryonic cells throughout embryogenesis and predominantly expressed in non-muscle tissues, while UNC-60B protein is mainly detected in body wall muscles [26]. Our biochemical and genetic studies demonstrated that the UNC-60 isoforms have distinct biochemical properties in the regulation of actin dynamics [27,28] and different *in vivo* functions during development and in muscle organization [26,29].

The structure of the *unc-60* gene and its expression patterns raise a question as to how the first exon and the two series of downstream exons are properly spliced in a tissue-specific manner. We previously reported genetic evidence that an RNA-binding protein SUP-12, which has only one RNA-recognition motif (RRM), is required for generation of muscle-specific UNC-60B mRNA [30]. However, the molecular mechanism by which SUP-12 regulates the muscle-specific alternative processing of the *unc-60* gene remains unclear. In this study, we applied a transgenic alternative splicing reporter system [31,32,33] to visualize muscle-specific alternative processing patterns of the *unc-60* pre-mRNA. We demonstrate that repression of excision of the intron between exon 1 and exon 2A is the fate-determining event for the *unc-60* transcript. We provide genetic and biochemical evidence that SUP-12 and another muscle-specific splicing regulator Alternative-Splicing-Defective-2 (ASD-2), a member of the signal transduction and activation of RNA (STAR) family of RNA-binding proteins [34], cooperatively repress excision of the first intron through specific binding to the intron. Our data provide *in vivo* evidence that combinatorial regulation of a single splice site by two tissue-specific splicing regulators determine the binary fate of the entire transcript that can potentially be processed into two alternative isoforms.

Results

Visualization of the muscle-specific alternative pre–mRNA processing of the *unc-60* gene

In order to visualize the binary processing patterns of the *unc-60* transcript *in vivo*, we intended to construct a pair of fluorescence alternative processing reporter minigenes. If the intron between exon 1 and exon 2A (hereafter called intron 1A) is excised prior to selection of exon 2B, it would be impossible to produce UNC-60B mRNA. We therefore assumed that excision of intron 1A should be repressed until exon 2B is transcribed in tissues where UNC-60B is expressed. On the basis of the assumption, we constructed an asymmetric pair of reporter minigenes, *unc-60E1-E2A-RFP* and *unc-60E1-E3B-GFP*. The *unc-60E1-E2A-RFP* cassette, carrying *unc-60* genomic DNA fragment from exon 1 through exon 2A (Figure 1B, top panel), was designed to monitor excision of intron 1A via expression of RFP-fusion protein (UNC-60A-RFP). If intron 1A is retained (UNC-60-I1A), RFP would not be expressed due to a premature termination codon in intron 1A (Figure 1B, top panel). On the other hand, the *unc-60E1-E3B-GFP* cassette, carrying *unc-60* genomic DNA fragment from exon 1 through exon 3B (Figure 1B, bottom panel), was designed to monitor UNC-60B-type processing via expression of GFP-fusion protein (UNC-60B-GFP). An intact UNC-60A isoform (UNC-60A-full) would be expressed in tissues where UNC-60A is expressed (Figure 1B, bottom panel).

We successfully visualized the alternative expression of the UNC-60 isoforms with the *unc-60* reporter cassettes under the control of the *unc-51* promoter that directs expression in a broad variety of tissues [35,36]. As expected, the expression patterns of UNC-60A-RFP and UNC-60B-GFP varied between muscle and non-muscle tissues (Figure 1C, 1D). Non-muscle tissues including the nervous system and intestine expressed UNC-60A-RFP (Figure 1C, 1D, left panels), and muscle tissues such as body wall muscles and pharyngeal muscles expressed UNC-60B-GFP (Figure 1C, 1D, right panels). This result is consistent with our previous immunohistochemical studies showing that UNC-60A and UNC-60B proteins were detected in non-muscle and muscle tissues, respectively [26,37]. We checked splicing patterns of mRNAs derived from the *unc-60* reporter cassettes by cloning and sequencing reverse transcription-polymerase chain reaction (RT-PCR) products, and confirmed that the four mRNA isoforms schematically shown in Figure 1B were actually generated in the transgenic worms (data not shown).

To focus on the muscle-specific control of the *unc-60* processing, we utilized *myo-3* promoter to drive expression of the *unc-60* reporter specifically in body wall muscles. Transgenic worms with an integrated transgene allele *ybIs1831 [myo-3::unc-60E1-E2A-RFP myo-3::unc-60E1-E3B-GFP]* predominantly expressed UNC-60B-GFP in

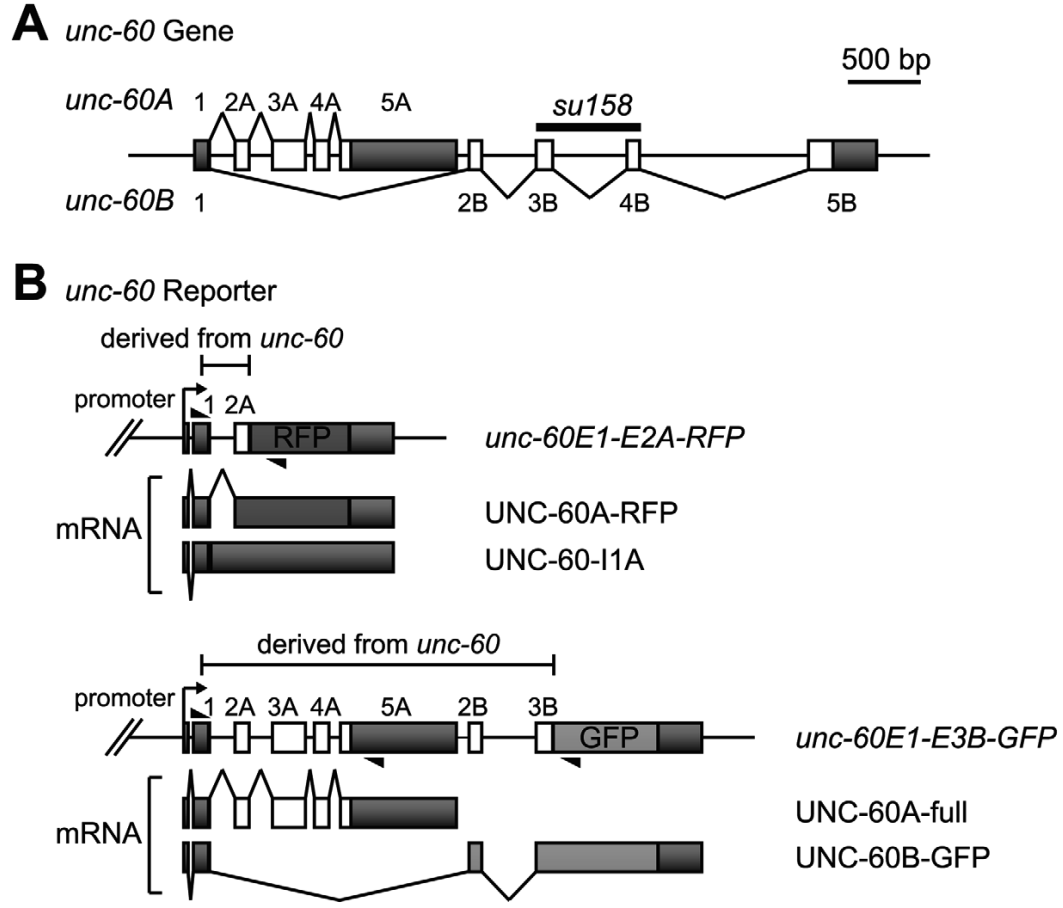
A unc-60 Gene
500 bp
unc-60A 1 2A 3A 4A 5A
su158
unc-60B 1 2B 3B 4B 5B
B unc-60 Reporter
derived from unc-60
promoter
1 2A
RFP
unc-60E1-E2A-RFP
mRNA
UNC-60A-RFP
UNC-60-I1A
derived from unc-60
promoter
1 2A 3A 4A 5A 2B 3B
GFP
unc-60E1-E3B-GFP
mRNA
UNC-60A-full
UNC-60B-GFP

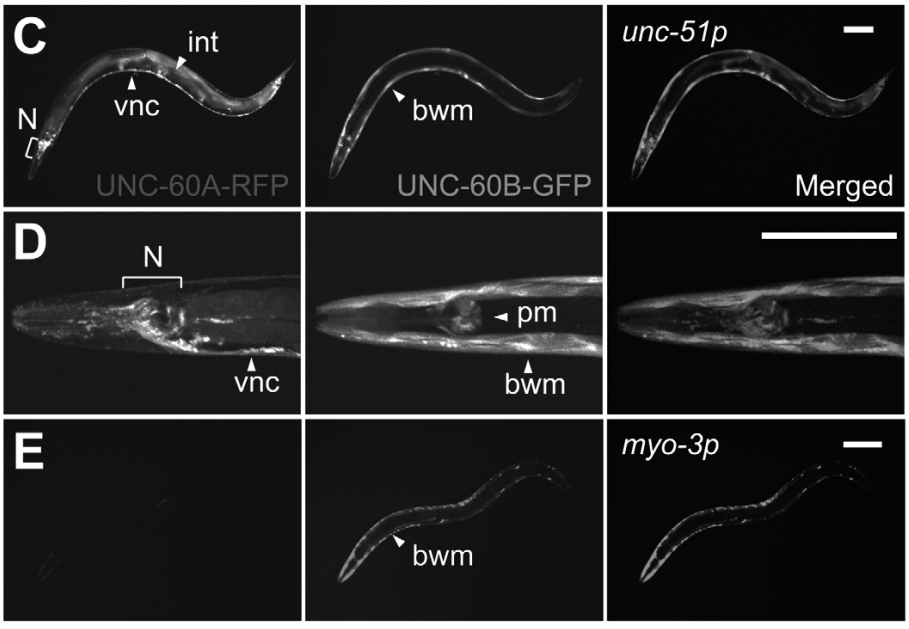
C
int
vnc
N
UNC-60A-RFP
bwm
UNC-60B-GFP
unc-51p
Merged
D
N
vnc
pm
bwm
E
bwm
myo-3p

Figure 1. Visualization of tissue-specific alternative processing patterns of the *unc-60* transcript. (*A*) Schematic structure of the *unc-60* gene. Numbered boxes indicate exons. Predicted open reading frames (ORFs) are coloured in white and untranslated regions (UTRs) are in gray. The deleted region in *unc-60 (su158)* is indicated. (*B*) Schematic illustration of a pair of *unc-60* reporter minigenes, *unc-60E1-E2A-RFP* and *unc-60E1-E3B-GFP*, and UNC-60A- and UNC-60B-type mRNAs derived from them. cDNA cassettes and predicted ORFs for RFP and GFP are coloured in magenta and green, respectively. Triangles indicate positions and directions of primers used to check splicing patterns of mRNAs derived from the minigenes by RT-PCR. (*C* and *D*) Confocal images of transgenic *unc-60* reporter worms *ybEx1812 [unc-51::unc-60E1-E2A-RFP unc-51::unc-60E1-E3B-GFP]*. UNC-60A-RFP (left), UNC-60B-GFP (middle) and merged images (right) of an adult worm (*C*) and a head region at higher magnification (*D*). Anterior is to the left and dorsal is to the top. bwm, body wall muscles; int, intestine; N, neurons in head ganglia; pm, pharyngeal muscles; vnc, ventral nerve cord. Scale bars, 50 μm. (*E*) Confocal images of a transgenic *unc-60* reporter worm *ybIs1831 [myo-3::unc-60E1-E2A-RFP myo-3::unc-60E1-E3B-GFP]* shown as in (*C*) and (*D*).
doi:10.1371/journal.pgen.1002991.g001

body wall muscles (Figure 1E), consistent with the *unc-60* reporter expression in muscles (Figure 1C, 1D). We therefore used the *myo-3* promoter for further analyses described below.

SUP-12 and another muscle-specific splicing factor ASD-2 regulate muscle-specific processing of the *unc-60* reporter

To test whether muscle-specific repression of UNC-60A-RFP and expression of UNC-60B-GFP from the *unc-60* reporter are similarly regulated by a muscle-specific splicing regulator SUP-12 to the endogenous mRNAs for UNC-60A and UNC-60B isoforms [30], we crossed the reporter allele *ybIs1831* with a presumptive null allele *sup-12 (yb1253)* [38]. As expected, the reporter worms clearly turned the colour from Green to Red in the *sup-12* background (Figure 2A), confirming that SUP-12 is required for the muscle-specific expression profile of the *unc-60* reporter.

In a previous study, we identified SUP-12 as a co-regulator of mutually exclusive exons of a fibroblast growth factor receptor gene *egg-laying-defective (egl)-15* [38]. In the case of repression of *egl-15* exon 5B, SUP-12 functions as a muscle-specific partner of the Fox-1 family proteins ASD-1 and FOX-1 [31,38]. We therefore speculated that other regulator(s) may also be involved in the muscle-specific regulation of *unc-60*. As direct interaction between SUP-12 and ASD-1 in a yeast two-hybrid system had been reported in a worm interactome study [39], we screened for a putative co-regulator of the *unc-60* reporter by knocking down genes encoding possible SUP-12-interactors ASD-1, ASD-2, ETR-1, MEC-8, R02F2.5 and W02A11.3, deposited in the database (http://interactome.dfci.harvard.edu/). We performed RNA interference (RNAi) by feeding the reporter worms with bacterial clones targeting the six genes, and found that knockdown of *asd-2* led to expression of UNC-60A-RFP (Figure S1).

We previously identified ASD-2, an RNA-binding protein belonging to the STAR family, as a regulator of muscle-specific and developmentally regulated alternative splicing of a collagen gene *let-2* [32,33]. The *asd-2* gene has alternative first exons and a non-lethal allele *asd-2 (yb1540)* has a nonsense mutation in the *asd-2b*-specific first exon (Figure 2B), which is used in body wall muscles and pharyngeal muscles [32]. The *unc-60* reporter worms exhibited weak Red phenotype in the *asd-2 (yb1540)* background (Figure 2C) and body wall muscle-specific expression of ASD-2b cDNA rescued the colour phenotype (Figure 2D), confirming that *asd-2b* is involved in the muscle-specific regulation of the *unc-60* reporter. To investigate subcellular localization of ASD-2, we raised polyclonal antibodies against recombinant full-length ASD-2b protein and stained wild-type and *asd-2 (yb1540)* worms with a purified immunoglobulin G (IgG) fraction (Figure 2E, 2F). Nuclei of body wall muscles, which are aligned along the dorsal and ventral periphery, are stained in the wild type (Figure 2E) and not in *asd-2* mutant (Figure 2F). In Western blotting, the same antibody detected a major band with an apparent molecular weight of 56 kDa in wild-type and not in *asd-2 (yb1540)* lysate (Figure 2G). These results indicated that ASD-2b is the major isoform and is predominantly localized in the nuclei of body wall muscles. RNAi by micro-injecting double-stranded RNA (dsRNA), a more effective method than feeding dsRNA-expressing bacteria, led to a stronger Red phenotype (Figure 2C), suggesting trace remaining activity of ASD-2 in *asd-2 (yb1540)* mutant.

To confirm splicing patterns of mRNAs derived from the *unc-60* reporter minigenes in body wall muscles, we performed RT-PCR analysis with minigene-specific primer sets (Figure 2H). In the wild-type background, UNC-60B-type mRNA, UNC-60B-GFP, was predominantly generated from *unc-60E1-E3B-GFP* (Figure 2H, middle panel, lane 1). A transcript derived from *unc-60E1-E2A-RFP* was almost undetectable (Figure 2H, top panel, lane 1), presumably due to rapid degradation of a non-productive mRNA isoform, UNC-60-I1A, by nonsense-mediated mRNA decay (NMD) [40]. On the other hand, the amount of UNC-60B-GFP was reduced and UNC-60A-type mRNAs, UNC60A-RFP and UNC-60A-full, were detected in *asd-2* and *sup-12* mutants (Figure 2H, lanes 2 and 3), consistent with their colour phenotypes shown in Figure 2C and 2A, respectively. These results confirmed that both SUP-12 and ASD-2 are responsible for switching the processing patterns of the *unc-60* reporter from UNC-60A-type to UNC-60B-type in body wall muscles.

CUAAC repeats and UGUGUG stretch in intron 1A control the muscle-specific alternative processing of the *unc-60* reporter

The experiments described above indicate that each of the *unc-60* reporter minigenes, even the shorter one, carries sufficient regulatory elements for ASD-2 and SUP-12 to switch from non-muscle-type to muscle-type processing. As regulatory elements for alternative splicing are often evolutionarily conserved in introns among nematodes [31,32,38,41], we searched for conserved stretches in *unc-60* intron 1A in the *Caenorhabditis* genus. Alignment of nucleotide sequences available in WormBase (http://www.wormbase.org/) revealed that CTAAC repeats and TGTGTG stretch are highly conserved just upstream of the splice acceptor site (Figure 3A). To evaluate the roles of these elements in the muscle-specific processing of the *unc-60* reporter, we constructed two pairs of modified *unc-60* reporter minigenes *M1* and *M2*. In the *M1* pair, CTAAC repeats were mutagenized to CAAAC (Figure 3B). In the *M2* pair, TGTGTG were mutagenized to TATATA (Figure 3B). Disruption of either of the two elements resulted in Red phenotype (Figure 3C), phenocopying *sup-12* mutant (Figure 2A) and *asd-2 (RNAi)* worms (Figure 2C). RT-PCR analysis of mRNAs derived from the mutant reporters revealed that both *M1* and *M2* mutations increased production of UNC-60A-RFP (Figure 3D, top panel) and decreased expression of UNC-60B-GFP (Figure 3D, bottom panel), consistent with their colour phenotypes. These results confirmed that the colour phenotypes observed with the mutant reporters are due to altered patterns of pre-mRNA processing. We concluded that both CUAAC repeats and UGUGUG stretch are required for muscle-specific repression of intron 1A excision. Notably,

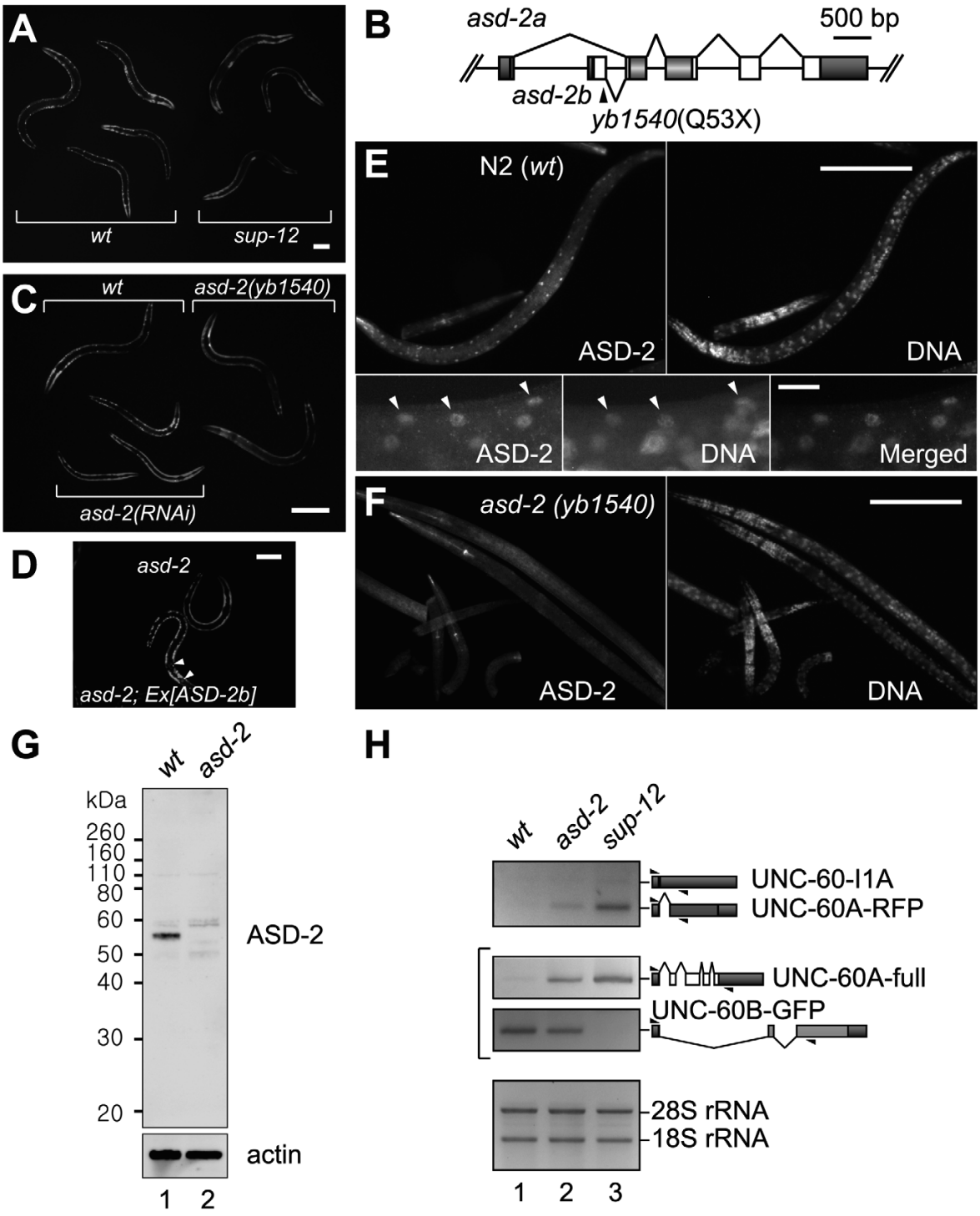

Figure 2. ASD-2 and SUP-12 regulate muscle-specific processing of the *unc-60* reporter in body wall muscles. (*A*) A micrograph of the *unc-60* reporter worms carrying the integrated allele *ybIs1831* in the wild-type (left) and *sup-12 (yb1253)* (right) backgrounds. (*B*) Schematic structure of the *asd-2* gene. The position of a nonsense mutation in *yb1540* is indicated. A region encoding STAR domain is coloured. (*C*) A micrograph of wild-type, *asd-2(yb1540)* mutant and *asd-2(RNAi)* worms carrying *ybIs1831*. (*D*) A micrograph of *asd-2(yb1540)* and *asd-2(yb1540); ybEx2266 [myo-2::mRFP myo-3::ASD-2b]* worms carrying *ybIs1831*. Arrowheads indicate RFP expression in pharynx as a marker for transgenesis. Scale bars in (*A*), (*C*) and (*D*),

50 μm. (*E*, *F*) Microphotographs of N2 (*E*) and *asd-2(yb1540)* (*F*) worms stained with anti-ASD-2b (ASD-2) and Hoechst 33258 (DNA). High-magnification and merged images are also indicated for N2 in bottom panels of (*E*). Arrowheads indicate nuclei of some of body wall muscle cells. Scale bars in (*E*) top panels and (*F*), 100 μm; in (*E*) bottom panels, 10 μm. (*G*) Western blotting with anti-ASD-2b. Lysates from synchronized L1 larvae of N2 (lane 1) and *asd-2(yb1540)* mutant (lane 2) were subjected to Western blotting with anti-ASD-2b (top) and anti-actin (bottom). (*H*) RT-PCR analysis of mRNAs derived from *ybIs1831* in the wild-type (lane 1), *asd-2 (yb1540)* (lane 2) and *sup-12 (yb1253)* (lane 3) backgrounds. RT-PCR products derived from *unc-60E1-E2A-RFP* (top) and *unc-60E1-E3B-GFP* (middle) and total RNAs (bottom) are shown. Splicing patterns of the mRNAs are schematically shown on the right. Triangles indicate positions and directions of the primers.
doi:10.1371/journal.pgen.1002991.g002

expression of UNC-60A-full mRNA from the *M1* and *M2* mutants of *unc-60E1-E3B-GFP* minigene increased compared to the wild-type minigene (Figure 3D), indicating that the repression of intron 1A excision via CUAAC repeats and UGUGUG stretch is a crucial event to switch the processing patterns of the entire *unc-60E1-E3B-GFP* minigene from UNC-60A-type to UNC-60B-type.

ASD-2 and SUP-12 cooperatively bind to *unc-60* intron 1A *in vitro* via direct and specific binding to CUAAC repeats and UGUGUG stretch, respectively

To confirm direct and specific binding of ASD-2 and SUP-12 to the *cis*-elements in *unc-60* intron 1A *in vitro*, we prepared radiolabelled RNA probes containing the intact sequence (WT) or those with mutations as in the mutant reporters (M1 and M2) (Figure 4A) and recombinant full-length ASD-2b and full-length SUP-12 proteins (Figure 4B) to perform electrophoretic mobility shift assays (EMSAs) (Figure 4C, 4D). Recombinant ASD-2b protein shifted the mobility of WT (Figure 4C, lanes 1–6) and M2 (Figure 4D, lanes 18–22) probes in a dose-dependent manner and not of M1 probe (Figure 4D, lanes 1–5), demonstrating direct and specific binding of ASD-2b to CUAAC repeats. On the other hand, recombinant SUP-12 protein shifted the mobility of WT (Figure 4C, lanes 13–18) and M1 (Figure 4D, lanes 6–9) probes to a similar extent in a dose-dependent manner and less efficiently of M2 probe (Figure 4D, lanes 23–26) to a less extent, demonstrating direct and specific binding of SUP-12 to UGUGUG stretch. The result also indicated that SUP-12 could bind to other site(s) in the probes with a lower affinity.

We next asked whether ASD-2b and SUP-12 cooperatively bind to *unc-60* intron 1A RNA. We analyzed supershifts of the mobility of the *unc-60* intron 1A probes by the combination of ASD-2b and SUP-12 in EMSAs (Figure 4C, 4D). ASD-2b efficiently supershifted the mobility of WT probe at lower concentrations in the presence of SUP-12 (Figure 4C, lanes 7–12) compared to ASD-2b alone (lanes 1–6). In the same way, SUP-12 supershifted the mobility of WT probe at lower concentrations in the presence of ASD-2b (lanes 19–24) compared to SUP-12 alone (lanes 13–18). These results indicated that ASD-2b and SUP-12 cooperatively form a stable ASD-2b/SUP-12/RNA ternary complex with *unc-60* intron 1A RNA. ASD-2b failed to supershift the mobility of M1 probe (Figure 4D, lanes 10–17), indicating that CUAAC repeats are essential for the ternary complex formation. SUP-12 less efficiently supershifted the mobility of M2 probe (Figure 4D, lanes 31–34) compared to WT probe (Figure 4C, lanes 21–24) in the presence of ASD-2b, indicating that UGUGUG stretch is involved in the ternary complex formation.

We finally asked whether ASD-2b and SUP-12 can preform a complex in the absence of *unc-60* intron 1A by pull-down experiments (Figure 4E). Glutathione-*S*-transferase (GST)-fused full-length ASD-2b protein pulled down a substantial amount of recombinant full-length SUP-12 protein in the absence of target RNAs (Figure 4E, lane 2) and wild-type (WT) *unc-60* intron 1A (*unc-60*-I1A) RNA enhanced the pull-down efficiency in a dose-dependent manner (lanes 3, 4). On the other hand, GST-fused monomeric RFP (mRFP) protein failed to pull down SUP-12 protein even in the presence of *unc-60*-I1A RNA (lanes 10–13), demonstrating specific interaction between ASD-2b and SUP-12. M1 and M2 mutant *unc-60*-I1A RNAs less effectively enhanced the interaction between ASD-2b and SUP-12 (lanes 5–8), consistent with their weaker or no ability to form a ternary complex (Figure 4D). We therefore concluded that ASD-2b and SUP-12 can weakly interact with each other and that *unc-60* intron 1A RNA promotes the formation of the stable ASD-2b/SUP-12/RNA ternary complex by providing juxtaposed CUAAC repeats and UGUGUG stretch that are specifically recognized by ASD-2b and SUP-12, respectively.

Depletion of ASD-2 leads to substantial expression of endogenous UNC-60A in body wall muscles and restores motility of *unc-60B* mutant

We examined whether ASD-2 regulates muscle-specific pre-mRNA processing of the endogenous *unc-60* gene. We have demonstrated that ASD-2 and SUP-12 cooperatively switch alternative processing of the *unc-60* reporter from UNC-60A-type to UNC-60B-type in body wall muscles. If this model can be applied to the endogenous *unc-60* gene, worms depleted of *asd-2* function should ectopically express UNC-60A in place of UNC-60B in body wall muscles. Indeed, RT-PCR analysis of the endogenous UNC-60 mRNAs revealed that relative amount of UNC-60B mRNA was decreased in *asd-2 (yb1540); asd-2 (RNAi)* worms (Figure S2). To further test the splicing change in body wall muscles, we investigated expression of UNC-60A protein by immunohistochemistry (Figure 5A, 5B). In wild-type worms, UNC-60A was undetectable in body wall muscles (Figure 5A, encircled) but was detected in other tissues (Figure 5A, left panel). Knockdown of the *asd-2* gene resulted in ectopic expression of UNC-60A in body wall muscles (Figure 5B, encircled), confirming that ASD-2 determines the processing patterns of the endogenous *unc-60* gene in body wall muscles.

Our previous work demonstrated that *sup-12* mutation strongly suppressed structural defects of body wall muscles and paralysis of UNC-60B-specific mutant, *unc-60B (su158)* [30]. The deletion allele *su158* lacks exons 3B and 4B (Figure 1A), and suppression of the phenotypes by *sup-12* mutation was likely due to ectopic expression of UNC-60A [30]. We therefore investigated whether knockdown of the *asd-2* gene also suppresses phenotypes of *unc-60B (su158)* mutant. Wild-type worms exhibited sinusoidal locomotion (Figure 5C, left panel), and actin filaments were organized in a striated pattern (Figure 5C, right panel). On the other hand, *unc-60B* (*su158)* worms were almost paralyzed (Figure 5D, left panel) with severe disorganization of actin filaments (Figure 5D, right panel). We found that *asd-2 (yb1540); unc-60B (su158)* double mutant slightly restored motility and actin filament organization (Figure 5E). Since *asd-2(RNAi)* worms showed a severer colour phenotype than *asd-2(yb1540)* allele (Figure 2C), we further knocked down remaining activity of *asd-2* by RNAi. As expected, *asd-2 (yb1540); unc-60B (su158); asd-2 (RNAi)* worms restored sinusoidal locomotion (Figure 5F, left panel) and actin filament organization was greatly improved

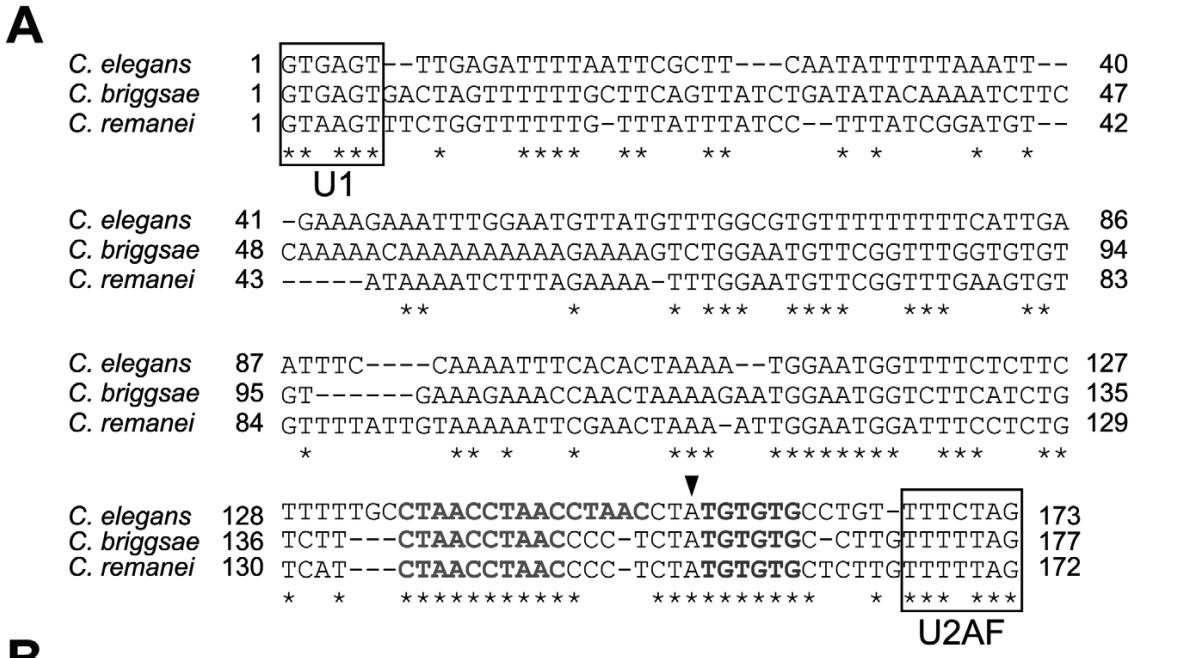
A
C. elegans 1 GTGAGT--TTGAGATTTTAATTCGCTT---CAATATTTTTAAATT-- 40
C. briggsae 1 GTGAGTGACTAGTTTTTTGCTTCAGTTATCTGATATACAAAATCTTC 47
C. remanei 1 GTAAGTTTCTGGTTTTTTG-TTTATTTATCC--TTTATCGGATGT-- 42
U1
C. elegans 41 -GAAAGAAATTTGGAATGTTATGTTTGGCGTGTTTTTTTTTCATTGA 86
C. briggsae 48 CAAAAACAAAAAAAAAAGAAAAGTCTGGAATGTTCGGTTTGGTGTGT 94
C. remanei 43 -----ATAAAATCTTTAGAAAA-TTTGGAATGTTCGGTTTGAAGTGT 83
C. elegans 87 ATTTC----CAAAATTTCACACTAAAA--TGGAATGGTTTTCTCTTC 127
C. briggsae 95 GT------GAAAGAAACCAACTAAAAGAATGGAATGGTCTTCATCTG 135
C. remanei 84 GTTTTATTGTAAAAATTCGAACTAAA-ATTGGAATGGATTTCCTCTG 129
C. elegans 128 TTTTTGCCTAACCTAACCTAACCTATGTGTGCCTGT-TTTCTAG 173
C. briggsae 136 TCTT---CTAACCTAACCCC-TCTATGTGTGC-CTTGTTTTTAG 177
C. remanei 130 TCAT---CTAACCTAACCCC-TCTATGTGTGCTCTTGTTTTTAG 172
U2AF
B
myo-3p
1 2A
RFP
unc-60E1-E2A-RFP-M1, -M2
myo-3p
1 2A 3A 4A 5A 2B 3B
GFP
unc-60E1-E3B-GFP-M1, -M2
Intron 1A
wt 5′-...TTTTTGCCTAACCTAACCTAACCTATGTGTGCCTGTTTTCTAG-3′
M1 5′-...TTTTTGCCAAACCAAACCAAACCTATGTGTGCCTGTTTTCTAG-3′
M2 5′-...TTTTTGCCTAACCTAACCTAACCTATATATACCTGTTTTCTAG-3′
C
wt
M1
M2
D
wt M1 M2
UNC-60-I1A
UNC-60A-RFP
UNC-60A-full
UNC-60B-GFP
1 2 3

Figure 3. CUAAC repeats and UGUGUG stretch are required for muscle-specific alternative processing of the *unc-60* reporter. (*A*) Nucleotide sequence alignment of *unc-60* intron 1A from *C. elegans*, *C. briggsae* and *C. remanei*. Asterisks denote residues conserved among three species. CTAAC repeats and TGTGTG stretch are coloured in magenta and blue, respectively. Binding regions for U1 snRNP (U1) and U2 snRNP auxiliary factor (U2AF) are boxed. Arrowhead indicates a putative branch site. (*B*) Schematic illustrations of mutated pairs of *unc-60* reporter minigenes, *-M1* and *-M2* (top), and nucleotide sequences of the modified regions (bottom). Red crosses indicate positions of modification. Mutated residues in the mutant minigenes are underlined. CTAAC repeats and TGTGTG stretch are coloured as in (*A*). (*C*) A micrograph of transgenic worms expressing wild-type (top), *M1* (middle) and *M2* (bottom) pairs of the *unc-60* reporter minigenes. Anterior is to the left. Scale bar, 50 μm. (*D*) RT-PCR analysis of mRNAs derived from wild-type (lane 1), *M1* (lane 2) and *M2* (lane 3) pairs of *myo-3p-unc-60E1-E2A-RFP* (top) and *myo-3p-unc-60E1-E3B-GFP* (bottom). Schematic structures of the mRNAs are indicated on the right.
doi:10.1371/journal.pgen.1002991.g003

(Figure 5F, right panel). We confirmed by immunohistochemistry that *asd-2 (yb1540)* mutation and/or *asd-2 (RNAi)* resulted in ectopic expression of UNC-60A in body wall muscles in the *unc-60B (su158)* background (Figure S3). Transgenic expression of UNC-60A (Figure 5G) as well as UNC-60B (Figure 5H) in body wall muscles restored sinusoidal locomotion of *unc-60B (su158)* mutant, indicating that UNC-60A can exert, at least in part, functions of muscle-specific UNC-60B isoform and that possible splicing change in other genes are not required for the phenotype suppression. These observations demonstrate that ASD-2 is a bona fide regulator of the muscle-specific pre-mRNA processing of the endogenous *unc-60* gene as well as SUP-12.

SUP-12 represses excision of intron 1A from the endogenous *unc-60* transcript

Finally, we analyzed splicing patterns of mature and partially spliced RNAs from the endogenous *unc-60* gene (Figure 6). For this experiment, we used wild-type and *sup-12 (yb1253)* worms because *asd-2 (yb1540)* mutation exhibited weaker effect on the *unc-60* reporter. In the wild type, mature UNC-60A and UNC-60B mRNAs were almost equally detected (Figure 6A, lane 3), while the latter was hardly detectable in *sup-12* mutant (lane 4), consistent with the result with the reporter (Figure 2H) and our previous study [30]. To analyze processing patterns of UNC-60B RNAs in body wall muscles, we amplified partially spliced RNAs carrying intron 2B, 3B or 4B with a forward primer in exon 1 and intronic reverse primers (Figure 6B). Partially spliced RNAs committed to UNC-60B, in which exon 1 was connected to exon 2B, were detected in the wild type (all panels, lane 3, bands 2 and 3) but were undetected in *sup-12* mutant (lane 4), consistent with the result shown in Figure 6A. These results indicated that SUP-12 is required for proper splicing between exon 1 and exon 2B in muscles. In *sup-12* mutant, all the introns, including intron 1A, were excised in the only detected RNAs (Figure 6B, all panels, lane 4, band 1), while in the wild type, intron 1A is retained in the longest detected RNAs (all panels, lane 3, band 1), indicating that SUP-12 represses excision of intron 1A.

We next analyzed partially spliced RNAs from the UNC-60A region (Figure 6C, 6D). Although the detected RNAs derived from this region were mixture of those in muscles and in non-muscle tissues, we assumed that differences in their relative amounts could be attributed to functions of SUP-12 in muscles. With a forward primer in intron 1A and a reverse primer in exon 5A (Figure 6C), we detected eight RNA species in *sup-12* mutant (lane 4, bands 1–6). These RNAs were all the theoretical intermediates in the UNC-60A processing. In the wild type (lane 3), two of the RNAs (bands 3 and 6) predominated, suggesting that SUP-12 represses their production. In these RNAs, intron 1A alone (band 6) or introns 1A and 2A were retained (band 3), supporting the idea that SUP-12 represses excision of intron 1A, and weakly of intron 2A, even after introns 3A and 4A are excised. We then analyzed the partially spliced RNAs with the forward primer in exon 1 and intronic reverse primers in introns 2A, 3A and 4A (Figure 6D). All the two (top panel, band 1–2), four (middle panel, bands 1–4) and eight (bottom panel, bands 1–7) theoretical intermediate RNA species were detected in *sup-12* mutant (lane 4), and relative amounts of the partially spliced RNAs to the pre-mRNAs (band 1) in the wild type (lane 3) and *sup-12* mutant (lane 4) were in good accordance with the idea that excision of introns 1A and 2A is facilitated in the absence of SUP-12. All these analyses of the partially spliced RNAs supported the model that SUP-12 represses excision of intron 1A to preserve exon 1 until exon 2B is transcribed in muscles.

Discussion

In this study, we have provided genetic and biochemical analyses of the mechanisms for regulation of the muscle-specific alternative processing of the *unc-60* pre-mRNA. Figure 7 illustrates models of the pre-mRNA processing deduced from this study. In non-muscle tissues (Figure 7A), intron 1A and the other introns are excised during or after transcription and UNC-60A mRNA is generated. The order of intron removal is not strictly regulated as suggested by the presence of all the theoretical partially spliced RNAs (Figure 6C, 6D). In muscles (Figure 7B), ASD-2b and SUP-12 cooperatively bind to CUAAC repeats and UGUGUG stretch, respectively, in intron 1A to repress excision of intron 1A and weakly of intron 2A during transcription of the UNC-60A region. When UNC-60B-specific region is being transcribed, exon 1 is readily spliced to exon 2B, and introns 3B and 4B are also readily removed in the order of transcription (Figure 6B). Introns 3A and 4A are properly and rapidly excised during the UNC-60B processing (Figure 6C) likely due to their small sizes (53 nt and 60 nt, respectively). This may explain why exon 1 is not aberrantly spliced to exons 3A or 4A but is exclusively spliced to exon 2B to form UNC-60B mRNA. Regulation of tissue-specific alternative polyadenylation may also be involved in the fate-decision of the *unc-60* transcript, although the results demonstrated above did not provide conclusive evidence that ASD-2 and/or SUP-12 regulate muscle-specific repression of the polyadenylation site for UNC-60A mRNA.

We have demonstrated that ASD-2 and SUP-12 cooperatively represses the 3′-splice site and not the 5′-splice site of intron 1A. Although *C. elegans* does not have a recognizable branch point consensus or a polypyrimidine tract [42], a putative branch site for intron 1A is the A at position -19, between CUAAC repeats and UGUGUG stretch (Figure 3A). This A is the first A upstream from the 3′ splice site and is close to the positions where the putative branch site A is frequently found [43]. It is therefore reasonable to suggest that formation of ASD-2b/SUP-12/RNA ternary complex sterically hinders U2 snRNP auxiliary factor (U2AF) bound to the 3′-splice site from recruiting U2 snRNP to the branch site. The situation is quite similar to muscle-specific repression of *egl-15* exon 5B, where the Fox-1 family proteins and SUP-12 cooperatively bind to juxtaposed *cis*-elements overlapping a putative branch site [20,38]. Recent microarray analyses of alternatively spliced exons in splicing factor mutants including *sup-12* identified many other splicing events affected by multiple splicing factors [44]. Combi-

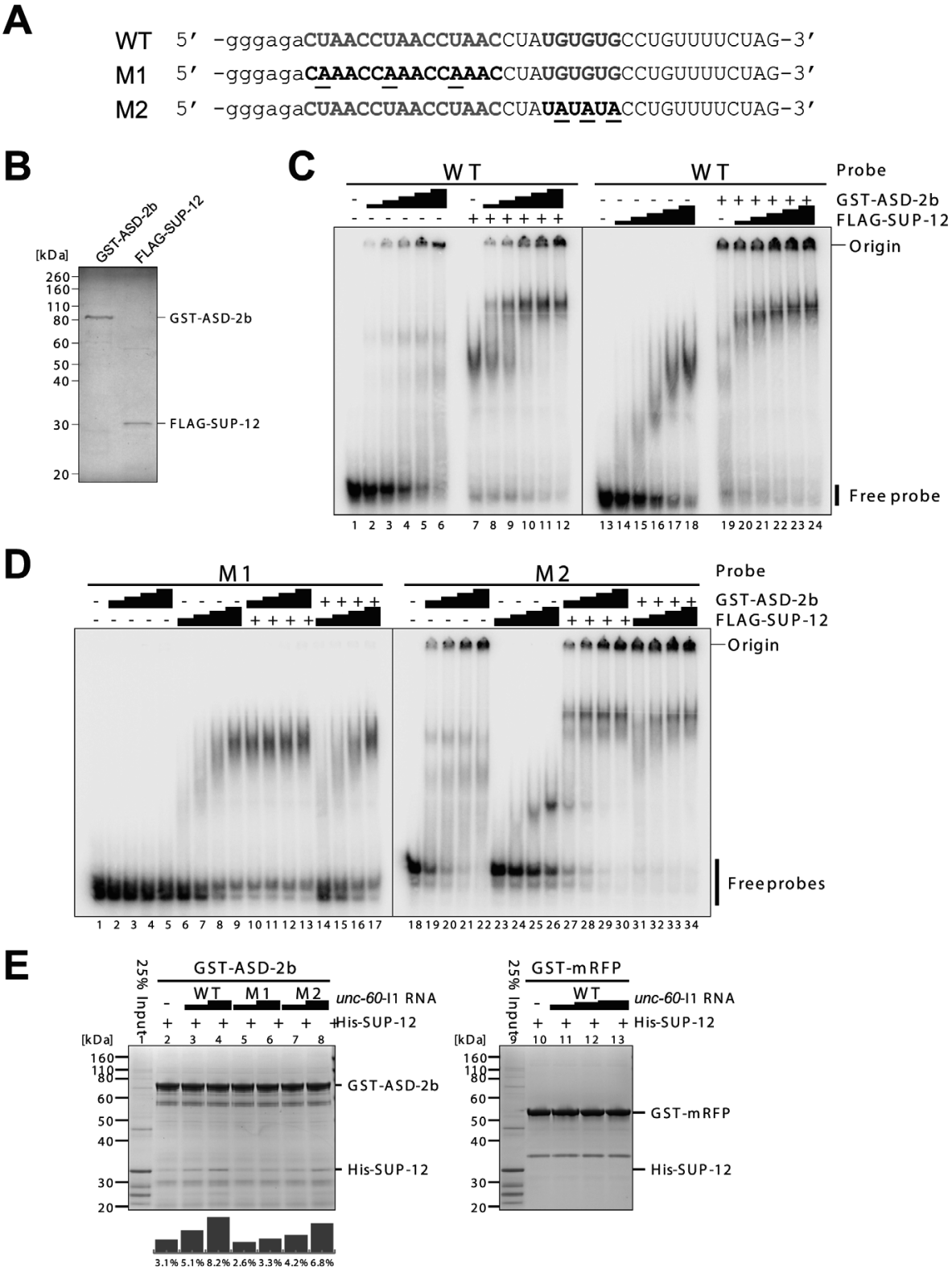
A
WT 5′ -gggagaCUAACCUAACCUAACCUAUGUGUGCCUGUUUUCUAG-3′
M1 5′ -gggagaCAAACCAAACCAAACCUAUGUGUGCCUGUUUUCUAG-3′
M2 5′ -gggagaCUAACCUAACCUAACCUAUAUAUACCUGUUUUCUAG-3′
B
[kDa]
GST-ASD-2b
FLAG-SUP-12
260
160
110
80
60
50
40
30
20
GST-ASD-2b
FLAG-SUP-12
C
WT
WT
Probe
GST-ASD-2b
FLAG-SUP-12
Origin
Free probe
1 2 3 4 5 6 7 8 9 10 11 12 13 14 15 16 17 18 19 20 21 22 23 24
D
M1
M2
Probe
GST-ASD-2b
FLAG-SUP-12
Origin
Free probes
1 2 3 4 5 6 7 8 9 10 11 12 13 14 15 16 17 18 19 20 21 22 23 24 25 26 27 28 29 30 31 32 33 34
E
25% Input
GST-ASD-2b
WT M1 M2
unc-60-I1 RNA
His-SUP-12
[kDa]
1 2 3 4 5 6 7 8
160
110
80
60
50
40
30
20
GST-ASD-2b
His-SUP-12
3.1% 5.1% 8.2% 2.6% 3.3% 4.2% 6.8%
25% Input
GST-mRFP
WT
unc-60-I1 RNA
His-SUP-12
[kDa]
9 10 11 12 13
160
110
80
60
50
40
30
20
GST-mRFP
His-SUP-12

Figure 4. ASD-2 and SUP-12 cooperatively bind to *unc-60* intron 1A *in vitro* via direct and specific binding to CUAAC repeats and UGUGUG stretch, respectively. (*A*) Sequences of radiolabelled WT, M1 and M2 probes used in EMSAs. The sequences are illustrated as in Figure 3B, bottom panel. Lowercase indicates residues derived from T7 promoter. (*B*) SDS-PAGE and CBB staining of recombinant GST-fused full-length ASD-2b (GST-ASD-2b) and FLAG-tagged full-length SUP-12 (FLAG-SUP-12) proteins used in (*C*) and (*D*). (*C* and *D*) EMSAs using WT (*C*), M1 (*D*, lanes 1–17) and M2 (*D*, lanes 18–34) probes with 2-fold dilution series of GST-ASD-2b or FLAG-SUP-12 protein alone or in combination. (+) indicates the maximal amounts of proteins used in the dilution series. (*E*) Pull-down experiments of recombinant His-tagged SUP-12 (His-SUP-12) protein with immobilized GST-fusion proteins. GST-ASD-2b (lanes 2–8) and GST-mRFP (lanes 10–13) were incubated with His-SUP-12, 25% of which was run in lanes 1 and 9, in the presence of various concentrations of wild-type (WT), M1 mutant and M2 mutant *unc-60* intron 1A (*unc-60*-I1A) RNAs. Bar graphs below the gel indicate the amounts of His-SUP-12 pulled down with GST-ASD-2b relative to the input (lane 1). A representative result from two repeated experiments is shown.
doi:10.1371/journal.pgen.1002991.g004

natorial regulation by multiple splicing factors may be the common feature in tissue-specific alternative pre-mRNA processing in *C. elegans*.

ASD-2 ortholog in *Drosophila*, Held out wings (How) [45,46,47], and that in zebrafish, Quaking A (QkA) [48], are known to be required for muscle development or activity by mutant analyses. Vertebrate orthologs of SUP-12, known as SEB-4 or RBM24, are also expressed in muscle tissues and have recently been shown to be involved in myogenic differentiation by knockdown experiments [49,50,51,52,53]. However, the target events that these orthologs regulate in muscles remain almost unclear. Considering the highly conserved amino acid sequences and their expression patterns, it is likely that the orthologs of ASD-2 and SUP-12 regulate alternative pre-mRNA processing to produce muscle-specific protein isoforms in higher organisms.

In this study, we have presented a model of complex alternative pre-mRNA processing of a gene generating two almost distinct mRNAs. An important aspect of this study is the successful application of a dichromatic fluorescence reporter system to analyze the complex alternative pre-mRNA processing. The asymmetric pair of fluorescence reporter minigenes utilized in this study offers an alternative option for visualizing complex processing patterns besides symmetric pairs of minigenes applied to mutually exclusive exons and cassette exons [32,33]. Another example of evolutionarily conserved genes with a structure similar to the *unc-60* gene is the cholinergic gene locus; genes encoding choline acetyltransferase (ChAT) and vesicular acetylcholine transporter (VAChT) share the common first exon, and the other exon(s) for VAChT reside in the first intron of the ChAT gene in mammals [54], *Drosophila* [55] and *C. elegans* [56]. The regulation mechanisms presented here would provide insight into the regulation of this kind of genes.

We demonstrated that ectopically expressed UNC-60A can compensate for the function of UNC-60B in sarcomeric actin organization in body wall muscles of *unc-60B* mutant. However, both UNC-60A and UNC-60B have characteristic actin-regulatory activities of ADF/cofilin *in vitro* with some quantitative differences [27,28,29]; UNC-60A has strong actin-monomer sequestering and only weak actin-filament severing activities, while UNC-60B has no actin-monomer sequestering and strong actin-filament severing activities. Although UNC-60A can compensate for the function of UNC-60B in body wall muscles, sarcomeric actin filaments in UNC-60A-complemented *unc-60B* mutant muscles still exhibit minor disorganization (unpublished data), suggesting that UNC-60B is a more suitable isoform. On the other hand, UNC-60B cannot compensate for the function of UNC-60A in the gonadal myoepithelial sheath [29]. This work and our previous works demonstrated that UNC-60A and UNC-60B are specifically adapted for functions in non-muscle and muscle cells, respectively, emphasizing that precise expression of appropriate ADF/cofilin isoforms, unravelled in this study, is important for development of tissue-specific actin-cytoskeletal structures [26,29].

Materials and Methods

Plasmid construction

To construct the *unc-60E1-E2A-RFP* and *unc-60E1-E3B-GFP* cassettes, *unc-60* genomic fragments spanning from exon 1 through 2A and exon 1 through 3B, respectively, were amplified from N2 genomic DNA and cloned into Gateway Entry vectors (Invitrogen) carrying either mRFP1 [57] or EGFP (Clontech) cDNA by using In-Fusion system (BD Biosciences). *M1* and *M2* mutations were introduced by mutagenesis with Quickchange II (Stratagene). Expression vectors were constructed by homologous recombination between the Entry vectors and Destination vectors [31,33] with LR Clonase II (Invitrogen). Sequences of the primers used in plasmid construction are available in Table S1.

Worm culture and microscopy

Worms were cultured following standard methods. Transgenic lines were prepared essentially as described [33] using *lin-15 (n765)* as a host or pmyo-2-mRFP as a marker. Integrant lines were generated by ultraviolet light irradiation as described previously [33,58]. Images of fluorescence reporter worms were captured using a fluorescence stereoscope (MZ16FA, Leica) with a dual and-pass filter GFP/DsRed equipped with a colour, cooled CCD camera (DP71, Olympus) or a confocal microscope (Fluoview FV500, Olympus) and processed with Metamorph (Molecular Devices) or Photoshop (Adobe).

RNA interference

RNAi experiments by feeding were performed essentially as described [59]. Briefly, L4 hermaphrodites were transferred to agar plates seeded with bacteria expressing dsRNAs of target genes and their progeny were scored for colour and behavioural phenotypes or used for staining. For RNAi experiment by micro-injection, sense and anti-sense *asd-2* RNAs were prepared as described preciously [32] and were annealed at room temperature and 1–5 μg/μl dsRNA was injected into the gonad of young adult hermaphrodites. Injected worms were cultured at 20°C and the colour phenotype of their progeny was evaluated.

RT–PCR

Total RNAs were extracted from worms by using RNeasy Mini kit (Qiagen) and DNase I (Promega). RNAs (300–500 ng) were reverse transcribed using random hexamers and Superscript II (Invitrogen) according to manufacturer's protocol. PCR was performed essentially as described previously [31,33]. For amplification of partially spliced RNAs, total RNAs were reverse transcribed with PrimeScript II and random hexamers (Takara), and amplified with BIOTAQ (Bioline) and analyzed by using BioAnalyzer (Agilent). Sequences of the RT-PCR products were confirmed either by direct sequencing or by cloning and sequencing. Sequences of the primers used in the RT-PCR assays are available in Table S2.

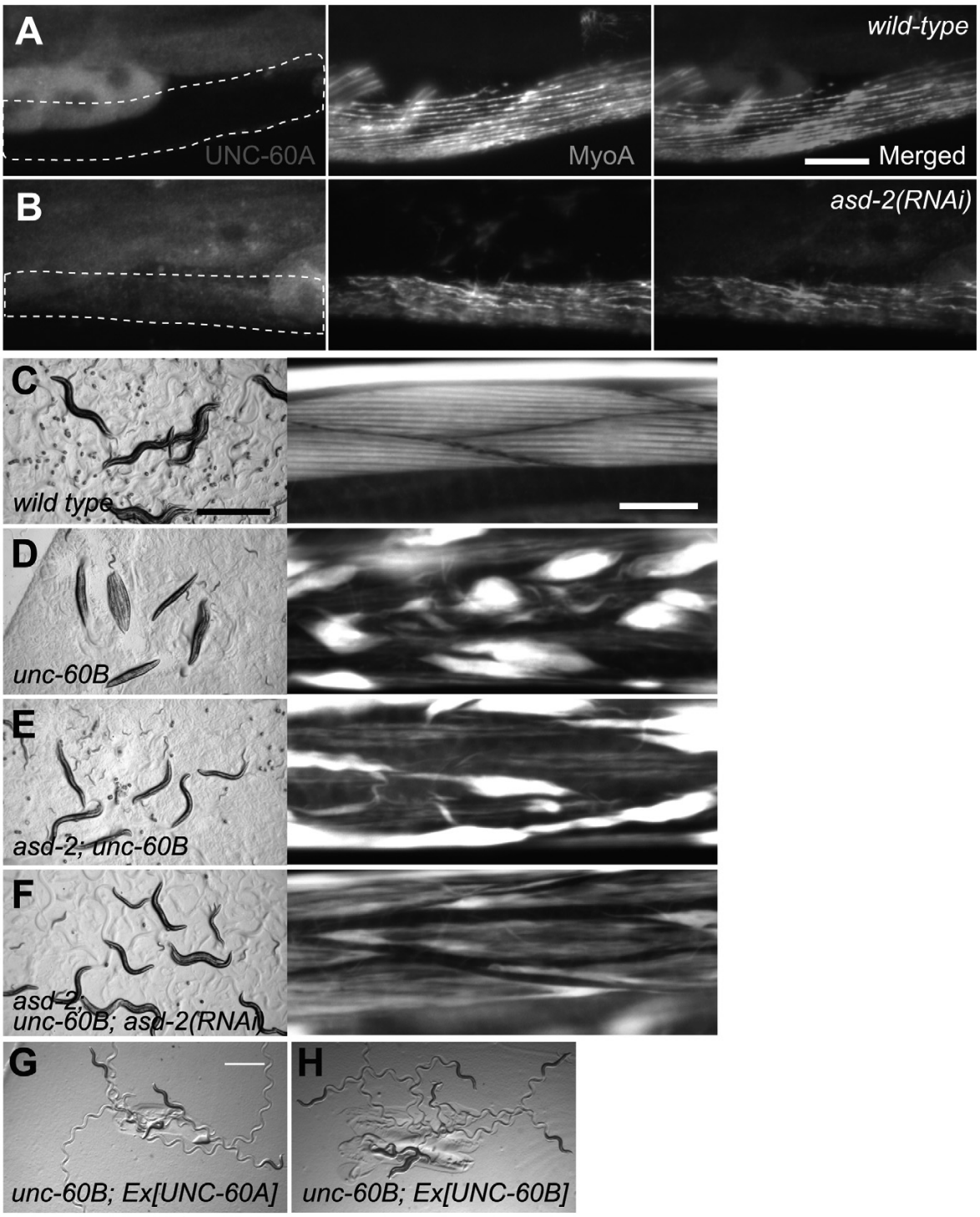

Figure 5. ASD-2 regulates alternative pre-mRNA processing of the endogenous *unc-60* gene in body wall muscles. (*A*, *B*) Immunofluorescence images of UNC-60A (left) and MyoA (middle) and merged images (right) of wild-type (*A*) and *asd-2(RNAi)* (*B*) worms. MyoA, a heavy chain of muscle-specific myosin, is a marker for body wall muscles (encircled with dotted lines). Scale bar, 20 μm. (*C*–*F*) Micrographs of worms on bacterial lawns (left) and actin filaments in body wall muscles stained with tetramethylrhodamine-phalloidin (right) of N2 (*C*), *unc-60 (su158)* (*D*),

asd-2 (yb1540); unc-60 (su158) (*E*) and *asd-2 (yb1540); unc-60 (su158); asd-2 (RNAi)* (*F*). Scale bars, 1 mm in left panels and 20 μm in right panels. (*G*, *H*) Micrographs of *unc-60 (su158); ybEx2149 [myo-3::UNC-60A]* (*G*) and *unc-60 (su158); ybEx2148 [myo-3::UNC-60B]* (*H*) worms on bacterial lawns. Scale bar, 1 mm.
doi:10.1371/journal.pgen.1002991.g005

Recombinant proteins

Denatured His-tagged full-length ASD-2b for immunization was purified from denatured bacterial lysate by using Ni-NTA agarose (QIAGEN). Cold-shock inducible expression vectors for His-GST-fused full-length ASD-2b and mRFP1 and FLAG-tagged full-length SUP-12 were constructed by using Destination vectors pDEST-Cold-GST and pDEST-Cold-FLAG (H.K.), respectively. GST-ASD-2b and FLAG-SUP-12 were purified by using Glutathione Sepharose 4B (GE Healthcare) and Anti-FLAG M2 Magnetic Beads (Sigma), respectively, and dialyzed against RNA binding buffer (see below). Purified proteins were separated by standard SDS-PAGE and stained with SimplyBlue SafeStain (Invitrogen).

Antibody production and Western blotting

Rabbit polyclonal anti-ASD-2b antiserum was generated with denatured recombinant His-ASD-2b protein by Operon Biotechnologies (Tokyo, Japan). IgG fraction (TD0135-02) was prepared from the antiserum by Medical & Biological Laboratories (Nagoya, Japan). Worm lysates were extracted from synchronized L1 larvae, separated by neutral polyacrylamide gel electrophoresis (NuPAGE, Invitrogen) and transferred to nitrocellulose membrane (Protran BA85, Whatman). Western blotting was performed with 15 μg/ml anti-ASD-2b (TD0135-02) or 1:40,000-diluted anti-actin monoclonal antibody (Ab-1, Calbiochem) and 1:1,000-diluted HRP-conjugated anti-rabbit IgG antibody (Pierce) or 1:10,000-diluted HRP-conjugated anti-mouse IgM antibody (Calbiochem). Chemiluminescence signals (West Dura, Thermo) were detected by using LAS4000 (GE Healthcare).

Immunohistochemistry

For staining with anti-ASD-2b, mixed stages of N2 and *asd-2 (yb1540)* worms were fixed with Bouin's fixative (15:5:1 mixture of saturated picric acid, formalin and acetic acid) supplemented with 25% methanol and 1.25% 2-mercaptoethanol for 60 min at room temperature, washed with phosphate-buffered saline (PBS) and permeabilized with 5% 2-mercaptoethanol and 1% Triton X-100 in PBS at 37°C for 30 hours. Fixed worms were treated with blocking buffer (0.5% skim milk and 0.5% bovine serum albumin (BSA) in PBS) for 2 hours at room temperature and stained with

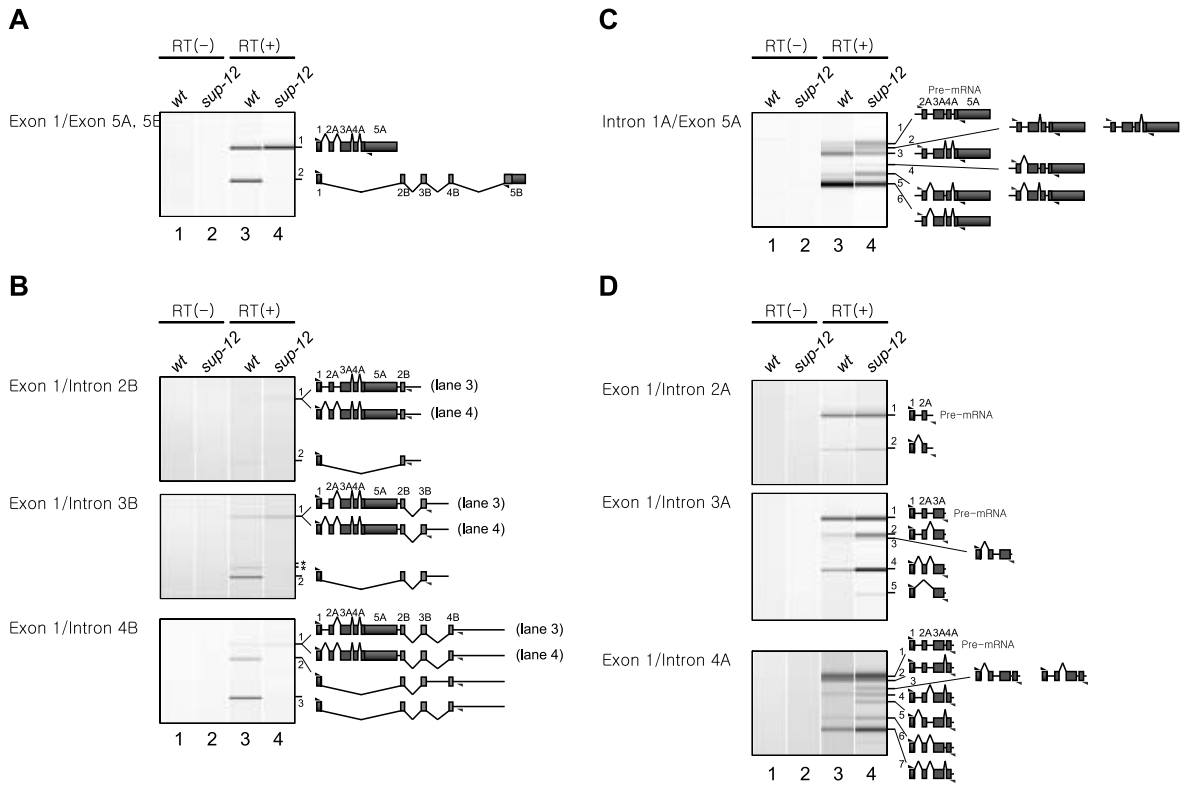

Figure 6. SUP-12 represses excision of intron 1A from the endogenous *unc-60* transcript. (*A–D*) RT-PCR analyses of mature mRNAs (*A*) and partially spliced RNAs (*B–D*) from the endogenous *unc-60* gene. Total RNAs from synchronized L1 larvae of N2 (lanes 1 and 3) and *sup-12 (yb1253)* mutant (lanes 2 and 4) were subjected to RT-PCR without (lanes 1 and 2) or with (lanes 3 and 4) reverse transcriptase (RT). Positions of the primers are indicated on the left. Each band is numbered in the order of size. Schematic structures of the RNAs are indicated on the right. Black and blue triangles indicate positions and directions of exonic and intronic primers, respectively. Asterisks denote artificially amplified fragments.
doi:10.1371/journal.pgen.1002991.g006

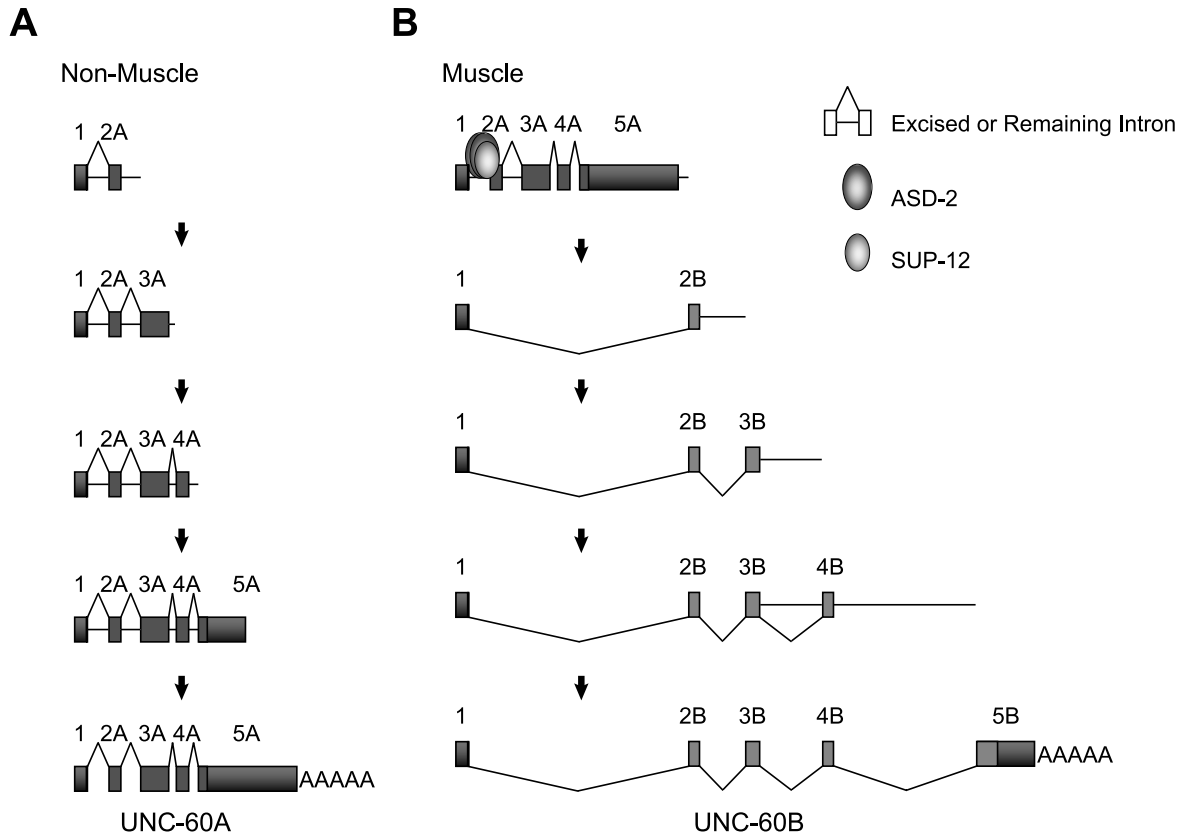

Figure 7. Schematic illustrations of the tissue-specific alternative processing of the *unc-60* pre-mRNA during the course of transcription. (*A*) A model of UNC-60A mRNA processing in non-muscle tissues. (*B*) A model of UNC-60B mRNA processing in muscles. See Discussion for detail.
doi:10.1371/journal.pgen.1002991.g007

6 μg/ml anti-ASD-2b (TD0135-02) as a primary antibody in blocking buffer for 24 hours at room temperature and then with 2 μg/ml Alexa488-conjugated goat anti-rabbit IgG (Invitrogen) as a secondary antibody together with 1 μg/ml Hoechst 33258 (Hoechst) in blocking buffer for 2 hours at room temperature. Fluorescence images were captured by using a compound microscope (DM6000B, Leica) equipped with a colour, cooled CCD camera (DFC310FX, Leica) or an inverted fluorescence microscope (Nikon TE2000) equipped with a monochrome CCD camera (SPOT RT, Diagnostic Instruments, Inc). Staining with anti-UNC-60A and anti-MyoA were performed as described previously [30]. Actin filaments were visualized by staining with tetramethylrhodamine-phalloidin as described previously [60].

Electophoretic mobility shift assay (EMSA)

^{32}P-labelled RNA probes were generated by *in vitro* transcription with [α^{32}P] UTP (Perkin Elmer) and T7 RNA polymerase (Takara). Sequences of template oligo DNAs are available in Table S3. Gel-purified RNA probes alone or with increasing amounts of recombinant protein(s) were incubated in 25 μl of RNA binding buffer (20 mM HEPES-KOH (pH7.9), 150 mM KCl, 5% glycerol, 1% Triton X-100, 1 mM DTT and 0.1 mM PMSF) supplemented with 100 ng/μl *E. coli* tRNA and 50 ng/μl BSA for 30 min at 20°C. Each sample was separated on a non-denaturing 4% polyacrylamide gel and analyzed with a fluoro-imaging analyzer (FLA-3000G, Fuji Film).

Pull-down

His-GST-fused recombinant full-length ASD-2b and mRFP1 proteins were immobilized on glutathione sepharose 4B beads (GE Healthcare) and incubated with His-SUP-12 in 100 μl of pull-down buffer (20 mM HEPES-KOH (pH7.9), 150 mM KCl, 1% Triton X-100, 1 mM DTT and 0.1 mM PMSF) supplemented with 100 ng/μl *E. coli* tRNA, 50 ng/μl BSA and 0, 30, 100, or 300 nM of *unc-60*-I1A RNAs (Operon Biotechnologies) for 30 min at 20°C. The sequences of the *unc-60*-I1A RNAs: *unc-60*-I1A-WT, 5′-UUUUUGCCUAACCUAACCUAACCUAUGUGUGCCU-GUUUU-3′; *unc-60*-I1A-M1, 5′-UUUUUGCCAAACCAAAC-CAAACCUAUGUGUGCCUGUUUU-3′; *unc-60*-I1-M2, 5′-UUUUUGCCUAACCUAACCUAACCUAUAUAUACCUGU-UUU-3′. Beads were washed four times with 1 ml pull-down buffer. Bound proteins were eluted with LDS sample buffer and separated by NuPAGE (Invitrogen). Gels were stained with SimplyBlue SafeStain (Invitrogen) and detected and analyzed by using LAS4000 (GE Healthcare).

Supporting Information

Figure S1 RNAi knockdown of SUP-12-interacting proteins revealed ASD-2 as a candidate regulator of the *unc-60* reporter expression. Microphotographs of *ybIs1831* worms fed with bacterial clones expressing dsRNAs for indicated genes. Images

in red channels are pseudo-coloured in magenta. Scale bar, 100 μm.
(PDF)

Figure S2 RT–PCR analysis of the endogenous *unc-60* mRNAs from synchronized L1 worms of N2 (lane 1), *asd-2 (yb1540)* (lane 2), *asd-2 (yb1540); ybIs1831; control (RNAi)* (lane 3) and *asd-2 (yb1540); ybIs1831; asd-2 (RNAi)* (lane 4). Splicing patterns of the mRNAs are schematically shown on the right. Triangles indicate positions and directions of the primers.
(PDF)

Figure S3 Immunofluorescence images of UNC-60A (left) and MyoA (middle) and merged images (right) of *unc-60 (su158)* (*A*), *unc-60 (su158); asd-2 (RNAi)* (*B*), *asd-2 (yb1540); unc-60 (su158)* (*C*) and *asd-2 (yb1540); unc-60 (su158); asd-2 (RNAi)* (*D*) worms. MyoA is a marker for body wall muscles (encircled with dotted lines in left panels). Scale bar, 20 μm.
(PDF)

Table S1 Sequences of primers used in plasmid construction.
(RTF)

Table S2 Sequences of primers used in RT–PCR assays.
(RTF)

Table S3 Sequences of oligo DNAs used in *in vitro* transcription.
(RTF)

Acknowledgments

We thank Roger Tsien of University of California San Diego for mRFP1 cDNA. We thank Monima Alam, Hajime Ito, Takayuki Yamada, Hideto Kudo, Satomi Takei, and Takako Ideue for technical assistance. We thank *Caenorhabditis* Genetics Center (CGC) for strains.

Author Contributions

Conceived and designed the experiments: GO SO MH HK. Performed the experiments: GO KO MT YW HK. Analyzed the data: GO SO HK. Contributed reagents/materials/analysis tools: GO KO YW SO HK. Wrote the paper: GO SO MH HK.

References

1. Licatalosi DD, Darnell RB (2010) RNA processing and its regulation: global insights into biological networks. Nat Rev Genet 11: 75–87.
2. Nilsen TW, Graveley BR (2010) Expansion of the eukaryotic proteome by alternative splicing. Nature 463: 457–463.
3. Pan Q, Shai O, Lee LJ, Frey BJ, Blencowe BJ (2008) Deep surveying of alternative splicing complexity in the human transcriptome by high-throughput sequencing. Nat Genet 40: 1413–1415.
4. Wang ET, Sandberg R, Luo S, Khrebtukova I, Zhang L, et al. (2008) Alternative isoform regulation in human tissue transcriptomes. Nature 456: 470–476.
5. Matlin AJ, Clark F, Smith CW (2005) Understanding alternative splicing: towards a cellular code. Nat Rev Mol Cell Biol 6: 386–398.
6. Black DL (2003) Mechanisms of alternative pre-messenger RNA splicing. Annu Rev Biochem 72: 291–336.
7. Witten JT, Ule J (2011) Understanding splicing regulation through RNA splicing maps. Trends Genet 27: 89–97.
8. McManus CJ, Graveley BR (2011) RNA structure and the mechanisms of alternative splicing. Curr Opin Genet Dev 21: 373–379.
9. Chen M, Manley JL (2009) Mechanisms of alternative splicing regulation: insights from molecular and genomics approaches. Nat Rev Mol Cell Biol 10: 741–754.
10. Schiaffino S, Reggiani C (1996) Molecular diversity of myofibrillar proteins: gene regulation and functional significance. Physiol Rev 76: 371–423.
11. Llorian M, Smith CW (2011) Decoding muscle alternative splicing. Curr Opin Genet Dev 21: 380–387.
12. Kalsotra A, Cooper TA (2011) Functional consequences of developmentally regulated alternative splicing. Nat Rev Genet 12: 715–729.
13. Gunning PW, Schevzov G, Kee AJ, Hardeman EC (2005) Tropomyosin isoforms: divining rods for actin cytoskeleton function. Trends Cell Biol 15: 333–341.
14. Wei B, Jin JP (2010) Troponin T isoforms and posttranscriptional modifications: Evolution, regulation and function. Arch Biochem Biophys 505: 144–154.
15. Kalsotra A, Xiao X, Ward AJ, Castle JC, Johnson JM, et al. (2008) A postnatal switch of CELF and MBNL proteins reprograms alternative splicing in the developing heart. Proc Natl Acad Sci U S A 105: 20333–20338.
16. Bland CS, Wang ET, Vu A, David MP, Castle JC, et al. (2010) Global regulation of alternative splicing during myogenic differentiation. Nucleic Acids Res 38: 7651–7664.
17. Brudno M, Gelfand MS, Spengler S, Zorn M, Dubchak I, et al. (2001) Computational analysis of candidate intron regulatory elements for tissue-specific alternative pre-mRNA splicing. Nucleic Acids Res 29: 2338–2348.
18. Sugnet CW, Srinivasan K, Clark TA, O'Brien G, Cline MS, et al. (2006) Unusual intron conservation near tissue-regulated exons found by splicing microarrays. PLoS Comput Biol 2: e4. doi:10.1371/journal.pcbi.0020004
19. Pascual M, Vicente M, Monferrer L, Artero R (2006) The Muscleblind family of proteins: an emerging class of regulators of developmentally programmed alternative splicing. Differentiation 74: 65–80.
20. Kuroyanagi H (2009) Fox-1 family of RNA-binding proteins. Cell Mol Life Sci 66: 3895–3907.
21. Vlasova IA, Bohjanen PR (2008) Posttranscriptional regulation of gene networks by GU-rich elements and CELF proteins. RNA Biol 5: 201–207.
22. Llorian M, Schwartz S, Clark TA, Hollander D, Tan LY, et al. (2010) Position-dependent alternative splicing activity revealed by global profiling of alternative splicing events regulated by PTB. Nat Struct Mol Biol 17: 1114–1123.
23. Chen CD, Kobayashi R, Helfman DM (1999) Binding of hnRNP H to an exonic splicing silencer is involved in the regulation of alternative splicing of the rat beta-tropomyosin gene. Genes Dev 13: 593–606.
24. McKim KS, Matheson C, Marra MA, Wakarchuk MF, Baillie DL (1994) The *Caenorhabditis elegans unc-60* gene encodes proteins homologous to a family of actin-binding proteins. Mol Gen Genet 242: 346–357.
25. Ono S (2007) Mechanism of depolymerization and severing of actin filaments and its significance in cytoskeletal dynamics. Int Rev Cytol 258: 1–82.
26. Ono K, Parast M, Alberico C, Benian GM, Ono S (2003) Specific requirement for two ADF/cofilin isoforms in distinct actin-dependent processes in *Caenorhabditis elegans*. J Cell Sci 116: 2073–2085.
27. Ono S, Benian GM (1998) Two *Caenorhabditis elegans* actin depolymerizing factor/cofilin proteins, encoded by the *unc-60* gene, differentially regulate actin filament dynamics. J Biol Chem 273: 3778–3783.
28. Yamashiro S, Mohri K, Ono S (2005) The two *Caenorhabditis elegans* actin-depolymerizing factor/cofilin proteins differently enhance actin filament severing and depolymerization. Biochemistry 44: 14238–14247.
29. Ono K, Yamashiro S, Ono S (2008) Essential role of ADF/cofilin for assembly of contractile actin networks in the *C. elegans* somatic gonad. J Cell Sci 121: 2662–2670.
30. Anyanful A, Ono K, Johnsen RC, Ly H, Jensen V, et al. (2004) The RNA-binding protein SUP-12 controls muscle-specific splicing of the ADF/cofilin pre-mRNA in *C. elegans*. J Cell Biol 167: 639–647.
31. Kuroyanagi H, Kobayashi T, Mitani S, Hagiwara M (2006) Transgenic alternative-splicing reporters reveal tissue-specific expression profiles and regulation mechanisms *in vivo*. Nat Methods 3: 909–915.
32. Ohno G, Hagiwara M, Kuroyanagi H (2008) STAR family RNA-binding protein ASD-2 regulates developmental switching of mutually exclusive alternative splicing *in vivo*. Genes Dev 22: 360–374.
33. Kuroyanagi H, Ohno G, Sakane H, Maruoka H, Hagiwara M (2010) Visualization and genetic analysis of alternative splicing regulation *in vivo* using fluorescence reporters in transgenic *Caenorhabditis elegans*. Nat Protoc 5: 1495–1517.
34. Volk T, Israeli D, Nir R, Toledano-Katchalski H (2008) Tissue development and RNA control: "HOW" is it coordinated? Trends Genet 24: 94–101.
35. Ogura K, Wicky C, Magnenat L, Tobler H, Mori I, et al. (1994) *Caenorhabditis elegans unc-51* gene required for axonal elongation encodes a novel serine/threonine kinase. Genes Dev 8: 2389–2400.
36. Tomoda T, Bhatt RS, Kuroyanagi H, Shirasawa T, Hatten ME (1999) A mouse serine/threonine kinase homologous to *C. elegans* UNC51 functions in parallel fiber formation of cerebellar granule neurons. Neuron 24: 833–846.
37. Ono S, Baillie DL, Benian GM (1999) UNC-60B, an ADF/cofilin family protein, is required for proper assembly of actin into myofibrils in *Caenorhabditis elegans* body wall muscle. J Cell Biol 145: 491–502.
38. Kuroyanagi H, Ohno G, Mitani S, Hagiwara M (2007) The Fox-1 family and SUP-12 coordinately regulate tissue-specific alternative splicing *in vivo*. Mol Cell Biol 27: 8612–8621.
39. Li S, Armstrong CM, Bertin N, Ge H, Milstein S, et al. (2004) A map of the interactome network of the metazoan *C. elegans*. Science 303: 540–543.
40. Pulak R, Anderson P (1993) mRNA surveillance by the *Caenorhabditis elegans smg* genes. Genes Dev 7: 1885–1897.
41. Kabat JL, Barberan-Soler S, McKenna P, Clawson H, Farrer T, et al. (2006) Intronic alternative splicing regulators identified by comparative genomics in nematodes. PLoS Comput Biol 2: e86. doi:10.1371/journal.pcbi.0020086

42. Hollins C, Zorio DA, MacMorris M, Blumenthal T (2005) U2AF binding selects for the high conservation of the *C. elegans* 3′ splice site. RNA 11: 248–253.
43. Blumenthal T, Steward K (1997) RNA processing and gene structure. In: Riddle D, Blumenthal T, Meyer B, Priess J, editors. *C elegans* II. Woodbury, N.Y.: Cold Spring Harbor Laboratory Press. pp. 117–145.
44. Barberan-Soler S, Medina P, Estella J, Williams J, Zahler AM (2011) Co-regulation of alternative splicing by diverse splicing factors in *Caenorhabditis elegans*. Nucleic Acids Res 39: 666–674.
45. Zaffran S, Astier M, Gratecos D, Semeriva M (1997) The *held out wings (how) Drosophila* gene encodes a putative RNA-binding protein involved in the control of muscular and cardiac activity. Development 124: 2087–2098.
46. Baehrecke EH (1997) *who* encodes a KH RNA binding protein that functions in muscle development. Development 124: 1323–1332.
47. Nir R, Grossman R, Paroush Z, Volk T (2012) Phosphorylation of the *Drosophila melanogaster* RNA-binding protein HOW by MAPK/ERK enhances its dimerization and activity. PLoS Genet 8: e1002632. doi:10.1371/journal.pgen.1002632
48. Lobbardi R, Lambert G, Zhao J, Geisler R, Kim HR, et al. (2011) Fine-tuning of Hh signaling by the RNA-binding protein Quaking to control muscle development. Development 138: 1783–1794.
49. Jin D, Hidaka K, Shirai M, Morisaki T (2010) RNA-binding motif protein 24 regulates myogenin expression and promotes myogenic differentiation. Genes Cells 15: 1158–1167.
50. Li HY, Bourdelas A, Carron C, Shi DL (2010) The RNA-binding protein Seb4/RBM24 is a direct target of MyoD and is required for myogenesis during *Xenopus* early development. Mech Dev 127: 281–291.
51. Maragh S, Miller RA, Bessling SL, McGaughey DM, Wessels MW, et al. (2011) Identification of RNA binding motif proteins essential for cardiovascular development. BMC Dev Biol 11: 62.
52. Poon KL, Tan KT, Wei YY, Ng CP, Colman A, et al. (2012) RNA-binding protein RBM24 is required for sarcomere assembly and heart contractility. Cardiovasc Res.
53. Miyamoto S, Hidaka K, Jin D, Morisaki T (2009) RNA-binding proteins Rbm38 and Rbm24 regulate myogenic differentiation via p21-dependent and -independent regulatory pathways. Genes Cells 14: 1241–1252.
54. Mallet J, Houhou L, Pajak F, Oda Y, Cervini R, et al. (1998) The cholinergic locus: ChAT and VAChT genes. J Physiol Paris 92: 145–147.
55. Kitamoto T, Wang W, Salvaterra PM (1998) Structure and organization of the *Drosophila* cholinergic locus. J Biol Chem 273: 2706–2713.
56. Alfonso A, Grundahl K, McManus JR, Asbury JM, Rand JB (1994) Alternative splicing leads to two cholinergic proteins in *Caenorhabditis elegans*. J Mol Biol 241: 627–630.
57. Campbell RE, Tour O, Palmer AE, Steinbach PA, Baird GS, et al. (2002) A monomeric red fluorescent protein. Proc Natl Acad Sci U S A 99: 7877–7882.
58. Mitani S (1995) Genetic regulation of *mec-3* gene expression implicated in the specification of the mechanosensory neuron cell types in *Caenorhabditis elegans*. Dev Growth & Diff 37: 551–557.
59. Kamath RS, Martinez-Campos M, Zipperlen P, Fraser AG, Ahringer J (2001) Effectiveness of specific RNA-mediated interference through ingested double-stranded RNA in *Caenorhabditis elegans*. Genome Biol 2: RESEARCH0002.
60. Ono S (2001) The *Caenorhabditis elegans unc-78* gene encodes a homologue of actin-interacting protein 1 required for organized assembly of muscle actin filaments. J Cell Biol 152: 1313–1319.

東京医科歯科大学

歯と骨の分子疾患科学 国際教育研究拠点

～デント・メドミクスのインテリジェンスハブ～

平成24年度 実績報告書